

Investigation of the Role of Ag salts in  
Pd-Catalysed Direct Arylation Reactions

Gayathri Athavan

Ph.D.

University of York

Chemistry

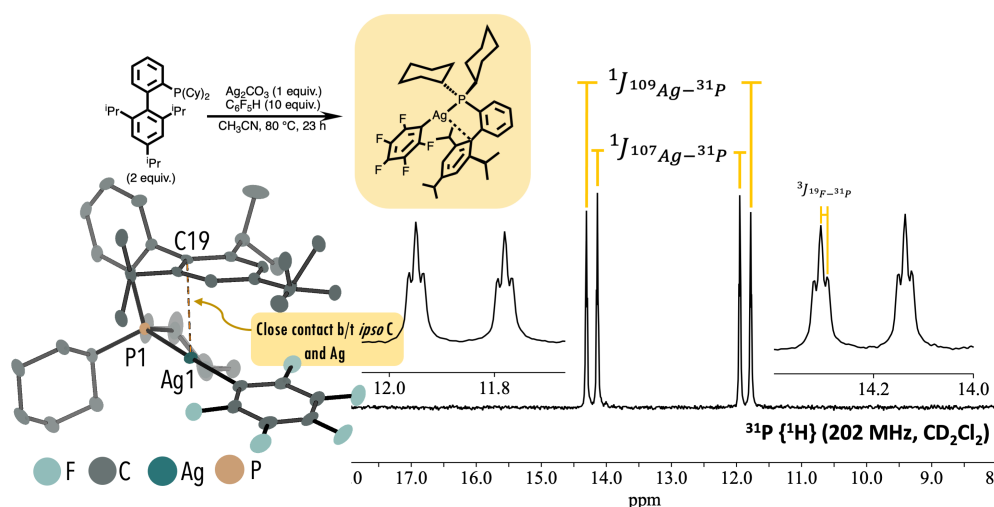
May 2022

## Abstract

$\text{Ag}^{\text{I}}$  salts are common additives in Pd-catalysed C–H functionalization reactions resulting in enhanced rates and yields compared to other metal salts. This was largely attributed to the ability of  $\text{Ag}^{\text{I}}$  to act as halide scavengers. However, recent evidence has shown that  $\text{Ag}^{\text{I}}$  salts can mediate the C–H bond activation step within reactions (Chapter 1). This thesis details the investigation of the role of  $\text{Ag}^{\text{I}}$  salt in the C–H direct arylation reaction of iodoarenes with fluoroarenes catalysed by Pd complexes in the presence of phosphine ligands. The stability of the Ag–P bond was determined by the choice of ligand.

Reaction of  $\text{Ag}_2\text{CO}_3$  with  $\text{C}_6\text{F}_5\text{H}$  and  $\text{PPh}_3$  resulted in the formation of the an  $\text{AgC}_6\text{F}_5(\text{PPh}_3)_n$  complex. The Ag– $\text{PPh}_3$  bond was highly labile at room-temperature, thus no  $^{107}\text{Ag}/^{109}\text{Ag}$  coupling information could be determined by NMR spectroscopy due to rapid phosphine-exchange, making it problematic for mechanistic investigation. Analysis by low-temperature NMR spectroscopy revealed complex speciation due to phosphine-exchange and binding modes with carbonate ligand (Chapter 2).

When the ligand was changed to Xphos, several reaction products could be isolated and characterised as single species in solution. Ag-intermediates were readily identified in solution by NMR spectroscopy, as the NMR active  $^{107}\text{Ag}$  and  $^{109}\text{Ag}$  provided diagnostic Ag–X coupling patterns. Key observations: a)  $\text{Ag}_2\text{CO}_3$  and Xphos react with  $\text{C}_6\text{F}_5\text{H}$  to form the C–H bond activation product  $\text{Ag}(\text{C}_6\text{F}_5)(\text{XPhos})$ , b) cross-coupling reaction between  $\text{Ag}(\text{C}_6\text{F}_5)(\text{XPhos})$  and  $\text{PdI}(\text{Ph})(\text{XPhos})$  produced  $\text{Ph-C}_6\text{F}_5$  at room-temperature. c) successful cross-coupling was accomplished using catalytic amounts of Ag salts as the sole silver source. A Pd/Ag co-catalytic mechanism was proposed wherein Ag mediates C–H bond activation and Pd performs cross-coupling (Chapter 3).



Further reaction optimisation was conducted and the haloarene and fluoroarene scope was explored. Strong dependence on the dialkylbiarylphosphine was noted, with Xphos being the optimal ligand (Chapter 4).

# Table of Contents

<b>Abstract</b> .....	<b>2</b>
<b>Table of Contents</b> .....	<b>3</b>
<b>List of Tables</b> .....	<b>6</b>
<b>List of Figures</b> .....	<b>9</b>
<b>List of Schemes</b> .....	<b>31</b>
<b>Acknowledgements</b> .....	<b>37</b>
<b>Declaration</b> .....	<b>39</b>
<b>Chapter 1: Introduction</b> .....	<b>40</b>
1.1 Pd-Catalysed C–H Functionalisation Reactions .....	40
1.2 Pd-Catalysed C–H Direct Arylation Reactions of Fluoroarenes .....	43
1.3 Proposed Mechanism of Pd-Catalysed Direct Arylation Reactions .....	46
1.4 The Role of Ag <sup>I</sup> Salts in the Pd-Catalysed C–H Bond Activation Reactions.....	52
1.4.1 C–H Bond Activation by Ag–Pd Heterometallic Complexes.....	53
1.4.2 C–H bond Activation by Ag Carbonate and Carboxylate salts .....	58
1.5 Introduction to Thesis Project.....	69
1.6 Project Aims and Objectives.....	71
<b>Chapter 2: Ag salts in Direct Arylation Reactions with Triphenylphosphine</b> .....	<b>72</b>
2.1 Introduction .....	72
2.1.1 Model Direct Arylation Reaction.....	72
2.1.2 Reported Synthesis and Reactivity of Pentafluorophenylsilver(I).....	75
2.1.3 Reported Synthesis and Structure of Phosphine-Coordinated Silver(I) Carbonate Complexes.....	81
2.2 Results: Detection of Pentafluorophenyl Silver Intermediate.....	84
2.3 Attempted Isolation and Characterization of the AgC <sub>6</sub> F <sub>5</sub> containing Intermediate	88
2.3 Synthesis of Phosphine–Coordinated Silver(I) Acetate Complexes.....	100
2.4 Synthesis of PPh <sub>3</sub> Coordinated Silver(I) Carbonate Complexes.....	104
2.5 Experiments with Reaction Intermediates .....	111
2.5.1 Cross-Coupling Reactions with Pd <sup>II</sup> Complexes.....	111

2.5.2 Reactions with Phosphine-Coordinated Silver(I) Complexes .....	116
2.5.3 Reactivity of Ag Intermediates within the Catalytic Direct Arylation Reaction .....	120
2.6 Discussion of Results .....	124
2.7 Conclusions .....	127
<b>Chapter 3: The Xphos Ag System .....</b>	<b>129</b>
3.1 Introduction .....	129
3.2: Synthesis and Characterisation of Ag(C <sub>6</sub> F <sub>5</sub> )(Xphos).....	132
3.3 Synthesis of the Silver(I) Carbonate Xphos Complex .....	142
3.4 Catalytic Direct Arylation Reactions with Xphos.....	147
3.5 Kinetic Isotope Effect .....	151
3.6 Ag <sup>I</sup> and Xphos Recycling Mechanism.....	161
3.7 Phosphine-Exchange and <sup>31</sup> P- <sup>31</sup> P EXSY Experiments.....	163
3.8 Proposed Catalytic Cycle.....	172
3.9 Summary and Conclusions.....	177
<b>Chapter 4: Optimisation of Catalytic Direct Arylation Reaction.....</b>	<b>179</b>
4.1 Introduction .....	179
4.2 Scope of Dialkylbiaryl Phosphine Ligands.....	185
4.3 AgC <sub>6</sub> F <sub>5</sub> Complexes of Various Dialkylbiaryl phosphines .....	186
4.4 The Effect of Haloarenes on the Direct Arylation Reaction .....	192
4.5 Substrate Scope of Iodoarenes .....	194
4.6 Substrate Scope of Fluoroarenes.....	202
4.7 Conclusions .....	207
<b>Chapter 5: Conclusions and Future work .....</b>	<b>208</b>
5.1 Key Conclusions .....	208
5.2 Future work .....	212
5.2.1 Further Reaction Optimization.....	212
5.2.2 Use of the Carbonate Complex 106 and its Analogues in Catalysis.....	214
5.2.3 Incorporating DFT modelling to Enhance Mechanistic Understanding .....	217

<b>Chapter 6: Experimental</b> .....	<b>218</b>
6.1 General Information on Instrumentation and Chemicals .....	218
6.2 General Experimental Procedures.....	221
6.3 Synthetic Procedures and Characterization of Compounds.....	222
6.3.1 Synthesis and characterization of Organic Compounds .....	222
6.3.1 Synthesis and characterization of Organometallic Complexes.....	231
6.4 Experimental Procedures for Chapter 2 .....	263
6.4.1 Reactions of Different Ag <sup>I</sup> salts with C <sub>6</sub> F <sub>5</sub> H in the presence of Different Additives .....	263
6.4.2 Cross-Coupling Reactions with Pd(II) Complexes .....	264
6.4.3 Reactions with Ag <sub>2</sub> (PPh <sub>3</sub> ) <sub>2</sub> (C <sub>6</sub> F <sub>5</sub> )(HCO <sub>3</sub> ) 91 and other reaction intermediates .....	271
6.4.4 Reactions with Phosphine-coordinated Silver(I) complexes .....	274
6.4.5: Reactions with Catalytic Amounts of Ag <sup>I</sup> salt .....	277
6.5 Experimental Procedures for Chapter 3 .....	280
6.5.1 Catalytic Direct Arylation Reactions with Varying Conditions .....	280
6.5.2 Stoichiometric Reactions with Reaction Intermediates .....	286
6.5.3 Kinetic Isotope Effect of Palladium-Catalysed Direct Arylation Reaction ...	314
6.5.4 Kinetic Isotope Effect of the Reaction between 106 and C <sub>6</sub> F <sub>5</sub> H 17/C <sub>6</sub> F <sub>5</sub> D 69 .....	315
6.5.5 <sup>t</sup> BuXphos Exchange Experiments with Ag <sup>I</sup> Complexes .....	321
6.5.6 Concentration Dependent EXSY Experiments .....	327
6.5.7 Temperature-Dependent EXSY experiments.....	332
6.6 Experimental Procedures for Chapter 4 .....	335
<b>Appendix A – Published Paper</b> .....	<b>346</b>
<b>Appendix B – NMR Spectroscopic Data for Synthesised Compounds</b> .....	<b>357</b>
<b>Appendix C – X-Ray Crystallographic Data</b> .....	<b>455</b>
<b>Abbreviation List</b> .....	<b>468</b>
<b>References</b> .....	<b>471</b>

## List of Tables

<b>Table 1:</b> Thermodynamic parameters experimentally measured by Platt <i>et al.</i> for the [C <sub>6</sub> F <sub>5</sub> H] dependent and independent process .....	71
<b>Table 2:</b> Summary of relevant parameters for Ag NMR spectroscopy <sup>96,97</sup> .....	73
<b>Table 3:</b> Screening the reaction of different silver salts and additives with pentafluorobenzene <b>17</b> .....	85
<b>Table 4:</b> The reaction of Ag <sub>2</sub> CO <sub>3</sub> and PPh <sub>3</sub> with C <sub>6</sub> F <sub>5</sub> H <b>17</b> in DMF at 60 °C .....	87
<b>Table 5:</b> Principal bond lengths and angles of the carbonate and acetate modelled versions of <b>91</b> .....	89
<b>Table 6:</b> <sup>31</sup> P{ <sup>1</sup> H} NMR data of the Ag–P resonance of Ag <sub>2</sub> (PPh <sub>3</sub> ) <sub>2</sub> (C <sub>6</sub> F <sub>5</sub> )(μ <sub>2</sub> -HCO <sub>3</sub> ) <b>91</b> . 93	
<b>Table 7:</b> <sup>31</sup> P{ <sup>1</sup> H} NMR data of the Ag–P resonances of <b>92</b> .....	96
<b>Table 8:</b> <sup>31</sup> P{ <sup>1</sup> H} NMR data of the Ag–P resonances of <b>93</b> .....	99
<b>Table 9:</b> Comparison of the closest matches for the peaks of <b>91</b> and <b>93</b> .....	100
<b>Table 10:</b> Principal bond lengths and angles for [Ag(DPPE)(κ <sup>2</sup> -OAc)] <sub>n</sub> <b>95</b> .....	103
<b>Table 11:</b> Principal bond lengths and angles for <b>89</b> and <b>90</b> .....	105
<b>Table 12:</b> Low temperature <sup>31</sup> P{ <sup>1</sup> H} NMR data of [Ag(PPh <sub>3</sub> ) <sub>2</sub> ] <sub>2</sub> CO <sub>3</sub> •2 H <sub>2</sub> O <b>88</b> at –100°C (173 K) .....	111
<b>Table 13:</b> Summary for the stoichiometric reaction of PPh <sub>3</sub> coordinated Ag complexes and 10 equivalents of C <sub>6</sub> F <sub>5</sub> H.....	120
<b>Table 14:</b> Influence of the addition of catalytic amounts of Ag containing salts and complexes on the direct arylation reaction of 4-iodotoluene <b>26</b> with pentafluorobenzene <b>17</b> . .....	123
<b>Table 15:</b> Principal bond lengths and angles of <b>101</b> , <b>106</b> and <b>105</b> .....	137
<b>Table 16:</b> Principal bond lengths and angles of <b>109</b> .....	147
<b>Table 17:</b> Catalytic direct arylation reactions with varying conditions.....	150
<b>Table 18:</b> T <sub>1</sub> values of the reactants and products in toluene at 233 K .....	155
<b>Table 19:</b> Slope and intercept of fast process and slow process for the reaction between <b>106</b> and C <sub>6</sub> F <sub>5</sub> H <b>17</b> /C <sub>6</sub> F <sub>5</sub> D <b>69</b> .....	158
<b>Table 20:</b> Summary of T <sub>1</sub> , chemical shift and coupling constant of the different phosphorus species in the reaction between <b>101</b> and <sup>t</sup> BuXphos.....	164
<b>Table 21:</b> T <sub>1</sub> values of Xphos and the Ag complexes used for EXSY experiments .....	169
<b>Table 22:</b> Values of k <sub>obs</sub> and V <sub>ex</sub> for <b>101</b> .....	169
<b>Table 23:</b> Summary of the T <sub>1</sub> values measured at different temperatures for the mixture of <b>101</b> and Xphos (5 equiv.).....	171
<b>Table 24:</b> Values of k <sub>obs</sub> and V <sub>ex</sub> for <b>101</b> in C <sub>6</sub> D <sub>6</sub> as a function of temperature. Data corrected for difference in relaxation times. ....	171

<b>Table 25:</b> Catalytic direct arylations where reaction intermediates are used as pre-catalysts .....	176
<b>Table 26:</b> Effect of different dialkylbiaryl phosphines ligands on the C–H direct arylation reaction between 4-iodotoluene <b>26</b> and pentafluorobenzene <b>17</b> . .....	185
<b>Table 27:</b> Synthesis and isolation of various Ag(C <sub>6</sub> F <sub>6</sub> )(PR <sub>2</sub> R') (where PR <sub>2</sub> R' = dialkylbiarylphosphines ligands).....	187
<b>Table 28:</b> Principal bond length and angles of all the AgC <sub>6</sub> F <sub>5</sub> PR <sub>3</sub> .....	190
<b>Table 29:</b> Difference in bond distance between Ag–C <sub>ipso</sub> and Ag–C <sub>α</sub> compared to 3 σ and 5 σ.....	190
<b>Table 30:</b> Distances between the carbon atoms of the distal ring of the biaryl of the phosphine and Ag metal centre from the crystal structure.....	191
<b>Table 31:</b> Bond lengths and distances of η <sup>2</sup> -complexes reported in the literature, and comparison with free ligand <sup>148,147</sup> .....	192
<b>Table 32:</b> Direct Arylation of 4-bromotoluene <b>13</b> with pentafluorobenzene <b>17</b> in DMF with varying ligand and temperatures. ....	193
<b>Table 33:</b> Direct arylation of 4-chlorotoluene <b>130</b> with pentafluorobenzene <b>17</b> in DMF with varying temperatures.....	194
<b>Table 34:</b> The <i>para</i> -substituted aryl iodides scope of direct arylation at 60 °C in DMF	198
<b>Table 35:</b> Substrate scope of bulky, heteroatom, <i>meta</i> - and <i>ortho</i> - substituted aryl iodides at 60 °C.....	200
<b>Table 36:</b> <sup>19</sup> F{ <sup>1</sup> H} NMR yield <sup>[a]</sup> of iodoarenes at 3 h, 23 h (yield after purification) <sup>[b]</sup> at 100 °C in DMF.....	201
<b>Table 37:</b> Fluoroarene substrate scope for the direct arylation reaction .....	203
<b>Table 38:</b> Principal bond length and angles of <b>165</b> , in comparison to <b>101</b> . .....	206
<b>Table 39:</b> Effect of reducing Ag and ligand amounts in the C–H direct arylation reaction .....	213
<b>Table 40:</b> Influence of the addition of catalytic amounts of Ag containing salts and complexes on the direct arylation reaction of 4-iodotoluene <b>26</b> with pentafluorobenzene <b>17</b> (comparison of % conversion calculated using starting material and product vs. calculated using the internal standard.) .....	279
<b>Table 41:</b> The chemical shift and coupling constant of authentic samples of Ag complexes in DMF .....	304
<b>Table 42:</b> Slope and intercept for the fast process for the reaction between <b>106</b> and C <sub>6</sub> F <sub>5</sub> H <b>17</b> /C <sub>6</sub> F <sub>5</sub> D <b>69</b> .....	319
<b>Table 43:</b> Slope and intercept for the slow process for the reaction between <b>106</b> and C <sub>6</sub> F <sub>5</sub> H <b>17</b> /C <sub>6</sub> F <sub>5</sub> D <b>69</b> .....	320

<b>Table 44:</b> Summary of T <sub>1</sub> , chemical shift and coupling constant of the different phosphorus species in <b>GA-5-385</b> .....	322
<b>Table 45:</b> Summary of T <sub>1</sub> , chemical shift and coupling constant of the different phosphorus species in <b>GA-5-385</b> .....	324
<b>Table 46:</b> Summary of T <sub>1</sub> , chemical shift and coupling constant of the different phosphorus species in <b>GA-5-384</b> .....	326
<b>Table 47:</b> T <sub>1</sub> values of the mixture of Ag complex and Xphos .....	327
<b>Table 48:</b> Mass of <b>101</b> and varying equiv. of Xphos used for the EXSY experiments .	328
<b>Table 49:</b> Relative integration of the Xphos peak wrt <b>101</b> at each mixing time .....	329
<b>Table 50:</b> Values of k <sub>obs</sub> and V <sub>ex</sub> for <b>101</b> .....	330
<b>Table 51:</b> The mass of <b>106</b> and varying equiv. of Xphos used for the EXSY experiments .....	330
<b>Table 52:</b> Relative integration of the Xphos peak wrt <b>106</b> at each mixing time .....	331
<b>Table 53:</b> The mass of <b>105</b> and varying equiv. of Xphos used for the EXSY experiments .....	331
<b>Table 54:</b> Relative integration of the Xphos peak wrt <b>105</b> at each mixing time .....	331
<b>Table 55:</b> Summary of the T <sub>1</sub> values measured at different temperatures for the mixture of <b>101</b> and Xphos (5 equiv.) .....	332
<b>Table 56:</b> Relative integration of the Xphos peak wrt <b>101</b> at each mixing time and at different temperatures .....	332
<b>Table 57:</b> Values of k <sub>obs</sub> and V <sub>ex</sub> for <b>101</b> in C <sub>6</sub> D <sub>6</sub> as a function of temperature. Data corrected for difference in relaxation times. ....	333
<b>Table 58:</b> Crystal data and structure refinement for <b>91</b> (carbonate structure) .....	455
<b>Table 59:</b> Crystal data and structure refinement for <b>91</b> (acetate structure).....	456
<b>Table 60:</b> Crystal data and structure refinement for <b>95</b> .....	457
<b>Table 61:</b> Crystal data and structure refinement for <b>89</b> .....	458
<b>Table 62:</b> Crystal data and structure refinement for <b>90</b> .....	459
<b>Table 63:</b> Crystal data and structure refinement for <b>101</b> .....	460
<b>Table 64:</b> Crystal data and structure refinement for <b>106</b> .....	461
<b>Table 65:</b> Crystal data and structure refinement for <b>109</b> .....	462
<b>Table 66:</b> Crystal data and structure refinement for <b>105</b> .....	463
<b>Table 67:</b> Crystal data and structure refinement for <b>122</b> .....	464
<b>Table 68:</b> Crystal data and structure refinement for <b>125</b> .....	465
<b>Table 69:</b> Crystal data and structure refinement for <b>124</b> .....	466
<b>Table 70:</b> Crystal data and structure refinement for <b>165</b> .....	467



## List of Figures

<b>Figure 1:</b> Comparison of chelate- and non-chelate-assisted C–H functionalisation strategies.....	41
<b>Figure 2:</b> Examples of commonly used <i>ortho</i> - and <i>meta</i> -selective directing groups used in Pd-catalysed C–H bond functionalization reactions. The functionalised C–H bonds are highlighted in orange.....	41
<b>Figure 3:</b> Potential positions for C–H functionalisation in 1,3-difluorobenzene <b>12</b> .....	42
<b>Figure 4:</b> Examples of fluorine-containing pharmaceutical and agricultural molecules.	44
<b>Figure 5:</b> The substitution of hydrogens for fluorine in peptoids has been found to be beneficial in controlling the cis/trans conformation of the resulting peptoid chain, without the use of chiral monomers. ....	44
<b>Figure 6:</b> AMLA-(6) transition state for C–H activation of C <sub>6</sub> F <sub>5</sub> H <b>17</b> computed by Fagnou <i>et al.</i> <sup>34</sup> .....	48
<b>Figure 7:</b> Example of a computationally-generated AMLA(4) and AMLA(6)-TS for Ir complex <sup>59,66</sup> .....	48
<b>Figure 8:</b> Summary of the different hypothesised roles of Ag <sup>I</sup> salts in C–H functionalization reactions. a) Ag <sup>I</sup> salts acting as a source of carboxylate ligand for Pd <i>via</i> halide abstraction reaction. b) C–H bond activation mediated by Ag <sup>I</sup> salts <i>via</i> AMLA(6) transition state, to produce an Ag-arene intermediate which can undergo transmetalation with Pd. c) Pd and Ag form bimetallic or polymetallic intermediates which are then responsible for C–H bond activation. <sup>74,75</sup> .....	53
<b>Figure 9:</b> The Pd-Ag dinuclear and trinuclear clusters <b>34</b> and <b>35</b> synthesized by Hor and co-workers by treating Pd(O <sub>2</sub> CCF <sub>2</sub> CF <sub>3</sub> ) <sub>2</sub> (dppf) with one or two equivalents of Ag(O <sub>2</sub> CCF <sub>2</sub> CF <sub>3</sub> ) <sub>2</sub> in dichloromethane respectively. <sup>76</sup> .....	54
<b>Figure 10:</b> The Pd/Ag bimetallic complexes isolated and characterized by Strassner and co-workers <sup>77</sup> and Kozitsyna and co-workers <sup>78</sup> respectively.....	54
<b>Figure 11:</b> The monomeric <b>38</b> , dimeric <b>39</b> , trimeric clusters <b>41</b> of Pd acetate and Pd-Ag acetate cluster <b>40</b> considered for the computational investigation of the mechanism of meta-C–H selective activation reactions. <sup>79</sup> .....	55
<b>Figure 12:</b> The transition states for meta-selective C–H activation by both a Pd <sub>2</sub> (OAc) <sub>4</sub> <b>39</b> and PdAg(OAc) <sub>3</sub> <b>40</b> cluster respectively. The nitrile group, of the bulky directing group, is shown to coordinate with one end of the metal cluster to aid in the formation of a cyclophane-like transition state which overrides the typical ortho-selectivity of the reaction. <sup>79</sup> .....	56
<b>Figure 13:</b> The transition states of C–H activation incorporating a PdAg(OAc) <sub>3</sub> (left) and Pd <sub>2</sub> (OAc) <sub>4</sub> (right) complex, with the corresponding Gibbs free energies. <sup>82</sup> .....	58

<b>Figure 14:</b> a) Plot of $k_{\text{obs}}$ against of the $[\text{C}_6\text{F}_5\text{H}]_{\text{ave}}$ between the concentration of 0.18M and 0.92M for the direct arylation of 4-iodotoluene. The non-zero y-intercept of the plot is usually indicative of a process which is independent of the concentration $\text{C}_6\text{F}_5\text{H}$ . b) Plot of $k_{\text{obs}}$ against $[\text{C}_6\text{F}_5\text{H}]_{\text{ave}}$ for the reaction in <b>Scheme 33</b> , at different temperatures. (adapted from G. Platt's PhD dissertation.) <sup>68</sup> .....	70
<b>Figure 15:</b> An example of a $^{31}\text{P}\{^1\text{H}\}$ NMR spectrum showing the coupling of $^{31}\text{P}$ with $^{107}\text{Ag}$ and $^{109}\text{Ag}$ .....	74
<b>Figure 16:</b> Solid state structure of neat $\text{AgC}_6\text{F}_5$ <b>55</b> <sup>113</sup> and the nitrile adducts isolated from $\text{MeCN}$ <sup>112</sup> and $\text{EtCN}$ <sup>95</sup> .....	80
<b>Figure 17:</b> Select examples of aryl- <sup>114,115,116</sup> and perfluoroalkenylsilver <sup>117</sup> complexes which are tetrameric in the crystal structure, and diarylargentate <sup>118</sup> and pentafluorophenyl(ylide)silver <sup>119</sup> complexes. ....	81
<b>Figure 18:</b> The $^{19}\text{F}\{^1\text{H}\}$ NMR (470.6 MHz, $\text{CD}_3\text{CN}$ , 25 °C) spectrum of <b>55</b> .....	84
<b>Figure 19:</b> The $^{19}\text{F}\{^1\text{H}\}$ (MHz, 25 °C, $\text{CH}_3\text{CN}$ ) spectrum of the reaction mixture of Entry 6, <b>Table 3</b> . The spectrum shows the ortho-F resonances of $\text{C}_6\text{F}_5\text{H}$ <b>17</b> and $\text{AgC}_6\text{F}_5(\text{PPh}_3)_n$ <b>91</b> used to calculate the % conversion. ....	86
<b>Figure 20:</b> The crystal structure of <b>91</b> with the bridging ligand modelled as hydrogen carbonate .....	89
<b>Figure 21:</b> The crystal structure of <b>91</b> with the bridging ligand modelled as acetate, which provided a better fit with the model. However, $^{13}\text{C}$ -labelling experiments support the presence of hydrogen carbonate within the structure. Some disorder around the bridging ligand present. ....	90
<b>Figure 22:</b> Comparison of various Ag---Ag bond distances (orange) found in different literature Ag complexes. <sup>112-116</sup> .....	90
<b>Figure 23:</b> The $^{19}\text{F}\{^1\text{H}\}$ NMR (470 MHz, $\text{C}_6\text{D}_6$ , 25 °C) spectrum of $\text{Ag}_2(\text{PPh}_3)_2(\text{C}_6\text{F}_5)(\mu_2\text{-HCO}_3)$ <b>91</b> .....	91
<b>Figure 24:</b> Variable-temperature $^{31}\text{P}\{^1\text{H}\}$ NMR (202 MHz, 128 scans, $\text{tol-d}_8$ ) spectrum of <b>91</b> .....	92
<b>Figure 25:</b> $^{31}\text{P}\{^1\text{H}\}$ NMR (202 MHz, $\text{tol-d}_8$ : $\text{DCM-d}_2$ (20:80), -100 °C) spectrum of <b>91</b> .....	94
<b>Figure 26:</b> $^{19}\text{F}\{^1\text{H}\}$ NMR (470 MHz, $\text{tol-d}_8$ :dichloromethane- $\text{d}_2$ (20:80), -100 °C) spectrum of <b>91</b> .....	94
<b>Figure 27:</b> Stack plot of the $^{13}\text{C}\{^1\text{H}\}$ NMR (125.7 MHz, $\text{C}_6\text{D}_6$ , 25 °C) spectrum of the $^{13}\text{C}$ -labelled $\text{Ag}_2(\text{PPh}_3)_2(\text{C}_6\text{F}_5)(\mu_2\text{-H}^{13}\text{CO}_3)$ <b>92</b> ( <b>Below</b> ) and the non-labelled $\text{Ag}_2(\text{PPh}_3)_2(\text{C}_6\text{F}_5)(\mu_2\text{-HCO}_3)$ <b>91</b> ( <b>Above</b> ) .....	95
<b>Figure 28:</b> Stack plot of the $^{31}\text{P}\{^1\text{H}\}$ NMR (202 MHz, $\text{tol-d}_8$ :dichloromethane- $\text{d}_2$ (20:80), -100 °C) spectrum of <b>91</b> ( <b>top</b> ) and <b>92</b> ( <b>bottom</b> ). ....	96

<b>Figure 29:</b> $^{13}\text{C}\{\text{H}\}$ NMR (125.7 MHz, $\text{tol-}d_8$ :dichloromethane- $d_2$ (20:80), $-100\text{ }^\circ\text{C}$ ) spectrum of <b>92</b> .....	97
<b>Figure 30:</b> $^{31}\text{P}\{\text{H}\}$ (202 MHz, toluene:dichloromethane, $-100\text{ }^\circ\text{C}$ ) spectrum of <b>93</b> .....	98
<b>Figure 31:</b> Stack plot of the $^{31}\text{P}\{\text{H}\}$ (202 MHz, Tol:dichloromethane, $-100\text{ }^\circ\text{C}$ ) spectrum of <b>91 (top)</b> and <b>93 (bottom)</b> .....	99
<b>Figure 32:</b> $^{31}\text{P}\{\text{H}\}$ (202 MHz, dichloromethane- $d_2$ , $-80\text{ }^\circ\text{C}$ ) of <b>94</b> .....	101
<b>Figure 33:</b> The crystal structure of the $[\text{Ag}(\text{DPPE})(\kappa^2\text{-OAc})]_n$ <b>95</b> complex which shows the DPPE ligand bridging two different Ag centres.....	102
<b>Figure 34:</b> The asymmetric unit of $[\text{Ag}(\text{DPPE})(\kappa^2\text{-OAc})]_n$ <b>95</b> showing H-bonding with MeOH.....	103
<b>Figure 35:</b> The crystal structure of $[\text{Ag}(\text{PPh}_3)_2(\kappa^2\text{-HCO}_3)]_2$ <b>89</b> isolated from reaction mixture of $\text{Ag}_2\text{CO}_3$ and $\text{PPh}_3$ with $\text{C}_6\text{F}_5\text{H}$ <b>17</b> in DMF. ....	106
<b>Figure 36:</b> $^{31}\text{P}\{\text{H}\}$ NMR (202 MHz, $\text{tol-}d_8$ :dichloromethane- $d_2$ (20:80), $-80\text{ }^\circ\text{C}$ ) spectrum of $[\text{Ag}(\text{PPh}_3)_2(\text{HCO}_3)]_2$ <b>89</b> .....	107
<b>Figure 37:</b> Stack plot of the $^{31}\text{P}\{\text{H}\}$ NMR (202 MHz, $\text{tol-}d_8$ :dichloromethane- $d_2$ (20:80), $-80\text{ }^\circ\text{C}$ ) spectrum of <b>91 (top)</b> and <b>89 (bottom)</b> .....	107
<b>Figure 38:</b> The X-ray crystal structure of <b>90</b> , the crystals isolated from the reaction between $\text{Ag}_2\text{CO}_3$ and $\text{PPh}_3$ in DMF.....	108
<b>Figure 39:</b> The $[\text{Ag}(\text{PPh}_2)_3\text{HCO}_3]_n$ <b>90</b> existed as a coordinate polymer connected via hydrogen bonding.....	109
<b>Figure 40:</b> The $^{31}\text{P}\{\text{H}\}$ NMR (202 MHz, dichloromethane- $d_2$ : $\text{tol-}d_8$ , $-100\text{ }^\circ\text{C}$ ) spectrum of $[(\text{PPh}_3)_2\text{Ag}]_2(\text{CO}_3)\cdot 2\text{H}_2\text{O}$ <b>88</b> .....	110
<b>Figure 41:</b> The synthesis of $\text{Pd}(\text{PPh}_3)_2(\text{I})(\text{phenyl})$ <b>97</b> and $\text{Pd}(\text{PPh}_3)_2(\text{I})(4\text{-tolyl})$ <b>98</b> .....	111
<b>Figure 42:</b> $^{31}\text{P}\{\text{H}\}$ NMR (202 MHz, Tol, $25\text{ }^\circ\text{C}$ ) spectrum of the reaction mixture of $\text{Ag}_2(\text{PPh}_3)_2(\text{C}_6\text{F}_5)(\mu\text{-HCO}_3)$ <b>91</b> and $\text{Pd}(\text{PPh}_3)_2(\text{I})(\text{tolyl})$ <b>98</b> .....	112
<b>Figure 43:</b> $^{19}\text{F}\{\text{H}\}$ NMR (470 MHz, DMF, $25\text{ }^\circ\text{C}$ ) spectrum of the reaction mixture of <b>91</b> and <b>98</b> .....	114
<b>Figure 44:</b> Reaction between <b>91</b> and <b>98</b> monitored by $^{31}\text{P}\{\text{H}\}$ and $^{19}\text{F}\{\text{H}\}$ NMR spectroscopy in a temperature range of $-75\text{ }^\circ\text{C}$ (198 K) to $-10\text{ }^\circ\text{C}$ (263 K) in toluene- $d_8$ ...	114
<b>Figure 45:</b> Reaction between <b>91</b> and <b>98</b> monitored by $^{31}\text{P}\{\text{H}\}$ and $^{19}\text{F}\{\text{H}\}$ NMR spectroscopy in a temperature range of $-40\text{ }^\circ\text{C}$ (233 K) to $0\text{ }^\circ\text{C}$ (273 K) in dichloromethane- $d_2$ .....	115
<b>Figure 46:</b> Reactivity of the above phosphine-coordinated Ag complexes were tested with 10 equivalents of $\text{C}_6\text{F}_5\text{H}$ <b>17</b> .....	117

<b>Figure 47:</b> $^{19}\text{F}\{^1\text{H}\}$ NMR (470 MHz, DMF, 25 °C) spectrum of the reaction mixture of <b>89</b> and <b>17</b> in the presence of $\text{Cs}_2\text{CO}_3$ with a D1 = 10 sec. The $\text{AgC}_6\text{F}_5$ containing product (orange) and <b>17</b> (green are highlighted).....	118
<b>Figure 48:</b> $^1\text{H}$ NMR (500MHz, $\text{CDCl}_3/\text{DMF}$ , 25 °C) spectrum of the reaction mixture in <b>Entry 4</b> at 3h showing the $-\text{CH}_3$ resonance of 1,3,5-trimethoxybenzene ( $\delta$ 3.78), product <b>18</b> ( $\delta$ 2.43) and 4-iodotoluene <b>26</b> ( $\delta$ 2.30). The two singlet off-scale peaks centred at $\delta$ 2.88 and 2.96 are solvent peaks belonging to DMF.....	121
<b>Figure 49:</b> The $^1\text{H}$ NMR (500MHz, $\text{CDCl}_3/\text{DMF}$ , 25 °C) spectrum of the reaction mixture of <b>Entry 1</b> after 23 h with product <b>18</b> (2.44), homocoupling side-product <b>99</b> (2.40) and 4-iodotoluene <b>26</b> (2.31). .....	121
<b>Figure 50:</b> Complexes synthesized to help understand the structure of <b>91</b> in solution..	125
<b>Figure 51:</b> Phosphine coordinated Ag complex incorporating acetate, hydrogen carbonate and carbonate ligands. ....	126
<b>Figure 52:</b> $^{31}\text{P}\{^1\text{H}\}$ (202.5 MHz, $\text{CD}_2\text{Cl}_2$ , 25 °C) spectrum of <b>101</b> .....	133
<b>Figure 53:</b> $^{19}\text{F}\{^1\text{H}\}$ NMR (470 MHz, $\text{CD}_2\text{Cl}_2$ , 25 °C) spectrum of <b>101</b> .....	133
<b>Figure 54:</b> $^{31}\text{P}\{^{109}\text{Ag}\}$ NMR (162 MHz, dichloromethane- $d_2$ , 25 °C) of a concentrated sample of $\text{Ag}(\text{C}_6\text{F}_5)(\text{Xphos})$ <b>101</b> .....	134
<b>Figure 55:</b> $^{31}\text{P}\{^{109}\text{Ag}\}$ - $^{109}\text{Ag}$ HMQC spectrum of <b>101</b> showing the $^{109}\text{Ag}$ resonance at $\delta$ 713 .....	134
<b>Figure 56:</b> Comparison of the $\text{M}-\text{C}_{\text{ipso}}$ bonds in various group 11 metal complexes dialkylbiarylphosphine ligands, reported by Maseras and Echavarren and co-workers. <sup>124</sup> .	135
<b>Figure 57:</b> The crystal structure of the $\text{Ag}(\text{C}_6\text{F}_5)(\text{Xphos})$ <b>101</b> .....	136
<b>Figure 58:</b> $^{31}\text{P}\{^1\text{H}\}$ (202.5 MHz, dichloromethane- $d_2$ , 25 °C) NMR spectrum of the reaction mixture of <b>101</b> (yellow) and <b>102</b> (pale yellow) showing the presence of <b>105</b> (blue) and unbound Xphos.....	138
<b>Figure 59:</b> $^{19}\text{F}\{^1\text{H}\}$ NMR (470 MHz, $\text{CD}_2\text{Cl}_2$ , 25 °C) of the reaction mixture of <b>101</b> and <b>102</b> immediately after sample preparation, showing the presence of the organic product <b>28</b> (yellow). .....	139
<b>Figure 60:</b> The crystal structure of $[\text{AgIXphos}]_2$ <b>105</b> .....	140
<b>Figure 61:</b> Decomposition of <b>55</b> and <b>101</b> to $\text{C}_6\text{F}_5\text{D}$ <b>69</b> with an excess of $\text{D}_2\text{O}$ in $\text{CD}_3\text{CN}$ and $\text{CD}_2\text{Cl}_2$ respectively .....	142
<b>Figure 62:</b> The crystal structure of $[\text{Ag}(\text{XPhos})]_2(\mu-\kappa^2,\kappa^2-\text{CO}_3)$ <b>106</b> .....	143
<b>Figure 63:</b> Brown crystals of $[\text{Ag}(\text{XPhos})]_2(\mu-\kappa^2,\kappa^2-\text{CO}_3)$ <b>106</b> in the round-bottom flask .....	143

<b>Figure 64:</b> $^{31}\text{P}\{\text{}^1\text{H}\}$ (202.5 MHz, $\text{C}_6\text{D}_6$ , 25 °C) NMR spectrum of the reaction mixture of <b>106</b> with <b>17</b> , at $t = 0$ h, RT. The mixture shows the presence of <b>106</b> (red) and <b>101</b> (yellow). .....	145
<b>Figure 65:</b> The crystal structure of $\text{AgOAcXphos}$ <b>109</b> .....	146
<b>Figure 66:</b> $^{19}\text{F}\{\text{}^1\text{H}\}$ NMR (470 MHz, $\text{CDCl}_3$ , 25 °C, 32 Sc) spectrum of the reaction mixture of the standard direct arylation reaction. The % $^{19}\text{F}$ NMR yields were calculated using the <i>ortho</i> -F resonance of the product ( $\delta -143.5$ , blue) wrt octafluoronaphthalene ( $\delta -145.2$ , internal standard, yellow), remaining $\text{C}_6\text{F}_5\text{H}$ shown in red.....	148
<b>Figure 67:</b> Initial rate of reaction for the direct arylation of 4-iodotoluene <b>26</b> with 10 equiv. of $\text{C}_6\text{F}_5\text{H}$ <b>17</b> (black) and $\text{C}_6\text{F}_5\text{D}$ <b>69</b> (red).....	154
<b>Figure 68:</b> $^{19}\text{F}\{\text{}^1\text{H}\}$ NMR (470 MHz, Tol, $-40$ °C) spectrum of the reaction mixture of <b>106</b> and $\text{C}_6\text{F}_5\text{H}$ <b>17</b> ( <i>Ortho</i> -F peak in red, peaks indicated by <b>b</b> ) producing <b>101</b> ( <i>Ortho</i> -F peak in yellow, peaks indicated by <b>a</b> ) at $-40$ °C (233 K). Octafluoronaphthalene (peak used for integration in green, peaks indicated by <b>c</b> ) was used as the internal standard. ....	156
<b>Figure 69:</b> Change in concentration of <b>101</b> over time for the reaction of $\text{Ag}_2(\mu\text{-CO}_3)(\text{Xphos})_2$ <b>106</b> and two equiv. of $\text{C}_6\text{F}_5\text{H}$ <b>17</b> or $\text{C}_6\text{F}_5\text{D}$ <b>69</b> in toluene at $-40$ °C .....	157
<b>Figure 70:</b> Initial rate for the reaction of $[\text{Ag}(\text{XPhos})]_2(\mu\text{-}\kappa^2, \kappa^2\text{-CO}_3)$ <b>106</b> and two equiv. of $\text{C}_6\text{F}_5\text{H}$ <b>17</b> or $\text{C}_6\text{F}_5\text{D}$ <b>69</b> in toluene at $-40$ °C (Fast process) .....	157
<b>Figure 71:</b> Rate for the reaction of $[\text{Ag}(\text{XPhos})]_2(\mu\text{-}\kappa^2, \kappa^2\text{-CO}_3)$ <b>106</b> and two equiv. of $\text{C}_6\text{F}_5\text{H}$ <b>17</b> or $\text{C}_6\text{F}_5\text{D}$ <b>69</b> in toluene at $-40$ °C (slow process).....	158
<b>Figure 72:</b> $^{31}\text{P}\{\text{}^1\text{H}\}$ NMR (202.5 MHz, Tol, $-40$ °C) time course of the reaction between <b>106</b> and $\text{C}_6\text{F}_5\text{H}$ (2 equiv.) to yield $\text{Ag}(\text{C}_6\text{F}_5)(\text{Xphos})$ <b>101</b> and unbound Xphos.....	159
<b>Figure 73:</b> $^{31}\text{P}\{\text{}^1\text{H}\}$ NMR (202.5 MHz, Tol, $-40$ °C) time course of the reaction between <b>106</b> and $\text{C}_6\text{F}_5\text{H}$ (2 equiv.) to yield $\text{Ag}(\text{C}_6\text{F}_5)(\text{Xphos})$ <b>101</b> and unbound Xphos, along with the integral graph calculated using MestReNova, demonstrating the change in each reagent. .	160
<b>Figure 74:</b> Change in the % conversion to $\text{Ag}(\text{C}_6\text{F}_5)(\text{Xphos})$ <b>101</b> over time in seconds. .....	160
<b>Figure 75:</b> Precipitation of a yellow solid (AgI) upon mixing <b>105</b> with <b>55</b> (Scheme 85b) in J young NMR tube .....	162
<b>Figure 76:</b> $^{31}\text{P}\{\text{}^1\text{H}\}$ (202.5 MHz, $\text{CD}_2\text{Cl}_2$ , 25 °C) spectrum of the mixture of $\text{Ag}(\text{C}_6\text{F}_5)(\text{Xphos})$ <b>101</b> (1 equiv.) and $^t\text{BuXphos}$ (1 equiv.).....	164
<b>Figure 77:</b> The four basic stages of all 2D experiments: Preparation, Evolution, Mixing and Detection. For EXSY experiments the exchange process occurs in the mixing period. <sup>130</sup> .....	165
<b>Figure 78:</b> Example EXSY spectrum, where the exchange between <b>b</b> and <b>c</b> is denoted by the presence of the exchange cross peaks (orange), while no exchange occurs with <b>a</b> . .....	166

<b>Figure 79:</b> 2D $^{31}\text{P}$ - $^{31}\text{P}$ EXSY spectrum of a mixture of $\text{Ag}(\text{C}_6\text{F}_5)(\text{Xphos})$ <b>101</b> and Xphos (5 equiv.) with a mixing time of 2 s .....	167
<b>Figure 80:</b> Stack plot from 1D EXSY experiment with <b>101</b> and Xphos (5 equiv.), with various mixing times in $\text{CD}_2\text{Cl}_2$ . Selective inversion of <b>101</b> resonance with a selective pulse width ca. 5 ppm, with 20 scans per mixing time.....	167
<b>Figure 81:</b> Plot of fractional transfer of magnetisation from <b>101</b> to free XPhos in dichloromethane against mixing time. a) plot without corrections for the difference in relaxation times. b) Plot with the corrections applied to the relaxation times. ....	169
<b>Figure 82:</b> Plot of exchange velocity $V_{\text{ex}}$ vs [XPhos]. The <b>black</b> plot shows the uncorrected data; <b>red</b> plot shows the corrected data.....	170
<b>Figure 83:</b> Plot of fractional transfer of magnetisation from <b>101</b> to free XPhos in $\text{C}_6\text{D}_6$ against mixing time for different temperatures. The slopes correspond to $k_{\text{obs}}$ for the exchange process. The data have been corrected for the differences in relaxation time at each temperature.....	171
<b>Figure 84:</b> Eyring plots for the phosphine-exchange rate. <b>a)</b> plot using values of $k_{\text{obs}}$ , <b>b)</b> using values of $V_{\text{ex}}$ . ....	172
<b>Figure 85:</b> Proposed catalytic cycle, illustrating the role of Ag within C–H direct arylation reactions .....	175
<b>Figure 86:</b> Structural features of dialkylbiarylphosphines and their effect on catalysis <sup>139,140,141</sup> .....	180
<b>Figure 87:</b> The effect of <i>para</i> -substituents of the aryl ring on the Pd–C <sub>ipso</sub> bond length derived from x-ray crystallographic analysis. <sup>127</sup> .....	181
<b>Figure 88:</b> Effect of substituents on the biaryl backbone on dearomative rearrangement <sup>127</sup> .....	183
<b>Figure 89:</b> Structure of <sup>t</sup> BuBrettphos, <sup>t</sup> BuXphos and RockPhos.....	184
<b>Figure 90:</b> Crystal structure of $\text{AgC}_6\text{F}_5\text{CyJohnphos}$ <b>122</b> .....	188
<b>Figure 91:</b> Crystal structure of $\text{AgC}_6\text{F}_5\text{Sphos}$ <b>124</b> .....	188
<b>Figure 92:</b> Crystal structure of $\text{AgC}_6\text{F}_5\text{Brettphos}$ <b>125</b> .....	189
<b>Figure 93:</b> $^{19}\text{F}\{^1\text{H}\}$ NMR (470 MHz, $\text{CDCl}_3$ , 25 °C) of the reaction mixture with 4-iodoanisole <b>50</b> depicting the <i>ortho</i> -F resonance of the product and <i>F</i> -resonance of octafluoronaphthalene used to calculate the $^{19}\text{F}\{^1\text{H}\}$ NMR yields. ....	195
<b>Figure 94:</b> Variation in $^{19}\text{F}\{^1\text{H}\}$ NMR yield with respect to the <i>para</i> -substituents of the aryl iodides .....	199
<b>Figure 95:</b> $^{19}\text{F}$ NMR chemical shift of the different F environments in <b>165</b> , <b>67</b> and <b>166</b> .....	205
<b>Figure 96:</b> Crystal structure of $\text{AgC}_5\text{F}_4\text{NXphos}$ <b>165</b> .....	206

<b>Figure 97:</b> $^{31}\text{P}\{^1\text{H}\}$ low-temperature VT NMR stack plot for $\text{Ag}_2(\text{PPh}_3)_2(\text{C}_6\text{F}_5)(\mu_2\text{-HCO}_3)$ <b>91</b> demonstrating the lability of the Ag–P bond at room temperature and complex equilibrium of species in solution when fully resolved. ....	209
<b>Figure 98:</b> Change in $^{19}\text{F}\{^1\text{H}\}$ NMR yield with respect to the <i>para</i> -substituents of the iodoarenes at 60 ° and 100 °C .....	211
<b>Figure 99:</b> Ag carbonate complex <b>106</b> is capable of C–H activation whereas Ag acetate <b>109</b> was found to be inactive for C–H activation.....	217
<b>Figure 100:</b> Experimental set-up for preparation of the sample for the low-temperature VT NMR monitoring of the transmetallation reaction .....	267
<b>Figure 101:</b> $^{31}\text{P}\{^1\text{H}\}$ (202.5 MHz, <i>tol-d</i> <sub>8</sub> ) stack plot of the <b>GA-1-087</b> reaction mixture at different temperatures (–75 °C to –40 °C) .....	268
<b>Figure 102:</b> $^{31}\text{P}\{^1\text{H}\}$ (202.5 MHz, <i>tol-d</i> <sub>8</sub> ) stack plot of the <b>GA-1-087</b> reaction mixture at different temperatures (–30 °C to –5 °C).....	268
<b>Figure 103:</b> $^{19}\text{F}\{^1\text{H}\}$ (470 MHz, <i>tol-d</i> <sub>8</sub> ) stack plot of the <b>GA-1-087</b> reaction mixture at different temperatures (–75 °C to –40 °C) .....	269
<b>Figure 104:</b> $^{19}\text{F}\{^1\text{H}\}$ (470 MHz, <i>tol-d</i> <sub>8</sub> ) stack plot of the <b>GA-1-087</b> reaction mixture at different temperatures (–30 °C to –5 °C) .....	269
<b>Figure 105:</b> $^{31}\text{P}\{^1\text{H}\}$ NMR (202.5 MHz, dichloromethane- <i>d</i> <sub>2</sub> , –40 °C) of the <b>GA-2-104</b> reaction mixture.....	270
<b>Figure 106:</b> $^{19}\text{F}\{^1\text{H}\}$ NMR (470 MHz, dichloromethane- <i>d</i> <sub>2</sub> , –40 °C) of the <b>GA-2-104</b> reaction mixture at different temperatures (–30 °C to –5 °C).....	271
<b>Figure 107:</b> $^{31}\text{P}\{^1\text{H}\}$ NMR (202.5 MHz, DMF (non-deuterated), –50 °C) spectrum of the reaction mixture of <b>GA-1-088</b> . Spectra could not be fully resolved at this temperature.....	274
<b>Figure 108 :</b> $^{19}\text{F}\{^1\text{H}\}$ NMR (470 MHz, $\text{CDCl}_3$ , 25 °C, 32 Sc) spectrum of the reaction mixture of the standard direct arylation reaction. The % $^{19}\text{F}\{^1\text{H}\}$ NMR yield were calculated using the <i>ortho</i> -F resonance of the product ( $\delta$ –143.5) wrt octafluoronaphthalene ( $\delta$ –145.2, internal standard).....	280
<b>Figure 109:</b> $^{19}\text{F}\{^1\text{H}\}$ NMR (470 MHz, $\text{CDCl}_3/\text{DMF}$ , 25 °C, 32 Sc) spectrum of the reaction mixture of <b>GA-4-296</b> (Table 25, Entry 1) at 3h.....	282
<b>Figure 110:</b> $^1\text{H}$ NMR (500 MHz, $\text{CDCl}_3$ , 25 °C, 32 Sc) spectrum of the reaction mixture of <b>GA-3-222</b> at 23h. The resonances used to calculate the % $^1\text{H}$ NMR yield were the methyl resonance of the product <b>18</b> ( $\delta$ 2.43) wrt 1,3,5-trimethoxybenzene ( $\delta$ 3.77, internal standard). .....	283
<b>Figure 111:</b> $^{31}\text{P}\{^1\text{H}\}$ (202.5 MHz, $\text{CD}_2\text{Cl}_2$ , 25 °C) spectrum of the reaction mixture of <b>GA-3-205</b> , collected at $t = 0$ h, RT, showing the presence of <b>101</b> , <b>102</b> , <b>105</b> and unbound Xphos. ....	287

<b>Figure 112:</b> $^{19}\text{F}\{^1\text{H}\}$ NMR (470 MHz, $\text{CD}_2\text{Cl}_2$ , 25 °C) of the reaction mixture <b>GA-3-205</b> immediately after sample preparation, showing the presence of the organic product. ....	287
<b>Figure 113:</b> Stack plot of the $^{31}\text{P}\{^1\text{H}\}$ NMR spectrum of the reaction mixture at –80, –60, –50, –40 °C showing unreacted starting material. ....	289
<b>Figure 114:</b> Stack plot of the $^{31}\text{P}\{^1\text{H}\}$ NMR spectrum of the reaction mixture at –35, –30, –25, –20 °C showing formation of <b>105</b> as the by-product. ....	289
<b>Figure 115:</b> Stack plot of the $^{19}\text{F}\{^1\text{H}\}$ NMR spectrum of the reaction mixture at –35, –30, –25, –20 °C showing formation of organic product <b>28</b> . ....	290
<b>Figure 116:</b> $^{31}\text{P}\{^1\text{H}\}$ (202.5 MHz, $\text{CD}_2\text{Cl}_2$ , –20 °C) NMR spectrum of the reaction mixture .....	290
<b>Figure 117:</b> $^{19}\text{F}\{^1\text{H}\}$ (470 MHz, $\text{CD}_2\text{Cl}_2$ , –20 °C) NMR spectrum of the reaction mixture .....	291
<b>Figure 118:</b> $^{19}\text{F}\{^1\text{H}\}$ NMR (470 MHz, DMF (unlocked), 25 °C) of the reaction mixture <b>GA-2-163</b> after heating at 130 °C for 1 h, showing the presence of <b>101</b> (yellow, peaks indicated by <b>a</b> ) and $\text{C}_6\text{F}_5\text{H}$ <b>17</b> (green, peaks indicated by <b>b</b> ) from slight decomposition of <b>101</b> . ....	292
<b>Figure 119:</b> $^{31}\text{P}\{^1\text{H}\}$ (202.5 MHz, $\text{C}_6\text{D}_6/\text{C}_6\text{H}_6$ , locked to $\text{C}_6\text{D}_6$ , 25 °C) spectrum of the reaction mixture of <b>GA-3-233</b> , collected at $t = 0$ h, RT. The mixture shows both the presence of <b>101</b> and <b>106</b> . ....	293
<b>Figure 120:</b> $^{19}\text{F}\{^1\text{H}\}$ NMR (470 MHz, $\text{C}_6\text{D}_6/\text{C}_6\text{H}_6$ , locked to $\text{C}_6\text{D}_6$ , 25 °C) of the reaction mixture <b>GA-3-233</b> showing presence of both <b>101</b> and trace amounts of <b>17</b> .....	294
<b>Figure 121:</b> $^{31}\text{P}\{^1\text{H}\}$ (202.5 MHz, $\text{C}_6\text{D}_6$ , 25 °C) spectrum of the reaction mixture of <b>GA-3-216</b> , collected at $t = 0$ h, RT. The mixture shows both the presence of <b>106</b> and <b>101</b> . ....	295
<b>Figure 122:</b> $^{19}\text{F}\{^1\text{H}\}$ NMR (470 MHz, $\text{C}_6\text{D}_6$ , 25 °C) of the reaction mixture <b>GA-3-216</b> . ....	295
<b>Figure 123:</b> $^{31}\text{P}\{^1\text{H}\}$ (202.5 MHz, $\text{CH}_3\text{CN}$ , 25 °C) spectrum of the reaction mixture of <b>GA-3-190</b> , collected after heating at 80 °C for 24 h. The mixture showed only the presence of <b>109</b> and no <b>101</b> or unbound Xphos. ....	296
<b>Figure 124:</b> $^{19}\text{F}\{^1\text{H}\}$ NMR (470 MHz, $\text{CH}_3\text{CN}$ , 25 °C) of the reaction mixture <b>GA-3-190</b> , showing unreacted $\text{C}_6\text{F}_5\text{H}$ <b>17</b> .....	297
<b>Figure 125:</b> $^{31}\text{P}\{^1\text{H}\}$ (202.5 MHz, $\text{CD}_2\text{Cl}_2$ , 25 °C) spectrum of the reaction mixture of <b>GA-4-271</b> after allowing it to react overnight. The mixture shows the presence of unreacted <b>105</b> . ....	298
<b>Figure 126:</b> $^{19}\text{F}\{^1\text{H}\}$ NMR (470 MHz, $\text{CD}_2\text{Cl}_2$ , 25 °C) of the reaction mixture <b>GA-4-271</b> , showing only unreacted $\text{C}_6\text{F}_5\text{H}$ <b>17</b> with no formation of any new species. ....	298
<b>Figure 127:</b> $^{31}\text{P}\{^1\text{H}\}$ (202.5 MHz, DMF (unlocked), 25 °C) spectrum of <b>GA-4-272</b> after it was heated at 60 °C for 19 h. The mixture shows the presence of unreacted <b>105</b> . ....	299



<b>Figure 128:</b> $^{19}\text{F}\{^1\text{H}\}$ NMR (470 MHz, DMF (unlocked), 25 °C) of the reaction mixture <b>GA-4-272</b> , showing only unreacted <b>C<sub>6</sub>F<sub>5</sub>H 17</b> with no formation of any new species. ....	300
<b>Figure 129:</b> $^{31}\text{P}\{^1\text{H}\}$ (202.5 MHz, DMF (unlocked), 25 °C) spectrum of <b>GA-4-276</b> at room temperature for 24 h. The mixture shows the presence of unreacted <b>105</b> .....	301
<b>Figure 130:</b> $^{31}\text{P}\{^1\text{H}\}$ (202.5 MHz, DMF (unlocked), 25 °C) spectrum of <b>GA-4-278</b> at 60 °C for 2 h. The mixture shows the presence of unreacted <b>105</b> , unbound Xphos and Xphos oxide. ....	302
<b>Figure 131:</b> $^{31}\text{P}\{^1\text{H}\}$ (202.5 MHz, DMF (unlocked), 25 °C) spectrum of <b>GA-4-298</b> at 60 °C for 4 h. The mixture shows the presence of unreacted <b>105</b> .....	303
<b>Figure 132:</b> $^{31}\text{P}\{^1\text{H}\}$ (202.5 MHz, DMF (unlocked), 25 °C) spectrum of the reaction mixture of <b>GA-5-354</b> . The Ag resonance was centred at $\delta$ 14.9 ( $1J$ 107Ag – $31P$ = 459.7 Hz, $1J$ 109Ag – $31P$ = 532.6 Hz) corresponding to <b>101</b> . ....	304
<b>Figure 133:</b> $^{19}\text{F}\{^1\text{H}\}$ NMR (470 MHz, DMF (unlocked), 25 °C) of the reaction mixture <b>GA-4-345</b> , showing the presence of <b>101</b> in the reaction mixture with remaining unreacted <b>C<sub>6</sub>F<sub>5</sub>H 17</b> .....	305
<b>Figure 134:</b> LIFDI-MS spectrum of the reaction mixture of <b>GA-4-321</b> . The major species with $m/z$ 752.25331 corresponds to <b>101</b> . ....	305
<b>Figure 135:</b> An expansion of the $m/z$ 752.25331 peak in the LIFDI spectrum of <b>GA-4-321</b> , showing the characteristic Ag isotopic pattern. ....	306
<b>Figure 136:</b> $^{31}\text{P}\{^1\text{H}\}$ (202.5 MHz, CD <sub>2</sub> Cl <sub>2</sub> , 25 °C) spectrum of the reaction mixture of <b>GA-4-318</b> , recorded immediately after the mixture was prepared in the glovebox. The resonance was centred at $\delta$ 13.0 ( $1J$ 107Ag – $31P$ = 443.5 Hz, $1J$ 109Ag – $31P$ = 512.3 Hz) which corresponds to <b>101</b> .....	307
<b>Figure 137:</b> $^{19}\text{F}\{^1\text{H}\}$ NMR (470 MHz, CD <sub>2</sub> Cl <sub>2</sub> , 25 °C) of the reaction mixture <b>GA-4-318</b> , showing the presence of <b>101</b> . ....	308
<b>Figure 138:</b> $^{31}\text{P}\{^1\text{H}\}$ (202.5 MHz, CD <sub>3</sub> CN, 25 °C) spectrum of the reaction mixture of <b>GA-4-303</b> , recorded immediately after the mixture was prepared in the glovebox. The resonance was centred at $\delta$ 14.2 ( $1J$ 107Ag – $31P$ = 492.1 Hz, $1J$ 109Ag – $31P$ = 569.0 Hz). ....	309
<b>Figure 139:</b> $^{19}\text{F}\{^1\text{H}\}$ NMR (470 MHz, CD <sub>3</sub> CN, 25 °C, 32 Sc) of the reaction mixture <b>GA-4-303</b> .....	309
<b>Figure 140:</b> $^{31}\text{P}\{^1\text{H}\}$ (202.5 MHz, CD <sub>2</sub> Cl <sub>2</sub> , 25 °C) spectrum of the reaction mixture of <b>GA-6-483</b> , recorded at $t$ = 5 d, RT. The spectrum shows the presence of unreacted <b>101</b> and the formation of unbound Xphos due to hydrolysis by D <sub>2</sub> O.....	310
<b>Figure 141:</b> $^{19}\text{F}\{^1\text{H}\}$ NMR (470 MHz, CD <sub>2</sub> Cl <sub>2</sub> , 25 °C) of the reaction mixture <b>GA-6-483</b> after 5 d at RT highlighting the <i>ortho</i> -F resonances of <b>101</b> and <b>C<sub>6</sub>F<sub>5</sub>D 69</b> . ....	311
<b>Figure 142:</b> $^{19}\text{F}\{^1\text{H}\}$ NMR (470 MHz, CD <sub>3</sub> CN, 25 °C) of the reaction mixture <b>GA-6-484</b> after 24 h at RT highlighting the <i>ortho</i> -F resonances of <b>55</b> (yellow, peaks labelled <b>a</b> ) and	

C <sub>6</sub> F <sub>5</sub> D <b>69</b> (green, peaks labelled <b>b</b> ) trace amounts of C <sub>6</sub> F <sub>5</sub> H <b>17</b> (red, only <i>Ortho</i> -F peak labelled <b>c</b> ).....	312
<b>Figure 143:</b> <sup>19</sup> F{ <sup>1</sup> H} NMR (470 MHz, C <sub>6</sub> D <sub>6</sub> , 25 °C) of the reaction mixture <b>GA-6-467</b> , key resonances are highlighted, <b>101</b> (yellow, peaks labelled a), C <sub>6</sub> F <sub>5</sub> H <b>17</b> (green, peaks labelled b), octafluoronaphthelene (red, peaks labelled c) .....	313
<b>Figure 144:</b> <sup>19</sup> F{ <sup>1</sup> H} NMR (470 MHz, C <sub>6</sub> D <sub>6</sub> , 25 °C) of the reaction mixture <b>GA-6-468</b> . key resonances are highlighted, <b>101</b> (yellow, peaks labelled a), C <sub>6</sub> F <sub>5</sub> D <b>69</b> (green, peaks labelled b), octafluoronaphthelene (red, peaks labelled c) and trace C <sub>6</sub> F <sub>5</sub> H <b>17</b> (blue, labelled d) .....	313
<b>Figure 145:</b> Initial rate of reaction for the direct arylation of 4-iodotoluene with 10 equiv. of C <sub>6</sub> F <sub>5</sub> H (black) and C <sub>6</sub> F <sub>5</sub> D (red).....	315
<b>Figure 146:</b> Experimental set-up for the kinetic monitoring of the reaction between Ag <sub>2</sub> (μ-CO <sub>3</sub> )(Xphos) <sub>2</sub> <b>106</b> and two equiv. of C <sub>6</sub> F <sub>5</sub> H <b>17</b> /C <sub>6</sub> F <sub>5</sub> D <b>69</b> .....	317
<b>Figure 147:</b> T <sub>1</sub> values of the reactants and products in toluene at 233 K .....	317
<b>Figure 148:</b> Change in concentration of <b>101</b> over time for the reaction of Ag <sub>2</sub> (μ-CO <sub>3</sub> )(Xphos) <sub>2</sub> <b>106</b> and two equiv. of C <sub>6</sub> F <sub>5</sub> H <b>17</b> or C <sub>6</sub> F <sub>5</sub> D <b>69</b> in toluene at – 40 °C .....	318
<b>Figure 149:</b> Initial rate for the reaction of Ag <sub>2</sub> (μ-CO <sub>3</sub> )(Xphos) <sub>2</sub> and two equiv. of C <sub>6</sub> F <sub>5</sub> H or C <sub>6</sub> F <sub>5</sub> D in toluene at – 40 °C (Fast process) .....	319
<b>Figure 150:</b> Rate for the reaction of Ag <sub>2</sub> (μ-CO <sub>3</sub> )(Xphos) <sub>2</sub> <b>106</b> and two equiv. of C <sub>6</sub> F <sub>5</sub> H <b>17</b> or C <sub>6</sub> F <sub>5</sub> D <b>69</b> in toluene at – 40 °C (slow process).....	320
<b>Figure 151:</b> <sup>31</sup> P{ <sup>1</sup> H} (202.5 MHz, CD <sub>2</sub> Cl <sub>2</sub> , 25 °C) spectrum of the reaction mixture of AgC <sub>6</sub> F <sub>5</sub> Xphos <b>101</b> (1 equiv.) and <sup>1</sup> BuXphos (1 equiv.) .....	321
<b>Figure 152:</b> <sup>31</sup> P{ <sup>1</sup> H} (202.5 MHz, C <sub>6</sub> D <sub>6</sub> , 25 °C) spectrum of the reaction mixture of Ag <sub>2</sub> CO <sub>3</sub> Xphos <sub>2</sub> <b>106</b> (1 equiv.) and <sup>1</sup> BuXphos (2 equiv.) .....	323
<b>Figure 153:</b> <sup>31</sup> P{ <sup>1</sup> H} (202.5 MHz, CD <sub>2</sub> Cl <sub>2</sub> , 25 °C) spectrum of the reaction mixture of AgIXphos <b>105</b> (1 equiv.) and <sup>1</sup> BuXphos (1 equiv.) .....	325
<b>Figure 154:</b> 2D EXSY spectrum of the mixture of <b>101</b> with Xphos (5 equiv.), with a mixing time of 2.0 sec. ....	327
<b>Figure 155:</b> Stack plot from a 1D EXSY experiment with <b>101</b> and Xphos (5 equiv.), with various mixing times, in CD <sub>2</sub> Cl <sub>2</sub> . ....	328
<b>Figure 156:</b> Plot of fractional transfer of magnetisation from <b>101</b> to free XPhos in CD <sub>2</sub> Cl <sub>2</sub> against mixing time. a) Plot without correction for the difference in relaxation times. b) plot with correction applied. The slopes correspond to k <sub>obs</sub> for the exchange process. ....	329
<b>Figure 157:</b> Plot of exchange velocity V <sub>ex</sub> vs [XPhos]. Black, uncorrected data, red corrected data. ....	330
<b>Figure 158:</b> Plot of fractional transfer of magnetisation from <b>101</b> to free XPhos in C <sub>6</sub> D <sub>6</sub> against mixing time for different temperatures. The slopes correspond to k <sub>obs</sub> for the exchange	

process. The data have been corrected for the differences in relaxation time at each temperature.....	333
<b>Figure 159:</b> Eyring plots for the exchange rate. a) using values of $k_{\text{obs}}$ , b) below using values of $V_{\text{ex}}$ .....	334
<b>Figure 160:</b> $^1\text{H}$ (400 MHz, $\text{C}_6\text{D}_6$ , 20 °C) spectrum of 2,3,4,5,6-pentafluoro-4'-(methyl)biphenyl <b>18</b> ( <i>JDF file reference: a6581gya</i> ).....	357
<b>Figure 161:</b> $^{19}\text{F}\{^1\text{H}\}$ (376 MHz, $\text{C}_6\text{D}_6$ , 20 °C) spectrum of 2,3,4,5,6-pentafluoro-4'-(methyl)biphenyl <b>18</b> ( <i>JDF file reference: a6581gya</i> ).....	357
<b>Figure 162:</b> $^1\text{H}$ NMR (500 MHz, $\text{CDCl}_3$ , 25°C) spectrum of 2,3,4,5,6-pentafluorobiphenyl <b>28</b> (spectrum collected on AV500, saved as 5 under GA-5-428).....	358
<b>Figure 163:</b> $^{19}\text{F}\{^1\text{H}\}$ NMR (470.6 MHz, $\text{CDCl}_3$ , 25 °C) spectrum of 2,3,4,5,6-pentafluorobiphenyl <b>28</b> (spectrum collected on AV500, saved as 6 under GA-5-428).....	358
<b>Figure 164:</b> HSQC spectrum of 2,3,4,5,6-pentafluorobiphenyl <b>28</b> in $\text{CDCl}_3$ (spectrum collected on AV500, saved as 7 under GA-5-428).....	359
<b>Figure 165:</b> $^{13}\text{C}\{^1\text{H}\}$ (125.8 MHz, $\text{CDCl}_3$ , 25 °C) spectrum of 2,3,4,5,6-pentafluorobiphenyl <b>28</b> (spectrum collected on AV500, saved as 8 under GA-5-428).....	359
<b>Figure 166:</b> $^1\text{H}$ NMR (500 MHz, $\text{CDCl}_3$ , 25°C) spectrum of 2,3,4,5,6-pentafluoro-4'-(fluoro)biphenyl <b>134</b> (spectrum collected on AV500, saved as 7 under GA-5-429).....	360
<b>Figure 167:</b> $^{19}\text{F}\{^1\text{H}\}$ NMR (470.6 MHz, $\text{CDCl}_3$ , 25 °C) spectrum of 2,3,4,5,6-pentafluoro-4'-(fluoro)biphenyl <b>134</b> (spectrum collected on AV500, saved as 8 under GA-5-429).....	360
<b>Figure 168:</b> HSQC spectrum of 2,3,4,5,6-pentafluoro-4'-(fluoro)biphenyl <b>134</b> in $\text{CDCl}_3$ (spectrum collected on AV500, saved as 9 under GA-5-429).....	361
<b>Figure 169:</b> $^{13}\text{C}\{^1\text{H}\}$ (125.8 MHz, $\text{CDCl}_3$ , 25 °C) spectrum of 2,3,4,5,6-pentafluoro-4'-(fluoro)biphenyl <b>134</b> (spectrum collected on AV500, saved as 13 under GA-5-429).....	361
<b>Figure 170:</b> Stack plot of the $^{13}\text{C}\{^1\text{H}\}$ NMR spectrum (top) of <b>134</b> with the $^{13}\text{C}\{^1\text{H}, ^{19}\text{F}\}$ spectrum with an O3P of $\delta -158$ (middle) and $\delta -111$ (bottom), in $\text{CDCl}_3$ (spectrum collected on AV500, the individual spectrum are saved as 13,12 and 10 under GA-5-429).....	362
<b>Figure 171:</b> $^1\text{H}$ NMR (500 MHz, $\text{CDCl}_3$ , 25°C) spectrum of 2',3',4',5',6'-pentafluorobiphenyl-4-carboxylate <b>140</b> (spectrum collected on AV500, saved as 5 under GA-6-518).....	363
<b>Figure 172:</b> $^{19}\text{F}\{^1\text{H}\}$ NMR (470.6 MHz, $\text{CDCl}_3$ , 25 °C) spectrum of 2',3',4',5',6'-pentafluorobiphenyl-4-carboxylate <b>140</b> (spectrum collected on AV500, saved as 6 under GA-6-518).....	363
<b>Figure 173:</b> HSQC spectrum of 2',3',4',5',6'-pentafluorobiphenyl-4-carboxylate <b>140</b> in $\text{CDCl}_3$ (spectrum collected on AV500, saved as 7 under GA-6-518).....	364

<b>Figure 174:</b> $^{13}\text{C}\{^1\text{H}\}$ (125.8 MHz, $\text{CDCl}_3$ , 25 °C) spectrum of 2',3',4',5',6'-pentafluorobiphenyl-4-carboxylate <b>140</b> (spectrum collected on AV500, saved as 8 under GA-6-518) .....	364
<b>Figure 175:</b> $^1\text{H}$ NMR (500 MHz, $\text{CDCl}_3$ , 25°C) spectrum of 1-(2',3',4',5',6'-pentafluoro-[1,1'-biphenyl]-4-yl)ethan-1-one <b>143</b> (spectrum collected on AV500, saved as 3 under GA-6-519).....	365
<b>Figure 176:</b> $^{19}\text{F}\{^1\text{H}\}$ NMR (470.6 MHz, $\text{CDCl}_3$ , 25 °C) spectrum of 1-(2',3',4',5',6'-pentafluoro-[1,1'-biphenyl]-4-yl)ethan-1-one <b>143</b> (spectrum collected on AV500, saved as 6 under GA-6-519).....	365
<b>Figure 177:</b> $^{13}\text{C}\{^1\text{H}\}$ (125.8 MHz, $\text{CDCl}_3$ , 25 °C) spectrum of 1-(2',3',4',5',6'-pentafluoro-[1,1'-biphenyl]-4-yl)ethan-1-one <b>143</b> (spectrum collected on AV500, saved as 9 under GA-6-519).....	366
<b>Figure 178:</b> $^1\text{H}$ NMR (500 MHz, $\text{CDCl}_3$ , 25°C) spectrum of 6-(Perfluorophenyl)Quinoline <b>148</b> (spectrum collected on AV500, saved as 3 under GA-6-520) .....	366
<b>Figure 179:</b> $^{19}\text{F}\{^1\text{H}\}$ NMR (470.6 MHz, $\text{CDCl}_3$ , 25 °C) spectrum of 6-(Perfluorophenyl)Quinoline <b>148</b> (spectrum collected on AV500, saved as 4 under GA-6-520) .....	367
<b>Figure 180:</b> $^1\text{H}$ NMR (500 MHz, $\text{CDCl}_3$ , 25°C) spectrum of 2,3,5,6-tetrafluoro-4-[-4-methylphenyl]pyridine <b>158</b> (spectrum collected on AV500, saved as 3 under GA-5-357). 367	
<b>Figure 181:</b> $^{19}\text{F}\{^1\text{H}\}$ NMR (470.6 MHz, $\text{CDCl}_3$ , 25 °C) spectrum of 2,3,5,6-tetrafluoro-4-[-4-methylphenyl]pyridine <b>158</b> (spectrum collected on AV500, saved as 4 under GA-5-357) .....	368
<b>Figure 182:</b> $^{13}\text{C}\{^1\text{H}\}$ (125.8 MHz, $\text{CDCl}_3$ , 25 °C) spectrum of 2,3,5,6-tetrafluoro-4-[-4-methylphenyl]pyridine <b>158</b> .....	368
<b>Figure 183:</b> $^2\text{H}$ (76 MHz, Tol (non-deuterated) 25 °C) spectrum of $\text{C}_6\text{F}_5\text{D}$ <b>69</b> (spectrum collected on AV500, saved as 9 under GA-4-277) .....	369
<b>Figure 184:</b> $^{19}\text{F}\{^1\text{H}\}$ (470.6 MHz, $\text{CDCl}_3$ , 25°C) spectrum of $\text{C}_6\text{F}_5\text{D}$ <b>69</b> (spectrum collected on AV500, saved as 8 under GA-4-277).....	369
<b>Figure 185:</b> $^{13}\text{C}\{^1\text{H}\}$ NMR (126 MHz, $\text{CDCl}_3$ , 25 °C) spectrum of $\text{C}_6\text{F}_5\text{D}$ <b>69</b> (spectrum collected on AV500, saved as 12 under GA-4-277) .....	370
<b>Figure 186:</b> $^1\text{H}$ NMR (500 MHz, $\text{CDCl}_3$ , 25 °C) spectrum of $\text{Ag}(\text{PPh}_3)_2(\kappa^2\text{-OAc})$ <b>94</b> (spectrum collected on AV500, saved as 3 under GA-1-001) .....	370
<b>Figure 187:</b> $^{13}\text{C}\{^1\text{H}\}$ NMR (126 MHz, $\text{CDCl}_3$ , 25 °C) spectrum of $\text{Ag}(\text{PPh}_3)_2(\kappa^2\text{-OAc})$ <b>94</b> (spectrum collected on AV500, saved as 5 under GA-1-001) .....	371
<b>Figure 188:</b> $^{31}\text{P}\{^1\text{H}\}$ NMR (202 MHz, $\text{CDCl}_3$ , 25 °C) spectrum of $\text{Ag}(\text{PPh}_3)_2(\kappa^2\text{-OAc})$ <b>94</b> , (spectrum collected on AV500, saved as 4 under GA-1-001) .....	371

<b>Figure 189:</b> $^{31}\text{P}\{^1\text{H}\}$ NMR (202 MHz, $\text{CD}_2\text{Cl}_2$ , $-80\text{ }^\circ\text{C}$ ) spectrum of $\text{Ag}(\text{PPh}_3)_2(\kappa^2\text{-OAc})$ <b>94</b> , (spectrum collected on AV500, saved as 2 under GA-1-001) .....	372
<b>Figure 190:</b> $^1\text{H}$ NMR (400 MHz, $\text{DMSO-}d_6$ , $25\text{ }^\circ\text{C}$ ) spectrum of $[\text{Ag}(\text{PPh}_3)_2]_2(\text{CO}_3)\cdot 2\text{ H}_2\text{O}$ <b>88</b> ( <i>JDF file reference: d8847gya</i> ).....	372
<b>Figure 191:</b> $^{13}\text{C}\{^1\text{H}\}$ NMR (101 MHz, $\text{DMSO-}d_6$ , $25\text{ }^\circ\text{C}$ ) spectrum of $[\text{Ag}(\text{PPh}_3)_2]_2(\text{CO}_3)\cdot 2\text{ H}_2\text{O}$ <b>88</b> ( <i>JDF file reference: d8847gya</i> ).....	373
<b>Figure 192:</b> $^{31}\text{P}\{^1\text{H}\}$ NMR (162 MHz, $\text{DMSO-}d_6$ , $25\text{ }^\circ\text{C}$ ) spectrum of $[\text{Ag}(\text{PPh}_3)_2]_2(\text{CO}_3)\cdot 2\text{ H}_2\text{O}$ <b>88</b> ( <i>JDF file reference: d8847gya</i> ) .....	373
<b>Figure 193:</b> $^{31}\text{P}\{^1\text{H}\}$ NMR (202 MHz, dichloromethane- $d_2$ :tol- $d_8$ , $-100^\circ\text{C}$ ) spectrum of $[\text{Ag}(\text{PPh}_3)_2]_2(\text{CO}_3)\cdot 2\text{ H}_2\text{O}$ <b>88</b> (spectrum collected on AV500, saved as 11 under GA-1-039) .....	374
<b>Figure 194:</b> $^1\text{H}$ NMR (400 MHz, $\text{DMSO-}d_6$ , $25\text{ }^\circ\text{C}$ ) spectrum of $[\text{Ag}(\text{PPh}_3)_2(\kappa^2\text{-HCO}_3)]_2$ <b>89</b> ( <i>JDF file reference: d7633gya</i> ) .....	374
<b>Figure 195:</b> $^{13}\text{C}\{^1\text{H}\}$ NMR (101 MHz, $\text{DMSO-}d_6$ , $25\text{ }^\circ\text{C}$ ) spectrum of $[\text{Ag}(\text{PPh}_3)_2(\kappa^2\text{-HCO}_3)]_2$ <b>89</b> ( <i>JDF file reference: d7633gya</i> ) .....	375
<b>Figure 196:</b> $^{31}\text{P}\{^1\text{H}\}$ NMR (162 MHz, $\text{DMSO-}d_6$ , $25\text{ }^\circ\text{C}$ ) spectrum of $[\text{Ag}(\text{PPh}_3)_2(\kappa^2\text{-HCO}_3)]_2$ <b>89</b> ( <i>JDF file reference: d7633gya</i> ).....	375
<b>Figure 197:</b> $^{31}\text{P}\{^1\text{H}\}$ NMR (202 MHz, tol- $d_8$ :dichloromethane- $d_2$ (20:80), $-80^\circ\text{C}$ ) spectrum of $[\text{Ag}(\text{PPh}_3)_2(\kappa^2\text{-HCO}_3)]_2$ <b>89</b> (spectrum collected on AV500, saved as 4 under GA-1-075) .....	376
<b>Figure 198:</b> $^1\text{H}$ NMR (500 MHz, $\text{CDCl}_3$ , $25\text{ }^\circ\text{C}$ ) spectrum of $\text{Pd}(\text{PPh}_3)_2(4\text{-tolyl})(\text{I})$ <b>98</b> (spectrum collected on AV500, saved as 2 under GA-1-038) .....	376
<b>Figure 199:</b> $^{13}\text{C}\{^1\text{H}\}$ NMR (126 MHz, $\text{CDCl}_3$ , $25\text{ }^\circ\text{C}$ ) spectrum of $\text{Pd}(\text{PPh}_3)_2(4\text{-tolyl})(\text{I})$ <b>98</b> (spectrum collected on AV500, saved as 6 under GA-1-038) .....	377
<b>Figure 200:</b> $^{31}\text{P}\{^1\text{H}\}$ NMR (202 MHz, $\text{CDCl}_3$ , $25\text{ }^\circ\text{C}$ ) spectrum of $\text{Pd}(\text{PPh}_3)_2(4\text{-tolyl})(\text{I})$ <b>98</b> (spectrum collected on AV500, saved as 3 under GA-1-038) .....	377
<b>Figure 201:</b> $^1\text{H}$ NMR (500 MHz, $\text{CDCl}_3$ , $25\text{ }^\circ\text{C}$ ) spectrum of $\text{Pd}(\text{PPh}_3)_2(\text{Ph})(\text{I})$ <b>97</b> (spectrum collected on AV500, saved as 3 under GA-1-055) .....	378
<b>Figure 202:</b> $^{13}\text{C}\{^1\text{H}\}$ NMR (126 MHz, $\text{CDCl}_3$ , $25\text{ }^\circ\text{C}$ ) spectrum of $\text{Pd}(\text{PPh}_3)_2(\text{Ph})(\text{I})$ <b>97</b> (spectrum collected on AV500, saved as 5 under GA-1-055) .....	378
<b>Figure 203:</b> $^{31}\text{P}\{^1\text{H}\}$ NMR (202 MHz, $\text{CDCl}_3$ , $25\text{ }^\circ\text{C}$ ) spectrum of $\text{Pd}(\text{PPh}_3)_2(\text{Ph})(\text{I})$ <b>97</b> (spectrum collected on AV500, saved as 4 under GA-1-055) .....	379
<b>Figure 204:</b> $^1\text{H}$ NMR (400 MHz, $\text{CDCl}_3$ , $25\text{ }^\circ\text{C}$ ) spectrum of $\text{Pd}(\text{PPh}_3)_2\text{Cl}_2$ <b>171</b> ( <i>JDF file reference: d8737gya</i> ).....	379
<b>Figure 205:</b> $^{31}\text{P}\{^1\text{H}\}$ NMR (162 MHz, $\text{CDCl}_3$ , $25\text{ }^\circ\text{C}$ ) spectrum of $\text{Pd}(\text{PPh}_3)_2\text{Cl}_2$ <b>171</b> ( <i>JDF file reference: d8737gya</i> ) .....	380

<b>Figure 206:</b> $^1\text{H}$ NMR (500 MHz, $\text{C}_6\text{D}_6$ , 25 °C) spectrum of $\text{Pd}(\text{PPh}_3)_4$ <b>172</b> (spectrum collected on AV500, saved as 3 under GA-1-067) .....	380
<b>Figure 207:</b> $^{31}\text{P}\{^1\text{H}\}$ NMR (202 MHz, $\text{C}_6\text{D}_6$ , 25 °C) spectrum of $\text{Pd}(\text{PPh}_3)_4$ <b>172</b> (spectrum collected on AV500, saved as 4 under GA-1-067) .....	381
<b>Figure 208:</b> $^1\text{H}$ NMR (500 MHz, $\text{C}_6\text{D}_6$ , 25 °C) spectrum of $\text{Ag}_2(\text{PPh}_3)_2(\text{C}_6\text{F}_5)(\mu\text{-HCO}_3)$ <b>91</b> (spectrum collected on AV500, saved as 37 under GA-1-070) .....	381
<b>Figure 209:</b> $^{13}\text{C}\{^1\text{H}\}$ NMR (125.7 MHz, $\text{C}_6\text{D}_6$ , 25 °C) spectrum of $\text{Ag}_2(\text{PPh}_3)_2(\text{C}_6\text{F}_5)(\mu\text{-HCO}_3)$ <b>91</b> (spectrum collected on AV500, saved as 40 under GA-1-070) .....	382
<b>Figure 210:</b> $^{31}\text{P}\{^1\text{H}\}$ NMR (202 MHz, $\text{C}_6\text{D}_6$ , 25 °C) spectrum of $\text{Ag}_2(\text{PPh}_3)_2(\text{C}_6\text{F}_5)(\mu\text{-HCO}_3)$ <b>91</b> (spectrum collected on AV500, saved as 38 under GA-1-070) .....	382
<b>Figure 211:</b> $^{19}\text{F}\{^1\text{H}\}$ NMR (470 MHz, $\text{C}_6\text{D}_6$ , 25 °C) spectrum of $\text{Ag}_2(\text{PPh}_3)_2(\text{C}_6\text{F}_5)(\mu\text{-HCO}_3)$ <b>91</b> (spectrum collected on AV500, saved as 39 under GA-1-070) .....	383
<b>Figure 212:</b> $^1\text{H}$ NMR (500 MHz, $\text{tol-}d_8$ :dichloromethane- $d_2$ (20:80), -100 °C) spectrum of $\text{Ag}_2(\text{PPh}_3)_2(\text{C}_6\text{F}_5)(\mu\text{-HCO}_3)$ <b>91</b> (spectrum collected on AV500, saved as 33 under GA-1-070) .....	383
<b>Figure 213:</b> $^{31}\text{P}\{^1\text{H}\}$ NMR (202 MHz, $\text{tol-}d_8$ : dichloromethane- $d_2$ (20:80), -100 °C) spectrum of $\text{Ag}_2(\text{PPh}_3)_2(\text{C}_6\text{F}_5)(\mu\text{-HCO}_3)$ <b>91</b> (spectrum collected on AV500, saved as 34 under GA-1-070) .....	384
<b>Figure 214:</b> $^{19}\text{F}\{^1\text{H}\}$ NMR (470 MHz, $\text{tol-}d_8$ : dichloromethane- $d_2$ (20:80), -100 °C) spectrum of <b>91</b> (spectrum collected on AV500, saved as 35 under GA-1-070) .....	384
<b>Figure 215:</b> $^{19}\text{F}$ COSY NMR (470 MHz, $\text{tol-}d_8$ :dichloromethane- $d_2$ (20:80), -100 °C) spectrum of <b>91</b> (spectrum collected on AV500, saved as 36 under GA-1-070) .....	385
<b>Figure 216:</b> The variable-temperature $^{13}\text{P}\{^1\text{H}\}$ NMR (202 MHz, 128 scans, $\text{tol-}d_8$ ) spectrum of <b>91</b> (spectrum collected on AV500 and saved under GA-1-070) .....	385
<b>Figure 217:</b> The variable-temperature $^{19}\text{F}\{^1\text{H}\}$ NMR (470 MHz, 64 scans, $\text{tol-}d_8$ ) spectrum of $\text{Ag}_2(\text{PPh}_3)_2(\text{C}_6\text{F}_5)(\mu\text{-HCO}_3)$ <b>91</b> (spectrum collected on AV500 and saved under GA-1-070) .....	386
<b>Figure 218:</b> $^1\text{H}$ NMR (500 MHz, $\text{C}_6\text{D}_6$ , 25 °C) spectrum of $\text{Ag}_2(\text{PPh}_3)_2(\text{C}_6\text{F}_5)(\mu\text{-H}^{13}\text{CO}_3)$ <b>92</b> (spectrum collected on AV500, saved as 1 under GA-2-095) .....	386
<b>Figure 219:</b> $^{13}\text{C}\{^1\text{H}\}$ NMR (125.7 MHz, $\text{C}_6\text{D}_6$ , 25 °C) spectrum of $\text{Ag}_2(\text{PPh}_3)_2(\text{C}_6\text{F}_5)(\mu\text{-H}^{13}\text{CO}_3)$ <b>92</b> (spectrum collected on AV500, saved as 5 under GA-2-095) .....	387
<b>Figure 220:</b> $^{31}\text{P}\{^1\text{H}\}$ NMR (202 MHz, $\text{C}_6\text{D}_6$ , 25 °C) spectrum of $\text{Ag}_2(\text{PPh}_3)_2(\text{C}_6\text{F}_5)(\mu\text{-H}^{13}\text{CO}_3)$ <b>92</b> (spectrum collected on AV500, saved as 2 under GA-1-095) .....	387
<b>Figure 221:</b> $^{19}\text{F}\{^1\text{H}\}$ NMR (470 MHz, $\text{C}_6\text{D}_6$ , 25 °C) spectrum of $\text{Ag}_2(\text{PPh}_3)_2(\text{C}_6\text{F}_5)(\mu\text{-H}^{13}\text{CO}_3)$ <b>92</b> (spectrum collected on AV500, saved as 3 under GA-1-095) .....	388

<b>Figure 222:</b> $^{13}\text{C}\{^1\text{H}\}$ NMR (125.7 MHz, <i>tol-d</i> <sub>8</sub> :dichloromethane- <i>d</i> <sub>2</sub> (20:80), -100 °C) spectrum of $\text{Ag}_2(\text{PPh}_3)_2(\text{C}_6\text{F}_5)(\mu\text{-H}^{13}\text{CO}_3)$ <b>92</b> (spectrum collected on AV500, saved as 13 under GA-1-095).....	388
<b>Figure 223:</b> $^{13}\text{C}$ NMR (125.7 MHz, <i>tol-d</i> <sub>8</sub> :dichloromethane- <i>d</i> <sub>2</sub> (20:80) spectrum of $\text{Ag}_2(\text{PPh}_3)_2(\text{C}_6\text{F}_5)(\mu\text{-H}^{13}\text{CO}_3)$ <b>92</b> (spectrum collected on AV500, saved as 14 under GA-1-095).....	389
<b>Figure 224:</b> $^{31}\text{P}\{^1\text{H}\}$ NMR (202 MHz, <i>tol-d</i> <sub>8</sub> :dichloromethane- <i>d</i> <sub>2</sub> (20:80), -100 °C) spectrum of $\text{Ag}_2(\text{PPh}_3)_2(\text{C}_6\text{F}_5)(\mu\text{-H}^{13}\text{CO}_3)$ <b>92</b> (spectrum collected on AV500, saved as 11 under GA-1-095).....	389
<b>Figure 225:</b> $^{19}\text{F}\{^1\text{H}\}$ NMR (470 MHz, <i>tol-d</i> <sub>8</sub> :dichloromethane- <i>d</i> <sub>2</sub> (20:80), -100 °C) spectrum of $\text{Ag}_2(\text{PPh}_3)_2(\text{C}_6\text{F}_5)(\mu\text{-H}^{13}\text{CO}_3)$ <b>92</b> (spectrum collected on AV500, saved as 12 under GA-1-095).....	390
<b>Figure 226:</b> The $^{19}\text{F}\{^1\text{H}\}$ NMR (470.6 MHz, $\text{CD}_3\text{CN}$ , 25 °C) spectrum of $\text{AgC}_6\text{F}_5$ <b>55</b> (spectrum collected on AV500, saved as 4 under GA-4-258) .....	390
<b>Figure 227:</b> The $^{13}\text{C}\{^1\text{H}\}$ (125.8 MHz, $\text{CD}_3\text{CN}$ , 25 °C) spectrum of $\text{AgC}_6\text{F}_5$ <b>55</b> . Trace amount of EtCN (blue) is also present in the solution. EtCN and $\text{CD}_3\text{CN}$ tend to coordinate strongly with $\text{AgC}_3\text{F}_6$ , the CN $^{13}\text{C}$ peaks of the coordinated species is also present in the $^{13}\text{C}$ spectra. (spectrum collected on AV500, saved as 7 under GA-4-258).....	391
<b>Figure 228:</b> The Stack plot of the $^{13}\text{C}\{^1\text{H}\}$ NMR spectrum (bottom), $^{13}\text{C}\{^1\text{H}, ^{19}\text{F}\}$ NMR spectrum with O3P = -107 (middle) and $^{13}\text{C}\{^1\text{H}, ^{19}\text{F}\}$ NMR spectrum (top) of $\text{AgC}_6\text{F}_5$ <b>55</b> . (spectra collected on AV500, saved under GA-4-258).....	392
<b>Figure 229:</b> $^{31}\text{P}\{^1\text{H}\}$ NMR (202 MHz, <i>tol-d</i> <sub>8</sub> :dichloromethane- <i>d</i> <sub>2</sub> (20:80), 25 °C ) spectrum of $\text{Ag}_2(\text{PPh}_3)_n(\text{C}_6\text{F}_5)$ <b>93</b> (spectrum collected on AV500, saved as 2 under GA-4-268) .....	392
<b>Figure 230:</b> $^{19}\text{F}\{^1\text{H}\}$ NMR (470 MHz, <i>tol-d</i> <sub>8</sub> :dichloromethane- <i>d</i> <sub>2</sub> (20:80), 25 °C) spectrum of $\text{Ag}_2(\text{PPh}_3)_n(\text{C}_6\text{F}_5)$ <b>93</b> (spectrum collected on AV500, saved as 3 under GA-4-268) .....	393
<b>Figure 231:</b> $^{31}\text{P}\{^1\text{H}\}$ NMR (202 MHz, <i>tol-d</i> <sub>8</sub> :dichloromethane- <i>d</i> <sub>2</sub> (20:80), -100 °C ) spectrum of $\text{Ag}_2(\text{PPh}_3)_n(\text{C}_6\text{F}_5)$ <b>93</b> (spectrum collected on AV500, saved as 34 under GA-4-268).....	393
<b>Figure 232:</b> $^{19}\text{F}\{^1\text{H}\}$ NMR (470 MHz, <i>tol-d</i> <sub>8</sub> :dichloromethane- <i>d</i> <sub>2</sub> (20:80), -100 °C) spectrum of $\text{Ag}_2(\text{PPh}_3)_n(\text{C}_6\text{F}_5)$ <b>93</b> (spectrum collected on AV500, saved as 6 under GA-4-268) .....	394
<b>Figure 233:</b> $^1\text{H}$ NMR (500 MHz, $\text{CD}_2\text{Cl}_2$ , 25 °C) spectrum of <b>101</b> (spectrum collected on AV500, saved as 7 under GA-2-137).....	394
<b>Figure 234:</b> $^1\text{H}$ NMR (500 MHz, $\text{CD}_2\text{Cl}_2$ , 25°C) spectrum of <b>101</b> between $\delta$ 0.7 and $\delta$ 3.00 .....	395
<b>Figure 235:</b> $^1\text{H}$ NMR (500 MHz, $\text{CD}_2\text{Cl}_2$ , 25°C) spectrum of <b>101</b> between $\delta$ 7.00 and $\delta$ 8.00 .....	395

<b>Figure 236:</b> $^{31}\text{P}\{^1\text{H}\}$ (202.5 MHz, $\text{CD}_2\text{Cl}_2$ , 25 °C) spectrum of <b>101</b> (spectrum collected on AV500, saved as 8 under GA-2-137).....	396
<b>Figure 237:</b> $^{19}\text{F}\{^1\text{H}\}$ NMR (470.6 MHz, $\text{CD}_2\text{Cl}_2$ , 25 °C) spectrum of <b>101</b> (spectrum collected on AV500, saved as 9 under GA-2-137) .....	396
<b>Figure 238:</b> $^{13}\text{C}$ DEPT-135 (125.8 MHz, $\text{CD}_2\text{Cl}_2$ , 25 °C) spectrum of <b>101</b> (spectrum collected on AV500, saved as 15 under GA-2-138) .....	397
<b>Figure 239:</b> $^{13}\text{C}\{^1\text{H}\}$ (125.8 MHz, $\text{CD}_2\text{Cl}_2$ , 25 °C) spectrum of <b>101</b> (spectrum collected on AV500, saved as 20 under GA-2-138).....	397
<b>Figure 240:</b> $^{13}\text{C}\{^1\text{H}\}$ (125.8 MHz, $\text{CD}_2\text{Cl}_2$ , 25 °C) spectrum of <b>101</b> between $\delta$ 20 and $\delta$ 40 .....	398
<b>Figure 241:</b> Stack plot of the $^{13}\text{C}\{^1\text{H}\}$ NMR spectrum (bottom) and the $^{13}\text{C}$ DEPT-135 of <b>101</b> between $\delta$ 20 and $\delta$ 40 .....	398
<b>Figure 242:</b> $^{13}\text{C}\{^1\text{H}\}$ (125.8 MHz, $\text{CD}_2\text{Cl}_2$ , 25 °C) spectrum of <b>101</b> between $\delta$ 160 and $\delta$ 110.....	399
<b>Figure 243:</b> Stack plot of the $^{13}\text{C}\{^1\text{H}\}$ NMR spectrum (below) and the $^{13}\text{C}$ DEPT-135 (above) of <b>101</b> between $\delta$ 160 and $\delta$ 110 .....	399
<b>Figure 244:</b> Stack plot of the $^{13}\text{C}\{^1\text{H}\}$ NMR spectrum (bottom) with the $^{13}\text{C}\{^1\text{H}, ^{19}\text{F}\}$ spectrum with an O3P of $\delta$ -107 (top) and $\delta$ -160 (middle) in $\text{CD}_2\text{Cl}_2$ .....	400
<b>Figure 245:</b> Stack plot of the $^{13}\text{C}\{^1\text{H}\}$ NMR spectrum (bottom) with the $^{13}\text{C}\{^1\text{H}, ^{19}\text{F}\}$ spectrum with an O3P of $\delta$ -107 (middle) and $\delta$ -160 (top), in $\text{CDCl}_3$ .....	401
<b>Figure 246:</b> $^{31}\text{P}\{^{109}\text{Ag}\}$ (162 MHz, $\text{CD}_2\text{Cl}_2$ , 25 °C) spectrum of <b>101</b> .....	401
<b>Figure 247:</b> $^{31}\text{P}\{^{109}\text{Ag}\}$ - $^{109}\text{Ag}$ HMQC spectrum of <b>101</b> .....	402
<b>Figure 248:</b> HSQC spectrum of <b>101</b> in $\text{CD}_2\text{Cl}_2$ (spectrum collected on AV500, saved as 16 under GA-2-138) .....	402
<b>Figure 249:</b> HMBC spectrum of <b>101</b> in $\text{CD}_2\text{Cl}_2$ (spectrum collected on AV500, saved as 17 under GA-2-138) .....	403
<b>Figure 250:</b> $^1\text{H}$ NMR (500 MHz, $\text{CD}_2\text{Cl}_2$ , 25 °C) spectrum of the Pd(I)(Xphos)(Ph) <b>102</b> (spectrum collected on AV500, saved as 3 under GA-3-188) .....	403
<b>Figure 251:</b> $^1\text{H}$ NMR (500 MHz, $\text{CD}_2\text{Cl}_2$ , 25 °C) spectrum of <b>102</b> between $\delta$ - 0.2 to $\delta$ 3.5 .....	404
<b>Figure 252:</b> $^1\text{H}$ NMR (500 MHz, $\text{CD}_2\text{Cl}_2$ , 25 °C) spectrum of <b>102</b> between $\delta$ 6.6 to $\delta$ 7.9 .....	404
<b>Figure 253:</b> $^{31}\text{P}\{^1\text{H}\}$ (202.5 MHz, $\text{CD}_2\text{Cl}_2$ , 25 °C) spectrum of <b>102</b> (spectrum collected on AV500, saved as 4 under GA-3-188).....	405
<b>Figure 254:</b> DEPT-135 spectrum of <b>102</b> (spectrum collected on AV500, saved as 5 under GA-3-188) .....	405



<b>Figure 255:</b> $^{13}\text{C}\{^1\text{H}\}$ (125.8 MHz, $\text{CD}_2\text{Cl}_2$ , 25 °C) spectrum of <b>102</b> (spectrum collected on AV500, saved as 8 under GA-3-188).....	406
<b>Figure 256:</b> $^{13}\text{C}\{^1\text{H}\}$ (125.8 MHz, $\text{CD}_2\text{Cl}_2$ , 25 °C) spectrum of <b>102</b> between $\delta$ 20 and 40 .....	406
<b>Figure 257:</b> Stack plot of the $^{13}\text{C}$ NMR spectrum (bottom) and DEPT-135 of <b>102</b> between $\delta$ 20 and $\delta$ 40 .....	407
<b>Figure 258:</b> $^{13}\text{C}\{^1\text{H}\}$ (125.8 MHz, $\text{CD}_2\text{Cl}_2$ , 25 °C) spectrum of <b>102</b> between $\delta$ 163 and $\delta$ 117.....	407
<b>Figure 259:</b> Stack plot of the $^{13}\text{C}$ NMR spectrum (bottom) and DEPT-135 spectrum of <b>102</b> between $\delta$ 20 and $\delta$ 40 .....	408
<b>Figure 260:</b> HSQC spectrum of <b>102</b> (spectrum collected on AV500, saved as 10 under GA-3-188) .....	408
<b>Figure 261:</b> HMBC spectrum of <b>102</b> (spectrum collected on AV500, saved as 8 under GA-4-338) .....	409
<b>Figure 262:</b> $^1\text{H}$ NMR (500 MHz, $\text{C}_6\text{D}_6$ , 25 °C) spectrum of the <b>106</b> (spectrum collected on AV500, saved as 15 under GA-2-169).....	409
<b>Figure 263:</b> $^1\text{H}$ NMR (500 MHz, $\text{C}_6\text{D}_6$ , 25 °C) spectrum of the <b>106</b> between $\delta$ 0.9 to $\delta$ 3.6 .....	410
<b>Figure 264:</b> $^1\text{H}$ NMR (500 MHz, $\text{C}_6\text{D}_6$ , 25 °C) spectrum of the <b>106</b> between $\delta$ 0.9 to $\delta$ 3.6 .....	410
<b>Figure 265:</b> $^{31}\text{P}\{^1\text{H}\}$ (202.5 MHz, $\text{C}_6\text{D}_6$ , 25 °C) spectrum of the <b>106</b> (spectrum collected on AV500, saved as 17 under GA-2-169).....	411
<b>Figure 266:</b> $^{13}\text{C}$ DEPT – 135 (125.8 MHz, $\text{CD}_2\text{Cl}_2$ , 25 °C) spectrum of <b>106</b> (spectrum collected on AV500, saved as 18 under GA-2-169) .....	411
<b>Figure 267:</b> $^{13}\text{C}\{^1\text{H}\}$ (125.8 MHz, $\text{C}_6\text{D}_6$ , 25 °C) spectrum of <b>106</b> (spectrum collected on AV500, saved as 21 under GA-2-169).....	412
<b>Figure 268:</b> $^{13}\text{C}\{^1\text{H}\}$ (125.8 MHz, $\text{C}_6\text{D}_6$ , 25 °C) spectrum of <b>106</b> between $\delta$ 20 – $\delta$ 40 .....	412
<b>Figure 269:</b> Stack plot of the $^{13}\text{C}\{^1\text{H}\}$ Carbon DEPT spectrum (above) and the $^{13}\text{C}\{^1\text{H}\}$ spectrum (below) of <b>106</b> (between $\delta$ 20 – $\delta$ 40).....	413
<b>Figure 270:</b> $^{13}\text{C}\{^1\text{H}\}$ (125.8 MHz, $\text{C}_6\text{D}_6$ , 25 °C) spectrum of <b>106</b> between $\delta$ 120 and $\delta$ 156 .....	413
<b>Figure 271:</b> Stack plot of the $^{13}\text{C}\{^1\text{H}\}$ Carbon DEPT spectrum (above) and the $^{13}\text{C}\{^1\text{H}\}$ spectrum (below) of <b>106</b> between $\delta$ 120 and $\delta$ 154) .....	414
<b>Figure 272:</b> HSQC spectrum of <b>106</b> (spectrum collected on AV500, saved as 19 under GA-2-169) .....	414
<b>Figure 273:</b> HMBC spectrum of <b>106</b> (spectrum collected on AV500, saved as 20 under GA-2-169) .....	415

<b>Figure 274:</b> $^1\text{H}$ NMR (500 MHz, $\text{CD}_3\text{CN}$ , 25 °C) spectrum of <b>109</b> (spectrum collected on AV500, saved as 1 under GA-6-473).....	415
<b>Figure 275:</b> $^1\text{H}$ NMR (500 MHz, $\text{CD}_3\text{CN}$ , 25 °C) spectrum of <b>109</b> between $\delta$ 0.7 to $\delta$ 3.1.....	416
<b>Figure 276:</b> $^1\text{H}$ NMR (500 MHz, $\text{CD}_3\text{CN}$ , 25 °C) spectrum of <b>109</b> between $\delta$ 7.0 to $\delta$ 8.0.....	416
<b>Figure 277:</b> $^{31}\text{P}\{^1\text{H}\}$ (202.5 MHz, $\text{CD}_3\text{CN}$ , 25 °C) spectrum of <b>109</b> (spectrum collected on AV500, saved as 2 under GA-6-473).....	417
<b>Figure 278:</b> $^{13}\text{C}$ DEPT-135 (125.8 MHz, $\text{CD}_3\text{CN}$ , 25 °C) spectrum of <b>109</b> (spectrum collected on AV500, saved as 3 under GA-6-473).....	417
<b>Figure 279:</b> $^{13}\text{C}\{^1\text{H}\}$ (125.8 MHz, $\text{CD}_3\text{CN}$ , 25 °C) spectrum of <b>109</b> (spectrum collected on AV500, saved as 6 under GA-6-473).....	418
<b>Figure 280:</b> $^{13}\text{C}\{^1\text{H}\}$ (125.8 MHz, $\text{CD}_3\text{CN}$ , 25 °C) spectrum of <b>109</b> between $\delta$ 20 and $\delta$ 40.....	418
<b>Figure 281:</b> Stack plot of the $^{13}\text{C}\{^1\text{H}\}$ Carbon DEPT spectrum (above) and the $^{13}\text{C}\{^1\text{H}\}$ spectrum (below) of <b>109</b> between $\delta$ 20 and $\delta$ 40.....	419
<b>Figure 282:</b> $^{13}\text{C}\{^1\text{H}\}$ (125.8 MHz, $\text{CD}_3\text{CN}$ , 25 °C) spectrum of <b>109</b> between $\delta$ 120 and $\delta$ 183.....	419
<b>Figure 283:</b> Stack plot of the $^{13}\text{C}\{^1\text{H}\}$ Carbon DEPT spectrum (above) and the $^{13}\text{C}\{^1\text{H}\}$ spectrum (below) of <b>109</b> between $\delta$ 110 and $\delta$ 186.....	420
<b>Figure 284:</b> HSQC spectrum of <b>109</b> (spectrum collected on AV500, saved as 4 under GA-6-473).....	420
<b>Figure 285:</b> HMBC spectrum of <b>109</b> (spectrum collected on AV500, saved as 5 under GA-6-473).....	421
<b>Figure 286:</b> $^1\text{H}$ NMR (500 MHz, $\text{CD}_2\text{Cl}_2$ , 25 °C) spectrum of <b>105</b> (spectrum collected on AV500, saved as 4 under GA-2-148).....	421
<b>Figure 287:</b> $^1\text{H}$ NMR (500 MHz, $\text{CD}_2\text{Cl}_2$ , 25 °C) spectrum of <b>105</b> between $\delta$ 0.8 and $\delta$ 4.0.....	422
<b>Figure 288:</b> $^1\text{H}$ NMR (500 MHz, $\text{CD}_2\text{Cl}_2$ , 25 °C) spectrum of <b>105</b> between $\delta$ 7.0 and $\delta$ 8.0.....	422
<b>Figure 289:</b> $^{31}\text{P}\{^1\text{H}\}$ (202.5 MHz, $\text{CD}_2\text{Cl}_2$ , 25 °C) spectrum of <b>105</b> (spectrum collected on AV500, saved as 5 under GA-2-148).....	423
<b>Figure 290:</b> $^{13}\text{C}$ DEPT-135 (125.8 MHz, $\text{CD}_2\text{Cl}_2$ , 25 °C) spectrum of <b>105</b> (spectrum collected on AV500, saved as 6 under GA-2-148).....	423
<b>Figure 291:</b> $^{13}\text{C}\{^1\text{H}\}$ (125.8 MHz, $\text{CD}_2\text{Cl}_2$ , 25 °C) spectrum of <b>105</b> (spectrum collected on AV500, saved as 7 under GA-2-148).....	424

<b>Figure 292:</b> $^{13}\text{C}\{^1\text{H}\}$ (125.8 MHz, $\text{CD}_2\text{Cl}_2$ , 25 °C) spectrum of <b>105</b> between $\delta$ 20 and $\delta$ 40	424
<b>Figure 293:</b> Stack plot of the $^{13}\text{C}\{^1\text{H}\}$ Carbon DEPT spectrum (above) and the $^{13}\text{C}\{^1\text{H}\}$ spectrum (below) of <b>105</b> between $\delta$ 20 and $\delta$ 40	425
<b>Figure 294:</b> $^{13}\text{C}\{^1\text{H}\}$ (125.8 MHz, $\text{CD}_2\text{Cl}_2$ , 25 °C) spectrum of <b>105</b> between $\delta$ 118 and $\delta$ 155	425
<b>Figure 295:</b> Stack plot of the $^{13}\text{C}\{^1\text{H}\}$ Carbon DEPT spectrum (above) and the $^{13}\text{C}\{^1\text{H}\}$ spectrum (below) of <b>105</b> between $\delta$ 120 and $\delta$ 154)	426
<b>Figure 296:</b> $^{31}\text{P}\{^{109}\text{Ag}\}$ (162 MHz, $\text{CD}_2\text{Cl}_2$ , 25 °C) spectrum of <b>105</b>	426
<b>Figure 297:</b> $^{31}\text{P}\{^{109}\text{Ag}\}$ - $^{109}\text{Ag}$ HMQC spectrum of <b>105</b>	427
<b>Figure 298:</b> HSQC spectrum of <b>105</b> (spectrum collected on AV500, saved as 8 under GA-2-148)	427
<b>Figure 299:</b> HMBC spectrum of <b>105</b> (spectrum collected on AV500, saved as 9 under GA-2-148)	428
<b>Figure 300:</b> $^1\text{H}$ NMR (500 MHz, $\text{CD}_2\text{Cl}_2$ , 25 °C) spectrum of $\text{AgC}_6\text{F}_5\text{CyJohnPhos}$ <b>122</b>	428
<b>Figure 301:</b> $^{31}\text{P}\{^1\text{H}\}$ (202.5 MHz, $\text{CD}_2\text{Cl}_2$ , 25 °C) spectrum of $\text{AgC}_6\text{F}_5\text{CyJohnPhos}$ <b>122</b>	429
<b>Figure 302:</b> $^{19}\text{F}\{^1\text{H}\}$ NMR (470.6 MHz, $\text{CD}_2\text{Cl}_2$ , 25 °C) spectrum of $\text{AgC}_6\text{F}_5\text{CyJohnPhos}$ <b>122</b>	429
<b>Figure 303:</b> $^{13}\text{C}$ DEPT-135 (125.8 MHz, $\text{CD}_2\text{Cl}_2$ , 25 °C) spectrum of $\text{AgC}_6\text{F}_5\text{CyJohnPhos}$ <b>122</b>	430
<b>Figure 304:</b> $^{13}\text{C}\{^1\text{H}\}$ (125.8 MHz, $\text{CD}_2\text{Cl}_2$ , 25 °C) spectrum of $\text{AgC}_6\text{F}_5\text{CyJohnPhos}$ <b>122</b>	430
<b>Figure 305:</b> $^{13}\text{C}\{^1\text{H}\}$ (125.8 MHz, $\text{CD}_2\text{Cl}_2$ , 25 °C) spectrum of $\text{AgC}_6\text{F}_5\text{CyJohnPhos}$ <b>122</b> between $\delta$ 25 and $\delta$ 36	431
<b>Figure 306:</b> Stack plot p the $^{13}\text{C}\{^1\text{H}\}$ NMR spectrum (bottom) and the $^{13}\text{C}$ DEPT-135 (top) of $\text{AgC}_6\text{F}_5\text{CyJohnPhos}$ <b>122</b> between $\delta$ 20 and $\delta$ 40	431
<b>Figure 307:</b> $^{13}\text{C}\{^1\text{H}\}$ (125.8 MHz, $\text{CD}_2\text{Cl}_2$ , 25 °C) spectrum of $\text{AgC}_6\text{F}_5\text{CyJohnPhos}$ <b>122</b> between $\delta$ 124 and $\delta$ 153	432
<b>Figure 308:</b> Stack plot of the $^{13}\text{C}\{^1\text{H}\}$ NMR spectrum (below) and the $^{13}\text{C}$ DEPT-135 (above) of $\text{AgC}_6\text{F}_5\text{CyJohnPhos}$ <b>122</b> between $\delta$ 160 and $\delta$ 110	432
<b>Figure 309:</b> HSQC spectrum of $\text{AgC}_6\text{F}_5\text{CyJohnPhos}$ <b>122</b> in $\text{CD}_2\text{Cl}_2$	433
<b>Figure 310:</b> HMBC spectrum of $\text{AgC}_6\text{F}_5\text{CyJohnPhos}$ <b>122</b> in $\text{CD}_2\text{Cl}_2$	433
<b>Figure 311:</b> Stack plot of <b>122</b> the $^{13}\text{C}\{^1\text{H}\}$ NMR spectrum (top) with the $^{13}\text{C}\{^1\text{H}, ^{19}\text{F}\}$ spectrum with specific $^{19}\text{F}$ coupling of $^{19}\text{F}$ peak (indicated by O3) at $\delta$ -107 (bottom) and $\delta$ -162 (middle), in $\text{CD}_2\text{Cl}_2$	434

<b>Figure 312:</b> $^1\text{H}$ NMR (500 MHz, $\text{CD}_2\text{Cl}_2$ , 25 °C) spectrum of $\text{AgC}_6\text{F}_5\text{Sphos}$ <b>124</b> .....	434
<b>Figure 313:</b> $^{31}\text{P}\{^1\text{H}\}$ (202.5 MHz, $\text{CD}_2\text{Cl}_2$ , 25 °C) spectrum of $\text{AgC}_6\text{F}_5\text{Sphos}$ <b>124</b> .....	435
<b>Figure 314:</b> $^{19}\text{F}\{^1\text{H}\}$ NMR (470.6 MHz, $\text{CD}_2\text{Cl}_2$ , 25 °C) spectrum of $\text{AgC}_6\text{F}_5\text{Sphos}$ <b>124</b> .....	435
<b>Figure 315:</b> $^{13}\text{C}$ DEPT-135 (125.8 MHz, $\text{CD}_2\text{Cl}_2$ , 25 °C) spectrum of $\text{AgC}_6\text{F}_5\text{Sphos}$ <b>124</b> .....	436
<b>Figure 316:</b> $^{13}\text{C}\{^1\text{H}\}$ (125.8 MHz, $\text{CD}_2\text{Cl}_2$ , 25 °C) spectrum of $\text{AgC}_6\text{F}_5\text{Sphos}$ <b>124</b> .....	436
<b>Figure 317:</b> $^{13}\text{C}\{^1\text{H}\}$ (125.8 MHz, $\text{CD}_2\text{Cl}_2$ , 25 °C) spectrum of $\text{AgC}_6\text{F}_5\text{Sphos}$ <b>124</b> between $\delta$ 23 and $\delta$ 58 .....	437
<b>Figure 318:</b> Stack plot of the $^{13}\text{C}\{^1\text{H}\}$ NMR spectrum (bottom) and the $^{13}\text{C}$ DEPT-135 (top) of $\text{AgC}_6\text{F}_5\text{Sphos}$ <b>124</b> between $\delta$ 23 and $\delta$ 58.....	437
<b>Figure 319:</b> $^{13}\text{C}\{^1\text{H}\}$ (125.8 MHz, $\text{CD}_2\text{Cl}_2$ , 25 °C) spectrum of $\text{AgC}_6\text{F}_5\text{Sphos}$ <b>124</b> between $\delta$ 20 and $\delta$ 40 .....	438
<b>Figure 320:</b> Stack plot of the $^{13}\text{C}\{^1\text{H}\}$ NMR spectrum (bottom) and the $^{13}\text{C}$ DEPT-135 of $\text{AgC}_6\text{F}_5\text{Sphos}$ <b>124</b> between $\delta$ 20 and $\delta$ 40.....	438
<b>Figure 321:</b> HSQC spectrum of $\text{AgC}_6\text{F}_5\text{Sphos}$ <b>124</b> in $\text{CD}_2\text{Cl}_2$ .....	439
<b>Figure 322:</b> HMBC spectrum of $\text{AgC}_6\text{F}_5\text{Sphos}$ <b>124</b> in $\text{CD}_2\text{Cl}_2$ .....	439
<b>Figure 323:</b> Stack plot of <b>124</b> the $^{13}\text{C}\{^1\text{H}\}$ NMR spectrum (top) with the $^{13}\text{C}\{^1\text{H}, ^{19}\text{F}\}$ spectrum with specific $^{19}\text{F}$ coupling of $^{19}\text{F}$ peak (indicated by O3) at $\delta$ -107 (bottom) and $\delta$ - 160 (middle), in $\text{CD}_2\text{Cl}_2$ .....	440
<b>Figure 324:</b> $^1\text{H}$ NMR (500 MHz, $\text{CD}_2\text{Cl}_2$ , 25 °C) spectrum of $\text{Ag}(\text{C}_6\text{F}_5)(\text{BrettPhos})$ <b>125</b> .....	440
<b>Figure 325:</b> $^1\text{H}$ NMR (500 MHz, $\text{CD}_2\text{Cl}_2$ , 25°C) spectrum of $\text{Ag}(\text{C}_6\text{F}_5)(\text{BrettPhos})$ <b>125</b> between $\delta$ 0.5 and $\delta$ 4.0.....	441
<b>Figure 326:</b> $^1\text{H}$ NMR (500 MHz, $\text{CD}_2\text{Cl}_2$ , 25°C) spectrum of $\text{Ag}(\text{C}_6\text{F}_5)(\text{BrettPhos})$ <b>125</b> between $\delta$ 6.6 and $\delta$ 7.3.....	441
<b>Figure 327:</b> $^{31}\text{P}\{^1\text{H}\}$ (202.5 MHz, $\text{CD}_2\text{Cl}_2$ , 25 °C) spectrum of $\text{Ag}(\text{C}_6\text{F}_5)(\text{BrettPhos})$ <b>125</b> .....	442
<b>Figure 328:</b> $^{19}\text{F}\{^1\text{H}\}$ NMR (470.6 MHz, $\text{CD}_2\text{Cl}_2$ , 25 °C) spectrum of $\text{Ag}(\text{C}_6\text{F}_5)(\text{BrettPhos})$ <b>125</b> .....	442
<b>Figure 329:</b> $^{13}\text{C}$ DEPT-135 (125.8 MHz, $\text{CD}_2\text{Cl}_2$ , 25 °C) spectrum of $\text{Ag}(\text{C}_6\text{F}_5)(\text{BrettPhos})$ <b>125</b> .....	443
<b>Figure 330:</b> $^{13}\text{C}\{^1\text{H}\}$ (125.8 MHz, $\text{CD}_2\text{Cl}_2$ , 25 °C) spectrum of $\text{Ag}(\text{C}_6\text{F}_5)(\text{BrettPhos})$ <b>125</b> .....	443
<b>Figure 331:</b> $^{13}\text{C}\{^1\text{H}\}$ (125.8 MHz, $\text{CD}_2\text{Cl}_2$ , 25 °C) spectrum of $\text{Ag}(\text{C}_6\text{F}_5)(\text{BrettPhos})$ <b>125</b> between $\delta$ 20 and $\delta$ 40.....	444

<b>Figure 332:</b> Stack plot of the $^{13}\text{C}\{^1\text{H}\}$ NMR spectrum (bottom) and the $^{13}\text{C}$ DEPT-135 (top) of $\text{Ag}(\text{C}_6\text{F}_5)(\text{BrettPhos})$ <b>125</b> between $\delta$ 20 and $\delta$ 42 .....	444
<b>Figure 333:</b> $^{13}\text{C}\{^1\text{H}\}$ (125.8 MHz, $\text{CD}_2\text{Cl}_2$ , 25 °C) spectrum of $\text{Ag}(\text{C}_6\text{F}_5)(\text{BrettPhos})$ <b>125</b> between $\delta$ 50 and $\delta$ 60 .....	445
<b>Figure 334:</b> $^{13}\text{C}\{^1\text{H}\}$ (125.8 MHz, $\text{CD}_2\text{Cl}_2$ , 25 °C) spectrum of $\text{Ag}(\text{C}_6\text{F}_5)(\text{BrettPhos})$ <b>125</b> between $\delta$ 108 and $\delta$ 170 .....	445
<b>Figure 335:</b> Stack plot of the $^{13}\text{C}\{^1\text{H}\}$ NMR spectrum (bottom) and the $^{13}\text{C}$ DEPT-135 (top) of $\text{Ag}(\text{C}_6\text{F}_5)(\text{BrettPhos})$ <b>125</b> between $\delta$ 100 and $\delta$ 170 .....	446
<b>Figure 336:</b> HSQC spectrum of $\text{Ag}(\text{C}_6\text{F}_5)(\text{BrettPhos})$ <b>125</b> in $\text{CD}_2\text{Cl}_2$ .....	446
<b>Figure 337:</b> HMBC spectrum of $\text{Ag}(\text{C}_6\text{F}_5)(\text{BrettPhos})$ <b>125</b> in $\text{CD}_2\text{Cl}_2$ .....	447
<b>Figure 338:</b> Stack plot of <b>125</b> the $^{13}\text{C}\{^1\text{H}\}$ NMR spectrum (top) with the $^{13}\text{C}\{^1\text{H}, ^{19}\text{F}\}$ spectrum with specific $^{19}\text{F}$ coupling of $^{19}\text{F}$ peak (indicated by O3) at $\delta$ -106 (middle) and $\delta$ -162 (bottom), in $\text{CD}_2\text{Cl}_2$ .....	447
<b>Figure 339:</b> $^1\text{H}$ NMR (500 MHz, $\text{CD}_2\text{Cl}_2$ , 25 °C) spectrum of $\text{Ag}(\text{C}_5\text{F}_4\text{N})(\text{Xphos})$ <b>165</b>	448
<b>Figure 340:</b> $^1\text{H}$ NMR (500 MHz, $\text{CD}_2\text{Cl}_2$ , 25 °C) spectrum of $\text{Ag}(\text{C}_5\text{F}_4\text{N})(\text{Xphos})$ <b>165</b> between $\delta$ 0.5 and $\delta$ 3.0 .....	448
<b>Figure 341:</b> $^1\text{H}$ NMR (500 MHz, $\text{CD}_2\text{Cl}_2$ , 25 °C) spectrum of $\text{Ag}(\text{C}_5\text{F}_4\text{N})(\text{Xphos})$ <b>165</b> between $\delta$ 6.8 and $\delta$ 7.4 .....	449
<b>Figure 342:</b> $^{31}\text{P}\{^1\text{H}\}$ (202.5 MHz, $\text{CD}_2\text{Cl}_2$ , 25 °C) spectrum of $\text{Ag}(\text{C}_5\text{F}_4\text{N})(\text{Xphos})$ <b>165</b> .....	449
<b>Figure 343:</b> $^{19}\text{F}\{^1\text{H}\}$ NMR (470.6 MHz, $\text{CD}_2\text{Cl}_2$ , 25 °C) spectrum of $\text{Ag}(\text{C}_5\text{F}_4\text{N})(\text{Xphos})$ <b>165</b> .....	450
<b>Figure 344:</b> $^{13}\text{C}$ DEPT-135 (125.8 MHz, $\text{CD}_2\text{Cl}_2$ , 25 °C) spectrum of $\text{Ag}(\text{C}_5\text{F}_4\text{N})(\text{Xphos})$ <b>165</b> .....	450
<b>Figure 345:</b> $^{13}\text{C}\{^1\text{H}\}$ (125.8 MHz, $\text{CD}_2\text{Cl}_2$ , 25 °C) spectrum of $\text{Ag}(\text{C}_5\text{F}_4\text{N})(\text{Xphos})$ <b>165</b> .....	451
<b>Figure 346:</b> $^{13}\text{C}\{^1\text{H}\}$ (125.8 MHz, $\text{CD}_2\text{Cl}_2$ , 25 °C) spectrum of $\text{Ag}(\text{C}_5\text{F}_4\text{N})(\text{Xphos})$ <b>165</b> between $\delta$ 20 and $\delta$ 40 .....	451
<b>Figure 347:</b> Stack plot of the $^{13}\text{C}\{^1\text{H}\}$ NMR spectrum (bottom) and the $^{13}\text{C}$ DEPT-135 (top) of $\text{Ag}(\text{C}_5\text{F}_4\text{N})(\text{Xphos})$ <b>165</b> between $\delta$ 19 and $\delta$ 43 .....	452
<b>Figure 348:</b> $^{13}\text{C}\{^1\text{H}\}$ (125.8 MHz, $\text{CD}_2\text{Cl}_2$ , 25 °C) spectrum of $\text{Ag}(\text{C}_5\text{F}_4\text{N})(\text{Xphos})$ <b>165</b> between $\delta$ 120 and $\delta$ 137 .....	452
<b>Figure 349:</b> Stack plot of the $^{13}\text{C}\{^1\text{H}\}$ NMR spectrum (bottom) and the $^{13}\text{C}$ DEPT-135 (top) of $\text{Ag}(\text{C}_5\text{F}_4\text{N})(\text{Xphos})$ <b>165</b> between $\delta$ 120 and $\delta$ 160 .....	453
<b>Figure 350:</b> $^{13}\text{C}\{^1\text{H}\}$ (125.8 MHz, $\text{CD}_2\text{Cl}_2$ , 25 °C) spectrum of $\text{Ag}(\text{C}_5\text{F}_4\text{N})(\text{Xphos})$ <b>165</b> between $\delta$ 138 and $\delta$ 154 .....	453
<b>Figure 351:</b> HSQC spectrum of $\text{Ag}(\text{C}_5\text{F}_4\text{N})(\text{Xphos})$ <b>165</b> in $\text{CD}_2\text{Cl}_2$ .....	454

**Figure 352:** HMBC spectrum of Ag(C<sub>5</sub>F<sub>4</sub>N)(Xphos) **165** in CD<sub>2</sub>Cl<sub>2</sub> ..... 454

## List of Schemes

<b>Scheme 1:</b> The synthesis of poly(3-hexyl)thiophenes using both adapted Suzuki cross-coupling conditions and direct arylation polymerization approaches. <sup>7,8</sup> .....	40
<b>Scheme 2:</b> Example of a ligand-accelerated non-directed C–H functionalisation reaction utilising a highly electron deficient ligand. <sup>26</sup> .....	42
<b>Scheme 3:</b> a) Pd-catalysed direct arylation of 1,3-difluorobenzene <b>12</b> with 4-bromotoluene <b>13</b> to form the C2-substituted biaryl product <b>14</b> . <sup>34</sup> b) Pd-catalysed dehydrogenative cross-coupling of 1,3-difluorobenzene <b>12</b> with benzene <b>15</b> to regioselectivity favour the formation of C2-substituted <b>16</b> . <sup>33</sup> .....	43
<b>Scheme 4:</b> The direct arylation reaction of 4-bromotoluene <b>13</b> using pentafluorobenzene <b>17</b> presented by Fagnou and co-workers. <sup>34</sup> .....	43
<b>Scheme 5:</b> The direct arylation polycondensation reaction of octafluorobiphenyl <b>23</b> with 1,2,4,5-tetrafluorobenzene <b>24</b> to synthesize the polymer PDOF-TP <b>25</b> , which is used as an OLED. <sup>49</sup> .....	45
<b>Scheme 6:</b> The Pd-catalysed direct arylation of polyfluorinated aromatics with aryl iodides, incorporating mild conditions. <sup>35</sup> .....	45
<b>Scheme 7:</b> The proposed catalytic cycle for the Pd-catalysed direct arylation reaction of fluorinated aromatics by Fagnou and co-workers. ....	47
<b>Scheme 8:</b> The Pd-catalysed direct arylation of 4-iodotoluene <b>26</b> with pentafluorobenzene <b>17</b> . <sup>68</sup> .....	49
<b>Scheme 9:</b> The proposed mechanism for the direct arylation of 4-iodotoluene with pentafluorobenzene based on mechanistic and kinetic studies. <sup>68</sup> .....	50
<b>Scheme 10:</b> Reaction of Pd carboxylate complexes with C <sub>6</sub> F <sub>5</sub> H <b>17</b> . Yields determined using <sup>1</sup> H NMR spectroscopy. <sup>68</sup> .....	51
<b>Scheme 11:</b> a) Direct arylation of 2-bromotoluene <b>30</b> with benzene <b>15</b> studied by Tan and Hartwig b) Reaction of Pd carboxylate intermediate <b>33</b> with benzene <b>15</b> . <sup>71</sup> .....	51
<b>Scheme 12:</b> Direct arylation of 2-bromotoluene <b>30</b> with and without 3 mol% of DavePhos <sup>71</sup> .....	52
<b>Scheme 13:</b> The meta-selective Pd-catalysed direct arylation of toluene, incorporating a bulky nitrile (blue) directing group. <sup>10</sup> .....	55
<b>Scheme 14:</b> a) The meta-selective olefination of benzoic acid derivatives using a conformationally flexible nitrile template to access the meta C–H bond. <sup>80</sup> b) Meta-selective olefination of aryl alcohols using a tethered nitrile template. <sup>81</sup> .....	57
<b>Scheme 15:</b> The Pd-catalysed oxidative ortho-selective amination of N-aryl benzamides <b>44</b> , where the amide group acts as a directing group. <sup>82,84</sup> .....	57

<b>Scheme 16:</b> The direct arylation of 4-iodoanisole <b>50</b> with (2-fluorotoluene)Cr(CO) <sub>3</sub> <b>49</b> to investigate the role of Pd and Ag. <sup>85</sup> .....	58
<b>Scheme 17:</b> Catalytic mechanism proposed by Larossa and co-workers based on their kinetic evidence.....	59
<b>Scheme 18:</b> Reaction used to evaluate the effect of Ag and group 1 metal carboxylate and carbonate salts. <sup>74</sup> .....	60
<b>Scheme 19:</b> Reaction of C <sub>6</sub> F <sub>5</sub> H <b>17</b> with AgOPiv to product AgC <sub>6</sub> F <sub>5</sub> <b>55</b> detected by <sup>19</sup> F NMR spectroscopy and compared to an authentic sample of AgC <sub>6</sub> F <sub>5</sub> <b>55</b> .....	60
<b>Scheme 20:</b> The Pd-catalysed direct allylation of fluorobenzene <b>58</b> with allylic pivalates <b>59</b> . <sup>87</sup> .....	61
<b>Scheme 21:</b> Synthesis of monophosphine-ligated AgOPiv <b>62</b> , which are isolated as a pair of rotamers by Hartwig and co-workers. <sup>87</sup> .....	61
<b>Scheme 22:</b> Preparation of monophosphine-ligated Ag-aryl complex, which is the proposed intermediate generated after C–H activation by the monophosphine-coordinated AgOPiv complex. <sup>87</sup> .....	62
<b>Scheme 23:</b> a) The Au/Ag co-catalysed cross dehydrogenative coupling of pyrazoles <b>66</b> and tetra-fluoropyridine <b>67</b> . b) The H/D exchange experiment with C <sub>6</sub> F <sub>5</sub> H <b>17</b> with D <sub>2</sub> O demonstrated the C–H activation capabilities of the AgOAc salt alone. c) The production of AgC <sub>6</sub> F <sub>5</sub> <b>55</b> from the reaction of C <sub>6</sub> F <sub>5</sub> H <b>17</b> with AgOAc in the presence of Cs <sub>2</sub> CO <sub>3</sub> . The AgC <sub>6</sub> F <sub>5</sub> <b>55</b> complex was detected by <sup>19</sup> F NMR spectroscopy.....	63
<b>Scheme 24:</b> The direct-arylation of benzo[ <i>b</i> ]thiophene <b>70</b> with 4-iodotoluene <b>26</b> , where the regioselectivity is determined by the catalyst-loading of Pd. <sup>89</sup> .....	63
<b>Scheme 25:</b> Optimized reaction conditions for the C2-selective direct arylation of benzo[ <i>b</i> ]thiophene which employs low catalytic loading of Pd. <sup>51</sup> .....	64
<b>Scheme 26:</b> Proposed mechanism for the synthesis of the C3 product <b>71</b> <i>via</i> Pathway A and of the C2 product <b>72</b> <i>via</i> Pathway B.....	65
<b>Scheme 27:</b> The synthesis of poly(3-hexylthiophene) <b>2</b> by a direct arylation polymerization reaction incorporating a Pd/Ag dual catalytic system. <sup>8</sup> .....	65
<b>Scheme 28:</b> The reaction of PEPPSI- <i>i</i> Pr <b>73</b> with excess pyridine <b>74</b> heated at 80 °C for 24 h resulted in 74 % of the 3-chloropyridine <b>76</b> being displaced by pyridine <b>74</b> . <sup>8</sup> .....	66
<b>Scheme 29:</b> Proposed mechanism for the synthesis of poly(3-hexylthiophene) <b>2</b> by a direct arylation polymerization reaction, incorporating a Pd/Ag dual catalytic system. <sup>8</sup> .....	67
<b>Scheme 30:</b> The Pd-catalysed direct arylation reaction between 4-bromotoluene <b>13</b> and (2-fluorotoluene)Cr(CO) <sub>3</sub> <b>49</b> in toluene, using AgBr as the co-catalyst. ....	67
<b>Scheme 31:</b> The proposed mechanism for the Pd/Ag co-catalyst system with catalytic amounts of Ag .....	68



<b>Scheme 32:</b> Ag-mediated deuteration of fluorinated aromatics in the presence of D <sub>2</sub> O <sup>93,94</sup>	69
<b>Scheme 33:</b> Direct arylation reaction of 4-iodotoluene <b>26</b> and pentafluorobenzene <b>17</b> studied by Platt <i>et al.</i> <sup>68</sup>	69
<b>Scheme 34:</b> The standard model reaction of the direct arylation of 4-iodotoluene with pentafluorobenzene in DMF at 60 °C.	72
<b>Scheme 35:</b> Synthesis of AgC <sub>6</sub> F <sub>5</sub> <b>55</b> outlined by Sun and Miller. <sup>108</sup>	75
<b>Scheme 36:</b> Reactivity of <b>55</b> examined by Sun and Miller <sup>108</sup> (No yields reported.)	76
<b>Scheme 37:</b> Synthesis of AgC <sub>6</sub> F <sub>5</sub> <b>55</b> outlined by Abad and co-workers. <sup>109</sup>	77
<b>Scheme 38:</b> Synthesis of AgC <sub>6</sub> F <sub>5</sub> <b>55</b> and other methylphenyl derivatives using diarylzinc outlined by Van Der Kerk and co-workers. <sup>110</sup>	78
<b>Scheme 39:</b> Synthesis of AgC <sub>6</sub> F <sub>5</sub> <b>55</b> reported by Villinger and co-workers <sup>112</sup>	78
<b>Scheme 40:</b> Synthesis of AgC <sub>6</sub> F <sub>5</sub> <b>55</b> outlined by Wickleder and co-workers <sup>95</sup>	79
<b>Scheme 41:</b> Reaction of AgC <sub>6</sub> F <sub>5</sub> <b>55</b> with various group 12 – 16 elements <sup>95</sup>	79
<b>Scheme 42:</b> The synthesis of [Ag(PPh <sub>3</sub> ) <sub>2</sub> ](CO <sub>3</sub> )•2H <sub>2</sub> O <b>88</b> outlined by White and co-workers. <sup>121</sup>	82
<b>Scheme 43:</b> The synthesis of [Ag(PPh <sub>3</sub> ) <sub>2</sub> (κ <sup>2</sup> -HCO <sub>3</sub> )] <sub>2</sub> <b>89</b> outlined by White and co-workers. <sup>121</sup>	82
<b>Scheme 44:</b> Synthesis of AgC <sub>6</sub> F <sub>5</sub> <b>55</b> from the reaction of <b>81</b> and AgF in EtCN	84
<b>Scheme 45:</b> The synthesis of an aryl-silver complex from the reaction between Ag <sub>2</sub> CO <sub>3</sub> and PPh <sub>3</sub> with 10 equivalences of C <sub>6</sub> F <sub>5</sub> H <b>17</b> in acetonitrile.	88
<b>Scheme 46:</b> Synthesis of <sup>13</sup> C- labelled The Ag <sub>2</sub> (PPh <sub>3</sub> ) <sub>2</sub> (C <sub>6</sub> F <sub>5</sub> )(μ <sup>2</sup> -H <sup>13</sup> CO <sub>3</sub> ) <b>92</b>	95
<b>Scheme 47:</b> The synthesis of AgC <sub>6</sub> F <sub>5</sub> (PPh <sub>3</sub> ) <sub>n</sub> <b>93</b> from the reaction between AgC <sub>6</sub> F <sub>5</sub> <b>55</b> and PPh <sub>3</sub>	98
<b>Scheme 48:</b> The synthesis of (PPh <sub>3</sub> ) <sub>2</sub> Ag(κ <sup>2</sup> -OAc) <b>94</b> complex from AgOAc and 2 equiv. PPh <sub>3</sub> in toluene.	101
<b>Scheme 49:</b> The synthesis of [Ag(DPPE)(κ <sup>2</sup> -OAc)] <sub>n</sub> <b>95</b> from AgOAc and DPPE in toluene.	101
<b>Scheme 50:</b> Crystals of [Ag(PPh <sub>3</sub> ) <sub>2</sub> HCO <sub>3</sub> ] <sub>2</sub> <b>89</b> isolated from the synthesis of Ag <sub>2</sub> (PPh <sub>3</sub> ) <sub>2</sub> (C <sub>6</sub> F <sub>5</sub> )(μ <sup>2</sup> -HCO <sub>3</sub> ) <b>91</b>	104
<b>Scheme 51:</b> Synthesis of the [Ag(PPh <sub>3</sub> ) <sub>2</sub> (κ <sup>2</sup> -HCO <sub>3</sub> )] <sub>2</sub> <b>89</b> from PPh <sub>3</sub> , AgNO <sub>3</sub> and Na <sub>2</sub> CO <sub>3</sub> in a mixed solvent system of EtOH and H <sub>2</sub> O.	105
<b>Scheme 52:</b> Reaction of Ag <sub>2</sub> CO <sub>3</sub> with 2 equiv. of PPh <sub>3</sub> in DMF at 60°C for 16 h to yield <b>90</b>	108
<b>Scheme 53:</b> The synthesis of the [(PPh <sub>3</sub> ) <sub>2</sub> Ag] <sub>2</sub> (CO <sub>3</sub> ) <b>88</b> from the reaction of Ag <sub>2</sub> CO <sub>3</sub> with 6 equiv. of PPh <sub>3</sub> in CH <sub>3</sub> CN. <sup>121</sup>	110

<b>Scheme 54:</b> The transmetallation and subsequent reductive elimination reaction between <b>91</b> and Pd(PPh <sub>3</sub> ) <sub>2</sub> (I)(R <sup>1</sup> ) where R <sup>1</sup> = H, Me. (Solvent = toluene, dichloromethane).....	112
<b>Scheme 55:</b> The in situ generation of <b>91</b> from <b>17</b> and subsequent reaction of <b>91</b> with <b>98</b> in DMF .....	113
<b>Scheme 56:</b> The in situ generation of AgC <sub>6</sub> F <sub>5</sub> <b>55</b> from the reaction between Ag <sub>2</sub> CO <sub>3</sub> and C <sub>6</sub> F <sub>5</sub> H <b>17</b> , and subsequent reaction with 4-iodotoluene <b>26</b> .....	116
<b>Scheme 57:</b> The reaction between C <sub>6</sub> F <sub>5</sub> H <b>17</b> and 4-Iodotoluene <b>26</b> in the presence of Ag <sub>2</sub> CO <sub>2</sub> and PPh <sub>3</sub> in DMF.....	116
<b>Scheme 58:</b> The reaction between Ag(PPh <sub>3</sub> ) <sub>2</sub> (κ <sup>2</sup> -OAc) and 10 equivalents of C <sub>6</sub> F <sub>5</sub> H in DMF heated to 60 °C .....	117
<b>Scheme 59:</b> Reaction between [Ag(PPh <sub>3</sub> ) <sub>2</sub> (HCO <sub>3</sub> ) <sub>2</sub> ] <b>89</b> with C <sub>6</sub> F <sub>5</sub> H <b>17</b> in DMF .....	118
<b>Scheme 60:</b> Reaction of [Ag(PPh <sub>3</sub> ) <sub>2</sub> (HCO <sub>3</sub> ) <sub>2</sub> ] <b>89</b> with C <sub>6</sub> F <sub>5</sub> H <b>17</b> in the presence of Cs <sub>2</sub> CO <sub>3</sub> (1 equiv.) DMF.....	118
<b>Scheme 61:</b> Reaction between <b>88</b> and 10 equivalents of C <sub>6</sub> F <sub>5</sub> H <b>17</b> in DMF at both 60 °C and room temperature.....	119
<b>Scheme 62:</b> The synthesis and isolation of <b>91</b> from acetonitrile .....	124
<b>Scheme 63:</b> Direct arylation reaction of 4-iodotoluene <b>26</b> with pentafluorobenzene <b>17</b> with catalytic amounts of Ag additives (10 to 1 mol%) and Cs <sub>2</sub> CO <sub>3</sub> (0.75 equiv. as the base)...	127
<b>Scheme 64:</b> Reaction of AgOPiv with <b>61</b> to produce <b>62</b> as a pair of rotamers <sup>87</sup> .....	129
<b>Scheme 65:</b> Preparation of monophosphine-ligated silver-aryl complex, which is the proposed intermediate generated after C–H activation by the monophosphine-coordinated AgOPiv complex <sup>87</sup> .....	130
<b>Scheme 66:</b> Cross-coupling reaction between <b>100</b> and <b>64</b> in toluene at room-temperature <sup>87</sup> .....	130
<b>Scheme 67:</b> Effect of different phosphine ligands on the C–H direct arylation of 4-iodotoluene <b>26</b> with pentafluorobenzene <b>17</b> . <sup>68</sup> .....	131
<b>Scheme 68:</b> Synthesis of Ag(C <sub>6</sub> F <sub>5</sub> )(Xphos) <b>101</b> from the reaction between Xphos, Ag <sub>2</sub> CO <sub>3</sub> and C <sub>6</sub> F <sub>5</sub> H <b>17</b> .....	132
<b>Scheme 69:</b> The synthesis of <b>102</b> from the reaction of <b>103</b> and Xphos and <b>96</b> in cyclohexane at room temperature <sup>127</sup> .....	136
<b>Scheme 70:</b> The stoichiometric reaction between <b>101</b> and <b>102</b> in dichloromethane-d <sub>2</sub> at room temperature .....	138
<b>Scheme 71:</b> The synthesis of <b>105</b> from the reaction between AgI and Xphos in dichloromethane .....	140
<b>Scheme 72:</b> Reaction of a) <b>101</b> with 4-iodotoluene <b>26</b> and b) <b>102</b> with C <sub>6</sub> F <sub>5</sub> H <b>17</b> as control experiments .....	141

<b>Scheme 73:</b> The synthesis of <b>106</b> from the reaction between Xphos and Ag <sub>2</sub> CO <sub>3</sub> in acetonitrile.....	142
<b>Scheme 74:</b> Isolation of Ag carbonate complexes <b>107</b> and <b>108</b> by Hartwig and co-workers. <sup>94</sup> .....	144
<b>Scheme 75:</b> Reaction of <b>106</b> with C <sub>6</sub> F <sub>5</sub> H <b>17</b> at room temperature to produce <b>101</b> .....	145
<b>Scheme 76:</b> Selective deuteration by Ag carbonate complex <b>108</b> demonstrated by Hartwig and co-workers <sup>94</sup> .....	145
<b>Scheme 77:</b> Synthesis of AgOAcXphos complex <b>109</b> from acetonitrile .....	146
<b>Scheme 78:</b> Standard model reaction of the direct arylation of 4-iodotoluene <b>26</b> with pentafluorobenzene <b>17</b> in DMF at 60 °C with Xphos as the ligand.....	148
<b>Scheme 79:</b> Few select examples of the KIE of various reactions involving C–H activation, including a) direct arylation of 4-iodoanisole <b>50</b> with (2-fluorotoluene)Cr(CO) <sub>3</sub> <b>49</b> <sup>128</sup> b) Ag catalysed C–H deuteration <sup>94</sup> c) direct arylation of 4-iodotoluene <b>26</b> with pentafluorobenzene <b>17</b> . <sup>68</sup> .....	152
<b>Scheme 80:</b> Synthesis of deuteropentafluorobenzene <b>69</b> <sup>129</sup> .....	153
<b>Scheme 81:</b> Direct arylation of 4-iodotoluene <b>26</b> (0.085 M) with C <sub>6</sub> F <sub>5</sub> H <b>17</b> /C <sub>6</sub> F <sub>5</sub> D <b>69</b> (0.85 M) in DMF at 60 ° for 3 h.....	153
<b>Scheme 82:</b> Reaction of <b>106</b> with C <sub>6</sub> F <sub>5</sub> H or C <sub>6</sub> F <sub>5</sub> D at room temperature in toluene.....	154
<b>Scheme 83:</b> Reaction conditions used to monitor the kinetic profile and calculate the KIE of the reaction of <b>106</b> with C <sub>6</sub> F <sub>5</sub> H <b>17</b> and C <sub>6</sub> F <sub>5</sub> D <b>69</b> .....	155
<b>Scheme 84:</b> Reaction of <b>105</b> with an excess of C <sub>6</sub> F <sub>5</sub> H <b>17</b> (20 equiv.) and carbonate salts such as Ag <sub>2</sub> CO <sub>3</sub> and K <sub>2</sub> CO <sub>3</sub> , did not result in the formation of the expected product.....	161
<b>Scheme 85:</b> Reaction demonstrating a possible phosphine and Ag recycling mechanism to regenerate <b>101</b> .....	162
<b>Scheme 86:</b> Reaction of AgC <sub>6</sub> F <sub>5</sub> <b>55</b> with Xphos to generate Ag(C <sub>6</sub> F <sub>5</sub> )(Xphos) <b>101</b> .....	163
<b>Scheme 87:</b> Phosphine-exchange analysed by 1D EXSY to reveal parameters consistent with associative exchange .....	174
<b>Scheme 88:</b> Silver carbonate acting as base in CMD mechanism.....	177
<b>Scheme 89:</b> General synthetic methodology for the production of dialkylbiarylphosphines <sup>140,141</sup> .....	179
<b>Scheme 90:</b> plausible general mechanism for the synthesis of dialkylbiarylphosphines	180
<b>Scheme 91:</b> Dearomative rearrangement of the Pd- <sup>1</sup> BuBrettPhos complex <b>118</b> to <b>119</b> <sup>127</sup> .....	181
<b>Scheme 92:</b> Reductive elimination of <b>119</b> with base and subsequent oxidative addition with excess aryl bromide to produce <b>120</b> <sup>127</sup> .....	182
<b>Scheme 93:</b> Synthesis of <b>121</b> from the reaction of <sup>1</sup> BuXphos and Pd <sub>2</sub> (dba) <sub>3</sub> •CHCl <sub>3</sub> by Allgeier and co-workers <sup>145</sup> .....	182

<b>Scheme 94:</b> Effect of dialkyl groups on the dearomative rearrangement <sup>127</sup> .....	183
<b>Scheme 95:</b> Catalytic direct arylation conditions used for the substrate scope of aryl iodides .....	194
<b>Scheme 96:</b> The C–H direct arylation reaction conditions used by a) Platt <i>et al.</i> <sup>68</sup> and b) Zhang and co-workers <sup>35</sup> when performing their respective aryl iodide substrate scopes ....	196
<b>Scheme 97:</b> Direct arylation reaction of chloro-4-iodobenzene <b>135</b> with pentafluorobenzene <b>17</b> in DMF at 60 °C .....	196
<b>Scheme 98:</b> <sup>19</sup> F{ <sup>1</sup> H} NMR (470 MHz, CDCl <sub>3</sub> , 25 °C) spectrum of mixture of a) reaction between chloro-4-iodobenzene <b>135</b> with pentafluorobenzene <b>17</b> , showing the <i>ortho</i> -F resonances of <b>136</b> and <b>137</b> . b) Reaction between bromo-4-iodobenzene with pentafluorobenzene <b>17</b> , showing the overlapping <i>F</i> -resonances of multiple products. ....	197
<b>Scheme 99:</b> The C–H direct arylation reaction conditions used by a) Platt <i>et al.</i> <sup>68</sup> and b) Zhang and co-workers <sup>35</sup> when performing their respective fluoroarene substrate scope ....	202
<b>Scheme 100:</b> Direct arylation reaction of <b>26</b> with <b>12</b> (10 equiv.) outlined by Platt <i>et al.</i> .....	204
<b>Scheme 101:</b> Direct arylation reaction of 4-iodotoluene <b>26</b> with 1,3-difluorobenzene ( <b>12</b> , 10 equiv.) at 80 °C, using Xphos as the ligand. ....	204
<b>Scheme 102:</b> Synthesis of Ag(C <sub>5</sub> F <sub>4</sub> N)(Xphos) <b>165</b> .....	205
<b>Scheme 103:</b> Summary of key reactions from chapter 2, where PPh <sub>3</sub> was used as the ligand .....	209
<b>Scheme 104:</b> Proposed mechanism incorporating both Pd and Ag as co-catalysts.....	210
<b>Scheme 105:</b> reaction of <b>106</b> with 1,2-difluorobenzene <b>12</b> depicting the formation of various regioisomers .....	212
<b>Scheme 106:</b> Hypothesised effect of <sup>n</sup> Bu <sub>4</sub> NI on the direct arylation reaction with chloroarene .....	214
<b>Scheme 107:</b> Use of Ag <sub>2</sub> CO <sub>3</sub> in the deuteration reactions by a) Hartwig and co-workers <sup>94</sup> and b) Haung and co-workers. <sup>93</sup> .....	214
<b>Scheme 108:</b> Examples of a) Pd-catalysed decarboxylative Heck-type reaction <sup>152</sup> , b) Pd-catalysed decarboxylative heterocoupling between aryl carboxylic acids <sup>155</sup> .....	215
<b>Scheme 109:</b> Examples of silver-catalysed a) homocoupling reaction of (hetero)aryl/alkyl alkynes <sup>162</sup> b) ligand-free carboxylation reaction of aryl/alkyl terminal alkynes with CO <sub>2</sub> . <sup>163</sup> .....	215
<b>Scheme 110:</b> Proposed mechanism of Ag catalysed carboxylation reactions by Lu and co-workers using DFT studies <sup>160</sup> .....	216
<b>Scheme 111:</b> a) Pd/Ag catalysed synthesis of enynes b) reaction of AgOTf with an alkyne and DIPEA and chemical shift (δ) to the reaction intermediates detected by <sup>109</sup> Ag NMR spectroscopy in DMF- <i>d</i> <sub>7</sub> and C <sub>6</sub> D <sub>6</sub> . <sup>159</sup> .....	216

## Acknowledgements

First and foremost, I would like to thank my two wonderful supervisors, Robin Perutz and Ian Fairlamb. Their unwavering support through thick and thin was paramount in helping me grow as both a chemist and a person. This project was carried out during the daunting time of COVID-19 and endless cycles of lockdowns. Thus, I am especially grateful for how patient and kind they were in providing both emotional and academic support during these unprecedented times. I really appreciate Robin for taking the time to provide detailed explanations for my million and one questions, which helped shape my understanding of inorganic and organometallic chemistry. Also, Ian's insights and thorough understanding of Pd reactivity and organic chemistry were unparalleled and critical for this project. Overall, I am grateful to my supervisors for constantly finding new ways to challenge my understanding of chemistry and making these three years a unique adventure.

This project would not have been possible without the financial support provided by my parents and the Wild Fund Scholarship (Dr. Tony Wild), for which I am immensely grateful.

During my time at York, I had the pleasure of being a part of the Fairlamb and Perutz groups who were an infinite source of knowledge, support, and humour. Morning coffee, group meetings and pub adventures provided numerous opportunities to discuss new theories, examine data and talk about chemistry in a relaxed and friendly manner. I would also like to thank them for enthusiastically humouring all my weird comics and drawings, bad jokes, and terrible Star Wars references.

I would especially like to thank Anders Hammarbäck and Neil Scott for being two major pillars of support during my humble beginnings as a PhD student. Anders really challenged and shaped the way I designed experiments, engaged with the literature, and my work ethic within the lab. Meanwhile Neil was a ray of positivity who also had the misfortune of being my mentor at York. He patiently suffered through my constant complaints about trivial life problems while providing thoughtful insights about chemistry and life. These two people were pivotal in shaping my approach and standard for everyday lab work.

While by no means an exhaustive list, I would like to thank these notable people for brightening my time in lab:

- Neda Jeddi – My partner-in-crime for NMR tomfoolery and providing solidarity by looking just as stressed as I felt every day.
- Jonny Eastwood – For gloating about the superiority of using balloons over Schlenk lines for air-sensitive chemistry and stress-chugging endless cups of coffee with me.
- James Firth – For patting me on the back while I cried over organic reactions and simple manual column chromatography.

- Tom Burden – For patting me on the back while I cried over simple Grignard reactions, TLC analysis and automated column chromatography.
- David Husbands – For his scathing sense of humour, brutally correcting my grammar and crying over the horrors of Schlenk and glovebox chemistry with me.
- George Clarke – For brightening the day with his hilarious anecdotes and facts.

I would especially like to thank Heather Fish and Alex Heyam (NMR) for all their patient and kind technical guidance with NMR instrumentation. Without them, half the weird and wild NMR shenanigans in this thesis would not have been possible. I would also extend my gratitude towards Adrian Whitwood and Theo Tanner (XRD) for all the XRD wizardry, and Karl Heaton (MS) for humouring all my annoying air- and light-sensitive LIFDI samples. I would also like to thank Charlotte Lee for always helping me fix my Schlenk line with infinite patience and ensuring the entire lab ran smoothly.

I would also like to acknowledge my friends from Canada: Alex, Dylan, Jonathan, Chae and Jasmyne. They may live an ocean away but still managed to be ever-present when I needed a sympathetic ear. I am grateful for the fountain of hilarious memes, Book Club events and encouragement they have provided. I can never thank my parents Athavan Rajendran and Nigithra Athavan enough for always encouraging me to follow my dreams!

Finally, I would like to thank all the cups of coffee I consumed in the past three years for providing the concentrated dose of caffeine I needed to survive my life as a frazzled insomniac.

## Declaration

The work presented in this thesis is my own original work, except where referenced or clearly indicated in the body of text. This work has not been previously presented for an award at this, or any other, University. The work was carried out at the University of York between October 2018 and May 2022.

Part of this work has been reproduced in a published peer-reviewed journal, a copy of which can be found in Appendix A:

Athavan, G.; Tanner, T.F.N.; Whitwood, A.C; Fairlamb, I.J.S; Perutz, R. N; Direct Evidence for Competitive C–H Activation by a Well-Defined Silver Xphos Complex in Palladium-Catalyzed C–H Functionalization. *Organometallics*, **2022**, XX, XX–XX

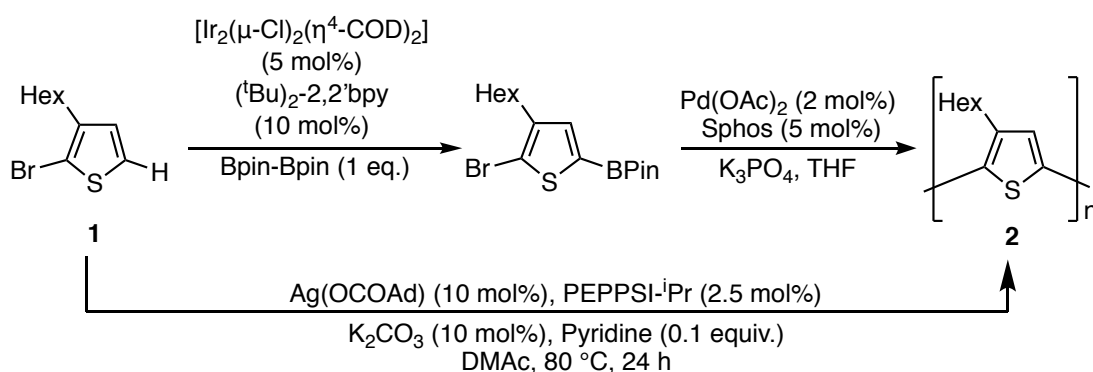
Gayathri Athavan

May 2022

## Chapter 1: Introduction

### 1.1 Pd-Catalysed C–H Functionalisation Reactions

Pd-catalysed C–H direct functionalization reactions are powerful synthetic transformations as they allow for the construction of complex compounds by activating and functionalizing relatively inert C–H bonds.<sup>1–3</sup> By design, the reactions bypass the need for a pre-functionalized organometallic coupling partner, which is often required in Pd-catalysed cross-coupling reactions.<sup>4</sup> In general, it is considered to be a more atom economic and cost-efficient alternative to traditional cross-coupling reactions, with less metal waste.<sup>5,6</sup> For example, the synthesis of poly(3-hexyl)thiophene **1** *via* Pd-catalysed direct arylation does not require the C4 position to be pre-functionalized with a metal (**Scheme 1**).<sup>7,8</sup>



**Scheme 1:** The synthesis of poly(3-hexyl)thiophenes using both adapted Suzuki cross-coupling conditions and direct arylation polymerization approaches.<sup>7,8</sup>

The primary limitation of C–H direct functionalisation reactions is regioselective control of the C–H bond cleavage process. To overcome this challenge, there are two approaches: chelated-assisted and non-chelated assisted C–H functionalisation reactions. These reactions are also referred to as directed and undirected C–H functionalisation reactions (**Figure 1**).<sup>9</sup>

Chelate-assisted C–H functionalisation reactions utilise metal-coordinating functional groups incorporated within the substrate to act as directing groups (DG). The DGs makes use of heteroatoms, such as nitrogen, sulfur, phosphorus and oxygen, to coordinate with and direct the metal centre toward the appropriate C–H bond for functionalisation (**Figure 2**). Thus, methodologies using DGs are most frequently *ortho*-selective, however examples of *meta*-<sup>10,11</sup> and *para*-<sup>12</sup> selective methods have been reported.<sup>13–15</sup> The chief limitation with DG is the requirement to install and later remove the DG from the substrate after C–H functionalisation. Nevertheless, recent strategies with traceless directing group (*i.e.* C–H functionalisation and removal of DG occurs in an one-pot protocol) have helped address this limitation.<sup>13</sup> The use



of heteroatoms poses another problem with DG as often the coordination of the heteroatoms to the catalyst could potentially result in catalyst poisoning.<sup>15</sup>

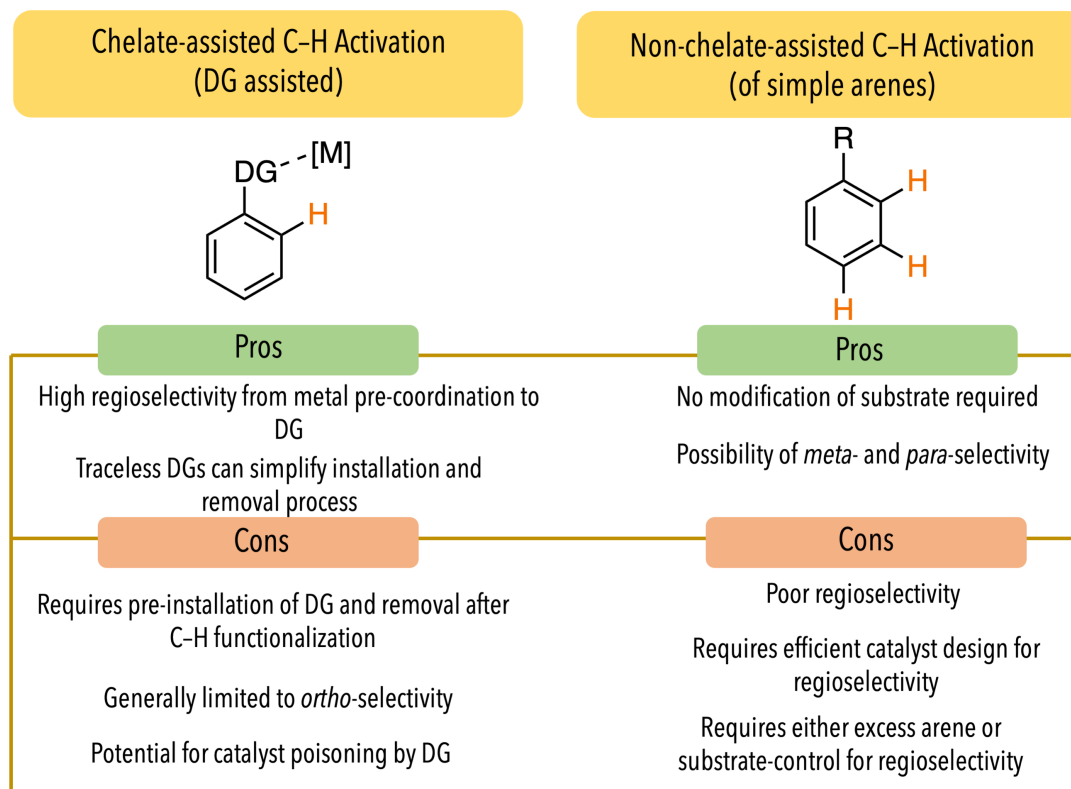


**Figure 1:** Comparison of chelate- and non-chelate-assisted C–H functionalisation strategies.

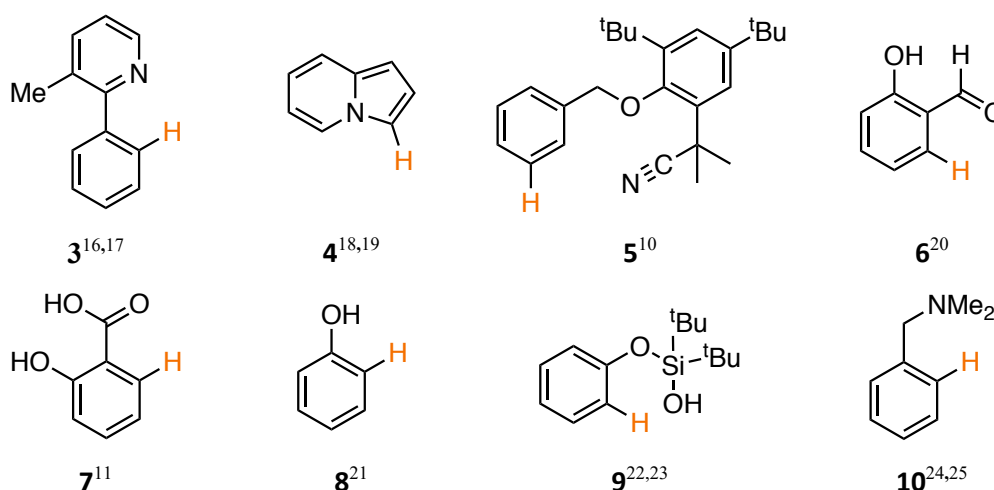
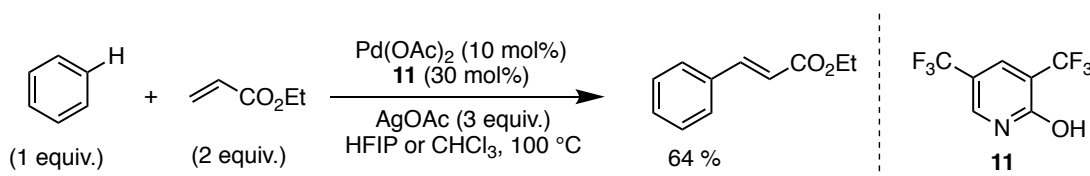


**Figure 2:** Examples of commonly used *ortho*- and *meta*-selective directing groups used in Pd-catalysed C–H bond functionalization reactions. The functionalised C–H bonds are highlighted in orange.

In contrast, non-chelate assisted C–H functionalisation protocols avoid the use of DG, by instead relying on substrate- or catalyst-controlled regioselectivity. When examples of these reactions are known they often require high catalyst loadings, and/or efficient catalyst and ligand design for regioselectivity (**Scheme 2**).<sup>26,27</sup> In the absence of catalyst-controlled regioselectivity, substrate controlled regioselectivity or an excess of substrate are used.<sup>9</sup>



**Scheme 2:** Example of a ligand-accelerated non-directed C–H functionalisation reaction utilising a highly electron deficient ligand.<sup>26</sup>

A class of compounds which employ substrate-controlled regioselectivity are polyfluorinated aromatics. The presence of fluorines in the aromatic ring imposes a form of substrate-controlled regioselectivity where, instead of a DG, the electronic and steric properties of the substrate controls regioselectivity. This effect is referred to as *ortho*-fluorine effect. The C–H bond *ortho*- to or in-between two F atoms is favoured as the site of C–H functionalisation.<sup>28–30</sup> This is best illustrated by the coupling of 1,3-difluorobenzene **12** and 4-bromotoluene **13** and benzene **15** (**Scheme 3**). 1,3-Difluorobenzene **12** offers three potential sites for C–H functionalisation (**Figure 3**), and both experimental competition experiments and DFT studies have shown that the C–H bond in the C2 position is favoured over the C4 position.<sup>31–33</sup> The direct arylation reaction of **12** and **13** selectively produces the C2-product **14** in 85% yield after purification.<sup>34</sup> Similarly, the dehydrogenative cross-coupling of **12** with benzene **15**, affords the C2-product **16** over the C4 product.

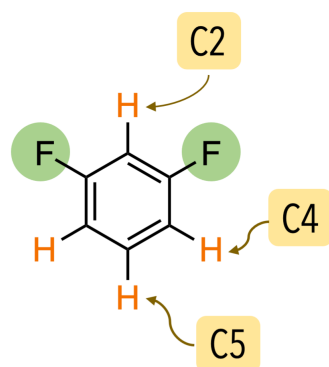
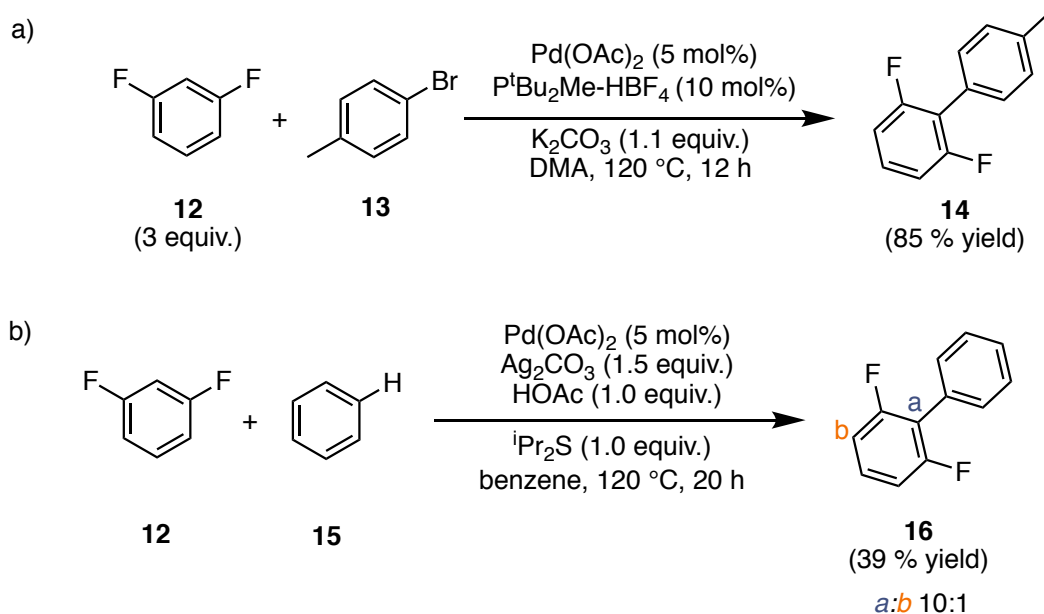


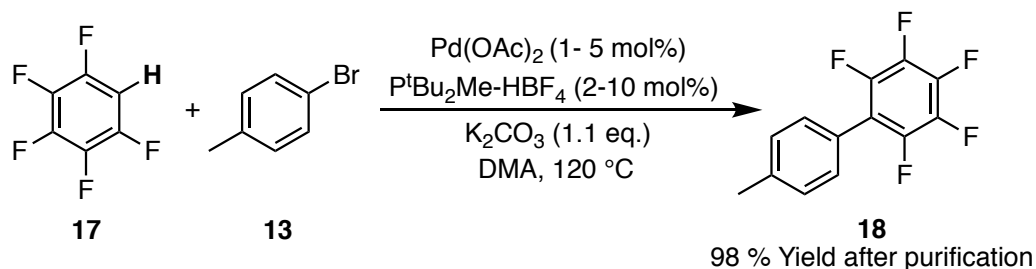
**Figure 3:** Potential positions for C–H functionalisation in 1,3-difluorobenzene **12**



**Scheme 3:** a) Pd-catalysed direct arylation of 1,3-difluorobenzene **12** with 4-bromotoluene **13** to form the C2-substituted biaryl product **14**.<sup>34</sup> b) Pd-catalysed dehydrogenative cross-coupling of 1,3-difluorobenzene **12** with benzene **15** to regioselectivity favour the formation of C2-substituted **16**.<sup>33</sup>

## 1.2 Pd-Catalysed C–H Direct Arylation Reactions of Fluoroarenes

While Pd-catalysed direct arylation has found a wide range of applications, it has become especially prominent in the synthesis of electron-deficient aromatic systems.<sup>35–38</sup> In 2006, Fagnou and co-workers published their finding on one of the first examples of the Pd-catalysed direct arylation of fluorinated aromatics, in the following reaction (**Scheme 4**).<sup>34</sup> Prior to this publication, the most widely used direct arylation reaction was electrophilic aromatic substitution which heavily restricted the substrate scope to highly nucleophilic arenes rendering most electron-deficient aromatics inaccessible.<sup>34</sup>



**Scheme 4:** The direct arylation reaction of 4-bromotoluene **13** using pentafluorobenzene **17** presented by Fagnou and co-workers.<sup>34</sup>

The incorporation of fluorine or fluorinated analogues of common functional groups in synthetic molecules is highly relevant in the pharmaceutical,<sup>39,40</sup> agricultural<sup>41–43</sup> and biological applications<sup>44,45</sup> (**Figure 4**). The inclusion of fluorine often dramatically alters the binding affinity, pharmacokinetic properties and biological activity of natural products and drug candidates. For example, the lipophilicity of a drug candidate can often be altered by the inclusion of fluorine containing groups such as  $-\text{CF}_3$ ,  $-\text{S}-\text{CF}_3$  or  $\text{O}-\text{CF}_3$ .<sup>40</sup>

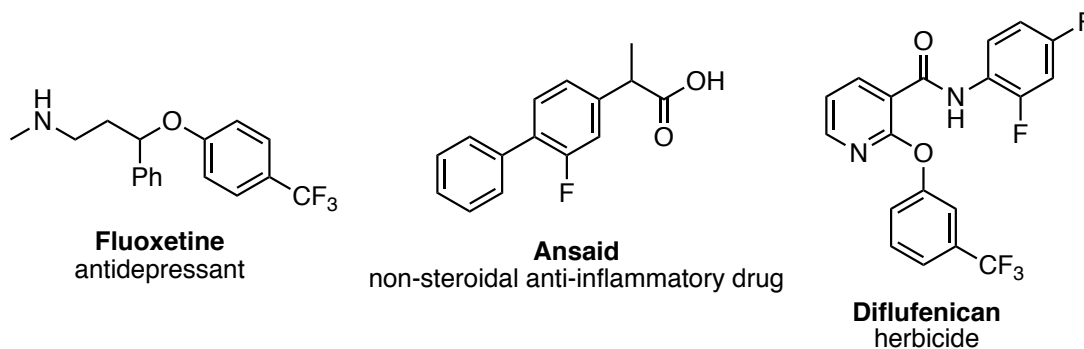


**Figure 4:** Examples of fluorine-containing pharmaceutical and agricultural molecules.

The small size and high electronegativity of fluorine also allows for unique electrostatic interactions which can lead to significant chemical and structural changes. One study in 2019, found that the substitution of phenyl **19** with tetrafluoropyridine **20** and methyl **21** with trifluoromethyl **22** in peptoid monomers (**Figure 5**) allowed for greater control of the *cis/trans* conformer and structure of the resulting peptoid chain. The inclusion of fluorine generated highly electron-deficient systems which favoured stronger  $n \rightarrow \pi^*_{\text{Ar}}$  delocalisation allowing for this unique steric control.<sup>46</sup>

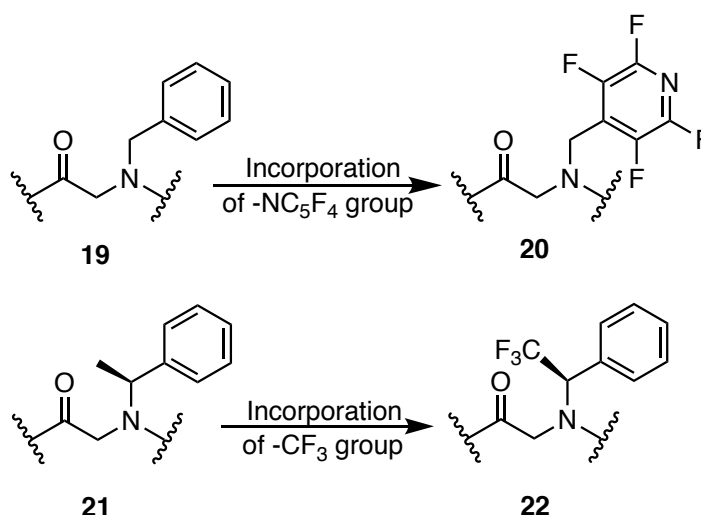
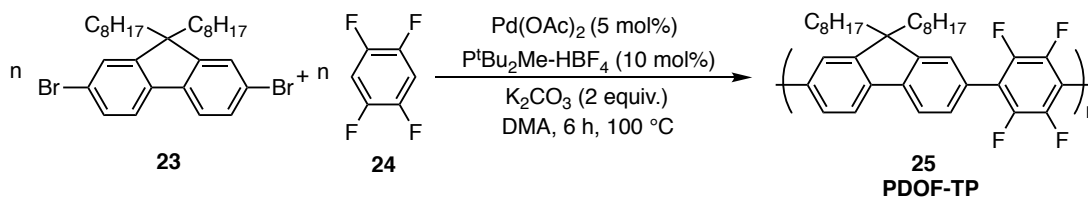


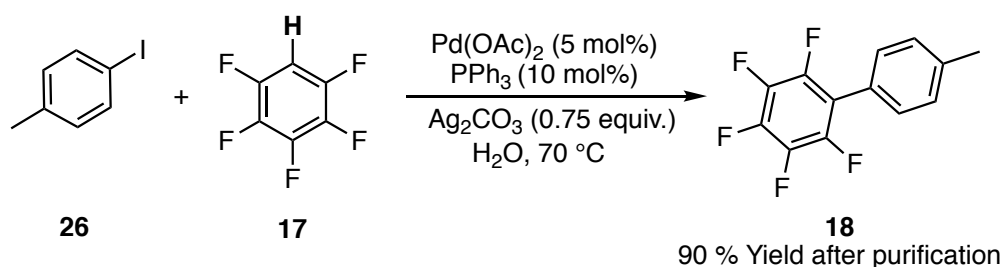
**Figure 5:** The substitution of hydrogens for fluorine in peptoids has been found to be beneficial in controlling the *cis/trans* conformation of the resulting peptoid chain, without the use of chiral monomers.

Similarly, fluorine-containing molecules are ubiquitous in the field of polymerization and materials science.<sup>47,48</sup> The strong electron-withdrawing nature and electron density of fluorine is known to lower the energy of orbitals thereby allowing precise control of the HOMO and LUMO orbitals in the design of organic semi-conductors, photovoltaics, and OLEDs.<sup>47</sup> Thus, direct arylation polycondensation reactions, have become a routine, atom-economic way of synthesizing conjugated polymers which are integral in the production of OLEDs, organic photovoltaic and other materials (**Scheme 5**).<sup>49,5</sup>



**Scheme 5:** The direct arylation polycondensation reaction of octafluorobiphenyl **23** with 1,2,4,5-tetrafluorobenzene **24** to synthesize the polymer PDOF-TP **25**, which is used as an OLED.<sup>49</sup>

Thus, the Pd-catalysed C–H direct arylation reaction has gained significant academic and industrial interest, as it provides a relatively mild and atom-economic synthetic methodology.<sup>6</sup> As a result, the reaction conditions have been highly optimized since the initial publication by Fagnou and co-workers. For example, Zhang and co-workers demonstrated that direct arylation reactions can be performed under aqueous conditions, enabled by cheap, commercially available PPh<sub>3</sub> and Ag<sub>2</sub>CO<sub>3</sub> (**Scheme 6**).<sup>35</sup>



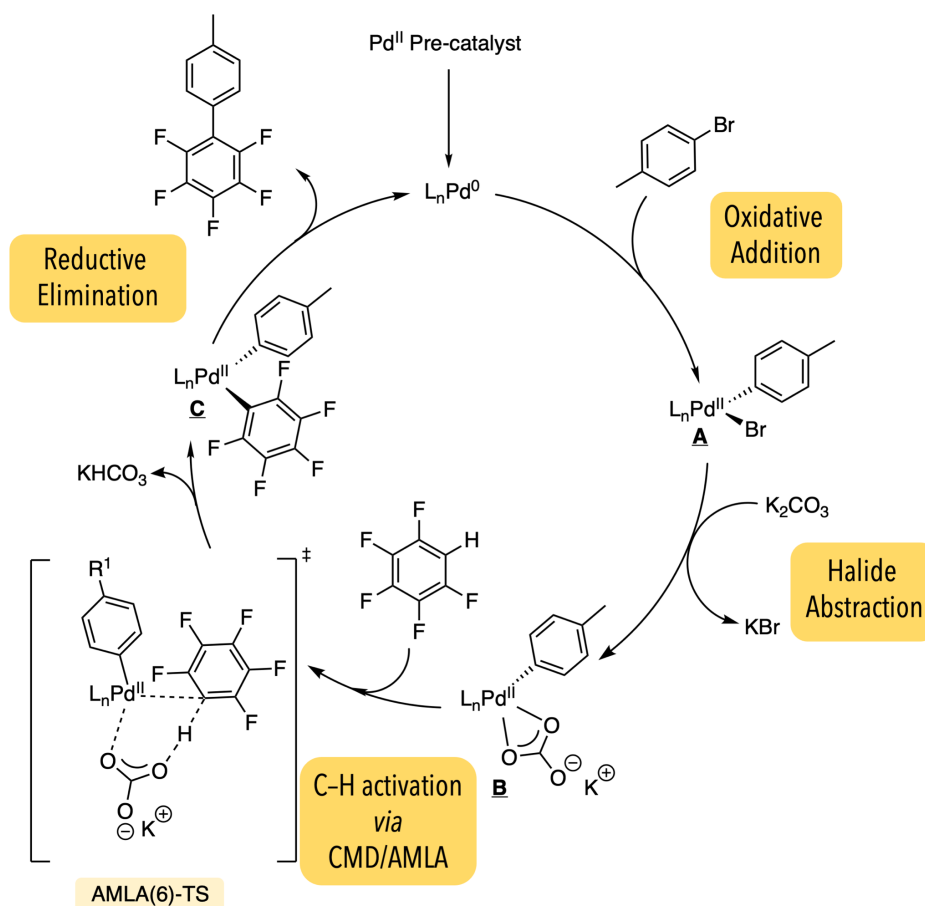
**Scheme 6:** The Pd-catalysed direct arylation of polyfluorinated aromatics with aryl iodides, incorporating mild conditions.<sup>35</sup>

## 1.3 Proposed Mechanism of Pd-Catalysed Direct Arylation Reactions

C–H direct arylation reactions provide insight into the activation and functionalization of relatively inert C–H bonds and have been the subject of numerous mechanistic investigations. Over the years, a number of reaction mechanisms have been proposed, such as oxidative C–H insertion,<sup>50</sup> Heck-like mechanism,<sup>51</sup> electrophilic aromatic substitution<sup>52,53</sup> and concerted metalation deprotonation (CMD) which is also known as 6-membered ambiphilic metal-ligand activation AMLA(6).<sup>54</sup> The general consensus has favoured an electrophilic aromatic substitution ( $S_{EAr}$ ) for electron rich,  $\pi$ -nucleophilic aromatic systems and the AMLA mechanism is thought to be active for electron-deficient aromatics.<sup>53,55–58</sup> However, examples of the AMLA mechanism being operative in electron-rich arene systems also exist.<sup>54</sup>

Fagnou and co-workers, in their 2006 publication, showed that the direct arylation of polyfluorinated aromatics takes place *via* AMLA, and proposed the mechanism in **Scheme 7**. The direct arylation reaction of polyfluorinated aromatics occurred preferentially with more electron-deficient aromatics, which is an inversion of the reactivity observed with electrophilic aromatic substitution reactions. The reaction displayed a primary kinetic isotope effect with a KIE of 3.0, indicating that the C–H bond cleavage is the rate-limiting step. During their investigation, mechanisms of oxidative addition of the C–H bond to the Pd centre, and the  $S_{EAr}$  mechanism were also considered. However the computational models did not support these mechanisms (**Scheme 5**).<sup>34</sup>

Activation of the Pd<sup>II</sup> pre-catalyst generates the catalytically active Pd<sup>0</sup> species which undergoes oxidative addition with the aryl halide to generate species (**A**). Species (**A**) then undergoes ligand exchange with the carbonate or carboxylate-type base such as K<sub>2</sub>CO<sub>3</sub>, resulting in the production of a  $\kappa^2$ -CO<sub>3</sub> coordinated Pd species (**B**). The carbonate-ligand coordinated to species (**B**) enables it to activate the most acidic C–H bond of the polyfluorinated arene *via* the AMLA(6) mechanism to generate bis(aryl)-Pd species (**C**) and releases a hydrogen-carbonate as a by-product. Species (**C**) then undergoes reductive elimination to yield the product and regenerate the Pd<sup>0</sup> species.<sup>34</sup>



**Scheme 7:** The proposed catalytic cycle for the Pd-catalysed direct arylation reaction of fluorinated aromatics by Fagnou and co-workers.

The key step is the C–H bond activation of the electron deficient arene, which was shown to proceed *via* AMLA(6)-TS. AMLA is a concerted mechanism where the acidic C–H of the polyfluorinated substrate is deprotonated by the  $\kappa^1$ -carboxylate Pd<sup>II</sup> centre, while the resulting carbanion is stabilized by and eventually forms a bond with the Pd centre.<sup>54</sup> A H–bonding interaction between the C–H of the substrate and un-coordinated oxygen of the  $\kappa^1$ -OAc, results in an agostic interaction which polarises the C–H bond. This allows the acetate ligand to cleave the C–H with relative ease. Thus, AMLA relies on the synergy between a strong H-bond interaction which facilitates an agostic interaction that allows for the proton transfer from the substrate to acetate ligand.<sup>59,60</sup> The AMLA mechanism proceeds *via* a cyclic transition state, with no change in oxidation state, and the number of atoms present in this transition state is often denoted with brackets, following the term AMLA(*n*) (*n* is typically 4 or 6).<sup>54</sup> An example of an AMLA(4) and AMLA(6)-TS for the C–H activation by an Ir complex is shown in **Figure 7**. This mechanism has also been referred to as Internal Electrophilic Substitution (IES)<sup>61,62</sup> and CMD<sup>63,64</sup>, and has been found to be operative with a range of different ligands and other transition metals such as Ru<sup>64,65</sup> and Ir<sup>59,66</sup>.<sup>54,67</sup>

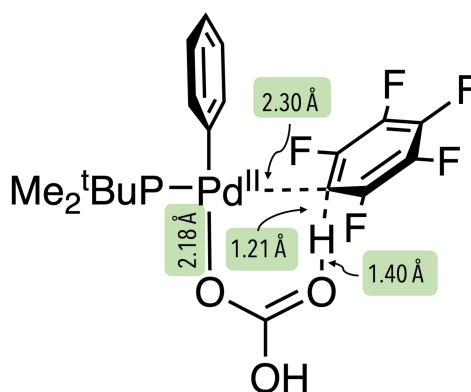


**Figure 6:** AMLA-(6) transition state for C–H activation of  $C_6F_5H$  **17** computed by Fagnou *et al.*<sup>34</sup>

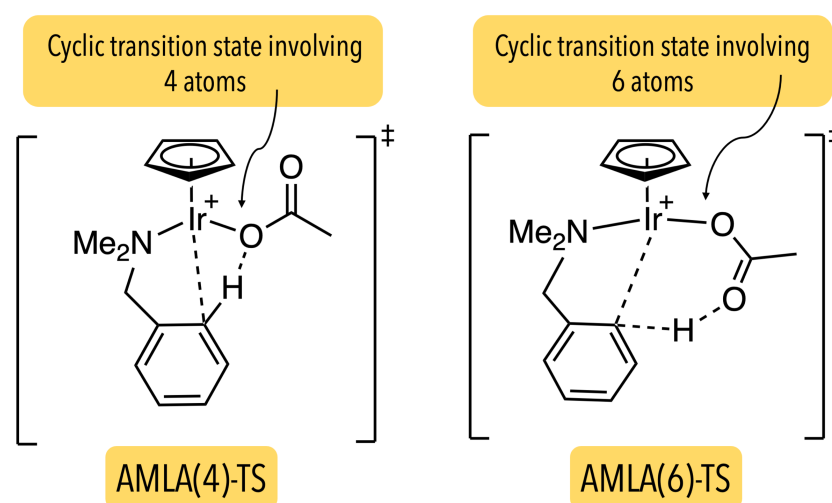
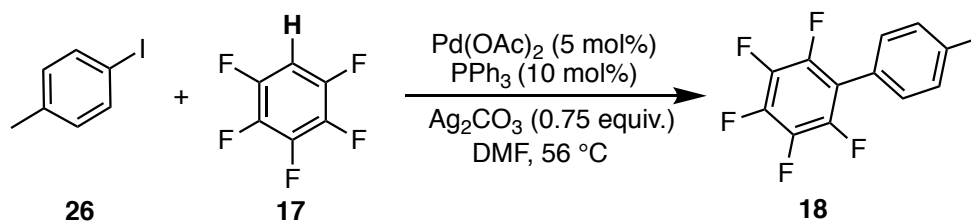


**Figure 7:** Example of a computationally-generated AMLA(4) and AMLA(6)-TS for Ir complex<sup>59,66</sup>

Following the work of Fagnou<sup>34</sup> and Zhang,<sup>35</sup> work in York by Platt *et al.* attempted to rigorously elucidate the mechanism of Pd-catalysed direct arylation reactions of polyfluorinated aromatics using the reaction conditions outlined by Zhang and co-workers. The direct arylation of 4-iodotoluene **26** (1 equiv.) and pentafluorobenzene **17** (1.5 equiv.), involves using 5 mol%  $Pd(OAc)_2$  as the precatalyst with 10 mol% of  $PPh_3$  as the ligand and 0.75 equiv. of  $Ag_2CO_3$  as the base. The reaction was carried out in DMF at 56 or 60 °C (**Scheme 8**). The primary challenge when analysing systems incorporating Ag carbonate and carboxylates arises from the poor solubility of these salts. Hence, to overcome this challenge, the following reaction was specifically tailored to be monitored using *in situ* FT-IR spectroscopic analysis.<sup>68</sup>

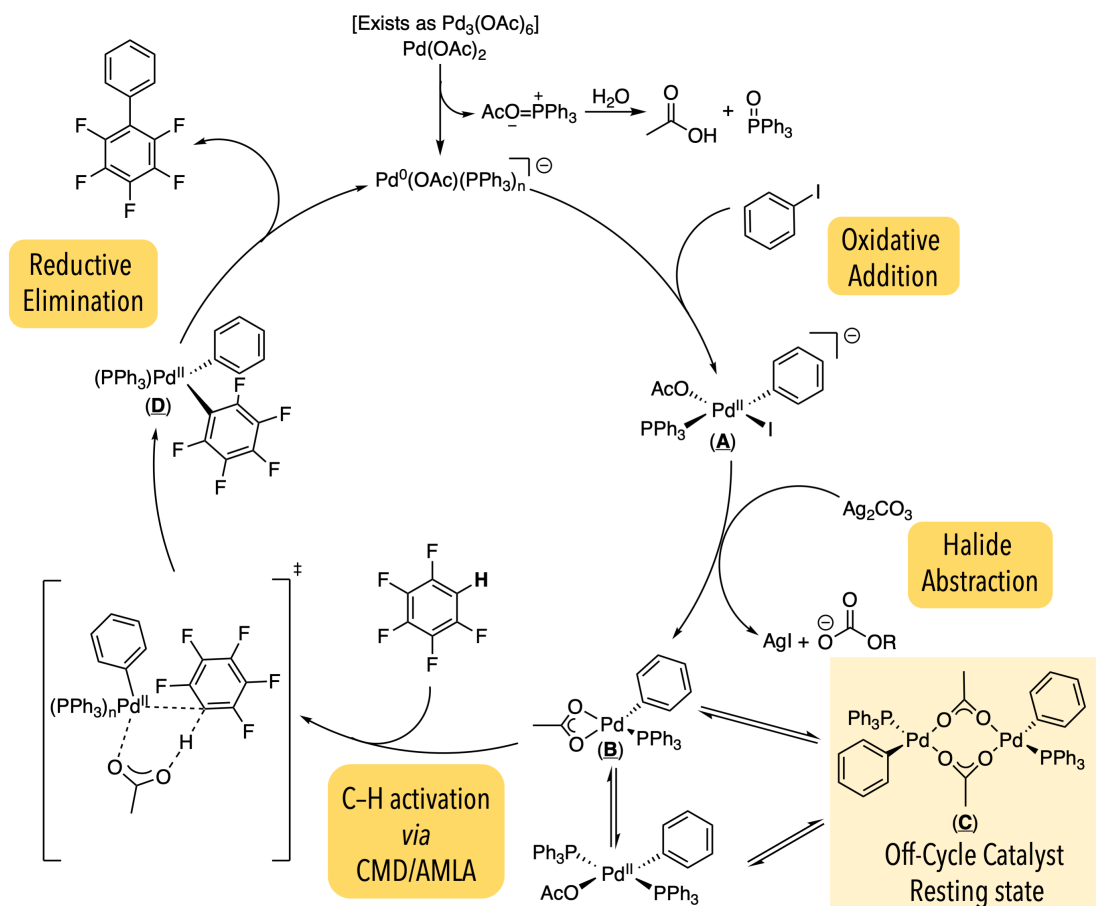




**Scheme 8:** The Pd-catalysed direct arylation of 4-iodotoluene **26** with pentafluorobenzene **17**<sup>68</sup>

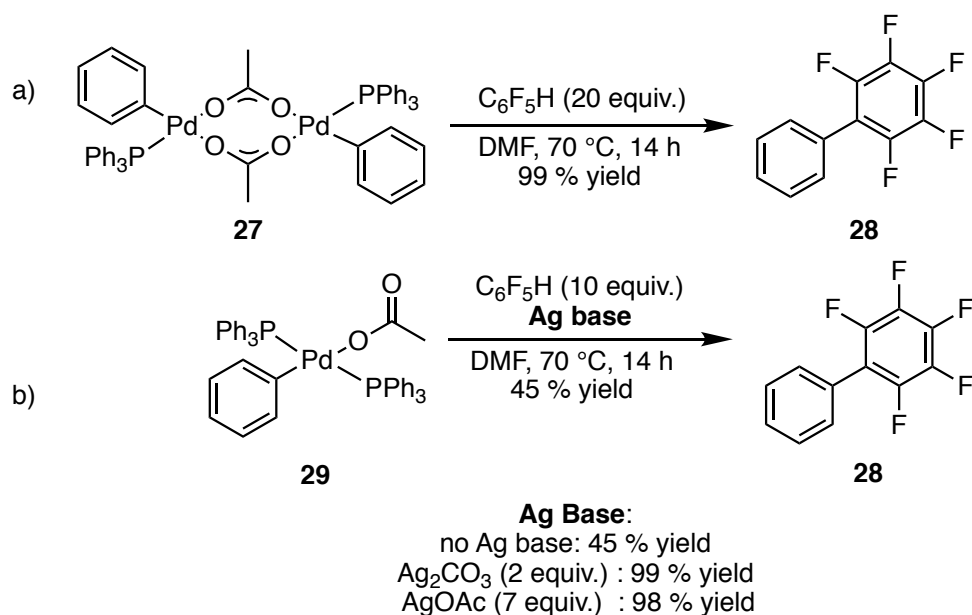
The substrates and products have observable infrared spectra bands in DMF, hence making *in situ* FT-IR spectroscopy an ideal technique for reaction monitoring. Using reaction progress kinetic analysis (RPKA<sup>69</sup>) and variable-time normalized analysis (VTNA<sup>70</sup>), in conjunction with isolated reaction intermediates and *ex situ* ESI(±)-MS and LIFDI-MS studies on reaction aliquots, Platt *et al.* were able to thoroughly examine several steps of the reaction mechanism and proposed for the following reaction mechanism (**Scheme 9**).<sup>68</sup>

The proposed mechanism closely followed Fagnou and co-worker's initial proposal (**Scheme 7**). After pre-catalyst activation, the active catalytic species undergoes oxidative addition to generate (**A**). The stoichiometric reaction between complex (**A**) with silver carbonate resulted in halide abstraction and detection of (**B**) by <sup>1</sup>H and <sup>31</sup>P{<sup>1</sup>H} NMR spectroscopic analysis and LIFDI-MS, and the precipitation of solid silver(I) iodide. A dinuclear Pd<sup>II</sup> species (**C**) was found to be the catalyst resting state, which is consistent with the measured 0.5 order with respect to Pd. Species (**C**) was found to be in equilibrium with the mononuclear species (**B**). The pentafluorobenzene reacts with (**B**) to generate (**D**) which undergoes reductive elimination to yield the organic product, with concomitant regeneration of the active catalytic species. The reaction displayed a primary KIE which suggested that the C–H bond cleavage is the rate-determining state; kinetic activation parameters suggested that an AMLA(6) mechanism is operative.<sup>68</sup>



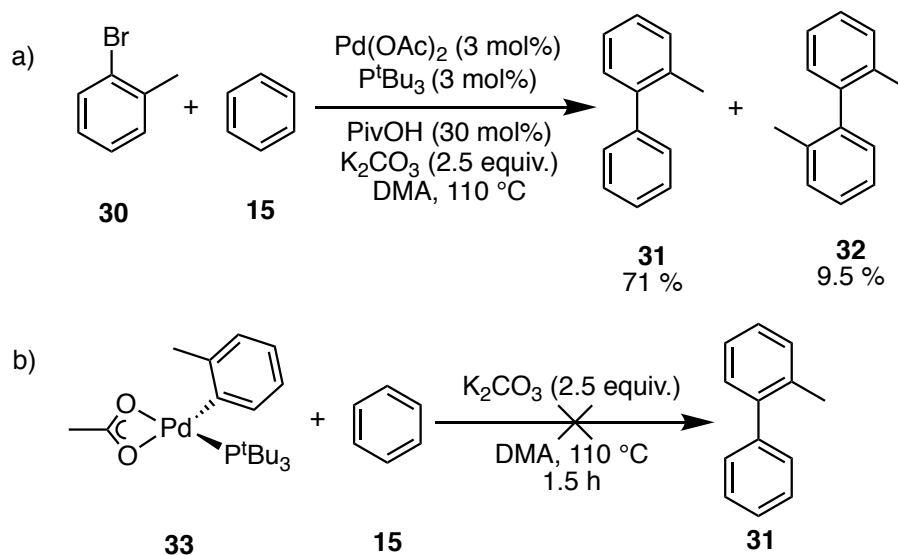
**Scheme 9:** The proposed mechanism for the direct arylation of 4-iodotoluene with pentafluorobenzene based on mechanistic and kinetic studies.<sup>68</sup>

$\text{Pd}^{\text{II}}$ -carboxylate complexes have been shown to be capable of C–H bond activation, both computationally<sup>54</sup> and experimentally<sup>68</sup>. Platt *et al.* were able to react the dimeric  $[\text{Pd}(\text{Ph})(\mu\text{-OAc})(\text{PPh}_3)_2]$  **27** with pentafluorobenzene **17** (20 equiv.) which led to quantitative production of organic product, when heated at 70 °C in DMF for 14 h (**Scheme 10a**). In comparison, the monomeric  $\text{Pd}(\text{Ph})(\kappa^1\text{-OAc})(\text{PPh}_3)_2$  **29** reacted much more sluggishly, with only a 45 % yield of **28**. However, the addition of either  $\text{Ag}_2\text{CO}_3$  or  $\text{AgOAc}$ , vastly improved yields of cross-coupled product (**Scheme 10b**).<sup>68</sup>



**Scheme 10:** Reaction of Pd carboxylate complexes with C<sub>6</sub>F<sub>5</sub>H **17**. Yields determined using <sup>1</sup>H NMR spectroscopy.<sup>68</sup>

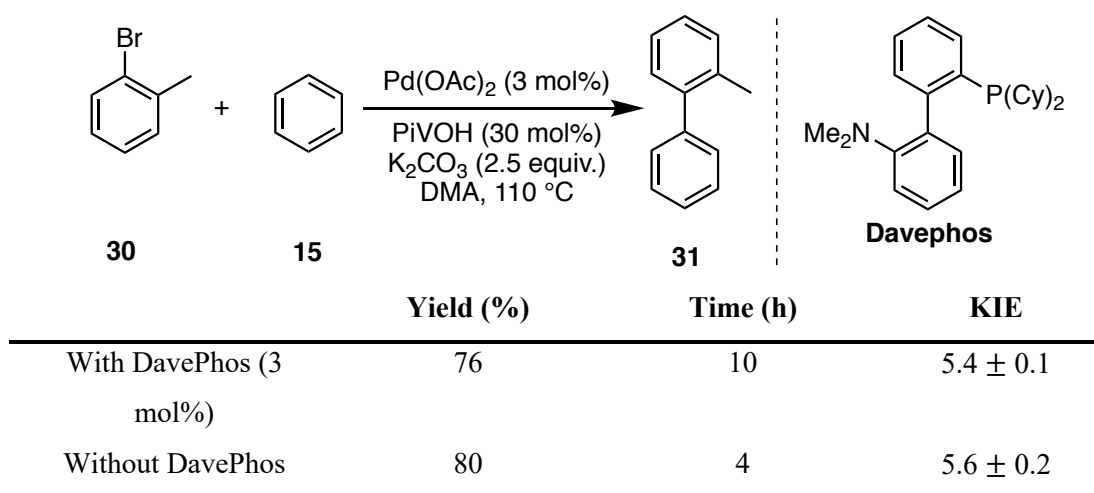
Other mechanisms of C–H activation by Pd have also been identified. When studying the direct arylation of 2-bromotoluene **30** with benzene **15**, Tan and Hartwig found that the expected Pd carboxylate intermediate **33** alone was incapable of C–H bond functionalisation of benzene **15** (Scheme 11).<sup>71</sup>



**Scheme 11:** a) Direct arylation of 2-bromotoluene **30** with benzene **15** studied by Tan and Hartwig b) Reaction of Pd carboxylate intermediate **33** with benzene **15**.<sup>71</sup>

Additives such as carboxylate ligand (*n*-hept<sub>4</sub>OPiv), halide (*n*-hept<sub>4</sub>Br), or oxygen sources were required for successful C–H activation of benzene **15** and production of the organic

product. Based on their observations, Tan and Hartwig propose that the additive aids in the displacement of the phosphine ligand, which is essential to generate the proposed ligand-less aryl Pd<sup>0</sup> species responsible for the C–H cleavage step. This finding suggests removing the phosphine-ligand from the reaction should increase the rate of C–H bond activation by Pd, and, as C–H activation was the rate-limiting step, this would result in an overall increase in the rate of reaction. Indeed, as suggested by this hypothesis, the removal of phosphine ligands such as DavePhos resulted in an increased rate, while the overall KIE of the reaction remained the same with or without phosphine ligand (**Scheme 12**).<sup>71</sup>



**Scheme 12:** Direct arylation of 2-bromotoluene **30** with and without 3 mol% of DavePhos<sup>71</sup>

## 1.4 The Role of Ag<sup>I</sup> Salts in the Pd-Catalysed C–H Bond Activation Reactions

Silver carbonate and carboxylate salts are common additives in Pd-catalysed C–H functionalization reactions, often dramatically improving cross-coupling yields and reaction rates. While the exact role of the Ag<sup>I</sup> salts was not well understood, it was initially proposed that they acted as halide scavengers, terminal oxidants, or a source of carboxylate ligand. However, attempts to replace the Ag<sup>I</sup> salts with other halide scavengers or terminal oxidants did not yield the same results.<sup>72,73</sup> Hence, other proposals such as Ag<sup>I</sup> salts forming bimetallic or polymetallic complexes with Pd, thereby promoting C–H bond activation, or the AgCO<sub>2</sub>R being able to directly activate the C–H bond of the electron-deficient arene *via* AMLA(6)-TS, were also made (**Figure 8**).<sup>74,75</sup>

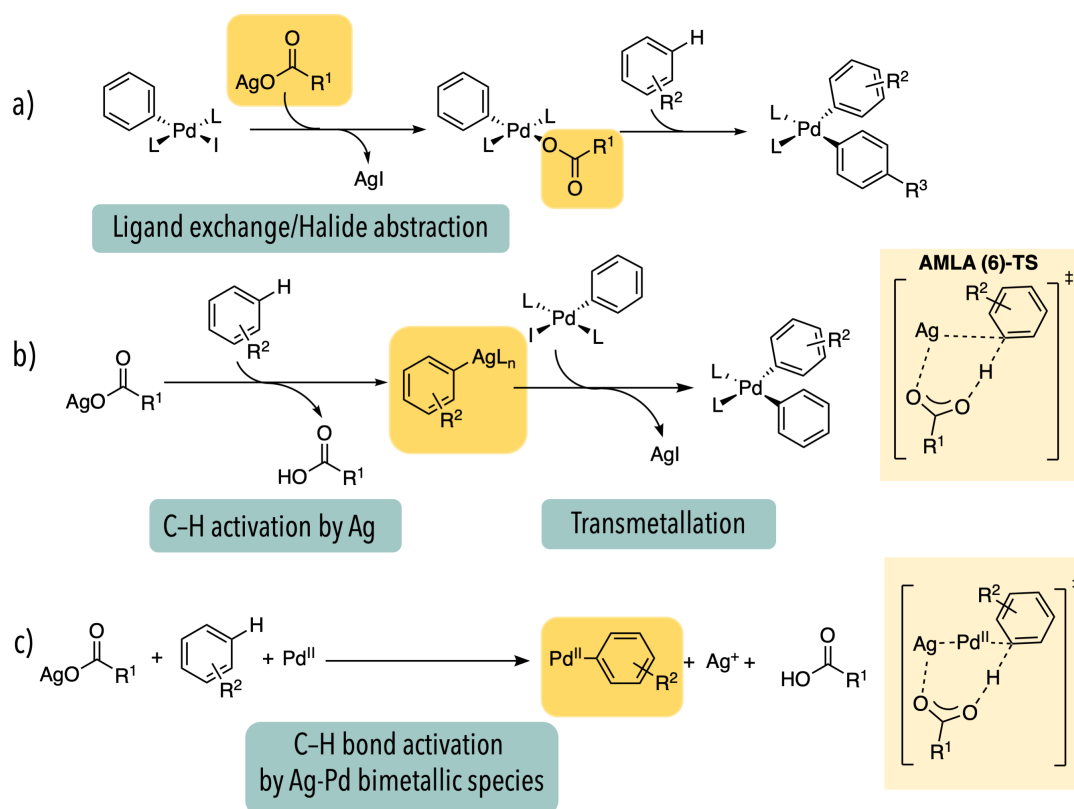


**Figure 8:** Summary of the different hypothesised roles of  $\text{Ag}^{\text{I}}$  salts in C–H functionalization reactions. a)  $\text{Ag}^{\text{I}}$  salts acting as a source of carboxylate ligand for Pd *via* halide abstraction reaction. b) C–H bond activation mediated by  $\text{Ag}^{\text{I}}$  salts *via* AMLA(6) transition state, to produce an Ag-arene intermediate which can undergo transmetalation with Pd. c) Pd and Ag form bimetallic or polymetallic intermediates which are then responsible for C–H bond activation.<sup>74,75</sup>

#### 1.4.1 C–H Bond Activation by Ag–Pd Heterometallic Complexes

Examples of  $\text{Ag}^{\text{I}}/\text{Pd}^{\text{II}}$  bi- and polymetallic clusters are known, especially those incorporating carboxylate-type ligands. Hor and co-workers isolated and characterised  $\text{Ag}^{\text{I}}/\text{Pd}^{\text{II}}$  binuclear and trinuclear clusters incorporating phosphine and carboxylate-type ligands (**Figure 9**). The complexes were structurally characterised using low temperature NMR spectroscopy and XRD analysis, showing that, in solution, these complexes rapidly fluctuate between different coordination modes of the fluoropropanoate ligand.<sup>76</sup>

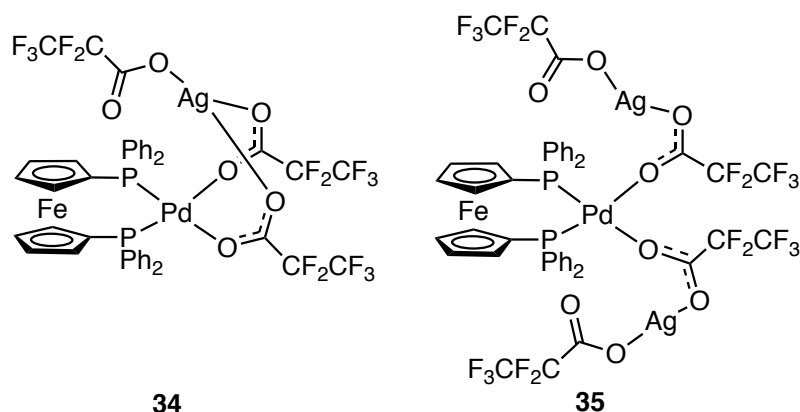


**Figure 9:** The Pd-Ag dinuclear and trinuclear clusters **34** and **35** synthesized by Hor and co-workers by treating  $\text{Pd}(\text{O}_2\text{CCF}_2\text{CF}_3)_2(\text{dppf})$  with one or two equivalents of  $\text{Ag}(\text{O}_2\text{CCF}_2\text{CF}_3)_2$  in dichloromethane respectively.<sup>76</sup>

Strassner and co-workers reported the characterization of a Pd-Ag trinuclear N-heterocyclic carbene acetate complex **36**<sup>77</sup> and Kozitsyna and co-workers showed that  $\text{Ag}^{\text{I}}/\text{Pd}^{\text{II}}$  trinuclear acetate cluster **37** can be synthesized by reacting  $\text{Pd}_3(\text{OAc})_6$  with  $\text{AgOAc}$  in acetic acid (**Figure 10**).<sup>78</sup> These clusters exist as infinite polymeric chains with repeat units being linked by hydrogen bonding. Strassner and co-workers found that the Pd/Ag carbene acetato-complex **36** existed as an infinite anionic polymer chain, and repeating units were hydrogen bonded by water molecules.<sup>77</sup> Similarly, Kozitsyna and co-workers found that their complex **37** existed as a linear metallic chain where the AcOH moiety acts as the H-bond donor and the bridging acetate of the adjacent unit acts as the H-bond acceptor.<sup>78</sup>

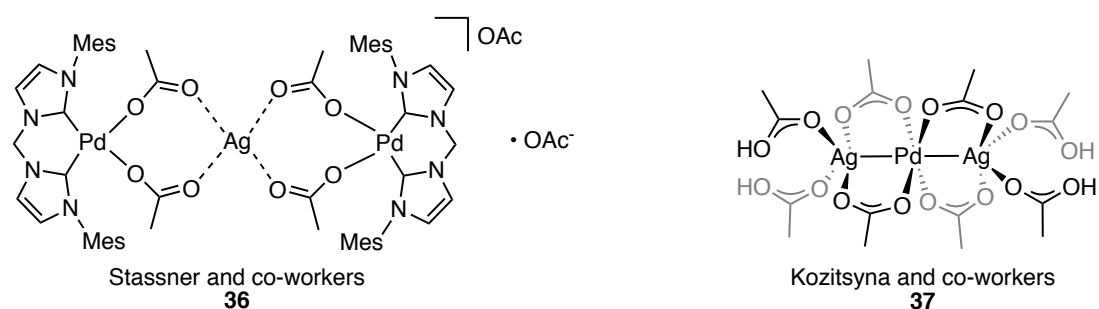
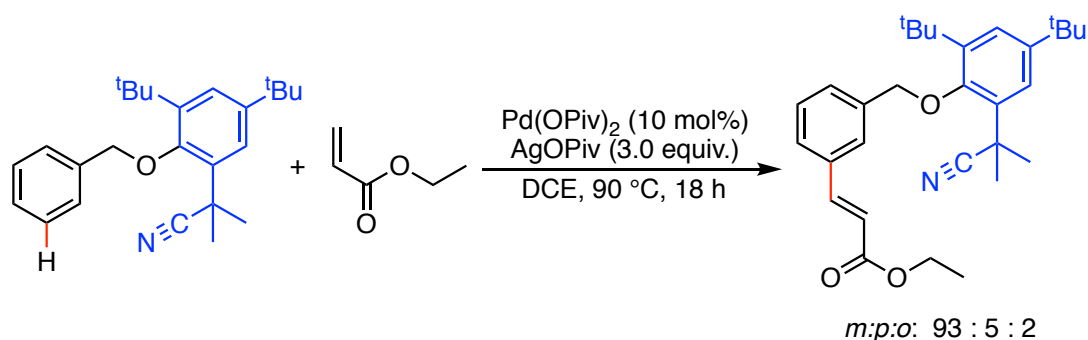


**Figure 10:** The Pd/Ag bimetallic complexes isolated and characterized by Strassner and co-workers<sup>77</sup> and Kozitsyna and co-workers<sup>78</sup> respectively.

While the synthesis and characterization of Ag/Pd clusters have been reported, their relevance in catalysis has been only examined computationally, with limited experimental evidence. In 2002, Yu and co-workers developed a synthetic methodology for the *meta*-selective Pd-catalysed C–H olefination of toluene derivatives (**Scheme 13**). The use of a bulky

nitrile template (blue), acted as a directing group which allowed for the selective olefination of the *meta*-C–H bond of various toluene derivatives.<sup>10</sup>



**Scheme 13:** The *meta*-selective Pd-catalysed direct arylation of toluene, incorporating a bulky nitrile (blue) directing group.<sup>10</sup>

It is proposed the selectivity is a result of the nitrile group coordinating with the Pd centre of the catalytic species and forming a cyclophane-like transition state that is large enough to activate the *meta*-C–H bond.<sup>10</sup> To support this mechanism and elucidate the active catalytic species, Yu and Tan *et al.* investigated the mechanism of *meta*-C–H direct arylation of toluene using computational methods. Palladium acetate is known to exist as monomeric **38**, dimeric **39** and trimeric clusters **41**; thus, all three structures were considered as potential active catalytic species. Additionally, the Ag salt used in the reaction was critical for both high yields and *meta*-selectivity. Attempts to replace the Ag additive with other terminal oxidants resulted in poor yields or loss of *meta*-selectivity. Thus, a Pd/Ag acetate cluster **40** was also evaluated as a potential catalytic species computationally in the study (**Figure 11**)<sup>79</sup>

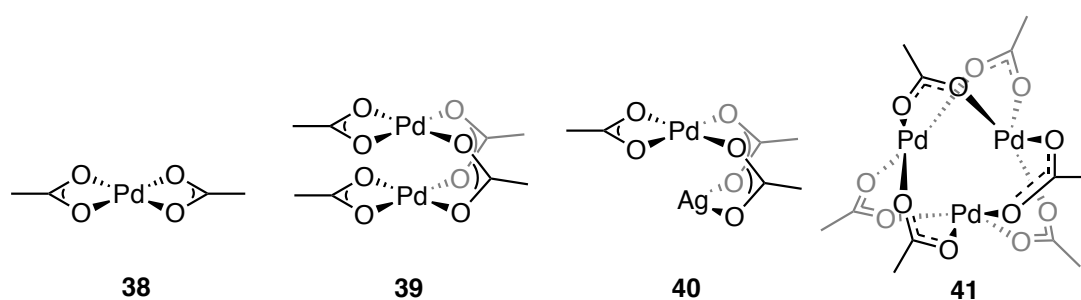


**Figure 11:** The monomeric **38**, dimeric **39**, trimeric clusters **41** of Pd acetate and Pd-Ag acetate cluster **40** considered for the computational investigation of the mechanism of *meta*-C–H selective activation reactions.<sup>79</sup>

The transition state involving monomeric Pd(OAc)<sub>2</sub> **38** was found to be too strained to allow for *meta*-C–H activation, whereas all transition states involving the trimeric Pd<sub>3</sub>(OAc)<sub>6</sub> **41** had

very high energy barriers. Transition states involving bimetallic catalytic species such as  $\text{Pd}_2(\text{OAc})_4$  **39** and  $\text{PdAg}(\text{OAc})_3$  **40** allowed for the formation of a larger macrocycle, thus alleviating the ring strain of *meta*-C–H activation. When the reaction pathways incorporating  $\text{Pd}_2(\text{OAc})_4$  **39** and  $\text{PdAg}(\text{OAc})_3$  **40** were compared, the transition state of *meta*-C–H activation, **43** involving  $\text{PdAg}(\text{OAc})_3$  **40** was found to be more favourable as it required a lower  $\Delta G^\ddagger(363.15\text{ K}) = 24.8\text{ kcal/mol}$  versus transition state **42** with  $\text{Pd}_2(\text{OAc})_4$  which required  $\Delta G^\ddagger(363.15\text{ K}) = 29.3\text{ kcal/mol}$  (Figure 12).<sup>79</sup>

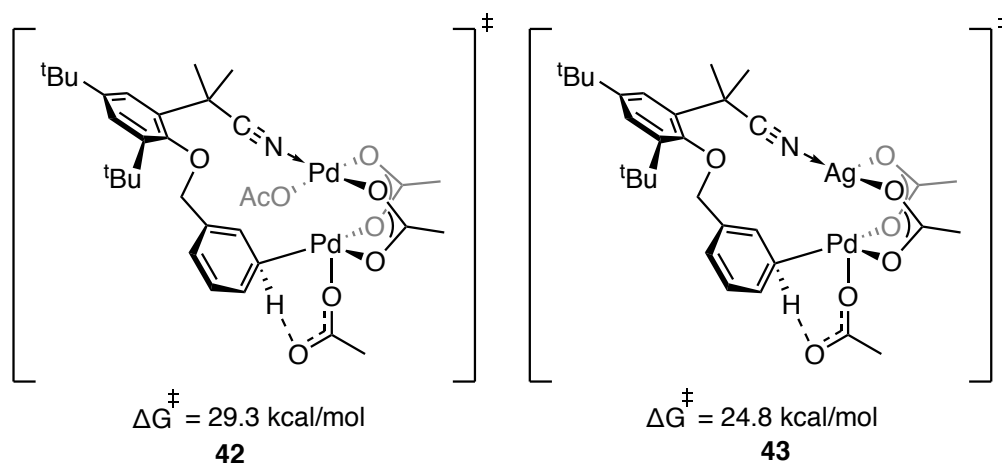
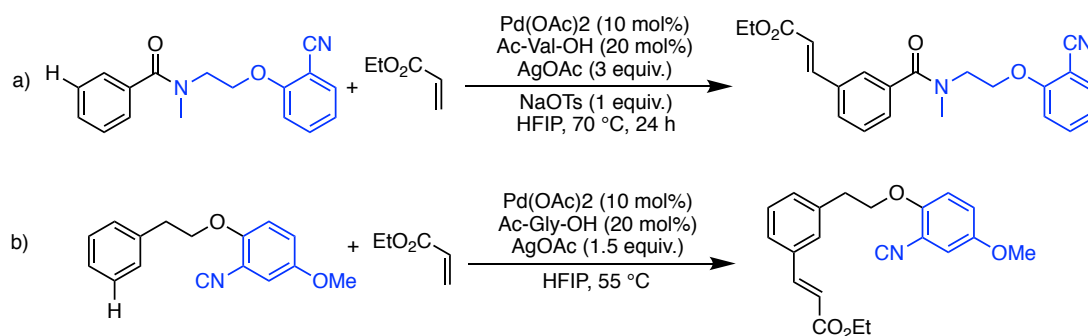


**Figure 12:** The transition states for *meta*-selective C–H activation by both a  $\text{Pd}_2(\text{OAc})_4$  **39** and  $\text{PdAg}(\text{OAc})_3$  **40** cluster respectively. The nitrile group, of the bulky directing group, is shown to coordinate with one end of the metal cluster to aid in the formation of a cyclophane-like transition state which overrides the typical *ortho*-selectivity of the reaction.<sup>79</sup>

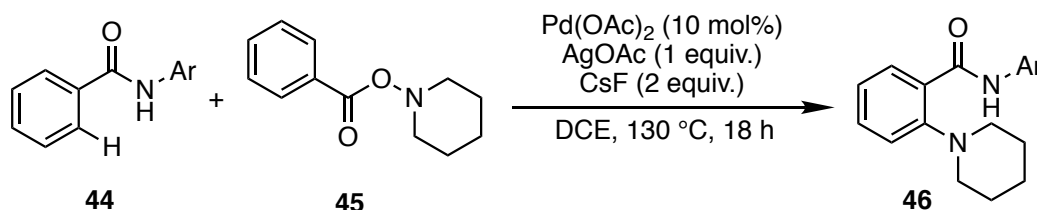
Similar reactions incorporating bulky or tethered nitrile groups for *meta*-selective C–H activation and functionalization have since been proposed to proceed *via* Pd/Ag bimetallic transition state.<sup>80</sup> For example, the *meta*-selective C–H olefination of benzoic acid derivatives such as amide<sup>80</sup> and remote *meta*-selective olefination of alcohols<sup>81</sup> (Scheme 14). In both reactions, the C–H activation of the *meta*-C–H bond is shown to proceed *via* an Ag/Pd bimetallic TS, using computational studies. The involvement of a bimetallic complex allows for the formation of a much larger macrocyclic transition state that is found to favour *meta*-selectivity.<sup>80,81</sup>





**Scheme 14:** a) The *meta*-selective olefination of benzoic acid derivatives using a conformationally flexible nitrile template to access the *meta* C–H bond.<sup>80</sup> b) *Meta*-selective olefination of aryl alcohols using a tethered nitrile template.<sup>81</sup>

The involvement of Pd/Ag bimetallic clusters in C–H activation has also been proposed in the Pd-catalysed *ortho*-C–H amination of N-aryl benzamides **44** (Scheme 15).<sup>82,83</sup> In this reaction, the amide acts as the directing group, allowing for the selective C–H functionalization of the *ortho*-C–H bond.<sup>84</sup>



**Scheme 15:** The Pd-catalysed oxidative *ortho*-selective amination of N-aryl benzamides **44**, where the amide group acts as a directing group.<sup>82,84</sup>

To investigate the mechanism, Schaefer and co-workers evaluated the free energy of various transition states (TS) involving monomeric and dimeric Pd acetate complexes and a Pd/Ag heterometallic cluster. The most stable transition state with the lowest Gibbs free energy, involved a Pd/Ag bimetallic complex in the TS **47**. Close contact distance between 2.90 – 2.96 Å was noted between the Pd and Ag metal centres, in the TS, which allowed for favourable electronic interactions between the two metal centres. Additionally, C–H activation was primarily facilitated by the Pd<sup>II</sup> centre, attempts to switch the position of the Pd and Ag centre resulted in a higher energy state transition state. The C–H activation by similar TS **48**, using a dimeric Pd acetate complex, resulted in a higher free energy intermediate (Figure 13). The caesium fluoride in the reaction is proposed to help in the deprotonation of the amide or acetic acid found in the reaction.<sup>82,83</sup> When computing the overall energy profile of reaction without the inclusion of AgOAc and CsF, the C–H activation step was rate-determining step for the C–H amination reaction. However, when the involvement of the AgOAc and CsF

additives were considered, the energy barrier of the C–H activation step lowers and the N–O activation step becomes the rate-determining step.<sup>83</sup>

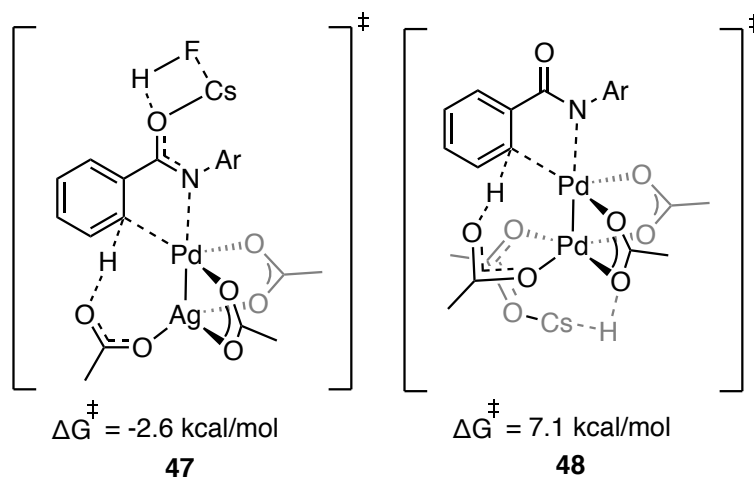
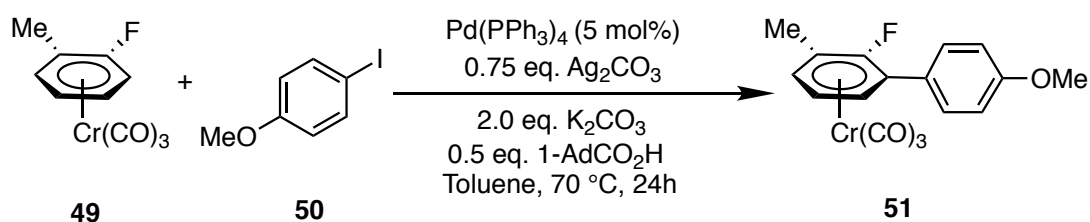


**Figure 13:** The transition states of C–H activation incorporating a PdAg(OAc)<sub>3</sub> (left) and Pd<sub>2</sub>(OAc)<sub>4</sub> (right) complex, with the corresponding Gibbs free energies.<sup>82</sup>

While numerous studies have proposed the involvement of Pd/Ag bimetallic species in C–H activation and functionalization reactions, the evidence for the mechanism mostly remains computational. Experimental studies involving isolated intermediates or detailed kinetic studies remain to be undertaken.<sup>75</sup>

#### 1.4.2 C–H bond Activation by Ag Carbonate and Carboxylate salts

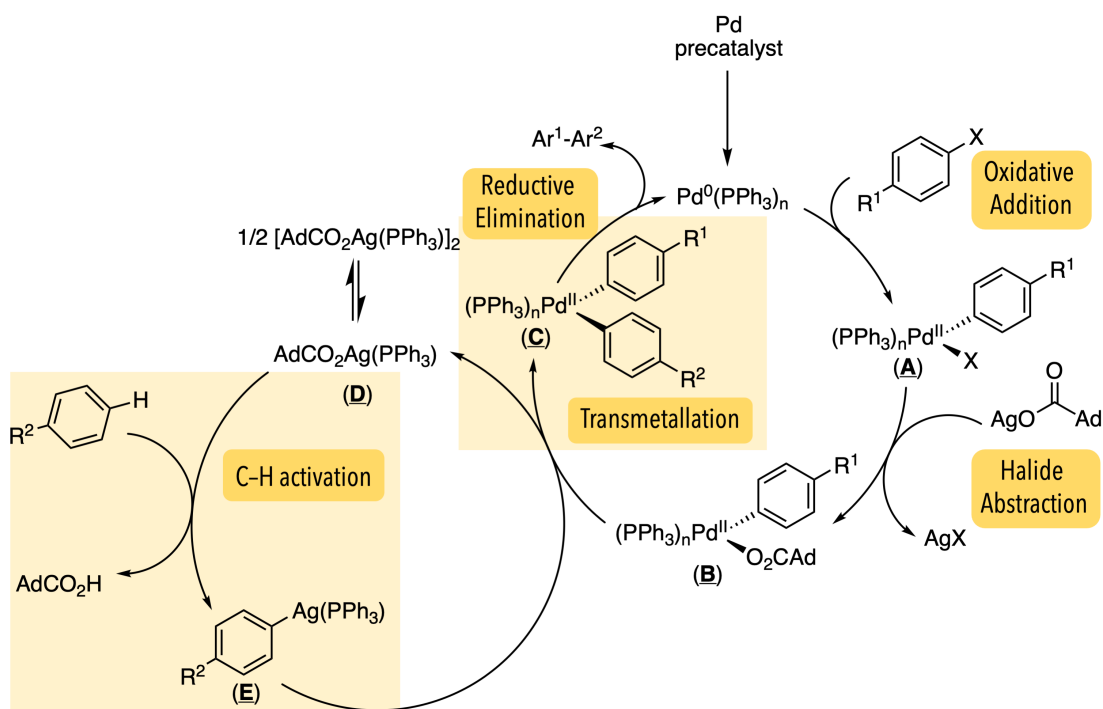
In 2016, Larrosa and co-workers showed that the Ag carboxylate salts were capable of activating C–H bonds (**Scheme 16**).<sup>85</sup>



**Scheme 16:** The direct arylation of 4-iodoanisole **50** with (2-fluorotoluene)Cr(CO)<sub>3</sub> **49** to investigate the role of Pd and Ag.<sup>85</sup>

When determining the order of each reagent, for the direct arylation of 4-iodoanisole **50** with (2-fluorotoluene)Cr(CO)<sub>3</sub> **49**, they found the order with respect to Pd was zero. This is inconsistent with the C–H bond activation by Pd. In contrast, Platt *et al.*'s system which proceeds predominantly *via* Pd facilitated C–H activation, has an order of 0.5 with respect to Pd which accounts for a dimeric catalytic resting state.<sup>68</sup> Larrosa's reaction also showed zero-

order dependence on Pd and aryl halide **50**, a first order and positive order dependence on fluoroarene **49** and PPh<sub>3</sub> respectively. H/D exchange experiments demonstrated that a combination of AgOCOAd (0.5 equiv.) and PPh<sub>3</sub> (0.5 equiv.) resulted in a 75 % deuteration of fluoroarene **49** when reacted with 10 equivalents of D<sub>2</sub>O in toluene at 70 °C after 2 h. When only AgOCOAd (Ad = adamantyl) was used, only 5 % deuteration of **49** was achieved. This provided indirect evidence for the C–H bond activation capability of AgOCOAd, in the presence of PPh<sub>3</sub>. Based on these observations, Larossa and co-workers proposed a dual Ag/Pd co-catalytic mechanism where, in addition to its role as a halide abstraction agent, C–H bond activation is primarily mediated by Ag (**Scheme 17**).<sup>86</sup>

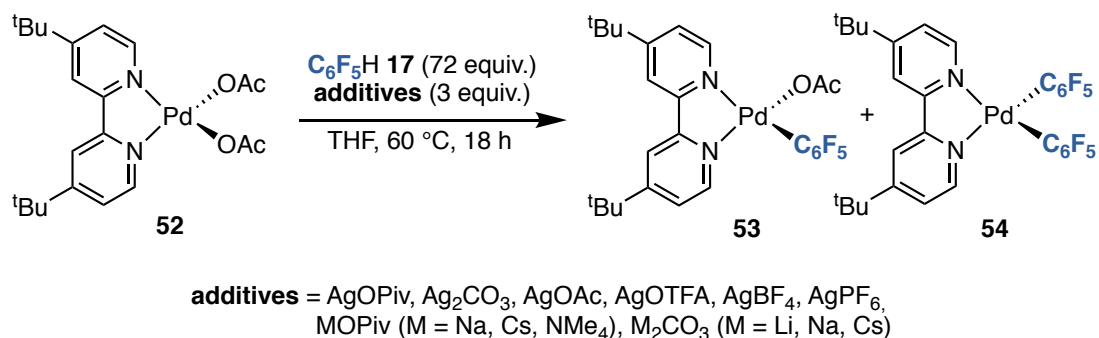


**Scheme 17:** Catalytic mechanism proposed by Larossa and co-workers based on their kinetic evidence.

The catalytically active Pd<sup>0</sup> species undergoes oxidative addition with the aryl halide, to generate species (A). AgCO<sub>2</sub>Ad then abstracts a halide from species (A), generating species (B) with a carboxylate coordinated to the Pd centre. However, as opposed to species (B) undergoing C–H bond activation *via* an ALMA-(6) mechanism, Larossa and co-workers propose that a (PPh<sub>3</sub>)<sub>n</sub>AgO<sub>2</sub>CAd (D) species, generated *in situ* from the Ag<sub>2</sub>CO<sub>3</sub>, AdCO<sub>2</sub>H and free PPh<sub>3</sub> present in the solution, was responsible for the C–H activation of the arene coupling partner. The coordination of the carboxylate ligand would make the Ag species capable of C–H activation *via* an AMLA(6) mechanism. This would result in the formation of an Ag-aryl species (E), which would be capable of undergoing transmetalation with species (B) to form species (C). Ultimately species (C) would undergo reductive elimination to generate the

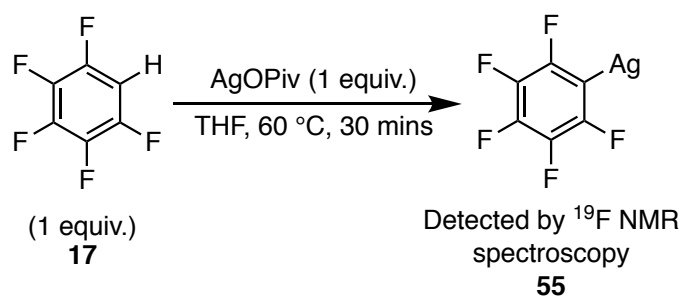
product and active catalytic species. While Larossa and co-workers were able to indirectly prove the existence of the Ag-aryl (**E**) using stoichiometric reactions, they were unable to isolate or detect the proposed  $(\text{PPh}_3)_n\text{AgO}_2\text{CAd}$  (**D**) or Ag-Aryl complex (**E**).<sup>85</sup>

Sanford and co-workers evaluated the C–H activation capabilities of a wide range of metal carboxylate and carbonate salts, using a Pd-precursor  $\text{Pd}(\text{dtbpy})(\text{OAc})_2$  **52** which yielded stable  $\text{Pd}(\text{dtbpy})(\text{C}_6\text{F}_5)(\text{OAc})$  **53** and  $\text{Pd}(\text{dtbpy})(\text{C}_6\text{F}_5)_2$  **54** upon transmetalation (**Scheme 18**).<sup>74</sup>



**Scheme 18:** Reaction used to evaluate the effect of Ag and group 1 metal carboxylate and carbonate salts.<sup>74</sup>

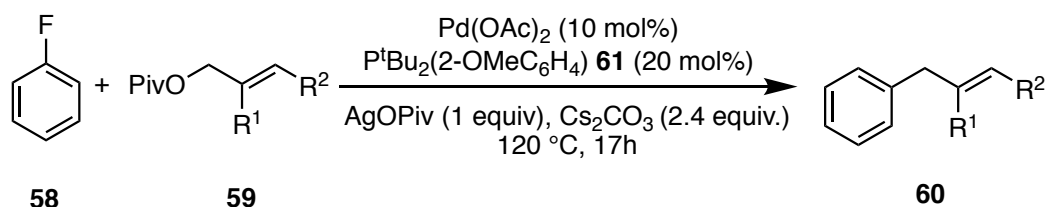
The reaction of **52** with  $\text{C}_6\text{F}_5\text{H}$  in the presence of Ag carboxylate and carbonate salts such as AgOPiv, Ag<sub>2</sub>CO<sub>3</sub>, AgOAc, and AgOTFA resulted in a mixture of **53** and **54**. Use of AgOPiv yielded the greatest amount of **54** (88%). In contrast, group 1 MOPiv and M<sub>2</sub>CO<sub>3</sub> salts and Ag salts with weakly coordinating anions such as BF<sub>4</sub><sup>−</sup> and PF<sub>6</sub><sup>−</sup> yielded little to no product. Additionally, when AgOPiv was reacted with  $\text{C}_6\text{F}_5\text{H}$  at 60 °C, formation of the C–H bond activation product: a  $\text{AgC}_6\text{F}_5$  **55** complex, was detected by <sup>19</sup>F NMR spectroscopy *via* its  $\delta - 105$  ppm resonance (**Scheme 19**). The identity of **55** was compared and confirmed using an authentic sample of  $\text{AgC}_6\text{F}_5$  **55**, synthesized from the reaction between AgOTFA **56** and LiC<sub>6</sub>F<sub>5</sub> **57**. When CsOPiv was reacted with  $\text{C}_6\text{F}_5\text{H}$  **17**, no products were detected by <sup>19</sup>F NMR spectroscopy.



**Scheme 19:** Reaction of  $\text{C}_6\text{F}_5\text{H}$  **17** with AgOPiv to product  $\text{AgC}_6\text{F}_5$  **55** detected by <sup>19</sup>F NMR spectroscopy and compared to an authentic sample of  $\text{AgC}_6\text{F}_5$  **55**.

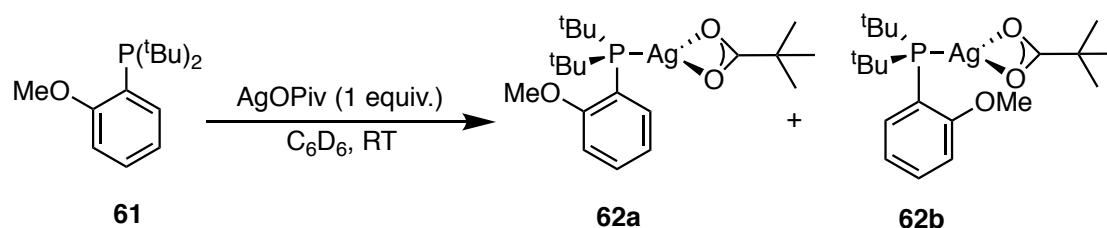
Using the aforementioned reactions in conjunction with H/D exchange reactions and DFT calculations, Sanford and co-workers were able to demonstrate that Ag carboxylates and carbonates were capable of C–H activation of fluorinated aromatics and it was a plausible pathway for the Ag additives within Pd/Ag C–H bond functionalization reactions.<sup>74</sup>

Hartwig and co-workers, while studying the Pd-catalysed direct allylation of aryl C–H bonds (**Scheme 20**), have also found that the AgOPiv salts within their system were directly responsible for the C–H bond activation of the arene coupling partner.<sup>87</sup> H/D exchange reactions of 1-fluoronaphthalene with 10 equivalents of D<sub>2</sub>O, showed that AgOPiv in the presence of the bulky phosphine ligand allowed for the highest deuteration of the C–H bond *ortho*- to the fluorine in 1-fluoronaphthalene (66% deuteration). With the addition of Pd(OAc)<sub>2</sub>, the % deuteration dropped to 44 %.

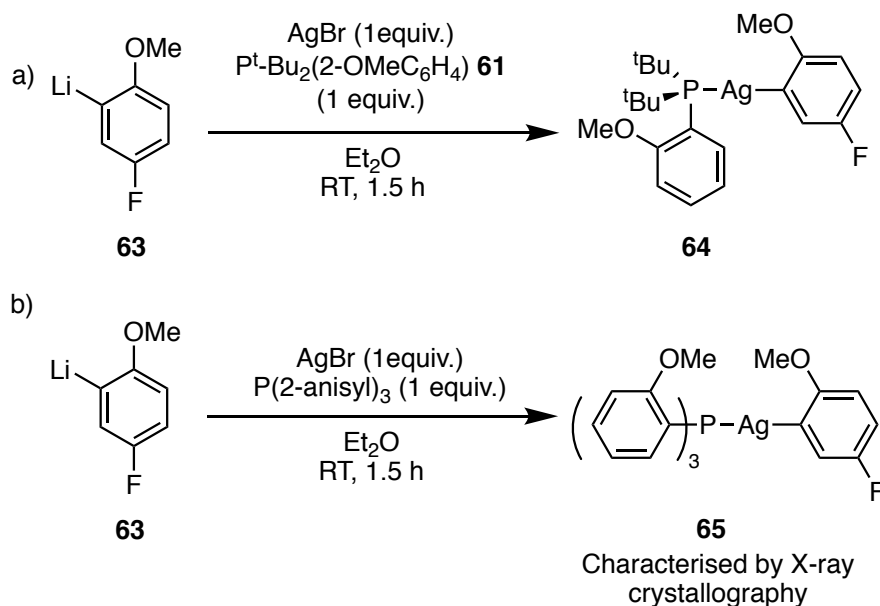


**Scheme 20:** The Pd-catalysed direct allylation of fluorobenzene **58** with allylic pivalates **59**.<sup>87</sup>

In support of their hypothesis, Hartwig and co-workers isolated and fully characterised the monophosphine-ligated AgOPiv **62** complex as a pair of rotamers from the reaction of AgOPiv with the phosphine ligand **61**. The presence of **62** was also detected *in operando* by <sup>31</sup>P NMR spectroscopy when monitoring the catalytic reaction (**Scheme 21**). They also prepared a phosphine ligated Ag-aryl complex and examined the transmetalation of the aryl-group from the Ag complex to Pd (**Scheme 22**). Using these reactions, Hartwig and co-workers proposed that the monophosphine-ligated AgOPiv complex within their reaction was capable of C–H activation, generating a Ag-aryl complex which could later undergo transmetalation to transfer the aryl group from the Ag to Pd.<sup>87</sup>

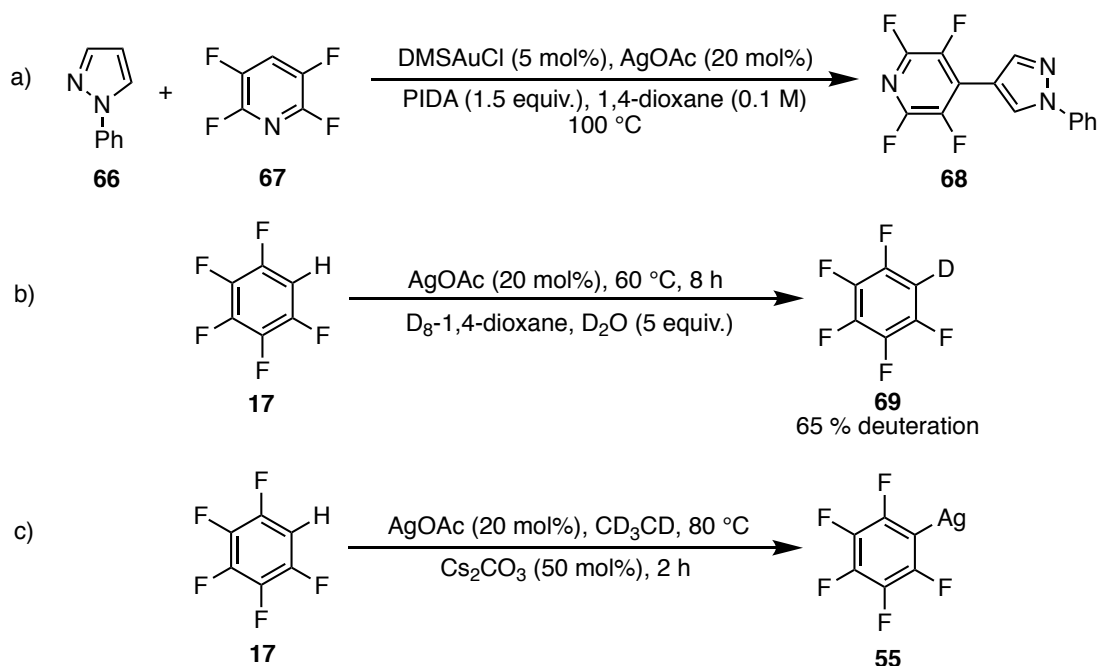


**Scheme 21:** Synthesis of monophosphine-ligated AgOPiv **62**, which are isolated as a pair of rotamers by Hartwig and co-workers.<sup>87</sup>



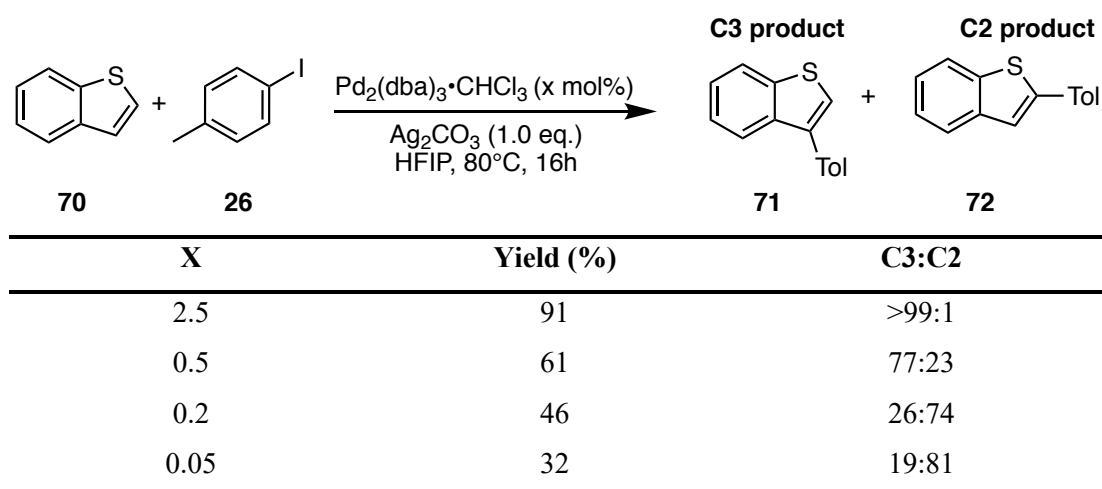
**Scheme 22:** Preparation of monophosphine-ligated Ag-aryl complex, which is the proposed intermediate generated after C–H activation by the monophosphine-coordinated AgOPiv complex.<sup>87</sup>

When investigating the mechanism of cross-dehydrogenative biaryl coupling reactions between pyrazoles and fluoroarenes (**Scheme 23a**), Zhu and co-workers found the reaction was carried out by an Au/Ag dual catalytic system. The AgOAc was responsible for the C–H activation of the electron-deficient arenes as demonstrated by H/D exchange experiments. The reaction of AgOAc with 5 equivalents of pentafluorobenzene **17** in the presence of a large excess of D<sub>2</sub>O, resulted in 65 % deuteration of the pentafluorobenzene (**Scheme 23b**). Additionally, the reaction of AgOAc with pentafluorobenzene in the presence of Cs<sub>2</sub>CO<sub>3</sub> resulted in the production of the AgC<sub>6</sub>F<sub>5</sub> **55** complex, which was easily detected by <sup>19</sup>F NMR spectroscopy, due to the significantly deshielded *ortho*-F resonance of AgC<sub>6</sub>F<sub>5</sub> **55** at  $\delta -107$  (in CD<sub>3</sub>CN). While AgOAc alone was capable of C–H bond activation, according to Zhu and co-workers, the presence of Cs<sub>2</sub>CO<sub>3</sub> aids in the production of AgC<sub>6</sub>F<sub>5</sub> **55** by acting as a base and deprotonating the AcOH produced to regenerate AcO<sup>−</sup> anions.<sup>88</sup>



**Scheme 23:** a) The Au/Ag co-catalysed cross dehydrogenative coupling of pyrazoles **66** and tetra-fluoropyridine **67**. b) The H/D exchange experiment with  $C_6F_5H$  **17** with  $D_2O$  demonstrated the C–H activation capabilities of the AgOAc salt alone. c) The production of  $AgC_6F_5$  **55** from the reaction of  $C_6F_5H$  **17** with AgOAc in the presence of  $Cs_2CO_3$ . The  $AgC_6F_5$  **55** complex was detected by  $^{19}F$  NMR spectroscopy.

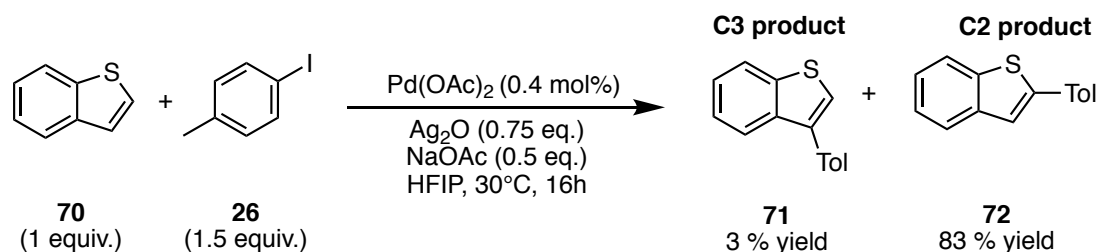
During the development of a C3-selective direct arylation of benzo[*b*]thiophenes **70** with iodoarenes, Larrosa and co-workers found that the regioselectivity of the system was determined by the catalyst loading of Pd (**Scheme 24**).<sup>51,89</sup>



**Scheme 24:** The direct-arylation of benzo[*b*]thiophene **70** with 4-iodotoluene **26**, where the regioselectivity is determined by the catalyst-loading of Pd.<sup>89</sup>

Decreasing the Pd loading resulted in an increased selectivity towards the C2 arylated product **72**; however, this effect was lost when loadings as low as 0.05 mol% Pd are employed. Based on this observation, Larossa and co-workers proposed that under low concentrations of Pd, the C–H activation of benzo[*b*]thiophene **70** was mediated by Ag<sup>I</sup>, which resulted in the production of the C2 product **72**, whereas under high-concentration of Pd, catalysis was dominated by Pd, proceeding *via* a Heck-type pathway, resulting in the formation of the C3-product **71** (Scheme 26).<sup>51,89</sup>

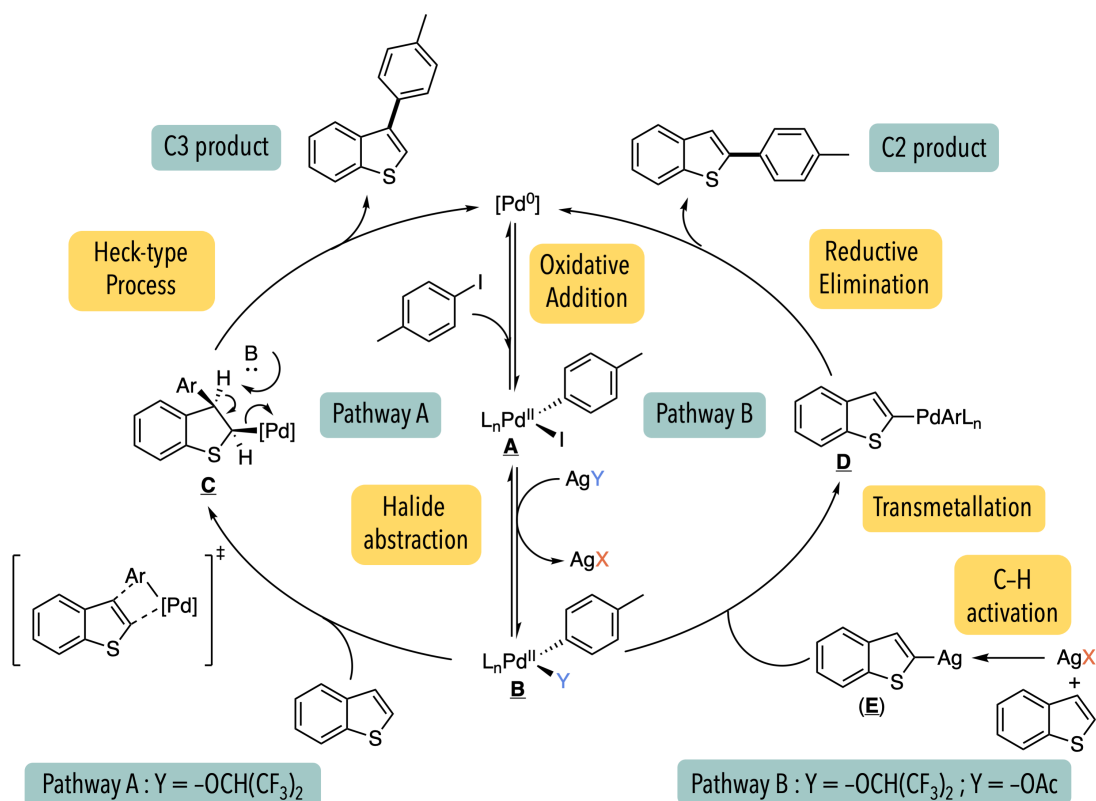
To support their proposal, Larossa and co-workers optimized the conditions required for the C2-selective direct arylation reaction of benzo[*b*]thiophene **70** and found that the reaction proceeded at room-temperature which allowed for excellent functional group tolerance (Scheme 25). They then investigated the mechanism of the C2-selective process.



**Scheme 25:** Optimized reaction conditions for the C2-selective direct arylation of benzo[*b*]thiophene which employs low catalytic loading of Pd.<sup>51</sup>

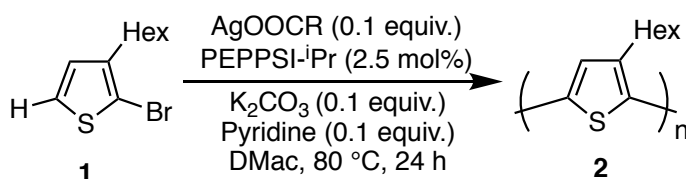
The KIEs of the C3 and C2 selective processes were different, with the KIE of the C2 process being consistent with the rate-limiting C–H activation step *via* AMLA(6). Furthermore, using RPKA and VTNA, they were able to show that in the C2-selective process, the order with respect to Pd is zero and benzo[*b*]thiophene **70** has an order of one. This showed that the rate-determining C–H bond activation step of the C2-selective process does not involve Pd. The order with respect to Ag was complicated by the low solubility of Ag<sub>2</sub>O in HFIP. Additionally, slowing down the rate of the C2-selective process resulted in the C3-process becoming competitive, impeding the reaction. Hence 3-bromobenzo[*b*]thiophene was used in place of benzo[*b*]thiophene, and the order with respect to Ag was determined to be 0.5 within a concentration range of 0.6 M to 0.4 M, which implies a dimeric resting state, consistent with their proposal. This demonstrates how understanding the non-innocent role of Ag salts can be crucial for the understanding and development of C–H activation protocols.





**Scheme 26:** Proposed mechanism for the synthesis of the C3 product **71** via Pathway A and of the C2 product **72** via Pathway B.

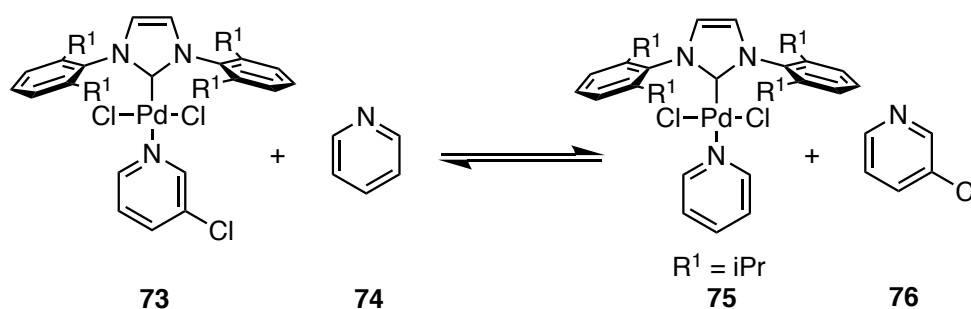
Luscombe and co-workers developed a Pd/Ag co-catalytic system for the direct arylation polymerization of 2-bromo-3-hexylthiophene **1** (**Scheme 27**). Bulky Ag<sup>I</sup> carboxylate salts such as silver(I) adamantanoate (AgAd) and silver(I) neodecanoate (AgNDA) were used for their efficiency in direct arylation polymerization and to reduce the undesired C–H activation of the 4-position of the thiophene which leads to branching.<sup>8</sup>



**Scheme 27:** The synthesis of poly(3-hexylthiophene) **2** by a direct arylation polymerization reaction incorporating a Pd/Ag dual catalytic system.<sup>8</sup>

Based on the findings of Larossa<sup>86</sup> and Sanford,<sup>90</sup> Luscombe and co-workers suggest both the Pd catalyst and the Ag carboxylate salt within their reaction systems are capable of C–H activation. H/D exchange studies with the 0.1 equivalents of AgNDA and 1 equivalent of 2-bromo-3-hexylthiophene and D<sub>2</sub>O in DMAc heated at 80 °C for 24 h, resulted in 64 %

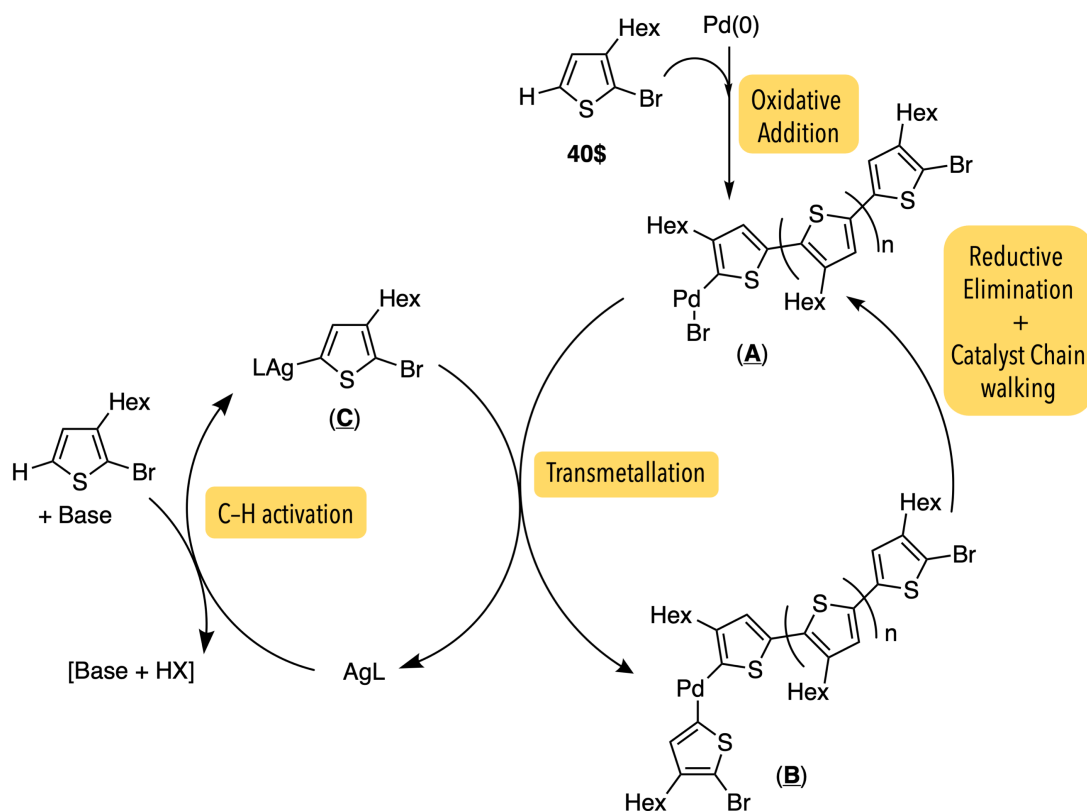
deuteration. When the Ag salt in the system was replaced with other carboxylate bases, the reactivity decreased, only yielding oligomers. C–H bond activation by AgNDA was preferred over the Pd-mediated pathway, as the former generates polymers with low dispersities ( $< 1.5$ ) whereas the latter lead to unfavourable polymerization. Thus, to suppress C–H bond activation by the PEPPSI-<sup>i</sup>Pr **73**, pyridine **74** was introduced into the system. The active catalytic species is generated when 3-chloropyridine **76** dissociates from PEPPSI-<sup>i</sup>Pr **73**, the addition of pyridine **74** plays as inhibitory role for pre-catalyst activation, coordinating to the Pd<sup>II</sup> centre (Scheme 28).<sup>8</sup>



**Scheme 28:** The reaction of PEPPSI-<sup>i</sup>Pr **73** with excess pyridine **74** heated at 80 °C for 24 h resulted in 74 % of the 3-chloropyridine **76** being displaced by pyridine **74**.<sup>8</sup>

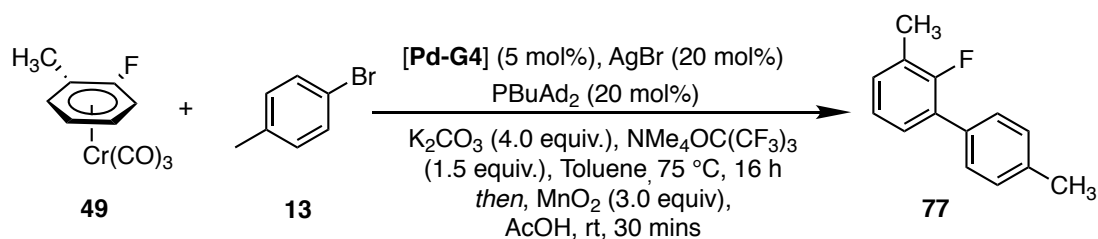
The inhibitory effect of pyridine **74** is hypothesized to suppress C–H bond activation at Pd<sup>II</sup>, relegating the C–H activation of 2-bromo-3-hexylthiophene **1** primarily to Ag. This helped optimise the reaction to synthesize the poly(3-hexylthiophene) **2** with the desired molar mass distribution ( $M_n$ ) and low dispersities. Luscombe and co-workers proposed the following reaction catalytic mechanism, albeit based on limited experimental data (Scheme 29).<sup>8</sup>

After Pd pre-catalyst activation, the 2-bromo-3-hexylthiophene **1** undergoes oxidative addition to generate (**A**). The C–H bond in the 5-position of 2-bromo-3-hexylthiophene **1** is activated by Ag-carboxylate salt to generate an Ag aryl complex (**C**) which undergoes transmetalation with (**A**) to generate (**B**). Species (**B**) is then thought to undergoes reductive elimination and subsequent catalyst ring-walking *via* a metal-polymer  $\pi$ -complex, allowing for catalyst migration and intramolecular oxidative addition to regenerate (**A**). However, further kinetic and mechanistic studies are required to verify this mechanism.<sup>8,91</sup>

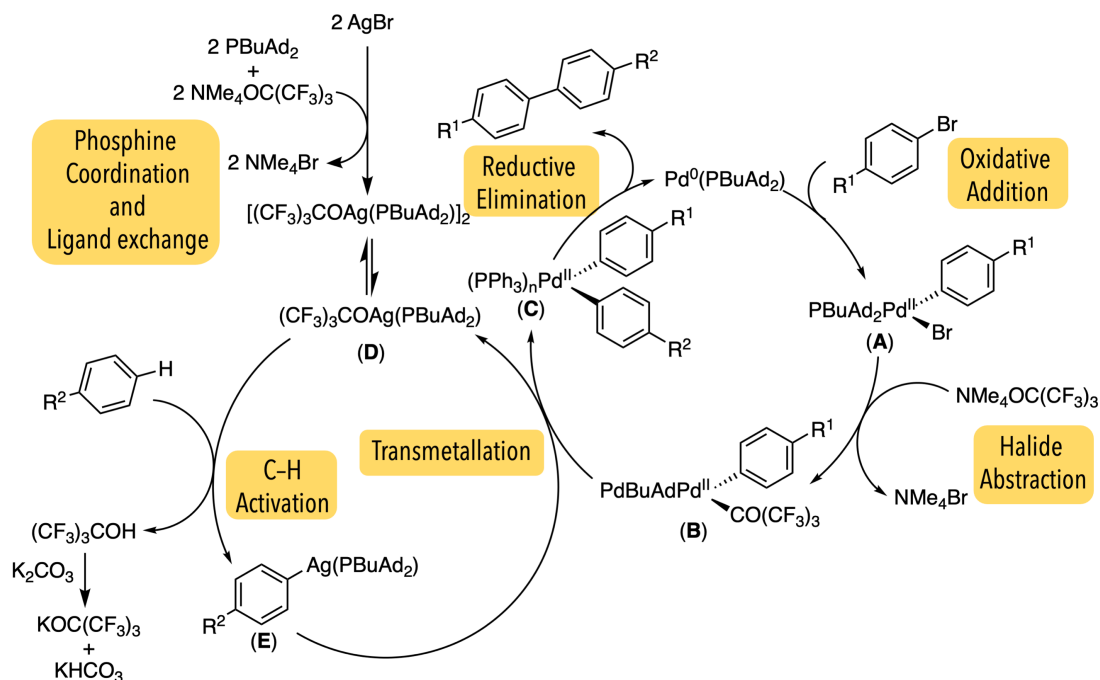


**Scheme 29:** Proposed mechanism for the synthesis of poly(3-hexylthiophene) **2** by a direct arylation polymerization reaction, incorporating a Pd/Ag dual catalytic system.<sup>8</sup>

In 2020, Larossa and co-workers were able specifically tailor a Pd/Ag co-catalytic system where catalytic amounts of Ag was used for C–H bond activation, and a different additive was used as the halide abstraction agent (**Scheme 30**).<sup>92</sup>



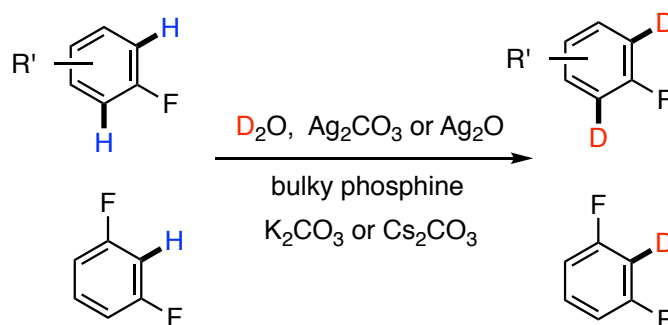
**Scheme 30:** The Pd-catalysed direct arylation reaction between 4-bromotoluene **13** and (2-fluorotoluene)Cr(CO)<sub>3</sub> **49** in toluene, using AgBr as the co-catalyst.



**Scheme 31:** The proposed mechanism for the Pd/Ag co-catalyst system with catalytic amounts of Ag

During their investigation, Larossa and co-workers were able to show that AgBr in conjunction with  $\text{NMe}_4\text{OC}(\text{CF}_3)_3$  and  $\text{PBUAd}_2$  generated a phosphine-coordinated  $\text{AgOC}(\text{CF}_3)_3(\text{PBUAd}_2)$  (characterized by XRD and NMR spectroscopy) which was then capable of C–H activation. They were able to demonstrate this using H/D scrambling experiments and that  $[\text{Me}_4\text{N}]\text{OC}(\text{CF}_3)_3$  acts as the halide abstraction agent in the system as it can also abstract the halide from Ag, allowing for catalyst regeneration.<sup>92</sup>

Overall, a combination of experimental and computational evidence has demonstrated the diverse roles that  $\text{Ag}^{\text{I}}$  salts can play within Pd catalysed C–H functionalisation reactions. Numerous studies have used H/D exchange experiments to demonstrate the ability of Ag salts to C–H activate fluorinated aromatics (**Scheme 32**). This has been used as basis for  $\text{Ag}^{\text{I}}$  mediated deuteration for the alteration of therapeutic molecules and heteroatoms.<sup>93,94</sup> Kinetic and mechanistic investigations performed on direct arylation reactions have shown that Ag salts have the capability to enable efficient C–H activation of resulting in enhanced yields and rate of reaction.<sup>74,86,92</sup> Evidence of catalytically competent Ag intermediates have also been isolated. For instance, Hartwig and co-workers isolated a phosphine-coordinated Ag precursor **62** (**Scheme 21**) and used lithiation reactions to synthesise the expected Ag arene product after C–H activation (**64**, **65**) (**Scheme 22**). The Ag arene intermediate was then able to participate in transmetalation with Pd to generate the C–H functionalised product.<sup>87</sup>

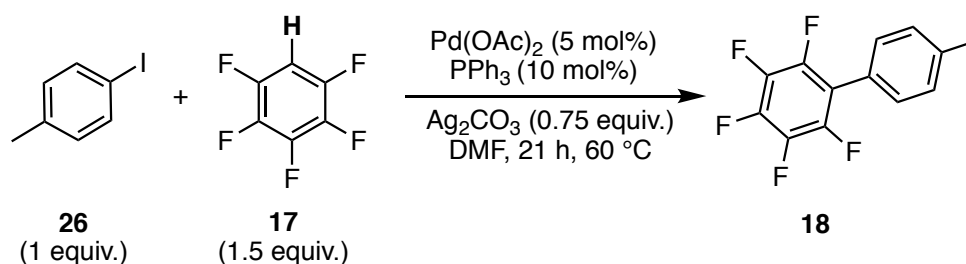


**Scheme 32:** Ag-mediated deuteration of fluorinated aromatics in the presence of  $\text{D}_2\text{O}$ <sup>93,94</sup>

The role of  $\text{Ag}^{\text{I}}$  salts in reactions involving C–H activation have been partially delineated in some cases, however a holistic understanding of the role of Ag in these reactions and interactions with the Pd co-catalyst has hitherto not been realised.

## 1.5 Introduction to Thesis Project

As seen from the range of publications from 2016 summarised previously in this introduction, the Ag carbonate and carboxylate salts have been shown to play a non-innocent role in the Pd-catalysed direct arylation reactions. Thus, when studying the mechanism of these reactions, it is critical to determine the role of the  $\text{Ag}^{\text{I}}$  salt. This project aims to elucidate the mechanism of C–H bond activation of fluorinated aromatics by  $\text{Ag}^{\text{I}}$  salts. For this purpose, the Pd-catalysed direct arylation reaction of 4-iodotoluene **26** and pentafluorobenzene **17** studied by Platt *et al.* was used as the standard model system (**Scheme 33**). In concert with a  $\text{Pd}(\text{OAc})_2$  pre-catalyst source,  $\text{PPh}_3$  was primarily used as the ligand for their studies, and while this reaction is used as a starting point, the tertiary phosphine ligand was varied later in the study.



**Scheme 33:** Direct arylation reaction of 4-iodotoluene **26** and pentafluorobenzene **17** studied by Platt *et al.*<sup>68</sup>

The kinetics and mechanism of the Pd intermediates of the reaction have already been investigated, thus providing an ideal environment to focus the project on the role of the  $\text{Ag}^{\text{I}}$  salts within the system. Additionally, there is evidence in the pre-existing data to suggest that

the Ag<sup>I</sup> salts may be playing a non-innocent role. For instance, when elucidating the order with respect to pentafluorobenzene, the concentration dependence of the rate of reaction on pentafluorobenzene **17** was found to have a significant non-zero y-intercept (**Figure 14a**). Typically, this is indicative of the presence of multiple rate constants, one of which is dependent on [C<sub>6</sub>F<sub>5</sub>H] and another alternate process, which is independent of the concentration of pentafluorobenzene **17**. It is hypothesised that the alternate [C<sub>6</sub>F<sub>5</sub>H] independent process could be the result of C–H bond activation by an organometallic Ag complex. When studying the effect of temperature on the reaction rate (**Scheme 14b**), Platt *et al.* was able to determine the activation parameters of the [C<sub>6</sub>F<sub>5</sub>H] dependent and independent processes under pseudo-zeroth-order conditions (**Table 1**). The negative entropy measured for both processes suggests that the TS is more-ordered than the preceding reaction intermediate. Based on the kinetic parameters derived from the temperature dependent studies, Platt *et al.* proposed that the [C<sub>6</sub>F<sub>5</sub>H] independent alternate process likely proceeds through an AMLA(6)-TS.<sup>68</sup> Additionally, Platt *et al.* also noted that the addition of PPh<sub>3</sub> accelerated the rate of reaction of the alternate pathway.<sup>68</sup> A similar observation was made by Larossa and co-workers, a positive order with respect to PPh<sub>3</sub> was observed in the direct arylation reaction of 4-iodoanisole **50** and (2-fluorotoluene)Cr(CO)<sub>3</sub> **49**, where C–H bond activation was primarily carried out by Ag.<sup>86</sup>

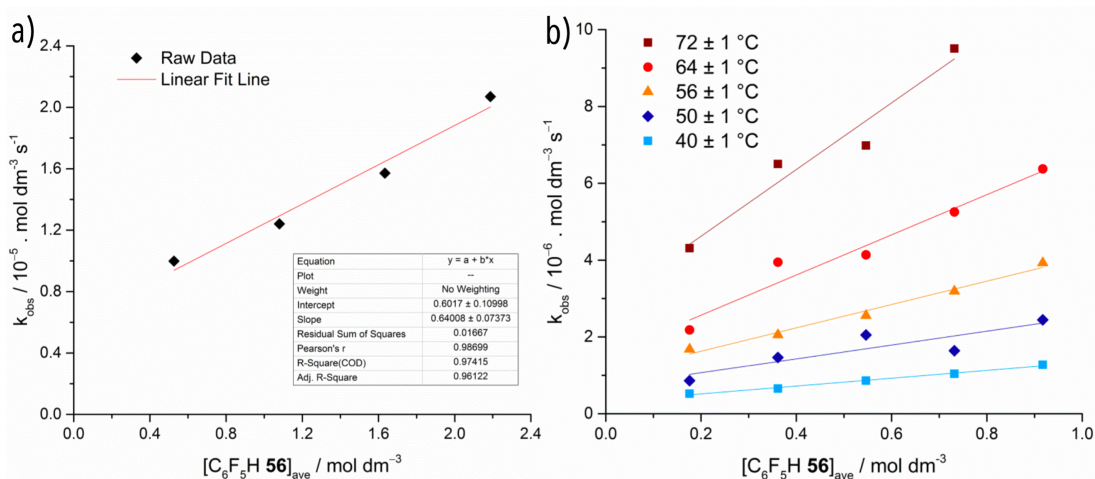


**Figure 14:** a) Plot of  $k_{\text{obs}}$  against of the  $[\text{C}_6\text{F}_5\text{H}]_{\text{ave}}$  between the concentration of 0.18M and 0.92M for the direct arylation of 4-iodotoluene. The non-zero y-intercept of the plot is usually indicative of a process which is independent of the concentration C<sub>6</sub>F<sub>5</sub>H. b) Plot of  $k_{\text{obs}}$  against  $[\text{C}_6\text{F}_5\text{H}]_{\text{ave}}$  for the reaction in **Scheme 33**, at different temperatures. (*adapted from G. Platt's PhD dissertation.*)<sup>68</sup>

**Table 1:** Thermodynamic parameters experimentally measured by Platt *et al.* for the [C<sub>6</sub>F<sub>5</sub>H] dependent and independent process

Activation parameter	[C <sub>6</sub> F <sub>5</sub> H] dependent process	[C <sub>6</sub> F <sub>5</sub> H] independent process
E <sub>a</sub> (KJ mol <sup>-1</sup> ) <sup>[a]</sup>	61.9 ± 2.6	60.9 ± 3.0
A (s <sup>-1</sup> ) <sup>[a]</sup>	6.59 × 10 <sup>5</sup>	1.51 × 10 <sup>5</sup>
ΔH <sup>‡</sup> (J mol <sup>-1</sup> ) <sup>[b]</sup>	59.1 ± 2.6	58.2 ± 3.0
ΔS (J K <sup>-1</sup> mol <sup>-1</sup> ) <sup>[b]</sup>	-143 ± 8	-155 ± 9
ΔG (298 K) <sup>‡</sup> (J mol <sup>-1</sup> ) <sup>[b]</sup>	102 ± 5	104 ± 6

<sup>[a]</sup> values determined from Arrhenius plot. <sup>[b]</sup> values determined from Eyring plot.

## 1.6 Project Aims and Objectives

The aim of this project is to investigate and elucidate the mechanism of C–H bond activation by Ag carbonate and carboxylate salts in a typical Pd-catalysed direct arylation reaction. The focus is to understand the structure and reactivity of the Ag reaction intermediates involved in catalysis and integrate this data in a proposed reaction mechanism for the C–H activation of fluorinated aromatics by Ag<sup>I</sup> salts. The following objectives were designed to meet the aims of the project and where relevant further surveys of the literature were also included in the introduction of each chapter.

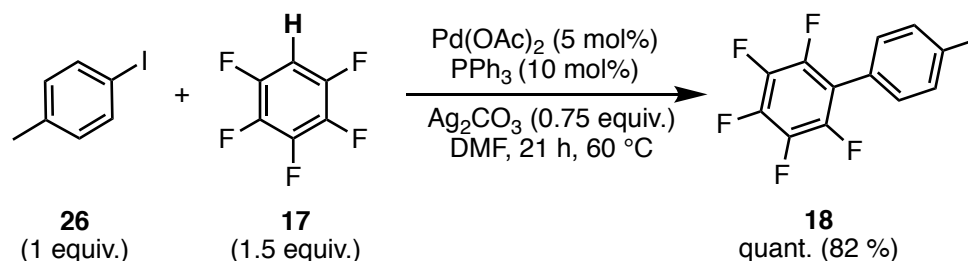
- I. The characterization and reactivity of the silver intermediates involved in the direct arylation reaction when PPh<sub>3</sub> is used as the ligand (Chapter 2).
- II. Study of the direct arylation reaction with Xphos as the ligand, and isolation and mechanistic investigation with silver intermediates to elucidate a proposed mechanism for C–H bond activation by a Ag well-defined species (Chapter 3).
- III. Further optimization of the direct arylation protocol with Xphos, scope of fluoroarenes and iodoarenes, and study of silver complexes with various dialkylarylphosphine ligands (Chapter 4).
- IV. Conclusions and Future work (Chapter 5)

## Chapter 2: Ag salts in Direct Arylation Reactions with Triphenylphosphine

### 2.1 Introduction

#### 2.1.1 Model Direct Arylation Reaction

To study the effect of silver carbonate and carboxylate salts, the palladium catalysed direct arylation of 4-iodotoluene **26** with pentafluorobenzene **17** was selected as the model system. Platt *et al.* already established the kinetics of the reaction and elucidated the role of palladium within the catalytic cycle.<sup>68</sup> Thus, this study was able to focus on the role and effect of the silver salts within the direct arylation reaction of interest (**Scheme 34**).



**Scheme 34:** The standard model reaction of the direct arylation of 4-iodotoluene with pentafluorobenzene in DMF at 60 °C.

The standard model reaction is typically carried out at 0.9 mmol of 4-iodotoluene **26** with 1.5 equiv. of pentafluorobenzene **17** with 5 mol% palladium acetate and 10 mol% triphenylphosphine as the pre-catalyst and ligand respectively and 0.75 equivalents of silver carbonate as the base. The reaction is carried out in DMF at 60 °C. The conversion of reaction was calculated by comparing the methyl <sup>1</sup>H peak of the 4-iodotoluene **26** with the product **18** in the <sup>1</sup>H NMR spectrum of the crude reaction mixture diluted in CDCl<sub>3</sub>. The conversion after heating for 21 h was quantitative, and the yield of the product after purification by flash chromatography (100 % Petroleum ether 40-60 °C) was 82 %. None of the homocoupled product was detected by <sup>1</sup>H NMR spectroscopy or by GC-MS analysis of the reaction mixture.

Due to the use of pentafluorobenzene **17** and triphenylphosphine, the standard model reaction is suitable to be studied by <sup>19</sup>F{<sup>1</sup>H} NMR and <sup>31</sup>P{<sup>1</sup>H} NMR spectroscopy, respectively. The expected product of the C–H activation of pentafluorobenzene **17** by Ag, would contain AgC<sub>6</sub>F<sub>5</sub> motif, which can be easily detected by <sup>19</sup>F{<sup>1</sup>H} NMR spectroscopy.<sup>95</sup> The coordination of phosphine ligand to the silver salt within the system is proposed to generate a more soluble phosphine-coordinated silver complex which is then capable of C–H



activation of pentafluorobenzene. Thus,  $^{31}\text{P}\{^1\text{H}\}$  NMR spectroscopy was used to probe any potential silver-phosphine interactions.

Silver is composed of two naturally occurring stable isotopes,  $^{107}\text{Ag}$  and  $^{109}\text{Ag}$  with a natural abundance of 51.8 % and 48.2 % respectively. Both isotopes are NMR active, with nuclear spins of  $\frac{1}{2}$ , and gyromagnetic ratios of  $\gamma = -1.0828 \times 10^7 \text{ T}^{-1} \text{ s}^{-1}$  ( $^{107}\text{Ag}$ ) and  $\gamma = -1.2449 \times 10^7 \text{ T}^{-1} \text{ s}^{-1}$  ( $^{109}\text{Ag}$ ). Despite the slightly lower abundance,  $^{109}\text{Ag}$  is the preferred nucleus for NMR spectroscopy due to its slightly higher receptivity and gyromagnetic ratio.<sup>96</sup> However, the direct detection of  $^{109}\text{Ag}$  by NMR spectroscopy remains a challenge and the reason for this is two-fold. A consequence of the low gyromagnetic ratio ( $\gamma$ ) of both isotopes is that  $^{109}\text{Ag}$  has low sensitivity, and the negative gyromagnetic ratio also makes it impossible to use signal enhancement techniques such as NOE. Additionally, both silver nuclei suffer from long relaxation times ( $T_1$ ), often in the order of several 100 seconds. For example, aqueous solutions of  $\text{AgNO}_3$  have  $^{109}\text{Ag}$   $T_1$  values between 900 to 1000 seconds. Thus,  $^{109}\text{Ag}$  NMR experiments are often time-intensive, as long relaxation delays are required to avoid saturation effects during signal acquisition.<sup>97</sup>

**Table 2:** Summary of relevant parameters for Ag NMR spectroscopy<sup>96,97</sup>

Isotope	Natural abundance (%)	Nuclear spin	Gyromagnetic ratio ( $\gamma$ ) $\text{T}^{-1} \text{ s}^{-1}$	Relative receptivity to $^{13}\text{C}$	Resonance Frequency at 11.7467 T (500 MHz for $^1\text{H}$ )
$^{107}\text{Ag}$	51.8	$\frac{1}{2}$	$-1.0828 \times 10^7$	0.205	20.244
$^{109}\text{Ag}$	48.2	$\frac{1}{2}$	$-1.2449 \times 10^7$	0.290	23.274

As a result, the direct detection of  $^{109}\text{Ag}$  is often limited to highly concentrated samples or the use of paramagnetic relaxation agents.<sup>98,97</sup> For instance, Berger and co-workers used  $^{109}\text{Ag}$  NMR to carry out mechanistic NMR studies the reaction of  $\text{AgOTf}$  with alkynes and were able to observe the  $\pi$ -alkyne- and alkynyl-Ag intermediates. To observe these species by  $^{109}\text{Ag}$ , all reactions were carried out in 1 M concentration using 10 mm diameter NMR tube and recorded using a 600 MHz Bruker spectrometer fitted with a 10 mm TBI probe.<sup>99</sup> Alternatively, indirect detection of Ag, using polarization transfer techniques such as INEPT<sup>100,101</sup> (insensitive Nuclei Enhancement by Polarization Transfer), HSQC<sup>102</sup> (Heteronuclear Single Quantum Coherence) or HMQC<sup>103</sup> (Heteronuclear Multiple Quantum Coherence) is also often used. This helps alleviate the long relaxation delays required for  $^{109}\text{Ag}$

NMR spectroscopy by instead relying on the  $T_1$  of the other NMR active nuclei within the system.<sup>97</sup>

The coupling of  $^{107}\text{Ag}$  and  $^{109}\text{Ag}$  with surrounding NMR active nuclei, also produces diagnostic coupling patterns, which reflect the natural abundance of the two silver isotopes.<sup>96,97</sup> This method is used to characterize silver complexes and determine the coupling of silver to proximal NMR active nuclei. For example, phosphine-coordinated silver complexes can be characterized using  $^{31}\text{P}\{^1\text{H}\}$  NMR spectroscopy. The coupling of  $^{107}\text{Ag}$  and  $^{109}\text{Ag}$  with  $^{31}\text{P}$  gives rise to a pair of overlapping doublets, with the  $^{107}\text{Ag}$ - $^{31}\text{P}$  resonance being of slightly greater intensity due to the slightly larger abundance, but smaller coupling constant when compared to the  $^{109}\text{Ag}$ - $^{31}\text{P}$  coupling (**Figure 15**). The  $^{107}\text{Ag}$ - $^{31}\text{P}$  and  $^{109}\text{Ag}$ - $^{31}\text{P}$  coupling constants have also been shown to decrease as the coordination number of Ag increases.<sup>104–107</sup> As a phosphine-coordinated silver complex is thought to be involved in the C–H bond activation of pentafluorobenzene, the use of  $^{31}\text{P}\{^1\text{H}\}$  NMR spectroscopy can be used to detect the presence of any silver complexes.

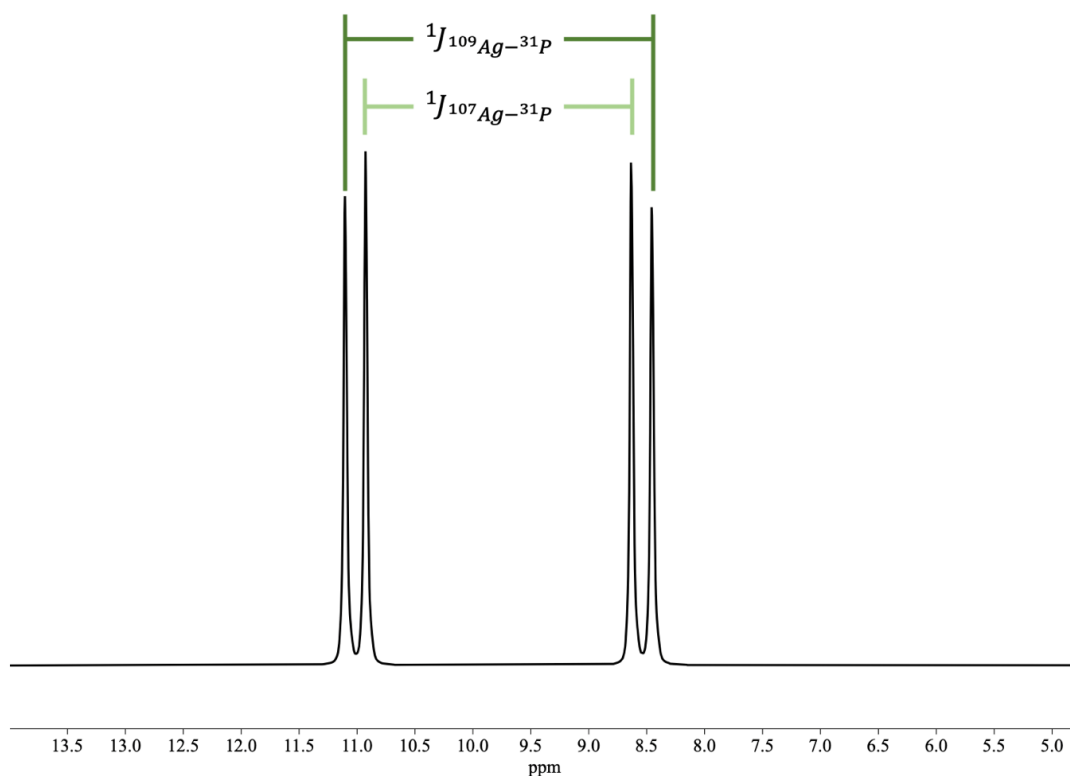
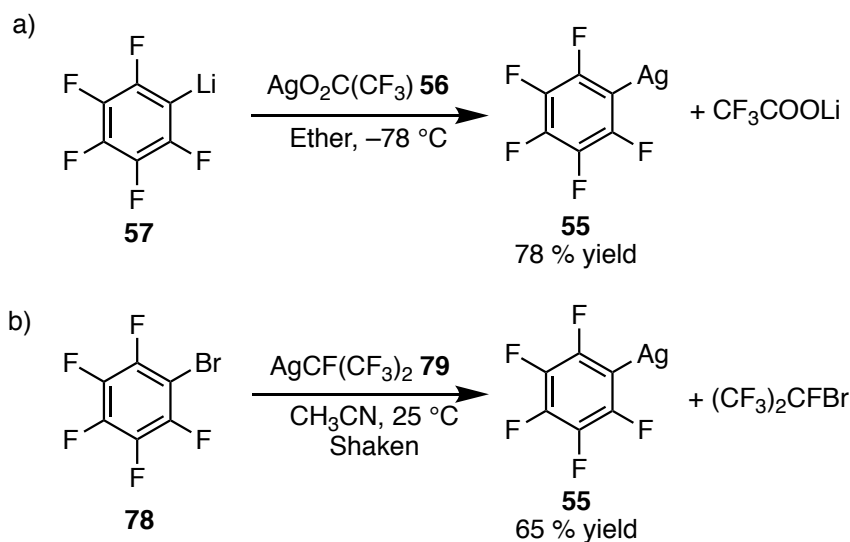


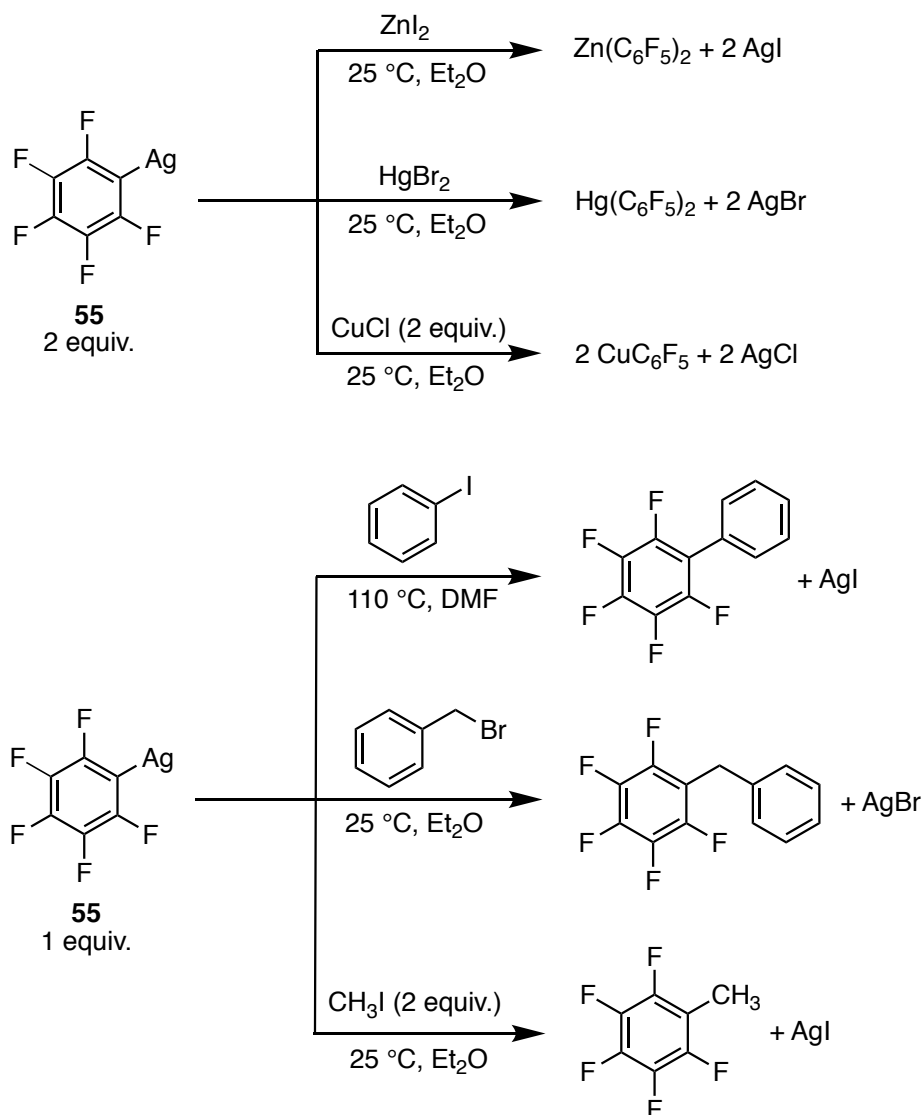
**Figure 15:** An example of a  $^{31}\text{P}\{^1\text{H}\}$  NMR spectrum showing the coupling of  $^{31}\text{P}$  with  $^{107}\text{Ag}$  and  $^{109}\text{Ag}$

## 2.1.2 Reported Synthesis and Reactivity of Pentafluorophenylsilver(I)

The first reported synthesis of  $\text{AgC}_6\text{F}_5$  **55** was by Sun and Miller, where they showed that **55** can be isolated either from the reaction of pentafluorophenyllithium **57** and silver(I) trifluoroacetate **56** or the reaction between pentafluorophenyl bromide **78** and pentafluoroisopropylsilver(I) **79** (Scheme 35).<sup>108</sup> The complex more stable and easier to isolate than the analogous  $\text{AgC}_6\text{H}_5$  complex which decomposed at  $-18\text{ }^\circ\text{C}$  and was light and air sensitive. Complex **55** was found to be a useful synthetic intermediate capable of transferring a  $-\text{C}_6\text{F}_5$  group to form new C–C or C–M. When reacted with various halide salts such as  $\text{ZnI}_2$ ,  $\text{CuCl}$  and  $\text{HgBr}_2$ , or aryl halide, **55** was capable of undergoing a ligand-exchange reaction generating an arylated product and the expected silver salt (Scheme 36).<sup>108</sup> This highlights the potential ability of  $\text{AgC}_6\text{F}_5$  **55** or  $\text{AgC}_6\text{F}_5$ -containing complex to act as a potential reaction intermediate capable of either undergoing transmetalation with a  $\text{Pd}(\text{aryl})(\text{I})(\text{PR}_3)_n$  type complex or directly reacting with the aryl halide.

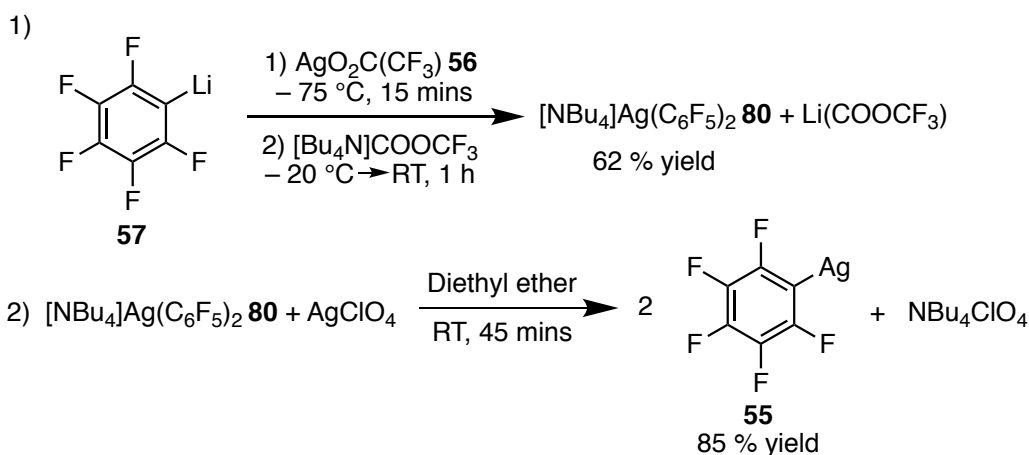


Scheme 35: Synthesis of  $\text{AgC}_6\text{F}_5$  **55** outlined by Sun and Miller.<sup>108</sup>



**Scheme 36:** Reactivity of **55** examined by Sun and Miller<sup>108</sup> (No yields reported.)

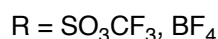
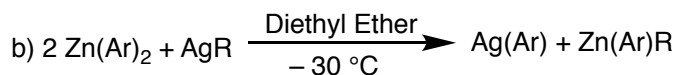
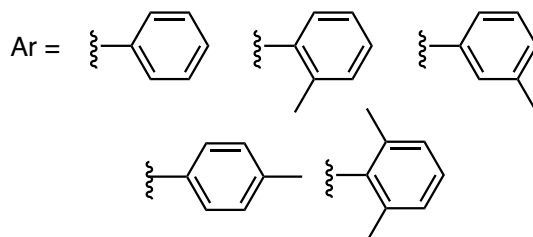
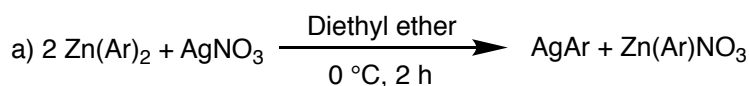
Since the original isolation of  $\text{AgC}_6\text{F}_5$  **55** published by Sun and Miller, a variety of different synthetic methodologies to prepare **55** were developed. When studying a range of anionic organometallic silver(I) complexes with the type of  $\text{Bu}_4\text{N}[\text{AgR}_2]$  ( $\text{R} = \text{C}_6\text{F}_5, \text{C}_6\text{Cl}_5$ ) among others, Abad and co-workers isolated  $\text{AgC}_6\text{F}_5$  **55** as a white solid when  $[\text{Bu}_4\text{N}]\text{Ag}(\text{C}_6\text{F}_5)_2$  **80** was reacted with  $\text{AgClO}_4$  in dry diethyl ether at room temperature. This synthetic method provided a variation on the one developed by Sun and Miller, as the  $[\text{Bu}_4\text{N}]\text{Ag}(\text{C}_6\text{F}_5)_2$  **80** is synthesised from the reaction between  $\text{LiC}_6\text{F}_5$  **57** and silver trifluoroacetate **56** and  $[\text{Bu}_4\text{N}]\text{CO}_2\text{CF}_3$  (**Scheme 37**).<sup>109</sup>



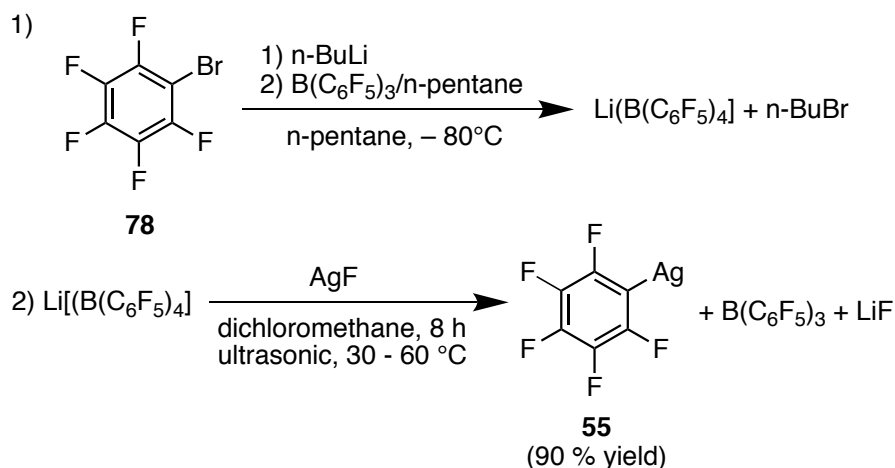
**Scheme 37:** Synthesis of  $\text{AgC}_6\text{F}_5$  **55** outlined by Abad and co-workers.<sup>109</sup>

Arylating agents such as diarylzinc,<sup>110</sup> trialkylphenyltin and -lead compounds<sup>111</sup> were also used in the synthesis of arylsilver(I) complexes. Van Der Kerk and co-workers synthesised  $\text{AgC}_6\text{H}_5$  and other methylphenylsilver(I) derivatives to high yields of 90 – 95 % using the reaction of diarylzinc with different silver salts such as  $\text{AgNO}_3$ ,  $\text{AgSO}_3\text{CF}_3$  and  $\text{AgBF}_4$  at low temperatures in diethyl ether (**Scheme 38**).<sup>110</sup> Beverwijk and Van Der Kerk have also shown that  $\text{AgNO}_3$  can be reacted with an excess of trialkylphenyltin and -lead compounds in ethanol to synthesise  $\text{AgC}_6\text{H}_5$ .<sup>111</sup> Similarly, the reaction of  $\text{AgNO}_3$  with arylating agents such as pentafluorophenyl zinc and cadmium can also be used in the synthesis of  $\text{AgC}_6\text{F}_5$  **55**.<sup>95</sup>

When studying the structure and reactivity of lithium and silver tetrakis(pentafluorophenyl)borate salts in various solvents, Villinger and co-workers found that solvent-free  $\text{Li}[\text{B}(\text{C}_6\text{F}_5)_4]$  reacts with  $\text{AgF}$  when irradiated with ultrasonic for 8 h in dichloromethane to yield  $\text{AgC}_6\text{F}_5$  **55** (90 % yield). The original  $\text{Li}[\text{B}(\text{C}_6\text{F}_5)_4]$  is synthesised from the reaction of perfluorophenyl bromide **78** with  $n\text{-BuLi}$  and  $\text{B}(\text{C}_6\text{F}_5)_3$  in pentane (**Scheme 39**). The driving force for the synthesis of  $\text{AgC}_6\text{F}_5$  **55** is proposed to be instability of the solvent-free  $\text{Ag}[\text{B}(\text{C}_6\text{F}_5)_4]$  intermediate which decomposes by abstracting a  $-\text{C}_6\text{F}_5$  group from the  $[\text{B}(\text{C}_6\text{F}_5)_4]^-$  anion. Typically,  $\text{Li}[\text{B}(\text{C}_6\text{F}_5)_4]$  is synthesized in diethyl ether or toluene and isolated as solvent adducts  $\text{Li}[\text{B}(\text{C}_6\text{F}_5)_4] \cdot \text{Et}_2\text{O}$  or  $\text{Li}[\text{B}(\text{C}_6\text{F}_5)_4] \cdot 2$  toluene. When the solvent coordinated analogues of  $\text{Li}[\text{B}(\text{C}_6\text{F}_5)_4]$  are reacted with  $\text{AgNO}_3$ , the solvent stabilized complexes/adducts  $\text{Ag}[\text{B}(\text{C}_6\text{F}_5)_4] \cdot \text{Et}_2\text{O}$  or  $\text{Ag}[\text{B}(\text{C}_6\text{F}_5)_4] \cdot 3$  toluene are then isolated.<sup>112</sup>

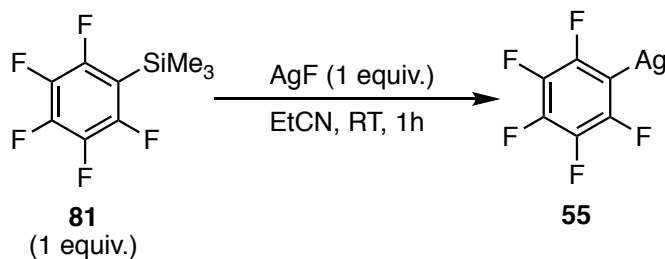


**Scheme 38:** Synthesis of  $\text{AgC}_6\text{F}_5$  **55** and other methylphenyl derivatives using diarylzinc outlined by Van Der Kerk and co-workers.<sup>110</sup>



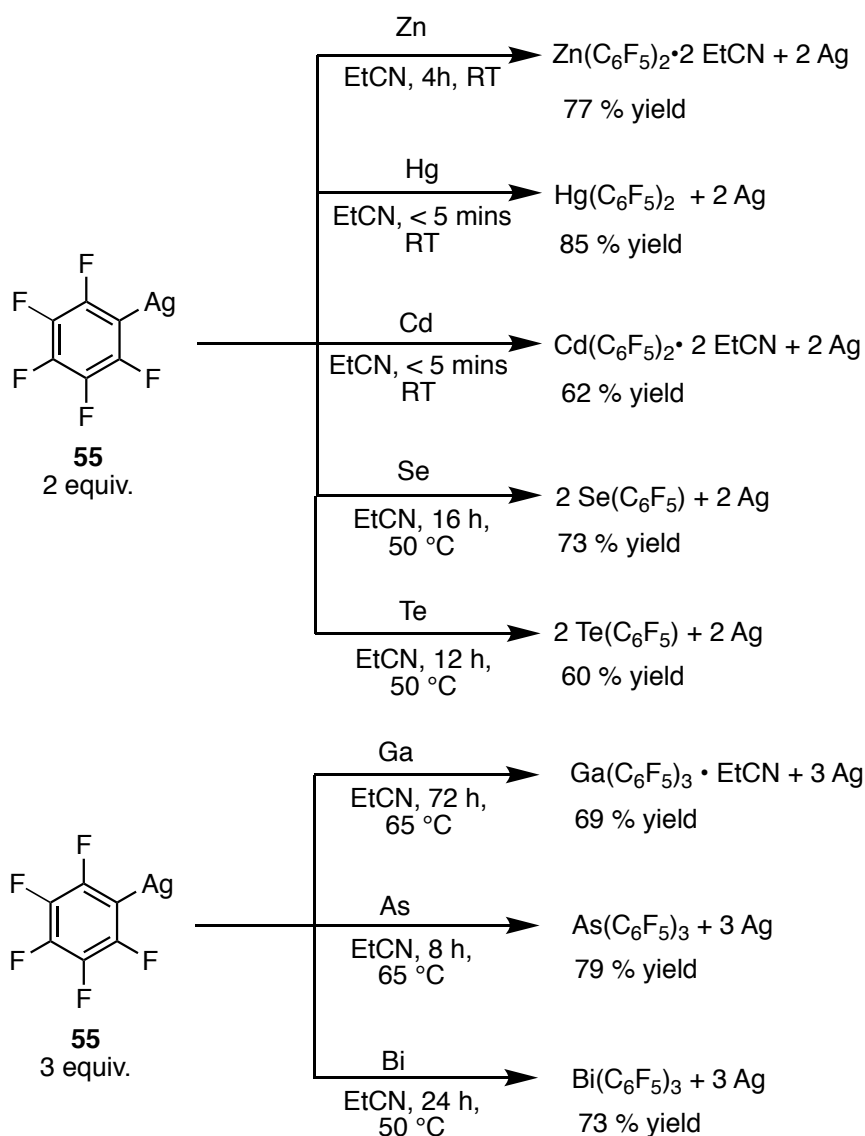
**Scheme 39:** Synthesis of  $\text{AgC}_6\text{F}_5$  **55** reported by Villinger and co-workers<sup>112</sup>

Most synthetic routes to  $\text{AgC}_6\text{F}_5$  **55** unfortunately involve the use of inconvenient to handle, explosive and toxic reagents. For example, the organolithium intermediate  $\text{LiC}_6\text{F}_5$  **57**, generated from the reaction between  $\text{C}_6\text{F}_5\text{Br}$  **78** and  $^n\text{BuLi}$ , is infamous for being highly explosive.<sup>112,95</sup> The best-known synthesis for  $\text{AgC}_6\text{F}_5$  **55** was published in 2002 by Wickleder and co-workers, where  $\text{AgC}_6\text{F}_5$  **55** is synthesised from the reaction of  $\text{AgF}$  and  $\text{SiMe}_3\text{C}_6\text{F}_5$  **81** in EtCN at room temperature (**Scheme 40**). The product was isolated as a solvent coordinated adduct,  $\text{AgC}_6\text{F}_5 \cdot \text{EtCN}$ . Heating the solvent coordinated  $\text{AgC}_6\text{F}_5 \cdot \text{EtCN}$  complex to 87 – 93 °C, causes it to lose the EtCN donor to yield  $\text{AgC}_6\text{F}_5$  **55**.<sup>95</sup>



**Scheme 40:** Synthesis of  $\text{AgC}_6\text{F}_5$  **55** outlined by Wickleder and co-workers<sup>95</sup>

Wickleder and co-workers determined the oxidative capabilities of  $\text{AgC}_6\text{F}_5$  **55** by reacting it a tenfold excess of group 12 – 16 elements, including Zn, Cd, Hg, Ga, In, Sn, As, Sb, Bi, Se, Te, Tl, Pb. This resulted in the oxidation of the element, transfer of the  $-\text{C}_6\text{F}_5$  group and production of elemental Ag. Selective few examples are depicted in **Scheme 41**.<sup>95</sup>



**Scheme 41:** Reaction of  $\text{AgC}_6\text{F}_5$  **55** with various group 12 – 16 elements<sup>95</sup>

Crystals of  $\text{AgC}_6\text{F}_5$  **55** isolated from EtCN by Wickleder and co-workers which revealed that the complex existed as an infinite polymeric chain (by XRD analysis), with the  $-\text{C}_6\text{F}_5$  acting as bridging ligands. The structure was also found to contain two crystallographically unique Ag centres, where  $\text{Ag}^1$  existed in a linear coordination with two  $-\text{C}_6\text{F}_5$  bridging ligands while  $\text{Ag}^2$  existed as a distorted tetrahedron with coordination to two EtCN ligands and two bridging  $\text{C}_6\text{F}_5$  groups.<sup>95</sup> The structure of  $\text{AgC}_6\text{F}_5$  **55** isolated from MeCN, contained a structure very similar to the EtCN analogue (**Figure 16**).<sup>112</sup> In 2015, Villinger and co-workers were able to grow colourless crystals of neat  $\text{AgC}_6\text{F}_5$  by slowly cooling saturated solution of  $\text{AgC}_6\text{F}_5$  in propyl benzene, isopropyl benzene and hexamethylbenzene. They found that neat  $\text{AgC}_6\text{F}_5$  exists as a perfectly linear infinite coordination polymer with each Ag metal centre being bridged by  $-\text{C}_6\text{F}_5$  ligands. In contrast, the nitrile coordinated  $\text{AgC}_6\text{F}_5$  XRD crystal structure alternated between bent and linear arrangements due to the distorted tetrahedron structure adopted by the  $\text{Ag}^2$  centre (**Figure 16**).<sup>113</sup>

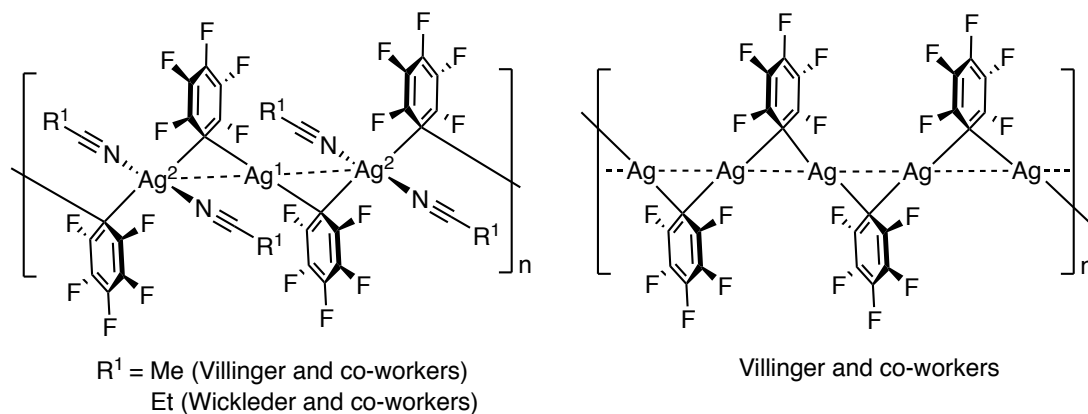


**Figure 16:** Solid state structure of neat  $\text{AgC}_6\text{F}_5$  **55**<sup>113</sup> and the nitrile adducts isolated from MeCN<sup>112</sup> and EtCN<sup>95</sup>

The structure determined by Wickleder and co-workers provided one of the first examples of an arylsilver(I) complex which exists as an infinite polymeric chain.<sup>95</sup> Previously reported arylsilver (**82**,<sup>114</sup> **83**<sup>115</sup>, **84**<sup>116</sup>) and perfluoroalkenylsilver(I) (**87**<sup>117</sup>) complexes exist as tetramers in the solid-state. Examples of diarylargentates (**85**<sup>118</sup>) crystallise as two separate ion pairs, and pentafluorophenyl(ylide)silver(I) complexes (**86**<sup>119</sup>) exist as monomers in the solid-state. A few select examples of these structures have been illustrated in **Figure 17**.



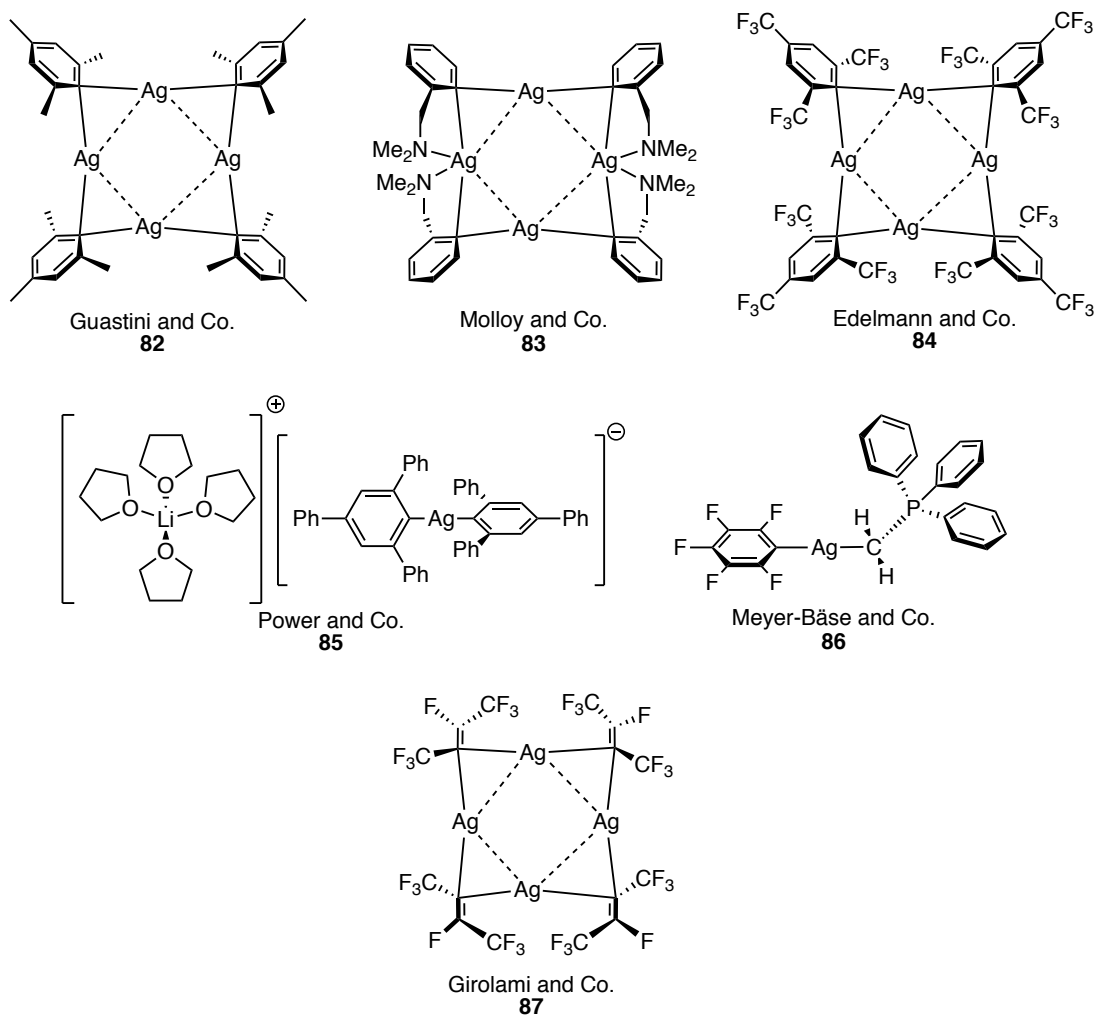


**Figure 17:** Select examples of aryl-<sup>114,115,116</sup> and perfluoroalkenylsilver<sup>117</sup> complexes which are tetrameric in the crystal structure, and diarylargentate<sup>118</sup> and pentafluorophenyl(ylide)silver<sup>119</sup> complexes.

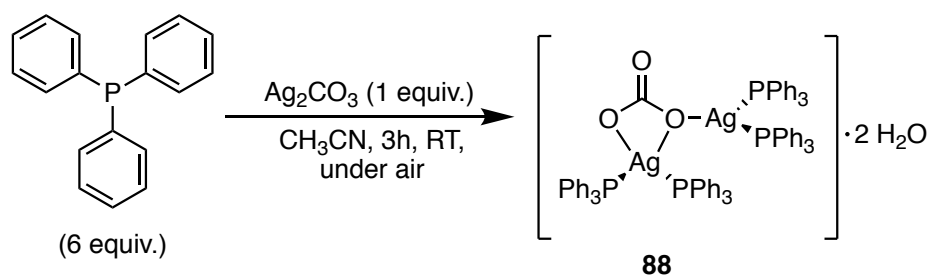
### 2.1.3 Reported Synthesis and Structure of Phosphine-Coordinated Silver(I)

#### Carbonate Complexes

Many phosphine-coordinated Ag complexes are known and well-characterised in the literature, however examples of complexes containing carbonate ligands are rare.<sup>120,104</sup> In 2011, White and co-workers outlined the synthesis of several triphenylphosphine-coordinated silver complexes with carbonate and hydrogen carbonate ligands using both mechanochemically and from solution-based methods. The solid-state structures of the complexes were determined by X-ray diffraction, IR spectroscopy and <sup>31</sup>P CP MAS NMR spectroscopy.<sup>121</sup>

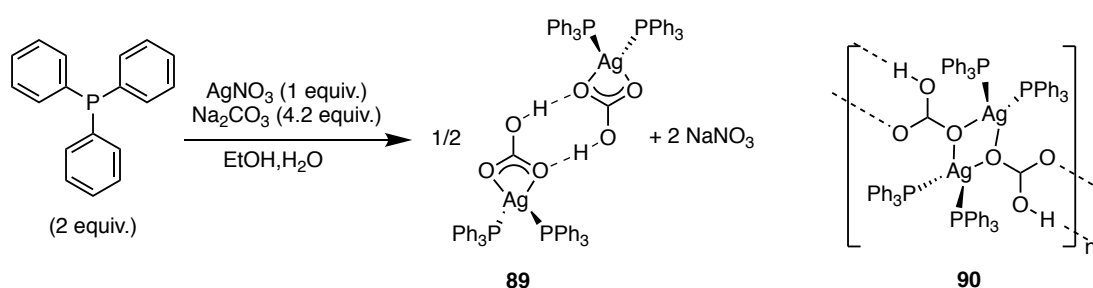
They isolated one of the first examples of triphenylphosphine-coordinated silver(I) carbonate complex [Ag(PPh<sub>3</sub>)<sub>2</sub>]<sub>2</sub>(CO<sub>3</sub>)•2H<sub>2</sub>O **88** as an adduct of water from the reaction

between silver carbonate with 6 equivalents of PPh<sub>3</sub> in acetonitrile under air. Carrying out the reaction under rigorous air- and water free conditions resulted in no formation of product. The crystal structure of **88** revealed that complex was binuclear with both the silver centres coordinated to two PPh<sub>3</sub> ligands. The <sup>31</sup>P CP MAS NMR spectrum of **88** revealed the presence of a doublet centred at δ 6.8 with <sup>1</sup>J<sub>107,109Ag-31P</sub> = 421 Hz, indicating the four P atoms are equivalent in the solid-state.<sup>121</sup>



**Scheme 42:** The synthesis of [Ag(PPh<sub>3</sub>)<sub>2</sub>]<sub>2</sub>(CO<sub>3</sub>)·2H<sub>2</sub>O **88** outlined by White and co-workers.<sup>121</sup>

White and co-workers also found that the reaction between AgNO<sub>3</sub> and 4.2 equivalents of Na<sub>2</sub>CO<sub>3</sub> with 2 equivalents of PPh<sub>3</sub> in a mixture of ethanol and water resulted in the formation of triphenylphosphine-coordinated hydrogen-carbonate complex [Ag(PPh<sub>3</sub>)<sub>2</sub>(κ<sup>2</sup>-HCO<sub>3</sub>)]<sub>2</sub> **89** with [Ag(PPh<sub>3</sub>)<sub>3</sub>HCO<sub>3</sub>]<sub>n</sub> **90** being isolated only once adventitiously from the same experimental procedure. X-ray analysis of **89** and **90** was used to confirm the structure of the complex. The two phosphorus atoms of the **89** monomeric unit were found to be inequivalent by <sup>31</sup>P CP MAS NMR spectroscopy, resulting in an ABX spin system (A,B = <sup>31</sup>P, X = <sup>107,109</sup>Ag). The spectrum revealed the presence of two AB quartets centred at δ 6.1 (<sup>1</sup>J<sub>107,109Ag-31P</sub> = 475 Hz) and δ 7.2 (<sup>1</sup>J<sub>107,109Ag-31P</sub> = 469 Hz) with <sup>2</sup>J<sub>PP</sub> = 147 Hz. The coupling of <sup>31</sup>P to the <sup>107</sup>Ag and <sup>109</sup>Ag isotopes could not be resolved.<sup>121</sup>

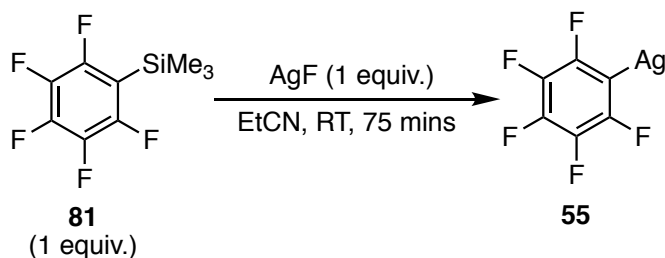


**Scheme 43:** The synthesis of [Ag(PPh<sub>3</sub>)<sub>2</sub>(κ<sup>2</sup>-HCO<sub>3</sub>)]<sub>2</sub> **89** outlined by White and co-workers.<sup>121</sup>

In contrast, the  $^{31}\text{P}$  CP MAS NMR spectrum of two  $\text{PPh}_3$  ligands **90** were equivalents, with a pair of doublets centred at  $\delta$  5.4 ( $^1J_{^{107,109}\text{Ag}-^{31}\text{P}} = 432$  Hz) and the coupling of  $^{31}\text{P}$  to  $^{107}\text{Ag}$  and  $^{109}\text{Ag}$  isotopes remained unresolved. The presence of monomeric  $[\text{Ag}(\text{PPh}_3)_2(\kappa^2\text{-HCO}_3)]_2$  **89** was detected in the spectrum of **90**. While the CPMAS NMR spectra of **89** and **90** were distinctly different, the IR spectrum of the two complexes were almost identical.

## 2.2 Results: Detection of Pentafluorophenyl Silver Intermediate

As a starting point, an authentic sample of  $\text{AgC}_6\text{F}_5$  **55** was prepared, using the synthetic procedure outlined by Wickleder and co-workers.<sup>95</sup> The reaction of  $\text{AgF}$  and  $\text{SiMe}_3\text{C}_6\text{F}_5$  **81** in EtCN was carried out at room temperature and the desired  $\text{AgC}_6\text{F}_5$  **55** complex was isolated as a lilac solid (78% yield) (Scheme 44). The  $^{19}\text{F}\{^1\text{H}\}$  NMR spectrum of **55** in acetonitrile showed three resonances at  $\delta$   $-107.4$  (2 F, m, 2,6-F),  $-160.6$  (1 F, t,  $J = 19.4$  Hz, 4-F),  $-163.1$  (2 F, m, 3,5-F). Due to the complex splitting pattern of the *ortho*-F resonance, the  $^3J_{\text{Ag-F}}$  coupling could not be identified. The LIFDI-MS spectrum of **55** dissolved in DMF contained the molecular ion peak  $[\text{AgC}_6\text{F}_5]^+$  but also revealed the presence of  $[\text{Ag}_2\text{C}_6\text{F}_5]^+$  and solvent coordinated silver clusters such as  $([\text{Ag}_2\text{C}_6\text{F}_5\text{DMF}]^+)$ .



**Scheme 44:** Synthesis of  $\text{AgC}_6\text{F}_5$  **55** from the reaction of **81** and  $\text{AgF}$  in EtCN

Wickleder and co-workers isolated crystals of **55** as a 1:1 adduct of EtCN and coordination of EtCN was also observed in the crystal structure. Due to the strongly coordinating nature of **55**, they also found the chemical shift of the  $\text{AgC}_6\text{F}_5$  **55** to be strongly solvent dependent.<sup>95</sup>

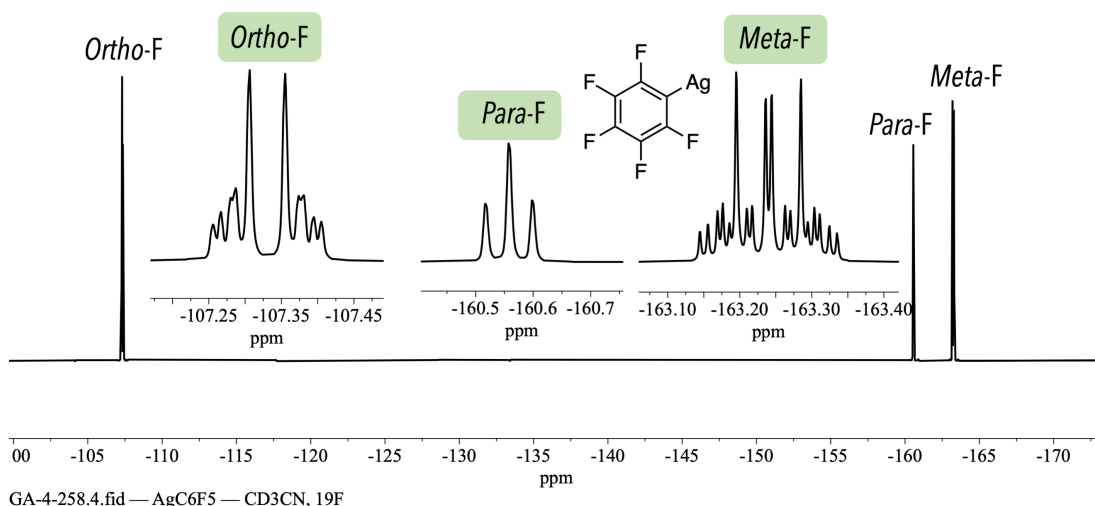
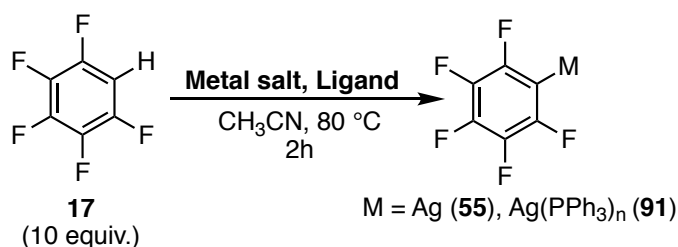


**Figure 18:** The  $^{19}\text{F}\{^1\text{H}\}$  NMR (470.6 MHz,  $\text{CD}_3\text{CN}$ , 25 °C) spectrum of **55**

An initial screening was conducted to determine if the silver salts used in the direct arylation of 4-iodotoluene **26** could activate the C–H bond of pentafluorobenzene **17**. In the

standard catalytic reaction studied by Platt *et al.*, Ag<sub>2</sub>CO<sub>3</sub> was the preferred base under the optimized reaction conditions. However, the pre-catalyst Pd<sub>3</sub>(OAc)<sub>6</sub> has a much higher solubility in DMF, as opposed to Ag<sub>2</sub>CO<sub>3</sub>, thus, the possibility of *in situ* generation of AgOAc cannot be ignored. The C–H bond activation capability of both Ag<sub>2</sub>CO<sub>3</sub> and AgOAc was considered, in a reaction with 10 equivalents of pentafluorobenzene **17**, in acetonitrile. The product of C–H activation is expected to contain a AgC<sub>6</sub>F<sub>5</sub> motif which was compared to the authentic sample of **55**. The % conversion to AgC<sub>6</sub>F<sub>5</sub> **55** from pentafluorobenzene **17** was monitored using <sup>19</sup>F{<sup>1</sup>H} NMR spectroscopy. The expected product AgC<sub>6</sub>F<sub>5</sub> **55** had a distinct *ortho*-F resonance which is significantly deshielded at δ –107.4 in CH<sub>3</sub>CN, whereas the *ortho*-F resonance for C<sub>6</sub>F<sub>5</sub>H **17** appears at δ –139 (**Figure 19**). The AgC<sub>6</sub>F<sub>5</sub> **55** complex exists as infinite polymer chains which are stabilized by highly coordinating nitrile solvents.<sup>95</sup> Hence, for ease of detecting and to stabilize the potential AgC<sub>6</sub>F<sub>5</sub> **55** intermediate, CH<sub>3</sub>CN was chosen as the preferred solvent. The reactions carried out are summarised in **Table 3**.

**Table 3:** Screening the reaction of different silver salts and additives with pentafluorobenzene **17**



Entry	Metal salt	Ligand	Conversion <sup>[a]</sup> (%)
1	AgOAc (1 equiv.)	-	0
2	Ag <sub>2</sub> CO <sub>3</sub> (1 equiv.)	-	Trace
3	Ag <sub>2</sub> CO <sub>3</sub> (1 equiv.) + AgOAc (1 equiv.)	-	Trace
4	AgOAc (1 equiv.)	PPh <sub>3</sub> (2 equiv.)	0
5	Ag <sub>2</sub> CO <sub>3</sub> (1 equiv.) + AgOAc (1 equiv.)	PPh <sub>3</sub> (2 equiv.)	25
6	Ag <sub>2</sub> CO <sub>3</sub> (1 equiv.)	PPh <sub>3</sub> (2 equiv.)	100
7	AgOAc (1 equiv.) + Cs <sub>2</sub> CO <sub>3</sub> (1 equiv.)	-	83
8 <sup>[b]</sup>	AgOAc (1 equiv.) + Cs <sub>2</sub> CO <sub>3</sub> (2.5 equiv.)	-	45
9	AgNO <sub>3</sub> (1 equiv.) + Cs <sub>2</sub> CO <sub>3</sub> (1 equiv.)	-	Trace

<sup>[a]</sup> The % conversion was calculated by integrating the *ortho*-F resonance of the starting material C<sub>6</sub>F<sub>5</sub>H (δ –139) with respect to **55** (δ –107.4). For reactions with PPh<sub>3</sub>, the *ortho*-F resonance of **91** (δ –106.4) is used.

<sup>[b]</sup> 5 equivalents of pentafluorobenzene used in this experiment.

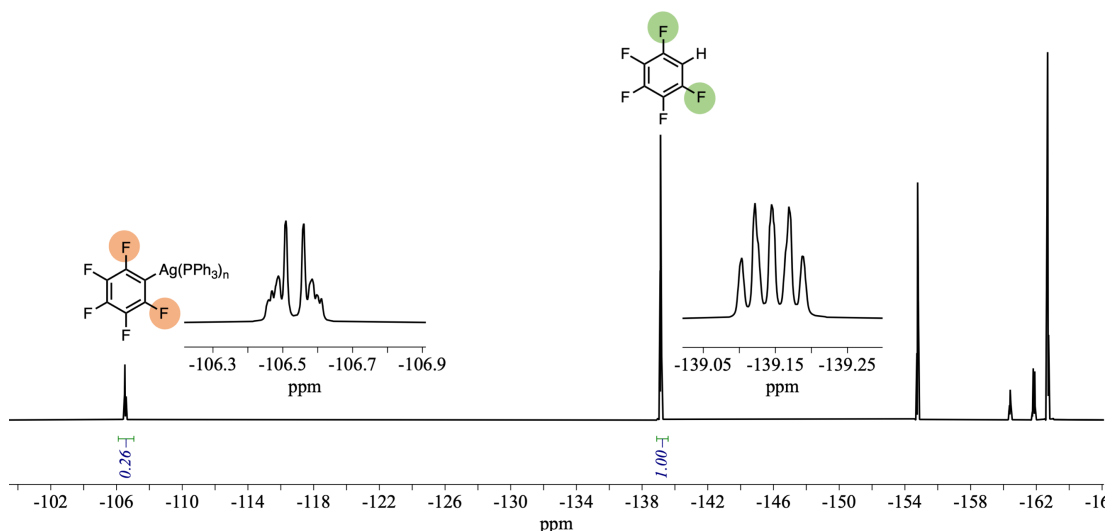


**Figure 19:** The  $^{19}\text{F}\{^1\text{H}\}$  (MHz, 25 °C,  $\text{CH}_3\text{CN}$ ) spectrum of the reaction mixture of Entry 6, Table 3. The spectrum shows the *ortho*-F resonances of  $\text{C}_6\text{F}_5\text{H}$  **17** and  $\text{AgC}_6\text{F}_5(\text{PPh}_3)_n$  **91** used to calculate the % conversion.

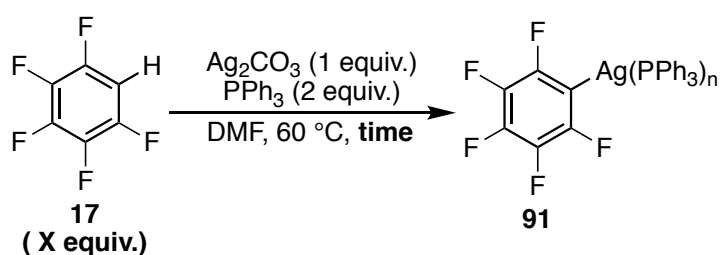
The reaction of  $\text{Ag}_2\text{CO}_3$  with 10 equivalents of  $\text{C}_6\text{F}_5\text{H}$ , resulted in trace production of  $\text{AgC}_6\text{F}_5$  **55** detected by the appearance of a multiplet at  $\delta -107.4$  in the  $^{19}\text{F}\{^1\text{H}\}$  NMR spectrum of the reaction mixture after heating at 80 °C for 2 h. This region was completely silent when  $\text{AgOAc}$  was used as the silver salt (Table 3, Entry 1 and 2). Zhu and co-workers found that the addition of a carbonate base such as  $\text{Cs}_2\text{CO}_3$  was a required additive for C–H activation by  $\text{AgOAc}$ .<sup>88</sup> Hence in Entry 3, both  $\text{AgOAc}$  and  $\text{Ag}_2\text{CO}_3$  were added, and this also resulted in trace production of  $\text{AgC}_6\text{F}_5$  **55**.

When  $\text{AgOAc}$  is used in conjunction with 1 equiv. of  $\text{Cs}_2\text{CO}_3$  the percent conversion of  $\text{C}_6\text{F}_5\text{H}$  to  $\text{AgC}_6\text{F}_5$  **55** is 83 % and the conversion drops to 45% with 2.5 equiv. of  $\text{Cs}_2\text{CO}_3$  (Entry 7 and 8). These reactions are similar to the conditions employed by Zhu and co-workers, and it can be concluded that the presence of  $\text{Cs}_2\text{CO}_3$  or another soluble base is required for C–H bond activation by  $\text{AgOAc}$ . Since solubility is an issue with Ag salts such as  $\text{Ag}_2\text{CO}_3$ , a combination of  $\text{AgNO}_3$  and  $\text{Cs}_2\text{CO}_3$  was incorporated as a more soluble counterpart to  $\text{Ag}_2\text{CO}_3$ , with the assumption that  $\text{NO}_3$  does not have a detrimental effect on C–H activation. The reaction between  $\text{AgNO}_3$  and  $\text{Cs}_2\text{CO}_3$  also resulted in only trace amount of  $\text{AgC}_6\text{F}_5$  production (Entry 9).

The addition of  $\text{PPh}_3$  to the reaction has a beneficial effect on C–H bond activation, when used in conjunction with  $\text{Ag}_2\text{CO}_3$  as 100 % conversion to  $\text{AgC}_6\text{F}_5(\text{PPh}_3)_n$  **91** with respect to  $\text{C}_6\text{F}_5\text{H}$  (Figure 19) was detected (Entry 6) by its *ortho*-F resonance at  $\delta -106.4$ . The bond between silver and  $\text{PPh}_3$  is highly labile at room temperature; thus, only a singlet at  $\delta 9.5$  was detected in the  $^{31}\text{P}\{^1\text{H}\}$  NMR spectrum. The chemical shift of  $\text{PPh}_3$  is  $\delta -5$ , which indicates

that the PPh<sub>3</sub> is interacting with and coordinating to the silver complex present in solution. AgOAc seems to have a detrimental effect (**Entry 5**), as the addition of 1 equivalent of AgOAc resulted in the % conversion dropping to 25%. The reaction of AgOAc and PPh<sub>3</sub> resulted in no product, indicating that the AgOAc is not capable of C–H activation in this system (**Entry 4**).

**Table 4:** The reaction of Ag<sub>2</sub>CO<sub>3</sub> and PPh<sub>3</sub> with C<sub>6</sub>F<sub>5</sub>H **17** in DMF at 60 °C



Entry	Equivalents of C <sub>6</sub> F <sub>5</sub> H	Time (h)	Conversion <sup>[a]</sup> (%)
1	10	2	80
		4	90
		24	100
2	1	2	77
		4	83
		24	90
		48	90

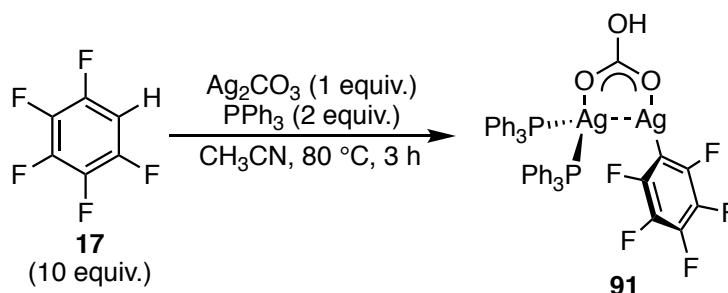
<sup>[a]</sup> The % conversion was calculated by integrating the *ortho*-F resonance of the starting material C<sub>6</sub>F<sub>5</sub>H ( $\delta$  –139.2) with respect to the AgC<sub>6</sub>F<sub>5</sub> complex ( $\delta$  –106.2) in DMF.

The reaction of Ag<sub>2</sub>CO<sub>3</sub> and PPh<sub>3</sub> with 10 equivalents of C<sub>6</sub>F<sub>5</sub>H resulted in quantitative conversion to the silver intermediate. Hence these conditions were used in the reactions performed in DMF, with both 10 equiv. and 1 equiv. of C<sub>6</sub>F<sub>5</sub>H. When 10 equiv. of C<sub>6</sub>F<sub>5</sub>H was used, the reaction reached 100% conversion within 24 h (**Entry 1**). With **Entry 2**, a maximum of 90% conversion was achieved with the stoichiometric reaction in 24 h, further heating for an additional 24 h resulted in the decomposition of complex which can be seen in the <sup>19</sup>F{<sup>1</sup>H} NMR spectrum.

These results show that Ag<sub>2</sub>CO<sub>3</sub> in the presence of PPh<sub>3</sub> can mediate the C–H bond activation of C<sub>6</sub>F<sub>5</sub>H and the expected intermediate is observed *via* <sup>19</sup>F{<sup>1</sup>H} NMR spectroscopy. Thus, under the catalytic conditions it is possible that the Ag<sub>2</sub>CO<sub>3</sub> and PPh<sub>3</sub> present in the solution activates the C–H bond of C<sub>6</sub>F<sub>5</sub>H. During the standard reaction, there is a far greater excess of Ag<sub>2</sub>CO<sub>3</sub> (0.75 equiv. with respect to 4-iodotoluene) than PPh<sub>3</sub> (10 mol% or 20 mol%); thus, the process is likely dependent on the amount of PPh<sub>3</sub> present.

## 2.3 Attempted Isolation and Characterization of the $\text{AgC}_6\text{F}_5$ containing Intermediate

To determine the structure of **91**, the reaction of  $\text{Ag}_2\text{CO}_3$  with  $\text{C}_6\text{F}_5\text{H}$  **17** in the presence of 2 equiv. of  $\text{PPh}_3$  was carried out in acetonitrile (**Scheme 45**). Dark brown crystals of **91** were grown by slowly cooling a saturated solution of the complex in acetonitrile to  $-18\text{ }^\circ\text{C}$ .



**Scheme 45:** The synthesis of an aryl-silver complex from the reaction between  $\text{Ag}_2\text{CO}_3$  and  $\text{PPh}_3$  with 10 equivalents of  $\text{C}_6\text{F}_5\text{H}$  **17** in acetonitrile.

The x-ray diffraction analysis of single crystals revealed that **91** exists as a dimeric structure  $\text{Ag}_2(\text{PPh}_3)_2(\text{C}_6\text{F}_5)(\mu_2\text{-HCO}_3)$  in the solid-state (**Figure 20**). Two silver metal centres were bridged by a hydrogen carbonate ligand. The  $\text{Ag}\cdots\text{Ag}$  bond length is  $2.9576(8)\text{ \AA}$ , is longer than the  $\text{Ag}\text{-Ag}$  bond in metallic Ag ( $2.89\text{ \AA}$ ), and some of the other Ag complexes previously reported (**Figure 22**).<sup>112–116</sup> However, it is shorter than  $2r_w$  ( $3.44\text{ \AA}$ ), where  $r_w = 1.72\text{ \AA}$  is the van der Waals radius of Ag, suggesting a weak interaction between the two metal centres. One of the silver centres contained the  $-\text{C}_6\text{F}_5$  moiety and the  $\text{Ag}\text{-}(\text{C}_6\text{F}_5)$  bond length is  $2.056(10)\text{ \AA}$ . For comparison, the  $\text{Ag}\text{-}(\text{C}_6\text{F}_5)$  distance in the neat polymeric structure of  $\text{AgC}_6\text{F}_5$  is  $2.195(3)\text{ \AA}$ .<sup>113</sup> The MeCN coordinated  $\text{AgC}_6\text{F}_5\cdot\text{MeCN}$  structure contained two crystallographically unique Ag metal centres with the  $\text{Ag}(1)\text{-C}_6\text{F}_5$  bond distance  $2.381(2)\text{ \AA}$  being longer than the  $\text{Ag}(2)\text{-C}_6\text{F}_5$  bond distance of  $2.147(2)\text{ \AA}$ .<sup>112</sup>

The second silver centre was coordinated to two  $\text{PPh}_3$  ligands with an  $\text{Ag}\text{-PPh}_3$  bond of  $2.4317(18)$ . The  $\text{O}\text{-Ag}(\text{C}_6\text{F}_5)$  bond length is  $2.075(9)\text{ \AA}$  and the distance between the  $\text{O}\text{-Ag}(\text{PPh}_3)_2$  is  $2.301(5)\text{ \AA}$ . However, the quality of the crystal was found to be quite poor, with a final R factor of 0.0885, which leads to some ambiguity in the identity of the bridging ligand when refining the crystal structure. This is also evident in the large distortions around the carbonyl carbon of **91** (**Figure 20**). The replacement of the hydrogen carbonate with acetate, led to an improvement in the refinement with as R factor of 0.0881 (**Figure 21**). There was no acetate used in the reaction, and later  $^{13}\text{C}$  labelling experiments helped support the presence of hydrogen carbonate within the structure. Thus, the structure of the complex is assumed to be **91** in the solid state.



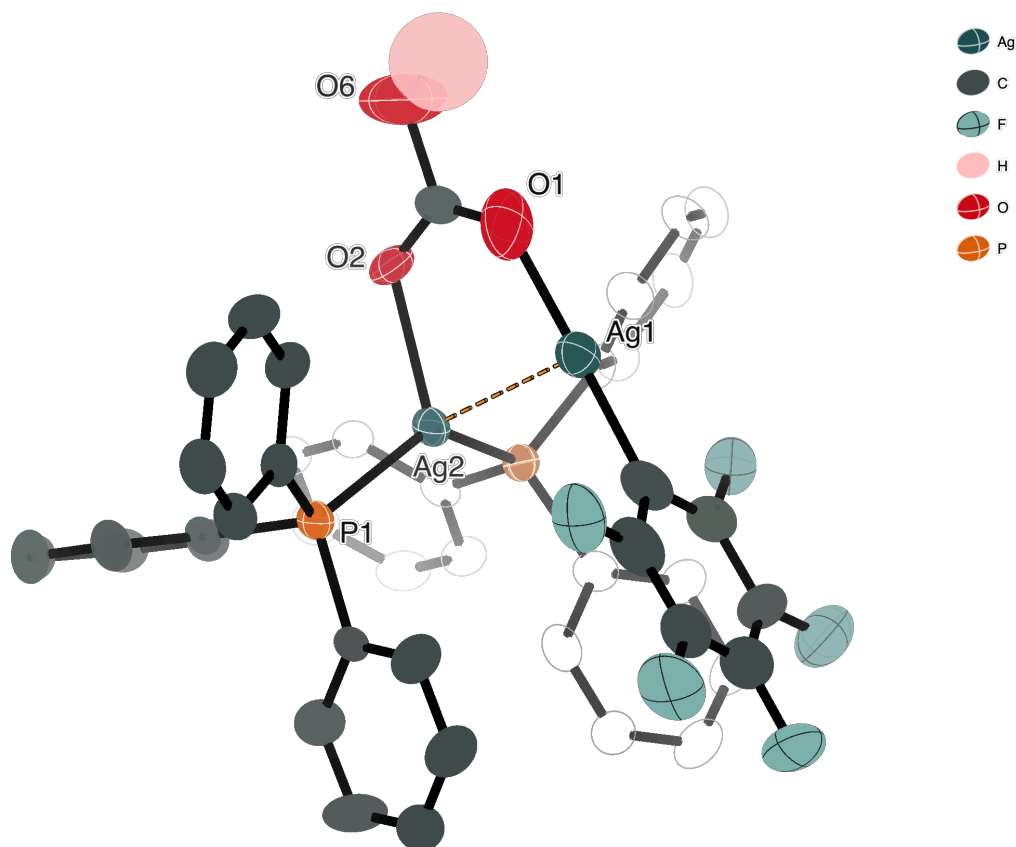


**Figure 20:** The crystal structure of **91** with the bridging ligand modelled as hydrogen carbonate

**Table 5:** Principal bond lengths and angles of the carbonate and acetate modelled versions of **91**

Bond	Carbonate modelled <b>91</b>	Acetate modelled <b>91</b>
	Bond length (Å)	
Ag(1)–O(1)	2.075(1)	2.074(1)
Ag(1)–C(1)	2.056(1)	2.056(1)
Ag(2)–O(2)	2.301(5)	2.302(5)
Ag(2)–P(1)	2.432(2)	2.431(2)
Ag(2)–P(2)	2.432(2)	2.431(2)
Ag(1)–Ag(2)	2.958(9)	2.958(9)
Bond angles	Angle (°)	
O(2)–Ag(2)–Ag(1)	79.3(2)	79.3(1)
O(1)–Ag(1)–Ag(2)	82.6(2)	82.6(2)
O(1)–Ag(1)–C(1)	178.5(4)	178.5(9)
O(2)–Ag(2)–P(1)	109.8(2)	109.8(2)
O(2)–Ag(2)–P(2)	110.4(2)	110.5(2)

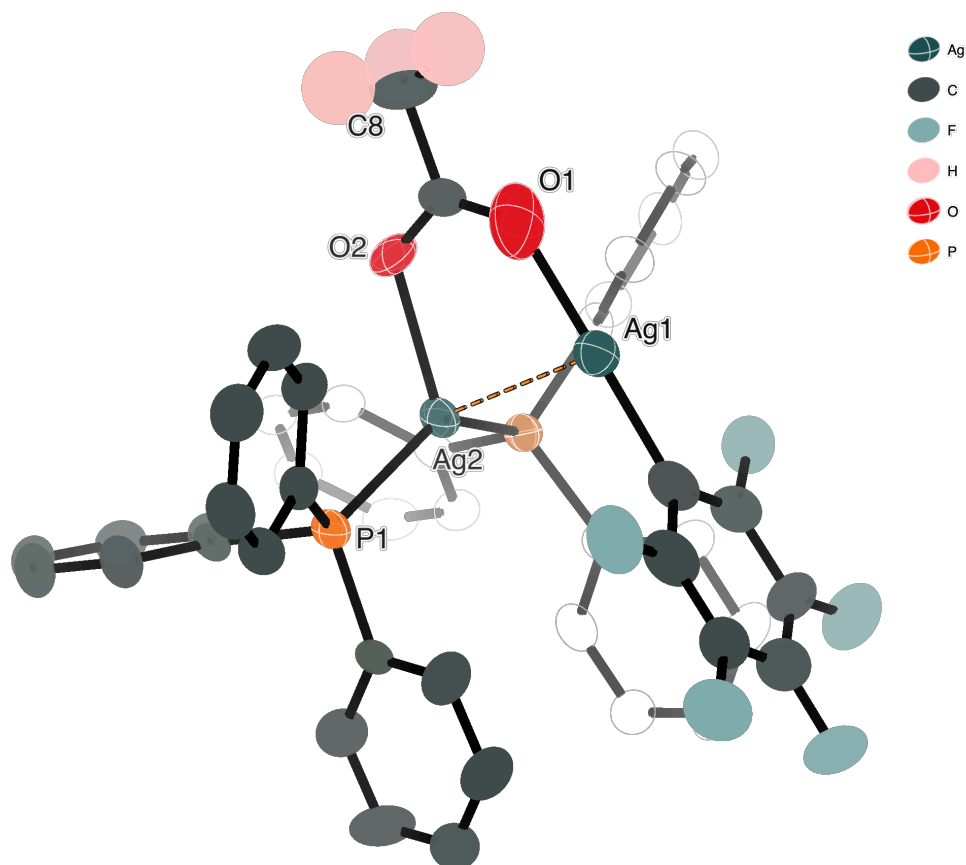


**Figure 21:** The crystal structure of **91** with the bridging ligand modelled as acetate, which provided a better fit with the model. However,  $^{13}\text{C}$ -labelling experiments support the presence of hydrogen carbonate within the structure. Some disorder around the bridging ligand present.

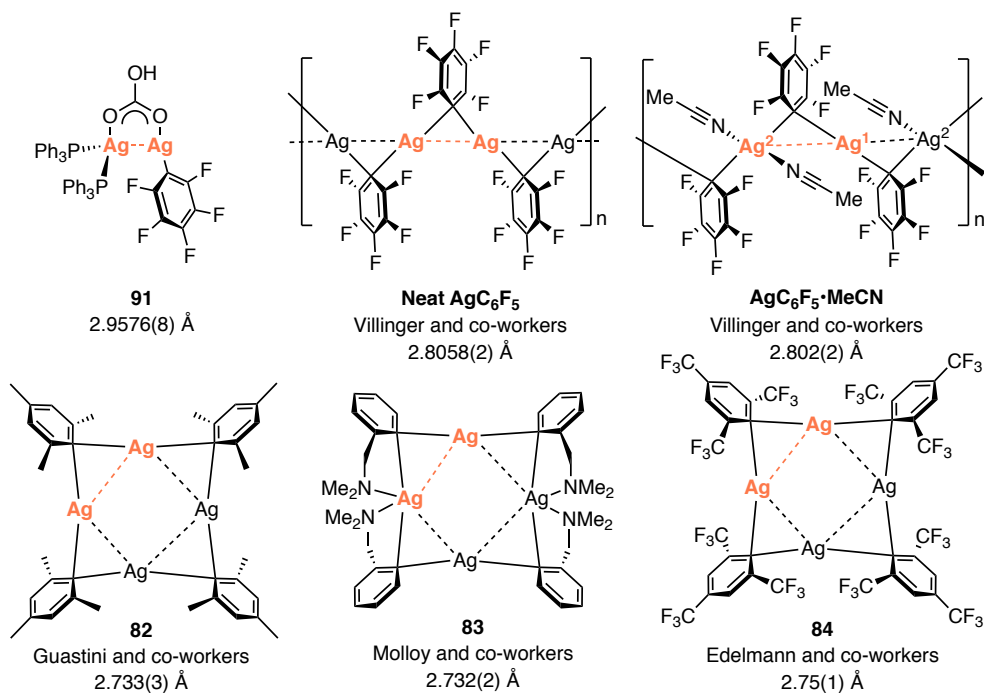


**Figure 22:** Comparison of various Ag---Ag bond distances (orange) found in different literature Ag complexes. <sup>112–116</sup>

The  $^{19}\text{F}\{^1\text{H}\}$  NMR spectrum of  $\text{Ag}_2(\text{PPh}_3)_2(\text{C}_6\text{F}_5)(\mu_2\text{-HCO}_3)$  **91** crystals, showed the characteristic *ortho*-F resonance at  $\delta -106.3$  as well as the corresponding *para*-F and *meta*-F peaks at  $\delta -159.2$  and  $\delta -161.4$  respectively. However, the dark brown crystals were also contaminated with a 30 %  $\text{C}_6\text{F}_5\text{H}$  **17** impurity, as determined by  $^{19}\text{F}\{^1\text{H}\}$  NMR spectroscopy (**Figure 23**). Attempts to remove the impurity using subsequent recrystallizations or a high vacuum Schlenk line were unsuccessful. The  $^{31}\text{P}\{^1\text{H}\}$  NMR spectrum of the complex at room temperature contained only a singlet at  $\delta 9$ , suggesting a very rapid exchange due to the lability of the Ag–PPh<sub>3</sub> bond. To understand the bonding mode of the PPh<sub>3</sub> in **91**, low-temperature NMR spectroscopy was used to freeze the rapid exchange of the PPh<sub>3</sub> ligand and gain information of the complex in solution.

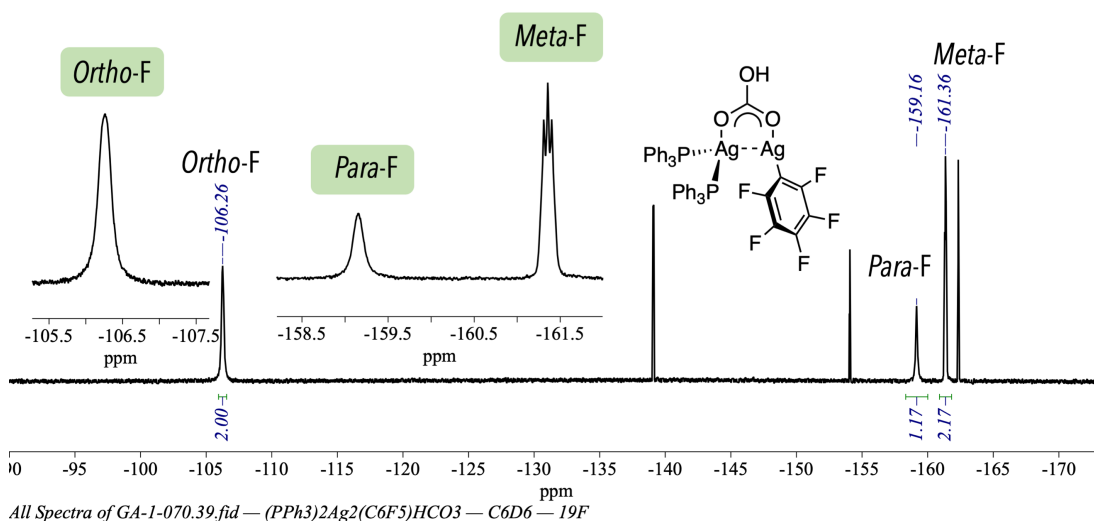


**Figure 23:** The  $^{19}\text{F}\{^1\text{H}\}$  NMR (470 MHz,  $\text{C}_6\text{D}_6$ , 25 °C) spectrum of  $\text{Ag}_2(\text{PPh}_3)_2(\text{C}_6\text{F}_5)(\mu_2\text{-HCO}_3)$  **91**

A sample of  $\text{Ag}_2(\text{PPh}_3)_2(\text{C}_6\text{F}_5)(\mu_2\text{-HCO}_3)$  **91** was prepared in toluene- $d_8$  and was cooled down to  $-60^\circ\text{C}$  (213 K) and the temperature was gradually decreased incrementally:  $-70^\circ\text{C}$  (203 K),  $-80^\circ\text{C}$  (193 K),  $-85^\circ\text{C}$  (188 K) and  $-90^\circ\text{C}$  (183 K). At room temperature (298 K), the complex is observed as a sharp singlet at  $\delta 9.42$  in the  $^{31}\text{P}\{^1\text{H}\}$  NMR spectrum, however upon cooling this peak gradually broadened and resolved into multiple resonances (**Figure 24**). At  $-80^\circ\text{C}$  (193 K), a pair of sharp doublets at  $\delta 9.79$  were observed. These doublets are characteristic of Ag–P coupling and resulted from the phosphorus coupling with  $^{107}\text{Ag}$  and  $^{109}\text{Ag}$  (natural abundance of 51% and 49% respectively). The coupling constants of  $^{31}\text{P} - ^{107}\text{Ag}$  and  $^{31}\text{P} - ^{109}\text{Ag}$  were determined to be  $^1J_{^{31}\text{P}-^{107}\text{Ag}} = 410$  Hz and  $^1J_{^{31}\text{P}-^{109}\text{Ag}} = 475$  Hz, respectively.

Unfortunately, even at  $-90\text{ }^{\circ}\text{C}$  (183 K), all the peaks of the  $\text{Ag}_2(\text{PPh}_3)_2(\text{C}_6\text{F}_5)(\mu_2\text{-HCO}_3)$  **91** could not be fully resolved. Furthermore, cooling the sample to  $-85\text{ }^{\circ}\text{C}$  (188 K) and  $-90\text{ }^{\circ}\text{C}$  (183 K), resulted in poor resolution of the peaks (**Figure 24**). This is likely because these temperatures are very close to the melting point of toluene ( $-95\text{ }^{\circ}\text{C}$ , 178 K), hence resulting in a very poor shim.

Thus, to reach lower temperatures,  $\text{Ag}_2(\text{PPh}_3)_2(\text{C}_6\text{F}_5)(\mu_2\text{-HCO}_3)$  **91** was dissolved in a mixed solvent system of dichloromethane- $d_2$  and toluene- $d_8$  (80:20) and cooled to  $-100\text{ }^{\circ}\text{C}$  (173 K) on the AV500 spectrometer. At this temperature the  $^{31}\text{P}\{^1\text{H}\}$  NMR spectrum displayed multiple resonances within a range of  $\delta$  0 to  $\delta$  30 and appears to be fully resolved (**Figure 25**). It showed that  $\text{Ag}_2(\text{PPh}_3)_2(\text{C}_6\text{F}_5)(\mu_2\text{-HCO}_3)$  **91** exists in an equilibrium of multiple species in solution. The Ag–P containing species were readily identified by the characteristic  $^{107}\text{Ag}/^{109}\text{Ag}$  coupling pattern with  $^{31}\text{P}$ . This, in conjunction with relative integrals allowed for the tentative identification of a total of 8 different phosphorus – coordinated silver species in the  $^{31}\text{P}\{^1\text{H}\}$  NMR spectrum with 3 major species, 3 minor species and 2 species in trace amounts. The approximate chemical shifts, coupling constants and integrations of these peaks have been summarized in **Table 6**. However, these are rather unreliable, due to the large overlaps between the peaks.

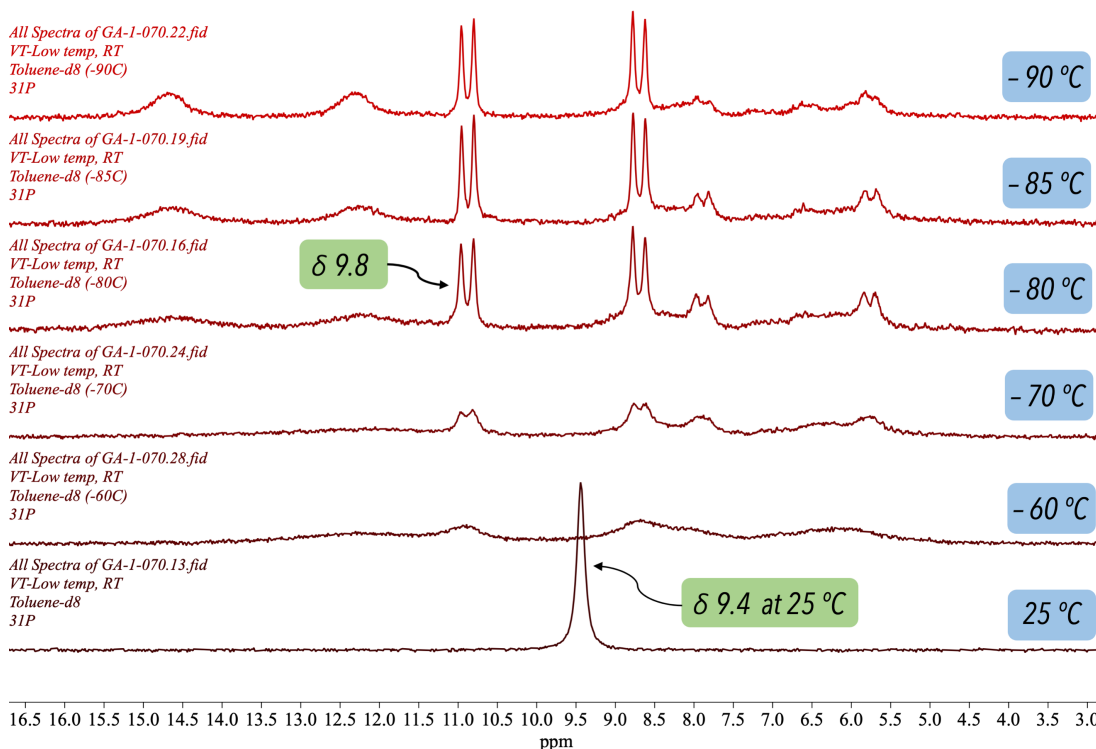


**Figure 24:** Variable-temperature  $^{31}\text{P}\{^1\text{H}\}$  NMR (202 MHz, 128 scans, tol- $d_8$ ,) spectrum of **91**

At  $-100\text{ }^{\circ}\text{C}$  (173 K), the  $^{19}\text{F}\{^1\text{H}\}$  resonances assigned to  $\text{Ag}_2(\text{PPh}_3)_2(\text{C}_6\text{F}_5)(\mu_2\text{-HCO}_3)$  **91**, also split into multiple resonances, indicating multiple  $\text{AgC}_6\text{F}_5$  species exist in equilibrium in solution (**Figure 26**). The *ortho*-F resonance of the  $\text{AgC}_6\text{F}_5$  has split into 4 distinct resonances; the same is true for the *para*- and *meta*- F resonances; however, these resonances are more difficult to distinguish due to overlap. The *ortho*-F resonance centred at  $\delta -106$  at room temperature, had split into 4 distinct resonances centred at  $\delta -105.2$ ,  $\delta -105.7$ ,  $\delta -107.7$  and  $\delta -108.1$  at low temperature. Due to the chemical shift of these resonances, they have been tentatively assigned as *ortho*-F resonances. The major species appears with an *ortho*-F resonance at  $\delta -107.7$ . The corresponding *para*-F ( $\delta -160.4$ ) and *meta*-F ( $\delta -161.8$ ) peaks can also be identified using the relative integrations and low-temperature  $^{19}\text{F}$  COSY spectrum (in **Appendix**). However, for the other species, it is difficult to do the same due to the poor resolution and overlap of the peaks.

**Table 6:**  $^{31}\text{P}\{^1\text{H}\}$  NMR data of the Ag–P resonance of  $\text{Ag}_2(\text{PPh}_3)_2(\text{C}_6\text{F}_5)(\mu_2\text{-HCO}_3)$  **91**

Entry <sup>[a]</sup>	Chemical shift of $^{31}\text{P} - ^{107}\text{Ag}$ peaks		Chemical shift of $^{31}\text{P} - ^{109}\text{Ag}$ peaks		Resonance centered at: ( $\delta$ )	Integration		Coupling constant $^{31}\text{P} - ^{107}\text{Ag}$ (Hz)	Coupling constant $^{31}\text{P} - ^{109}\text{Ag}$ (Hz)
	Peak 1	Peak 2	Peak 1	Peak 2		Peak 1	Peak 2		
1	2.61	1.25	2.71	1.14	1.9	0.06	0.06	275	317
2	2.97	1.55	3.07	1.45	2.3	0.04	0.04	287	327
3	6.96	4.98	7.11	4.83	6.0	0.97	0.93	400	461
4	7.85	5.78	8.01	5.62	6.8	1.43	0.61	418	483
5	8.35	6.22	8.50	6.06	7.4	1.00	1.04	460	493
6	10.03	7.95	10.19	7.79	9.0	0.78	1.43	420	485
7	14.65	12.4	14.81	12.26	13.5	0.62	0.61	455	515
8	19.12	15.74	19.38	15.48	17.4	0.29	0.30	683	788

<sup>[a]</sup> The coupling constants of **Entry 1, 2, 4, 7** and **8**, can be assigned easily as these doublets do not overlap with each other and the integrations aid in easily distinguishing the peaks. However, with **Entry 3, 5** and **6**, there is some uncertainty when assigning the peaks as their integration values are very similar and the doublets tend to overlap with each other.

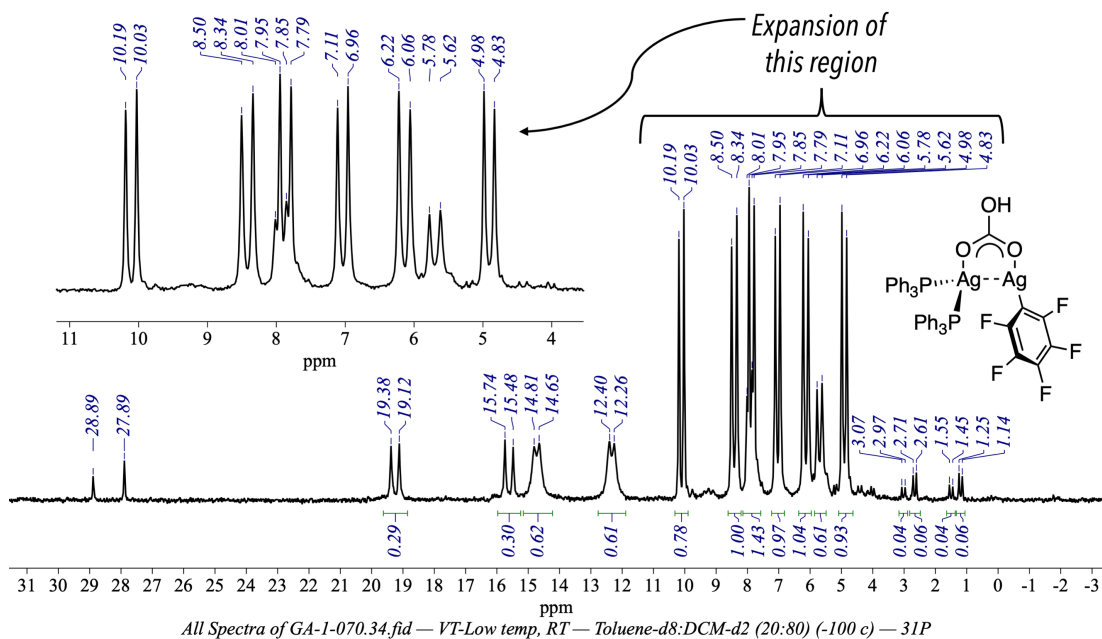


**Figure 25:**  $^{31}\text{P}\{^1\text{H}\}$  NMR (202 MHz, tol-*d*<sub>8</sub>:DCM-*d*<sub>2</sub> (20:80), -100 °C) spectrum of **91**

Considering the highly complex speciation of **91**, the solid-state structure of the complex can only give very limited insight into the reactivity of the complex, as the structure in solution is very different. Attempts to use mass spectroscopy to understand the complex were also unsuccessful as even a gentle technique such as LIFDI-MS resulted in fragmentation of the complex. An additional complication is the presence of the 30 % contamination of C<sub>6</sub>F<sub>5</sub>H **17** which makes it difficult to conduct detailed kinetic experiments.

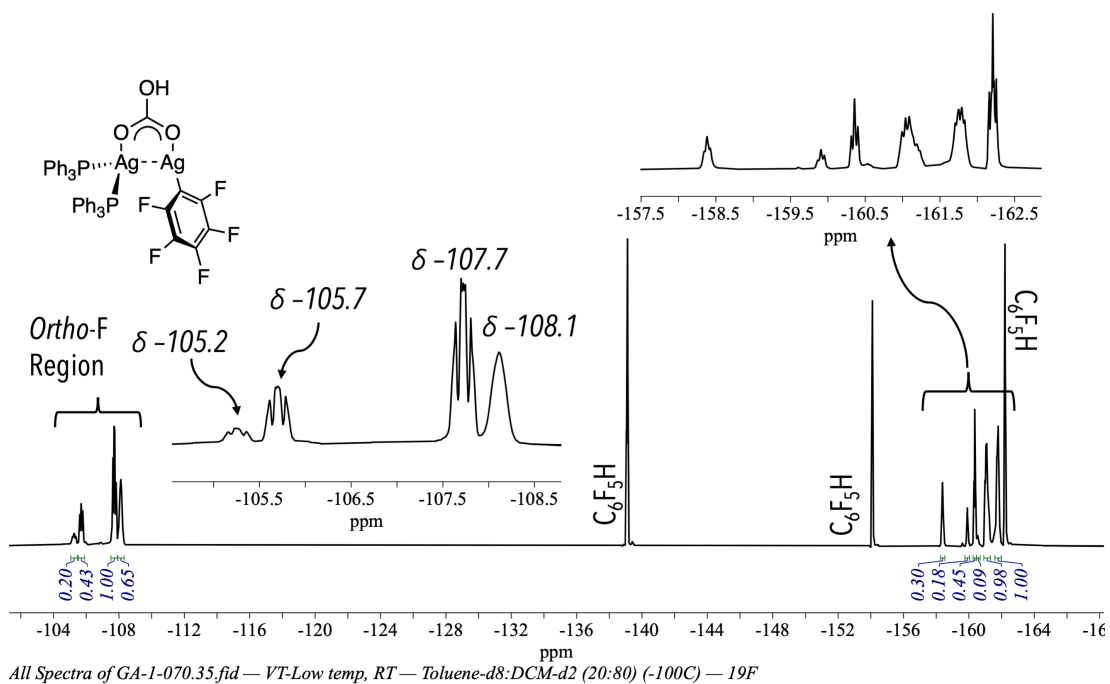
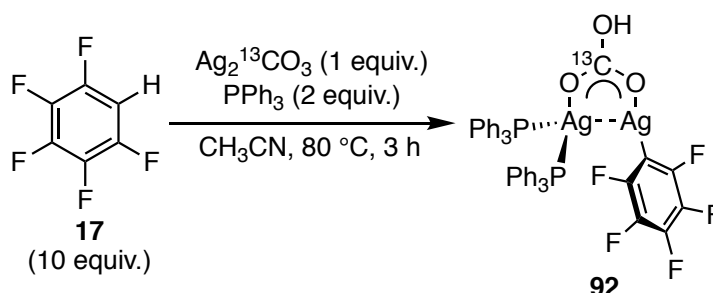


**Figure 26:**  $^{19}\text{F}\{^1\text{H}\}$  NMR (470 MHz, tol-*d*<sub>8</sub>:dichloromethane-*d*<sub>2</sub> (20:80), -100 °C) spectrum of **91**

Nevertheless, to obtain information of the structure of complex **91** in solution, the carbonyl carbon of the bridging hydrogen carbonate of the complex was  $^{13}\text{C}$  labelled.  $\text{C-13}$  labelled  $\text{Ag}_2^{13}\text{CO}_3$  was prepared from the reaction between  $\text{Na}_2^{13}\text{CO}_3$  and 2 equivalents of  $\text{AgNO}_3$  in deionised water and isolated as a bright yellow solid with 85 % yield. The  $\text{Ag}_2(\text{PPh}_3)_2(\text{C}_6\text{F}_5)(\mu_2\text{-H}^{13}\text{CO}_3)$  **92** was synthesized from the reaction of  $\text{Ag}_2^{13}\text{CO}_3$  with 2 equivalence of  $\text{PPh}_3$  and 10 equivalence of  $\text{C}_6\text{F}_5\text{H}$  (**Scheme 46**).



**Scheme 46:** Synthesis of  $^{13}\text{C}$ -labelled The  $\text{Ag}_2(\text{PPh}_3)_2(\text{C}_6\text{F}_5)(\mu_2\text{-H}^{13}\text{CO}_3)$  **92**

The complex was characterised in  $\text{C}_6\text{D}_6$  by NMR spectroscopy and the  $^{13}\text{C}\{^1\text{H}\}$  spectrum of **92** at room temperature contained two singlet resonances at  $\delta$  172 and  $\delta$  168, which were absent in the non-labelled complex (**Figure 27**). Complex **92** was dissolved in a mixed solvent system of dichloromethane- $d_2$  and toluene- $d_8$  (80:20) and characterised at  $-100^\circ\text{C}$  (173 K).

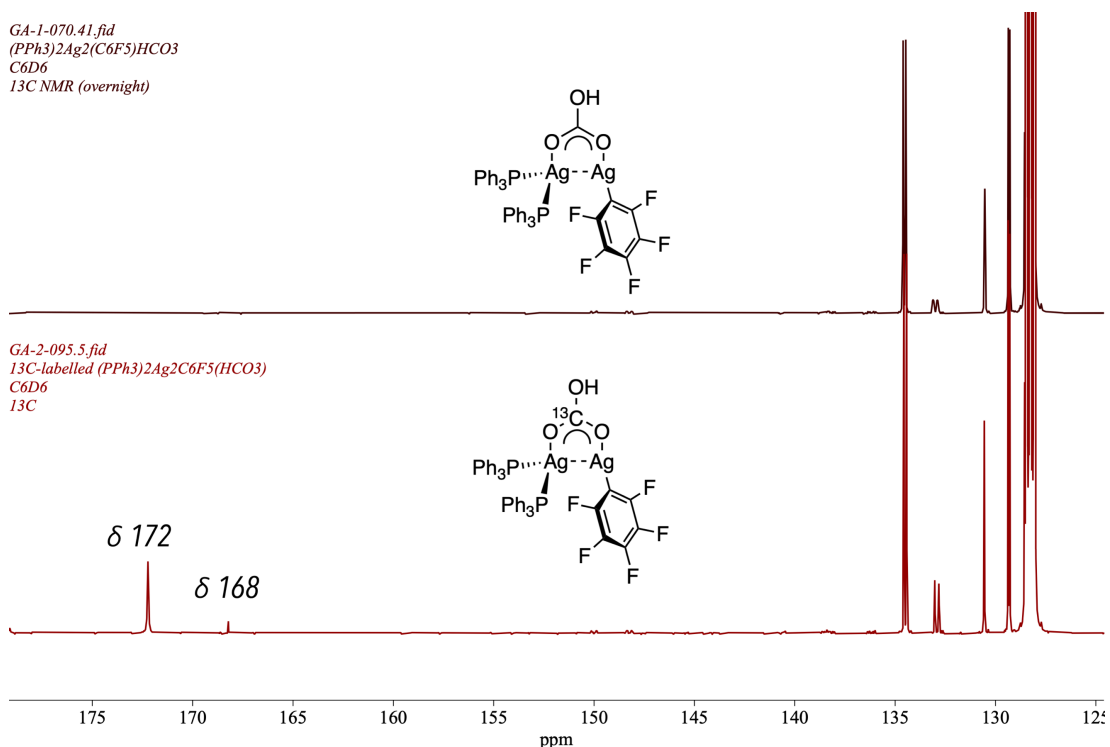


**Figure 27:** Stack plot of the  $^{13}\text{C}\{^1\text{H}\}$  NMR (125.7 MHz,  $\text{C}_6\text{D}_6$ ,  $25^\circ\text{C}$ ) spectrum of the  $^{13}\text{C}$ -labelled  $\text{Ag}_2(\text{PPh}_3)_2(\text{C}_6\text{F}_5)(\mu_2\text{-H}^{13}\text{CO}_3)$  **92** (**Below**) and the non-labelled  $\text{Ag}_2(\text{PPh}_3)_2(\text{C}_6\text{F}_5)(\mu_2\text{-HCO}_3)$  **91** (**Above**)

All Spectra of GA-1-070.34.fid  
VT-Low temp, RT  
Toluene-d8:DCM-d2 (20:80) (-100 c)  
31P

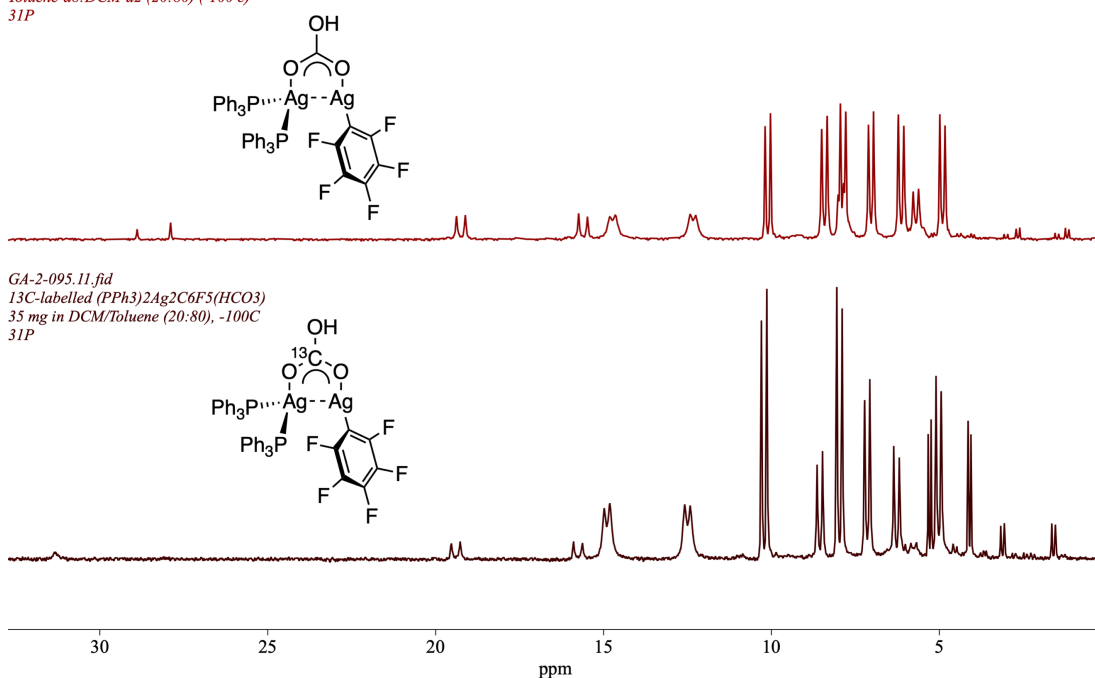


**Figure 28:** Stack plot of the  $^{31}\text{P}\{^1\text{H}\}$  NMR (202 MHz, tol- $d_8$ :dichloromethane- $d_2$  (20:80),  $-100\text{ }^\circ\text{C}$ ) spectrum of **91** (top) and **92** (bottom).

**Table 7:**  $^{31}\text{P}\{^1\text{H}\}$  NMR data of the Ag–P resonances of **92**

Entry	Chemical shift of $^{31}\text{P}$ – $^{107}\text{Ag}$ ( $\delta$ )		Chemical shift of $^{31}\text{P}$ – $^{109}\text{Ag}$ ( $\delta$ )		Resonance Centered at ( $\delta$ )	Integration		Coupling constant $^1J_{^{31}\text{P}-^{107}\text{Ag}}$ (Hz)	Coupling Constant $^1J_{^{31}\text{P}-^{109}\text{Ag}}$ (Hz)
	Peak 1	Peak 2	Peak 1	Peak 2		Peak 1	Peak 2		
1	3.06	1.65	3.17	1.54	2.4	0.13	0.13	285	330
2	5.25	4.14	5.33	4.06	4.7	0.4	0.4	225	257
3	7.07	5.1	7.22	4.95	6.1	1	1.05	399	460
4	8.48	6.36	8.64	6.19	7.4	0.61	0.71	429	496
5	10.14	8.05	10.3	7.89	9.1	1.23	1.36	423	488
6	14.81	12.58	14.98	12.42	13.7	0.9	0.9	451	518
7	19.27	15.89	19.53	15.63	17.6	0.15	0.15	684	790

The  $^{31}\text{P}\{^1\text{H}\}$  NMR spectrum of **92** at 173 K, has some minor differences to the spectrum of **91**. Notably **92** seems to contain 7 distinct Ag–P species, whereas the un-labelled complex **91** contains 8 and the concentration of the species of **92** were different when compared to **91** (Figure 28). The unlabelled sample **91** was prepared using 15 mg in 0.5 mL of solvent, whereas 35 mg of  $^{13}\text{C}$ -labelled complex **92** was dissolved in 0.5 mL of solvent to obtain a



better  $^{13}\text{C}$  spectra. The integrations and chemical shifts of the Ag–P species present in  $^{31}\text{P}\{^1\text{H}\}$  NMR spectrum are summarized in **Table 7**. In contrast, the low-temperature  $^{19}\text{F}\{^1\text{H}\}$  NMR spectra of the  $^{13}\text{C}$ -labelled and un-labelled complex show little difference in the peaks and relative integration values.

The  $^{13}\text{C}\{^1\text{H}\}$  NMR spectrum of **92** at 173K contained 6 singlet resonances centred around  $\delta$  170, with two major ( $\delta$  –171.3 and –170.8) and four very minor carbonate containing complexes. No Ag- $^{13}\text{C}$  coupling observed with the carbonyl signals (**Figure 29**). The  $^{13}\text{C}$  proton coupled spectrum was collected to observe any potential  $^{13}\text{C}$ - $^1\text{H}$  coupling; however, no  $^1\text{H}$ - $^{13}\text{C}$  splitting patterns were observed and the carbonate signals remained singlets.

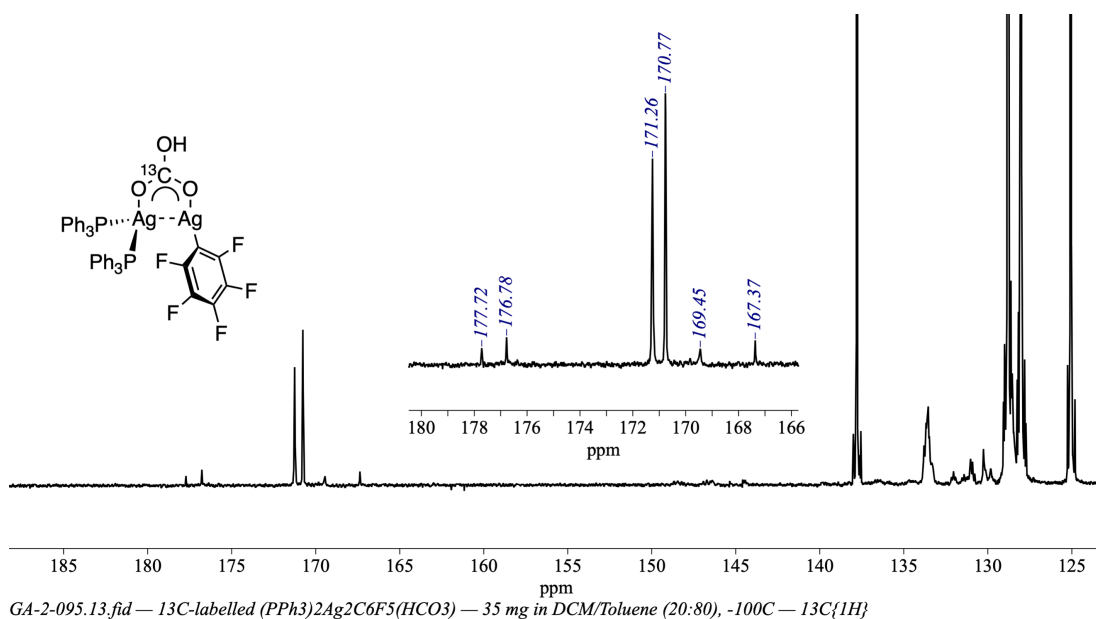
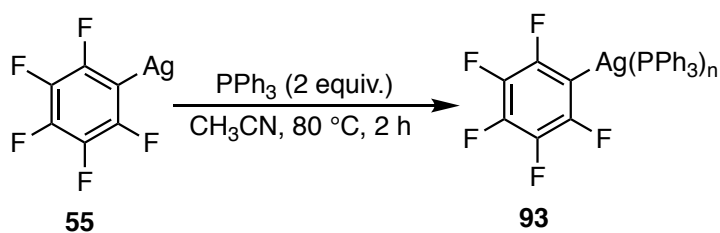


**Figure 29:**  $^{13}\text{C}\{^1\text{H}\}$  NMR (125.7 MHz,  $\text{tol-}d_8$ :dichloromethane- $d_2$  (20:80),  $-100^\circ\text{C}$ ) spectrum **92**

The presence of multiple carbonate signals suggests that the **91** and **92** not only exist in a complex equilibrium coordinated to various phosphines, but also exists in equilibrium with various binding modes with the hydrogen-carbonate ligand.<sup>122</sup> This likely contributes to complex equilibrium of various species in solution.

To gain more insight into the behaviour of the equilibrium species, the  $\text{AgC}_6\text{F}_5$  **55** was treated with 2 equivalents of  $\text{PPh}_3$  to help simplify the system by removing the carbonate ligand. The complex **55** was stirred with two equivalents of  $\text{PPh}_3$  in acetonitrile at  $80^\circ\text{C}$  for 2 h, and brown crystals of the product **93** were isolated at 73 % yield after cooling the reaction mixture to  $-18^\circ\text{C}$  (**Scheme 47**). The number of phosphines coordinated to the  $\text{AgC}_6\text{F}_5$  motif in **93** is ill-defined, thus the structure is represented as  $\text{Ag}(\text{PPh}_3)_n\text{C}_6\text{F}_5$ .



**Scheme 47:** The synthesis of  $\text{AgC}_6\text{F}_5(\text{PPh}_3)_n$  **93** from the reaction between  $\text{AgC}_6\text{F}_5$  **55** and  $\text{PPh}_3$

The complex **93** was characterized by  $^{19}\text{F}\{^1\text{H}\}$  and  $^{31}\text{P}\{^1\text{H}\}$  NMR spectroscopy at  $-100^\circ\text{C}$  in a mixture of dichloromethane and toluene 80:20 mixture. Much like the **91**, the complex was found to exist in an equilibrium of different Ag–P species with approximately 5 species in solution (**Figure 30**). The chemical shifts, coupling constants and integrations of these peaks are summarized (**Table 8**). However, most of the  $^{31}\text{P}$  resonances of **93** matched did not match with the peaks of **91**, the closest matches only shared similar coupling constants but had different chemical shifts. The comparison of the closest match peaks of **93** and **91** are summarized in **Table 9**. The vastly dissimilar  $^{31}\text{P}\{^1\text{H}\}$  spectra imply that **91** and **93** have very different equilibrium species. Interestingly, the  $^{19}\text{F}\{^1\text{H}\}$  NMR of **93** spectrum mainly remains unchanged at 173 K. LIFDI-MS analysis of **93** in DMF resulted in fragmentation of the complex with  $[\text{Ag}(\text{PPh}_3)_2]^+$  being the highest intensity peak.

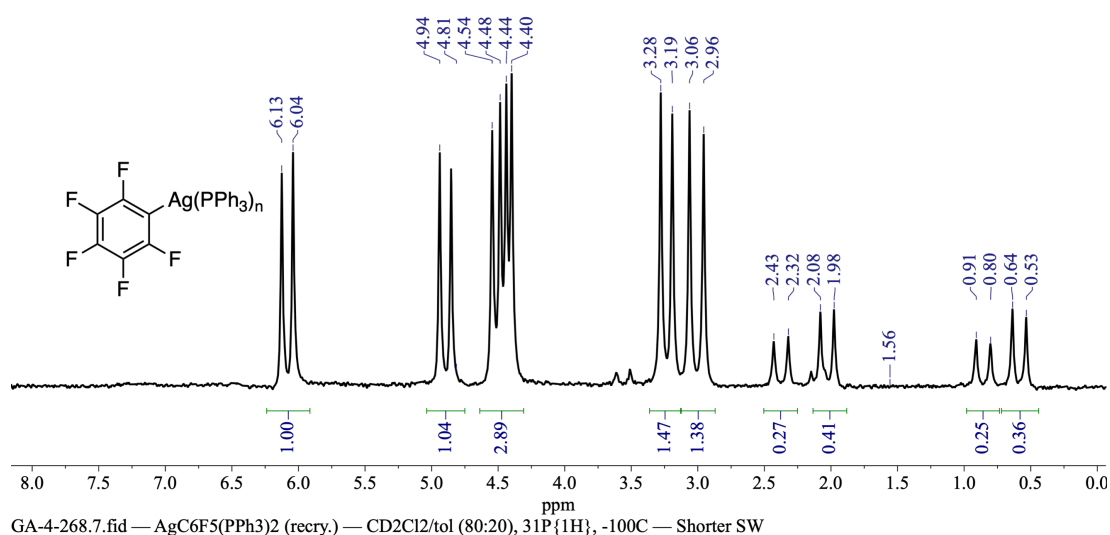


**Figure 30:**  $^{31}\text{P}\{^1\text{H}\}$  (202 MHz, toluene:dichloromethane,  $-100^\circ\text{C}$ ) spectrum of **93**

**Table 8:**  $^{31}\text{P}\{^1\text{H}\}$  NMR data of the Ag–P resonances of **93**

Entry	Chemical shift of $^{31}\text{P}$ – $^{107}\text{Ag}$ ( $\delta$ )		Chemical shift of $^{31}\text{P}$ – $^{109}\text{Ag}$ ( $\delta$ )		Resonance Centered at ( $\delta$ )	Integration		Coupling constant $^1J_{^{31}\text{P}-^{107}\text{Ag}}$ (Hz)	Coupling Constant $^1J_{^{31}\text{P}-^{109}\text{Ag}}$ (Hz)
	Peak 1	Peak 2	Peak 1	Peak 2		Peak 1	Peak 2		
1	1.98	0.64	2.08	0.53	1.3	0.41	0.36	271	313
2	2.32	0.91	2.43	0.80	1.6	0.27	0.25	285	329
3	4.4	3.28	4.44	3.19	3.8	2.89*	1.47	226	253
4	4.48	3.06	4.54	2.96	3.8		1.38	287	319
5	6.04	4.94	6.13	4.81	5.5	1.00	1.04	222	267

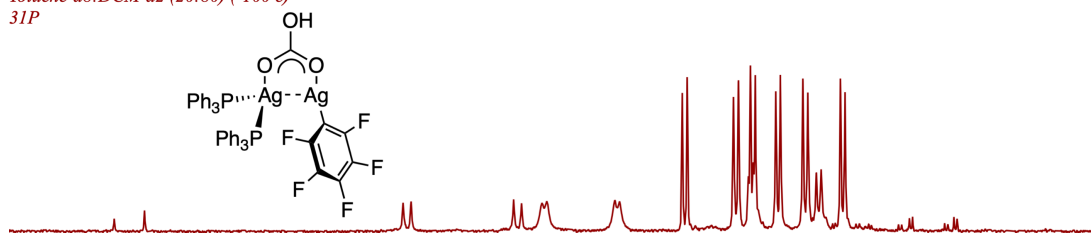
\* Peaks 1 for Entry 3 and 4 overlap, so have same integration value

All Spectra of GA-1-070.34.fid

VT-Low temp, RT

Toluene-d8:DCM-d2 (20:80) (-100 c)

$^{31}\text{P}$



GA-4-268.5.fid

AgC6F5(PPh3)2 (recry.)

CD2Cl2/tol (80:20),  $^{31}\text{P}\{^1\text{H}\}$ , -100C

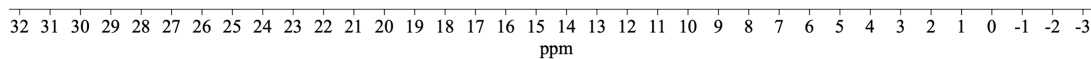


**Figure 31:** Stack plot of the  $^{31}\text{P}\{^1\text{H}\}$  (202 MHz, Tol:dichloromethane,  $-100\text{ }^\circ\text{C}$ ) spectrum of **91** (top) and **93** (bottom)

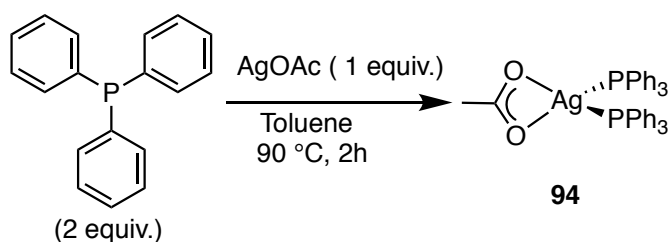
**Table 9:** Comparison of the closest matches for the peaks of **91** and **93**

Entry	Complex	Chemical shift ( $\delta$ )	Coupling	Coupling constant
			constant (Hz)	(Hz)
			$^1J_{31P-107Ag}$	$^1J_{31P-109Ag}$
1	$Ag_2(PPh_3)_2(C_6F_5)(\mu_2-HCO_3)$			
	<b>91</b>	1.9	275	317
	$Ag(C_6F_5)(PPh_3)_n$ <b>93</b>	1.3	271	313
2	$Ag_2(PPh_3)_2(C_6F_5)(\mu_2-HCO_3)$			
	<b>91</b>	2.3	287	327
	$AgC_6F_5(PPh_3)_n$ <b>93</b>	1.6	285	329

## 2.3 Synthesis of Phosphine-Coordinated Silver(I) Acetate Complexes

From the literature, it is implied that prior to C–H activation, the silver salt coordinates with a phosphine to form a more soluble phosphine-coordinated silver complex.<sup>87,86</sup> Thus, a range of phosphine coordinated silver complexes were synthesized to identify potential intermediates. The complexes were characterized by  $^1H$ ,  $^{31}P\{^1H\}$  NMR spectroscopy at both room temperature and low temperature, MS, XRD and CHN analysis.

The combination of  $AgOAc$  and  $PPh_3$  was found to be inactive for C–H bond activation; nevertheless, the speculated triphenylphosphine coordinated silver acetate complex was synthesized using a procedure outlined by Molloy and co-workers, which included full characterization of the product.<sup>123</sup> An  $Ag(PPh_3)_2(\kappa^2-OAc)$  **94** complex was synthesized from  $AgOAc$  and 2 equivalents of  $PPh_3$  in toluene, using a modified literature procedure (**Scheme 48**). The desired product was isolated as an off-white solid in 76 % yield. As observed with previous complexes, the  $Ag-PPh_3$  bond was very labile and only a singlet at  $\delta$  9.0 was observed in the  $^{31}P\{^1H\}$  NMR spectrum at room temperature. When the sample was cooled to  $-80^\circ C$ , the resonance resolved into a pair of doublets centred at  $\delta$  8.48 and with  $^1J_{31P-107Ag} = 370.6$  Hz and  $^1J_{31P-109Ag} = 506.2$  Hz (**Figure 32**). In contrast to **91** and **93**, complex **94** exists as a single species in solution where the two phosphines are equivalent. The LIFDI-MS spectrum of **94** in dichloromethane, showed the presence of  $[M-OAc]^+$  fragment.



**Scheme 48:** The synthesis of  $(\text{PPh}_3)_2\text{Ag}(\kappa^2\text{-OAc})$  **94** complex from AgOAc and 2 equiv.  $\text{PPh}_3$  in toluene.

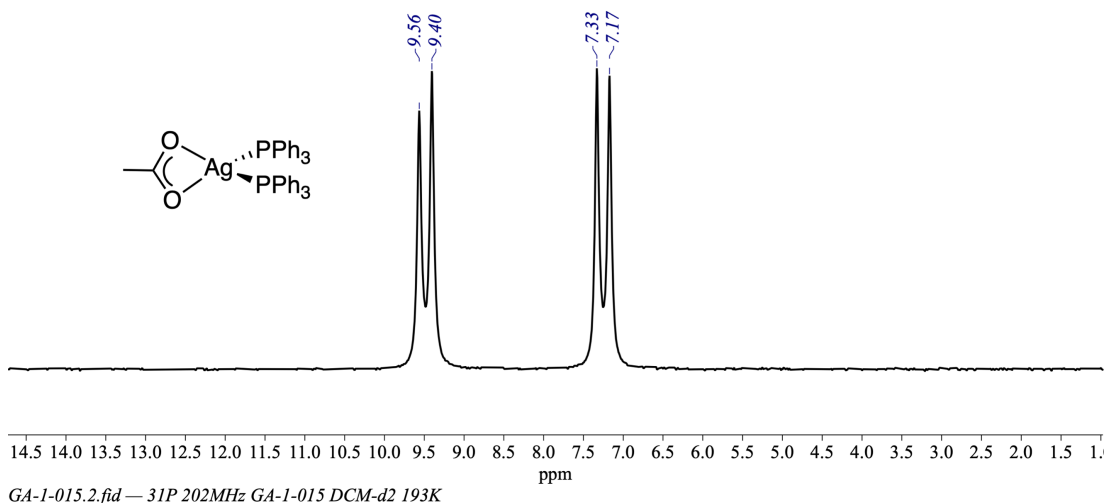
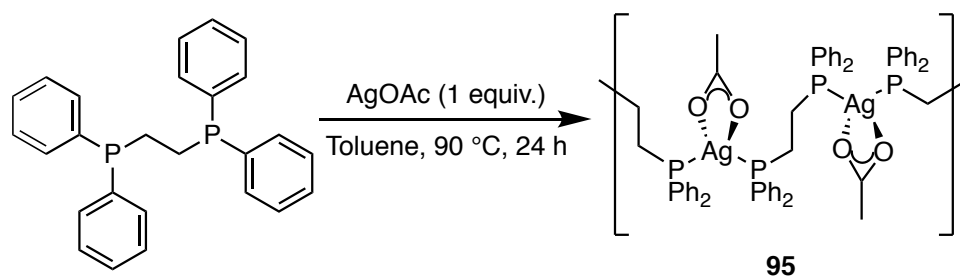


**Figure 32:**  $^{31}\text{P}\{^1\text{H}\}$  (202 MHz, dichloromethane- $d_2$ ,  $-80^\circ\text{C}$ ) of **94**

Due to the lability of the  $\text{Ag-PPh}_3$  at room temperature, a brief attempt to was made to synthesize a complex with a chelating ligand. Due to the chelate effect, a bidentate ligand such as 1,2-bis(diphenylphosphino)ethane (DPPE) would be much less labile than  $\text{PPh}_3$ . Thus, an analogous complex to  $\text{Ag}(\text{PPh}_3)_2(\kappa^2\text{-OAc})$  using a chelating phosphine such as DPPE could theoretically afford extra stability of the resulting  $\text{Ag}(\kappa^2\text{-DPPE})(\text{C}_6\text{F}_5)$ . As there was no pre-existing literature procedure present for the synthesis of  $\text{Ag}(\text{DPPE})(\kappa^2\text{-OAc})$  complex, the synthetic procedure for  $\text{Ag}(\text{PPh}_3)_2(\kappa^2\text{-OAc})$  **94** was modified to produce the  $[\text{Ag}(\text{DPPE})(\kappa^2\text{-OAc})]_n$  **95** complex (**Scheme 49**).



**Scheme 49:** The synthesis of  $[\text{Ag}(\text{DPPE})(\kappa^2\text{-OAc})]_n$  **95** from AgOAc and DPPE in toluene.

The resulting complex **95** was found to be insoluble in most common solvents such as dichloromethane, chloroform, ethyl acetate, acetone, THF, DMSO and only sparingly soluble in methanol. The complex was recrystallized from a saturated solution of MeOH and was analysed using X-ray crystallography diffraction methods. The structure of the  $[\text{Ag}(\text{DPPE})(\kappa^2\text{-OAc})]_n$  **95** complex was found to be a coordination polymer, which rationalized the insolubility of the complex (**Figure 33**). The Ag–P(1) and Ag–P(2) distance are 2.4543(7) Å and 2.4457(7) Å respectively. There is asymmetry in the bond distance with Ag–O(1) having a shorter bond length of 2.358(2) Å and Ag–O(2) with a longer distance of 2.746(3) Å. The O(1) of the acetate ligand also hydrogen bonds with the H3A proton of methanol with the O···H distance of 1.72(4) Å (**Figure 34**). The LIFDI-MS analysis only showed a peak at  $m/z$  903.24 with an isotopic pattern containing only one silver centre which corresponded to  $[\text{Ag}(\text{DPPE})_2]^+$ . Due to the complicated structure of  $[\text{Ag}(\text{DPPE})(\kappa^2\text{-OAc})]_n$  **95** complex and its insolubility in most solvents, no further stoichiometric reactions were performed with the complex.

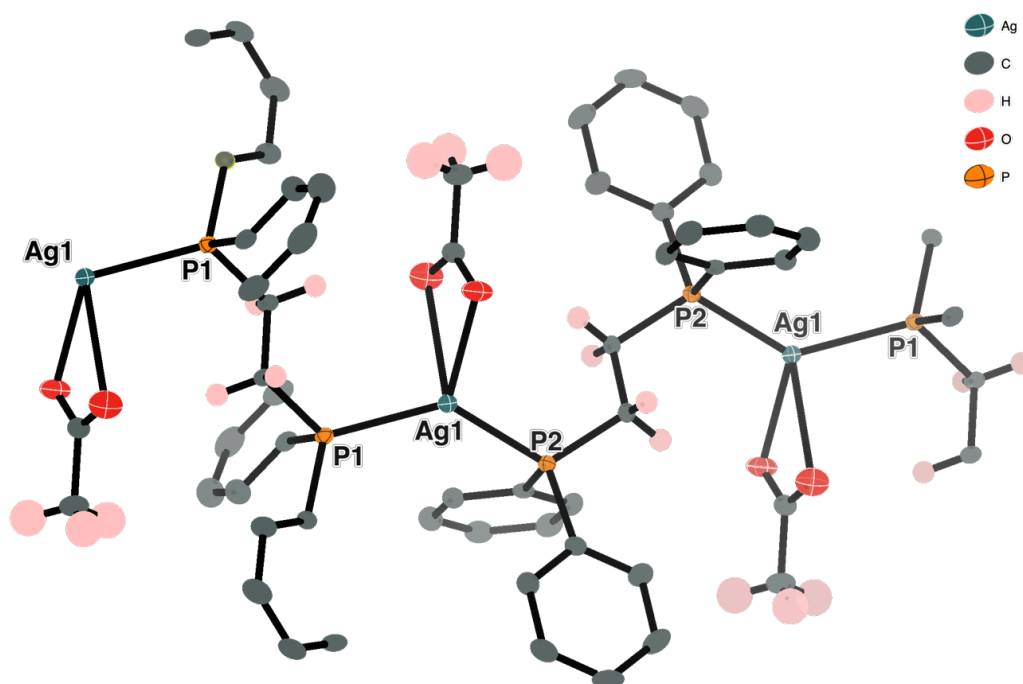


**Figure 33:** The crystal structure of the  $[\text{Ag}(\text{DPPE})(\kappa^2\text{-OAc})]_n$  **95** complex which shows the DPPE ligand bridging two different Ag centres.

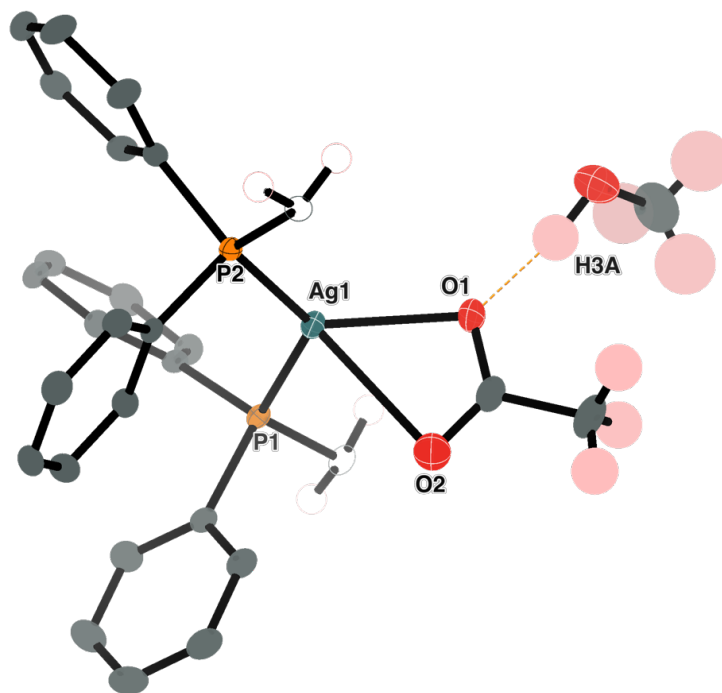


**Figure 34:** The asymmetric unit of  $[\text{Ag}(\text{DPPE})(\kappa^2\text{-OAc})]_n$  **95** showing H-bonding with MeOH

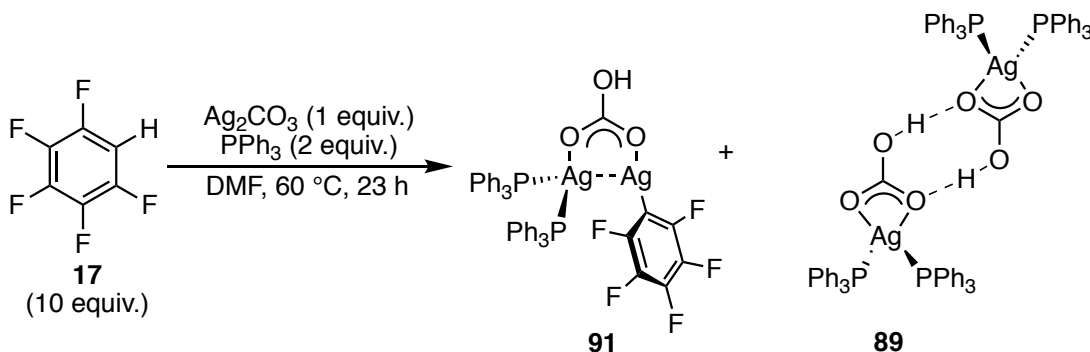
**Table 10:** Principal bond lengths and angles for  $[\text{Ag}(\text{DPPE})(\kappa^2\text{-OAc})]_n$  **95**

Bond	Bond lengths (Å)
Ag(1)–P(1)	2.454(6)
Ag(1)–P(2)	2.446(9)
Ag(1)–O(1)	2.357(2)
Ag(1)–O(2)	2.746(3)
O(1) ... O(3)	2.719(3)
O(1) ... H3A	1.725(4)
Bond angles	Bond Angles (°)
O(1)–Ag(1)–O(2)	50.47(7)
O(1)–Ag(1)–P(1)	116.75(6)
O(1)–Ag(1)–P(2)	112.03(6)

## 2.4 Synthesis of PPh<sub>3</sub> Coordinated Silver(I) Carbonate Complexes

Examples of silver-phosphine complexes incorporating carbonate are, generally, sparse in the literature. However in 2002, Bowmaker *et al.* reported the synthesis of various triphenylphosphine-ligated silver(I) bicarbonate complexes and were able to characterize these complexes using infrared spectroscopy, X-ray diffraction and solid-state <sup>31</sup>P MAS NMR spectroscopy.<sup>121</sup>

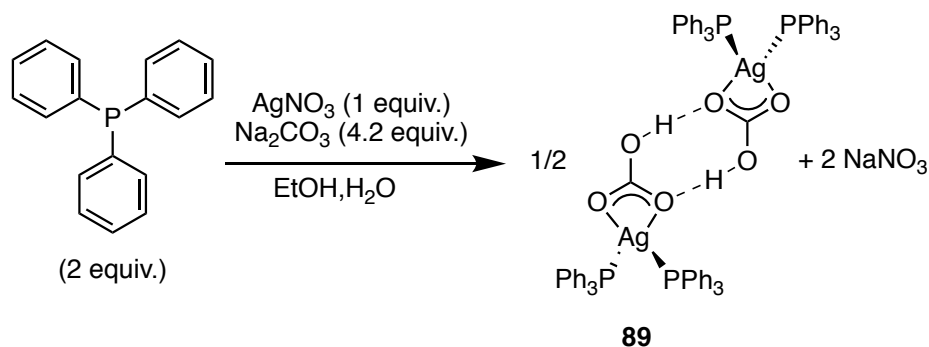
Crystals of [Ag(PPh<sub>3</sub>)<sub>2</sub>HCO<sub>3</sub>]<sub>2</sub> **89** were isolated from the reaction mixture of Ag<sub>2</sub>CO<sub>3</sub>, PPh<sub>3</sub> and 10 equivalents of C<sub>6</sub>F<sub>5</sub>H which was used to synthesis Ag<sub>2</sub>(PPh<sub>3</sub>)<sub>2</sub>(C<sub>6</sub>F<sub>5</sub>)(μ<sub>2</sub>-HCO<sub>3</sub>) **91** (Scheme 50). The presence of the Ag<sub>2</sub>(PPh<sub>3</sub>)<sub>2</sub>(C<sub>6</sub>F<sub>5</sub>)(μ<sub>2</sub>-HCO<sub>3</sub>) **91** was confirmed by <sup>19</sup>F {<sup>1</sup>H} NMR spectroscopy. The crystals of [Ag(PPh<sub>3</sub>)<sub>2</sub>HCO<sub>3</sub>]<sub>2</sub> **89** were obtained from the reaction mixture *via* vapour diffusion recrystallization method.



**Scheme 50:** Crystals of [Ag(PPh<sub>3</sub>)<sub>2</sub>HCO<sub>3</sub>]<sub>2</sub> **89** isolated from the synthesis of Ag<sub>2</sub>(PPh<sub>3</sub>)<sub>2</sub>(C<sub>6</sub>F<sub>5</sub>)(μ<sub>2</sub>-HCO<sub>3</sub>) **91**

The formation of [Ag(PPh<sub>3</sub>)<sub>2</sub>(κ<sup>2</sup>-HCO<sub>3</sub>)]<sub>2</sub> **89** suggests that phosphine-coordinated silver(I) carbonate complexes are also involved in the C–H bond activation of C<sub>6</sub>F<sub>5</sub>H. The structure of the complex was determined using X-ray diffraction analysis. The complex was found to exist as centrosymmetric hydrogen bonded dimers (**Figure 35**). The central H-bonded Ag(κ<sup>2</sup>-HCO<sub>3</sub>) unit of the dimer lies in a plane, with the PPh<sub>3</sub> groups lying out of the plane. The C(37)–O(2)–Ag(1)–P(1) torsional angle is 95.9(1)°. The distance between the donor and acceptor O(1)⋯O(3) of the hydrogen bond is 2.614(2) Å. The Ag–O bond distance is 2.408(2) and the Ag–P distance is 2.431(6) Å. The synthesis of this complex has been previously reported by Bowmaker *et al* in their 2002 paper where they rigorously characterized the [Ag(PPh<sub>3</sub>)<sub>2</sub>(κ<sup>2</sup>-HCO<sub>3</sub>)]<sub>2</sub> **89** using solid-state methods such as X-ray crystallography, IR, and <sup>31</sup>P MAS NMR spectroscopy.<sup>121</sup> This procedure was reproduced, and the desired [Ag(PPh<sub>3</sub>)<sub>2</sub>HCO<sub>3</sub>]<sub>2</sub> **89** complex was prepared with a 76 % yield as a white solid (**Scheme 51**).





**Scheme 51:** Synthesis of the  $[\text{Ag}(\text{PPh}_3)_2(\kappa^2\text{-HCO}_3)]_2$  **89** from  $\text{PPh}_3$ ,  $\text{AgNO}_3$  and  $\text{Na}_2\text{CO}_3$  in a mixed solvent system of  $\text{EtOH}$  and  $\text{H}_2\text{O}$ .

**Table 11:** Principal bond lengths and angles for **89** and **90**

Bond	$[\text{Ag}(\text{PPh}_3)_2(\kappa^2\text{-HCO}_3)]_2$ <b>89</b>	$[\text{Ag}(\text{PPh}_3)_2\text{HCO}_3]_n$ <b>90</b>
	Bond length (Å)	
Ag(1)–O(1)	2.408(2)	2.343(19)
Ag(1)–O(2) <sup>[a]</sup> / Ag(1)–O(3) <sup>[b]</sup>	2.594(2)	2.346(18)
Ag(1)–P(1)	2.4309(6)	2.445(7)
Ag(1)–P(2)	2.4279(5)	2.419(7)
O(1) ... O(3) <sup>[a]</sup> / O(2) ... O(4) <sup>[b]</sup>	2.614(2)	2.582(3)
Bond Angles	Angle (°)	
O(1)–Ag1–O(2)/ O(1)–Ag1–O(3)	52.57(6)	75.81(8)
P(1)–Ag(1)–O(1)	109.80(4)	101.00(3)
P(2)–Ag1–O(2)	100.44(4)	122.21(3)
Torsional angles		
C(37)–O(2)–Ag(1)–P(1) <sup>[a]</sup> / C(1)–O(1)–Ag(1)–P(2) <sup>[b]</sup>	95.9(1)	72.7(1)

[a] is for **89** and [b] for **90** (different atom labels in the crystal structure but the same bond)

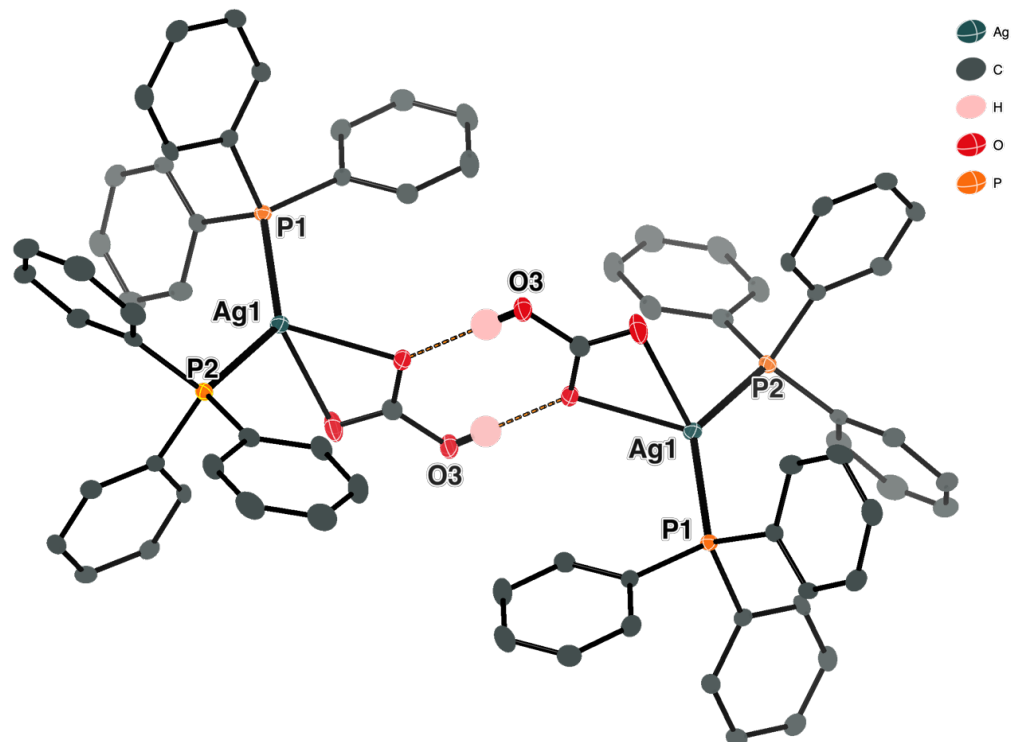


**Figure 35:** The crystal structure of  $[\text{Ag}(\text{PPh}_3)_2(\kappa^2\text{-HCO}_3)]_2$  **89** isolated from reaction mixture of  $\text{Ag}_2\text{CO}_3$  and  $\text{PPh}_3$  with  $\text{C}_6\text{F}_5\text{H}$  **17** in DMF.

Due to the lability of the  $\text{Ag-PPh}_3$  bond at room temperature, the complex was characterized using low temperature  $^{31}\text{P}\{^1\text{H}\}$  NMR spectroscopy at  $-80^\circ\text{C}$  in a mixed solvent system of toluene- $d_8$ : dichloromethane- $d_2$  (20:80). The spectrum of the complex contains a pair of doublet resonances centred at  $\delta$  9.78 with coupling constants  $^1J_{^{31}\text{P}-^{107}\text{Ag}} = 465.1$  Hz and the  $^1J_{^{31}\text{P}-^{109}\text{Ag}} = 536.8$  Hz and the two  $\text{PPh}_3$  coordinated to the Ag are chemically equivalent (**Figure 36**). As the  $[\text{Ag}(\text{PPh}_3)_2(\kappa^2\text{-HCO}_3)]_2$  **89** complex was isolated from the reaction mixture  $\text{Ag}_2\text{CO}_3$  and  $\text{PPh}_3$  with  $\text{C}_6\text{F}_5\text{H}$  **17** in DMF, it was hypothesized that this species could be one of the equilibrium species present in the solution of  $\text{Ag}_2(\text{PPh}_3)_2(\text{C}_6\text{F}_5)(\mu_2\text{-HCO}_3)$  **91**. However, it was found that the chemical shift and coupling constant of **89** was not in agreement with any of the  $\text{Ag-P}$  species present in the  $\text{Ag}_2(\text{PPh}_3)_2(\text{C}_6\text{F}_5)(\mu_2\text{-HCO}_3)$  **91**.

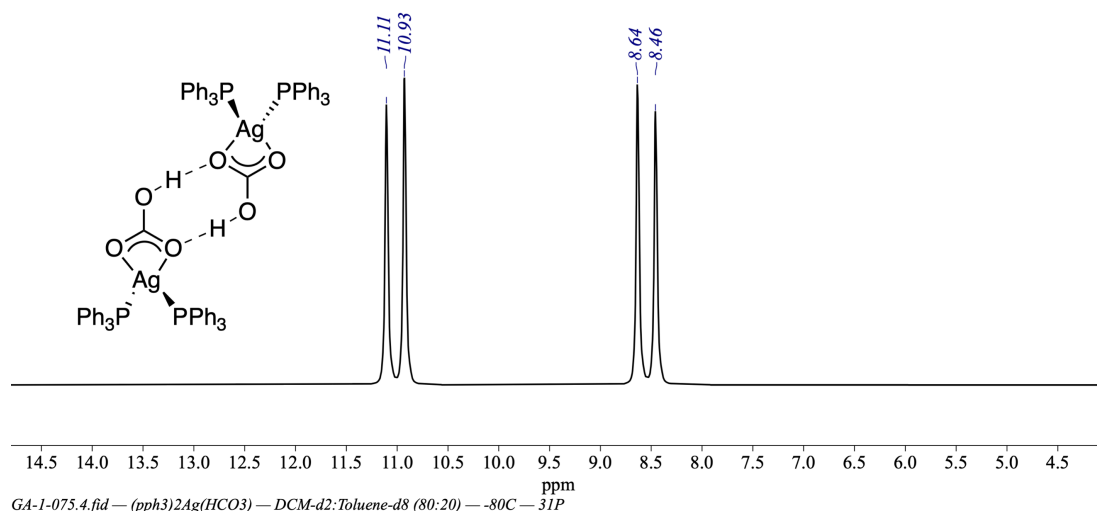


**Figure 36:**  $^{31}\text{P}\{^1\text{H}\}$  NMR (202 MHz, tol- $d_8$ :dichloromethane- $d_2$  (20:80),  $-80^\circ\text{C}$ ) spectrum of  $[\text{Ag}(\text{PPh}_3)_2(\text{HCO}_3)]_2$  **89**.

All Spectra of GA-1-070.34.fid  
VT-Low temp, RT  
Toluene- $d_8$ :DCM- $d_2$  (20:80) (-100 c)  
31P

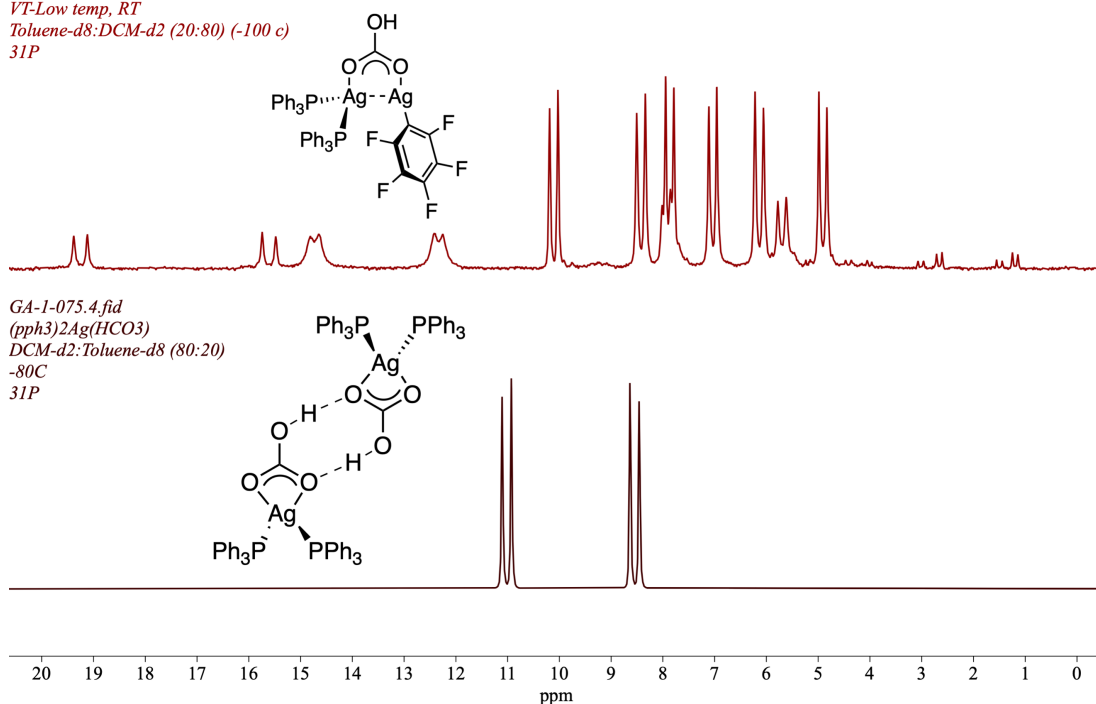
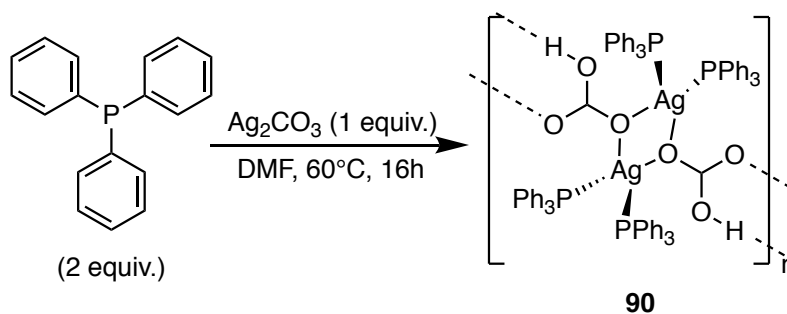


**Figure 37:** Stack plot of the  $^{31}\text{P}\{^1\text{H}\}$  NMR (202 MHz, tol- $d_8$ :dichloromethane- $d_2$  (20:80),  $-80^\circ\text{C}$ ) spectrum of **91** (top) and **89** (bottom)

A polymorph of  $[\text{Ag}(\text{PPh}_3)_2(\kappa^2\text{-HCO}_3)]_2$  **89** was isolated when studying the reaction between  $\text{Ag}_2\text{CO}_3$  and  $\text{PPh}_3$  in DMF to observe the formation of phosphine-coordinated silver species in DMF under standard reaction conditions (**Scheme 52**). After heating at  $60^\circ\text{C}$  for 16 h, a single resonance at  $\delta$  5.8 was observed in the  $^{31}\text{P}\{^1\text{H}\}$  NMR spectrum with no unbound phosphines remaining. Attempts to characterize the complex in DMF using low temperature

$^{31}\text{P}\{^1\text{H}\}$  NMR spectroscopy failed as the lowest temperature possible to achieve with DMF is  $-50\text{ }^\circ\text{C}$  which was not cold enough to resolve any silver-phosphorus coupling.



**Scheme 52:** Reaction of  $\text{Ag}_2\text{CO}_3$  with 2 equiv. of  $\text{PPh}_3$  in DMF at  $60^\circ\text{C}$  for 16 h to yield **90**

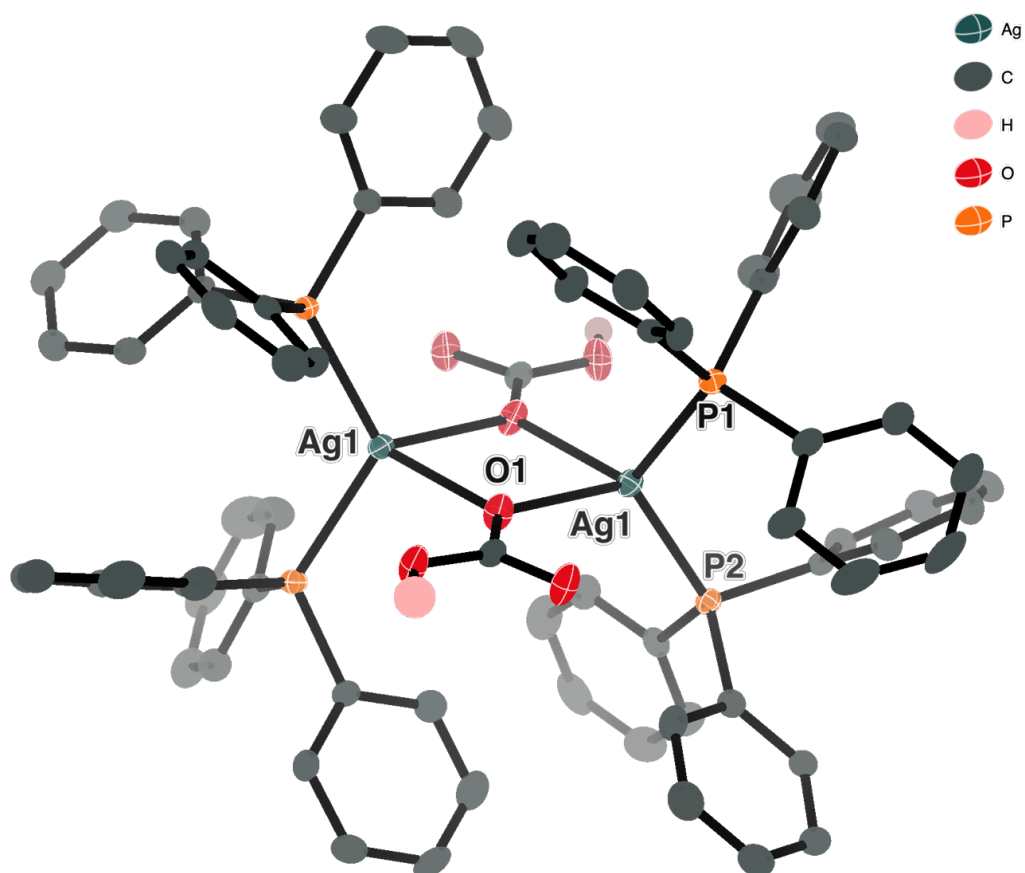


**Figure 38:** The X-ray crystal structure of **90**, the crystals isolated from the reaction between  $\text{Ag}_2\text{CO}_3$  and  $\text{PPh}_3$  in DMF.

The complex was isolated from the reaction mixture (in DMF) *via* vapour-diffusion recrystallization using hexane as an anti-solvent and the crystals were analysed using X-ray diffraction (**Figure 38**) and revealed to be a polymorph of **89**.  $[\text{Ag}(\text{PPh}_3)_3\text{HCO}_3]_n$  **90** was found to be a hydrogen-bond polymer, where the units are bound by hydrogen carbonate groups. The

distance between the oxygen of the donor -OH and acceptor -O is 2.582(3) Å and the O···H is 1.77 Å. Bowmaker *et al.* isolated a similar compound  $[(\text{PPh}_3)_2\text{Ag}(\mu\text{-O-COOH})_2\text{Ag}(\text{PPh}_3)_2]$ , with similar crystal parameters. However, they were only able to isolate this complex once serendipitously when attempting to synthesize  $\text{Ag}(\text{PPh}_3)_2(\text{HCO}_3)$ . Subsequent attempts to reproduce this synthesis by Bowmaker *et al.* failed.

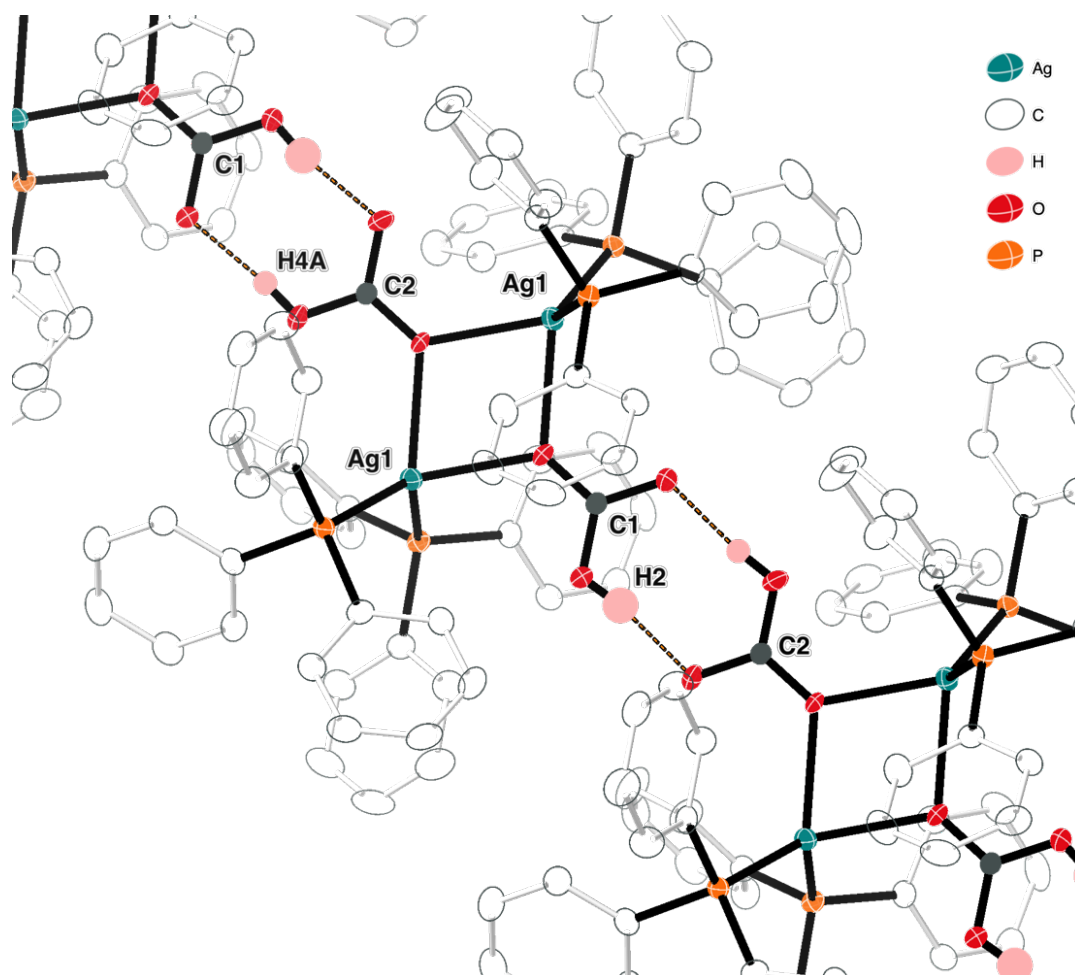
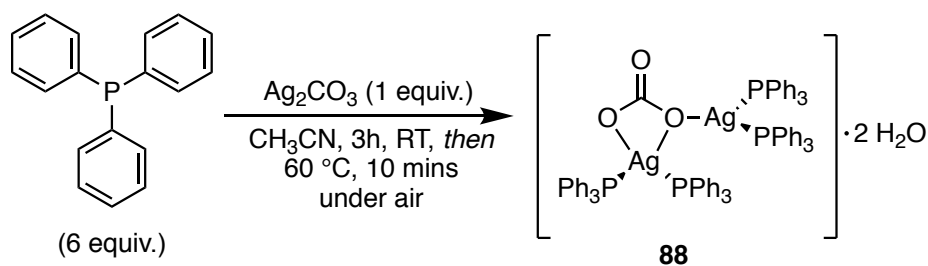


**Figure 39:** The  $[\text{Ag}(\text{PPh}_2)_3\text{HCO}_3]_n$  **90** existed as a coordinate polymer connected *via* hydrogen bonding.

Bowmaker *et al.* also published the synthesis of a phosphine-ligated silver carbonate  $[\text{Ag}(\text{PPh}_3)_2]_2(\text{CO}_3)$  **88**. Their synthesis was repeated to examine if this complex was capable of C–H activation (**Scheme 53**). A mixture of  $\text{Ag}_2\text{CO}_3$  with 6 equivalents of  $\text{PPh}_3$  in  $\text{CH}_3\text{CN}$  at room temperature in an open flask, and the gradually heated to 60 °C for 10 minutes to precipitate a white solid within 10 minutes of heating. This solid was redissolved in hot acetonitrile, and was slowly cooled to ambient temperature to yielded  $[\text{Ag}(\text{PPh}_3)_2]_2(\text{CO}_3)$  **88** as a white flaky solid with 37 % yield. Interestingly, Bowmaker *et al.* observed no formation of **88** when the reaction was carried out under an inert atmosphere and moisture-free

conditions. They postulate that contact with ambient air is required and the source of the H<sub>2</sub>O incorporated in the complex.<sup>121</sup>



**Scheme 53:** The synthesis of the [(PPh<sub>3</sub>)<sub>2</sub>Ag]<sub>2</sub>(CO<sub>3</sub>) **88** from the reaction of Ag<sub>2</sub>CO<sub>3</sub> with 6 equiv. of PPh<sub>3</sub> in CH<sub>3</sub>CN.<sup>121</sup>

The complex was characterised in a solvent mixture of toluene-*d*<sub>8</sub>:dichloromethane-*d*<sub>2</sub> (20:80), and characterised at -100 °C (173 K). Much like **91** and **93** complex, the product exists as an equilibrium with multiple Ag–PPh<sub>3</sub> species, with most peaks contained between δ -3 to δ 21. Most of the resonances exist as pairs of doublets characteristic of Ag–P coupling (Table 12). However, some of the peaks were difficult to distinguish due to peak overlap.

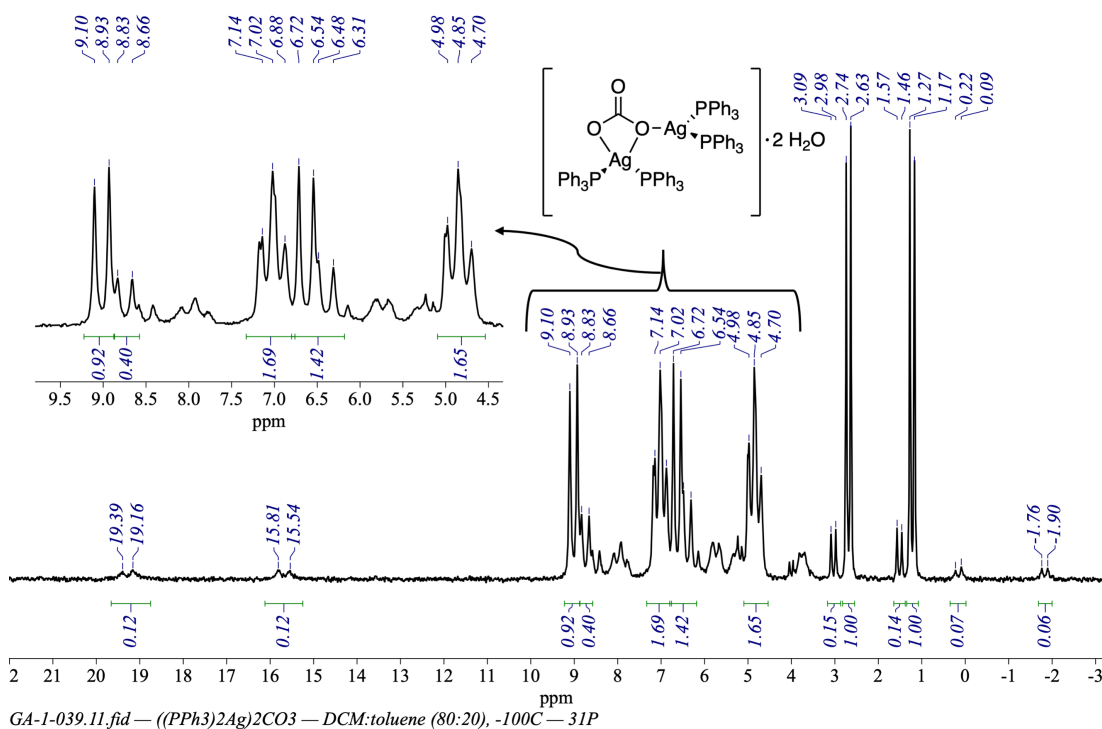


**Figure 40:** The <sup>31</sup>P{<sup>1</sup>H} NMR (202 MHz, dichloromethane-*d*<sub>2</sub>:tol-*d*<sub>8</sub>, -100°C) spectrum of [(PPh<sub>3</sub>)<sub>2</sub>Ag]<sub>2</sub>(CO<sub>3</sub>)·2H<sub>2</sub>O **88**

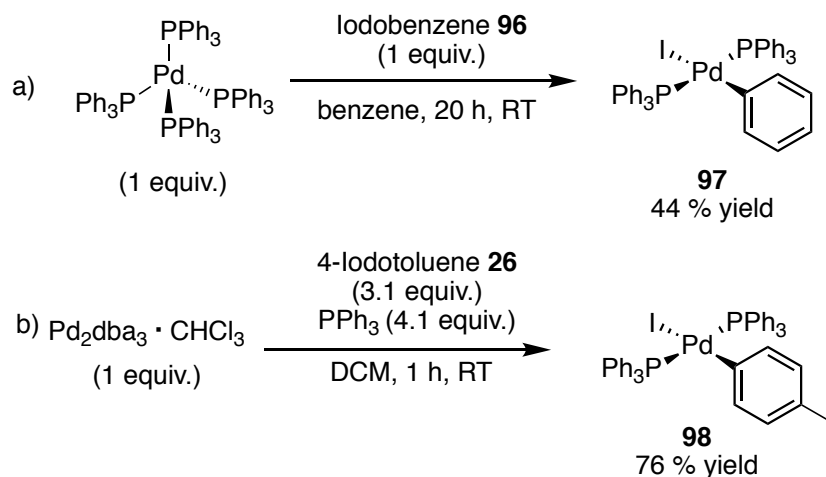
**Table 12:** Low temperature  $^{31}\text{P}\{^1\text{H}\}$  NMR data of  $[\text{Ag}(\text{PPh}_3)_2]_2\text{CO}_3 \cdot 2 \text{H}_2\text{O}$  **88** at  $-100^\circ\text{C}$  (173 K)

Entry	Chemical shift of $^{31}\text{P}$ – $^{107}\text{Ag}$ ( $\delta$ )		Chemical shift of $^{31}\text{P}$ – $^{109}\text{Ag}$ ( $\delta$ )		Resonance Centered at ( $\delta$ )	Integration		Coupling constant $^1J_{^{31}\text{P}-^{107}\text{Ag}}$ (Hz)	Coupling Constant $^1J_{^{31}\text{P}-^{109}\text{Ag}}$ (Hz)
	Peak 1	Peak 2	Peak 1	Peak 2		Peak 1	Peak 2		
1	0.09	-1.76	0.22	-1.90	-0.8	0.07	0.06	374	428
2	2.63	1.27	2.74	1.17	2.0	1.00	1.00	275	317
3	2.98	1.57	3.09	1.46	2.3	0.15	0.14	285	329
4	8.66	6.48	8.83	6.31	7.6	1.42	1.42	440	509
5	8.93	6.72	9.1	6.54	7.8			446	517
6	19.16	15.81	19.39	15.54	17.5	0.12	0.12	677	778

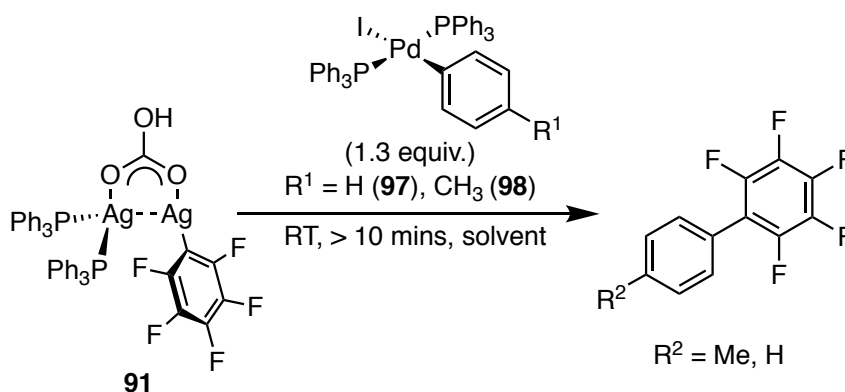
## 2.5 Experiments with Reaction Intermediates

### 2.5.1 Cross-Coupling Reactions with $\text{Pd}^{\text{II}}$ Complexes

The current hypothesis suggests that the product of C–H activation by Ag, such as  $\text{Ag}_2(\text{PPh}_3)_2(\text{C}_6\text{F}_5)(\mu_2\text{-HCO}_3)$  **91** is capable of undergoing transmetalation with the oxidative addition product  $\text{Pd}(\text{PPh}_3)_2(\text{aryl})(\text{I})$ , to generate a Pd biaryl complex which can reductively eliminate to form the organic product and regenerate the active catalytic species. To examine this, the oxidative addition products of  $\text{Pd}^0$  into iodobenzene **96** and 4-iodotoluene **26** were prepared. The reaction of  $\text{Pd}(\text{PPh}_3)_4$  with iodobenzene **96** in benzene at room temperature, resulted in the isolation of the *trans*- $\text{Pd}(\text{PPh}_3)_2(\text{I})(\text{Ph})$  **97** with a yield of 44 %. Complex **98** was isolated at 74 % yield from the reaction between  $\text{Pd}_2(\text{dba})_3 \cdot \text{CHCl}_3$  with 4-iodotoluene **26** and  $\text{PPh}_3$  in dichloromethane.

**Figure 41:** The synthesis of  $\text{Pd}(\text{PPh}_3)_2(\text{I})(\text{phenyl})$  **97** and  $\text{Pd}(\text{PPh}_3)_2(\text{I})(4\text{-tolyl})$  **98**

The  $\text{Ag}_2(\text{PPh}_3)_2(\text{C}_6\text{F}_5)(\mu_2\text{-HCO}_3)$  **91** reacted rapidly with the  $\text{Pd}(\text{PPh}_3)_2(\text{R})(\text{I})$ , ( $\text{R}$  = phenyl, 4-tolyl) complex to undergo transmetalation and subsequent reductive elimination at room temperature (**Scheme 54**). The reaction occurred within 10 min as a solution of **91** was added to  $\text{Pd}(\text{PPh}_3)_2(\text{R})(\text{I})$  complex. The reaction was accompanied by a colour change from a cloudy grey colour to moss green. All of the  $\text{Ag}_2(\text{PPh}_3)_2(\text{C}_6\text{F}_5)(\mu_2\text{-HCO}_3)$  **91** was fully consumed before the first  $^{19}\text{F}\{^1\text{H}\}$  NMR spectra could be recorded ( $> 10$  min), and the  $^{19}\text{F}\{^1\text{H}\}$  NMR spectrum showed full conversion to the organic product, along with the 30% of  $\text{C}_6\text{F}_5\text{H}$  contaminant from the **91** complex.



**Scheme 54:** The transmetalation and subsequent reductive elimination reaction between **91** and  $\text{Pd}(\text{PPh}_3)_2(\text{I})(\text{R}^1)$  where  $\text{R}^1 = \text{H}$ , Me. (Solvent = toluene, dichloromethane)

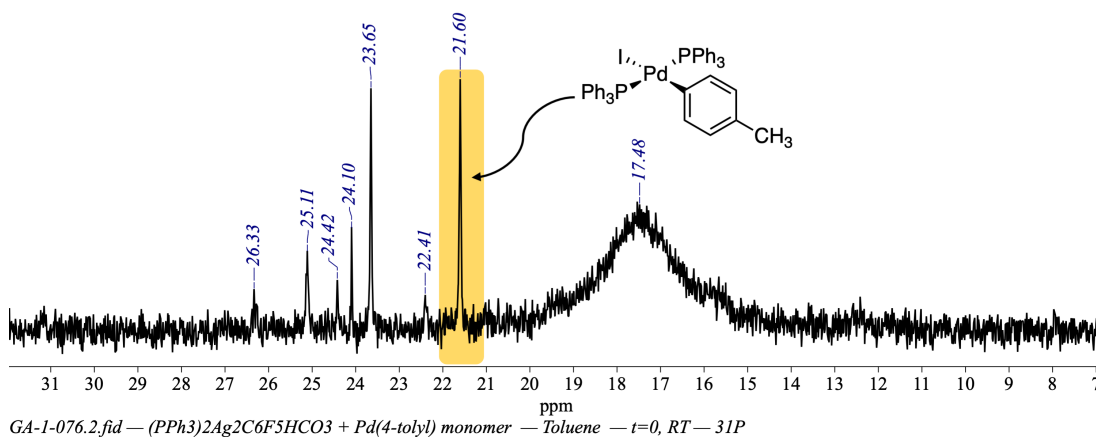


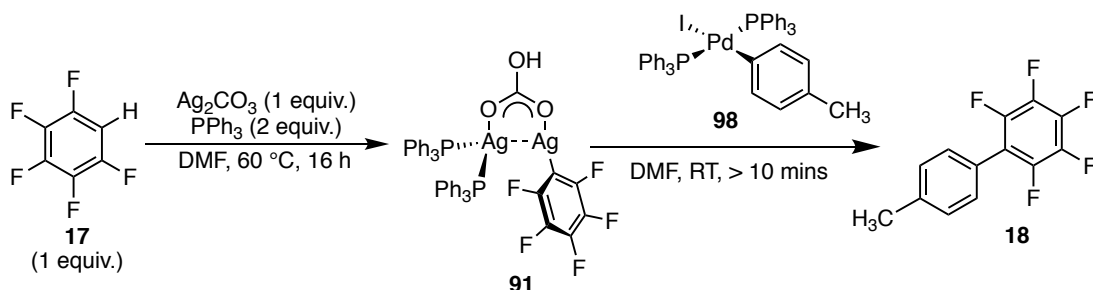
**Figure 42:**  $^{31}\text{P}\{^1\text{H}\}$  NMR (202 MHz, Tol, 25 °C) spectrum of the reaction mixture of  $\text{Ag}_2(\text{PPh}_3)_2(\text{C}_6\text{F}_5)(\mu_2\text{-HCO}_3)$  **91** and  $\text{Pd}(\text{PPh}_3)_2(\text{I})(\text{tolyl})$  **98**

No evidence of the product of transmetalation,  $\text{Pd}(\text{PPh}_3)_2(\text{R})(\text{C}_6\text{F}_5)$  ( $\text{R}$  = phenyl or 4-tolyl) was detected at room temperature by either  $^{31}\text{P}\{^1\text{H}\}$  or  $^{19}\text{F}\{^1\text{H}\}$  NMR spectroscopy. Additionally, it should be noted that transmetalation and reductive elimination occurred rapidly at room temperature, whereas the standard catalytic reaction with 4-iodotoluene **26**



and pentafluorobenzene **17** is carried out at 60 °C. The  $^{31}\text{P}\{^1\text{H}\}$  NMR spectrum of the reaction mixture of **91** and **98** showed multiple phosphorus containing species, with unreacted *trans*-Pd(PPh<sub>3</sub>)<sub>2</sub>(4-tolyl)(I) **98** at  $\delta$  21.6 and a unassigned broad peak centred at  $\delta$  17.5 (**Figure 42**). At room temperature, in toluene Ag<sub>2</sub>(PPh<sub>3</sub>)<sub>2</sub>(C<sub>6</sub>F<sub>5</sub>)( $\mu_2$ -HCO<sub>3</sub>) **91** appears as a singlet at  $\delta$  9.44, however due to the lability of the PPh<sub>3</sub> and within a complex mixture such as this it is difficult to detect the presence of any silver species. As a result of the lability of the Ag–PPh<sub>3</sub> bond and complexity of the  $^{31}\text{P}\{^1\text{H}\}$  NMR spectrum, not many conclusions could be drawn.

The reaction was also carried out in DMF; **91** was generated *in situ* in DMF and was directly reacted with **98** without isolation (**Scheme 55**). Heating a mixture of Ag<sub>2</sub>CO<sub>3</sub> and PPh<sub>3</sub> with 1 equiv. of **17** in DMF for 16 h resulted in an 83 % conversion to **91** which was subsequently reacted with 1.2 equiv. of *trans*-Pd(PPh<sub>3</sub>)<sub>2</sub>(tolyl)(I) (**98**). In a similar way to the reactions carried out in toluene and dichloromethane, **91** reacted immediately with **98** and the  $^{19}\text{F}\{^1\text{H}\}$  NMR spectrum collected within less than 10 min showed full consumption of **91** and the presence of **18**. However, an additional broad peak at  $\delta$  –117.2 was also detected (**Figure 43**). This could potentially be *trans*-Pd(PPh<sub>3</sub>)<sub>2</sub>(4-tolyl)(C<sub>6</sub>F<sub>5</sub>), but this is difficult to confirm due to the low concentration of the species. Additionally, the  $^{31}\text{P}\{^1\text{H}\}$  NMR spectrum was too complex to easily detect the corresponding phosphorus resonance of the Pd(PPh<sub>3</sub>)<sub>2</sub>(tolyl)(C<sub>6</sub>F<sub>5</sub>).



**Scheme 55:** The *in situ* generation of **91** from **17** and subsequent reaction of **91** with **98** in DMF

In an attempt to observe any of the intermediates involved in transmetalation and reductive elimination, the reaction between **91** and **98** was prepared at –78 °C using an acetone/dry ice cold bath and placed in the pre-cooled probe (–75 °C) on the AV 500 MHz instrument. At –75 °C, the Ag<sub>2</sub>(PPh<sub>3</sub>)<sub>2</sub>(C<sub>6</sub>F<sub>5</sub>)( $\mu_2$ -HCO<sub>3</sub>) (**91**) and *trans*-Pd(PPh<sub>3</sub>)<sub>2</sub>(4-tolyl)(I) **98** remained unreacted and the  $^{31}\text{P}\{^1\text{H}\}$  and  $^{19}\text{F}\{^1\text{H}\}$  resonances of the Ag<sub>2</sub>(PPh<sub>3</sub>)<sub>2</sub>(C<sub>6</sub>F<sub>5</sub>)( $\mu_2$ -HCO<sub>3</sub>) **91** were partially resolved. The temperature was gradually increased in increments of 10 °C from –70 °C to 0 °C. Formation of the organic product was detected in the  $^{19}\text{F}\{^1\text{H}\}$  NMR spectrum at –10 °C. Unfortunately, during the course of the experiment, *trans*-Pd(PPh<sub>3</sub>)<sub>2</sub>(4-tolyl)(I) **98** complex partially precipitated from solution.

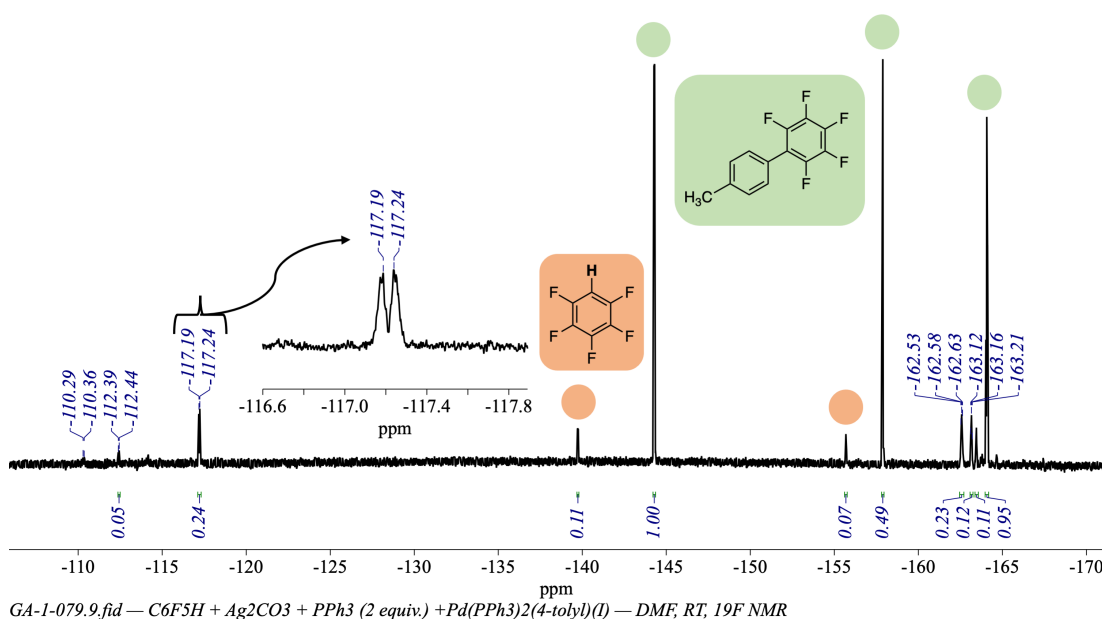


**Figure 43:**  $^{19}\text{F}\{^1\text{H}\}$  NMR (470 MHz, DMF, 25 °C) spectrum of the reaction mixture of **91** and **98**

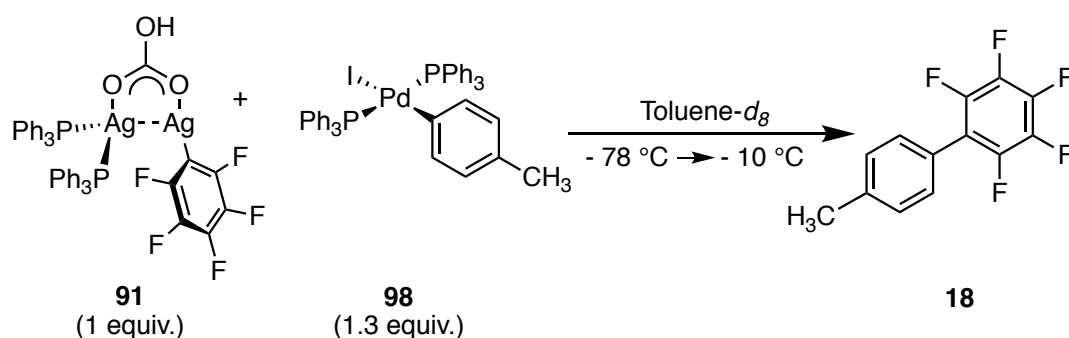


**Figure 44:** Reaction between **91** and **98** monitored by  $^{31}\text{P}\{^1\text{H}\}$  and  $^{19}\text{F}\{^1\text{H}\}$  NMR spectroscopy in a temperature range of  $-75\text{ °C}$  (198 K) to  $-10\text{ °C}$  (263 K) in toluene- $d_8$ .

The experiment was repeated using dichloromethane as both **91** and **98** have a higher solubility in this solvent. The  $^{31}\text{P}\{^1\text{H}\}$  and  $^{19}\text{F}\{^1\text{H}\}$  NMR spectrum of the reaction mixture were collected for a temperature range between  $-40\text{ °C}$  (233 K) to  $0\text{ °C}$  (273 K) with  $5\text{ °C}$  increments. The sample was prepared at  $-78\text{ °C}$  and placed in the pre-cooled probe ( $-40\text{ °C}$ ) on the AV 500 MHz instrument. Likely due to the increased solubility, transmetalation and reductive elimination occurred at  $-40\text{ °C}$  as generation of the organic product (6% conversion) was observed in the  $^{19}\text{F}\{^1\text{H}\}$  NMR spectrum. The formation and consumption of new peaks were observed in the  $^{19}\text{F}\{^1\text{H}\}$  and  $^{31}\text{P}\{^1\text{H}\}$  NMR spectrum, however it was difficult to reliably assign these peaks due to the complexity of the spectra and peak overlap. Additionally, the resonances corresponding to Ag complexes are not fully resolved at the chosen temperature

range of  $-40\text{ }^{\circ}\text{C}$  (233 K) to  $0\text{ }^{\circ}\text{C}$  (273 K). Without any Ag–P coupling information it is difficult to assign which peaks correspond to Ag and which to Pd and to detect if any Ag or Pd containing by-products are being formed.

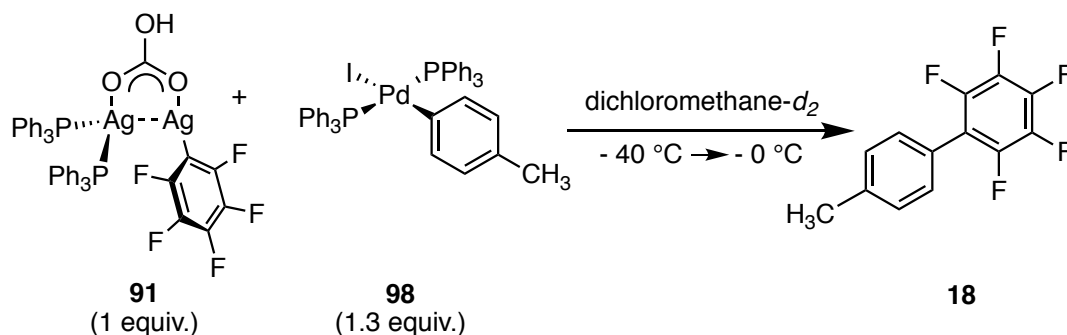
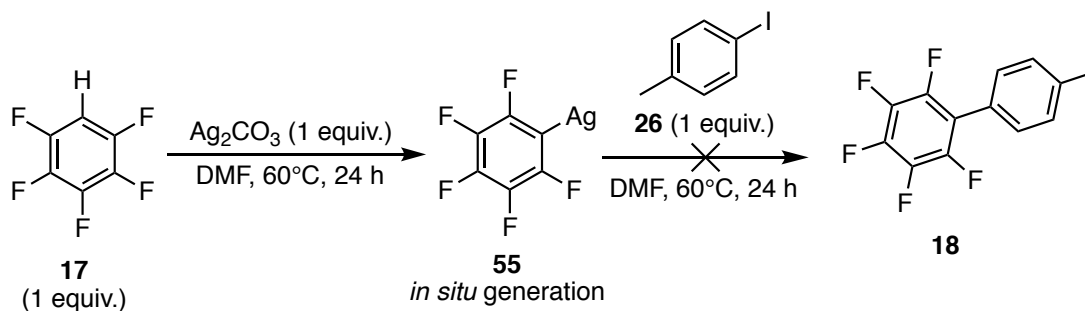


**Figure 45:** Reaction between **91** and **98** monitored by  $^{31}\text{P}\{^1\text{H}\}$  and  $^{19}\text{F}\{^1\text{H}\}$  NMR spectroscopy in a temperature range of  $-40\text{ }^{\circ}\text{C}$  (233 K) to  $0\text{ }^{\circ}\text{C}$  (273 K) in dichloromethane- $d_2$ .

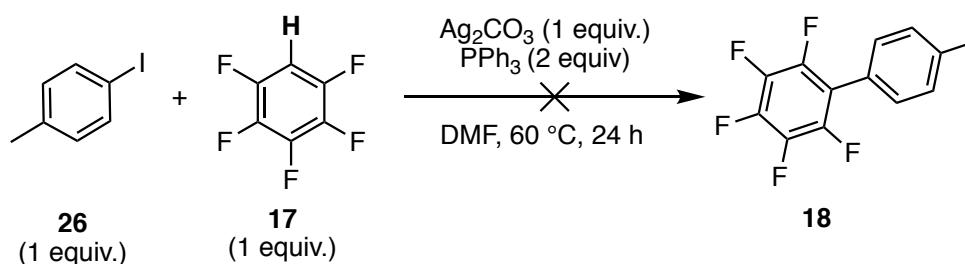
As a control, **91** was reacted directly with 4-iodotoluene **26** and monitored by  $^{19}\text{F}\{^1\text{H}\}$  at 1 h, 24 h and at 48 h. Only trace formation of product was detected after heating at  $60\text{ }^{\circ}\text{C}$  for 48 h, indicating that the direct reaction of **91** with 4-iodotoluene **26** unlikely to occur under catalytic conditions.

Previously, it was noted that the reaction between 1 equiv. of  $\text{Ag}_2\text{CO}_3$  with  $\text{C}_6\text{F}_5\text{H}$  in  $\text{CH}_3\text{CN}$  resulted in the formation of trace amounts of  $\text{AgC}_6\text{F}_5$  **55** (Table 3, Entry 2). Thus, an experiment was conducted to observe if the  $\text{AgC}_6\text{F}_5$  **55** generated *in situ*, is capable of directly reaction with 4-iodotoluene **26** (Scheme 56). A mixture of  $\text{Ag}_2\text{CO}_3$  and 1 equivalent of  $\text{C}_6\text{F}_5\text{H}$  **17** was stirred at  $60\text{ }^{\circ}\text{C}$  for 24 h, and the  $^{19}\text{F}\{^1\text{H}\}$  NMR spectrum showed approximately 1% conversion of  $\text{C}_6\text{F}_5\text{H}$  to  $\text{AgC}_6\text{F}_5$  **55**. 4-Iodotoluene **26** was added to this reaction mixture and was heated for an additional 24 h. None of the resonances associated with the organic product was observed *via*  $^{19}\text{F}\{^1\text{H}\}$  NMR spectroscopy and the  $\text{AgC}_6\text{F}_5$  (approximately 1%) remained unreacted in solution, indicating that any  $\text{AgC}_6\text{F}_5$  generated is unlikely to reaction directly with 4-iodotoluene **26**.



**Scheme 56:** The *in situ* generation of  $\text{AgC}_6\text{F}_5$  **55** from the reaction between  $\text{Ag}_2\text{CO}_3$  and  $\text{C}_6\text{F}_5\text{H}$  **17**, and subsequent reaction with 4-iodotoluene **26**

As another control, the reaction between  $\text{C}_6\text{F}_5\text{H}$  **17** and 4-iodotoluene **26** was carried out with 1 equivalent of  $\text{Ag}_2\text{CO}_3$  and 2 equivalent of  $\text{PPh}_3$ , without the inclusion of  $\text{Pd}(\text{OAc})_2$  (**Scheme 57**). After heating for 24 h at  $60^\circ\text{C}$ , the  $^{19}\text{F}\{^1\text{H}\}$  NMR spectrum of the reaction mixture showed 80% conversion of **17** to  $\text{Ag}_2(\text{PPh}_3)_2(\text{C}_6\text{F}_5)(\mu_2\text{-HCO}_3)$  **91** with only trace amounts of organic product detected.  $\text{Pd}(\text{OAc})_2$  is required for the direct arylation reaction to occur, and additionally **91** generated *in situ* is incapable of directly reacting with 4-iodotoluene **26**.



**Scheme 57:** The reaction between  $\text{C}_6\text{F}_5\text{H}$  **17** and 4-Iodotoluene **26** in the presence of  $\text{Ag}_2\text{CO}_2$  and  $\text{PPh}_3$  in DMF

### 2.5.2 Reactions with Phosphine-Coordinated Silver(I) Complexes

A phosphine-coordinated Ag complex is often proposed to be responsible for C–H activation.<sup>86,87</sup> To test this hypothesis, the following complexes were reacted with 10 equivalents of  $\text{C}_6\text{F}_5\text{H}$  **17** in DMF at  $60^\circ\text{C}$  for 24 h (**Figure 46**). Due to the lability of the Ag– $\text{PPh}_3$  bond, no useful information could be derived from the  $^{31}\text{P}\{^1\text{H}\}$  NMR spectra of the reaction mixtures at room temperature. Principally, the  $^{19}\text{F}\{^1\text{H}\}$  NMR spectrum was used to detect the presence of the  $\text{AgC}_6\text{F}_5$  containing products. As the  $\text{PPh}_3$  coordinated Ag species undergo complex speciation in solution, the products of C–H activation are typically ill-defined in solution. This makes it impossible to calculate % conversion or yields. Instead,

qualitative observations such as the presence of  $\text{AgC}_6\text{F}_5$  containing product in the  $^{19}\text{F}\{^1\text{H}\}$  NMR spectrum and the integral of this peak with respect to  $\text{C}_6\text{F}_5\text{H}$  is reported.

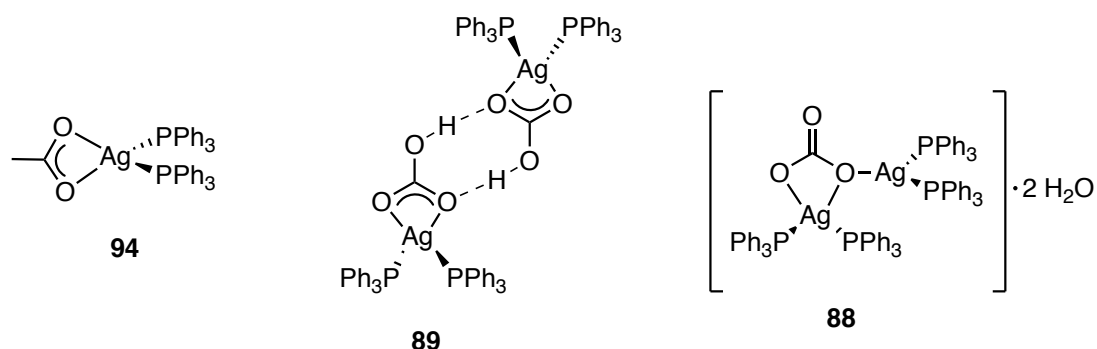
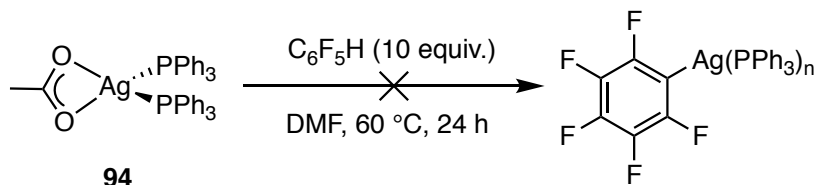


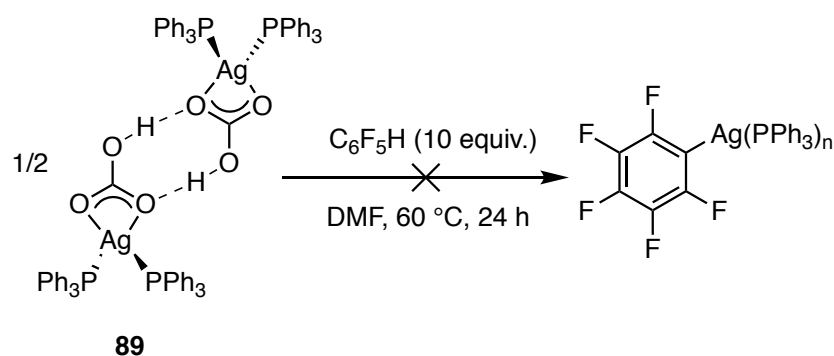
**Figure 46:** Reactivity of the above phosphine-coordinated Ag complexes were tested with 10 equivalents of  $\text{C}_6\text{F}_5\text{H}$  17

The  $\text{Ag}(\text{PPh}_3)_2(\kappa^2\text{-OAc})$  94 complex was unable to C–H activate  $\text{C}_6\text{F}_5\text{H}$  17 when reacted with 10 equivalents  $\text{C}_6\text{F}_5\text{H}$  in DMF (Scheme 58). The reaction mixture was heated for 2 h and 24 h and in both instances, no formation of a  $\text{AgC}_6\text{F}_5$  complex was detected by  $^{19}\text{F}\{^1\text{H}\}$  NMR spectroscopy. This is consistent, as the reaction of 10 equivalents of  $\text{C}_6\text{F}_5\text{H}$  17 with  $\text{AgOAc}$  and  $\text{PPh}_3$  in acetonitrile also did not yield any  $\text{AgC}_6\text{F}_5$  complex. Thus, it was concluded that  $\text{AgOAc}$  was not capable of C–H activation within this system.

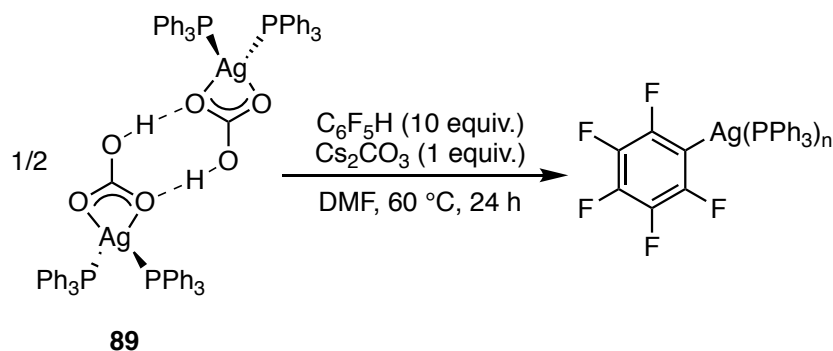


**Scheme 58:** The reaction between  $\text{Ag}(\text{PPh}_3)_2(\kappa^2\text{-OAc})$  and 10 equivalents of  $\text{C}_6\text{F}_5\text{H}$  in DMF heated to  $60\text{ }^\circ\text{C}$

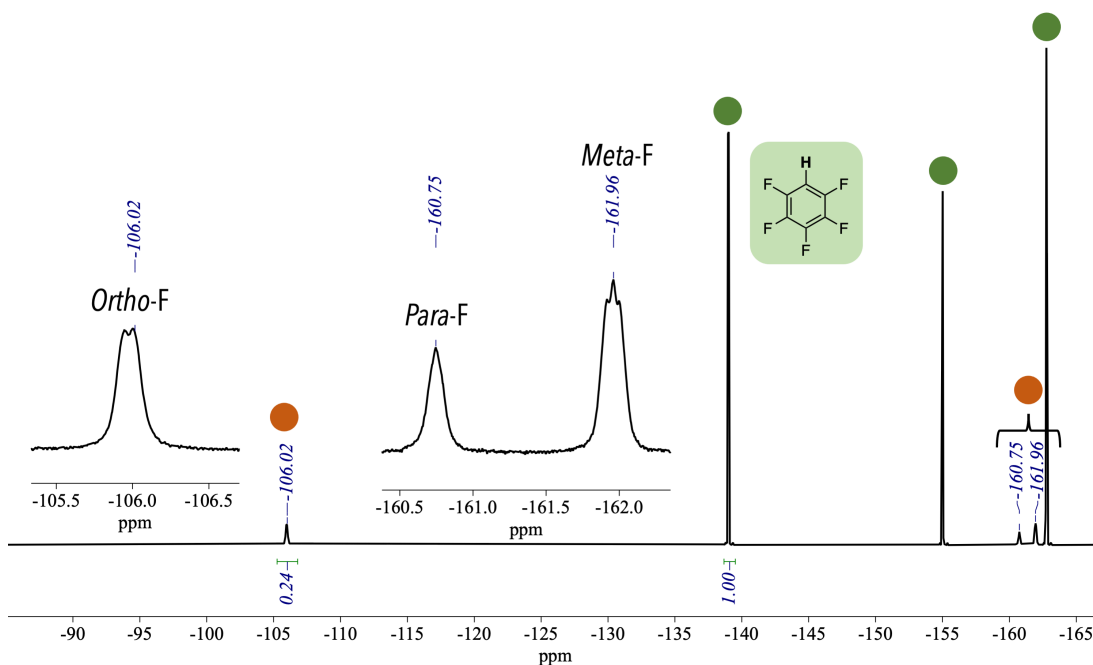
When reacted with 10 equivalents of  $\text{C}_6\text{F}_5\text{H}$  17,  $[\text{Ag}(\text{PPh}_3)_2(\text{HCO}_3)]_2$  89 was found to be incapable of C–H activation, as no formation of an  $\text{AgC}_6\text{F}_5$  containing product was detected by  $^{19}\text{F}\{^1\text{H}\}$  NMR spectroscopy (Scheme 59). However, when 1 equivalent of  $\text{Cs}_2\text{CO}_3$  was added, production of a  $\text{AgC}_6\text{F}_5$  containing product was detected by  $^{19}\text{F}\{^1\text{H}\}$  NMR spectroscopy (Scheme 60). A broad resonance at  $\delta - 106.0$  was detected and assigned as the *ortho*-F peak, with the corresponding *para*-F and *meta*-F at  $\delta - 160.7$  and  $- 162.0$  respectively. The % consumption of  $\text{C}_6\text{F}_5\text{H}$  (Ag:  $\text{C}_6\text{F}_5\text{H}$  is 1:10) after 24 h was 17% and was calculated by integrating the broad resonance at  $- 106.4$  ppm corresponding to the *ortho*-F resonance of the  $\text{AgC}_6\text{F}_5$  motif was integrated with respect to the *ortho*-F resonance of  $\text{C}_6\text{F}_5\text{H}$ . The D1 for the  $^{19}\text{F}\{^1\text{H}\}$  NMR spectrum was set to 10 sec. However, as the product of C–H activation is ill-defined, the % consumption can only be tentatively calculated (Figure 47).



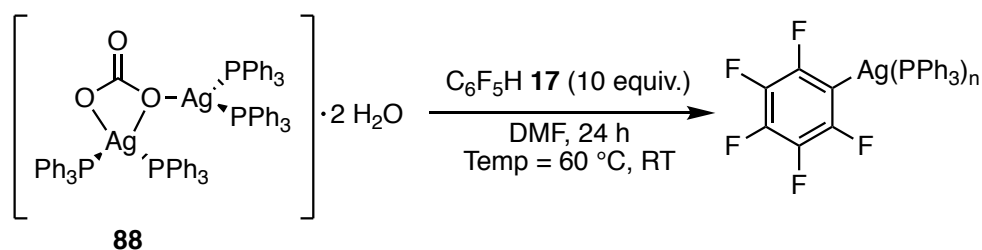
**Scheme 59:** Reaction between  $[\text{Ag}(\text{PPh}_3)_2(\text{HCO}_3)]_2$  **89** with  $\text{C}_6\text{F}_5\text{H}$  **17** in DMF



**Scheme 60:** Reaction of  $[\text{Ag}(\text{PPh}_3)_2(\text{HCO}_3)]_2$  **89** with  $\text{C}_6\text{F}_5\text{H}$  **17** in the presence of  $\text{Cs}_2\text{CO}_3$  (1 equiv.) DMF

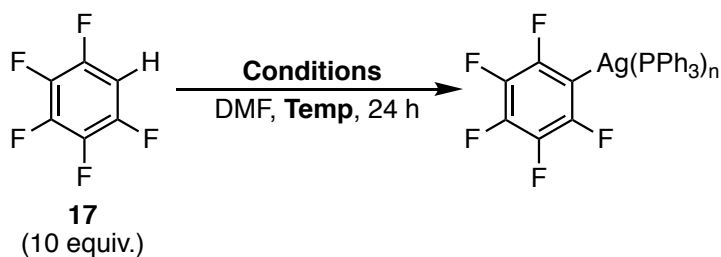


**Figure 47:**  $^{19}\text{F}\{^1\text{H}\}$  NMR (470 MHz, DMF, 25 °C) spectrum of the reaction mixture of **89** and **17** in the presence of  $\text{Cs}_2\text{CO}_3$  with a  $\text{D}_1 = 10$  sec. The  $\text{AgC}_6\text{F}_5$  containing product (orange) and **17** (green) are highlighted.



**Scheme 61:** Reaction between **88** and 10 equivalents of  $C_6F_5H$  **17** in DMF at both 60 °C and room temperature

The carbonate complex  $[(PPh_3)_2Ag]_2(CO_3)$  **88** was found to be capable of C–H bond activation of  $C_6F_5H$  to produce a  $AgC_6F_5$  containing product when reacted with 10 equivalents of  $C_6F_5H$  **17** at 60 °C in DMF. The % consumption of  $C_6F_5H$  was calculated to be 22%, in a similar manner to the reaction with **89**. Interestingly, the complex was capable of C–H activation at room temperature, only more sluggishly than at 60 °C, the % consumption of  $C_6F_5H$  calculated as 6% after 24 h. However, it was difficult to elucidate any more information about the system due to the ill-defined structures of both **88** and  $AgC_6F_5$  containing complex. Nevertheless, this demonstrates that phosphine-coordinated silver carbonate complex, such as **88**, could potentially be active for C–H activation within catalytic direct arylation reaction. Additionally, **88** was partially soluble at RT in DMF and completely soluble at 60 °C compared to  $Ag_2CO_3$  which has very low solubility in DMF. The coordination of  $PPh_3$  helps solubilise  $Ag_2CO_3$  by generating **88**.

**Table 13:** Summary for the stoichiometric reaction of PPh<sub>3</sub> coordinated Ag complexes and 10 equivalents of C<sub>6</sub>F<sub>5</sub>H

Entry	Conditions	Temperature (°C)	Detection of AgC <sub>6</sub> F <sub>5</sub> product	Consumption of C <sub>6</sub> F <sub>5</sub> H (%) <sup>[a]</sup>
1	Ag(PPh <sub>3</sub> ) <sub>2</sub> (κ <sup>2</sup> -OAc) <b>94</b> (1 equiv.)	60	No	-
2	[Ag(PPh <sub>3</sub> ) <sub>2</sub> (κ <sup>2</sup> -HCO <sub>3</sub> ) <sub>2</sub> <b>89</b> (0.5 equiv.)	60	No	-
3	[Ag(PPh <sub>3</sub> ) <sub>2</sub> (κ <sup>2</sup> -HCO <sub>3</sub> ) <sub>2</sub> <b>89</b> (0.5 equiv.) + Cs <sub>2</sub> CO <sub>3</sub> (1 equiv.)	60	Yes	17
4	[Ag(PPh <sub>3</sub> ) <sub>2</sub> ] <sub>2</sub> CO <sub>3</sub> •2 H <sub>2</sub> O <b>88</b>	60	Yes	22
5	[Ag(PPh <sub>3</sub> ) <sub>2</sub> ] <sub>2</sub> CO <sub>3</sub> •2 H <sub>2</sub> O <b>88</b>	RT	Yes	6

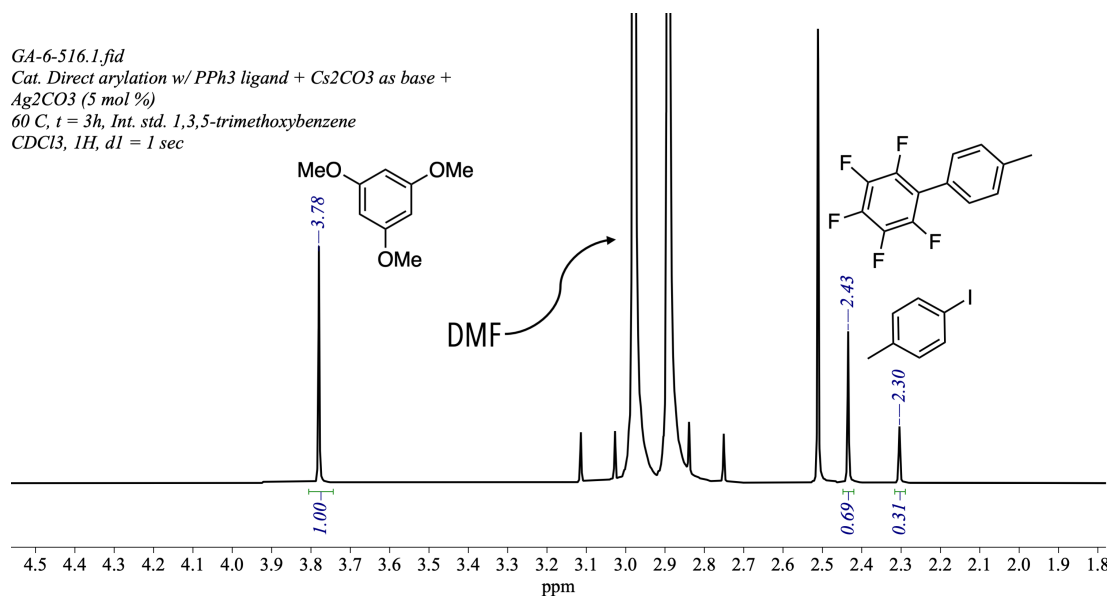
<sup>[a]</sup> Consumption of C<sub>6</sub>F<sub>5</sub>H was calculated by integrating the *ortho*-F resonance of C<sub>6</sub>F<sub>5</sub>H (δ -139) with respect to AgC<sub>6</sub>F<sub>5</sub> containing product (δ -106.02), however due to the ill-defined nature of the AgC<sub>6</sub>F<sub>5</sub> containing product in solution, the % consumption can only be tentatively calculated.

### 2.5.3 Reactivity of Ag Intermediates within the Catalytic Direct Arylation Reaction

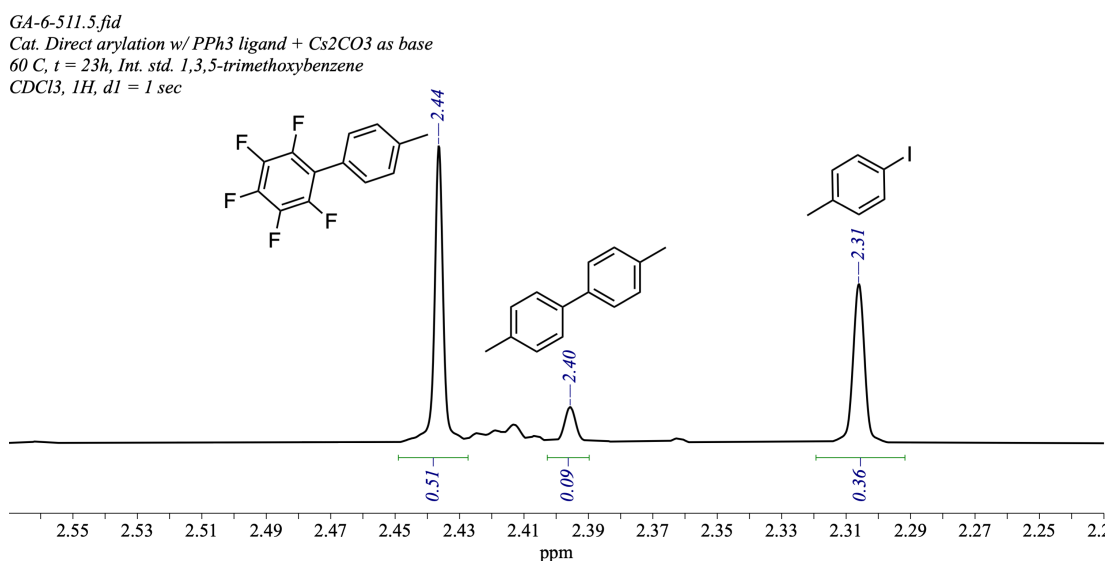
From the stoichiometric reactions, both the phosphine-coordinated Ag carbonate complex **89** (in conjunction with Cs<sub>2</sub>CO<sub>3</sub>) and **88** were found to be capable of C–H activation of C<sub>6</sub>F<sub>5</sub>H. Thus, their activity with the catalytic system was examined. As the standard point of comparison, the Pd-catalysed direct arylation reaction of 4-iodotoluene **26** and pentafluorobenzene **17** with Cs<sub>2</sub>CO<sub>3</sub> as the base was used (**Table 14, Entry 1**). The <sup>1</sup>H NMR conversions were reported using 1,3,5-trimethoxybenzene as the internal standard and were calculated by integrating the -CH<sub>3</sub> peak of 4-iodotoluene (δ 2.30) with respect to the -CH<sub>3</sub> peak of 1,3,5-trimethoxybenzene (δ 3.78) (**Figure 48**). The -CH<sub>3</sub> peak of the product **18** (δ 2.43) could not be reliably integrated in all cases due to peak overlap and was not used. However, where possible the % conversion by integrating the starting material (δ 2.30) and product (δ 2.43) was calculated and was found to be in good agreement with <sup>1</sup>H NMR conversion with internal standard (see **Appendix**). Unless shown otherwise, the reactions were



carried out at 0.9 mmol of 4-iodotoluene **26** in 2.6 mL of DMF. The progress of the reaction was monitored using reaction aliquots which were collected at 3 and 23 h time points. The reaction aliquots were prepared by collecting approximately 0.1 mL of the reaction mixture and filtering it through Celite® using CDCl<sub>3</sub> as the eluent. The sample was locked to CDCl<sub>3</sub> and the spectrum was referenced using the -CH<sub>3</sub> peak of 1,3,5-trimethoxybenzene ( $\delta$  3.78).



**Figure 48:** <sup>1</sup>H NMR (500MHz, CDCl<sub>3</sub>/DMF, 25 °C) spectrum of the reaction mixture in **Entry 4** at 3h showing the -CH<sub>3</sub> resonance of 1,3,5-trimethoxybenzene ( $\delta$  3.78), product **18** ( $\delta$  2.43) and 4-iodotoluene **26** ( $\delta$  2.30). The two singlet off-scale peaks centred at  $\delta$  2.88 and 2.96 are solvent peaks belonging to DMF.

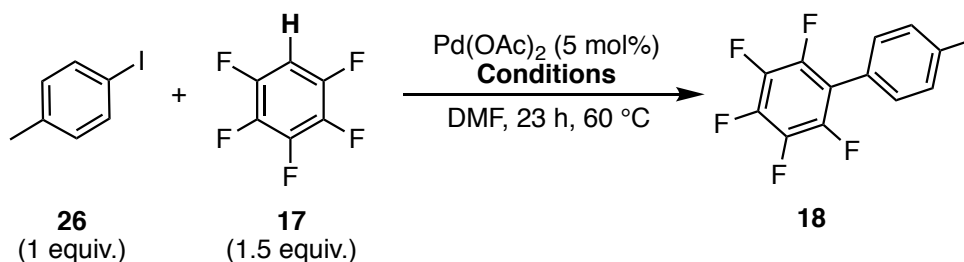


**Figure 49:** The <sup>1</sup>H NMR (500MHz, CDCl<sub>3</sub>/DMF, 25 °C) spectrum of the reaction mixture of **Entry 1** after 23 h with product **18** (2.44), homocoupling side-product **99** (2.40) and 4-iodotoluene **26** (2.31).

When Cs<sub>2</sub>CO<sub>3</sub> was used as the base for the standard catalytic direct arylation reaction, the % conversion after heating for 23 h is 69 %. Trace amounts of the methyl peak of the homocoupling side-product (CH<sub>3</sub>)C<sub>6</sub>H<sub>4</sub>-C<sub>6</sub>H<sub>4</sub>(CH<sub>3</sub>) (4,4'-dimethylbiphenyl, **99**) were also detected at  $\delta$  2.40 (~ 4% <sup>1</sup>H NMR yield) (**Figure 49**). Platt *et al.* observed that when no Ag or over 10 mol% of catalyst loading were used, the reaction produced trace quantities of the biaryl homocoupling side-product.<sup>68</sup>

When 5 mol% of either [Ag(PPh<sub>3</sub>)<sub>2</sub>( $\kappa^2$ -HCO<sub>3</sub>)]<sub>2</sub> **89** or [Ag(PPh<sub>3</sub>)<sub>2</sub>]<sub>2</sub>CO<sub>3</sub>•2 H<sub>2</sub>O **88** was used with Cs<sub>2</sub>CO<sub>3</sub> (0.75 equiv.) as the base, the conversion improved to 98 % and 99 % respectively (**Table 14, Entry 2 and 3**). While no kinetic information was obtained, for the reactions with Ag complexes, the % conversion at 3 h is significantly higher when compared to **Entry 1** with no Ag additives. Additionally, the presence of the side-product **99** was not noticeably detected by the <sup>1</sup>H NMR spectroscopy. With 5 mol% Ag<sub>2</sub>CO<sub>3</sub> the greatest conversion at 3 h (73 %) was obtained and reaction reaches near completion by 23 h (94 % conversion) (**Table 14, Entry 4**). Trace amounts of the homocoupling side-product **99** were also detected but were difficult to quantify due to peak overlap. The amount of Ag used can be decreased to 2.5 mol% without an appreciable decrease in the % conversion. When 1 mol% of Ag<sub>2</sub>CO<sub>3</sub> was used, the <sup>1</sup>H NMR yield dropped from 94 % to 80 % (**Entry 4 and 8**). This result suggests that even the presence of trace amounts of Ag is sufficient to improve the yield and rate of reaction. The result also demonstrates that Ag act as a co-catalyst also with Pd for the direct arylation reaction.

The use of 10 mol% AgC<sub>6</sub>F<sub>5</sub> **55** resulted an almost identical % conversion to when [Ag(PPh<sub>3</sub>)<sub>2</sub>( $\kappa^2$ -HCO<sub>3</sub>)]<sub>2</sub> **89**, [Ag(PPh<sub>3</sub>)<sub>2</sub>]<sub>2</sub>CO<sub>3</sub>•2 H<sub>2</sub>O **88** and Ag<sub>2</sub>CO<sub>3</sub> were used as co-catalysts in the direct arylation reaction (**Entry 2,3,4 and 9**).

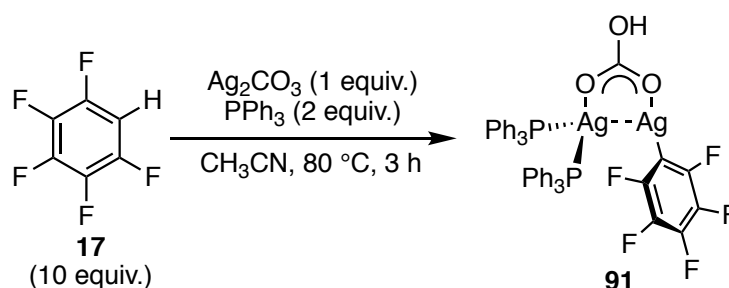
**Table 14:** Influence of the addition of catalytic amounts of Ag containing salts and complexes on the direct arylation reaction of 4-iodotoluene **26** with pentafluorobenzene **17**.

Entry	Conditions	<sup>1</sup> H NMR	
		Conversion <sup>[a]</sup> (%)	
		3 h	23 h
1	PPh <sub>3</sub> (10 mol%) + Cs <sub>2</sub> CO <sub>3</sub> (0.75 equiv.)	15	69
2	PPh <sub>3</sub> (5 mol%) + [Ag(PPh <sub>3</sub> ) <sub>2</sub> (κ <sup>2</sup> -HCO <sub>3</sub> ) <sub>2</sub> <b>89</b> (5 mol%) + Cs <sub>2</sub> CO <sub>3</sub> (0.75 equiv.)	51	98
3	PPh <sub>3</sub> (5 mol%) + [Ag(PPh <sub>3</sub> ) <sub>2</sub> ] <sub>2</sub> CO <sub>3</sub> •2 H <sub>2</sub> O <b>88</b> (5 mol%) + Cs <sub>2</sub> CO <sub>3</sub> (0.75 equiv.)	62	99
4	PPh <sub>3</sub> (10 mol%) + Ag <sub>2</sub> CO <sub>3</sub> (5 mol%) + Cs <sub>2</sub> CO <sub>3</sub> (0.75 equiv.)	73	94
5	PPh <sub>3</sub> (5 mol%) + [Ag(PPh <sub>3</sub> ) <sub>2</sub> (κ <sup>2</sup> -HCO <sub>3</sub> ) <sub>2</sub> <b>89</b> (2.5 mol%) + Cs <sub>2</sub> CO <sub>3</sub> (0.75 equiv.)	54	93
6	PPh <sub>3</sub> (5 mol%) + [Ag(PPh <sub>3</sub> ) <sub>2</sub> ] <sub>2</sub> CO <sub>3</sub> •2 H <sub>2</sub> O <b>88</b> (2.5 mol%) + Cs <sub>2</sub> CO <sub>3</sub> (0.75 equiv.)	59	96
7	PPh <sub>3</sub> (10 mol%) + Ag <sub>2</sub> CO <sub>3</sub> (2.5 mol%) + Cs <sub>2</sub> CO <sub>3</sub> (0.75 equiv.)	57	89
8	PPh <sub>3</sub> (10 mol%) + Ag <sub>2</sub> CO <sub>3</sub> (1 mol%) + Cs <sub>2</sub> CO <sub>3</sub> (0.75 equiv.)	44	80
9	PPh <sub>3</sub> (10 mol%) + AgC <sub>6</sub> F <sub>5</sub> <b>55</b> (10 mol%) + Cs <sub>2</sub> CO <sub>3</sub> (0.75 equiv.)	70	96

<sup>[a]</sup> The <sup>1</sup>H NMR conversion was calculated by integrating the methyl -CH<sub>3</sub> resonance of the starting material 4-iodotoluene **26** (δ 2.30) with respect to 1,3,5-trimethoxybenzene (δ 3.78) in the <sup>1</sup>H NMR spectrum of the reaction mixture with D1 = 1 sec.

## 2.6 Discussion of Results

To understand the role of Ag in the Pd-catalysed direct arylation reactions, the reaction between 4-iodotoluene **26** and pentafluorobenzene **17** was selected, with 5 mol% palladium acetate and 10 mol% triphenylphosphine as the pre-catalyst and ligand respectively. Silver carbonate (0.75 equivalents) was used as the base. It was found that  $\text{Ag}_2\text{CO}_3$  in the presence of  $\text{PPh}_3$  can activate the C–H bond pentafluorobenzene **17** to produce a  $\text{AgC}_6\text{F}_5$ -containing product **91** which was easily recognised *via* the *ortho*-fluorine resonance using  $^{19}\text{F}\{^1\text{H}\}$  NMR spectroscopy. Without the addition of  $\text{PPh}_3$ , only a trace amount of  $\text{AgC}_6\text{F}_5$  **55** was detected. In contrast,  $\text{AgOAc}$  was incapable of C–H bond activation, both in the presence and absence of  $\text{PPh}_3$ .



**Scheme 62:** The synthesis and isolation of **91** from acetonitrile

The  $\text{AgC}_6\text{F}_5$ -containing product **91** was isolated as brown crystals from acetonitrile, and the structure of the complex was determined by X-ray diffraction (**Scheme 62**). During the refinement of the crystal structure, there was some ambiguity in the identity of the bridging ligand, due to the poor quality of the crystals. However, the presence of the hydrogen carbonate as the bridging ligand was later confirmed by  $^{13}\text{C}$  labelling experiments. Unfortunately, the complex was generally contaminated with 25–30% of pentafluorobenzene **17** which, despite numerous purification attempts, could not be removed. The lack of purity complicated any effort to perform detailed kinetic studies with **91**.

At room temperature, the  $^{31}\text{P}\{^1\text{H}\}$  NMR spectrum of all the  $\text{PPh}_3$  coordinated Ag complexes only contained a sharp singlet typically within the range of  $\delta$  11 – 8, (depending on the complex) due to the lability of the  $\text{Ag}-\text{PPh}_3$ . Low temperature NMR spectroscopy was used to resolve the  $^{31}\text{P}\{^1\text{H}\}$  NMR spectrum, and temperatures as low as  $-80\text{ }^\circ\text{C}$  (193 K) to  $-100\text{ }^\circ\text{C}$  (173 K) were required to fully freeze the rapid phosphine exchange. The  $^{31}\text{P}\{^1\text{H}\}$  NMR spectrum of **91** in a mixed solvent system of dichloromethane- $d_2$  and toluene- $d_8$  (80:20) required a temperature of  $-100\text{ }^\circ\text{C}$  (173 K) to be fully resolved. The  $\text{Ag}-\text{P}$  containing species were readily identified by the characteristic  $^{107}\text{Ag}/^{109}\text{Ag}$  coupling pattern with  $^{31}\text{P}$ . The  $^{31}\text{P}\{^1\text{H}\}$  spectrum revealed that **91** exists in an equilibrium of multiple species in solution. A total of 8

different phosphorus-coordinated silver species were tentatively identified in the  $^{31}\text{P}\{^1\text{H}\}$  NMR spectrum but could not be rigorously assigned due to the overlap of the various peaks. Due to the complex speciation of **91** in solution, the solid-state X-ray crystal structure is not representative of the structure in solution. To better understand the structures of the equilibrium species of **91** in solution, the  $^{13}\text{C}$ -labelled analogue of **91**,  $\text{AgC}_6\text{F}_5$  **55** and  $\text{AgC}_6\text{F}_5(\text{PPh}_3)_2$  **93** complex were synthesized and studied using low-temperature NMR spectroscopy. However, only limited information was obtained due to the complex speciation (**Figure 50**).

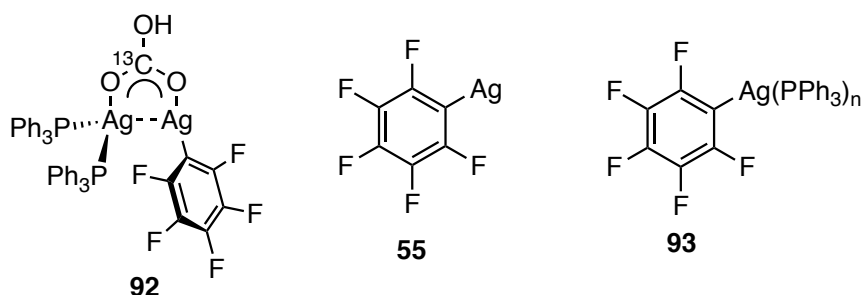


**Figure 50:** Complexes synthesized to help understand the structure of **91** in solution

The carbonate complex **91** reacted rapidly with the  $\text{Pd}(\text{PPh}_3)_2(\text{R})(\text{I})$ , ( $\text{R}$  = phenyl, 4-tolyl), undergoing transmetallation and subsequent reductive elimination at room temperature within 10 min. It should be noted that transmetallation with  $\text{Pd}(\text{PPh}_3)_2(\text{R})(\text{I})$  occurs rapidly at room temperature whereas the standard direct arylation reaction occurs at  $60\text{ }^\circ\text{C}$ . The reaction was also monitored at low temperature in toluene and dichloromethane using  $^{31}\text{P}\{^1\text{H}\}$  and  $^{19}\text{F}\{^1\text{H}\}$  NMR spectroscopy. In dichloromethane, it was found that the transmetallation and reductive elimination occurs at temperatures as low as  $-40\text{ }^\circ\text{C}$  (233 K). However, due to the complexity of the spectrum it was difficult to reliably identify any reaction intermediates. It was also determined that **91** does not react directly with 4-iodotoluene **26** alone and that without the presence of  $\text{Pd}(\text{OAc})_2$ ,  $\text{Ag}_2\text{CO}_3$  and  $\text{PPh}_3$ , is not capable of facilitating the direct arylation reaction between pentafluorobenzene and 4-iodotoluene.

From the literature, it is implied that prior to C–H bond activation, the silver salt coordinates with a phosphine to form a more soluble complex. Thus, a range of phosphine-coordinated silver complexes incorporating both carbonate- and acetate-type ligands were synthesised to identify potential intermediates (**Figure 51**).  $\text{Ag}(\text{PPh}_3)_2(\kappa^2\text{-OAc})$  **94** was synthesized from the reaction between  $\text{AgOAc}$  and 2 equivalents of  $\text{PPh}_3$ , and was found to be incapable of C–H activation when reacted with 10 equivalents of  $\text{C}_6\text{F}_5\text{H}$  **17** at  $60\text{ }^\circ\text{C}$  in DMF. In contrast to **91**,  $\text{Ag}(\text{PPh}_3)_2(\kappa^2\text{-OAc})$  **94** exists as a well-defined species in solution. The  $^{31}\text{P}\{^1\text{H}\}$  NMR spectrum of **94** in dichloromethane- $d_2$  was fully resolved to reveal a pair

of doublets at  $\delta$  8.48 with  $^1J_{31\text{P}-107\text{Ag}} = 370.6$  Hz and  $^1J_{31\text{P}-109\text{Ag}} = 506.2$  Hz. The complex was not active for C–H activation when reacted with  $\text{C}_6\text{F}_5\text{H}$  in DMF at 24 h, this is consistent with the reaction of 10 equivalents of  $\text{C}_6\text{F}_5\text{H}$  **17** with  $\text{AgOAc}$  and  $\text{PPh}_3$ , which did not produce a  $\text{AgC}_6\text{F}_5$  intermediate.

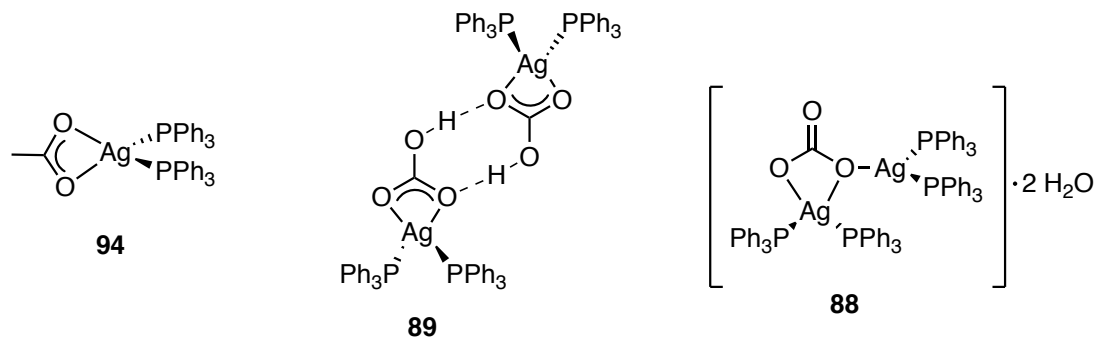


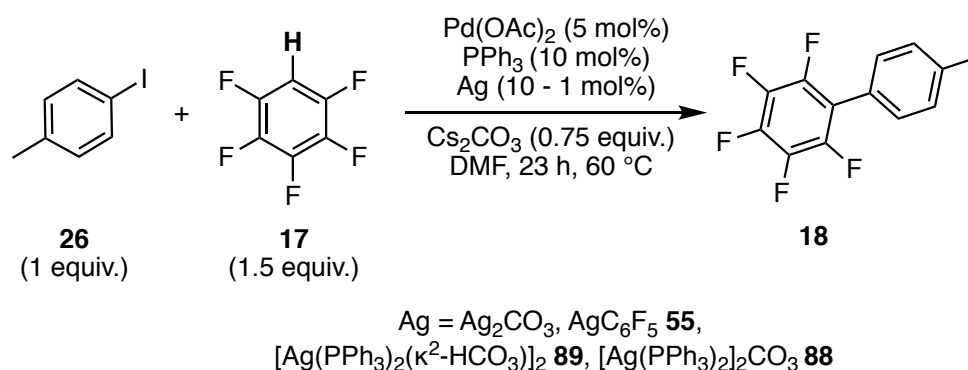
**Figure 51:** Phosphine coordinated Ag complex incorporating acetate, hydrogen carbonate and carbonate ligands.

In contrast,  $[(\text{PPh}_3)_2\text{Ag}]_2(\text{CO}_3)$  **88**, isolated from the reaction between  $\text{Ag}_2\text{CO}_3$  and 6 equivalents of  $\text{PPh}_3$ , was found to be capable of C–H activation when reacted with 10 equivalents of  $\text{C}_6\text{F}_5\text{H}$  **17** at 60 °C in both toluene and DMF. Interestingly, the complex was capable of slow C–H bond activation at room temperature. However, it was difficult to elucidate more information about the system due to the ill-defined structure of both **88** and  $\text{AgC}_6\text{F}_5$  containing complex. Like **91**, **88** was characterised at –100 °C (173 K) and exists in a complex equilibrium with multiple  $\text{Ag}-\text{PPh}_3$  species in solution. The various species could not be assigned with accuracy due to large peak overlaps. Nevertheless, this demonstrates that phosphine-coordinated silver carbonate complex, such as **88**, could potentially be active for C–H activation within the catalytic direct arylation reaction. Additionally, **88** was partially soluble at RT in DMF and completely soluble at 60 °C compared to  $\text{Ag}_2\text{CO}_3$  which has very low solubility in DMF.

The complex  $[\text{Ag}(\text{PPh}_3)_2(\text{HCO}_3)]_2$  **89** was isolated from the reaction between  $\text{AgNO}_3$  and  $\text{Na}_2\text{CO}_3$  with  $\text{PPh}_3$  in a mixture of ethanol and water. The  $^{31}\text{P}\{^1\text{H}\}$  NMR spectrum of  $[\text{Ag}(\text{PPh}_3)_2(\text{HCO}_3)]_2$  **89** in dichloromethane- $d_2$ :toluene- $d_8$  (80:20) was resolved at –80 °C (193 K) and the two  $\text{PPh}_3$  ligands coordinated to the Ag are chemically equivalent. This complex appears to be free of the complicated equilibria present in the other carbonate or bicarbonate complexes. Crystals of the complex were formed when attempting to isolate **91** from DMF *via* vapour diffusion recrystallization methods and a polymorph of **89**, i.e **90** was isolated from the reaction mixture between  $\text{Ag}_2\text{CO}_3$  and 2 equivalents of  $\text{PPh}_3$ . This strongly suggests that **89** is a potential intermediate in the C–H bond activation mechanism of  $\text{C}_6\text{F}_5\text{H}$  **17** by Ag. The  $[\text{Ag}(\text{PPh}_3)_2(\kappa^2\text{-HCO}_3)]_2$  complex **89** was found to be incapable of C–H activation when reacted

with 10 equivalents of  $C_6F_5H$  **17**. However, in the presence of 1 equivalent of  $Cs_2CO_3$ , **89** was found to be capable of C–H activation. Further analysis beyond this was impossible due to the rapid exchange of  $PPh_3$  in solution and complex speciation of the product of C–H activation in solution.

When considering the effect of Ag salts on the direct arylation reaction, the reaction with 0.75 equivalents of  $Cs_2CO_3$  was used a standard point of comparison. When  $Cs_2CO_3$  was used as the base, 69 % conversion was achieved after heating at 60 °C for 23 h. When catalytic amounts of Ag (either in the form of  $Ag_2CO_3$  or using  $AgC_6F_5$  **55**,  $[Ag(PPh_3)_2(\kappa^2-HCO_3)]_2$  **89**  $[Ag(PPh_3)_2]_2CO_3 \cdot 2 H_2O$  **88**) was added in conjunction with  $Cs_2CO_3$  the % conversion after 23 h was typically 95 % or above (**Scheme 63**). The mol% of Ag can be decreased to as low as 2.5 mol% without a significant drop in yield.



**Scheme 63:** Direct arylation reaction of 4-iodotoluene **26** with pentafluorobenzene **17** with catalytic amounts of Ag additives (10 to 1 mol%) and  $Cs_2CO_3$  (0.75 equiv. as the base)

## 2.7 Conclusions

- $Ag_2CO_3$ , in the presence of  $PPh_3$ , can form a more soluble phosphine-coordinated Ag carbonate complex **88**, which undergoes C–H bond activation of  $C_6F_5H$  **17** at both 60 °C and room temperature in DMF.
- The reaction of  $Ag_2CO_3$ ,  $PPh_3$  and  $C_6F_5H$  in DMF yields **91**, which is capable of undergoing transmetalation with  $Pd(PPh_3)_2(Ph)(I)$  and subsequent reductive elimination at room temperature within 10 minutes to generate the organic product.
- Under catalytic conditions, C–H activation by Ag could be a process competing with C–H activation by Pd.
- The Ag– $PPh_3$  bond of the  $PPh_3$  coordinated Ag complexes studied were highly labile, and prone to rapid phosphine exchange in solution.
- Temperatures as low as – 80 °C (193 K) or – 100 °C (173 K) were required to fully resolve the  $^31P\{^1H\}$  NMR spectra in dichloromethane- $d_2$  or a mixed solvent system

of dichloromethane:toluene (80:20). When fully resolved, most of the  $\text{PPh}_3$  coordinated Ag complexes existed as equilibria between multiple species.

- The complicated speciation with multiple equilibrium species makes it difficult to study the structure of these complexes in solution, despite the multiple NMR active nuclei present in the system. The NMR spectra indicated that the solid-state structures obtained from X-ray crystallography could not be used to assess the structure of the complex in solution. As the structure of the species in solution is ill-defined, it is impossible to design rigorous mechanistic or kinetic experiments to elucidate any information about the mechanism of C–H activation by Ag.
- For these reasons, this system was found to be unsuitable to understand and elucidate the catalytic reactions. The main conclusion from this study is that the reactions of  $\text{Ag}^{\text{I}}$  in a triphenylphosphine system are consistent with C-H bond activation by  $\text{Ag}^{\text{I}}$  but they are very complicated and difficult to understand. This conclusion stimulated a search for a more amenable Ag system.

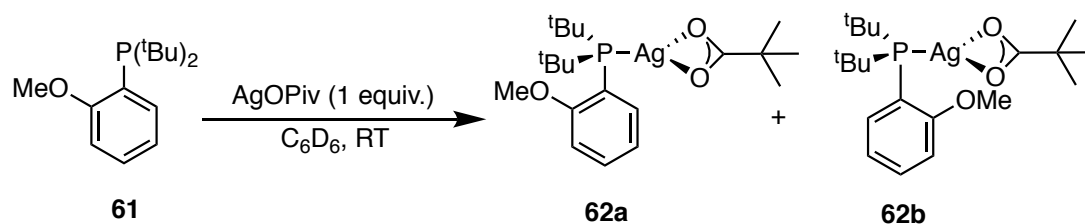


## Chapter 3: The Xphos Ag System

### 3.1 Introduction

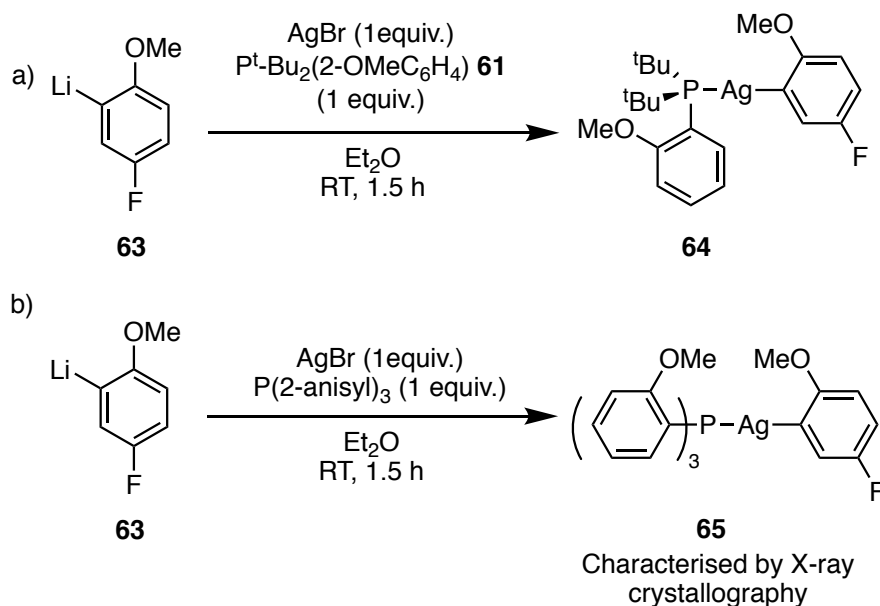
In Chapter 1, the general evidence of the non-innocent role of Ag<sup>I</sup> salts used in C–H functionalization reactions was discussed. Following this, in Chapter 2, the literature on the synthesis and structures of silver arene and silver carbonate complexes was summarised in the introduction. From the work done in Chapter 2, PPh<sub>3</sub> was found to be an unsuitable ligand for mechanistic investigations largely due to the highly labile Ag–PPh<sub>3</sub> bond and different coordination modes of the carbonate ligand. This made it difficult to characterise Ag containing reaction intermediates which were often undergoing complicated speciation in solution. The poorly defined nature of potential reaction intermediates prohibited detailed mechanistic or kinetic studies. To mitigate this problem, it was theorised that substituting PPh<sub>3</sub> with a more electron-donating phosphine would help stabilise the Ag–P bond, allowing for better characterisation of the Ag–P containing reaction intermediates.

Literature precedence for stable Ag–P bonds often contain bulky phosphines with electron-donating substitutions. When studying the Pd-catalysed direct allylation of aryl C–H bonds, Hartwig and co-workers were able to isolate phosphine-liganded Ag arene (**64**, **65**) and pivalate (**62**) complexes. The reaction of the phosphine **61** with AgOPiv yielded **62** as a pair of rotamers at room temperature in benzene-*d*<sub>6</sub>. **62** existed as a pair of distinct rotamers in solution, which were assigned using NOESY at 0 °C and the Ag–P bond was stable at room temperature, allowing for ease of assignment and identification.<sup>87</sup>



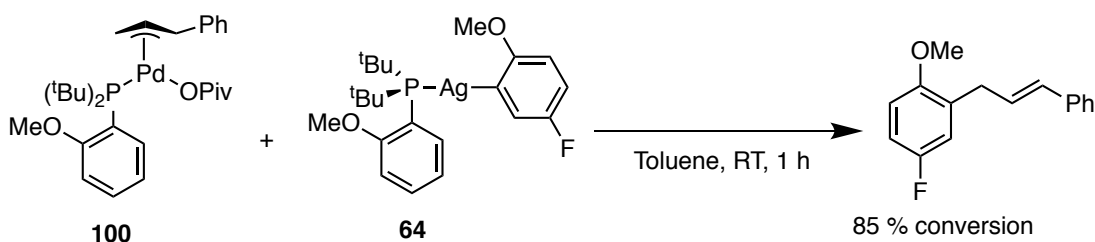
**Scheme 64:** Reaction of AgOPiv with **61** to produce **62** as a pair of rotamers<sup>87</sup>

Complexes **64** and **65** were isolated from the reaction of AgBr with lithium arene **63**. Much like **62**, **64** existed as a pair of rotamers, however crystals of this complex could not be isolated. Instead, the analogous **65** was prepared and the structure was determined by x-ray crystallography and used for stoichiometric reactions.<sup>87</sup>



**Scheme 65:** Preparation of monophosphine-ligated silver-aryl complex, which is the proposed intermediate generated after C–H activation by the monophosphine-coordinated AgOPiv complex<sup>87</sup>

These complexes contained stable Ag–P bonds at room temperature, and existed as well-defined species in solution, making it a convenient system to study the reactivity of the Ag complexes. For instance, the well-defined **64** was reacted with **100** at room temperature to obtain the cross-coupling product. Additionally, **62** was also detected *in operando* by  $^{31}\text{P}\{^1\text{H}\}$  NMR monitoring of the catalytic reaction. Using these reactions, Hartwig and co-workers proposed that the monophosphine-ligated AgOPiv complex within their reaction was capable of C–H activation, generating a silver-aryl complex which can later undergo transmetalation to transfer the aryl group from the silver to palladium.<sup>87</sup>



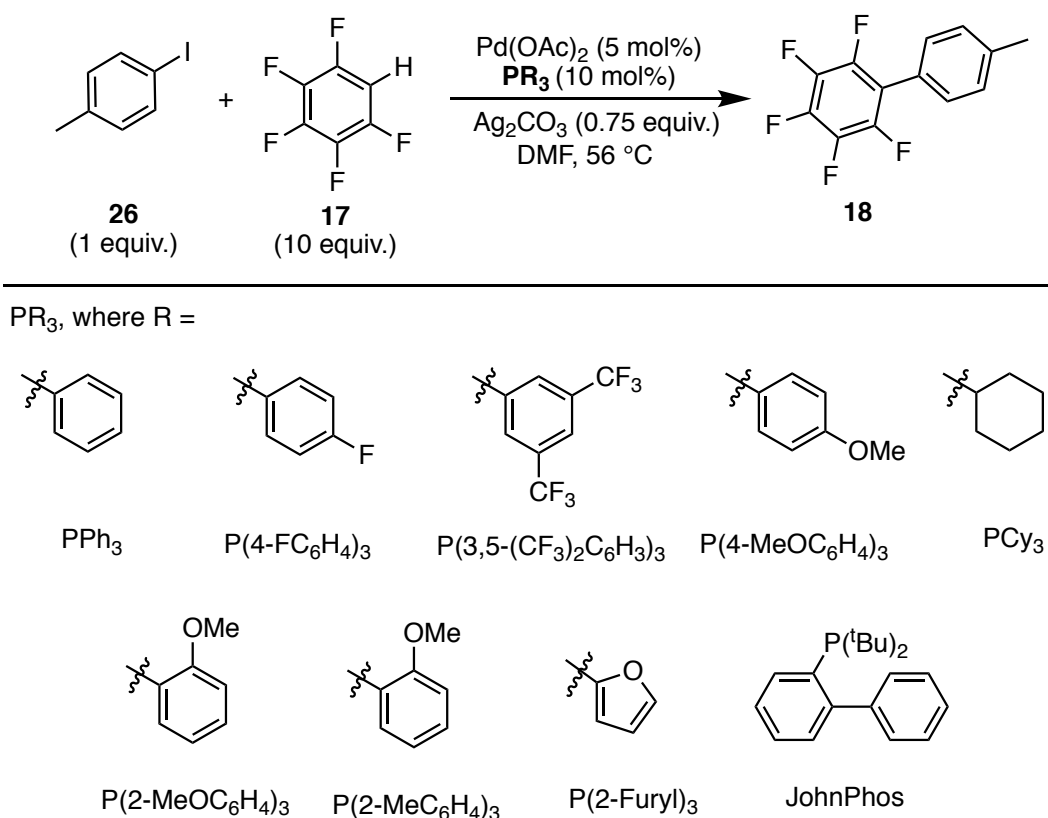
**Scheme 66:** Cross-coupling reaction between **100** and **64** in toluene at room-temperature<sup>87</sup>

In contrast to the Ag–PPh<sub>3</sub> bond seen in Chapter 2, the Ag–P bond in **62** and **64** is highly stable which allowed for ease of complex characterization and detection of intermediates by  $^{31}\text{P}\{^1\text{H}\}$  NMR spectroscopy. This result suggests that a bulkier and electron-donating phosphine likely results in a more stable Ag–PR<sub>3</sub> bond that is beneficial in the mechanistic

investigation. Thus, replacing PPh<sub>3</sub> in the standard direct arylation reaction with a more electron-rich phosphine could generate a more stable Ag–P bond.

The effect of phosphine ligands on the reaction rate and % conversion of the direct arylation of 4-iodotoluene **26** and pentafluorobenzene **17** has been previously studied by Platt *et al.* The rate of reaction was determined by following the kinetic profile between 5 – 50 % conversion using *in situ* IR spectroscopy. The final conversion of the reaction was determined by the integration of methyl peaks of 4-iodotoluene **26** and the product **18** in the <sup>1</sup>H NMR spectrum of the reaction mixture. Quantitative conversion was achieved when electron-poor ligands such as PPh<sub>3</sub>, P(3,5-(CF<sub>3</sub>)<sub>2</sub>C<sub>6</sub>H<sub>3</sub>)<sub>3</sub>, P(4-F C<sub>6</sub>H<sub>4</sub>)<sub>3</sub>, and P(2-furyl)<sub>3</sub> were used. In contrast more electron rich phosphines such as P(2-OMeC<sub>6</sub>H<sub>4</sub>)<sub>3</sub>, P(4-OMeC<sub>6</sub>H<sub>4</sub>)<sub>3</sub>, P(2-MeC<sub>6</sub>H<sub>4</sub>)<sub>3</sub> and PCy<sub>3</sub> resulted in a drop in % conversion. The greatest rate acceleration was observed with steric hindrance at the *ortho*-position, such as P(2-OMeC<sub>6</sub>H<sub>4</sub>)<sub>3</sub> and P(2-MeC<sub>6</sub>H<sub>4</sub>)<sub>3</sub>; however the reaction did not reach quantitative conversion in either case.<sup>68</sup>

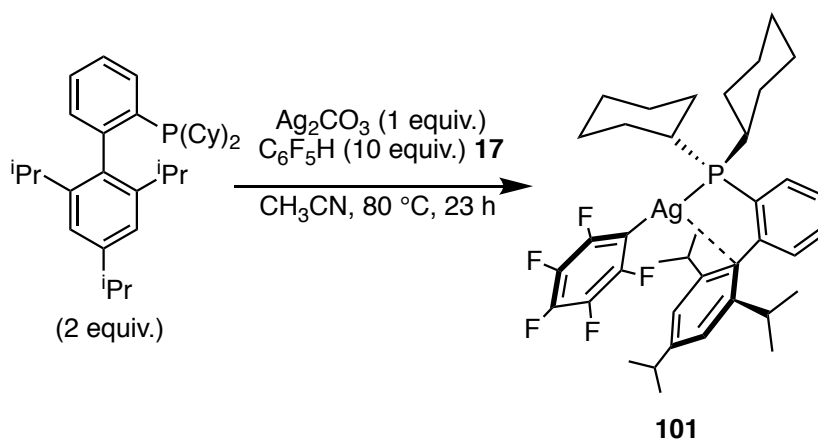
The data collected by Platt *et al.* provided a basis for selecting a small substrate scope of phosphines as the rate of reaction and % conversion of the reaction is well known.



**Scheme 67:** Effect of different phosphine ligands on the C–H direct arylation of 4-iodotoluene **26** with pentafluorobenzene **17**.<sup>68</sup>

### 3.2: Synthesis and Characterisation of $\text{Ag}(\text{C}_6\text{F}_5)(\text{Xphos})$

The  $\text{PPh}_3$  system proved to be problematic due to the lability of the  $\text{Ag}-\text{P}$  bond which made it difficult to establish a well-defined system, which is required for detailed mechanistic and kinetic studies. It was theorised that replacing  $\text{PPh}_3$  with a more electron donating phosphine would help form a more stable  $\text{Ag}-\text{P}$  bond. A short survey of phosphines more electron-donating than  $\text{PPh}_3$  was conducted. When  $\text{P}(4\text{-OMeC}_6\text{H}_4)_3$  was considered, the results were very similar to  $\text{PPh}_3$ . The  $^{19}\text{F}\{^1\text{H}\}$  NMR spectrum showed a new peak at  $-100$  ppm, consistent with the *ortho*-F resonance of  $\text{AgC}_6\text{F}_5$  containing complex. However, the  $^{31}\text{P}\{^1\text{H}\}$  spectrum only revealed a singlet with no evidence for coupling to  $^{107}\text{Ag}$  or  $^{109}\text{Ag}$  at room temperature, indicating the lability of the  $\text{Ag}-\text{P}$  bond. A more electron withdrawing phosphine,  $\text{P}(\text{furyl})_3$ , did not react at all. Finally, reaction with a strongly electron-donating and sterically hindered phosphine Xphos, revealed a pair of doublets of triplets in the  $^{31}\text{P}\{^1\text{H}\}$  NMR spectrum at room temperature characteristic of a product **101** containing an  $\text{Ag}(\text{XPhos})(\text{C}_6\text{F}_5)$  unit. Reaction of  $\text{Ag}_2\text{CO}_3$  with 2 equivalents of Xphos and 10 equivalents of  $\text{C}_6\text{F}_5\text{H}$  at  $80^\circ\text{C}$  yielded **101** as brown crystals with 66 % yield (**Scheme 68**).



**Scheme 68:** Synthesis of  $\text{Ag}(\text{C}_6\text{F}_5)(\text{Xphos})$  **101** from the reaction between Xphos,  $\text{Ag}_2\text{CO}_3$  and  $\text{C}_6\text{F}_5\text{H}$  **17**

The  $^{31}\text{P}\{^1\text{H}\}$  NMR spectrum recorded in dichloromethane- $d_2$  exhibited a pair of doublets of triplets at 13.0 ppm ( $^1J_{^{107}\text{Ag} \ ^{31}\text{P}} = 444$ ,  $^1J_{^{109}\text{Ag} \ ^{31}\text{P}} = 512$ ,  $^4J_{\text{PF}} = 3.0$  Hz), where the phosphorus resonance was split by both of the NMR active nuclei of  $^{107}\text{Ag}/^{109}\text{Ag}$  and the  $^{19}\text{F}$  from the  $\text{C}_6\text{F}_5$ - ring (**Figure 52**). The  $^{19}\text{F}\{^1\text{H}\}$  NMR spectrum showed three resonances at  $-107.0$  ppm (2 F, m, 2,6-F),  $-161.5$  (1 F, t,  $J = 19.8$  Hz, 4-F),  $-163.2$  (2 F, m, 3,5-F) (**Figure 53**). The LIFDI mass spectrum showed a parent ion at  $m/z = 752.251$  ( $^{107}\text{Ag}$  isotopologue) with an isotope pattern consistent with monomeric  $\text{Ag}(\text{C}_6\text{F}_5)(\text{XPhos})$ .

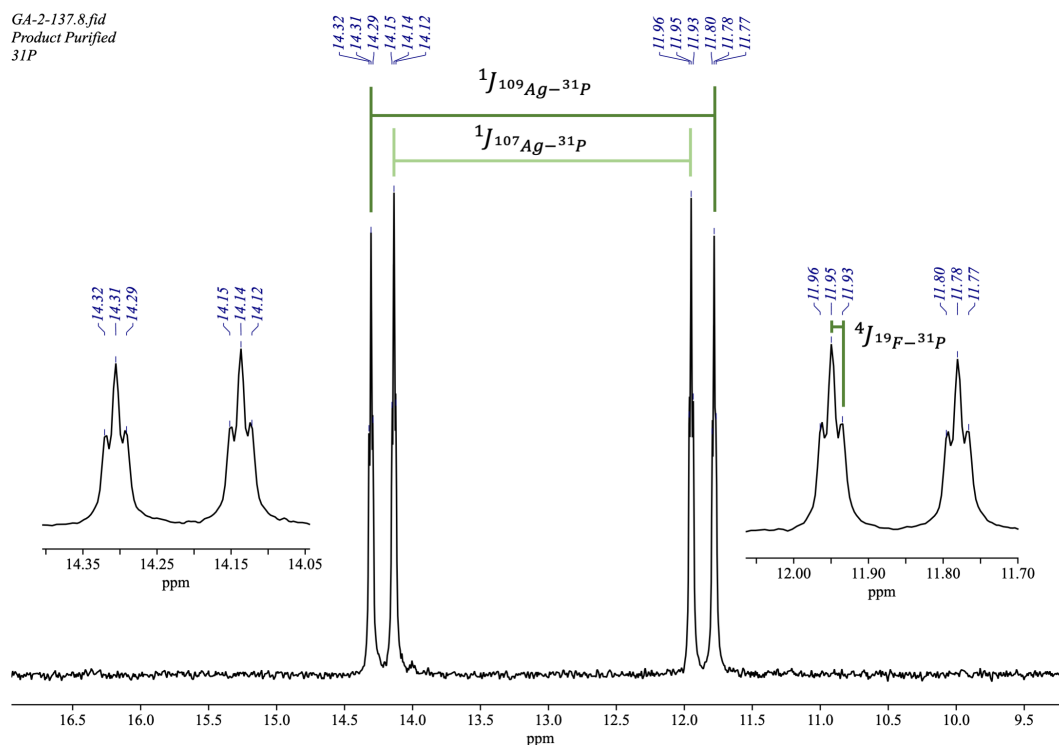


**Figure 52:**  $^{31}\text{P}\{^1\text{H}\}$  (202.5 MHz,  $\text{CD}_2\text{Cl}_2$ , 25 °C) spectrum of **101**

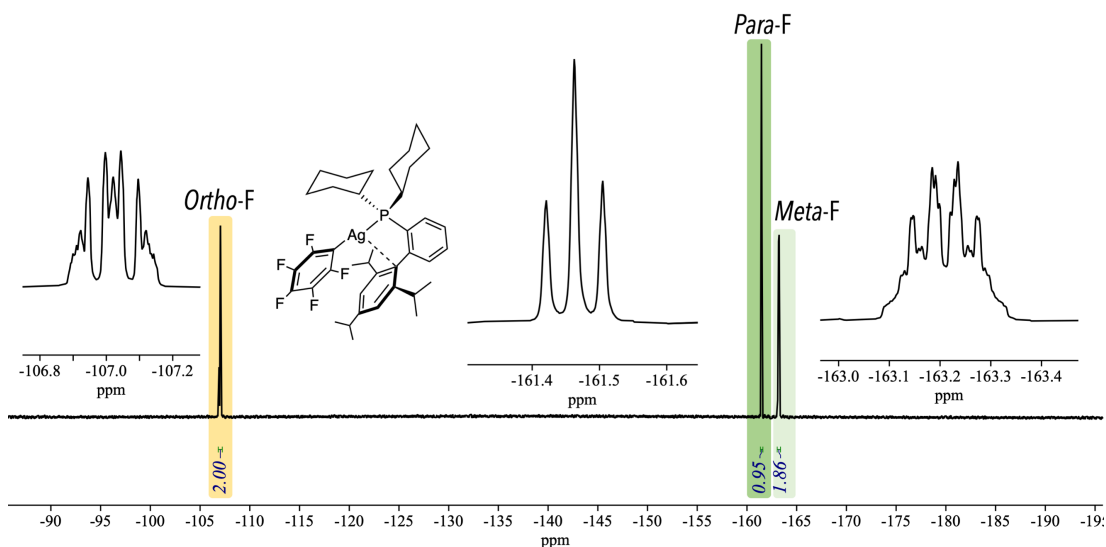


**Figure 53:**  $^{19}\text{F}\{^1\text{H}\}$  NMR (470 MHz,  $\text{CD}_2\text{Cl}_2$ , 25 °C) spectrum of **101**

Furthermore, the stability of the complex allowed for the characterisation by  $^{31}\text{P}\{^{109}\text{Ag}\}$  NMR and  $^{31}\text{P}\{^{109}\text{Ag}\}$ - $^{109}\text{Ag}$  HMQC. Typically, the direct observation of  $^{109}\text{Ag}$  is made challenging by the long  $T_1$  and negative NOE to protons, which makes these experiments taxing on instrument time. However, the  $^{31}\text{P}\{^{109}\text{Ag}\}$ - $^{109}\text{Ag}$  HMQC experiment depends on the  $T_1$  and sensitivity of the  $^{31}\text{P}$  signal, allowing for the indirect observation of the  $^{109}\text{Ag}$  signal. The  $^{31}\text{P}\{^{109}\text{Ag}\}$  NMR spectrum showed the  $^{109}\text{Ag}$  decoupled  $^{31}\text{P}$  centred at  $\delta$  13.0 in dichloromethane- $d_2$ , while the  $^{31}\text{P}$  coupled to  $^{107}\text{Ag}$  remained unaffected (**Figure 54**). The

$^{31}\text{P}\{^{109}\text{Ag}\}\text{-}^{109}\text{Ag}$  HMQC allowed for the indirect detection of the  $^{109}\text{Ag}$  resonance centred at  $\delta$  713 in the F1 domain.

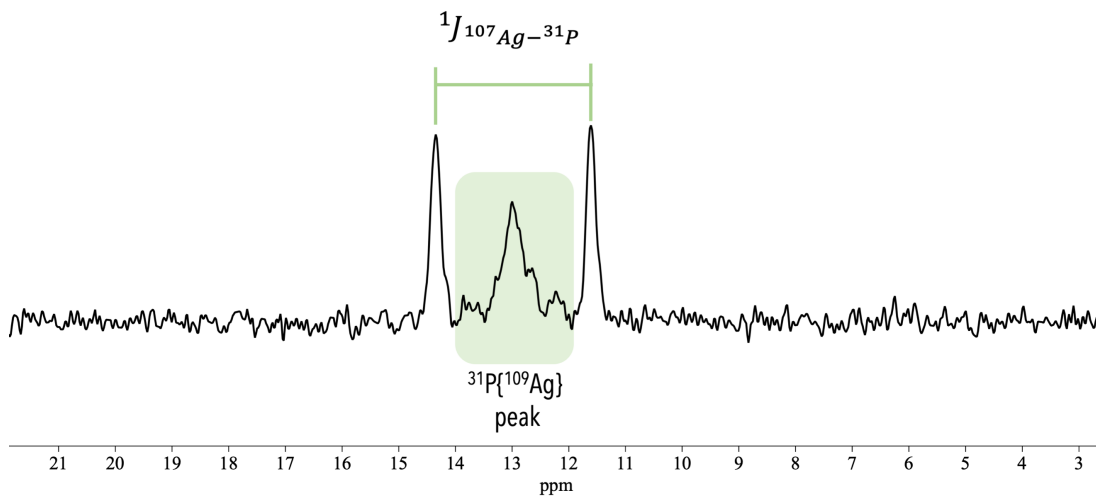


**Figure 54:**  $^{31}\text{P}\{^{109}\text{Ag}\}$  NMR (162 MHz, dichloromethane- $d_2$ , 25 °C) of a concentrated sample of  $\text{Ag}(\text{C}_6\text{F}_5)(\text{Xphos})$  **101**

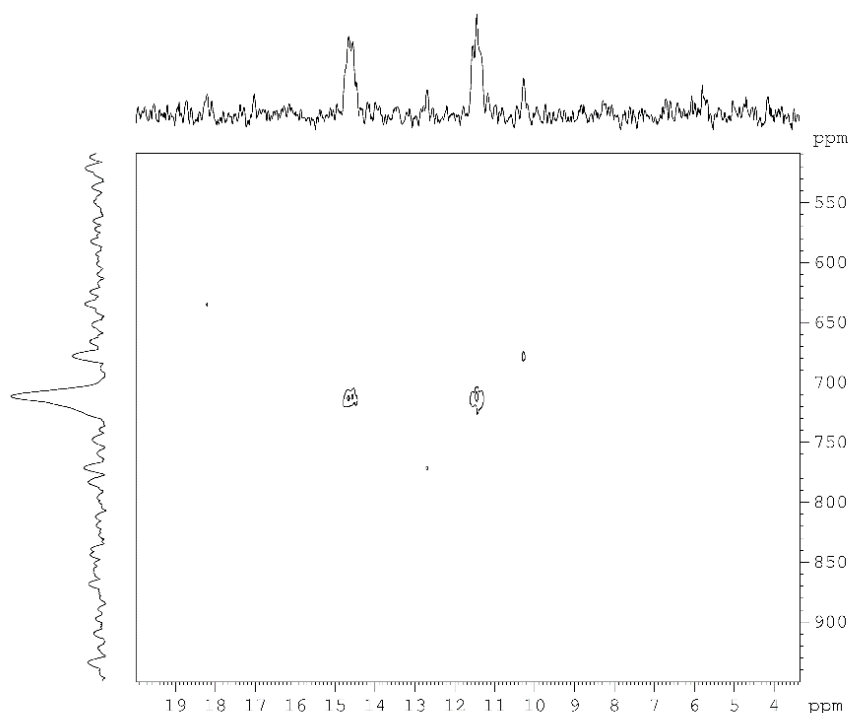


**Figure 55:**  $^{31}\text{P}\{^{109}\text{Ag}\}\text{-}^{109}\text{Ag}$  HMQC spectrum of **101** showing the  $^{109}\text{Ag}$  resonance at  $\delta$  713

Brown crystals of **101** were isolated by slow cooling in acetonitrile and analysed by single-crystal X-ray crystallography which revealed that  $\text{Ag}(\text{C}_6\text{F}_5)(\text{XPhos})$  **101** is monomeric with Ag–C and Ag–P distances of 2.124(2) and 2.380(6) Å, respectively (**Figure 57, Table 15**). The coordination at Ag<sup>I</sup> is close to linear [C–Ag–P 168.86(6)°]. The distal ring of the biphenyl

shows an approach between the ipso carbon C(7) and Ag [3.062(2) Å]. Such interactions are longer and hence weaker when compared to examples of Ag<sup>I</sup>(arene) complexes with η<sup>2</sup> interactions [Ag–C interactions *ca.* 2.30 – 2.40 Å]. For metal complexes containing dialkylbiarylphosphine ligands, interactions between the metal centre and distal ring of the biaryl are common. For Ag<sup>I</sup> complexes, the typical Ag<sup>I</sup>–C<sub>ipso</sub> distance falls within the range of 2.9 – 3.0 Å. Comparing <sup>t</sup>BuXphos-containing isoleptic complexes of group 11 metals, the M–C<sub>ipso</sub> bond length increases from Cu<sup>I</sup> (2.58 Å), Ag<sup>I</sup> (2.91 Å) to Au<sup>I</sup> (3.04 Å) (**Figure 56**).<sup>124,125</sup> In contrast related Pd<sup>II</sup> complexes, often have C(ipso)-Pd interactions *ca.* 2.45 Å.

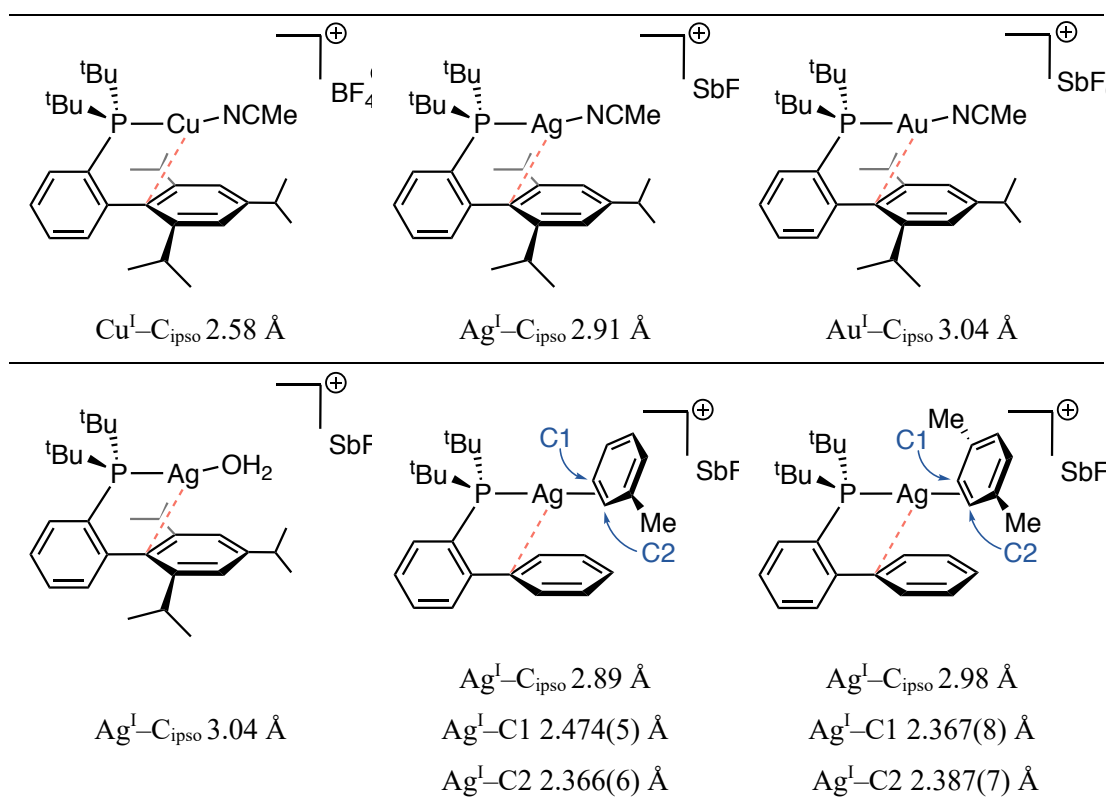


**Figure 56:** Comparison of the M–C<sub>ipso</sub> bonds in various group 11 metal complexes dialkylbiarylphosphine ligands, reported by Maseras and Echavarren and co-workers.<sup>124</sup>

The C<sub>6</sub>F<sub>5</sub> ring exhibits π-stacking with the adjacent molecule, with a centroid-to-centroid distance of 3.336(2) Å. Other Ag(C<sub>6</sub>F<sub>5</sub>)L (L = nitrile) complexes are known but have polymeric structures.<sup>126,112</sup> Hartwig and co-workers have isolated a monomeric silver fluoroaryl phosphine, Ag{C<sub>6</sub>H<sub>3</sub>(2-OMe)(4-F)}{P(o-anisyl)<sub>3</sub>} **65**, from the reaction of AgBr with a lithiated arene and phosphine, with a similar structure to **101**.<sup>87</sup> The direct isolation of **101** from the reaction of Ag<sub>2</sub>CO<sub>3</sub> with Xphos and pentafluorobenzene **17** demonstrates the C–H activation capability of silver carbonate.

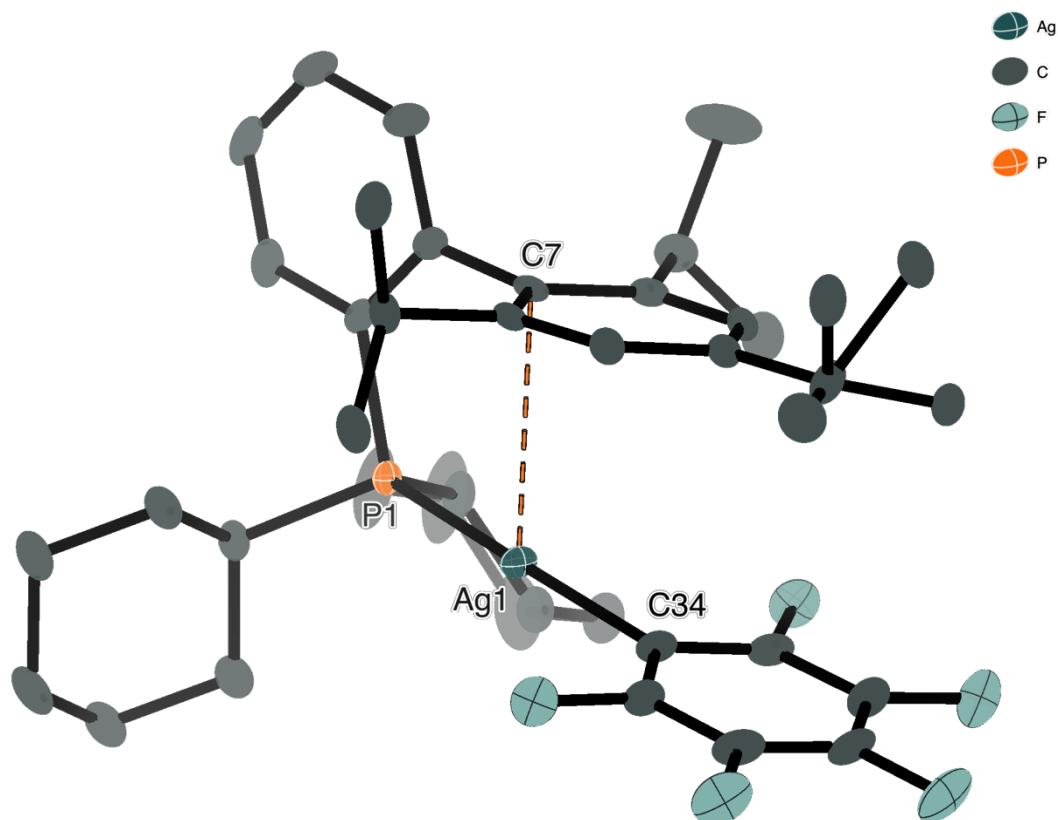
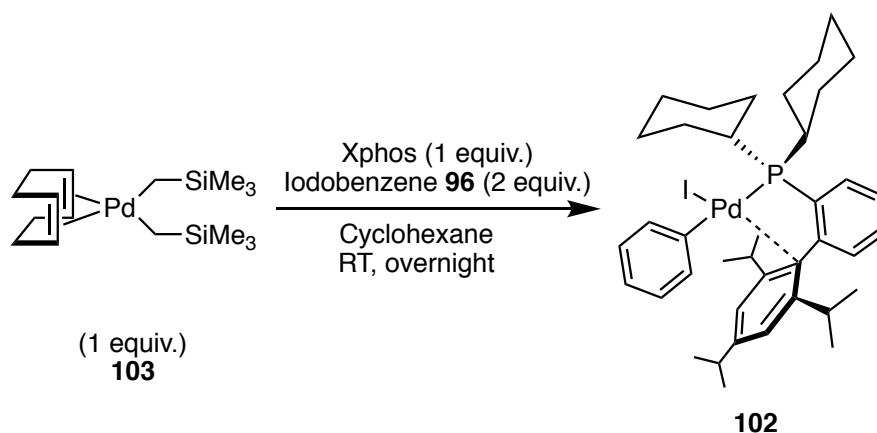


**Figure 57:** The crystal structure of the  $\text{Ag}(\text{C}_6\text{F}_5)(\text{Xphos})$  **101**

To test whether **101** was competent for cross-coupling under stoichiometric conditions, the product of oxidative addition by Pd,  $\text{PdI}(\text{C}_6\text{H}_5)(\text{Xphos})$  **102** was synthesized. Employing a literature procedure outlined by Hartwig and co-workers, the  $\text{Pd}^{\text{II}}$  complex  $\text{PdI}(\text{C}_6\text{H}_5)(\text{XPhos})$  **102** was prepared as a yellow solid from the reaction of  $(\text{COD})\text{Pd}(\text{CH}_2\text{SiMe}_3)_2$  **103** and Xphos with iodobenzene **96** in cyclohexane at room temperature and isolated with a yield of 90 % (Scheme 69).<sup>127</sup>



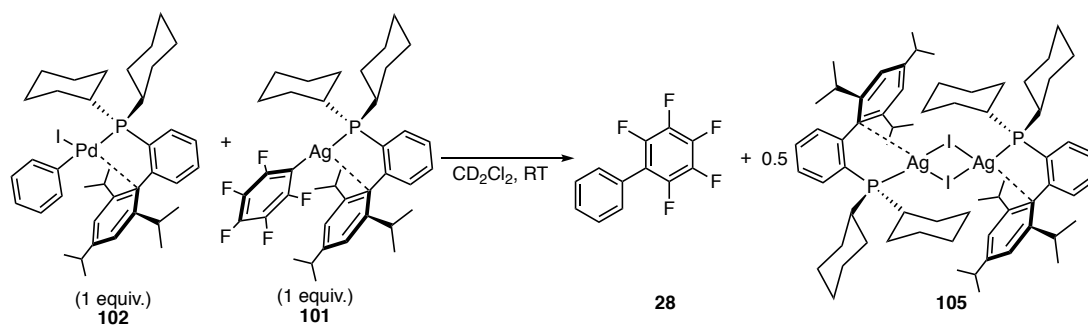
**Scheme 69:** The synthesis of **102** from the reaction of **103** and Xphos and **96** in cyclohexane at room temperature<sup>127</sup>



**Table 15:** Principal bond lengths and angles of **101**, **106** and **105**

	<b>101</b>	<b>106</b>	<b>105</b>
Bond	Bond length (Å)		
Ag(1)–P(1)	2.3801(5)	2.3328(9)	2.4255(7)
Ag(1)–C(34)	2.124(2)	2.678(2)	-
Ag(1)–C(7)ipso	3.062(2)	3.071(3)	3.277(3)
Ag(1)–O(1)	-	2.249(2)	-
Ag(1)–O(2)	-	2.3572(2)	-
C(34)–O(1)	-	1.281(3)	-
C(34)–O(2)	-	1.303(5)	-
Ag(1)–I(1)	-	-	2.8357(3)
Bond angles	Angle (°)		
C(34)–Ag(1)–P(1)	168.85(6)	167.29(3)	-
P(1)–Ag(1)–O(1)	-	150.85(7)	-
C(34)–Ag(1)–O(1)	-	28.48(10)	-
O(1)–Ag(1)–O(2)	-	57.56(8)	-
C(34)–Ag(1)–O(1)	-	28.48(10)	-
Ag(1)–O(2)–Ag(1')	-	178.444(13)	-
I(1)–Ag(1)–I(1')	-	-	100.057(8)
P(1)–Ag(1)–I(1)	-	-	128.803(18)
P(1)–Ag–I(1)–I(1)	-	-	151.26(3)

When reacted stoichiometrically in dichloromethane- $d_2$ , the transmetalation reaction between PdI(C<sub>6</sub>H<sub>5</sub>)(XPhos) **102** and Ag(C<sub>6</sub>F<sub>5</sub>)(XPhos) **101** and subsequent reductive elimination reaction of Pd(C<sub>6</sub>F<sub>5</sub>)(Ph)(Xphos) **104** took place rapidly at room temperature (**Scheme 70**). Almost immediately approximately 90 % conversion to the organic product **28** occurred. The presence of the Pd(C<sub>6</sub>F<sub>5</sub>)(Ph)(Xphos) **104** could not be detected by <sup>31</sup>P{<sup>1</sup>H} and <sup>19</sup>F{<sup>1</sup>H} NMR spectroscopy. Along with the organic product, the concomitant formation of [AgI(XPhos)]<sub>2</sub> **105** was also detected in <sup>31</sup>P{<sup>1</sup>H} NMR (CD<sub>2</sub>Cl<sub>2</sub>) spectrum by a pair of concentric doublets at  $\delta$  16.89 with  $^1J_{107Ag^{31P}} = 542$  Hz,  $^1J_{109Ag^{31P}} = 627$  Hz (**Figure 58**).



**Scheme 70:** The stoichiometric reaction between **101** and **102** in dichloromethane- $d_2$  at room temperature

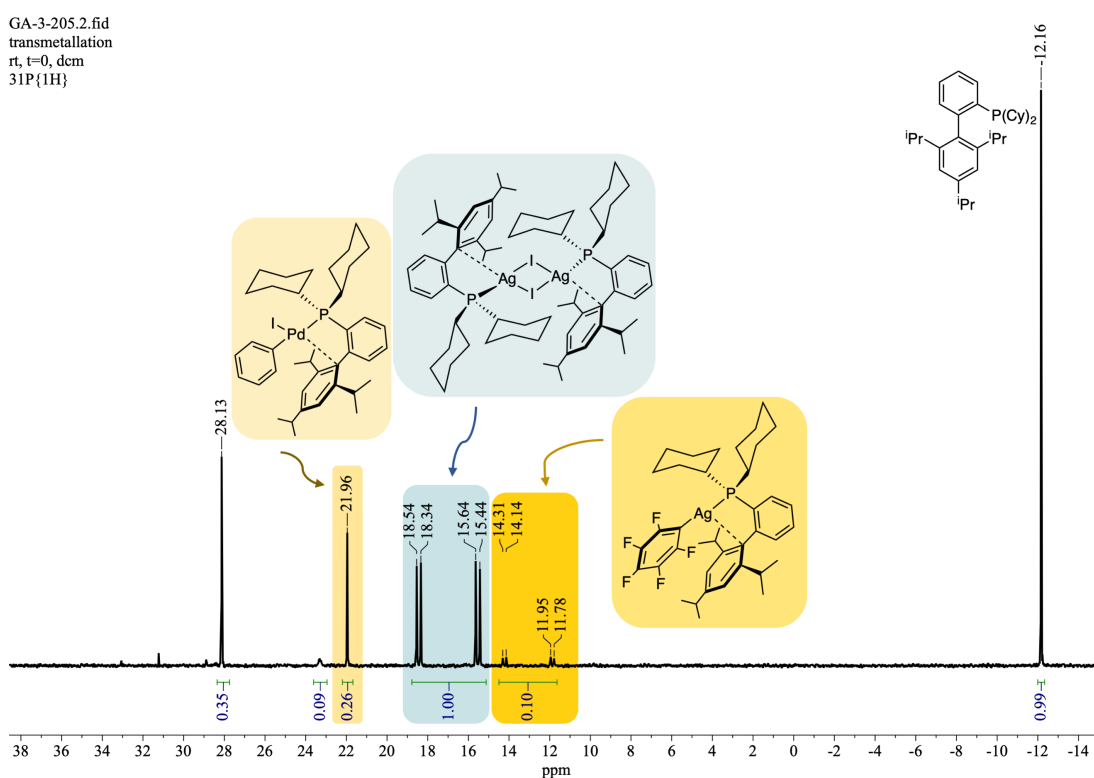


**Figure 58:**  $^{31}\text{P}\{^1\text{H}\}$  (202.5 MHz, dichloromethane- $d_2$ , 25 °C) NMR spectrum of the reaction mixture of **101** (yellow) and **102** (pale yellow) showing the presence of **105** (blue) and unbound Xphos.

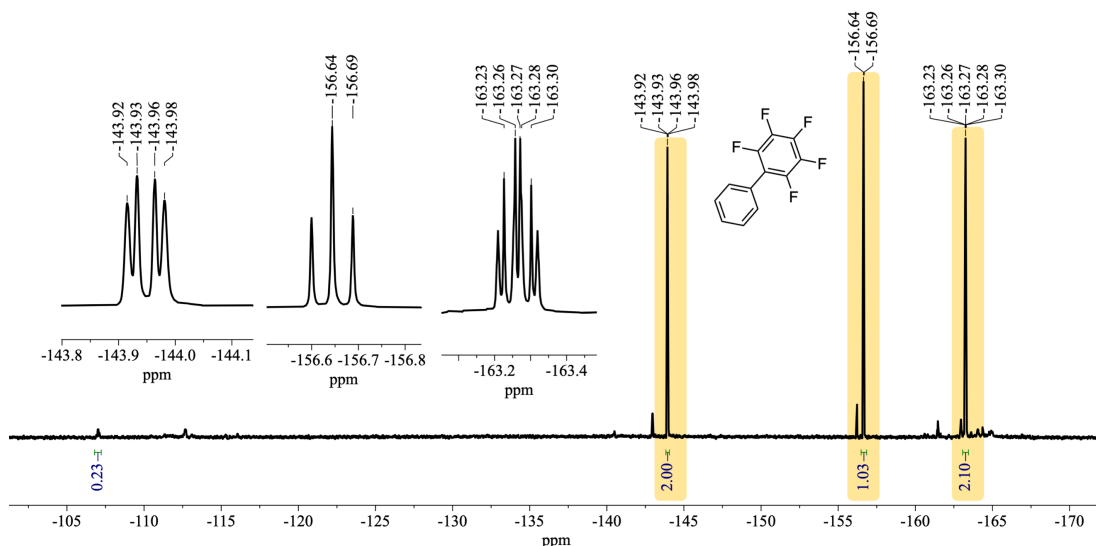
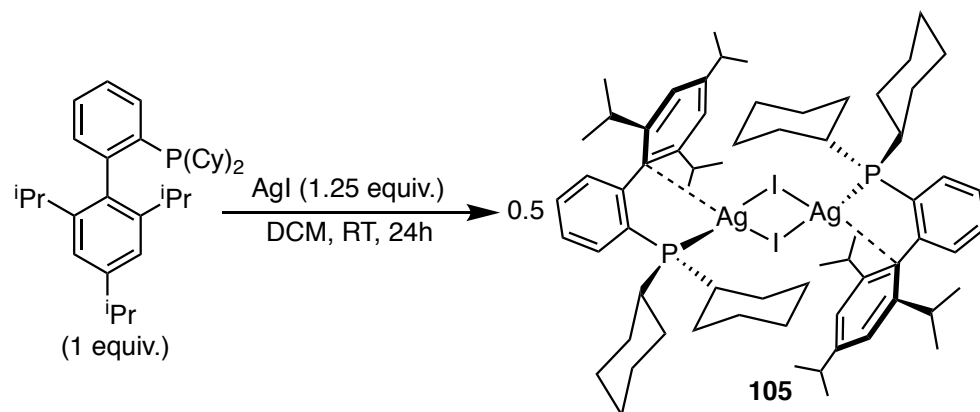


**Figure 59:**  $^{19}\text{F}\{^1\text{H}\}$  NMR (470 MHz,  $\text{CD}_2\text{Cl}_2$ , 25 °C) of the reaction mixture of **101** and **102** immediately after sample preparation, showing the presence of the organic product **28** (yellow).

The identity of  $[\text{AgI}(\text{XPhos})]_2$  **105** was confirmed by preparing an authentic sample by the reaction of  $\text{AgI}$  with XPhos in  $\text{CD}_2\text{Cl}_2$  at room temperature for 24 h (**Scheme 71**). The desired product was isolated as clear colourless crystals, with a yield of 72 %, by layering the reaction mixture in dichloromethane with dry hexane. A saturated solution of **105** in dichloromethane- $d_2$  was also analysed by  $^{31}\text{P}\{^{109}\text{Ag}\}$  NMR and  $^{31}\text{P}\{^{109}\text{Ag}\}$ - $^{109}\text{Ag}$  HMQC. The  $^{31}\text{P}\{^{109}\text{Ag}\}$ - $^{109}\text{Ag}$  HMQC showed that the  $^{109}\text{Ag}$  resonance of the dimer is centred at  $\delta$  590. The LIFDI mass spectrum of **105** dissolved in dichloromethane, shows  $m/z = 1295.459$  (100%,  $[\text{M-I}]^+$ ) with isotope pattern consistent with two silver atoms (quoted for  $^{107}\text{Ag}^{109}\text{Ag}$ ) and a much smaller peak at  $m/z = 710.183$  (12%,  $[\text{AgI}(\text{XPhos})]^+$ ) for the monomer (quoted for  $^{107}\text{Ag}$ ). This spectrum suggests that **105** exists as a dimer in solution or in an equilibrium between monomer and dimer. The molecular structure determined crystallographically reveals a  $C_2$ -symmetric dimer with bridging iodides. The central  $\text{Ag}_2(\mu\text{-I}_2)$  unit is planar, but the phosphorus atoms lie out of that plane with a  $\text{P}(1)\text{-Ag-I}(1)\text{-I}(1')$  torsional angle of  $151.26(3)^\circ$  (**Figure 60**). Similar to **101**, close contact between the distal benzene ring  $\text{C}(7)^{\text{ipso}}$  and the Ag atom [ $3.277(3)$  Å] are found in **105**.



**Scheme 71:** The synthesis of **105** from the reaction between AgI and Xphos in dichloromethane

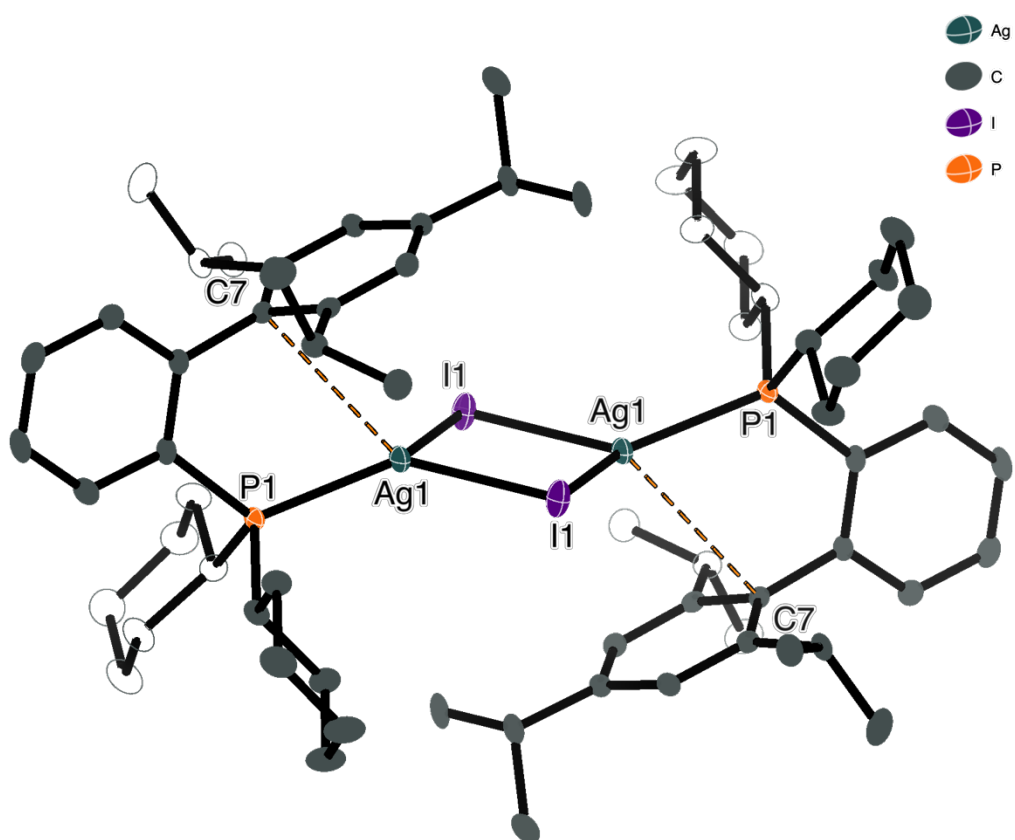
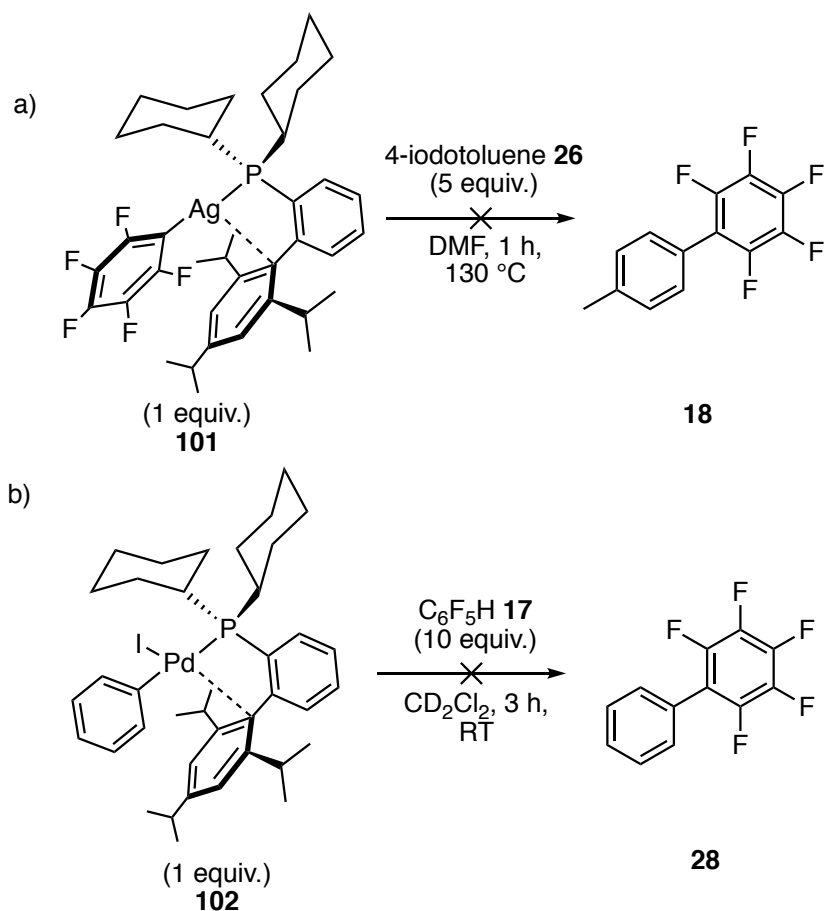


**Figure 60:** The crystal structure of  $[\text{AgIXphos}]_2$  **105**

In an attempt to detect the product of transmetallation  $\text{Pd}(\text{C}_6\text{F}_5)(\text{Ph})(\text{Xphos})$  **104** by NMR spectroscopy, a mixture of **101** and **102** was prepared at  $-80\text{ }^\circ\text{C}$  (193 K) in dichloromethane- $d_2$  and analyzed by NMR spectroscopy from a temperature range of  $-80\text{ }^\circ\text{C}$  (193 K) to  $-20\text{ }^\circ\text{C}$  (253 K). Formation of **28** was observed from  $-30\text{ }^\circ\text{C}$ , but no transmetallation product was detected in the  $^{31}\text{P}\{^1\text{H}\}$  and  $^{19}\text{F}\{^1\text{H}\}$  NMR spectroscopy. For comparison, Hartwig and co-

workers reacted  $\text{Ag}\{\text{C}_6\text{H}_3(2\text{-OMe})(4\text{-F})\}\{\text{P}(\text{tBu})_2(2\text{-OMeC}_6\text{H}_4)\}$  **64** with  $\text{Pd}(\eta^3\text{-allyl-Ph})(\text{OPiv})\{\text{P}(\text{tBu})_2(2\text{-OMeC}_6\text{H}_4)\}$  **100** at room temperature for 1 h to obtain the cross-coupling product with 85% conversion.<sup>87</sup> As a control, the reaction between **101** and 4-iodotoluene **26** was attempted, but no evidence of the cross-coupling product was detected by  $^{19}\text{F}\{^1\text{H}\}$  NMR spectroscopy, up to 130 °C (**Scheme 72a**). In contrast, Sun and Miller, showed that  $\text{AgC}_6\text{F}_5$  **55** was able to directly react with iodobenzene **96** to form a biaryl product  $\text{C}_6\text{H}_5\text{-C}_6\text{F}_5$  and  $\text{AgI}$  in DMF at 110 °C.<sup>108</sup> As another control, **102** was reacted with 10 equivalents of  $\text{C}_6\text{F}_5\text{H}$  **17** without any Ag complexes or base, resulting in no reaction at room temperature (**Scheme 72b**).



**Scheme 72:** Reaction of a) **101** with 4-iodotoluene **26** and b) **102** with  $\text{C}_6\text{F}_5\text{H}$  **17** as control experiments

The decomposition of  $\text{Ag}(\text{C}_6\text{F}_5)(\text{Xphos})$  **101** and  $\text{AgC}_6\text{F}_5$  **55** by  $\text{D}_2\text{O}$  in  $\text{CD}_2\text{Cl}_2$  and  $\text{CD}_3\text{CN}$  respectively was also examined at room temperature. The hydrolysis of  $\text{AgC}_6\text{F}_5$  **55** was monitored by  $^{19}\text{F}\{^1\text{H}\}$  NMR spectroscopy by integrating the *ortho*-F resonance of  $\text{AgC}_6\text{F}_5$  **55** with respect to the *ortho*-F peak of  $\text{C}_6\text{F}_5\text{D}$  **69** at  $-140$  ppm in acetonitrile- $d_3$ . After 24 h at room temperature, 83 % conversion to  $\text{C}_6\text{F}_5\text{D}$  **69** was observed. In comparison, **101** was far more robust to hydrolysis as only 12% decomposition to  $\text{C}_6\text{F}_5\text{D}$  **69** was observed after 24 h

and 20 % decomposition after 5 days. Evidently, coordination to Xphos affords increase stability to **101** compared to **55**.

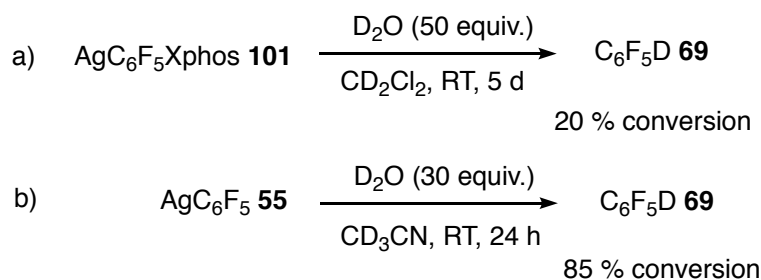
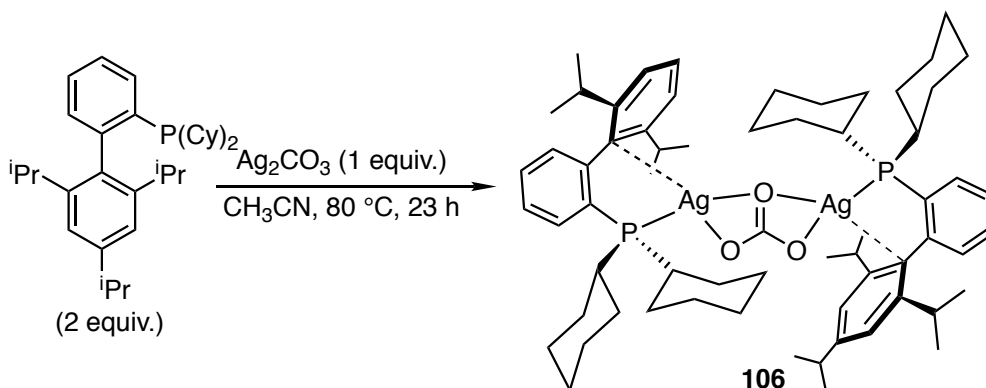


**Figure 61:** Decomposition of **55** and **101** to  $\text{C}_6\text{F}_5\text{D}$  **69** with an excess of  $\text{D}_2\text{O}$  in  $\text{CD}_3\text{CN}$  and  $\text{CD}_2\text{Cl}_2$  respectively

### 3.3 Synthesis of the Silver(I) Carbonate Xphos Complex

Silver carbonate is highly insoluble in both acetonitrile and DMF, so the anticipated first step in the reaction with  $\text{C}_6\text{F}_5\text{H}$  **17** and Xphos may be the coordination of Xphos to  $\text{Ag}_2\text{CO}_3$  to form a more soluble silver XPhos carbonate complex. Indeed, the reaction of silver carbonate with 2 equivalents of Xphos at  $80^\circ\text{C}$  in acetonitrile yielded an amber solution, which upon cooling formed brown crystals with a 24 % yield (**Scheme 73**). The product was identified as  $[\text{Ag}(\text{XPhos})]_2(\mu\text{-}\kappa^2, \kappa^2\text{-CO}_3)$  **106** by NMR, CHN analysis and X-ray crystallography. The  $^{31}\text{P}\{^1\text{H}\}$  NMR spectrum recorded in  $\text{C}_6\text{D}_6$  showed a pair of doublets at  $\delta$  15.9 ( $^1J_{^{107}\text{Ag}^{31}\text{P}} = 634$ ,  $^1J_{^{109}\text{Ag}^{31}\text{P}} = 731$  Hz).



**Scheme 73:** The synthesis of **106** from the reaction between Xphos and  $\text{Ag}_2\text{CO}_3$  in acetonitrile

The molecular structure of **106** shows a  $C_2$ -symmetric complex with an  $\text{Ag}(\mu\text{-CO}_3)\text{Ag}$  unit that is almost planar with one oxygen bridging the two silver atoms [ $\text{Ag}(1)\text{-O}(2)\text{-Ag}(1)'$   $178.444(13)^\circ$ ] and the O(1) oxygens bonded to one silver each. The  $\text{Ag-O}(2)$  distances [ $2.3572(2)$  Å] are longer than the  $\text{Ag-O}(1)$  distances [ $2.249(2)$  Å]. The  $\text{C}(34)\text{-O}(1)$  and  $\text{C}(34)\text{-O}(2)$  distances are  $1.281(3)$  and  $1.303(5)$  Å, respectively. The sum of the angles around

C(34) is  $360.0(5)$ , indicating trigonal planar coordination. The coordination at Ag is Y-shaped with  $O(1)\text{--Ag}\text{--}O(2) = 57.56(8)^\circ$ . The ipso carbon on the distal benzene ring C(9) lies in close contact [ $3.071(3) \text{ \AA}$ ] with the silver atom bearing the corresponding phosphorus (**Figure 62**). The CHN analysis shows one acetonitrile of crystallization per Ag, in agreement with the crystal structure.

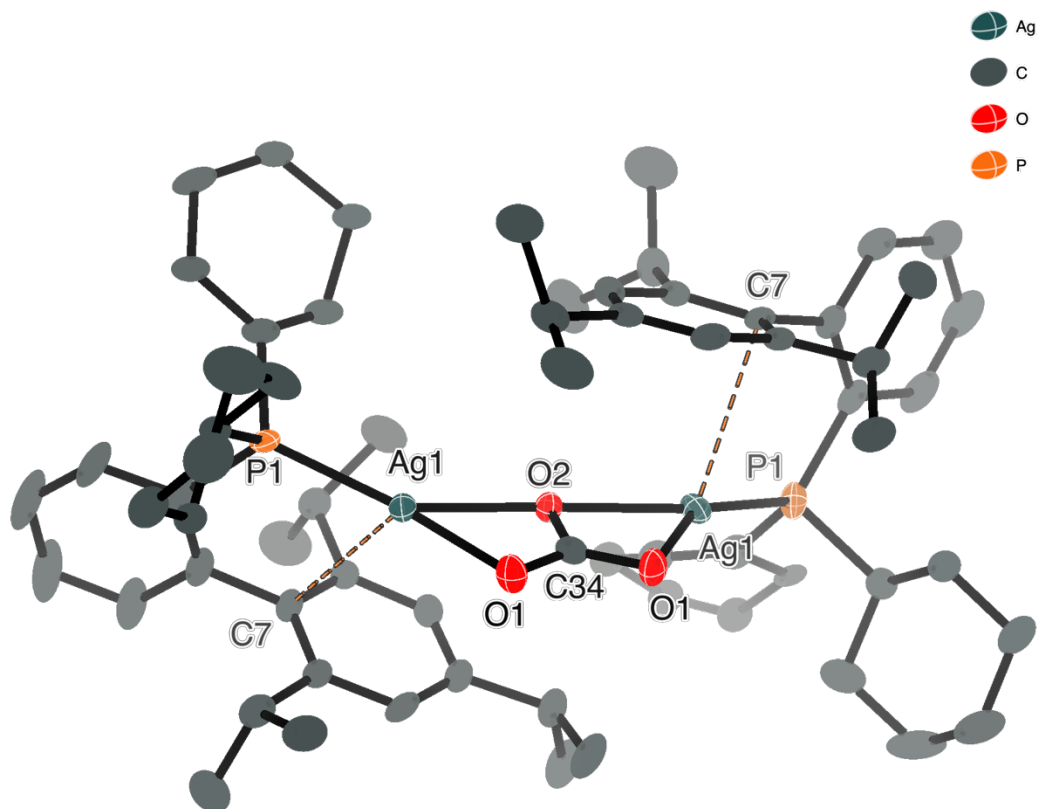


**Figure 62:** The crystal structure of  $[\text{Ag}(\text{XPhos})]_2(\mu\text{-}\kappa^2, \kappa^2\text{-CO}_3)$  **106**

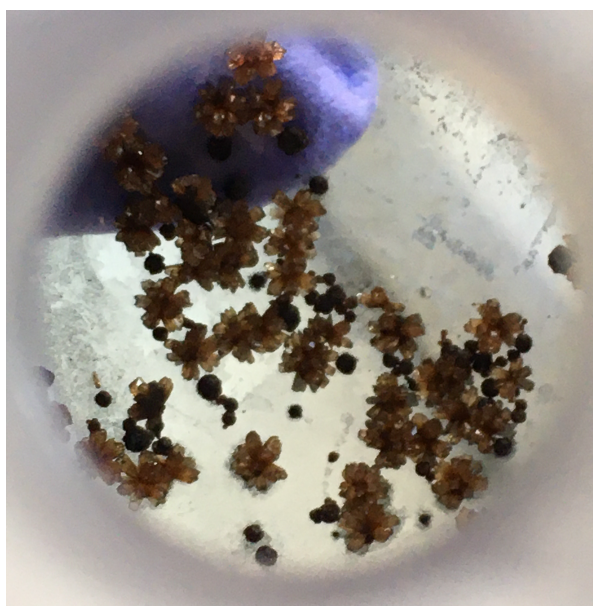
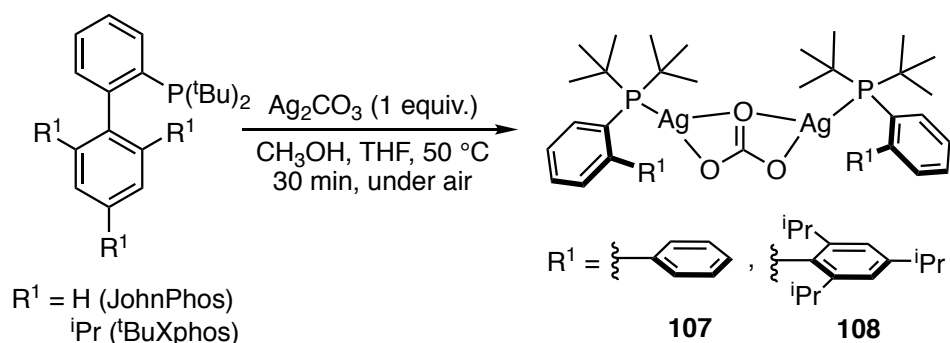


**Figure 63:** Brown crystals of  $[\text{Ag}(\text{XPhos})]_2(\mu\text{-}\kappa^2, \kappa^2\text{-CO}_3)$  **106** in the round-bottom flask

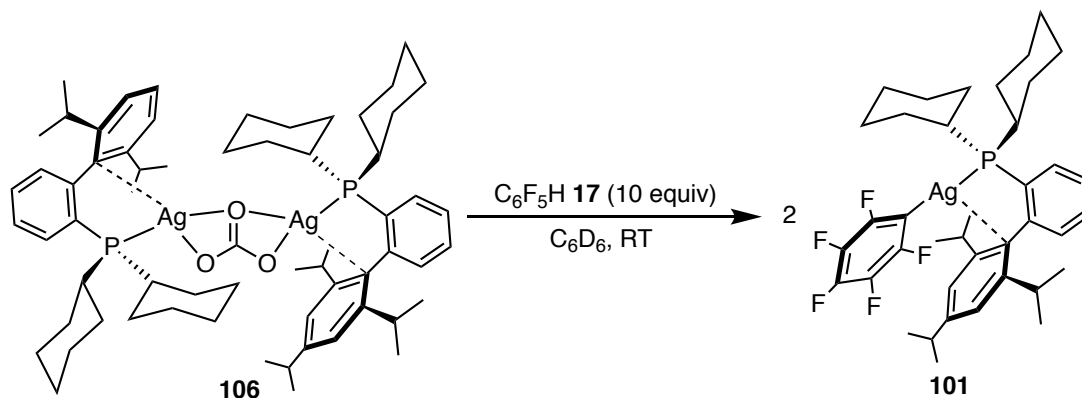
During the progress of this work, Hartwig and co-workers in 2021, demonstrated that a combination of  $\text{Ag}_2\text{CO}_3$  and Johnphos was capable of the site-selective C–H bond deuteration of 5-membered heterocycles, and pharmaceuticals using  $\text{CH}_3\text{OD}$  as the source of deuterium. They isolated two Ag complexes which are analogous to **106**: **107** (using Johnphos) and **108** (using  ${}^t\text{BuXphos}$ ). Complex **108** was characterized in  $\text{CH}_3\text{OH-}d_4$  and had a  $\delta$  43.5 with  ${}^1J_{107\text{Ag}^{31}\text{P}} = 649$  and  ${}^1J_{109\text{Ag}^{31}\text{P}} = 748$  Hz, which is similar to **106**.<sup>94</sup>



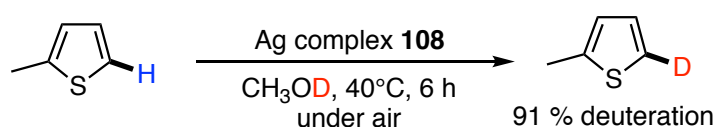
**Scheme 74:** Isolation of Ag carbonate complexes **107** and **108** by Hartwig and co-workers.<sup>94</sup>

Complex **106** reacts with pentafluorobenzene **17** (5 equiv. wrt Ag) in  $\text{C}_6\text{D}_6$  at room temperature to form **101** as the sole product containing the  $\text{Ag}(\text{XPhos})$  moiety (**Scheme 75**). Benzene was used as solvent since mass spectra show that **106** reacts with chlorine sources such as chloroform or dichloromethane to form  $[\text{Ag}(\text{XPhos})]_2(\mu\text{-Cl})_2$ . Almost full conversion to **101** was detected within minutes, as seen in the  ${}^{31}\text{P}\{^1\text{H}\}$  NMR spectrum recorded immediately after sample preparation (**Figure 64**). The sample was then monitored at 2 h and 24 h, with little to no change detected at room temperature. This demonstrates the capability of **106** to undergo C–H activation with  $\text{C}_6\text{F}_5\text{H}$  **17** to yield **101** rapidly. Similar to **106**, the Ag carbonate complexes isolated by Hartwig and co-workers were capable of C–H bond activation. The complexes isolated by Hartwig and co-workers were capable of catalyzing the deuteration five-membered heteroatoms rapidly at 40 °C. They demonstrated that the analogous  $\text{Ag}_2\text{CO}_3{}^t\text{BuXphos}_2$  **108** was competent at selective deuteration of 2-methyl thiophene to 91% in  $\text{CH}_3\text{OD}$  at 40 °C for 6 h under air (**Scheme 76**)<sup>94</sup>





**Scheme 75:** Reaction of **106** with  $\text{C}_6\text{F}_5\text{H } \mathbf{17}$  at room temperature to produce **101**



**Scheme 76:** Selective deuteration by Ag carbonate complex **108** demonstrated by Hartwig and co-workers<sup>94</sup>

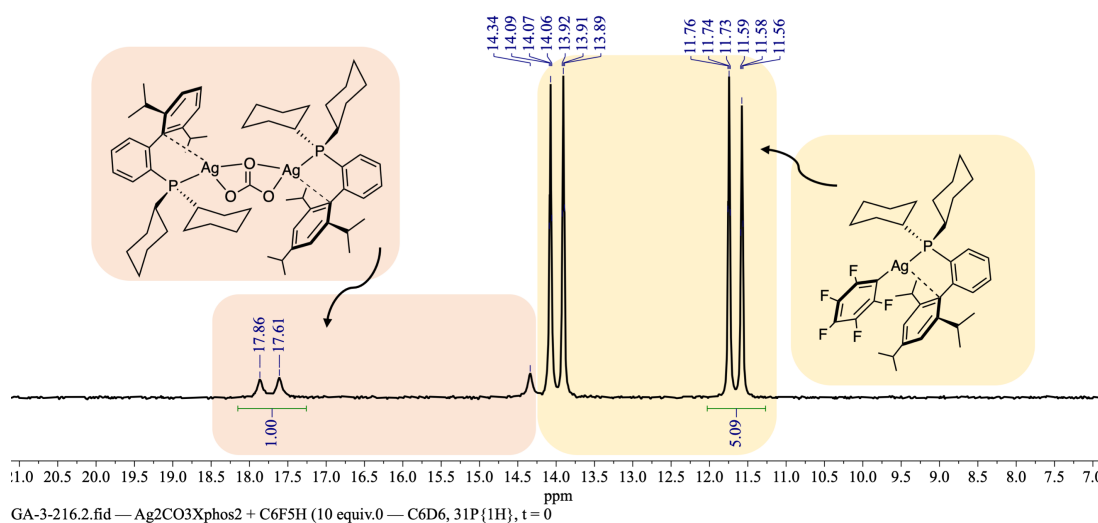
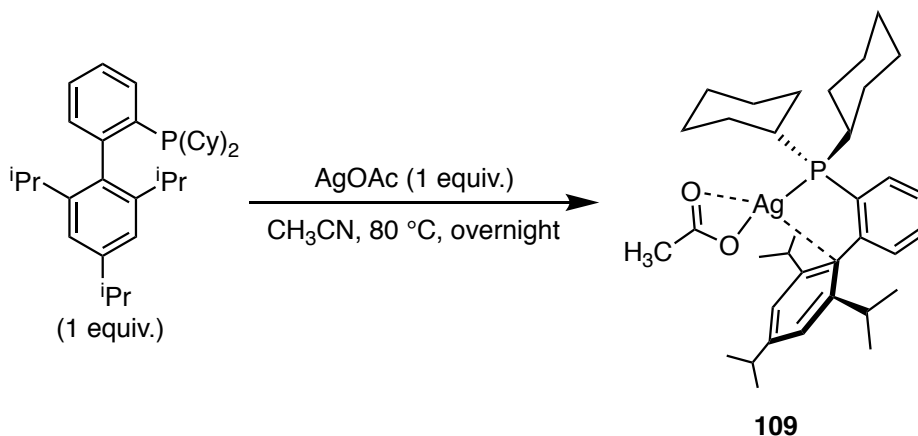


**Figure 64:**  $^{31}\text{P}\{^1\text{H}\}$  (202.5 MHz,  $\text{C}_6\text{D}_6$ , 25 °C) NMR spectrum of the reaction mixture of **106** with **17**, at  $t = 0$  h, RT. The mixture shows the presence of **106** (red) and **101** (yellow).

The reaction of  $\text{AgOAc}$  in the presence of Xphos (1 equiv.) and  $\text{C}_6\text{F}_5\text{H } \mathbf{17}$  (10 equiv.) did not produce any **101** (none detected by  $^{31}\text{P}\{^1\text{H}\}$  or  $^{19}\text{F}\{^1\text{H}\}$  NMR spectroscopy); instead the presence of **109** was detected by  $^{31}\text{P}\{^1\text{H}\}$  NMR spectroscopy with a signal at  $\delta$  16.55 (pair of d,  $^1J_{107\text{Ag}^{31}\text{P}} = 643.9$  Hz,  $^1J_{109\text{Ag}^{31}\text{P}} = 743.2$  Hz, 1 *P*). The identity of **109** was confirmed by preparing an authentic sample, using the reaction of  $\text{AgOAc}$  with Xphos in acetonitrile (**Scheme 77**). This is consistent with the reactivity of  $\text{AgOAc}$  found in the  $\text{PPh}_3$  system in Chapter 2.



**Scheme 77:** Synthesis of AgOAcXphos complex **109** from acetonitrile

The structure of **109** was confirmed by x-ray crystallography and existed as a monomer in contrast to the dimeric carbonate complex  $[\text{Ag}(\text{XPhos})]_2(\mu\text{-}\kappa^2, \kappa^2\text{-CO}_3)$  **106**. The Ag–C(9)ipso bond in **109** is longer than the similar bond distance observed in  $[\text{Ag}(\text{XPhos})]_2(\mu\text{-}\kappa^2, \kappa^2\text{-CO}_3)$  **106** of 3.071(3) Å but is still shorter than the distance observed in  $[\text{Ag}(\text{IXphos})]_2$  **105** of 3.277(3) Å (Table 16). The Ag–O bonds in **109** (Ag(1)–O(1) 2.108(3) Å and Ag(1)–O(2) 2.982(3)) are shorter than the analogous bonds in **106** which has Ag(1)–O(1) of 2.249(2) and Ag(1)–O(2) of 2.3572(2).

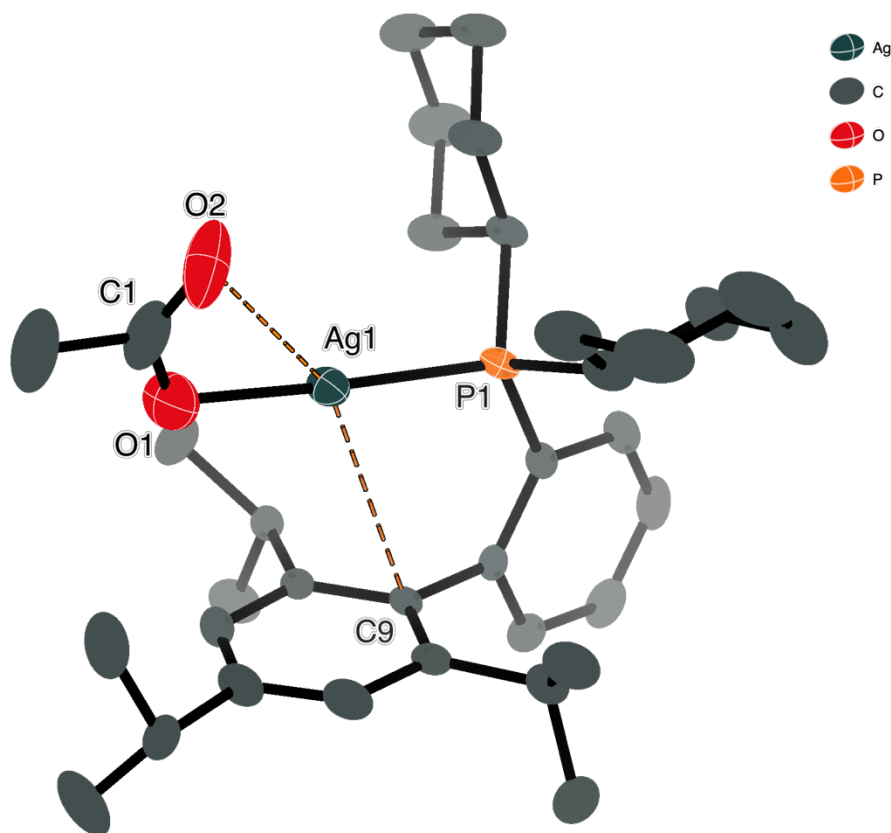


**Figure 65:** The crystal structure of AgOAcXphos **109**

**Table 16:** Principal bond lengths and angles of **109**

<b>109</b>	
<b>Bond</b>	<b>Bond length (Å)</b>
Ag(1)–P(1)	2.3563(7)
Ag(1)–O(1)	2.108(3)
Ag(1)–O(2)	2.982(3)
O(1)–C(1)	1.253(5)
O(2)–C(1)	1.212(5)
Ag(1)–C(9) <sup>ipso</sup>	3.161(2)
<b>Bond angles</b>	<b>Angle (°)</b>
P(1)–Ag(1)–O(1)	176.61(8)
Ag(1)–O(1)–C(1)	115.5(2)
C(1)–O(2)–Ag(1)	73.4(2)

### 3.4 Catalytic Direct Arylation Reactions with Xphos

In contrast to the PPh<sub>3</sub> ligand, Xphos has been established as a more suitable ligand for mechanistic investigations due to the stability of Ag–Xphos bond at room temperature. This allows for the easy detection and isolation of key intermediates in the reaction, especially due to the characteristic <sup>107</sup>Ag/<sup>109</sup>Ag splitting pattern with NMR active nuclei. Thus, the ability of XPhos as a suitable phosphine for catalytic C–H bond arylation was examined.

The standard catalytic reaction was monitored using both <sup>1</sup>H and <sup>19</sup>F{<sup>1</sup>H} NMR spectroscopy. Where possible, the <sup>19</sup>F{<sup>1</sup>H} NMR conversions were calculated by integrating the *ortho*-F resonance of the product ( $\delta$  –143.5) with respect to octafluoronaphthalene ( $\delta$  –145.2) as the internal standard. <sup>19</sup>F T<sub>1</sub> – inversion recovery experiments were used to accurately determined the T<sub>1</sub> of all the components in the reaction mixture, and a D1 of 20 seconds was selected based on this data. Octafluoronaphthalene was found to be a suitable and consistent internal standard when Ag bases were used. However, it was observed to co-precipitate from solution when non-Ag based carbonate bases such as Cs<sub>2</sub>CO<sub>3</sub> and K<sub>2</sub>CO<sub>3</sub> were incorporated. In these cases, the <sup>1</sup>H NMR spectrum of the reaction mixture was used to calculate the % conversion.

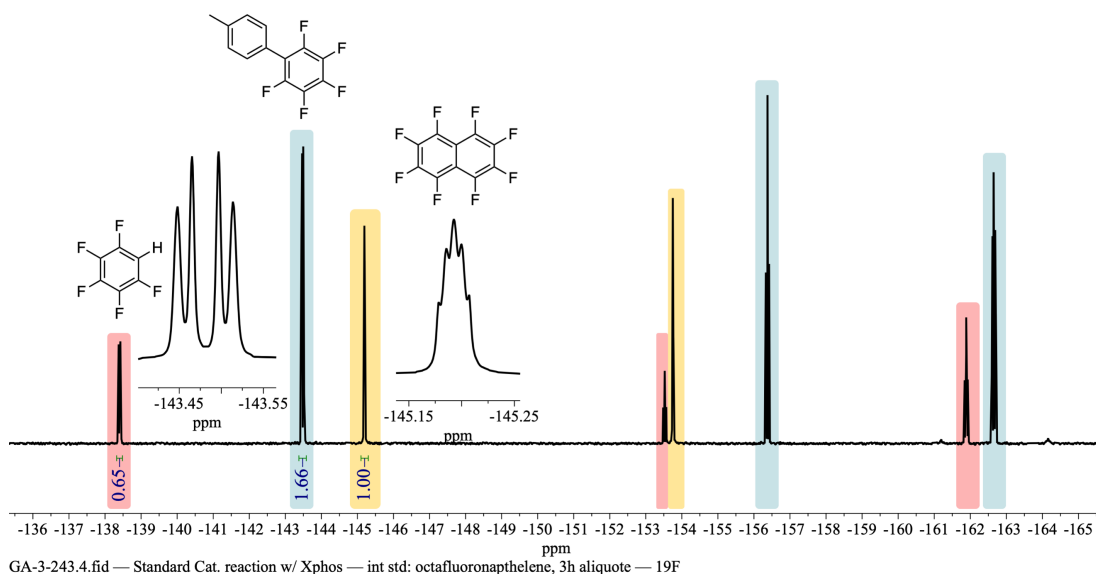
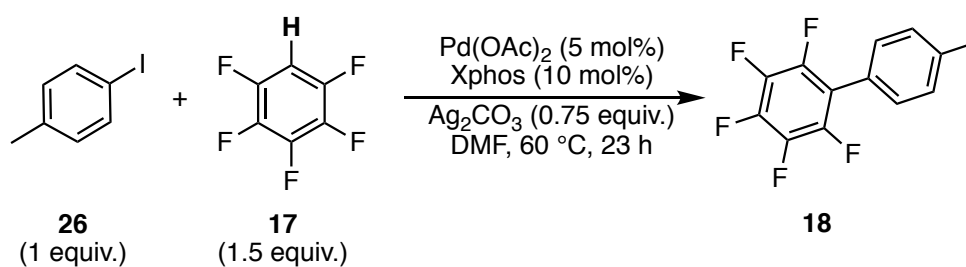


**Figure 66:**  $^{19}\text{F}\{^1\text{H}\}$  NMR (470 MHz,  $\text{CDCl}_3$ , 25 °C, 32 Sc) spectrum of the reaction mixture of the standard direct arylation reaction. The %  $^{19}\text{F}$  NMR yields were calculated using the *ortho*-F resonance of the product ( $\delta$  -143.5, blue) wrt octafluoronaphthalene ( $\delta$  -145.2, internal standard, yellow), remaining  $\text{C}_6\text{F}_5\text{H}$  shown in red.

$^1\text{H}$  NMR yields were reported using 1,3,5-trimethoxybenzene as the internal standard and were calculated by integrating the  $-\text{CH}_3$  peak of 4-iodotoluene **26** ( $\delta$  2.30) or product **18** ( $\delta$  2.43) with respect to the  $-\text{OCH}_3$  peak of 1,3,5-trimethoxybenzene ( $\delta$  3.78). The % NMR yields calculated using  $^1\text{H}$  and  $^{19}\text{F}\{^1\text{H}\}$  NMR spectrum of the reaction mixture were in good agreement with each other.

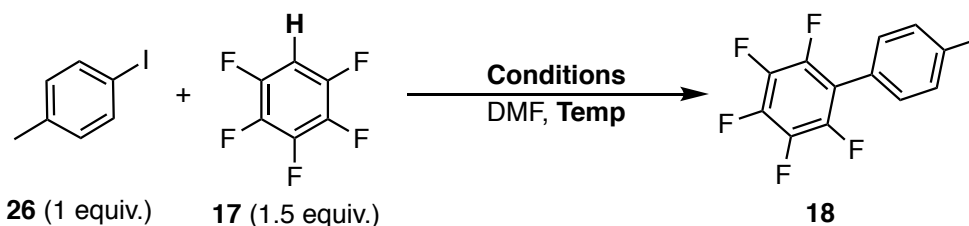


**Scheme 78:** Standard model reaction of the direct arylation of 4-iodotoluene **26** with pentafluorobenzene **17** in DMF at 60 °C with Xphos as the ligand

Pentafluorobenzene **17** was reacted with 4-iodotoluene **26** with  $\text{Pd(OAc)}_2$  (5 mol%), XPhos (10 mol%) and  $\text{Ag}_2\text{CO}_3$  (0.75 equiv.) in DMF at 60 °C, and the reaction reached 96% NMR yield (measured by both  $^1\text{H}$  and  $^{19}\text{F}\{^1\text{H}\}$  NMR) after 3 h. The yield of the product **18** after purification by flash chromatography (100 % petroleum ether 40-60 °C) was 84 %. When repeated at room temperature, the reaction resulted in 72 % ( $^1\text{H}$ ) and 77% ( $^{19}\text{F}\{^1\text{H}\}$ ) NMR

yield after 23 h (**Table 17, Entry 2**), whereas a control reaction without Pd(OAc)<sub>2</sub> at 60 °C gave no product (**Table 17, Entry 3**). Reducing the amount of Xphos added to 5 mol% from 10 mol%, results in only 19 % NMR yield even after prolonged heating at 60 °C for 23 h (**Table 17, Entry 4**). This suggests that 10 mol% of Xphos ligand is optimal for this reaction.

When the quantity of Ag<sub>2</sub>CO<sub>3</sub> was reduced to 0.1 equiv. or 10 mol%, the NMR yield after 3 h was 21% at 60 °C and it barely increased after 23 h. When this reaction was carried out at both 60 °C or room temperature, the NMR yield after 23 h is 21 % indicating that carbonate ligand becomes limiting (**Table 17, Entry 5 and 6**). Use of catalytic amounts of Ag<sub>2</sub>CO<sub>3</sub> (10 mol%) with K<sub>2</sub>CO<sub>3</sub> (0.75 equiv.) at 60 °C (23 h) restored the conversion to 65% (<sup>1</sup>H NMR, **Table 17, Entry 7**). When this reaction is repeated at room-temperature, a conversion of 31 % (<sup>1</sup>H NMR yield) was achieved (**Table 17, Entry 8**). When a similar experiment was performed with Ag(C<sub>6</sub>F<sub>5</sub>)(XPhos) **101** (5 mol%) as the sole source of Ag<sup>I</sup> and K<sub>2</sub>CO<sub>3</sub> (0.75 equiv.) at 60 °C (23 h), the conversion was 57% (**Entry 7**). Replacement of Ag<sub>2</sub>CO<sub>3</sub> by either Cs<sub>2</sub>CO<sub>3</sub> or AgOAc gave conversions under 10% when heated for 3 h at 60 °C (**Table 17, Entry 9 and 10**).

**Table 17:** Catalytic direct arylation reactions with varying conditions

Entry	Conditions <sup>[a]</sup>	Temp. (°C)	NMR Yield (isolated yield) (%) <sup>[a]</sup>	
			3 h	23 h
1	Pd(OAc) <sub>2</sub> (5 mol%) + Xphos (10 mol%) + Ag <sub>2</sub> CO <sub>3</sub> (0.75 equiv.)	60	96 (84)	96
2	Pd(OAc) <sub>2</sub> (5 mol%) + Xphos (10 mol%) + Ag <sub>2</sub> CO <sub>3</sub> (0.75 equiv.)	20	-	75
3	Xphos (10 mol%) + Ag <sub>2</sub> CO <sub>3</sub> (0.75 equiv.)	60	-	0
4	Pd(OAc) <sub>2</sub> (5 mol%) + Xphos (5 mol%) + Ag <sub>2</sub> CO <sub>3</sub> (0.75 equiv.)	60	19	19
5	Pd(OAc) <sub>2</sub> (5 mol%) + Xphos (10 mol%) + Ag <sub>2</sub> CO <sub>3</sub> (10 mol%)	60	21	22
6	Pd(OAc) <sub>2</sub> (5 mol%) + Xphos (10 mol%) + Ag <sub>2</sub> CO <sub>3</sub> (10 mol%)	20	5	21
7	Pd(OAc) (5 mol%) + Xphos (10 mol%) + Ag <sub>2</sub> CO <sub>3</sub> (10 mol%) + K <sub>2</sub> CO <sub>3</sub> (0.75 equiv.)	60	60	65
8	Pd(OAc) (5 mol%) + Xphos (10 mol%) + Ag <sub>2</sub> CO <sub>3</sub> (10 mol%) + K <sub>2</sub> CO <sub>3</sub> (0.75 equiv.)	20	9	31
9	Pd(OAc) <sub>2</sub> (5 mol%) + Xphos (10 mol%) + Cs <sub>2</sub> CO <sub>3</sub> (0.75 equiv.)	60	9	-
10	Pd(OAc) <sub>2</sub> + Xphos (10 mol%) + AgOAc (1.5 equiv.)	60	7	37
11	Pd(OAc) <sub>2</sub> (5 mol%) + Xphos (10 mol%) + K <sub>2</sub> CO <sub>3</sub> (0.75 equiv.)	60	19	-
12	Pd(OAc) <sub>2</sub> + Xphos (10 mol%) + Ag(C <sub>6</sub> F <sub>5</sub> )(Xphos) <b>101</b> (5 mol%) + K <sub>2</sub> CO <sub>3</sub> (0.75 equiv.)	60	28	57
13	Pd(OAc) <sub>2</sub> + Xphos (10 mol%) + Ag(C <sub>6</sub> F <sub>5</sub> )(Xphos) <b>101</b> (5 mol%) + K <sub>2</sub> CO <sub>3</sub> (0.75 equiv.)	20	8	16

<sup>[a]</sup> For methods of determining NMR yields, see Experimental; Yield of isolated product obtained following chromatography on silica-gel.

### 3.5 Kinetic Isotope Effect

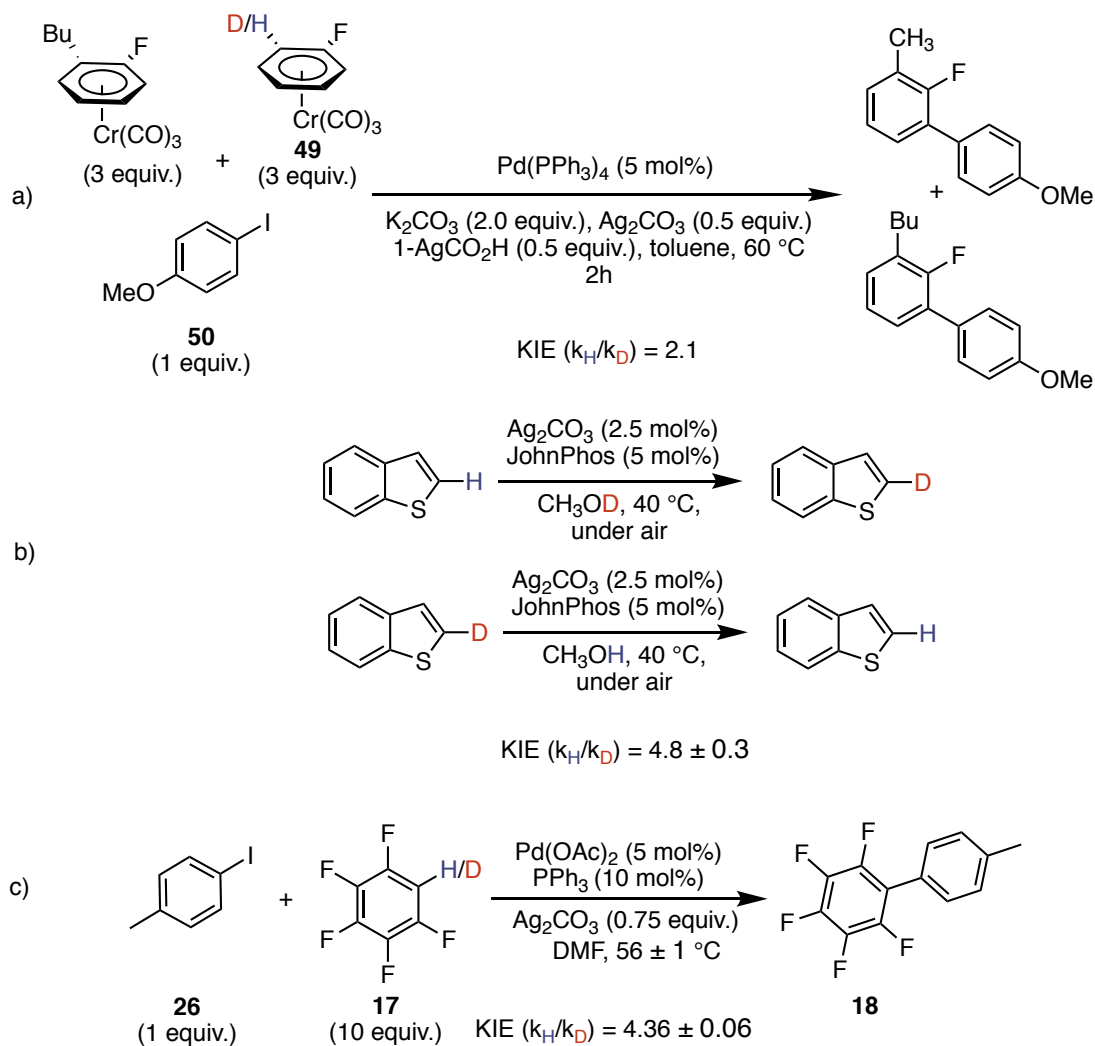
A Kinetic Isotope Effect is observed when the replacement of an isotope within the reaction leads to a change in the rate of reaction. Typically, a naturally abundant isotope such as  $^1\text{H}$ ,  $^{12}\text{C}$  and  $^{18}\text{O}$  is replaced with their less abundant counterpart ( $^2\text{H}$ ,  $^{13}\text{C}$ ,  $^{17}\text{O}$ ). If the site of isotopic labelling is at or near the reaction site, a change in the rate of reaction is observed. This is an effect of quantum mechanics due to zero-point energies where bonds to heavier isotopes have lower vibrational frequencies and require greater energy input to achieve the transition state, resulting in a slower reaction rate. However, if the site of isotopic labeling is far from or uninvolved in the rate-determining step, no KIE will be observed. Thus, by studying the magnitude of the ratio of the rate of reaction between the two isotopes, inferences can be made about the transition state and rate-determining step of the reaction.

$$KIE = \frac{k_{light}}{k_{heavy}}$$

Where,  $k_{light}$  = rate constant for reaction with lighter isotope (eg.  $^1\text{H}$ )

$k_{heavy}$  = rate constant for reaction with heavier isotope (eg.  $^2\text{H}$  or D)

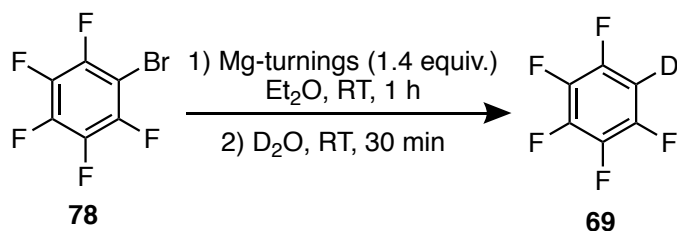
The study of KIEs have become a staple mechanistic tool for C–H functionalization reactions as they help determine if C–H bond cleavage plays a significant role in the rate-determining step. In reactions proposed proceed *via* an AMLA(6)-TS, a primary KIE is observed due to bond breaking/formation in the TS. Larossa and co-workers determined the KIE of the direct arylation of 4-iodoanisole **50** with (2-fluorotoluene)Cr(CO)<sub>3</sub> **49**, as 2.1 using intermolecular competition reactions with isotopically labelled substrate (**Scheme 79a**).<sup>128</sup> Hartwig and co-workers when studying the Ag catalysed C–H deuteration reactions, measured the KIE using parallel reactions with and without isotopically labelled substrates (**Scheme 79b**).<sup>94</sup> Platt *et al.* used *in situ* ReactIR® to monitor the kinetics of the direct arylation of 4-iodotoluene **26**, using PPh<sub>3</sub> as the ligand, and determined the KIE of the reaction to be  $4.36 \pm 0.06$  (**Scheme 79c**).<sup>68</sup>



**Scheme 79:** Few select examples of the KIE of various reactions involving C–H activation, including a) direct arylation of 4-iodoanisole **50** with (2-fluorotoluene) $\text{Cr(CO)}_3$  **49**<sup>128</sup> b) Ag catalysed C–H deuteration<sup>94</sup> c) direct arylation of 4-iodotoluene **26** with pentafluorobenzene **17**.<sup>68</sup>

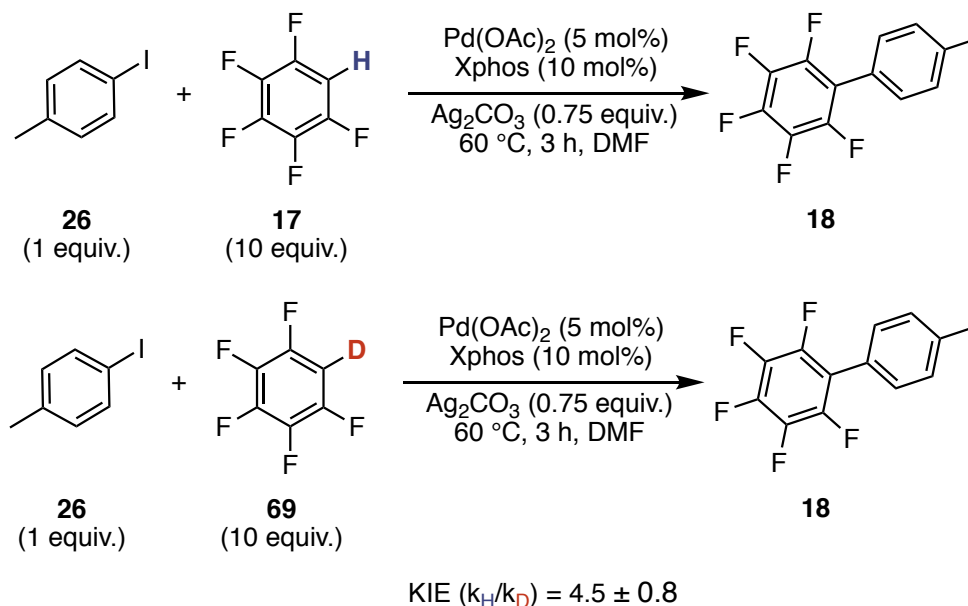
Compared to  $\text{PPh}_3$ , Xphos has very different steric and electronic parameters. Thus, the KIE of the direct arylation with Xphos as the ligand was measured to gain insight into the rate-determining step and C–H bond breaking event. Deuteropentafluorobenzene **69** was prepared by deuteration of pentafluorobenzene using  $\text{D}_2\text{O}$  (Scheme 80).<sup>129</sup> The product **69** was isolated using simple distillation and the purity was determined by  $^1\text{H}$ ,  $^2\text{H}$  and  $^{19}\text{F}\{^1\text{H}\}$  NMR spectroscopy.





**Scheme 80:** Synthesis of deuteriopentafluorobenzene **69**<sup>129</sup>

The standard direct arylation reaction of 4-iodotoluene **26** was carried out under pseudo-zero order conditions with a 10-fold excess of pentafluorobenzene **17**/deuteriopentafluorobenzene **69** (10 equiv.) (**Scheme 81**). The progress of the reaction was monitored using reaction aliquots (details in Experimental). The concentration of product was calculated using the integration of the *ortho*-F resonance of the product ( $\delta -143.5$ ) in comparison to octafluoronaphthalene ( $\delta -145.2$ ) (internal standard) in the  $^{19}\text{F}\{^1\text{H}\}$  NMR spectrum using a  $D1 = 5$  sec. The initial rates of the reaction were calculated using the first 8 data points of the kinetic plot. The KIE of the catalytic reaction was determined from the initial rate of reaction as  $4.5 \pm 0.8$ , making this a primary KIE with a significant C–H bond cleavage step occurring at the rate-determining step of the reaction (**Figure 67**). This is comparable to Platt *et al.*'s KIE of  $4.36 \pm 0.06$  (**Scheme 79c**).<sup>68</sup>



**Scheme 81:** Direct arylation of 4-iodotoluene **26** (0.085 M) with  $\text{C}_6\text{F}_5\text{H}$  **17**/ $\text{C}_6\text{F}_5\text{D}$  **69** (0.85 M) in DMF at  $60^\circ$  for 3 h

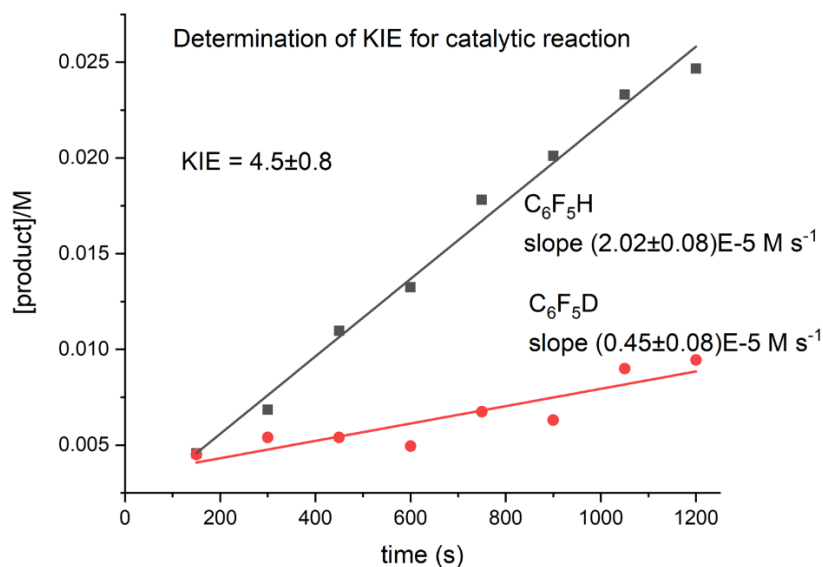
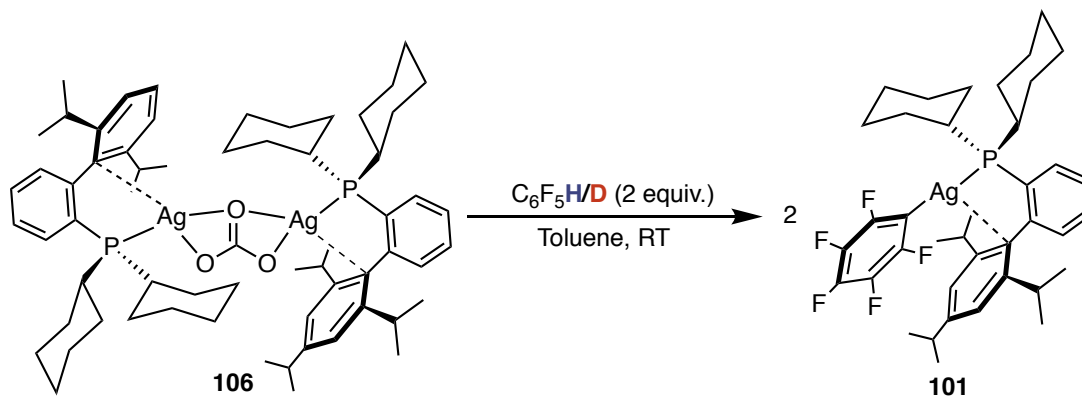


**Figure 67:** Initial rate of reaction for the direct arylation of 4-iodotoluene **26** with 10 equiv. of  $C_6F_5H$  **17** (black) and  $C_6F_5D$  **69** (red)

To obtain further information about the C–H activation by Ag, the KIE of the C–H activation of  $C_6F_5H$  **17** by **106** was also measured. The reaction between **106** and stoichiometric amounts of  $C_6F_5H$  **17** or  $C_6F_5D$  **69** occurs almost instantaneously at room temperature, with a  $^{19}F\{^1H\}$  NMR yield of 85 % and 73 % respectively (**Scheme 82**).



**Scheme 82:** Reaction of **106** with  $C_6F_5H$  or  $C_6F_5D$  at room temperature in toluene

Entry	Isotope	$^{19}F\{^1H\}$ NMR yield (%) <sup>[a]</sup>
1	H	85 %
2	D	73 %

<sup>[a]</sup>  $^{19}F\{^1H\}$  NMR yield calculated by integrating the *ortho*-F resonance of **101** ( $\delta$  -106.7) with respect to octafluoronaphthalene ( $\delta$  -145.2) with a D1 = 20 sec

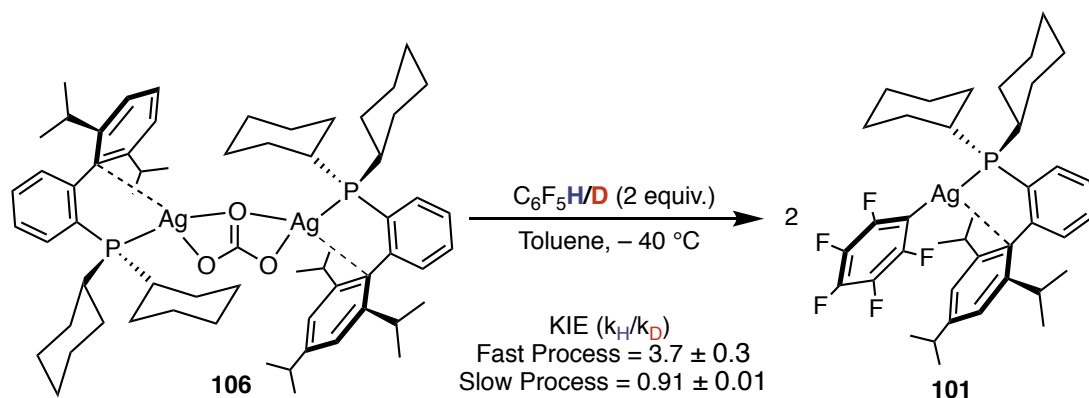
Thus, to slow down the rate of reaction, different low temperatures, and equivalents of  $C_6F_5H$  **17** were trialed, and the kinetic of the reaction was monitored by  $^{19}F\{^1H\}$  NMR spectroscopy. The reaction progressed too quickly at  $0\text{ }^\circ\text{C}$ ,  $-20\text{ }^\circ\text{C}$ ,  $-30\text{ }^\circ$  and with 10 and 20 equivalents of  $C_6F_5H$  **17** (5 equiv. and 10 equiv. per Ag atom) to obtain good kinetics data. However,  $-40\text{ }^\circ\text{C}$  was identified as a suitable temperature with 2 equivalents of  $C_6F_5H$  (1 equiv. of  $C_6F_5H$  per Ag atom) to carry out kinetic analysis.

$^{19}F\{^1H\}$   $T_1$  inversion recovery experiments were performed on a reaction mixture with all the fluorine-containing products and reactants in toluene at  $-40\text{ }^\circ\text{C}$  to accurately determine the  $T_1$  value at the desired temperature (**Table 18**). Using this data, a d1 of 2 s was selected. Data points were collected every 3.06 minutes. The *ortho*-F resonance of the  $Ag(C_6F_5)(Xphos)$  **101** ( $\delta -106.7$ ) was integrated with respect to the internal standard peak ( $\delta -146.7$ ) to determine the concentration of product in the reaction mixture and calculate the rate of reaction (**Figure 68**).

**Table 18:**  $T_1$  values of the reactants and products in toluene at 233 K

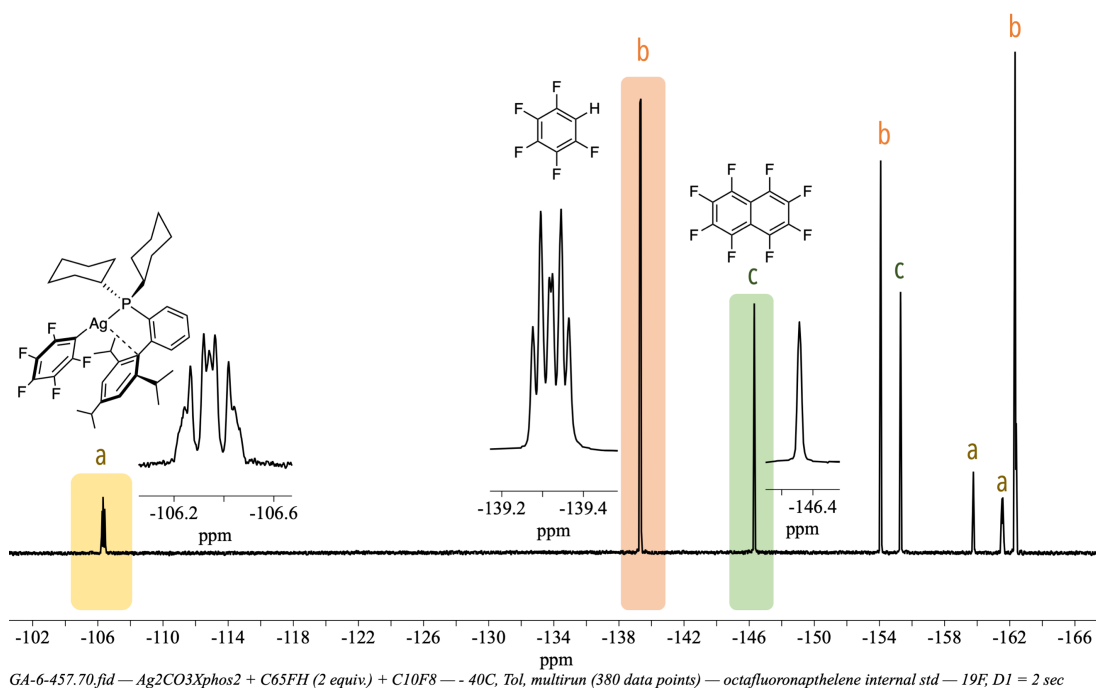
Reagent	$T_1$ (s)
$Ag(C_6F_5)(XPhos)$ <b>101</b>	0.54
$C_6F_5H$ <b>17</b>	1.82
Octafluoronaphthalene	0.50

To monitor the kinetics of the reaction and calculate the KIE, a mixture of **106** and  $C_6F_5H$  **17** (or  $C_6F_5D$  **69**) was prepared in a J-young NMR tube at  $-78\text{ }^\circ\text{C}$  using an ethyl acetate/liq. nitrogen cold bath. Octafluoronaphthalene was used as an internal standard. The final reaction mixture was a light brown colour with no precipitation observed of starting material observed upon leaving the reaction mixture at  $-78\text{ }^\circ\text{C}$  for 10 – 15 mins. The sample was then placed directly in the pre-cooled ( $-40\text{ }^\circ\text{C}/233\text{K}$ ) probe on the Bruker AVIHD 500 instrument. Data collection was initiated immediately after tuning and shimming the sample (**Scheme 83**).

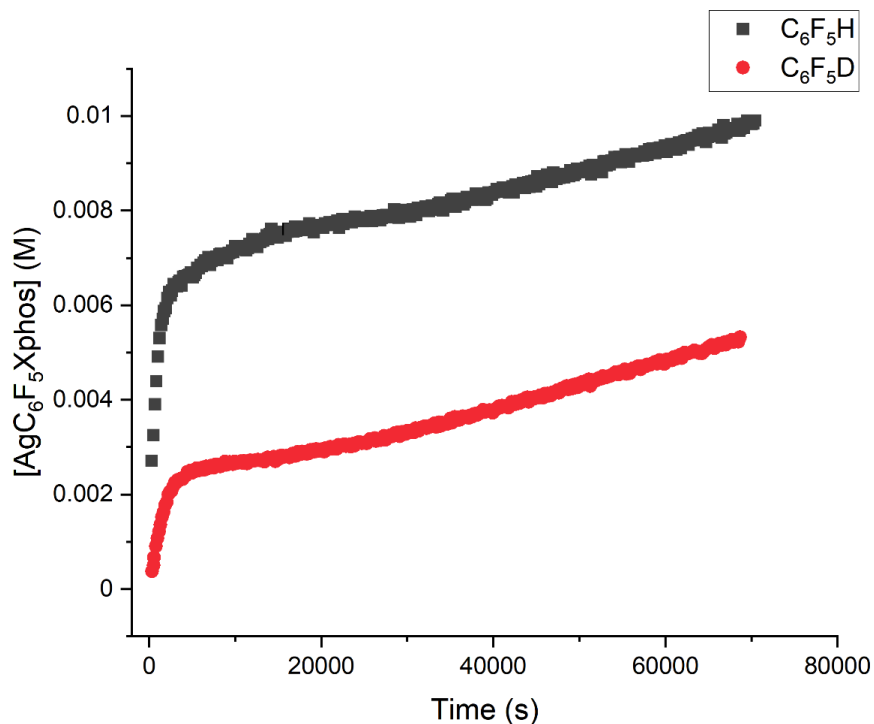


**Scheme 83:** Reaction conditions used to monitor the kinetic profile and calculate the KIE of the reaction of **106** with  $C_6F_5H$  **17** and  $C_6F_5D$  **69**.

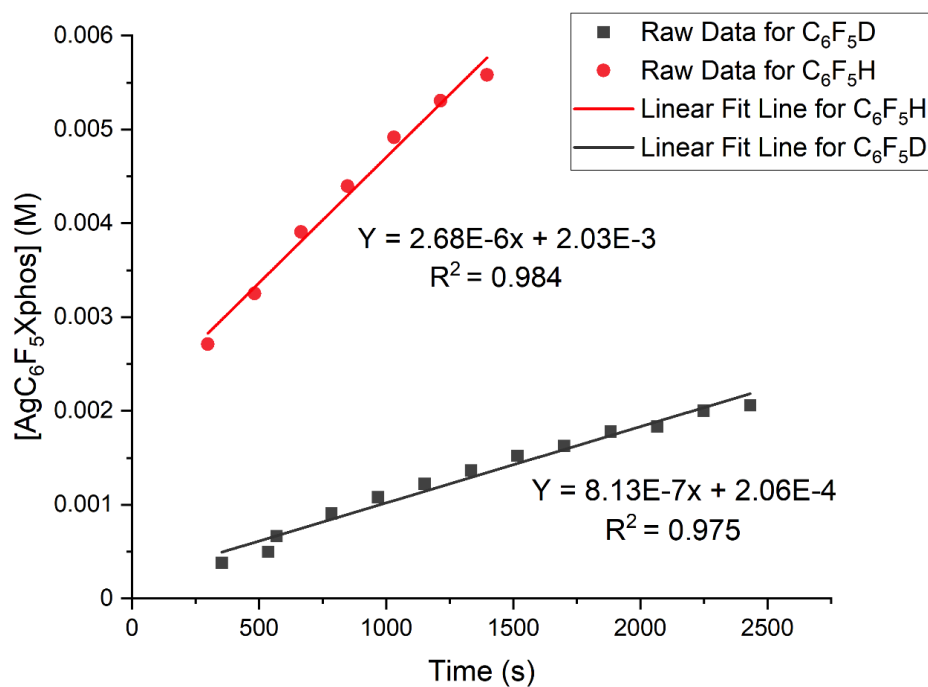
The kinetic profile of the reaction was composed of a fast initial process lasting *ca.* 20 mins followed by a much slower process. This rate of reaction was determined by fitting a linear equation to the data, and the rate was determined using the slope. The data is tabulated in **Table 19**. The KIEs were calculated for the two different processes separately, with a KIE of  $3.7 \pm 0.3$  for the fast process (**Figure 70**) and  $0.91 \pm 0.01$  for the slow process (**Figure 71**). The KIE for the fast process indicates significant C–H bond breaking in the TS state. However, the change in rate could be indicative of a change in the mechanism later in the reaction. Based on the limited kinetic data obtained, it is difficult to determine the origin of the slow process.



**Figure 68:**  $^{19}\text{F}\{^1\text{H}\}$  NMR (470 MHz, Tol,  $-40\text{ }^\circ\text{C}$ ) spectrum of the reaction mixture of **106** and  $\text{C}_6\text{F}_5\text{H}$  **17** (*Ortho*-F peak in red, peaks indicated by **b**) producing **101** (*Ortho*-F peak in yellow, peaks indicated by **a**) at  $-40\text{ }^\circ\text{C}$  (233 K). Octafluoronaphthalene (peak used for integration in green, peaks indicated by **c**) was used as the internal standard.



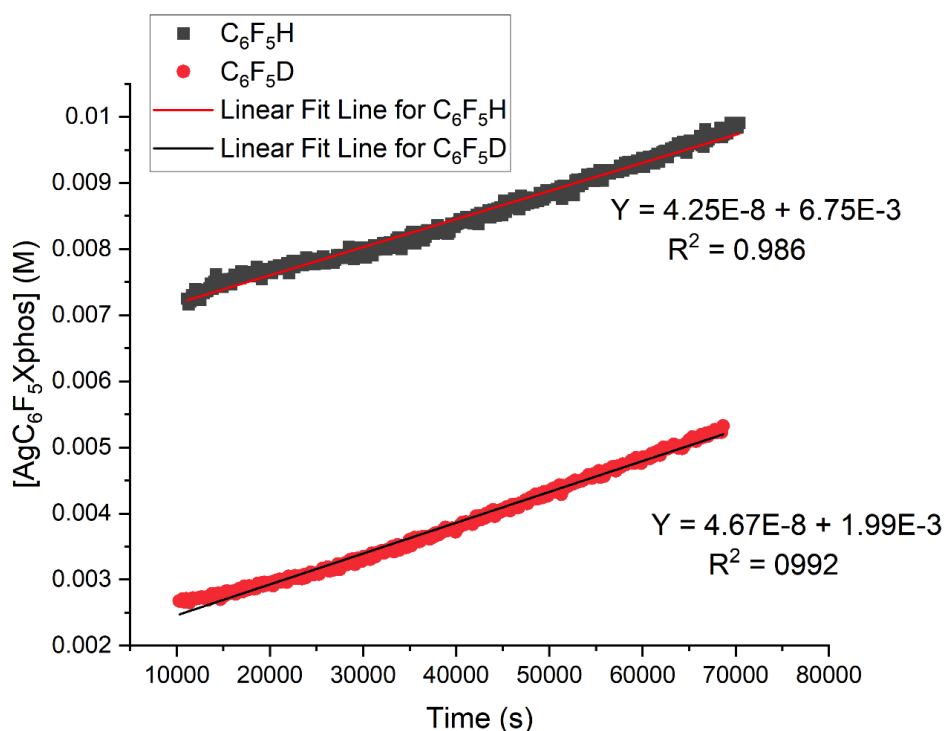
**Figure 69:** Change in concentration of **101** over time for the reaction of  $\text{Ag}_2(\mu\text{-CO}_3)(\text{Xphos})_2$  **106** and two equiv. of  $\text{C}_6\text{F}_5\text{H}$  **17** or  $\text{C}_6\text{F}_5\text{D}$  **69** in toluene at  $-40\text{ }^\circ\text{C}$



**Figure 70:** Initial rate for the reaction of  $[\text{Ag}(\text{XPhos})]_2(\mu\text{-}\kappa^2,\kappa^2\text{-CO}_3)$  **106** and two equiv. of  $\text{C}_6\text{F}_5\text{H}$  **17** or  $\text{C}_6\text{F}_5\text{D}$  **69** in toluene at  $-40\text{ }^\circ\text{C}$  (Fast process)

**Table 19:** Slope and intercept of fast process and slow process for the reaction between **106** and C<sub>6</sub>F<sub>5</sub>H **17**/C<sub>6</sub>F<sub>5</sub>D **69**

	Isotope	Slope	Standard	Intercept	Standard	R <sup>2</sup>
		M s <sup>-1</sup>	Error		Error	
<b>Fast Process</b>	H	2.68E-				
	06		1.4E-07	2.03E-03	1.3E-04	0.98435
	D	8.13E-				
	07		3.7E-08	2.06E-04	5.6E-05	0.97558
	KIE				3.7 ± 0.3	
	Slope	Standard	Intercept	Standard	R <sup>2</sup>	
	M s <sup>-1</sup>	Error		Error		
<b>Slow Process</b>	H	4.25E-				
	08		2.8E-10	0.00675	1.2E-05	0.98599
	D	4.67E-				
	08		2.4E-10	1.99E-03	1.0E-05	0.99168
	KIE				0.91 ± 0.01	

**Figure 71:** Rate for the reaction of [Ag(XPhos)]<sub>2</sub>(μ-κ<sup>2</sup>,κ<sup>2</sup>-CO<sub>3</sub>) **106** and two equiv. of C<sub>6</sub>F<sub>5</sub>H **17** or C<sub>6</sub>F<sub>5</sub>D **69** in toluene at -40 °C (slow process)

To elucidate more information about the fast and slow process, the reaction was also separately monitored using  $^{31}\text{P}\{^1\text{H}\}$  NMR spectroscopy, which showed the consumption of **106**, gradual production of **101** and the presence of unbound Xphos (**Figure 72**). The  $T_1$  values of phosphorus complexes are typically very long, for example at room temperature the  $T_1$  value of Xphos and **101** are 7.61 and 4.26 secs respectively. As a  $90^\circ$  pulse is used in these  $^{31}\text{P}\{^1\text{H}\}$  NMR experiments (*zgpg*), a  $D1 = T_1 \times 5$  is required to improve the accuracy of the integrations. At  $-40^\circ\text{C}$ , the  $T_1$  of Xphos and **101** in toluene were 2.22 and 1.73 seconds respectively, which would require a D1 of 12 seconds. As the initial fast process occurs rapidly with the first 20 mins, a long D1 would greatly limit the number of data points that could be collected. Thus, the default D1 of 2 seconds was used, and instead to help improve the data, the number of scans was set to 128, and the data point was collected every 5.45 min. Additionally, at lower temperatures peak broadening and poor shimming was observed.

The integral graphs produced using MestReNova show the approximate trend with respect to each  $^{31}\text{P}$  containing species (**Figure 73**). The resonances of **106** and **101** partially overlap, thus the unobscured aspect of the signal was integrated. The % conversion can only be calculated tentatively using the  $^{31}\text{P}\{^1\text{H}\}$  NMR spectrum from the integrations of **106**, **101** and Xphos. However, the kinetic profile derived from the  $^{31}\text{P}\{^1\text{H}\}$  NMR spectrum is consistent with the  $^{19}\text{F}\{^1\text{H}\}$  NMR spectrum; the reaction initially begins with a fast process and is then followed by a slower process (**Figure 74**). Additionally, no new reaction intermediates were detected by low-temperature  $^{31}\text{P}\{^1\text{H}\}$  and  $^{19}\text{F}\{^1\text{H}\}$  NMR spectroscopy.

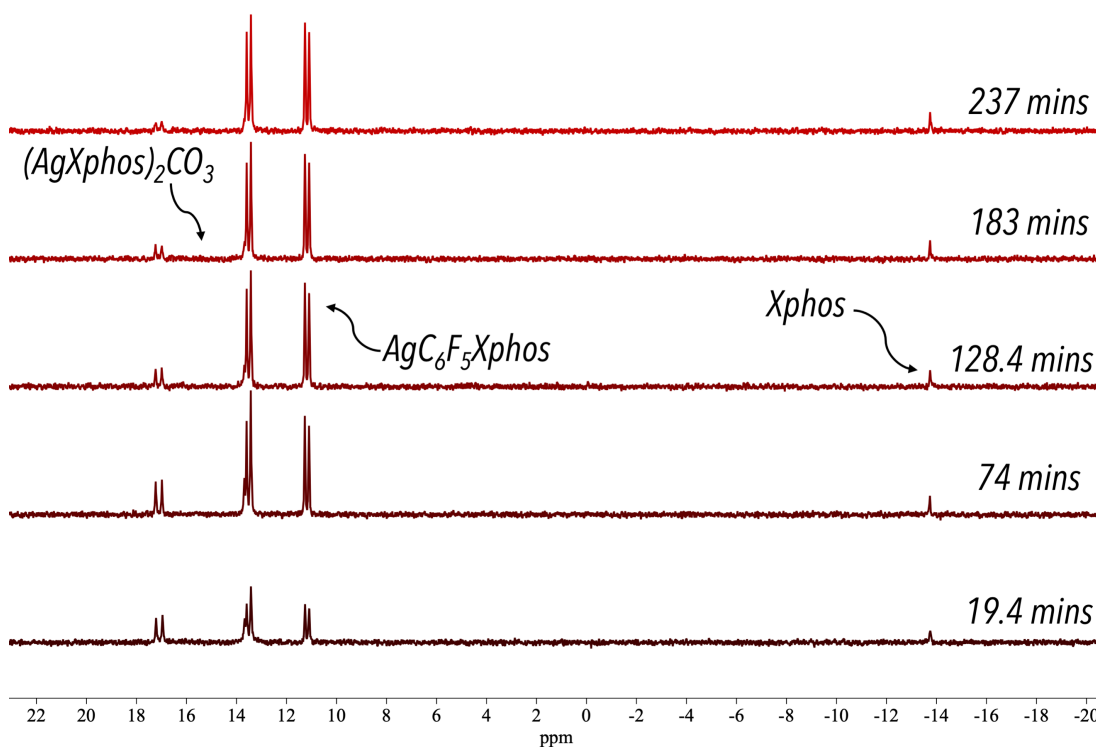


**Figure 72:**  $^{31}\text{P}\{^1\text{H}\}$  NMR (202.5 MHz, Tol,  $-40^\circ\text{C}$ ) time course of the reaction between **106** and  $\text{C}_6\text{F}_5\text{H}$  (2 equiv.) to yield  $\text{Ag}(\text{C}_6\text{F}_5)(\text{Xphos})$  **101** and unbound Xphos.

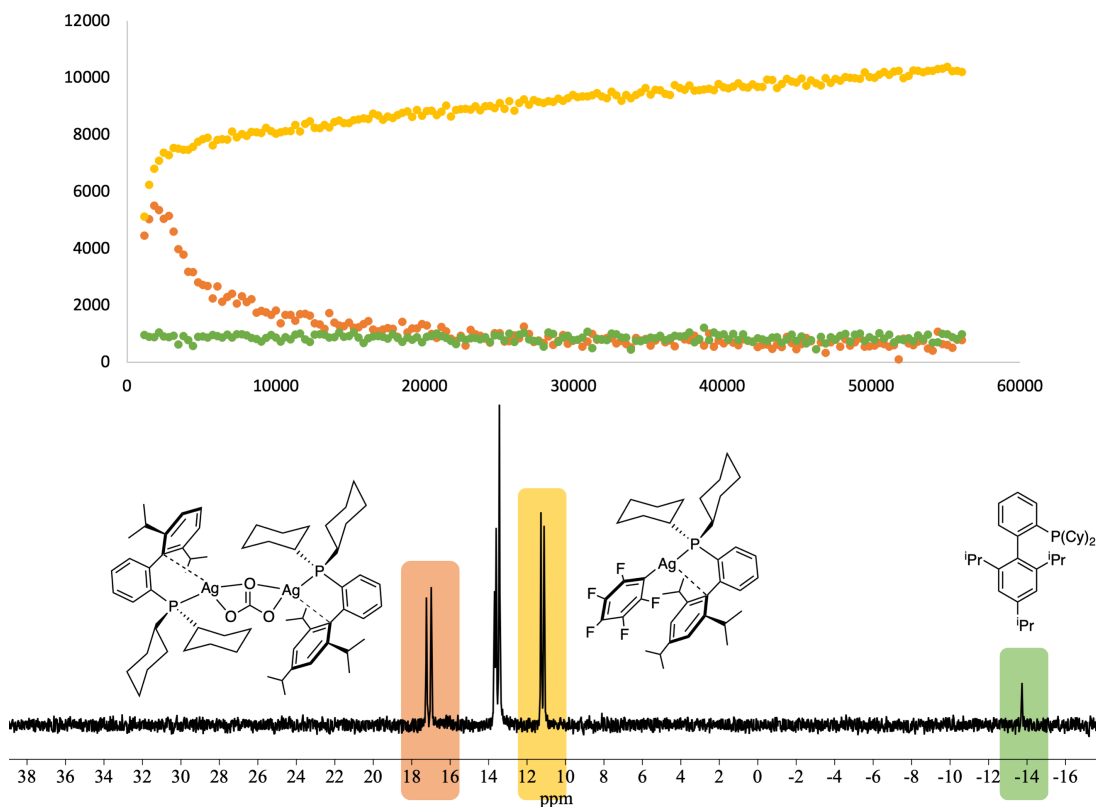


**Figure 73:**  $^{31}\text{P}\{^1\text{H}\}$  NMR (202.5 MHz, Tol,  $-40\text{ }^\circ\text{C}$ ) time course of the reaction between **106** and  $\text{C}_6\text{F}_5\text{H}$  (2 equiv.) to yield  $\text{Ag}(\text{C}_6\text{F}_5)(\text{Xphos})$  **101** and unbound Xphos, along with the integral graph calculated using MestReNova, demonstrating the change in each reagent.

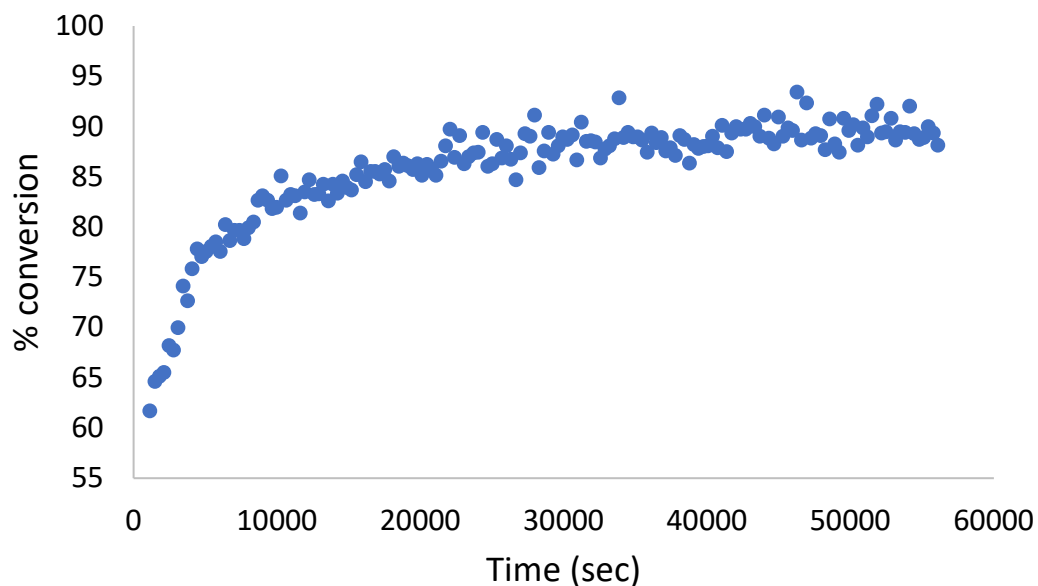
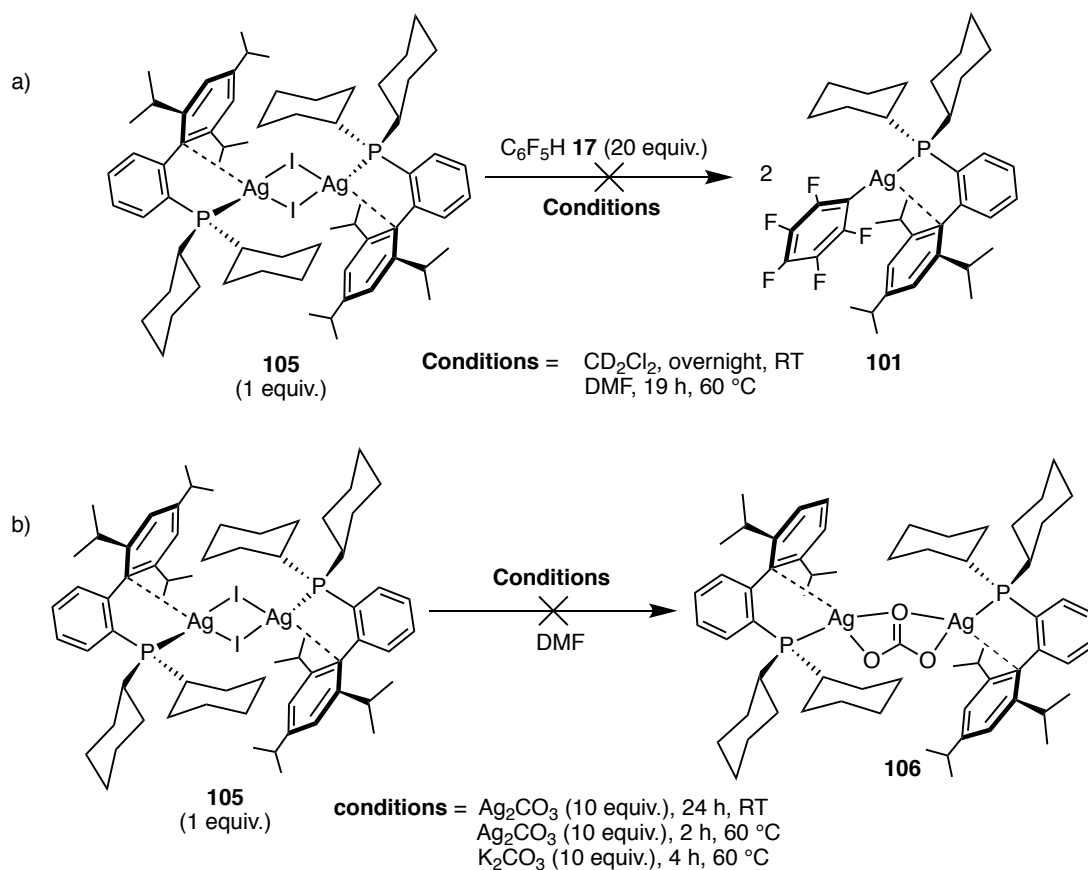


**Figure 74:** Change in the % conversion to  $\text{Ag}(\text{C}_6\text{F}_5)(\text{Xphos})$  **101** over time in seconds.



### 3.6 Ag<sup>I</sup> and Xphos Recycling Mechanism

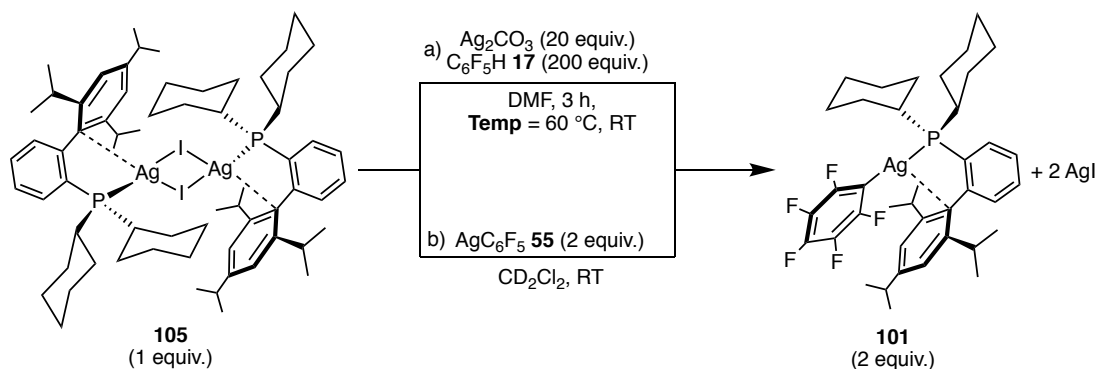
The ability to use catalytic amounts of Ag in the standard direct arylation reaction suggests that the Ag and the Xphos within the system are being recycled in some manner. Thus far it has been demonstrated that Ag<sub>2</sub>CO<sub>3</sub> coordinates with Xphos to form **106**, which is capable of C–H activation at room temperature to yield **101** which contains an -AgC<sub>6</sub>F<sub>5</sub> motif. Complex **101** can undergo transmetallation with **102** to generate the organic product **28** and an Ag iodide by-product **105**. Thus, it was postulated that [AgIXphos]<sub>2</sub> **105** is somehow capable of regenerating either species **106** or **101** within the catalytic cycle. Initial attempts involved reacting C<sub>6</sub>F<sub>5</sub>H with **105** but found no reaction in either DMF at 60 °C or dichloromethane at room temperature (**Scheme 84a**). Similarly, the reaction of **105** with Ag<sub>2</sub>CO<sub>3</sub> or K<sub>2</sub>CO<sub>3</sub> did not form any of the expected **106** product instead the **105** remained unreacted according to the <sup>31</sup>P{<sup>1</sup>H} NMR spectrum (**Scheme 84b**).



**Scheme 84:** Reaction of **105** with an excess of C<sub>6</sub>F<sub>5</sub>H **17** (20 equiv.) and carbonate salts such as Ag<sub>2</sub>CO<sub>3</sub> and K<sub>2</sub>CO<sub>3</sub>, did not result in the formation of the expected product.

However, the reaction of **105** with excess Ag<sub>2</sub>CO<sub>3</sub> (10 equiv.) and a large excess of pentafluorobenzene (100 equiv.) generated **101** and precipitation of silver iodide. The presence of **101** within the reaction mixture was confirmed by <sup>31</sup>P{<sup>1</sup>H}, <sup>19</sup>F{<sup>1</sup>H} NMR spectroscopy and LIFDI-MS analysis (details in Experimental). This reaction also takes place rapidly at

room temperature as full conversion of **105** to **101** was observed within 3 h (**Scheme 85a**). In a similar vein, the mixture of **105** with  $\text{AgC}_6\text{F}_5$  **55** in dichloromethane, resulted in the immediate precipitation of AgI as a yellow solid (**Figure 75**) and formation of **101** (**Scheme 85b**). This provides a plausible recycling mechanism for the Xphos ligand, and the formation of AgI as the final by-product by the end of the reaction.



**Scheme 85:** Reaction demonstrating a possible phosphine and Ag recycling mechanism to regenerate **101**

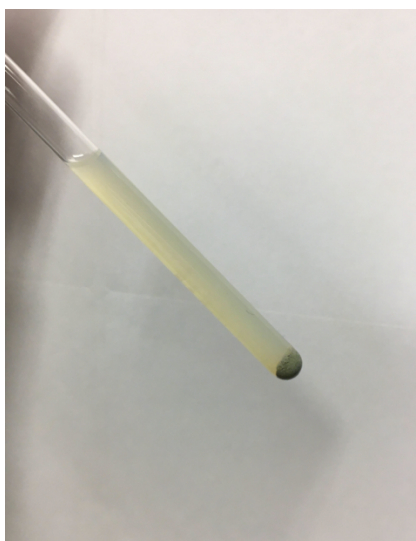
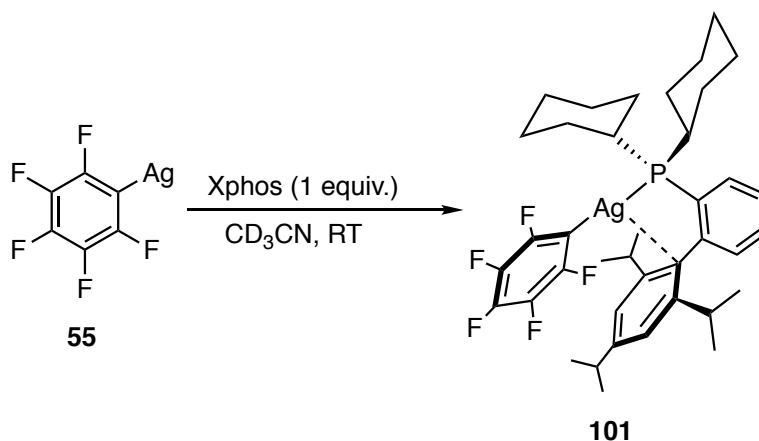


**Figure 75:** Precipitation of a yellow solid (AgI) upon mixing **105** with **55** (**Scheme 85b**) in J young NMR tube

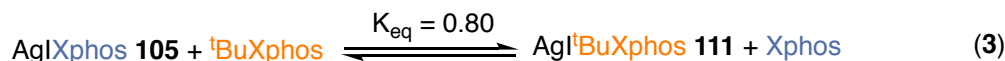
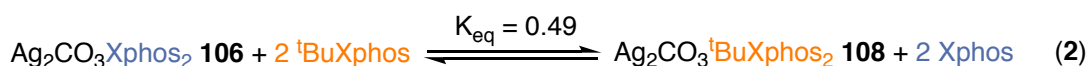
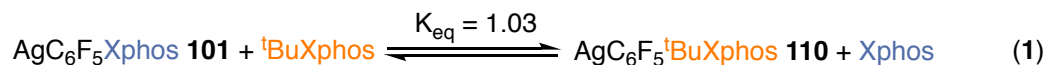
Finally, as expected, the reaction of  $\text{AgC}_6\text{F}_5$  **55** reacts rapidly with Xphos, at room temperature in acetonitrile, to form **101** quantitatively (**Scheme 86**). This suggests that the formation of **101** is highly favourable. Additionally, in Chapter 2, it was noted that  $\text{Ag}_2\text{CO}_3$  was capable of reacting with  $\text{C}_6\text{F}_5\text{H}$  **17** to produce trace amounts of  $\text{AgC}_6\text{F}_5$  **55**. Thus, this provides an additional mechanism by which **101** could be regenerated.



**Scheme 86:** Reaction of  $\text{AgC}_6\text{F}_5$  **55** with Xphos to generate  $\text{Ag}(\text{C}_6\text{F}_5)(\text{Xphos})$  **101**

### 3.7 Phosphine-Exchange and $^{31}\text{P}$ - $^{31}\text{P}$ EXSY Experiments

To understand the lability of the Ag–Xphos bond in the Ag complexes, **101**, **106** and **105** were reacted with  $^t\text{BuXphos}$ . To improve the accuracy of the integrations of the  $^{31}\text{P}\{^1\text{H}\}$  NMR spectrum,  $^{31}\text{P}\{^1\text{H}\}$   $T_1$  – inversion recovery experiments were carried out to determine the  $T_1$  of the different phosphorus species and the D1 was set to  $T_1 \times 5$ . Addition of  $^t\text{BuXphos}$  (1 equiv.) to **101** resulted in immediate formation of a new silver phosphine species at room temperature ( $^{31}\text{P}$  NMR  $\delta$  38.5, pair of dt,  $^1J_{107\text{Ag}^{31}\text{P}} = 448$  Hz,  $^1J_{109\text{Ag}^{31}\text{P}} = 516$  Hz,  $J_{\text{PF}} = 2.7$  Hz, compared to free ligand at  $\delta$  21.4) in 50% conversion consistent with exchange of the phosphine to form the  $^t\text{BuXphos}$  analogue  $\text{Ag}(\text{C}_6\text{F}_5)(^t\text{BuXphos})$  **110**. Assuming this is an equilibrium reaction, the equilibrium constant was deduced to be  $1.03 \pm 0.05$  for formation of **110** (see eq. 1). Similar behavior was observed for **106** and **105** (eq 2-3).



(**105** and **111** assumed to be monomer in solution for calcn of  $K_{\text{eq}}$ )

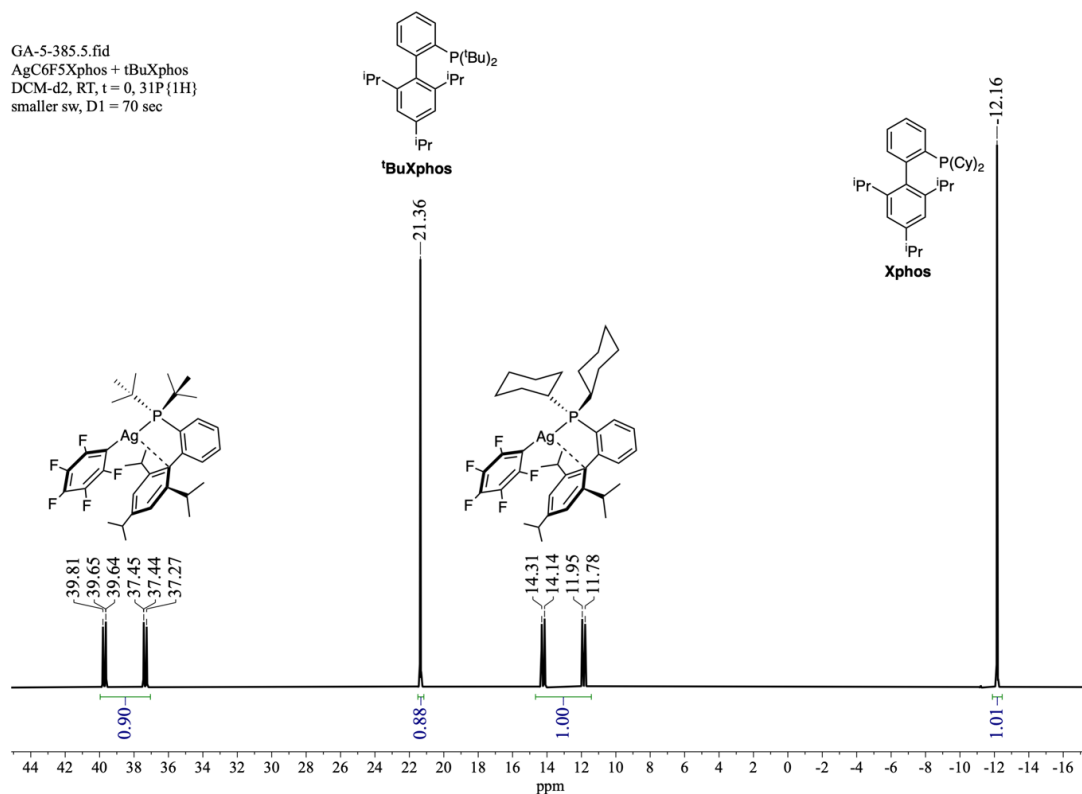
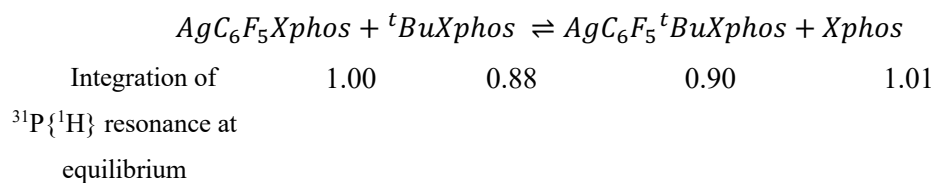


**Figure 76:**  $^{31}\text{P}\{^1\text{H}\}$  (202.5 MHz,  $\text{CD}_2\text{Cl}_2$ , 25 °C) spectrum of the mixture of  $\text{Ag}(\text{C}_6\text{F}_5)(\text{Xphos})$  **101** (1 equiv.) and <sup>t</sup>BuXphos (1 equiv.)

**Table 20:** Summary of  $T_1$ , chemical shift and coupling constant of the different phosphorus species in the reaction between **101** and <sup>t</sup>BuXphos

Reagent	$T_1$ (s)	Chemical Shift (ppm)	$J(^{107}\text{Ag} - ^{31}\text{P})$ (Hz)	$J(^{109}\text{Ag} - ^{31}\text{P})$ (Hz)
Xphos	7.61	-12.16	-	-
$\text{Ag}(\text{C}_6\text{F}_5)(\text{Xphos})$	4.26	13.00	443	512
<sup>t</sup> BuXphos	13.36	21.36	-	-
$\text{Ag}(\text{C}_6\text{F}_5)^{\text{t}}\text{BuXphos}$	8.68	38.53	447	516

#### Calculating the Equilibrium constant ( $K_{\text{eq}}$ )



$$K_{eq} = \frac{[AgC_6F_5^tBuXphos][Xphos]}{[AgC_6F_5Xphos][^tBuXphos]} = \frac{0.90 \times 1.01}{1.00 \times 0.88} = 1.03$$

The results of these experiments, suggest that the Ag–Xphos bond is labile enough to allow intermolecular exchange, but in contrast to the PPh<sub>3</sub> ligand, is stable at room temperature to allow for ease of characterization at room temperature. The experiments with <sup>t</sup>BuXPhos encouraged further study to better understand the exchange between Ag(XPhos) complexes and free XPhos using <sup>31</sup>P-<sup>31</sup>P EXSY experiments.

A <sup>31</sup>P-<sup>31</sup>P EXchange SpectroscopY (EXSY) uses the same pulse sequence as an NOESY experiment but is used to detect chemical or conformational exchange rather than structural information. Like NOESY, EXSY utilizes a set of three radio frequency 90° pulses which are divided among four distinct stages (**Figure 77**).<sup>130</sup>

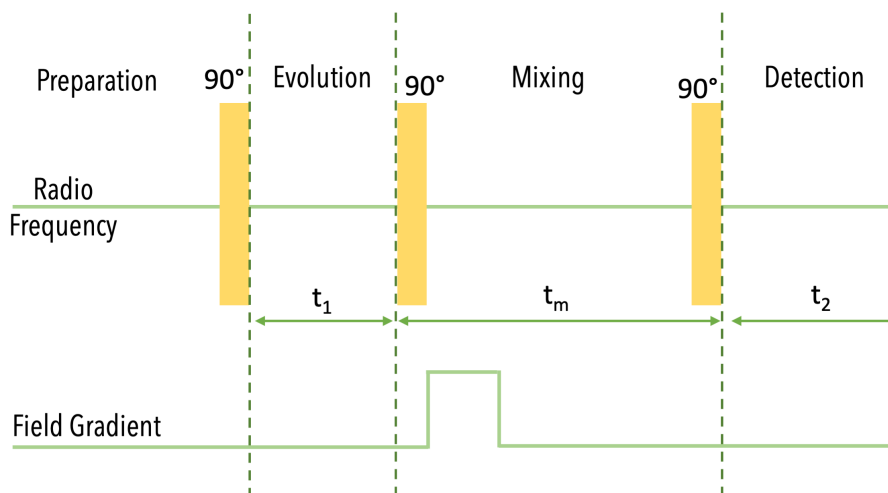


**Figure 77:** The four basic stages of all 2D experiments: Preparation, Evolution, Mixing and Detection. For EXSY experiments the exchange process occurs in the mixing period.<sup>130</sup>

The first 90° pulse excites the spin-active nuclei to their characteristic frequencies, resulting in transverse magnetization during the preparation period. This is followed by the evolution period lasting for  $t_1$  where the nuclei are allowed to precess and acquire precession frequency information. The second 90° occurs at the start of the mixing period, lasting for  $t_m$  which is also known as the mixing time. This is predominantly when the exchange process occurs, and results in transfer of longitudinal magnetization. The final 90° pulse during the detection period, rotates the longitudinal magnetization after exchange, and allows for detection of the FID by the spectrometer. The mixing time  $t_m$  is a particularly important parameter, as it is the time during which the exchange process occurs.<sup>130</sup> Thus, EXSY experiments are often recorded with a range of different mixing times. Exchange processes are denoted by the presence of exchange cross peaks, which occur away from the diagonal line

and directly correlate the two exchanging peaks (**Figure 78**). Exchange peaks have the opposite sign to NOE peaks.

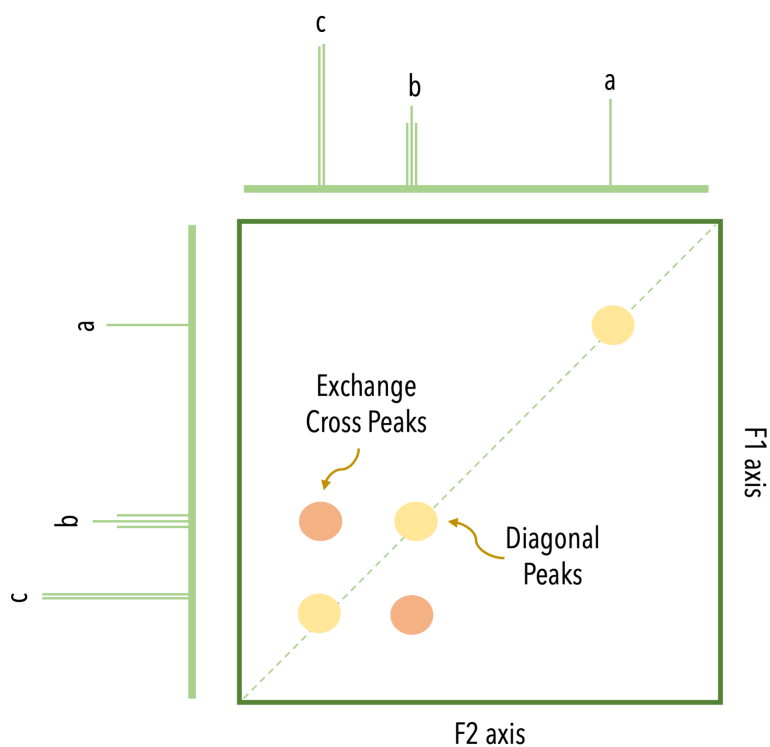


**Figure 78:** Example EXSY spectrum, where the exchange between **b** and **c** is denoted by the presence of the exchange cross peaks (orange), while no exchange occurs with **a**.

To study the exchange process between  $\text{Ag}(\text{C}_6\text{F}_5)(\text{Xphos})$  **101** and Xphos, a sample of **101** and 5 equiv. of Xphos in dichloromethane- $d_2$  and the  $T_1$  all the species involved were measured to help set the D1 and select an appropriate range of mixing times. The 2D  $^{31}\text{P}$ - $^{31}\text{P}$  EXSY spectrum (mixing time: 2 s) revealed cross peaks consistent with intermolecular exchange between **101** and XPhos on the timescale of seconds (**Figure 79**). However, due to the long mixing times and D1 relaxation delays, each 2D EXSY experiment required very long experiment times in the order of 18 – 22 h per mixing time.

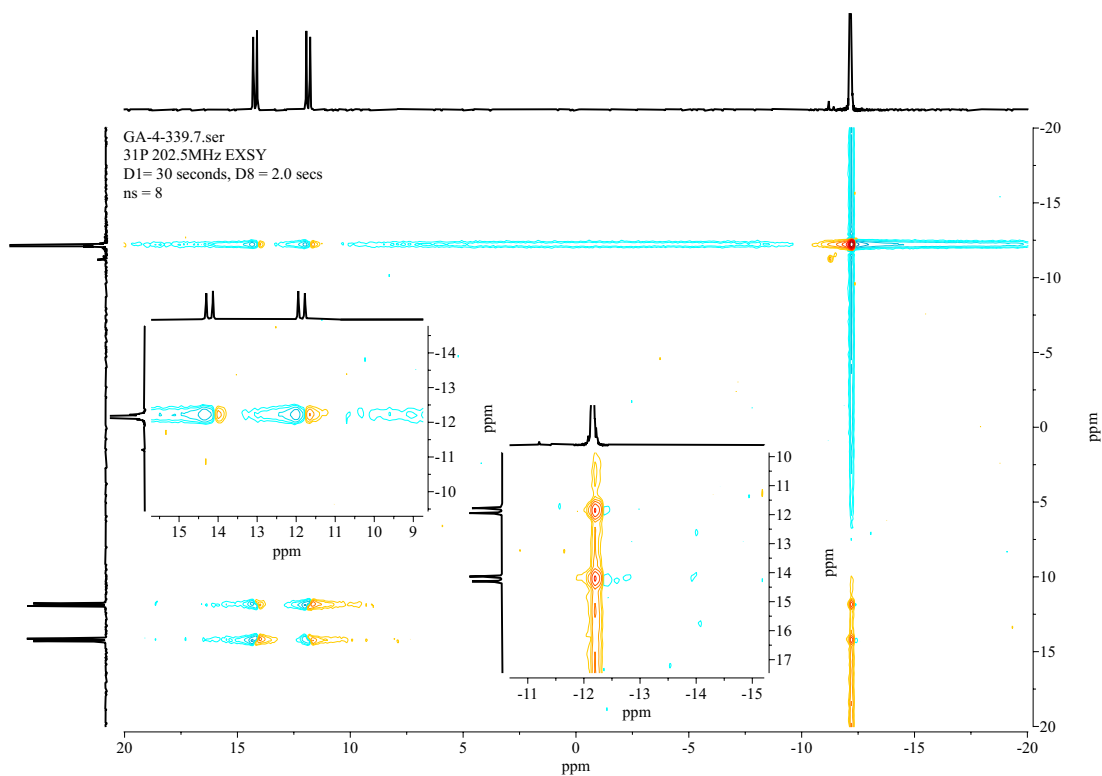


**Figure 79:** 2D  $^{31}\text{P}$ - $^{31}\text{P}$  EXSY spectrum of a mixture of  $\text{Ag}(\text{C}_6\text{F}_5)(\text{Xphos})$  **101** and Xphos (5 equiv.) with a mixing time of 2 s

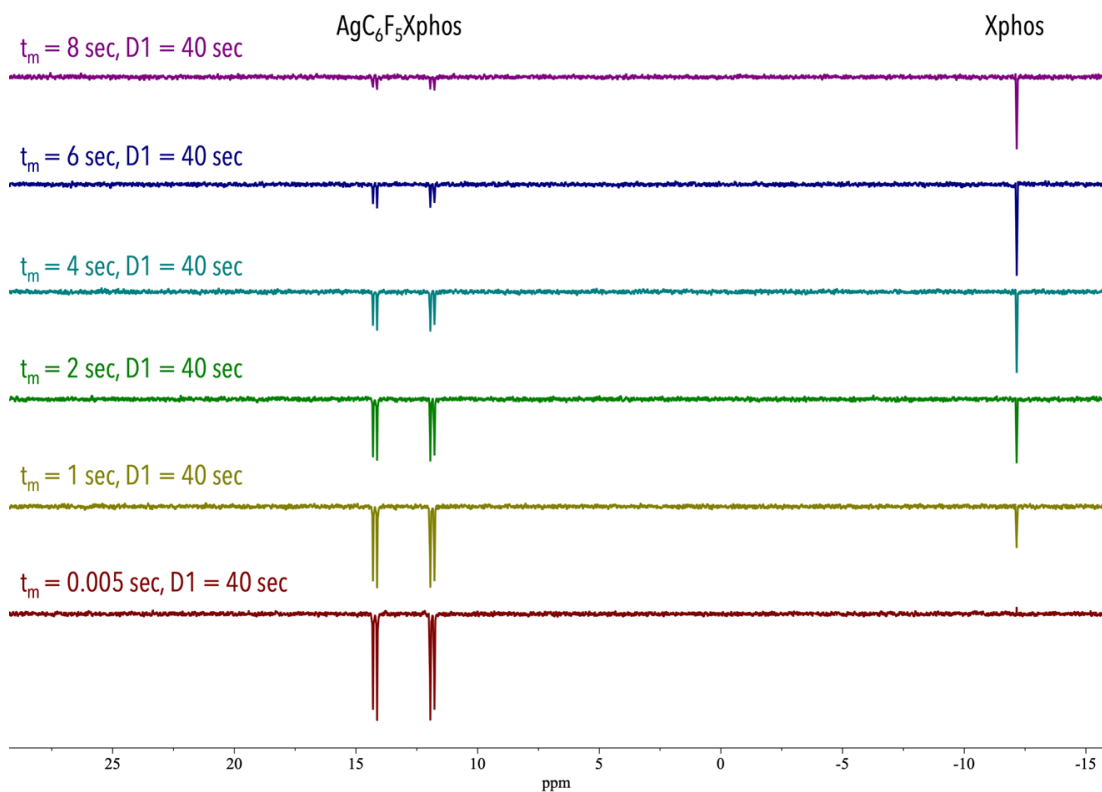


**Figure 80:** Stack plot from 1D EXSY experiment with **101** and Xphos (5 equiv.), with various mixing times in  $\text{CD}_2\text{Cl}_2$ . Selective inversion of **101** resonance with a selective pulse width ca. 5 ppm, with 20 scans per mixing time.

Since there is exchange between two sites only, 1D-EXSY is suitable and is more economical in instrument time.<sup>131</sup> In a 1D-EXSY experiments, one resonance is selectively excited and as it undergoes exchange during the mixing time, the magnetization is gradually transferred to the nuclei it is in chemical exchange with. In this case, the resonance of **101** was selectively excited, and exchange with Xphos allows for magnetization transfer to the Xphos signal<sup>131,132</sup> (**Figure 80**). Exchange between Ag(C<sub>6</sub>F<sub>5</sub>)(Xphos) **101** and Xphos (both in excess and stoichiometric) was detected with mixing times 1 s onwards. Similarly, when **106** and **105** were reacted with stoichiometric and excess Xphos, exchange was detected by 1D EXSY at mixing times of 0.5 s and 1 s respectively. This suggests the AgXphos complexes are all capable of undergoing intermolecular exchange, on a timescale of seconds with Xphos.

To gain insight into the kinetics of the exchange process, 1D-EXSY experiments on **101** in the presence of a range of concentrations of free XPhos were conducted in dichloromethane-*d*<sub>2</sub> yielding evidence that the rate of exchange  $V_{ex}$  depends linearly on [XPhos] and  $k_{obs}$  is derived from the variation of fractional integration of [XPhos] with mixing time  $t_m$  on selective excitation of **101**. EXSY data were also collected for [Ag(XPhos)]<sub>2</sub>(μ-κ<sup>2</sup>,κ<sup>2</sup>-CO<sub>3</sub>) **106** and Ag<sub>2</sub>(μ-I)<sub>2</sub>(Xphos)<sub>2</sub> **105** but were not analysed further because of ambiguities in concentrations cause by dissociation of dimer species. The analysis of both the concentration and temperature-dependent EXSY data was carried out by Prof. Robin Perutz, and the procedure for data analysis is explained below.

$$V_{ex} = k_{obs} \frac{[Xphos][AgC_6F_5Xphos \mathbf{101}]}{[Xphos] + [AgC_6F_5Xphos \mathbf{101}]}$$

**Equation 1:** Rate of exchange by McKay equation<sup>133</sup>

The integration ratios of Xphos with respect to Ag(C<sub>6</sub>F<sub>5</sub>)(Xphos) **101** were converted to integration fractions I(XPhos)/[I(XPhos) + I(Ag(XPhos)(C<sub>6</sub>F<sub>5</sub>))] which were then plotted against mixing time. A linear equation was fitted to the data up until a mixing time of 6 s. A correction factor had to be applied to the data due to the large difference in relaxation times (T<sub>1</sub>) of **101** and Xphos in dichloromethane-*d*<sub>2</sub> (**Table 21**). The correction factor was given as:

$$e^{-t(T_{1A}^{-1} - T_{1B}^{-1})}$$

**Equation 2:** Correction factor applied to the data due the large difference in relaxation times for **101** and Xphos

For mixing times between 0 to 6 s, the correct factors for the data varied from 1 to 1.78. The correction factor for a mixing time of 8 s was very large (2.16), and thus this data point was excluded from the calculations. The plot of integration fractions vs the mixing times with



and without the corrections is showing in **Figure 81**, and the  $k_{\text{obs}}$  of the exchange process is given by the slope of the linear equation.

**Table 21:**  $T_1$  values of Xphos and the Ag complexes used for EXSY experiments

Compound	Benzene- $d_6$		dichloromethane- $d_2$		dichloromethane- $d_2$	
	<b>106</b>	Xphos	<b>105</b>	Xphos	<b>101</b>	Xphos
$T_1$ (s)	1.79	5.35	4.97	6.11	4.46	7.75

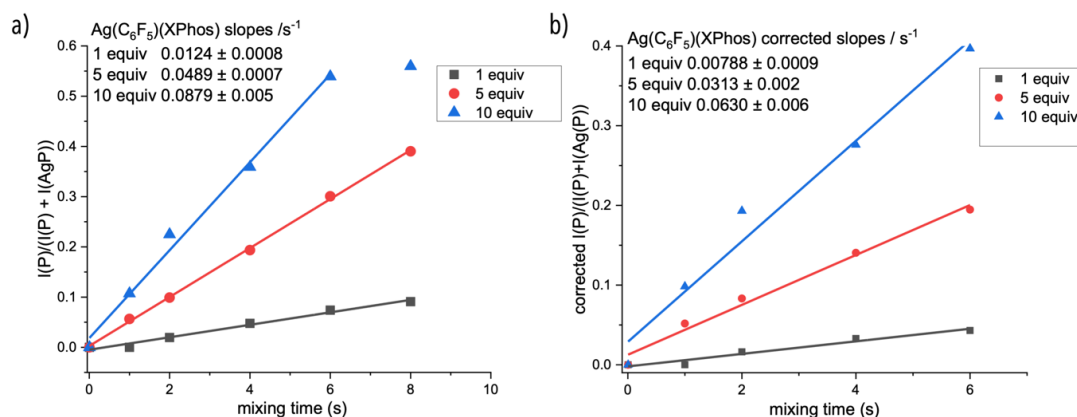


**Figure 81:** Plot of fractional transfer of magnetisation from **101** to free XPhos in dichloromethane against mixing time. a) plot without corrections for the difference in relaxation times. b) Plot with the corrections applied to the relaxation times.

The **Figure 81** shows a dependence of  $k_{\text{obs}}$  on  $[\text{XPhos}]$  which points to an associative reaction. Using the  $k_{\text{obs}}$ , the rate of exchange ( $V_{\text{ex}}$ ) was calculated using **Equation 1**, and the values of  $k_{\text{obs}}$  and  $V_{\text{ex}}$  for the corrected and uncorrected data are shown in **Table 22**. The application of the correction factor in **Equation 2** resulted in a reduction of about 30% in both  $k_{\text{obs}}$  and  $V_{\text{ex}}$ .

**Table 22:** Values of  $k_{\text{obs}}$  and  $V_{\text{ex}}$  for **101**

	Equiv. of Xphos	Concentration (M)		Slope/ $k_{\text{obs}}$ ( $s^{-1}$ )		$V_{\text{ex}}$ ( $\times 10^{-4} \text{M}^{-1} \text{s}^{-1}$ )	
		[ <b>101</b> ]	[XPhos]	Uncorrected	Corrected	Uncorrected	Corrected
		1	1	0.025	0.024	$0.0124 \pm 0.0008$	$0.0079 \pm 0.0009$
2	5	0.023	0.12	$0.0489 \pm 0.0007$	$0.0313 \pm 0.002$	$9.43 \pm 0.14$	$6.0 \pm 0.4$
3	10	0.024	0.24	$0.0879 \pm 0.005$	$0.0630 \pm 0.006$	$19.5 \pm 1.1$	$14 \pm 1.0$

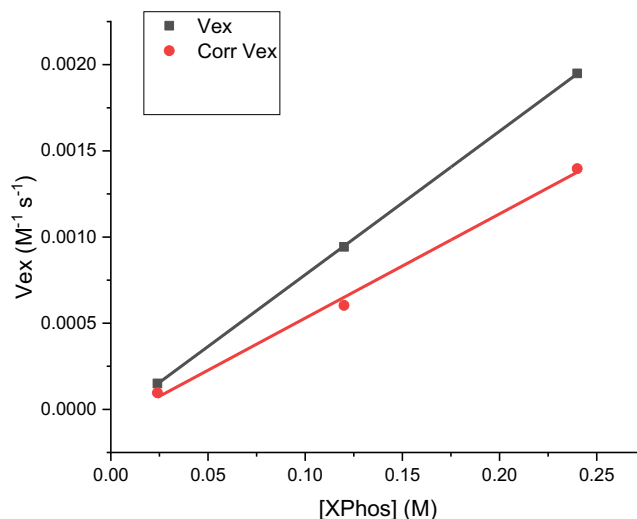


**Figure 82:** Plot of exchange velocity  $V_{\text{ex}}$  vs  $[\text{XPhos}]$ . The **black** plot shows the uncorrected data; **red** plot shows the corrected data.

To calculate the activation parameters of the phosphine exchange, variable temperature 1D-EXSY experiments with a mixture of **101** and excess XPhos (5 equiv.) were performed in  $\text{C}_6\text{D}_6$ . The solvent was changed from dichloromethane to benzene to access a suitable temperature range of 20 °C to 60 °C with 10 °C increments. The data was processed in the same manner as the concentration dependent EXSY experiments described above (analysis by Prof. Robin Perutz). The variation of the  $T_1$  of **101** and Xphos in different temperatures is summarized in **Table 23**. The correction factor varied from 1.0 to 1.3 except for the data at 60 °C which was less than 1. The  $k_{\text{obs}}$  were once again derived from the slope of the plot of integration fractions and mixing time over a range of temperatures (**Figure 83**). The Eyring equation was used to derive the activation parameters. Following the conversion to exchange velocities ( $V_{\text{ex}}$ ), a second Eyring plot was calculated to determine of activation parameters yielding  $\Delta H^\ddagger = 40.0 \pm 1.2 \text{ kJ/mol}$  and  $\Delta S^\ddagger = -162 \pm 4 \text{ J/K}\cdot\text{mol}$ , providing clear evidence for associative exchange (**Figure 84**).

$$\ln \frac{k}{T} = \frac{\Delta H^\ddagger}{R} \cdot \frac{1}{T} + \ln \frac{k_B}{h} + \frac{\Delta S^\ddagger}{R}$$

Where:  $k$  = rate constant,  $T$  = absolute temperature,  $\Delta H^\ddagger$  = enthalpy of activation,  $R$  = gas constant,  $k_B$  = Boltzmann constant,  $h$  = Planck's constant,  $\Delta S^\ddagger$  = entropy of activation

**Equation 3:** Eyring equation

**Table 23:** Summary of the  $T_1$  values measured at different temperatures for the mixture of **101** and Xphos (5 equiv.)

Reagent	$T_1$ (s)				
	20 °C	30 °C	40 °C	50 °C	60 °C
<b>101</b>	2.70	3.95	4.39	5.33	8.10
Xphos	4.45	5.18	5.80	6.48	7.43

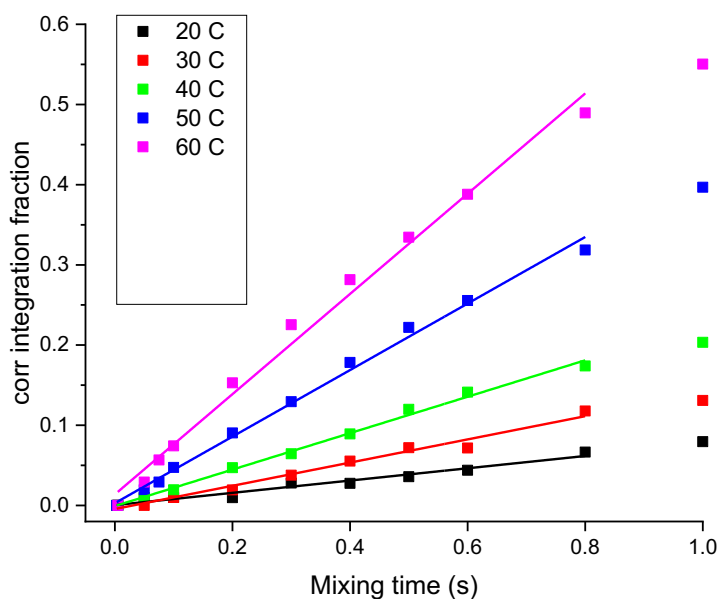


**Figure 83:** Plot of fractional transfer of magnetisation from **101** to free XPhos in  $C_6D_6$  against mixing time for different temperatures. The slopes correspond to  $k_{obs}$  for the exchange process. The data have been corrected for the differences in relaxation time at each temperature.

**Table 24:** Values of  $k_{obs}$  and  $V_{ex}$  for **101** in  $C_6D_6$  as a function of temperature. Data corrected for difference in relaxation times.

Temp (K)	Corrected Slope $k_{obs}$ ( $s^{-1}$ )	Corrected $V_{ex}$ ( $M^{-1} s^{-1}$ )
293	0.077	0.00144
303	0.145	0.00272
313	0.227	0.00426
323	0.415	0.00779
333	0.625	0.0117

Measured with  $[Ag(C_6F_5)XPhos] = 0.0226$  M,  $[XPhos] = 0.111$

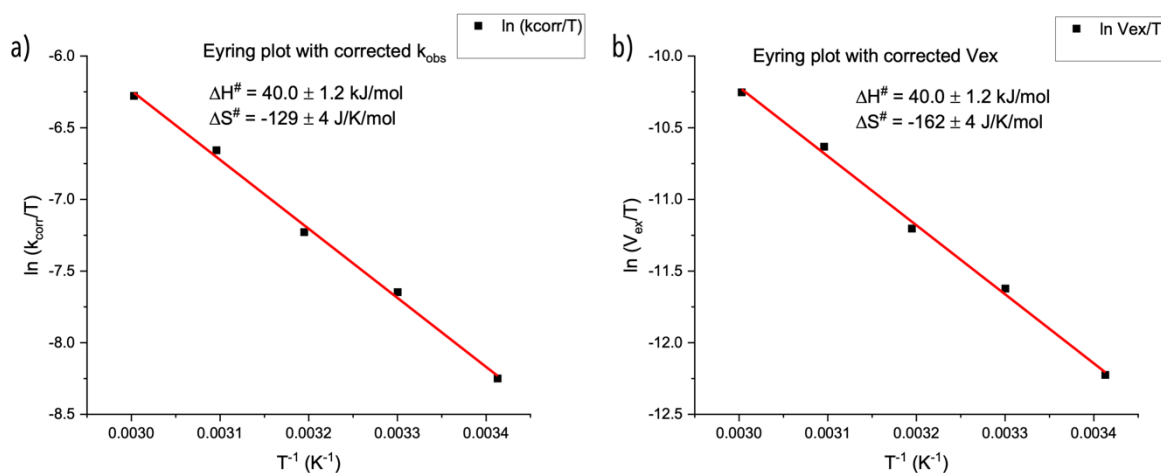


**Figure 84:** Eyring plots for the phosphine-exchange rate. **a)** plot using values of  $k_{\text{obs}}$ , **b)** using values of  $V_{\text{ex}}$ .

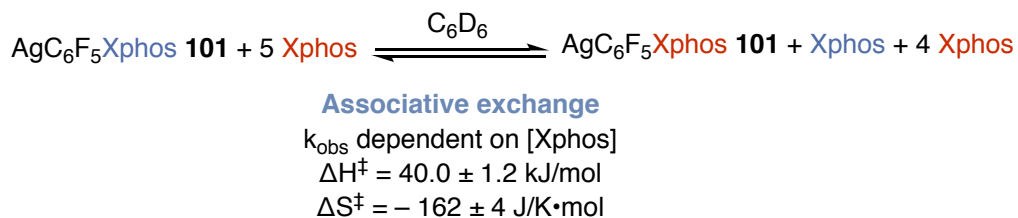
### 3.8 Proposed Catalytic Cycle

Based on the experimental evidence accumulated so far, the following observations can be made:

- ❖  $\text{Ag}_2\text{CO}_3$  is capable of coordinating with Xphos to form a more soluble  $[\text{Ag}(\text{XPhos})]_2(\mu-\kappa^2, \kappa^2-\text{CO}_3)$  **106** complex which is highly active at C–H activation of  $\text{C}_6\text{F}_5\text{H}$  **17**.
  - At room temperature, the reaction between **106** and **17** (2 equiv.) immediately generates **101** (85 %  $^{19}\text{F}\{^1\text{H}\}$  NMR yield)
  - The kinetic profile of the reaction, followed by  $^{19}\text{F}\{^1\text{H}\}$  NMR spectroscopy at  $-40^\circ\text{C}$ , revealed a fast initial reaction, followed by a slower process after 20 min
    - KIE of the fast process:  $3.7 \pm 0.3$
    - KIE of the slow process:  $0.97 \pm 0.01$
  - The primary KIE of the fast process suggests a significant C–H cleavage bond breakage event in the TS.
  - Following the reaction by  $^{31}\text{P}\{^1\text{H}\}$  NMR spectroscopy revealed a similar kinetic profile and no additional reaction intermediates were identified by  $^{31}\text{P}\{^1\text{H}\}$  or  $^{19}\text{F}\{^1\text{H}\}$  NMR spectroscopy at low temperatures.
- ❖ The product of C–H activation  $\text{Ag}(\text{C}_6\text{F}_5)(\text{Xphos})$  **101** was readily isolated from the reaction of  $\text{Ag}_2\text{CO}_3$  and Xphos (2 equiv.) with  $\text{C}_6\text{F}_5\text{H}$  **17**.

- Unlike the PPh<sub>3</sub> system, the Ag–Xphos was found to be stable at room-temperature and the complex was found to exist as a monomeric complex in solution.
- ❖ **101** was capable of undergoing transmetallation with PdI(C<sub>6</sub>H<sub>5</sub>)(Xphos) **102** and at room temperature. Subsequent reductive elimination also occurred rapidly, to generate the organic product **28** and AgI containing product **105**.
  - The presence of **105** was detected by <sup>31</sup>P{<sup>1</sup>H} NMR spectroscopy and its identity was confirmed with an authentic sample.
  - The mixture of **101** and **102** was prepared at –80 °C and analysed by low-temperature <sup>19</sup>F{<sup>1</sup>H} and <sup>31</sup>P{<sup>1</sup>H} NMR spectroscopy which revealed transmetallation and subsequent reductive elimination occurred at –30 °C, but the product of transmetallation Pd(C<sub>6</sub>F<sub>5</sub>)(C<sub>6</sub>H<sub>5</sub>)(Xphos) **104** was not detected.
- ❖ When the catalytic direct arylation reaction of 4-iodotoluene **26** and pentafluorobenzene **17** was carried out with Pd(OAc)<sub>2</sub> (5 mol%), Xphos (10 mol%, ligand) and Ag<sub>2</sub>CO<sub>3</sub> (0.75 equiv., base) in DMF, the reaction reaches 96% conversion within 3 h at 60 °C.
  - The reaction reached 77 % conversion within 23 h at room temperature.
  - KIE of the catalytic direct arylation reaction with Xphos as the ligand was calculated to be 4.5 ± 0.8 showing a primary kinetic isotope effect.
    - This is in line with the KIE measured by Platt *et al.* of 4.36 ± 0.06 for the direct arylation reaction using PPh<sub>3</sub> as the ligand.<sup>68</sup>
  - Replacing Ag<sub>2</sub>CO<sub>3</sub> with Cs<sub>2</sub>CO<sub>3</sub> (0.75 equiv.) or AgOAc (1.5 equiv.) resulted in < 10 % NMR yield.
  - The room temperature reactivity of the catalytic reaction is consistent with stoichiometric reactions of C–H activation of C<sub>6</sub>F<sub>5</sub>H **17** by **106** and transmetallation between **101** and **102**, both of which occurred at room-temperature.
- ❖ Experimenting further with the reaction conditions revealed that catalytic amounts of Ag<sub>2</sub>CO<sub>3</sub> (10 mol%) and K<sub>2</sub>CO<sub>3</sub> (0.75 equiv.) to yield 65 % conversion to organic product at 60 °C after 23 h.
- ❖ The ability to use catalytic amounts of Ag<sup>I</sup> demonstrates that [AgIXphos]<sub>2</sub> **105** is likely not a thermodynamic sink for Ag<sup>I</sup> and Xphos ligand and is capable of regenerating either **106** or **101**.

- Reacting [AgIXphos]<sub>2</sub> **105** with an excess C<sub>6</sub>F<sub>5</sub>H **17** or Ag<sub>2</sub>CO<sub>3</sub>/K<sub>2</sub>CO<sub>3</sub> in DMF did not produce the expected Ag containing product (**101** and **106** respectively).
  - However, the reaction of [AgIXphos]<sub>2</sub> **105** with Ag<sub>2</sub>CO<sub>3</sub> (20 equiv.) and C<sub>6</sub>F<sub>5</sub>H **17** (200 equiv.) in DMF at 3 h resulted in quantitative conversion to Ag(C<sub>6</sub>F<sub>5</sub>)(Xphos) **101** at both 60 °C and room temperature.
  - The reaction of AgC<sub>6</sub>F<sub>5</sub> **55** and [AgIXphos]<sub>2</sub> **105** in dichloromethane resulted in the immediate and quantitative conversion to Ag(C<sub>6</sub>F<sub>5</sub>)(Xphos) **101** and formation of AgI as a yellow solid.
  - This provides a plausible mechanism by which **101** could be regenerated within the catalytic cycle.
- ❖ The regeneration of **101** from either [AgIXphos]<sub>2</sub> **105** suggests that the Xphos within these complexes are capable of phosphine-exchange.
- Phosphine-exchange reactions with <sup>t</sup>BuXphos revealed that Ag intermediates **101**, **106** and **105** were capable of undergoing exchange.
  - Further insight into the phosphine-exchange process with Xphos specifically was gained using <sup>31</sup>P-<sup>31</sup>P 1D EXSY experiments to analyse mixtures of Ag complexes with an excess of free Xphos.
    - This revealed that **101**, **106** and **105** are all capable of undergoing intermolecular exchange with free Xphos (under both stoichiometric and excess conditions).
  - Variable-temperature 1D EXSY experiments performed on **101** with an excess of Xphos (5 equiv.) in C<sub>6</sub>D<sub>6</sub> helped determine the activation parameters of the exchange process which were ΔH<sup>‡</sup> = 40.0 ± 1.2 kJ/mol and ΔS<sup>‡</sup> = -162 ± 4 J/K·mol, providing clear evidence for associative exchange (**Scheme 87**).



**Scheme 87:** Phosphine-exchange analysed by 1D EXSY to reveal parameters consistent with associative exchange

Based on all the experimental evidence summarized, the following catalytic cycle involving Pd, and Ag is postulated (**Figure 85**). It is proposed that Ag is primarily responsible for C–H activation, while Pd effects cross-coupling. Ag<sub>2</sub>CO<sub>3</sub> coordinates with Xphos, to

generate **106** which reacts with  $C_6F_5H$  **17** to generate **101**. This species undergoes transmetalation with **102**, which is produced from the oxidative addition of the  $Pd^0$  active catalytic species and aryl halide, resulting in the generation of  $[AgIXphos]_2$  **105** and  $Pd(C_6F_5)(C_6H_5)(Xphos)$  **104**. Reductive elimination of  $Pd(C_6F_5)(C_6H_5)(Xphos)$  **104** produces the organic product and regenerates the  $Pd^0$  active catalytic species. The  $[AgIXphos]_2$  **105** complex reacts with  $C_6F_5H$  and  $Ag_2CO_3$  (or  $K_2CO_3$  when catalytic amounts of  $Ag_2CO_3$  is used) to regenerate the  $Ag(C_6F_5)(Xphos)$  **101** complex.

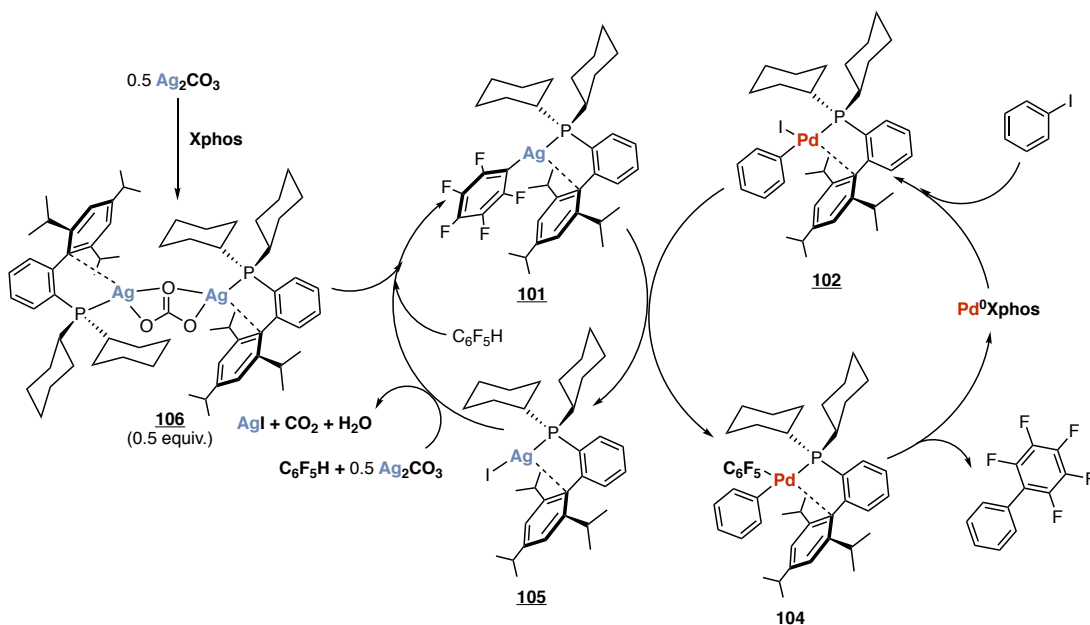


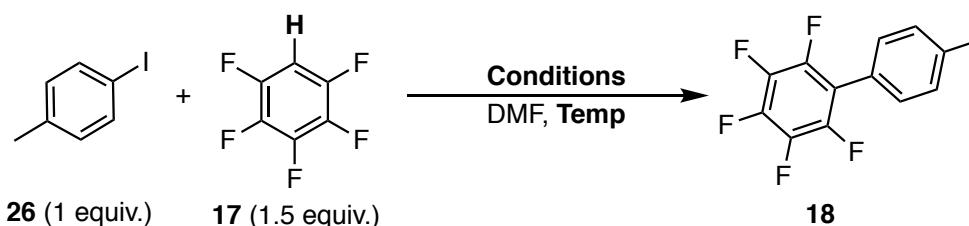
**Figure 85:** Proposed catalytic cycle, illustrating the role of Ag within C–H direct arylation reactions

Based on this proposal,  $PdI(C_6H_5)(XPhos)$  (**102**, 5 mol%) could be substituted as a catalyst for the coupling of 4-iodotoluene **26** with pentafluorobenzene **17** in the presence of 5 mol% XPhos and  $Ag_2CO_3$  (0.75 equiv.). When  $PdI(C_6F_5)(Xphos)$  **102** was used as the source of Pd instead of  $Pd(OAc)_2$ , the conversion after 3 h and 23 h was 83 % and quantitative respectively at 60 °C (**Table 25, Entry 1**). When repeated at room temperature, 63 %  $^{19}F\{^1H\}$  NMR yield was achieved after 23 h (**Table 25, Entry 2**). These results are comparable to those when  $Pd(OAc)_2$  is used as the pre-catalyst. Also consistent with the 5 mol% of **102** used, the expected  $C_6H_5-C_6F_5$  **28** product was also formed with a  $^{19}F\{^1H\}$  NMR yield of 5% with respect to  $C_7H_7-C_6F_5$  **18** product. The ability to use  $Ag(C_6F_5)(Xphos)$  **101** (5 mol%) as the sole source of  $Ag^I$ , also supports the proposed mechanism (**Table 17, Entry 12**). The direct arylation reaction can be carried out with both **102** and **101** as pre-catalysts and results in 63% conversion after 7 d at 60 °C. However, the reaction is quite sluggish under these conditions (**Table 25, Entry 3**).

All the steps in the catalytic cycle have been verified stoichiometrically other than the formation and reaction of a Pd<sup>0</sup> species which is not expected to be detectable under our conditions (oxidative addition being fast). Similarly the product of transmetalation Pd(C<sub>6</sub>H<sub>5</sub>)(C<sub>6</sub>F<sub>5</sub>)(Xphos) **104** complex could also not be detected under the reaction conditions. The cycle shows two alternative routes from Ag<sub>2</sub>CO<sub>3</sub> to form **101** reflecting the experiments described above. The experiments with reduced Ag<sub>2</sub>CO<sub>3</sub> with and without K<sub>2</sub>CO<sub>3</sub> confirm that carbonate is required for the C-H bond activation acting as the Brønsted base (**Table 17, Entry 5 and 6**). The postulated alternative mechanism invoking Ag<sup>I</sup> as a base and Pd as being involved in a CMD process is expected to involve Ag-carbonato-Pd **112** as an intermediate (**Scheme 88**).

Finally, while the experiments provide clear evidence for C-H bond activation by Ag, it does not exclude competing C-H bond activation steps at Pd or a role for higher order catalyst species.<sup>134-138</sup>

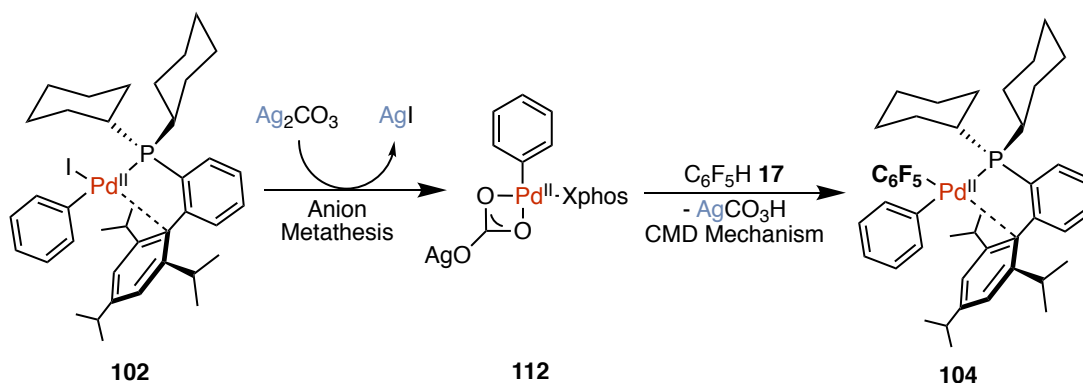
**Table 25:** Catalytic direct arylations where reaction intermediates are used as pre-catalysts



Entry	Conditions	Temp.	NMR Yield (%)			
			3 h	23 h	48 h	7 d
1	PdI(C <sub>6</sub> H <sub>5</sub> )(Xphos) <b>102</b> (5 mol%) + Xphos (5 mol%) + Ag <sub>2</sub> CO <sub>3</sub> (0.75 equiv.)	60	86	Quant.	-	-
2	PdI(C <sub>6</sub> H <sub>5</sub> )(Xphos) <b>102</b> (5 mol%) + Xphos (5 mol%) + Ag <sub>2</sub> CO <sub>3</sub> (0.75 equiv.)	20	6	63	-	-
3	PdI(C <sub>6</sub> H <sub>5</sub> )(Xphos) <b>102</b> (5 mol%) + Ag(C <sub>6</sub> F <sub>5</sub> )(Xphos) <b>101</b> (5 mol%) + Xphos (5 mol%) + K <sub>2</sub> CO <sub>3</sub> (0.75 equiv.)	60	1	23	49	63
4	PdI(C <sub>6</sub> H <sub>5</sub> )(Xphos) <b>102</b> (5 mol%) + Ag(C <sub>6</sub> F <sub>5</sub> )(Xphos) <b>101</b> (5 mol%) + Xphos (5 mol%) + K <sub>2</sub> CO <sub>3</sub> (0.75 equiv.)	20	2	5	11	29

<sup>[a]</sup> details on the calculation of NMR yields in Experimental





**Scheme 88:** Silver carbonate acting as base in CMD mechanism.

### 3.9 Summary and Conclusions

The use of Xphos as the ligand provided an excellent model system to study the role of  $\text{Ag}^{\text{I}}$  in the C–H direct arylation reaction. This is largely attributed to the stability of the Ag–P bond due to the use of an electron-rich, sterically hindered ligand. The Ag–Xphos bond was stable at room-temperature, allowing for ease of identification and characterization of reaction intermediates.

The silver carbonate is capable of C–H bond activation of pentafluorobenzene in the presence of XPhos yielding discrete and well-defined  $\text{Ag}(\text{C}_6\text{F}_5)(\text{Xphos})$  **101**. This reaction can also be carried out stepwise yielding first the carbonate complex  $[\text{Ag}(\text{XPhos})]_2(\mu\text{-}\kappa^2, \kappa^2\text{-CO}_3)$  **106** and then upon reaction of **106** with  $\text{C}_6\text{F}_5\text{H}$ , generates **101**. The **101** complex was found to be competent at cross-coupling: upon reacting with  $\text{PdI}(\text{C}_6\text{H}_5)(\text{XPhos})$  **102**, transmetalation and subsequent reductive elimination occurred rapidly generating the organic product instantly at room-temperature. An additional by-product of transmetalation is the generation of  $[\text{Ag}(\text{XPhos})(\mu\text{-I})]_2$  **105**. The identity of this complex was confirmed by preparing an authentic sample from the reaction between  $\text{AgI}$  with XPhos in dichloromethane. All three silver complexes have been characterized in solution and crystallographically. They are all labile with respect to associative exchange with free XPhos or with  $^t\text{BuXPhos}$  and all participate in cross-coupling.

Catalytic cross-coupling of 4-iodotoluene to pentafluorobenzene may be achieved in the presence of palladium(II) acetate, XPhos and silver carbonate at 60 °C or at room temperature. Catalytic cross-coupling also occurs with **102** as catalyst in the presence of  $\text{Ag}_2\text{CO}_3$  and a reduced quantity of XPhos. A catalytic cycle involving C–H bond activation at silver has been proposed consistent with the set of tested stoichiometric reactions. It is now clear how the phosphine solubilizes silver carbonate and silver iodide, however, the phosphine is labile

enough to allow precipitation of silver iodide as the final by-product of catalysis. It is stressed that the study does not exclude competing C–H bond activation steps at palladium or a role for higher order catalyst species. Nevertheless, the evidence for the C–H bond activation abilities of silver carbonate in the presence of a suitable phosphine is now conclusive and is shown to involve well-defined mononuclear and dinuclear silver phosphine complexes.

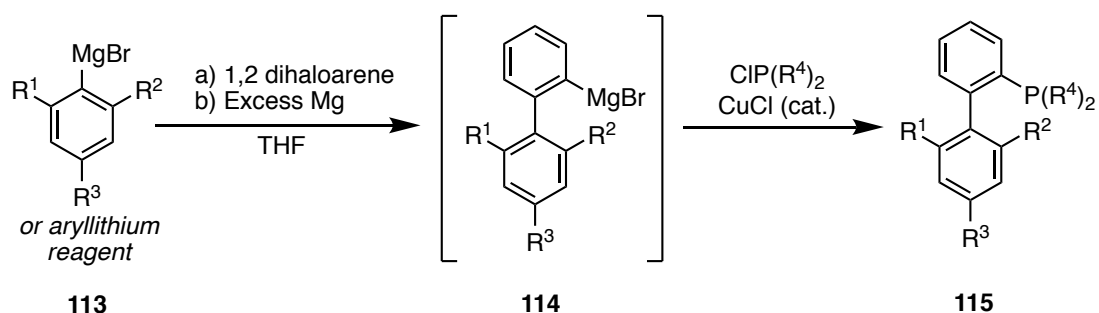
## Chapter 4: Optimisation of Catalytic Direct Arylation Reaction

### Reaction

#### 4.1 Introduction

The experimental evidence from Chapter 3 was sufficient to propose a mechanism outlining the role of  $\text{Ag}^{\text{I}}$  in the C–H bond direct arylation reaction. Thus, the focus of this chapter is on trying to compare the standard catalytic reaction with Xphos as the ligand to analogues with other phosphines and develop an optimised synthetic method which takes advantage of the mechanistic insights obtained in the previous chapter. As a starting point, a survey of dialkylbiarylphosphine ligands was conducted to identify the optimal ligand for C–H activation of fluorinated aromatics.

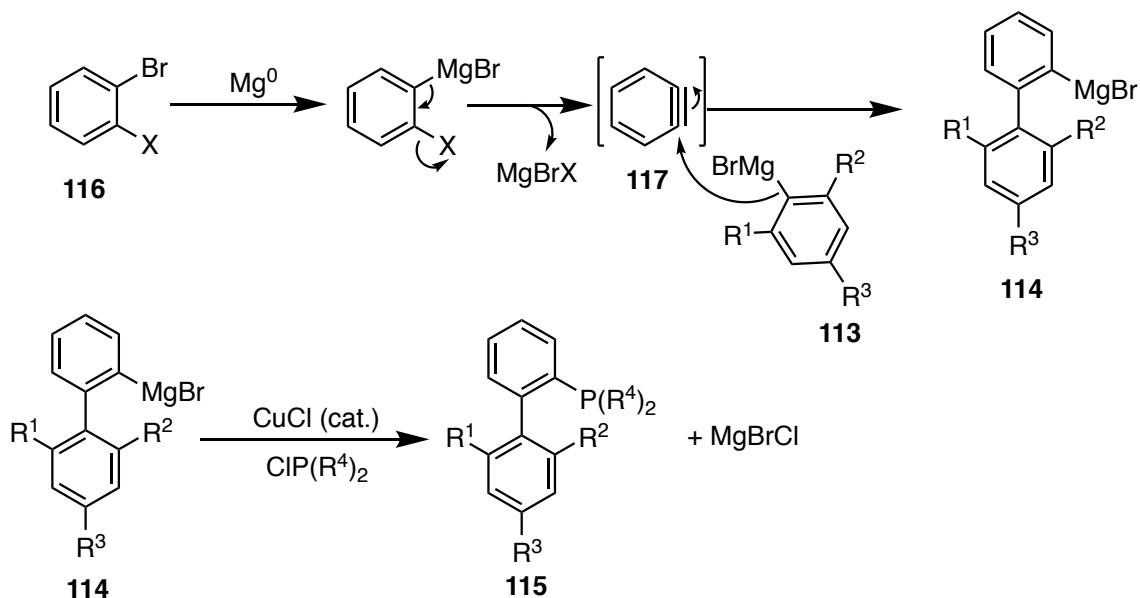
Dialkylbiarylphosphines form a highly versatile class of bulky, electron-rich ligands utilised in a diverse variety of transition-metal catalysed reactions. They were first introduced in 1998 by Buchwald and co-workers and grew into prominence in Pd catalysed C–C,<sup>139</sup> C–N<sup>140,141</sup> and C–O bond-forming transformations. The versatility of these ligands is largely attributed to their highly tunability, ease of synthesis and good air- and thermal stability. Dialkylbiarylphosphines ligands can readily be accessed using a one-pot protocol wherein an aryl Grignard or aryllithium reagent is treated with 1,2-dihaloarene and excess magnesium metal followed by a copper(I) chloride catalysed reaction with dialkyl chlorophosphine (**Scheme 89**).<sup>139–141</sup>



**Scheme 89:** General synthetic methodology for the production of dialkylbiarylphosphines<sup>140,141</sup>

The reaction of the 1,2-dihaloarene **116** with magnesium metal generates a benzyne **117** *in situ*, which reacts with the aryl Grignard **113** (or aryllithium) reagent to generate a biaryl Grignard reagent **114**. This subsequently reacts with dialkylchlorophosphine  $\text{CIP}(\text{R}^4)_2$  under a catalytic amounts of copper(I) chloride, to generate the desired dialkylbiarylphosphine ligand **115**.<sup>140</sup> The  $\text{CuCl}$  was used to catalyse the coupling of aryl Grignard reagents with the hindered

chlorophosphines and improve the yield of the reaction.<sup>142</sup> A plausible generalised mechanism is provided in **Scheme 90**; however, the details of the reaction vary based on the type of substituents and conditions of the reaction. The versatility and availability of Grignard and organolithium reagents has allowed for diverse functionalization of the dialkylbiarylphosphines. The crystalline ligands are easy to handle, robust against oxidation<sup>143</sup> and commercially available.<sup>140,141</sup>



**Scheme 90:** plausible general mechanism for the synthesis of dialkylbiarylphosphines

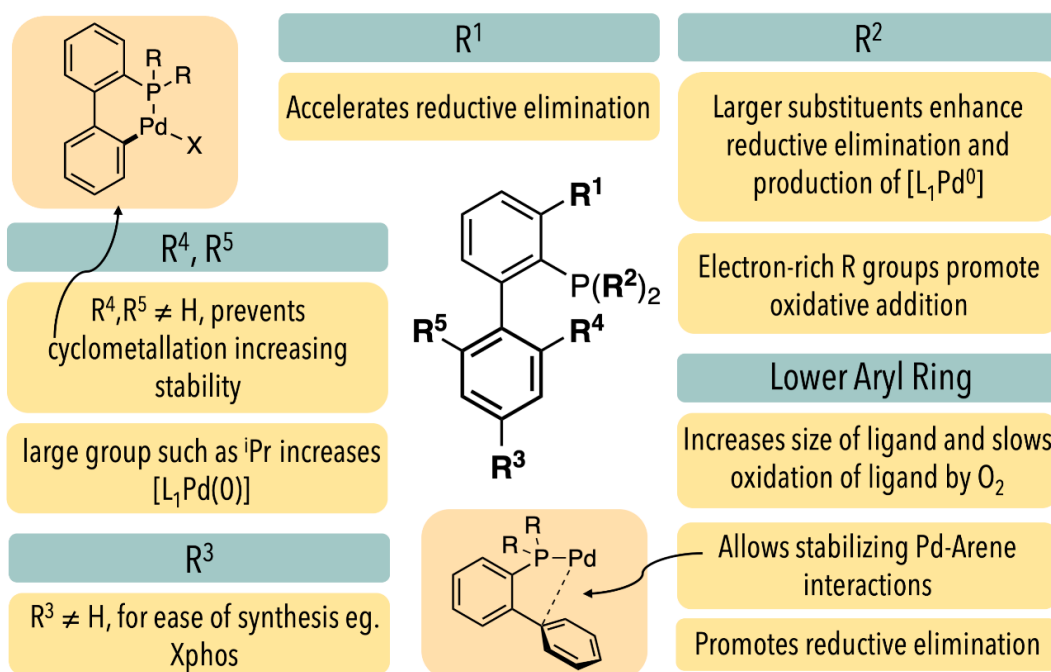
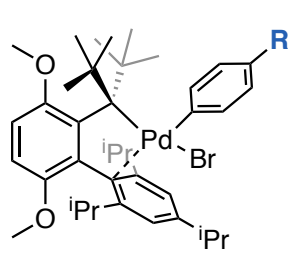


**Figure 86:** Structural features of dialkylbiarylphosphines and their effect on catalysis<sup>139,140,141</sup>

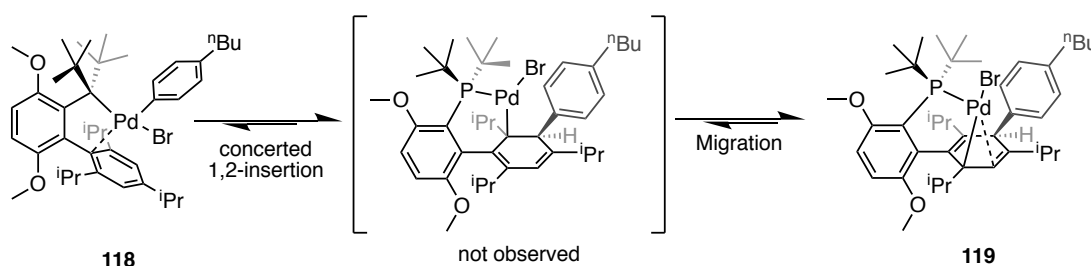
The structural and electronic features of dialkylbiarylphosphines have a documented effect on catalysis, based on their impact on the metal centre (**Figure 86**). For instance, steric bulk and electron-rich nature of these ligands is believed to aid in formation of the highly reaction  $[L_1Pd^0]$  active catalytic species. The distal ring of the biaryl provides a weak Pd-arene interaction, stabilising the metal centre by providing additional electron density. This interaction has been observed in x-ray crystal structure of Pd- dialkylbiarylphosphines complexes, where the *ipso* carbon of the distal ring often lies in close-contact with the metal centre.<sup>140</sup> In  $LPd^{II}(Ar)X$  type complexes, where L = dialkylbiarylphosphine ligand, generally the Pd-C<sub>ipso</sub> interactions are of the order or 2.5 Å – 2.4 Å. Electron-rich *para*-substituents on aryl ligand tend to increase the Pd-C<sub>ipso</sub> distance, due to a stronger trans influence (**Figure 87**).<sup>127</sup> Additionally, as expected, the increased electron density provided by large R-group substituents on the distal ring have been observed to promote  $[L_1Pd^0]$  production and reductive elimination.<sup>140,127,144</sup>



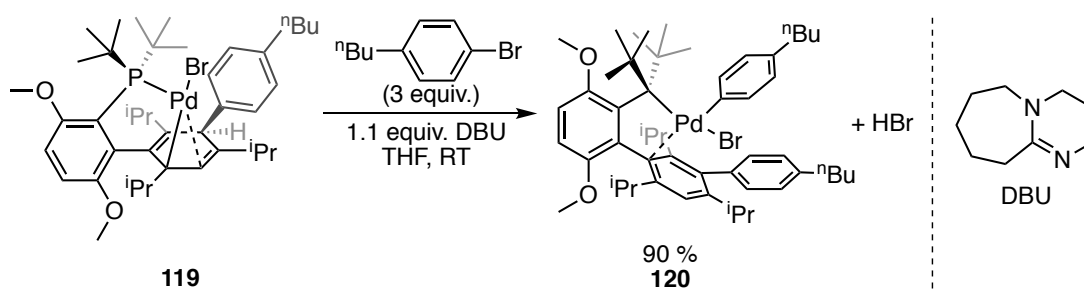
R group	Pd-C <sub>ipso</sub> (Å)
- <sup>n</sup> Bu	2.50(4)
-H	2.50(0)
-F	2.47(0)
-CN	2.45(2)

**Figure 87:** The effect of *para*-substituents of the aryl ring on the Pd-C<sub>ipso</sub> bond length derived from x-ray crystallographic analysis.<sup>127</sup>

When studying mono-ligated  $LPd^{II}(Ar)X$  complexes, Buchwald and co-workers observed the Pd<sup>t</sup>BuBrettPhos complex **118** undergo an unusual dearomative rearrangement reactions at room temperature to produce **119** (**Scheme 91**). When the mixture of **118/119** was treated with excess aryl bromide and DBU, reductive elimination and subsequent oxidative addition occurred, likely *via*  $LPd^0$  to generate **120** (**Scheme 92**).<sup>127</sup>

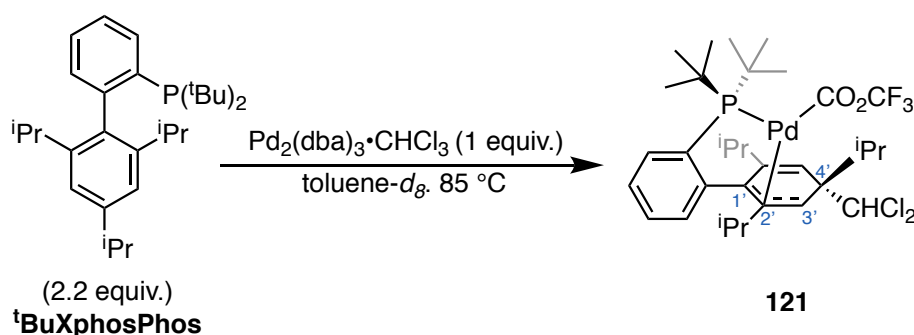


**Scheme 91:** Dearomative rearrangement of the Pd-<sup>t</sup>BuBrettPhos complex **118** to **119**<sup>127</sup>



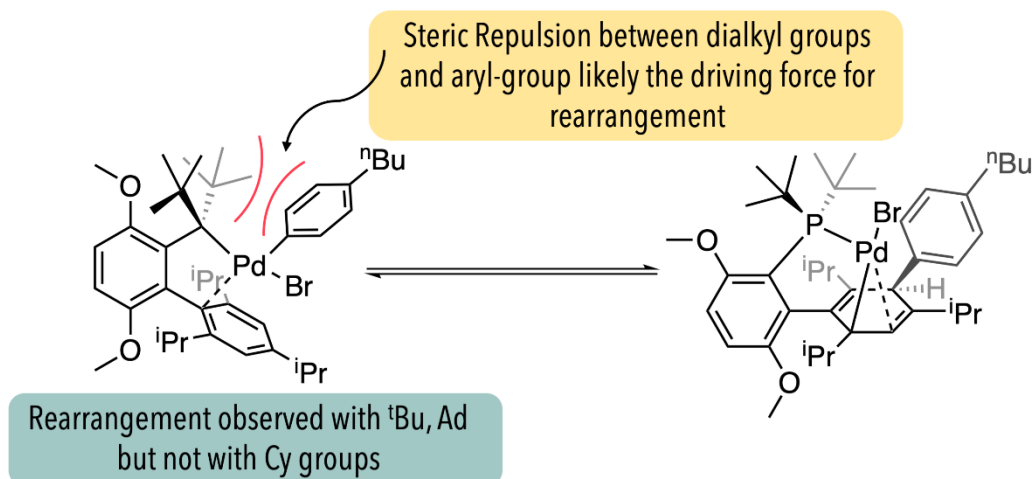
**Scheme 92:** Reductive elimination of **119** with base and subsequent oxidative addition with excess aryl bromide to produce **120**<sup>127</sup>

Allgeier and co-workers isolated a similar complex **121**, when studying the degradation product of the reaction between <sup>t</sup>BuXphos and Pd<sub>2</sub>(dba)<sub>3</sub>•CHCl<sub>3</sub> (**Scheme 93**). They proposed a carbene insertion mechanism originating from dichloromethane, resulting in the dearomatization of the 4'-position of the distal biaryl ring.<sup>145</sup>



**Scheme 93:** Synthesis of **121** from the reaction of <sup>t</sup>BuXphos and Pd<sub>2</sub>(dba)<sub>3</sub>•CHCl<sub>3</sub> by Allgeier and co-workers<sup>145</sup>

Buchwald and co-workers further investigated the unusual aromatic rearrangement reaction of **118** (**Figure 94**). The effect of various parameters such as solvent, aryl substituent, halide etc. on the rearrangement reaction was investigated. They found that the ligand structure significantly impacted the rate and extent of dearomatization rearrangements, specifically the dialkyl groups on the phosphorus and substituents on the biaryl backbone. Dialkylbiaryl phosphines ligands with bulkier groups such as tert-butyl or adamantyl dialkyl groups on the phosphorus promoted dearomative rearrangement, whereas no rearrangement was observed when cyclohexyl groups were incorporated. The unfavourable steric repulsion between larger dialkyl groups (<sup>t</sup>Bu, Ad) and the aryl-group likely acts as the driving force for dearomatization rearrangement to relieve the steric strain (**Scheme 94**).<sup>127</sup>



**Scheme 94:** Effect of dialkyl groups on the dearomative rearrangement<sup>127</sup>

The effect of the substituents on the biaryl backbone was dependent on the position of the substituent. The substituent on the 3-position ( $R^1$ ) increased the rate of dearomative rearrangement. This is likely a steric effect where the repulsion caused by the  $R^1$ -group ‘pushes’ the <sup>t</sup>Bu groups towards the Pd centre increasing the steric encumbrance and favouring rearrangement. In contrast, the substituent on the 6-position ( $R^2$ ) inhibited the rate of dearomative rearrangement, due to the interaction between the  $R^2$ -group and the *ortho*-isopropyl groups which ‘tilts’ the distal ring in the complex in a manner which destabilises the dearomatized complex (**Figure 88**).<sup>127</sup>

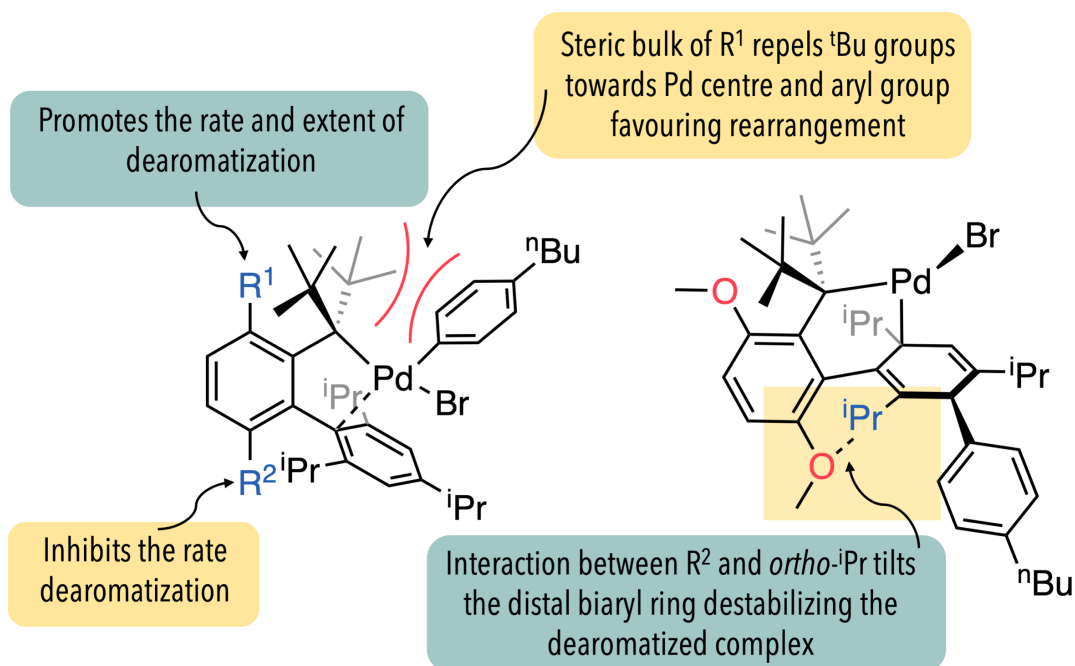


**Figure 88:** Effect of substituents on the biaryl backbone on dearomative rearrangement<sup>127</sup>

Most of these observations were primarily carried out on Pd<sup>II</sup> complexes with a <sup>t</sup>BuBrettphos (or its analogues) but was also applicable to Pd<sup>II</sup> complexes with <sup>t</sup>BuXphos and RockPhos and can be generalised (**Figure 89**).

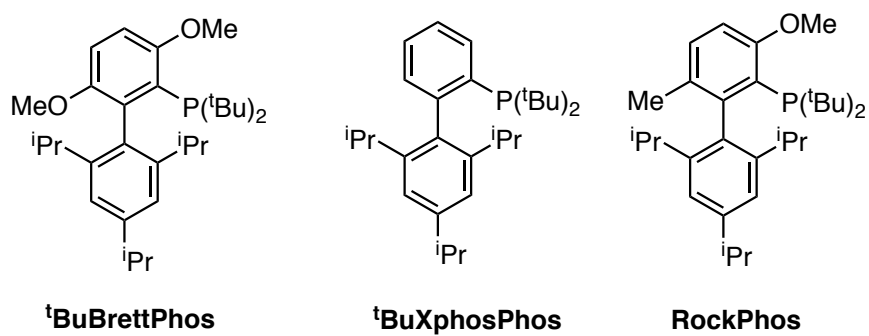


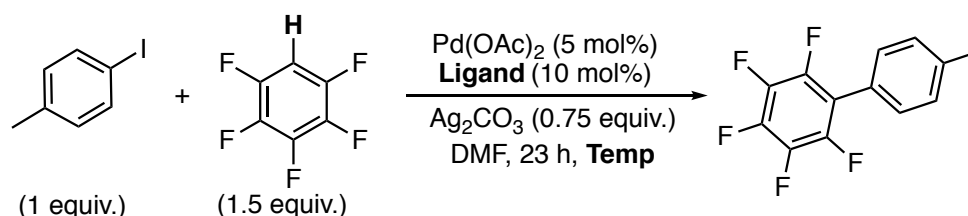
**Figure 89:** Structure of <sup>t</sup>BuBrettphos, <sup>t</sup>BuXphos and RockPhos



## 4.2 Scope of Dialkylbiaryl Phosphine Ligands

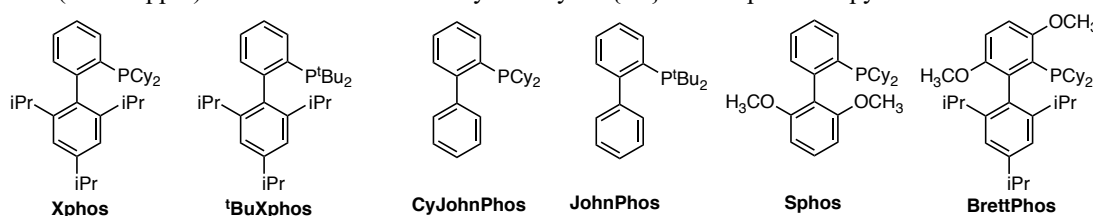
To conduct a survey of dialkylbiaryl phosphines ligands, the direct arylation reaction between 4-iodotoluene **26** and pentafluorobenzene **17** were carried out with Pd(OAc)<sub>2</sub> (5 mol%) and Ag<sub>2</sub>CO<sub>3</sub> (0.75 equiv.) with different Buchwald type ligands (10 mol%) in DMF. As silver carbonate is used as the base, octafluoronaphthalene was found to be an appropriate internal standard. The reactions were carried out at both room temperature (20 °C) and at 60 °C, and the reaction with PPh<sub>3</sub> as the ligand was used as the point of comparison (**Table 26**). The reaction was monitored using reaction aliquots collected at 3 h and 23 h. Platt *et al.* has investigated the effect of trialkyl phosphine ligand on the % conversion and reaction rate of the direct arylation reaction of interest.<sup>68</sup>

**Table 26:** Effect of different dialkylbiaryl phosphines ligands on the C–H direct arylation reaction between 4-iodotoluene **26** and pentafluorobenzene **17**.



Entry	Ligand	% Yield by <sup>19</sup> F{ <sup>1</sup> H} NMR spectroscopy <sup>[a]</sup>			
		60 °C Reaction		Room temperature reaction (20 °C)	
		3 h	23 h	3 h	23 h
1	PPh <sub>3</sub>	83	100	10	43
2	Xphos	96	96	-	75
3	<sup>t</sup> BuXphos	3	6	0	0
4	CyJohnPhos	67	100	13	16
5	JohnPhos	64	100	5	34
6	Sphos	66	70	15	73
7	BrettPhos	5	5	0	3

[a] The % <sup>19</sup>F{<sup>1</sup>H} NMR yield was calculated using octafluoronaphthalene as the internal standard. The Internal standard resonance at –145.0 ppm was used and compared to the ortho-*F* peak of the product (–143.8 ppm) to calculate the % NMR yields by <sup>19</sup>F{<sup>1</sup>H} NMR spectroscopy.

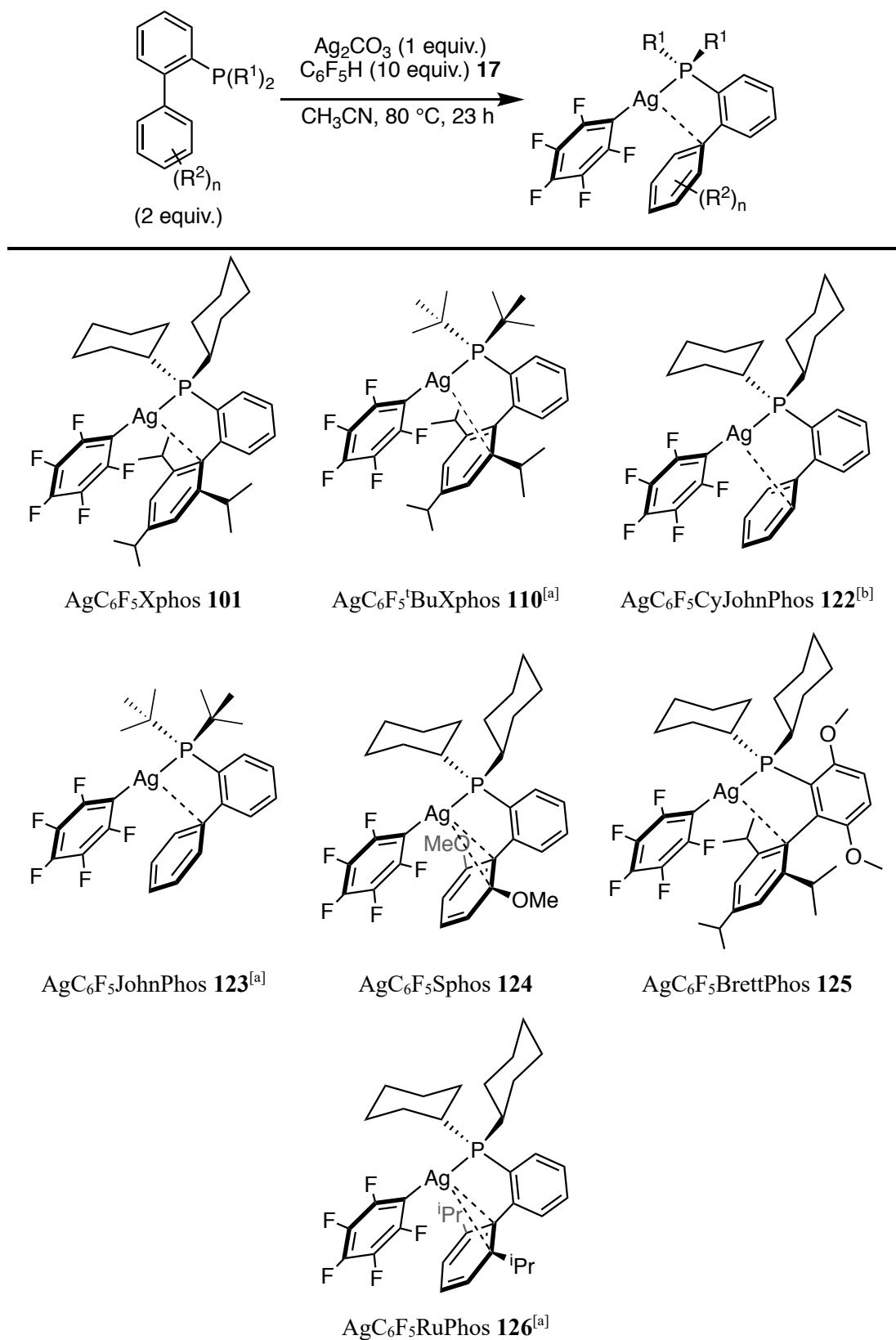


The reaction with PPh<sub>3</sub> reached 83 % <sup>19</sup>F{<sup>1</sup>H} NMR yield at 3 h and quantitative conversion by 23 h. The reaction at room temperature was much more sluggish reaching 43% conversion

after 23 h (**Entry 1**). In contrast, the reaction with Xphos as the ligand reached 96%  $^{19}\text{F}\{^1\text{H}\}$  NMR yield when heated for 3 h at 60 °C and 75 %  $^{19}\text{F}\{^1\text{H}\}$  NMR yield at room temperature after 23 h (**Entry 2**). Interestingly, the  $^t\text{BuXphos}$  ligand, which is similar in structure to Xphos but with  $^t\text{Bu}$  groups instead of Cy, performed poorly only achieving 6 %  $^{19}\text{F}\{^1\text{H}\}$  NMR yield after heating at 60 °C for 23 h (**Entry 3**). This might be the result of the steric of the ligand or due to the concerted dearomative rearrangement of the Pd oxidative addition product<sup>127</sup>, at least in the case of  $^t\text{BuXphos}$ . Both CyJohnphos and Johnphos show excellent and similar reactivity, reaching full conversion by 23 h at 60 °C, but produced lower  $^{19}\text{F}\{^1\text{H}\}$  NMR yields at room temperature. When Sphos is used as the ligand, a  $^{19}\text{F}\{^1\text{H}\}$  NMR yield of 70 % is achieved at both 60 °C and at room temperature. Finally, BrettPhos, like  $^t\text{BuXphos}$ , achieved low conversions with 5 %  $^{19}\text{F}\{^1\text{H}\}$  NMR yield after heating at 60 °C for 23 h. From the data collected, the reaction with Xphos has the greatest rate, achieving a  $^{19}\text{F}\{^1\text{H}\}$  NMR yield of 96% by 3 h at 60 °C, followed by  $\text{PPh}_3$ . Additionally, Xphos allowed for the highest conversion of 77 % after 23 h at room temperature. Thus, Xphos was selected as the optimal ligand to carry out future reactions. In Chapter 3, when the amount of Xphos was reduced from 10 mol% to 5 mol% the  $^{19}\text{F}\{^1\text{H}\}$  NMR yield dropped to 19 %, indicating that 10 mol% is the optimal amount required for successful catalysis.

### 4.3 $\text{AgC}_6\text{F}_5$ Complexes of Various Dialkylbiaryl phosphines

The effect of dialkylbiarylphosphine ligands on the Pd has already been characterised however its effect on the Ag centre remains to be explored. For this purpose, the reaction of  $\text{Ag}_2\text{CO}_3$  and  $\text{C}_6\text{F}_5\text{H}$  (10 equiv.) was carried out with various dialkylbiarylphosphines ligands, and the  $\text{Ag}(\text{C}_6\text{F}_5)(\text{PR}_2\text{R}')$  intermediates were isolated and their crystal structures determined using XRD analysis. This work was carried out in conjunction with an MChem project student Alex Heald and where appropriate Heald's contribution has been highlighted.<sup>146</sup> An inventory of the isolated silver complexes is provided in **Table 27**.

**Table 27:** Synthesis and isolation of various  $\text{Ag}(\text{C}_6\text{F}_5)(\text{PR}_2\text{R}')$  (where  $\text{PR}_2\text{R}' =$  dialkylbiarylphosphines ligands)

<sup>[a]</sup> Complex and Crystal structures isolated by Heald *et al.*<sup>146</sup> <sup>[b]</sup> complex synthesised by Heald *et al.*<sup>146</sup>, crystals isolated by GA.

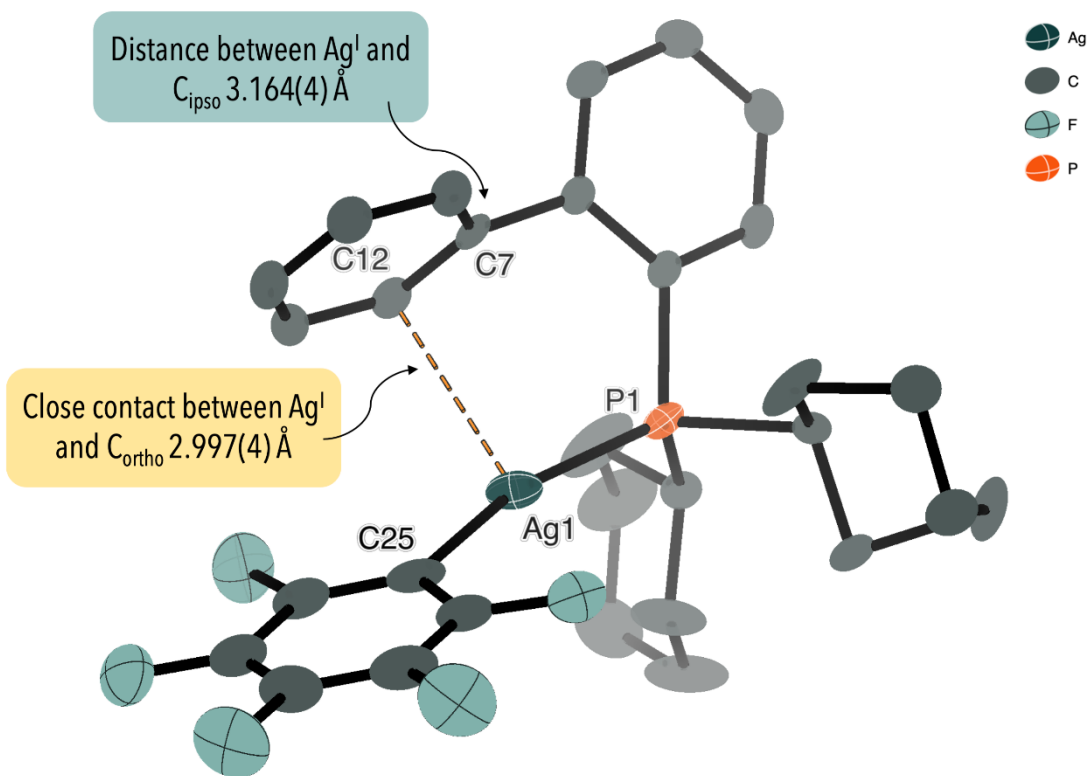


Figure 90: Crystal structure of  $\text{AgC}_6\text{F}_5\text{CyJohnphos}$  122

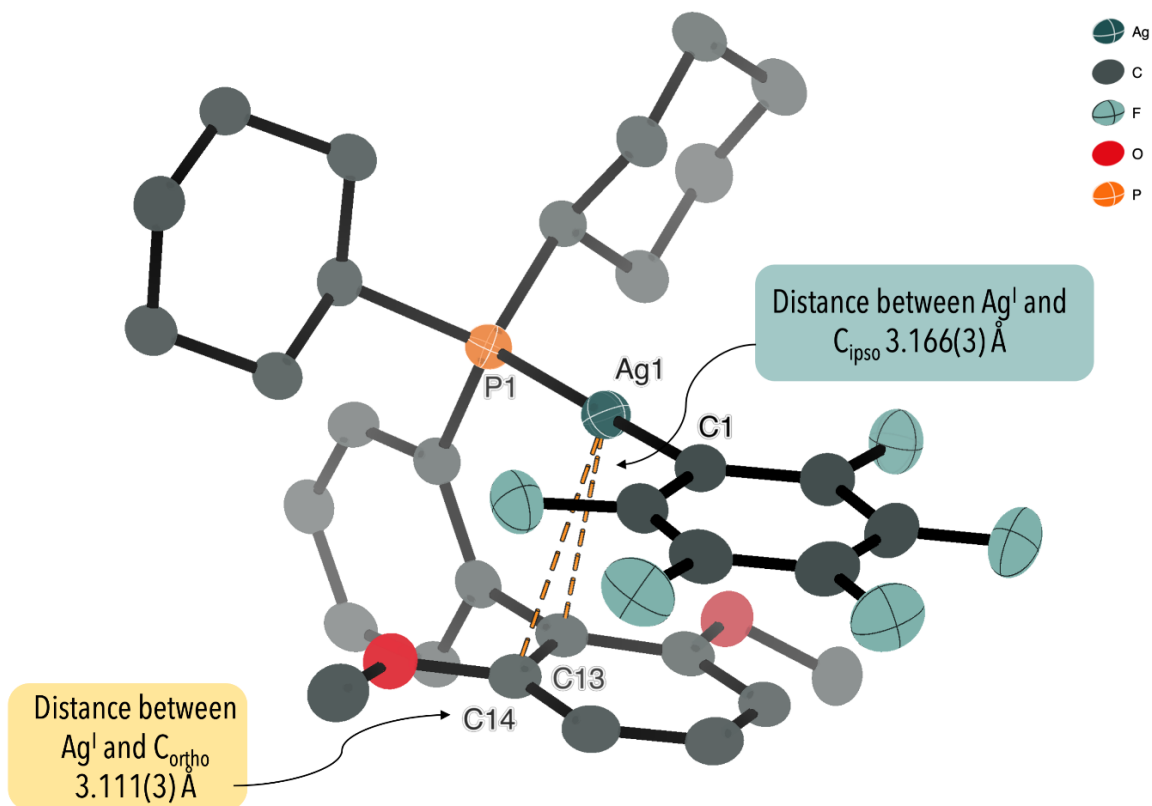
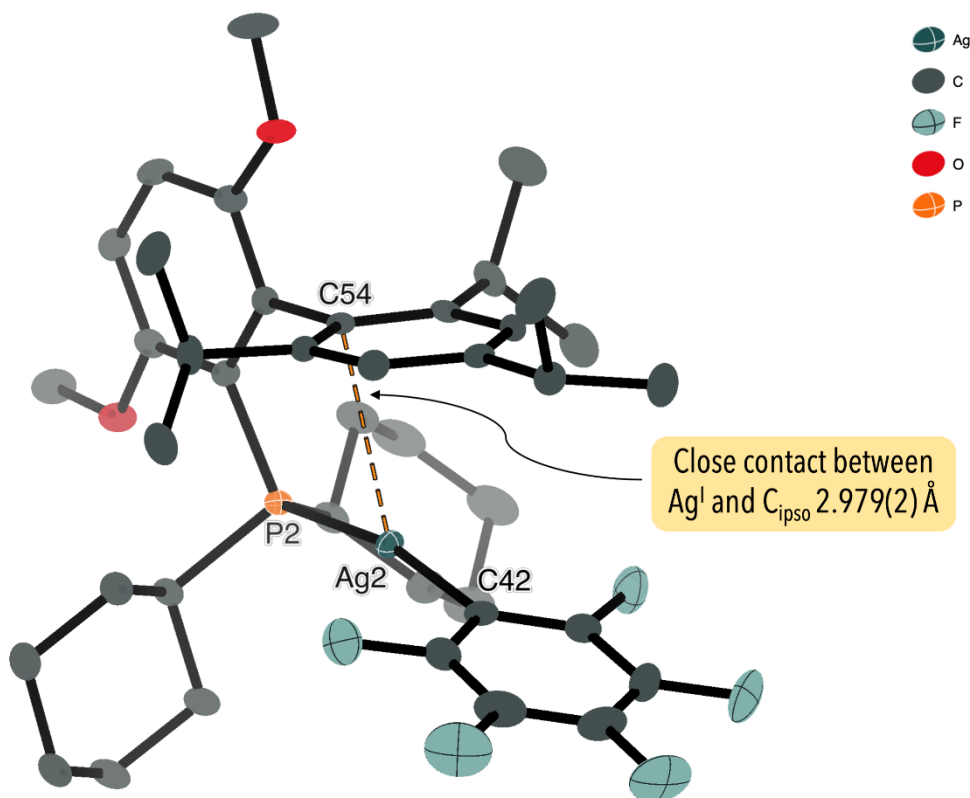


Figure 91: Crystal structure of  $\text{AgC}_6\text{F}_5\text{Sphos}$  124



**Figure 92:** Crystal structure of  $\text{AgC}_6\text{F}_5\text{Brettphos}$  **125**

The crystal structures of  $\text{Ag}(\text{C}_6\text{F}_5)(\text{PR}_2\text{R}')$  complexes share many characteristic features; the principal bond lengths and angles of the different structures are summarised in **Table 28**. The coordination of  $\text{Ag}^{\text{I}}$  to phosphine ligand and  $-\text{C}_6\text{F}_5$  unit is close to linear with the  $\text{C}-\text{Ag}-\text{P}$  angle falling within the range of  $162.8 - 175.3^\circ$ . The  $\text{Ag}-\text{P}$  and  $\text{Ag}-\text{C}_6\text{F}_5$  bond distances are also similar across the different structures. Much like **101**, the distal ring of the dialkylbiarylphosphine ligands in all the  $\text{Ag}(\text{C}_6\text{F}_5)(\text{PR}_2\text{R}')$  structures is oriented towards and is in close contact with the metal centre. With monoligated  $\text{Pd}^{\text{II}}(\text{Ar})(\text{X})(\text{PR}_2\text{R}')$  complexes, the  $\text{Pd}-\text{C}_{\text{ipso}}$  distance varies between  $2.45 - 2.50 \text{ \AA}$  depending on the substituents<sup>127</sup>. In contrast, the interactions between the  $\text{Ag}^{\text{I}}$  centre and  $\text{C}_{\text{ipso}}$  vary within the range of  $2.979(2)$  (**125**) to  $3.166(3)$  (**124**), suggesting a weaker interaction.

In **101**, the close contact interaction lies between the  $\text{Ag}^{\text{I}}$  metal centre and the *ipso* carbon of distal ring and the same is true for the Ag complexes of Johnphos (**123**) and BrettPhos (**125**, **Figure 92**). However, in certain cases, it was noted that the metal centre was in close contact with the *ortho*-C instead of the *ipso*-C of the distal ring. This is most notable in the crystal structures of <sup>t</sup>BuXphos (**110**) and CyJohnPhos (**122**, **Figure 90**) where the distance between one of the *ortho*-carbons and the Ag centre is  $3.052(2)$  for **110** and  $2.997(4)$  for **122**

respectively. In the case of the Ag structures of Sphos **124** and RuPhos **126**, close contact of both the *ipso*- and *ortho*-C with the metal centre is observed.

To examine the significance of the Ag–C<sub>ipso</sub> and Ag–C<sub>ortho</sub> bond distances, the difference between the two bonds were compared to 3σ and 5σ (where σ = standard deviation which is the e.s.d of the crystal structure bond distance). Bond differences greater than 3σ indicate a confidence interval of 99.73% and 5σ is 99.99994%. When compared to 3σ, all the Ag–C<sub>ipso</sub> and Ag–C<sub>ortho</sub> bond were found to be significant. When the threshold for significance is increased to 5σ, all the Ag–C<sub>ipso</sub> and Ag–C<sub>ortho</sub> bond differences, except for **126**, were found to be significant. Similarly, the various bond distance between Ag and the carbon atoms of the distal ring of the biaryl were all found to be significant up to 5σ (Table 30).

**Table 28:** Principal bond length and angles of all the AgC<sub>6</sub>F<sub>5</sub>PR<sub>3</sub>

Complex <sup>[a],[b]</sup>	Bond length (Å)				Bond Angle
	Ag–P	Ag–C <sub>6</sub> F <sub>5</sub>	Ag–C <sub>ipso</sub>	Ag–C <sub>α</sub>	(°)
AgC <sub>6</sub> F <sub>5</sub> Xphos <b>101</b>	2.3801(5)	2.124(2)	3.062(2)	3.152(2)	168.85(6)
AgC <sub>6</sub> F <sub>5</sub> <sup>t</sup> BuXphos <b>110</b>	2.3746(5)	2.106(1)	3.157(1)	3.052(2)	162.88(4)
AgC <sub>6</sub> F <sub>5</sub> CyJohnphos <b>122</b>	2.375(1)	2.114(4)	3.164(4)	2.997(4)	165.2(1)
AgC <sub>6</sub> F <sub>5</sub> Johnphos <b>123</b>	2.3968(7)	2.121(3)	3.055(2)	3.119(2)	164.10(8)
AgC <sub>6</sub> F <sub>5</sub> Sphos <b>124</b>	2.3742(8)	2.120(3)	3.166(3)	3.111(3)	175.37(8)
AgC <sub>6</sub> F <sub>5</sub> BrettPhos <b>125</b>	2.3727(6)	2.121(2)	2.979(2)	3.100(2)	167.94(6)
AgC <sub>6</sub> F <sub>5</sub> RuPhos <b>126</b>	2.3777(7)	2.120(2)	3.014(2)	3.028(2)	171.97(6)

<sup>[a]</sup> Complex and Crystal structures isolated by Heald *et al.*<sup>146</sup> highlighted in green in the table. <sup>[b]</sup> Complex isolated by Heald *et al* and crystal structure isolated by GA.

**Table 29:** Difference in bond distance between Ag–C<sub>ipso</sub> and Ag–C<sub>α</sub> compared to 3 σ and 5 σ

Complex	Ag–C <sub>ipso</sub> (Å)		Ag–C <sub>α</sub> (Å)		Bond distance difference	3 σ	5 σ
	Bond distance	e.s.d	Bond distance	e.s.d			
<b>101</b>	3.062	0.002	3.152	0.002	0.090	0.006	0.010
<b>110</b>	3.157	0.001	3.052	0.002	0.110	0.006	0.010
<b>122</b>	3.164	0.004	2.997	0.004	0.170	0.012	0.020
<b>123</b>	3.055	0.002	3.119	0.002	0.060	0.006	0.010
<b>124</b>	3.166	0.003	3.111	0.003	0.050	0.009	0.015
<b>125</b>	3.022	0.002	3.100	0.002	0.080	0.006	0.010
<b>126</b>	3.014	0.002	3.028	0.002	0.010	0.006	0.010

<sup>[a]</sup> e.s.d. = estimated standard deviation of bond distances from crystal structures

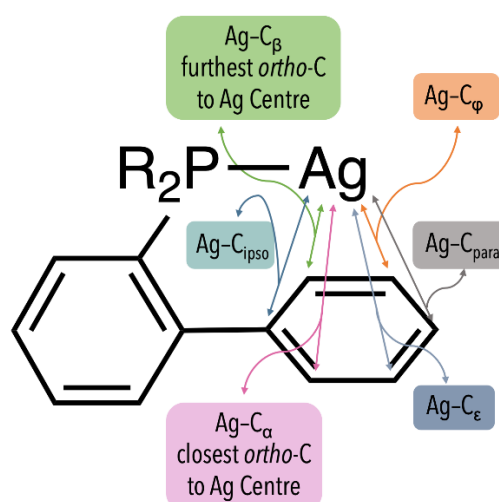


**Table 30:** Distances between the carbon atoms of the distal ring of the biaryl of the phosphine and Ag metal centre from the crystal structure

Complex	Bond length (Å)						$5 \sigma$
	Ag-C <sub>ipso</sub>	Ag-C <sub>α</sub>	Ag-C <sub>β</sub>	Ag-C <sub>φ</sub>	Ag-C <sub>ε</sub>	Ag-C <sub>para</sub>	
<b>101</b>	3.062(2)	3.152(2)	3.356(2)	3.686(2)	3.522(2)	3.574(2)	0.01
<b>110</b>	3.157(1)	3.052(2)	3.710(2)	4.036(2)	3.466(2)	3.951(2)	0.01
<b>122</b>	3.164(4)	2.997(4)	3.637(4)	3.943(4)	3.359(4)	3.822(4)	0.02
<b>123</b>	3.055(2)	3.119(2)	3.313(3)	3.606(3)	3.436(3)	3.665(2)	0.01
<b>124</b>	3.166(3)	3.111(3)	3.569(3)	3.819(3)	3.422(3)	3.737(3)	0.01
<b>125</b>	3.022(2)	3.100(2)	3.273(2)	3.521(2)	3.365(2)	3.574(2)	0.01
<b>126</b>	3.014(2)	3.028(2)	3.421(2)	3.793(2)	3.453(2)	3.797(2)	0.01

The close contact between the Ag<sup>I</sup> centre and the *ipso*- and *ortho*-C suggests a type of secondary  $\eta^2$ -arene interaction with the distal ring of the biaryl. Examples of true  $\eta^2$ -complexes with Ag and Rh, typically have much shorter bond distances between the arene bond and metal centre, along with bond elongation along the C–C bond<sup>147</sup>. For example, **127** reported by Zsolnai and co-workers, features an  $\eta^2$ -alkynyl–Ag<sup>I</sup> interaction with a bond distance in the order of 2.30 – 2.40 Å.<sup>148</sup> Chin *et al.* isolated examples of  $\eta^2$ -arene complexes with Rh, such as **128** and **129**, feature bond distances of 2.13 – 2.16 Å.<sup>147</sup> The C–C participating in the  $\eta^2$  interactions is also observed to be elongated when compared to the free ligand (**Table 31**). In contrast, the shortest bond distance between arene ring and Ag centre in the AgC<sub>6</sub>F<sub>5</sub>PR<sub>3</sub> complex are in the order of 3.00 Å, which is considerably longer. No elongation of the C–C bond was also observed in these complexes, as the interaction is much weaker. However, as the bond distance between the Ag<sup>I</sup> centre and *ipso*- and *ortho*-C are significant, it is likely a secondary  $\eta^2$ -arene interaction.

**Table 31:** Bond lengths and distances of  $\eta^2$ -complexes reported in the literature, and comparison with free ligand<sup>148,147</sup>

Bond	Bond distance (Å)		
	127 <sup>148</sup>	128 <sup>147</sup>	129 <sup>147</sup>
C <sup>1</sup> -M	2.29(2)	2.128(4)	2.16(1)
C <sup>2</sup> -M	2.41(2)	2.144(4)	2.13(1)
C <sup>1</sup> -C <sup>2</sup>	1.26(2)	1.428(6)	1.45(2)
free ligand C <sup>1</sup> -C <sup>2</sup>	1.21	1.372	1.370
C <sup>3</sup> -M	2.33(2)	-	-
C <sup>4</sup> -M	2.43(2)	-	-
C <sup>3</sup> -C <sup>4</sup>	1.27(3)	-	-
free ligand C <sup>3</sup> -C <sup>4</sup>	1.20	-	-

#### 4.4 The Effect of Haloarenes on the Direct Arylation Reaction

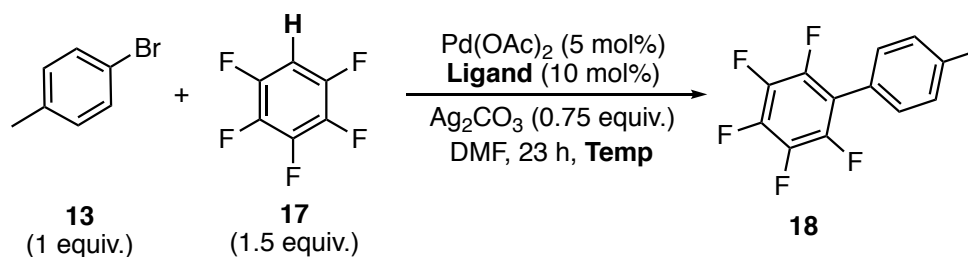
The reactivity of bromo- and chloroarenes was examined using 4-bromotoluene **13** and 4-chlorotoluene **130** as exemplar reagents. This allows the results to be directly compared to the reactions using 4-iodotoluene **26**. The reactions between 4-bromotoluene **13** and pentafluorobenzene **17** were carried out in DMF, using Pd(OAc)<sub>2</sub> (5 mol%) as the pre-catalyst and Ag<sub>2</sub>CO<sub>3</sub> (0.75 equiv.) as the base. A range of different temperatures and dialkylbiaryl phosphine ligands were also used. Sluggish reactivity was observed when 4-bromotoluene was used, where catalyst turnover generally ceased after approximately 30 % conversion to product **18** (Table 32). From the dialkylbiarylphosphine ligand scope, the three most active ligands for catalysis were Xphos, CyJohnphos and Johnphos. Xphos was found to be the most efficient ligand, for reactions with 4-bromotoluene **13** followed by Johnphos and CyJohnphos. Increasing the temperature to 60 °C from room temperature resulted in a slight increase in % <sup>19</sup>F {<sup>1</sup>H} NMR yield from approximately 10 % NMR yield to 30 %, however increasing the



temperature to 80 °C or 100 °C did not result in a major improvement in NMR yield (**Table 32**).

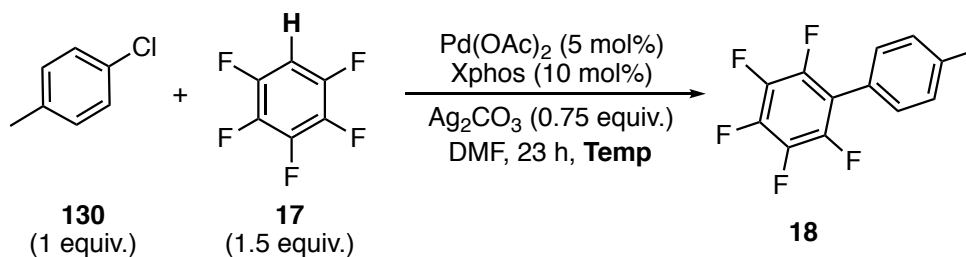
No conversion to product **18** was observed from the reaction of 4-chlorotoluene **13** with pentafluorobenzene **17** under the standard catalytic direct arylation reaction conditions with Xphos as the ligand (**Table 33**). No reactivity was observed even when the temperature was increased to 100 °C. Optimal reactivity was achieved with iodoarenes, bromoarenes resulted in sluggish reactivity, while chloroarenes did not react at all.

**Table 32:** Direct Arylation of 4-bromotoluene **13** with pentafluorobenzene **17** in DMF with varying ligand and temperatures.



Ligand	$^{19}\text{F}\{^1\text{H}\}$ NMR yield (%) <sup>[a]</sup>							
	Room temperature		60 °C		80 °C		100 °C	
	3 h	23 h	3 h	23 h	3 h	23 h	3 h	23 h
Xphos	6	11	30	29	26	27	23	27
JohnPhos	2	3	11	11	-	-	-	-
CyJohnPhos	0	0	2	2	-	-	-	-

<sup>[a]</sup> The %  $^{19}\text{F}\{^1\text{H}\}$  NMR was calculated using Octafluoronaphthelene as the internal standard. The Internal standard resonance at -145 ppm was used and compared to the ortho-*F* peak of the product (-143.8 ppm) to calculate the % NMR yields by  $^{19}\text{F}\{^1\text{H}\}$  NMR spectroscopy.

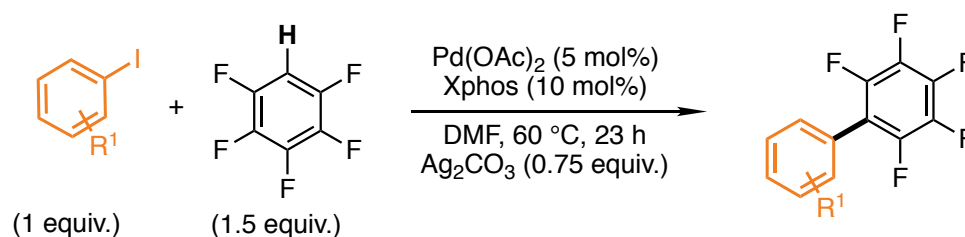
**Table 33:** Direct arylation of 4-chlorotoluene **130** with pentafluorobenzene **17** in DMF with varying temperatures.

Time (h)	$^{19}\text{F}\{^1\text{H}\}$ NMR yield (%) <sup>[a]</sup>		
	Temperature ( °C)		
	60	80	100
3	0	0	0
23	0	0	0

<sup>[a]</sup> The %  $^{19}\text{F}\{^1\text{H}\}$  NMR was calculated using Octafluoronaphthelene as the internal standard. The Internal standard resonance at  $-145$  ppm was used and compared to the *ortho-F* peak of the product ( $-143.8$  ppm) to calculate the % NMR yields by  $^{19}\text{F}\{^1\text{H}\}$  NMR spectroscopy.

## 4.5 Substrate Scope of Iodoarenes

With the currently optimised conditions, a brief substrate scope with aryl iodides was conducted to gain further understanding of the reactivity of the system (**Scheme 95**). For this purpose, aryl iodides bearing different functional groups in the *para*-, *meta*- and *ortho*-positions were considered. The reaction mixture was heated for 23 h, however reaction aliquots at both 3 h and 23 h were collected to monitor the progress of the reaction using  $^{19}\text{F}\{^1\text{H}\}$  NMR spectroscopy (**Figure 93**). While previous reactions (in chapter 4) were carried out in Schlenk tubes using rigorous air and moisture free conditions. It was found that these reactions could also be carried out in screw top 7 mL vials, with a PTFE silicon septum with no effect on the yield of the reaction. The reagents could also be used directly from the bottle without drying or further purification.

**Scheme 95:** Catalytic direct arylation conditions used for the substrate scope of aryl iodides

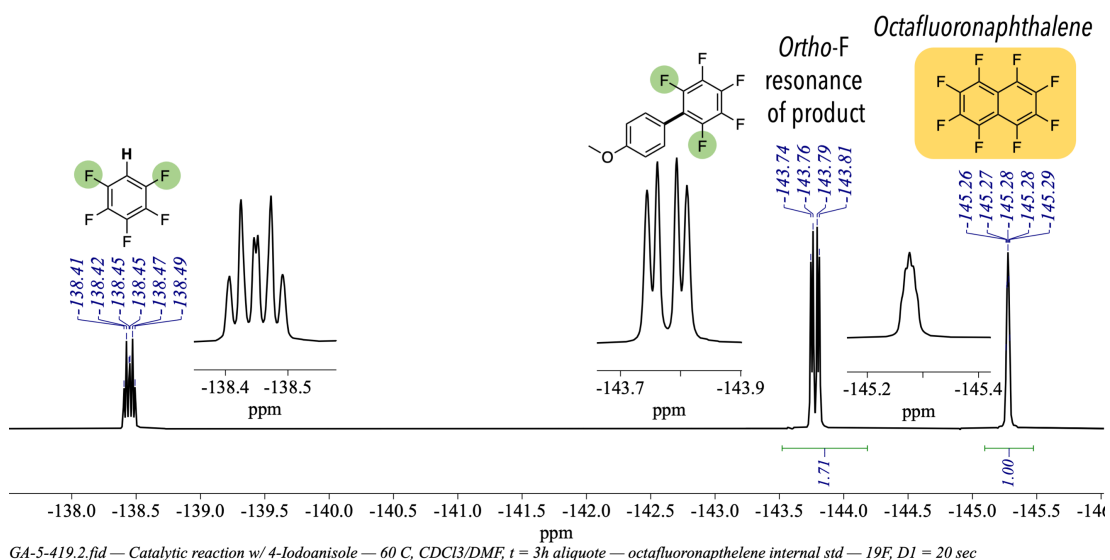
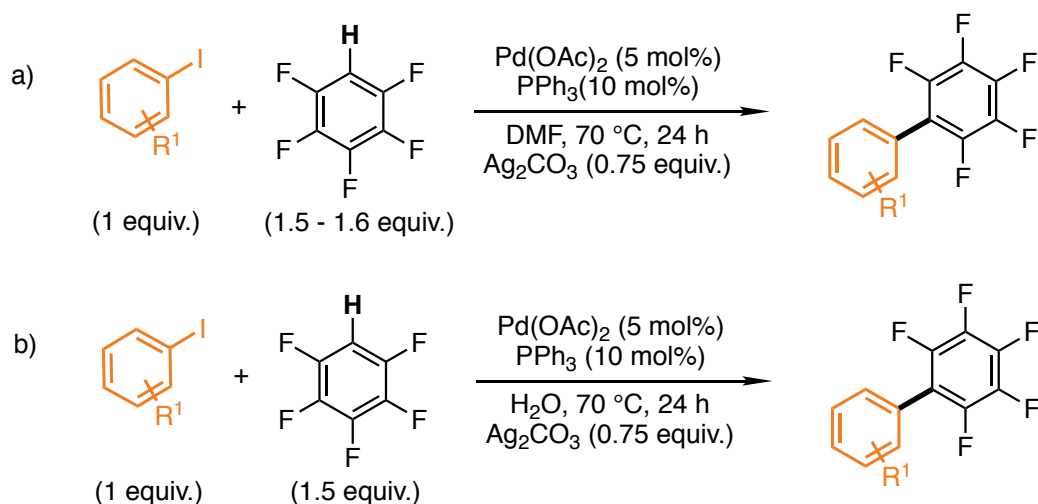


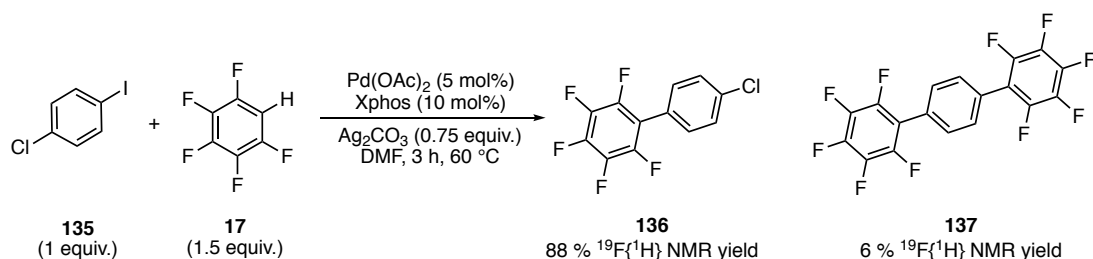
**Figure 93:**  $^{19}\text{F}\{^1\text{H}\}$  NMR (470 MHz,  $\text{CDCl}_3$ , 25 °C) of the reaction mixture with 4-iodoanisole **50** depicting the *ortho*-F resonance of the product and *F*-resonance of octafluoronaphthalene used to calculate the  $^{19}\text{F}\{^1\text{H}\}$  NMR yields.

The effect of the *para*-substituents of the iodoarenes on the  $^{19}\text{F}\{^1\text{H}\}$  NMR yield of the direct arylation at both 60 °C and 100 °C (when data is available) has been plotted in **Figure 94**. Little to no conversion to **131** and **132** was obtained when 4-iodoaniline and 4-iodophenol, respectively. This is likely indicative of a reaction sensitivity towards protic substrates which is similar to the reactivity observed in Platt *et al.*'s direct arylation reaction where  $\text{PPh}_3$  was used as the ligand (**Scheme 96a**).<sup>68</sup> This could be due catalyst deactivation by coordination of the 1° amine or hydroxyl group to Pd metal centre. The hydroxyl group is also sensitive to redox reactions under the given conditions. The reaction of  $-\text{OMe}$  (4-iodoanisole),  $-\text{Me}$  (4-iodotoluene) and  $-\text{H}$  (iodobenzene) resulted in almost quantitative conversion within 3 h of heating at 60 °C. Surprisingly a  $^{19}\text{F}\{^1\text{H}\}$  NMR yield of 66 % of **134** was obtained with fluoro-4-iodobenzene and after purification by column chromatography a yield of 49 % of **134** was obtained. In contrast, under the reaction conditions of Platt *et al.*<sup>68</sup> and Zhang and co-workers<sup>35</sup> (**Scheme 96**), yields (after purification by column chromatography) of **134** were 78 % and 73 % were obtained respectively.

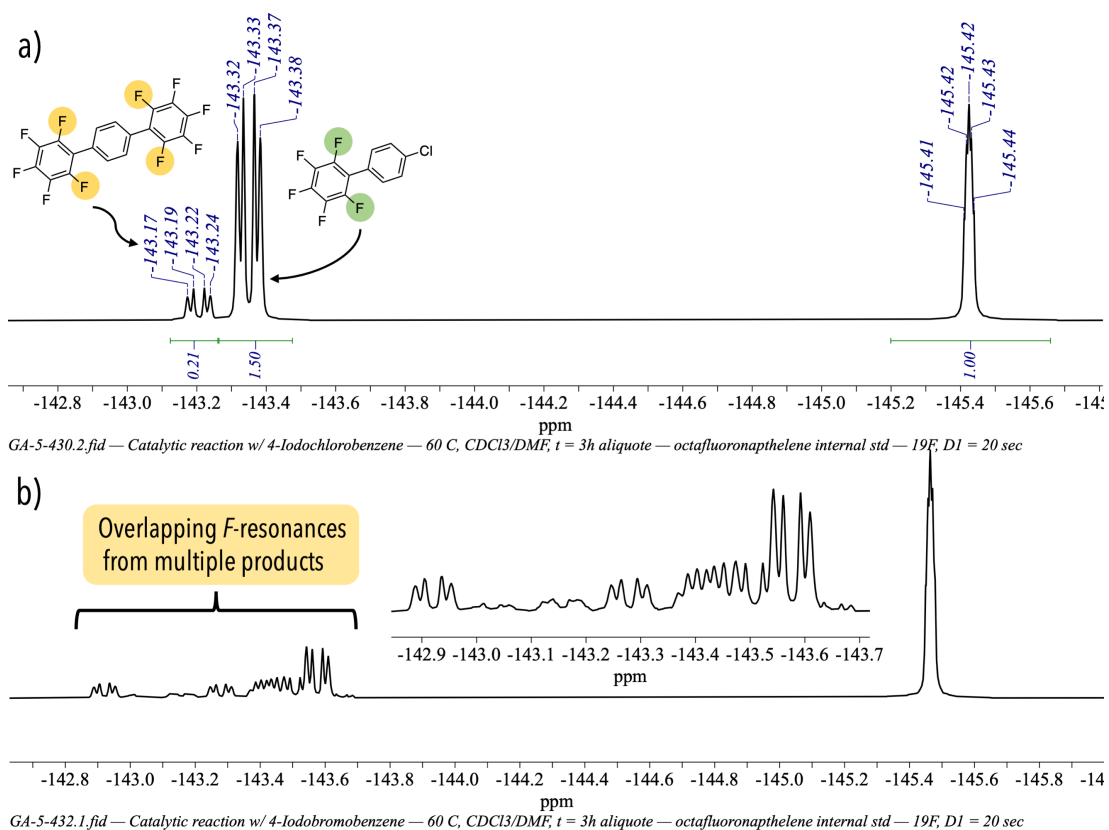


**Scheme 96:** The C–H direct arylation reaction conditions used by a) Platt *et al.*<sup>68</sup> and b) Zhang and co-workers<sup>35</sup> when performing their respective aryl iodide substrate scopes

The reaction between chloro-4-iodobenzene **135** and pentafluorobenzene **17** resulted in the formation of a major product **136** to 88 % and a minor diarylated product **137** of 6 % by  $^{19}\text{F}\{^1\text{H}\}$  NMR yield after heating at 60 °C (**Scheme 97**). The *F*-resonances of both products were detected in the  $^{19}\text{F}\{^1\text{H}\}$  NMR spectrum (**Scheme 98a**) and the identity was confirmed by *m/z* and fragmentation pattern by GC-EI. The presence of the diarylated product **137** is of particular interest as it involves the activation of the Cl–C bond of the major product **136** to yield the minor product **137**. In contrast, 4-chlorotoluene **130** did not react at all under the model reaction conditions at even 100 °C. This suggests varying the haloarene or reaction conditions could help access chloroarenes or bromoarenes.



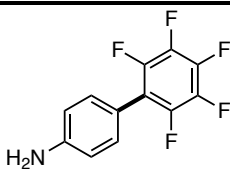
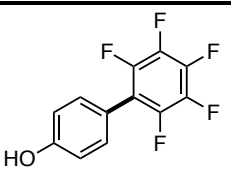
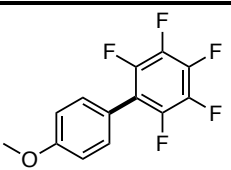
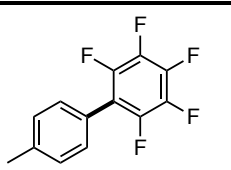
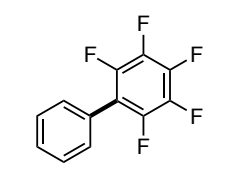
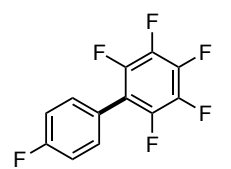
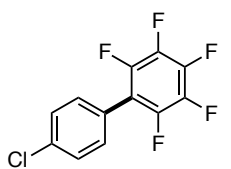
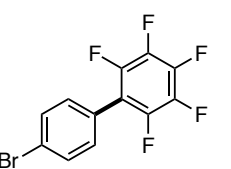
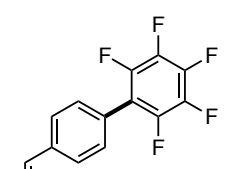
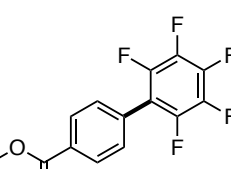
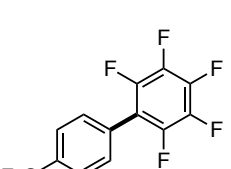
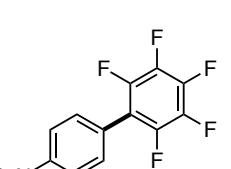
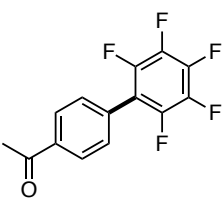
**Scheme 97:** Direct arylation reaction of chloro-4-iodobenzene **135** with pentafluorobenzene **17** in DMF at 60 °C



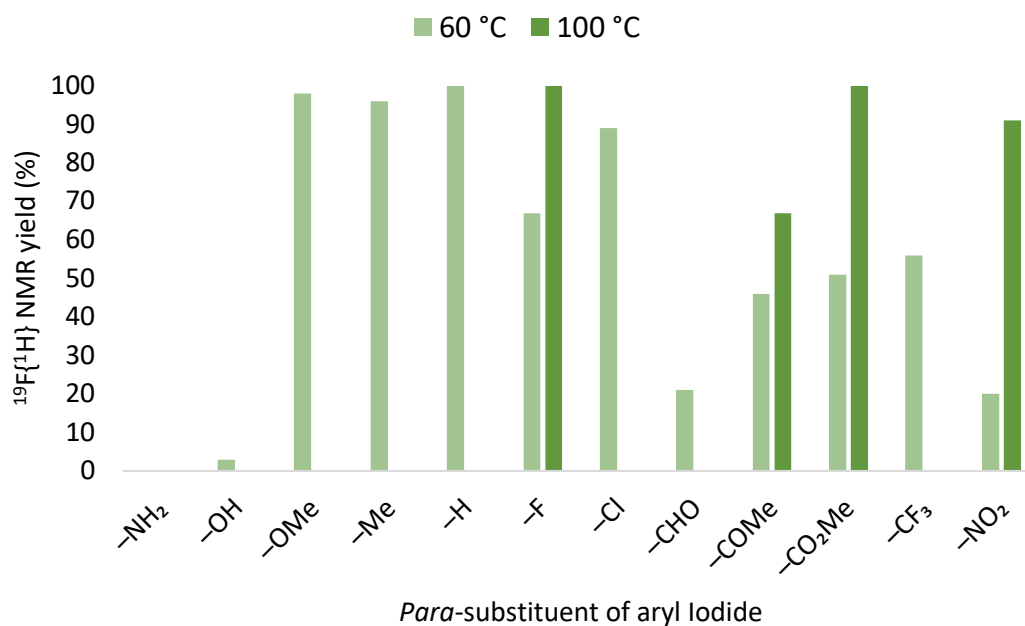
**Scheme 98:**  $^{19}\text{F}\{^1\text{H}\}$  NMR (470 MHz,  $\text{CDCl}_3$ , 25 °C) spectrum of mixture of a) reaction between chloro-4-iodobenzene **135** with pentafluorobenzene **17**, showing the *ortho*-F resonances of **136** and **137**. b) Reaction between bromo-4-iodobenzene with pentafluorobenzene **17**, showing the overlapping F-resonances of multiple products.

The reaction of bromo-4-iodobenzene resulted in multiple products which were difficult to identify and/or quantify using the  $^{19}\text{F}\{^1\text{H}\}$  NMR spectrum, due to peak overlap (**Scheme 98b**). The GC-EI trace was also complex and difficult to analyse. This is likely due to activation of both the Br-C and I-C bonds of the substrate. Moderate to low yields were obtained when carbonyl functional groups were positioned in the *para*-position. The reaction with methyl-4-iodobenzoate and 4-iodoacetophenone resulted in a  $^{19}\text{F}\{^1\text{H}\}$  NMR yield of 51 % and 40 % respectively, after heating at 60 °C for 3 h. When 4-iodobenzaldehyde was used, only a sluggish  $^{19}\text{F}\{^1\text{H}\}$  NMR yield of 20 % was obtained after 3 h of heating at 60 °C. The use of highly electron-withdrawing *para*-substituents, such as  $-\text{CF}_3$  and  $-\text{NO}_2$ , also resulted in moderate to low yields. Overall, with electron-deficient *para*-substituents, mixed results were obtained.

**Table 34:** The *para*-substituted aryl iodides scope of direct arylation at 60 °C in DMF

$^{19}\text{F}\{^1\text{H}\}$ NMR yield <sup>[a]</sup> of <i>Para</i> substituted aryl iodides at 3 h, 23 h (yield after purification) <sup>[b]</sup>			
			
<b>131</b> 0 %, 0%	<b>132</b> 3 %, 3 %	<b>133</b> 98 %, 97 %	<b>18</b> 96%, 96% (84)
			
<b>28</b> 98%, 100% (74)	<b>134</b> 66%, 67% (49)	<b>136</b> 88 %, 89 %	<b>138</b> multiple products
			
<b>139</b> 20 %, 21 %	<b>140</b> 51 %, 51 %	<b>141</b> 53 %, 56 %	<b>142</b> 19%, 20 %
			
<b>143</b> 40 %, 46 %, 52 % <sup>[c]</sup>			

<sup>[a]</sup>  $^{19}\text{F}\{^1\text{H}\}$  NMR yield was calculated using octafluoronaphthalene as the internal standard. The Internal standard resonance at  $-145$  ppm was used and compared to the *ortho-F* peak of the product to calculate the % yields by  $^{19}\text{F}\{^1\text{H}\}$  NMR spectroscopy. <sup>[b]</sup>  $^{19}\text{F}\{^1\text{H}\}$  NMR yield after 3 h is denoted by the first values followed by the yield at 23 h <sup>[c]</sup>  $^{19}\text{F}\{^1\text{H}\}$  NMR yield after 46 h.

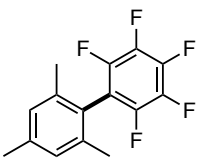
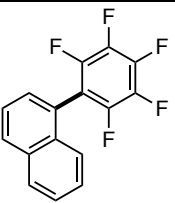
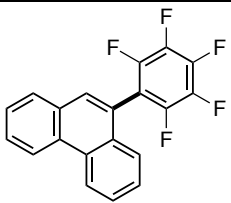
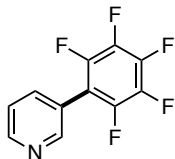
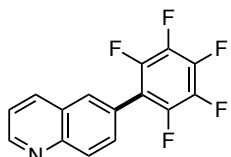
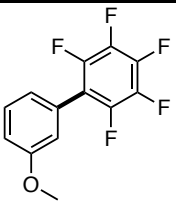
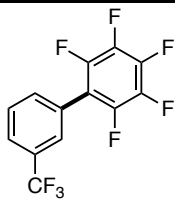
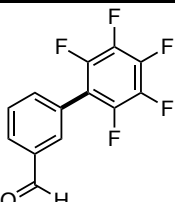
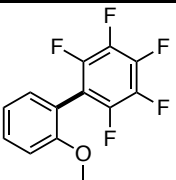
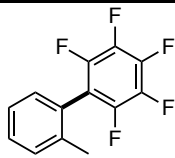
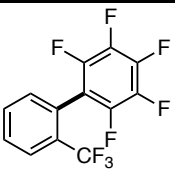


**Figure 94:** Variation in  $^{19}\text{F}\{^1\text{H}\}$  NMR yield with respect to the para-substituents of the aryl iodides

The use of bulky aryl iodides (2-iodo-1,3,5-trimethylbenzene, 1-iodonaphthalene, 9-iodophenanthrene) and nitrogen-containing heteroatoms (2-iodopyridine, 6-iodoquinoline) results in little to no yield of product by  $^{19}\text{F}\{^1\text{H}\}$  NMR spectroscopy. An increase in steric bulk in the *ortho*-position ( $-\text{Me}$ ,  $-\text{CF}_3$ ,  $-\text{OMe}$ ) also proved to be problematic for catalysis. In contrast, the reaction was more tolerant towards *meta*-substituents, resulting in moderately good yields. However, the use of 3-iodobenzaldehyde still resulted in sluggish  $^{19}\text{F}\{^1\text{H}\}$  NMR yield indicating some functional group sensitivity.

To examine if an increase in the temperature could result in better yields and help expand the substrate scope, the temperature of the reaction was increased to 100 °C. In some cases, the increase in temperature resulted in vastly improved yields. Most notably, methyl-4-iodobenzoate where the  $^{19}\text{F}\{^1\text{H}\}$  NMR yield at 3 h and 23 h at 60 °C was 40 % and 46 % respectively but upon heating to 100 °C, the  $^{19}\text{F}\{^1\text{H}\}$  NMR yield improved to 89 % at 3 h and 100 % at 23 h. Similarly, with 6-iodoquinoline, the reaction was extremely sluggish at 60 °C culminating in only 11 %  $^{19}\text{F}\{^1\text{H}\}$  NMR yield after 23 h, whereas at 100 °C, a 97 %  $^{19}\text{F}\{^1\text{H}\}$  NMR yield was recorded after heating for 23 h. This is similarly true for fluoro-4-iodobenzene and iodo-4-nitrobenzene and *meta*-substituted aryl iodides, where the  $^{19}\text{F}\{^1\text{H}\}$  NMR yields are vastly improved compared to the reaction at 60 °C. However, even at an elevated temperature, no improvement in yield was observed with *ortho*-substituted aryl iodides.

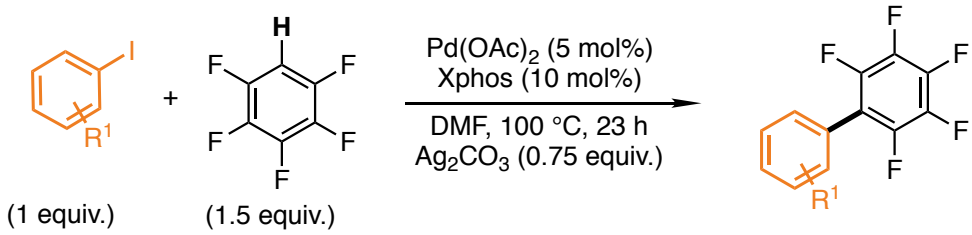
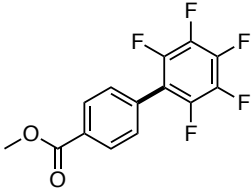
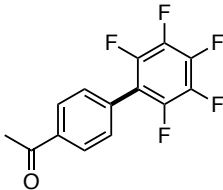
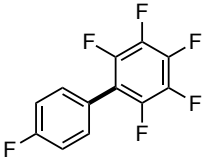
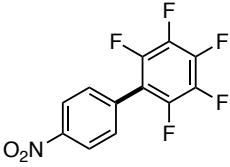
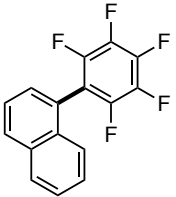
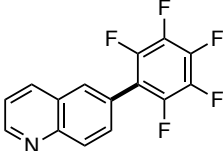
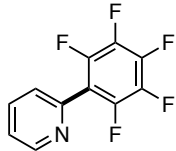
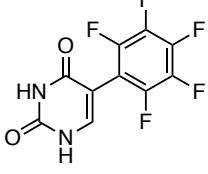
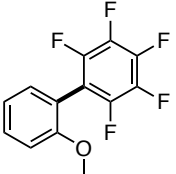
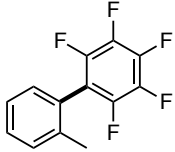
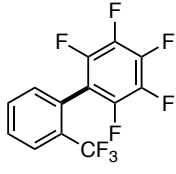
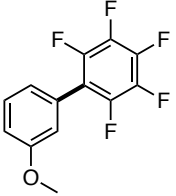
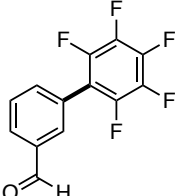
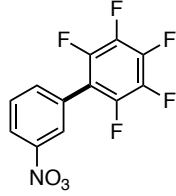
**Table 35:** Substrate scope of bulky, heteroatom, *meta*- and *ortho*- substituted aryl iodides at 60 °C

$^{19}\text{F}\{^1\text{H}\}$ NMR yield of bulky and heteroaromatic substituents at 3 h, 23 h <sup>[a][b]</sup>			
			
<b>144</b> 0 %, 0 %	<b>145</b> 15 %, 14%	<b>146</b> 6%, 6%	<b>147</b> 2 %, 3 %
			
<b>148</b> 10 %, 11 %			
$^{19}\text{F}\{^1\text{H}\}$ NMR yield of <i>meta</i> substituents			
			
<b>149</b> 82 %, 85 % <sup>[b]</sup>	<b>150</b> 69 %, 73 %	<b>151</b> 14 %, 14%	
$^{19}\text{F}\{^1\text{H}\}$ NMR yield of <i>ortho</i> substituents			
			
<b>152</b> 6 %, 6%	<b>153</b> 27 %, 27 % <sup>[c]</sup>	<b>154</b> 0 % <sup>[d]</sup>	

<sup>[a]</sup> The %  $^{19}\text{F}\{^1\text{H}\}$  NMR Yield was calculated using octafluoronaphthalene as the internal standard. The internal standard resonance at  $-145$  ppm was used and compared to the *ortho*-*F* peak of the product to calculate the % NMR yields by  $^{19}\text{F}\{^1\text{H}\}$  NMR spectroscopy. <sup>[b]</sup>  $^{19}\text{F}\{^1\text{H}\}$  NMR yield after 3 h is denoted by the first values followed by the yield at 23 h <sup>[c]</sup>  $^{19}\text{F}\{^1\text{H}\}$  NMR yield at 69 h instead of 23 h. <sup>[d]</sup>  $^{19}\text{F}\{^1\text{H}\}$  NMR yield at 23 h only.



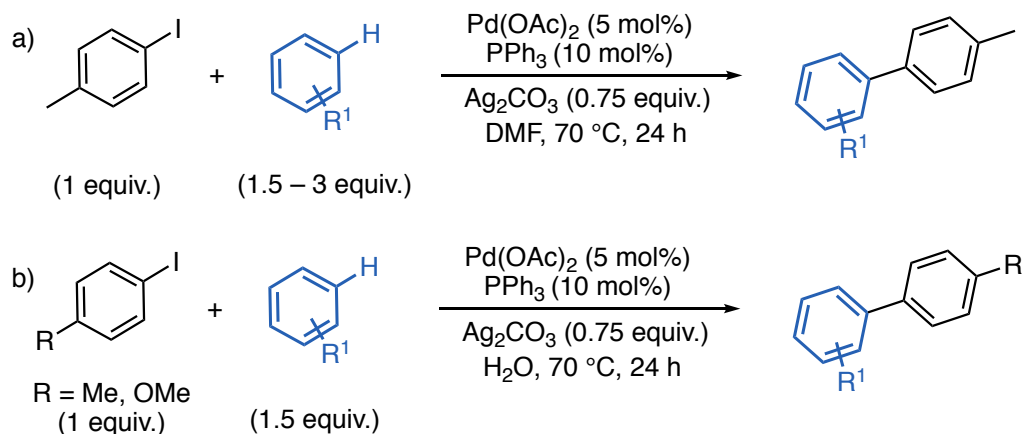
**Table 36:**  $^{19}\text{F}\{^1\text{H}\}$  NMR yield<sup>[a]</sup> of iodoarenes at 3 h, 23 h (yield after purification)<sup>[b]</sup> at 100 °C in DMF

			
(1 equiv.)	(1.5 equiv.)		
<i>Para</i> substituents			
			
<b>140</b> 89%, 100% (66)	<b>143</b> 62 %, 67 % (54)	<b>134</b> 96 %, 100 % (80)	<b>142</b> 71 %, 91 %
<i>Bulky and heteroaromatic</i> substituents			
			
<b>145</b> 24 %, 27 %	<b>148</b> 86 %, 97 % (50)	<b>155</b> 2%, 3 %	<b>156</b> 0 %, 0%
<i>Ortho</i> substituents			
			
<b>152</b> 11 %, 15 %	<b>153</b> 29 %, 33 %	<b>154</b> 0 %, 0%	
<i>Meta</i> substituents			
			
<b>149</b> 86 %, 92 %	<b>151</b> 58 %, 88 %	<b>157</b> 75 %, 93 %	

<sup>[a]</sup> The %  $^{19}\text{F}\{^1\text{H}\}$  yield was calculated using  $^{19}\text{F}$  the internal standard. Details in Experimental. <sup>[b]</sup>  $^{19}\text{F}\{^1\text{H}\}$  NMR yield after 3 h is denoted by the first values followed by the yield at 23 h.

## 4.6 Substrate Scope of Fluoroarenes

A variety of fluorinated arenes and pyridines were tested in the direct arylation reaction with 4-iodotoluene **26** (Table 37). The reaction with 2,3,4,5-tetrafluoropyridine **67** was surprisingly slow when compared to pentafluorobenzene **17**, reaching an  $^{19}\text{F}\{^1\text{H}\}$  NMR yield of 73 % after heating at 60 °C for 3 h. In comparison, with **17** an  $^{19}\text{F}\{^1\text{H}\}$  NMR yield of 96 % of **18** was reached after 3 h. The use of other dialkylphosphine ligands such as JohnPhos or CyJohnphos does not improve the %  $^{19}\text{F}\{^1\text{H}\}$  NMR yield obtained with **67**. Under Zhang and co-worker's conditions (Scheme 99b), with  $\text{PPh}_3$  as the ligand, 86% yield of **157** was obtained after purification. No reaction took place with 1,3-difluorobenzene **12** and 1,2,3,4-tetrafluorobenzene **159**. This is consistent with the results obtained with Platt *et al.*'s conditions (Scheme 99a). Under these conditions, Platt *et al.* only detected trace amounts of the biaryl product for difluorinated aromatics.



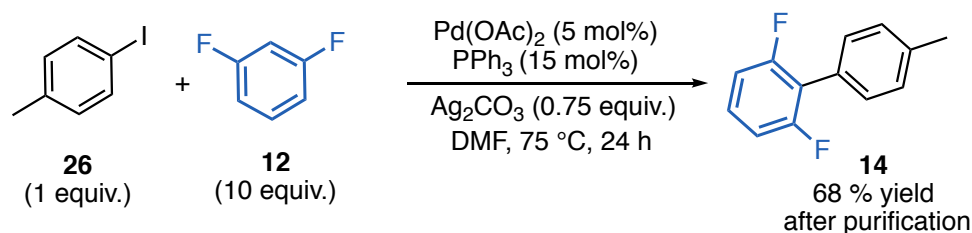
**Scheme 99:** The C–H direct arylation reaction conditions used by a) Platt *et al.*<sup>68</sup> and b) Zhang and co-workers<sup>35</sup> when performing their respective fluoroarene substrate scope

When attempting to improve the fluoroarene substrate scope of the reaction, Platt *et al.* found that increasing the reaction temperature to 75 °C and amount of ligand ( $\text{PPh}_3$ , 15 mol%), along with using a large excess of the fluoroarene (10 equiv.) allowed for the successful regioselective direct arylation of 1,3-difluorobenzene **12** to yield **14** to 68% after purification by column chromatography (Scheme 100). However, the reactivity of other fluoroarenes (1,2-difluorobenzene 1,4-difluorobenzene, fluorobenzene) under these modified conditions only led to trace quantities of biaryl product formation.

**Table 37:** Fluoroarene substrate scope for the direct arylation reaction

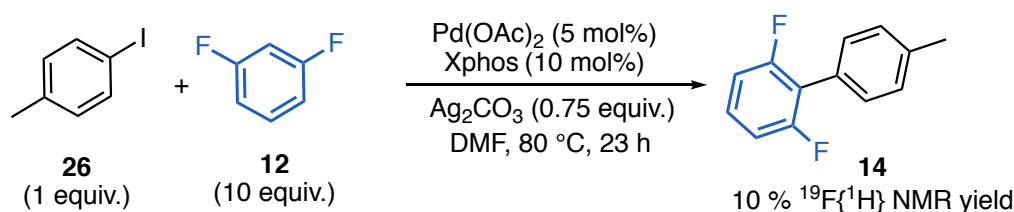
Entry	Fluorinated aromatics	Product	Ligand	Temperature (°C)	<sup>19</sup> F{ <sup>1</sup> H}	
					NMR yield <sup>[a]</sup>	
					3 h	23 h
1			Xphos	RT	-	77
				60	96	96
2			Xphos	RT	-	27
			Xphos	60	73	93
			JohnPhos	60	61	69
			CyJohnPhos	60	67	67
3			PPh <sub>3</sub>	70	3	12
			Xphos	RT	0	0
				70	0	2
				80	1	3
4			Xphos	RT	0	0
				60	0	0
5			Xphos	60	5	23
				100	36	46
6			Xphos	60	0	0
				100	5	5

<sup>[a]</sup> The % <sup>19</sup>F{<sup>1</sup>H} yield was calculated using octafluoronaphthalene as the internal standard. The internal standard resonance ( $\delta$  -145 ppm) compared to the ortho-*F* peak of the product to calculate the % yields by <sup>19</sup>F{<sup>1</sup>H} NMR spectroscopy. Details provided in the experimental.



**Scheme 100:** Direct arylation reaction of **26** with **12** (10 equiv.) outlined by Platt *et al.*

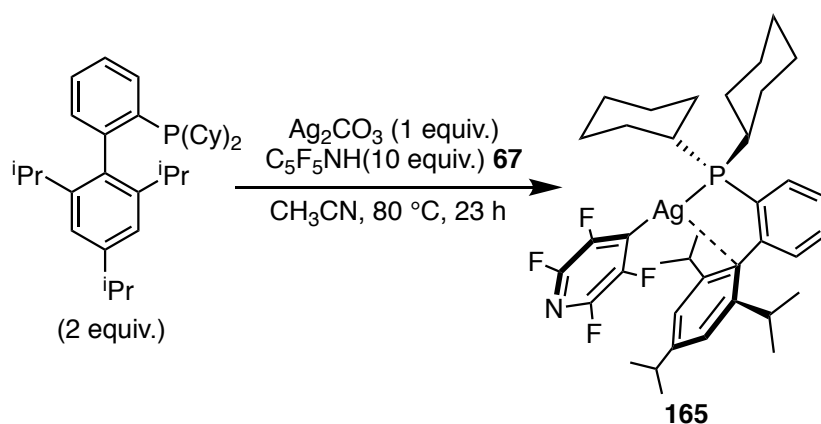
Employing conditions similar to Platt *et al.*'s, the direct arylation reaction between 4-iodotoluene **26** and 1,3-difluorobenzene **12** was repeated at 80 °C using 10 equivalents of fluoroarene (**Scheme 101**). Unfortunately, under these conditions, only low <sup>19</sup>F{<sup>1</sup>H} NMR yields of 5 % after 3 h and 10 % after 23 h were observed. An increase in Xphos ligand is likely also required to improve conversion.



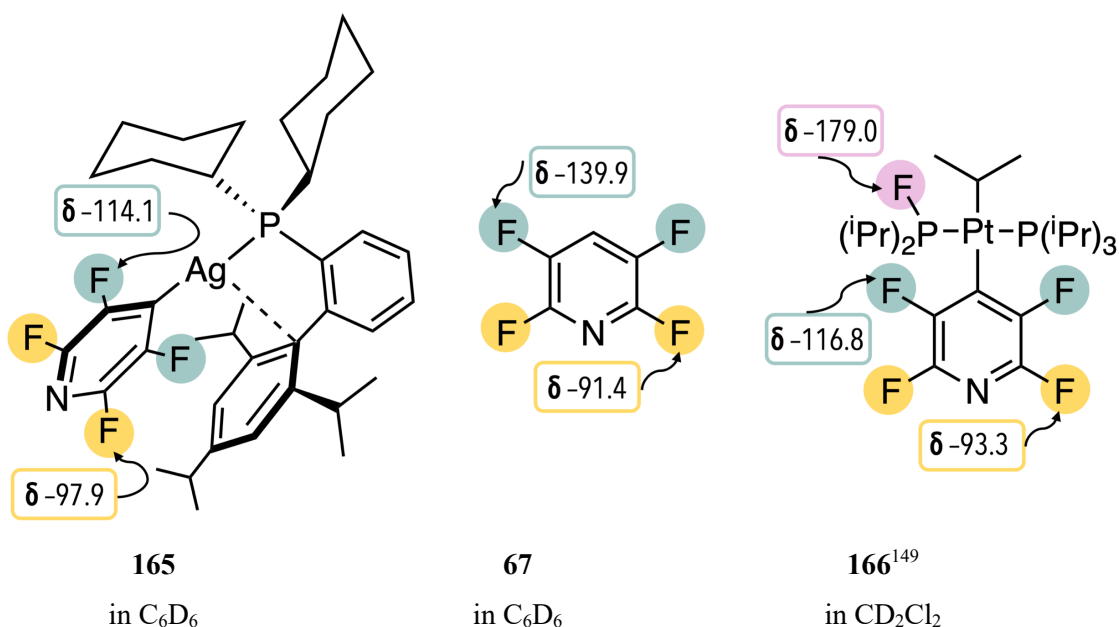
**Scheme 101:** Direct arylation reaction of 4-iodotoluene **26** with 1,3-difluorobenzene (**12**, 10 equiv.) at 80 °C, using Xphos as the ligand.

With difluorinated pyridines, a temperature of 60 °C resulted in little to modest conversions by <sup>19</sup>F{<sup>1</sup>H} NMR spectroscopy, thus the reaction was increased to 100 °C. The reaction with 3,5-difluoropyridine **161** resulted in the regioselective arylation of the C4 position to produce **162**, but only a moderate conversion of 46 % was obtained after heating at 100 °C for 23 h. Only trace amounts of the product **164** (5 % <sup>19</sup>F{<sup>1</sup>H} NMR yield) was detected when 2,6-difluoropyridine **163** was reacted. Selective arylation of the C3-position of the 2,6-difluoropyridine **163** seems to have occurred based on the presence of two <sup>19</sup>F resonances with equal integral values in the <sup>19</sup>F{<sup>1</sup>H} NMR spectrum of the reaction mixture.

To understand the effect of the different fluoroarenes on the structure of the Ag-arene complexes, the Ag<sub>2</sub>CO<sub>3</sub> and Xphos (2 equiv.) was reacted with 10 equivalents of 2,3,4,5-tetrafluoropyridine to produce **165** as dark brown crystals (55 % yield) (**Scheme 102**).

Scheme 102: Synthesis of  $\text{Ag}(\text{C}_5\text{F}_4\text{N})(\text{Xphos})$  **165**

The resulting complex was characterised using benzene- $d_6$  and exhibited pair of doublets of triplets at  $\delta$  13.2 ppm ( $^1J_{107\text{Ag } 31\text{P}} = 440$ ,  $^1J_{109\text{Ag } 31\text{P}} = 509$ ,  $^4J_{\text{PF}} = 4.0$  Hz). The  $^{19}\text{F}\{^1\text{H}\}$  NMR spectrum displayed two resonances at  $\delta$  -97.9 (2 F, m, 2,5-F) and -114.1 (2 F, m, 3,5-F). The  $^{19}\text{F}$  NMR resonances of 2,3,5,6-tetrafluoropyridine in  $\text{C}_6\text{D}_6$  appear at  $\delta$  -91.4 (m, 2,6-F) and -139.9 (m, 3,5-F). C-H activation and consequent coordination to  $\text{Ag}^{\text{I}}$  causes the 3,5-F atoms to become more deshielded and move to  $\delta$  -114.1. For comparison, Jasim *et al.* isolated a tetrafluoropyridyl-containing Pt complex **166**, where the F resonances of the tetrafluoropyridyl ring appeared at  $\delta$  -93.3 (m, 2,6-F) and -116.8 (m,  $J_{\text{PtF}} = 180$  Hz).<sup>149</sup> The presence of Pt satellites in the  $^{19}\text{F}$  NMR spectrum aided in the assignment of the resonances (Scheme 99).

Figure 95:  $^{19}\text{F}$  NMR chemical shift of the different F environments in **165**, **67** and **166**

The structure of **165** exhibits similar bond lengths and angles to those of **101** (Table 38). The Ag<sup>I</sup> metal centre lines in close contact with the *ipso* carbon of the distal ring of the biaryl ring.

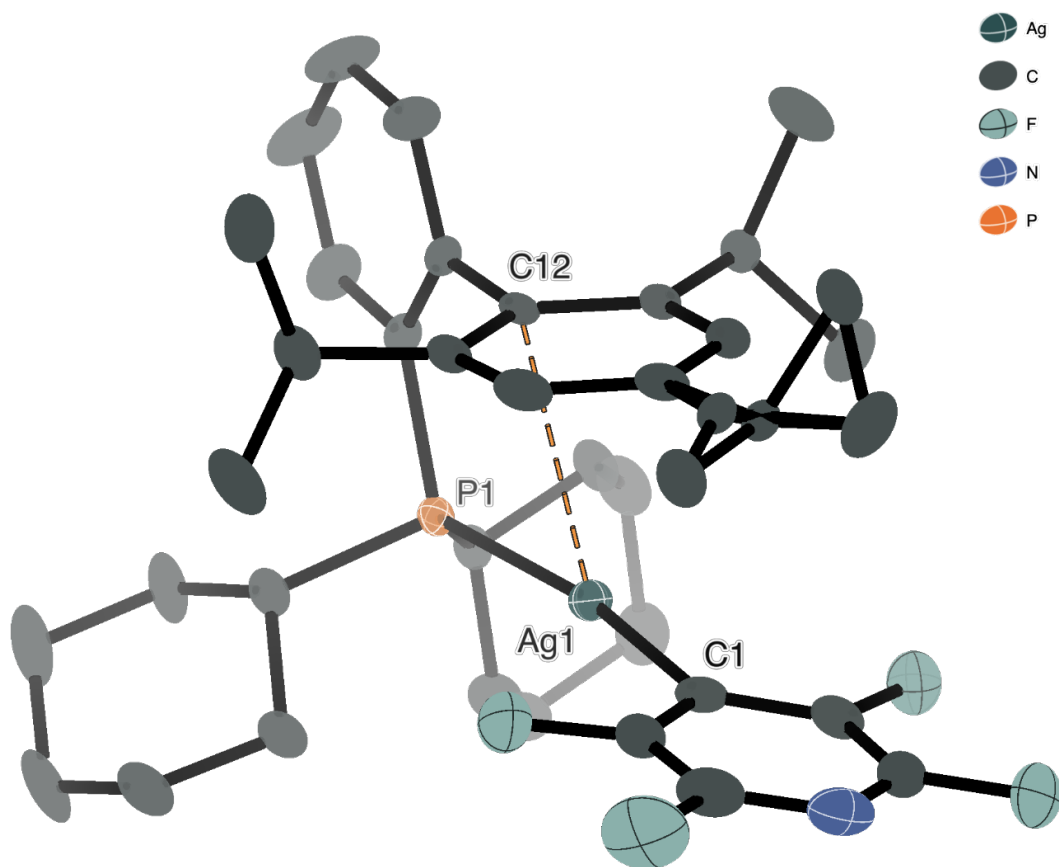


**Figure 96:** Crystal structure of AgC<sub>5</sub>F<sub>4</sub>NXphos **165**

**Table 38:** Principal bond length and angles of **165**, in comparison to **101**.

Bond	165	101
	Bond length (Å)	
Ag(1)–P(1)	2.3876(6)	2.3801(5)
Ag(1)–C(1)	2.134(3)	2.124(2)
Ag(1)–C(12) <sub>ipso</sub>	3.069(2)	3.062(2)
Bond angles	Angle (°)	
C(1)–Ag(1)–P(1)	170.65(7)	168.85(6)

## 4.7 Conclusions

A range of dialkylbiaryl phosphines was screened for the direct arylation reaction with PPh<sub>3</sub> as the benchmark ligand. Xphos was found to be the optimal ligand, with the greatest conversion (96 %) by 3 h at 60 °C. Additionally it allowed for the highest conversions of 77 % after 23 h at room temperature. The effect of dialkylbiaryl phosphines on Ag C–H activation intermediates was studied by synthesizing a library of Ag(C<sub>6</sub>F<sub>5</sub>)(PR<sub>2</sub>R') complexes and characterising these complexes by X-ray crystallography. Most of these complexes shared similar structures, with linear P–Ag–C<sub>6</sub>F<sub>5</sub> bonds and close contact of the Ag<sup>I</sup> centre with the distal ring of the biaryl. While in **101** a close contact between the Ag<sup>I</sup> metal centre and the *ipso* carbon of distal ring was observed, this was not consistent across all the Ag complexes. For example, the Ag structures with tBuXphos and CyJohnPhos featured close contact interaction between the *ortho*-C and Ag centre. The Ag structures of Sphos **124** and RuPhos **126**, contained close contact of the Ag<sup>I</sup> centre with both the *ipso*- and *ortho*-C of the distal ring. In general, for most of the structures, the close contact of the Ag<sup>I</sup> metal centre to the *ipso*-C and *ortho*-C seems to suggest a secondary η<sup>2</sup>-arene interaction.

The substrate scope for the direct arylation reaction was investigated at 60 °C. The reaction yields are good with 4-iodotoluene **26**, sluggish with 4-bromotoluene **13** and no reaction was observed with 4-chlorotoluene **130**. An iodoarene substrate scope showed that the reaction was generally tolerant towards weakly donating and withdrawing *para*-substituted iodoarenes and sensitive to strongly donating (–NH<sub>2</sub>, –OH) or withdrawing groups (–NO<sub>2</sub>). The reaction was also sensitive to bulky, heteroaromatic and *ortho*-substituents. Increasing the temperature to 100 °C improved the tolerance of the reaction towards strongly withdrawing groups (–NO<sub>2</sub>) *para*-substituted-, *meta*-substituted- and some heteroaromatic iodoarenes.

The fluoroarene scope for the direct arylation reaction was not as extensive as the aryl iodide scope. However, based on the data collected, high yields were achieved with only pentafluorobenzene **17** and 2,3,5,6-tetrafluoropyridine **67**. Further work is required to improve the tolerance toward other fluoroarenes. Finally, the Ag C–H activated intermediate with 2,3,5,6-tetrafluoropyridine **67** and Xphos was synthesised and characterised by X-ray crystallography. The structure of **165** is very similar to that of **101**, but clearly has a very different reactivity in catalysis.

## Chapter 5: Conclusions and Future work

### 5.1 Key Conclusions

This project was designed to understand the role of Ag<sup>I</sup> salts in the catalytic mechanism of C–H direct arylation reaction of iodoarenes with fluoroarenes. A key step in the direct arylation reaction is the C–H activation of the fluorinated arene *via* ALMA(6) mechanism which was originally thought to be carried out by Pd. However, publications since 2016, have since demonstrated the ability of Ag carbonate and carboxylate salts to undergo C–H activation of fluorinated aromatics (Chapter 1).

Platt *et al.* has previously investigated the role of Pd in the mechanism of C–H direct arylation of 4-iodotoluene **26** and pentafluorobenzene **17** with PPh<sub>3</sub> as the ligand.<sup>68</sup> This provided an ideal model system which allowed the project to focus solely on the role of Ag. Unfortunately, the use of PPh<sub>3</sub> proved to be problematic for mechanistic investigations. The Ag–PPh<sub>3</sub> bond was highly labile in solution, thus no bonding or characteristic <sup>107</sup>Ag/<sup>109</sup>Ag–<sup>31</sup>P coupling information could be derived from the <sup>31</sup>P{<sup>1</sup>H} NMR spectrum. Even when the spectra were fully resolved at – 100 °C, it was difficult to obtain structural information of the complexes due to speciation (**Figure 97**).

The Ag complexes existed in an exchange equilibrium with multiple (PPh<sub>3</sub>)<sub>n</sub> coordinated to Ag and also in different coordination modes with the carboxylate ligand (Chapter 2). Thus, this system was found to be unsuitable for further mechanistic study. However, based on the limited stoichiometric experiments carried out, it was observed that Ag<sub>2</sub>CO<sub>3</sub>, in the presence of PPh<sub>3</sub>, formed a more soluble complex **88**, which was capable of C–H activation of C<sub>6</sub>F<sub>5</sub>H **17** at both 60 °C and room temperature in DMF. Additionally, the reaction of Ag<sub>2</sub>CO<sub>3</sub>, PPh<sub>3</sub> and C<sub>6</sub>F<sub>5</sub>H in DMF yielded **91**, which is capable of undergoing transmetallation with Pd(PPh<sub>3</sub>)<sub>2</sub>(-tolyl)(I) **98** and subsequent reductive elimination at room temperature within 10 minutes to generate the organic product **18**. These results imply C–H activation by Ag is possible within the given system. Additionally, Platt *et al.* provided clear evidence that C–H activation can also be carried out by Pd and Pd based intermediates.<sup>68</sup> Thus, under catalytic conditions, C–H activation by Ag could be a process competing with C–H activation by Pd (**Scheme 104**).

Substituting the PPh<sub>3</sub> ligand for the more sterically hindering and electron donating Xphos ligand was effective in reducing the lability of the Ag–P bond. Ag complexes incorporating Xphos remained stable at room temperature and were easily characterised. Thus, the direct arylation reaction between 4-iodotoluene **26** and pentafluorobenzene **17** with Xphos as the ligand proved to be an ideal system to carry out mechanistic investigations. Based on the experiments performed, a Pd/Ag co-catalysed mechanism was proposed (**Scheme 104**).



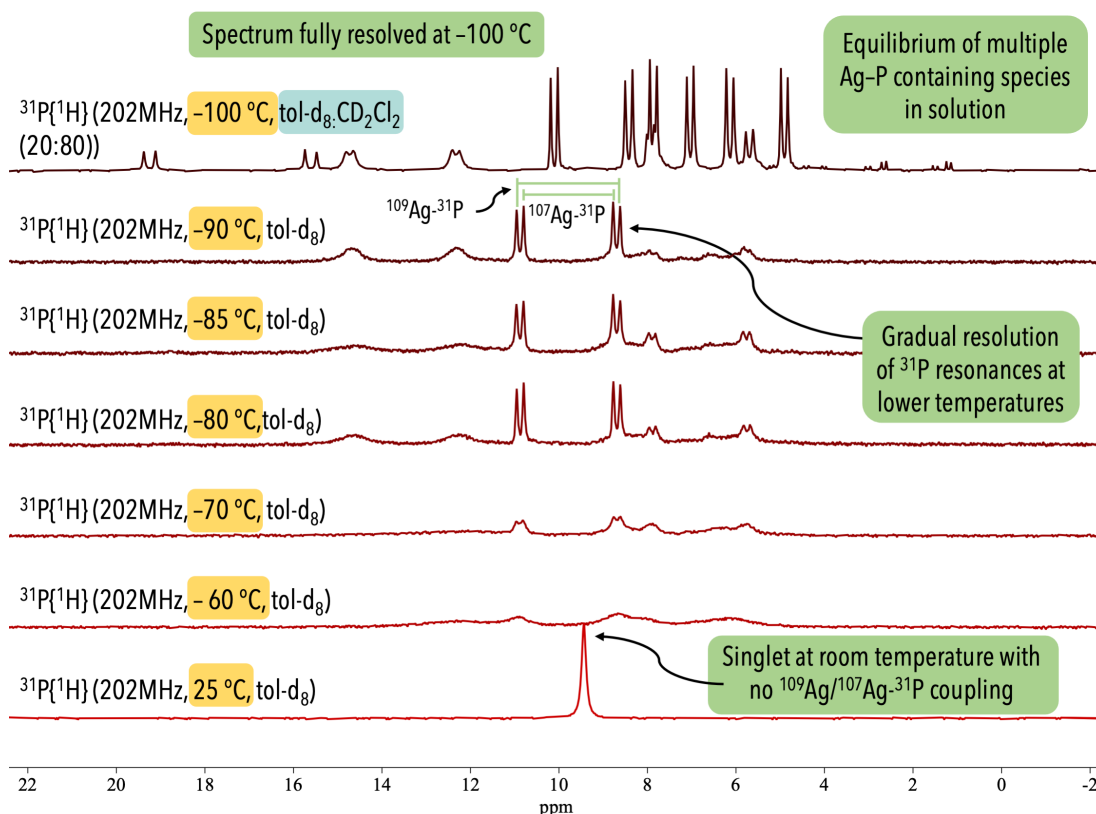
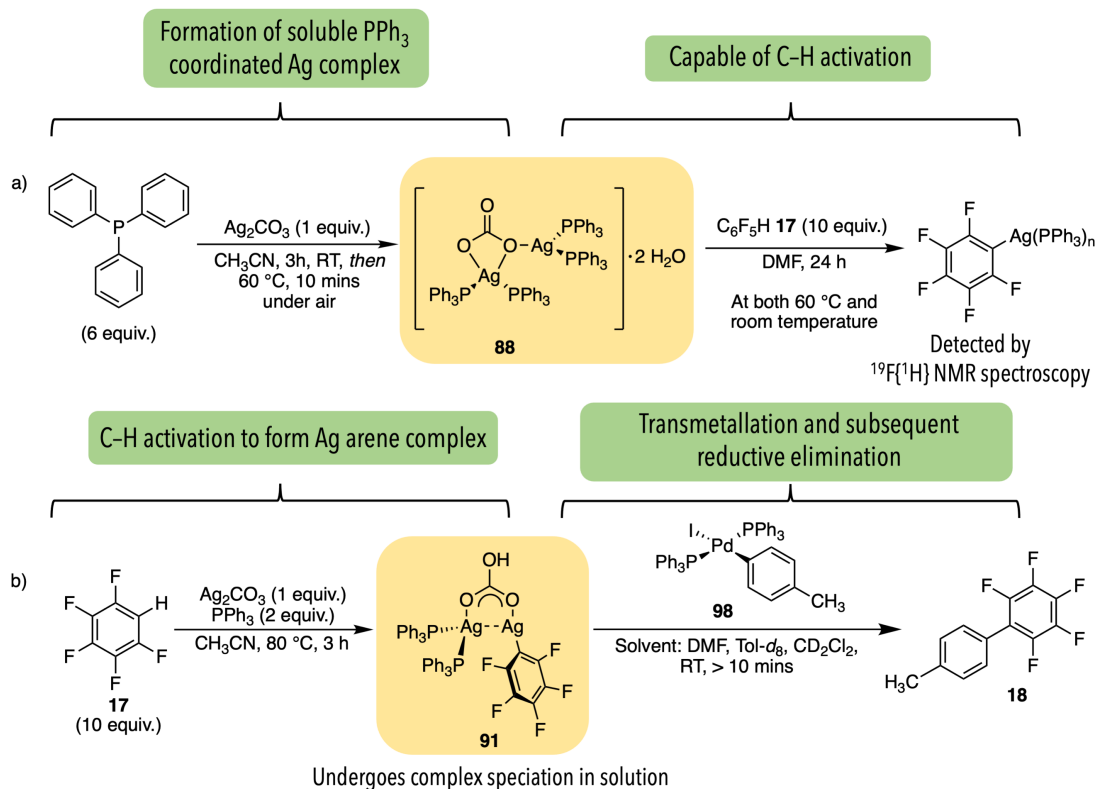
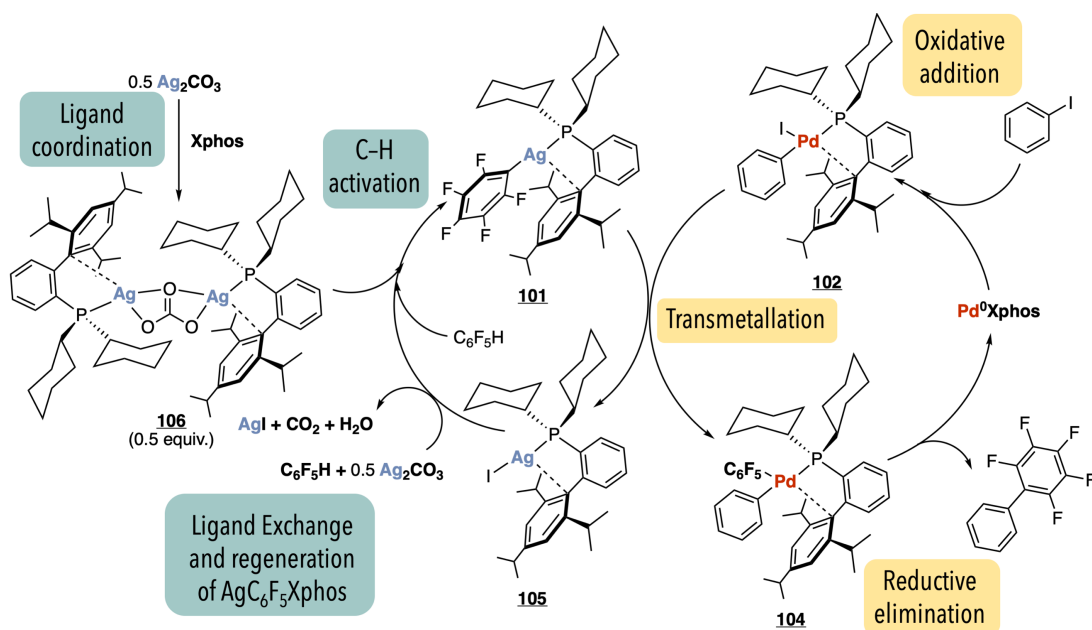


**Figure 97:**  $^{31}\text{P}\{^1\text{H}\}$  low-temperature VT NMR stack plot for  $\text{Ag}_2(\text{PPh}_3)_2(\text{C}_6\text{F}_5)(\mu_2\text{-HCO}_3)$  **91** demonstrating the lability of the Ag–P bond at room temperature and complex equilibrium of species in solution when fully resolved.



**Scheme 103:** Summary of key reactions from chapter 2, where  $\text{PPh}_3$  was used as the ligand

The individual steps of the catalytic cycles were verified stoichiometrically, except for the formation of the  $\text{Pd}^0$  species, and oxidative addition which are not expected to be detectable under these conditions (oxidative addition being fast). Silver carbonate, in the presence of Xphos, is capable of undergoing C–H activation with pentafluorobenzene to produce **101** as a discrete, well-defined complex. The production of **101** can also be carried out stepwise by reaction  $\text{Ag}_2\text{CO}_3$  with Xphos to isolate **106**, which can be further reacted with  $\text{C}_6\text{F}_5\text{H}$  **17** to generate **101**. When reacted with the Pd product of oxidative addition **102**, **101** could undergo rapid transmetalation to produce **105** as a by-product. The subsequent reductive elimination occurred rapidly to generate the organic product, and even at low temperatures the intermediate **104** could not be detected by NMR spectroscopy. When **105** treated with a large excess of  $\text{Ag}_2\text{CO}_3$  and  $\text{C}_6\text{F}_5\text{H}$  **17**, or reacted with  $\text{AgC}_5\text{F}_5$  **55**, production of **101** is detected, along with precipitation of AgI. This reactivity implied phosphine exchange between the Ag complexes, which was confirmed by detailed EXSY studies to be an associative exchange process. This also provided a route by which **101** could be regenerated. The amount of  $\text{Ag}_2\text{CO}_3$  or **101** used in the direct arylation can be reduced to catalytic amounts in conjugation with  $\text{K}_2\text{CO}_3$  (0.75 equiv.) as the base. This mechanistic investigation provides clear evidence for C–H activation by Ag, however it does not exclude competing C–H bond activation steps at Pd or the role of higher order catalyst species<sup>134–138</sup> (Chapter 3).



**Scheme 104:** Proposed mechanism incorporating both Pd and Ag as co-catalysts

The next step of the project was to use these mechanistic insights to aid in further reaction optimisation. For this purpose, a range of dialkylbiaryl phosphines was screened for the direct arylation reaction with  $\text{PPh}_3$  as the benchmark ligand and Xphos was found to be the optimal ligand. The reaction, however, demonstrated a strong dependence on the nature of the

dialkylbiaryl phosphine ligand. Thus to study this effect, a library of  $\text{Ag}(\text{C}_6\text{F}_5)(\text{PR}_2\text{R}')$  complexes were isolated and characterised using X-ray crystallography. Following this, the substrate scope of aryl iodides at 60 °C for the direct arylation revealed that the reaction was generally tolerant electron-donating *para*-substituted aryl iodides and sensitive to protic substrates ( $-\text{NH}_2$ ,  $-\text{OH}$ ). Results with electron-withdrawing groups were generally mixed. The reaction was also sensitive to bulky, heteroaromatic and *ortho*-substituents. Increasing the temperature to 100 °C improved the tolerance of the reaction to electron-withdrawing groups ( $-\text{F}$ ,  $-\text{NO}_2$ ), *meta*-substituted aryl iodides and some heteroaromatic aryl iodides (**Figure 98**). The fluoroarene scope was quite limited, achieving high yields with only pentafluorobenzene **17** and 2,3,5,6-tetrafluoropyridine **67**. Finally, the Ag C–H activated intermediate with 2,3,5,6-tetrafluoropyridine **67** and Xphos was synthesised, and its structure was found to be very similar to **101** (Chapter 4).

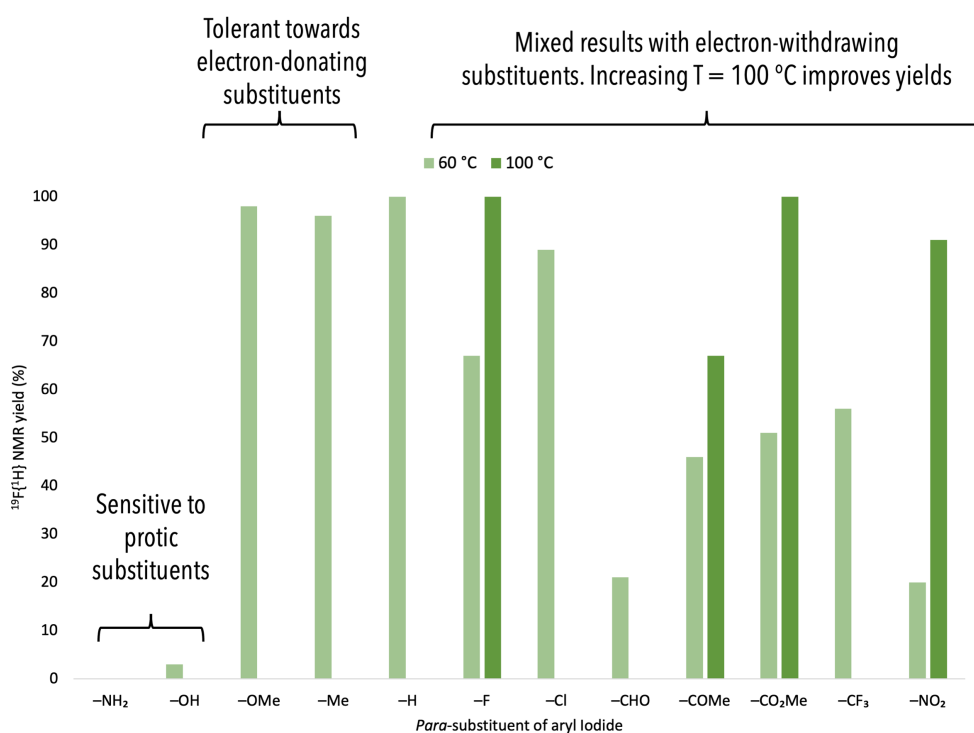
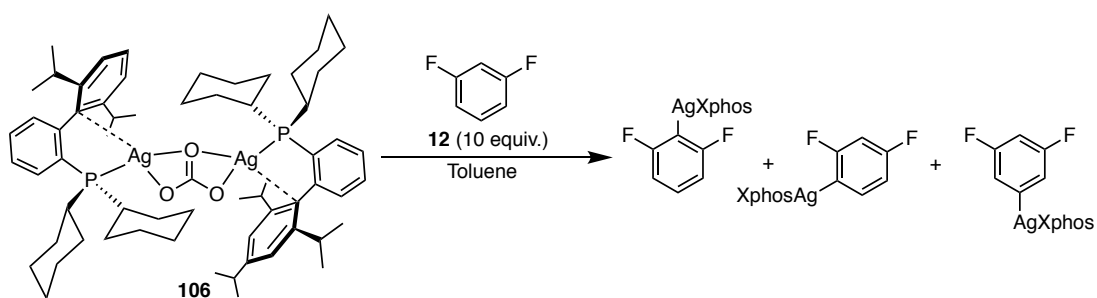


**Figure 98:** Change in  $^{19}\text{F}\{^1\text{H}\}$  NMR yield with respect to the *para*-substituents of the iodoarenes at 60 ° and 100 °C

## 5.2 Future work

### 5.2.1 Further Reaction Optimization

In this thesis, an initial substrate scope and preliminary reaction optimisation of the direct arylation, with Xphos as the ligand, was carried out. However further avenues for optimisation remain. For instance, the scope of iodoarenes, increasing the temperature to 100 °C helped improve the yield for challenging substrates and this can also be further expanded upon. Further work is required to improve the tolerance toward other fluoroarenes. Varying reaction conditions such as equivalents of arene, mol% of ligand or temperature could potentially improve the scope of the reaction. This problem can also be addressed by first reacting the carbonate complex **106** with a range of fluoroarenes before using the products for C–H functionalization and catalysis. In cases where multiple regioisomers can be formed (eg. 1,2-difluorobenzene and 3,5-difluoropyridine), it will be interesting to investigate if the products are kinetically or thermodynamically determined (**Scheme 105**). If the reaction is under thermodynamic control, the expected product with preference for fluorine to lie ortho to silver is expected.<sup>150,31</sup>



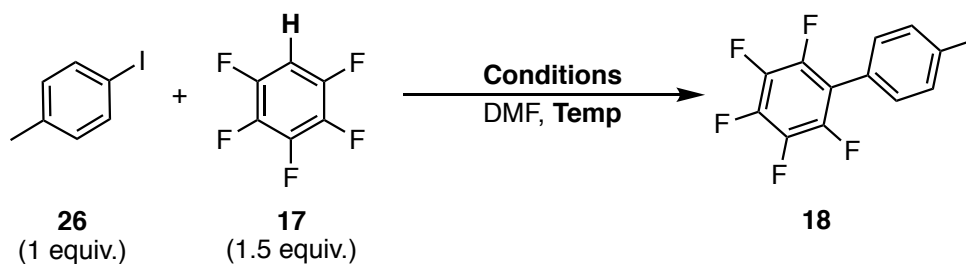
**Scheme 105:** reaction of **106** with 1,2-difluorobenzene **12** depicting the formation of various regioisomers

The amount of Ag used within the reaction could also be further optimised. Previous work from Chapter 2 and 3 has shown that the amount of Ag used can be reduced to catalytic amounts, provided an additional source of carbonate ligand is provided. In the direct arylation reaction, with PPh<sub>3</sub> as the ligand, the amount of Ag<sub>2</sub>CO<sub>3</sub> can be reduced to 5 mol% without any decrease in % NMR yield, when Cs<sub>2</sub>CO<sub>3</sub> (0.75 equiv.) is used as the base. Reducing the Ag<sub>2</sub>CO<sub>3</sub> to 1 mol% resulted in a slight drop in yield from 94 % to 80 %.

When Xphos is used as the ligand, decreasing the amount of Ag<sub>2</sub>CO<sub>3</sub> to 10 mol% and using K<sub>2</sub>CO<sub>3</sub> (0.75 equiv.) as the base resulted in the loss of yield from 96 % (with 0.75 equiv. of Ag<sub>2</sub>CO<sub>3</sub>) to 65 %. This could be the result of the difference in the rate of phosphine exchange in the PPh<sub>3</sub> and Xphos system. From the proposed catalytic cycle (**Scheme 104**), phosphine exchange is important in regeneration of the Ag catalytically active species. The Ag–PPh<sub>3</sub> bond is far more labile and thus, regeneration of the Ag catalytically active species in the

reaction with PPh<sub>3</sub> is likely faster and results in a faster rate. This is not the case with Xphos, where exchange occurs at an NMR timescale at room temperature. This, further optimisation can be carried out were the amount of Ag<sub>2</sub>CO<sub>3</sub> for the reaction with Xphos can be decrease from 0.75 equiv. The amount of phosphine used seems to be optimised for the Xphos system, as decreasing the Xphos used from 10 mol% to 5 mol% resulted in a drop in yield from 96 % to 19 % after heating at 3 h at 60°C.

**Table 39:** Effect of reducing Ag and ligand amounts in the C–H direct arylation reaction



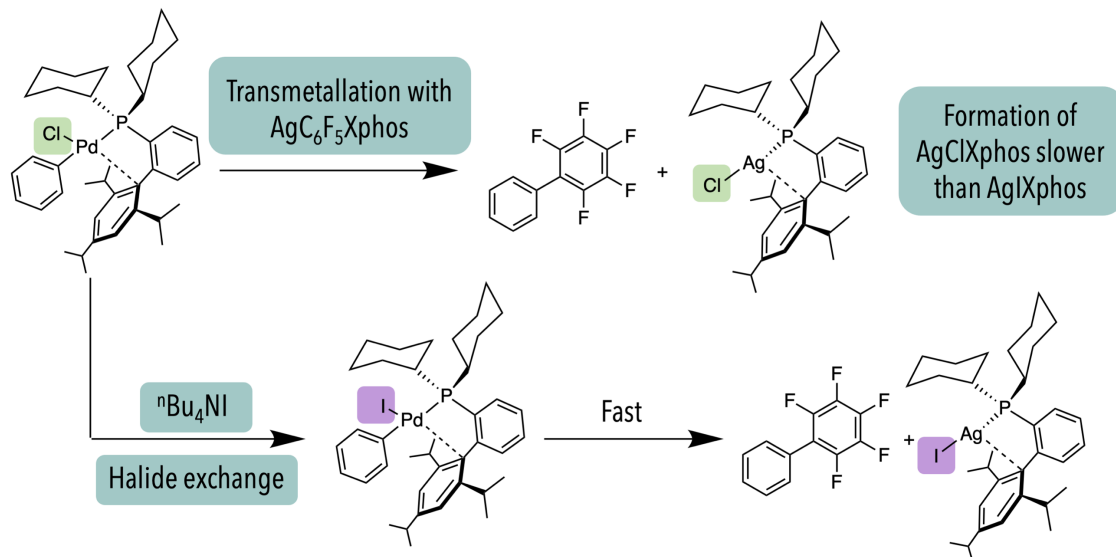
Entry	Conditions <sup>[a]</sup>	Temp. (°C)	NMR Yield (%) <sup>[b]</sup>	
			3 h	23 h
1	Pd(OAc) <sub>2</sub> (5 mol%) + PPh <sub>3</sub> (10 mol%) + Ag <sub>2</sub> CO <sub>3</sub> (5 mol%) + Cs <sub>2</sub> CO <sub>3</sub> (0.75 equiv.)	60	73	94
2	Pd(OAc) <sub>2</sub> (5 mol%) + PPh <sub>3</sub> (10 mol%) + Ag <sub>2</sub> CO <sub>3</sub> (1 mol%) + Cs <sub>2</sub> CO <sub>3</sub> (0.75 equiv.)	60	44	80
3	Pd(OAc) <sub>2</sub> (5 mol%) + Xphos (10 mol%) + Ag <sub>2</sub> CO <sub>3</sub> (0.75 equiv.)	60	96	96
4	Pd(OAc) <sub>2</sub> (5 mol%) + Xphos (10 mol%) + Ag <sub>2</sub> CO <sub>3</sub> (10 mol%) + K <sub>2</sub> CO <sub>3</sub> (0.75 equiv.)	60	60	65
5	Pd(OAc) <sub>2</sub> (5 mol%) + Xphos (5 mol%) + Ag <sub>2</sub> CO <sub>3</sub> (0.75 equiv.)	60	19	19

<sup>[a]</sup> Conditions unless shown otherwise, C<sub>6</sub>F<sub>5</sub>H (1.5 equiv.) + 4-iodotoluene (1 equiv. at 0.9 mmol scale); <sup>[b]</sup> For methods of determining NMR yields, see Experimental.

#### The use of <sup>n</sup>BuNI as an additive to access chloroarenes

Based on the reaction mechanism from **Scheme 104**, the oxidative addition into the X–C bond of the haloarenes is controlled by Pd and the ligand. Xphos has been used in numerous cross-coupling reactions to access inactivated aryl chlorides.<sup>139</sup> Thus, the complete lack of reactivity towards chloroarenes in the direct arylation reaction was rather unusual and suggests a different step within the catalytic cycle is halting catalysis. Thus, it is hypothesised that perhaps the formation of AgCl(Xphos) from the transmetallation reaction between Pd(Xphos)(Ph)Cl and Ag(C<sub>6</sub>F<sub>5</sub>)(Xphos), is very slow, hindering catalysis. Theoretically the

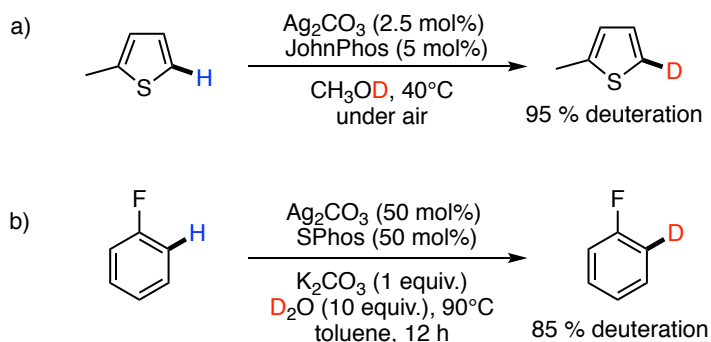
use of an additive such as *n*-tetrabutylammonium iodide  ${}^n\text{Bu}_4\text{NI}$  could react with  $\text{Pd}(\text{Xphos})(\text{Ph})\text{Cl}$  to generate  $\text{Pd}(\text{Xphos})(\text{Ph})\text{I}$  which would increase the rate of formation of  $\text{AgIXphos}$ . In addition, other additives could also be used to further optimise catalysis (Scheme 106).



**Scheme 106:** Hypothesised effect of  ${}^n\text{Bu}_4\text{NI}$  on the direct arylation reaction with chloroarene

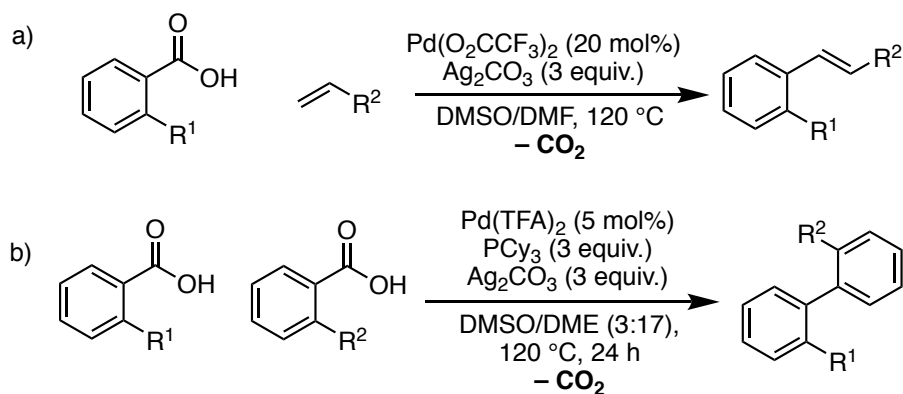
### 5.2.2 Use of the Carbonate Complex 106 and its Analogues in Catalysis

As  $\text{Ag}^{\text{I}}$  salts are proximately used in multiple catalytic systems, it would be interesting to investigate the use of **106** or the combination of  $\text{Ag}_2\text{CO}_3$  and different phosphines as either catalysts or co-catalysts in different cross-coupling reactions.<sup>73,151</sup> For instance, the combination of  $\text{Ag}_2\text{CO}_3$  and dialkybiaryl phosphines have been used as catalysts for deuteration of various fluorinated aromatics. Hartwig and co-workers have shown that an analogue of **106** with Johnphos is catalytically active for H/D exchange.<sup>94</sup> While Haung and co-workers used a combination of  $\text{Ag}_2\text{CO}_3$  with Sphos in toluene for the deuteration of various monofluorinated arenes.<sup>93</sup>



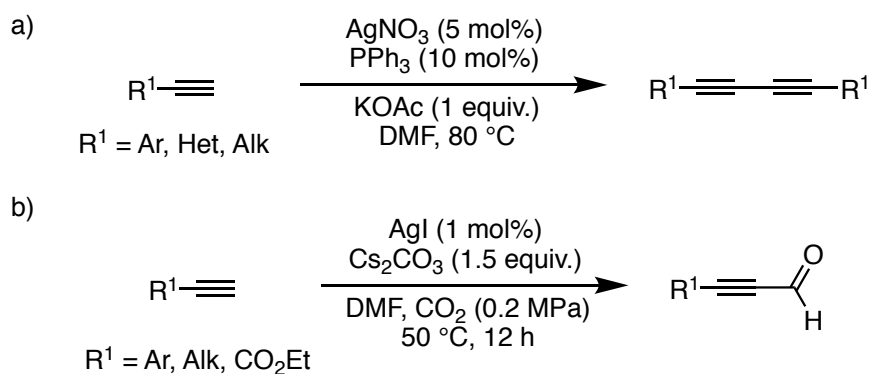
**Scheme 107:** Use of  $\text{Ag}_2\text{CO}_3$  in the deuteration reactions by a) Hartwig and co-workers<sup>94</sup> and b) Haung and co-workers.<sup>93</sup>

Ag<sup>I</sup> salts are critical additives commonly used in Pd-catalysed decarboxylative Heck-type<sup>152,153</sup> and coupling reactions<sup>154,155</sup> (**Scheme 108**). The reactions mechanism for these reactions typically involves a decarboxylation step where the carboxylic acid is released as CO<sub>2</sub> along with cross-coupling. Mechanistic studies have demonstrated the ability of Pd to mediate decarboxylation of electron-rich benzoic acids.<sup>153,156</sup> Whereas Ag is thought to be operative in the decarboxylative step in electron-deficient benzoic acids.<sup>157,158</sup>

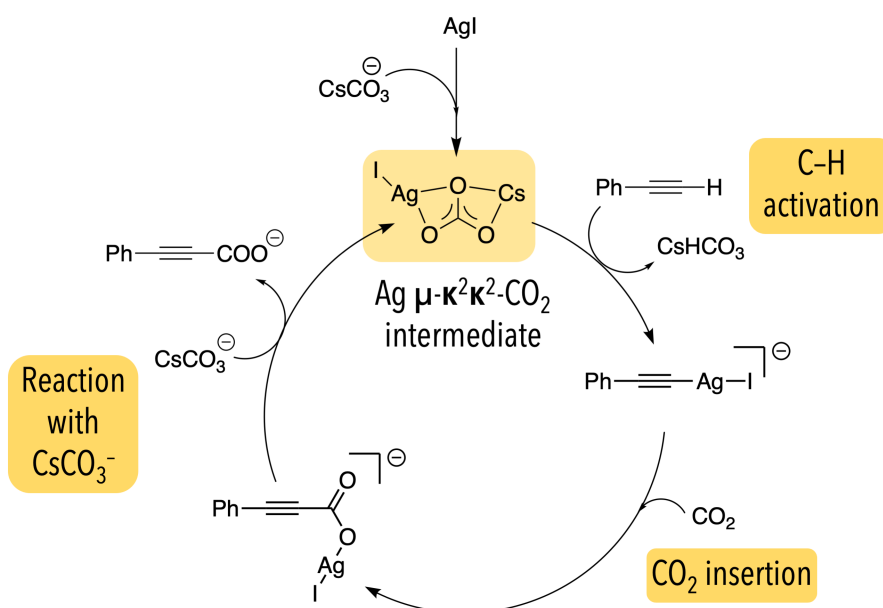


**Scheme 108:** Examples of a) Pd-catalysed decarboxylative Heck-type reaction<sup>152</sup>, b) Pd-catalysed decarboxylative heterocoupling between aryl carboxylic acids<sup>155</sup>.

Ag pre-catalysts are also prominently used in alkyne reactions. The alkynophilic nature of Ag helps promote the activation of alkynes *via*  $\pi$ -coordination of metal to the C–C triple bond. Examples of Ag<sup>I</sup> salts being used in a variety of transformations is well-known (**Scheme 109**).<sup>159</sup> Generally, reactions involving Ag<sup>I</sup> and alkynes are predominately thought to proceed *via* silver(I) acetylide intermediate. However, other reaction intermediates have also been proposed, for instance: using DFT studies Lu and co-workers found an unexpected  $\mu$ - $\kappa^2, \kappa^2$ -CO<sub>2</sub> Ag intermediate to be active in Ag-catalysed carboxylation reactions (**Scheme 110**).<sup>160</sup> A similar intermediate was calculated by Maseras and co-workers using DFT, and highlighted possibility of DMSO acting as a ligand within the system.<sup>161</sup>

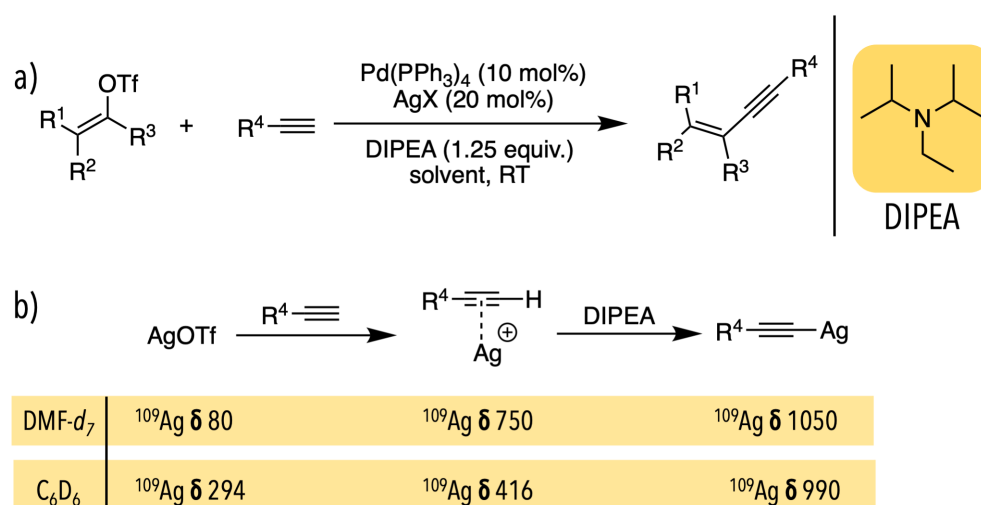


**Scheme 109:** Examples of silver-catalysed a) homocoupling reaction of (hetero)aryl/alkyl alkynes<sup>162</sup> b) ligand-free carboxylation reaction of aryl/alkyl terminal alkynes with CO<sub>2</sub>.<sup>163</sup>



**Scheme 110:** Proposed mechanism of Ag catalysed carboxylation reactions by Lu and co-workers using DFT studies<sup>160</sup>

When elucidating the role of Ag in Pd/Ag catalysed synthesis of enynes,<sup>164,165</sup> Berger and co-workers used <sup>1</sup>H, <sup>31</sup>C and <sup>109</sup>Ag NMR studies to study the reaction between various Ag<sup>I</sup> salts and alkynes. They reacted AgOTf sequentially hexyne and DIPEA and there were able to detect the  $\pi$ -coordinated alkyne-Ag intermediate and the resulting alkyn-1-yl silver complex<sup>166</sup> by <sup>109</sup>Ag NMR spectroscopy (**Scheme 111**).<sup>159</sup> Furthermore, as Pd(PPh<sub>3</sub>)<sub>4</sub> was used as the pre-catalyst, Berger and co-workers also investigated the interaction between PPh<sub>3</sub> and hexyn-1-yl silver complex and characterised the resulting complex by low-temperature <sup>109</sup>Ag and <sup>31</sup>P NMR spectroscopy.<sup>167</sup>



**Scheme 111:** a) Pd/Ag catalysed synthesis of enynes b) reaction of AgOTf with an alkyne and DIPEA and chemical shift ( $\delta$ ) to the reaction intermediates detected by <sup>109</sup>Ag NMR spectroscopy in DMF-*d*<sub>7</sub> and C<sub>6</sub>D<sub>6</sub>.<sup>159</sup>



Investigating the use of **106** and its analogues within these reactions could potentially lead to new synthetic methodology. Additionally, due to the stability of the Ag–Xphos bond makes it an ideal tool for any future mechanistic investigations.

### 5.2.3 Incorporating DFT modelling to Enhance Mechanistic Understanding

DFT studies can be used to complement the experimental work within this thesis. The crystal structures of the catalytically relevant intermediates have been determined. This can be used to model the reaction and identify key transition states. DFT studies incorporating Ag carboxylate complexes are known in the literature.<sup>86,74</sup> Thus, modelling transition state using the Ag carbonate complex **106** could also provide interesting insights. The kinetic profile of C–H activation by **106** and crystal structure is also known, and the experimental evidence could help with the refinement of the DFT model. A key question is whether the reaction of **106** with pentafluorobenzene can be described as an AMLA(6) reaction. In contrast to the Ag carbonate complex **106**, the Ag acetate complex **109** was found to be incapable at C–H activation, and it could be interesting to explore these differences by calculating the energies of the different transition states.

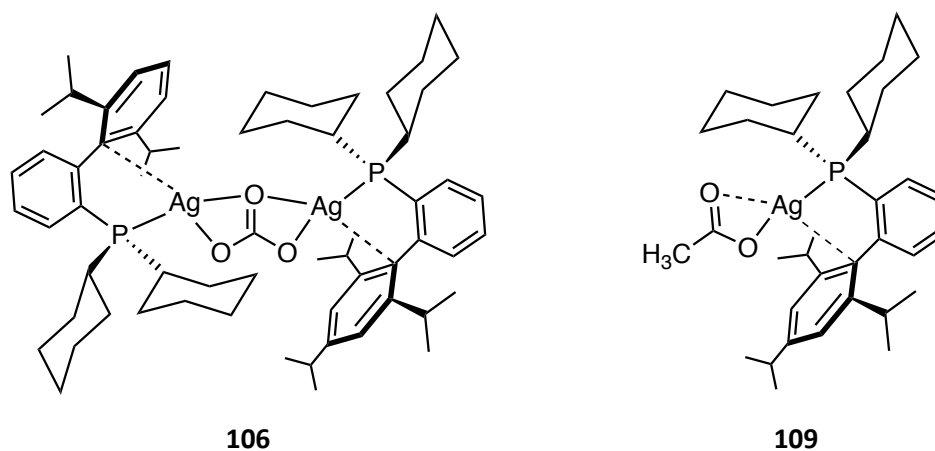


**Figure 99:** Ag carbonate complex **106** is capable of C–H activation whereas Ag acetate **109** was found to be inactive for C–H activation.

Furthermore, this work can also be used as the basis for understanding the effect of different phosphines and fluoroarenes on C–H activation by Ag. A library of different phosphine coordinated to the Ag complex has been isolated, and DFT calculations can be used to correlate ligand parameters with any trends within the data. Additionally, the crystal structures of **101** with pentafluorobenzene and **165** with 2,3,5,6-tetrafluoropyridine have been isolated. Together, this can help enhance the understanding of the effect of different phosphines and fluoroarene in the C–H activation by Ag mechanism.

## Chapter 6: Experimental

### 6.1 General Information on Instrumentation and Chemicals

#### Solvents and Reagents

All reagents were purchased from commercial sources such as Acros Organics, Alfa Aesar, Fisher Scientific, Fluorochem, Sigma-Aldrich or TCI, and were used without any further purification, unless stated otherwise. Pd(OAc)<sub>2</sub> (nitrite-free) was purchased from Precious Metals Online (note high purity Pd<sub>3</sub>(OAc)<sub>6</sub>). Iodobenzene and pentafluorobenzene were degassed using three cycles of freeze-pump-thaw and stored over activated 4 Å molecular sieves, under an atmosphere of nitrogen. Dry DMF (99.8 %, water <50 ppm) was purchased from Acros Organics and was deoxygenated by bubbling nitrogen gas for 1 hour before being stored over activated 4 Å molecular sieves. Acetonitrile was dried by refluxing over CaH<sub>2</sub> (1 week) before being distilled, transferred into an ampule, and deoxygenated by bubbling with argon gas for 30 mins. Chloroform-*d* and dichloromethane-*d*<sub>2</sub> were dried by stirring over CaH<sub>2</sub> for 48 h and degassed by three cycles of freeze-pump-thaw and distilled at high vacuum and stored under argon. Similarly, benzene-*d*<sub>6</sub> and toluene-*d*<sub>8</sub> were also dried over CaH<sub>2</sub> for 48 h and degassed by three cycles of freeze-pump-thaw and distilled at high vacuum and stored under argon. Synthesized silver and palladium complexes were stored in a -30°C freezer inside an argon-filled glovebox. All synthesized silver complexes were stored in light-protected vials wrapped in foil.

#### Reaction Conditions

Unless specified, all reactions were carried out under an inert atmosphere (Ar or N<sub>2</sub>) using either a dry argon-filled glovebox (<0.1 ppm O<sub>2</sub>) or using a standard Schlenk line (typically 10<sup>-2</sup> mbar) techniques. The standard Schlenk lines are connected to nitrogen gas taken from liquid nitrogen tanks and passed through a column of sodium hydroxide pellets and silica prior to use. All glassware required for air and moisture sensitive protocols is oven- or flame dried prior to use. Reactions using light-sensitive reagents (Ag salts and complexes) were carried out in foiled Schlenk tubes or amberized J-Young tubes. The ambient room temperature fluctuates between 21-24 °C, and room-temperature reactions were carried out without thermostatic control.

Some of the experiments pertaining to Chapter 4, were carried out in Supelco® 7 mL clear vials with a screw cap which has a hole with a PTFEE silicone septa. When required reactions in these vials were heated using a 7 well aluminium heating block set to the desired temperature.

### Nuclear Magnetic Resonances (NMR) Spectroscopy

Solution NMR spectra were recorded using a Bruker AVIHD 500 instrument ( $^1\text{H}$  500 MHz,  $^{31}\text{C}$  125 MHz,  $^{31}\text{P}$  202 MHz,  $^{19}\text{F}$  470 MHz) or JEOL ECX400 or JEOL ECS400 spectrometer ( $^1\text{H}$  400 MHz,  $^{31}\text{C}$  101 MHz,  $^{31}\text{P}$  162 MHz,  $^{19}\text{F}$  376 MHz). The  $^1\text{H}$  chemical shifts are quoted in parts per million (ppm,  $\delta$ ) and are referenced to the residual protio solvent resonances of the deuterated solvent. Carbon-13 NMR spectra were internally referenced to solvent resonances used and are reported to one decimal place. Fluorine-19 NMR spectra were externally referenced to  $\text{CFCl}_3$ . Phosphorus-31 NMR spectra were externally referenced to  $\text{H}_3\text{PO}_4$ . The  $^{31}\text{P}\{^{109}\text{Ag}\}$  and  $^{31}\text{P}\{^{109}\text{Ag}\}\text{-}^{109}\text{Ag}$  HMQC spectra were recorded on a Bruker Avance 400 MHz instrument on a TXI probe with an *HMQCGP* sequence for  $^{31}\text{P}\{^{109}\text{Ag}\}\text{-}^{109}\text{Ag}$  HMQC without  $^1\text{H}$  decoupling. The  $^{109}\text{Ag}$  resonance is referenced to aqueous  $\text{AgNO}_3$  at  $\delta$  0.

Inversion recovery experiments were used to determine  $T_1$  values, using the standard Bruker *tlir* and *tlrig* pulse programs for  $^{19}\text{F}$  and  $^{31}\text{P}$  respectively. The relaxation delay,  $d_1$ , was set to 30 s. The results were analysed using MestReNova, where the 1D peak integral graphs were fitted to a three-parameter exponential fit  $B + F \cdot \exp(-x \cdot G)$  ( $I(t) = I^0 + P \cdot \exp(-t/T_1)$ ,  $G^{-1} = T_1$ ).

2D and 1D EXSY spectra were recorded on the Bruker AVIHD 500 instrument using the *noesygpphpp* and *selnospig* pulse program. A range of different mixing times,  $d_8$ , were recorded for EXSY experiments. The mixing times ( $d_8$ ) and relaxation delay ( $d_1$ ) used are discussed in the EXSY experiments section.

### Mass Spectrometry

EI and LIFDI mass spectrometry were carried out on a JEOL T200 AccuTOF GCx-Plus and Agilent 7890B GC instrument. ESI mass spectrometry was carried out on a Bruker compact MS – Agilent 1260 infinity series LC. Mass spectra are listed for  $^{107}\text{Ag}$  and  $^{107}\text{Ag}^{109}\text{Ag}$ , in the case of dimers.

### Single crystal X-ray diffraction

Diffraction data were collected at 110 K on an Oxford Diffraction SuperNova diffractometer with  $\text{Cu-K}\alpha$  radiation ( $\lambda = 1.54184 \text{ \AA}$ ) using a EOS CCD camera. The crystal was cooled with an Oxford Instruments Cryojet. Diffractometer control, data collection, initial unit cell determination, frame integration and unit-cell refinement were carried out with “CrysAlis”.<sup>168</sup> Face-indexed absorption corrections were applied using spherical harmonics, implemented in SCALE3 ABSPACK scaling algorithm.<sup>169</sup> OLEX2<sup>c</sup> was used for overall structure solution, refinement and preparation of computer graphics and publication data. Within OLEX2, the algorithm used for structure solution was “ShelXT dual-space”.<sup>170</sup> Refinement by full-matrix least-squares used the SHELXL-97<sup>171</sup> algorithm within OLEX2.<sup>170</sup>

All non-hydrogen atoms were refined anisotropically. Hydrogen atoms were placed using a “riding model” and included in the refinement at calculated positions.

For **90**, the bicarbonate hydrogens were each disordered over two sites related by a mirror plane. The O-H bond lengths for these bicarbonates were fixed at 0.825, this being the average distance determined when these hydrogens were located by difference map.

For **101**, one of the isopropyl groups was disordered with the methyl groups being modelled in two positions of equal occupancy.

For **106**, one of the cyclohexyl groups was disordered and modelled over two positions with refined occupancies of 0.652:0.348(4). With the disordered cyclohexyl group, the Atomic Displacement Parameters (ADPs) of adjacent atoms were constrained to be equal. The acetonitrile was disordered and modeled in three positions. One position had the carbons and nitrogen on special positions and the other two were related by a symmetry rotation.

For **105**, the dichloromethane was disordered with the carbon and one chlorine modelled in two positions with refined occupancies of 0.78:0.22(2). The C-Cl bond-lengths were restrained to be the same and the ADP of the carbons were constrained to be equal.

For **109**, the structure exhibited disorder of both the silver acetate and one of the isopropyl groups modelled in two positions. In addition, there was a partial occupied water distributed over 3 sites. The silver acetate was modelled in two positions in refined occupancies of 0.9305:0.0695(16). The ADPs of equivalent pairs of disordered atoms were constrained to be equal (Ag1 & Ag1a, C1 & C1a, C2 & C2a, O1 & O1a, O2 & O2a). The C-O bond lengths were constrained to be equal (C1-O1 & C1a-O1a) as were the C=O bond lengths (C1=O2 & C1a=O2a). One isopropyl was modelled in two positions with refined occupancies of 0.579:0.421(6). The ADP of two pairs of disordered carbons were constrained to be equal (C18 & C18A, C20 & C20A). A partially-occupied disordered water was modelled in three positions with occupancies of 0.480(6), 0.162(4) & 0.162(4), the latter two occupancies being constrained to be the same.

For **165**, one of the isopropyl groups was disordered and modelled in two positions with refined occupancies of 0.516:0.484(5). The ADPs of C21a and C21b were constrained to be equal.

### Flash Chromatography

Merck aluminum backed TLC plates with silica gel 60 F254 were used for thin layer chromatography (TLC) and the spots were visualized under ultraviolet lights ( $\lambda_{max} = 254$  nm). Retention factors ( $R_f$ ) are reported to two decimal places with the solvent system used for purification. High purity grade silica gel from Sigma-Aldrich (Pore size 60 Å, 220 – 440 mesh particle size, 35 – 75  $\mu\text{m}$  particle size) was used for flash column chromatography.

## 6.2 General Experimental Procedures

### General Procedure A: Synthesis of Fluorinated Biaryls with Solid Aryl Halides

To a light-protected air-tight vial equip with a stirrer bar, Pd(OAc)<sub>2</sub> (10 mg, 0.045 mmol, 5 mol%) Xphos (43 mg, 0.09 mmol, 0.1 equiv.), Ag<sub>2</sub>CO<sub>3</sub> (186 mg, 0.68 mmol, 0.75 equiv.) and the solid aryl halide (0.9 mmol, 1 equiv.) were added. The vial cap with silicone septum was screwed on and the vial was purged with nitrogen for 10 minutes. Then, dry DMF (2.6 mL) and pentafluorobenzene (227 mg, 1.35 mmol, 1.5 equiv., 150  $\mu$ L) were added and the reaction mixture was placed in a pre-heated aluminium heated block at the desired temperature. After 23 h, deionized water (40 mL) was added, and the reaction mixture was extracted with ethyl acetate (80 mL  $\times$  1, 40 mL  $\times$  2). The combined organic layer was dried over Na<sub>2</sub>SO<sub>4</sub>, filtered and the solvent was removed under reduced pressure to give the crude product.

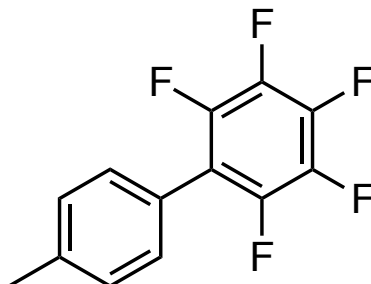
### General Procedure B: Synthesis of Fluorinated Biaryls with Liquid Aryl Halides

To a light-protected air-tight vial equip with a stirrer bar, Pd(OAc)<sub>2</sub> (10 mg, 0.045 mmol, 5 mol%) Xphos (43 mg, 0.09 mmol, 0.1 equiv.), Ag<sub>2</sub>CO<sub>3</sub> (186 mg, 0.68 mmol, 0.75 equiv.) were added. The vial cap with silicone septum was screwed on and the vial was purged with nitrogen for 10 minutes. Then, dry DMF (2.6 mL), the liquid aryl halide (0.9 mmol, 1 equiv.) and pentafluorobenzene (227 mg, 1.35 mmol, 1.5 equiv., 150  $\mu$ L) were added and the reaction mixture was placed in a pre-heated aluminium heated block at the desired temperature. After 23 h, deionized water (40 mL) was added, and the reaction mixture was extracted with ethyl acetate (80 mL  $\times$  1, 40 mL  $\times$  2). The combined organic layer was dried over Na<sub>2</sub>SO<sub>4</sub>, filtered and the solvent was removed under reduced pressure to give the crude product.

## 6.3 Synthetic Procedures and Characterization of Compounds

### 6.3.1 Synthesis and characterization of Organic Compounds

#### Synthesis of 2,3,4,5,6-pentafluoro-4'-(methyl) biphenyl (**18**)



In a light-protected Schlenk tube,  $\text{PPh}_3$  (50 mg, 0.2 mmol, 0.1 equiv.),  $\text{Pd}(\text{OAc})_2$  (21 mg, 0.1 mmol, 0.05 equiv.) and  $\text{Ag}_2\text{CO}_3$  (388 mg, 1.4 mmol, 0.75 equiv.) were added and the Schlenk tube was evacuated and refilled with nitrogen three times. The 4-iodotoluene **26** (414 mg, 1.9 mmol, 1 equiv.) was added against a positive flow of nitrogen, followed by the pentafluorobenzene **17** (477 mg, 315  $\mu\text{L}$ , 2.8 mmol, 1.5 equiv.) which was transferred using a gas-tight microsyringe (500  $\mu\text{L}$ ), and DMF (5.2 mL). The Schlenk tube was then submerged in a pre-heated oil bath (60  $^\circ\text{C}$ ) for 21 hours, under an atmosphere of nitrogen. Once the reaction mixture had cooled down to ambient temperature, deionized water (50 mL) was added and the aqueous layer was extracted with EtOAc (80 mL  $\times$  1, 40 mL  $\times$  2). The organic layer was dried over  $\text{Na}_2\text{SO}_4$ , filtered and the solvent was removed using rotatory evaporation. The product was purified using flash column chromatography ( $\text{SiO}_2$ ,  $R_f = 0.49$ , petroleum ether 40-60  $^\circ\text{C}$ ) to yield **18** as a white crystalline solid (402 mg, 82%).

(Lab book reference number: GA-1-029)

A light-protected Schlenk tube with  $\text{Ag}_2\text{CO}_3$  (186 mg, 0.68 mmol, 0.75 equiv.),  $\text{Pd}(\text{OAc})_2$  (10 mg, 0.045 mmol, 0.05 equiv., 5 mol%) and Xphos (43 mg, 0.09 mmol, 0.1 equiv., 10 mol%) was evacuated and refilled three times with nitrogen. To this, 4-iodotoluene **26** (196 mg, 0.9 mmol, 1 equiv.) was added followed by DMF (2.6 mL) and pentafluorobenzene **17** (227 mg, 1.35 mmol, 1.5 equiv., 150  $\mu\text{L}$ ) were added under the flow of nitrogen. The mixture was heated at 60  $^\circ\text{C}$  for 3 h under a gentle flow of nitrogen. The reaction mixture was cooled to ambient temperature and extracted with EtOAc (80 mL) and deionized water (40 mL). The aqueous layer was then extracted with EtOAc (2  $\times$  40 mL), which were then combined, dried over  $\text{Na}_2\text{SO}_4$ , and vacuum filtered through a cotton plug. The solvent was removed under

vacuum to give the crude product. Purification by flashchromatography ( $\text{SiO}_2$ ,  $R_f = 0.42$ , petroleum ether  $40^\circ\text{C}$ – $60^\circ\text{C}$ ) afforded **18** (196 mg, 84 %) as a white crystalline solid.

(Lab book reference number: GA-3-184)

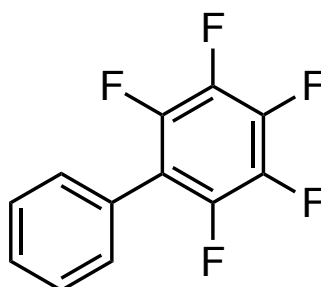
IR:  $\nu_{\text{max}}/\text{cm}^{-1}$  (ATR) 3030 (C–H aromatic str.), 2930 ( $\text{CH}_3$  str.), 1653 (C=C aromatic str.), 1484 (C=C aromatic str.), 1054 (C–F str.), 976 (=C–H in-plane bend), 824 (=C–H *oop* bend);

NMR:  $^1\text{H}$  (400 MHz, 16 scans,  $\text{C}_6\text{D}_6$ ):  $\delta = 7.10$  (2 *H*, d,  $J = 8.1$  Hz, 2',6'-H), 6.91 (2 *H*, d,  $J = 7.9$  Hz, 3',5'-H), 2.06 (3 *H*, s, 4'- $\text{CH}_3$ );

$^{19}\text{F}$  (376 MHz,  $\text{C}_6\text{D}_6$ ):  $-144.1$  (2 *F*, dd,  $J = 23.6, 8.0$  Hz, 2,6-F),  $-156.7$  (1 *F*, t,  $J = 21.6$  Hz, 4-F),  $-162.8$  (2 *F*, td,  $J = 23.3, 8.0$  Hz, 3,5-F);

MS (EI)  $m/z$  (%) 258.04681 ( $[\text{M}]^+$ , 100) ( $\text{C}_{13}\text{H}_7\text{F}_5$  requires 258.0468, diff 0.00001).

The analytical data obtained was in agreement with literature.<sup>35,172</sup>

Synthesis of 2,3,4,5,6-pentafluorobiphenyl (**28**)

Iodobenzene **96** (184 mg, 0.9 mmol, 1 equiv., 100  $\mu$ L) was reacted with pentafluorobenzene **17** (227 mg, 1.35 mmol, 1.5 equiv., 150  $\mu$ L) at 60  $^{\circ}$ C following **General Procedure B**. The product was purified by flash chromatography ( $\text{SiO}_2$ ,  $R_f = 0.35$ , petroleum-ether 40–60  $^{\circ}$ C) to give the product **28** (162.6 mg, 74 %) as a white crystalline solid.

IR:  $\nu_{max}/\text{cm}^{-1}$  (ATR) 1652 (–C=C– ring str.), 1487 (C=C aromatic str.), 1060 (aryl C–F str.), 976 (=C–H in-plane bend), 848 (=C–H *oop* bend), 743 (mono sub. *oop*), 693 (mono sub. *oop*);

NMR:  $^1\text{H}$  (500 MHz,  $\text{CDCl}_3$ , 25  $^{\circ}$ C):  $\delta = 7.10$  (2 H, d,  $J = 8.1$  Hz, 2',6'-H), 6.91 (2 H, d,  $J = 7.9$  Hz, 3',5'-H), 2.06 (3 H, s, 4'- $\text{CH}_3$ );

$^{13}\text{C}\{^1\text{H}\}$  NMR (126 MHz,  $\text{CDCl}_3$ , 25  $^{\circ}$ C): 144.3 (dm,  $^1J_{CF} = 247.7$  Hz, CF), 140.5 (dm,  $^1J_{CF} = 253.9$  Hz, 4-CF), 138.0 (dm,  $^1J_{CF} = 250.4$  Hz, CF), 130.3 (t,  $J = 1.9$  Hz, 3',5'-CH), 129.5 (s, 4'-CH);

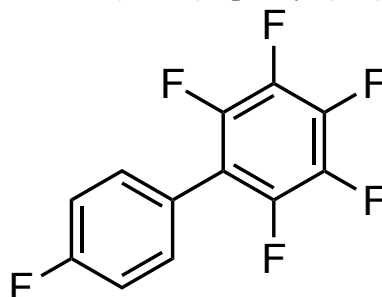
$^{19}\text{F}\{^1\text{H}\}$  NMR (471 MHz,  $\text{CDCl}_3$ , 25  $^{\circ}$ C)  $\delta -143.2$  (2 F, dd,  $J = 22.9, 8.2$  Hz, 2,6-F),  $-155.6$  (1 F, t,  $J = 20.9$  Hz, 4-F),  $-162.3$  (2 F, m, 3,5-F);

MS (EI)  $m/z$  (%) 244.03005 ( $[\text{M}]^+$ , 100) ( $\text{C}_{12}\text{H}_5\text{F}_5$  requires 244.03059, diff 0.00054).

The analytical data obtained was in agreement with literature.<sup>35,172</sup>

(Lab book reference number: GA-5-428)



**Synthesis of 2,3,4,5,6-pentafluoro-4'-(fluoro)biphenyl (134)**

1-fluoro-4-iodobenzene **167** (200 mg, 0.9 mmol, 1 equiv., 104  $\mu$ L) was reacted with pentafluorobenzene **17** (227 mg, 1.35 mmol, 1.5 equiv., 150  $\mu$ L) at 60  $^{\circ}$ C following **General Procedure B**. The crude product was purified by manual flash chromatography ( $\text{SiO}_2$ ,  $R_f = 0.30$ , hexanes) to give the product **134** (116.3 mg, 49 %) as a white crystalline solid.

(Lab book reference number: GA-5-429)

1-fluoro-4-iodobenzene **167** (200 mg, 0.9 mmol, 1 equiv., 104  $\mu$ L) was reacted with pentafluorobenzene **17** (227 mg, 1.35 mmol, 1.5 equiv., 150  $\mu$ L) at 100  $^{\circ}$ C following **General Procedure B**. The crude product was purified by automated flash chromatography ( $\text{SiO}_2$ ,  $R_f = 0.34$ , hexanes) to give the product **134** (187.8 mg, 80 %) as a white crystalline solid.

(Lab book reference number: GA-6-528)

IR:  $\nu_{max}/\text{cm}^{-1}$  (ATR) 2951 (C–H aromatic str.), 1603 (C=C aromatic str.), 1225 (aryl C–F), 1488 (C=C aromatic str.), 1064, 980, 842 (para disub. aromatic =C–H *oop*);

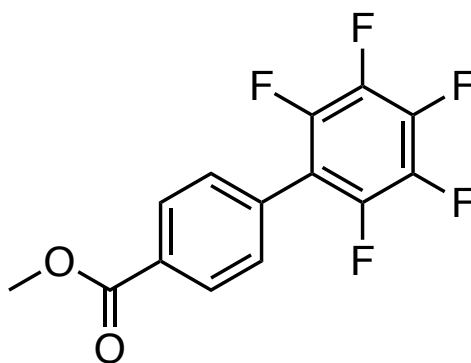
NMR:  $^1\text{H}$  NMR (500 MHz,  $\text{CDCl}_3$ , 25  $^{\circ}$ C)  $\delta$  7.41 (2 H, m, 3',5'-H), 7.19 (2 H, m, 2',6'-H);

$^{13}\text{C}\{^1\text{H}\}$  NMR (126 MHz,  $\text{CDCl}_3$ , 25  $^{\circ}$ C):  $\delta$  163.3 (dm,  $^1J_{CF} = 249.9$  Hz, 4'-CF<sub>3</sub>), 144.3 (dm,  $J = 247.8$  Hz, 2,6-CF), 140.6 (dm,  $J = 254.5$  Hz, 4-CF), 138.2 (dm,  $J = 250.8$  Hz, 3,5-CF), 132.2 (td,  $J = 8.5, 2.3$  Hz, 3',5'-C), 116.1 (d,  $J = 21.9$  Hz, 2',6'-C);

$^{19}\text{F}\{^1\text{H}\}$  NMR (471 MHz,  $\text{CDCl}_3$ , 25  $^{\circ}$ C)  $\delta$  -111.3 (1 F, tt,  $J = 8.6, 5.2$  Hz, 4'-F), -143.3 (2 F, dd,  $J = 22.9, 8.2$  Hz, 2,6-F), -155.2 (1 F, t,  $J = 20.9$  Hz, 4-F), -162.0 (2 F, m, 3,5-F);

MS (EI)  $m/z$  (%) 262.02047 ([M]<sup>+</sup>, 100) ( $\text{C}_{12}\text{H}_4\text{F}_6$  requires 262.02117, diff 0.0007).

The analytical data obtained was in agreement with literature.<sup>35,172</sup>

Synthesis of methyl 2',3',4',5',6'-pentafluorobiphenyl-4-carboxylate (**140**)

Methyl-4-iodobenzoate **168** (235.8 mg, 0.9 mmol, 1 equiv.) was reacted with pentafluorobenzene **17** (227 mg, 1.35 mmol, 1.5 equiv., 150  $\mu$ L) at 100  $^{\circ}$ C following **General Procedure A**. The crude product was purified by automated flash chromatography ( $\text{SiO}_2$ ,  $R_f = 0.42$ , EtOAc:hexanes (20:80)) to give the product **140** (178.6 mg, 66 %) as a white flaky solid.

IR:  $\nu_{\text{max}}/\text{cm}^{-1}$  (ATR) 2963 (C–H aromatic str.), 2847 (C–H aromatic str.), 1727 (C=O str.), 1653 (–C=C– aromatic str.), 1484 (–C=C– aromatic str.), 1437, 1278 (aryl C–F str.), 980, 960, 856 (para disub. aromatic =C–H *oop* bend), 815, 754;

NMR:  $^1\text{H}$  (500 MHz,  $\text{CDCl}_3$ , 25  $^{\circ}$ C):  $\delta$  8.16 (2 H, m, 3,5-H), 7.51 (2 H, m, 2,6-H), 3.96 (3 H, s,  $\text{CH}_3$ );

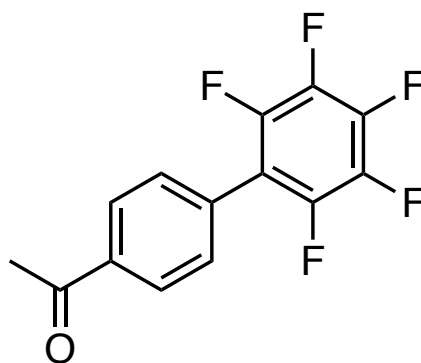
$^{13}\text{C}\{^1\text{H}\}$  NMR (126 MHz,  $\text{CDCl}_3$ , 25  $^{\circ}$ C):  $\delta$  166.4 (s, C=O), 144.1 (dm,  $^1J_{\text{CF}} \approx 255.1$  Hz, CF), 140.8 (dm,  $^1J_{\text{CF}} \approx 258.7$  Hz, CF), 137.8 (dm,  $^1J_{\text{CF}} \approx 246.8$  Hz, CF), 130.9 (s, 4-C), 130.2 (t,  $J = 2.3$  Hz, 3,5-CH), 129.9 (s, 2,6-CH), 52.4 (s,  $\text{CH}_3$ );

$^{19}\text{F}\{^1\text{H}\}$  NMR (471 MHz,  $\text{CDCl}_3$ , 25  $^{\circ}$ C)  $\delta$  –142.8 (2 F, dd,  $J = 22.9, 8.2$  Hz, 2,6-F), –154.1 (1 F, t,  $J = 20.9$  Hz, 4-F), –161.6 (2 F, m, 3,5-F);

MS (EI)  $m/z$  (%) 302.03486 ( $[\text{M}]^+$ , 43) ( $\text{C}_{14}\text{H}_7\text{F}_5\text{O}_2$  requires 302.03607, diff 0.00121), 271.01694 ( $[\text{M} - \text{CH}_3\text{O}]^+$ , 100) ( $\text{C}_{13}\text{H}_4\text{F}_5\text{O}$  requires 271.0182, diff 0.00126).

The analytical data obtained was in agreement with literature.<sup>172</sup>

(Lab book reference number: GA-6-518)

**Synthesis of 1-(2',3',4',5',6'-pentafluoro-[1,1'-biphenyl]-4-yl)ethan-1-one (143)**


4-iodoacetophenone **169** (221 mg, 0.9 mmol, 1 equiv.) was reacted with pentafluorobenzene **17** (227 mg, 1.35 mmol, 1.5 equiv., 150  $\mu$ L) at 100  $^{\circ}$ C following **General Procedure A**. The crude product was purified by automated flash chromatography (SiO<sub>2</sub>, R<sub>f</sub> = 0.36, EtOAc:hexanes (20:80)) to give the product **143** (138.6 mg, 54 %) as an off-white flaky solid.

IR:  $\nu_{max}/\text{cm}^{-1}$  (ATR) 2922 (C–H str.), 2855 (C–H str.), 1682 (conj. C=O), 1486 (–C=C– aromatic str.), 1266 (aryl C–F str.), 1062, 983 (=C–H *oop*), 856 (para disub. aromatic =C–H *oop* bend), 838;

NMR: <sup>1</sup>H NMR (500 MHz, CDCl<sub>3</sub>, 25  $^{\circ}$ C)  $\delta$  8.08 (2 H, m, 3,5-H), 7.54 (2 H, m, 2,6-H), 2.66 (3 H, s, CH<sub>3</sub>);

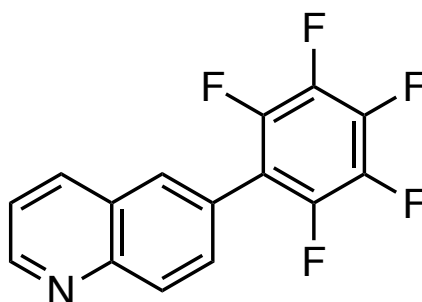
<sup>13</sup>C{<sup>1</sup>H} NMR (126 MHz, CDCl<sub>3</sub>, 25  $^{\circ}$ C):  $\delta$  197.5 (s, C=O), 144.2 (dm, <sup>1</sup>J<sub>CF</sub>  $\approx$  248.3 Hz, CF), 141.1 (dm, <sup>1</sup>J<sub>CF</sub>  $\approx$  255.0 Hz, 4-CF), (dm, <sup>1</sup>J<sub>CF</sub>  $\approx$  251.3 Hz, CF), 137.6 (s, 4-C), 130.6 (t, J = 2.3 Hz, 3,5-CH), 128.7 (s, 2,6-CH), 26.8 (s, CH<sub>3</sub>);

<sup>19</sup>F{<sup>1</sup>H} NMR (471 MHz, CDCl<sub>3</sub>, 25  $^{\circ}$ C)  $\delta$  – 142.8 (2 F, dd, J = 22.6, 8.3 Hz, 2,6-F), – 154.0 (1 F, t, J = 20.9 Hz, 4-F), –161.5 (2 F, m, 3,5-F);

MS (EI) *m/z* (%) 286.04001 ([M]<sup>+</sup>, 25) (C<sub>14</sub>H<sub>7</sub>F<sub>5</sub>O requires 286.04116, diff 0.00115), 271.01666 ([M – CH<sub>3</sub>]<sup>+</sup>, 100) (C<sub>13</sub>H<sub>4</sub>F<sub>5</sub>O requires 271.0182, diff 0.00154), 243.02180 ([M – C<sub>2</sub>H<sub>3</sub>O]<sup>+</sup>, 25) (C<sub>12</sub>H<sub>4</sub>F<sub>5</sub> requires 243.0233, diff 0.0015)

The analytical data obtained was in agreement with literature.<sup>173</sup>

(Lab book reference number: GA-6-519)

Synthesis of 6-(perfluorophenyl)quinoline (**148**)

6-Iodoquinoline **170** (230 mg, 0.9 mmol, 1 equiv.) was reacted with pentafluorobenzene **17** (227 mg, 1.35 mmol, 1.5 equiv., 150  $\mu$ L) at 100 °C following **General Procedure A**. The crude product was purified by automated flash chromatography (SiO<sub>2</sub>, R<sub>f</sub> = 0.12, EtOAc:hexanes (20:80)) to give the product **148** (132 mg, 50 %) as an off-white flaky solid.

IR:  $\nu_{max}/\text{cm}^{-1}$  (ATR) 2918 (C–H str.), 2863 (C–H str.), 1652 (C=C aromatic str.), 1592, 1484 (C=C aromatic str.), 1460, 1354, 1050 (aryl C–F), 1021, 978, 964, 897, 846, 801, 787, 619;

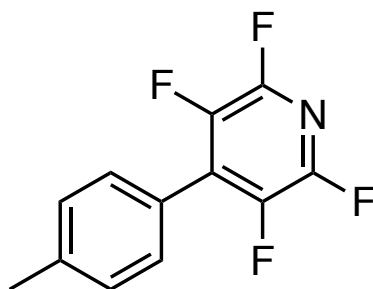
NMR: <sup>1</sup>H NMR (500 MHz, CDCl<sub>3</sub>, 25 °C)  $\delta$  9.01 (1 H, dd,  $J$  = 4.3, 1.7 Hz), 8.4 – 8.1 (2 H, m), 7.93 (1 H, q,  $J$  = 1.5 Hz), 7.74 (1 H, dq,  $J$  = 8.8, 1.7 Hz), 7.49 (1 H, dd,  $J$  = 8.3, 4.2 Hz).

<sup>19</sup>F{<sup>1</sup>H} NMR (471 MHz, CDCl<sub>3</sub>, 25 °C)  $\delta$  – 142.9 (2 F, dd,  $J$  = 22.9, 8.2 Hz, 2,6-F), – 154.5 (1 F, t,  $J$  = 20.9 Hz, 4-F), – 161.7 (2 F, td,  $J$  = 22.5, 8.1 Hz, 3,5-F);

MS (EI)  $m/z$  (%) 295.04058 ([M]<sup>+</sup>, 100) (C<sub>15</sub>H<sub>6</sub>F<sub>5</sub>N requires 295.04149, diff 0.00091).

The analytical data obtained was in agreement with literature.<sup>174</sup>

(Lab book reference number: GA-6-520)

Synthesis of 2,3,5,6-tetrafluoro-4-[4-methylphenyl]pyridine (**158**)

4-Iodotoluene **26** (196 mg, 0.9 mmol, 1 equiv.) was reacted with 2,3,5,6-tetrafluoropyridine **67** (203 mg, 1.35 mmol, 1.5 equiv., 136  $\mu\text{L}$ ) at 60  $^{\circ}\text{C}$  following **General Procedure A**. The reaction was only carried out for 3 h. The crude product was purified by manual flash chromatography ( $\text{SiO}_2$ ,  $R_f = 0.42$ , pet ether:diethylether (90:10)) to give the product **158** (161.2 mg, 74 %) as a white flaky solid.

IR:  $\nu_{\text{max}}/\text{cm}^{-1}$  (ATR) 2928 (C–H str.), 2863 (C–H str.), 1641 (C=C aromatic str.), 1445 (C=C aromatic str.), 1403, 1286 (aryl C–F str.), 1146, 942, 815 (para disub. aromatic =C–H *oop* bend);

NMR:  $^1\text{H}$  NMR (500 MHz,  $\text{CDCl}_3$ , 25  $^{\circ}\text{C}$ )  $\delta$  7.43 (2 H, m, 3,5-H), 7.35 (2 H, m, 2,6-H), 2.45 (3 H, s,  $-\text{CH}_3$ );

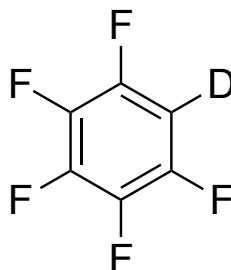
$^{13}\text{C}\{^1\text{H}\}$  NMR (126 MHz,  $\text{CDCl}_3$ , 25  $^{\circ}\text{C}$ )  $\delta$  120.8 (dm,  $^1J_{\text{CF}} \approx 244.9$  Hz, CF), 117.8 (2, 3,5-CH), 116.1 (dm,  $^1J_{\text{CF}} \approx 257.0$  Hz, CF), 110.4 (tm,  $^2J_{\text{CF}} \approx 14.8$  Hz, 4-C of tetrafluoropyridine ring), 106.5 (s, 2,6-CH), 99.8 (s, quat C of phenyl ring),  $-1.7$  (s,  $-\text{CH}_3$ )

$^{19}\text{F}\{^1\text{H}\}$  NMR (471 MHz,  $\text{CDCl}_3$ , 25  $^{\circ}\text{C}$ )  $\delta$   $-19.1$  (2 F, m, 2,6-F),  $-145.4$  (2 F, m, 3,5-F);

MS (EI)  $m/z$  (%) 241.05000 ( $[\text{M}]^+$ , 100) ( $\text{C}_{12}\text{H}_7\text{F}_4\text{N}$  requires 241.0515, diff 0.0015).

The analytical data obtained was in agreement with literature.<sup>34</sup>

(Lab book reference number: GA-5-357)

Synthesis of Pentafluorodeuterobenzene (69)<sup>129</sup>

To a three-neck round bottom flask (500 mL) was fitted with a condenser, dropping flask (150 mL), and an adaptor to connect to the Schlenk-line. Magnesium-turnings (5.50 g, 0.23 mol, 1.4 equiv.) and dry diethylether (160 mL) were sequentially added to a three-neck round bottom flask under an atmosphere of nitrogen. The reaction was then cooled to 0 °C and initiated by the dropwise addition of pentafluorobromobenzene (40 g, 0.16 mol, 1 equiv., 20 mL). The reaction mixture was then stirred at room temperature for 2 h. D<sub>2</sub>O (15 g, 0.77 mol, 4.8 equiv., 14 mL) was added to the dark brown reaction mixture and for stirred for 30 min, and the organic layer was separated, dried over Mg<sub>2</sub>SO<sub>4</sub> and filtered. Most of the solvent was removed on the rotary evaporator and purified by simple distillation under nitrogen at 100 °C. The product was obtained as a clear colourless liquid (9.25 g, 6 mL, 34 %).

B.p 86 °C (760 mmHg);

NMR: <sup>2</sup>H (76 MHz, tol (non-deuterated), 25 °C) δ 5.97 (s);

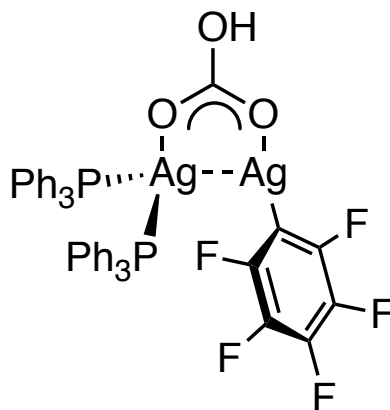
<sup>19</sup>F{<sup>1</sup>H} (470.6 MHz, CDCl<sub>3</sub>, 25°C): δ -138.7 (2 F, dd, *J* = 22.1, 8.3 Hz, 2,6-F), -153.5 (1 F, t, *J* = 20.1 Hz, 4-F), -161.9 (2 F, td, *J* = 21.2, 8.5 Hz, 3,5-F);

<sup>13</sup>C{<sup>1</sup>H} NMR (126 MHz, CD<sub>3</sub>CN, 25 °C): δ 146.2 (dm, *J* = 248.9, 11.7, 4.2 Hz, CF), 141.8 (dtt, *J* = 254.2, 13.3, 5.3 Hz, CF), 137.6 (dm, *J* ≈ 251 Hz, CF), 100.0 (qui of m, CD).

This compound was synthesized using a literature procedure. The analytical data obtained was in agreement with the literature.<sup>129</sup>

(Lab book reference number: GA-4-277)

## 6.3.1 Synthesis and characterization of Organometallic Complexes

Attempted Synthesis of  $\text{Ag}_2(\text{PPh}_3)_2(\text{C}_6\text{F}_5)(\mu_2\text{-HCO}_3)$  (91)

In an oven-dried Schlenk tube,  $\text{Ag}_2\text{CO}_3$  (139 mg, 0.5 mmol, 1 equiv.) and  $\text{PPh}_3$  (262 mg, 0.5 mmol, 1 equiv.) were added and the Schlenk tube was evacuated and refilled three times with nitrogen. Dry  $\text{CH}_3\text{CN}$  (5 mL) was added, and the reaction mixture was submerged in a pre-heated oil bath ( $80^\circ\text{C}$ ) before  $\text{C}_6\text{F}_5\text{H}$  (840 mg, 5 mmol,  $555\ \mu\text{L}$ , 10 equiv.) was added. After 3 h, the reaction mixture was allowed to cool down to room temperature, and the solvent and excess  $\text{C}_6\text{F}_5\text{H}$  was removed under reduced pressure to yield the product (322.4 mg)<sup>[a]</sup> as a peach coloured solid. The solid (100 mg) was dissolved in hot acetonitrile ( $80^\circ\text{C}$ ) and then gradually cooled to  $-18\ ^\circ\text{C}$  to yield the product as dark brown crystals (81.2 mg).<sup>[b]</sup> Crystal suitable for X-ray diffraction were isolated from a saturated solution of Acetonitrile.

NMR:  $^1\text{H}$  NMR (500 MHz, 16 scans,  $\text{C}_6\text{D}_6$ ,  $25.0\ ^\circ\text{C}$ ):  $\delta = 7.37$  (12 H, m,  $\text{PPh}_3$ ), 6.95 (18 H, m,  $\text{PPh}_3$ );

$^{31}\text{P}\{^1\text{H}\}$  NMR (202 MHz, 128 scans,  $\text{C}_6\text{D}_6$ ,  $25\ ^\circ\text{C}$ ):  $\delta = 9.42$  (s, 2 P);

$^{19}\text{F}\{^1\text{H}\}$  NMR (470 MHz, 128 scans,  $\text{C}_6\text{D}_6$ ,  $25\ ^\circ\text{C}$ ):  $\delta = -106.3$  (br, 2 F, 2,6-F),  $-159.2$  (br, 1 F, 4-F),  $-161.4$  (br t,  $J = 22.04$  Hz, 2 F, 3,5-F);<sup>[c]</sup>

$^{13}\text{C}$  NMR (125.7 MHz, 16000 scans,  $\text{C}_6\text{D}_6$ ,  $25^\circ\text{C}$ ):  $\delta = 1343.0$  (d,  $J = 16.76$  Hz, 2-C of  $\text{P}(\text{C}_6\text{H}_5)_3$ ), 132.7 (d,  $J = 26.00$  Hz, 1-C of  $\text{P}(\text{C}_6\text{H}_5)_3$ ), 130.4 (s, 4-C of  $\text{P}(\text{C}_6\text{H}_5)_3$ ), 129.2 (d,  $J = 9.50$ , 3-C of  $\text{P}(\text{C}_6\text{H}_5)_3$ );

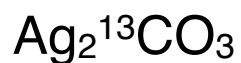
<sup>[a]</sup> The complex was found to be contaminated with approximately 25 – 30%  $\text{C}_6\text{F}_5\text{H}$  (purity determined by  $^{19}\text{F}\{^1\text{H}\}$  NMR spectroscopy. The yield of the complex  $\sim 46\%$  when accounted for the 30 %  $\text{C}_6\text{F}_5\text{H}$  contamination.

<sup>[b]</sup> Attempts to remove the  $\sim 30\%$   $\text{C}_6\text{F}_5\text{H}$  contamination by recrystallization, by drying the solid using a high vacuum Schlenk line (for 1 week, or by heating to  $80\ ^\circ\text{C}$  under vacuum for 3 h) have all failed. Recrystallized attempts included: layering with hexane/acetonitrile, ether/acetonitrile, ether/DMF, hexane/DMF, hexane/dichloromethane. Diffusion with ether/acetonitrile, hexane/acetonitrile, ether/DMF, hexane/DMF.

[c] The  $^{19}\text{F}\{^1\text{H}\}$  NMR spectrum contained 30%  $\text{C}_6\text{F}_5\text{H}$  and the corresponding  $^{19}\text{F}$  resonances. Only the resonances corresponding to **91** are reported.

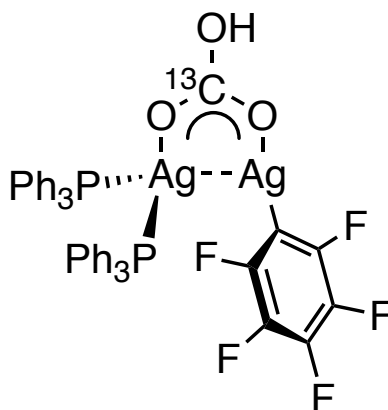
(Lab book reference number: GA-1-070, GA-1-089, GA-2-126, GA-2-129)



**Synthesis of  $^{13}\text{C}$ -labelled  $\text{Ag}_2^{13}\text{CO}_3$** 

In a 250 mL light-protected conical flask,  $^{13}\text{C}$ -labelled  $\text{Na}_2^{13}\text{CO}_3$  (267 mg, 2.5 mmol, 1 equiv.) was dissolved in deionized water (100 mL). Once all the solid had been dissolved,  $\text{AgNO}_3$  (849 mg, 5 mmol, 2 equiv.) was added and the solution was stirred at room temperature overnight, resulting in the formation of the precipitate. The solid was filtered, washed with deionized water ( $10\text{ cm}^3 \times 3$ ) and ethanol ( $10\text{ cm}^3 \times 3$ ) and was dried under vacuum to yield the product (591.5 mg, 85.5 %). The product was characterized using ATR-IR spectroscopy.  $\nu_{\text{max}}/\text{cm}^{-1}$  (ATR): 1785, 1230, 1070 (CO str. of  $\text{CO}_3^{2-}$ ), 815 (CO *oop* bend of  $\text{CO}_3^{2-}$ ), 776, 719, 710

(Lab book reference number: GA-1-082, GA-2-151)

Synthesis of  $^{13}\text{C}$  – labelled  $\text{Ag}_2(\text{PPh}_3)_2(\text{C}_6\text{F}_5)(\mu_2\text{-H}^{13}\text{CO}_3)$  (**92**)

In an oven-dried Schlenk tube,  $\text{Ag}_2^{13}\text{CO}_3$  (Synthesized from **GA-1-082**, 138 mg, 0.5 mmol, 1 equiv.) and  $\text{PPh}_3$  (262 mg, 0.5 mmol, 1 equiv.) were added and the Schlenk tube was evacuated and refilled three times with nitrogen. Dry  $\text{CH}_3\text{CN}$  (4.5 mL) was added, and the reaction mixture was submerged in a pre-heated oil bath ( $80^\circ\text{C}$ ) before  $\text{C}_6\text{F}_5\text{H}$  (840 mg, 5 mmol, 555  $\mu\text{L}$ , 10 equiv.) was added. After, the reaction mixture was allowed to cool down to room temperature, and the solvent and excess  $\text{C}_6\text{F}_5\text{H}$  was removed under reduced pressure to yield the product (330 mg, 67 %)<sup>[a]</sup> as a peach coloured solid. The solid (300 mg) was dissolved in hot acetonitrile ( $80^\circ\text{C}$ ) and then gradually cooled to  $-18^\circ\text{C}$  to yield the product as dark brown crystals (232.5 mg).

NMR:  $^1\text{H}$  NMR (500 MHz, 16 scans,  $\text{C}_6\text{D}_6$ ,  $25.0^\circ\text{C}$ ):  $\delta = 7.35$  (12 H, m,  $\text{PPh}_3$ ), 6.95 (18 H, m,  $\text{PPh}_3$ ).

$^{31}\text{P}\{^1\text{H}\}$  NMR (202 MHz, 128 scans,  $\text{C}_6\text{D}_6$ ,  $25^\circ\text{C}$ ):  $\delta = 9.2$  (s, 2 P);

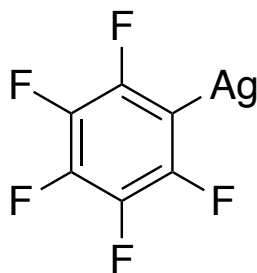
$^{19}\text{F}\{^1\text{H}\}$  NMR (470 MHz, 128 scans,  $\text{C}_6\text{D}_6$ ,  $25^\circ\text{C}$ ):  $\delta = -106.4$  (br, 2 F, 2,6-F),  $-158.9$  (br, 1 F, 4-F),  $-161.2$  (br t,  $J = 21.7$  Hz, 2 F, 3,5-F);<sup>[b]</sup>

$^{13}\text{C}\{^1\text{H}\}$  NMR (125.7 MHz, 16000 scans,  $\text{C}_6\text{D}_6$ ,  $25^\circ\text{C}$ ):  $\delta = 172.0$  (s), 168.03 (s), 134.3 (d,  $J = 16.7$  Hz, 2-C of  $\text{P}(\text{C}_6\text{H}_5)_3$ ), 132.7 (d,  $J = 25.7$  Hz, 1-C of  $\text{P}(\text{C}_6\text{H}_5)_3$ ), 130.4 (s, 4-C of  $\text{P}(\text{C}_6\text{H}_5)_3$ ), 129.1 (d,  $J = 9.73$ , 3-C of  $\text{P}(\text{C}_6\text{H}_5)_3$ );

<sup>[a]</sup> The complex was found to be contaminated with approximately 25 – 30%  $\text{C}_6\text{F}_5\text{H}$  (purity determined by  $^{19}\text{F}\{^1\text{H}\}$  NMR spectroscopy. The yield of the complex 47 % when accounted for the 30 %  $\text{C}_6\text{F}_5\text{H}$  contamination.

<sup>[b]</sup> The  $^{19}\text{F}\{^1\text{H}\}$  NMR spectrum contained 30%  $\text{C}_6\text{F}_5\text{H}$  and the corresponding  $^{19}\text{F}$  resonances. Only the resonances corresponding to **92** are reported.

(Lab book reference number: GA-2-095)

Synthesis of  $\text{AgC}_6\text{F}_5$  (**55**)<sup>95</sup>

In an argon glovebox, AgF (317 mg, 2.5 mmol, 1 equiv.) followed by dry EtCN (5 mL) was added to a light protected Schlenk tube. The mixture was stirred for 5 minutes before the addition of  $\text{Me}_3\text{SiC}_6\text{F}_5$  (600 mg, 2.5 mmol, 1.02 equiv. 476  $\mu\text{L}$ ). The reaction mixture was stirred at room temperature for 75 minutes. The reaction mixture was then removed from the glovebox and the solvent and other volatile compounds were removed under vacuum at 40 °C on the Schlenk line to yield the product **55** as a pale lilac solid (534.5 mg, 78 % yield).

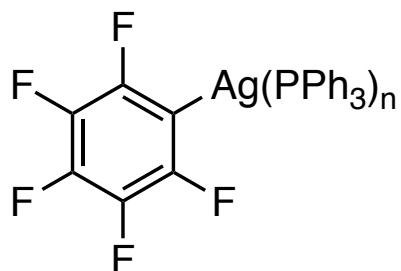
NMR:  $^{19}\text{F}\{^1\text{H}\}$  (470.6 MHz,  $\text{CD}_3\text{CN}$ , 25 °C):  $\delta = -107.4$  (2 F, m, 2,6-F),  $-160.6$  (1 F, t,  $J = 19.4$  Hz, 4-F),  $-163.1$  (2 F, m, 3,5-F);

$^{13}\text{C}\{^1\text{H}\}$  (126 MHz,  $\text{CD}_3\text{CN}$ , 25 °C):  $\delta = -148.8$  (ddm,  $^1J_{\text{CF}} = 220$  Hz,  $^3J_{\text{CF}} = 31$  Hz, 2,6-C),  $-138.8$  (dm,  $^1J_{\text{CF}} = 243$  Hz, 4-C),  $-136.0$  (dm, 253 Hz, 3,5-C);

MS (LIFDI)  $m/z$  (%) 273.89564 ( $[\text{M}]^+$ , 1.03) (calcd for  $\text{AgC}_6\text{F}_5$  273.89656, diff 0.00316), 382.79758 ( $[\text{Ag}_2\text{C}_6\text{F}_5]^+$ , 2.39), (calcd for  $[\text{Ag}_2\text{C}_6\text{F}_5]^+$  382.8019, diff 0.00432), 455.84981 ( $[\text{Ag}_2\text{C}_6\text{F}_5\text{DMF}]^+$ , 3.07), (calcd for  $[\text{Ag}_2\text{C}_6\text{F}_5\text{DMF}]^+$  455.8548, diff 0.00499).

A literature procedure was followed for the synthesis of this compound. The analytical data obtained were in agreement with the literature.<sup>95</sup>

(Lab book reference number: GA-4-258)

**Synthesis of Ag (C<sub>6</sub>F<sub>5</sub>)(PPh<sub>3</sub>)<sub>n</sub> (93)**

In an argon glovebox, AgC<sub>6</sub>F<sub>5</sub> (100 mg, 0.36 mmol, 1 equiv.) and PPh<sub>3</sub> (189 mg, 0.72 mmol, 2 equiv.) were weighed out and transferred to a foil wrapped Schlenk tube. A suba seal was fitted to the mouth of the Schlenk tube, the side-arm was closed, and then the Schlenk tube was removed from the glovebox. The Schlenk tube was connect to a Schlenk line, and the side arm was evacuated and refilled three time. Under a flow of nitrogen, CH<sub>3</sub>CN (2 mL) was added and the Schlenk tube was submerged in a pre-heated oil bath (80 °C). The reaction mixture was heated at 80 °C for 2 h before being filter canula transferred to another hot Schlenk tube (80 °C) while the reaction mixture was still hot. The reaction mixture was slowly cooled to room temperature to yield the product as dark brown crystals (42.2 mg, 15 %). The crystals were filtered and dried under reduced pressure. The filtrate was transferred into another Schlenk tube and slowly cooled to – 18 °C, to yield more product as brown crystals (167.8 mg, 58%). The total yield of product is 210 mg, 73 %.

NMR: <sup>31</sup>P{<sup>1</sup>H} NMR (202 MHz, Tol:CD<sub>2</sub>Cl<sub>2</sub> (20:80), 25 °C) δ = 4.9 (s)

<sup>19</sup>F{<sup>1</sup>H} NMR (471 MHz, Tol:CD<sub>2</sub>Cl<sub>2</sub> (20:80), 25 °C) δ –107.5 (2 *F*, m, 2,6-F), –159.6 (1 *F*, br s, 4-F), –161.9 (2 *F*, m, 3,5-F);

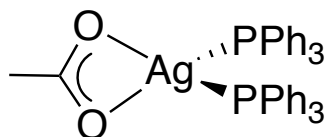
<sup>31</sup>P{<sup>1</sup>H} NMR (202 MHz, Tol:CD<sub>2</sub>Cl<sub>2</sub> (20:80), –100 °C): spectra complex, discussed in chapter 2.

<sup>19</sup>F{<sup>1</sup>H} NMR (471 MHz, Tol:CD<sub>2</sub>Cl<sub>2</sub> (20:80), –100 °C): –107.0 (2 *F*, m, 2,6-F), –159.6 (1 *F*, t, *J* = 23.5 Hz, 4-F), –161.0 (2 *F*, m, 3,5-F)

MS (LIFDI) *m/z* (%) 262.09055 ([PPh<sub>3</sub>]<sup>+</sup>, 100) (calcd for C<sub>18</sub>H<sub>15</sub>P 262.0911, diff 0.00055), 631.08782 ([Ag(PPh<sub>3</sub>)<sub>2</sub>]<sup>+</sup>, 98.5) (calcd for C<sub>36</sub>H<sub>30</sub>AgP 631.0874, diff 0.00042), 798.07929 ([M]<sup>+</sup>, 0.68) (calcd for C<sub>42</sub>H<sub>30</sub>AgF<sub>5</sub>P<sub>2</sub> 798.07883, diff 0.00046), 893.18357 ([Ag(PPh<sub>3</sub>)<sub>3</sub>]<sup>+</sup>, 5.46) (calcd for C<sub>59</sub>H<sub>95</sub>AgP<sub>3</sub> 893.1785, diff 0.00507), 906.98600 ([Ag<sub>2</sub>C<sub>6</sub>F<sub>5</sub>(PPh<sub>3</sub>)<sub>2</sub>]<sup>+</sup>, 6.34) (calcd for C<sub>42</sub>H<sub>30</sub>Ag<sub>2</sub>F<sub>5</sub>P<sub>2</sub> 906.9841, diff 0.0019).

(Lab book reference number: GA-4-268)

### Synthesis of $\text{Ag}(\text{PPh}_3)_2(\kappa^2\text{-OAc})$ (94)



In a foil wrapped Schlenk tube,  $\text{AgOAc}$  (1.0 g, 6.02 mmol, 1 equiv.) and  $\text{PPh}_3$  (3.5 g, 13.2 mmol, 2.2 equiv.) were added and the Schlenk tube was evacuated and refilled three times. Dry toluene (20 mL) was added, and the reaction mixture was stirred and heated at 90 °C for 24 h. The reaction mixture was then cooled to room-temperature, and the resulting white solid was suction filtered. The solid was then dissolved in DCM (50 mL), filtered through celite, and concentrated under reduced pressure to yield the product (3.15 g, 76 %) as a white solid.

Anal. Calc. for  $\text{C}_{38}\text{H}_{33}\text{AgO}_2\text{P}_2$ : C 66.00, H 4.81, observed C 65.91, H 4.95.

NMR:  $^1\text{H}$  (500 MHz, 32 scans,  $\text{CDCl}_3$ ):  $\delta = 7.43 - 7.27$  (30 H, m,  $\text{PC}_6\text{H}_5$ ), 1.93 (3 H, s,  $\text{CO}_2\text{CH}_3$ );

$^{13}\text{C}\{^1\text{H}\}$  NMR (126 MHz, 16048 scans,  $\text{CDCl}_3$ ):  $\delta = 178.5$  (s,  $\text{CO}_2\text{CH}_3$ ), 134.1 (d,  $J = 16.8$  Hz,  $\text{PC}_6\text{H}_5$ ), 132.8 (d,  $J = 25.3$  Hz,  $\text{PC}_6\text{H}_5$ ), 130.1 (s,  $\text{PC}_6\text{H}_5$ ), 128.9 (d,  $J = 9.7$  Hz), 23.8 (s,  $\text{CO}_2\text{CH}_3$ );

$^{31}\text{P}\{^1\text{H}\}$  (202 MHz, 128 scans,  $\text{CDCl}_3$ ):  $\delta = 8.4$  (s);

$^{31}\text{P}\{^1\text{H}\}$  (202 MHz, 64 scans, dichloromethane- $d_2$ ,  $-80^\circ\text{C}$ ):  $\delta = 8.5$  (pair of doublets  $d$ ,  $^1J_{^{31}\text{P}-^{107}\text{Ag}} = 370.6$  Hz,  $^1J_{^{31}\text{P}-^{109}\text{Ag}} = 506.2$  Hz, 2 P,  $\text{PPh}_3$ ).

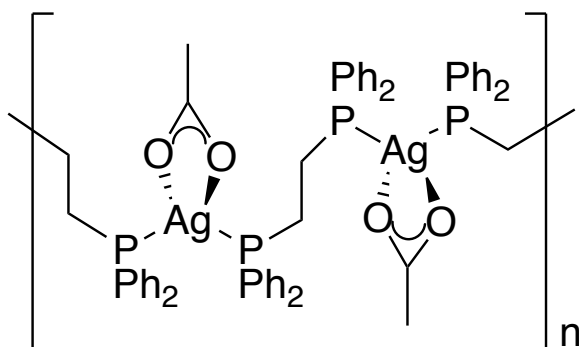
MS (LIFDI) (%)  $m/z$  (%) 631.13 ( $[\text{M}-\text{OAc}]^+$ , 86 %) ( $\text{C}_{36}\text{H}_{30}\text{AgP}_2$  requires 631.09).

$\nu_{\text{max}}/\text{cm}^{-1}$  (ATR): 3056 ( $\text{C}_{\text{aryl}}-\text{H}$  str.), 3003 (C=C str.), 2921, 1550 ( $-\text{CH}=\text{CH}-$  str.), 1478 (C=C aromatic str.), 1434 (P- $\text{C}_{\text{aryl}}$  str.), 1396, 1094 (P- $\text{C}_{\text{aryl}}$  str.), 742, 692, 503;

A modified version of a literature procedure was followed for the synthesis of this compound. The analytical data obtained was in agreement with the literature.<sup>123</sup>

(Lab book reference number: GA-1-001, GA-1-015)

### Synthesis of $[\text{AgDPPE}(\kappa^2\text{-OAc})]_n$ (95)



To a light-protected Schlenk tube equip with a stirrer bar, AgOAc (0.330 g, 1.98 mmol, 1 equiv.) and DPPE (0.934 g, 2.37 mmol, 1.2 equiv.) were added and the Schlenk tube was evacuated and refilled three times with nitrogen. Dry toluene (10 mL) was added, and the mixture was heated to 90°C for 24 h, and then allowed to cool down to room temperature slowly. This resulted in the formation of white crystalline powder, which was then suction filtered, in air, and washed with cold toluene (5 mL  $\times$  2) and DCM (10 mL  $\times$  2) to yield the product (840 mg, 75 % yield).

Anal. Calc. for  $\text{C}_{28}\text{H}_{28}\text{AgO}_2\text{P}_2$ : C 59.38, H 4.98, observed C 59.49, H 4.81.

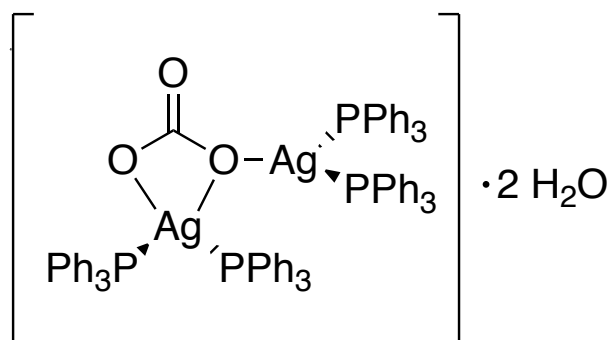
MS (LIFDI) (%)  $m/z$  (%) 903.24257 ( $[\text{AgDPPE}_2]^+$ , 92 %) ( $\text{C}_{52}\text{H}_{48}\text{AgP}_4$  requires 903.1757).

$\nu_{\text{max}}/\text{cm}^{-1}$  (ATR): 3048 ( $\text{C}_{\text{aryl}}\text{-H}$  str.), 2951 (C-H str.), 2916 (C-H str.), 1552, 1481 ( $-\text{CH}_2$  methylene bend), 1432 (P- $\text{C}_{\text{aryl}}$  str.), 1401, 1097 (P- $\text{C}_{\text{aryl}}$  str.), 731, 691, 513, 477.

Due to poor solubility of complex most NMR solvents, high quality NMR spectrum could not be obtained.

Crystals suitable for X-ray diffraction were grown from a saturated solution of the product in MeOH.

(Lab book reference number: GA-1-016)

Synthesis of  $((\text{PPh}_3)_2\text{Ag})_2\text{CO}_3 \cdot 2\text{H}_2\text{O}$  (88)

In a light-protected 50 mL round-bottom flask,  $\text{PPh}_3$  (787 mg, 3.0 mmol, 6 equiv.) was dissolved in warm acetonitrile (15 mL, 60 °C).  $\text{Ag}_2\text{CO}_3$  (136 mg, 0.50 mmol, 1 equiv.) was added and the reaction mixture was stirred for 3 h at room temperature in an open flask. The reaction mixture was gradually heated to 60 °C, resulting in the formation of a white precipitation within 10 minutes of heating. The white solid was re-dissolved by adding an additional 15 mL of acetonitrile and the warm solution was vacuum filtered through a cotton plug to remove insoluble grey residuals. The solution was allowed to cool in air to yield the product (246 mg, 37 %) as a white flaky solid.

Anal. Calc. for  $\text{C}_{78}\text{H}_{64}\text{Ag}_2\text{O}_2\text{P}_4$ : C 64.43, H 4.74, observed C 64.343, H 4.747.

NMR:  $^1\text{H}$  (400 MHz, 32 scans,  $\text{DMSO}-d_6$ ):  $\delta = 7.45 - 7.39$  (12 H, m,  $\text{PC}_6\text{H}_5$ ),  $7.38 - 7.29$  (48 H, m,  $\text{PC}_6\text{H}_5$ )

$^{13}\text{C}\{^1\text{H}\}$  (101 MHz, 2048 scans,  $\text{DMSO}-d_6$ ):  $\delta = 133.5$  (d,  $J = 17.3$  Hz,  $\text{PC}_6\text{H}_5$ )  $132.9$  (d,  $J = 20.9$ ,  $\text{PC}_6\text{H}_5$ ),  $130.2$  (s,  $\text{PC}_6\text{H}_5$ ),  $128.9$  (d,  $J = 9.2$  Hz,  $\text{PC}_6\text{H}_5$ ).

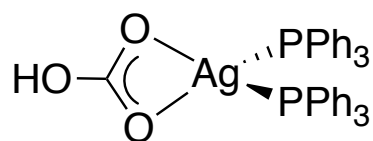
$^{31}\text{P}\{^1\text{H}\}$  NMR (162 MHz, 128 scans,  $\text{DMSO}-d_6$ ):  $\delta = 7.09$  (s).

MS (LIFDI) (%)  $m/z$  (%) 1297.15348 ( $[\text{M}-\text{CH}_3\text{O}_3]^+$ , 0.7 %) ( $\text{C}_{72}\text{H}_{61}\text{Ag}_2\text{O}_2\text{P}_4$  requires 1297.1721)

$\nu_{\text{max}}/\text{cm}^{-1}$  (ATR): 3061, 1660, 1582, 1476 (CO str. of  $\text{CO}_3^{2-}$ ), 1431 (P- $\text{C}_{\text{aryl}}$  str.), 1305 (CO str. of  $\text{CO}_3^{2-}$ ), 1093 (P- $\text{C}_{\text{aryl}}$  str.), 854 (CO *oop* bend of  $\text{CO}_3^{2-}$ ), 742, 691, 511, 497, 499, 430

A literature procedure was followed for the synthesis of this compound. The analytical data obtained was in agreement with the literature.<sup>121</sup>

(Lab book reference number: GA-1-039, GA-1-081, GA-2-099)

**Synthesis of  $\text{Ag}(\text{PPh}_3)_2(\kappa^2\text{-HCO}_3)$  (89)**

Under rapid stirring, a boiling solution of  $\text{PPh}_3$  (524 mg, 2.0 mmol, 2 equiv.) in ethanol (10 mL) was added to a hot solution of  $\text{AgNO}_3$  (154 mg, 1.0 mmol, 1 equiv.) in water (1.6 mL). This solution is then transferred to a room temperature solution of  $\text{Na}_2\text{CO}_3$  (445 mg, 4.2 mmol, 4.2 equiv.) in water (10 mL). This resulted in the formation of a white solid as the solution was gradually allowed to cool down to room temperature. The white solid was collected *via* vacuum filtration and was washed with a 1:1 mixture of  $\text{EtOH}:\text{H}_2\text{O}$  (10 mL  $\times$  3). The crude product was further purified *via* recrystallization from a saturated hot solution of acetonitrile, to yield the product (1.64 g, 73 % yield) as colourless prisms.

NMR:  $^1\text{H}$  (400 MHz, 32 scans,  $\text{DMSO-}d_6$ ):  $\delta = 7.52 - 7.45$  (6 *H*, m,  $\text{PC}_6\text{H}_5$ ),  $7.42 - 7.35$  (12 *H*, m,  $\text{PC}_6\text{H}_5$ ),  $7.33 - 7.25$  (12 *H*, m,  $\text{PC}_6\text{H}_5$ ),  $3.32$  (1 *H*, s, *OH*).

$^{13}\text{C}\{^1\text{H}\}$  (101 MHz, 2048 scans,  $\text{DMSO-}d_6$ ):  $\delta = 133.9$  (d,  $J = 16.7$  Hz,  $\text{PC}_6\text{H}_5$ ),  $132.6$  (d,  $J = 24.5$  Hz,  $\text{PC}_6\text{H}_5$ ),  $131.1$  (s,  $\text{PC}_6\text{H}_5$ ),  $129.6$  (d,  $J = 9.4$  Hz,  $\text{PC}_6\text{H}_5$ );

$^{31}\text{P}\{^1\text{H}\}$  NMR (162 MHz, 128 scans,  $\text{DMSO-}d_6$ ,  $25^\circ\text{C}$ ):  $\delta = 7.8$  (s).

$^{31}\text{P}\{^1\text{H}\}$  (202 MHz, 128 scans, *tol-}d\_8*: dichloromethane-*d}\_2* (20:80),  $25^\circ\text{C}$ ):  $\delta = 10.8$  (s, 2  $\text{PPh}_3$ ).

$^{31}\text{P}\{^1\text{H}\}$  (202 MHz, 512 scans, *tol-}d\_8*: dichloromethane-*d}\_2* (20:80),  $-80^\circ\text{C}$ ):  $\delta = 9.8$  (pair of doublets d,  $^1J_{31\text{P}-107\text{Ag}} = 465.1$  Hz,  $^1J_{31\text{P}-109\text{Ag}} = 536.8$  Hz, 2 *P*,  $\text{PPh}_3$ ).

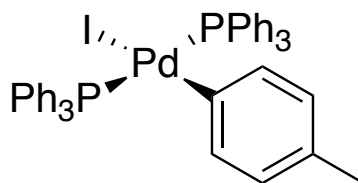
MS (LIFDI) (%) *m/z* (%) 631.09928 ( $[\text{M-HCO}_3]^+$ , 86 %) ( $\text{C}_{36}\text{H}_{30}\text{AgP}_2$  requires 631.0874).

$\nu_{\text{max}}/\text{cm}^{-1}$  (ATR): 3058 ( $\text{C}_{\text{aryl}}\text{-H}$  str.), 2928 (C-H str.), 1478 (C=C aromatic str.), 1435 (P-C<sub>aryl</sub> str.), 1397, 1293, 1095 (P-C<sub>aryl</sub> str.), 750, 692, 502, 426.

A literature procedure was followed for the synthesis of this compound. The analytical data obtained was in agreement with the literature.<sup>121</sup>

(Lab book reference number: GA-1-040, GA-1-075)



Synthesis of  $(\text{PPh}_3)_2\text{Pd}(4\text{-tolyl})(\text{I})$  (**98**)

An oven-dried Schlenk tube with 4-iodotoluene (176 mg, 0.80 mmol, 3.1 equiv.) was evacuated and refilled with nitrogen three times. Dry DCM (120 mL) was cannula transferred into the Schlenk tube and the solution was stirred for 10 minutes before  $\text{Pd}_2(\text{dba})_3 \cdot \text{CHCl}_3$  (270 mg, 0.26 mmol, 1 equiv.) and  $\text{PPh}_3$  (280 mg, 1.07 mmol, 4.1 equiv.) was added under a positive flow of nitrogen. The solution was stirred for 1 hour, during which time the dark purple solution changed colour to an opaque dark yellow colour. The solvent was removed under reduced pressure on the Schlenk line leaving behind a yellow solid which was subsequently washed with dry diethyl ether (20 mL  $\times$  5) under an atmosphere of nitrogen. The resulting product was found to be a dark grey solid (337mg, 76 %).

$\nu_{\text{max}}/\text{cm}^{-1}$  (ATR) 3047 (C–H aromatic str.), 2916 ( $\text{CH}_3$  str.), 1477 (–CH=CH– str.), 1432 (C=C aromatic str.), 1093 (=C–H in-plane bend), 687, 507, 494;

NMR:  $^1\text{H}$  (500 MHz, 32 scans,  $\text{CDCl}_3$ ):  $\delta$  = 7.58 – 7.47 (12 H, m, 2,6- $\text{PC}_6\text{H}_5$ ), 7.33 (6 H, t,  $J$  = 7.4 Hz, 4- $\text{PC}_6\text{H}_5$ ), 7.25 (12 H, t,  $J$  = 7.6 Hz, 3,4- $\text{PC}_6\text{H}_5$ ), 6.43 (2 H, d,  $J$  = 6.6 Hz, 2,6- $\text{C}_6\text{H}_5$ ) 6.09 (2 H, d,  $J$  = 7.2 Hz, 3,5- $\text{C}_6\text{H}_5$ ), 1.93 (3 H, s, 4- $\text{CH}_3$ ).

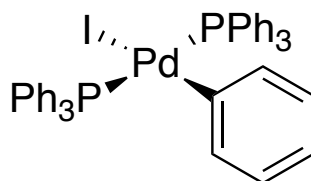
$^{13}\text{C}\{^1\text{H}\}$  NMR (126 MHz, 2048 scans,  $\text{CDCl}_3$ ):  $\delta$  = 135.7 (t,  $J$  = 5.1 Hz, CH), 135.1 (t,  $J$  = 6.2 Hz, CH), 132.1 (t), 132.4 (t,  $J$  = 23.0 Hz, CH), 129.7 (s, CH), 129.1 (s, CH), 127.8 (t,  $J$  = 5.1 Hz, CH), 20.3 Hz (s, 4- $\text{CH}_3$ ).

$^{31}\text{P}\{^1\text{H}\}$  NMR (202 MHz, 128 scans,  $\text{CDCl}_3$ ):  $\delta$  = 22.5 (s).

MS (ESI) (%)  $m/z$  (%) 721.1513 ([M–I], 100) ( $\text{C}_{43}\text{H}_{37}\text{P}_2\text{Pd}$  requires 721.1405, diff 0.0108)

A literature procedure was followed for the synthesis of this compound.<sup>175</sup> The analytical data obtained was in agreement with the literature.<sup>68</sup>

(Lab book reference number: GA-1-032, GA-1-038)

**Synthesis of  $(\text{PPh}_3)_2\text{Pd}(\text{Ph})(\text{I})$  (97)**

Under an atmosphere of nitrogen, a yellow suspension of  $\text{Pd}(\text{PPh}_3)_4$  (242 mg, 0.21 mmol, 1 equiv.) in dry benzene (3 mL) was produced under rapid stirring. To this suspension, dry iodobenzene (23  $\mu\text{L}$ , 43 mg, 0.21 mmol, 1 equiv.) was added and the reaction mixture was stirred under a flow of nitrogen, at room temperature for 20 h. The reaction mixture was then filtered under an atmosphere of nitrogen and washed with hexane (5 mL  $\times$  5) to yield the product as a white solid (77 mg, 44%).

$\nu_{\text{max}}/\text{cm}^{-1}$  (ATR) 3050 (C–H aromatic str.), 1558 (–CH=CH– str.), 1464 (C=C aromatic str.), 1094 (=C–H in-plane bend), 727, 698, 491;

NMR:  $^1\text{H}$  (500 MHz, 32 scans,  $\text{CDCl}_3$ ):  $\delta$  = 7.44 – 7.37 (12 H, m, 2,6- $\text{PC}_6\text{H}_5$ ), 7.21 (6 H, t,  $J$  = 7.3 Hz, 4- $\text{PC}_6\text{H}_5$ ), 7.13 (12 H, t,  $J$  = 7.4 Hz, 3,5- $\text{PC}_6\text{H}_5$ ), 6.51 (2 H, d,  $J$  = 6.9 Hz, 2,6- $\text{C}_6\text{H}_5\text{Pd}$ ), 6.23 (1 H, t,  $J$  = 7.2 Hz, 4- $\text{C}_6\text{H}_5\text{Pd}$ ), 6.12 (2 H, t,  $J$  = 7.4 Hz, 3,5- $\text{C}_6\text{H}_5\text{Pd}$ ).

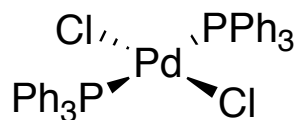
$^{13}\text{C}\{^1\text{H}\}$  (126 MHz, 16048 scans,  $\text{CDCl}_3$ ):  $\delta$  = 136.1 (t,  $J$  = 5.0 Hz, CH), 135.0 (t,  $J$  = 6.2 Hz, CH), 132.3 (t,  $J$  = 23.1 Hz, CH), 129.8 (s, CH), 128.5 (s, CH), 127.9 (t,  $J$  = 5.1 Hz, CH), 122.0 (s, CH).

$^{31}\text{P}\{^1\text{H}\}$  (202 MHz, 128 scans,  $\text{CDCl}_3$ ):  $\delta$  = 22.9 (s);

MS (LIFDI) m/z (%) 834.03296 ( $[\text{M}]^+$ , 100) ( $\text{C}_{42}\text{H}_{35}\text{IP}_2\text{Pd}$  requires 834.02880, diff 0.00416)

A literature procedure was followed for the synthesis of this compound. The analytical data obtained was in agreement with the literature.<sup>176</sup>

(Lab book reference number: GA-1-055)

**Synthesis of  $(\text{PPh}_3)_2\text{PdCl}_2$  (171)**

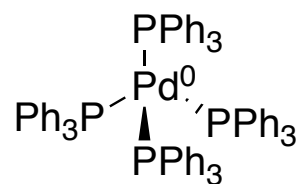
Under an atmosphere of nitrogen, a yellow suspension of  $\text{PdCl}_2$  (1.51 g, 8.50 mmol, 1 equiv.) in deoxygenated, anhydrous DMSO (150 mL) was produced with rapid stirring. The anhydrous DMSO (extra dry, 99.7+%) was purchased from acros organics and deoxygenated by bubbling with  $\text{N}_2$  for 1 h. Against a positive flow of nitrogen,  $\text{PPh}_3$  (4.46 g, 17.0 mol, 2 equiv.) was added and the reaction mixture was submerged in a preheated oil bath  $90\text{ }^\circ\text{C}$ , resulting in an orange solution. The reaction mixture was heated at  $90\text{ }^\circ\text{C}$  for 6 hours under a continuous flow of nitrogen. The reaction mixture was then cooled to room-temperature, resulting in the formation of a bright yellow solid in an orange solution. The rest of the workup was performed in air. The reaction mixture was then suction filtered and washed with DMSO ( $\text{mL} \times 2$ ) and  $\text{Et}_2\text{O}$  ( $50\text{ mL} \times 5$ ) to yield the product (5.28 g, 88%) as a yellow solid.

NMR:  $^1\text{H}$  (400 MHz, 32 scans,  $\text{CDCl}_3$ ):  $\delta = 7.79 - 7.67$  (12 H, m, 2,6- $\text{C}_6\text{H}_5\text{P}$ ),  $7.47 - 7.35$  (18 H, m, 3,4,5- $\text{C}_6\text{H}_5\text{P}$ ).

$^{31}\text{P}\{^1\text{H}\}$  NMR (162 MHz, 128 scans,  $\text{CDCl}_3$ ): 23.9 (s).

A literature procedure was followed for the synthesis of this compound. The analytical data obtained was in agreement with the literature.<sup>68</sup>

(Lab book reference number: GA-1-066)

**Synthesis of Pd(PPh<sub>3</sub>)<sub>4</sub> (172)**

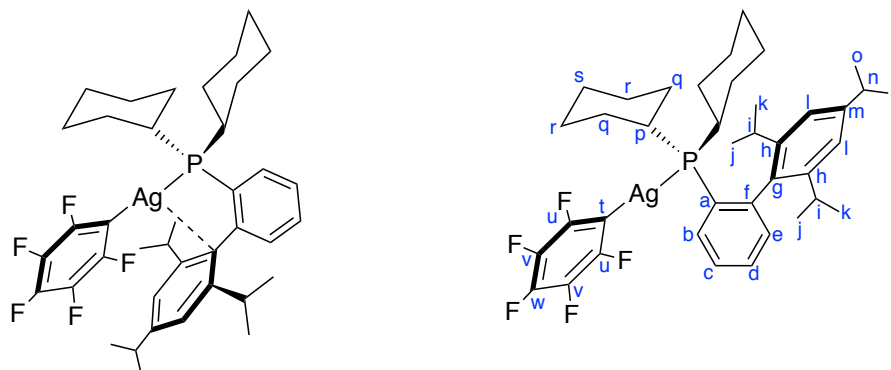
To an oven-dried Schlenk tube, PdCl<sub>2</sub> (502 mg, 2.83 mmol, 1 equiv.) and PPh<sub>3</sub> (3710 mg, 14.1 mmol, 5 equiv.) was added and the Schlenk tube was evacuated and refilled three times with nitrogen. To this, deoxygenated anhydrous DMSO (40 mL) was added, and the reaction mixture was heated (*ca.* 150 °C) until all the solid material had fully dissolved to produce an orange solution. The heat was then removed and hydrazine monohydrate (569 mg, 11.3 mmol, 4 equiv., 0.55 mL) was added dropwise over a minute, resulting in a dark red solution. The reaction mixture was cooled to room temperature before being filtered under an atmosphere of nitrogen. The resulting yellow solid was washed with EtOH (20 mL × 4) and diethyl ether (15 mL × 4) and dried under vacuum yielding the product as dark yellow crystalline powder (2.93 g, 79 % yield).

NMR: <sup>1</sup>H (500 MHz, 32 scans, C<sub>6</sub>D<sub>6</sub>): δ = 7.49 – 7.45 (24 H, m, 2,6-C<sub>6</sub>H<sub>5</sub>P), 6.98 – 6.97 (12 H, m, 4-C<sub>6</sub>H<sub>5</sub>P), 6.94 – 6.91 (24 H, m, 3,5-C<sub>6</sub>H<sub>5</sub>P).

<sup>31</sup>P{<sup>1</sup>H} (202 MHz, 128 scans, C<sub>6</sub>D<sub>6</sub>): δ = 16.72 (s, 4 P) ;

A literature procedure was followed for the synthesis of this compound. The analytical data obtained was in agreement with the literature.<sup>68</sup>

(Lab book reference number: GA-1-067)

Synthesis of  $\text{Ag}(\text{C}_6\text{F}_5)(\text{Xphos})$  (**101**)

In a light protected Schlenk tube,  $\text{Ag}_2\text{CO}_3$  (156 mg, 0.6 mmol, 1 equiv.) and Xphos (572 mg, 1.2 mmol, 2 equiv.) was added, which was evacuated and refilled three times with nitrogen. Under a flow of nitrogen,  $\text{CH}_3\text{CN}$  (6 mL), followed by  $\text{C}_6\text{F}_5\text{H}$  (1008 mg, 6.0 mmol, 10 equiv.  $665 \mu\text{L}$ ) was added and the reaction mixture was submerged in a pre-heated oil bath ( $80^\circ\text{C}$ ) and allowed to react for 23 h. The mixture was removed from the oil bath and filtered under an atmosphere of nitrogen. The solvent and excess volatile reagents were removed under reduced pressure on the Schlenk line to produce a dark grey solid. The remaining dark grey solid was then re-dissolved in  $\text{CH}_3\text{CN}$  (80 mL), while being stirred and heated to  $80^\circ\text{C}$ . The hot solution was cannula filtered into another light protected Schlenk tube which was pre-heated ( $80^\circ\text{C}$ ). The solution was allowed to cool down gradually to ambient temperature to produce small dark brown crystals on the walls of the Schlenk tube. The crystals were filtered and dried under reduced pressure to yield the product as dark brown crystals (594 mg, 66 %). Dark-brown crystals suitable for X-ray analysis were grown by preparing a saturated solution of **101** in hot acetonitrile ( $80^\circ\text{C}$ ) which was then slowly cooled to ambient temperature (with no external cooling).

Anal. Calc. for  $\text{C}_{39}\text{H}_{49}\text{AgF}_5\text{P}$ : C 62.32, H 6.57, observed C 62.20, H 6.57.

$^1\text{H}$  NMR (500 MHz,  $\text{CD}_2\text{Cl}_2$ ,  $25^\circ\text{C}$ ):  $\delta$  7.74 (1 H, m,  $\text{H}^b$ ), 7.55 – 7.53 (2 H, m,  $\text{H}^c + \text{H}^d$ ), 7.25 (1 H, m,  $\text{H}^e$ ), (2 H, s,  $\text{H}^f$ ), 2.55 (1 H, sept,  $J = 6.9$  Hz,  $\text{H}^n$ ) 2.38 (2 H, sept,  $J = 6.8$  Hz,  $\text{H}^i$ ), 2.17 – 2.08 (4 H, br,  $\text{Cy}$ ), 1.91 – 1.68 (8 H, br,  $\text{Cy}$ ), 1.49 – 1.21 (16 H, br  $\text{Cy}$  peak overlapping with d from  $^i\text{Pr}$  ( $\text{H}^o$ ),  $J_{iPr} = 6.9$  Hz,  $\text{Cy} + \text{H}^o$ ), 0.99 – 0.98 (12 H, overlapping d,  $J = 6.9$  Hz,  $\text{H}^k + \text{H}^j$ ).

$^{31}\text{P}\{^1\text{H}\}$  (202.5 MHz,  $\text{CD}_2\text{Cl}_2$ ,  $25^\circ\text{C}$ ):  $\delta$  13.0 (pair of dt,  $^1J_{107\text{Ag}-31\text{P}} = 443.5$  Hz,  $^1J_{109\text{Ag}-31\text{P}} = 512.3$  Hz,  $^4J_{FP} = 3.0$  Hz, 1 P).

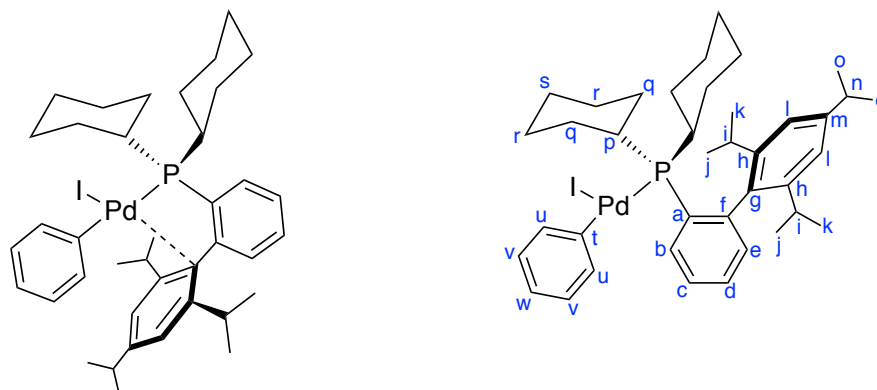
$^{19}\text{F}\{^1\text{H}\}$  (470.6 MHz,  $\text{CD}_2\text{Cl}_2$ ,  $25^\circ\text{C}$ ):  $\delta$  -107.0 (2 F, m, 2,6-F), -160.4 (1 F, t,  $J = 19.8$  Hz, 4-F), -162.5 (2 F, m, 3,5-F).

$^{13}\text{C}\{^1\text{H}\}$  NMR (126 MHz,  $\text{CD}_2\text{Cl}_2$ , 25 °C)  $\delta$  148.8 (s,  $\text{C}_m$ ), 147.5 (br ddm,  $^1J_{CF} \approx 219$  Hz,  $^3J_{CF} \approx 32$  Hz,  $\text{C}_u$ ), 147.3 (d,  $^2J_{CP} = 21.6$  Hz,  $\text{C}_f$ ), 145.8 (s,  $\text{C}_n$ ), 137.9 (br dm,  $^1J_{CF} \approx 239$  Hz,  $\text{C}_w$ ), 135.8 (br dm,  $^1J_{CF} \approx 225$  Hz,  $\text{C}_v$ ), 134.8 (d,  $^3J_{CP} = 8.6$  Hz,  $\text{C}_g$ ), 132.8 (d,  $^2J_{CP} = 7.0$  Hz,  $\text{C}_b$ ), 132.5 (d,  $^3J_{CP} = 4.3$  Hz,  $\text{C}_e$ ), 130.1 (d,  $^4J_{CP} = 2.0$  Hz,  $\text{C}_d$ ), 128.9 (dd,  $^1J_{CP} = 32.5$  Hz,  $^2J_{107/109\text{Ag}^{13}\text{C}} = 3.1$  Hz,  $\text{C}_a$ ), 127.3 (d,  $^3J_{CP} = 4.6$  Hz,  $\text{C}_c$ ), 122.1 (s,  $\text{C}_i$ ), 35.9 (dd,  $J = 17.7, 3.6$  Hz,  $\text{C}_p$ ), 33.4 (s,  $\text{C}_n$ ), 31.5 (dd,  $J = 7.2, 1.25$  Hz,  $\text{C}_y \text{CH}_2$ ), 30.8 (s,  $\text{C}_i$ ), 30.4 (dd,  $J = 6.1, 2.3$  Hz,  $\text{C}_y \text{CH}_2$ ), 27.2 (d,  $J = 13.6$  Hz,  $\text{C}_y \text{CH}_2$ ), 26.8 (d,  $J = 12.3$  Hz,  $\text{C}_y \text{CH}_2$ ), 25.9 (d,  $J = 1.5$  Hz,  $\text{C}_y \text{CH}_2$ ), 25.4 (s,  $\text{C}_k/\text{C}_j$ ), 22.9 (s,  $\text{C}_o$ ), 22.8 (s,  $\text{C}_k/\text{C}_j$ ).

$^{31}\text{P}\{^{109}\text{Ag}\}$ - $^{109}\text{Ag}$  HMQC} indirect detection of the  $^{109}\text{Ag}$  resonance at  $\delta$  713

MS (LIFDI) m/z (%) 750.2507 ( $[\text{M}]^+$ , 100) (calcd for  $\text{C}_{39}\text{H}_{49}\text{F}_5\text{PAg}$  750.2538, diff 0.003)

(Lab book reference number: GA-2-137, GA-2-138, and GA-2-139)

Synthesis of Pd(Xphos)(Ph)(I) (**102**)<sup>127</sup>

A procedure adapted from literature was followed for the synthesis of this compound.<sup>127</sup> In the glovebox, Xphos (48 mg, 0.10 mmol, 1.0 equiv.) was weighed in a 7 mL air-tight vial, and cyclohexane (~ 4 mL) was added dropwise until all the ligand was dissolved. Then iodobenzene (61 mg, 0.30 mmol, 3.0 equiv., 34  $\mu$ L) was then added using a gas tight syringe followed by (COD)Pd(CH<sub>2</sub>TMS)<sub>2</sub> (40 mg, 0.10 mmol, 1 equiv.). Upon the addition of the (COD)Pd(CH<sub>2</sub>TMS) the reaction mixture instantly changed to a clear pale yellow solution. The reaction was left stirring overnight at room temperature resulting in the formation of a pale-yellow suspension. Pentane (~ 2 mL) was added, and the reaction mixture was stirred well before being removed from the glovebox; the rest of the workup was performed under air. The mixture was evenly distributed between 6 centrifuge vials (2 mL vials) and the mixture was centrifuged (6000 rpm) for 5 min. This resulted in the mixture separating into a clear colourless solution and a pale-yellow solid. The colourless solution was removed using a pipette and the pale-yellow solid was suspended in pentane (dry) before being centrifuged again for 5 minutes. This process was repeated three times in total and the solid was dried under vacuum to yield **102** as a pale-yellow solid (71 mg, 90 %).

Anal. Calc. for C<sub>39</sub>H<sub>54</sub>IPPd: C 59.51, H 6.91, observed C 59.88, H 6.93.

<sup>1</sup>H NMR (500 MHz, CD<sub>2</sub>Cl<sub>2</sub>)  $\delta$  7.70 (1 H, m, **H<sup>b</sup>**), 7.45 – 7.39 (2 H, m, **H<sup>c</sup>** + **H<sup>d</sup>**), 7.15 (2 H, s, **H<sup>l</sup>**), 7.01 (2 H, m, **H<sup>a</sup>**), 6.90 (2 H, m, **H<sup>v</sup>**), 6.83 – 6.75 (2 H, m, overlapping **H<sup>e</sup>** + **H<sup>w</sup>**), 3.16 (1 H, sept,  $J = 6.9$  Hz, **H<sup>n</sup>**), 2.48 (2 H, sept,  $J = 6.8$  Hz, **H<sup>i</sup>**), 2.25 (2 H, tdt,  $J = 12.8, 10.4, 2.9$  Hz, **H<sup>p</sup>**), 1.95 (2 H, br, Cy), 1.82 – 1.55 (16 H, br,  $J_{\text{ipr}} = 6.8$  Hz, br Cy peaks overlapping with d from <sup>i</sup>Pr (**H<sup>k</sup>** or **H<sup>j</sup>**)), 1.40 (6 H, d,  $J_{\text{ipr}} = 6.9$  Hz, **H<sup>k</sup>** or **H<sup>j</sup>**), 1.31 – 1.05 (6 H, m, Cy), 0.88 (6 H, d,  $J_{\text{ipr}} = 6.7$  Hz, **H<sup>o</sup>**), 0.58 (2 H, qt,  $J = 12.8, 3.7$  Hz, Cy).

<sup>31</sup>P{<sup>1</sup>H} (202.5 MHz, CD<sub>2</sub>Cl<sub>2</sub>, 25°C):  $\delta$  21.96 (s).

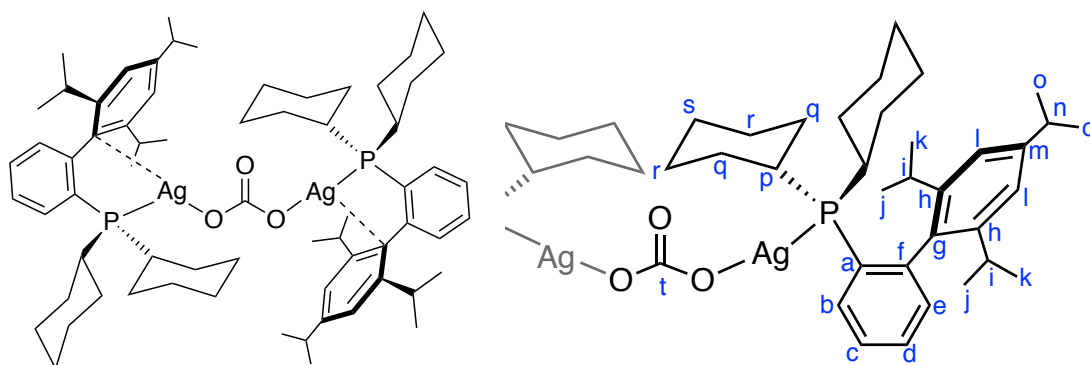
<sup>13</sup>C{<sup>1</sup>H} NMR (126 MHz, CD<sub>2</sub>Cl<sub>2</sub>)  $\delta$  156.2 (s, **C<sub>m</sub>**), 150.0 (s, **C<sub>h</sub>**), 147.3 (d,  $J = 20.6$  Hz, **C<sub>a</sub>**), 138.5 (d,  $^3J_{\text{CP}} = 3.8$  Hz, **C<sub>u</sub>**), 134.6 (s, quaternary C), 134.3 (s, quaternary C), 134.1 (d,  $J_{\text{CP}} = 11.2$  Hz, **C<sub>b</sub>**), 132.6 (s, **C<sub>e</sub>**), 130.8 (d,  $J_{\text{CP}} = 2.3$  Hz, **C<sub>d</sub>**), 130.0 (s, quaternary C), 127.1 (d,  $^3J_{\text{CP}} = 4.8$  Hz, **C<sub>c</sub>**), 127.0 (s, **C<sub>v</sub>**), 126.7 (d,  $^2J_{\text{CP}} = 3.8$  Hz, **C<sub>t</sub>**), 125.7 (s, **C<sub>i</sub>**), 123.4 (s, **C<sub>w</sub>**),

35.5 (d,  $^1J_{CP} = 24.7$  Hz, **C<sub>p</sub>**), 34.5 (s, **C<sub>n</sub>**), 31.9 (s, **C<sub>i</sub>**), 28.4 (d,  $J_{CP} = 2.4$  Hz, **Cy CH<sub>2</sub>**), 28.1 (d,  $J_{CP} = 13.0$  Hz, **Cy CH<sub>2</sub>**), 28.0 (d,  $J_{CP} = 1.9$  Hz, **Cy CH<sub>2</sub>**), 27.6 (d,  $J_{CP} = 10.7$  Hz, **Cy CH<sub>2</sub>**), 26.2 (d,  $J_{CP} = 1.4$  Hz, **Cy CH<sub>2</sub>**), 25.5 (s, **C<sub>k</sub>/C<sub>j</sub>**), 24.7 (s, **C<sub>o</sub>**), 24.7 (s, **C<sub>k</sub>/C<sub>j</sub>**).

MS (LIFDI) m/z (%) 786.20682 ( $[M]^+$ , 100) (calcd for C<sub>39</sub>H<sub>54</sub>PPdI 786.20372, diff 0.0031)

(Lab book reference number: GA-3-188, GA-4-338, GA-4-293)



Synthesis of  $\text{Ag}_2(\mu\text{-CO}_3)(\text{Xphos})_2$  (**106**)

In a light protected Schlenk tube,  $\text{Ag}_2\text{CO}_3$  (138 mg, 0.5 mmol, 1 equiv.) and Xphos (477 mg, 1 mmol, 2 equiv.) were added and the Schlenk tube was evacuated and refilled three times with nitrogen. Dry  $\text{CH}_3\text{CN}$  (20 mL) was added, and the reaction mixture was submerged in a pre-heated oil bath and allowed to react for 24 h. This resulted in the formation of a dark brown solution which was vacuum filtered through a cotton plug while hot, into a round-bottom flask (50 mL). The solvent was allowed to evaporate slowly in an open round-bottom flask overnight to yield dark brown crystals which were filtered and washed with cyclohexane (2 mL  $\times$  2) to yield the product (148 mg, 24 %). Crystals suitable for X-ray diffraction were grown by dissolving **106** in acetonitrile and allowing the acetonitrile to evaporate gradually at room temperature.

Anal. Calc. for  $\text{C}_{69}\text{H}_{101}\text{Ag}_2\text{O}_3\text{P}_2\text{N}$ : C 65.24, H 8.01, N 1.10 observed C 64.86, H 8.29, N 0.69.

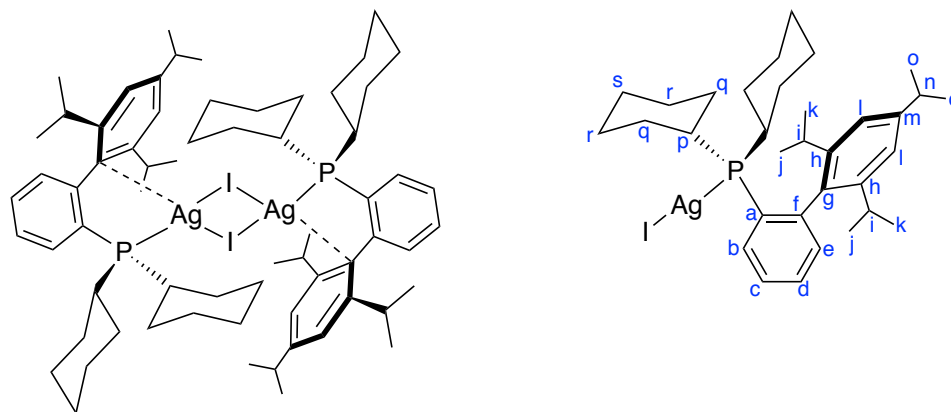
$^1\text{H}$  NMR (500 MHz,  $\text{C}_6\text{D}_6$ , 25°C):  $\delta$  = 7.46 (4 H, s,  $\text{H}^{\text{d}}$ ), 7.30 (2 H, m,  $\text{H}^{\text{b}}$ ), 7.25 (2 H, m,  $\text{H}^{\text{c}}$ ), 7.09 – 7.03 (4 H, m,  $\text{H}^{\text{d}}$  +  $\text{H}^{\text{e}}$ ), 3.31 (2 H, sept,  $J$  = 6.9 Hz,  $\text{H}^{\text{m}}$ ), 2.50 (4 H, sept,  $J$  = 6.9 Hz,  $\text{H}^{\text{i}}$ ), 1.96 – 1.87 (4 H, br, Cy), 1.87 – 1.51 (45 H, br,  $J_{\text{ipr}}$  = 6.9 Hz, br Cy peak overlapping with d from  $^{\text{i}}\text{Pr}$  of  $\text{H}^{\text{n}}$  and  $\text{H}^{\text{k}}$  or  $\text{H}^{\text{j}}$ ), 1.51 – 1.24 (9 H, br m, Cy), 1.22 – 1.03 (24 H, br m, br Cy peak overlapping with d from  $^{\text{i}}\text{Pr}$  of  $\text{H}^{\text{k}}$  or  $\text{H}^{\text{j}}$ ).

$^{31}\text{P}\{^1\text{H}\}$  (202.5 MHz,  $\text{C}_6\text{D}_6$ , 25°C):  $\delta$  = 15.9 (pair of d,  $^1J_{^{107}\text{Ag}-^{31}\text{P}}$  = 634.2 Hz,  $^1J_{^{109}\text{Ag}-^{31}\text{P}}$  = 731.2 Hz, 2 P).

$^{13}\text{C}\{^1\text{H}\}$  NMR (126 MHz,  $\text{CDCl}_3$ )  $\delta$  = 150.9 (s,  $\text{C}_m$ ), 148.5 (d,  $^2J_{\text{CP}}$  = 21.1 Hz,  $\text{C}_t$ ), 145.4 (s,  $\text{C}_h$ ), 134.4 (d,  $^3J_{\text{CP}}$  = 8.3 Hz,  $\text{C}_g$ ), 133.1 (d,  $^3J_{\text{CP}}$  = 6.4 Hz,  $\text{C}_e$ ), 132.3 (d,  $^3J_{\text{CP}}$  = 6.1 Hz,  $\text{C}_b$ ), 130.3 (dd,  $^1J_{\text{CP}}$  = 30.8 Hz,  $^2J_{^{13}\text{C}-^{107/109}\text{Ag}}$  = 6.0 Hz,  $\text{C}_a$ ), 129.7 (s,  $\text{C}_d/\text{C}_c$ ), 127.1 (d,  $^3J_{\text{CP}}$  = 4.3 Hz,  $\text{C}_f/\text{C}_d$ ), 122.5 (s,  $\text{C}_l$ ), 35.9 (dd,  $J$  = 17.1, 4.1 Hz,  $\text{C}_p$ ), 35.1 (s,  $\text{C}_n$ ), 31.5 (s, Cy  $\text{CH}_2$ ), 31.5 (s,  $\text{C}_i$ ), 30.2 (dd,  $J$  = 6.7 Hz, 2.2 Hz, Cy  $\text{CH}_2$ ), 27.7 (d,  $J$  = 13.8 Hz, Cy  $\text{CH}_2$ ), 27.3 (d,  $J$  = 12.2 Hz, Cy  $\text{CH}_2$ ), 26.4 (s,  $\text{C}_k/\text{C}_j$ ), 26.2 (s, Cy  $\text{CH}_2$ ), 24.8 (s,  $\text{C}_o$ ), 23.4 (s,  $\text{C}_k/\text{C}_j$ ).

$\nu_{\text{max}}/\text{cm}^{-1}$  (ATR-IR) 2924, 2849, 1605, 1444, 1429, 1382, 1360, 1344, 1001, 869, 854, 840, 773, 744, 514, 487

*(Lab book reference number: GA-2-169, GA-4-279)*

Synthesis of  $\text{Ag}_2(\mu\text{-I})_2(\text{Xphos})_2$  (**105**)

In a light protected Schlenk tube, AgI (234 mg, 1.0 mmol, 1.0 equiv.) and Xphos (477 mg, 1.0 mmol, 1 equiv.) were added and the Schlenk tube was evacuated and refilled three times with nitrogen. Dichloromethane (6 mL) was then then added, and the reaction mixture was stirred at room temperature for 24 h. The reaction mixture was then filtered under nitrogen, layered with dry hexane (~ 20 mL) and placed in a  $-18\text{ }^\circ\text{C}$  freezer. The resulting colourless needles were filtered under nitrogen using a cannula filter and dried under reduced pressure to yield the product as a white crystalline solid (511.3 mg, 72 %). Crystals suitable for X-ray diffraction were grown in a glovebox, by dissolving **105** in dichloromethane and layering with hexane in a light-protected vial cooled in a  $-30\text{ }^\circ\text{C}$  freezer.

Anal. Calc. for  $\text{C}_{33}\text{H}_{49}\text{AgIP}$ : C 55.71, H 6.91, observed C 55.69, H 7.25.

NMR  $^1\text{H}$  (500 MHz,  $\text{CD}_2\text{Cl}_2$ ,  $25\text{ }^\circ\text{C}$ )  $\delta$  7.72 (1 H, m,  $\text{H}^b$ ), 7.58 – 7.51 (2 H, m,  $\text{H}^c + \text{H}^d$ ), 7.28 (1 H, m,  $\text{H}^e$ ), 7.21 (2 H, s,  $\text{H}^f$ ), 3.07 (1 H, sept,  $J = 7.0$  Hz,  $\text{H}^g$ ), 2.34 (2 H, sept,  $J = 6.8$  Hz,  $\text{H}^i$ ), 2.20 – 2.04 (4 H, br, Cy), 1.97 – 1.65 (8 H, br, Cy), 1.56 – 1.12 (22 H, br Cy peak overlapping with d from  $^i\text{Pr}$ ,  $J_{iPr} = 6.9$  Hz, Cy +  $\text{H}^o + \text{H}^k/\text{H}^l$ ), 0.98 (6 H, d,  $J = 6.7$  Hz,  $\text{H}^k/\text{H}^l$ ).

$^{31}\text{P}\{^1\text{H}\}$  NMR (202.5 MHz,  $\text{CD}_2\text{Cl}_2$ ,  $25\text{ }^\circ\text{C}$ ):  $\delta$  16.58 (pair of d,  $^1J_{107\text{Ag}-31\text{P}} = 542.7$  Hz,  $^1J_{109\text{Ag}-31\text{P}} = 627.7$  Hz, 1 P).

$^{13}\text{C}\{^1\text{H}\}$  NMR (126 MHz,  $\text{CD}_2\text{Cl}_2$ ,  $25\text{ }^\circ\text{C}$ )  $\delta$  = 150.4 (s,  $\text{C}_m$ ), 147.4 (d,  $^2J_{\text{CP}} = 21.0$  Hz,  $\text{C}_f$ ), 145.8 (s,  $\text{C}_h$ ), 134.9 (d,  $^3J_{\text{CP}} = 8.6$  Hz,  $\text{C}_g$ ), 133.1 (d,  $^3J_{\text{CP}} = 6.8$  Hz,  $\text{C}_b$ ), 132.9 (d,  $^2J_{\text{CP}} = 5.5$  Hz,  $\text{C}_e$ ), 130.6 (d,  $^4J_{\text{CP}} = 1.9$  Hz,  $\text{C}_d$ ), 128.6 (dd,  $^1J_{\text{CP}} = 32.5$  Hz,  $^2J_{107/109\text{Ag}^{13}\text{C}} = 4.6$  Hz,  $\text{C}_a$ ), 127.8 (d,  $^3J_{\text{CP}} = 4.5$  Hz,  $\text{C}_c$ ), 123.1 (s,  $\text{C}_i$ ), 35.9 (dd,  $J = 17.0, 4.0$  Hz,  $\text{C}_p$ ), 34.4 (s,  $\text{C}_n$ ), 31.7 (d,  $J_{\text{CP}} = 7.3$  Hz, Cy  $\text{CH}_2$ ), 31.2 (s,  $\text{C}_i$ ), 30.5 (dd,  $J_{\text{CP}} = 5.7, 2.2$  Hz, Cy  $\text{CH}_2$ ), 27.6 (d,  $J_{\text{CP}} = 13.6$  Hz, Cy  $\text{CH}_2$ ), 27.2 (d,  $J_{\text{CP}} = 12.4$  Hz, Cy  $\text{CH}_2$ ), 26.1 (d,  $J_{\text{CP}} = 1.4$  Hz, Cy  $\text{CH}_2$ ), 25.9 (s,  $\text{C}_o$ ), 24.2 (s,  $\text{C}_k/\text{C}_j$ ), 23.6 (s,  $\text{C}_k/\text{C}_j$ ).

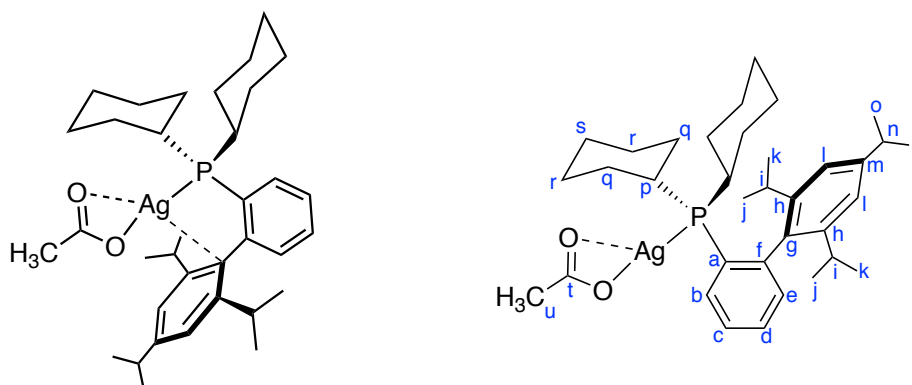
$^{31}\text{P}\{^{109}\text{Ag}\}$ - $^{109}\text{Ag}$  HMQC} indirect detection of the  $^{109}\text{Ag}$  resonance at  $\delta$  590

MS (LIFDI)  $m/z$  (%) 1295.45593 ( $[\text{M-I}]^+$ , 100) (calcd for  $\text{C}_{66}\text{H}_{98}\text{Ag}_2\text{IP}_2$  1295.4287, diff 0.027), 710.18300 ( $[\text{M}/2]^+$ , 12) (calcd for  $\text{C}_{33}\text{H}_{49}\text{AgIP}$  710.1667, diff 0.016).

$\nu_{\text{max}}/\text{cm}^{-1}$  (ATR-IR) 2957, 2924, 2853, 1607, 1445, 1382, 1360, 1003, 868, 766, 483.

(Lab book reference number: GA-2-148 and GA-4-317)

## Synthesis of AgOAcXphos (109)



To a light-protected Schlenk tube, AgOAc (83.4 mg, 0.5 mmol, 1 equiv.) and Xphos (238 mg, 0.5 mmol, 1 equiv.) were added, and the Schlenk tube was evacuated and refilled with nitrogen three times. Against a flow of nitrogen, CH<sub>3</sub>CN (10 mL) was added, and the reaction mixture was submerged in a pre-heated oil bath (80 °C) and allowed to react overnight. The reaction mixture was then vacuum filtered through a cotton plug, while hot, into a round-bottom flask (25 mL). The solvent was allowed to evaporate slowly in an open round-bottom flask to yield **109** as white prisms (317.6 mg, 98 %). Crystals suitable for X-ray diffraction were grown by dissolving **109** in hot acetonitrile and allowing the acetonitrile to evaporate gradually at room temperature.

NMR <sup>1</sup>H (500 MHz, CD<sub>3</sub>CN, 25 °C) δ 7.80 (1 H, m, **H<sup>b</sup>**), 7.55 – 7.50 (2 H, m, **H<sup>c</sup>** + **H<sup>d</sup>**), 7.23 (1 H, m, **H<sup>e</sup>**), 7.14 (2 H, s, **H<sup>f</sup>**), 2.90 (1 H, sept, *J* = 7.0 Hz, **H<sup>g</sup>**), 2.28 (2 H, sept, *J* = 6.8 Hz, **H<sup>i</sup>**), 2.14 – 1.96 (4 H, br, Cy), 1.82 – 1.61 (11 H, br Cy peak overlapping with *s* of -CH<sup>u</sup>), 1.33 – 1.10 (22 H, br Cy peak overlapping with *d* from <sup>1</sup>Pr, *J*<sub>*i*Pr</sub> = 6.9 Hz, Cy + **H<sup>o</sup>** + **H<sup>k</sup>**/**H<sup>j</sup>**), 0.91 (6 H, d, *J* = 6.7 Hz, **H<sup>k</sup>**/**H<sup>j</sup>**).

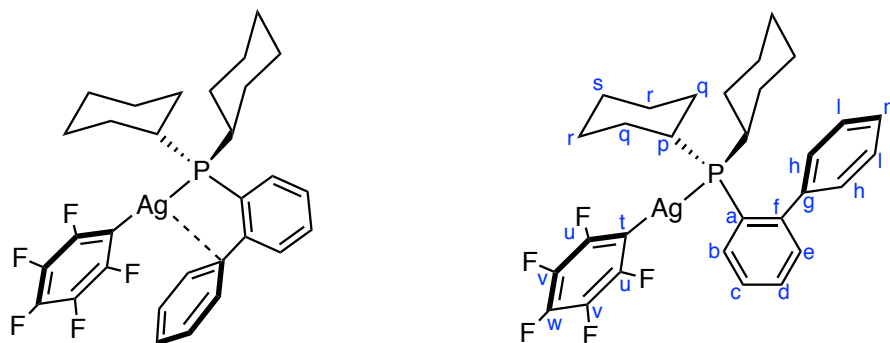
<sup>31</sup>P{<sup>1</sup>H} NMR (202.5 MHz, CD<sub>3</sub>CN, 25 °C): δ 16.55 (pair of d, <sup>1</sup>*J*<sub>107Ag-31P</sub> = 643.9 Hz, <sup>1</sup>*J*<sub>109Ag-31P</sub> = 743.2 Hz, 1 *P*).

<sup>13</sup>C{<sup>1</sup>H} NMR (126 MHz, CD<sub>3</sub>CN, 25 °C) δ = 177.9 (s, **C<sub>t</sub>**), 150.5 (s, **C<sub>m</sub>**), 147.6 (d, <sup>2</sup>*J*<sub>CP</sub> = 21.4 Hz, **C<sub>f</sub>**), 146.8 (s, **C<sub>h</sub>**), 135.6 (d, <sup>3</sup>*J*<sub>CP</sub> 8.8 Hz, **C<sub>g</sub>**), 133.9 (d, <sup>3</sup>*J*<sub>CP</sub> 6.3 Hz, **C<sub>b</sub>**), 133.5 (d, <sup>2</sup>*J*<sub>CP</sub> = 7.6 Hz, **C<sub>e</sub>**), 131.1 (d, <sup>4</sup>*J*<sub>CP</sub> = 2.5 Hz, **C<sub>d</sub>**), 129.3 (dd, <sup>1</sup>*J*<sub>CP</sub> = 34.8 Hz, <sup>2</sup>*J*<sub>107/109Ag-13C</sub> = 5.4 Hz, **C<sub>a</sub>**), 128.5 (dd, *J* = 4.7, 1.9 Hz, **C<sub>c</sub>**), 122.6 (s, **C<sub>i</sub>**), 36.0 (dd, *J* = 18.9, 4.5 Hz, **C<sub>p</sub>**), 35.0 (s, **C<sub>n</sub>**), 32.2 (d, *J*<sub>CP</sub> = 7.6 Hz, **Cy CH<sub>2</sub>**), 31.7 (s, **C<sub>i</sub>**), 31.1 (dd, *J*<sub>CP</sub> = 6.4, 2.6 Hz, **Cy CH<sub>2</sub>**), 27.7 (d, *J*<sub>CP</sub> = 13.9 Hz, **Cy CH<sub>2</sub>**), 27.3 (d, *J*<sub>CP</sub> = 12.6 Hz, **Cy CH<sub>2</sub>**), 26.5 (d, *J*<sub>CP</sub> = 1.3 Hz, **Cy CH<sub>2</sub>**), 25.8 (s, **C<sub>o</sub>**), 24.1 (s, **C<sub>k</sub>**/**C<sub>j</sub>**), 23.2 (s, **C<sub>k</sub>**/**C<sub>j</sub>**), 22.8 (s, **C<sub>u</sub>**).

MS (LIFDI) *m/z* (%) 642.27209 ([M]<sup>+</sup>, 100) (calcd for C<sub>35</sub>H<sub>52</sub>AgO<sub>2</sub>P 642.27504, diff 0.00295);

$\nu_{\max}/\text{cm}^{-1}$  (ATR-IR) 2955, 2918, 2851, 1568, 1399, 1378, 1003, 919, 872, 770, 762, 666, 615, 515

(Lab book reference number: GA-6-454 and GA-6-473)

Synthesis of  $\text{Ag}(\text{C}_6\text{F}_5)(\text{CyJohnPhos})$  (**122**)

In a light protected Schlenk tube,  $\text{Ag}_2\text{CO}_3$  (138 mg, 0.5 mmol, 1 equiv.) and CyJohnphos (350 mg, 1.0 mmol, 2 equiv.) were added, and the Schlenk tube was evacuated and refilled three times and nitrogen. Under a flow of nitrogen,  $\text{CH}_3\text{CN}$  (5 mL), followed by  $\text{C}_6\text{F}_5\text{H}$  (840 mg, 5.0 mmol, 10 equiv., 555  $\mu\text{L}$ ) was added and the reaction mixture was submerged in a pre-heated oil bath (80  $^\circ\text{C}$ ) and allowed to react for 23 h. The mixture was removed from the oil bath and filtered under an atmosphere of nitrogen using a filter cannula. The solvent and excess reagents were removed under-reduced pressure to produce a white solid which was then re-dissolved in  $\text{CH}_3\text{CN}$  (5 mL), while being stirred and heated to 80  $^\circ\text{C}$ . The hot solution was cannula filtered into another light protected Schlenk tube which was heated to 80  $^\circ\text{C}$ . The solution was allowed to cool down gradually to ambient temperature and then placed in  $-18$   $^\circ\text{C}$  freezer to produce small white crystals on the walls of the Schlenk tube. The crystals were filtered and dried under reduced pressure to yield the product as white crystals **122** (363.6 mg, 58 %). Colourless crystals suitable for X-ray analysis were grown by preparing a saturated solution of **122** in hot acetonitrile (80  $^\circ\text{C}$ ) which was initially slowly cooled to ambient temperature and then cooled to  $-18$   $^\circ\text{C}$ .

$^1\text{H}$  NMR (500 MHz,  $\text{CD}_2\text{Cl}_2$ , 25 $^\circ\text{C}$ )  $\delta$  7.66 (1 H, m,  $\text{H}^b$ ), 7.51 (2 H, m,  $\text{H}^c + \text{H}^d$ ), 7.38 (2 H, m,  $\text{H}^h$ ), 7.32 (1 H, m,  $\text{H}^e$ ), 7.23 (2 H, m,  $\text{H}^l$ ), 7.12 (1 H, m,  $\text{H}^m$ ), 2.24 – 2.09 (2 H, m, Cy), 2.05 – 1.95 (2 H, m, Cy), 1.89 – 1.59 (8 H, m, Cy), 1.42 – 1.11 (9 H, m, Cy);

$^{31}\text{P}\{^1\text{H}\}$  (202.5 MHz,  $\text{CD}_2\text{Cl}_2$ , 25 $^\circ\text{C}$ )  $\delta$  15.5 (pair of d,  $^1J_{107\text{Ag}-31\text{P}} = 449.6$  Hz,  $^1J_{109\text{Ag}-31\text{P}} = 518.4$  Hz, 1 P);

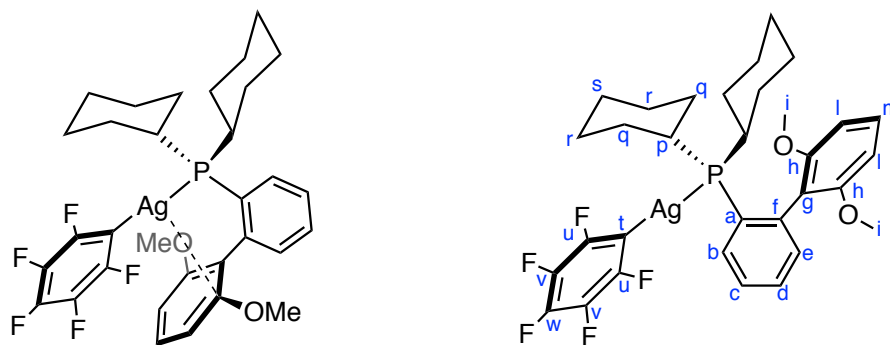
$^{19}\text{F}\{^1\text{H}\}$  (470.6 MHz,  $\text{CD}_2\text{Cl}_2$ , 25 $^\circ\text{C}$ )  $\delta$   $-107.5$  (2 F, m, 2,6-F),  $-160.8$  (1 F, t,  $J = 19.8$  Hz, 4-F),  $-162.9$  (2 F, m, 3,5-F);

$^{13}\text{C}\{^1\text{H}\}$  NMR (126 MHz,  $\text{CD}_2\text{Cl}_2$ , 25  $^\circ\text{C}$ )  $\delta$  150.3 (d,  $J = 18.6$  Hz,  $\text{C}_f$ ), 147.9 (ddm,  $^1J_{\text{CF}} \approx 220$  Hz,  $^3J_{\text{CF}} \approx 36$  Hz,  $\text{C}_u$ ), 141.6 (d,  $J = 7.6$  Hz,  $\text{C}_g$ ), 138.4 (dm,  $^1J_{\text{CF}} \approx 243$  Hz,  $\text{C}_w$ ), 136.3 (dm,  $^1J_{\text{CF}} \approx 250$  Hz,  $\text{C}_v$ ), 133.2 (d,  $J = 3.7$  Hz,  $\text{C}_b$ ), 131.9 (d,  $J = 6.6$  Hz,  $\text{C}_e$ ), 130.6 (d,  $J = 1.9$  Hz,  $\text{C}_d$ ), 129.5 (s,  $\text{C}_h$ ), 129.3 (s,  $\text{C}_i$ ), 128.4 (s,  $\text{C}_m$ ), 128.0 (d,  $J = 4.8$  Hz,  $\text{C}_c$ ), 126.7 (d,  $J = 30.2$  Hz,  $\text{C}_a$ ), 35.6 (dd,  $J = 18.1, 2.7$  Hz,  $\text{C}_p$ ), 31.7 (d,  $J = 9.5$  Hz, Cy), 30.2 (d,  $J = 3.4$  Hz, Cy), 27.4 – 27.0 (m, Cy), 26.3 (d,  $J = 1.6$  Hz, Cy).

MS (LIFDI) m/z (%) 624.11194 ( $[M]^+$ , 100) (calcd for  $C_{30}H_{31}F_5PAg$  624.1134, diff 0.00146

(Lab book reference number: GA-5-386)



Synthesis of  $\text{Ag}(\text{C}_6\text{F}_5)(\text{Sphos})$  (**124**)

In a light protected Schlenk tube,  $\text{Ag}_2\text{CO}_3$  (137 mg, 0.5 mmol, 1 equiv.) and Sphos (410 mg, 1 mmol, 2 equiv.) was added, which was then evacuated and refilled three times with nitrogen. Under a flow of nitrogen,  $\text{CH}_3\text{CN}$  (5 mL), followed by  $\text{C}_6\text{F}_5\text{H}$  (840 mg, 5 mmol, 10 equiv., 555  $\mu\text{L}$ ) was added and the reaction mixture was submerged in a pre-heated oil bath (80  $^\circ\text{C}$ ) and allowed to react for 23 h. The mixture was removed from the oil bath and filtered under an atmosphere of nitrogen. The solvent and excess reagents were removed under reduced pressure to produce an off-white solid which was then dissolved in  $\text{CH}_3\text{CN}$  (5 mL), while being stirred and heated to 80  $^\circ\text{C}$ . The hot solution was cannula filtered into another hot light protected Schlenk tube (80  $^\circ\text{C}$ ). The solution was allowed to cool down gradually to ambient temperature and then placed in  $-18$   $^\circ\text{C}$  freezer to produce small white crystals on the walls of the Schlenk tube. The crystals were cannula filtered and dried under reduced pressure to yield the product as white crystals (435.1 mg, 63 %). Colourless crystals suitable for X-ray analysis were grown by preparing a saturated solution of **124** in hot acetonitrile (80  $^\circ\text{C}$ ) which was initially slowly cooled to ambient temperature and then further cooled to  $-18$   $^\circ\text{C}$  in the freezer.

$^1\text{H}$  NMR (500 MHz,  $\text{CD}_2\text{Cl}_2$ , 25 $^\circ\text{C}$ ):  $\delta$  7.65 (1 H, m,  $\text{H}^{\text{b}}$ ), 7.51 (1 H, tt,  $J = 7.5, 1.4$  Hz,  $\text{H}^{\text{d}}$ ), 7.46 (1 H, m,  $\text{H}^{\text{e}}$ ), 7.15 (1 H, m,  $\text{H}^{\text{e}}$ ), 6.98 (1 H, t,  $J = 8.4$  Hz,  $\text{H}^{\text{m}}$ ), 6.55 (2 H, d,  $J = 8.4$  Hz,  $\text{H}^{\text{f}}$ ), 3.70 (6 H, s,  $\text{H}^{\text{t}}$ ), 2.24 – 1.60 (12 H, m, Cy), 1.43 – 1.08 (10 H, m, Cy);

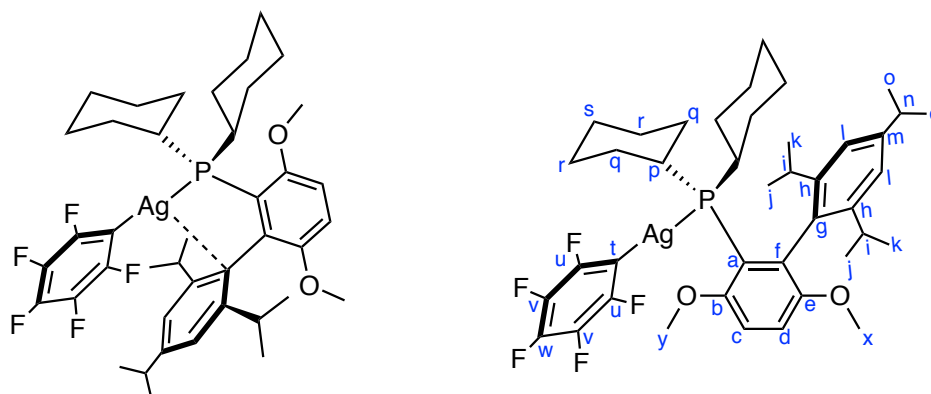
$^{31}\text{P}\{^1\text{H}\}$  (202.5 MHz,  $\text{CD}_2\text{Cl}_2$ , 25 $^\circ\text{C}$ ):  $\delta$  17.25 (pair of dt,  $^1J_{^{107}\text{Ag}-^{31}\text{P}} = 451.6$  Hz,  $^1J_{^{109}\text{Ag}-^{31}\text{P}} = 520.4$  Hz,  $^4J_{\text{FP}} = 2.0$  Hz, 1 P);

$^{19}\text{F}\{^1\text{H}\}$  (470.6 MHz,  $\text{CD}_2\text{Cl}_2$ , 25 $^\circ\text{C}$ ):  $\delta$   $-107.7$  (2 F, m, 2,6-F),  $-160.9$  (1 F, t,  $J = 19.9$  Hz, 4-F),  $-162.9$  (2 F, m, 3,5-F);

$^{13}\text{C}\{^1\text{H}\}$  NMR (126 MHz,  $\text{CD}_2\text{Cl}_2$ , 25  $^\circ\text{C}$ )  $\delta$  157.4 (s,  $\text{C}_g$ ), 147.9 (ddm,  $^1J_{\text{CF}} \approx 218$  Hz,  $^3J_{\text{CF}} \approx 35$  Hz,  $\text{C}_u$ ), 143.4 (d,  $J = 19.6$  Hz,  $\text{C}_f$ ), 138.4 (dm,  $^1J_{\text{CF}} \approx 239$  Hz,  $\text{C}_w$ ), 136.3 (dm,  $^1J_{\text{CF}} \approx 248$  Hz,  $\text{C}_v$ ), 133.0 (d,  $J = 4.6$  Hz,  $\text{C}_b$ ), 132.8 (d,  $J = 7.0$  Hz,  $\text{C}_e$ ), 130.8 (d,  $J = 2.1$  Hz,  $\text{C}_d$ ), 130.5 (s,  $\text{C}_m$ ), 129.0 (dd,  $J = 33.7, 4.0$  Hz,  $\text{C}_a$ ), 127.6 (d,  $J = 4.8$  Hz,  $\text{C}_c$ ), 118.2 (d,  $J = 8.2$  Hz,  $\text{C}_h$ ), 104.7 (s,  $\text{C}_i$ ), 55.7 (s,  $\text{C}_i$ ), 35.3 (dd,  $J = 18.9, 3.3$  Hz,  $\text{C}_p$ ), 31.4 (dd,  $J = 9.3, 1.6$  Hz, Cy), 30.2 (dd,  $J = 4.0, 1.9$  Hz, Cy), 27.7 – 27.0 (m, Cy), 26.4 (d,  $J = 1.4$  Hz, Cy)

MS (LIFDI) m/z (%) 684.13586 ( $[M]^+$ , 100) (calcd for  $C_{32}H_{35}F_5PO_2Ag$  684.13403, diff 0.00183)

(Lab book reference number: GA-5-383)

Synthesis of  $\text{Ag}(\text{C}_6\text{F}_5)(\text{BrettPhos})$  (**125**)

In a light protected Schlenk tube,  $\text{Ag}_2\text{CO}_3$  (83 mg, 0.3 mmol, 1 equiv.) and BrettPhos (322 mg, 0.6 mmol, 2 equiv.) was added, which was then evacuated and refilled three times with nitrogen. Under a flow of nitrogen,  $\text{CH}_3\text{CN}$  (3 mL), followed by  $\text{C}_6\text{F}_5\text{H}$  (504 mg, 3.0 mmol, 10 equiv., 333  $\mu\text{L}$ ) was added and the reaction mixture was submerged in a pre-heated oil bath (80 °C) and allowed to react for 23 h. The mixture was removed from the oil bath and filtered under an atmosphere of nitrogen. The solvent and excess reagents were removed under reduced pressure to produce an off-white solid which was then dissolved in  $\text{CH}_3\text{CN}$  (3 mL), while being stirred and heated to 80 °C. The hot solution was cannula filtered into another light protected Schlenk tube which was heated to 80 °C. The solution was allowed to cool down gradually to ambient temperature and then placed in –18 °C freezer to produce small peach-coloured crystals on the walls of the Schlenk tube. The crystals were filtered and dried under reduced pressure to yield the product as peach-coloured crystals (296.8 mg, 61 %). Peach-coloured crystals suitable for X-ray analysis were grown by preparing a saturated solution of **125** in hot acetonitrile (80 °C) which was initially slowly cooled to ambient temperature and then cooled further to –18 °C.

$^1\text{H}$  NMR (500 MHz,  $\text{CD}_2\text{Cl}_2$ , 25 °C):  $\delta$  7.06 – 7.02 (3 H, d of  $\text{H}^{\text{d}}$  overlapping with s of  $\text{H}^{\text{l}}$ ,  $\text{H}^{\text{d}}$  +  $\text{H}^{\text{l}}$ ), 6.96 (1 H,  $J = 9.1, 2.1$  Hz,  $\text{H}^{\text{c}}$ ), 3.90 (3 H, s,  $\text{H}^{\text{y}}$ ), 3.58 (3 H, s,  $\text{H}^{\text{x}}$ ), 2.59 – 2.35 (5 H, br Cy peak overlapping with sept of  $\text{H}^{\text{n}}$  and  $\text{H}^{\text{i}}$ ,  $J_{\text{iPr}} = 6.8$  Hz, Cy +  $\text{H}^{\text{n}}$  +  $\text{H}^{\text{i}}$ ), 1.98 – 1.87 (2 H, br, Cy), 1.80 – 1.46 (8 H, br, Cy), 1.45 – 1.04 (16 H, br Cy peak overlapping with d from  $\text{iPr}$  ( $\text{H}^{\text{k}}$  +  $\text{H}^{\text{j}}$ ),  $J_{\text{iPr}} = 6.8$  Hz, Cy +  $\text{H}^{\text{k}}$  +  $\text{H}^{\text{j}}$ ), 0.96 – 0.86 (12 H, overlapping d,  $J_{\text{iPr}} = 6.8$  Hz,  $\text{H}^{\text{k}}$  +  $\text{H}^{\text{j}}$  +  $\text{H}^{\text{o}}$ )

$^{31}\text{P}\{^1\text{H}\}$  (202.5 MHz,  $\text{CD}_2\text{Cl}_2$ , 25 °C):  $\delta$  18.14 (pair of dt,  $^1J_{107\text{Ag}-31\text{P}} = 441.5$  Hz,  $^1J_{109\text{Ag}-31\text{P}} = 510.3$  Hz,  $^4J_{\text{FP}} = 2.5$  Hz, 1 P).

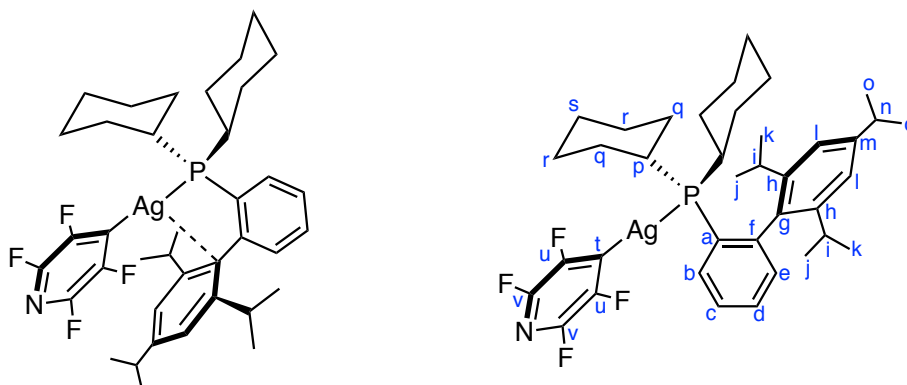
$^{19}\text{F}\{^1\text{H}\}$  (470.6 MHz,  $\text{CD}_2\text{Cl}_2$ , 25 °C):  $\delta$  –106.8 (2 F, m, 2,6-F), –161.9 (1 F, t,  $J = 20.0$  Hz, 4-F), –163.3 (2 F, m, 3,5-F).

$^{13}\text{C}\{^1\text{H}\}$  NMR (126 MHz,  $\text{CD}_2\text{Cl}_2$ , 25 °C)  $\delta$  156.2 (dd,  $J = 4.0, 2.5$  Hz,  $\text{C}_{\text{b}}$ ), 153.1 (d,  $J = 11.0$  Hz,  $\text{C}_{\text{e}}$ ), 148.5 (s,  $\text{C}_{\text{m}}$ ), 147.5 (br dm,  $^1J_{\text{CF}} \approx 250$  Hz,  $^3J_{\text{CF}} \approx 31$  Hz,  $\text{C}_{\text{u}}$ ), 146.6 (s,  $\text{C}_{\text{h}}$ ),

138.1 (d,  $J = 22.4$  Hz,  $C_f$ ), 137.7 (br dm,  $^1J_{CF} \approx 227$  Hz,  $C_w$ ), 135.8 (br dm,  $^1J_{CF} \approx 255$  Hz,  $C_v$ ), 130.9 (dd,  $J = 9.8, 1.4$  Hz,  $C_g$ ), 122.7 (s,  $C_i$ ), 118.6 (dd,  $J = 27.7, 4.2$  Hz,  $C_a$ ), 113.9 (d,  $J = 1.9$  Hz,  $C_d$ ), 110.2 (d,  $J = 3.7$  Hz,  $C_c$ ), 56.0 (s,  $C_y$ ), 55.2 (s,  $C_x$ ), 37.8 (dd,  $J = 19.2, 3.3$  Hz,  $C_p$ ), 35.0 (dd,  $J = 14.9, 2.9$  Hz,  $C_y$ ), 33.5 (s,  $C_n$ ), 31.1 (s,  $C_i$ ), 30.8 (d,  $J = 2.4$ ,  $C_y$ ), 27.8 (d,  $J = 11.3$  Hz,  $C_y$ ), 27.4 (d,  $J = 16.7$  Hz,  $C_y$ ), 26.4 (d,  $J = 1.2$  Hz,  $C_y$ ), 25.1 (s,  $C_k/C_j$ ), 24.4 (s,  $C_k/C_j$ ), 22.9 (s,  $C_o$ )

MS (LIFDI) m/z (%) 810.27734 ( $[M]^+$ , 100) (calcd for  $C_{41}H_{53}F_5PO_2Ag$  810.2754, diff 0.002)

(Lab book reference number: GA-5-382)

Synthesis of Ag(C<sub>5</sub>F<sub>4</sub>N)(Xphos) (165)

In a light protected Schlenk tube, Ag<sub>2</sub>CO<sub>3</sub> (83 mg, 0.3 mmol, 1 equiv.) and Xphos (286 mg, 0.6 mmol, 2 equiv.) was added, which was evacuated and refilled three times with nitrogen. Under a flow of nitrogen, CH<sub>3</sub>CN (10 mL), followed by C<sub>6</sub>F<sub>5</sub>H (453 mg, 3 mmol, 10 equiv., 300 μL) was added and the reaction mixture was submerged in a pre-heated oil bath (80 °C) and allowed to react for 23 h. The mixture was removed from the oil bath and filtered under an atmosphere of nitrogen. The solvent and excess reagents were removed under-reduced pressure to produce a dark brown solid. The solid was then dissolved in CH<sub>3</sub>CN (10 mL), while being stirred and heated to 80 °C. The hot solution was cannula filtered into another light protected Schlenk tube which was heated to 80 °C. The solution was allowed to cool down gradually to ambient temperature and then placed in –18 °C freezer to produce small dark brown crystals on the walls of the Schlenk tube. The crystals were filtered and dried under reduced pressure to yield the product as dark brown crystals (240.6 mg, 55 %). Brown plate-like crystals suitable for X-ray analysis were grown by preparing a saturated solution of **165** in hot acetonitrile (80 °C) which was initially slowly cooled to ambient temperature and then cooled further to –18 °C.

NMR <sup>1</sup>H (500 MHz, C<sub>6</sub>D<sub>6</sub>, 25 °C): δ 7.22 (2 H, s, **H<sup>a</sup>**), 7.13 – 7.17 (1 H, m, **H<sup>b</sup>** overlapped with *protio* peak of C<sub>6</sub>D<sub>6</sub>), 7.06 (1 H, m, **H<sup>c</sup>**), 7.02 – 6.98 (2 H, m, **H<sup>c</sup>** + **H<sup>d</sup>**), 2.61 (1 H, sept, *J* = 6.9 Hz, **H<sup>n</sup>**), 2.44 (2 H, sept, *J* = 6.8 Hz, **H<sup>i</sup>**), 1.86 – 1.70 (6 H, br, **Cy**), 1.62 – 1.43 (12 H, br **Cy** peak overlapping *d*, *J* = 6.9 Hz, **H<sup>k</sup>** + **H<sup>j</sup>**), 1.39 – 0.82 (23 H, br **Cy** peak overlapping with *d* from <sup>i</sup>Pr (**H<sup>o</sup>**), *J*<sub>*iPr*</sub> = 6.9 Hz, and **H<sup>k</sup>** + **H<sup>j</sup>**, *J* = 6.9 Hz).

<sup>31</sup>P {<sup>1</sup>H} (202.5 MHz, C<sub>6</sub>D<sub>6</sub>, 25 °C): δ 13.24 (pair of dt, <sup>1</sup>*J*<sub>107Ag–31P</sub> = 440.4 Hz, <sup>1</sup>*J*<sub>109Ag–31P</sub> = 509.0 Hz, <sup>4</sup>*J*<sub>FP</sub> = 4.0 Hz, 1 *P*).

<sup>19</sup>F {<sup>1</sup>H} (470.6 MHz, C<sub>6</sub>D<sub>6</sub>, 25 °C): δ –97.9 (2 F, m, 2,6-F(**F<sub>v</sub>**)), –114.9 (2 F, m, 3,5-F(**F<sub>u</sub>**)).

<sup>13</sup>C {<sup>1</sup>H} NMR (126 MHz, C<sub>6</sub>D<sub>6</sub>, 25 °C): δ 149.9 (s, **C<sub>m</sub>**), 147.8 (d, <sup>3</sup>*J*<sub>CP</sub> = 12.6 Hz, **Quat. C**), 146.1 (s, **C<sub>h</sub>**), 145.9 (dm, <sup>1</sup>*J*<sub>CF</sub> ≈ 226.8 Hz, **CF**), 143.6 (ddm, <sup>1</sup>*J*<sub>CF</sub> ≈ 253.3 Hz, **CF**), 135.1 (d, *J* = 8.8 Hz, **Quat. C**), 133.0 (d, *J* = 6.3 Hz, **C<sub>e</sub>**), 132.4 (d, *J* = 5.0 Hz, **C<sub>b</sub>**), 130.3 (d, *J* = 2.5

Hz, **C<sub>c</sub>**), 129.2 (dd,  $J = 32.9, 2.9$  Hz, **Quat. C**), 127.5 (d,  $J = 4.5$  Hz, **C<sub>d</sub>**), 122.8 (s, **C<sub>i</sub>**), 36.1 (dd,  $J = 17.7, 3.7$  Hz, **C<sub>p</sub>**), 33.9 (s, **C<sub>n</sub>**), 31.9 (dd,  $J = 8.8, 1.1$  Hz, **Cy CH<sub>2</sub>**), 31.4 (s, **C<sub>i</sub>**), 30.6 (dd,  $J = 6.1, 2.4$  Hz, **Cy CH<sub>2</sub>**), 27.5 (d,  $J = 13.8$  Hz, **Cy CH<sub>2</sub>**), 27.0 (d,  $J = 11.3$  Hz, **Cy CH<sub>2</sub>**), 26.0 (br d, **Cy CH<sub>2</sub>**), 25.9 (s, **C<sub>o</sub>**), 23.6 (s, **C<sub>k</sub>/ C<sub>j</sub>**), 23.4 (s, **C<sub>k</sub>/ C<sub>j</sub>**).

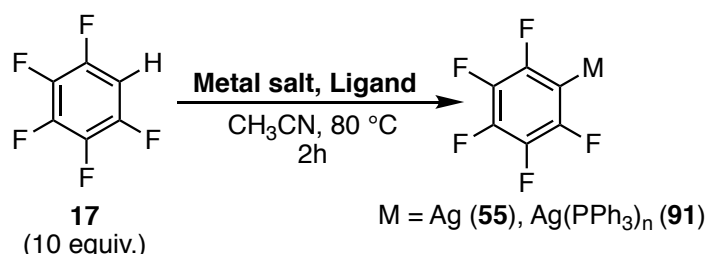
MS (LIFDI)  $m/z$  (%) 733.25683 ( $[M]^+$ , 100) (calcd for  $C_{38}H_{49}F_4NPAg$  733.2590, diff 0.00217)

(Lab book reference number: GA-4-280)

## 6.4 Experimental Procedures for Chapter 2

### 6.4.1 Reactions of Different Ag<sup>I</sup> salts with C<sub>6</sub>F<sub>5</sub>H in the presence of Different Additives

#### General Procedure for reactions of Ag<sup>I</sup> salts in acetonitrile



In a light-protected Schlenk tube, the desired Ag<sup>I</sup> salt, and additives (if required) were added and the Schlenk tube was evacuated and refilled three times with nitrogen. Under an atmosphere of nitrogen, dry acetonitrile (1 mL) was added and the Schlenk tube was submerged in a pre-heated oil bath (80 °C). Using a gas-tight microsyringe (250 μL), pentafluorobenzene (168 mg, 1 mmol, 10 equiv., 111 μL) was added and the reaction was stirred at 80 °C for 2 h. Then, 0.6 mL of the reaction mixture was transferred to a J-Young NMR tube, under an atmosphere of nitrogen and the mixture was immediately analysed by <sup>1</sup>H and <sup>19</sup>F{<sup>1</sup>H} NMR spectroscopy. If phosphine was added, the reaction mixture was also analysed by <sup>31</sup>P{<sup>1</sup>H} NMR spectroscopy. Results presented in **Table 3**.

**GA-1-049 (Entry 1):** The desired Ag<sup>I</sup> salt used was AgOAc (17 mg, 0.1 mmol, 1 equiv.) and no phosphine was added.

**GA-1-046 (Entry 2):** The desired Ag<sup>I</sup> salt used was Ag<sub>2</sub>CO<sub>3</sub> (28 mg, 0.1 mmol, 1 equiv.) and no phosphine was added.

**GA-1-043 (Entry 3):** The desired Ag<sup>I</sup> salts added were AgOAc (17 mg, 0.1 mmol, 1 equiv.) and Ag<sub>2</sub>CO<sub>3</sub> (28 mg, 0.1 mmol, 1 equiv.) and no phosphine was added.

**GA-1-052 (Entry 4):** The desired Ag<sup>I</sup> salt used was AgOAc (17 mg, 0.1 mmol, 1 equiv.), followed by PPh<sub>3</sub> (52 mg, 0.2 mmol, 2 equiv.).

**GA-1-044 (Entry 5):** The desired Ag<sup>I</sup> salts added were AgOAc (17 mg, 0.1 mmol, 1 equiv.) and Ag<sub>2</sub>CO<sub>3</sub> (28 mg, 0.1 mmol, 1 equiv.), followed by PPh<sub>3</sub> (52 mg, 0.2 mmol, 2 equiv.).

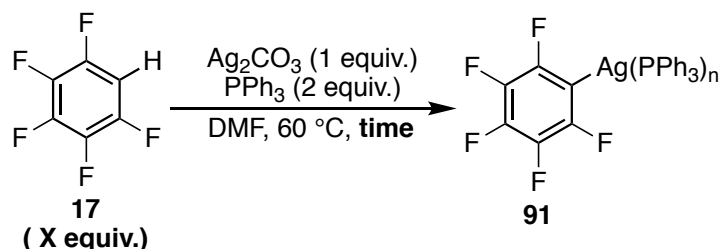
**GA-1-047 (Entry 6):** The desired Ag<sup>I</sup> salt added was Ag<sub>2</sub>CO<sub>3</sub> (28 mg, 0.1 mmol, 1 equiv.), followed by PPh<sub>3</sub> (52 mg, 0.2 mmol, 2 equiv.).

**GA-1-083 (Entry 7):** The desired Ag<sup>I</sup> salt added was AgOAc (17 mg, 0.1 mmol, 1 equiv.), followed by Cs<sub>2</sub>CO<sub>3</sub> (33 mg, 0.1 mmol, 1 equiv.).

**GA-1-084 (Entry 8):** The desired  $\text{Ag}^{\text{I}}$  salt added was  $\text{AgOAc}$  (33 mg, 0.2 mmol, 1 equiv.), followed by  $\text{Cs}_2\text{CO}_3$  (163 mg, 0.5 mmol, 2.5 equiv.). 5 equivalences of  $\text{C}_6\text{F}_5\text{H}$  used with respect to  $\text{AgOAc}$ .

**GA-1-085 (Entry 9):** The desired  $\text{Ag}^{\text{I}}$  salt added was  $\text{AgNO}_3$  (17 mg, 0.1 mmol, 1 equiv.), followed by  $\text{Cs}_2\text{CO}_3$  (33 mg, 0.1 mmol, 1 equiv.).

**The reaction of  $\text{Ag}_2\text{CO}_3$  and  $\text{PPh}_3$  with  $\text{C}_6\text{F}_5\text{H}$  in DMF at 60 °C**



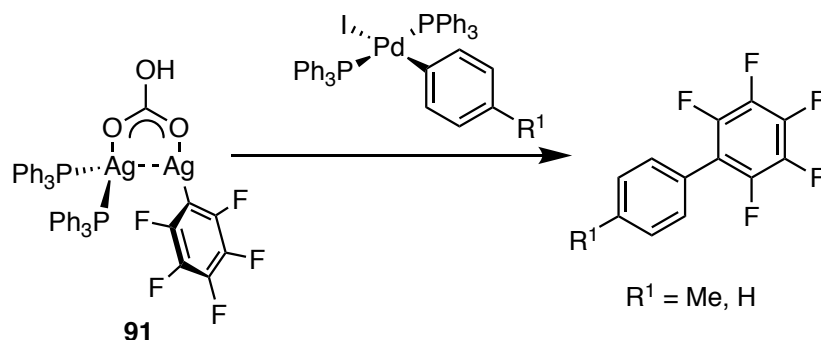
In a light-protected Schlenk tube,  $\text{Ag}_2\text{CO}_3$  (82 mg, 0.3 mmol, 1 equiv.) and  $\text{PPh}_3$  (157 mg, 0.6 mmol, 2 equiv.) were added and the Schlenk tube was evacuated and refilled three times with nitrogen. Dry DMF (3 mL) and  $\text{C}_6\text{F}_5\text{H}$  were added and the Schlenk tube was submerged in a pre-heated oil bath (60 °C) and allowed to react for 24 h. The progress of the reaction was monitored using reaction aliquots. The reaction aliquots were prepared by transferring 0.5 mL of the reaction mixture into a J-Young NMR tube using a syringe, under an atmosphere of nitrogen. The reaction aliquots were collected at 2 h, 4 h, 24 h, and 48 h analysed using  $^1\text{H}$ ,  $^{31}\text{P}\{^1\text{H}\}$  and  $^{19}\text{F}\{^1\text{H}\}$  NMR spectroscopy. Results presented in **Table 4**.

**GA-1-050 (Entry 1):** The equivalence of the  $\text{C}_6\text{F}_5\text{H}$  is 10 with respect to the  $\text{Ag}_2\text{CO}_3$ . The  $\text{C}_6\text{F}_5\text{H}$  (504 mg, 3 mmol, 10 equiv. 330  $\mu\text{L}$ ) was added with a 500  $\mu\text{L}$  gas-tight syringe.

**GA-1-053 (Entry 2):** The equivalence of the  $\text{C}_6\text{F}_5\text{H}$  is 1 with respect to the  $\text{Ag}_2\text{CO}_3$ . The  $\text{C}_6\text{F}_5\text{H}$  (50 mg, 0.3 mmol, 1 equiv. 35  $\mu\text{L}$ ) was added with a 50  $\mu\text{L}$  gas-tight syringe.

#### 6.4.2 Cross-Coupling Reactions with Pd(II) Complexes

Stoichiometric reaction between the  $\text{Ag}_2(\text{PPh}_3)_2(\text{C}_6\text{F}_5)(\text{HCO}_3)$  **91** and  $\text{Pd}(\text{PPh}_3)_2(\text{I})(\text{R}^1)$  ( $\text{R}^1$  = phenyl **97**, tolyl **98**), at room temperature



In a glovebox,  $\text{Ag}_2(\text{PPh}_3)_2(\text{C}_6\text{F}_5)(\text{HCO}_3)$  **91** (9.7 mg,<sup>[a]</sup>) and  $\text{Pd}(\text{PPh}_3)_2(\text{I})(\text{R}^1)$  were weighed out in two separate vials, and the silver complex was dissolved in solvent (0.5 mL) and then



mixed with the palladium complex. The reaction mixture was then transferred to a J-Young NMR tube, and immediately taken to the AV 500 MHz instrument to monitor the reaction by  $^{31}\text{P}\{^1\text{H}\}$  and  $^{19}\text{F}\{^1\text{H}\}$  NMR spectroscopy.

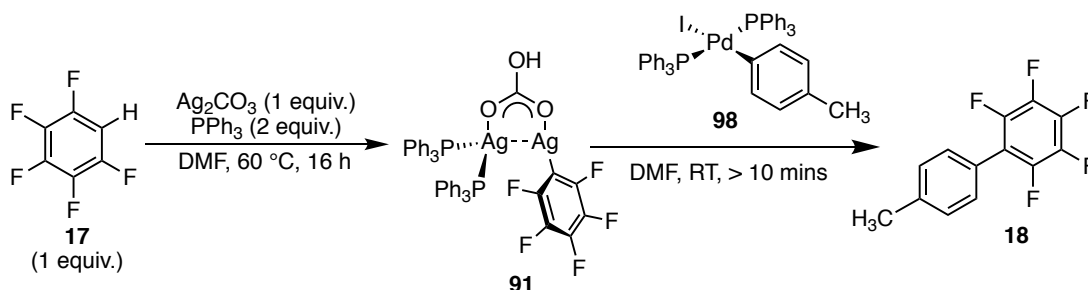
[a] The sample of  $\text{Ag}_2(\text{PPh}_3)_2(\text{C}_6\text{F}_5)(\text{HCO}_3)$  **91** used was contaminated with 25 %  $\text{C}_6\text{F}_5\text{H}$ , the actual amount of  $\text{Ag}_2(\text{PPh}_3)_2(\text{C}_6\text{F}_5)(\text{HCO}_3)$  **91** used is 7.3 mg, 0.0075 mmol, 1 equiv.

**GA-1-076:** The stoichiometric reaction between  $\text{Ag}_2(\text{PPh}_3)_2(\text{C}_6\text{F}_5)(\text{HCO}_3)$  **91** and  $\text{Pd}(\text{PPh}_3)_2(\text{I})(\text{tolyl})$  **98** at room temperature in toluene. The  $\text{Pd}(\text{PPh}_3)_2(\text{I})(\text{tolyl})$  **98** complex (8.5 mg, 0.01 mmol, 1.3 equiv.) was used and toluene was the solvent. All the  $\text{Ag}_2(\text{PPh}_3)_2(\text{C}_6\text{F}_5)(\text{HCO}_3)$  **91** was fully consumed in less than 10 minutes at room temperature (determined by  $^{19}\text{F}\{^1\text{H}\}$  NMR spectroscopy).

**GA-1-102:** The stoichiometric reaction between  $\text{Ag}_2(\text{PPh}_3)_2(\text{C}_6\text{F}_5)(\text{HCO}_3)$  **91** and  $\text{Pd}(\text{PPh}_3)_2(\text{I})(\text{phenyl})$  **97** at room temperature in toluene. The  $\text{Pd}(\text{PPh}_3)_2(\text{I})(\text{Ph})$  complex **97** (8.3 mg, 0.01 mmol, 1.3 equiv.) was used and toluene was the solvent. All the  $\text{Ag}_2(\text{PPh}_3)_2(\text{C}_6\text{F}_5)(\text{HCO}_3)$  **91** was fully consumed in less than 10 min at room temperature (determined by  $^{19}\text{F}\{^1\text{H}\}$  NMR spectroscopy).

**GA-1-103:** The stoichiometric reaction between  $\text{Ag}_2(\text{PPh}_3)_2(\text{C}_6\text{F}_5)(\text{HCO}_3)$  **91** and  $\text{Pd}(\text{PPh}_3)_2(\text{I})(\text{Ph})$  **97** at room temperature in dichloromethane. The  $\text{Pd}(\text{PPh}_3)_2(\text{I})(\text{Ph})$  **97** complex (8.3 mg, 0.01 mmol, 1.3 equiv.) was used and dichloromethane was the solvent. All the  $\text{Ag}_2(\text{PPh}_3)_2(\text{C}_6\text{F}_5)(\text{HCO}_3)$  **91** was fully consumed in less than 10 min at room temperature (determined by  $^{19}\text{F}\{^1\text{H}\}$  NMR spectroscopy).

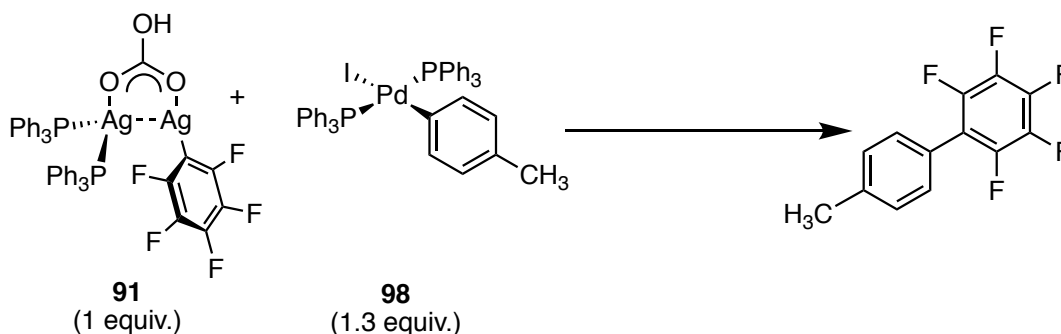
**GA-1-079:** *in situ* generation of  $\text{Ag}_2(\text{PPh}_3)_2(\text{C}_6\text{F}_5)(\text{HCO}_3)$  **91** in DMF, and subsequent reaction with  $\text{Pd}(\text{PPh}_3)_2(\text{I})(4\text{-tolyl})$  **98** at room temperature.



In a light-protected Schlenk tube,  $\text{Ag}_2\text{CO}_3$  (83 mg, 0.3 mmol, 1 equiv.),  $\text{PPh}_3$  (157 mg, 0.6 mmol, 2 equiv.) were added and the Schlenk tube was evacuated and refilled three times with nitrogen. Against a flow of nitrogen, dry DMF (3 mL) and  $\text{C}_6\text{F}_5\text{H}$  (50 mg, 0.30 mmol, 1 equiv.  $\mu\text{L}$ ) was added and the reaction mixture was submerged in a pre-heated oil bath and allowed to react for 16 h. After 16 h, 0.5 mL of the reaction mixture was transferred to a J-Young NMR

tube and the % conversion of  $C_6F_5H$  to  $Ag_2(PPh_3)_2(C_6F_5)(\mu_2-HCO_3)$  **91** was determined. The reaction mixture was diluted by transferring 0.3 mL of the reaction mixture into another Schlenk tube and adding dry DMF (2.7 mL). To this,  $Pd(PPh_3)_2(I)(4-tolyl)$  **98** (25 mg, 0.03 mmol,) was added and the mixture was stirred for 2 minutes before 0.5 mL of the diluted reaction mixture was transferred to a J-Young NMR tube and analysed by  $^{31}P\{^1H\}$  and  $^{19}F\{^1H\}$  NMR spectroscopy.

**The reaction between  $Ag_2(PPh_3)_2(C_6F_5)(\mu_2-HCO_3)$  **91** and  $Pd(PPh_3)_2(I)(4-tolyl)$  **98** monitored by low temperature  $^{31}P\{^1H\}$  and  $^{19}F\{^1H\}$  NMR spectroscopy.**



In a glovebox, a stock solution of  $Ag_2(PPh_3)_2(C_6F_5)(HCO_3)$  **91** (39 mg, 0.04 mmol)<sup>[a]</sup> was prepared in the desired solvent (0.8 mL, 0.05 M) and transferred to a J-Young tube. In another vial,  $Pd(PPh_3)_2(I)(4-tolyl)$  **98** (8.5 mg, 0.01 mmol, 1.3 equiv.) was dissolved in the desired solvent (300  $\mu$ L) and transferred into another J-Young NMR tube. Both NMR tubes were connected to the Schlenk line using a suitable adaptor, and the headspace of the adaptor was evacuated and refilled three times with nitrogen. The J-Young NMR tubes submerged in a  $-78^\circ C$  (195 K) dry ice/acetone cold bath. The temperature of the cold bath was monitored using a temperature probe. Under an atmosphere of nitrogen, the J-Young caps were removed, and the cold  $Ag_2(PPh_3)_2(C_6F_5)(HCO_3)$  solution (200  $\mu$ L) was transferred to the  $Pd(PPh_3)_2(I)(4-tolyl)$  solution using a 250  $\mu$ L gas tight syringe (**Figure 100**). The J young cap of the reaction mixture was screwed back on, and the reaction mixture was carried in a cold bath dewar (dry ice/acetone,  $-78^\circ C$ ) to the NMR centre and monitored using the AV 500 instrument

<sup>[a]</sup> The sample of  $Ag_2(PPh_3)_2(C_6F_5)(HCO_3)$  was contaminated with 25 %  $C_6F_5H$ , the actual mass of  $C_6F_5H$  actually being weight out is (29 mg, 0.03 mmol)

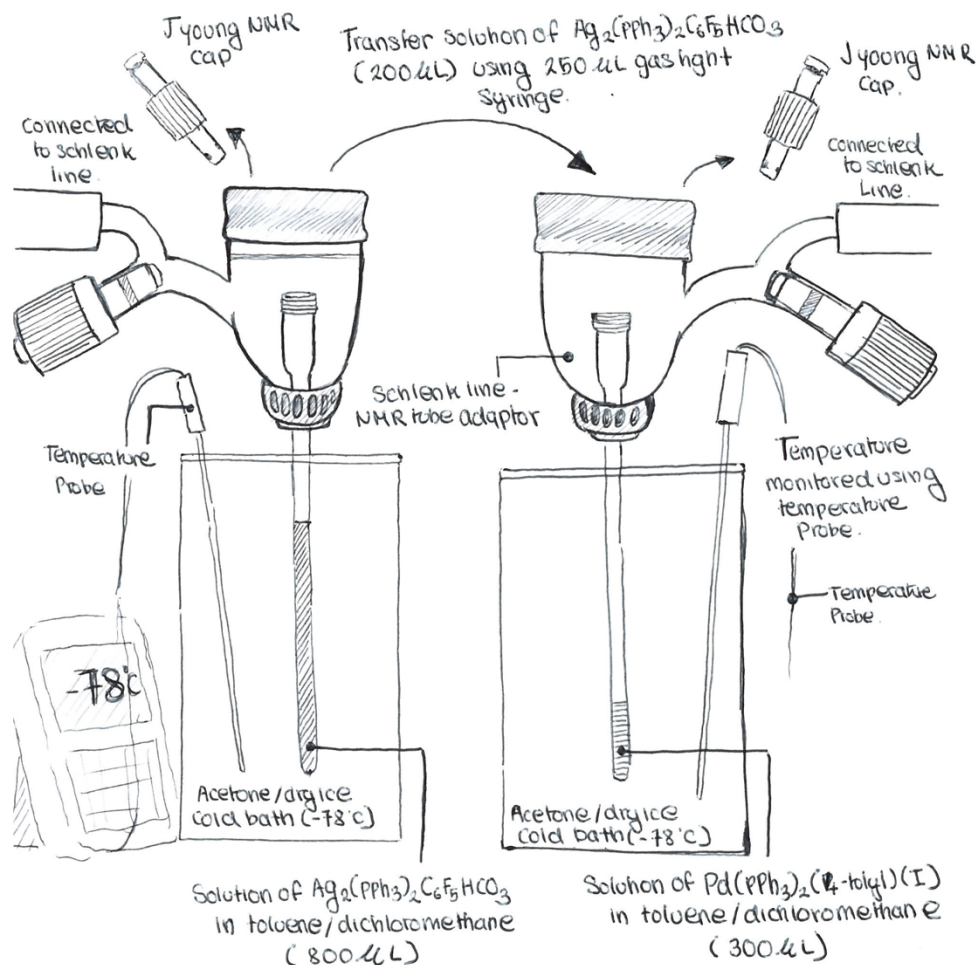


**Figure 100:** Experimental set-up for preparation of the sample for the low-temperature VT NMR monitoring of the transmetalation reaction

**GA-1-087:** The low temperature monitoring of the reaction between  $\text{Ag}_2(\text{PPh}_3)_2(\text{C}_6\text{F}_5)(\text{HCO}_3)$  **91** and  $\text{Pd}(\text{PPh}_3)_2(\text{I})(4\text{-tolyl})$  **98** in toluene- $d_8$ . The sample was prepared at  $-78\text{ }^\circ\text{C}$ , and place in a pre-cooled probe ( $-75\text{ }^\circ\text{C}$ , 198 K) on the AV 500 MHz instrument. The  $^{31}\text{P}\{^1\text{H}\}$  and  $^{19}\text{F}\{^1\text{H}\}$  NMR spectrum of the reaction mixture were collected for a temperature range between  $-70\text{ }^\circ\text{C}$  (203 K) to  $0\text{ }^\circ\text{C}$  (273 K) with  $10\text{ }^\circ\text{C}$  increments. (all spectra collected on AV500, saved under GA-1-087)

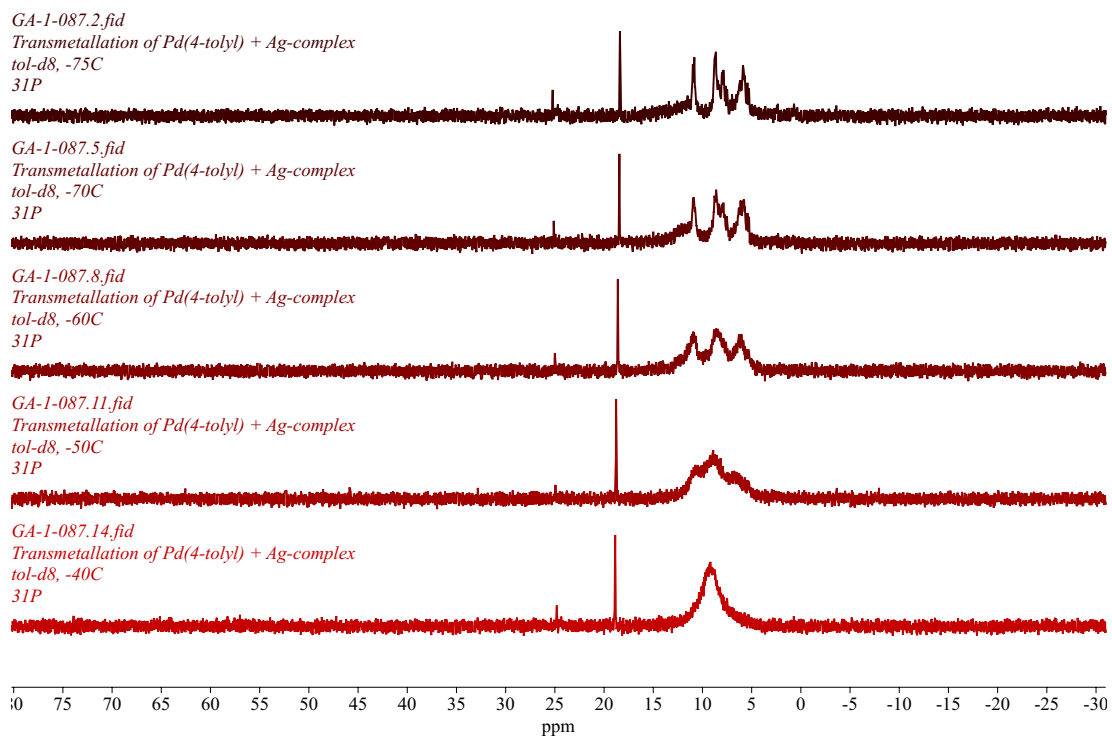


**Figure 101:**  $^{31}\text{P}\{^1\text{H}\}$  (202.5 MHz, tol- $d_8$ ) stack plot of the **GA-1-087** reaction mixture at different temperatures ( $-75\text{ }^\circ\text{C}$  to  $-40\text{ }^\circ\text{C}$ )

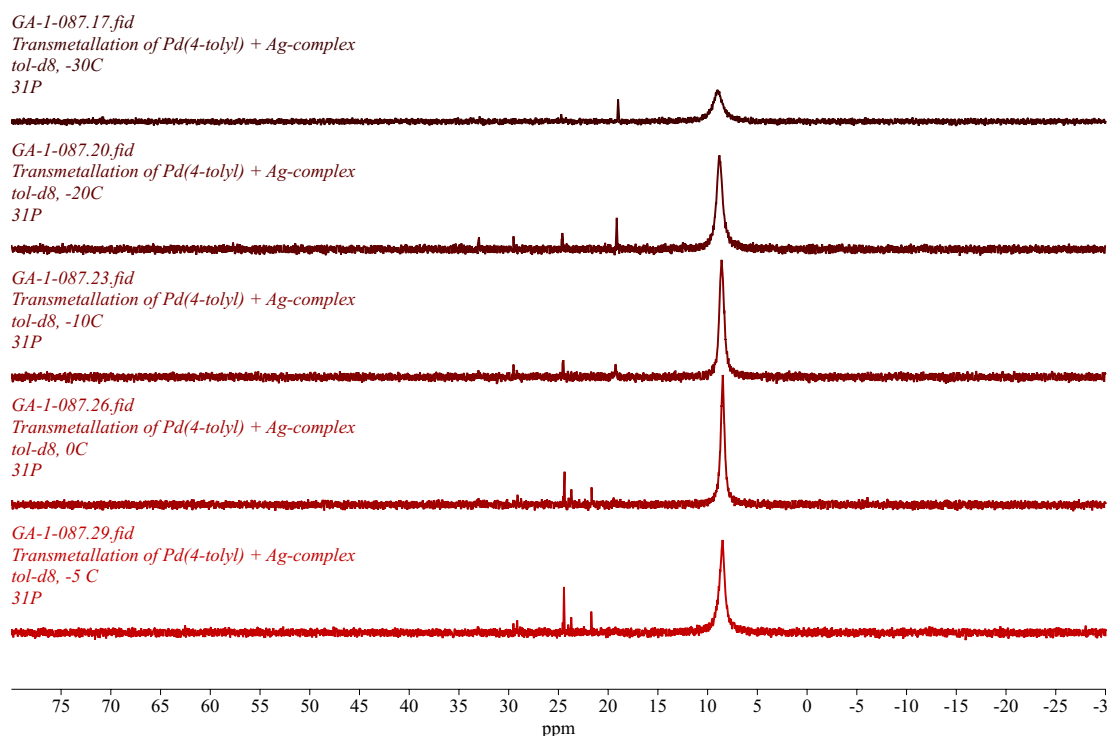


**Figure 102:**  $^{31}\text{P}\{^1\text{H}\}$  (202.5 MHz, tol- $d_8$ ) stack plot of the **GA-1-087** reaction mixture at different temperatures ( $-30\text{ }^\circ\text{C}$  to  $-5\text{ }^\circ\text{C}$ )

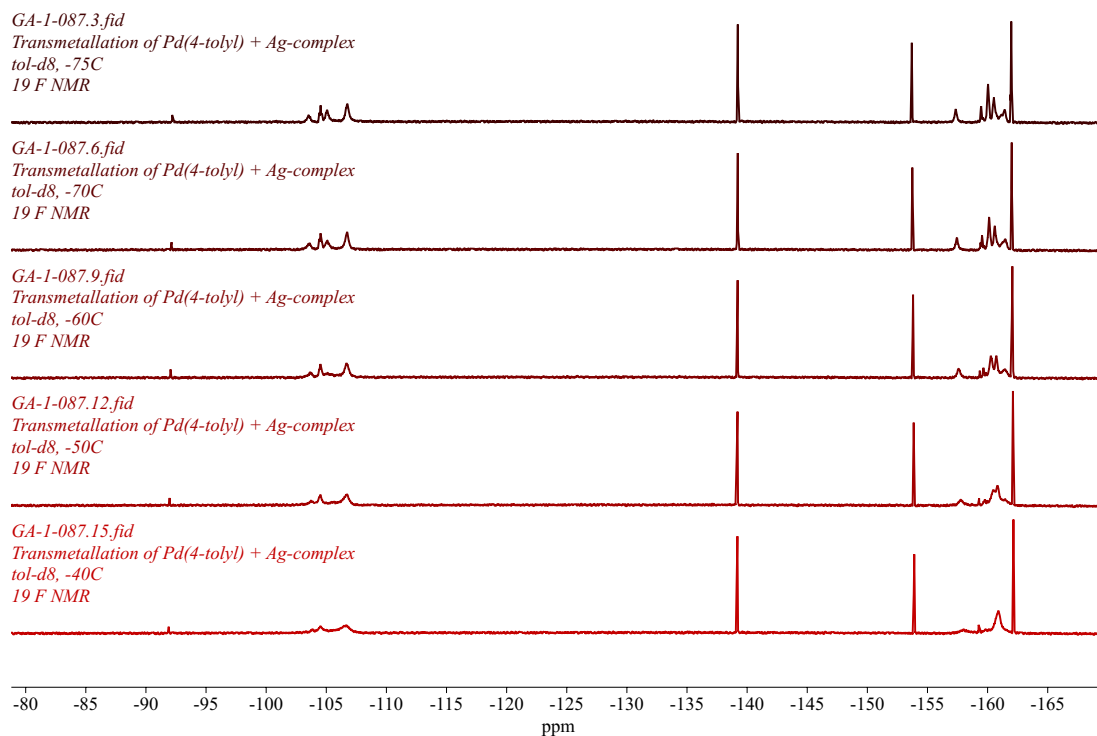


**Figure 103:**  $^{19}\text{F}\{^1\text{H}\}$  (470 MHz, tol- $d_8$ ) stack plot of the GA-1-087 reaction mixture at different temperatures ( $-75\text{ }^\circ\text{C}$  to  $-40\text{ }^\circ\text{C}$ )

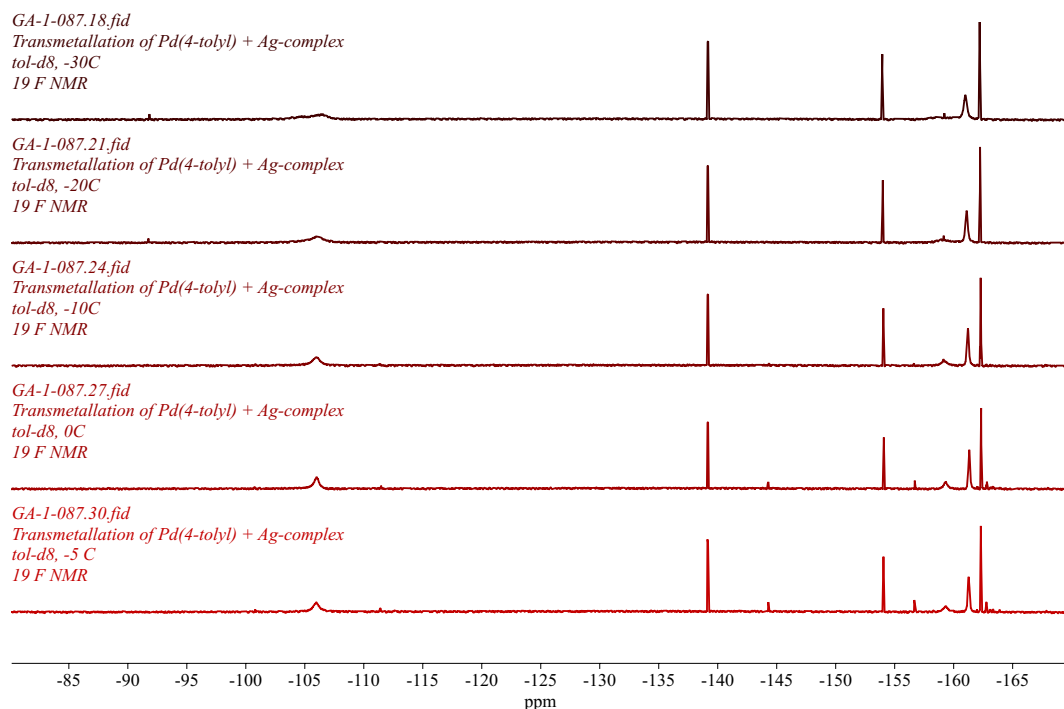


**Figure 104:**  $^{19}\text{F}\{^1\text{H}\}$  (470 MHz, tol- $d_8$ ) stack plot of the GA-1-087 reaction mixture at different temperatures ( $-30\text{ }^\circ\text{C}$  to  $-5\text{ }^\circ\text{C}$ )

**GA-2-104:** The low temperature monitoring of the reaction between  $\text{Ag}_2(\text{PPh}_3)_2(\text{C}_6\text{F}_5)(\text{HCO}_3)$  **91** and  $\text{Pd}(\text{PPh}_3)_2(\text{I})(4\text{-tolyl})$  **98** in dichloromethane- $d_2$ . The sample was prepared at  $-78\text{ }^\circ\text{C}$ , and placed in a pre-cooled probe ( $-40\text{ }^\circ\text{C}$ , 233 K) on the AV 500 MHz instrument. The  $^{31}\text{P}\{^1\text{H}\}$  and  $^{19}\text{F}\{^1\text{H}\}$  NMR spectrum of the reaction mixture were collected for a temperature range between  $-40\text{ }^\circ\text{C}$  (233 K) to  $0\text{ }^\circ\text{C}$  (273 K) with  $5\text{ }^\circ\text{C}$  increments. (all spectra collected on AV500, saved under GA-2-104)

GA-2-104.2.fid  
 $(\text{PPh}_3)_2\text{Ag}_2(\text{C}_6\text{F}_5)(\text{HCO}_3) + \text{Pd}(\text{Ph})(\text{I})(\text{PPh}_3)_2$   
 DCM,  $-40\text{ }^\circ\text{C}$   
 $^{31}\text{P}$

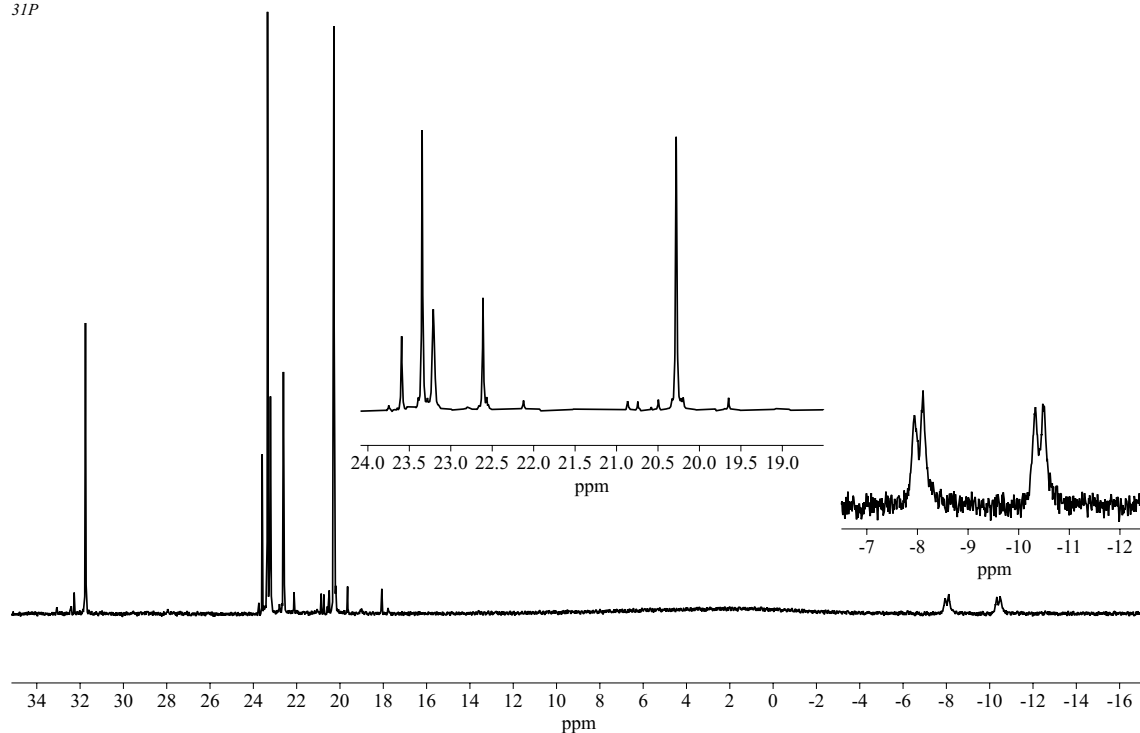


**Figure 105:**  $^{31}\text{P}\{^1\text{H}\}$  NMR (202.5 MHz, dichloromethane- $d_2$ ,  $-40\text{ }^\circ\text{C}$ ) of the **GA-2-104** reaction mixture.

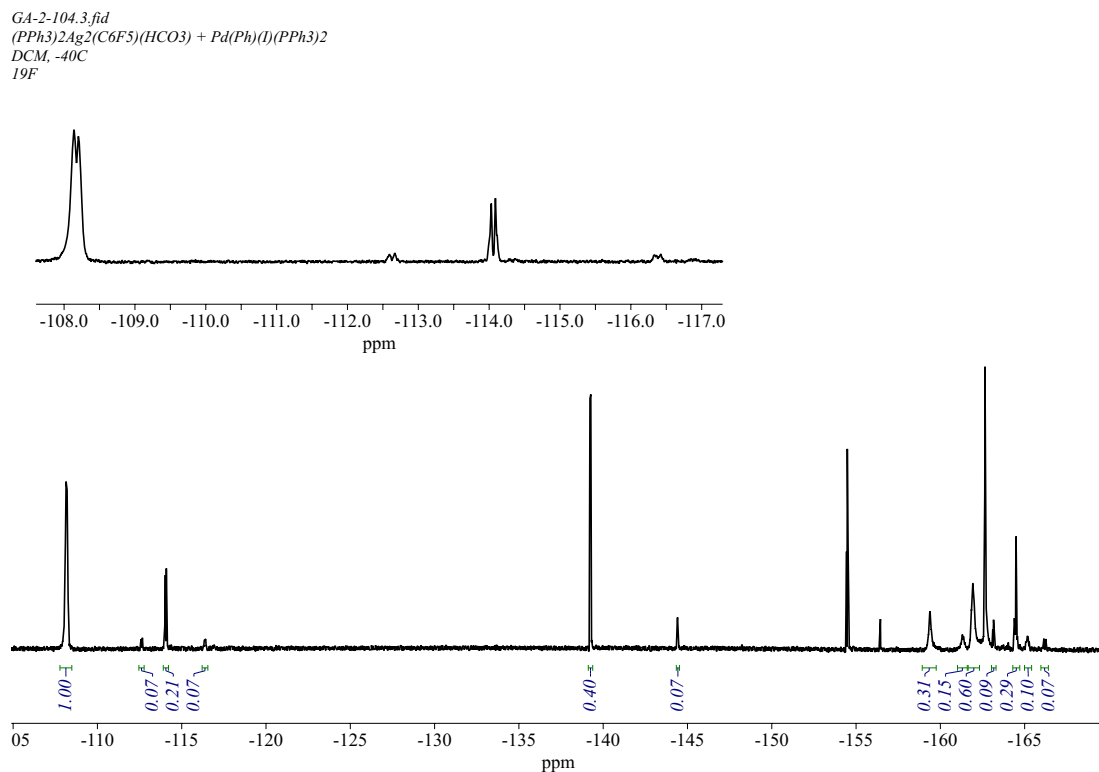
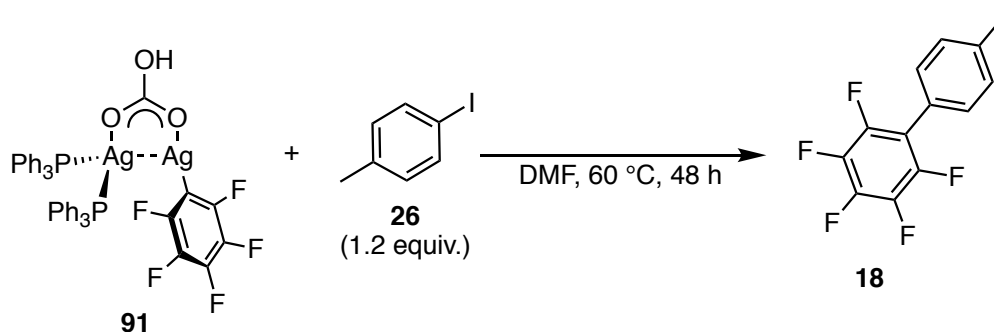


**Figure 106:** <sup>19</sup>F{<sup>1</sup>H} NMR (470 MHz, dichloromethane-*d*<sub>2</sub>, -40 °C) of the **GA-2-104** reaction mixture at different temperatures (-30 °C to -5 °C)

### 6.4.3 Reactions with Ag<sub>2</sub>(PPh<sub>3</sub>)<sub>2</sub>(C<sub>6</sub>F<sub>5</sub>)(HCO<sub>3</sub>) **91** and other reaction intermediates

#### GA-2-110: The reaction of Ag<sub>2</sub>(PPh<sub>3</sub>)<sub>2</sub>(C<sub>6</sub>F<sub>5</sub>)(HCO<sub>3</sub>) **91** with 4-iodotoluene in DMF

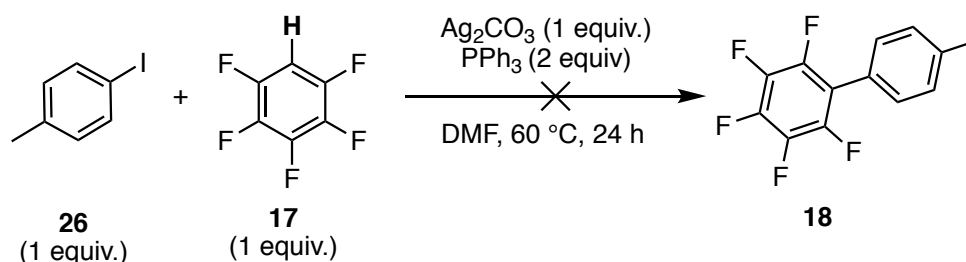


In a glovebox, 4-iodotoluene **26** (13 mg, 0.06 mmol, 1.2 equiv.) and Ag<sub>2</sub>(PPh<sub>3</sub>)<sub>2</sub>(C<sub>6</sub>F<sub>5</sub>)(HCO<sub>3</sub>) **91** (49 mg, 0.05 mmol, 1 equiv.)<sup>[a]</sup> were weighed out in separate vials. The 4-iodotoluene **26** was dissolved in DMF (0.6 mL) and this solution was used to dissolve the silver complex producing a peach reaction mixture. The reaction mixture was then transferred to a J-Young tube and analysed by <sup>31</sup>P{<sup>1</sup>H} and <sup>19</sup>F{<sup>1</sup>H} prior to submerging the J-

Young tube in a pre-heated oil bath (60 °C). Upon heating to 60 °C, the reaction mixture was monitored at 1 h, 2 h and 48 h.

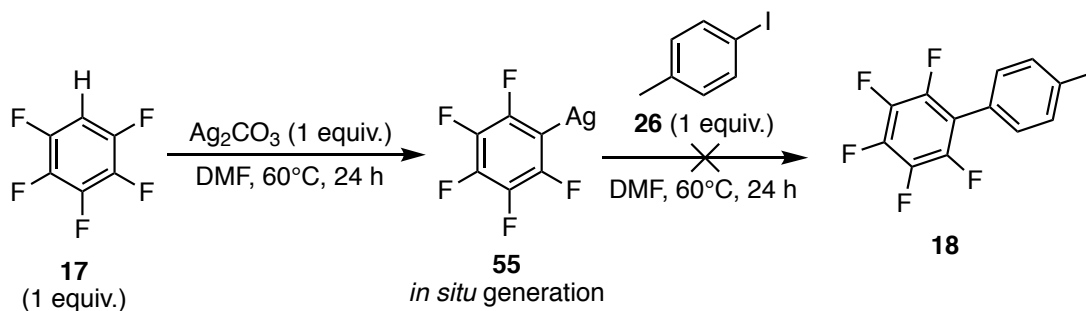
[a] The sample of  $\text{Ag}_2(\text{PPh}_3)_2(\text{C}_6\text{F}_5)(\text{HCO}_3)$  **91** used was contaminated with 30 %  $\text{C}_6\text{F}_5\text{H}$ , thus the mass of solid weighed out is 70 mg.

**GA-1-060:** The reaction of 4-Iodotoluene **26** and  $\text{C}_6\text{F}_5\text{H}$  **17** in the presence of  $\text{Ag}_2\text{CO}_3$  and  $\text{PPh}_3$



To a light-protected Schlenk tube equip with a stirrer bar,  $\text{Ag}_2\text{CO}_3$  (83 mg, 0.3 mmol, 1 equiv.) and  $\text{PPh}_3$  (157 mg, 0.6 mmol, 2 equiv.) were added and the Schlenk tube was evacuated and refilled three times with  $\text{N}_2$ . Against a flow of  $\text{N}_2$ , 4-iodotoluene **26** (65 mg, 0.3 mmol, 1 equiv.) was added followed by DMF (3 mL). The reaction mixture was submerged in a pre-heated oil bath (60 °C) and initiated by the addition of  $\text{C}_6\text{F}_5\text{H}$  **17**. After 24 h, 0.5 mL of the reaction mixture was transferred to a J-Young NMR tube under an atmosphere of  $\text{N}_2$  and analysed by  $^{31}\text{P}\{^1\text{H}\}$  and  $^{19}\text{F}\{^1\text{H}\}$  NMR spectroscopy.

**GA-1-058:** The reaction of  $\text{Ag}_2\text{CO}_3$  with  $\text{C}_6\text{F}_5\text{H}$  **17** in DMF at 60 °C followed by the addition of 4-iodotoluene **26**

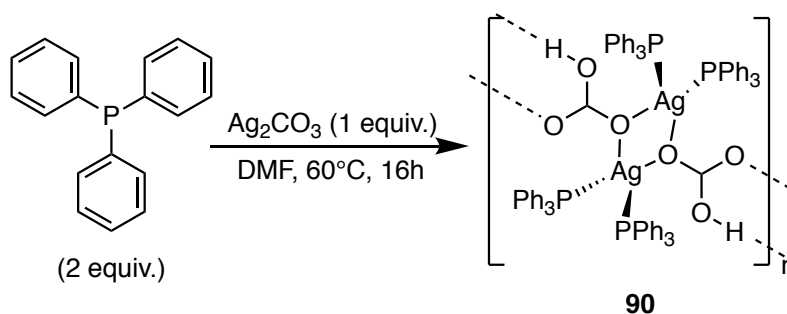


To a light-protected Schlenk tube equipped with a stirrer bar,  $\text{Ag}_2\text{CO}_3$  (83 mg, 0.3 mmol, 1 equiv.) was added, and the Schlenk tube was evacuated and refilled three times with  $\text{N}_2$ . Under an atmosphere of nitrogen, dry DMF (3 mL) was added with a 5 mL syringe fitted with a long needle. The reaction mixture was submerged in a pre-heated oil bath at 60 °C, before adding the  $\text{C}_6\text{F}_5\text{H}$  **17** (50.4 mg, 0.3 mmol, 1 equiv. 35  $\mu\text{L}$ ). The reaction mixture was then stirred at 60 °C for 24 h. After 24 h, precisely 0.5 mL of the reaction mixture was carefully transferred to a J-Young NMR tube under an atmosphere of nitrogen and the reaction mixture was analysed by  $^{31}\text{P}\{^1\text{H}\}$  and  $^{19}\text{F}\{^1\text{H}\}$  NMR spectroscopy. 4-Iodotoluene **26** (54.5 mg, 0.24



mmol, 1 equiv.) was added to the remaining reaction mixture (2.5 mL) and stirred at 60 °C for another 24 h. The amount of 4-iodotoluene **26** was corrected to the 2.5 mL volume of reaction mixture remaining after collecting the first reaction aliquot. After heating for 24 h, another reaction aliquot was collected to analyse the reaction mixture by  $^{31}\text{P}\{^1\text{H}\}$  and  $^{19}\text{F}\{^1\text{H}\}$  NMR spectroscopy.

**GA-1-088:** The reaction between  $\text{Ag}_2\text{CO}_3$  and  $\text{PPh}_3$  in DMF at 60 °C



To a light-protected Schlenk tube equip with a stirrer bar,  $\text{Ag}_2\text{CO}_3$  (83 mg, 0.3 mmol, 1 equiv.) and  $\text{PPh}_3$  (157 mg, 0.6 mmol, 2 equiv.) were added and the Schlenk tube was evacuated and refilled three times with  $\text{N}_2$ . Dry DMF (3 mL) was added, and the reaction mixture was submerged in a pre-heated oil bath (60 °C) and allowed to react for 16 h. After 16 h, 0.5 mL of the reaction mixture was transferred to a J-Young NMR tube under an atmosphere of  $\text{N}_2$  and analysed by  $^{31}\text{P}\{^1\text{H}\}$  NMR spectroscopy at both room temperature and at – 50 °C (223 K). At room temperature, only a singlet ( $\delta$  5.8) with no Ag-P coupling information was observed. Unfortunately, – 50 °C was not low enough to fully resolve the  $^{31}\text{P}\{^1\text{H}\}$  NMR spectrum. Crystals of **90** were isolated using vapour diffusion techniques using a combination of DMF and hexane.

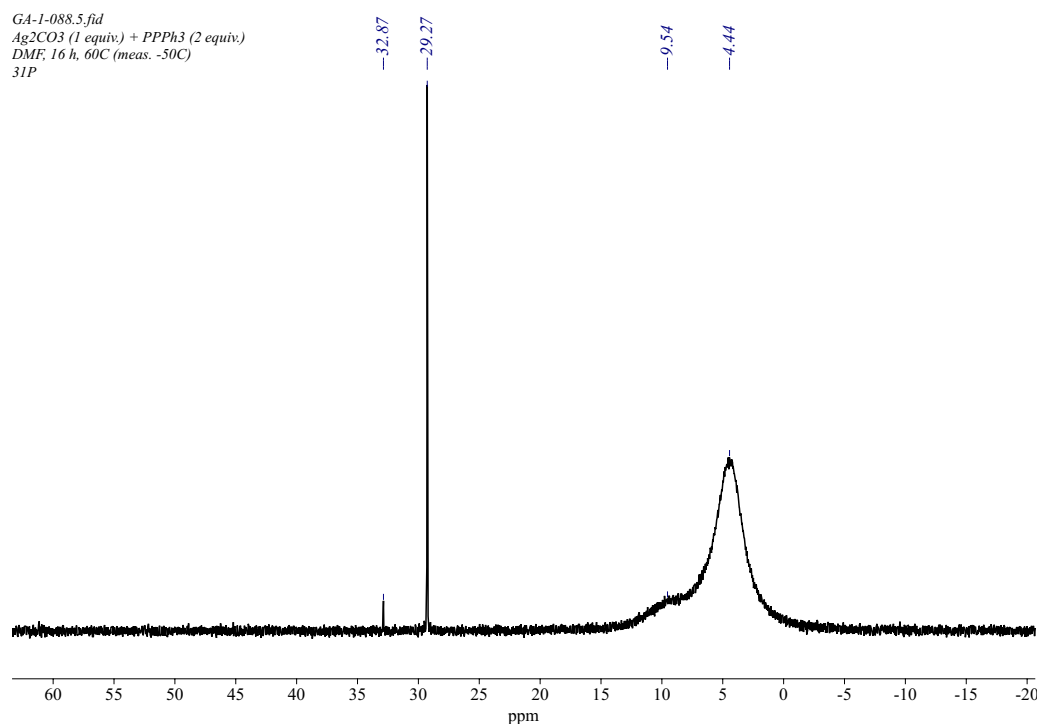
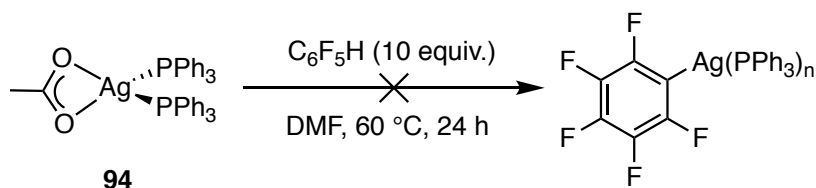


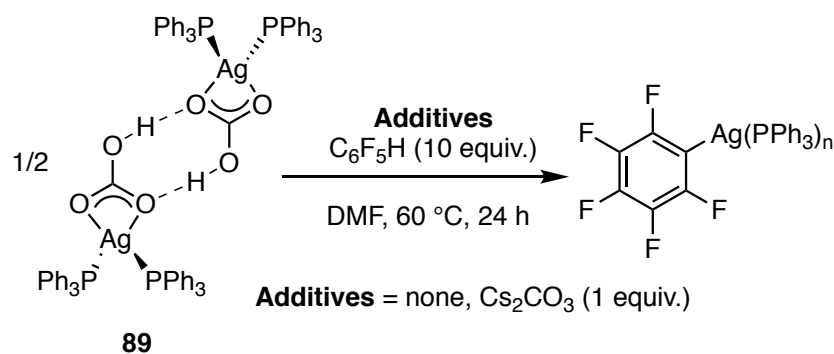
**Figure 107:**  $^{31}\text{P}\{^1\text{H}\}$  NMR (202.5 MHz, DMF (non-deuterated),  $-50\text{ }^\circ\text{C}$ ) spectrum of the reaction mixture of **GA-1-088**. Spectra could not be fully resolved at this temperature.

#### 6.4.4 Reactions with Phosphine-coordinated Silver(I) complexes

To a light-protected Schlenk tube, the desired silver complex (0.1 mmol, 1 equiv.) and any required additives were added and the Schlenk tube as evacuated and refilled three times with nitrogen. Against a flow of nitrogen, dry DMF (3 mL) and  $\text{C}_6\text{F}_5\text{H}$  **17** (168 mg, 1.0 mmol, 10 equiv. 110  $\mu\text{L}$ ) were added mixture was allowed to react for 24 h at the desired temperature. The reaction was monitored using a reaction aliquot which was prepared by transferring 0.5 mL of the reaction mixture into a J Young tube after 24 h. The reaction mixture was monitored by  $^{31}\text{P}\{^1\text{H}\}$  and  $^{19}\text{F}\{^1\text{H}\}$  NMR spectroscopy. Results presented in **Table 13**.

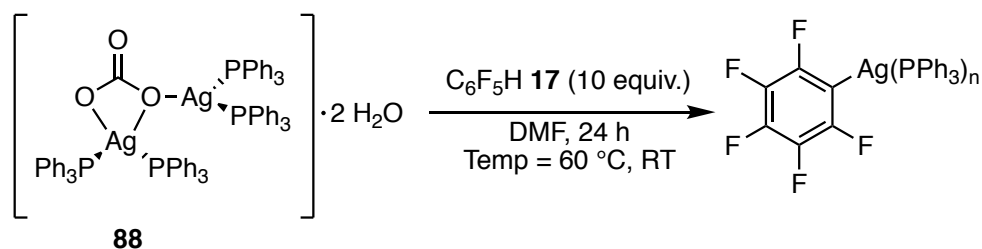


**GA-6-505** (Entry 1): The reaction of  $\text{Ag}(\text{PPh}_3)_2(\kappa^2\text{-OAc})$  **94** (69 mg, 0.1 mmol, 1 equiv.) with 10 equivalents of  $\text{C}_6\text{F}_5\text{H}$  (**17**) in DMF heated to  $60\text{ }^\circ\text{C}$  for 24 h. No formation of an  $\text{AgC}_6\text{F}_5$  containing product was detected in the  $^{19}\text{F}\{^1\text{H}\}$  NMR spectrum.



**GA-6-504 (Entry 2):** The reaction of  $\text{Ag}(\text{PPh}_3)_2(\kappa^2\text{-HCO}_3)$  **89** (69 mg, 0.1 mmol, 1 equiv.) with 10 equivalents of  $\text{C}_6\text{F}_5\text{H}$  **17** in DMF heated to 60 °C for 24 h. No formation of an  $\text{AgC}_6\text{F}_5$  containing product was detected in the  $^{19}\text{F}\{^1\text{H}\}$  NMR spectrum.

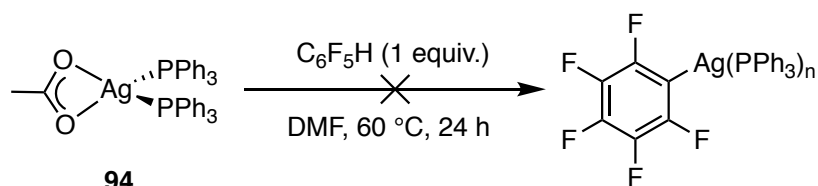
**GA-6-501 (Entry 3):** The reaction of  $\text{Ag}(\text{PPh}_3)_2(\kappa^2\text{-HCO}_3)$  **89** (69 mg, 0.1 mmol, 1 equiv.) and  $\text{Cs}_2\text{CO}_3$  (32 mg, 0.1 mmol, 1 equiv.) with 10 equivalents of  $\text{C}_6\text{F}_5\text{H}$  **17** in DMF heated to 60 °C for 24 h. The formation of an  $\text{AgC}_6\text{F}_5$  containing product was detected in the  $^{19}\text{F}\{^1\text{H}\}$  NMR spectrum, but a % conversion was not calculated due to the ill-defined nature of the product in solution.



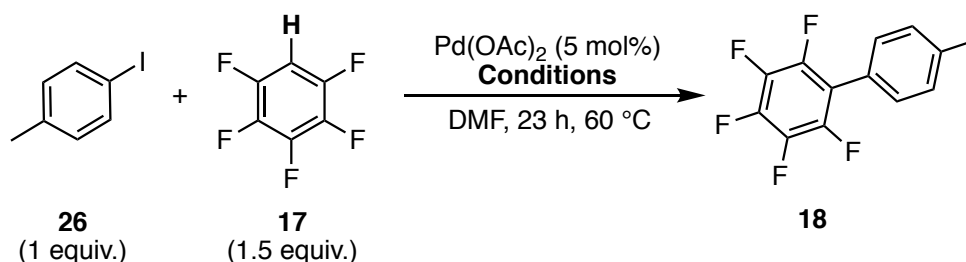
**GA-6-499 (Entry 4):** The reaction between  $[\text{Ag}(\text{PPh}_3)_2]_2\text{CO}_3 \cdot 2 \text{H}_2\text{O}$  **88** (132 mg, 0.1 mmol, 1 equiv.) with 10 equivalents of  $\text{C}_6\text{F}_5\text{H}$  **17** in DMF heated to 60 °C in DMF. After the addition of  $\text{C}_6\text{F}_5\text{H}$  **17**, the reaction mixture was submerged in a pre-heated oil bath (60 °C) for 24 h. The formation of an  $\text{AgC}_6\text{F}_5$  containing product was detected in the  $^{19}\text{F}\{^1\text{H}\}$  NMR spectrum, but a % conversion was not calculated due to the ill-defined nature of both **88** and product in solution.

**GA-6-500 (Entry 5):** The reaction between  $[\text{Ag}(\text{PPh}_3)_2]_2\text{CO}_3 \cdot 2 \text{H}_2\text{O}$  **88** (132 mg, 0.1 mmol, 1 equiv.) with 10 equivalents of  $\text{C}_6\text{F}_5\text{H}$  **17** in DMF was stirred at room temperature for 24 h. The formation of a  $\text{AgC}_6\text{F}_5$  containing product was detected in the  $^{19}\text{F}\{^1\text{H}\}$  NMR spectrum, but a % conversion was not calculated due to the ill-defined nature of both **88** and product in solution. However, from the relative integration with respect to  $\text{C}_6\text{F}_5\text{H}$ , was able to determine that the reaction at room temperature is more sluggish than at 60 °C.

**Reaction between  $\text{Ag}(\text{PPh}_3)_2(\kappa^2\text{-OAc})(\mathbf{94})$  with 1 equivalents of  $\text{C}_6\text{F}_5\text{H}$  ( $\mathbf{17}$ ) in DMF for 24 h**



In a light-protected Schlenk tube,  $\text{Ag}(\text{PPh}_3)_2(\kappa^2\text{-OAc})$  **94** (138.3 mg, 0.2 mmol, 1 equiv.) was added and the Schlenk tube was evacuated and refilled three times with nitrogen. Dry DMF (2 mL) was added, and the reaction mixture was submerged in a pre-heated oil bath ( $60\text{ }^\circ\text{C}$ ).  $\text{C}_6\text{F}_5\text{H}$  **17** (35 mg, 0.2 mmol, 1 equiv., 25  $\mu\text{L}$ ) was added and the mixture was stirred at  $60\text{ }^\circ\text{C}$  for 24 h. After 24 h, 0.5 mL of the reaction mixture was transferred into a J Young tube under nitrogen and analysed by monitored by  $^{31}\text{P}\{^1\text{H}\}$  and  $^{19}\text{F}\{^1\text{H}\}$  NMR spectroscopy.

6.4.5: Reactions with Catalytic Amounts of Ag<sup>I</sup> salt**Direct arylation reaction with Cs<sub>2</sub>CO<sub>3</sub> as the base and catalytic amounts of Ag<sup>I</sup> salts and complexes**

In a light-protected Schlenk tube Pd(OAc)<sub>2</sub> (10 mg, 0.045 mmol, 5 mol%), PPh<sub>3</sub> (as required), Ag additive, 1,3,5-trimethoxybenzene (44 mg, 0.26 mmol, 0.28 equiv., internal standard) and Cs<sub>2</sub>CO<sub>3</sub> (221 mg, 0.68 mmol, 0.75 equiv.) was added and the Schlenk tube was evacuated and refilled three times with nitrogen. Against a strong flow of nitrogen, 4-iodotoluene (196 mg, 0.9 mmol, 1 equiv.) was added followed by DMF (2.6 mL) and pentafluorobenzene (227 mg, 1.35 mmol, 1.5 equiv., 150 μL). The reaction mixture was then left stirring at the required temperature and reaction aliquots were collected to monitor the reaction using <sup>1</sup>H NMR spectroscopy. The reaction aliquots were prepared by collecting approximately 0.1 mL of the reaction mixture and filtering it through celite using CDCl<sub>3</sub> as the eluent. The sample was locked to CDCl<sub>3</sub> and the <sup>1</sup>H NMR spectrum of the reaction mixture was collected using a d1 = 1 sec, sw = 16, O1P = 6.175, 32 scans. The results are presented in **Table 14**.

**GA-6-509 (Entry 2):** PPh<sub>3</sub> (12 mg, 0.045 mmol, 5 mol%), [Ag(PPh<sub>3</sub>)<sub>2</sub>]<sub>2</sub>CO<sub>3</sub>•2 H<sub>2</sub>O **88** (60 mg, 0.045 mmol, 5 mol%) was added along with the other reagents, and the Schlenk tube was evacuated and refilled three times with nitrogen. After the addition of all the remaining reagents, the reaction mixture was submerged in a preheated oil bath (60 °C) and stirred for 23 h.

**GA-6-510 (Entry 3):** PPh<sub>3</sub> (12 mg, 0.045 mmol, 5 mol%), [Ag(PPh<sub>3</sub>)<sub>2</sub>(κ<sup>2</sup>-HCO<sub>3</sub>)]<sub>2</sub> **89** (62 mg, 0.045 mmol, 5 mol%) was added along with the other reagents, and the Schlenk tube was evacuated and refilled three times with nitrogen. After the addition of all the remaining reagents, the reaction mixture was submerged in a preheated oil bath (60 °C) and stirred for 23 h.

**GA-6-511 (Entry 1):** Only PPh<sub>3</sub> (23.6 mg, 0.09 mmol, 10 mol%) added along with the other reagents with no added Ag additive. The Schlenk tube was evacuated and refilled three times

with nitrogen. After the addition of all the remaining reagents, the reaction mixture was submerged in a preheated oil bath (60 °C) and stirred for 23 h.

**GA-6-514 (Entry 6):** PPh<sub>3</sub> (12 mg, 0.045 mmol, 5 mol%), [Ag(PPh<sub>3</sub>)<sub>2</sub>]<sub>2</sub>CO<sub>3</sub>•2 H<sub>2</sub>O **88** (30 mg, 0.023 mmol, 2.5 mol%) was added along with the other reagents, and the Schlenk tube was evacuated and refilled three times with nitrogen. After the addition of all the remaining reagents, the reaction mixture was submerged in a preheated oil bath (60 °C) and stirred for 23 h.

**GA-6-515 (Entry 5):** PPh<sub>3</sub> (12 mg, 0.045 mmol, 5 mol%), [Ag(PPh<sub>3</sub>)<sub>2</sub>(κ<sup>2</sup>-HCO<sub>3</sub>)]<sub>2</sub> **89** (31 mg, 0.023 mmol, 2.5 mol%) was added along with the other reagents, and the Schlenk tube was evacuated and refilled three times with nitrogen. After the addition of all the remaining reagents, the reaction mixture was submerged in a preheated oil bath (60 °C) and stirred for 23 h.

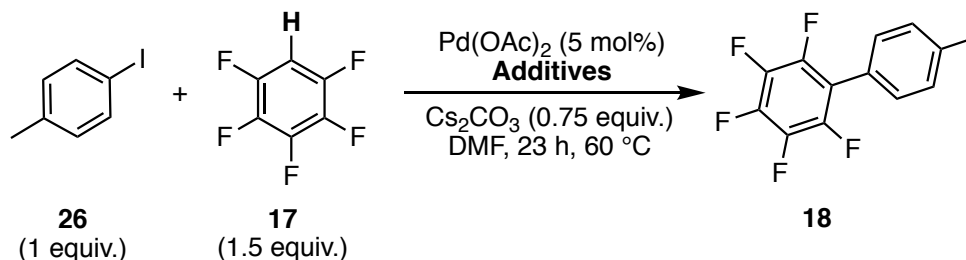
**GA-6-516 (Entry 4):** PPh<sub>3</sub> (23 mg, 0.09 mmol, 10 mol%), Ag<sub>2</sub>CO<sub>3</sub> (12 mg, 0.045 mmol, 5 mol%) was added along with the other reagents, and the Schlenk tube was evacuated and refilled three times with nitrogen. After the addition of all the remaining reagents, the reaction mixture was submerged in a preheated oil bath (60 °C) and stirred for 23 h.

**GA-6-521 (Entry 7):** PPh<sub>3</sub> (23 mg, 0.09 mmol, 10 mol%), Ag<sub>2</sub>CO<sub>3</sub> (6.2 mg, 0.023 mmol, 2.5 mol%) was added along with the other reagents, and the Schlenk tube was evacuated and refilled three times with nitrogen. After the addition of all the remaining reagents, the reaction mixture was submerged in a preheated oil bath (60 °C) and stirred for 23 h.

**GA-6-521 (Entry 8):** PPh<sub>3</sub> (23 mg, 0.09 mmol, 10 mol%), Ag<sub>2</sub>CO<sub>3</sub> (2.5 mg, 0.009 mmol, 1 mol%) was added along with the other reagents, and the Schlenk tube was evacuated and refilled three times with nitrogen. After the addition of all the remaining reagents, the reaction mixture was submerged in a preheated oil bath (60 °C) and stirred for 23 h.

**GA-7-533 (Entry 9):** PPh<sub>3</sub> (23.6 mg, 0.09 mmol, 10 mol%), AgC<sub>6</sub>F<sub>5</sub> **55** (25 mg, 0.09 mmol, 10 mol%) was added along with the other reagents, and the Schlenk tube was evacuated and refilled three times with nitrogen. After the addition of all the remaining reagents, the reaction mixture was submerged in a preheated oil bath (60 °C) and stirred for 23 h.

**Table 40:** Influence of the addition of catalytic amounts of Ag containing salts and complexes on the direct arylation reaction of 4-iodotoluene **26** with pentafluorobenzene **17** (comparison of % conversion calculated using starting material and product vs. calculated using the internal standard.)



Entry	Conditions	Conversion (%) <sup>[a]</sup>		<sup>1</sup> H NMR Conversion <sup>[b]</sup> (%)	
		3 h	23 h	3 h	23 h
		1	PPh <sub>3</sub> (10 mol%)	11	59
2	PPh <sub>3</sub> (5 mol%) + [Ag(PPh <sub>3</sub> ) <sub>2</sub> (κ <sup>2</sup> -HCO <sub>3</sub> ) <sub>2</sub> ] <b>89</b> (5 mol%)	48	98	51	98
3	PPh <sub>3</sub> (5 mol%) + [Ag(PPh <sub>3</sub> ) <sub>2</sub> ] <sub>2</sub> CO <sub>3</sub> •2 H <sub>2</sub> O <b>88</b> (5 mol%)	60	99	62	99
4	PPh <sub>3</sub> (10 mol%) + Ag <sub>2</sub> CO <sub>3</sub> (5 mol%)	69	93	73	94
5	PPh <sub>3</sub> (5 mol%) + [Ag(PPh <sub>3</sub> ) <sub>2</sub> (κ <sup>2</sup> -HCO <sub>3</sub> ) <sub>2</sub> ] <b>89</b> (2.5 mol%)	57	91	54	93
6	PPh <sub>3</sub> (5 mol%) + [Ag(PPh <sub>3</sub> ) <sub>2</sub> ] <sub>2</sub> CO <sub>3</sub> •2 H <sub>2</sub> O <b>88</b> (2.5 mol%)	56	94	59	96
7	PPh <sub>3</sub> (10 mol%) + Ag <sub>2</sub> CO <sub>3</sub> (2.5 mol%)	55	86	57	89
8	PPh <sub>3</sub> (10 mol%) + Ag <sub>2</sub> CO <sub>3</sub> (1 mol%)	49	79	44	80
9	PPh <sub>3</sub> (10 mol%) + AgC <sub>6</sub> F <sub>5</sub> <b>55</b> (10 mol%)	69	96	70	96

<sup>[a]</sup> The % conversion was calculated by integrating the methyl-CH<sub>3</sub> resonance of the starting material of 4-iodotoluene **26** ( $\delta$  2.30) with respect to product ( $\delta$  2.43) in the <sup>1</sup>H NMR spectrum of the reaction mixture with D1 = 1 sec.

<sup>[b]</sup> The <sup>1</sup>H NMR conversion was calculated by integrating the methyl -CH<sub>3</sub> resonance of the starting material 4-iodotoluene **26** ( $\delta$  2.30) with respect to 1,3,5-trimethoxybenzene ( $\delta$  3.78) in the <sup>1</sup>H NMR spectrum of the reaction mixture with D1 = 1 sec.

## 6.5 Experimental Procedures for Chapter 3

### 6.5.1 Catalytic Direct Arylation Reactions with Varying Conditions

#### General Experimental Procedure for the reaction with octafluoronaphthalene as $^{19}\text{F}\{^1\text{H}\}$ NMR internal standard

In a light-protected Schlenk tube  $\text{Pd}(\text{OAc})_2$  (10 mg, 0.045 mmol, 5 mol%), Xphos (43 mg, 0.09 mmol, 10 mol%) and the desired base were added and the Schlenk tube was evacuated and refilled three times with nitrogen. Against a strong flow of nitrogen, 4-iodotoluene **26** (196 mg, 0.9 mmol, 1 equiv.) and octafluoronaphthalene (71 mg, 0.26 mmol, 0.29 equiv., internal standard) were added followed by DMF (2.6 mL) and pentafluorobenzene **17** (227 mg, 1.35 mmol, 1.5 equiv., 150  $\mu\text{L}$ ). The reaction mixture was then left stirring at the required temperature and reaction aliquots were collected to monitor the reaction using  $^{19}\text{F}\{^1\text{H}\}$  NMR spectroscopy. The reaction aliquots were prepared by collecting approximately 0.1 mL of the reaction mixture and filtering it through Celite® using  $\text{CDCl}_3$  as the eluent. The sample was locked to  $\text{CDCl}_3$  and the  $^{19}\text{F}\{^1\text{H}\}$  NMR spectrum of the reaction mixture was collected using a  $d1 = 20$  secs,  $sw = 100$ ,  $\text{O1P} = -150$  and 32 scans. Data presented in **Table 17** unless stated otherwise.

GA-3-243.4.fid  
Standard Cat. reaction w/ Xphos  
int std: octafluoronaphthalene, 3h aliquote  
19F

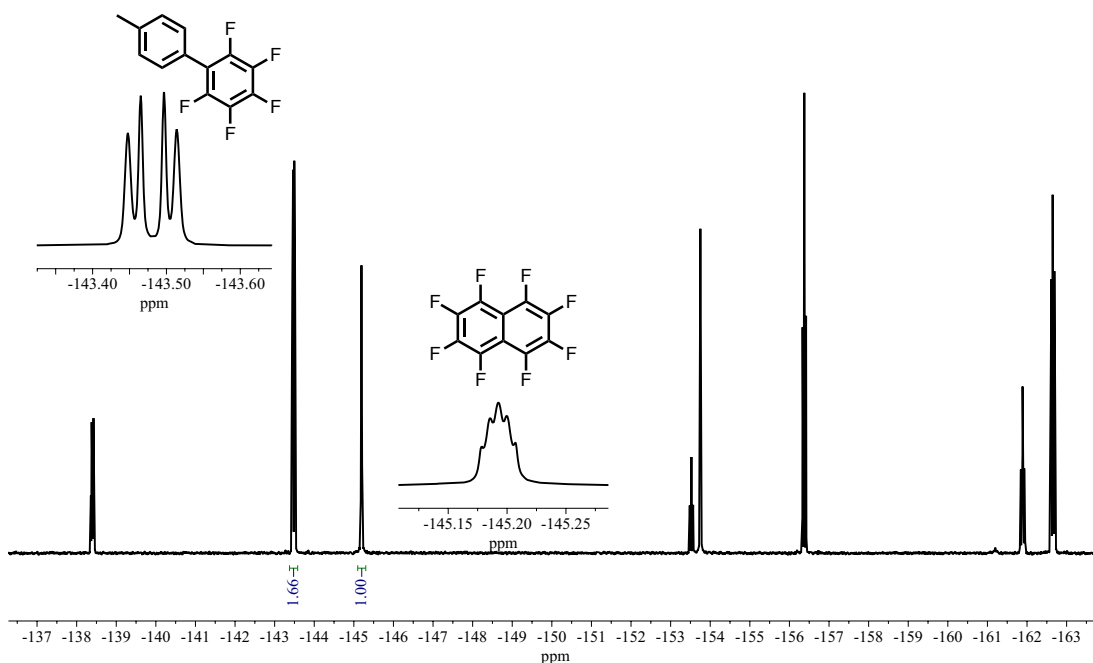


**Figure 108** :  $^{19}\text{F}\{^1\text{H}\}$  NMR (470 MHz,  $\text{CDCl}_3$ , 25  $^\circ\text{C}$ , 32 Sc) spectrum of the reaction mixture of the standard direct arylation reaction. The %  $^{19}\text{F}\{^1\text{H}\}$  NMR yield were calculated using the *ortho*-F resonance of the product ( $\delta -143.5$ ) wrt octafluoronaphthalene ( $\delta -145.2$ , internal standard).



**GA-3-243 (Entry 1):** The desired base used was  $\text{Ag}_2\text{CO}_3$  (186 mg, 0.68 mmol, 0.75 equiv.) and after the addition of all the reagents, the reaction mixture was submerged in a preheated oil bath (60 °C) and stirred for 23 h. Reaction aliquots at 3 h and 23 h were collected to calculate the %  $^{19}\text{F}\{^1\text{H}\}$  NMR yield at these times. The %  $^{19}\text{F}\{^1\text{H}\}$  NMR yield at 3 h = 96, 23 h = 96

- **GA-3-251:** Replicate of **GA-3-243** with a reaction aliquot collected at 3 h only to ensure the results are reproducible. The %  $^{19}\text{F}\{^1\text{H}\}$  NMR yield at 3 h = 93

**GA-3-244 (Entry 2):** The desired base used was  $\text{Ag}_2\text{CO}_3$  (186 mg, 0.68 mmol, 0.75 equiv.) and after the addition of all the reagents, the reaction mixture was stirred at room temperature for 23 h. A reaction aliquot 23 h was collected to calculate the %  $^{19}\text{F}\{^1\text{H}\}$  NMR yield. The %  $^{19}\text{F}\{^1\text{H}\}$  NMR yield at 23 h = 75.

**GA-5-392 (Entry 3):** Control experiment with no  $\text{Pd}(\text{OAc})_2$  added. The desired base used was  $\text{Ag}_2\text{CO}_3$  (186 mg, 0.68 mmol, 0.75 equiv.) and after the addition of all the reagents, the reaction mixture was stirred at 60 °C for 23 h. A reaction aliquot at 23 h was collected to calculate the %  $^{19}\text{F}\{^1\text{H}\}$  NMR yield. The %  $^{19}\text{F}\{^1\text{H}\}$  NMR yield at 23 h = 0.

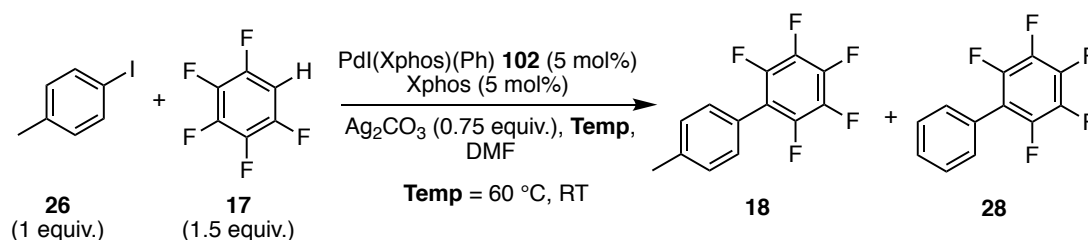
**GA-5-391 (Entry 4):** Experiment with 5 mol% of Xphos instead of 10 mol%. Added Xphos (21 mg, 0.045, 5 mol%) along with the desired base  $\text{Ag}_2\text{CO}_3$  (186 mg, 0.68 mmol, 0.75 equiv.) and after the addition of all the reagents, the reaction mixture was stirred at 60 °C for 23 h. A reaction aliquot at 3 h and 23 h was collected to calculate the %  $^{19}\text{F}\{^1\text{H}\}$  NMR yield. The %  $^{19}\text{F}\{^1\text{H}\}$  NMR yield at 3 h = 19, 23 h = 19.

**GA-4-311 (Entry 5):** Experiment with 10 mol% of  $\text{Ag}_2\text{CO}_3$ ; added  $\text{Ag}_2\text{CO}_3$  (25 mg, 0.09 mmol, 0.1 equiv., 10 mol%) and after the addition of all the reagents, the reaction mixture was stirred at 60 °C for 23 h. A reaction aliquot at 3h and 23 h was collected to calculate the %  $^{19}\text{F}\{^1\text{H}\}$  NMR yield. The %  $^{19}\text{F}\{^1\text{H}\}$  NMR yield at 3 h = 21, 23 h = 22.

**GA-4-312 (Entry 6):** Experiment with 10 mol% of  $\text{Ag}_2\text{CO}_3$ ; added  $\text{Ag}_2\text{CO}_3$  (25 mg, 0.09 mmol, 0.1 equiv., 10 mol%) and after the addition of all the reagents, the reaction mixture was stirred at RT for 23 h. A reaction aliquot at 3h and 23 h was collected to calculate the %  $^{19}\text{F}\{^1\text{H}\}$  NMR yield. The %  $^{19}\text{F}\{^1\text{H}\}$  NMR yield at 3 h = 5, 23 h = 21.

**GA-3-253 (Entry 10):** The desired base used was  $\text{AgOAc}$  (225 mg, 1.35 mmol, 1.5 equiv.) and after the addition of all the reagents, the reaction mixture was submerged in a preheated oil bath (60 °C) and stirred for 23 h. Reaction aliquots at 3 h and 23 h were collected to calculate the %  $^{19}\text{F}\{^1\text{H}\}$  NMR yield at these times. The %  $^{19}\text{F}\{^1\text{H}\}$  NMR yield at 3 h = 7, 23 h = 37.

**GA-4-296:** Using PdI(C<sub>6</sub>H<sub>5</sub>)(Xphos) **102** as the pre-catalyst for the standard catalytic direct arylation reaction between 4-iodotoluene **26** and pentafluorobenzene **17**



To a light-protected Schlenk tube, PdI(C<sub>6</sub>H<sub>5</sub>)(Xphos) **102** (35 mg, 0.045 mmol, 0.05 equiv.), Ag<sub>2</sub>CO<sub>3</sub> (186 mg, 0.67 mmol, 0.75 equiv.) and Xphos (21 mg, 0.045 mmol, 0.05 equiv.) were added and the Schlenk tube was evacuated and refilled three times with nitrogen. Against a flow of N<sub>2</sub>, 4-iodotoluene **26** (196 mg, 0.9 mmol, 1 equiv.) and octafluoronaphthalene (71 mg, 0.26 mmol, 0.29 equiv. internal standard) followed by DMF (2.6 mL) and C<sub>6</sub>F<sub>5</sub>H (227 mg, 1.35 mmol, 1.5 equiv. 150 μL) were added. The reaction mixture was heated at 60 °C for 23 h and reaction aliquots were collected at 3 h and 23 h. The reaction aliquots were prepared by collecting approximately 0.1 mL of the reaction mixture and filtering it through Celite® using CDCl<sub>3</sub> as the eluent. The sample was locked to CDCl<sub>3</sub> and the <sup>19</sup>F{<sup>1</sup>H} NMR spectrum of the reaction mixture was collected using a d1 = 20 secs, sw = 100, O1P = -150 and 32 scans.

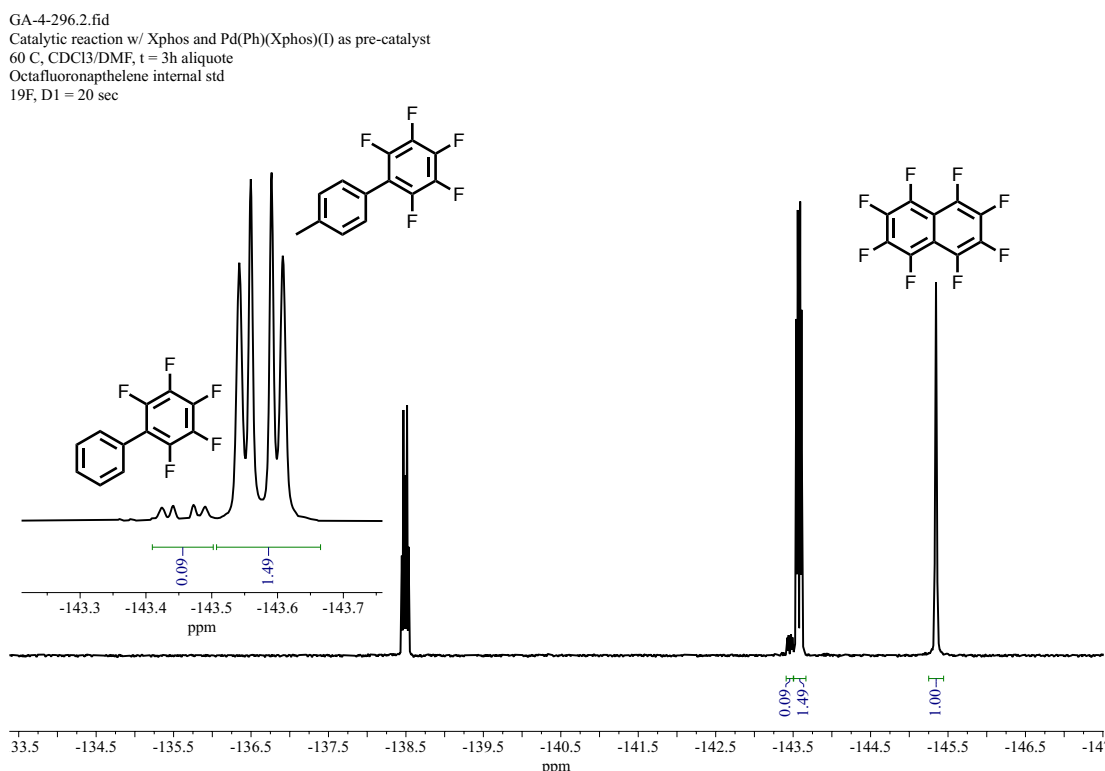


**Figure 109:** <sup>19</sup>F{<sup>1</sup>H} NMR (470 MHz, CDCl<sub>3</sub>/DMF, 25 °C, 32 Sc) spectrum of the reaction mixture of **GA-4-296** (Table 25, Entry 1) at 3h.

At 3 h, the  $^{19}\text{F}\{^1\text{H}\}$  NMR spectrum showed the presence of both **18** (86 %  $^{19}\text{F}\{^1\text{H}\}$  NMR yield) and the **28** (5 %  $^{19}\text{F}\{^1\text{H}\}$  NMR yield, compared to mmol of **18**). The  $^{19}\text{F}\{^1\text{H}\}$  NMR yield of **18** at 3 h = 86, 23 h = 100 and yield of **28** at 3 h = 5, 23 h = 5.

**GA-4-297** (Table 25, Entry 2): Reaction **GA-4-296**, repeated at room temperature. The  $^{19}\text{F}\{^1\text{H}\}$  NMR yield of **18** at 3 h = 6, 23 h = 63 and yield of **28** at 3 h = 3, 23 h = 5.

### General Experimental Procedure with 1,3,5-trimethoxybenzene as the $^1\text{H}$ NMR internal standard

In a light-protected Schlenk tube  $\text{Pd}(\text{OAc})_2$  (10 mg, 0.045 mmol, 5 mol%), Xphos (43 mg, 0.09 mmol, 10 mol%), 1,3,5-trimethoxybenzene (44 mg, 0.26 mmol, 0.28 equiv., internal standard) and the desired base was added and the Schlenk tube was evacuated and refilled three times with nitrogen. Against a strong flow of nitrogen, 4-iodotoluene (196 mg, 0.9 mmol, 1 equiv.) was added followed by DMF (2.6 mL) and pentafluorobenzene (227 mg, 1.35 mmol, 1.5 equiv., 150  $\mu\text{L}$ ). The reaction mixture was then left stirring at the required temperature and reaction aliquots were collected to monitor the reaction using  $^1\text{H}$  NMR spectroscopy. The reaction aliquots were prepared by collecting approximately 0.1 mL of the reaction mixture and filtering it through Celite® using  $\text{CDCl}_3$  as the eluent. The sample was locked to  $\text{CDCl}_3$  and the  $^1\text{H}$  NMR spectrum of the reaction mixture was collected using a  $d1 = 1$  sec,  $sw = 16$ ,  $\text{O1P} = 6.175$ , 32 scans. Data presented in **Table 17**, unless stated otherwise.

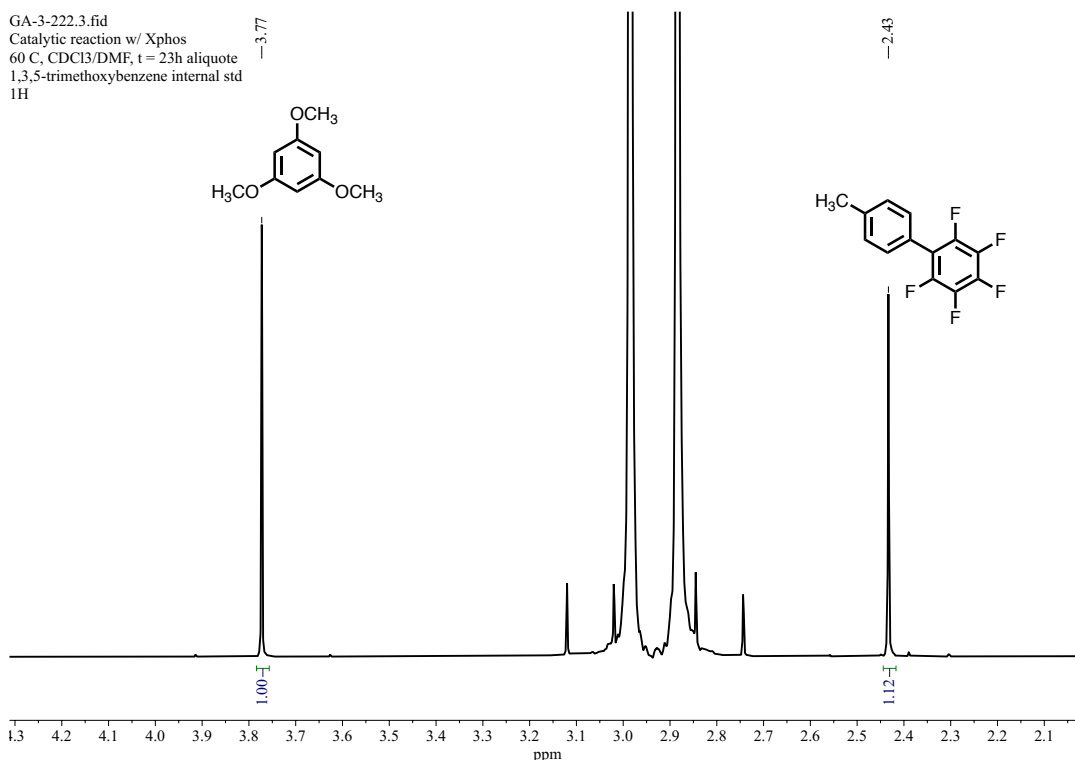


**Figure 110:**  $^1\text{H}$  NMR (500 MHz,  $\text{CDCl}_3$ , 25  $^\circ\text{C}$ , 32 Sc) spectrum of the reaction mixture of **GA-3-222** at 23h. The resonances used to calculate the %  $^1\text{H}$  NMR yield were the methyl resonance of the product **18** ( $\delta$  2.43) wrt 1,3,5-trimethoxybenzene ( $\delta$  3.77, internal standard).

**GA-3-222:** The desired base used was  $\text{Ag}_2\text{CO}_3$  (186 mg, 0.68 mmol, 0.75 equiv.) and after the addition of all the reagents, the reaction mixture was submerged in a preheated oil bath (60 °C) and stirred for 23 h. Reaction aliquots at 3 h and 23 h were collected to calculate the %  $^1\text{H}$  NMR yield. The %  $^1\text{H}$  NMR yield at 3 h = 96, 23 h = 97.

**GA-3-223:** The desired base used was  $\text{Ag}_2\text{CO}_3$  (186 mg, 0.68 mmol, 0.75 equiv.) and after the addition of all the reagents, the reaction mixture was stirred at room temperature for 23 h. A reaction aliquot 23 h was collected to calculate the %  $^1\text{H}$  NMR yield. The %  $^1\text{H}$  NMR yield at 23 h = 72.

**GA-4-304 (Entry 7):** Both  $\text{Ag}_2\text{CO}_3$  (25mg, 0.09 mmol, 0.1 equiv., 10 mol%) and  $\text{K}_2\text{CO}_3$  (93 mg, 0.67 mmol, 0.75 equiv.) were added and after the addition of all the reagents, the reaction mixture was submerged in a preheated oil bath (60 °C) and stirred for 23 h. Reaction aliquot at 3 h and 23 h was collected to calculate the %  $^1\text{H}$  NMR yield at this time. The %  $^1\text{H}$  NMR yield at 3 h = 60\*, 23 h = 65. \*  $^1\text{H}$  NMR yield at 3 h was calculated by integrating the methyl- $\text{CH}_3$  of 4-iodotoluene **26** ( $\delta$  2.30) wrt 1,3,5-trimethoxybenzene ( $\delta$  3.77, internal standard), as there was peak overlap for product peak in this spectrum.

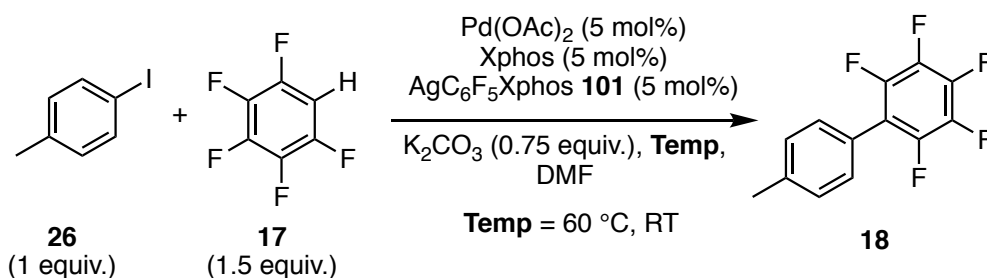
**GA-4-308 (Entry 8):** Both  $\text{Ag}_2\text{CO}_3$  (25mg, 0.09 mmol, 0.1 equiv., 10 mol%) and  $\text{K}_2\text{CO}_3$  (93 mg, 0.67 mmol, 0.75 equiv.) were added and after the addition of all the reagents, the reaction mixture was stirred at RT for 23 h. Reaction aliquot at 3 h and 23 h was collected to calculate the %  $^1\text{H}$  NMR yield. The %  $^1\text{H}$  NMR yield at 3 h = 9, 23 h = 21.

**GA-4-263 (Entry 9):** The desired base used was  $\text{Cs}_2\text{CO}_3$  (221 mg, 0.68 mmol, 0.75 equiv.) and after the addition of all the reagents, the reaction mixture was submerged in a preheated oil bath (60 °C) and stirred for 3 h. Reaction aliquots at 3 h was collected to calculate the %  $^1\text{H}$  NMR. The %  $^1\text{H}$  NMR yield at 3 h = 9.

**GA-4-262 (Entry 10):** The desired base used was  $\text{AgOAc}$  (225 mg, 1.35 mmol, 1.50 equiv.) and after the addition of all the reagents, the reaction mixture was submerged in a preheated oil bath (60 °C) and stirred for 23 h. Reaction aliquot at 3 h and 23 h were collected to calculate the %  $^1\text{H}$  NMR. The %  $^1\text{H}$  NMR yield at 3 h = 7 and 23 h = 37.

**GA-4-262 (Entry 11):** The desired base used was  $\text{K}_2\text{CO}_3$  (94 mg, 0.68 mmol, 0.75 equiv.) and after the addition of all the reagents, the reaction mixture was submerged in a preheated oil bath (60 °C) and stirred for 3 h. Reaction aliquot at 3 h was collected to calculate the %  $^1\text{H}$  NMR. The %  $^1\text{H}$  NMR yield at 3 h = 19.

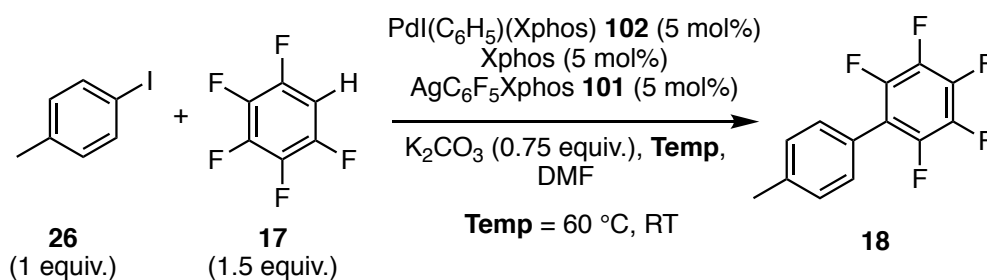
**GA-6-502** (Entry 12, 13): Using catalytic amounts of  $\text{AgC}_6\text{F}_5\text{Xphos}$  **101** for the standard catalytic direct arylation reaction between 4-iodotoluene **26** and pentafluorobenzene **17**



To a light-protected Schlenk tube,  $\text{Pd}(\text{OAc})_2$  (10 mg, 0.045 mmol, 0.05 equiv.),  $\text{Xphos}$  (21 mg, 0.045 mmol, 0.05 equiv.), 1,3,5-trimethoxybenzene (44 mg, 0.26 mmol, internal standard) and  $\text{K}_2\text{CO}_3$  (93 mg, 0.67 mmol, 0.75 equiv.) were added and the Schlenk tube was evacuated and refilled three times with nitrogen. Then  $\text{Ag}(\text{C}_6\text{F}_5)(\text{Xphos})$  **101** (34 mg, 0.045 mmol, 0.05 equiv.) was added and the Schlenk tube was once again evacuated refilled with nitrogen. Against a flow of  $\text{N}_2$ , 4-iodotoluene **26** (196 mg, 0.9 mmol, 1 equiv.) was added followed by DMF (2.6 mL) and  $\text{C}_6\text{F}_5\text{H}$  **17** (227 mg, 1.35 mmol, 1.5 equiv. 150  $\mu\text{L}$ ). The reaction mixture was heated at 60 °C for 23 h and reaction aliquots were collected at 3 h and 23 h. The reaction aliquots were prepared by collecting approximately 0.1 mL of the reaction mixture and filtering it through celite using  $\text{CDCl}_3$  as the eluent. The sample was locked to  $\text{CDCl}_3$  and the  $^1\text{H}$  NMR spectrum of the reaction mixture was collected using a  $d1 = 1$  sec,  $sw = 16$ ,  $\text{O1P} = 6.175$ , 32 scans. The resonances used to calculate the %  $^1\text{H}$  NMR yield were the methyl resonance of 4-iodotoluene ( $\delta$  2.30) wrt 1,3,5-trimethoxybenzene ( $\delta$  3.77, internal standard).

After being heated at 60 °C for 3 h, the % conversion to  $\text{C}_6\text{F}_5\text{-C}_7\text{H}_7$  was 28%, and after 23 h was 57%. The reaction was repeated at room temperature (**GA-6-503**), and at 3 h, the  $^1\text{H}$  NMR spectrum showed 8% conversion and at 23 h, the conversion was 16 % to  $\text{C}_6\text{F}_5\text{-C}_7\text{H}_7$ .

**GA-7-536** (Table 25, Entry 3, 4): Using catalytic amounts of  $\text{PdI}(\text{Ph})(\text{Xphos})$  **102** and  $\text{AgC}_6\text{F}_5\text{Xphos}$  **101** for the standard catalytic direct arylation reaction between 4-iodotoluene and pentafluorobenzene



To a light-protected Schlenk tube,  $\text{PdI}(\text{Ph})(\text{Xphos})$  **102** (35 mg, 0.045 mmol, 0.05 equiv.),  $\text{Xphos}$  (21 mg, 0.045 mmol, 0.05 equiv.), 1,3,5-trimethoxybenzene (44 mg, 0.26 mmol, internal standard), and  $\text{K}_2\text{CO}_3$  (93 mg, 0.67 mmol, 0.75 equiv.) were added and the Schlenk

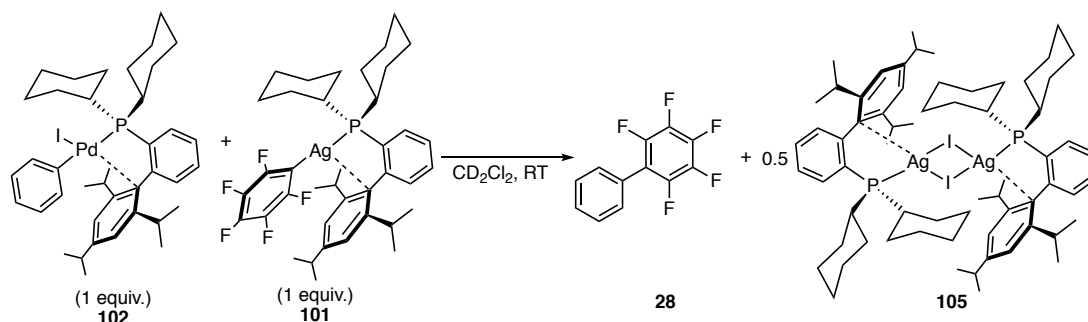
tube was evacuated and refilled three times with nitrogen. Then Ag(Xphos)C<sub>6</sub>F<sub>5</sub> **101** (34 mg, 0.045 mmol, 0.05 equiv.) was added and the Schlenk tube was once again evacuated refilled with nitrogen three times. Against a flow of N<sub>2</sub>, 4-iodotoluene (196 mg, 0.9 mmol, 1 equiv.) was added followed by DMF (2.6 mL) and C<sub>6</sub>F<sub>5</sub>H (227 mg, 1.35 mmol, 1.5 equiv. 150 μL). The reaction mixture was heated at 60 °C for 7 d and reaction aliquots were collected at 3 h, 23 h, 48 and 7d. The reaction aliquots were prepared by collecting approximately 0.1 mL of the reaction mixture and filtering it through celite using CDCl<sub>3</sub> as the eluent. The sample was locked to CDCl<sub>3</sub> and the <sup>1</sup>H NMR spectrum of the reaction mixture was collected using a d1 = 1 sec, sw = 16, O1P = 6.175, 32 scans. The resonances used to calculate the % <sup>1</sup>H NMR yield were the methyl resonance of 4-iodotoluene (δ 2.30) and product (δ 2.44) wrt 1,3,5-trimethoxybenzene (δ 3.77, internal standard).

After being heated at 60 °C for 7 d, the <sup>1</sup>H NMR conversion is 3 h = 1 %, 23 h = 23 %, 48 h = 49 % and 7 d = 63 %.

The reaction was repeated at room temperature (**GA-6-537**), the <sup>1</sup>H NMR conversion is 3 h = 2 %, 23 h = 5 %, 48 h = 11 % and 7 d = 29 %.

### 6.5.2 Stoichiometric Reactions with Reaction Intermediates

**GA-3-205:** The reaction of **101** and **102** in dichloromethene-*d*<sub>2</sub> at room temperature



In the glovebox, **102** (10 mg, 0.013 mmol, 1 equiv.) and **101** (10 mg, 0.013 mmol, 1 equiv.) were weighed out in two separate vials. **101** was dissolved in dichloromethane-*d*<sub>2</sub> (0.5 mL) to produce an amber solution and the solution was then transferred to dissolve all of **102** in the second vial. The mixture immediately changed colour from amber/yellow to deep moss green and then finally dark brown. The reaction mixture was quickly transferred to a J-Young NMR tube and was analysed by <sup>1</sup>H, <sup>31</sup>P{<sup>1</sup>H} and <sup>19</sup>F{<sup>1</sup>H} NMR spectroscopy.

The transmetalation between **101** and **102** and subsequent reductive elimination reaction of Pd(C<sub>6</sub>F<sub>5</sub>)(Ph)(Xphos) **104** complex took place rapidly at room temperature. The Pd(C<sub>6</sub>F<sub>5</sub>)(Ph)(Xphos) **104** complex was not detected by <sup>31</sup>P{<sup>1</sup>H} and <sup>19</sup>F{<sup>1</sup>H} NMR. The <sup>31</sup>P{<sup>1</sup>H} NMR spectrum showed the consumption of **101** and **102** and presence of **105** and unbound Xphos. The <sup>19</sup>F{<sup>1</sup>H} NMR showed to presence of the organic product **28** (90 % conversion) with some amounts of **101** remaining.

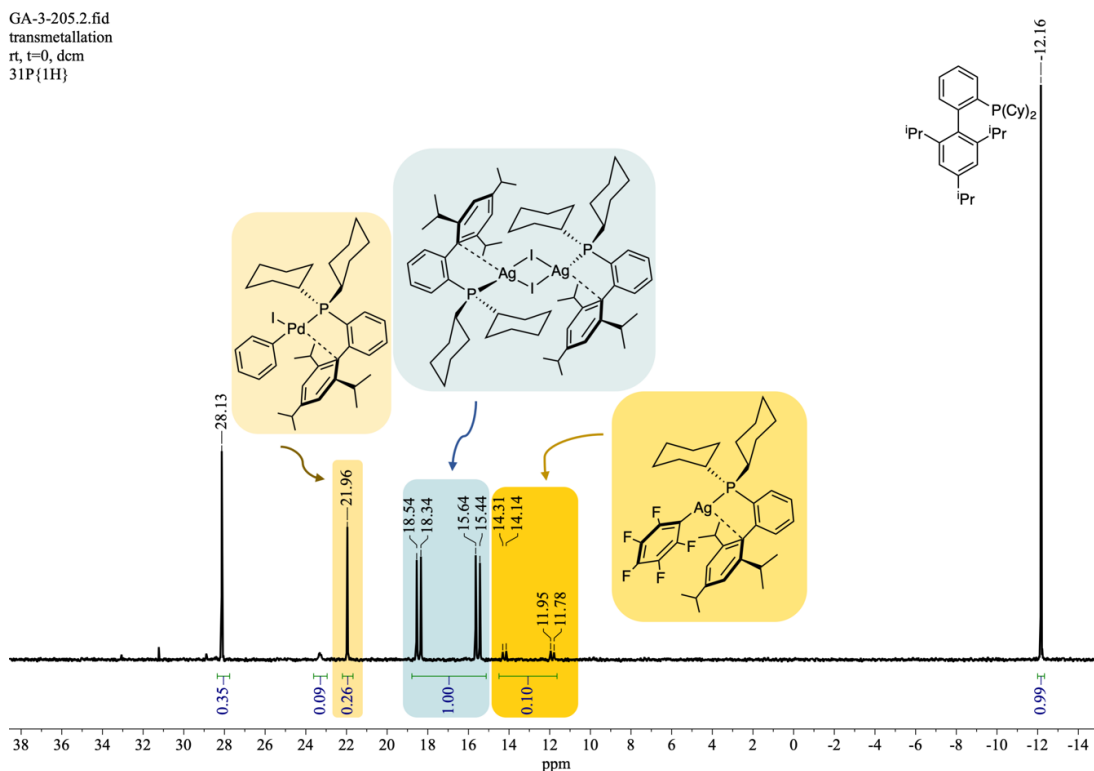


**Figure 111:**  $^{31}\text{P}\{^1\text{H}\}$  (202.5 MHz,  $\text{CD}_2\text{Cl}_2$ , 25 °C) spectrum of the reaction mixture of GA-3-205, collected at  $t = 0$  h, RT, showing the presence of **101**, **102**, **105** and unbound XPhos.

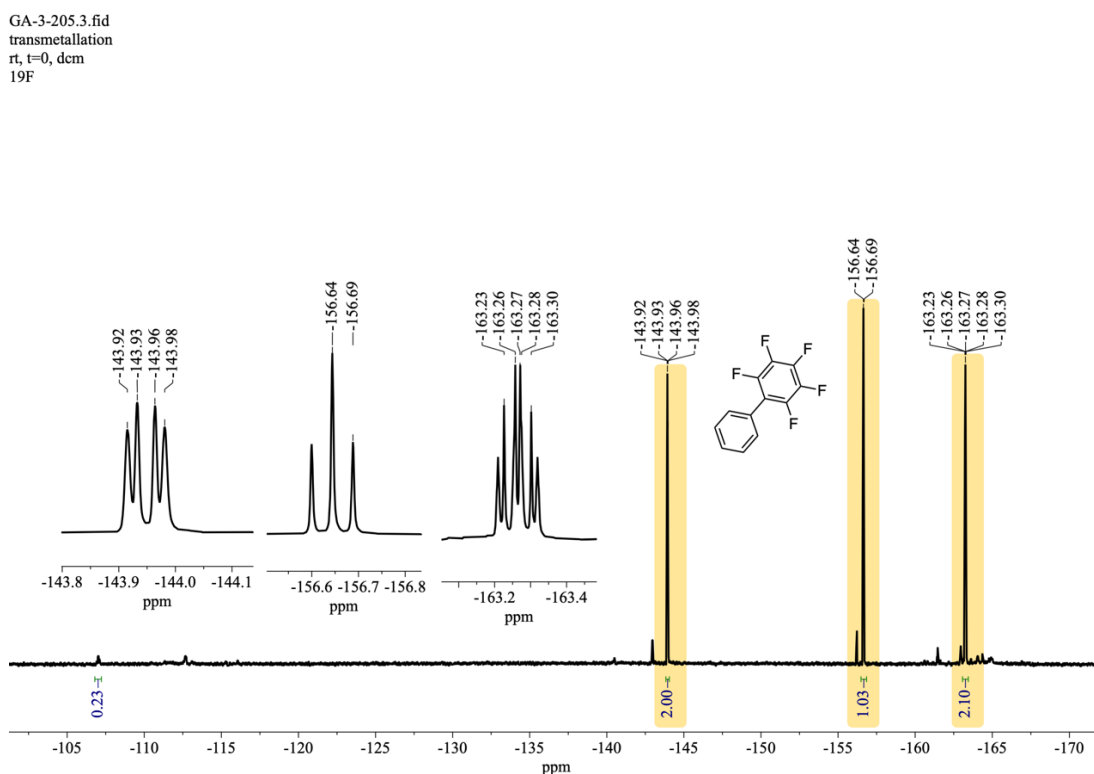
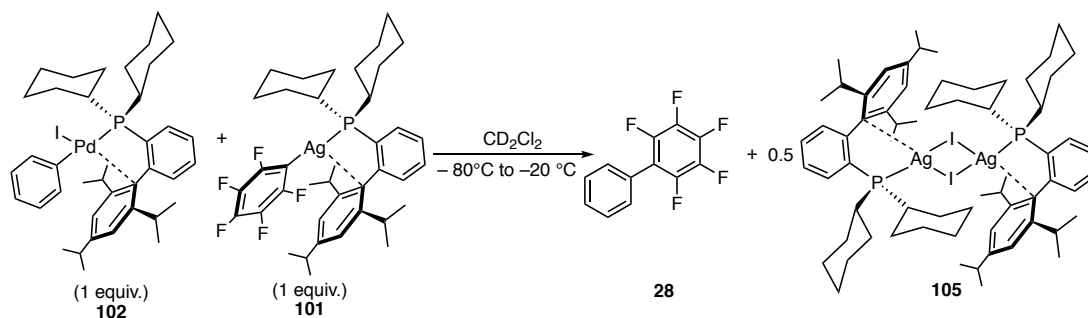


**Figure 112:**  $^{19}\text{F}\{^1\text{H}\}$  NMR (470 MHz,  $\text{CD}_2\text{Cl}_2$ , 25 °C) of the reaction mixture GA-3-205 immediately after sample preparation, showing the presence of the organic product.

**GA-4-328:** Low-temperature *in situ* monitoring of the transmetallation reaction between **101** and **102**



In the glovebox, two J-Young tubes, one with a solution of **102** (10 mg, 0.013 mmol, 1 equiv.) in dichloromethane- $d_2$  (0.3 mL) and in the other a solution of **101** (14 mg, 0.019 mmol) in dichloromethane- $d_2$  (0.3 mL), were prepared. Both the J-Young tubes were removed from the glovebox and connected to a Schlenk line using a suitable adaptor and the reaction mixtures in both tubes were cooled to  $-78^\circ\text{C}$  using a dry ice/acetone bath. The temperature of the cold bath was constantly monitored using a temperature probe. After the head space of the adaptor was evacuated and refilled three times with  $\text{N}_2$ , taps of J-Young tubes containing the solution of **101** and **102** were opened under an atmosphere of nitrogen and 0.2 mL of the solution of **101** was transferred to the solution of **102**, while cold, using a 250  $\mu\text{L}$  gas tight syringe. The set-up of the J young NMR tubes is similar to experimental set-up in **Figure 100**. The Bruker AVIHD 500 was used to record the low-temperature VT spectra of the reaction mixture. The NMR probe was pre-cooled to  $-80^\circ\text{C}$  (193 K) and the sample temperature was maintained at  $-78^\circ\text{C}$  until it was placed in the spectrometer. The temperature of the probe was gradually increased from  $-80^\circ\text{C}$  to  $-60$ ,  $-50$ ,  $-40$ ,  $-30^\circ\text{C}$ ,  $-35$ ,  $-25$  and  $-20^\circ\text{C}$ . At each temperature the  $^1\text{H}$ ,  $^{31}\text{P}\{^1\text{H}\}$  and  $^{19}\text{F}\{^1\text{H}\}$  NMR spectrum was recorded to monitor the reaction progress at each temperature.



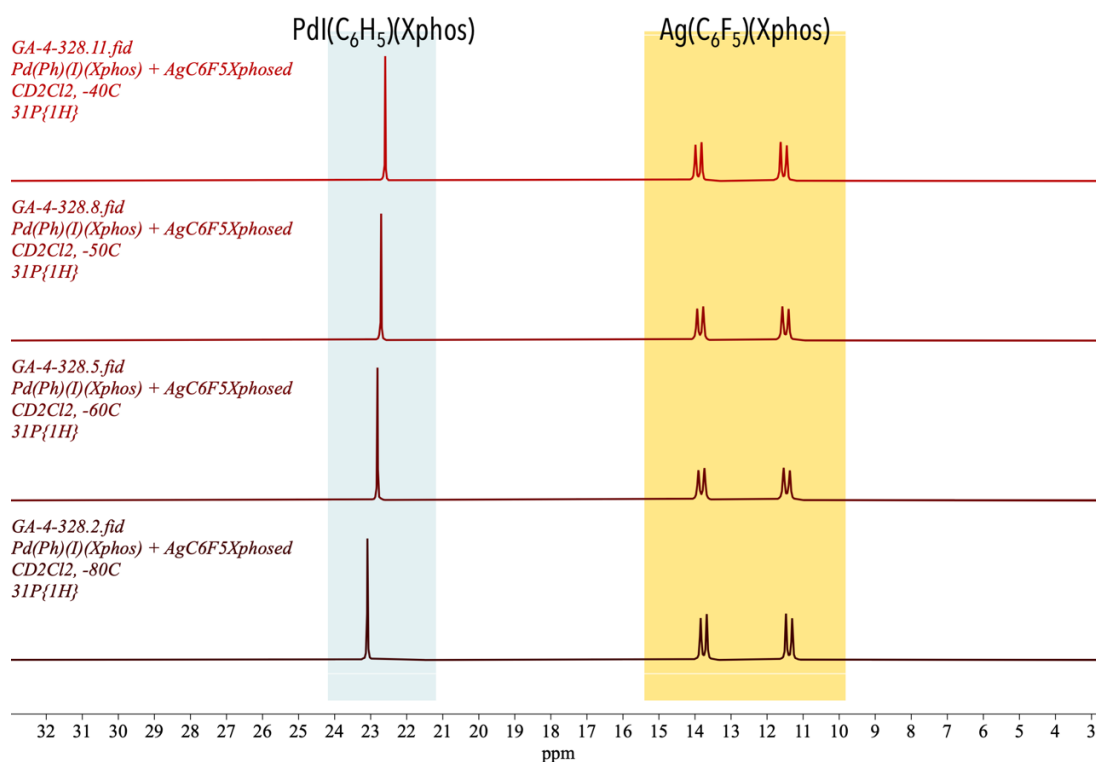


**Figure 113:** Stack plot of the  $^{31}\text{P}\{^1\text{H}\}$  NMR spectrum of the reaction mixture at  $-80$ ,  $-60$ ,  $-50$ ,  $-40$  °C showing unreacted starting material.

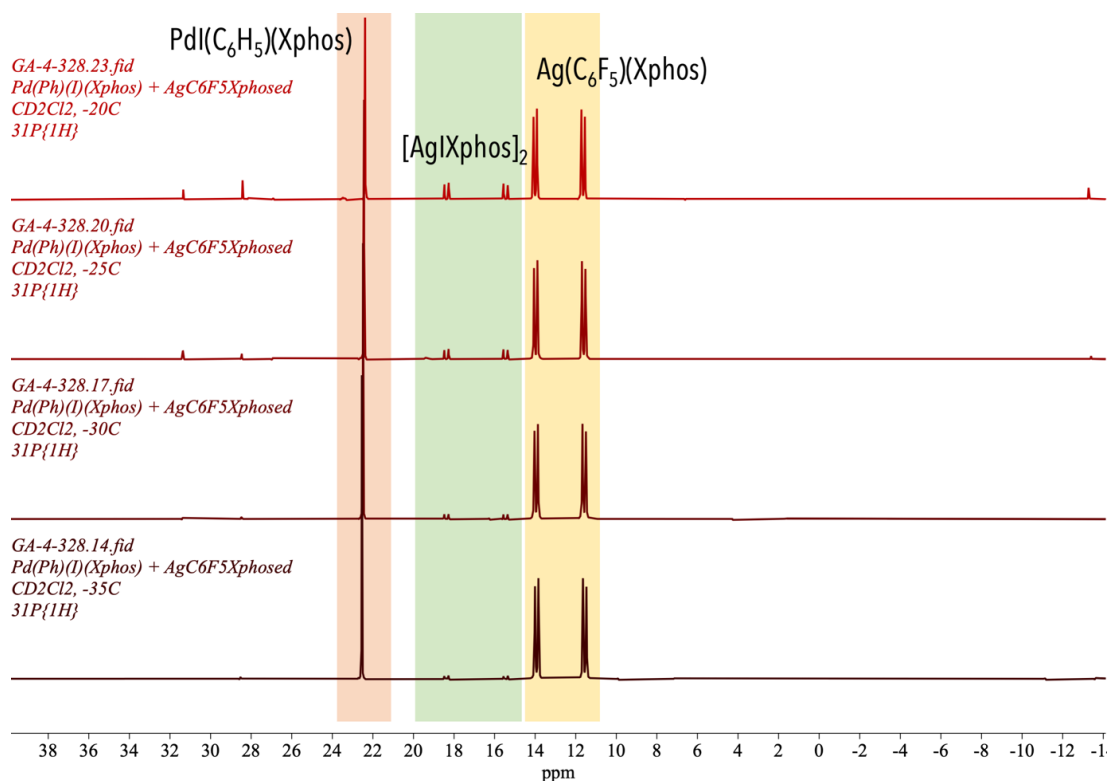


**Figure 114:** Stack plot of the  $^{31}\text{P}\{^1\text{H}\}$  NMR spectrum of the reaction mixture at  $-35$ ,  $-30$ ,  $-25$ ,  $-20$  °C showing formation of **105** as the by-product.

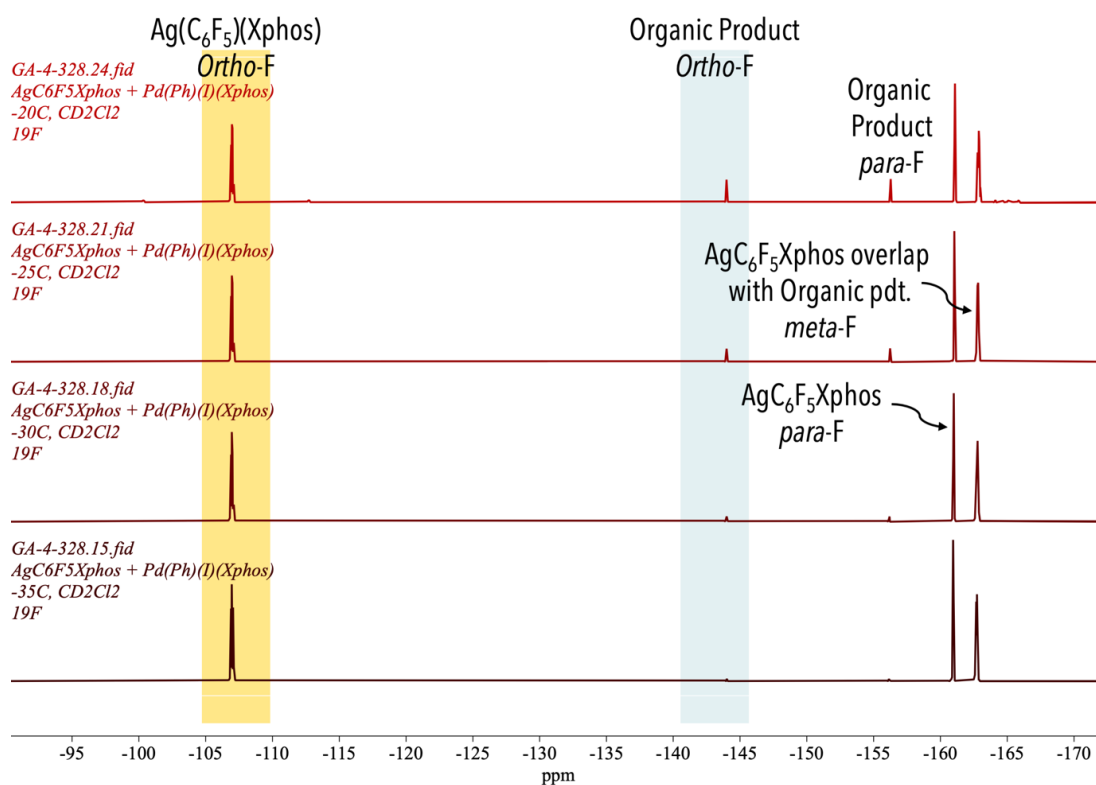


**Figure 115:** Stack plot of the  $^{19}\text{F}\{^1\text{H}\}$  NMR spectrum of the reaction mixture at  $-35$ ,  $-30$ ,  $-25$ ,  $-20$  °C showing formation of organic product **28**.

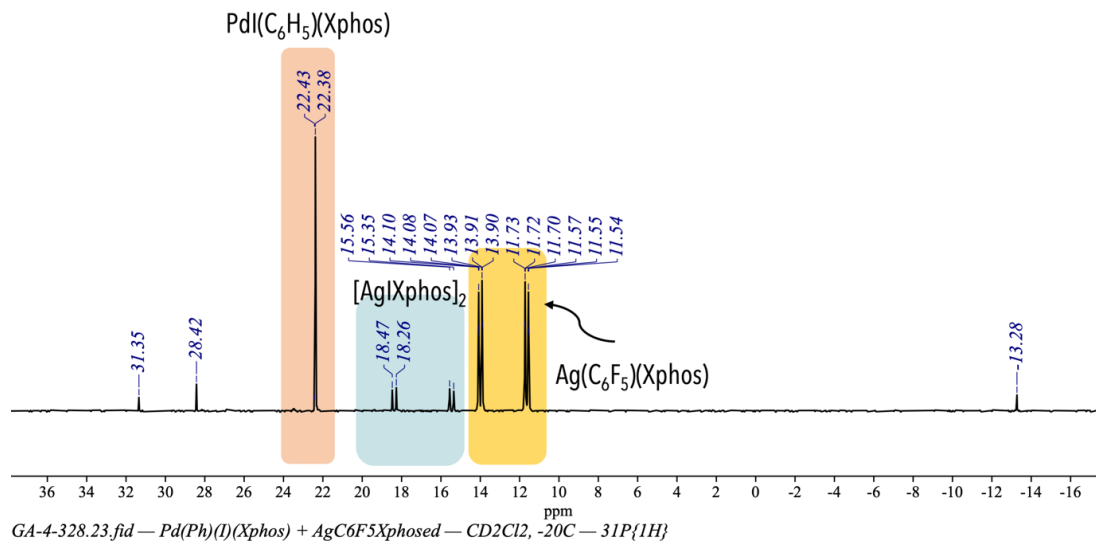


**Figure 116:**  $^{31}\text{P}\{^1\text{H}\}$  (202.5 MHz,  $\text{CD}_2\text{Cl}_2$ ,  $-20$  °C) NMR spectrum of the reaction mixture

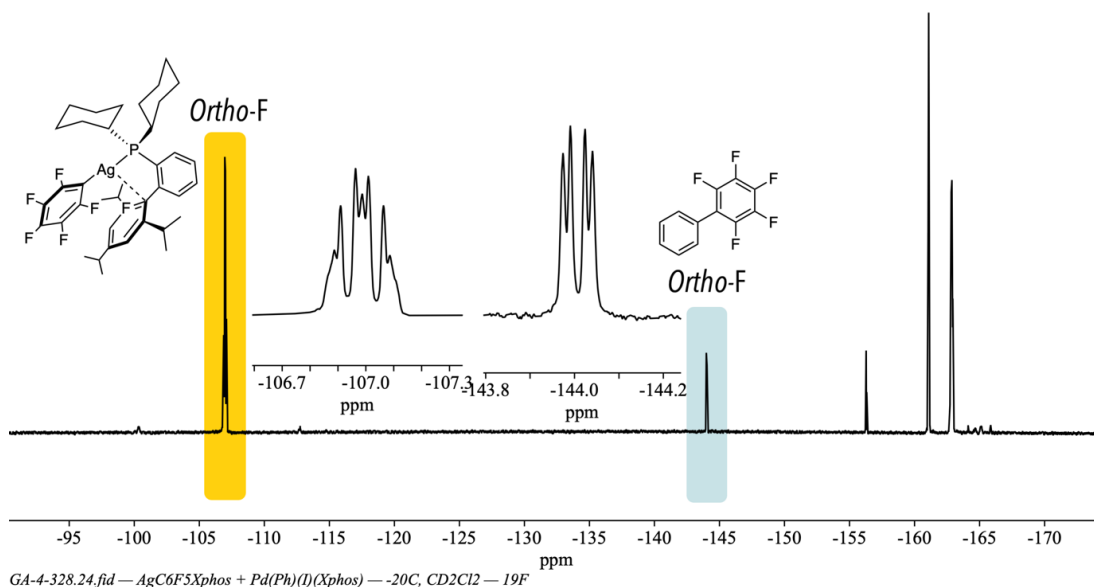
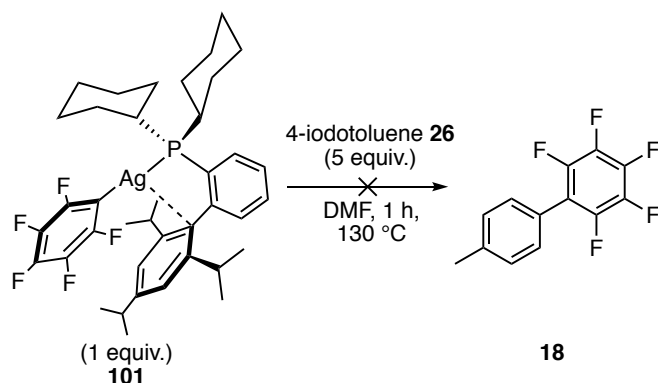


**Figure 117:**  $^{19}\text{F}\{^1\text{H}\}$  (470 MHz,  $\text{CD}_2\text{Cl}_2$ ,  $-20^\circ\text{C}$ ) NMR spectrum of the reaction mixture

**GA-2-163:** Reaction between **101** and 4-iodotoluene **26** in DMF at  $130^\circ\text{C}$



To a J-Young tube under nitrogen, 4-iodotoluene **26** (11 mg, 0.05 mmol, 5 equiv.) was added on the Schlenk line, followed by DMF (0.6 mL) and the J-Young tube was sealed and taken into the glovebox. In the glovebox, a large vial, **101** (7.5 mg, 0.01 mmol, 1 equiv.) was weighed out and dissolved using the solution of 4-iodotoluene **26** in DMF from the J-Young NMR tube to produce a light brown solution. The reaction mixture was analysed by  $^{31}\text{P}\{^1\text{H}\}$  and  $^{19}\text{F}\{^1\text{H}\}$  NMR spectroscopy before and after being submerged in a preheated oil bath ( $130^\circ\text{C}$ ) for 1 h. The  $^{19}\text{F}\{^1\text{H}\}$  NMR spectrum showed no evidence of the formation of the organic biaryl product **18** before or after heating. Heating the reaction mixture at  $130^\circ\text{C}$  for 1 h, only resulted in slight decomposition of **101** to  $\text{C}_6\text{F}_5\text{H}$  and elemental silver.

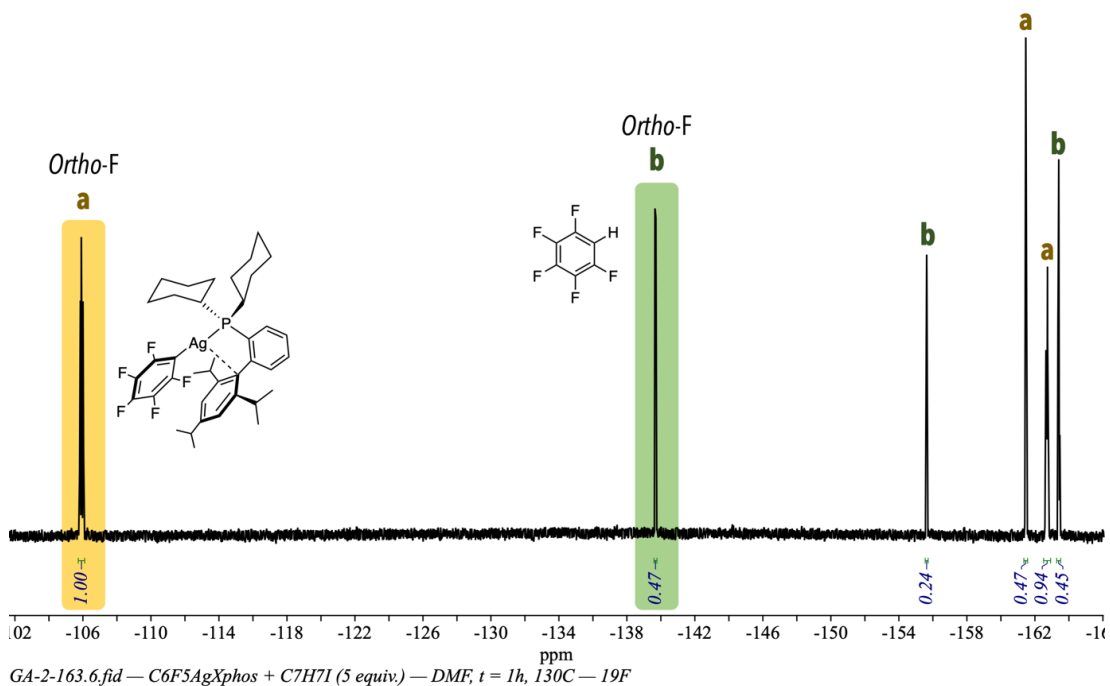
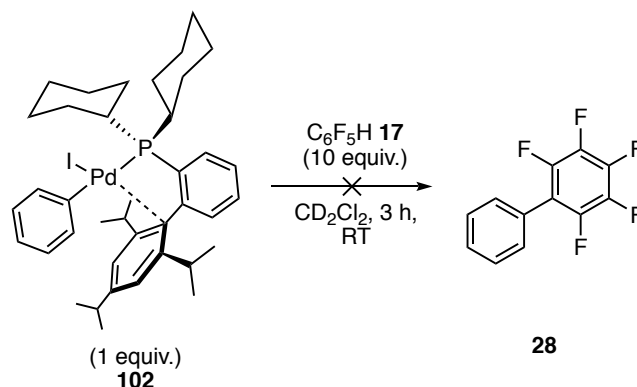


**Figure 118:**  $^{19}\text{F}\{^1\text{H}\}$  NMR (470 MHz, DMF (unlocked), 25 °C) of the reaction mixture **GA-2-163** after heating at 130 °C for 1 h, showing the presence of **101** (yellow, peaks indicated by a) and  $\text{C}_6\text{F}_5\text{H}$  **17** (green, peaks indicated by b) from slight decomposition of **101**.

**GA-3-185:** Reaction between **102** and  $\text{C}_6\text{F}_5\text{H}$  **17** in dichloromethane- $d_2$  at room temperature

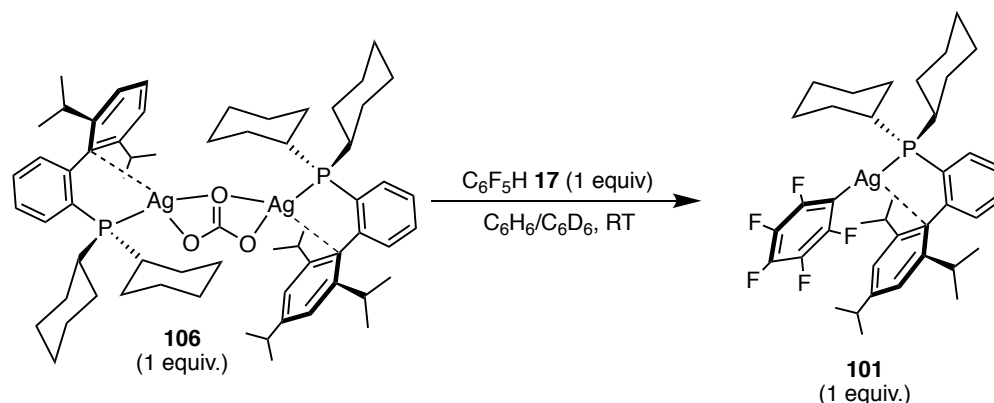


In the glovebox **102** (10 mg, 0.012 mmol, 1 equiv.) was weighed out in a vial, and  $\text{C}_6\text{F}_5\text{H}$  **17** (20 mg, 0.12 mmol, 10 equiv., 13  $\mu\text{L}$ ) was added with a 25  $\mu\text{L}$  gas-tight syringe. The reaction mixture was dissolved in dichloromethane- $d_2$  (0.5 mL) to produce a cloudy bright yellow solution which was transferred into a J-Young tube. The mixture was analysed by  $^1\text{H}$ ,  $^{31}\text{P}\{^1\text{H}\}$  and  $^{19}\text{F}\{^1\text{H}\}$  NMR spectroscopy before and after being allowed to react at room temperature for 3 h.

There was no reaction observed by  $^{31}\text{P}\{^1\text{H}\}$  and  $^{19}\text{F}\{^1\text{H}\}$  NMR spectroscopy. The  $^{31}\text{P}\{^1\text{H}\}$  spectrum only showed unreacted **102**, and the  $^{19}\text{F}\{^1\text{H}\}$  NMR spectrum only showed unreacted  $\text{C}_6\text{F}_5\text{H}$  **17** with no trace of the organic product being formed.

**The Reaction of 106 with C<sub>6</sub>F<sub>5</sub>H 17 in benzene**

**GA-3-233:** The reaction of **106** (1 equiv.) with C<sub>6</sub>F<sub>5</sub>H **17** (1 equiv.) in benzene at room temperature. (Ag: C<sub>6</sub>F<sub>5</sub>H ratio is 1:0.5, C<sub>6</sub>F<sub>5</sub>H is limiting)



In the glovebox, C<sub>6</sub>F<sub>5</sub>H **17** (16 mg, 0.11 mmol) was dissolved in C<sub>6</sub>H<sub>6</sub> (2 mL) to produce a 0.052 M stock solution. In a vial, 0.3 mL of this solution was added to another vial with **106** (20 mg, 0.016 mmol, 1 equiv.) followed by C<sub>6</sub>D<sub>6</sub> (0.2 mL). Once all the solid was completely dissolved, the reaction mixture was analysed by <sup>1</sup>H, <sup>31</sup>P{<sup>1</sup>H} and <sup>19</sup>F{<sup>1</sup>H} NMR spectroscopy.

The reaction reached ~ 50% conversion to **101** within minutes, as seen by the <sup>31</sup>P{<sup>1</sup>H} NMR spectrum recorded immediately after sample preparation. The sample was then monitored at 2 h and 24 h, but there was little to no change detected at room temperature.

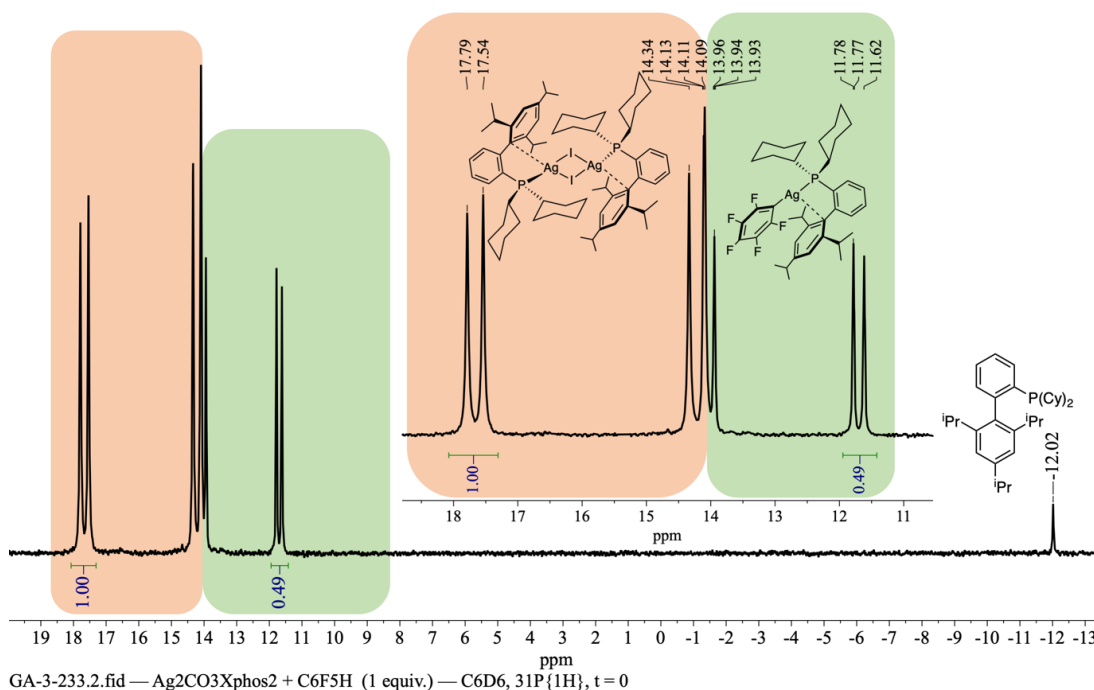


**Figure 119:** <sup>31</sup>P{<sup>1</sup>H} (202.5 MHz, C<sub>6</sub>D<sub>6</sub>/C<sub>6</sub>H<sub>6</sub>, locked to C<sub>6</sub>D<sub>6</sub>, 25 °C) spectrum of the reaction mixture of **GA-3-233**, collected at t = 0 h, RT. The mixture shows both the presence of **101** and **106**.

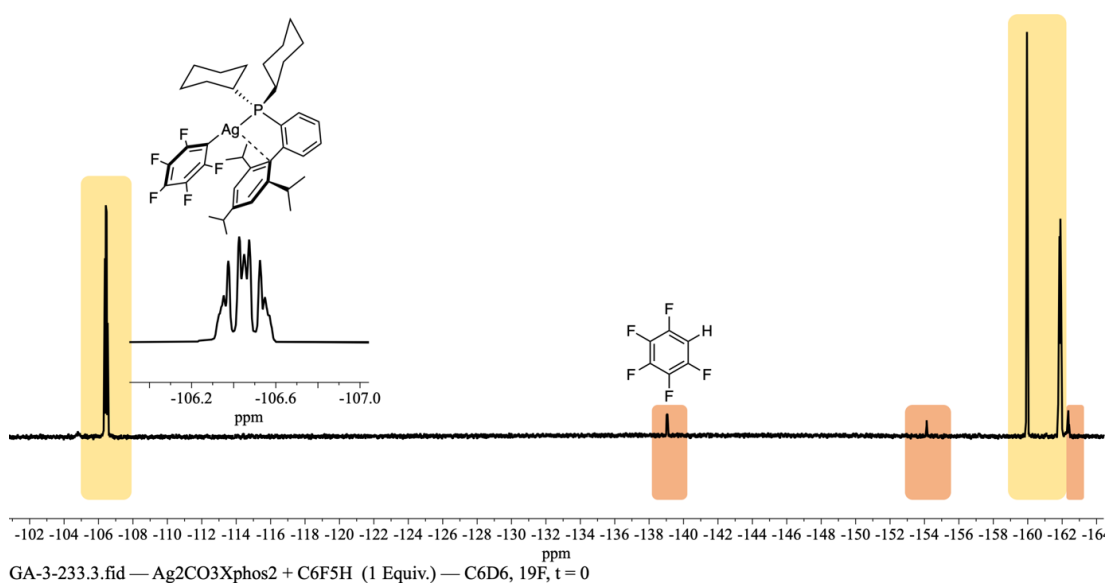
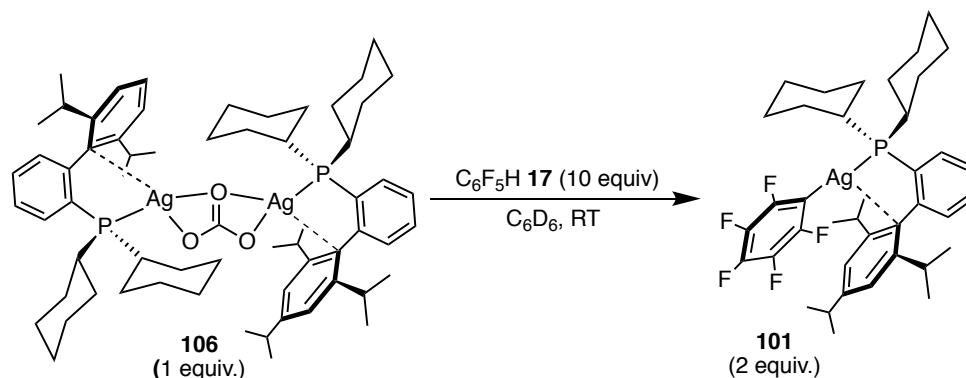


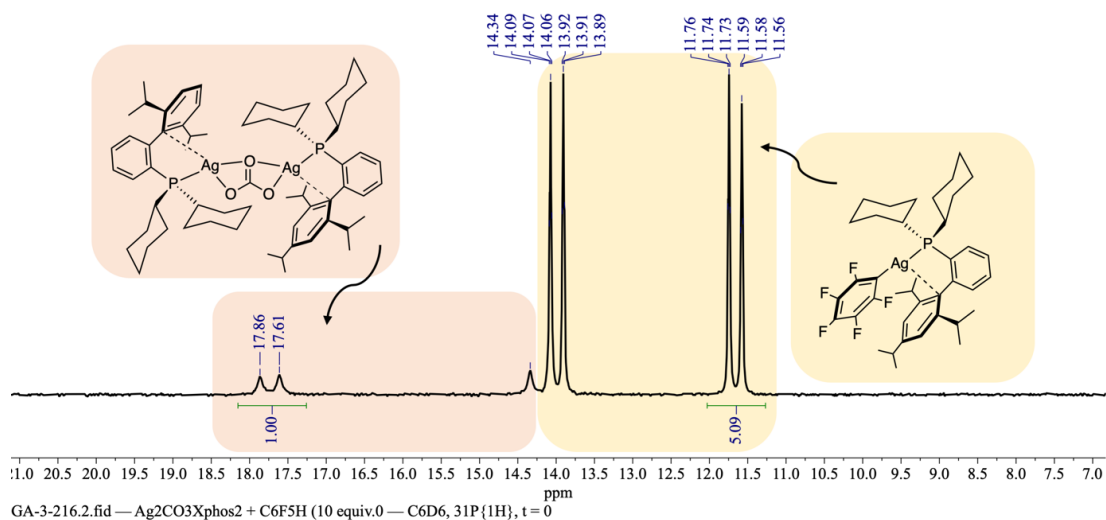
**Figure 120:**  $^{19}\text{F}\{^1\text{H}\}$  NMR (470 MHz,  $\text{C}_6\text{D}_6/\text{C}_6\text{H}_6$ , locked to  $\text{C}_6\text{D}_6$ , 25 °C) of the reaction mixture **GA-3-233** showing presence of both **101** and trace amounts of **17**

**GA-3-216:** Reaction of **106** (1 equiv.) with  $\text{C}_6\text{F}_5\text{H}$  **17** (10 equiv.) in benzene at room temperature.

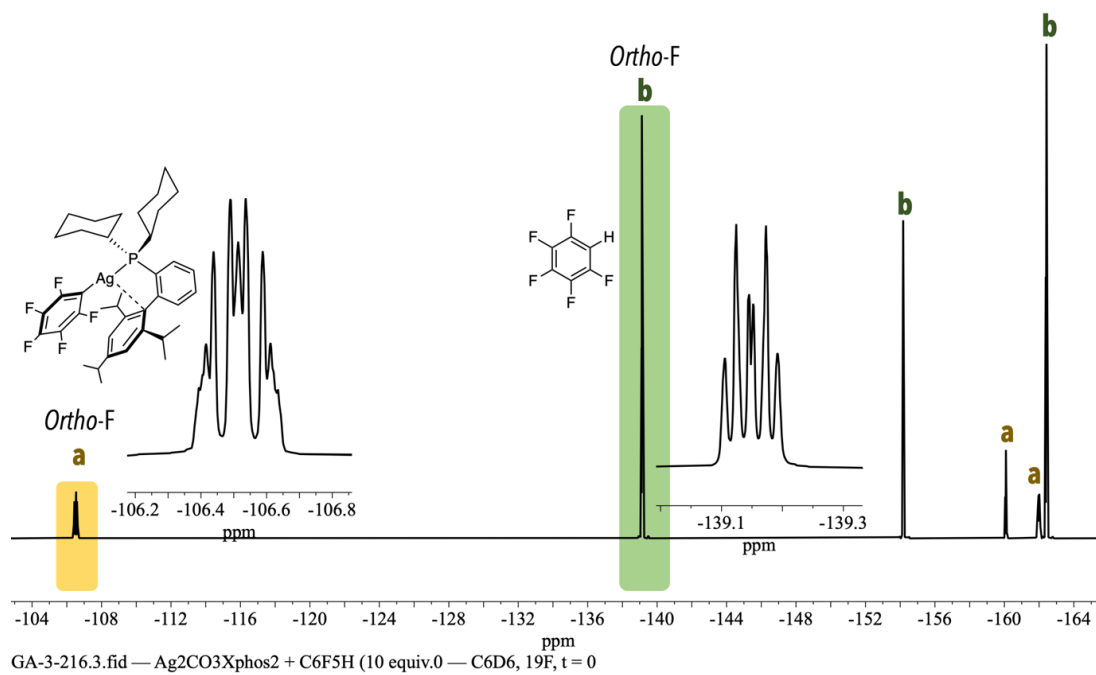


In a glovebox, **106** (20 mg, 0.016 mmol, 1 equiv.) was weighed out in a vial.  $\text{C}_6\text{F}_5\text{H}$  **17** (27 mg, 0.16 mmol, 10 equiv. 18  $\mu\text{L}$ ) was added and the reaction mixture was dissolved in  $\text{C}_6\text{D}_6$  (0.5 mL). The reaction mixture was then transferred to a J-Young NMR tube and monitored using  $^1\text{H}$ ,  $^{31}\text{P}\{^1\text{H}\}$  and  $^{19}\text{F}\{^1\text{H}\}$  NMR spectroscopy.

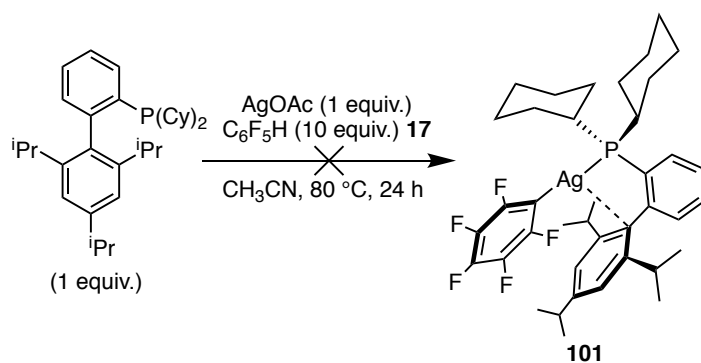
There was almost full conversion to **101** within minutes, as seen by the  $^{13}\text{P}\{^1\text{H}\}$  NMR spectrum recorded immediately after sample preparation. The sample was then monitored at 2 h and 24 h, but there was little to no change detected at room temperature.



**Figure 121:** <sup>31</sup>P{<sup>1</sup>H} (202.5 MHz, C<sub>6</sub>D<sub>6</sub>, 25 °C) spectrum of the reaction mixture of GA-3-216, collected at t = 0 h, RT. The mixture shows both the presence of **106** and **101**.



**Figure 122:** <sup>19</sup>F{<sup>1</sup>H} NMR (470 MHz, C<sub>6</sub>D<sub>6</sub>, 25 °C) of the reaction mixture GA-3-216.

**GA-3-190:** Reaction of AgOAc and Xphos with C<sub>6</sub>F<sub>5</sub>H (10 equiv.) in DMF

To a Schlenk tube, AgOAc (35 mg, 0.3 mmol, 1 equiv.) and Xphos (143 mg, 0.3 mmol, 1 equiv.) was added and the Schlenk tube was evacuated and refilled three times with nitrogen. CH<sub>3</sub>CN (3 mL) and C<sub>6</sub>F<sub>5</sub>H **17** (504 mg, 3 mmol, 10 equiv., 333 μL) were added and the reaction mixture was submerged in a pre-heated oil bath (80 °). After 24 h, 0.5 mL of the reaction mixture was transferred to a J-Young tube under an atmosphere of nitrogen and analysed by <sup>31</sup>P{<sup>1</sup>H} and <sup>19</sup>F{<sup>1</sup>H} NMR spectroscopy. The <sup>31</sup>P{<sup>1</sup>H} NMR spectrum showed the presence of a new Ag–P containing species, which was confirmed to be AgOAcXphos **109** after preparing an authentic sample. The <sup>19</sup>F{<sup>1</sup>H} NMR spectrum also showed no presence of **101**

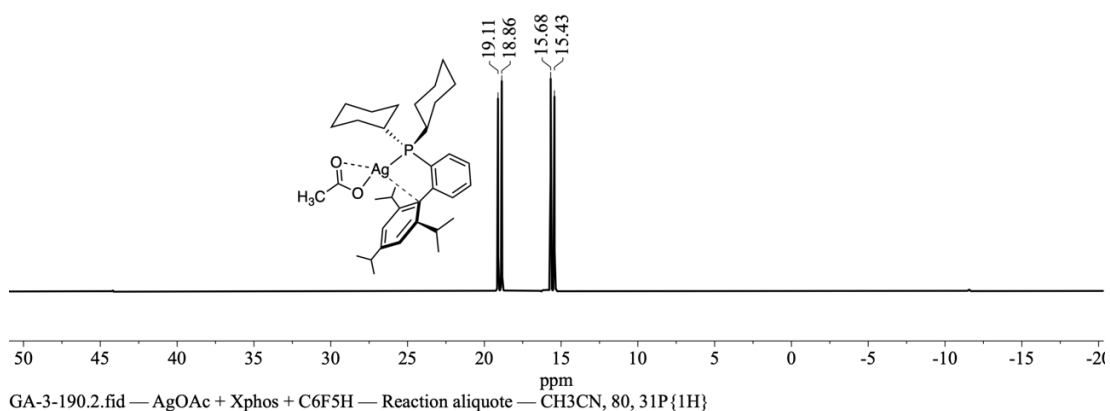


**Figure 123:** <sup>31</sup>P{<sup>1</sup>H} (202.5 MHz, CH<sub>3</sub>CN, 25 °C) spectrum of the reaction mixture of **GA-3-190**, collected after heating at 80°C for 24 h. The mixture showed only the presence of **109** and no **101** or unbound Xphos.



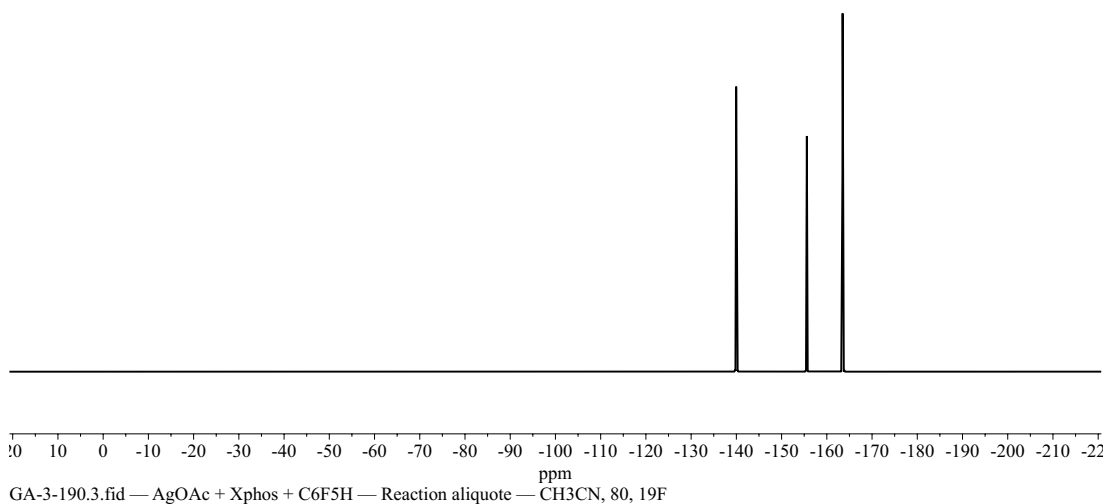
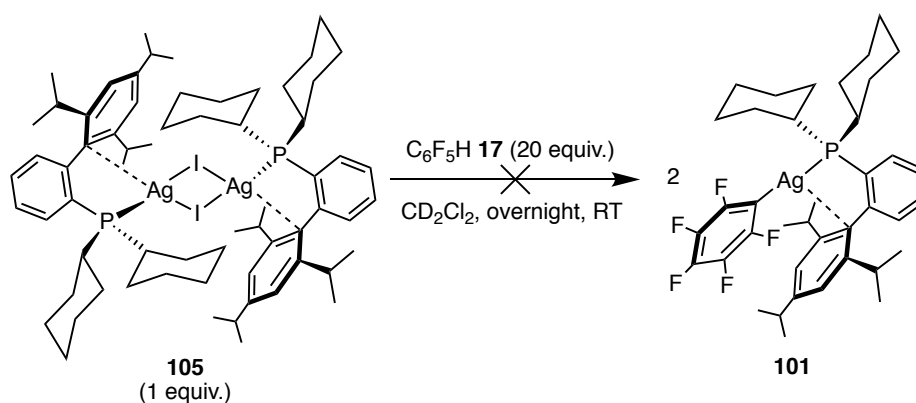


**Figure 124:**  $^{19}\text{F}\{^1\text{H}\}$  NMR (470 MHz,  $\text{CH}_3\text{CN}$ , 25 °C) of the reaction mixture **GA-3-190**, showing unreacted  $\text{C}_6\text{F}_5\text{H}$  **17**

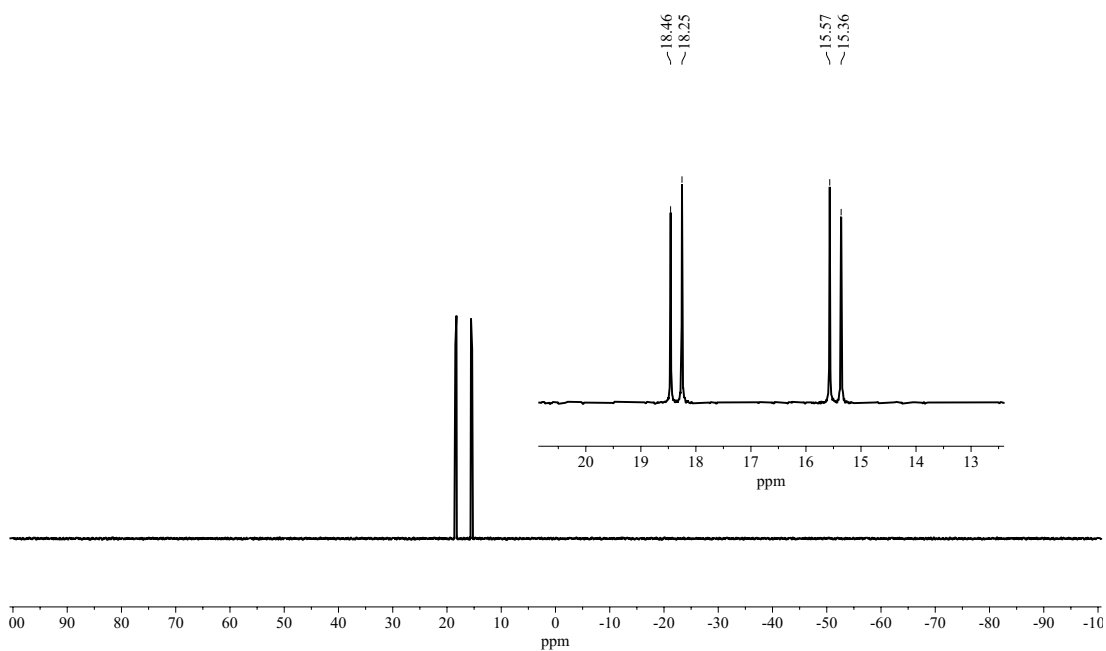
#### Reaction of **105** with $\text{C}_6\text{F}_5\text{H}$ **17**

**GA-4-271:** The Reaction of **105** with  $\text{C}_6\text{F}_5\text{H}$  **17** (20 equiv.) in  $\text{CD}_2\text{Cl}_2$  at room temperature



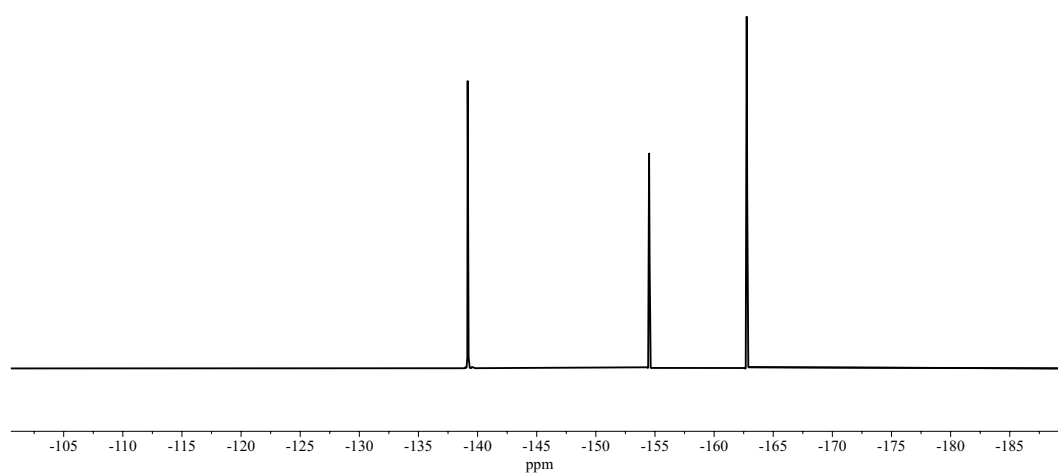
In a glovebox, **105** (10 mg, 0.007 mmol, 1 equiv.) was weighed out in a vial followed by  $\text{C}_6\text{F}_5\text{H}$  **17** (24 mg, 0.14 mmol, 20 equiv. 16  $\mu\text{L}$ ) (10 equiv. per Ag). The mixture was dissolved in dichloromethane- $d_2$  (0.5 mL) and transferred into a J-Young NMR tube and analysed by  $^1\text{H}$ ,  $^{31}\text{P}\{^1\text{H}\}$  and  $^{19}\text{F}\{^1\text{H}\}$  NMR spectroscopy. No formation of new species was detected by  $^{19}\text{F}\{^1\text{H}\}$  NMR at  $t = 0$  h or after leaving the reaction to react at room temperature overnight. There was also no change by  $^{31}\text{P}\{^1\text{H}\}$  NMR spectroscopy.

GA-4-271.5.fid  
 AgIXphos + C6F5H (10 equiv.)  
 CD2Cl2, 31P{1H}, t = overnight, RT

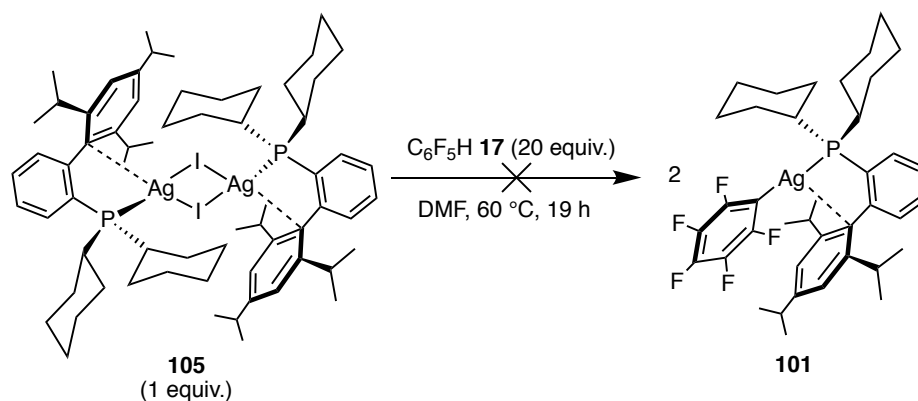


**Figure 125:**  $^{31}\text{P}\{^1\text{H}\}$  (202.5 MHz,  $\text{CD}_2\text{Cl}_2$ , 25 °C) spectrum of the reaction mixture of **GA-4-271** after allowing it to react overnight. The mixture shows the presence of unreacted **105**.

GA-4-271.6.fid  
 IAgXphos + C6F5H (10 equiv.)  
 DCM-d2,  $^{19}\text{F}$ , t = overnight, RT



**Figure 126:**  $^{19}\text{F}\{^1\text{H}\}$  NMR (470 MHz,  $\text{CD}_2\text{Cl}_2$ , 25 °C) of the reaction mixture **GA-4-271**, showing only unreacted  $\text{C}_6\text{F}_5\text{H}$  **17** with no formation of any new species.

GA-4-272: Reaction of **105** with  $C_6F_5H$  **17** (20 equiv.) in DMF at 60 °C

In a glovebox, **105** (10 mg, 0.007 mmol, 1 equiv.) was weighed out in a vial followed by  $C_6F_5H$  **17** (24 mg, 0.14 mmol, 20 equiv. 16  $\mu$ L) (10 equiv. per Ag). The mixture was dissolved in DMF (0.5 mL) and transferred into a J-Young NMR tube and analysed by  $^1H$ ,  $^{31}P\{^1H\}$  and  $^{19}F\{^1H\}$  NMR spectroscopy. No formation of new species was detected by  $^{19}F\{^1H\}$  NMR at  $t = 0$  h, RT or heating to 60 °C for 19 h. There was also no change by  $^{31}P\{^1H\}$  NMR spectroscopy.

GA-4-272.6.fid  
 AgIXphos + C6F5H (10 equiv.)  
 DMF, unlocked,  $^{31}P\{^1H\}$ ,  $t = 19$  h, 60C

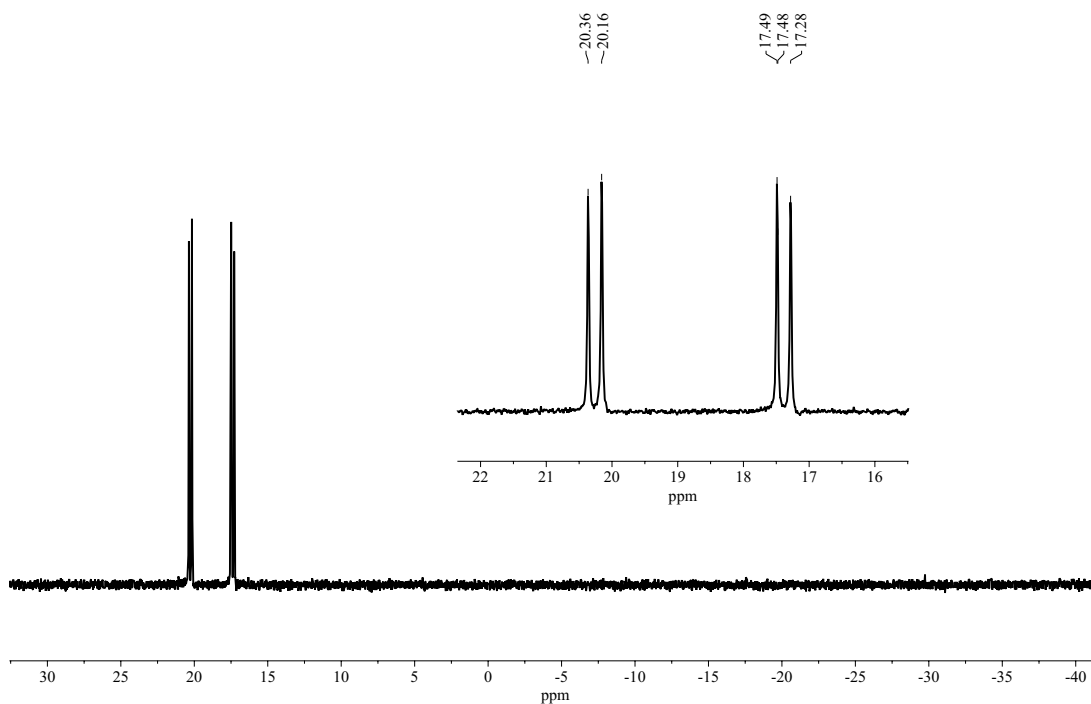


**Figure 127:**  $^{31}P\{^1H\}$  (202.5 MHz, DMF (unlocked), 25 °C) spectrum of GA-4-272 after it was heated at 60 °C for 19 h. The mixture shows the presence of unreacted **105**.

GA-4-272.7.fid  
 1AgXphos + C6F5H (10 equiv.)  
 DMF, unlocked, 19F, t = 19 h, 60C

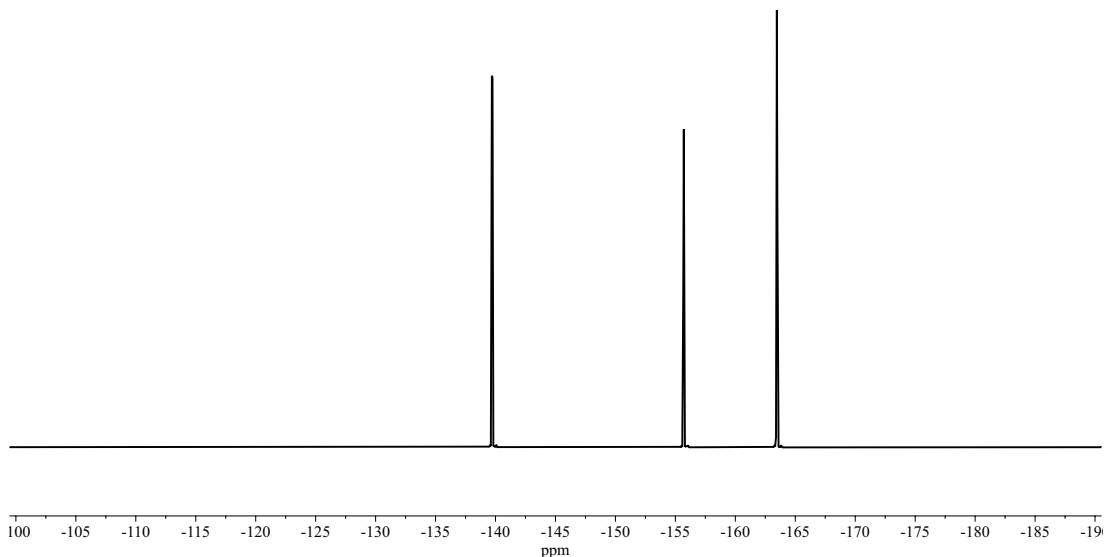
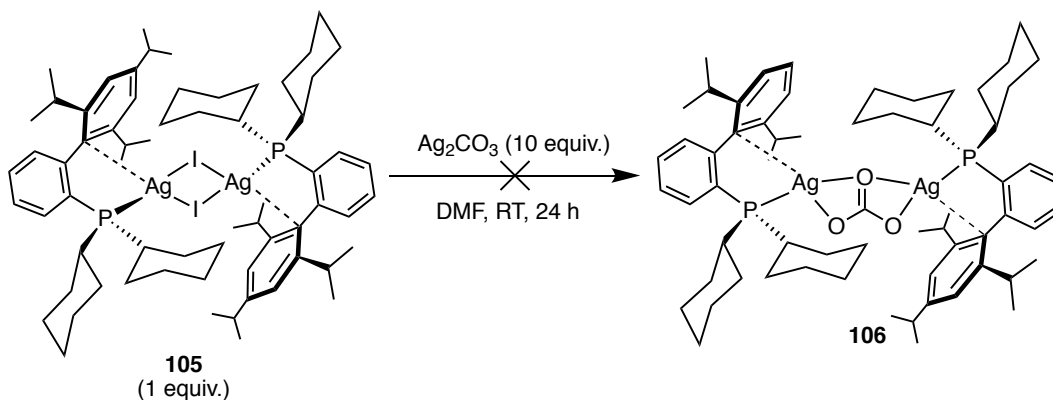


**Figure 128:**  $^{19}\text{F}\{^1\text{H}\}$  NMR (470 MHz, DMF (unlocked), 25 °C) of the reaction mixture **GA-4-272**, showing only unreacted  $\text{C}_6\text{F}_5\text{H}$  **17** with no formation of any new species.

**GA-4-276:** Reaction of **105** with  $\text{Ag}_2\text{CO}_3$  (10 equiv.) in DMF at room-temperature



To an oven dried Schlenk tube, **105** (15 mg, 0.010 mmol, 1 equiv.) and  $\text{Ag}_2\text{CO}_3$  (29 mg, 0.10 mmol, 10 equiv.) was added, and the Schlenk tube was evacuated and re-filled three times with nitrogen. Dry DMF (1 mL) was added, and the reaction mixture was stirred at room-temperature for 24 h. A reaction aliquot was prepared by filtering 0.5 mL of the reaction mixture under nitrogen to a J-young NMR tube. The reaction mixture was analysed by  $^{31}\text{P}\{^1\text{H}\}$  NMR spectroscopy. The mixture showed the presence of a slightly broad pair of doublets at  $\delta$  18.9 ( $^1J_{^{107}\text{Ag}^{31}\text{P}} = 558$  Hz,  $^1J_{^{109}\text{Ag}^{31}\text{P}} = 689$  Hz) which corresponds to **105** in DMF.

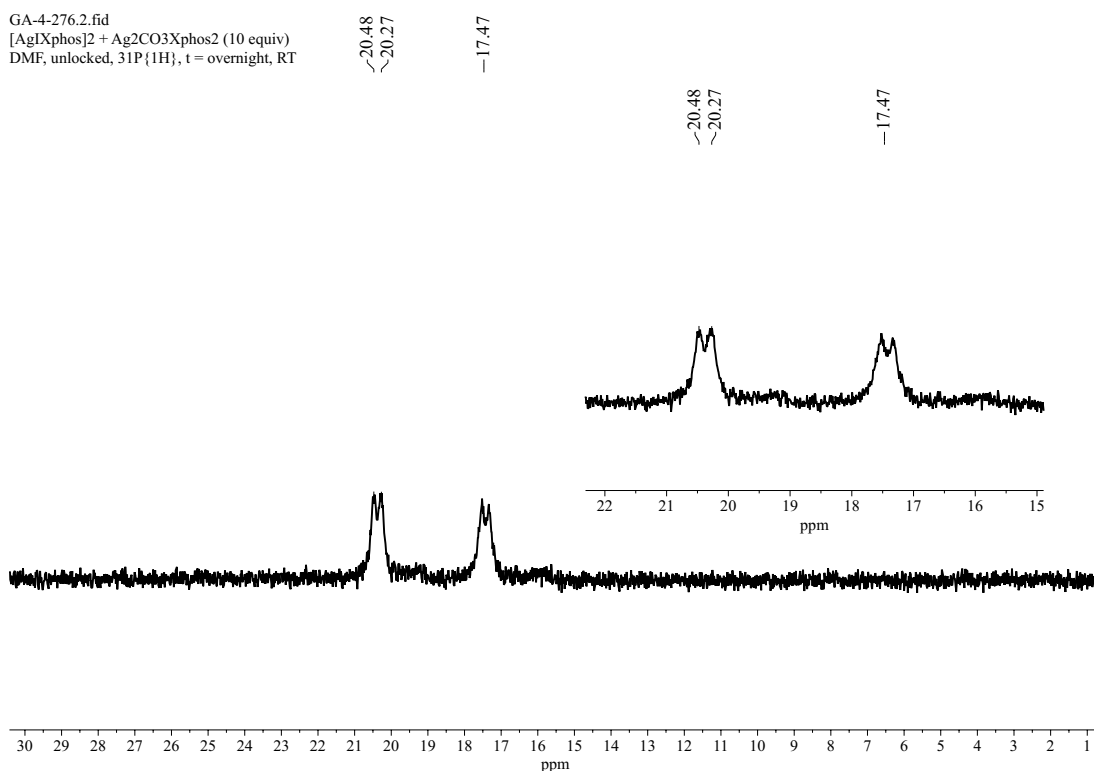
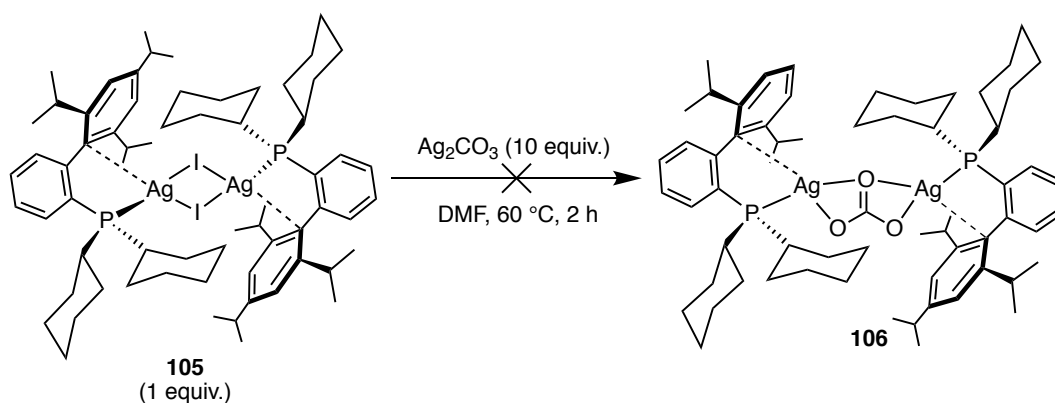


**Figure 129:**  $^{31}\text{P}\{^1\text{H}\}$  (202.5 MHz, DMF (unlocked), 25 °C) spectrum of **GA-4-276** at room temperature for 24 h. The mixture shows the presence of unreacted **105**.

**GA-4-278:** Reaction of **105** with  $\text{Ag}_2\text{CO}_3$  (10 equiv.) in DMF at 60 °C for 2 h



To an oven dried Schlenk tube, **105** (15 mg, 0.010 mmol, 1 equiv.) and  $\text{Ag}_2\text{CO}_3$  (29 mg, 0.10 mmol, 10 equiv.) was added, and the Schlenk tube was evacuated and re-filled three times with nitrogen. Dry DMF (1 mL) was added, and the reaction mixture was submerged in a pre-heated oil bath (60 °C) for 2 h. A reaction aliquot was prepared by filtering 0.5 mL of the reaction mixture under nitrogen to a J-young NMR tube. The reaction mixture was analysed by  $^{31}\text{P}\{^1\text{H}\}$  NMR spectroscopy. The mixture showed the presence of a slightly broad pair of doublets at  $\delta$  18.6 ( $^1J_{107\text{Ag}^{31}\text{P}} = 558$  Hz,  $^1J_{109\text{Ag}^{31}\text{P}} = 689$  Hz) which corresponds to **105** in DMF. Some of the  $\text{Ag}_2\text{CO}_3$  escaped through the filter and was present in the final NMR sample, which is likely contributed to the broadness of the peak.

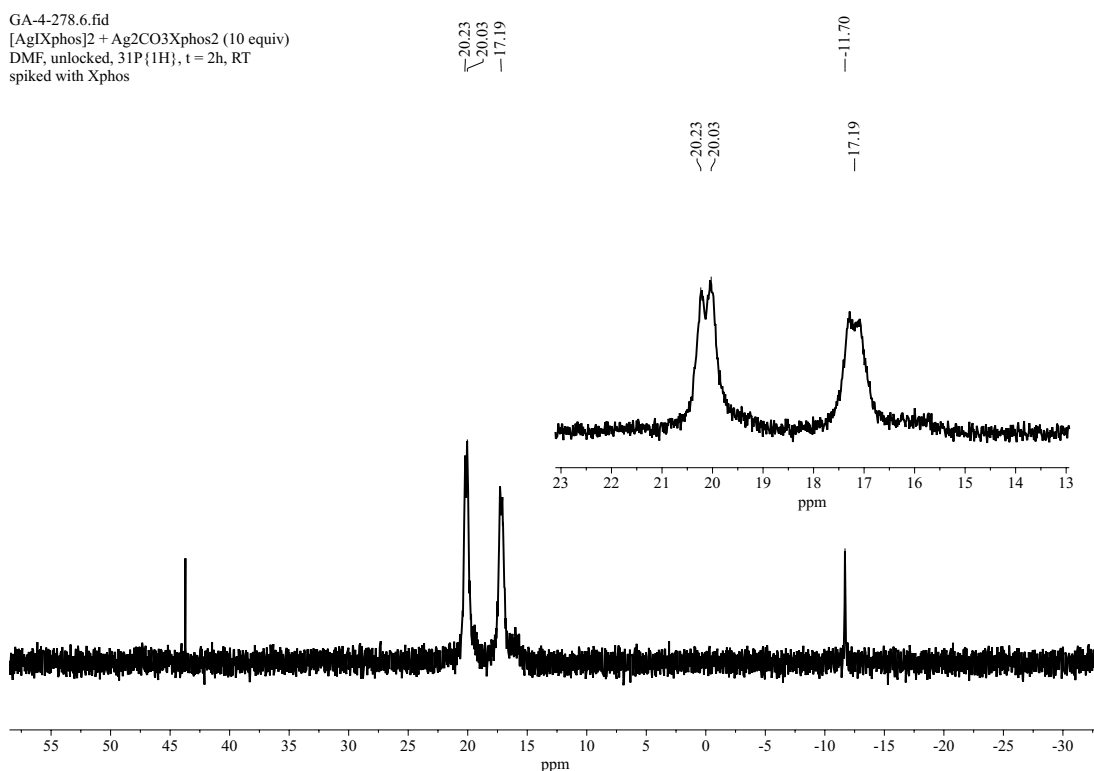
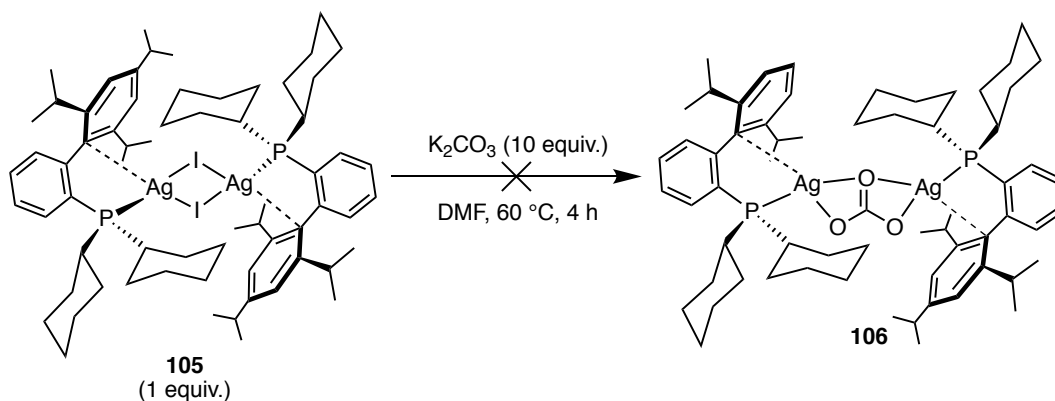


**Figure 130:** <sup>31</sup>P{<sup>1</sup>H} (202.5 MHz, DMF (unlocked), 25 °C) spectrum of **GA-4-278** at 60 °C for 2 h. The mixture shows the presence of unreacted **105**, unbound Xphos and Xphos oxide.

**GA-4-298:** Reaction of **105** with K<sub>2</sub>CO<sub>3</sub> (10 equiv.) in DMF at 60 °C for 4 h



To an oven dried Schlenk tube, **105** (15 mg, 0.010 mmol, 1 equiv.) and K<sub>2</sub>CO<sub>3</sub> (14 mg, 0.10 mmol, 10 equiv.) was added, and the Schlenk tube was evacuated and re-filled three times with nitrogen. Dry DMF (1 mL) was added, and the reaction mixture was submerged in a pre-heated oil bath (60 °C) for 4 h. A reaction aliquot was prepared by filtering 0.5 mL of the reaction mixture to a NMR tube. The reaction mixture was analysed by <sup>31</sup>P{<sup>1</sup>H} NMR spectroscopy. The mixture showed the presence of a broad doublet at δ 18.5 which corresponds to **105** in DMF. Some of the K<sub>2</sub>CO<sub>3</sub> escaped through the filter and was present in the final

NMR sample, which is likely contributed to the broadness of the peak and lack of  $^{107}\text{Ag}/^{109}\text{Ag}$  coupling information.

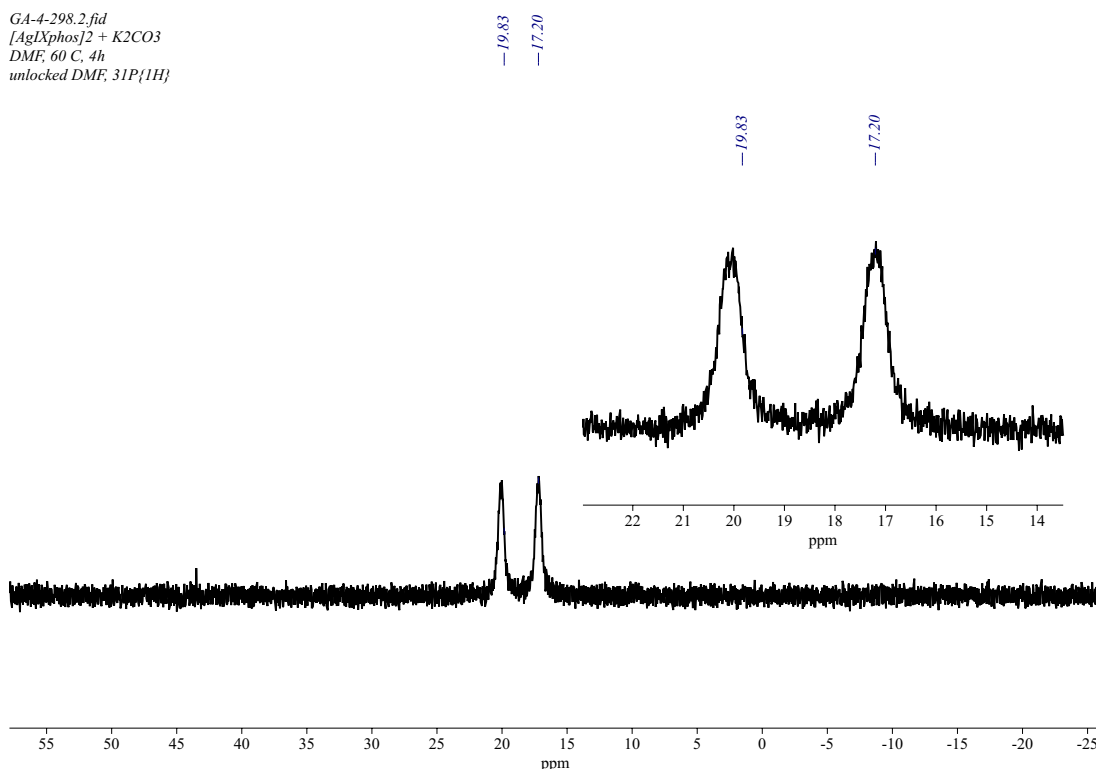
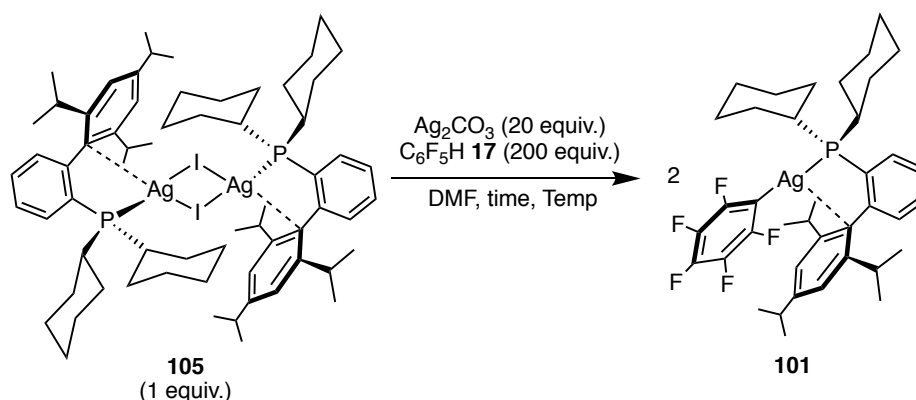


**Figure 131:**  $^{31}\text{P}\{^1\text{H}\}$  (202.5 MHz, DMF (unlocked), 25 °C) spectrum of **GA-4-298** at 60 °C for 4 h. The mixture shows the presence of unreacted **105**.

### The Reaction of **105** with $\text{Ag}_2\text{CO}_3$ and $\text{C}_6\text{F}_5\text{H}$ **17** conducted in DMF

#### General Experimental Procedure



In a light-protected Schlenk tube (wrapped in foil), **105** (15 mg, 0.005 mmol, 1 equiv.) and  $\text{Ag}_2\text{CO}_3$  (29 mg, 0.10 mmol, 20 equiv.) (10 equiv. per Ag) was added and the Schlenk tube was evacuated and refilled with nitrogen three times. Dry DMF (1 mL) and  $\text{C}_6\text{F}_5\text{H}$  (168 mg, 1.0 mmol, 200 equiv. 110  $\mu\text{L}$ ) (100 equiv. per Ag) were added and the Schlenk tube was set to the desired temperature and allowed to react for the required amount of time. The reaction mixture (0.5 mL) was then filtered under nitrogen and transferred to a J-Young NMR tube and

was analysed by  $^1\text{H}$ ,  $^{31}\text{P}\{^1\text{H}\}$  and  $^{19}\text{F}\{^1\text{H}\}$  NMR spectroscopy, unlocked in non-deuterated DMF.

**GA-4-321/GA-5-354:** After the addition of all the reagents, the reaction mixture was submerged in a per-heated oil bath (60 °C) and allowed to react for 4 h (**GA-4-321**)/ 3 h (**GA-5-354**.) After heating at 60 °C for 3 h, the formation of **101** was detected by  $^{31}\text{P}\{^1\text{H}\}$  and  $^{19}\text{F}\{^1\text{H}\}$  NMR spectroscopy, and LIFDI.

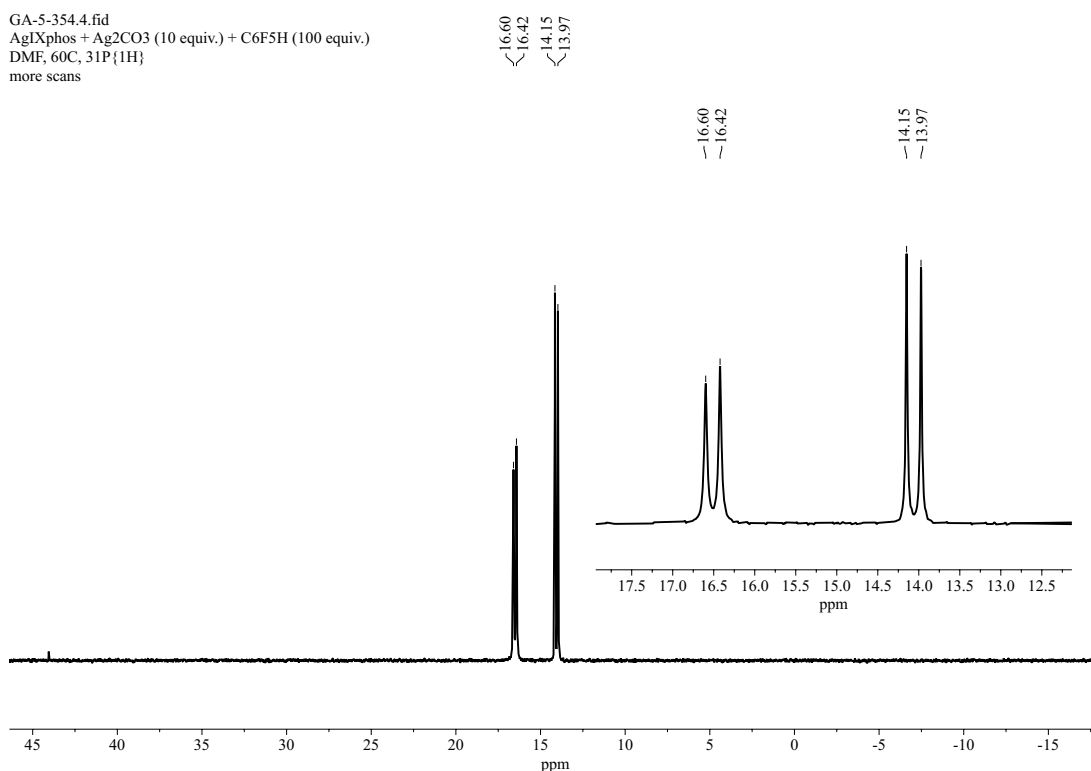


**Figure 132:**  $^{31}\text{P}\{^1\text{H}\}$  (202.5 MHz, DMF (unlocked), 25 °C) spectrum of the reaction mixture of **GA-5-354**. The Ag resonance was centred at  $\delta$  14.9 ( $^1J_{107\text{Ag}-^{31}\text{P}} = 459.7$  Hz,  $^1J_{109\text{Ag}-^{31}\text{P}} = 532.6$  Hz) corresponding to **101**.

**Table 41:** The chemical shift and coupling constant of authentic samples of Ag complexes in DMF

Authentic sample in DMF	Chemical Shift $\delta$	$^1J_{107\text{Ag}-^{31}\text{P}}$ (Hz)	$^1J_{109\text{Ag}-^{31}\text{P}}$ (Hz)	$^3J_{19\text{F}-^{31}\text{P}}$ (Hz)
<b>101</b> <sup>[a]</sup>	14.8	445.5	514.3	2.0
<b>105</b> <sup>[a]</sup>	18.6	552.8	619.6	-
<b>106</b> <sup>[b]</sup>	17.3	639.9	739.1	-

<sup>[a]</sup> An authentic sample was dissolved in DMF-*d*<sub>7</sub> to determine the chemical shift and coupling constants.

<sup>[b]</sup> An authentic sample recorded in non-deuterated DMF with Xphos added to aid sample referencing.



GA-5-354.5.fid  
 AgIXphos + Ag<sub>2</sub>CO<sub>3</sub> (10 equiv.) + C<sub>6</sub>F<sub>5</sub>H (100 equiv.)  
 DMF, 60C, 19F  
 more scans

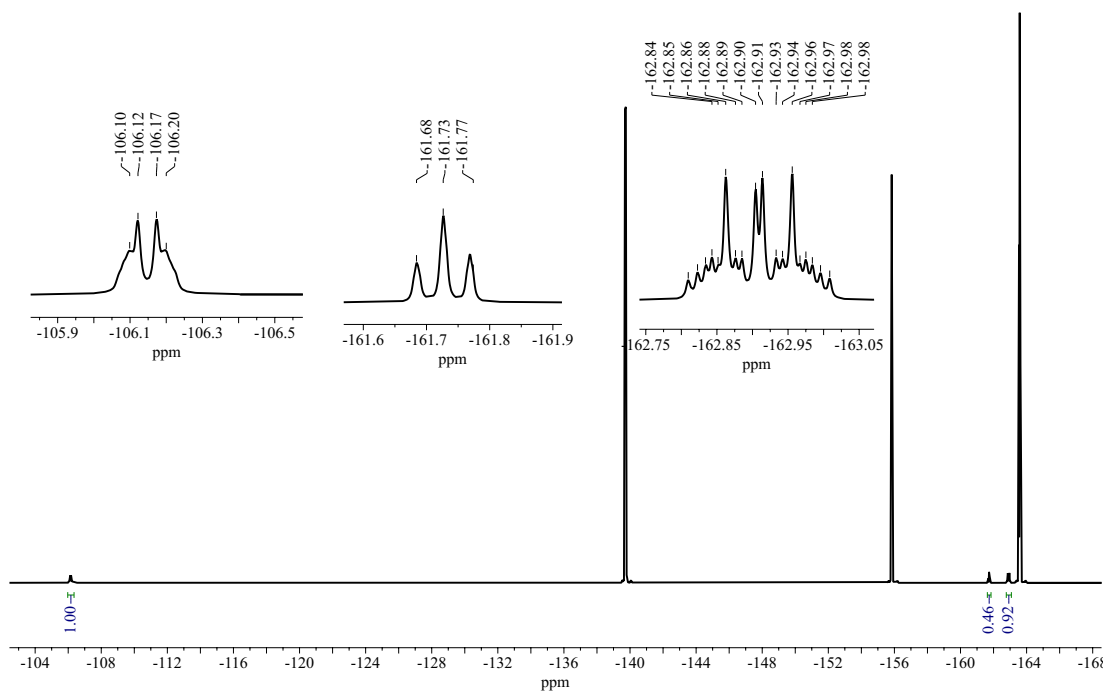


**Figure 133:**  $^{19}\text{F}\{^1\text{H}\}$  NMR (470 MHz, DMF (unlocked), 25 °C) of the reaction mixture **GA-4-345**, showing the presence of **101** in the reaction mixture with remaining unreacted  $\text{C}_6\text{F}_5\text{H}$  **17**.

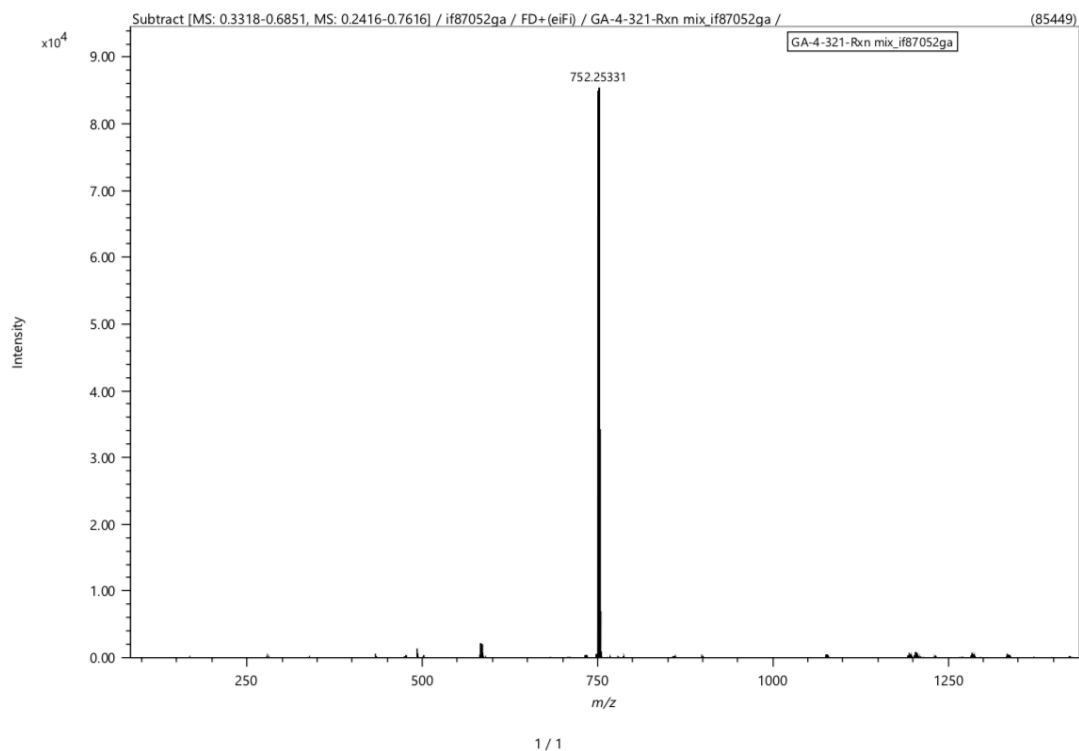


**Figure 134:** LIFDI-MS spectrum of the reaction mixture of **GA-4-321**. The major species with  $m/z$  752.25331 corresponds to **101**.

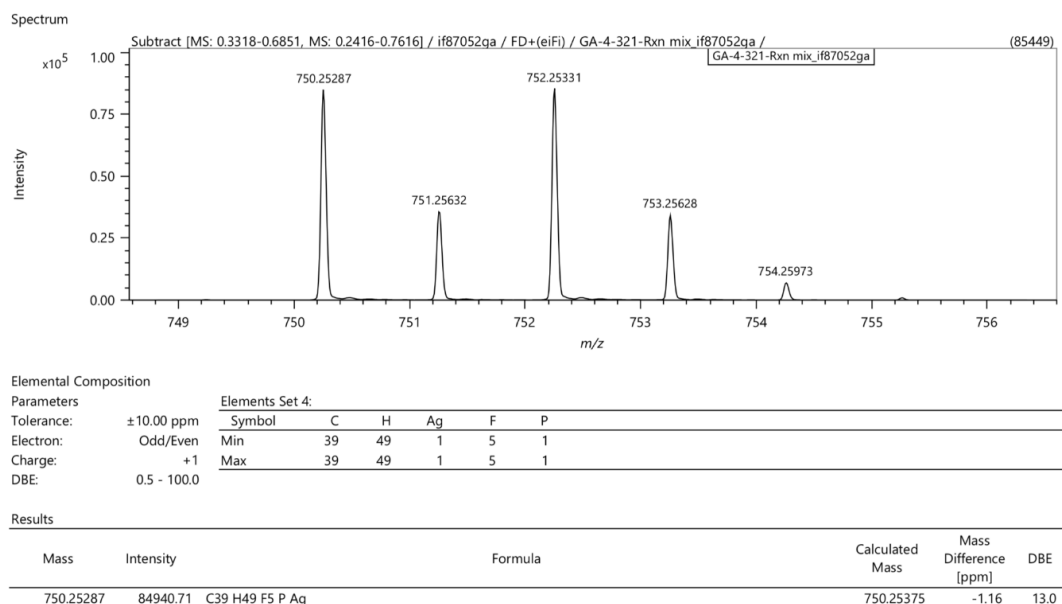
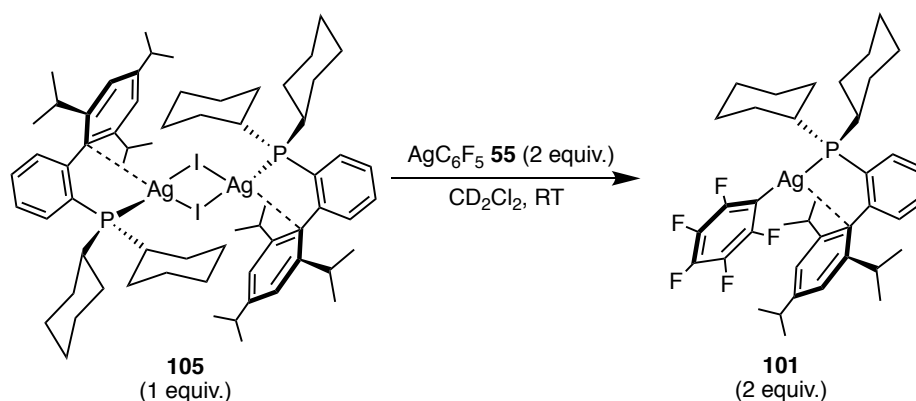


**Figure 135:** An expansion of the  $m/z$  752.25331 peak in the LIFDI spectrum of **GA-4-321**, showing the characteristic Ag isotopic pattern.

**GA-4-334/GA-4-349:** After the addition of all the reagents, the reaction mixture was stirred at room temperature for 22 h (**GA-4-334**)/ 3 h (**GA-4-349**). After 3h, the reaction mixture shows complete formation of **101** with no traces of **105** present by  $^{31}\text{P}\{^1\text{H}\}$  NMR spectroscopy. The  $^{19}\text{F}\{^1\text{H}\}$  NMR complements this by showing the presence of **101** along with unreacted  $\text{C}_6\text{F}_5\text{H}$ . This demonstrates that the reaction between **105**,  $\text{Ag}_2\text{CO}_3$  and  $\text{C}_6\text{F}_5\text{H}$  can occur at room temperature after 3 hours.

**GA-4-318:** The reaction between **105** and  $\text{AgC}_6\text{F}_5$  **55** in dichloromethane- $d_2$  at room temperature



In two separate foiled vials, **105** (15 mg, 0.011 mmol, 1 equiv.) and  $\text{AgC}_6\text{F}_5$  **55** (6 mg, 0.021 mmol, 2 equiv.) (1 equiv. per Ag) were weighed out in a glovebox, with the lights dimmed. **105** was dissolved in dichloromethane- $d_2$  (0.5 mL) to produce a clear colourless solution was then transferred to the vial containing the  $\text{AgC}_6\text{F}_5$  **55**. This resulted in the

immediate colour change to a pale-yellow solution. The solution was quickly transferred into a J-Young NMR tube and analysed by  $^1\text{H}$ ,  $^{31}\text{P}\{^1\text{H}\}$  and  $^{19}\text{F}\{^1\text{H}\}$  NMR spectroscopy. The  $^{31}\text{P}\{^1\text{H}\}$  and  $^{19}\text{F}\{^1\text{H}\}$  NMR spectrum of the reaction mixture showed the instant formation of **101**. It was also noted that a yellow solid precipitated from the solution, which is likely AgI.

GA-4-318.2.fid  
AgC6F5 + AgIXphos  
DCM-d2, RT, t = 0, 1H  
smaller SW

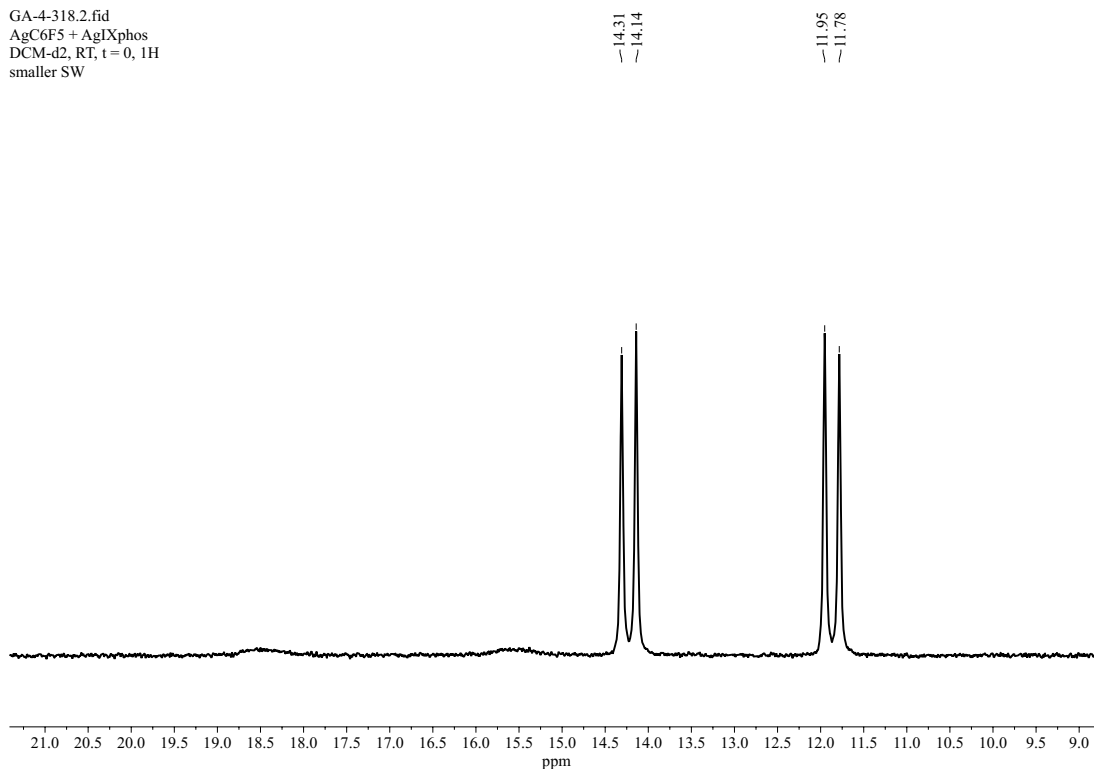


**Figure 136:**  $^{31}\text{P}\{^1\text{H}\}$  (202.5 MHz,  $\text{CD}_2\text{Cl}_2$ , 25 °C) spectrum of the reaction mixture of **GA-4-318**, recorded immediately after the mixture was prepared in the glovebox. The resonance was centred at  $\delta$  13.0 ( $^1J_{^{107}\text{Ag}-^{31}\text{P}} = 443.5$  Hz,  $^1J_{^{109}\text{Ag}-^{31}\text{P}} = 512.3$  Hz) which corresponds to **101**

GA-4-318.3.fid  
 AgC6F5 + AgIXphos  
 DCM-d2, RT, t = 0, 19F

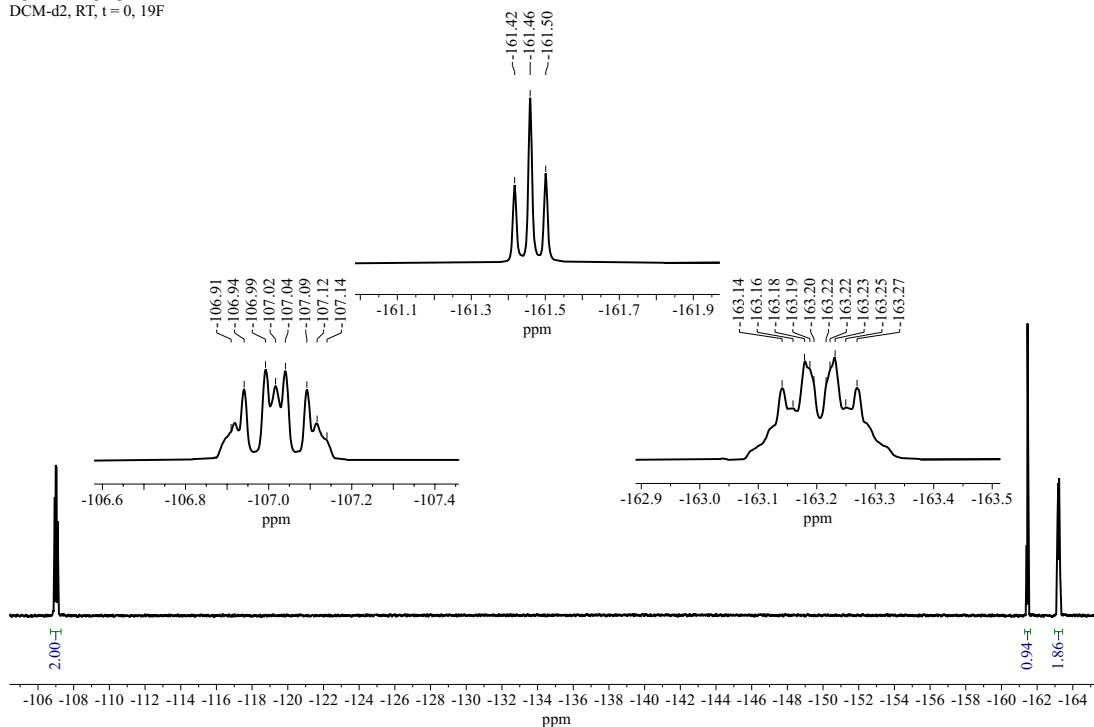
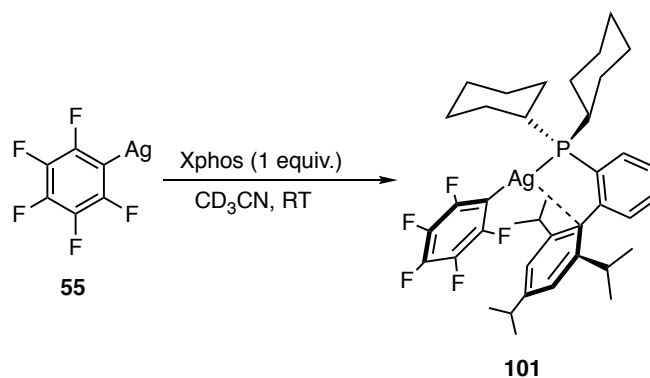


**Figure 137:**  $^{19}\text{F}\{^1\text{H}\}$  NMR (470 MHz,  $\text{CD}_2\text{Cl}_2$ , 25 °C) of the reaction mixture **GA-4-318**, showing the presence of **101**.

**GA-4-303:** Reaction between  $\text{AgC}_6\text{F}_5$  **55** and Xphos in  $\text{CD}_3\text{CN}$



In two separate vials,  $\text{AgC}_6\text{F}_5$  **55** (10 mg, 0.036 mmol, 1 equiv.) (weighed out in a foiled vial in the glovebox, with the lights dimmed) and Xphos (17 mg, 0.036 mmol, 1 equiv.) were weighed out in a glovebox. The  $\text{AgC}_6\text{F}_5$  **55** was then dissolved in  $\text{CD}_3\text{CN}$  (0.5 mL) before the solution was transferred to the vial containing the Xphos and all the solid was dissolved. The reaction mixture transferred into a J-Young NMR tube and analysed by  $^1\text{H}$ ,  $^{31}\text{P}\{^1\text{H}\}$  and  $^{19}\text{F}\{^1\text{H}\}$  NMR spectroscopy. The  $^{31}\text{P}\{^1\text{H}\}$  and  $^{19}\text{F}\{^1\text{H}\}$  NMR analysis showed almost instantaneous conversion to **101** with no traces of unreacted Xphos and  $\text{AgC}_6\text{F}_5$  **55** in the  $^{31}\text{P}\{^1\text{H}\}$  and  $^{19}\text{F}\{^1\text{H}\}$  NMR spectrum, respectively.

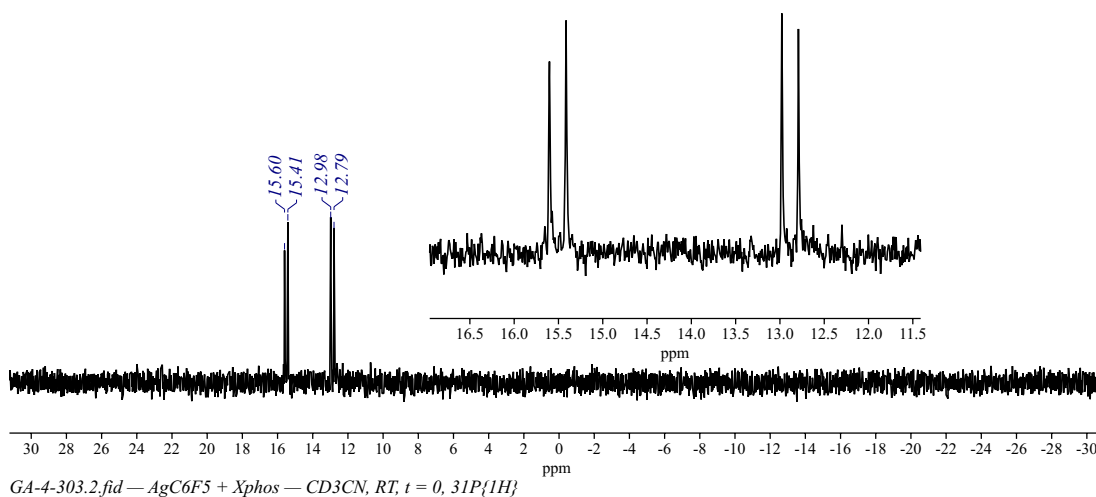


**Figure 138:**  $^{31}\text{P}\{^1\text{H}\}$  (202.5 MHz, CD<sub>3</sub>CN, 25 °C) spectrum of the reaction mixture of GA-4-303, recorded immediately after the mixture was prepared in the glovebox. The resonance was centred at  $\delta$  14.2 ( $^1J_{^{107}\text{Ag}-^{31}\text{P}} = 492.1$  Hz,  $^1J_{^{109}\text{Ag}-^{31}\text{P}} = 569.0$  Hz)

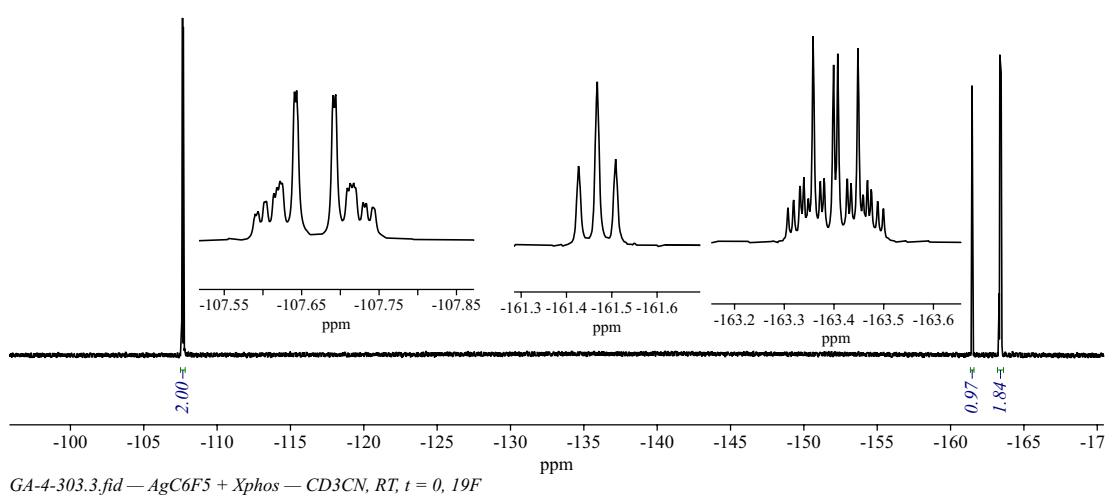
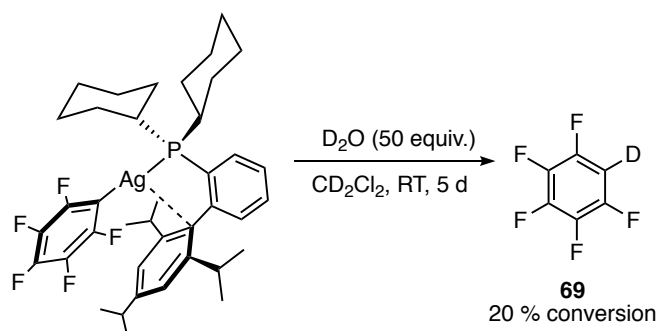


**Figure 139:**  $^{19}\text{F}\{^1\text{H}\}$  NMR (470 MHz, CD<sub>3</sub>CN, 25 °C, 32 Sc) of the reaction mixture GA-4-303.

**GA-6-483:** The reaction of **101** (1 equiv.) with D<sub>2</sub>O (50 equiv.) in dichloromethane-*d*<sub>2</sub>



In the glovebox, **101** (8 mg, 0.010 mmol, 1 equiv.) was dissolved in dichloromethane- $d_2$  (0.5 mL) and transferred to a J-Young NMR tube. The J-Young tube was then removed from the glovebox and affixed onto an NMR tube Schlenk line adaptor and connected to the Schlenk line. Under an atmosphere of nitrogen, the J-Young cap was removed and  $D_2O$  (10 mg, 0.50 mmol, 50 equiv., 9  $\mu$ L) was added. The J-Young cap was removed, and the reaction mixture was monitored by  $^1H$ ,  $^{31}P\{^1H\}$  and  $^{19}F\{^1H\}$  NMR spectroscopy at  $t = 0$  h (recorded immediately after sample preparation), 24 h and after 5 d.

The decomposition of **101** to  $C_6F_5D$  **69** was monitored using  $^{19}F\{^1H\}$  NMR spectroscopy. At  $t = 0$  h, 7 % conversion to  $C_6F_5D$  **69** was calculated by integrating the *ortho*-F resonance of **101** wrt the *ortho*-F peak of  $C_6F_5D$  **69** at  $\delta -139$  in dichloromethane- $d_2$ . The reaction mixture was then allowed to react for 24 h at room temperature, after which a 12 % conversion to  $C_6F_5D$  **69** was observed. Reacting at room temperature for 5 d resulted in a 20 % decomposition of **101** to  $C_6F_5D$  **69**. The  $^{31}P\{^1H\}$  NMR revealed a corresponding increase in the presence of unbound Xphos.

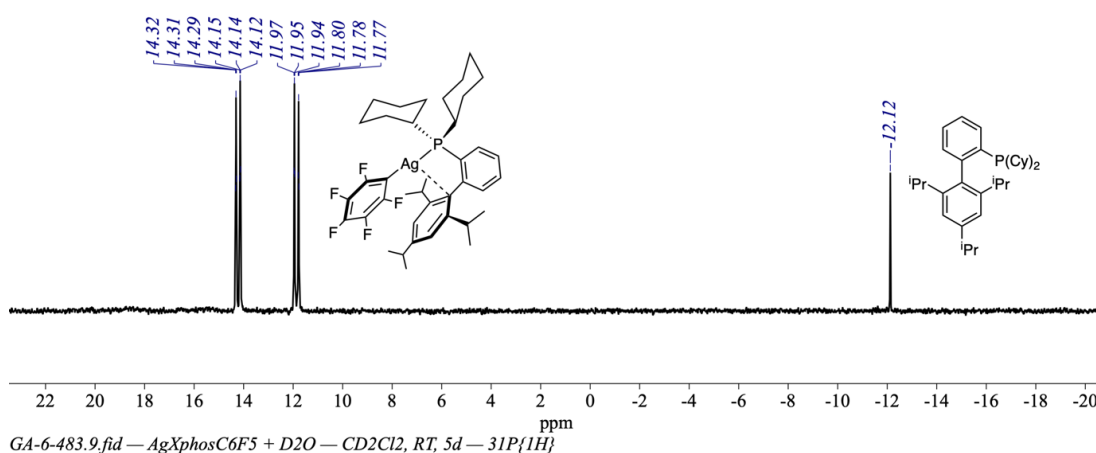


**Figure 140:**  $^{31}P\{^1H\}$  (202.5 MHz,  $CD_2Cl_2$ , 25 °C) spectrum of the reaction mixture of **GA-6-483**, recorded at  $t = 5$  d, RT. The spectrum shows the presence of unreacted **101** and the formation of unbound Xphos due to hydrolysis by  $D_2O$ .

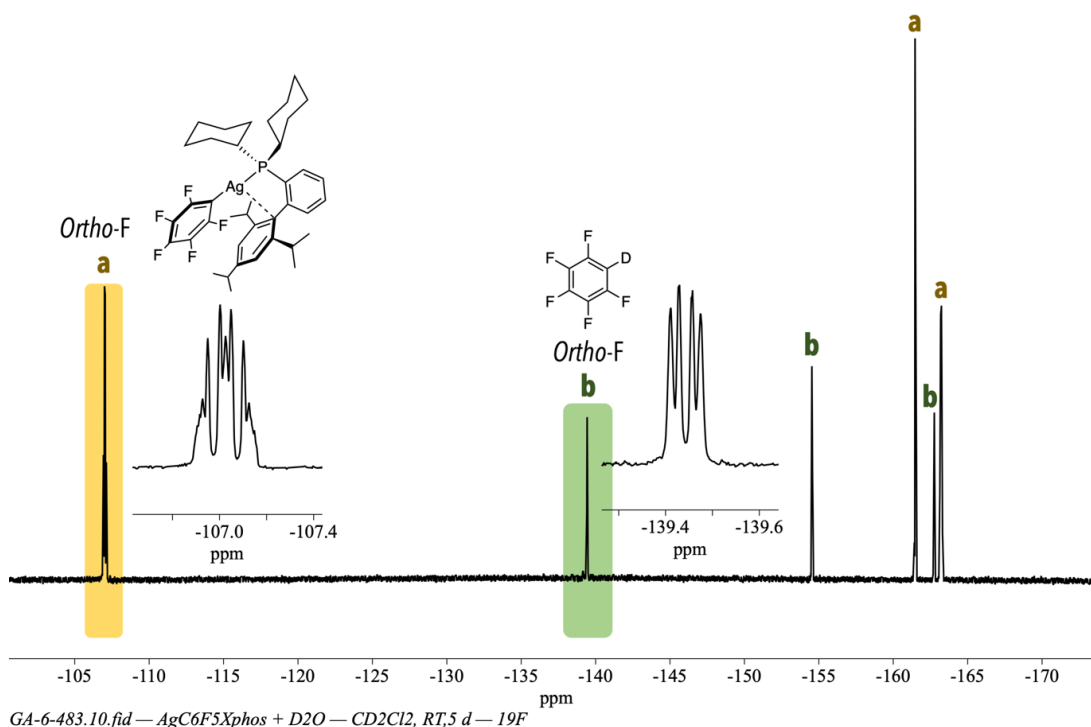


**Figure 141:**  $^{19}\text{F}\{^1\text{H}\}$  NMR (470 MHz,  $\text{CD}_2\text{Cl}_2$ , 25 °C) of the reaction mixture **GA-6-483** after 5 d at RT highlighting the *ortho*-F resonances of **101** and  $\text{C}_6\text{F}_5\text{D} **69**.$

**GA-6-484:** The reaction of  $\text{AgC}_6\text{F}_5$  **55** (1 equiv.) with  $\text{D}_2\text{O}$  (30 equiv.) in acetonitrile- $d_3$



In the glovebox,  $\text{AgC}_6\text{F}_5$  **55** (10 mg, 0.036 mmol, 1 equiv.) was dissolved in acetonitrile- $d_3$  (0.5 mL) and transferred to a J-Young NMR tube. The J-Young tube was then removed from the glovebox and affixed onto an NMR tube Schlenk line adaptor and connected to the Schlenk line. Under an atmosphere of nitrogen, the J-Young cap was removed and  $\text{D}_2\text{O}$  (22 mg, 1.10 mmol, 30 equiv., 20  $\mu\text{L}$ ) was added. The J-Young cap was re-capped, and the reaction mixture was monitored by  $^{19}\text{F}\{^1\text{H}\}$  NMR spectroscopy at  $t = 0$  h (recorded immediately after sample preparation) and 24 h.

The hydrolysis of the  $\text{AgC}_6\text{F}_5$  **55** complex was far more rapid compared to **101**, as shown by monitoring by  $^{19}\text{F}\{^1\text{H}\}$  NMR spectroscopy. At  $t = 0$  h, 6 % conversion to  $\text{C}_6\text{F}_5\text{D}$  **69** was calculated by integrating the *ortho*-F resonance of  $\text{AgC}_6\text{F}_5$  **55** wrt the *ortho*-F peak of  $\text{C}_6\text{F}_5\text{D}$  **69** at  $\delta -140$  in acetonitrile- $d_3$ . The reaction mixture was then allowed to react for 24 h at room temperature, after which gave 83 % conversion to  $\text{C}_6\text{F}_5\text{D}$  **69** was observed. A  $^{19}\text{F}\{^1\text{H}\}$  NMR spectrum collected after 5 d, showed complete decomposition of **55**.

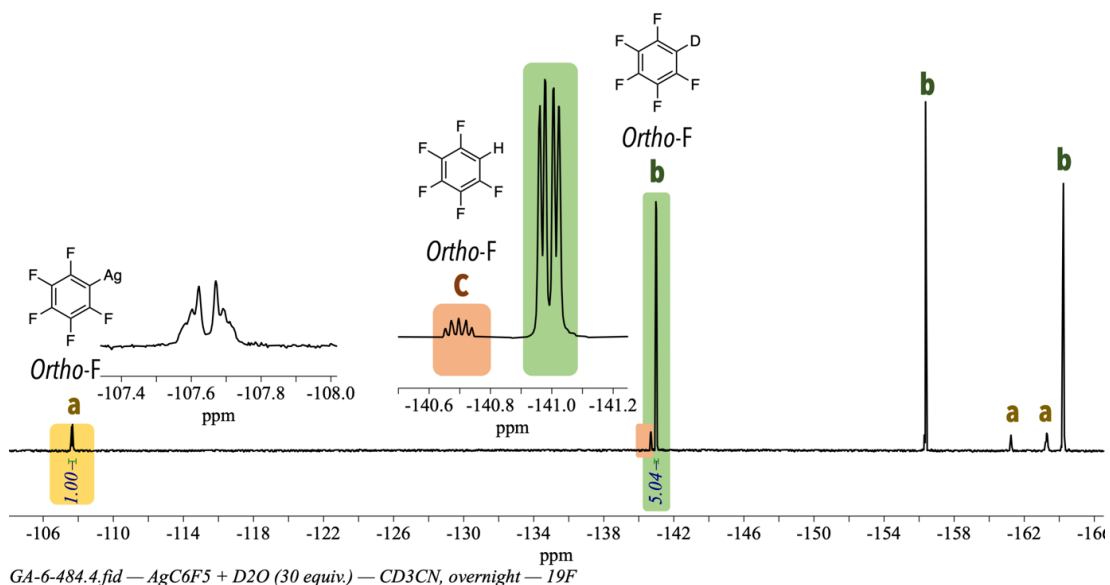
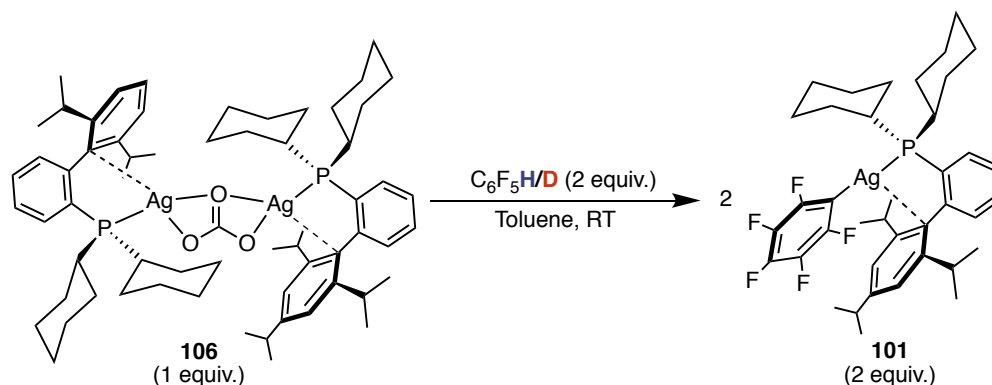


**Figure 142:**  $^{19}\text{F}\{^1\text{H}\}$  NMR (470 MHz,  $\text{CD}_3\text{CN}$ , 25 °C) of the reaction mixture **GA-6-484** after 24 h at RT highlighting the *ortho*-F resonances of **55** (yellow, peaks labelled **a**) and  $\text{C}_6\text{F}_5\text{D}$  **69** (green, peaks labelled **b**) trace amounts of  $\text{C}_6\text{F}_5\text{H}$  **17** (red, only *Ortho*-F peak labelled **c**)

#### Reaction between **106** and $\text{C}_6\text{F}_5\text{H}/\text{C}_6\text{F}_5\text{D}$ (2 equiv.) at room temperature in toluene



In the glovebox,  $\text{Ag}_2(\mu\text{-CO}_3)(\text{Xphos})_2$  **106** (10 mg, 0.0081 mmol, 1 equiv.) was dissolved in toluene (400  $\mu\text{L}$ ), to produce an amber solution. To this a solution of  $\text{C}_6\text{F}_5\text{H}$  **17**/ $\text{C}_6\text{F}_5\text{D}$  **69** and octafluoronaphthalene in toluene (100  $\mu\text{L}$ )<sup>[a]</sup> was added and transferred in a J-Young NMR tube using a gas-tight microlitre syringe. Immediately after preparation, the reaction mixture was analysed by  $^{31}\text{P}\{^1\text{H}\}$  and  $^{19}\text{F}\{^1\text{H}\}$  NMR spectroscopy. The %  $^{19}\text{F}\{^1\text{H}\}$  NMR yield was calculated by integrating the *ortho*-F resonance of the resulting complex **101** with respect to the internal standard, octafluoronaphthalene.

<sup>[a]</sup> A stock solution of  $\text{C}_6\text{F}_5\text{H}$  **17** (55 mg, 0.32 mmol, 0.16 M) and octafluoronaphthalene (10 mg, 0.037 mmol, 0.018 M) dissolved in toluene (2 mL) was prepared in a glovebox. The solution was stored in an ampule. A similar stock solution was prepared for the reaction with  $\text{C}_6\text{F}_5\text{D}$  **69**.



**GA-6-467:** The %  $^{19}\text{F}\{^1\text{H}\}$  NMR yield of the reaction of **106** with 2 equiv. of  $\text{C}_6\text{F}_5\text{H}$  is 85 %

**GA-6-468:** The %  $^{19}\text{F}\{^1\text{H}\}$  NMR yield of the reaction of **106** with 2 equiv. of  $\text{C}_6\text{F}_5\text{D}$  is 73 %

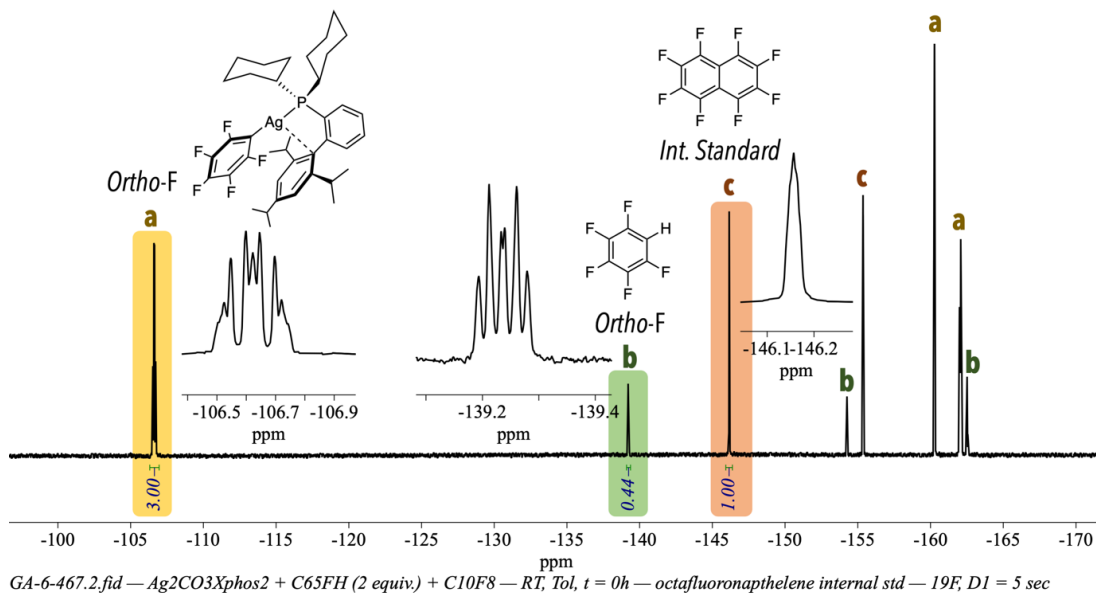


**Figure 143:**  $^{19}\text{F}\{^1\text{H}\}$  NMR (470 MHz,  $\text{C}_6\text{D}_6$ , 25 °C) of the reaction mixture **GA-6-467**, key resonances are highlighted, **101** (yellow, peaks labelled a),  $\text{C}_6\text{F}_5\text{H}$  **17** (green, peaks labelled b), octafluoronaphthalene (red, peaks labelled c)

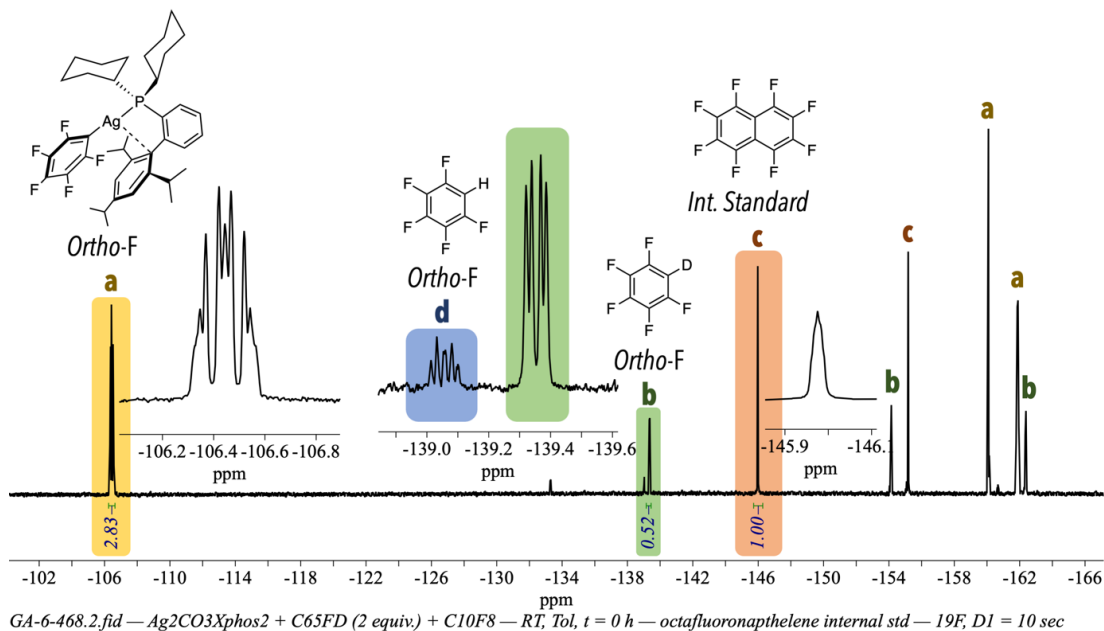
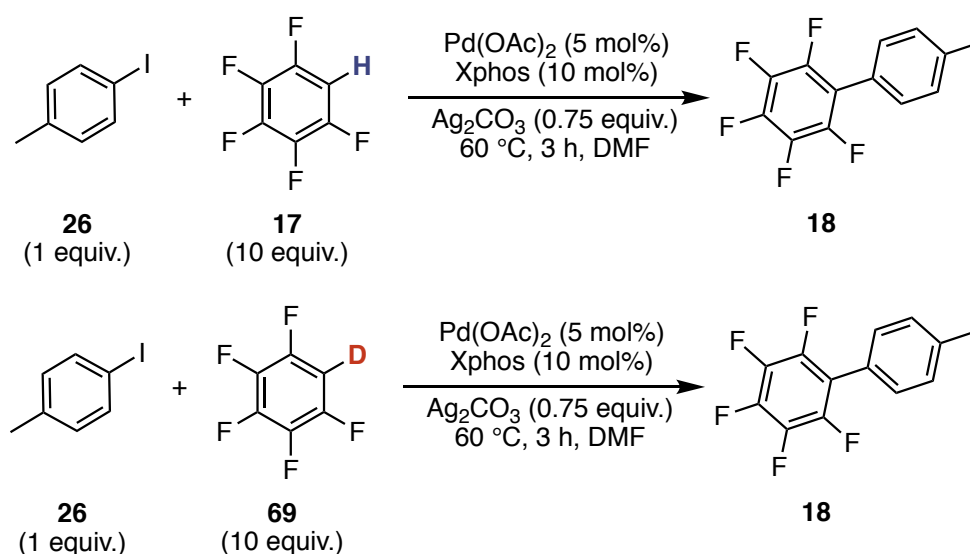


**Figure 144:**  $^{19}\text{F}\{^1\text{H}\}$  NMR (470 MHz,  $\text{C}_6\text{D}_6$ , 25 °C) of the reaction mixture **GA-6-468**. key resonances are highlighted, **101** (yellow, peaks labelled a),  $\text{C}_6\text{F}_5\text{D}$  **69** (green, peaks labelled b), octafluoronaphthalene (red, peaks labelled c) and trace  $\text{C}_6\text{F}_5\text{H}$  **17** (blue, labelled d)

## 6.5.3 Kinetic Isotope Effect of Palladium-Catalysed Direct Arylation Reaction



$$\text{KIE } (k_{\text{H}}/k_{\text{D}}) = 4.5 \pm 0.8$$

To a clean Schlenk tube, Pd(OAc)<sub>2</sub> (6 mg, 0.028 mmol, 5 mol%), Xphos (26 mg, 0.055 mmol, 10 mol%), Ag<sub>2</sub>CO<sub>3</sub> (114 mg, 0.41 mmol, 0.75 equiv.) were added and the Schlenk tube was evacuated and refilled three times with nitrogen. Then against a flow of nitrogen, 4-iodotoluene **26** (120 mg, 0.55 mmol, 1 equiv., 0.085 M) and octafluoronaphthalene (43 mg, 0.29 mmol, 0.29 equiv.) were added, followed by dry DMF (6.5 mL). The reaction mixture was submerged in a preheated oil bath (60 °C) and stirred at this temperature for 10 min. The temperature of the reaction mixture was monitored using a temperature probe inserted into the reaction vessel. After 10 min, fluoroarene (5.50 mmol, 10 equiv., 0.85 M) was added, and the progress of the reaction was monitored using reaction aliquots and the % NMR yield of the product was calculated using the <sup>19</sup>F{<sup>1</sup>H} NMR spectrum. The reaction aliquots were prepared by filtering ~ 0.1 mL of the reaction mixture through a Celite® pipette, using CDCl<sub>3</sub> as the eluent. Reaction aliquots were collected every 2.5 min for the first 40 minutes and then collected every 5 min for the next hour. The reaction was monitored for 90 min in total, and a final reaction aliquot was collected at ~24 h to check the final conversion of the reaction.

The sample was locked to CDCl<sub>3</sub> and the <sup>19</sup>F{<sup>1</sup>H} NMR spectrum of the reaction mixture was collected using a d1 = 5 secs, sw = 100 and O1P = -150. The progress of the reaction was monitored by calculating the % <sup>19</sup>F NMR yield using the *ortho*-F resonance of the product (δ -143.5) wrt octafluoronaphthalene (δ -145.2, internal standard). Initial rates were calculated using the first 8 data points of the kinetic curve and yielded a KIE of 4.5 ± 0.8.

**GA-6-491:** C<sub>6</sub>F<sub>5</sub>H **17** (925 mg, 5.50 mmol, 10 equiv., 610 μL) was added, the  $k_{\text{obs}} = 2.02 \pm 0.08 \times 10^{-5} \text{ M s}^{-1}$  and the final <sup>19</sup>F{<sup>1</sup>H} NMR yield was 63 %

**GA-6-492:** C<sub>6</sub>F<sub>5</sub>D **69** (930 mg, 5.50 mmol, 10 equiv. 610 μL) was added, the  $k_{\text{obs}} = 0.45 \pm 0.08 \times 10^{-5} \text{ M s}^{-1}$  and the final <sup>19</sup>F{<sup>1</sup>H} NMR yield was 17 %

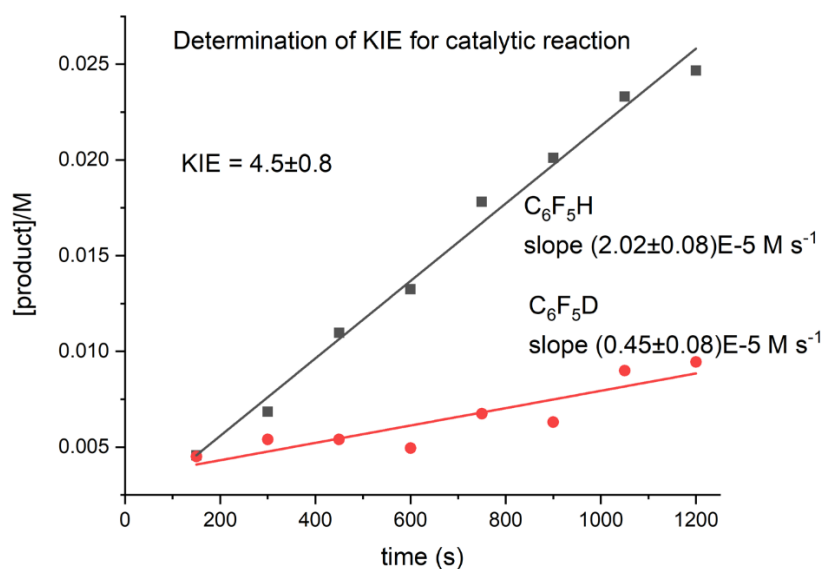
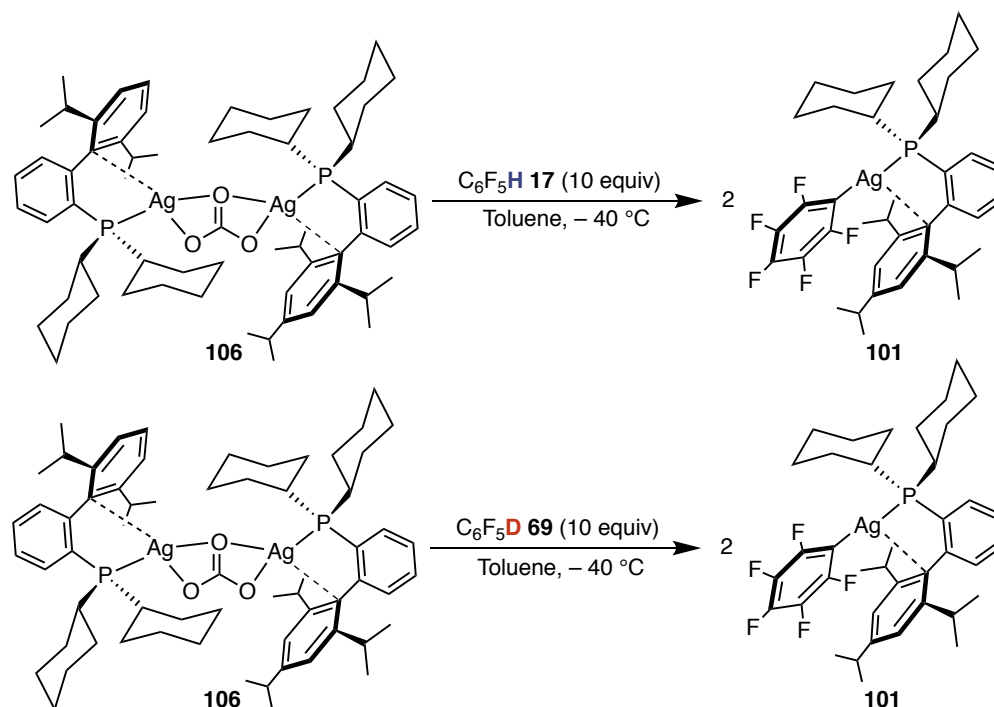


**Figure 145:** Initial rate of reaction for the direct arylation of 4-iodotoluene with 10 equiv. of C<sub>6</sub>F<sub>5</sub>H (black) and C<sub>6</sub>F<sub>5</sub>D (red)

#### 6.5.4 Kinetic Isotope Effect of the Reaction between **106** and C<sub>6</sub>F<sub>5</sub>H **17**/C<sub>6</sub>F<sub>5</sub>D

69



In the glovebox, **106** (10 mg, 0.0081 mmol, 1 equiv.) was dissolved in toluene (400  $\mu$ L) and transferred in a J-Young NMR tube using a gas-tight microlitre syringe. The J-Young

NMR tube was then removed from the glovebox and connected to the Schlenk line (**Figure 146**). The J-Young NMR tube was then cooled to  $-78\text{ }^{\circ}\text{C}$  using an ethyl acetate/liq. nitrogen cold bath and the temperature was monitored using a temperature probe.

Under an atmosphere of nitrogen, the cap of the J-Young tube was removed and a solution of  $\text{C}_6\text{F}_5\text{H}$  or  $\text{C}_6\text{F}_5\text{D}$  and octafluoronaphthalene in toluene ( $100\text{ }\mu\text{L}$ , from stock solution) was added cold ( $-78\text{ }^{\circ}\text{C}$ ) using a gas-tight microlitre syringe. The ampule of  $\text{C}_6\text{F}_5\text{H}/\text{C}_6\text{F}_5\text{D}$  and octafluoronaphthalene stock solution in toluene was pre-cooled using an ethyl acetate/liq. nitrogen cold bath to maintain temperature, prior to addition of the  $100\text{ }\mu\text{L}$  of stock solution. The J-Young cap was sealed, and sample was carried to the NMR centre placed in a dewar filled with ethyl acetate/liq. nitrogen ( $-78\text{ }^{\circ}\text{C}$ ). The spectra were collected on the Bruker AVIHD 500 instrument. The probe was pre-cooled to the required temperature and a timer was started as soon as the cold sample was placed in the probe.

**GA-6-457:** Reaction carried out at  $-40\text{ }^{\circ}\text{C}$  (233 K) with  $\text{C}_6\text{F}_5\text{H}$  **17** (2 equiv.) wrt **106**. A stock solution of  $\text{C}_6\text{F}_5\text{H}$  **17** (55 mg, 0.32 mmol, 0.16 M,  $36\text{ }\mu\text{L}$ ) and octafluoronaphthalene (10 mg, 0.037 mmol, 0.018 M) dissolved in toluene (2 mL) was prepared in a glovebox. The solution was stored in an ampule which was cooled to  $-78\text{ }^{\circ}\text{C}$  prior to the addition of  $100\text{ }\mu\text{L}$  of the solution to the solution of **106**. (*data used for calculation of KIE*)

- **GA-6-463:** Repeat of **GA-6-457**; to check reproducibility.

**GA-6-460:** Reaction carried out at  $-40\text{ }^{\circ}\text{C}$  (233K) with  $\text{C}_6\text{F}_5\text{D}$  **69** (2 equiv.) wrt **106**. A stock solution of  $\text{C}_6\text{F}_5\text{D}$  **69** (55 mg, 0.32 mmol, 0.16 M,  $36\text{ }\mu\text{L}$ ) and octafluoronaphthalene (10 mg, 0.037 mmol, 0.018 M) dissolved in toluene (2 mL) was prepared in a glovebox. The solution was stored in an ampule which was cooled to  $-78\text{ }^{\circ}\text{C}$  prior to the addition of  $100\text{ }\mu\text{L}$  of the solution to the solution of **106**. (*data used for calculation of KIE*)

**GA-6-461:** Reaction carried out at  $-40\text{ }^{\circ}\text{C}$  (233 K) with  $\text{C}_6\text{F}_5\text{H}$  **17** (10 equiv.) wrt **106**. A stock solution of  $\text{C}_6\text{F}_5\text{H}$  **17** (273 mg, 1.63 mmol, 0.81 M,  $181\text{ }\mu\text{L}$ ) and octafluoronaphthalene (10 mg, 0.037 mmol, 0.018 M) dissolved in toluene (2 mL) was prepared in a glovebox. The solution was stored in an ampule which was cooled to  $-78\text{ }^{\circ}\text{C}$  prior to the addition of  $100\text{ }\mu\text{L}$  of the solution to the solution of **106**.

**GA-6-462:** Reaction carried out at  $-40\text{ }^{\circ}\text{C}$  (233 K) with  $\text{C}_6\text{F}_5\text{H}$  **17** (2 equiv.) wrt **106** monitored by  $^{31}\text{P}\{^1\text{H}\}$ . Sample preparation identical to **GA-6-457**. The reaction was monitored by  $^{31}\text{P}\{^1\text{H}\}$  NMR spectroscopy instead of  $^{19}\text{F}\{^1\text{H}\}$  NMR spectroscopy. The D1 = 2 sec, with each data point being collected 5 mins, 27 sec and with 128 sc.

**GA-6-466:** Reaction carried out at  $-40\text{ }^{\circ}\text{C}$  (233 K) with  $\text{C}_6\text{F}_5\text{H}$  **17** (2 equiv.) wrt **106** and monitored using  $^{19}\text{F}\{^1\text{H}\}$  NMR spectroscopy but with a longer D1 of 5 sec. Sample preparation identical to **GA-6-457**.

**GA-6-470:** Reaction carried out at  $-30\text{ }^{\circ}\text{C}$  (243 K) with  $\text{C}_6\text{F}_5\text{H}$  **17** (2 equiv.) wrt **106**. Sample preparation identical to **GA-6-457**.

**GA-6-471:** Reaction carried out at  $-20\text{ }^{\circ}\text{C}$  (253 K) with  $\text{C}_6\text{F}_5\text{H}$  **17** (2 equiv.) wrt **106**. Sample preparation identical to **GA-6-457**.

**GA-6-474:** Reaction carried out at  $-0\text{ }^{\circ}\text{C}$  (273 K) with  $\text{C}_6\text{F}_5\text{H}$  **17** (2 equiv.) wrt **106**. Sample preparation identical to **GA-6-457**.

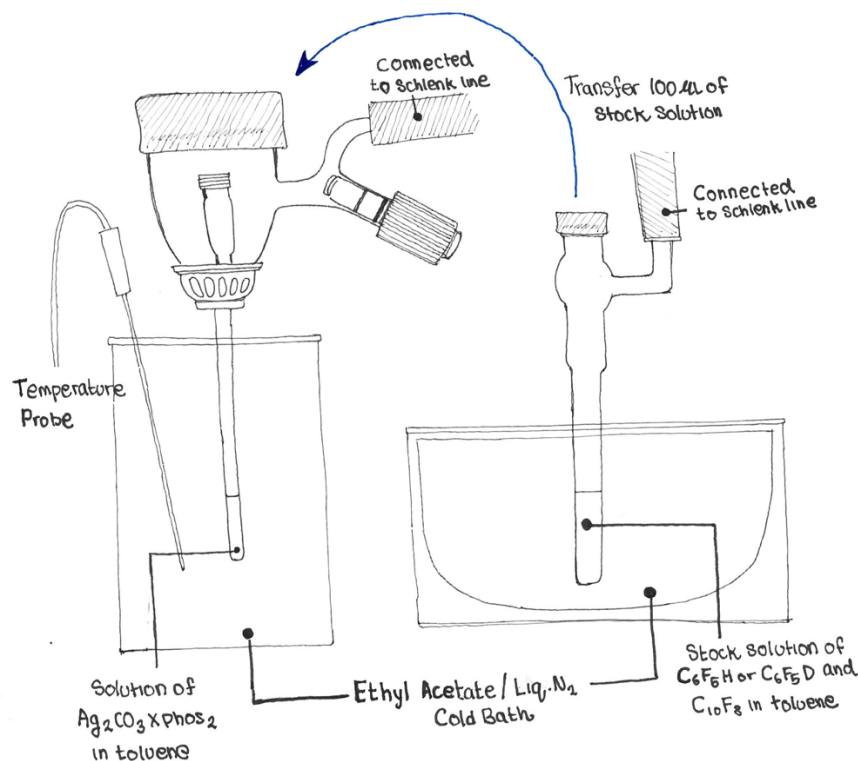


**Figure 146:** Experimental set-up for the kinetic monitoring of the reaction between  $\text{Ag}_2(\mu\text{-CO}_3)(\text{Xphos})_2$  **106** and two equiv. of  $\text{C}_6\text{F}_5\text{H}$  **17**/ $\text{C}_6\text{F}_5\text{D}$  **69**

Prior to carrying out the low-temperature experiment, a  $^{19}\text{F}\{^1\text{H}\}$   $T_1$  inversion recovery experiment was carried out for the reactants and products in toluene at  $-40\text{ }^{\circ}\text{C}$  to accurately determine the  $T_1$  value at the desired temperature (**Figure 147**). The  $^{19}\text{F}\{^1\text{H}\}$  pulse program used in zg30, with d1 of 2 s, sw = 90 and O1P = 135 with 32 scans. Unless specified otherwise, data points for the kinetic runs were collected every 3.06 minutes. The *ortho*-F resonance of the product ( $\delta -106.7$ ) was integrated with respect to the internal standard peak ( $\delta -146.7$ ) and was used to calculate the rate of reaction.

**Figure 147:**  $T_1$  values of the reactants and products in toluene at 233 K

Reagent	$T_1$ (s)
<b>101</b>	0.54
$\text{C}_6\text{F}_5\text{H}$	1.82
Octafluoronaphthalene	0.50

The kinetic profile of the reaction between  $\text{Ag}_2(\mu\text{-CO}_3)(\text{Xphos})_2$  and two equiv. of  $\text{C}_6\text{F}_5\text{H}$  in toluene at  $-40\text{ }^\circ\text{C}$  revealed two process, a fast initial process and a slow process. The KIE has been determined for both processes giving values of  $3.7 \pm 0.3$  and  $0.91 \pm 0.01$ , respectively, for the fast and slow processes (**Figure 148**, **Figure 149**).

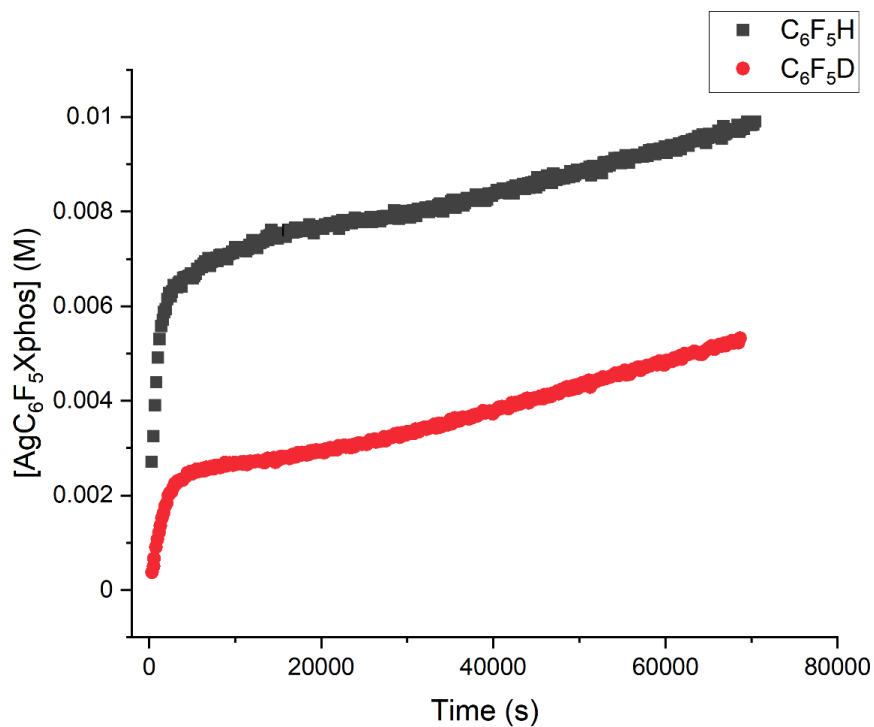


**Figure 148:** Change in concentration of **101** over time for the reaction of  $\text{Ag}_2(\mu\text{-CO}_3)(\text{Xphos})_2$  **106** and two equiv. of  $\text{C}_6\text{F}_5\text{H}$  **17** or  $\text{C}_6\text{F}_5\text{D}$  **69** in toluene at  $-40\text{ }^\circ\text{C}$

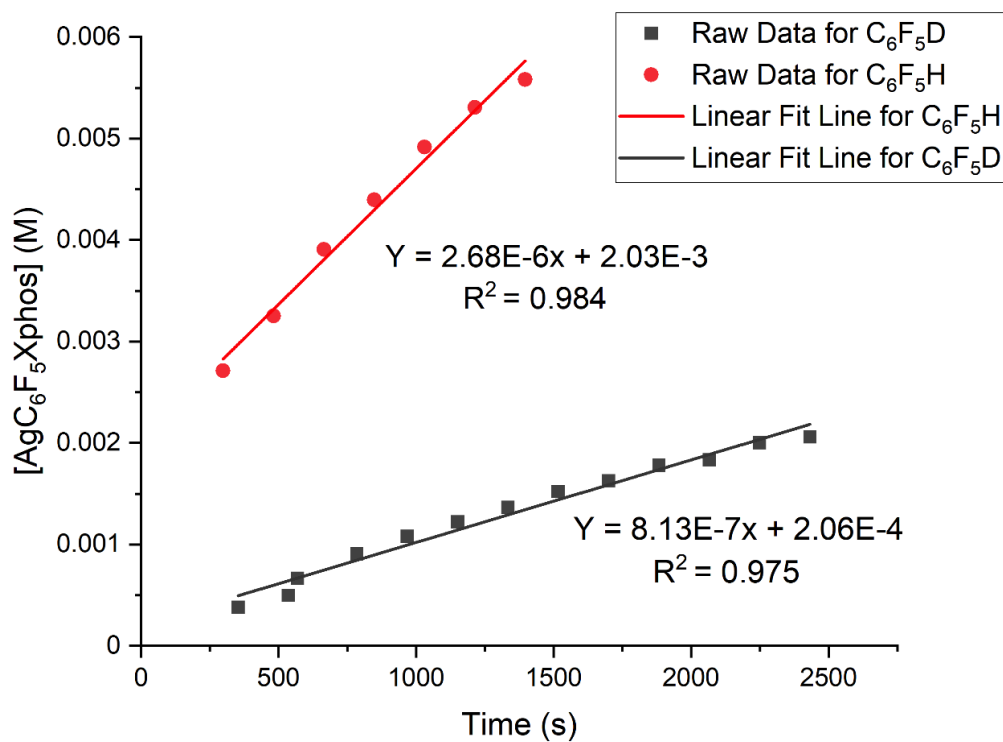


**Figure 149:** Initial rate for the reaction of  $\text{Ag}_2(\mu\text{-CO}_3)(\text{Xphos})_2$  and two equiv. of  $\text{C}_6\text{F}_5\text{H}$  or  $\text{C}_6\text{F}_5\text{D}$  in toluene at  $-40\text{ }^\circ\text{C}$  (Fast process)

**Table 42:** Slope and intercept for the fast process for the reaction between **106** and  $\text{C}_6\text{F}_5\text{H}$  **17/C<sub>6</sub>F<sub>5</sub>D 69**

	Slope M $\text{s}^{-1}$	Standard Error	Intercept	Standard Error	$\text{R}^2$
H	2.68E-06	1.38E-07	2.03E-03	1.27E-04	0.98435
D	8.13E-07	3.71E-08	2.06E-04	5.57E-05	0.97558
KIE				3.7 ± 0.3	

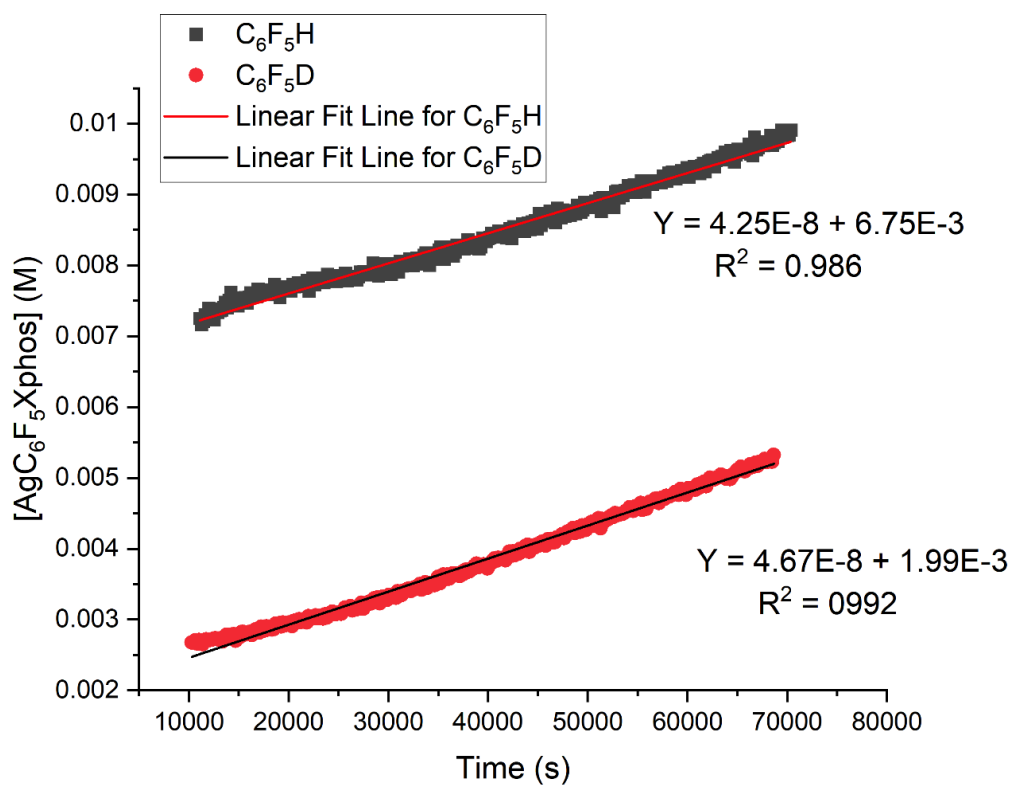


**Figure 150:** Rate for the reaction of  $\text{Ag}_2(\mu\text{-CO}_3)(\text{Xphos})_2$  **106** and two equiv. of  $\text{C}_6\text{F}_5\text{H}$  **17** or  $\text{C}_6\text{F}_5\text{D}$  **69** in toluene at  $-40\text{ }^\circ\text{C}$  (slow process)

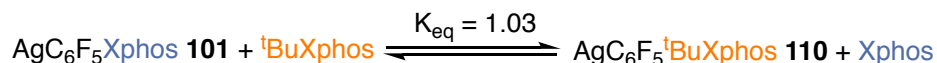
**Table 43:** Slope and intercept for the slow process for the reaction between **106** and  $\text{C}_6\text{F}_5\text{H}$  **17**/ $\text{C}_6\text{F}_5\text{D}$  **69**

	Slope M $\text{s}^{-1}$	Standard Error	Intercept	Standard Error	$\text{R}^2$
H	4.25E-08	2.82E-10	0.00675	1.24E-05	0.98599
D	4.67E-08	2.39E-10	1.99E-03	1.03E-05	0.99168
KIE				0.91 $\pm$ 0.01	



6.5.5 <sup>t</sup>BuXphos Exchange Experiments with Ag<sup>I</sup> Complexes

**GA-5-385:** The Phosphine-Exchange Reaction of AgC<sub>6</sub>F<sub>5</sub>Xphos **101** with <sup>t</sup>BuXphos

**Experimental Procedure**

In an argon glovebox, AgC<sub>6</sub>F<sub>5</sub>Xphos **101** (10 mg, 0.013 mmol, 1 equiv.) and <sup>t</sup>BuXphos (5.6 mg, 0.013 mmol, 1 equiv.) were weighed out in two separate vials. The Ag complex was dissolved in dichloromethane-*d*<sub>2</sub> and the solution was transferred to the vial containing the <sup>t</sup>BuXphos. Once all the ligand has dissolved, the solution was transferred into a J-young NMR tube and analysed by <sup>1</sup>H and <sup>31</sup>P{<sup>1</sup>H} NMR spectroscopy at 25 °C.

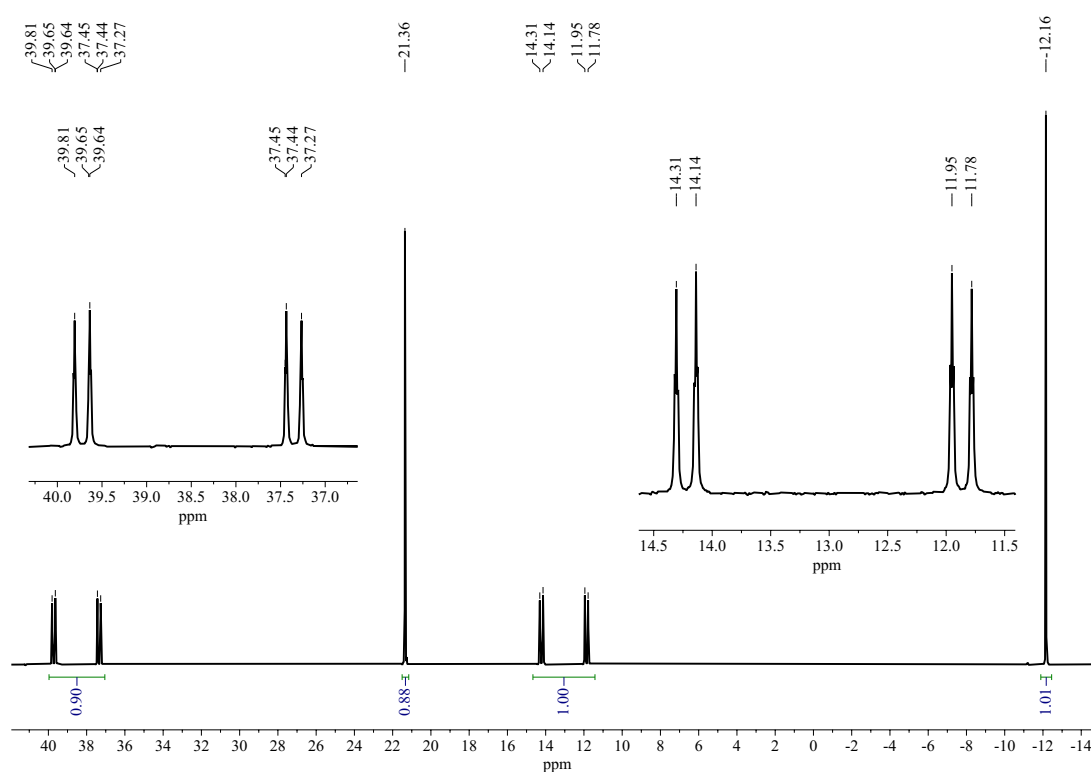


**Figure 151:** <sup>31</sup>P{<sup>1</sup>H} (202.5 MHz, CD<sub>2</sub>Cl<sub>2</sub>, 25 °C) spectrum of the reaction mixture of AgC<sub>6</sub>F<sub>5</sub>Xphos **101** (1 equiv.) and <sup>t</sup>BuXphos (1 equiv.)

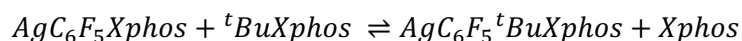
The <sup>31</sup>P{<sup>1</sup>H} NMR spectrum collected in dichloromethane-*d*<sub>2</sub> immediately after preparing the reaction mixture revealed that the system had already reached equilibrium. A <sup>31</sup>P{<sup>1</sup>H} T1 – inversion recovery experiment was carried out to determine the T1 of the different phosphorus species. The data was processed in Mnova and was used to determine the appropriate D1 for the phosphorus spectrum. The D1 for this experiment was set to 70 sec with 128 scans.

The chemical shifts and coupling constants of the species in the reaction mixture: Xphos (-12.2, s), AgC<sub>6</sub>F<sub>5</sub>Xphos **101** (13.0, pair of t,  $^1J_{107Ag-31P} = 443.4$  Hz,  $^1J_{109Ag-31P} = 512.3$  Hz,  $^3J_{19F-31P} = 3.0$  Hz), <sup>t</sup>BuXphos (21.4, s), AgC<sub>6</sub>F<sub>5</sub><sup>t</sup>BuXphos **110** (38.5, pair of t,  $^1J_{107Ag-31P} = 447.5$  Hz,  $^1J_{109Ag-31P} = 516.3$  Hz,  $^3J_{19F-31P} = 2.7$  Hz). The  $^{31}P\{^1H\}$  NMR spectrum of sample was collected at t = 0, RT, t = 23 h, RT, t ~ 48 h, RT. The integrals of the different species remained unchanged between the three spectra.

**Table 44:** Summary of T1, chemical shift and coupling constant of the different phosphorus species in GA-5-385

Reagent	G – value	T1 (sec)	Chemical Shift (ppm)	$^{107}Ag - ^{31}P$ J value (Hz)	$^{109}Ag - ^{31}P$ J value (Hz)
Xphos	0.131397	7.61	-12.16	-	-
AgC <sub>6</sub> F <sub>5</sub> Xphos <b>101</b>	0.234921	4.26	13.00	443.4	512.3
<sup>t</sup> BuXphos	0.0748435	13.36	21.36	-	-
AgC <sub>6</sub> F <sub>5</sub> <sup>t</sup> BuXphos <b>110</b>	0.115195	8.68	38.53	447.5	516.3

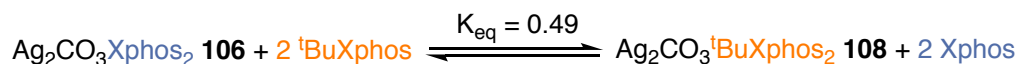
#### Calculating the Equilibrium constant ( $K_{eq}$ )



Integration of $^{31}P\{^1H\}$ resonance at equilibrium	1.00	0.88	0.90	1.01
---	------	------	------	------

$$K_{eq} = \frac{[AgC_6F_5{}^tBuXphos][Xphos]}{[AgC_6F_5Xphos][{}^tBuXphos]} = \frac{0.90 \times 1.01}{1.00 \times 0.88} = 1.03$$

**GA-5-390:** The Phosphine-Exchange Reaction between Ag<sub>2</sub>CO<sub>3</sub>Xphos<sub>2</sub> **106** and <sup>t</sup>BuXphos.



#### Experimental Procedure

In an argon glovebox, Ag<sub>2</sub>CO<sub>3</sub>Xphos<sub>2</sub> **106** (10 mg, 0.0081 mmol, 1 equiv.) and <sup>t</sup>BuXphos (7 mg, 0.016 mmol, 2 equiv.) were weighed out in two separate vials. The Ag complex **106** was dissolved in benzene-*d*<sub>2</sub> and the solution was transferred to the vial containing the

<sup>t</sup>BuXphos. Once all the ligand has dissolved, the solution was transferred into a J-young NMR tube and analysed by <sup>1</sup>H and <sup>31</sup>P{<sup>1</sup>H} NMR spectroscopy at 25 °C.

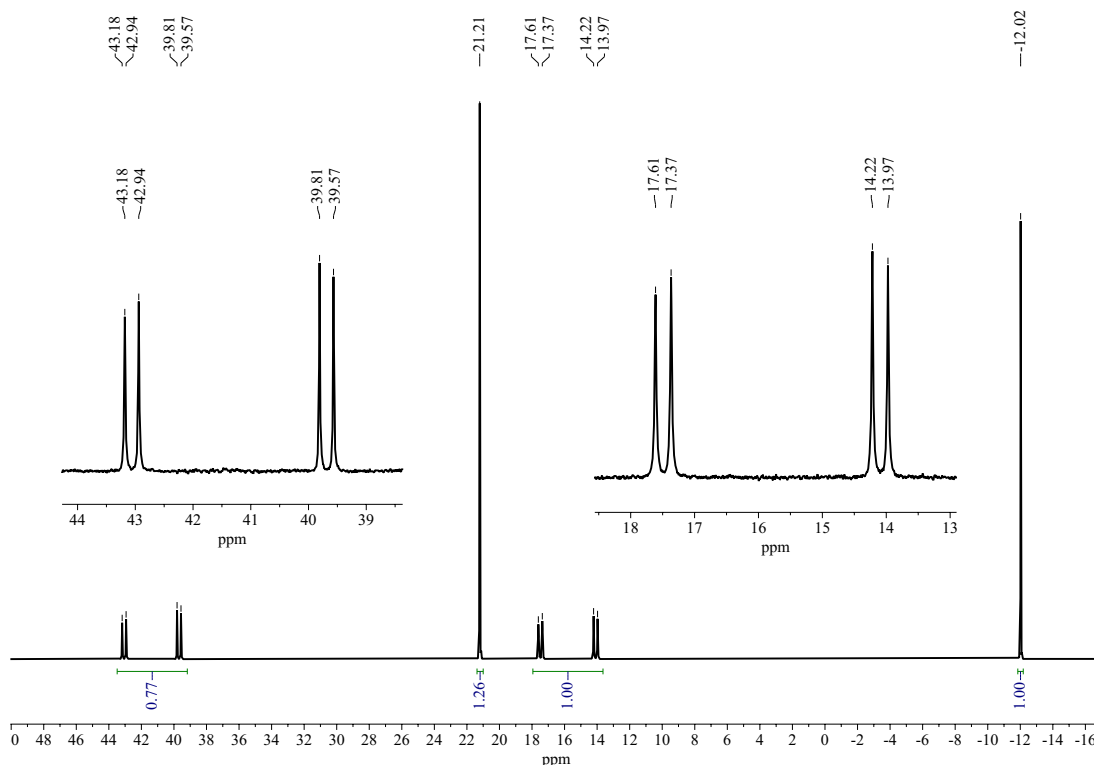


**Figure 152:** <sup>31</sup>P{<sup>1</sup>H} (202.5 MHz, C<sub>6</sub>D<sub>6</sub>, 25 °C) spectrum of the reaction mixture of Ag<sub>2</sub>CO<sub>3</sub>Xphos<sub>2</sub> **106** (1 equiv.) and <sup>t</sup>BuXphos (2 equiv.)

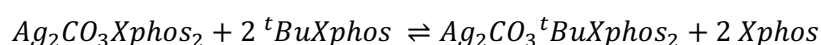
The <sup>31</sup>P{<sup>1</sup>H} NMR spectrum collected in benzene-*d*<sub>6</sub> immediately after preparing the reaction mixture revealed that the system had already reached equilibrium. A <sup>31</sup>P{<sup>1</sup>H} T1 – inversion recovery experiment was carried out to determine the T1 of the different phosphorus species. The data was processed in Mnova and was used to determine the appropriate D1 for the phosphorus spectrum. The D1 for this experiment was set to 50 sec with 128 scans.

The chemical shifts and coupling constants of the species in the reaction mixture: Xphos (–12.02, s), Ag<sub>2</sub>CO<sub>3</sub>Xphos<sub>2</sub> **106** (15.8, pair of d, <sup>1</sup>J<sub>107Ag–31P</sub> = 637.9 Hz, <sup>1</sup>J<sub>109Ag–31P</sub> = 737.1 Hz), <sup>t</sup>BuXphos (21.21, s), Ag<sub>2</sub>CO<sub>3</sub><sup>t</sup>BuXphos<sub>2</sub> **108** (41.4, pair of d, <sup>1</sup>J<sub>107Ag–31P</sub> = 633.8 Hz, <sup>1</sup>J<sub>109Ag–31P</sub> = 731.0 Hz). The <sup>31</sup>P{<sup>1</sup>H} NMR spectrum of sample was collected at t = 0, RT and t = 1 d, RT. The integrals of the different species remained unchanged.

**Table 45:** Summary of T1, chemical shift and coupling constant of the different phosphorus species in GA-5-385

Reagent	G – value	T1 (sec)	Chemical Shift (ppm)	<sup>107</sup> Ag – <sup>31</sup> P J value (Hz)	<sup>109</sup> Ag – <sup>31</sup> P J value (Hz)
Xphos	0.21762	4.60	-12.02	-	-
Ag <sub>2</sub> CO <sub>3</sub> Xphos <sub>2</sub> <b>106</b>	0.70504	1.42	15.80	637.9	737.1
<i>t</i> BuXphos	0.138344	7.23	21.21	-	-
Ag <sub>2</sub> CO <sub>3</sub> <i>t</i> BuXphos <sub>2</sub> <b>108</b>	0.389924	2.56	41.37	633.8	731.0

Calculating the Equilibrium constant (K<sub>eq</sub>)

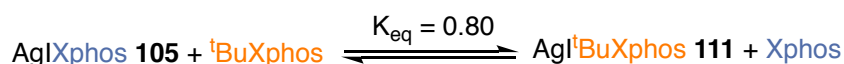


Integration of <sup>31</sup>P{<sup>1</sup>H} resonance at equilibrium

1.00	1.26	0.77	1.00
------	------	------	------

$$K_{eq} = \frac{[Ag_2CO_3\textit{t}BuXphos_2][Xphos]^2}{[Ag_2CO_3Xphos_2][\textit{t}BuXphos]^2} = \frac{0.77 \times 1.00^2}{1.00 \times 1.26^2} = 0.49$$

**GA-5-384:** The Phosphine-Exchange Reaction between AgIXphos **105** with <sup>1</sup>BuXphos.



(**105** and **111** assumed to be monomer in solution for calcn of K<sub>eq</sub>)

### Experimental Procedure

In an argon glovebox, AgIXphos **105** (10 mg, 0.014 mmol, 1 equiv.) and <sup>1</sup>BuXphos (6 mg, 0.014 mmol, 1 equiv.) were weighed out in two separate vials. The Ag complex **105** was dissolved in dichloromethane-*d*<sub>2</sub> and the solution was transferred to the vial containing the <sup>1</sup>BuXphos. Once all the ligand has dissolved, the solution was transferred into a J-young NMR tube and analysed by <sup>1</sup>H and <sup>31</sup>P{<sup>1</sup>H} NMR spectroscopy at 25 °C.

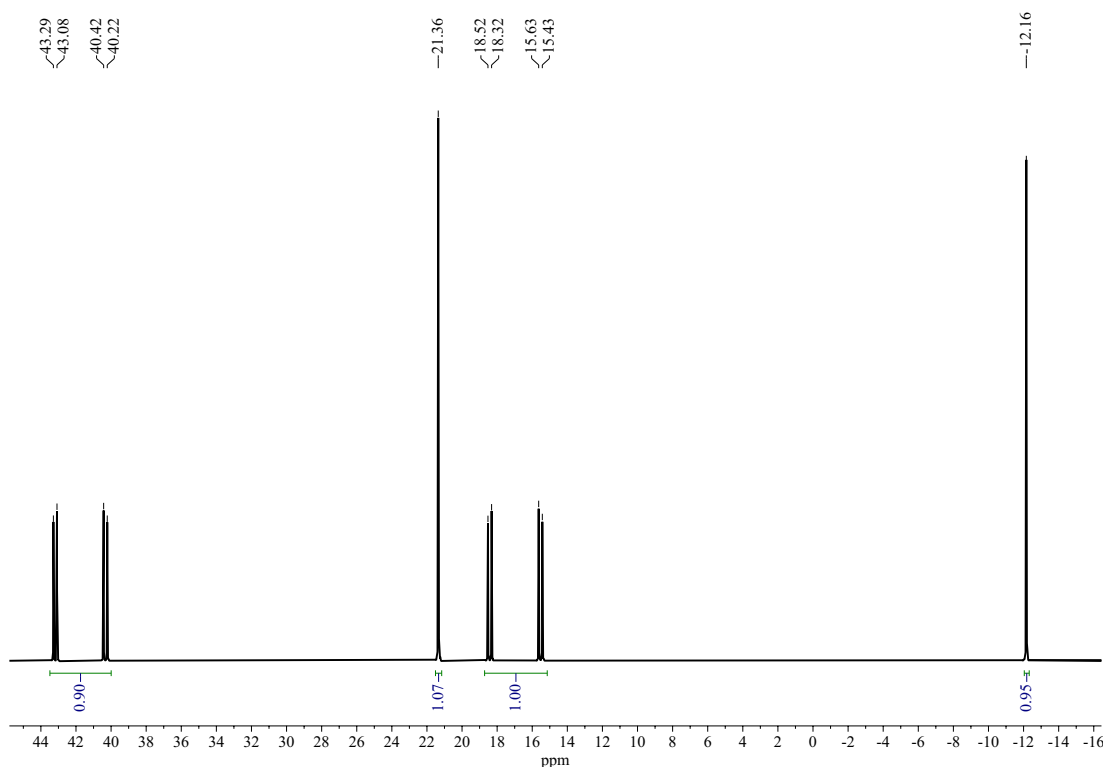


**Figure 153:**  $^{31}\text{P}\{^1\text{H}\}$  (202.5 MHz,  $\text{CD}_2\text{Cl}_2$ , 25 °C) spectrum of the reaction mixture of AgIXphos **105** (1 equiv.) and  $^t\text{BuXphos}$  (1 equiv.)

The  $^{31}\text{P}\{^1\text{H}\}$  NMR spectrum collected in dichloromethane- $d_2$  immediately after preparing the reaction mixture revealed that the system had already reached equilibrium. The chemical shifts and coupling constants of the species in the reaction mixture: Xphos (−12.2, s), AgIXphos **105** (16.9, pair of d,  $^1J_{107\text{Ag}-31\text{P}} = 542.7$  Hz,  $^1J_{109\text{Ag}-31\text{P}} = 627.7$  Hz),  $^t\text{BuXphos}$  (21.35, s), Ag $^t\text{BuXphos}$  **111** (41.8, pair of d,  $^1J_{107\text{Ag}-31\text{P}} = 538.6$  Hz,  $^1J_{109\text{Ag}-31\text{P}} = 621.7$  Hz). The  $^{31}\text{P}\{^1\text{H}\}$  NMR spectrum of sample was collected at  $t = 0$ , RT,  $t = 24$  h, RT, and  $t = 5$  d, RT. The integrals of the different species remained unchanged.

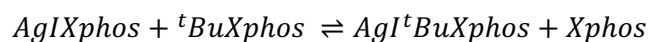
A  $^{31}\text{P}\{^1\text{H}\}$  T1 – inversion recovery experiment was carried out to determine the T1 of the different phosphorus species. The data was processed in Mnova and was used to determine the appropriate D1 for the phosphorus spectrum. The D1 for this experiment was set to 70 sec with 128 scans.

**Table 46:** Summary of T1, chemical shift and coupling constant of the different phosphorus species in GA-5-384

Reagent	G – value	T1 (sec)	Chemical Shift (ppm)	<sup>107</sup> Ag – <sup>31</sup> P J value (Hz)	<sup>109</sup> Ag – <sup>31</sup> P J value (Hz)
Xphos	0.133515	7.49	-12.16	-	-
AgIXphos <b>105</b>	0.195466	5.12	16.97	544.7	625.6
<sup>t</sup> BuXphos	0.119161	8.39	21.36	-	-
AgItBuXphos <b>111</b>	0.173772	5.75	41.75	538.6	621.6

Calculating the Equilibrium constant ( $K_{eq}$ )

- Calculation done assuming the AgIXphos **105** exists as a monomer in solution:



Integration of <sup>31</sup>P{<sup>1</sup>H} resonance at equilibrium

1.00	1.07	0.90	0.95
------	------	------	------

$$K_{eq} = \frac{[AgI{}^tBuXphos][Xphos]}{[AgIXphos][{}^tBuXphos]} = \frac{0.90 \times 0.95}{1.00 \times 1.07} = 0.80$$

## 6.5.6 Concentration Dependent EXSY Experiments

## General procedure

In a glovebox, the desired amount of Ag complex and Xphos were weighed out in two separate vials. The Xphos was then dissolved in the desired solvent and the solution was then used to transfer to a J-Young tube and a  $T_1$  inversion recovery experiment was used to measure the  $T_1$  of the Ag complex and the Xphos in the reaction mixture (Table 47). The  $T_1$  values were used to set the D1 ( $T_1 \times 5$ ) for the EXSY experiments. Initially, 2D EXSY experiments were used to analyse the sample, and exchange peaks were detected (Figure 154). However, each 2D EXSY experiment required very long experiment times ( $\sim 18 - 22$  h per mixing time), hence 1D EXSY was used for further analysis. **101**, **106**, and **105** were investigated with different number of equiv. of Xphos.

Table 47:  $T_1$  values of the mixture of Ag complex and Xphos

	Benzene- $d_6$		dichloromethane- $d_2$		dichloromethane- $d_2$	
Compound	<b>106</b>	Xphos	<b>105</b>	Xphos	<b>101</b>	Xphos
$T_1$ (s)	1.79	5.35	4.97	6.11	4.46	7.75

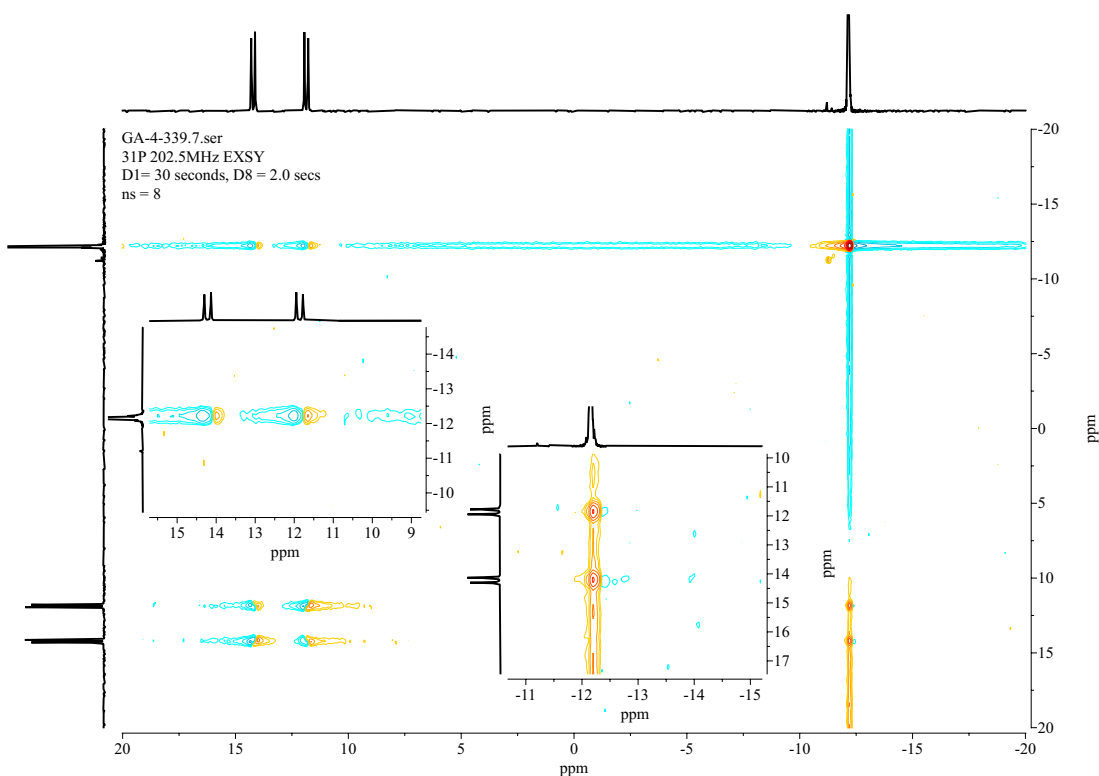
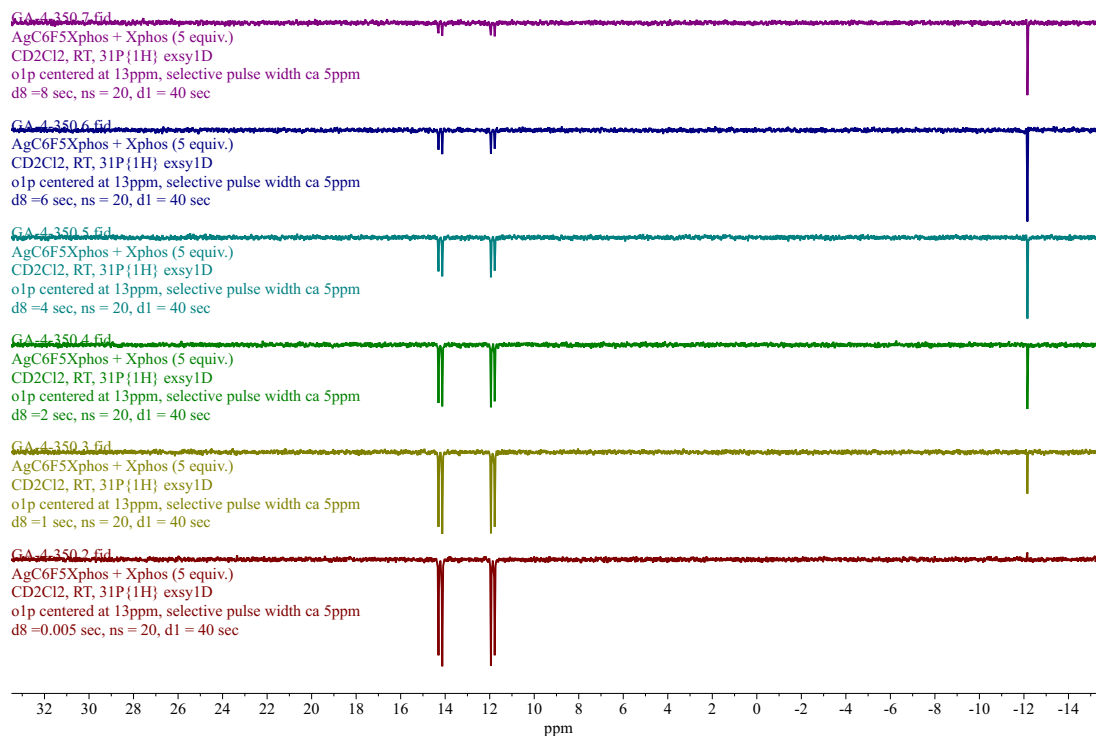


Figure 154: 2D EXSY spectrum of the mixture of **101** with Xphos (5 equiv.), with a mixing time of 2.0 sec.



**Figure 155:** Stack plot from a 1D EXSY experiment with **101** and Xphos (5 equiv.), with various mixing times, in CD<sub>2</sub>Cl<sub>2</sub>.

**Table 48:** Mass of **101** and varying equiv. of Xphos used for the EXSY experiments

Exp. Code	<b>101</b>				Xphos			
	Mass (mg)	Moles (mmol)	Equiv.	Conc. (M)	Mass (mg)	Moles (mmol)	Equiv.	Conc. (M)
GA-4-345	10.2	0.0136	1	0.025	6.3	0.0132	1	0.024
GA-4-350	9.5	0.0126	1	0.023	31.2	0.065	5	0.12
GA-4-346	10.1	0.0134	1	0.024	62.3	0.131	10	0.24
Volume of solvent (mL):					0.55			



**Table 49:** Relative integration of the Xphos peak wrt **101** at each mixing time

Solvent: Mixing time (s)	dichloromethane- $d_2$		
	Xphos equiv.		
	1 equiv.	5 equiv.	10 equiv.
0.005	0	0	0
1	0	0.06	0.12
2	0.02	0.11	0.29
4	0.05	0.24	0.56
6	0.08	0.43	1.17
8	0.1	0.64	1.27

**Treatment of Data** (calculations of EXSY data carried out by Prof. Robin Perutz)

The integration ratios were converted into integration fractions:

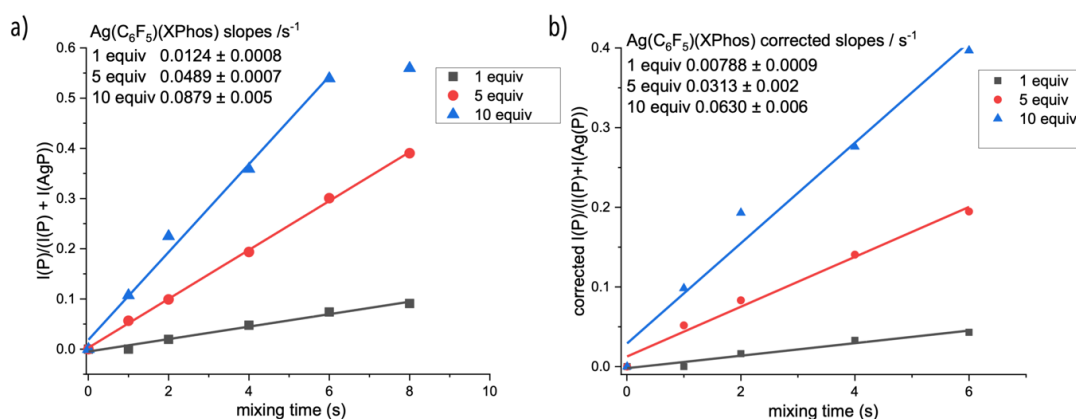
$$I(\text{XPhos})/[I(\text{XPhos}) + I(\text{Ag(XPhos)})(\text{C}_6\text{F}_5)]$$

Which were plotted against mixing time. A linear fit to the data was applied, up to a mixing time of 6 s. A correction factor was applied for the different relaxation times of the two components as  $\exp\{t(T_{1A}^{-1} - T_{1B}^{-1})\}$ . Correction factors vary from 1 to 1.78 for mixing times from 0 to 6 s. The mixing time of 8 s was ignored because the correction factor was too large (2.16). **Figure 156** shows plots of integration fractions vs mixing time without and with correction factors. The dependence of  $k_{\text{obs}}$  on  $[\text{XPhos}]$  clearly points to an associative reaction. Consequently, values of  $k_{\text{obs}}$  were converted to a second order exchange velocity ( $V_{\text{ex}}$ ) using the McKay equation. The conversion to exchange velocity  $V_{\text{ex}}$  follows Wilkins (page 39)<sup>133</sup> and the McKay equation:

$$V_{\text{ex}} = k_{\text{obs}} \times ab/(a+b)$$

Where a and b are the concentrations of **101** and XPhos, respectively

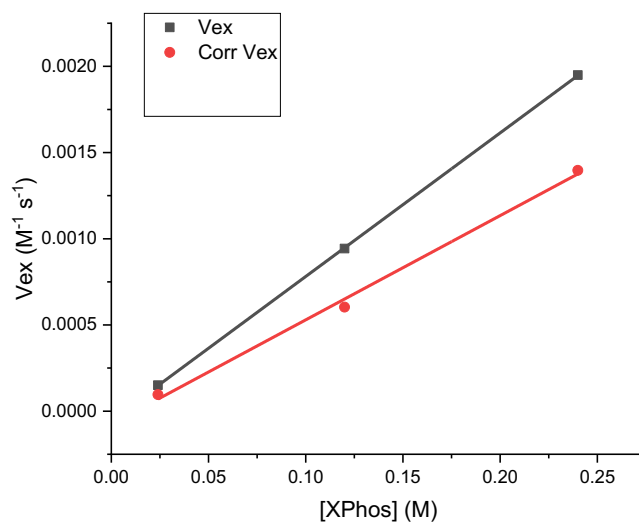
The resulting values of  $k_{\text{obs}}$  and  $V_{\text{ex}}$  are shown in **Table 50**. The corrections result in a reduction in  $k_{\text{obs}}$  and  $V_{\text{ex}}$  of about 30%.



**Figure 156:** Plot of fractional transfer of magnetisation from **101** to free XPhos in CD<sub>2</sub>Cl<sub>2</sub> against mixing time. a) Plot without correction for the difference in relaxation times. b) plot with correction applied. The slopes correspond to  $k_{\text{obs}}$  for the exchange process.

**Table 50:** Values of  $k_{\text{obs}}$  and  $V_{\text{ex}}$  for **101**

Equiv. of Xphos	Concentration (M)		Slope/ $k_{\text{obs}}$ ( $\text{s}^{-1}$ )		$V_{\text{ex}}$ ( $\times 10^{-4} \text{M}^{-1} \text{s}^{-1}$ )		
	[ <b>101</b> ]	[XPhos]	Uncorrected	Corrected	Uncorrected	Corrected	
1	1	0.025	0.024	0.0124 $\pm$ 0.0008	0.0079 $\pm$ 0.0009	1.51 $\pm$ 0.09	0.96 $\pm$ 0.11
2	5	0.023	0.12	0.0489 $\pm$ 0.0007	0.0313 $\pm$ 0.002	9.43 $\pm$ 0.14	6.0 $\pm$ 0.4
3	10	0.024	0.24	0.0879 $\pm$ 0.005	0.0630 $\pm$ 0.006	19.5 $\pm$ 1.1	14 $\pm$ 1.0

**Figure 157:** Plot of exchange velocity  $V_{\text{ex}}$  vs [XPhos]. Black, uncorrected data, red corrected data.

EXSY data were also collected for  $\text{Ag}_2(\mu\text{-CO}_3)(\text{Xphos})_2$  **106** and  $\text{Ag}_2(\mu\text{-I})_2(\text{Xphos})_2$  **105** but were not analysed further because of ambiguities in concentrations cause by dissociation of dimer species.

**Table 51:** The mass of **106** and varying equiv. of Xphos used for the EXSY experiments

Exp. Code	<b>106</b>				Xphos			
	Mass (mg)	Moles (mmol)	Equiv.	Conc. (M)	Mass (mg)	Moles (mmol)	Equiv.	Conc. (M)
GA-4- 348	10.4	0.00846	1	0.015	7.9	0.0166	2	0.030
GA-5- 353	9.4	0.00764	1	0.014	22.9	0.0480	6	0.087
GA-4- 352	10.9	0.00887	1	0.016	37.6	0.0789	10	0.14
Volume of Solvent (mL):				0.55				

**Table 52:** Relative integration of the Xphos peak wrt **106** at each mixing time

Solvent:	Benzene- <i>d</i> <sub>6</sub>		
Mixing time (sec)	Xphos equiv.		
	2 equiv.	6 equiv.	10 equiv.
0.003	0	n/a	n/a
0.005	0	0	0
0.3	0.06	n/a	n/a
0.5	0.05	0.19	0.33
1	0.15	0.48	0.71
2	0.35	1.26	2.11
3	0.52	2.26	3.85
4	0.6	4.91	-
5	0.9	-	-
6	-	-	-

**Table 53:** The mass of **105** and varying equiv. of Xphos used for the EXSY experiments

Exp. Code	<b>105</b>				Xphos			
	Mass (mg)	Moles (mmol)	Equiv.	Conc. (M)	Mass (mg)	Moles (mmol)	Equiv.	Conc. (M)
GA-3-335	10.2	0.00716	1	0.013	6.8	0.0143	2	0.026
GA-4-347	10.3	0.00724	1	0.013	33.1	0.0694	10	0.13
GA-4-351	10.4	0.00730	1	0.013	66.8	0.140	20	0.25
Volume of Solvent (mL):		0.55						

**Table 54:** Relative integration of the Xphos peak wrt **105** at each mixing time

Solvent:	Dichloromethane- <i>d</i> <sub>2</sub>		
Mixing time (sec)	Xphos equiv.		
	2 equiv. (1 equiv. per Ag atom)	10 equiv. (5 equiv. per Ag atom)	20 equiv. (10 equiv. per Ag atom)
0.003	0	0	0.01
0.005	0.01	n/a	n/a
0.5	n/a	n/a	2.15
1	0.93	2.07	7.44
2	0.91	4.46	21.84
4	0.99	13.76	10.36
6	1.04	13.38	-
8	1.33	-	-

## 6.5.7 Temperature-Dependent EXSY experiments

**General procedure**

In the glovebox, **101** (10 mg, 0.013 mmol, 1 equiv., 0.02 M) and Xphos (31 mg, 0.066 mmol, 5 equiv., 0.1 M) were weighed out in two separate vials. The Xphos was then dissolved in dichloromethane- $d_2$  (0.6 mL) and the solution was then used to transfer to a J-Young tube. The sample was placed in the NMR probe which was then heated to the desired temperature. Upon reaching temperature, a  $T_1$  inversion recovery experiment was used to measure the  $T_1$  of **101** and Xphos in the reaction mixture at the desired temperature. The  $T_1$  values at different temperatures were summarized in **Table 55**. The  $T_1$  values were used to set the D1 ( $T_1 \times 5$ ) for the 1D EXSY experiments.

**Table 55:** Summary of the  $T_1$  values measured at different temperatures for the mixture of **101** and Xphos (5 equiv.)

Reagent	$T_1$ (s)				
	20 °C	30 °C	40 °C	50 °C	60 °C
<b>101</b>	2.70	3.95	4.39	5.33	8.10
Xphos	4.45	5.18	5.80	6.48	7.43

**Table 56:** Relative integration of the Xphos peak wrt **101** at each mixing time and at different temperatures

Mixing times (sec)	Xphos Integration wrt Ag peak				
	20 °C	30 °C	40 °C	50 °C	60 °C
Exp. Code:	GA-5-372	GA-5-373	GA-5-374	GA-5-376	GA-5-377
0.003	0	0	0	0	-
0.005	0	0	0	0	0
0.05	0.01	0	0.01	0.02	0.03
0.075	-	-	-	0.03	0.06
0.1	0.01	0.01	0.02	0.05	0.08
0.2	0.01	0.02	0.05	0.10	0.18
0.3	0.03	0.04	0.07	0.15	0.29
0.4	0.03	0.06	0.10	0.22	0.39
0.5	0.04	0.08	0.14	0.29	0.50
0.6	0.05	0.08	0.17	0.35	0.63
0.8	0.08	0.14	0.22	0.48	0.95
1.0	0.10	0.16	0.27	0.68	1.21
2.0	0.23	0.36	0.69	1.71	2.93
3.0	-	-	1.13	-	-
4.0	-	-	1.80	-	-
6.0	-	-	3.27	-	-

Data were analysed as described above with the concentration-dependent EXSY experiments. The correction factor varied from 1.0 to 1.3 except for the 60° C data when it

was less than 1. The resulting rate constants were used to derive activation parameters from an Eyring plot. These corrections caused changes to the activation parameters that were within experimental error. Following conversion to exchange velocities  $V_{\text{ex}}$ , a second Eyring plot was calculated giving an even more decisive negative entropy of activation. The Eyring plots are shown in **Figure 159**. The analysis of the temperature dependent EXSY data was carried out by Prof. Robin Perutz.

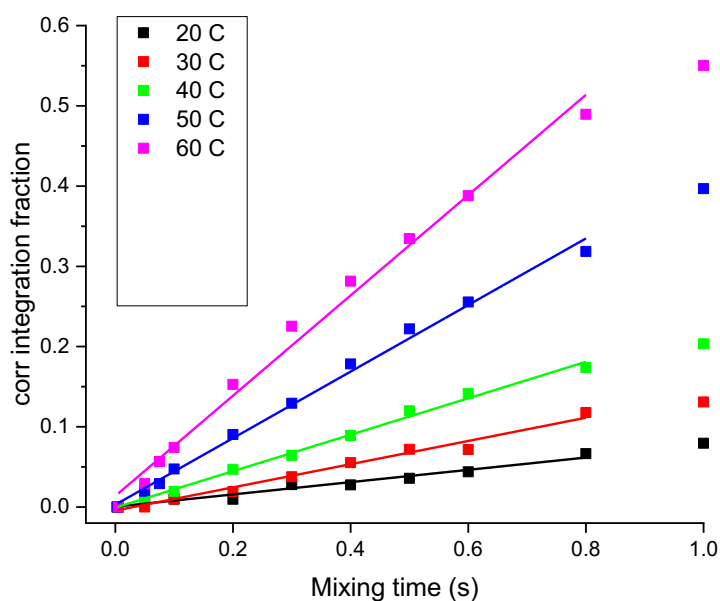


**Figure 158:** Plot of fractional transfer of magnetisation from **101** to free XPhos in  $\text{C}_6\text{D}_6$  against mixing time for different temperatures. The slopes correspond to  $k_{\text{obs}}$  for the exchange process. The data have been corrected for the differences in relaxation time at each temperature.

**Table 57:** Values of  $k_{\text{obs}}$  and  $V_{\text{ex}}$  for **101** in  $\text{C}_6\text{D}_6$  as a function of temperature. Data corrected for difference in relaxation times.

Temp (K)	Corrected Slope ( $k_{\text{obs}}$ )( $\text{s}^{-1}$ )	Corrected $V_{\text{ex}}$ ( $\text{M}^{-1} \text{s}^{-1}$ )
293	0.077	0.00144
303	0.145	0.00272
313	0.227	0.00426
323	0.415	0.00779
333	0.625	0.0117

Measured with  $[\text{Ag}(\text{C}_6\text{F}_5)\text{XPhos}] = 0.0226 \text{ M}$ ,  $[\text{XPhos}] = 0.111 \text{ M}$

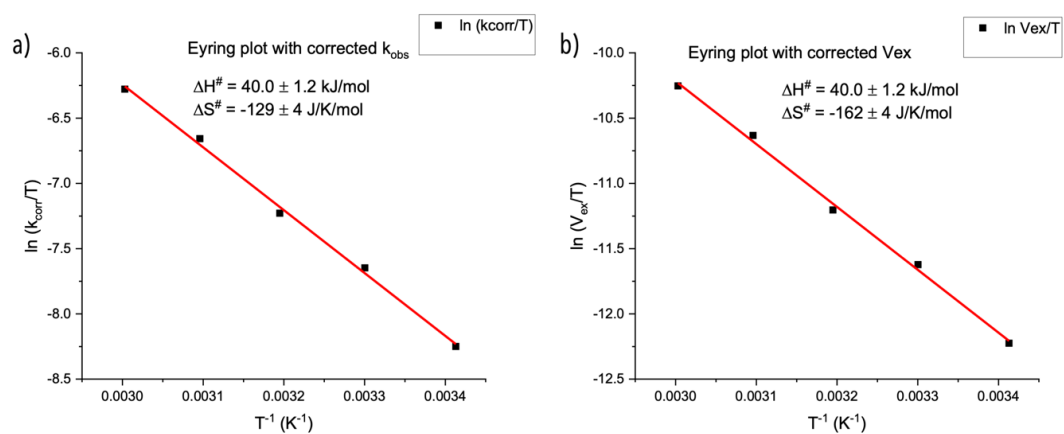
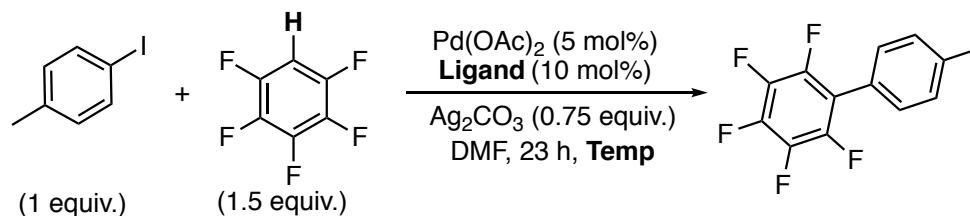


**Figure 159:** Eyring plots for the exchange rate. a) using values of  $k_{obs}$ , b) below using values of  $V_{ex}$ .

## 6.6 Experimental Procedures for Chapter 4

### General Experimental Procedure for Phosphine Ligand Substrate Scope



In a light-protected Schlenk tube Pd(OAc)<sub>2</sub> (10 mg, 0.045 mmol, 5 mol%), **ligand** (0.09 mmol, 10 mol%), Ag<sub>2</sub>CO<sub>3</sub> (186 mg, 0.68 mmol, 0.75 equiv.) was added and the Schlenk tube was evacuated and refilled three times with nitrogen. Against a strong flow of nitrogen, 4-iodotoluene **26** (196 mg, 0.9 mmol, 1 equiv.) and octafluoronaphthalene (71 mg, 0.26 mmol, 0.29 equiv., internal standard) were added followed by DMF (2.6 mL) and pentafluorobenzene **17** (227 mg, 1.35 mmol, 1.5 equiv., 150  $\mu$ L). The reaction mixture was then left stirring at the **required temperature** and reaction aliquots at 3 h and 23 h were collected to monitor the reaction using <sup>19</sup>F{<sup>1</sup>H} NMR spectroscopy. The reaction aliquots were prepared by collecting approximately 0.1 mL of the reaction mixture and filtering it through celite using CDCl<sub>3</sub> as the eluant. The sample was locked to CDCl<sub>3</sub> and the <sup>19</sup>F{<sup>1</sup>H} NMR spectrum of the reaction mixture was collected using a d1 = 20 secs, sw = 100, O1P = -150 and 32 scans.

**GA-3-243:** The desired ligand used was Xphos (43 mg, 0.09 mmol, 0.1 equiv.). The reaction mixture was submerged in a preheated oil bath (60 °C) and stirred for 23 h. The % <sup>19</sup>F{<sup>1</sup>H} NMR yield at 3 h = 96 %, 23 h = 96%.

**GA-3-344:** The desired ligand used was Xphos (43 mg, 0.09 mmol, 0.1 equiv.). The reaction mixture was stirred at ambient room temperature for 23 h. Only the reaction aliquots at 23 h was collected and the % <sup>19</sup>F{<sup>1</sup>H} NMR yield at 23 h = 75%.

**GA-5-358:** The desired ligand used was <sup>t</sup>BuXphos (38 mg, 0.09 mmol, 0.1 equiv.). The reaction mixture was submerged in a preheated oil bath (60 °C) and stirred for 23 h. The % <sup>19</sup>F{<sup>1</sup>H} NMR yield at 3 h = 3 %, 23 h = 6 %.

**GA-5-359:** The desired ligand used was <sup>t</sup>BuXphos (38 mg, 0.09 mmol, 0.1 equiv.). The reaction mixture was stirred at ambient room temperature for 23 h. The % <sup>19</sup>F{<sup>1</sup>H} NMR yield at 3 h = 0 %, 23 h = 0 %.

**GA-5-360:** The desired ligand used was CyJohnPhos (31 mg, 0.09 mmol, 0.1 equiv.). The reaction mixture was submerged in a preheated oil bath (60 °C) and stirred for 23 h. The % <sup>19</sup>F{<sup>1</sup>H} NMR yield at 3 h = 67 %, 23 h = 100 %.

**GA-5-361:** The desired ligand used was CyJohnPhos (31 mg, 0.09 mmol, 0.1 equiv.). The reaction mixture was stirred at ambient room temperature for 23 h. The %  $^{19}\text{F}\{^1\text{H}\}$  NMR yield at 3 h = 13 %, 23 h = 16%.

**GA-5-366:** The desired ligand used was JohnPhos (27 mg, 0.09 mmol, 0.1 equiv.). The reaction mixture was submerged in a preheated oil bath (60 °C) and stirred for 23 h. The %  $^{19}\text{F}\{^1\text{H}\}$  NMR yield at 3 h = 64 %, 23 h = 100 %.

**GA-5-363:** The desired ligand used was JohnPhos (27 mg, 0.09 mmol, 0.1 equiv.). The reaction mixture was stirred at ambient room temperature for 23 h. The %  $^{19}\text{F}\{^1\text{H}\}$  NMR yield at 3 h = 5 %, 23 h = 34 %.

**GA-5-364:** The desired ligand used was Sphos (37 mg, 0.09 mmol, 0.1 equiv.). The reaction mixture was submerged in a preheated oil bath (60 °C) and stirred for 23 h. The %  $^{19}\text{F}\{^1\text{H}\}$  NMR yield at 3 h = 66 %, 23 h = 70 %.

**GA-5-365:** The desired ligand used was Sphos (37 mg, 0.09 mmol, 0.1 equiv.). The reaction mixture was stirred at ambient room temperature for 23 h. The %  $^{19}\text{F}\{^1\text{H}\}$  NMR yield at 3 h = 15 %, 23 h = 73 %.

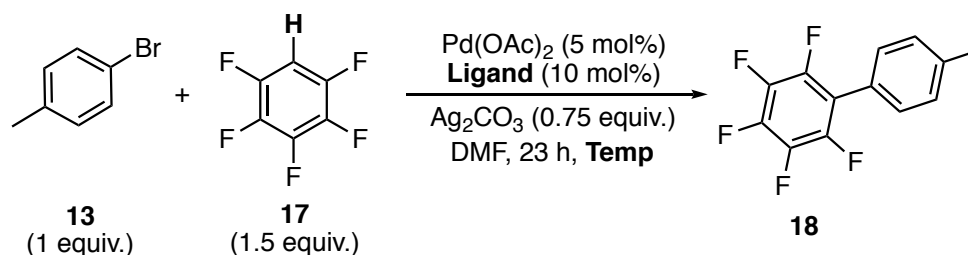
**GA-5-367:** The desired ligand used was BrettPhos (48 mg, 0.09 mmol, 0.1 equiv.). The reaction mixture was submerged in a preheated oil bath (60 °C) and stirred for 23 h. The %  $^{19}\text{F}\{^1\text{H}\}$  NMR yield at 3 h = 5 %, 23 h = 5 %.

**GA-5-368:** The desired ligand used was BrettPhos (48 mg, 0.09 mmol, 0.1 equiv.). The reaction mixture was stirred at ambient room temperature for 23 h. The %  $^{19}\text{F}\{^1\text{H}\}$  NMR yield at 3 h = 0 %, 23 h = 3 %.

**GA-5-369:** The desired ligand used was  $\text{PPh}_3$  (24 mg, 0.09 mmol, 0.1 equiv.). The reaction mixture was submerged in a preheated oil bath (60 °C) and stirred for 23 h. The %  $^{19}\text{F}\{^1\text{H}\}$  NMR yield at 3 h = 83 %, 23 h = 100 %.

**GA-5-370:** The desired ligand used was  $\text{PPh}_3$  (24 mg, 0.09 mmol, 0.1 equiv.). The reaction mixture was stirred at ambient room temperature for 23 h. The %  $^{19}\text{F}\{^1\text{H}\}$  NMR yield at 3 h = 10 %, 23 h = 43 %.

### General Experimental Procedure for Direct arylation with 4-bromotoluene **13** with varying ligands and temperatures





In a light-protected Schlenk tube Pd(OAc)<sub>2</sub> (10 mg, 0.045 mmol, 5 mol%), **ligand** (0.09 mmol, 10 mol%), Ag<sub>2</sub>CO<sub>3</sub> (186 mg, 0.68 mmol, 0.75 equiv.) was added and the Schlenk tube was evacuated and refilled three times with nitrogen. Against a strong flow of nitrogen, 4-bromotoluene **13** (153.9 mg, 0.9 mmol, 1 equiv.) and octafluoronaphthelene (71 mg, 0.26 mmol, 0.29 equiv., internal standard) were added followed by DMF (2.6 mL) and pentafluorobenzene **17** (227 mg, 1.35 mmol, 1.5 equiv., 150 μL). The reaction mixture was then left stirring at the **required temperature** and reaction aliquots at 3 h and 23 h were collected to monitor the reaction using <sup>19</sup>F{<sup>1</sup>H} NMR spectroscopy. The reaction aliquots were prepared by collecting approximately 0.1 mL of the reaction mixture and filtering it through celite using CDCl<sub>3</sub> as the eluant. The sample was locked to CDCl<sub>3</sub> and the <sup>19</sup>F{<sup>1</sup>H} NMR spectrum of the reaction mixture was collected using a d1 = 20 secs, sw = 100, O1P = - 150 and 32 scans.

**GA-5-399:** The desired ligand used was Xphos (43 mg, 0.09 mmol, 0.1 equiv.). The reaction mixture was submerged in a preheated oil bath (60 °C) and stirred for 23 h. The % <sup>19</sup>F{<sup>1</sup>H} NMR yield at 3 h = 30 %, 23 h = 29 %.

**GA-5-400/GA-5-402:** The desired ligand used was Xphos (43 mg, 0.09 mmol, 0.1 equiv.). The reaction mixture was stirred at ambient room temperature for 23 h. The % <sup>19</sup>F{<sup>1</sup>H} NMR yield at 3 h = 6 %, 23 h = 11 %.

**GA-5-417:** The desired ligand used was Xphos (43 mg, 0.09 mmol, 0.1 equiv.). The reaction mixture was submerged in a preheated oil bath (80 °C) and stirred for 23 h. The % <sup>19</sup>F{<sup>1</sup>H} NMR yield at 3 h = 26 %, 23 h = 27 %.

**GA-6-524:** The desired ligand used was Xphos (43 mg, 0.09 mmol, 0.1 equiv.). The reaction mixture was submerged in a preheated oil bath (100 °C) and stirred for 23 h. The % <sup>19</sup>F{<sup>1</sup>H} NMR yield at 3 h = 23 %, 23 h = 27 %.

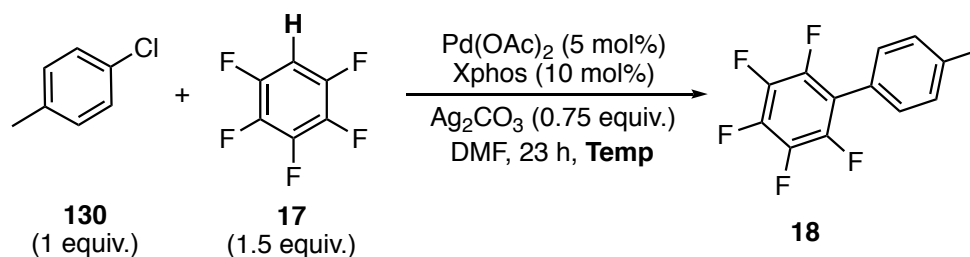
**GA-5-407:** The desired ligand used was CyJohnPhos (31 mg, 0.09 mmol, 0.1 equiv.). The reaction mixture was submerged in a preheated oil bath (60 °C) and stirred for 23 h. The % <sup>19</sup>F{<sup>1</sup>H} NMR yield at 3 h = 2 %, 23 h = 2 %.

**GA-5-408:** The desired ligand used was CyJohnPhos (31 mg, 0.09 mmol, 0.1 equiv.). The reaction mixture was stirred at ambient room temperature for 23 h. The % <sup>19</sup>F{<sup>1</sup>H} NMR yield at 3 h = 0 %, 23 h = 0 %.

**GA-5-410:** The desired ligand used was JohnPhos (27 mg, 0.09 mmol, 0.1 equiv.). The reaction mixture was submerged in a preheated oil bath (60 °C) and stirred for 23 h. The % <sup>19</sup>F{<sup>1</sup>H} NMR yield at 3 h = 11 %, 23 h = 11 %.

**GA-5-412:** The desired ligand used was JohnPhos (27 mg, 0.09 mmol, 0.1 equiv.). The reaction mixture was stirred at ambient room temperature for 23 h. The % <sup>19</sup>F{<sup>1</sup>H} NMR yield at 3 h = 2 %, 23 h = 3 %.

### General Experimental Procedure for Direct arylation with 4-chlorotoluene **130** with varying temperatures



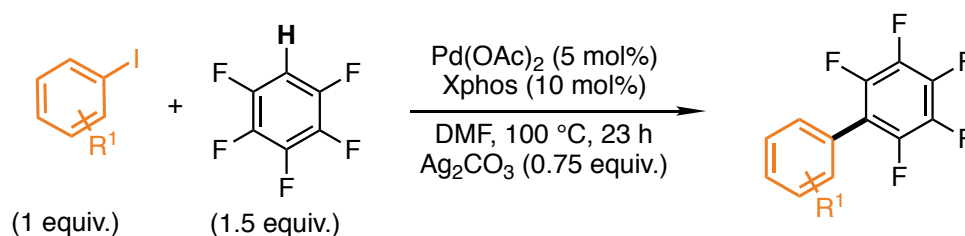
In a light-protected Schlenk tube Pd(OAc)<sub>2</sub> (10 mg, 0.05 mmol, 5 mol%), Xphos (43 mg, 0.09 mmol, 0.1 equiv., 10 mol%), Ag<sub>2</sub>CO<sub>3</sub> (186 mg, 0.68 mmol, 0.75 equiv.) was added and the Schlenk tube was evacuated and refilled three times with nitrogen. Against a strong flow of nitrogen, octafluoronaphthelene (71 mg, 0.26 mmol, 0.29 equiv., internal standard) was added followed by DMF (2.6 mL), 4-chlorotoluene **130** (114 mg, 0.9 mmol, 1 equiv., 106 μL) and pentafluorobenzene **17** (227 mg, 1.35 mmol, 1.5 equiv., 150 μL). The reaction mixture was then left stirring at the **required temperature** and reaction aliquots at 3 h and 23 h were collected to monitor the reaction using <sup>19</sup>F{<sup>1</sup>H} NMR spectroscopy. The reaction aliquots were prepared by collecting approximately 0.1 mL of the reaction mixture and filtering it through celite using CDCl<sub>3</sub> as the eluant. The sample was locked to CDCl<sub>3</sub> and the <sup>19</sup>F{<sup>1</sup>H} NMR spectrum of the reaction mixture was collected using a d1 = 20 secs, sw = 100, O1P = -150 and 32 scans.

**GA-5-413:** The reaction mixture was submerged in a preheated oil bath (60 °C) and stirred for 23 h. The % <sup>19</sup>F{<sup>1</sup>H} NMR yield at 3 h = 0 %, 23 h = 0 %.

**GA-5-416:** The reaction mixture was submerged in a preheated oil bath (80 °C) and stirred for 23 h. The % <sup>19</sup>F{<sup>1</sup>H} NMR yield at 3 h = 0 %, 23 h = 0 %.

**GA-5-525:** The reaction mixture was submerged in a preheated oil bath (100 °C) and stirred for 23 h. The % <sup>19</sup>F{<sup>1</sup>H} NMR yield at 3 h = 0 %, 23 h = 0 %.

#### Substrate scope for Aryl iodides



#### Solid Aryl Halides

To a light-protected air-tight vial (7 mL) equip with a stirrer bar, Pd(OAc)<sub>2</sub> (10 mg, 0.045 mmol, 5 mol%) Xphos (43 mg, 0.09 mmol, 0.1 equiv.), Ag<sub>2</sub>CO<sub>3</sub> (186 mg, 0.68 mmol, 0.75

equiv.) and the **solid aryl halide** (0.9 mmol, 1 equiv.) were added. The vial cap with silicone septum was screwed on and the vial was purged with nitrogen for 10 minutes. Then, dry DMF (2.6 mL) and pentafluorobenzene **17** (227 mg, 1.35 mmol, 1.5 equiv., 150  $\mu$ L) were added and the reaction mixture was placed in a pre-heated aluminium heating block at the **desired temperature**. The reaction mixture was then left stirring at the **required temperature** and reaction aliquots at 3 h and 23 h were collected to monitor the reaction using  $^{19}\text{F}\{^1\text{H}\}$  NMR spectroscopy. The reaction aliquots were prepared by collecting approximately 0.1 mL of the reaction mixture and filtering it through celite using  $\text{CDCl}_3$  as the eluant. The sample was locked to  $\text{CDCl}_3$  and the  $^{19}\text{F}\{^1\text{H}\}$  NMR spectrum of the reaction mixture was collected using a  $d1 = 20$  secs,  $sw = 100$ ,  $\text{O1P} = -150$  and 32 scans.

*Reactions are carried out at 60 °C*

**GA-5-411:** 4-Iodotoluene (196 mg, 0.9 mmol, 1 equiv.) was added, and the reaction mixture was heated to 60 °C for 23 h and the %  $^{19}\text{F}\{^1\text{H}\}$  NMR yield at 3 h = 96 %, 23 h = 96%.

**GA-5-415:** 4-Iodotoluene (196 mg, 0.9 mmol, 1 equiv.) was added, and the reaction mixture was heated to RT for 23 h and the %  $^{19}\text{F}\{^1\text{H}\}$  NMR yield at 23 h = 77 %.

**GA-5-419:** 4-Iodoanisole (211 mg, 0.9 mmol, 1 equiv.) was added, and the reaction mixture was heated to 60 °C for 23 h and the %  $^{19}\text{F}\{^1\text{H}\}$  NMR yield at 3 h = 98 %, 23 h = 97%.

**GA-5-420:** 4-Iodoaniline (197 mg, 0.9 mmol, 1 equiv.) was added and the reaction mixture was heated for 60 °C for 23 h and %  $^{19}\text{F}\{^1\text{H}\}$  NMR yield at 3 h = 0 %, 23 h = 0 %.

**GA-5-423:** 4-Iodophenol (198 mg, 0.9 mmol, 1 equiv.) was added the reaction mixture was heated to 60 °C for 23 h and the %  $^{19}\text{F}\{^1\text{H}\}$  NMR yield at 3 h = ~ 3 %, 23 h = ~ 3 %.

**GA-5-436:** 4-Iodobenzaldehyde (209 mg, 0.9 mmol, 1 equiv.) was added and the reaction mixture was heated to 60 °C for 23 h and the %  $^{19}\text{F}\{^1\text{H}\}$  NMR yield at 3 h = 20 %, 23 h = 21%.

**GA-5-425:** Iodo-4-nitrobenzene (224 mg, 0.9 mmol, 1 equiv.) was added and the reaction mixture was heated to 60 °C for 23 h and the %  $^{19}\text{F}\{^1\text{H}\}$  NMR yield at 3 h = 19 %, 23 h = 20 %.

**GA-5-426:** 4-Iodoacetophenone (221 mg, 0.9 mmol, 1 equiv.) was added and the reaction mixture was heated to 60 °C for 23 h and the %  $^{19}\text{F}\{^1\text{H}\}$  NMR yield at 3 h = 40 %, 23 h = 46 %. A reaction aliquot was also collected at 46 h,  $^{19}\text{F}\{^1\text{H}\}$  NMR yield = 52 %.

**GA-5-427:** 3-Iodopyridine (185 mg, 0.9 mmol, 1 equiv.) was added and the reaction mixture was heated to 60 °C for 23 h and the %  $^{19}\text{F}\{^1\text{H}\}$  NMR yield at 3 h = 2 %, 23 h = 3 %.

**GA-5-435:** Methyl-4-iodobenzoate (236 mg, 0.9 mmol, 1 equiv.) was added and the reaction mixture was heated to 60 °C for 23 h and the %  $^{19}\text{F}\{^1\text{H}\}$  NMR yield at 3 h = 51 %, 23 h = 51 %.

**GA-5-437:** 2-Iodo-1,3,5-trimethylbenzene (222 mg, 0.9 mmol, 1 equiv.) was added and the reaction mixture was heated to 60 °C for 23 h and the %  $^{19}\text{F}\{^1\text{H}\}$  NMR yield at 3 h = 0 %, 23 h = 0 %.

**GA-5-431:** 6-Iodoquinoline (230 mg, 0.9 mmol, 1 equiv.) was added and the reaction mixture was heated to 60 °C for 23 h and the %  $^{19}\text{F}\{^1\text{H}\}$  NMR yield at 3 h = 10 %, 23 h = 11 %.

**GA-5-439:** 9-Iodophenanthrene (274 mg, 0.9 mmol, 1 equiv.) was added and the reaction mixture was heated to 60 °C for 23 h and the %  $^{19}\text{F}\{^1\text{H}\}$  NMR yield at 3 h = 6 %, 23 h = 6 %.

**GA-6-477:** 3-Iodobenzaldehyde (208 mg, 0.9 mmol, 1 equiv.) was added and the reaction mixture was heated to 60 °C for 23 h and the %  $^{19}\text{F}\{^1\text{H}\}$  NMR yield at 3 h = 14 %, 23 h = 14 %.

**GA-5-430:** Chloro-4-Iodobenzene (215 mg, 0.9 mmol, 1 equiv.) was added and the reaction mixture was heated to 60 °C for 23 h. The reaction produced a major product ( $^{19}\text{F}\{^1\text{H}\}$  NMR yield at 3 h = 88 %, 23 h = 89 %) and a minor product ( $^{19}\text{F}\{^1\text{H}\}$  NMR yield at 3 h = 6 %, 23 h = 6 %).

**GA-5-434:** Bromo-4-Iodobenzene (254 mg, 0.9 mmol, 1 equiv.) was added and the reaction mixture was heated to 60 °C for 23 h. Multiple overlapping *F*-resonances were present in the  $^{19}\text{F}\{^1\text{H}\}$  NMR spectrum indicating the presence of multiple products.

*Reactions are carried out at 100 °C*

**GA-6-478:** Methyl-4-iodobenzoate (236 mg, 0.9 mmol, 1 equiv.) was added and the reaction mixture was heated to 100 °C for 23 h and the %  $^{19}\text{F}\{^1\text{H}\}$  NMR yield at 3 h = 89 %, 23 h = 100 %.

**GA-6-431:** 6-Iodoquinoline (230 mg, 0.9 mmol, 1 equiv.) was added and the reaction mixture was heated to 100 °C for 23 h and the %  $^{19}\text{F}\{^1\text{H}\}$  NMR yield at 3 h = 86 %, 23 h = 97 %.

**GA-6-482:** 4-Iodoacetophenone (221 mg, 0.9 mmol, 1 equiv.) was added and the reaction mixture was heated to 100 °C for 23 h and the %  $^{19}\text{F}\{^1\text{H}\}$  NMR yield at 3 h = 62 %, 23 h = 67 %.

**GA-6-488:** 3-Iodobenzaldehyde (208 mg, 0.9 mmol, 1 equiv.) was added and the reaction mixture was heated to 100 °C for 23 h and the %  $^{19}\text{F}$  NMR yield at 3 h = 58 %, 23 h = 88 %.

**GA-6-490:** Iodo-4-nitrobenzene (224 mg, 0.9 mmol, 1 equiv.) was added and the reaction mixture was heated to 100 °C for 23 h and the %  $^{19}\text{F}\{^1\text{H}\}$  NMR yield at 3 h = 71 %, 23 h = 91 %.

**GA-6-529:** Iodo-3-nitrobenzene (249 mg, 0.9 mmol, 1 equiv.) was added and the reaction mixture was heated to 100 °C for 23 h and the %  $^{19}\text{F}\{^1\text{H}\}$  NMR yield at 3 h = 75 %, 23 h = 93 %.

**GA-6-475:** 5-Iodouracil (238 mg, 0.9 mmol, 1 equiv.) was added and the reaction mixture was heated to 100 °C for 23 h and the %  $^{19}\text{F}\{^1\text{H}\}$  NMR yield at 3 h = 0 %, 23 h = 0 %.

### Liquid Aryl Halides (Procedure B)

To a light-protected air-tight vial (7 mL) equip with a stirrer bar, Pd(OAc)<sub>2</sub> (10 mg, 0.045 mmol, 5 mol%) Xphos (43 mg, 0.09 mmol, 0.1 equiv.), Ag<sub>2</sub>CO<sub>3</sub> (186 mg, 0.68 mmol, 0.75 equiv.) were added. The vial cap with silicone septum was screwed on and the vial was purged with nitrogen for 10 minutes. Then, dry DMF (2.6 mL), the **liquid aryl halide** (0.9 mmol, 1 equiv.) and pentafluorobenzene **17** (227 mg, 1.35 mmol, 1.5 equiv., 150 μL) were added and the reaction mixture was placed in a pre-heated aluminium heating block at the **desired temperature**. The reaction mixture was then left stirring at the **required temperature** and reaction aliquots at 3 h and 23 h were collected to monitor the reaction using  $^{19}\text{F}\{^1\text{H}\}$  NMR spectroscopy. The reaction aliquots were prepared by collecting approximately 0.1 mL of the reaction mixture and filtering it through celite using CDCl<sub>3</sub> as the eluant. The sample was locked to CDCl<sub>3</sub> and the  $^{19}\text{F}\{^1\text{H}\}$  NMR spectrum of the reaction mixture was collected using a d1 = 20 secs, sw = 100, O1P = -150 and 32 scans.

*Reactions are carried out at 60 °C*

**GA-5-422:** Iodobenzene (183.6 mg, 0.9 mmol, 1 equiv., 100 μL) was added, and the reaction mixture was heated to 60 °C for 23 h and the %  $^{19}\text{F}\{^1\text{H}\}$  NMR yield at 3 h = 98 %, 23 h = 100%.

**GA-5-421:** 4-Fluoroiodobenzene (200 mg, 0.9 mmol, 1 equiv. 105 μL) was added and the reaction mixture was heated to 60 °C for 23 h and the %  $^{19}\text{F}\{^1\text{H}\}$  NMR yield at 3 h = 66 %, 23 h = 67%.

**GA-5-438:** 2-Iodoanisole (210 mg, 0.9 mmol, 1 equiv. 117 μL) was added and the reaction mixture was heated to 60 °C for 23 h and the %  $^{19}\text{F}\{^1\text{H}\}$  NMR yield at 3 h = 6 %, 23 h = 6 %.

**GA-5-441:** 1-Iodonaphthalene (254 mg, 0.9 mmol, 1 equiv. 131 μL) was added and the reaction mixture was heated to 60 °C for 23 h and the %  $^{19}\text{F}\{^1\text{H}\}$  NMR yield at 3 h = 15 %, 23 h = 14 %.

**GA-5-442:** 3-Iodoanisole (234 mg, 0.9 mmol, 1 equiv. 107 μL) was added and the reaction mixture was heated to 60 °C for 69 h and the %  $^{19}\text{F}\{^1\text{H}\}$  NMR yield at 3 h = 82 %, 69 h = 85 %.

**GA-5-443:** 2-Iodotoluene (218 mg, 0.9 mmol, 1 equiv. 115 μL) was added and the reaction mixture was heated to 60 °C for 69 h and the %  $^{19}\text{F}\{^1\text{H}\}$  NMR yield at 3 h = 27 %, 69 h = 27 %.

**GA-5-447:** 4-Iodobenzotrifluoride (245 mg, 0.9 mmol, 1 equiv. 132 μL) was added and the reaction mixture was heated to 60 °C for 26 h and the %  $^{19}\text{F}\{^1\text{H}\}$  NMR yield at 3 h = 53 %, 26 h = 56 %.

**GA-5-448:** 3-Iodobenzotrifluoride (245 mg, 0.9 mmol, 1 equiv. 130  $\mu\text{L}$ ) was added and the reaction mixture was heated to 60  $^{\circ}\text{C}$  for 23 h and the %  $^{19}\text{F}\{^1\text{H}\}$  NMR yield at 3 h = 69 %, 23 h = 73 %.

**GA-6-459:** 2-Iodobenzotrifluoride (272 mg, 0.9 mmol, 1 equiv. 126  $\mu\text{L}$ ) was added and the reaction mixture was heated to 60  $^{\circ}\text{C}$  for 23 h and the %  $^{19}\text{F}\{^1\text{H}\}$  NMR yield at 23 h = 0 %.

*Reactions are carried out at 100  $^{\circ}\text{C}$*

**GA-6-479:** 2-Iodoanisole (210 mg, 0.9 mmol, 1 equiv. 117  $\mu\text{L}$ ) was added and the reaction mixture was heated to 100  $^{\circ}\text{C}$  for 23 h and the %  $^{19}\text{F}\{^1\text{H}\}$  NMR yield at 3 h = 11 %, 23 h = 15 %.

**GA-6-485:** 1-Iodonaphthalene (254 mg, 0.9 mmol, 1 equiv. 131  $\mu\text{L}$ ) was added and the reaction mixture was heated to 100  $^{\circ}\text{C}$  for 23 h and the %  $^{19}\text{F}\{^1\text{H}\}$  NMR yield at 3 h = 24 %, 23 h = 27 %.

**GA-6-486:** 2-Iodotoluene (218 mg, 0.9 mmol, 1 equiv. 115  $\mu\text{L}$ ) was added and the reaction mixture was heated to 100  $^{\circ}\text{C}$  for 23 h and the %  $^{19}\text{F}\{^1\text{H}\}$  NMR yield at 3 h = 29 %, 23 h = 33 %.

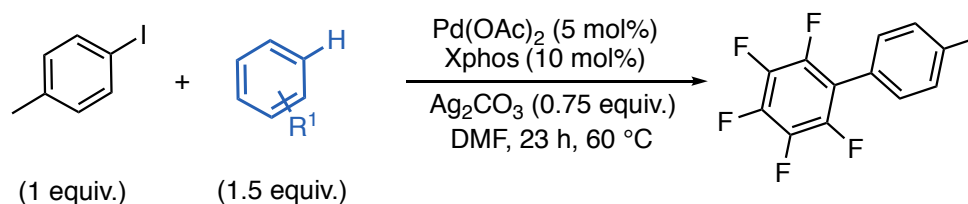
**GA-6-489:** 4-Fluoriodobenzene (200 mg, 0.9 mmol, 1 equiv. 105  $\mu\text{L}$ ) was added and the reaction mixture was heated to 100  $^{\circ}\text{C}$  for 23 h and the %  $^{19}\text{F}\{^1\text{H}\}$  NMR yield at 3 h = 96 %, 23 h = 100 %.

**GA-6-517:** 2-Iodopyridine (184 mg, 0.9 mmol, 1 equiv. 96  $\mu\text{L}$ ) was added and the reaction mixture was heated to 100  $^{\circ}\text{C}$  for 23 h and the %  $^{19}\text{F}\{^1\text{H}\}$  NMR yield at 3 h = 2 %, 23 h = 3 %.

**GA-6-487:** 2-Iodobenzotrifluoride (272 mg, 0.9 mmol, 1 equiv. 126  $\mu\text{L}$ ) was added and the reaction mixture was heated to 100  $^{\circ}\text{C}$  for 23 h and the %  $^{19}\text{F}\{^1\text{H}\}$  NMR yield at 3h = 0%, 23 h = 0 %.

**GA-6-530:** 3-Iodoanisole (211 mg, 0.9 mmol, 1 equiv. 107  $\mu\text{L}$ ) was added, and the reaction mixture was heated to 100  $^{\circ}\text{C}$  for 23 h and the %  $^{19}\text{F}\{^1\text{H}\}$  NMR yield at 3h = 86 %, 23 h = 92 %.

## General Experimental Procedure for fluoroaromatic substrate scope



To a light-protected air-tight vial (7 mL) equip with a stirrer bar, Pd(OAc)<sub>2</sub> (10 mg, 0.045 mmol, 5 mol%) Xphos (43 mg, 0.09 mmol, 0.1 equiv.), Ag<sub>2</sub>CO<sub>3</sub> (186 mg, 0.68 mmol, 0.75 equiv.) and 4-iodotoluene (196 mg, 0.9 mmol, 1 equiv.) were added. The vial cap with silicone septum was screwed on and the vial was purged with nitrogen for 10 minutes. Then, dry DMF (2.6 mL) and **fluoroarene** (1.35 mmol, 1.5 equiv.) were added and the reaction mixture was placed in a pre-heated aluminium heating block at the **desired temperature**. The reaction mixture was then left stirring at the **required temperature** and reaction aliquots at 3 h and 23 h were collected to monitor the reaction using <sup>19</sup>F{<sup>1</sup>H} NMR spectroscopy. The reaction aliquots were prepared by collecting approximately 0.1 mL of the reaction mixture and filtering it through celite using CDCl<sub>3</sub> as the eluant. The sample was locked to CDCl<sub>3</sub> and the <sup>19</sup>F{<sup>1</sup>H} NMR spectrum of the reaction mixture was collected using a d1 = 20 secs, sw = 100, O1P = -150 and 32 scans.

**GA-5-355:** 2,3,5,6-tetrafluoropyridine **67** (203 mg, 1.35 mmol, 1.5 equiv., 136 μL) was added and the reaction mixture was heated to 60 °C for 23 h. The % <sup>19</sup>F{<sup>1</sup>H} NMR yield was calculated by integrating the *ortho*-F resonance by the biaryl product **158** (δ -91.4) wrt octafluoronaphthalene (δ -145.2) and the NMR yield at 3 h = 76 %, 23 h = 93 %.

**GA-5-356:** 2,3,5,6-tetrafluoropyridine **67** (203 mg, 1.35 mmol, 1.5 equiv., 136 μL) was added and the reaction mixture was heated to RT for 23 h. The % <sup>19</sup>F{<sup>1</sup>H} NMR yield was calculated by integrating the *ortho*-F resonance by the biaryl product **158** (δ -91.4) wrt octafluoronaphthalene (δ -145.2) and the NMR yield at 23 h = 27 %. (*Only the 23 h reaction aliquot was collected*)

**GA-5-395:** *The ligand used is CyJohnPhos*, CyJohnPhos (31 mg, 0.09 mmol, 10 mol%) was added in place of Xphos. 2,3,5,6-tetrafluoropyridine **67** (203 mg, 1.35 mmol, 1.5 equiv., 136 μL) was added and the reaction mixture was heated to 60 °C for 23 h. The % <sup>19</sup>F{<sup>1</sup>H} NMR yield was calculated by integrating the *ortho*-F resonance by the biaryl product **158** (δ -91.4) wrt octafluoronaphthalene (δ -145.2) and the NMR yield at 3 h = 67 %, 23 h = 67 %.

**GA-5-397:** *The ligand used is JohnPhos*, JohnPhos (27 mg, 0.09 mmol, 10 mol%) was added in place of Xphos. 2,3,5,6-tetrafluoropyridine **67** (203 mg, 1.35 mmol, 1.5 equiv., 136 μL) was added and the reaction mixture was heated to 60 °C for 23 h. The % <sup>19</sup>F{<sup>1</sup>H} NMR

yield was calculated by integrating the *ortho*-F resonance by the biaryl product **67** ( $\delta$  -91.4) wrt octafluoronaphthalene ( $\delta$  -145.2) and the NMR yield at 3 h = 61 %, 23 h = 69 %.

**GA-5-375:** 1,3-difluorobenzene **12** (155 mg, 1.35 ml, 1.5 equiv., 180  $\mu$ L) was added and the reaction mixture was heated to 70 °C for 23 h. The %  $^{19}\text{F}\{^1\text{H}\}$  NMR yield was calculated by integrating the *ortho*-F resonance by the biaryl product **14** ( $\delta$  -114.7), wrt octafluoronaphthalene ( $\delta$  -145.2) and the NMR yield at 3 h = 0 %, 23 h = 2 %.

**GA-5-378:** 1,3-difluorobenzene **12** (155 mg, 1.35 ml, 1.5 equiv., 180  $\mu$ L) was added and the reaction mixture was stirred to RT for 23 h. The %  $^{19}\text{F}\{^1\text{H}\}$  NMR yield was calculated by integrating the *ortho*-F resonance by the biaryl product **14** ( $\delta$  -114.7), wrt octafluoronaphthalene ( $\delta$  -145.2) and the NMR yield at 3 h = 0 %, 23 h = 0 %.

**GA-5-379:** *The ligand used is PPh<sub>3</sub>*, PPh<sub>3</sub> (24 mg, 0.09 mmol, 10 mol%) was added in place of Xphos. 1,3-difluorobenzene **12** (155 mg, 1.35 ml, 1.5 equiv., 180  $\mu$ L) was added and the reaction mixture was stirred to 70 °C for 23 h. The %  $^{19}\text{F}\{^1\text{H}\}$  NMR yield was calculated by integrating the *ortho*-F resonance by the biaryl product **14** ( $\delta$  -114.7), wrt octafluoronaphthalene ( $\delta$  -145.2) and the NMR yield at 3 h = 3 %, 23 h = 12 %.

**GA-5-380:** 1,3-difluorobenzene **12** (155 mg, 1.35 ml, 1.5 equiv., 180  $\mu$ L) was added and the reaction mixture was heated to 80 °C for 23 h. The %  $^{19}\text{F}\{^1\text{H}\}$  NMR yield was calculated by integrating the *ortho*-F resonance by the biaryl product **14** ( $\delta$  -114.7), wrt octafluoronaphthalene ( $\delta$  -145.2) and the NMR yield at 3 h = 1 %, 23 h = 3 %.

**GA-5-405:** *10 equivalents of fluoroarene were used.* 1,3-difluorobenzene **12** (1027 mg, 9.0 ml, 10 equiv., 885  $\mu$ L) was added and the reaction mixture was heated to 80 °C for 23 h. The %  $^{19}\text{F}\{^1\text{H}\}$  NMR yield was calculated by integrating the *ortho*-F resonance by the biaryl product **14** ( $\delta$  -114.7), wrt octafluoronaphthalene ( $\delta$  -145.2) and the NMR yield at 3 h = 5 %, 23 h = 10 %.

**GA-5-388:** 1,2,3,4-tetrafluorobenzene **159** (204 mg, 1.35 ml, 1.5 equiv., 145  $\mu$ L) was added and the reaction mixture was heated to 60 °C for 23 h. The %  $^{19}\text{F}\{^1\text{H}\}$  NMR yield at 3 h = 0 %, 23 h = 0 %.

**GA-5-389:** 1,2,3,4-tetrafluorobenzene **159** (204 mg, 1.35 ml, 1.5 equiv., 145  $\mu$ L) was added and the reaction mixture was heated to RT °C for 23 h. The %  $^{19}\text{F}\{^1\text{H}\}$  NMR yield at 3 h = 0 %, 23 h = 0 %.

**GA-6-506:** 2,6-difluoropyridine **163** (155 mg, 1.35 ml, 1.5 equiv., 122  $\mu$ L) was added and the reaction mixture was heated to 60 °C for 23 h. The  $^{19}\text{F}\{^1\text{H}\}$  NMR spectrum of the reaction mixture was collected using sw = 240 and O1P = -100. The %  $^{19}\text{F}\{^1\text{H}\}$  NMR yield at 3 h = 0 %, 23 h = 0 %.

**GA-6-508:** 2,6-difluoropyridine **163** (155 mg, 1.35 ml, 1.5 equiv., 122  $\mu$ L) was added and the reaction mixture was heated to 100 °C for 23 h. The  $^{19}\text{F}\{^1\text{H}\}$  NMR spectrum of the reaction mixture was collected using sw = 240 and O1P = 100. The %  $^{19}\text{F}\{^1\text{H}\}$  NMR yield



was calculated by integrating the F resonance by the biaryl product **164** ( $\delta$  -71.6) wrt octafluoronaphthalene ( $\delta$  -145.2) and the NMR yield at 3 h = 5 %, 23 h = 5 %.

**GA-6-507:** 3,5-difluoropyridine **161** (155 mg, 1.35 mmol, 1.5 equiv., 123  $\mu$ L) was added and the reaction mixture was heated to 60 °C for 23 h. The  $^{19}\text{F}\{^1\text{H}\}$  NMR spectrum of the reaction mixture was collected using sw = 100 and O1P = -120. The %  $^{19}\text{F}\{^1\text{H}\}$  NMR yield was calculated by integrating the F resonance by the biaryl product **164** ( $\delta$  -130.5) wrt octafluoronaphthalene ( $\delta$  -145.2) and the NMR yield at 3 h = 5 %, 23 h = 23 %.

**GA-6-512:** 3,5-difluoropyridine **161** (155 mg, 1.35 mmol, 1.5 equiv., 123  $\mu$ L) was added and the reaction mixture was heated to 100 °C for 23 h. The  $^{19}\text{F}\{^1\text{H}\}$  NMR spectrum of the reaction mixture was collected using sw = 100 and O1P = -120. The %  $^{19}\text{F}\{^1\text{H}\}$  NMR yield was calculated by integrating the F resonance by the biaryl product **162** ( $\delta$  -130.5) wrt octafluoronaphthalene ( $\delta$  -145.2) and the NMR yield at 3 h = 36 %, 23 h = 46 %.

## Appendix A – Published Paper

Part of this work has been published in the following paper<sup>177</sup> and a copy has been provided.

Athavan, G.; Tanner, T.F.N.; Whitwood, A.C; Fairlamb, I.J.S; Perutz, R. N; Direct Evidence for Competitive C–H Activation by a Well-Defined Silver Xphos Complex in Palladium-Catalyzed C–H Functionalization. *Organometallics*, **2022**, XX, XX–XX

# Direct Evidence for Competitive C–H Activation by a Well-Defined Silver XPhos Complex in Palladium-Catalyzed C–H Functionalization

Gayathri Athavan, Theo F. N. Tanner, Adrian C. Whitwood, Ian J. S. Fairlamb,\* and Robin N. Perutz\*



Cite This: <https://doi.org/10.1021/acs.organomet.2c00063>



Read Online

ACCESS |



Metrics & More

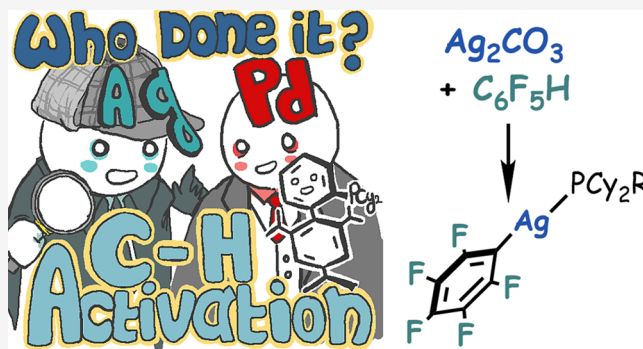


Article Recommendations



Supporting Information

**ABSTRACT:** Increasing evidence indicates that silver salts can play a role in the C–H activation step of palladium-catalyzed C–H functionalization. Here we isolate a silver(I) complex by C–H bond activation and demonstrate its catalytic competence for C–H functionalization. We demonstrate how silver carbonate, a common but highly insoluble additive, reacts with pentafluorobenzene in the presence of a bulky phosphine, XPhos, to form the C–H bond activation product  $\text{Ag}(\text{C}_6\text{F}_5)(\text{XPhos})$ . By isolating and fully characterizing this complex and the related carbonate and iodide complexes,  $[\text{Ag}(\text{XPhos})]_2(\mu-\kappa^2, \kappa^2-\text{CO}_3)$  and  $[\text{AgI}(\text{XPhos})]_2$ , we show how well-defined Ag(I) complexes can operate in conjunction with palladium complexes to achieve C–H functionalization even at ambient temperature. Reactions are tested against the standard cross-coupling of  $\text{C}_6\text{F}_5\text{H}$  with 4-iodotoluene, catalyzed by palladium acetate at 60 °C in the presence of silver carbonate and Xphos. Key observations are that (a)  $\text{PdI}(\text{C}_6\text{H}_5)(\text{XPhos})$  reacts stoichiometrically with  $\text{Ag}(\text{C}_6\text{F}_5)(\text{XPhos})$  to form  $\text{Ph}-\text{C}_6\text{F}_5$  instantly at room temperature; (b) catalytic cross coupling can be achieved using 5%  $\text{Ag}(\text{C}_6\text{F}_5)(\text{XPhos})$  as the sole silver source; and (c) palladium acetate (typical precatalyst) can be replaced for catalytic cross coupling by the expected oxidative addition compound  $\text{PdI}(\text{C}_6\text{H}_5)(\text{XPhos})$ . These investigations lead to a catalytic cycle in which Ag(I) plays the C–H bond activation role and palladium plays the coupling role. Moreover, we show how the phosphine can be exchanged between silver complexes, ensuring that it is recycled even though silver carbonate is consumed during catalytic cross-coupling.



## INTRODUCTION

The functionalization of C–H bonds of low reactivity has emerged as a powerful and selective strategy for the installation of a plethora of organic motifs, increasing structural complexity and diversity in applied chemical synthesis.<sup>1–3</sup> A variety of transition metals can be used to activate a C–H bond, from precious metals through to earth-abundant metals, each with their individual merits in terms of practical synthetic procedures.<sup>4,5</sup> There has been significant interest in palladium salts,<sup>6,7</sup> which catalyze the functionalization of a myriad of (hetero)arenes, with varying electronic and steric differences. Of interest are the electron-deficient fluorinated arenes,<sup>8–11</sup> which undergo reaction with iodoarenes in the presence of phosphines and bases such as carbonates and acetates. Extensive mechanistic studies have led to a consensus that C–H bond activation occurs by the concerted metalation deprotonation (CMD) mechanism,<sup>9,12–15</sup> alternatively described as ambiphilic metal–ligand assistance (AMLA-6).<sup>16,17</sup> Typically, these reactions are thought to involve mononuclear Pd species, operating homogeneously, with the caveat that there is some experimental evidence implicating hybrid homogeneous–heterogeneous behavior and higher order Pd species.<sup>18–21</sup> In early work, Fagnou et al. demonstrated the coupling of pentafluorobenzene to iodotoluene and studied its

mechanism; we also select this as an exemplar reaction. Fagnou et al. employed potassium carbonate as the base with  $\text{P}^t\text{Bu}_2\text{Me}$  as the ligand,<sup>9</sup> but later a variety of other bases were used, often including silver carbonate. Bulky phosphines continue to be employed, but even  $\text{PPh}_3$  is active.<sup>22</sup> In the past few years, Ag(I) has been demonstrated to play an active role in the critical C–H bond activation step in several reactions, starting with independent discoveries in 2016 by Lee and Hartwig<sup>23</sup> and by Larrosa et al.<sup>24</sup> Silver(I) can form several dinuclear complexes with triphenylphosphine with bridging carbonate or bicarbonate,<sup>25</sup> and silver(phosphine)halide complexes with bulky phosphines have been known since 1978. Notably, these silver complexes behave as neutral molecular species in dichloromethane solution.<sup>26</sup> In NMR spectra, they are characterized by large  $^{107}\text{Ag}-^{31}\text{P}$  and  $^{109}\text{Ag}-^{31}\text{P}$  coupling

**Special Issue:** Organometallic Chemistry Inspired by Maurice Brookhart

**Received:** February 2, 2022

constants that decrease as the coordination number of Ag increases.<sup>27–30</sup>

A series of papers implicated silver salts in the C–H bond activation of fluoroarenes, several of which are summarized in reviews.<sup>7,31–33</sup> We first consider the evidence in the absence of palladium. Simple silver salts have been shown to effect H/D exchange in pentafluorobenzene (or heptafluorotoluene) with D<sub>2</sub>O + AgOPiv (Piv = pivalate).<sup>34–36</sup> H/D exchange with D<sub>2</sub>O in the position ortho to the fluorine of a fluoroarene (or a metal complex of fluoroarene) was also reported, employing Ag<sub>2</sub>CO<sub>3</sub> (or Ag<sub>2</sub>O) and a bulky phosphine (Scheme 1, eq 1).<sup>37–39</sup> Similar studies including DFT calculations have been reported with AgOC(O)Ad + PPh<sub>3</sub> (Ad = adamantyl).<sup>24</sup>

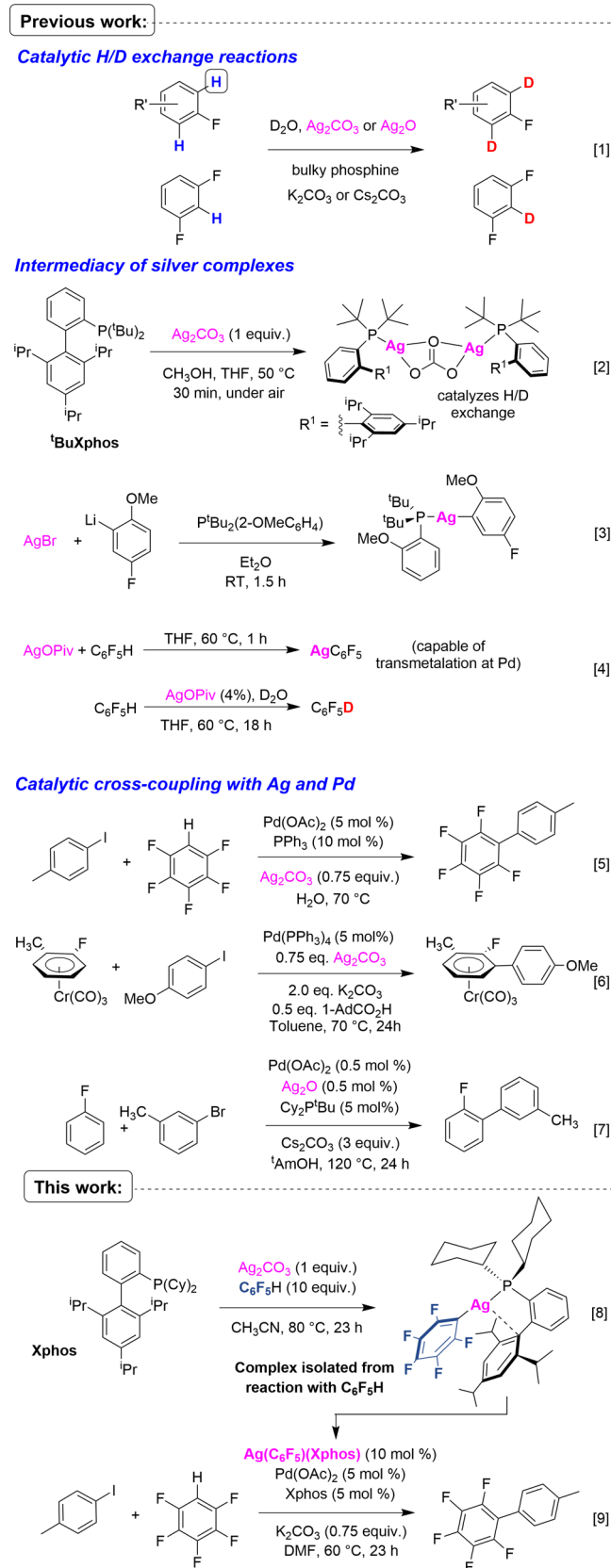
Such H/D exchange implicates the occurrence of a C–H bond activation process between a silver salt, a phosphine, and a substrate. Identification of such intermediates is important in understanding the catalytic exchange. A recent paper (published while our work was in progress) demonstrated that selective catalytic H/D exchange occurs between CH<sub>3</sub>OD and numerous heteroarenes in the presence of silver carbonate and certain bulky phosphines. Moreover, silver carbonate reacts with <sup>t</sup>BuXPhos to form a dinuclear silver phosphine carbonate complex which catalyzes H/D exchange of thiophene with CH<sub>3</sub>OD (Scheme 1, eq 2).<sup>40</sup> Thus, this complex is a likely intermediate in catalysis.

We now consider reactions in the presence of both silver and palladium. In the initial 2016 work, it was shown that a silver phosphine fluoroaryl complex reacts stoichiometrically with a palladium allyl complex to form the corresponding allyl arene. Notably, this silver complex was formed, not by reaction with the neutral arene but via lithium salt (Scheme 1, eq 3).<sup>23</sup> Nevertheless, this complex is again a plausible intermediate in catalysis. A further study focused on the reaction of palladium complexes with pentafluorobenzene in the presence of various silver salts, revealing the formation of Ag(C<sub>6</sub>F<sub>5</sub>) identified by its <sup>19</sup>F ortho-fluorine resonance. The same species could be formed by reaction of Ag(OPiv) (Piv = pivalate) with C<sub>6</sub>F<sub>5</sub>H in the absence of palladium complex. Silver pentafluorophenyl was shown to be capable of transmetalation at palladium and catalytic H/D exchange (Scheme 1, eq 4).<sup>34</sup> Ag(OPiv) has also been employed in the catalytic carboxylation of thiophene.<sup>41</sup>

We now turn to mechanisms of cross-coupling involving silver salts and palladium precatalysts. Such reactions are exemplified by the coupling of C<sub>6</sub>F<sub>5</sub>H and iodotoluene in the presence of Ag<sub>2</sub>CO<sub>3</sub>, PPh<sub>3</sub>, and Pd(OAc)<sub>2</sub> (Scheme 1, eq 5).<sup>22</sup> In one approach, supported by computational studies, there is direct formation of heterobimetallic Ag–Pd complexes;<sup>42</sup> although Ag–Pd clusters are known,<sup>43</sup> their role in C–H functionalization has not been established experimentally. In a second approach of more relevance here, silver(I) effects C–H bond activation as implicated by the ortho-selective H/D exchange mentioned above<sup>44</sup> and is followed by transmetalation. Several key observations support participation of silver in the second type of pathway. In addition to the evidence already cited (Scheme 1, eq 1–4), there is strong evidence from reaction kinetics, including kinetic isotope effects and rates dependent on concentrations of silver complex (Scheme 1, eq 6 and eq 7).<sup>33,39,24,23,45,46</sup> These studies are also supported by H/D exchange in the presence of both silver salts and palladium salts.

Notably, the catalytic cycles proposed in these papers address the use of alkyl carboxylic acids or acidic alcohols to displace the aryl group from silver, but the mechanism of

## Scheme 1. Involvement of Ag Salts in C–H Functionalization Chemistry



action of the silver carbonate was not clarified until 2021.<sup>40</sup> The cycles also implicate a requirement for sufficient

phosphine for coordination to both palladium and silver. In at least one proposed cycle, there is no mention that AgI may act as a sink for phosphine with potential implications for productive catalysis.<sup>24</sup> Furthermore, dynamic behavior involving phosphine ligand at both silver and palladium has not been explored, although it may have an important role in the reaction mechanism.

In this paper, we report the isolation of silver aryl and silver carbonate complexes derived directly from reaction of silver carbonate with a sterically hindered and commonly used phosphine, XPhos, and pentafluorobenzene (Scheme 1, eq 8). The aryl derivative can be formed directly or via isolation of the carbonate complex and is competent to form a cross-coupled product by reaction with a matching palladium phosphine complex. We also exemplify cross-coupling in the presence of catalytic quantities of the silver aryl complex without another silver source (Scheme 1, eq 9). These silver complexes undergo dynamic exchange with free phosphine. These studies lead to a proposal for a catalytic cycle in which the key steps have been verified stoichiometrically.

## RESULTS AND DISCUSSION

An initial survey of reactions of silver carbonate with pentafluorobenzene in acetonitrile or DMF in the presence of different phosphines at 60 °C was conducted to test for C–H bond activation. With PPh<sub>3</sub> and P(4-OMeC<sub>6</sub>H<sub>4</sub>)<sub>3</sub>, the <sup>19</sup>F NMR spectrum showed evidence of a new peak around δ –100 consistent with the ortho fluorine of an Ag(C<sub>6</sub>F<sub>5</sub>) complex,<sup>47</sup> but the <sup>31</sup>P{<sup>1</sup>H} NMR spectrum showed a singlet with no evidence for coupling to <sup>107</sup>Ag or <sup>109</sup>Ag at room temperature. Upon cooling to –100 °C, the sample with PPh<sub>3</sub> showed the presence of numerous species, each observed as a pair of concentric doublets with Ag–P coupling (Figure 1a). A more electron-withdrawing phosphine, P(furyl)<sub>3</sub>, did not react at all. The results show that use of PPh<sub>3</sub> as a ligand in C–H functionalization chemistry involving Ag may be complicated by the presence of multiple Ag–PPh<sub>3</sub> species. In contrast, the corresponding reaction with the strongly electron-donating and sterically hindered phosphine Xphos (Figure 1b) revealed a pair of doublets of triplets in the <sup>31</sup>P{<sup>1</sup>H} NMR spectrum at room temperature characteristic of a product **1** containing an Ag(C<sub>6</sub>F<sub>5</sub>)(Xphos) unit. We therefore selected this reaction for more detailed study. Without Xphos, only traces of an Ag(C<sub>6</sub>F<sub>5</sub>) product were formed.

Reaction of Ag<sub>2</sub>CO<sub>3</sub> with Xphos (2 equiv) and C<sub>6</sub>F<sub>5</sub>H (10 equiv) at 80 °C yielded **1** with 66% yield which crystallized on cooling (Scheme 2). The <sup>31</sup>P{<sup>1</sup>H} NMR spectrum recorded in CD<sub>2</sub>Cl<sub>2</sub> exhibited a pair of doublets of triplets at δ 13.0 (<sup>1</sup>J<sub>Ag<sup>107</sup>P</sub> = 444, <sup>1</sup>J<sub>Ag<sup>109</sup>P</sub> = 512, and <sup>3</sup>J<sub>PF</sub> = 3.0 Hz; Figure 1b). The <sup>19</sup>F NMR spectrum showed three resonances at δ –107.0 (m, 2F), –61.5 (t, J<sub>FF</sub> = 19.8 Hz, 1F), –163.3 (m, 2F). The <sup>31</sup>P–<sup>109</sup>Ag HMQC spectrum revealed the <sup>109</sup>Ag chemical shift as δ 713. The LIFDI mass spectrum showed a parent radical cation at *m/z* = 752.251 (<sup>107</sup>Ag isotopologue) with an isotope pattern consistent with monomeric Ag(C<sub>6</sub>F<sub>5</sub>)(Xphos).

The molecular structure of **1** determined by single-crystal X-ray crystallography confirmed that Ag(C<sub>6</sub>F<sub>5</sub>)(Xphos) is monomeric with Ag–C and Ag–P distances of 2.124(2) and 2.380(6) Å, respectively (Figure 2a). The coordination at Ag(I) is close to linear [C–Ag–P 168.86(6)°]. The distal ring of the biphenyl shows an approach between the ipso carbon C(7) and Ag [3.062(2) Å]. Such interactions are longer and hence weaker in our Ag complexes containing the Xphos

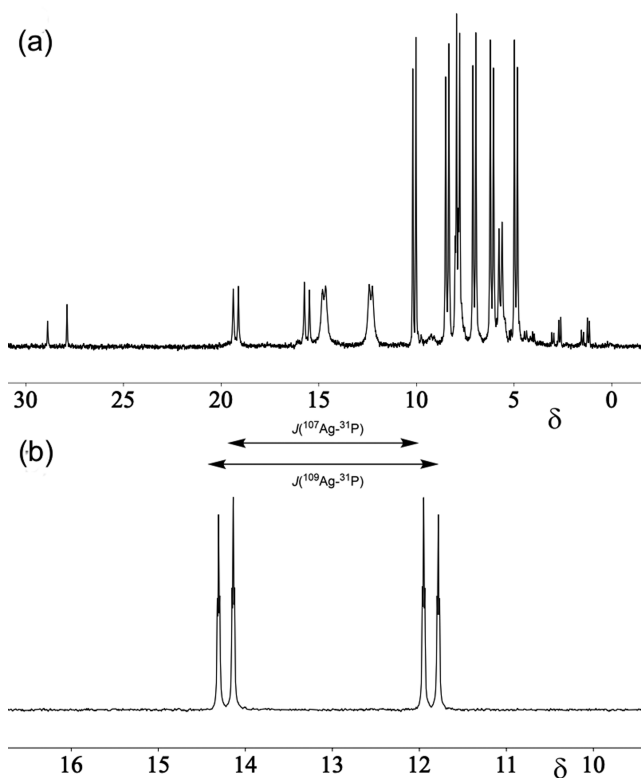
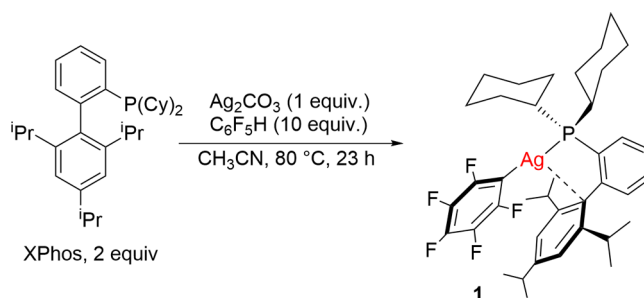


**Figure 1.** (a) <sup>31</sup>P{<sup>1</sup>H} NMR spectrum (202.5 MHz) at –100 °C in toluene-*d*<sub>8</sub>: CD<sub>2</sub>Cl<sub>2</sub> (20:80), following reaction of Ag<sub>2</sub>CO<sub>3</sub> with pentafluorobenzene in the presence of PPh<sub>3</sub>; (b) <sup>31</sup>P{<sup>1</sup>H} NMR spectrum at room temperature of **1** in CD<sub>2</sub>Cl<sub>2</sub> obtained by reaction of Ag<sub>2</sub>CO<sub>3</sub> with pentafluorobenzene in the presence of Xphos. (Cooling to –70 °C caused slight broadening but no new species were observed.)

## Scheme 2. Synthesis of Ag(C<sub>6</sub>F<sub>5</sub>)(Xphos) **1**



ligand than in related Pd(II) complexes [C(ipso)-Pd interactions ca. 2.45 Å].<sup>48</sup> The C<sub>6</sub>F<sub>5</sub> ring exhibits  $\pi$ -stacking with the adjacent molecule, with a centroid-to-centroid distance of 3.336(2) Å. Other Ag(C<sub>6</sub>F<sub>5</sub>)L (L = EtCN) complexes are known but have polymeric structures.<sup>49</sup> Hartwig et al. have isolated a monomeric silver fluoroaryl phosphine, Ag{C<sub>6</sub>H<sub>3</sub>(2-OMe)(4-F)}{P(o-anisyl)<sub>3</sub>}, with a similar structure to **1**.<sup>23</sup> Notably, their complex was not synthesized by a C–H bond activation process but by reaction of AgBr with the corresponding lithiated arene and phosphine.

The synthesis of **1** demonstrated that silver carbonate is capable of C–H bond activation with pentafluorobenzene. We now wanted to test whether this product was competent for cross-coupling under stoichiometric conditions. Employing a literature procedure,<sup>50</sup> we prepared the Pd(II) complex

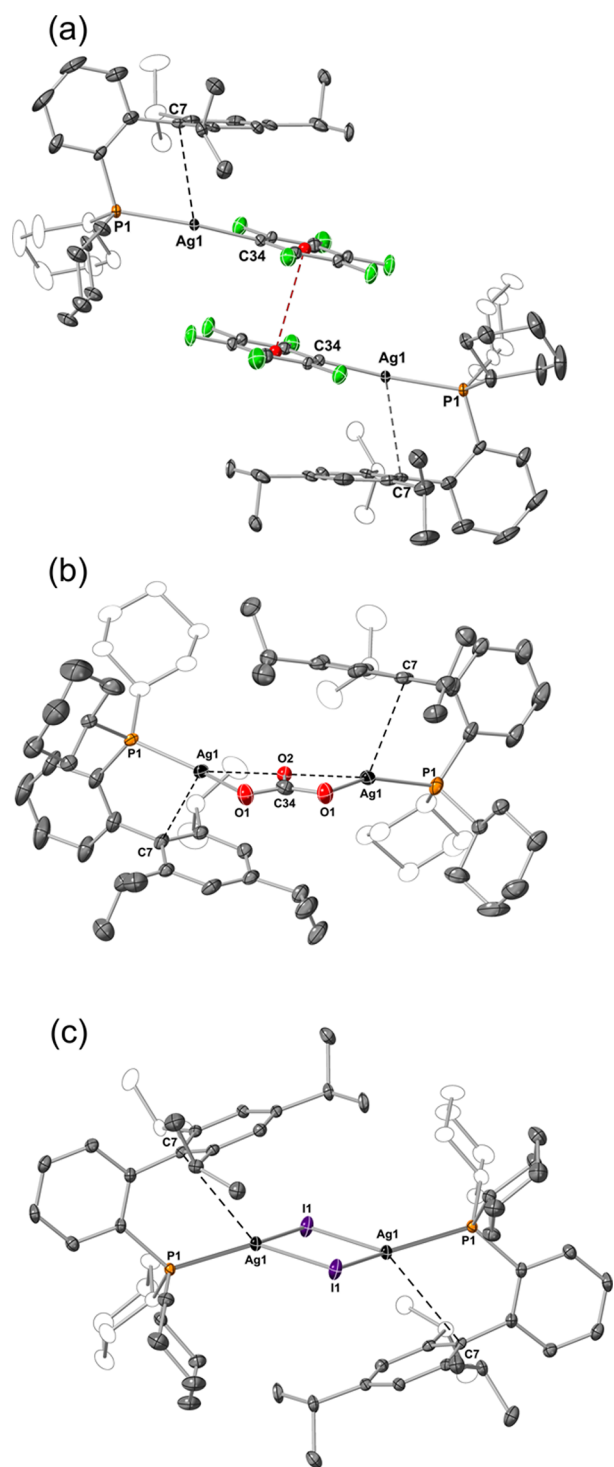
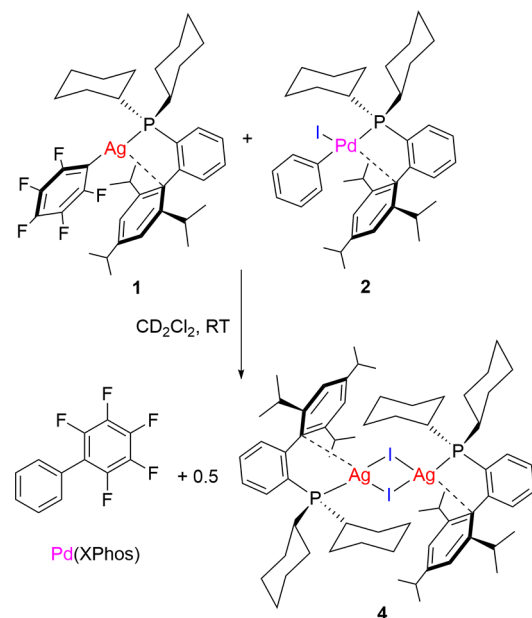


**Figure 2.** Molecular structures of (a)  $\text{Ag}(\text{C}_6\text{F}_5)(\text{Xphos})$ , **1**, (b)  $[\text{Ag}(\text{Xphos})_2](\mu\text{-}\kappa^2\text{-CO}_3)$ , **3**, (c)  $[\text{Ag}(\text{Xphos})_2](\mu\text{-I})$ , **4**. Hydrogen atoms are omitted; thermal ellipsoids are shown at the 50% level. Principal bond lengths and angles ( $\text{\AA}/\text{deg}$ ): **1**  $\text{Ag}(1)\text{-P}(1)$  2.3801(5),  $\text{Ag}(1)\text{-C}(34)$  2.124(2),  $\text{Ag}(1)\text{-C}(7)$  3.062(2),  $\text{C}(34)\text{-Ag}(1)\text{-P}(1)$  168.86(6); **3**  $\text{Ag}(1)\text{-P}(1)$  2.3328(9),  $\text{Ag}(1)\text{-O}(1)$  2.249(2),  $\text{Ag}(1)\text{-O}(2)$  2.3572(2),  $\text{Ag}(1)\text{-C}(34)$  2.678(2),  $\text{C}(34)\text{-O}(1)$  1.281(3),  $\text{C}(34)\text{-O}(2)$  1.303(5),  $\text{Ag}(1)\text{-C}(7)$  3.071(3),  $\text{P}(1)\text{-Ag}(1)\text{-C}(34)$  167.29(3),  $\text{P}(1)\text{-Ag}(1)\text{-O}(1)$  150.85(7),  $\text{C}(34)\text{-Ag}(1)\text{-O}(1)$  28.48(10),  $\text{O}(1)\text{-Ag}(1)\text{-O}(2)$  57.56(8),  $\text{Ag}(1)\text{-O}(2)\text{-Ag}(1')$  178.444(13); **4**  $\text{Ag}(1)\text{-I}(1)$  2.8357(3),  $\text{Ag}(1)\text{-P}(1)$  2.4255(7),  $\text{Ag}(1)\text{-C}(7)$  3.277(3),  $\text{I}(1)\text{-Ag}(1)\text{-I}(1')$  100.057(8),  $\text{P}(1)\text{-Ag}(1)\text{-I}(1)$  128.803(18),  $\text{P}(1)\text{-Ag}\text{-I}(1)\text{-I}(1')$  151.26(3).

$\text{PdI}(\text{C}_6\text{H}_5)(\text{Xphos})$  **2** analogous to  $\text{PdI}(\text{C}_6\text{H}_4\text{-F})(\text{Xphos})$  described previously [synthesized from  $(\text{COD})\text{Pd}(\text{CH}_2\text{SiMe}_3)_2$ ]<sup>51</sup> and reacted it stoichiometrically with  $\text{Ag}(\text{C}_6\text{F}_5)(\text{Xphos})$  in  $\text{CD}_2\text{Cl}_2$  at room temperature. Complete conversion to  $\text{Ph-C}_6\text{F}_5$ , as determined by NMR, occurred immediately (Scheme 3) with concomitant formation of  $[\text{AgI}(\text{Xphos})]_2$  (see below).

### Scheme 3. Stoichiometric Reaction of **1** and **2**



Furthermore, a mixture of **1** and **2** was prepared at  $-70\text{ }^\circ\text{C}$  in  $\text{CD}_2\text{Cl}_2$  and analyzed by NMR spectroscopy at  $-70$ ,  $-50$ , and  $-30\text{ }^\circ\text{C}$ . Formation of  $\text{Ph-C}_6\text{F}_5$  was observed from  $-30\text{ }^\circ\text{C}$ , but no transmetalation product was detected. For comparison, Hartwig et al. reacted  $\text{Ag}\{\text{C}_6\text{H}_3(2\text{-OMe})(4\text{-F})\}\{\text{P}(\text{o-anisyl})_3\}$  with  $\text{Pd}(\eta^3\text{-allyl-Ph})(\text{Opiv})\{\text{P}(\text{o-anisyl})_3\}$  at room temperature to obtain the cross-coupling product.<sup>23</sup> As a control, we attempted cross-coupling of **1** with iodotoluene but found no reaction up to  $130\text{ }^\circ\text{C}$  showing the requirement for Pd.<sup>52</sup> A further control reaction of  $\text{C}_6\text{F}_5\text{H}$  (10 equiv) with **2** without silver complexes or base showed no reaction at room temperature.

Since silver carbonate is highly insoluble in acetonitrile, we anticipated that the first step in the reaction with pentafluorobenzene and Xphos may be formation of a silver Xphos carbonate complex. Reaction of  $\text{Ag}_2\text{CO}_3$  with 2 equiv Xphos at  $80\text{ }^\circ\text{C}$  in MeCN yielded an amber solution from which brown crystals formed (yield 24%, Scheme 4). The product was identified as  $[\text{Ag}(\text{Xphos})_2](\mu\text{-}\kappa^2, \kappa^2\text{-CO}_3)$  **3** by

### Scheme 4. Synthesis and Reactivity of $[\text{Ag}(\text{Xphos})_2](\mu\text{-}\kappa^2\text{-CO}_3)$ **3**

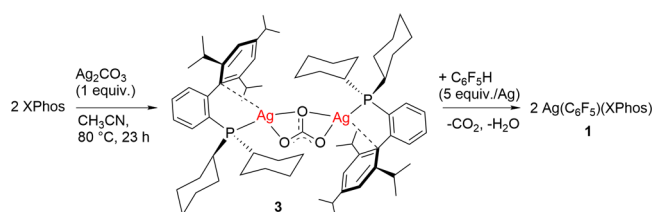
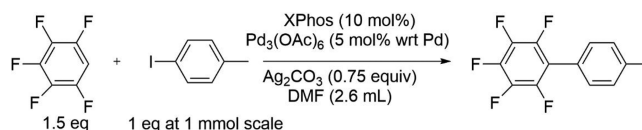


Table 1. Catalytic Reactions



variation of reaction conditions from standard above

entry	base or Ag source	ligand	Pd catalyst	temp (°C)	time (h)	NMR yield (isolated yield <sup>a</sup> )/%
1	standard	standard	standard	60	3	96 (84)
2	standard	standard	standard	20	23	75
3	standard	standard	no Pd(OAc) <sub>2</sub>	60	3	0
4	Ag <sub>2</sub> CO <sub>3</sub> (10 mol %)	standard	standard	60	3	21
5	Ag <sub>2</sub> CO <sub>3</sub> (10 mol %)	standard	standard	60	23	23
6	Ag <sub>2</sub> CO <sub>3</sub> (10 mol %) + K <sub>2</sub> CO <sub>3</sub> (0.75 equiv)	standard	standard	60	23	65
7	<b>1</b> (5 mol %) + K <sub>2</sub> CO <sub>3</sub> (0.75 equiv)	XPhos (5 mol %)	standard	60	23	57
8	Cs <sub>2</sub> CO <sub>3</sub>	standard	standard	60	3	<10
9	AgOAc	standard	standard	60	3	<10
10	standard	standard	intermediate Pd complex 2 (5 mol %)	20	23	63
11	standard	standard	intermediate Pd complex 2 (5 mol %)	60	3	86

<sup>a</sup>For methods of determining NMR yields, see the [Supporting Information](#); yield of isolated product obtained following chromatography on silica-gel.

NMR, CHN analysis, and X-ray crystallography.<sup>53</sup> The <sup>31</sup>P{<sup>1</sup>H} NMR spectrum recorded in C<sub>6</sub>D<sub>6</sub> showed a pair of doublets at δ 15.9 (<sup>1</sup>J<sub>Ag<sup>31</sup>P</sub> 634, <sup>1</sup>J<sub>Ag<sup>109</sup>P</sub> 731 Hz). The molecular structure of **3** (Figure 2b) shows a C<sub>2</sub>-symmetric complex with an Ag(μ-CO<sub>3</sub>)Ag unit that is almost planar with one oxygen bridging the two silver atoms [Ag(1)–O(2)–Ag(1)′ = 178.444(13)°] and the O(1) oxygens bonded to one silver each. The Ag–O(2) distances [2.3572(2) Å] are longer than the Ag–O(1) distances [2.249(2) Å]. The C(34)–O(1) and C(34)–O(2) distances are 1.281(3) and 1.303(5) Å, respectively. The sum of the angles around C(34) is 360.0(5), indicating trigonal planar coordination. The coordination at Ag is Y-shaped with O(1)–Ag–O(2) = 57.56(8)°. The ipso carbon on the distal benzene ring C(7) lies in close contact [3.071(3) Å] with the silver atom bearing the corresponding phosphorus. The CHN analysis shows one acetonitrile of crystallization per Ag, in agreement with the crystal structure. During the course of our work, Tlahuext-Aca and Hartwig reported two direct analogues of **3**, one with a P<sup>t</sup>BuXPhos ligand which was characterized crystallographically and one with a Johnphos ligand. Their <sup>31</sup>P–Ag coupling constants and metrics are similar to those of **3**.<sup>40</sup> The M<sub>2</sub>(μ-κ<sup>2</sup>,κ<sup>2</sup>-CO<sub>3</sub>) motif is quite common among first row transition metal carbonates from Mn to Zn and has also been observed for both Pd as well as Ag.<sup>54–61</sup>

Complex **3** reacts with pentafluorobenzene (5 equiv wrt Ag) in C<sub>6</sub>D<sub>6</sub> at room temperature to form **1** as the sole product containing the Ag(Xphos) moiety (Scheme 4). Benzene was used as the solvent since mass spectra show that **3** reacts with chlorine sources such as chloroform or dichloromethane to form [Ag(Xphos)]<sub>2</sub>(μ-Cl)<sub>2</sub>.

At this stage, we needed to establish Xphos as a suitable phosphine for catalytic C–H bond arylation. Pentafluorobenzene (1.5 equiv) was reacted with iodotoluene (1 equiv) with palladium(II) acetate (5 mol % wrt Pd, nitrite free Pd<sub>3</sub>(OAc)<sub>6</sub>),<sup>62</sup> Xphos (10 mol %), and Ag<sub>2</sub>CO<sub>3</sub> (0.75 equiv) in DMF at 60 °C for 3 h resulting in 96% conversion

(measured by both <sup>1</sup>H and <sup>19</sup>F NMR) to 4-MeC<sub>6</sub>H<sub>4</sub>–C<sub>6</sub>F<sub>5</sub> (Table 1, entry 1). Repetition of the reaction at room temperature resulted in 72% (<sup>1</sup>H) and 77% (<sup>19</sup>F) conversion after 23 h (entry 2). A fully worked-up reaction gave 84% isolated yield after 3 h reaction at 60 °C and separation by column chromatography on silica gel (entry 1), whereas a control reaction without palladium(II) acetate at 60 °C gave no product (entry 3). When the quantity of Ag<sub>2</sub>CO<sub>3</sub> was reduced to 0.1 equiv, the yield after 3 h was still 21%, but it barely increased after 23 h indicating that carbonate became limiting (entries 4 and 5). Use of a reduced quantity of Ag<sub>2</sub>CO<sub>3</sub> (10 mol %) with K<sub>2</sub>CO<sub>3</sub> (0.75 equiv) at 60 °C (23 h) restored the conversion to 65% (<sup>1</sup>H NMR, entry 6). When a similar experiment was performed with **1** (5 mol %) as the sole source of Ag(I) and K<sub>2</sub>CO<sub>3</sub> (0.75 equiv) at 60 °C (23 h), the conversion was 57% (entry 7). Replacement of Ag<sub>2</sub>CO<sub>3</sub> by either Cs<sub>2</sub>CO<sub>3</sub> or AgOAc gave conversions under 10% (entries 8 and 9).

These studies demonstrated that XPhos is active in catalytic cross-coupling as is **1**. Moreover, catalytic quantities of silver carbonate or **1** are sufficient in the presence of potassium carbonate. For comparison, Fagnou performed his C–H arylation reactions of pentafluorobenzene with PtBu<sub>2</sub>Me and K<sub>2</sub>CO<sub>3</sub> in DMA at 120 °C,<sup>9</sup> while Zhang et al. used PPh<sub>3</sub> and Ag<sub>2</sub>CO<sub>3</sub> in water at 70 °C for 16 h.<sup>22</sup> As mentioned above, Hartwig et al. demonstrated that their silver complex Ag{C<sub>6</sub>H<sub>3</sub>(2-OMe)(4-F)}{P(o-anisyl)<sub>3</sub>} is competent for cross-coupling in a stoichiometric reaction, but we did not find mention of its use in catalysis.<sup>23</sup>

The reaction of **1** with **2** yielded a silver iodide complex as a byproduct identified in the <sup>31</sup>P{<sup>1</sup>H} NMR (CD<sub>2</sub>Cl<sub>2</sub>) spectrum by a pair of concentric doublets. The same product [Ag(XPhos)(μ-I)]<sub>2</sub> **4** was formed by reaction of AgI with XPhos in CD<sub>2</sub>Cl<sub>2</sub> at room temperature for 24 h (<sup>31</sup>P{<sup>1</sup>H} NMR δ 16.89, pair of d, <sup>1</sup>J<sub>Ag<sup>31</sup>P</sub> = 542 Hz, <sup>1</sup>J<sub>Ag<sup>109</sup>P</sub> = 627 Hz, <sup>109</sup>Ag NMR δ 590) (Scheme 3). The LIFDI mass spectrum of **4** dissolved in dichloromethane shows *m/z* = 1295.459 (100%)

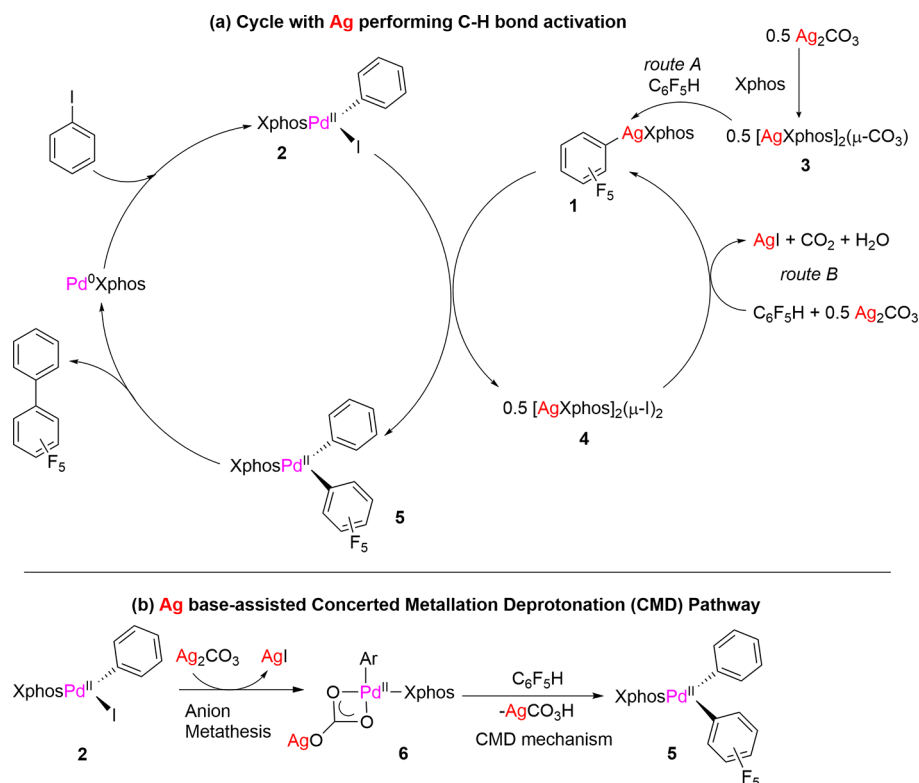


**Figure 3.** Proposed catalytic mechanisms. (a) Catalytic cycle with C–H bond activation by silver. (b) Silver carbonate acting as a base in the CMD mechanism. Note that **1** may be generated by reaction of  $C_6F_5H$  with **3** (route A) or by reaction with **4** (route B).

with isotope pattern consistent with two silver atoms (quoted for  $^{107}Ag^{109}Ag$ ) and a much smaller peak at  $m/z = 710.183$  (12%) for the monomer (quoted for  $^{107}Ag$ ). This spectrum suggests that this complex exists as a dimer in solution or as an equilibrium between monomer and dimer. The molecular structure determined crystallographically reveals a  $C_2$ -symmetric dimer with bridging iodides. The central  $Ag_2(\mu-I)_2$  unit is planar, but the phosphorus atoms lie out of that plane with a  $P(1)-Ag-I(1)-I(1')$  torsional angle of  $151.26(3)^\circ$ . Similar interactions between the distal benzene ring C(7) and the Ag atom [ $3.277(3)$  Å] are found to those in complexes **1** and **3** (Figure 2c).

Reaction of **4** with excess  $Ag_2CO_3$  (10 equiv) and a large excess of pentafluorobenzene (100 equiv) generates **1** and precipitates silver iodide (eq 1). As controls, we attempted to react  $C_6F_5H$  with **4** but found no reaction in either DMF at  $60^\circ C$  or  $CH_2Cl_2$  at room temperature. We also showed that **4** does not react with  $Ag_2CO_3$  in DMF at  $60^\circ C$ .

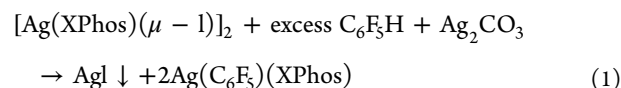
In addition, we investigated the acetate complex,  $Ag(OAc)(XPhos)$  **5**, formed by reaction of XPhos with  $AgOAc$  in  $CH_3CN$  at  $80^\circ C$ . Complex **5** exhibits a characteristic  $^{31}P\{^1H\}$  NMR resonance  $\delta$  16.55 (pair of d,  $^1J_{^{107}Ag^{31}P} = 643.9$  Hz,  $^1J_{^{109}Ag^{31}P} = 743.2$  Hz). The crystal structure of this complex revealed a monomer with  $\kappa^1$ -coordination of the acetate ligand (see the Supporting Information). In contrast to the behavior of **3**, the reaction of  $AgOAc$  in the presence of XPhos (1 equiv) and  $C_6F_5H$  (10 equiv) did not produce any **1** (none detected by  $^{31}P\{^1H\}$  or  $^{19}F\{^1H\}$  NMR spectroscopy) but generated **5** instead.

Further information was obtained from kinetic isotope effects measured both for the stoichiometric and for the catalytic reaction. For the stoichiometric reaction of **3** with  $C_6F_5H$  ( $C_6F_5D$ ), we employed a low temperature in order to

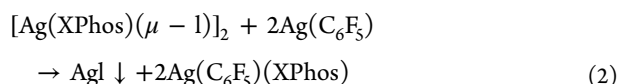
ensure a reasonable number of data points for the reaction with  $C_6F_5H$  which was monitored in situ by NMR. A temperature of  $-40^\circ C$  in toluene proved optimal, but, under these conditions, the reaction did not proceed to completion. A fast process lasting ca. 20 min was recorded, followed by a much slower process with KIEs were determined as  $3.7 \pm 0.3$  and  $0.91 \pm 0.01$ , respectively, for the fast and slow processes. The KIE for the fast process is consistent with rate-determining C–H bond breaking in this reaction of this silver–carbonate complex. The product of reaction was  $4-MeC_6H_4-C_6F_5$  as usual, but nature of the slow process has not been determined.

In separate experiments, catalytic reactions were conducted under the standard conditions (see Table 1) at  $60^\circ C$ , and the products were analyzed by NMR at different reaction times. The KIE for the catalytic reaction was determined from the initial rates of reaction as  $4.5 \pm 0.8$ .

The recycling of XPhos was clarified by synthesizing  $Ag(C_6F_5)$  independently.<sup>49</sup> With the authentic sample of  $Ag(C_6F_5)$ , we confirmed that this species is formed in low yield (ca. 10%) upon reaction of  $Ag_2CO_3$  with pentafluorobenzene in the absence of XPhos. Additionally, as expected,  $Ag(C_6F_5)$  reacts rapidly with XPhos at room temperature to form **1**. Of particular interest is the observation that  $Ag(C_6F_5)$  reacts with **4** to form **1** and a precipitate of AgI (eq 2). The reactions of eq 1 and eq 2 provide opportunities to recycle phosphine in the catalytic reactions and explain how AgI may be formed as a final product. The reactions of  $Ag(C_6F_5)$  in  $CD_3CN$  and **1** in  $CD_2Cl_2$  with  $D_2O$  at room temperature both give  $C_6F_5D$ ; however, the reaction of **1** takes several days.

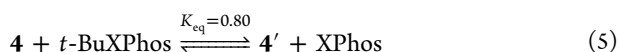
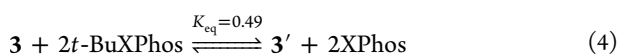
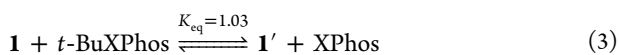






The observations described above lead us to postulate the catalytic cycle in Figure 3a in which Ag performs C–H bond activation and Pd effects cross-coupling.<sup>63</sup> According to this cycle, PdI(C<sub>6</sub>H<sub>5</sub>)(XPhos) (**2**, 5 mol %) should act as a catalyst for the coupling of 4-iodotoluene with pentafluorobenzene in the presence of 5 mol % XPhos and Ag<sub>2</sub>CO<sub>3</sub> (0.75 equiv). On testing this hypothesis at room temperature, we obtained yields of tol–C<sub>6</sub>F<sub>5</sub> after 3 and 23 h of 6% and 63%, respectively; at 60 °C, they increase to 86% and 100%, respectively (Table 1, entries 10, 11). As expected, Ph–C<sub>6</sub>F<sub>5</sub> was also formed with yield 5% wrt tol–C<sub>6</sub>F<sub>5</sub>. This cycle is also supported by the catalytic reaction with 5 mol % **1** as the source of Ag(I) (entry 7). All the steps in the catalytic cycle have been verified stoichiometrically other than the formation and reaction of a Pd(0) species which is not expected to be detectable under our conditions (oxidative addition being fast). The cycle shows two alternative routes from Ag<sub>2</sub>CO<sub>3</sub> to form **1** reflecting the experiments described above. The experiments with reduced Ag<sub>2</sub>CO<sub>3</sub> with and without K<sub>2</sub>CO<sub>3</sub> confirm that carbonate is required for the C–H bond activation acting as the Brønsted base. The postulated alternative mechanism invoking Ag(I) as a base and Pd as involved in a CMD process is expected to involve Ag–carbonato–Pd **6** as an intermediate (Figure 3b).

A further group of experiments illuminates the ability of XPhos to undergo exchange, thereby ensuring that its supply is not exhausted prematurely. To test the lability of the silver complexes, **1**, **3**, and **4**, we reacted each of them with *t*BuXPhos, in which the isopropyl groups are replaced by *t*butyl groups. Addition of *t*BuXPhos (1 equiv) to **1** resulted in immediate formation of a new silver phosphine species at room temperature (<sup>31</sup>P NMR δ 38.5, pair of dt, <sup>1</sup>J<sub>Ag<sup>31</sup>P</sub> = 448 Hz, <sup>1</sup>J<sub>Ag<sup>31</sup>P</sub> = 516 Hz, and J<sub>PF</sub> = 2.7 Hz, compared to free ligand at δ 21.4) in 50% conversion consistent with exchange of the phosphine to form the *t*BuXPhos analogue Ag(C<sub>6</sub>F<sub>5</sub>)-(*t*BuXPhos) **1'**. Assuming this is an equilibrium reaction, we deduce an equilibrium constant of 1.03 ± 0.05 for formation of **1'** (see eq 3). Similar behavior was observed for **3** and **4** (eqs 4 and 5).<sup>64</sup>



**4** and **4'** assumed to be monomers in solution for calcn of  $K_{\text{eq}}$

The experiments with *t*BuXPhos encouraged us to test for exchange between Ag(XPhos) complexes and free XPhos. A <sup>31</sup>P–<sup>31</sup>P EXSY spectrum of a sample of **1** in the presence of XPhos (5 equiv, mixing time 2 s) revealed cross peaks consistent with intermolecular exchange between **1** and XPhos on the time scale of seconds. Since there is exchange between two sites only, 1D-EXSY<sup>65</sup> is suitable and is more economical in instrument time. 1D-EXSY experiments on **1** in the presence of a range of concentrations of free XPhos were conducted in CD<sub>2</sub>Cl<sub>2</sub> yielding evidence that the rate of exchange  $V_{\text{ex}}$  depends linearly on [XPhos] (where  $V_{\text{ex}} = k_{\text{obs}}[\text{XPhos}][\mathbf{1}]/$

([XPhos] + [**1**]) and  $k_{\text{obs}}$  is derived from the variation of fractional integration of [XPhos] with mixing time  $\tau_{\text{m}}$  on selective excitation of **1**).<sup>66,67</sup> Variable temperature 1D-EXSY experiments with excess XPhos (5 equiv) were performed in C<sub>6</sub>D<sub>6</sub> in order to access a suitable temperature range to determine of activation parameters yielding  $\Delta H^\ddagger = 40.0 \pm 1.2$  kJ/mol and  $\Delta S^\ddagger = -162 \pm 4$  J/K mol, providing clear evidence for associative exchange.

## CONCLUSION

In conclusion, silver carbonate is capable of C–H bond activation of pentafluorobenzene in the presence of XPhos yielding discrete and well-defined Ag(C<sub>6</sub>F<sub>5</sub>)(XPhos) **1**. This reaction can also be carried out stepwise yielding first the carbonate complex [Ag(XPhos)]<sub>2</sub>(μ-κ<sup>2</sup>,κ<sup>2</sup>-CO<sub>3</sub>) **3** and then **1**. A third silver complex has been isolated by reaction of AgI with XPhos, [Ag(XPhos)(μ-I)]<sub>2</sub> **4**. All three silver complexes have been characterized in solution and crystallographically. They are all labile with respect to associative exchange with free XPhos or with *t*BuXPhos and all participate in cross-coupling. The viability of **1** for cross-coupling has been demonstrated stoichiometrically by reaction of **1** with PdI(C<sub>6</sub>H<sub>5</sub>)(XPhos) **2** yielding **4** as a byproduct; this reaction even occurs at –30 °C. Catalytic cross-coupling of 4-iodotoluene to pentafluorobenzene may be achieved in the presence of palladium(II) acetate, XPhos, and silver carbonate at 60 °C or at room temperature. Catalytic cross-coupling also occurs with **2** as the catalyst in the presence of Ag<sub>2</sub>CO<sub>3</sub> and a reduced quantity of XPhos. Catalytic quantities of silver in the form of Ag<sub>2</sub>CO<sub>3</sub> or **1** are active in conjunction with potassium carbonate as the stoichiometric base. A catalytic cycle involving C–H bond activation at silver has been proposed consistent with the set of tested stoichiometric reactions. It is now clear how the phosphine solubilizes silver carbonate and silver iodide; however, the phosphine is labile enough to allow precipitation of silver iodide as the final byproduct of catalysis. We stress that the study does not exclude competing C–H bond activation steps at palladium or a role for higher-order catalyst species. Nevertheless, the evidence for the C–H bond activation abilities of silver carbonate in the presence of a suitable phosphine is now conclusive and is shown to involve well-defined, soluble, mononuclear, and dinuclear silver phosphine complexes that are active in cross-coupling reactions with palladium complexes.

## ASSOCIATED CONTENT

### Supporting Information

The Supporting Information is available free of charge at <https://pubs.acs.org/doi/10.1021/acs.organomet.2c00063>.

Synthetic procedures, catalytic reactions, stoichiometric reactions, phosphine-exchange experiments, EXSY experiments, kinetic isotope effect experiments, crystallographic data, characterization data including NMR spectra (PDF)

### Accession Codes

CCDC 2110192– 2110194 and 2160367 contain the supplementary crystallographic data for this paper. These data can be obtained free of charge via [www.ccdc.cam.ac.uk/data\\_request/cif](http://www.ccdc.cam.ac.uk/data_request/cif), or by emailing [data\\_request@ccdc.cam.ac.uk](mailto:data_request@ccdc.cam.ac.uk), or by contacting The Cambridge Crystallographic Data Centre, 12 Union Road, Cambridge CB2 1EZ, UK; fax: + 44 1223 336033.

## AUTHOR INFORMATION

### Corresponding Authors

Ian J. S. Fairlamb – Department of Chemistry, University of York, York YO10 5DD, U.K.; [orcid.org/0000-0002-7555-2761](https://orcid.org/0000-0002-7555-2761); Email: [ian.fairlamb@york.ac.uk](mailto:ian.fairlamb@york.ac.uk)

Robin N. Perutz – Department of Chemistry, University of York, York YO10 5DD, U.K.; [orcid.org/0000-0001-6286-0282](https://orcid.org/0000-0001-6286-0282); Email: [robin.perutz@york.ac.uk](mailto:robin.perutz@york.ac.uk)

### Authors

Gayathri Athavan – Department of Chemistry, University of York, York YO10 5DD, U.K.

Theo F. N. Tanner – Department of Chemistry, University of York, York YO10 5DD, U.K.; [orcid.org/0000-0001-7563-9325](https://orcid.org/0000-0001-7563-9325)

Adrian C. Whitwood – Department of Chemistry, University of York, York YO10 5DD, U.K.; [orcid.org/0000-0002-5132-5468](https://orcid.org/0000-0002-5132-5468)

Complete contact information is available at:

<https://pubs.acs.org/10.1021/acs.organomet.2c00063>

### Notes

The authors declare no competing financial interest.

## ACKNOWLEDGMENTS

We are grateful to the Wild Fund of the University of York for a scholarship for G.A., to the University of York for funding a Ph.D. studentship for TFNT and laboratory equipment, and to Professor Simon Duckett for recording the  $^{31}\text{P}$ - $^{109}\text{Ag}$  NMR spectra.

## DEDICATION

We dedicate this paper to Professor Maurice Brookhart in admiration for his achievements in organometallic chemistry.

## REFERENCES

- (1) Baudoin, O. Multiple Catalytic C-H Bond Functionalization for Natural Product Synthesis. *Angew. Chem. Int. Ed* **2020**, *59*, 17798–17809.
- (2) Yu, C. J.; Sanjose-Orduna, J.; Patureau, F. W. W.; Perez-Temprano, M. H. Emerging unconventional organic solvents for C-H bond and related functionalization reactions. *Chem. Soc. Rev.* **2020**, *49*, 1643–1652.
- (3) Rej, S.; Ano, Y.; Chatani, N. Bidentate Directing Groups: An Efficient Tool in C-H Bond Functionalization Chemistry for the Expedient Construction of C-C Bonds. *Chem. Rev.* **2020**, *120*, 1788–1887.
- (4) Mihai, M. T.; Genov, G. R.; Phipps, R. J. Access to the meta position of arenes through transition metal catalyzed C-H bond functionalisation: a focus on metals other than palladium. *Chem. Soc. Rev.* **2018**, *47*, 149–171.
- (5) Ping, L.; Chung, D. S.; Bouffard, J.; Lee, S. G. Transition metal-catalyzed site- and regio-divergent C-H bond functionalization. *Chem. Soc. Rev.* **2017**, *46*, 4299–4328.
- (6) Ackermann, L. Carboxylate-Assisted Transition-Metal-Catalyzed C-H Bond Functionalizations: Mechanism and Scope. *Chem. Rev.* **2011**, *111*, 1315–1345.
- (7) Carrow, B. P.; Sampson, J.; Wang, L. Base-Assisted C-H Bond Cleavage in Cross-Coupling: Recent Insights into Mechanism, Speciation, and Cooperativity. *Isr. J. Chem.* **2020**, *60*, 230–258.
- (8) Eisenstein, O.; Milani, J.; Perutz, R. N. Selectivity of C-H Activation and Competition between C-H and C-F Bond Activation at Fluorocarbons. *Chem. Rev.* **2017**, *117*, 8710–8753.
- (9) Lafrance, M.; Rowley, C. N.; Woo, T. K.; Fagnou, K. Catalytic intermolecular direct arylation of perfluorobenzenes. *J. Am. Chem. Soc.* **2006**, *128*, 8754–8756.
- (10) Cao, M. N.; Wu, D. S.; Su, W. P.; Cao, R. Palladium nanocrystals stabilized by cucurbit[6]uril as efficient heterogeneous catalyst for direct C-H functionalization of polyfluoroarenes. *J. Catal.* **2015**, *321*, 62–69.
- (11) Ma, X. W.; Liu, Y.; Liu, P.; Xie, J. W.; Dai, B.; Liu, Z. Y. Palladium-catalyzed direct arylation of polyfluoroarene and facile synthesis of liquid crystal compounds. *Appl. Organomet. Chem.* **2014**, *28*, 180–185.
- (12) Garcia-Cuadrado, D.; Braga, A. A. C.; Maseras, F.; Echavarren, A. M. Proton abstraction mechanism for the palladium-catalyzed intramolecular arylation. *J. Am. Chem. Soc.* **2006**, *128*, 1066–1067.
- (13) Gorelsky, S. I.; Lapointe, D.; Fagnou, K. Analysis of the concerted metalation-deprotonation mechanism in palladium-catalyzed direct arylation across a broad range of aromatic substrates. *J. Am. Chem. Soc.* **2008**, *130*, 10848–10849.
- (14) Lafrance, M.; Lapointe, D.; Fagnou, K. Mild and efficient palladium-catalyzed intramolecular direct arylation reactions. *Tetrahedron* **2008**, *64*, 6015–6020.
- (15) Pascual, S.; de Mendoza, P.; Braga, A. A. C.; Maseras, F.; Echavarren, A. M. Bidentate phosphines as ligands in the palladium-catalyzed intramolecular arylation: the intermolecular base-assisted proton abstraction mechanism. *Tetrahedron* **2008**, *64*, 6021–6029.
- (16) Davies, D. L.; Donald, S. M. A.; Macgregor, S. A. Computational study of the mechanism of cyclometalation by palladium acetate. *J. Am. Chem. Soc.* **2005**, *127*, 13754–13755.
- (17) Davies, D. L.; Macgregor, S. A.; McMullin, C. L. Computational Studies of Carboxylate-Assisted C-H Activation and Functionalization at Group 8–10 Transition Metal Centers. *Chem. Rev.* **2017**, *117*, 8649–8709.
- (18) Pla, D.; Gomez, M. Metal and metal oxide nanoparticles: A lever for C-H functionalization. *ACS Catal.* **2016**, *6*, 3537–3552.
- (19) Reay, A. J.; Fairlamb, I. J. S. Catalytic C-H bond functionalisation chemistry: the case for quasi-heterogeneous catalysis. *Chem. Commun.* **2015**, *51*, 16289–16307.
- (20) Fairlamb, I. J. S.; Scott, N. W. J. Pd Nanoparticles in C-H Activation and Cross-coupling Catalysis. *Top. Organometal. Chem.* **2020**, *66*, 171–205.
- (21) Reay, A. J.; Neumann, L. K.; Fairlamb, I. J. S. Catalyst efficacy of homogeneous and heterogeneous palladium catalysts in the direct arylation of common heterocycles. *Synlett* **2016**, *27*, 1211–1216.
- (22) Chen, F.; Min, Q. Q.; Zhang, X. G. Pd-Catalyzed direct arylation of polyfluoroarenes on water under mild conditions using  $\text{PPh}_3$  ligand. *J. Org. Chem.* **2012**, *77*, 2992–2998.
- (23) Lee, S. Y.; Hartwig, J. F. Palladium-Catalyzed, Site-Selective Direct Allylation of Aryl C-H Bonds by Silver-Mediated C-H Activation: A Synthetic and Mechanistic Investigation. *J. Am. Chem. Soc.* **2016**, *138*, 15278–15284.
- (24) Whitaker, D.; Bures, J.; Larrosa, I. Ag(I)-Catalyzed C-H Activation: The Role of the Ag(I) Salt in Pd/Ag-Mediated C-H Arylation of Electron-Deficient Arenes. *J. Am. Chem. Soc.* **2016**, *138*, 8384–8387.
- (25) Bowmaker, G. A.; Effendy, Hanna, J. V.; Healy, P. C.; King, S. P.; Pettinari, C.; Skelton, B. W.; White, A. H. Solution and mechanochemical syntheses, and spectroscopic and structural studies in the silver(I) (bi-)carbonate: triphenylphosphine system. *Dalton Trans* **2011**, *40*, 7210–7218.
- (26) Goel, R. G.; Pilon, P. Tri-Tert-Butylphosphine Complexes of Silver(I) - Preparation, Characterization, and Spectral Studies. *Inorg. Chem.* **1978**, *17*, 2876–2879.
- (27) Muettterties, E. L.; Alegranti, C. W. Solution Structure and Kinetic Study of Metal-Phosphine and Metal-Phosphite Complexes 0.1. Silver(I) System. *J. Am. Chem. Soc.* **1972**, *94*, 6386–6391.
- (28) Bachman, R. E.; Andretta, D. F. Metal-ligand bonding in coinage metal-phosphine complexes: The synthesis and structure of some low-coordinate silver(I)-phosphine complexes. *Inorg. Chem.* **1998**, *37*, 5657–5663.

- (29) Patmore, N. J.; Hague, C.; Cotgreave, J. H.; Mahon, M. F.; Frost, C. G.; Weller, A. S. Silver phosphanes partnered with carborane monoanions: Synthesis, structures and use as highly active lewis acid catalysts in a hetero-Diels-Alder reaction. *Chem. - Eur. J.* **2002**, *8*, 2088–2098.
- (30) Keller, S.; Camenzind, T. N.; Abraham, J.; Prescimone, A.; Haussinger, D.; Constable, E. C.; Housecroft, C. E. Self-assembly of heteroleptic dinuclear silver(I) complexes bridged by bis-(diphenylphosphino)ethyne. *Dalton Trans* **2018**, *47*, 946–957.
- (31) Bay, K. L.; Yang, Y. F.; Houk, K. N. Multiple roles of silver salts in palladium-catalyzed C-H activations. *J. Organomet. Chem.* **2018**, *864*, 19–25.
- (32) Mudarra, A. L.; Martinez de Salinas, S.; Perez-Temprano, M. H. Beyond the traditional roles of Ag in catalysis: the transmetalating ability of organosilver(I) species in Pd-catalysed reactions. *Org. Biomol. Chem.* **2019**, *17*, 1655–1667.
- (33) Panigrahi, A.; Whitaker, D.; Vitorica-Yrezabal, I. J.; Larrosa, I. Ag/Pd Cocatalyzed Direct Arylation of Fluoroarene Derivatives with Aryl Bromides. *ACS Catal.* **2020**, *10*, 2100–2107.
- (34) Lotz, M. D.; Camasso, N. M.; Canty, A. J.; Sanford, M. S. Role of Silver Salts in Palladium-Catalyzed Arene and Heteroarene C-H Functionalization Reactions. *Organometallics* **2017**, *36*, 165–171.
- (35) Shimoyama, Y.; Kuwabara, J.; Kanbara, T. Mechanistic Study of Pd/Ag Dual-Catalyzed Cross-Dehydrogenative Coupling of Perfluoroarenes with Thiophenes. *ACS Catal.* **2020**, *10*, 3390–3397.
- (36) Li, W. P.; Yuan, D. D.; Wang, G. Q.; Zhao, Y.; Xie, J.; Li, S. H.; Zhu, C. J. Cooperative Au/Ag Dual-Catalyzed Cross-Dehydrogenative Biaryl Coupling: Reaction Development and Mechanistic Insight. *J. Am. Chem. Soc.* **2019**, *141*, 3187–3197.
- (37) Hu, G. Q.; Li, E. C.; Zhang, H. H.; Huang, W. Ag(I)-Mediated hydrogen isotope exchange of mono-fluorinated (hetero)arenes. *Org. Biomol. Chem.* **2020**, *18*, 6627–6633.
- (38) Wilkinson, L. A.; Pike, J. A.; Walton, J. W. C-H Activation of pi-Arene Ruthenium Complexes. *Organometallics* **2017**, *36*, 4376–4381.
- (39) Tlahuext-Aca, A.; Lee, S. Y.; Sakamoto, S.; Hartwig, J. F. Direct Arylation of Simple Arenes with Aryl Bromides by Synergistic Silver and Palladium Catalysis. *ACS Catal.* **2021**, *11*, 1430–1434.
- (40) Tlahuext-Aca, A.; Hartwig, J. F. Site-Selective Silver-Catalyzed C-H Bond Deuteration of Five-Membered Aromatic Heterocycles and Pharmaceuticals. *ACS Catal.* **2021**, *11*, 1119–1127.
- (41) Lee, M.; Hwang, Y. K.; Kwak, J. Ag(I)-Catalyzed C-H Carboxylation of Thiophene Derivatives. *Organometallics* **2021**, *40*, 3136–3144.
- (42) Bhaskararao, B.; Singh, S.; Anand, M.; Verma, P.; Prakash, P.; Athira, C.; Malakar, S.; Schaefer, H. F.; Sunoj, R. B. Is silver a mere terminal oxidant in palladium catalyzed C-H bond activation reactions? *Chem. Sci.* **2020**, *11*, 208–216.
- (43) Kozitsyna, N. Y.; Nefedov, S. E.; Klyagina, A. P.; Markov, A. A.; Dobrokhotova, Z. V.; Velikodny, Y. A.; Kochubey, D. I.; Zyubina, T. S.; Gekhman, A. E.; Vargaftik, M. N.; Moiseev, I. I. Novel heterometallic palladium-silver complex. *Inorg. Chim. Acta* **2011**, *370*, 382–387.
- (44) Clot, E.; Megret, C.; Eisenstein, O.; Perutz, R. N. Exceptional Sensitivity of Metal-Aryl Bond Energies to ortho-Fluorine Substituents: Influence of the Metal, the Coordination Sphere, and the Spectator Ligands on M-C/H-C Bond Energy Correlations. *J. Am. Chem. Soc.* **2009**, *131*, 7817–7827.
- (45) Colletto, C.; Panigrahi, A.; Fernandez-Casado, J.; Larrosa, I. Ag(I)-C-H Activation Enables Near-Room-Temperature Direct alpha-Arylation of Benzo b thiophenes. *J. Am. Chem. Soc.* **2018**, *140*, 9638–9643.
- (46) Batuecas, M.; Luo, J. F.; Gergelitsova, I.; Kramer, K.; Whitaker, D.; Vitorica-Yrezabal, I. J.; Larrosa, I. Catalytic Asymmetric C-H Arylation of (eta(6)-Arene)Chromium Complexes: Facile Access to Planar-Chiral Phosphines. *ACS Catal.* **2019**, *9*, 5268–5278.
- (47) Belt, S. T.; Helliwell, M.; Jones, W. D.; Partridge, M. G.; Perutz, R. N. Eta(2)-Coordination and C-F Activation of Hexafluorobenzene by Cyclopentadienylrhodium and Cyclopentadienyliridium Complexes. *J. Am. Chem. Soc.* **1993**, *115*, 1429–1440.
- (48) Bruno, N. C.; Tudge, M. T.; Buchwald, S. L. Design and preparation of new palladium precatalysts for C-C and C-N cross-coupling reactions. *Chem. Sci.* **2013**, *4*, 916–920.
- (49) Tyrre, W.; Wickleder, M. S. Silver compounds in synthetic chemistry. 1 - A facile preparative route for pentafluorophenylsilver, AgC<sub>6</sub>F<sub>5</sub> and its use as an oxidative pentafluorophenyl group transfer reagent in reactions with group 12 to 16 elements - the single crystal structure of AgC<sub>6</sub>F<sub>5</sub>. EtCN, the first arylsilver derivative crystallising in infinite chains. *Z. Anorg. Allg. Chem.* **2002**, *628*, 1841–1847.
- (50) Milner, P. J.; Maimone, T. J.; Su, M. J.; Chen, J. H.; Muller, P.; Buchwald, S. L. Investigating the Dearomative Rearrangement of Biaryl Phosphine-Ligated Pd(II) Complexes. *J. Am. Chem. Soc.* **2012**, *134*, 19922–19934.
- (51) Wagschal, S.; Perego, L. A.; Simon, A.; Franco-Espejo, A.; Tocqueville, C.; Albanese-Walker, J.; Jutand, A.; Grimaud, L. Formation of XPhos-Ligated Palladium(0) Complexes and Reactivity in Oxidative Additions. *Chem. - Eur. J.* **2019**, *25*, 6980–6987.
- (52) Ag(C<sub>6</sub>F<sub>5</sub>) reacts with iodobenzene at 110 °C. Sun, K. K.; Miller, W. T. Perfluorophenylsilver. *J. Am. Chem. Soc.* **1970**, *92*, 6985–6987.
- (53) Soltys-Brzostek, K.; Terlecki, M.; Sokolowski, K.; Lewinski, J. Chemical fixation and conversion of CO<sub>2</sub> into cyclic and cage-type metal carbonates. *Coord. Chem. Rev.* **2017**, *334*, 199–231.
- (54) Sattler, W.; Parkin, G. Structural characterization of zinc bicarbonate compounds relevant to the mechanism of action of carbonic anhydrase. *Chem. Sci.* **2012**, *3*, 2015–2019.
- (55) Dietrich, J.; Heinemann, F. W.; Schrodt, A.; Schindler, S. A new carbonate bridged dinuclear zinc complex with tripodal amine ligands. *Inorg. Chim. Acta* **1999**, *288*, 206–209.
- (56) Shopov, D. Y.; Sharninghausen, L. S.; Sinha, S. B.; Borowski, J. E.; Mercado, B. Q.; Brudvig, G. W.; Crabtree, R. H. Synthesis of pyridine-alkoxide ligands for formation of polynuclear complexes. *New J. Chem.* **2017**, *41*, 6709–6719.
- (57) Roy, L.; Al-Afyouni, M. H.; DeRoshia, D. E.; Mondal, B.; DiMucci, I. M.; Lancaster, K. M.; Shearer, J.; Bill, E.; Brennessel, W. W.; Neese, F.; Ye, S. F.; Holland, P. L. Reduction of CO<sub>2</sub> by a masked two-coordinate cobalt(I) complex and characterization of a proposed oxodicobalt(II) intermediate. *Chem. Sci.* **2019**, *10*, 918–929.
- (58) Stewart, J. A.; McKeown, P.; Driscoll, O. J.; Mahon, M. F.; Ward, B. D.; Jones, M. D. Tuning the Thiolen: Al(III) and Fe(III) Thiolen Complexes for the Ioselective ROP of rac-Lactide. *Macromolecules* **2019**, *52*, 5977–5984.
- (59) Kwak, C. H.; Kim, J. Preparation, characterization and X-ray structure of {[ (3,2,3-tet)Ni(mu-CO<sub>3</sub>)Ni(3,2,3-tet) ] [(3,2,3-tet)Cu]}-(ClO<sub>4</sub>)<sub>4</sub>: a heteronuclear trimetallic complex containing hydrogen bonds. *Inorg. Chem. Commun.* **2000**, *3*, 550–552.
- (60) Avdeeva, V. V.; Dziova, A. E.; Polyakova, I. N.; Malinina, E. A.; Goeva, L. V.; Kuznetsov, N. T. Copper(I), copper(II), and heterovalent copper(I,II) complexes with 1,10-phenanthroline and the closo-decaborate anion. *Inorg. Chim. Acta* **2015**, *430*, 74–81.
- (61) Muller, A.; Holzapfel, C. W. mu-carbonato bis{2'-di-tert-butylphosphanyl)biphenyl-2-yl}palladium(II) dichloromethane. *Acta Crystallogr. Sect. E: Crystallogr. Commun.* **2012**, *68*, m1574–m1575.
- (62) Bajwa, S. E.; Storr, T. E.; Hatcher, L. E.; Williams, T. J.; Baumann, C. G.; Whitwood, A. C.; Allan, D. R.; Teat, S. J.; Raitby, P. R.; Fairlamb, I. J. S. On the appearance of nitrite anion in [PdX(OAc)L<sub>2</sub>] and [Pd(X)(C<sup>^</sup>N)L] syntheses (X = OAc or NO<sub>2</sub>): photocrystallographic identification of metastable Pd(eta(1)-ONO)-(C<sup>^</sup>N)PPh<sub>3</sub>. *Chem. Sci.* **2012**, *3*, 1656–1661.
- (63) Interactions between arenes and silver(I) are well-known and probably precede C-H activation. Lindeman, S.; Rahore, R.; Kochi, J. K. Silver(I) Complexation of (Poly)aromatic Ligands. Structural Criteria for Depth Penetration into cis-Stilbenoid Cavities. *Inorg. Chem.* **2000**, *39*, 5707–5716.
- (64) **3** was treated as dinuclear, but **4** was considered mononuclear for calculation of equilibrium constants. Since **3** and **4** are dinuclear, we might expect separate resonances for the complex with one XPhos and one tBuXPhos, but they were not observed. At low temperature,

the resonances of **1** broadened while those of **1'** remained sharp, consistent with fluxionality.

(65) Perrin, C. L.; Engler, R. E. Accurate rate constants for chemical exchange from improved weighted linear-least-squares analysis of multiple 1D-EXSY data. *J. Magn. Reson., Ser. A* **1996**, *123*, 188–195.

(66) Wilkins, R. G. *Kinetics and mechanism of reactions of transition metal complexes*, 2nd ed.; VCH: Weinheim, 1992.

(67) McKay, H. A. C. Kinetics of some exchange reactions of the type  $RI + I^{*-}$  reversible arrow  $RI^* + I^-$  in alcoholic solution. *J. Am. Chem. Soc.* **1943**, *65*, 702–706.

## Appendix B – NMR Spectroscopic Data for Synthesised Compounds

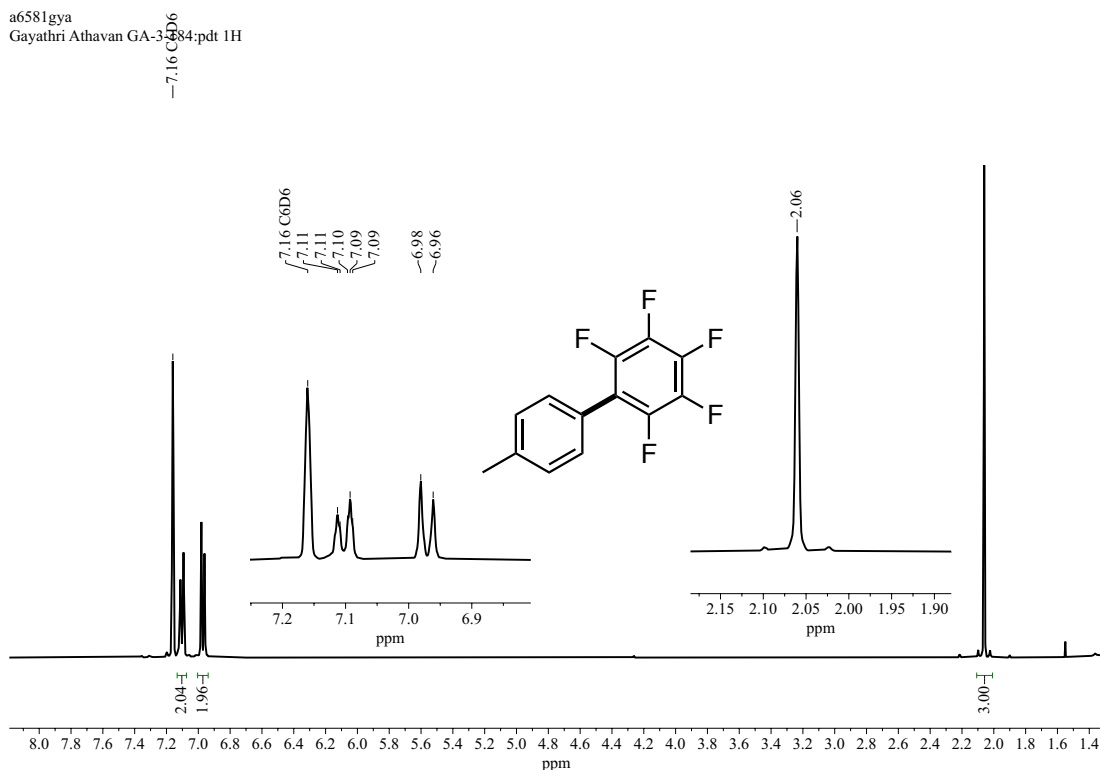


**Figure 160:**  $^1\text{H}$  (400 MHz,  $\text{C}_6\text{D}_6$ , 20 °C) spectrum of 2,3,4,5,6-pentafluoro-4'-(methyl)biphenyl **18** (*JDF* file reference: a6581gya)

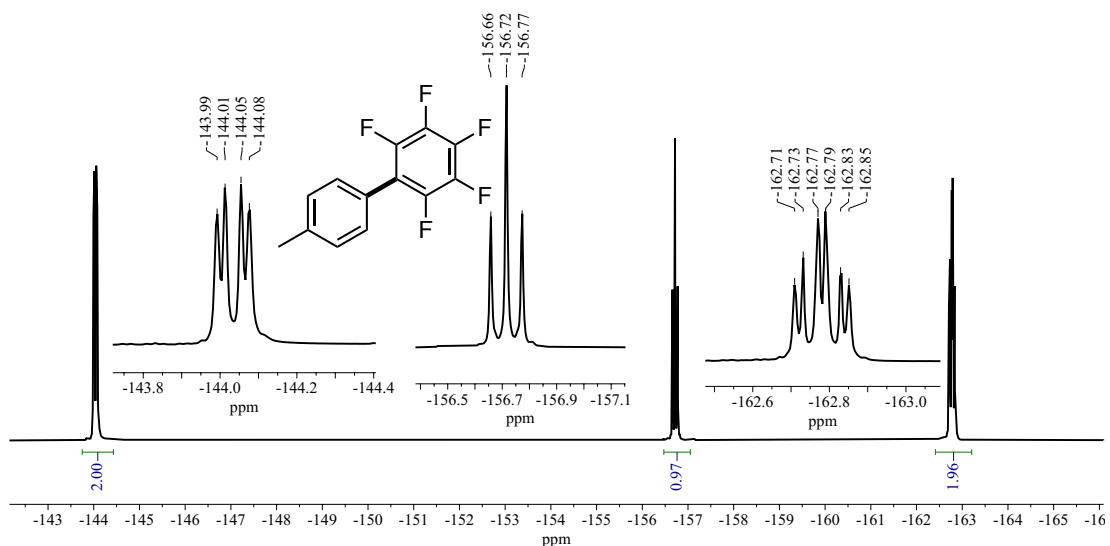


**Figure 161:**  $^{19}\text{F}\{^1\text{H}\}$  (376 MHz,  $\text{C}_6\text{D}_6$ , 20 °C) spectrum of 2,3,4,5,6-pentafluoro-4'-(methyl)biphenyl **18** (*JDF* file reference: a6581gya)

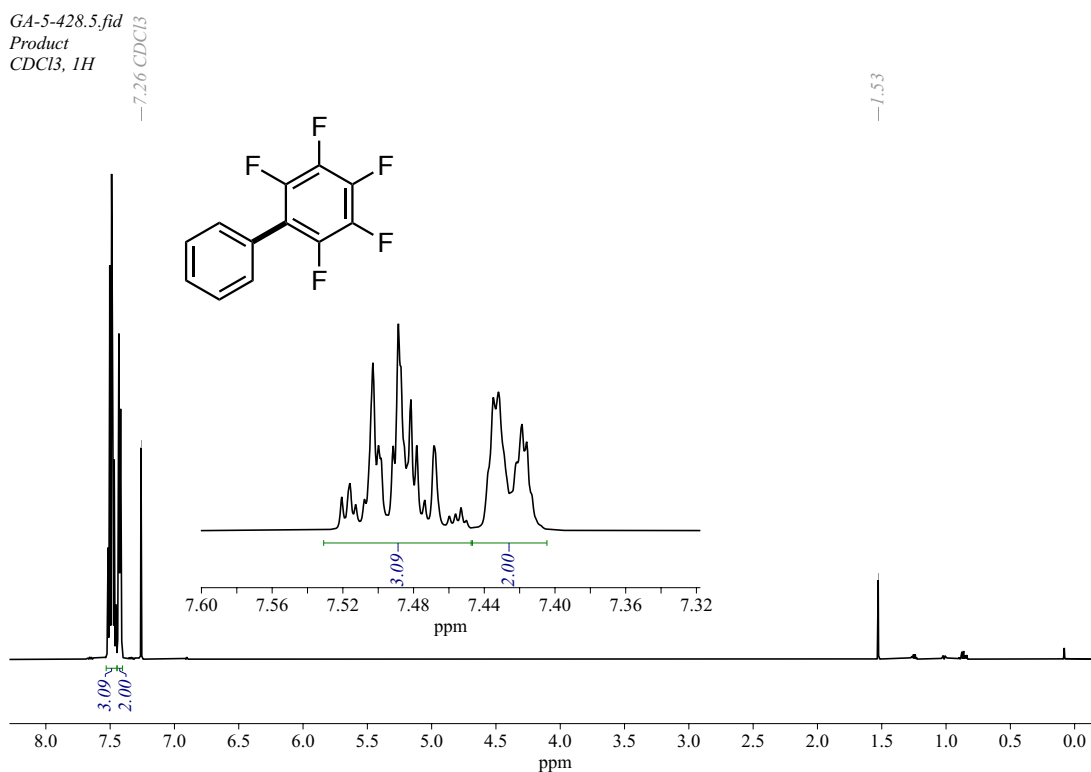


**Figure 162:** <sup>1</sup>H NMR (500 MHz, CDCl<sub>3</sub>, 25 °C) spectrum of 2,3,4,5,6-pentafluorobiphenyl **28** (spectrum collected on AV500, saved as 5 under GA-5-428)

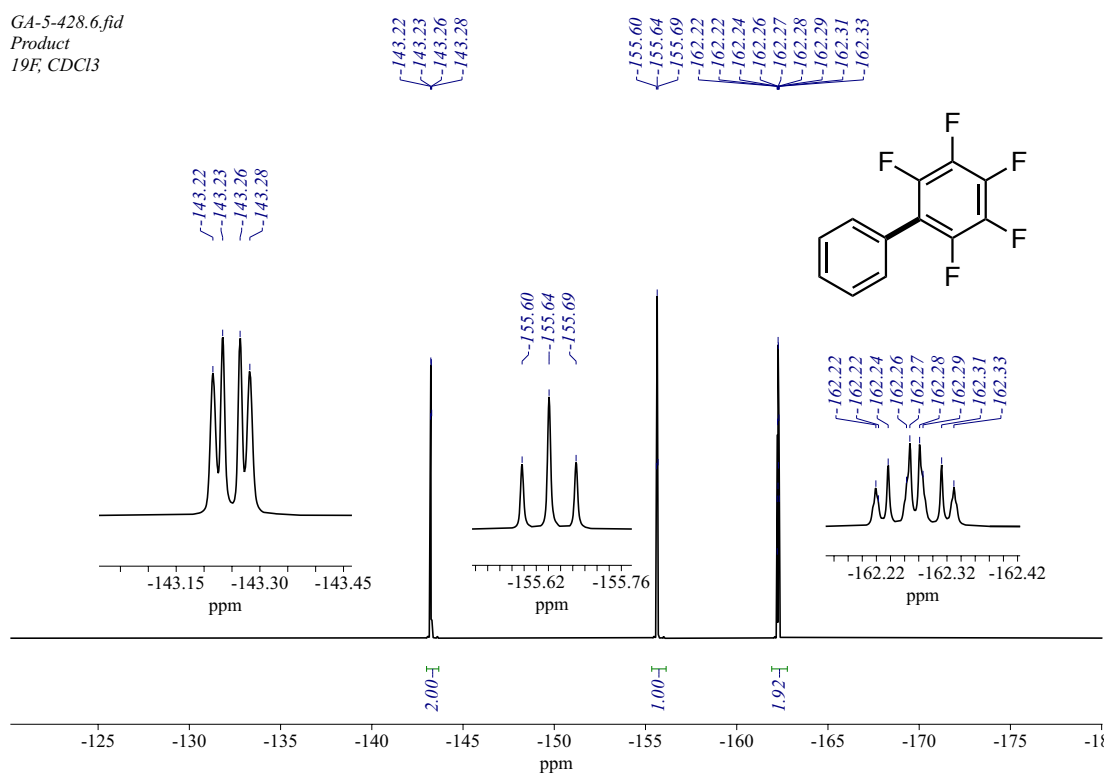


**Figure 163:** <sup>19</sup>F{<sup>1</sup>H} NMR (470.6 MHz, CDCl<sub>3</sub>, 25 °C) spectrum of 2,3,4,5,6-pentafluorobiphenyl **28** (spectrum collected on AV500, saved as 6 under GA-5-428)

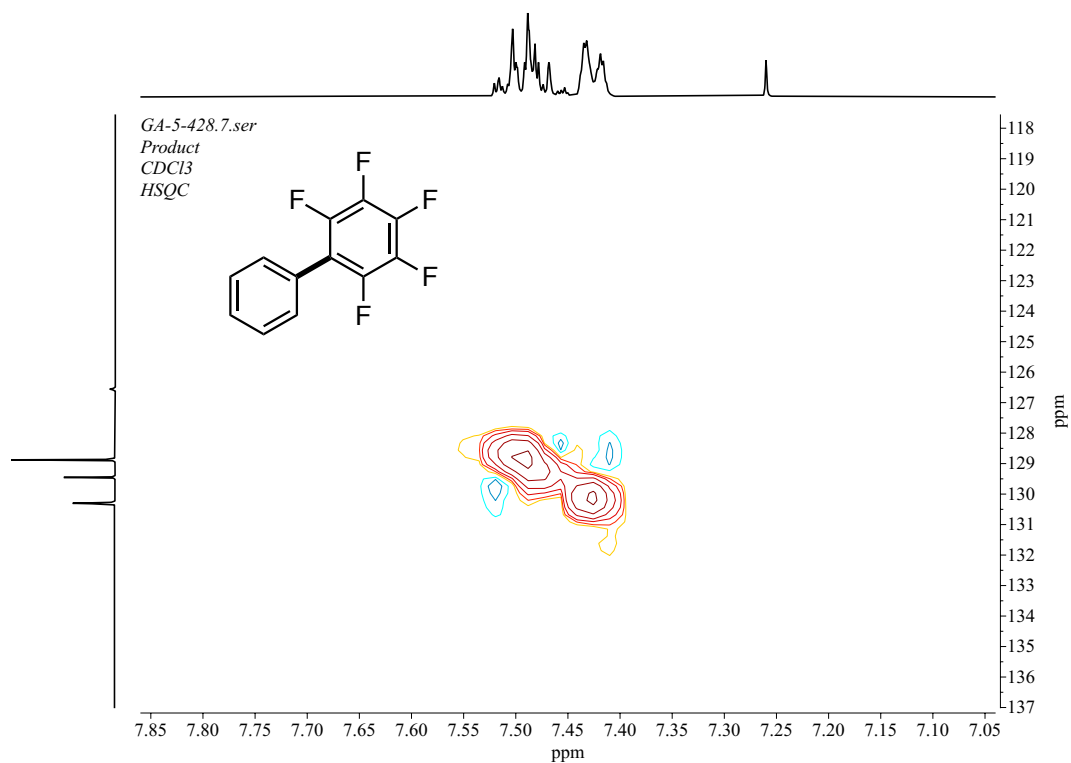


**Figure 164:** HSQC spectrum of 2,3,4,5,6-pentafluorobiphenyl **28** in CDCl<sub>3</sub> (spectrum collected on AV500, saved as 7 under GA-5-428)

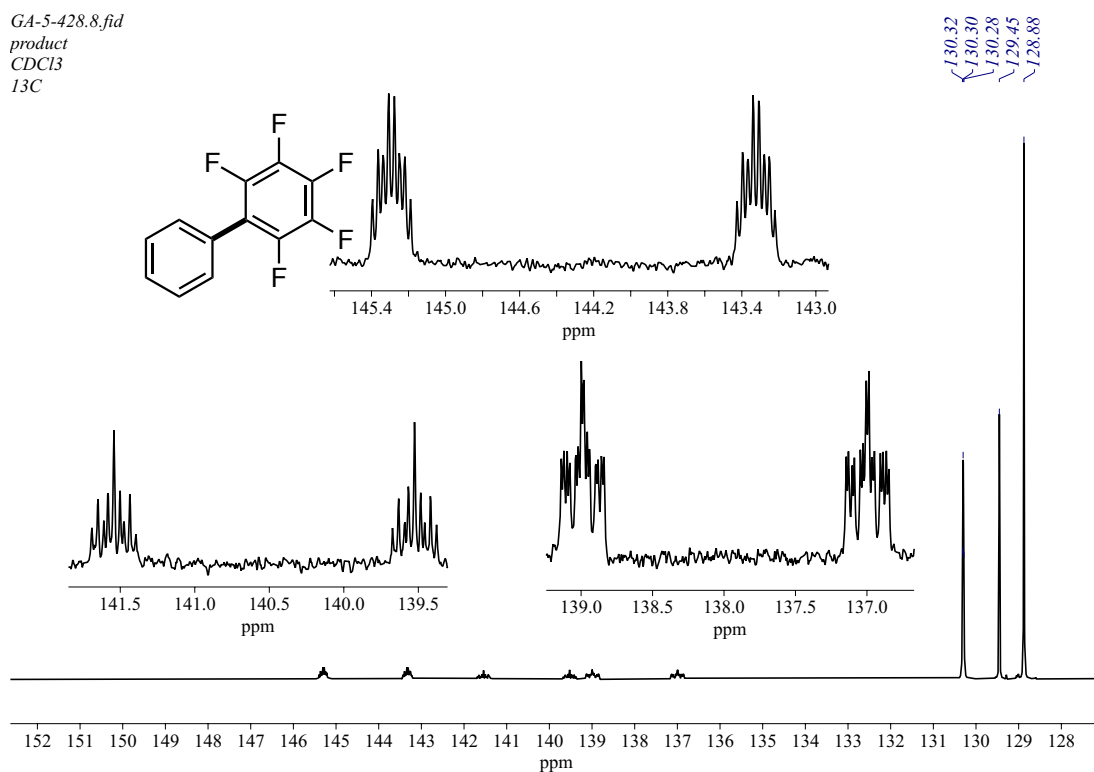


**Figure 165:** <sup>13</sup>C{<sup>1</sup>H} (125.8 MHz, CDCl<sub>3</sub>, 25 °C) spectrum of 2,3,4,5,6-pentafluorobiphenyl **28** (spectrum collected on AV500, saved as 8 under GA-5-428)

GA-5-429.7.fid  
(C6F5)(C6H4F)  
CDCl<sub>3</sub>, 1H

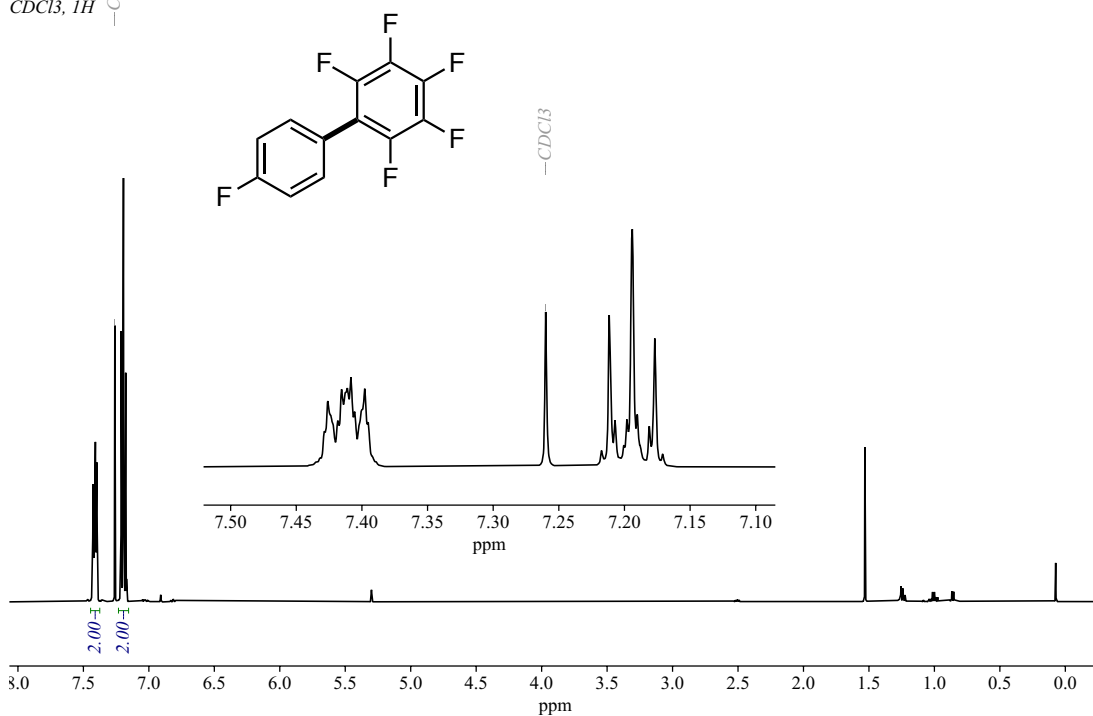


**Figure 166:** <sup>1</sup>H NMR (500 MHz, CDCl<sub>3</sub>, 25°C) spectrum of 2,3,4,5,6-pentafluoro-4'-(fluoro)biphenyl **134** (spectrum collected on AV500, saved as 7 under GA-5-429)

GA-5-429.8.fid  
(C6F5)(C6H4F)  
19F, CDCl<sub>3</sub>

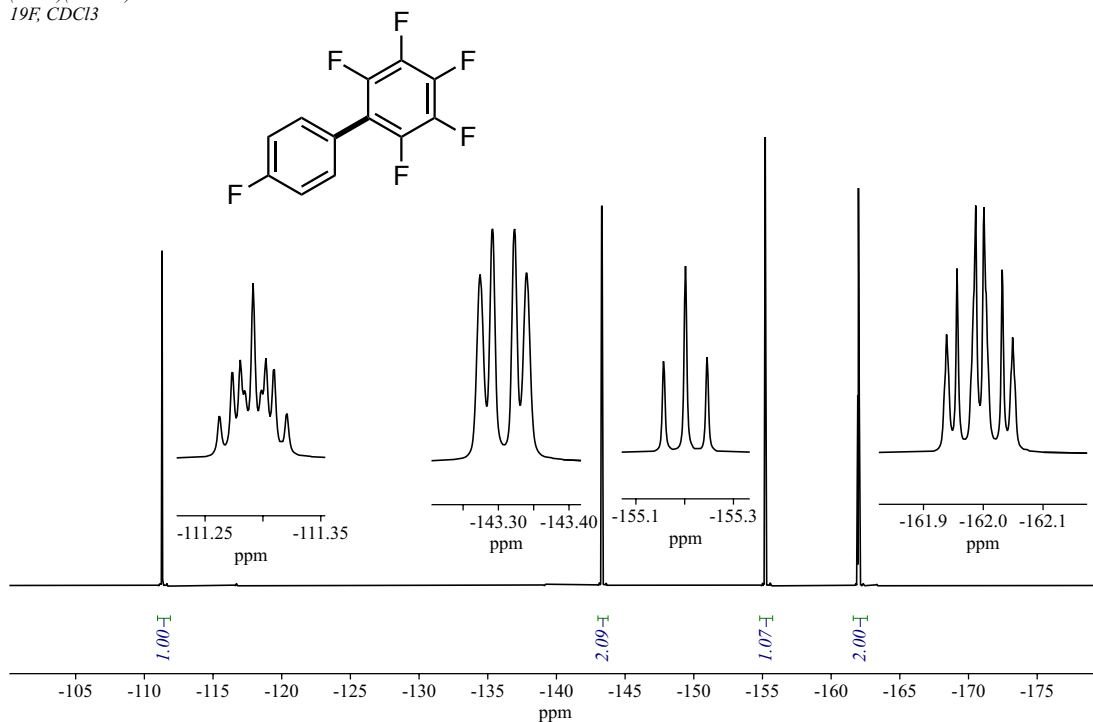


**Figure 167:** <sup>19</sup>F{<sup>1</sup>H} NMR (470.6 MHz, CDCl<sub>3</sub>, 25 °C) spectrum of 2,3,4,5,6-pentafluoro-4'-(fluoro)biphenyl **134** (spectrum collected on AV500, saved as 8 under GA-5-429)



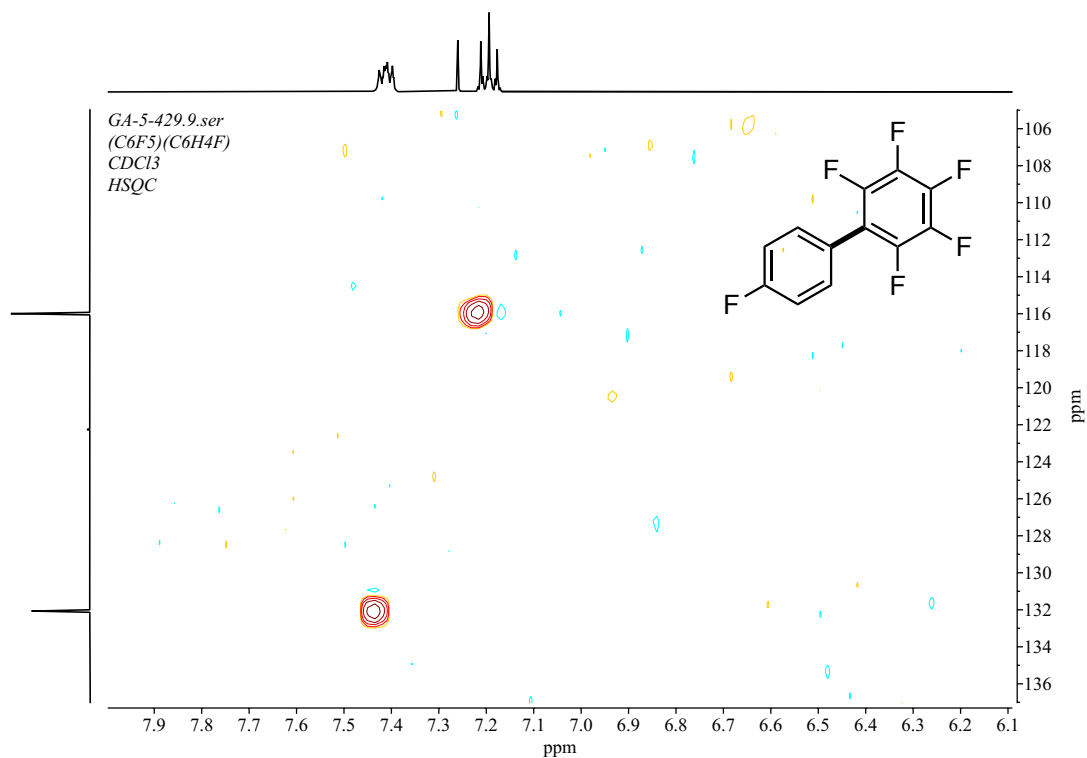


**Figure 168:** HSQC spectrum of 2,3,4,5,6-pentafluoro-4'-(fluoro)biphenyl **134** in CDCl<sub>3</sub> (spectrum collected on AV500, saved as 9 under GA-5-429)

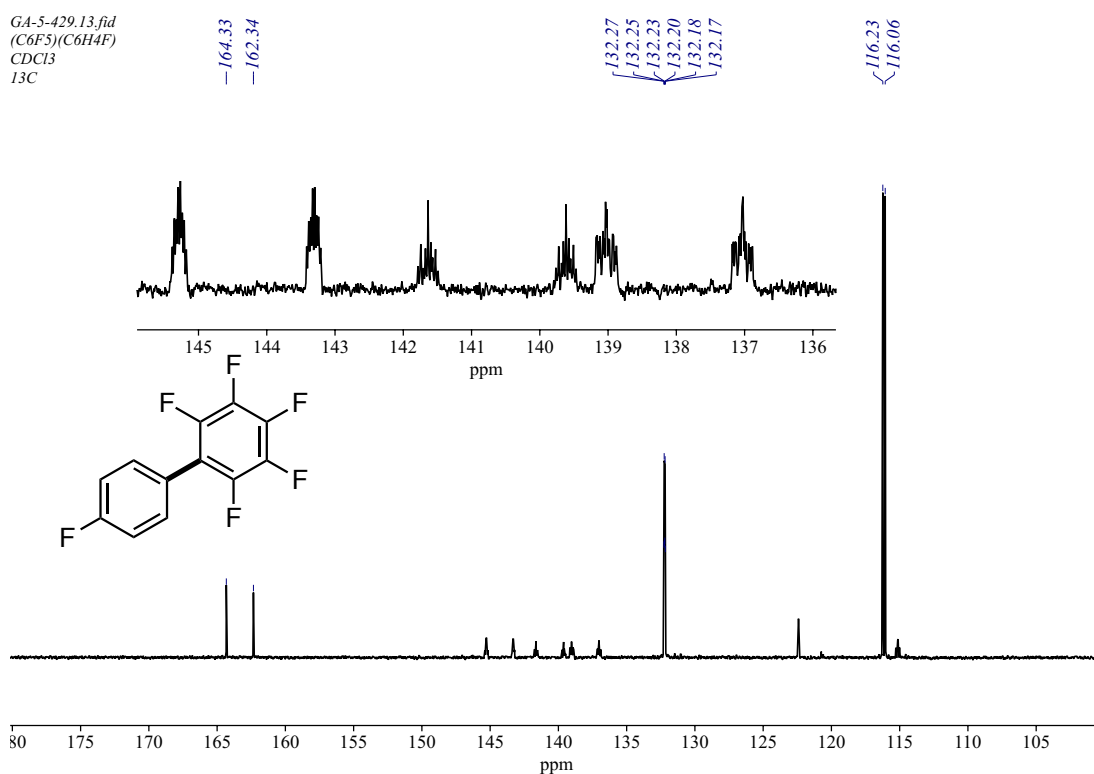


**Figure 169:** <sup>13</sup>C{<sup>1</sup>H} (125.8 MHz, CDCl<sub>3</sub>, 25 °C) spectrum of 2,3,4,5,6-pentafluoro-4'-(fluoro)biphenyl **134** (spectrum collected on AV500, saved as 13 under GA-5-429)

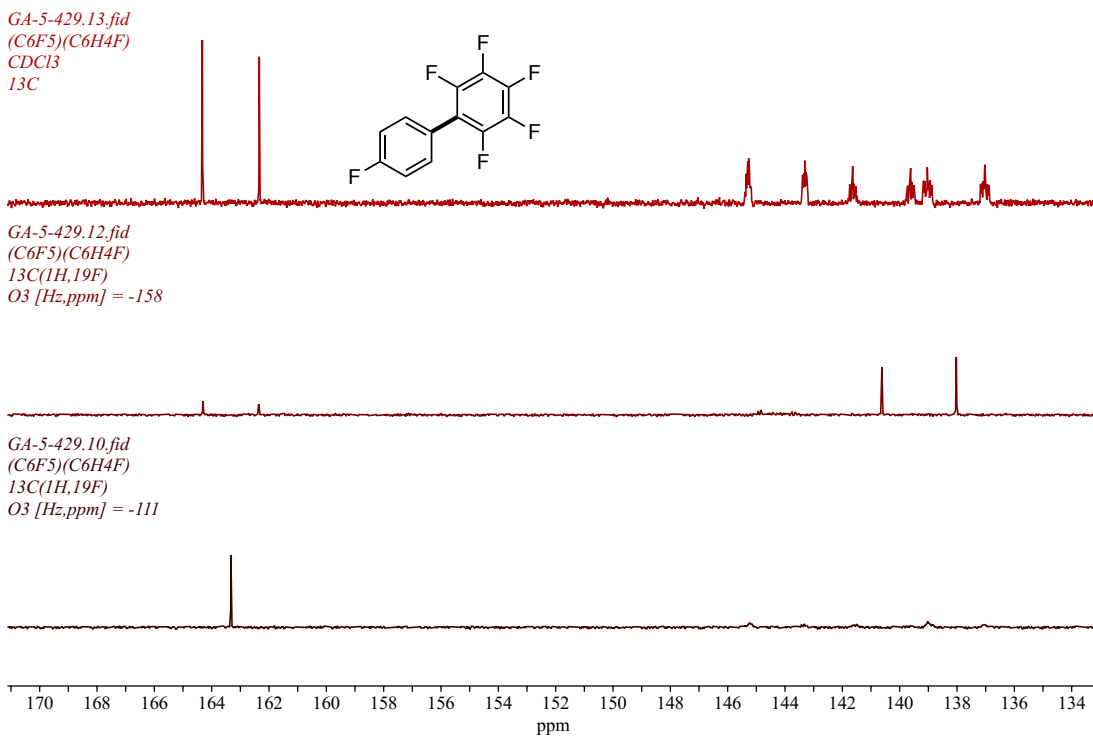


**Figure 170:** Stack plot of the  $^{13}\text{C}\{^1\text{H}\}$  NMR spectrum (top) of **134** with the  $^{13}\text{C}\{^1\text{H}, ^{19}\text{F}\}$  spectrum with an O3P of  $\delta -158$  (middle) and  $\delta -111$  (bottom), in  $\text{CDCl}_3$  (spectrum collected on AV500, the individual spectrum are saved as 13,12 and 10 under GA-5-429)

The assignments of the  $\text{C}_6\text{F}_5$  group carbon peaks were done using a  $^{13}\text{C}\{^1\text{H}, ^{19}\text{F}\}$  spectrum. Two different  $^{13}\text{C}\{^1\text{H}, ^{19}\text{F}\}$  experiments were set up, one with an irradiation frequency offset (O3P) at  $\delta -158$  and  $\delta -111$  (for  $^{19}\text{F}$ ). The O3P of  $\delta -111$  specifically decoupled the F signal from the carbon of  $\text{C}_6\text{H}_4\text{F}$  whereas the O3P of  $\delta -158$  offset decoupled the *meta*- and *para*- F from the carbon of  $\text{C}_6\text{F}_5$ . The stack plot of the three spectra has been shown in **Figure 170**.

GA-6-518.5.fid  
Purified compound  
CDCl<sub>3</sub>, 1H

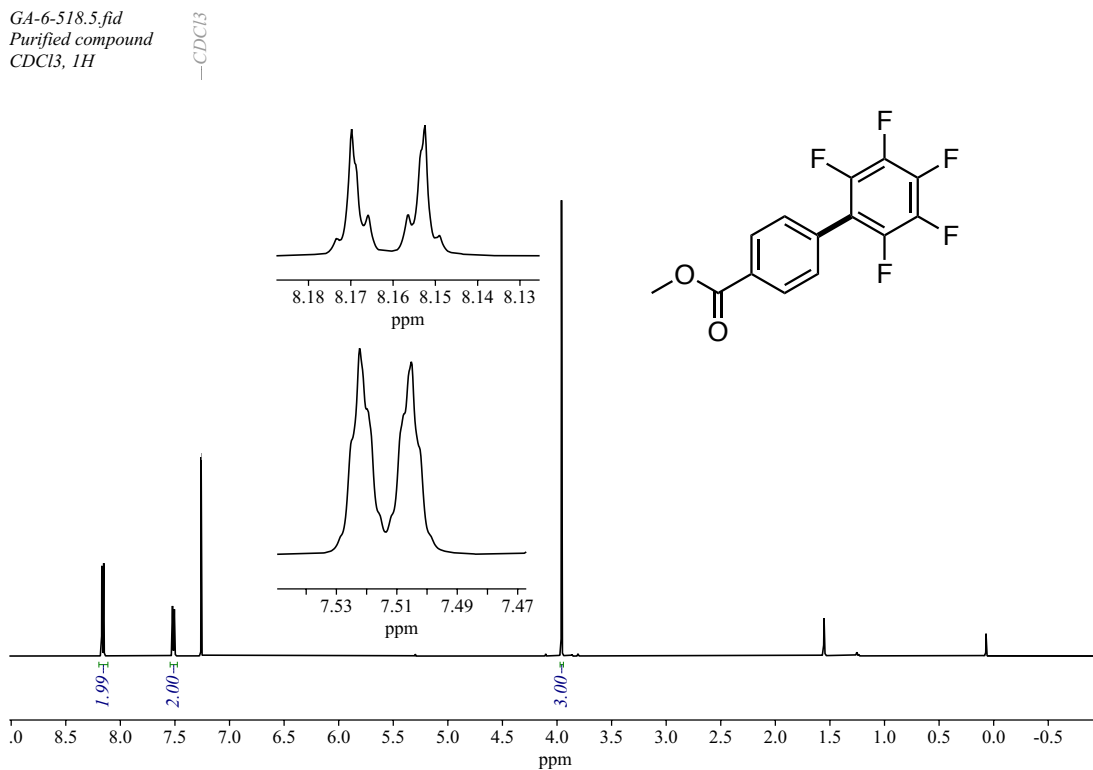


**Figure 171:** <sup>1</sup>H NMR (500 MHz, CDCl<sub>3</sub>, 25°C) spectrum of 2',3',4',5',6'-pentafluorobiphenyl-4-carboxylate **140** (spectrum collected on AV500, saved as 5 under GA-6-518)

GA-6-518.6.fid  
Purified compound  
Fraction 2 - 5  
CDCl<sub>3</sub>, <sup>19</sup>F{<sup>1</sup>H}

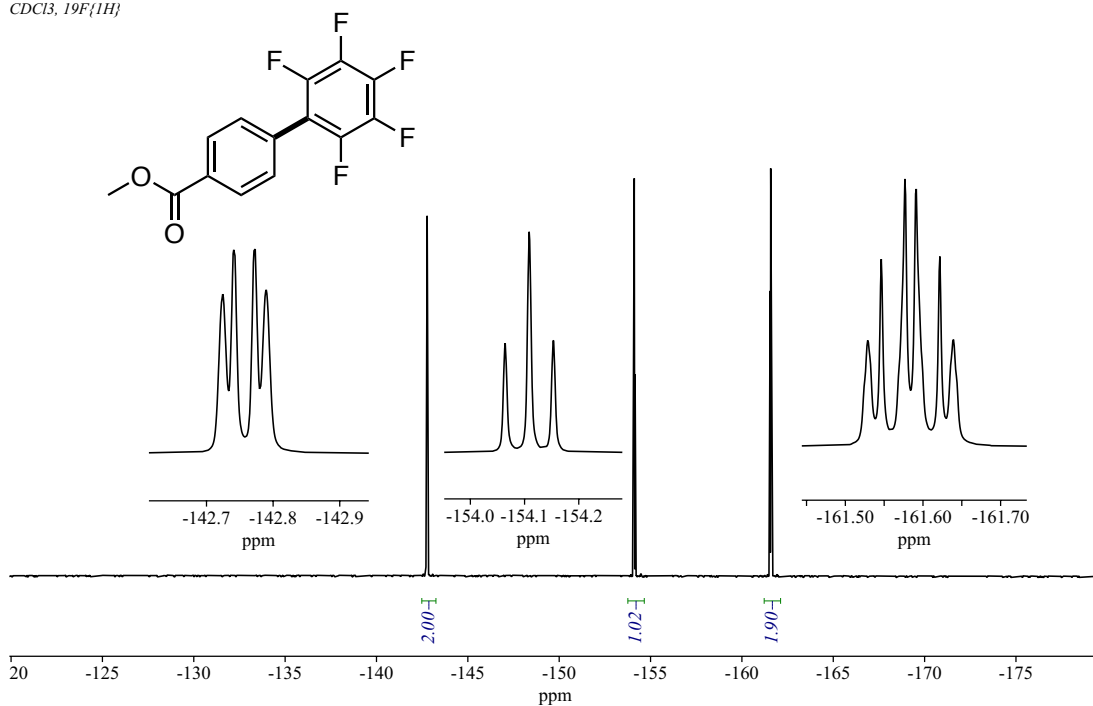


**Figure 172:** <sup>19</sup>F{<sup>1</sup>H} NMR (470.6 MHz, CDCl<sub>3</sub>, 25 °C) spectrum of 2',3',4',5',6'-pentafluorobiphenyl-4-carboxylate **140** (spectrum collected on AV500, saved as 6 under GA-6-518)

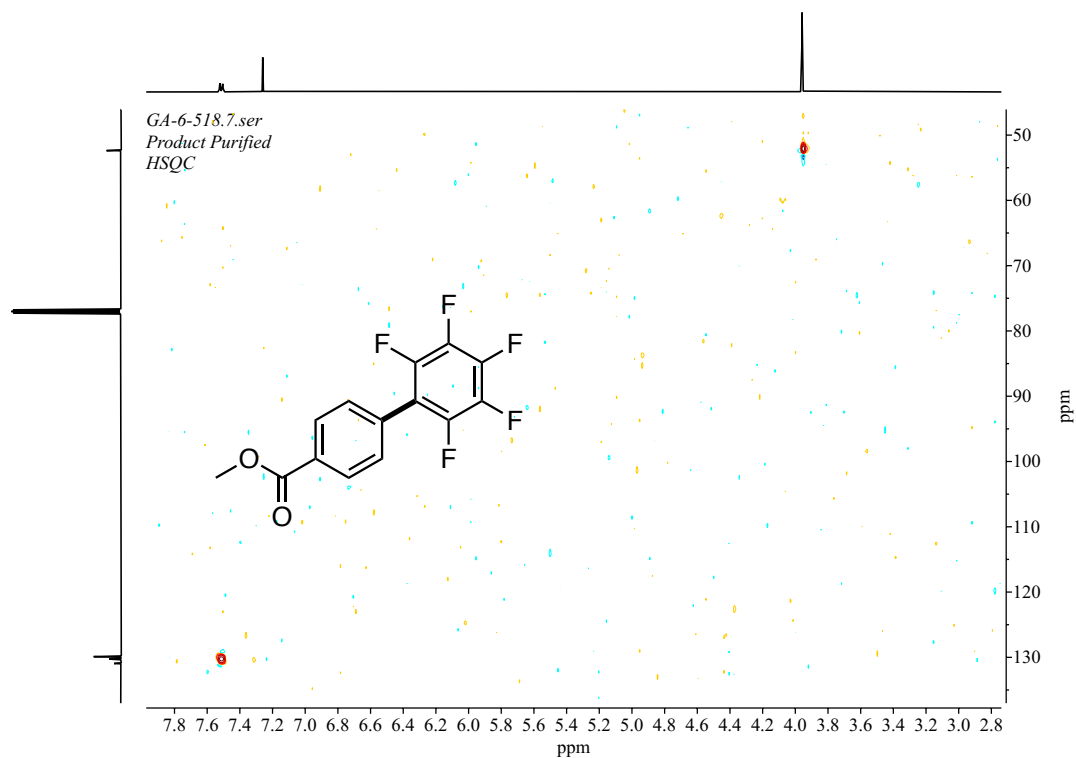


**Figure 173:** HSQC spectrum of 2',3',4',5',6'-pentafluorobiphenyl-4-carboxylate **140** in CDCl<sub>3</sub> (spectrum collected on AV500, saved as 7 under GA-6-518)

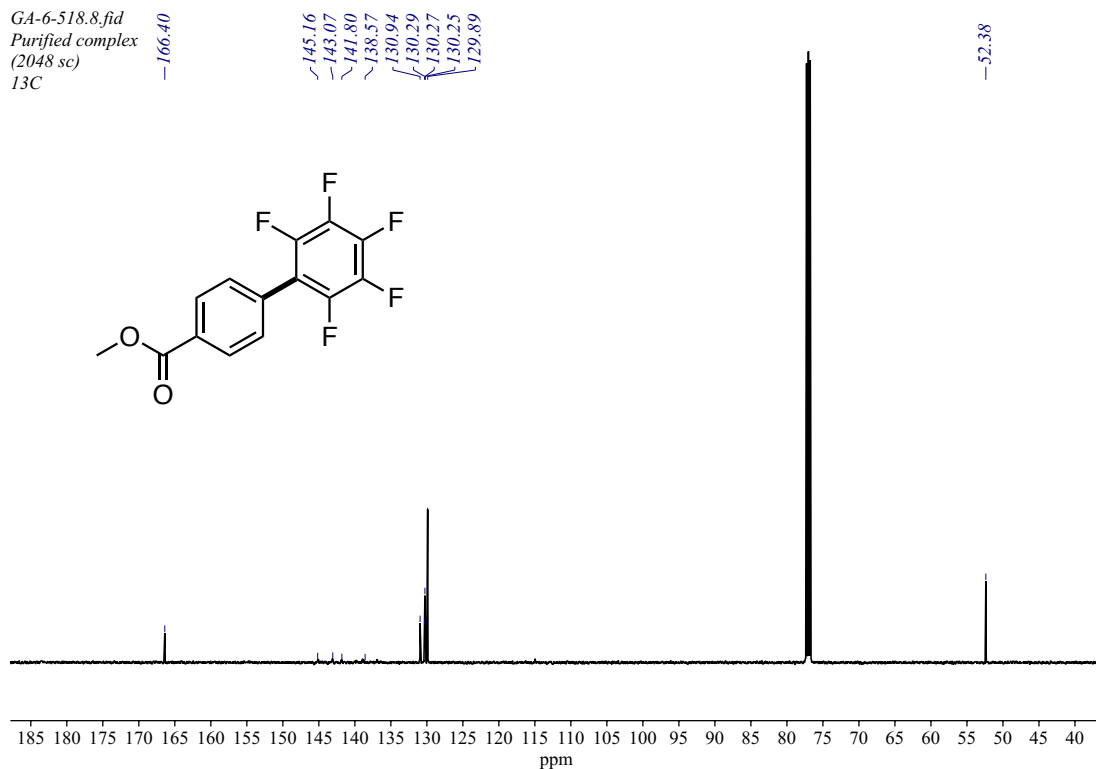


**Figure 174:** <sup>13</sup>C{<sup>1</sup>H} (125.8 MHz, CDCl<sub>3</sub>, 25 °C) spectrum of 2',3',4',5',6'-pentafluorobiphenyl-4-carboxylate **140** (spectrum collected on AV500, saved as 8 under GA-6-518)

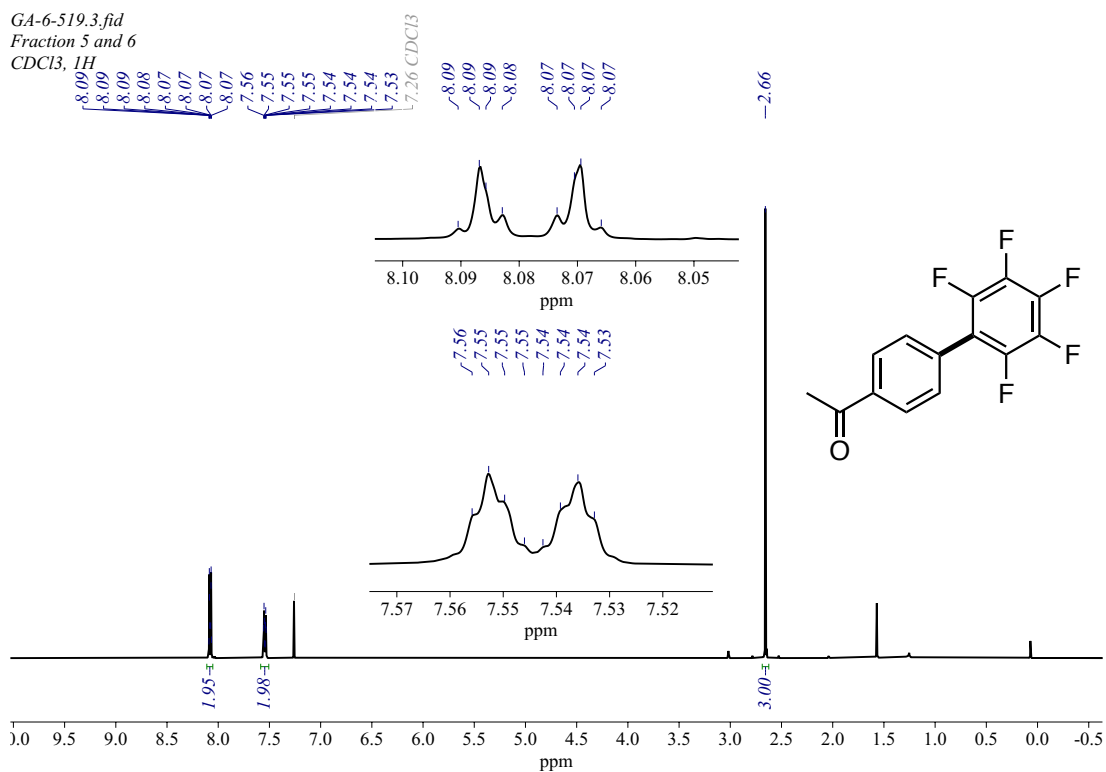


**Figure 175:** <sup>1</sup>H NMR (500 MHz, CDCl<sub>3</sub>, 25°C) spectrum of 1-(2',3',4',5',6'-pentafluoro-[1,1'-biphenyl]-4-yl)ethan-1-one **143** (spectrum collected on AV500, saved as 3 under GA-6-519)

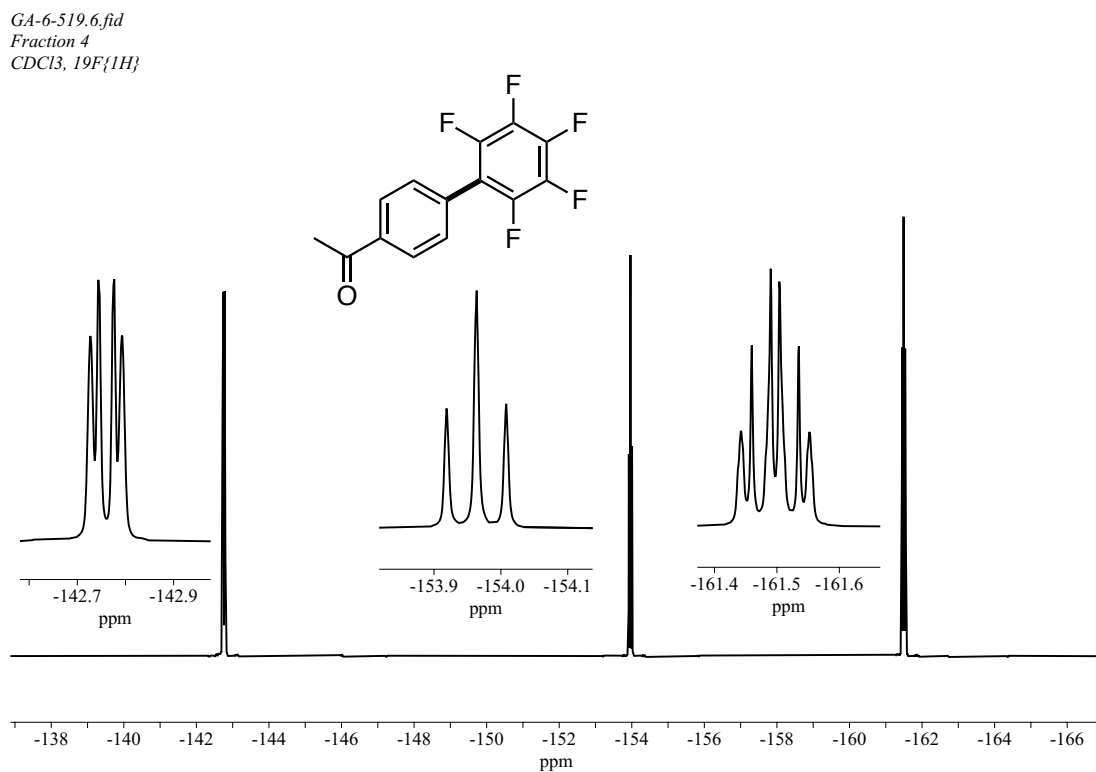


**Figure 176:** <sup>19</sup>F{<sup>1</sup>H} NMR (470.6 MHz, CDCl<sub>3</sub>, 25 °C) spectrum of 1-(2',3',4',5',6'-pentafluoro-[1,1'-biphenyl]-4-yl)ethan-1-one **143** (spectrum collected on AV500, saved as 6 under GA-6-519)

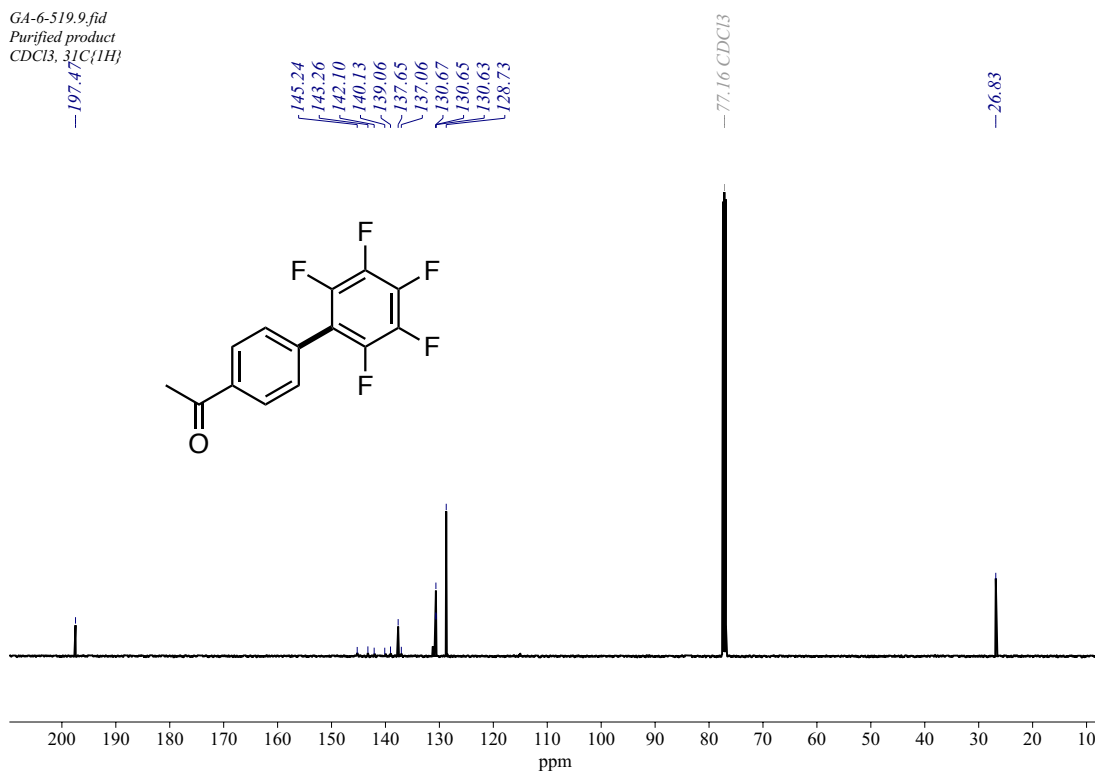


**Figure 177:** <sup>13</sup>C{<sup>1</sup>H} (125.8 MHz, CDCl<sub>3</sub>, 25 °C) spectrum of 1-(2',3',4',5',6'-pentafluoro-[1,1'-biphenyl]-4-yl)ethan-1-one **143** (spectrum collected on AV500, saved as 9 under GA-6-519)

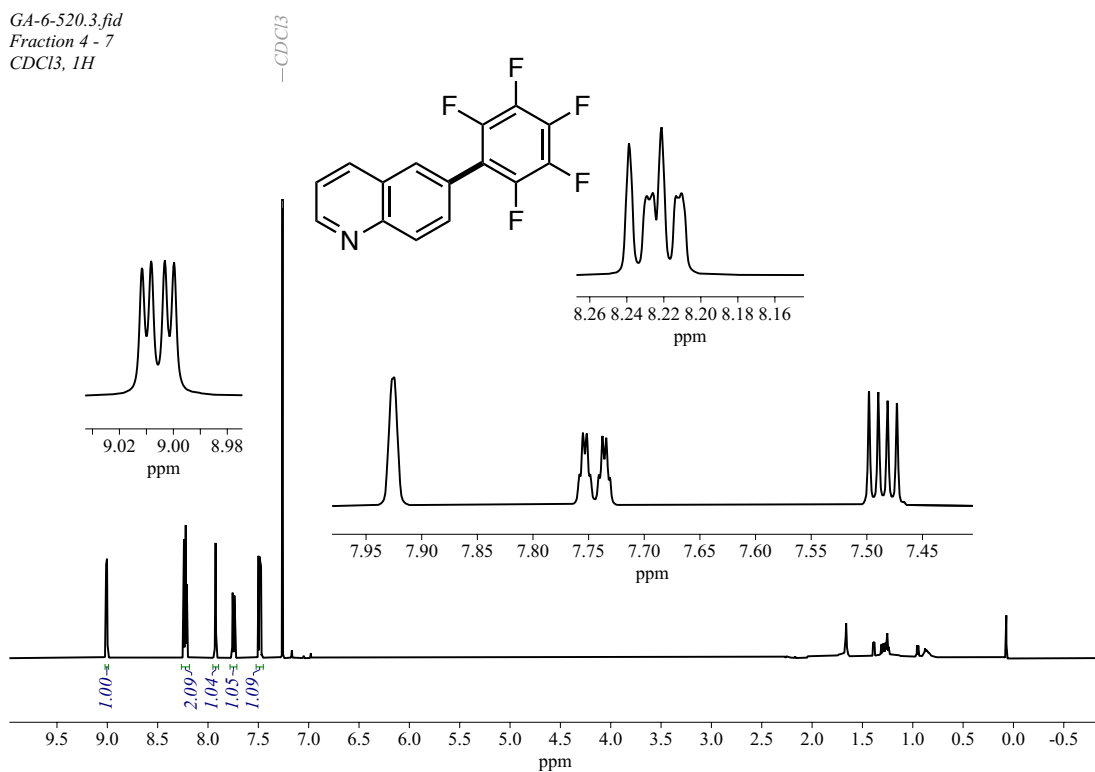


**Figure 178:** <sup>1</sup>H NMR (500 MHz, CDCl<sub>3</sub>, 25°C) spectrum of 6-(Perfluorophenyl)Quinoline **148** (spectrum collected on AV500, saved as 3 under GA-6-520)

GA-6-520.4.fid  
 Fraction 4 - 7  
 CDCl<sub>3</sub>, 19F{1H}

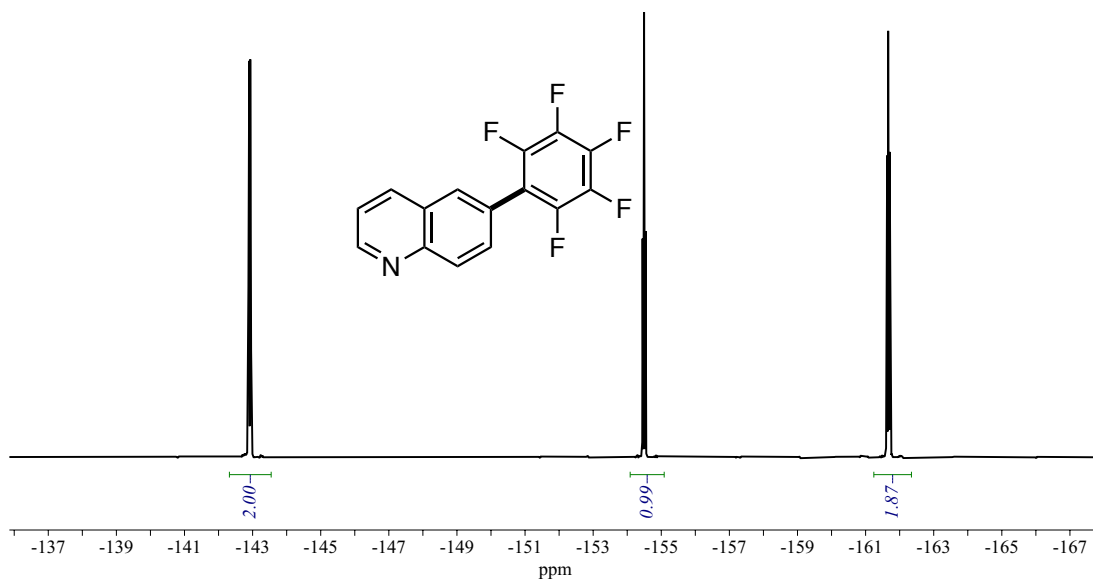


**Figure 179:** <sup>19</sup>F{<sup>1</sup>H} NMR (470.6 MHz, CDCl<sub>3</sub>, 25 °C) spectrum of 6-(Perfluorophenyl)Quinoline **148** (spectrum collected on AV500, saved as 4 under GA-6-520)

GA-5-357.3.fid  
 Purified product  
 CDCl<sub>3</sub>, 1H (32 sc)

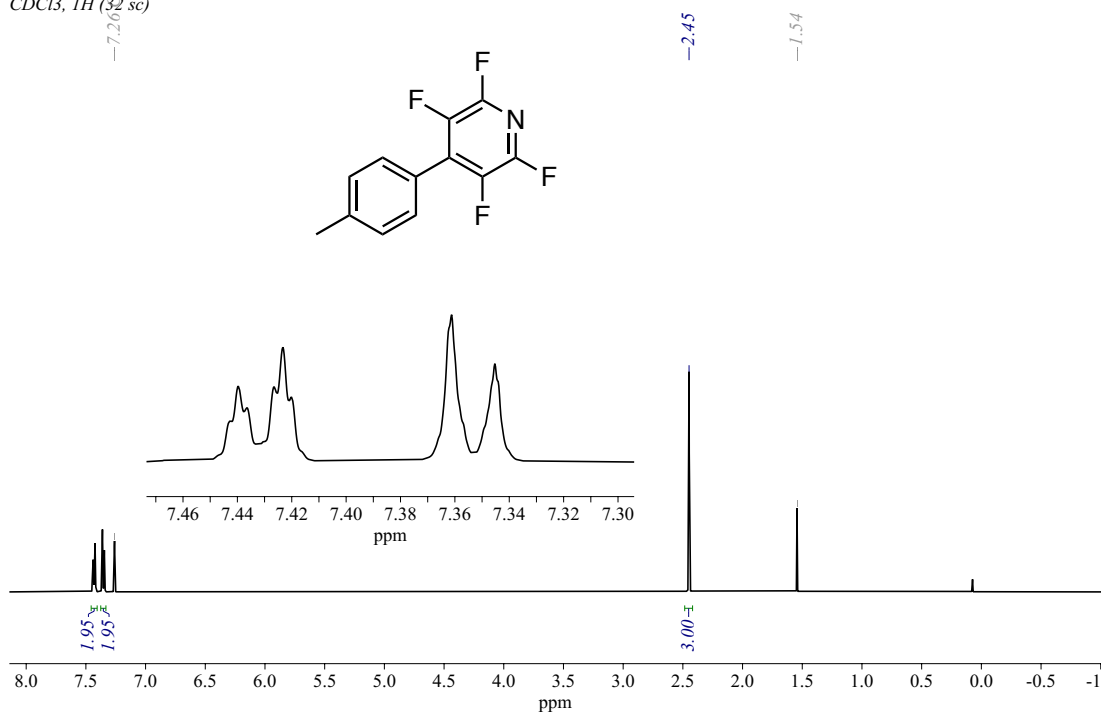


**Figure 180:** <sup>1</sup>H NMR (500 MHz, CDCl<sub>3</sub>, 25°C) spectrum of 2,3,5,6-tetrafluoro-4-[-4-methylphenyl]pyridine **158** (spectrum collected on AV500, saved as 3 under GA-5-357)

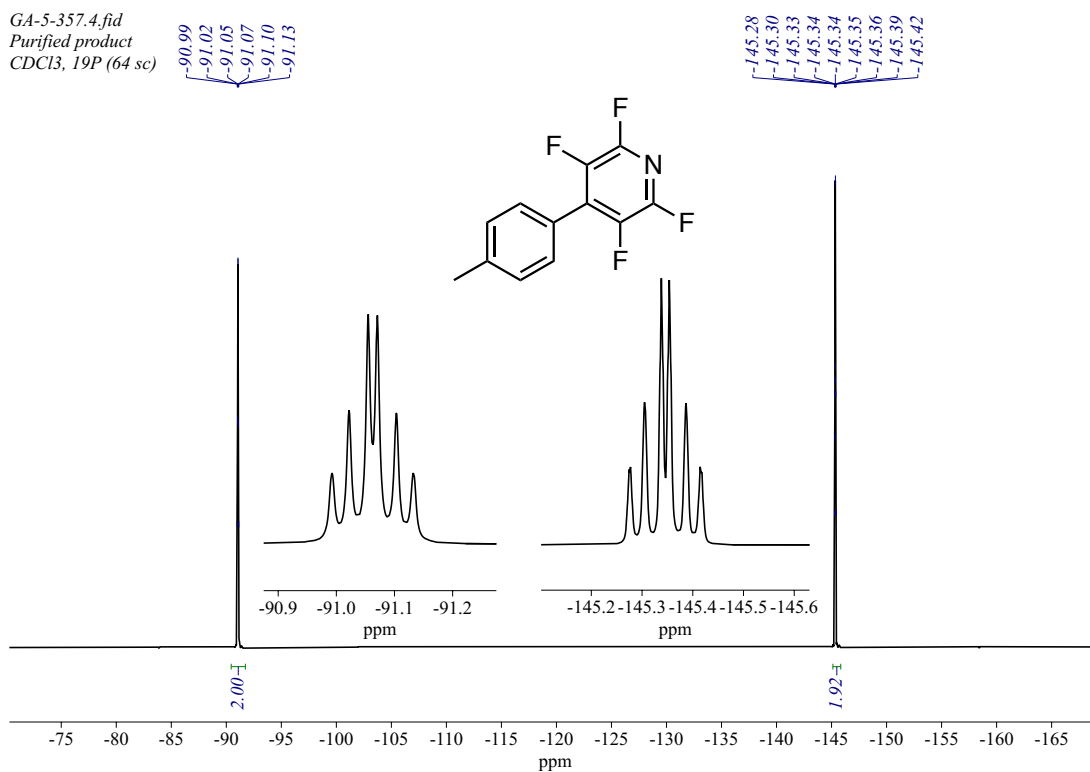


**Figure 181:** <sup>19</sup>F{<sup>1</sup>H} NMR (470.6 MHz, CDCl<sub>3</sub>, 25 °C) spectrum of 2,3,5,6-tetrafluoro-4-[4-methylphenyl]pyridine **158** (spectrum collected on AV500, saved as 4 under GA-5-357)

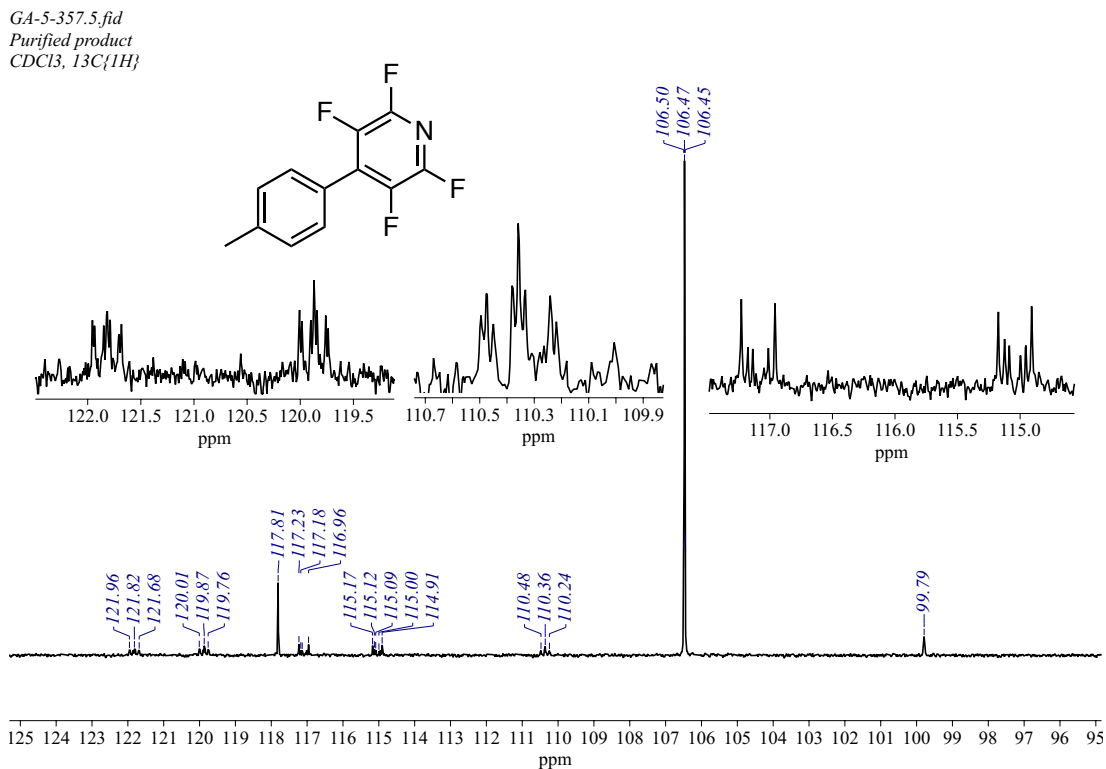


**Figure 182:** <sup>13</sup>C{<sup>1</sup>H} (125.8 MHz, CDCl<sub>3</sub>, 25 °C) spectrum of 2,3,5,6-tetrafluoro-4-[4-methylphenyl]pyridine **158**



GA-4-277.9.fid  
Purified C<sub>6</sub>F<sub>5</sub>D  
tol, 2H

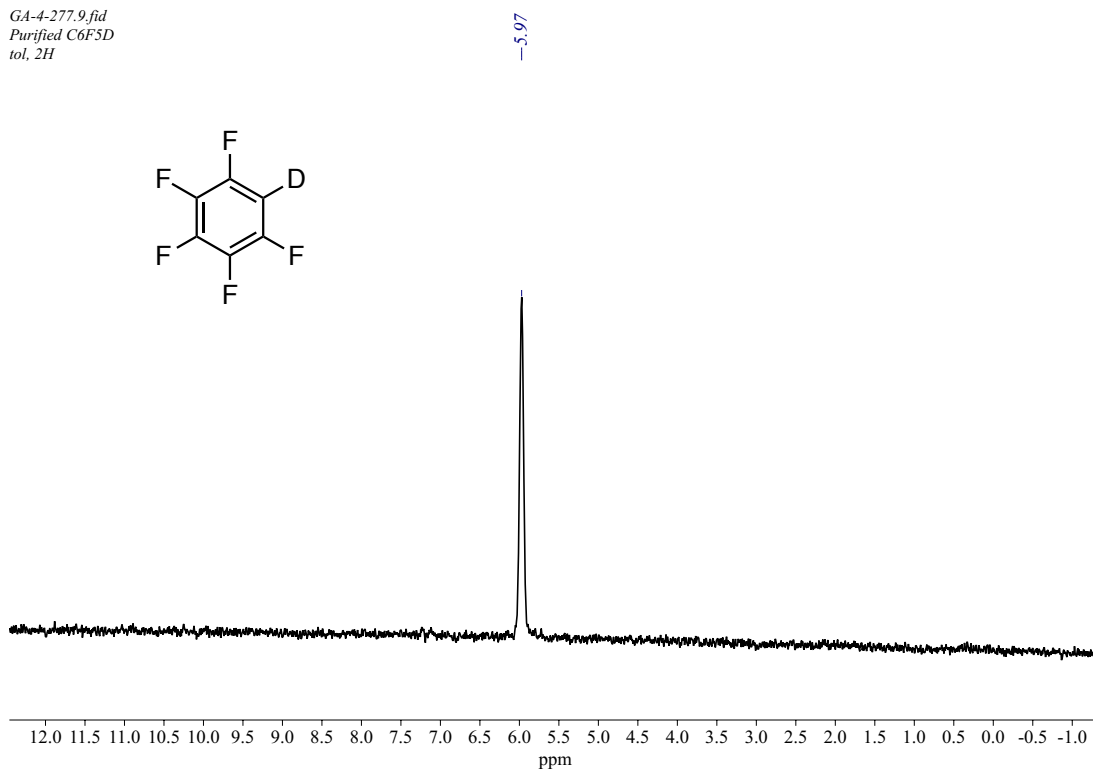


**Figure 183:** <sup>2</sup>H (76 MHz, Tol (non-deuterated) 25 °C) spectrum of C<sub>6</sub>F<sub>5</sub>D **69** (spectrum collected on AV500, saved as 9 under GA-4-277)

GA-4-277.8.fid  
Purified C<sub>6</sub>F<sub>5</sub>D  
CDCl<sub>3</sub>, 19F

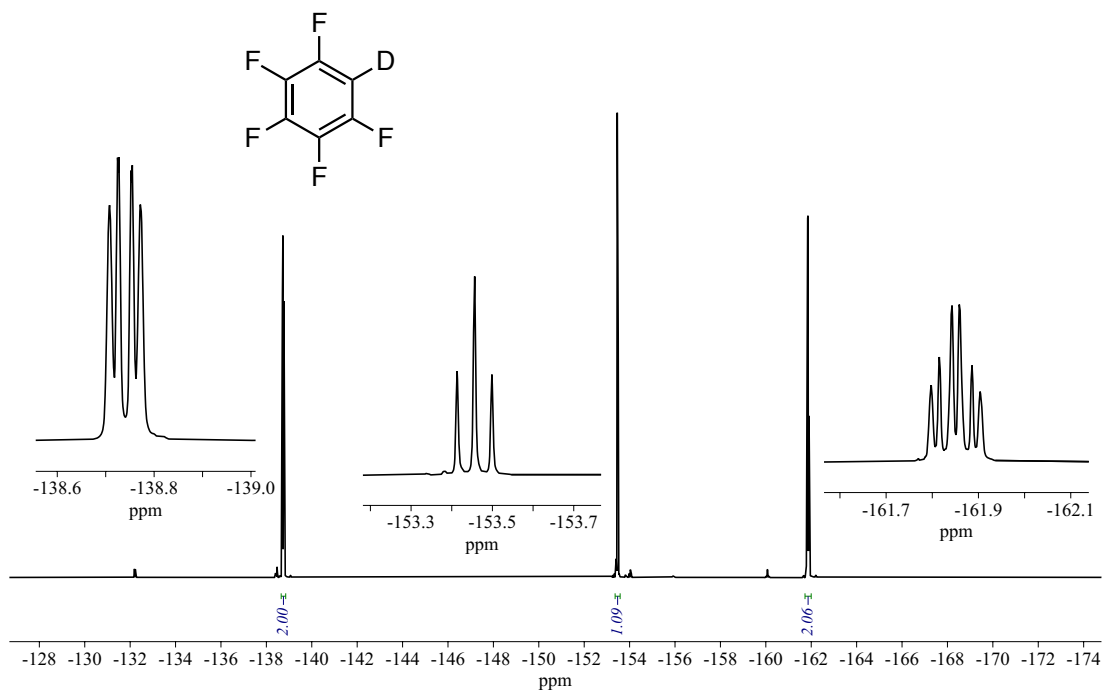


**Figure 184:** <sup>19</sup>F{<sup>1</sup>H} (470.6 MHz, CDCl<sub>3</sub>, 25°C) spectrum of C<sub>6</sub>F<sub>5</sub>D **69** (spectrum collected on AV500, saved as 8 under GA-4-277)

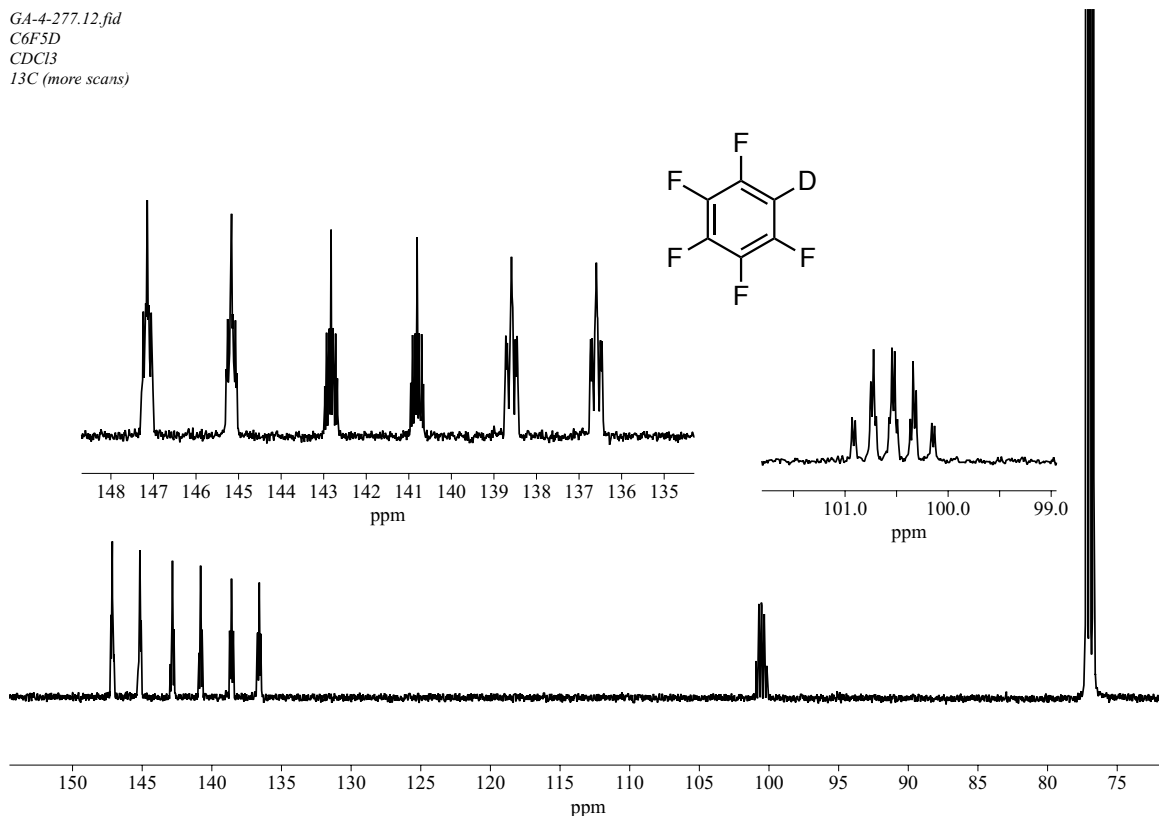


**Figure 185:**  $^{13}C\{^1H\}$  NMR (126 MHz,  $CDCl_3$ , 25 °C) spectrum of  $C_6F_5D$  **69** (spectrum collected on AV500, saved as 12 under GA-4-277)

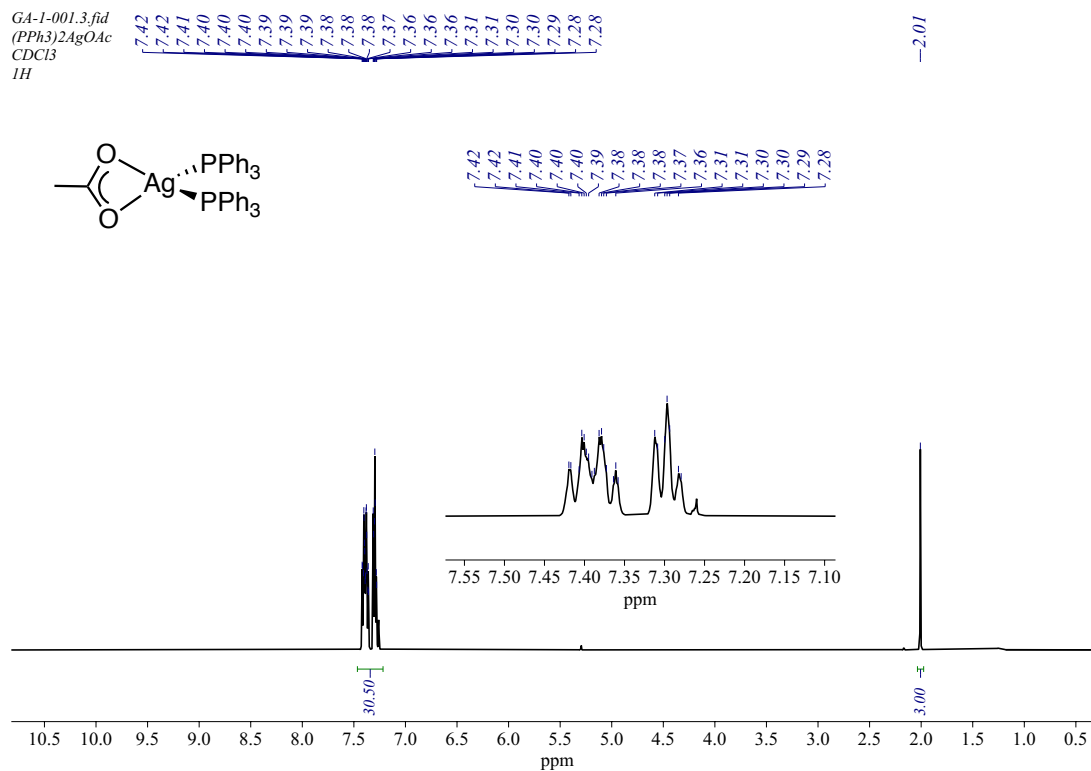


**Figure 186:**  $^1H$  NMR (500 MHz,  $CDCl_3$ , 25 °C) spectrum of  $Ag(PPh_3)_2(\kappa^2-OAc)$  **94** (spectrum collected on AV500, saved as 3 under GA-1-001)

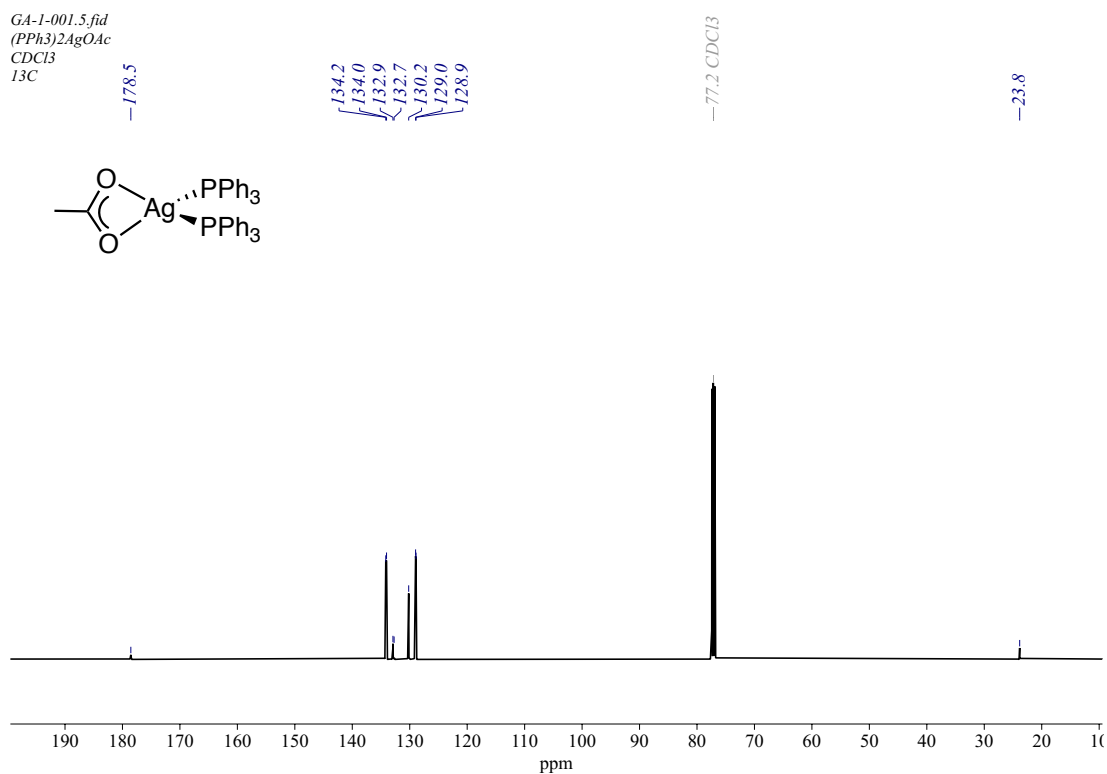


**Figure 187:**  $^{13}\text{C}\{^1\text{H}\}$  NMR (126 MHz,  $\text{CDCl}_3$ , 25 °C) spectrum of  $\text{Ag}(\text{PPh}_3)_2(\kappa^2\text{-OAc})$  **94** (spectrum collected on AV500, saved as 5 under GA-1-001)

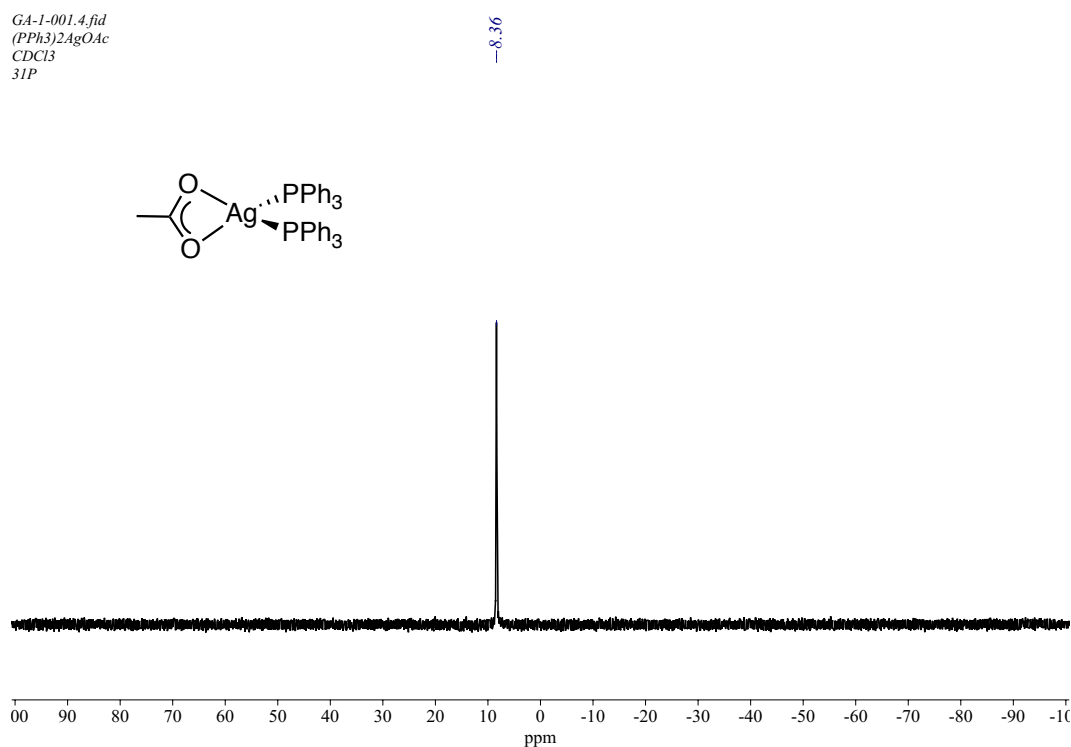


**Figure 188:**  $^{31}\text{P}\{^1\text{H}\}$  NMR (202 MHz,  $\text{CDCl}_3$ , 25 °C) spectrum of  $\text{Ag}(\text{PPh}_3)_2(\kappa^2\text{-OAc})$  **94**, (spectrum collected on AV500, saved as 4 under GA-1-001)

Appendix B – NMR Spectroscopic Data for Synthesised Compounds

GA-1-015.2.fid  
31P 202MHz GA-1-015 DCM-d2 193K

-9.67  
-9.40  
-7.57  
-7.17

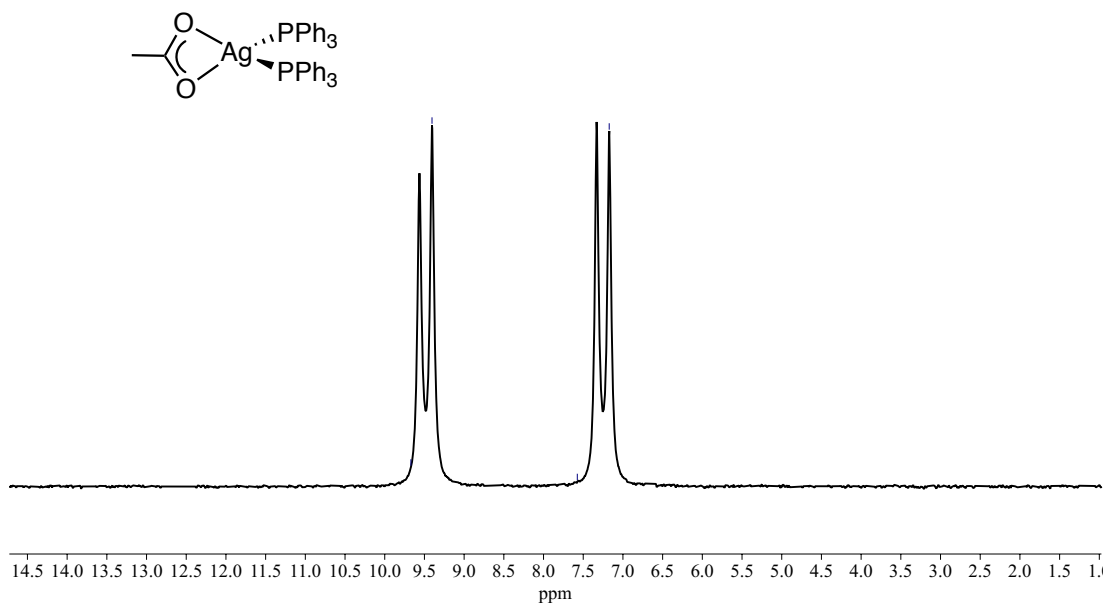


**Figure 189:**  $^{31}\text{P}\{^1\text{H}\}$  NMR (202 MHz,  $\text{CD}_2\text{Cl}_2$ ,  $-80^\circ\text{C}$ ) spectrum of  $\text{Ag}(\text{PPh}_3)_2(\kappa^2\text{-OAc})$

**94**, (spectrum collected on AV500, saved as 2 under GA-1-001)

d8847gya  
Gayathri Athavan GA-1-039 DMSO 1H

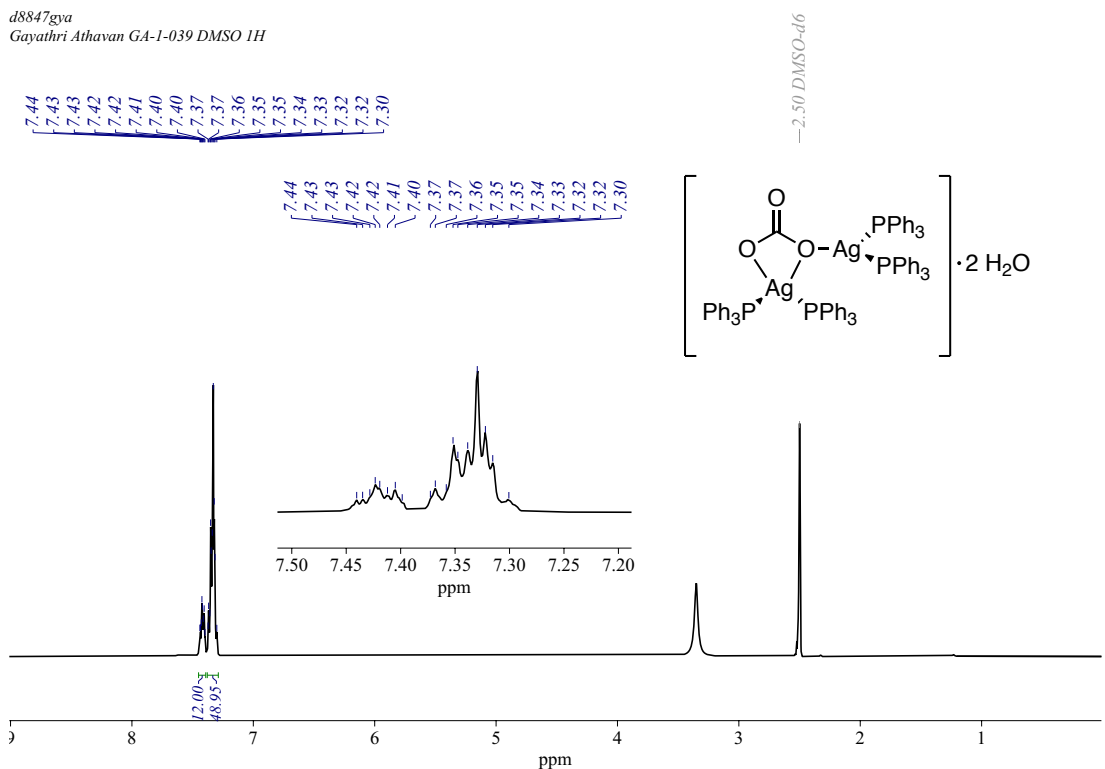


**Figure 190:**  $^1\text{H}$  NMR (400 MHz,  $\text{DMSO-}d_6$ ,  $25^\circ\text{C}$ ) spectrum of  $[\text{Ag}(\text{PPh}_3)_2]_2(\text{CO}_3)\cdot 2\text{H}_2\text{O}$  **88**

(JDF file reference: d8847gya)

Appendix B – NMR Spectroscopic Data for Synthesised Compounds

d8847gya  
Gayathri Athavan GA-1-039 DMSO 13C

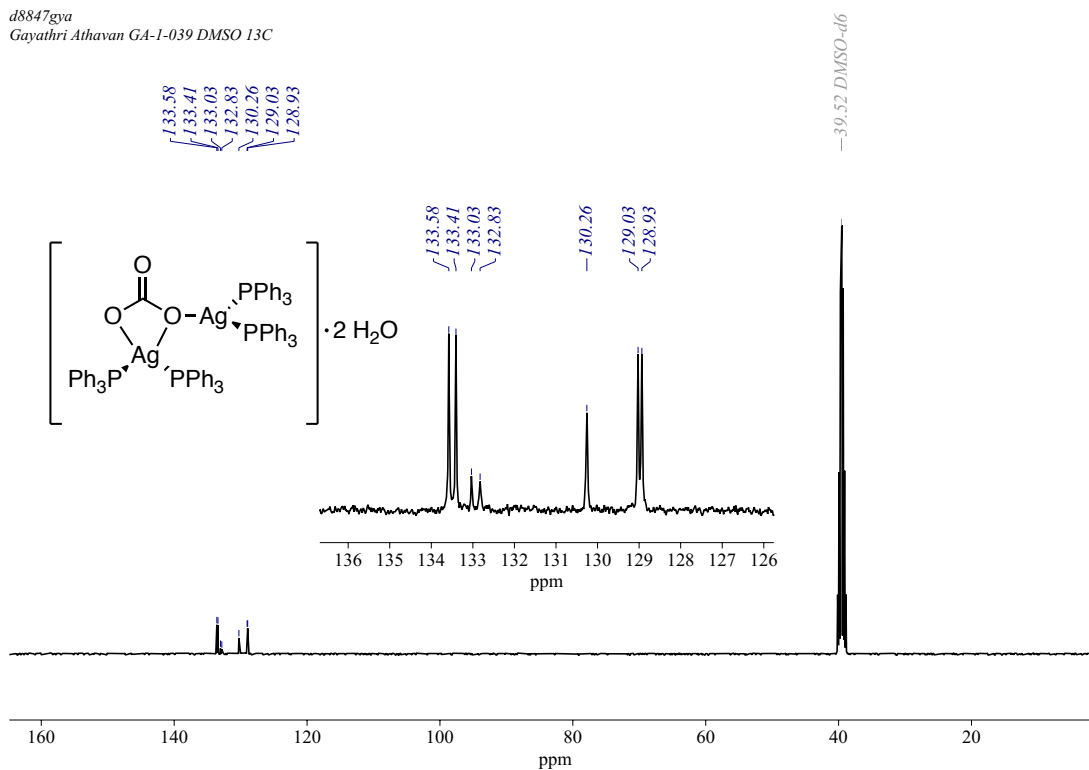


**Figure 191:**  $^{13}\text{C}\{^1\text{H}\}$  NMR (101 MHz, DMSO- $d_6$ , 25 °C) spectrum of  $[\text{Ag}(\text{PPh}_3)_2]_2(\text{CO}_3) \cdot 2 \text{H}_2\text{O}$  **88** (JDF file reference: d8847gya)

d8847gya  
Gayathri Athavan GA-1-039 DMSO 31P

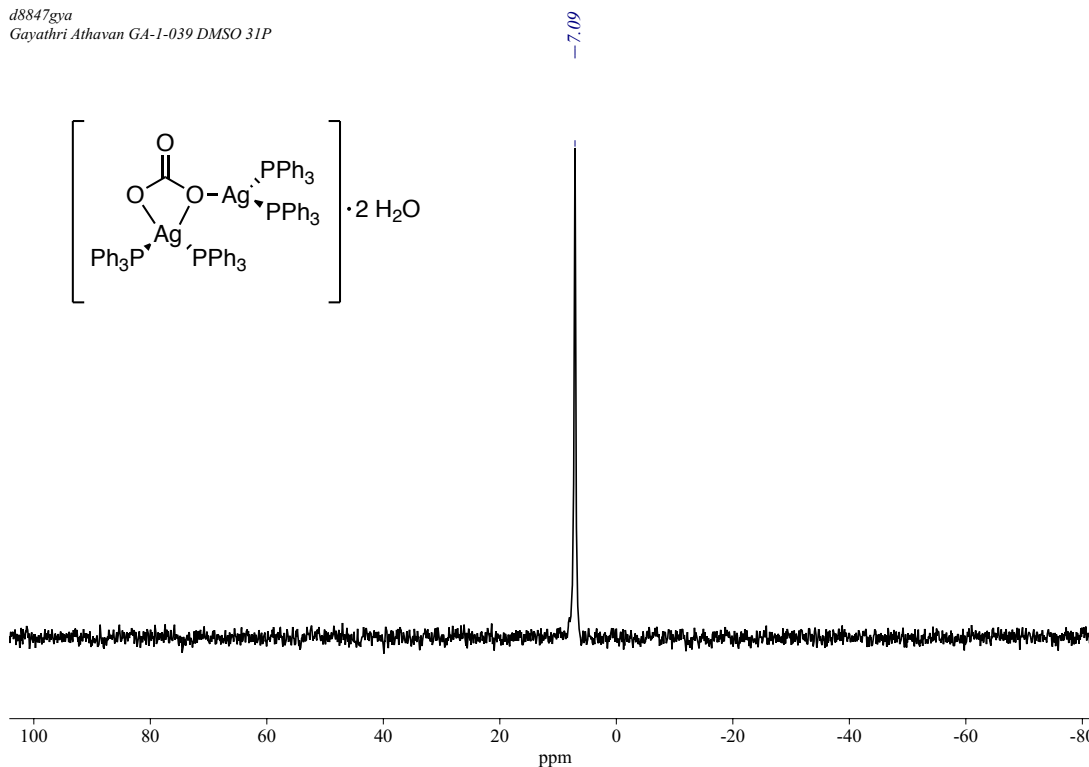


**Figure 192:**  $^{31}\text{P}\{^1\text{H}\}$  NMR (162 MHz, DMSO- $d_6$ , 25 °C) spectrum of  $[\text{Ag}(\text{PPh}_3)_2]_2(\text{CO}_3) \cdot 2 \text{H}_2\text{O}$  **88** (JDF file reference: d8847gya)

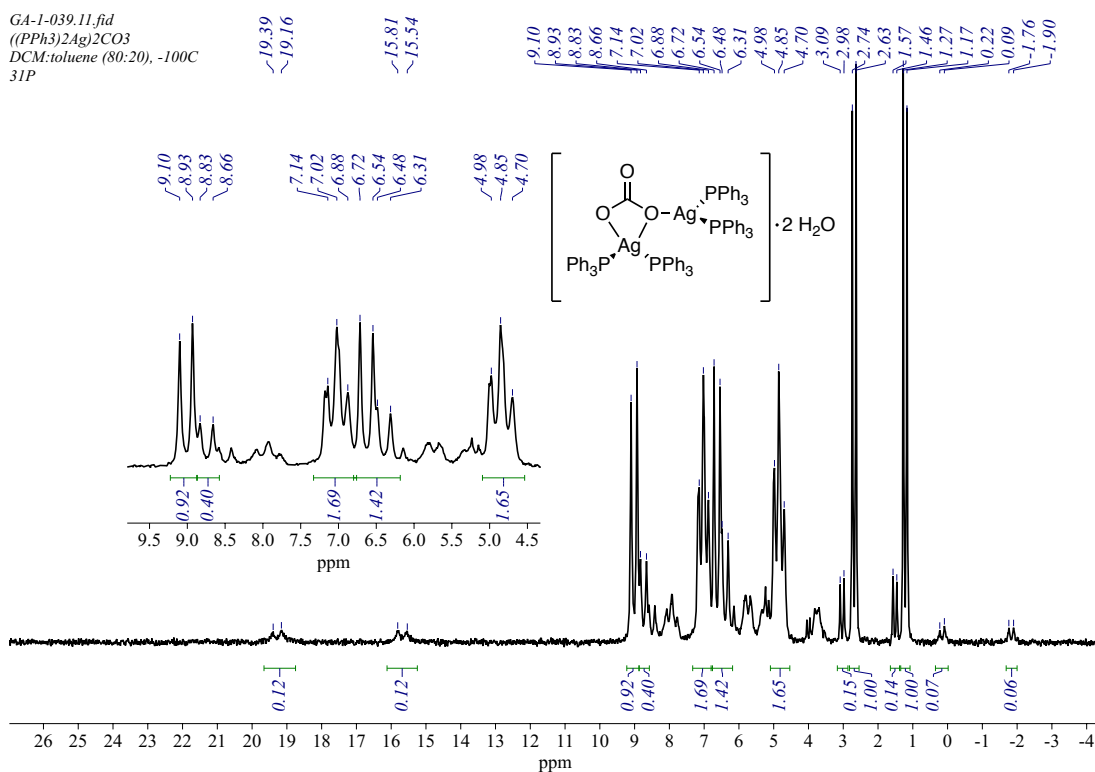


**Figure 193:** <sup>31</sup>P{<sup>1</sup>H} NMR (202 MHz, dichloromethane-d<sub>2</sub>:tol-d<sub>8</sub>, -100°C) spectrum of [Ag(PPh<sub>3</sub>)<sub>2</sub>]<sub>2</sub>(CO<sub>3</sub>)•2 H<sub>2</sub>O **88** (spectrum collected on AV500, saved as 11 under GA-1-039)

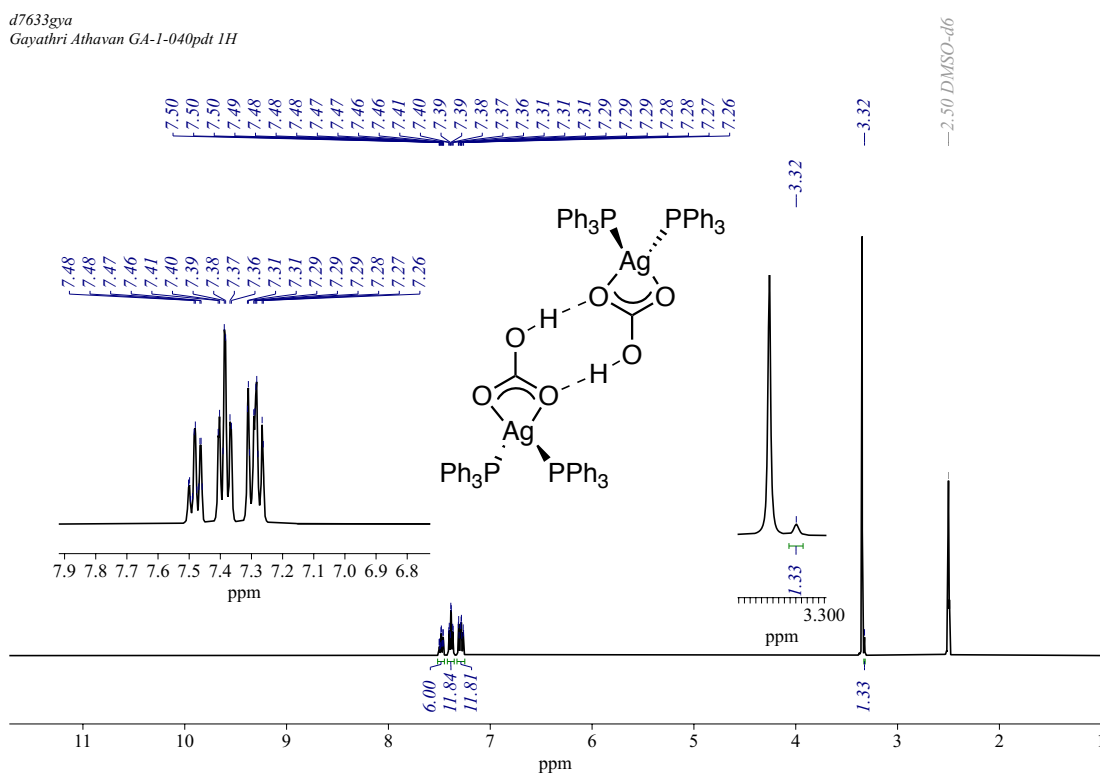


**Figure 194:** <sup>1</sup>H NMR (400 MHz, DMSO-d<sub>6</sub>, 25 °C) spectrum of [Ag(PPh<sub>3</sub>)<sub>2</sub>](κ<sup>2</sup>-HCO<sub>3</sub>)<sub>2</sub> **89** (JDF file reference: d7633gya)

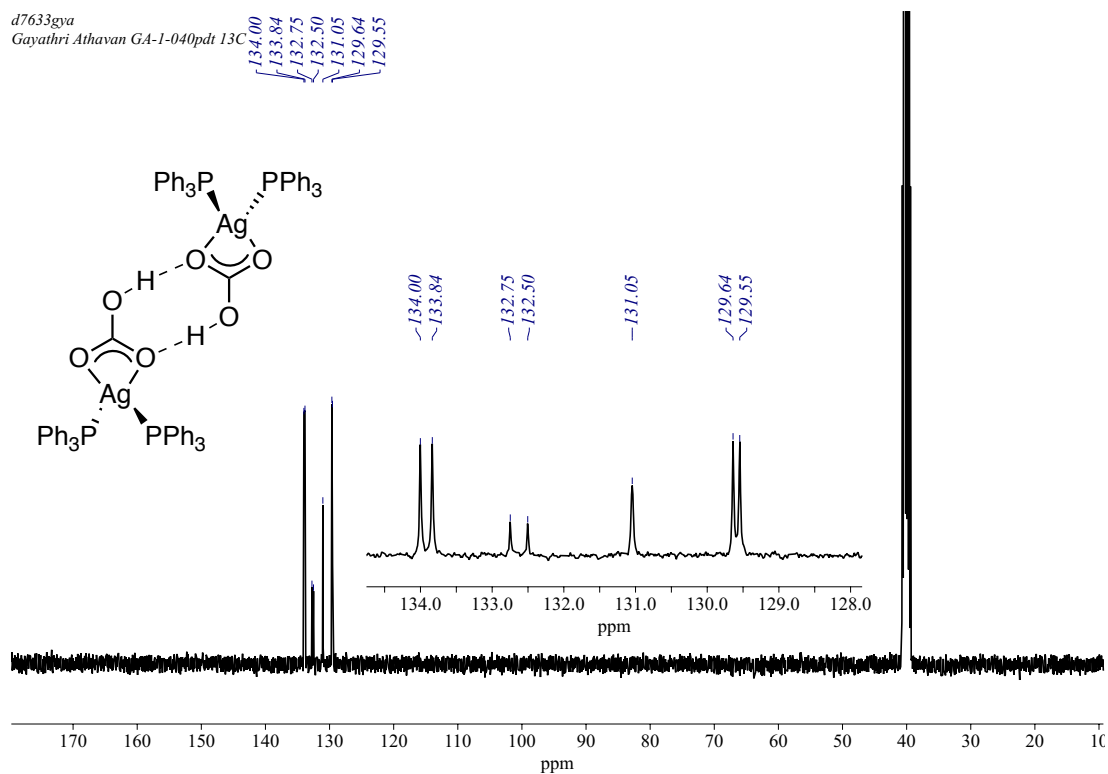


**Figure 195:**  $^{13}\text{C}\{^1\text{H}\}$  NMR (101 MHz,  $\text{DMSO-}d_6$ , 25 °C) spectrum of  $[\text{Ag}(\text{PPh}_3)_2(\kappa^2\text{-HCO}_3)_2]$  **89** (JDF file reference: d7633gya)

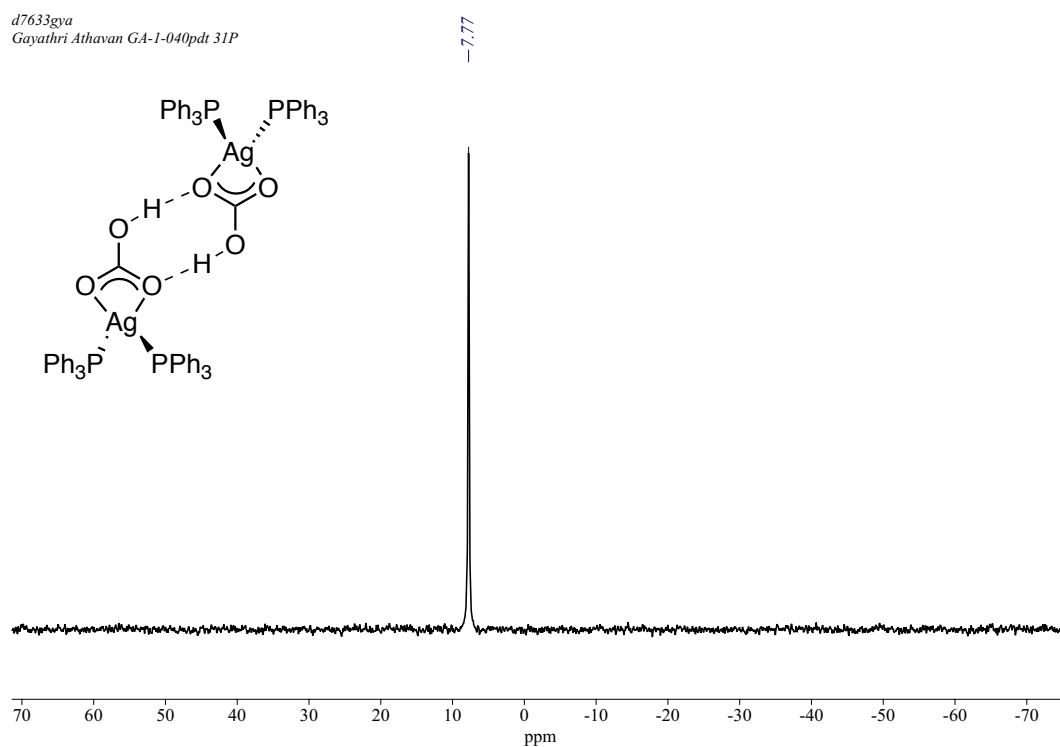


**Figure 196:**  $^{31}\text{P}\{^1\text{H}\}$  NMR (162 MHz,  $\text{DMSO-}d_6$ , 25 °C) spectrum of  $[\text{Ag}(\text{PPh}_3)_2(\kappa^2\text{-HCO}_3)_2]$  **89** (JDF file reference: d7633gya)

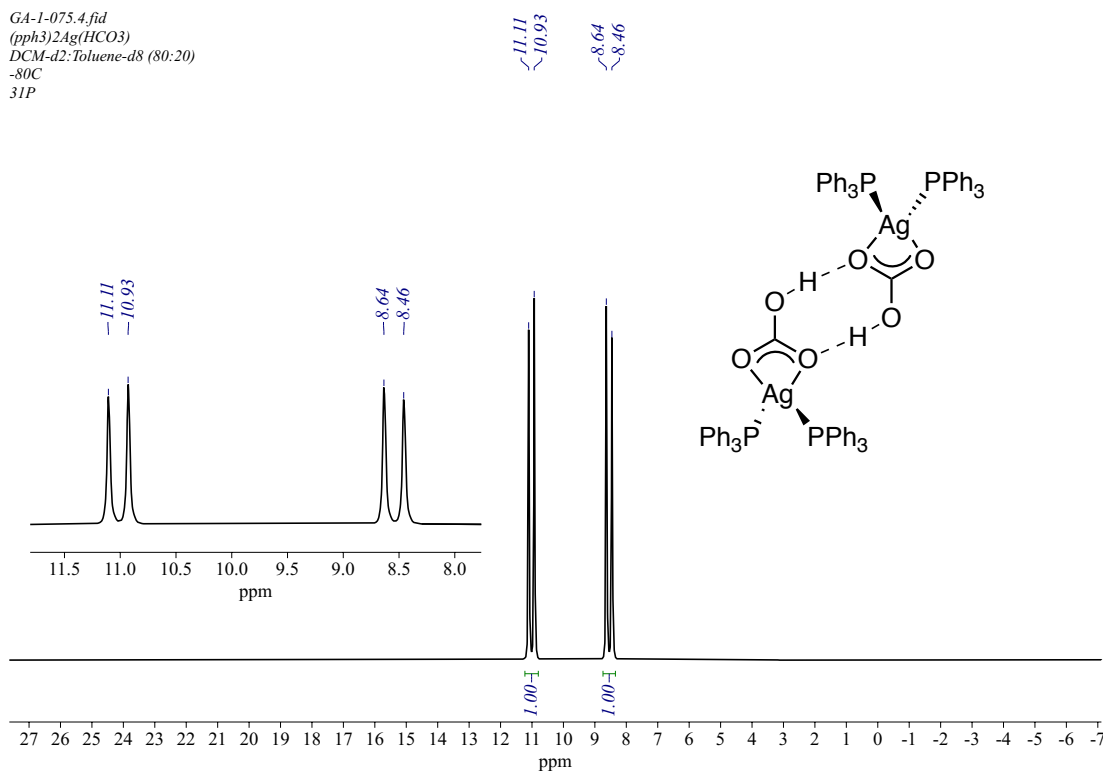


**Figure 197:**  $^{31}\text{P}\{^1\text{H}\}$  NMR (202 MHz,  $\text{tol-}d_8$ :dichloromethane- $d_2$  (20:80),  $-80^\circ\text{C}$ ) spectrum of  $[\text{Ag}(\text{PPh}_3)_2(\kappa^2\text{-HCO}_3)]_2$  **89** (spectrum collected on AV500, saved as 4 under GA-1-075)

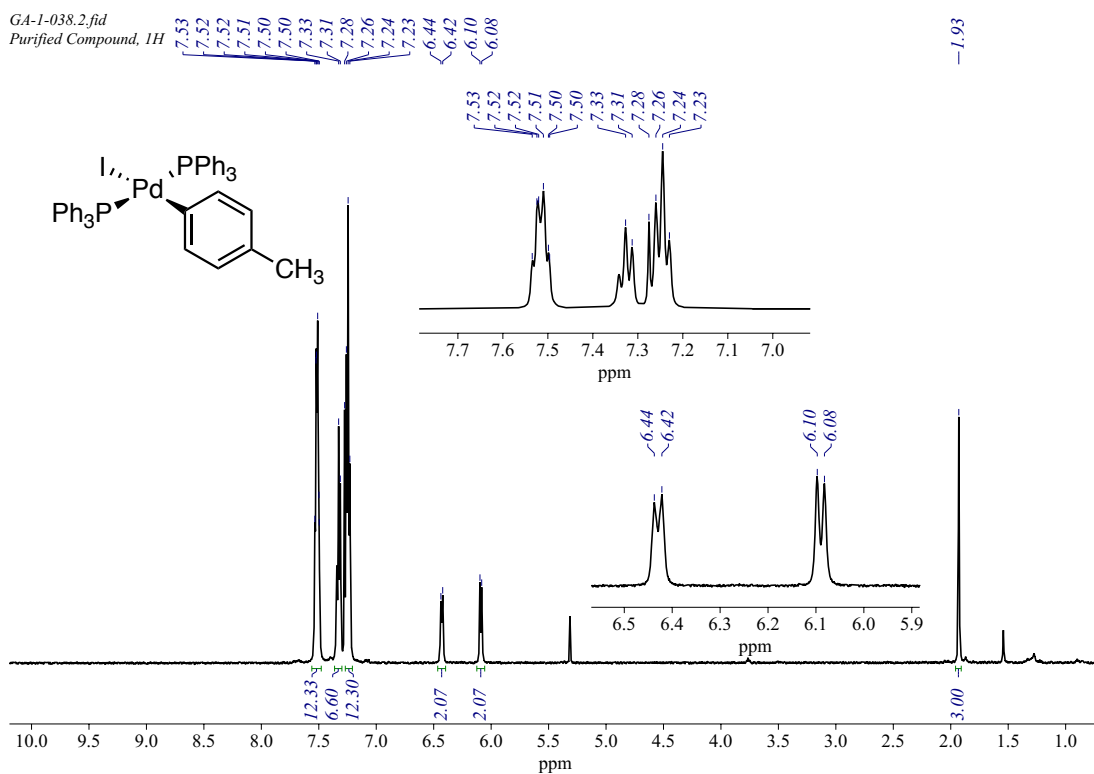


**Figure 198:**  $^1\text{H}$  NMR (500 MHz,  $\text{CDCl}_3$ ,  $25^\circ\text{C}$ ) spectrum of  $\text{Pd}(\text{PPh}_3)_2(4\text{-tolyl})(\text{I})$  **98** (spectrum collected on AV500, saved as 2 under GA-1-038)



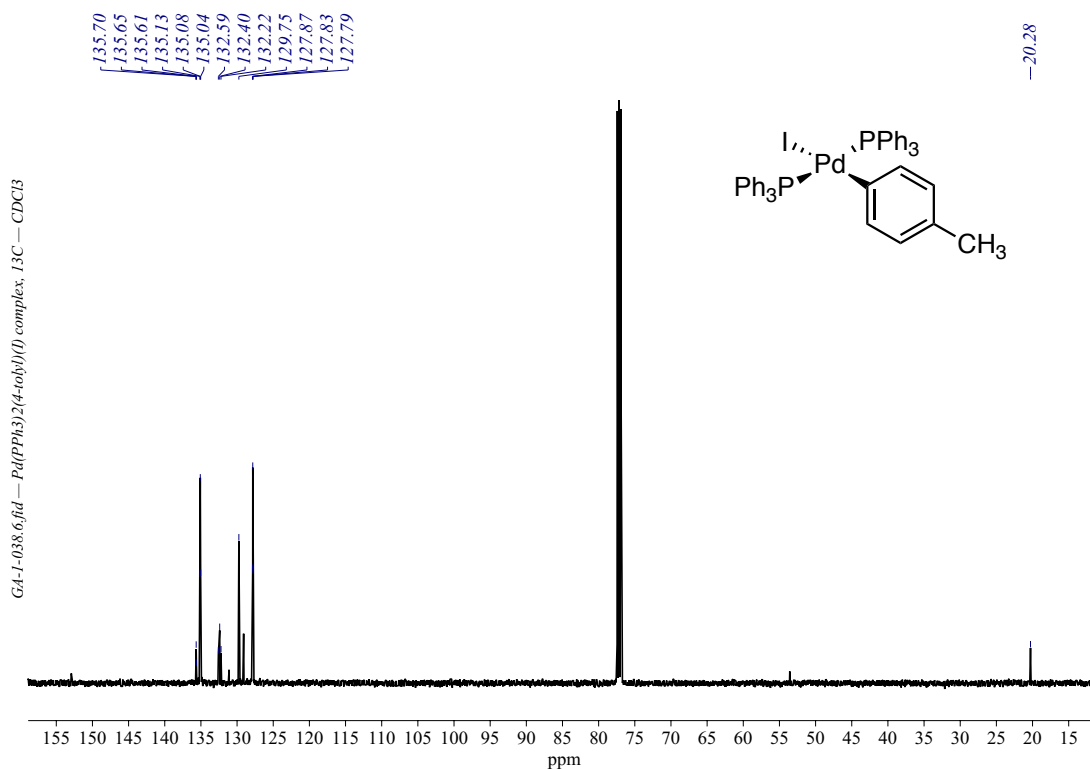


**Figure 199:** <sup>13</sup>C{<sup>1</sup>H} NMR (126 MHz, CDCl<sub>3</sub>, 25 °C) spectrum of Pd(PPh<sub>3</sub>)<sub>2</sub>(4-tolyl)(I) **98** (spectrum collected on AV500, saved as 6 under GA-1-038)

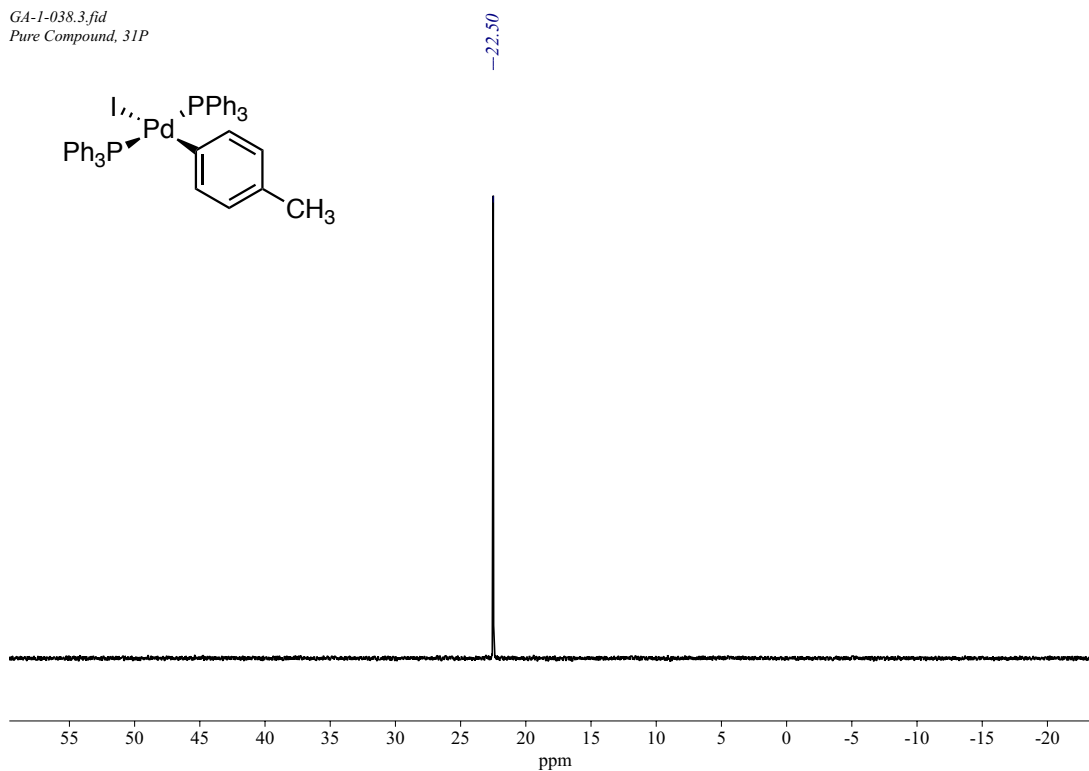


**Figure 200:** <sup>31</sup>P{<sup>1</sup>H} NMR (202 MHz, CDCl<sub>3</sub>, 25 °C) spectrum of Pd(PPh<sub>3</sub>)<sub>2</sub>(4-tolyl)(I) **98** (spectrum collected on AV500, saved as 3 under GA-1-038)

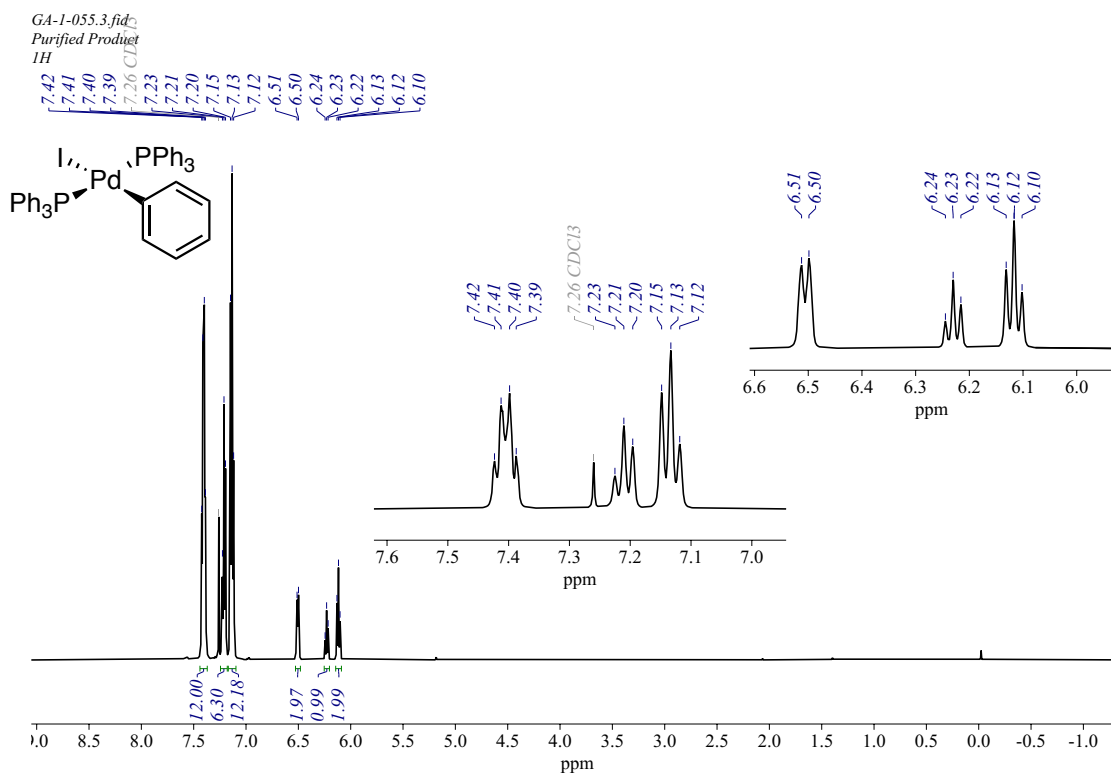


**Figure 201:**  $^1\text{H}$  NMR (500 MHz,  $\text{CDCl}_3$ , 25 °C) spectrum of  $\text{Pd}(\text{PPh}_3)_2(\text{Ph})(\text{I})$  **97** (spectrum collected on AV500, saved as 3 under GA-1-055)

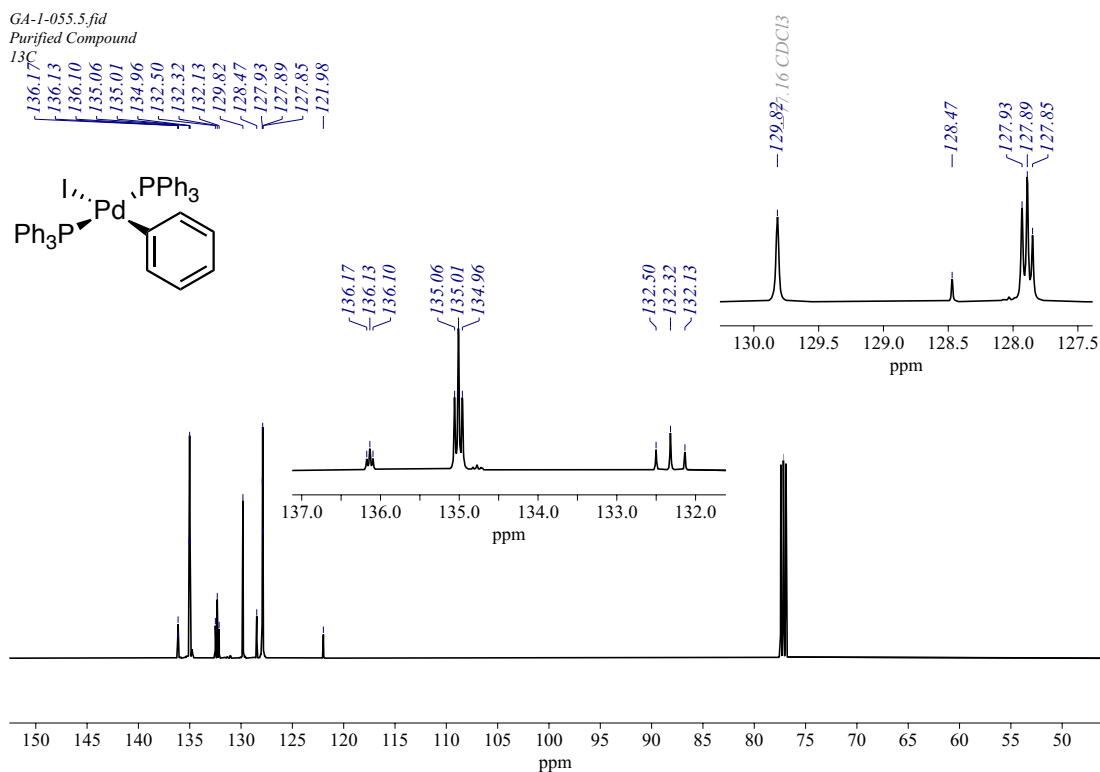


**Figure 202:**  $^{13}\text{C}\{^1\text{H}\}$  NMR (126 MHz,  $\text{CDCl}_3$ , 25 °C) spectrum of  $\text{Pd}(\text{PPh}_3)_2(\text{Ph})(\text{I})$  **97** (spectrum collected on AV500, saved as 5 under GA-1-055)

GA-1-055.4.fid  
Purified product  
31P

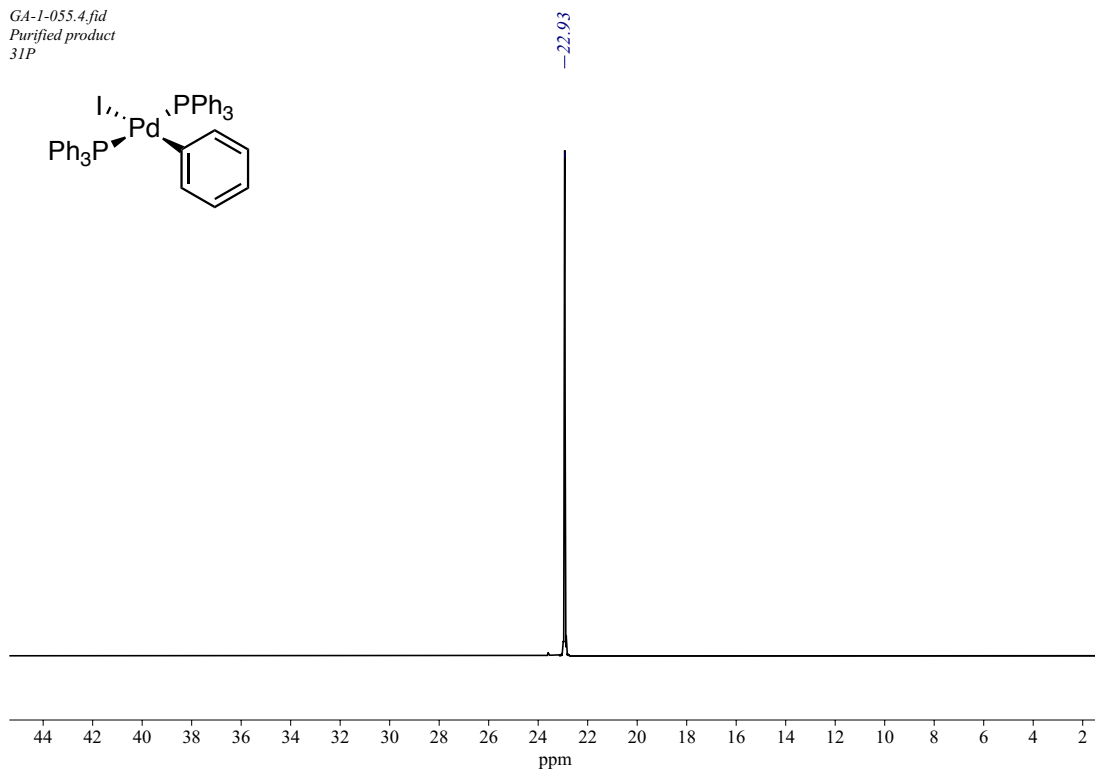
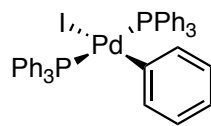


**Figure 203:**  $^{31}\text{P}\{^1\text{H}\}$  NMR (202 MHz,  $\text{CDCl}_3$ , 25 °C) spectrum of  $\text{Pd}(\text{PPh}_3)_2(\text{Ph})(\text{I})$  **97** (spectrum collected on AV500, saved as 4 under GA-1-055)

d8737gya  
Gayathri Athavan GA-1-066PufCPD 1H

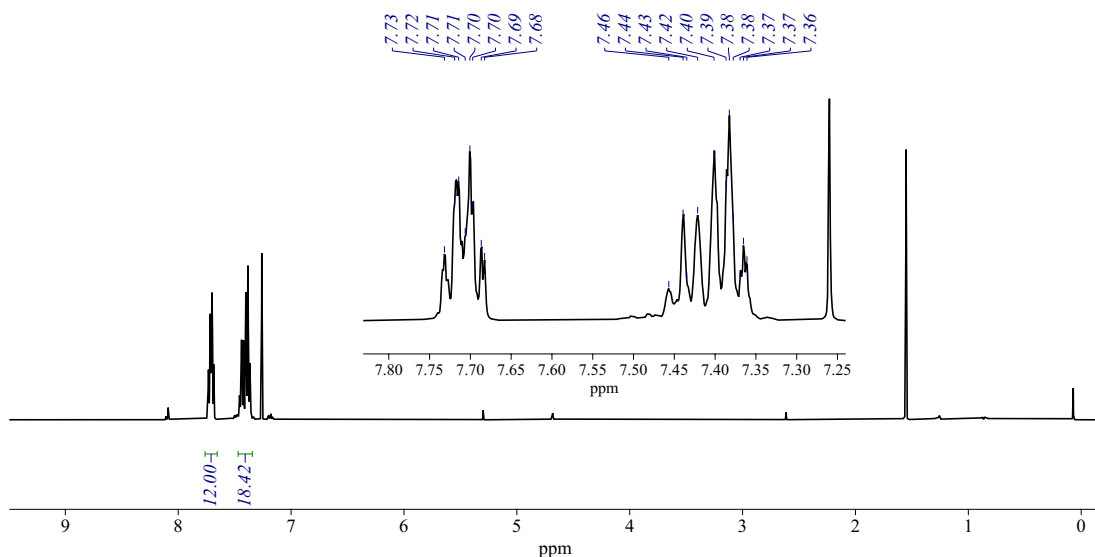
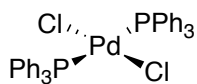


**Figure 204:**  $^1\text{H}$  NMR (400 MHz,  $\text{CDCl}_3$ , 25 °C) spectrum of  $\text{Pd}(\text{PPh}_3)_2\text{Cl}_2$  **171** (*JDF file reference: d8737gya*)

Appendix B – NMR Spectroscopic Data for Synthesised Compounds

d8737gya  
Gayathri Athavan GA-1-066PufCPD 31P

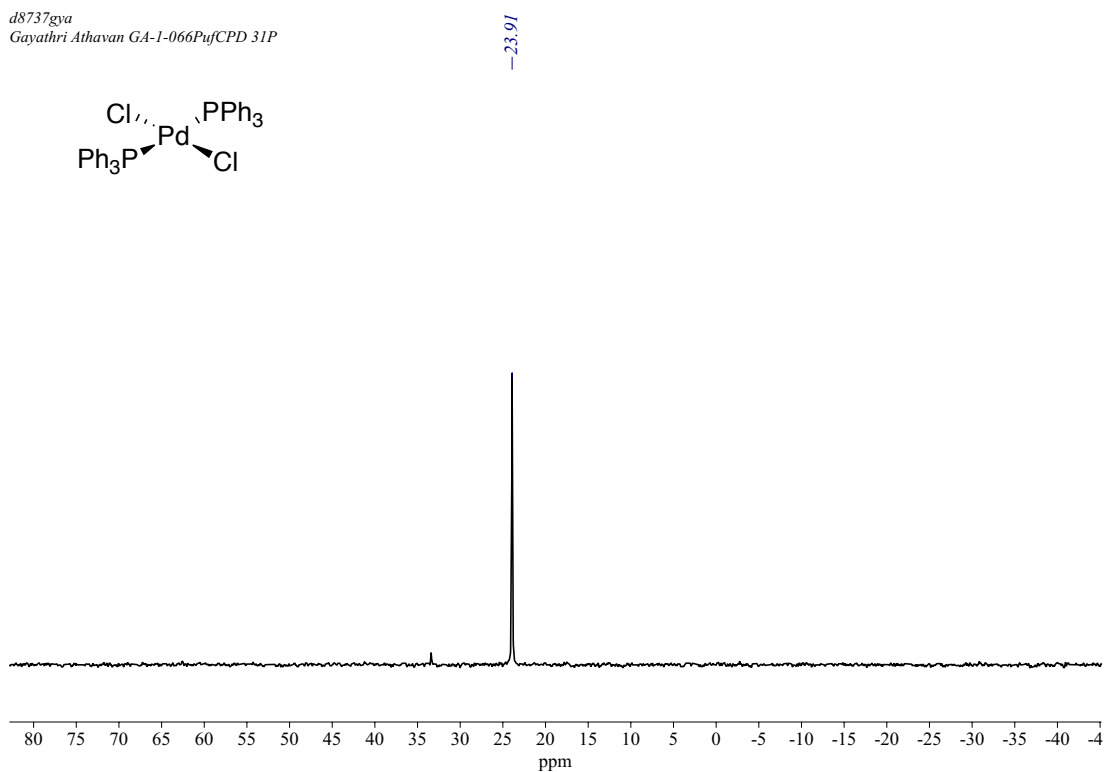


**Figure 205:**  $^{31}\text{P}\{^1\text{H}\}$  NMR (162 MHz,  $\text{CDCl}_3$ , 25 °C) spectrum of  $\text{Pd}(\text{PPh}_3)_2\text{Cl}_2$  **171** (JDF file reference: d8737gya)

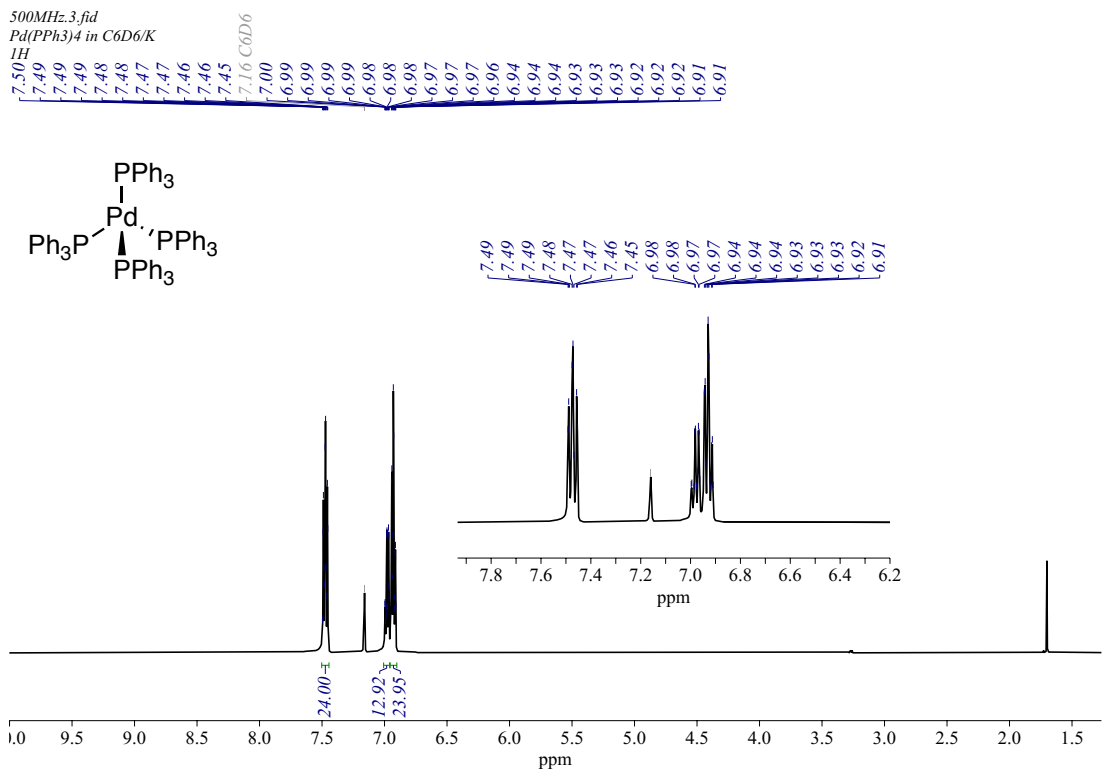


**Figure 206:**  $^1\text{H}$  NMR (500 MHz,  $\text{C}_6\text{D}_6$ , 25 °C) spectrum of  $\text{Pd}(\text{PPh}_3)_4$  **172** (spectrum collected on AV500, saved as 3 under GA-1-067)

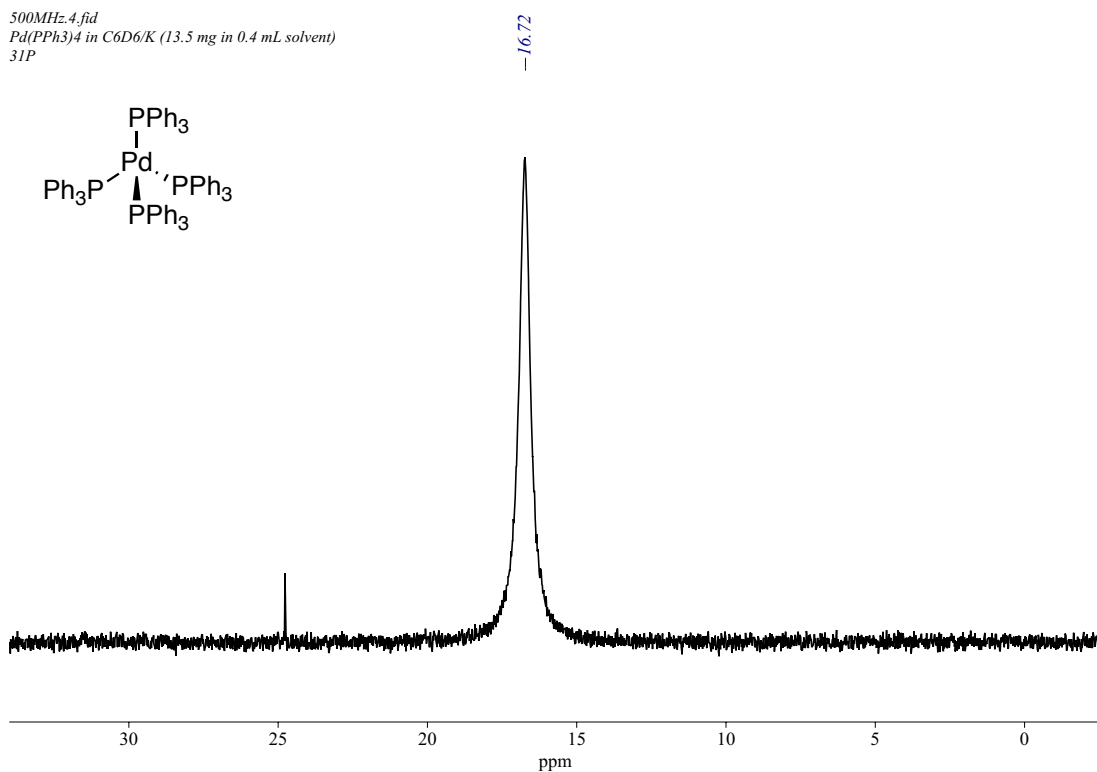


**Figure 207:** <sup>31</sup>P {<sup>1</sup>H} NMR (202 MHz, C<sub>6</sub>D<sub>6</sub>, 25 °C) spectrum of Pd(PPh<sub>3</sub>)<sub>4</sub> **172** (spectrum collected on AV500, saved as 4 under GA-1-067)

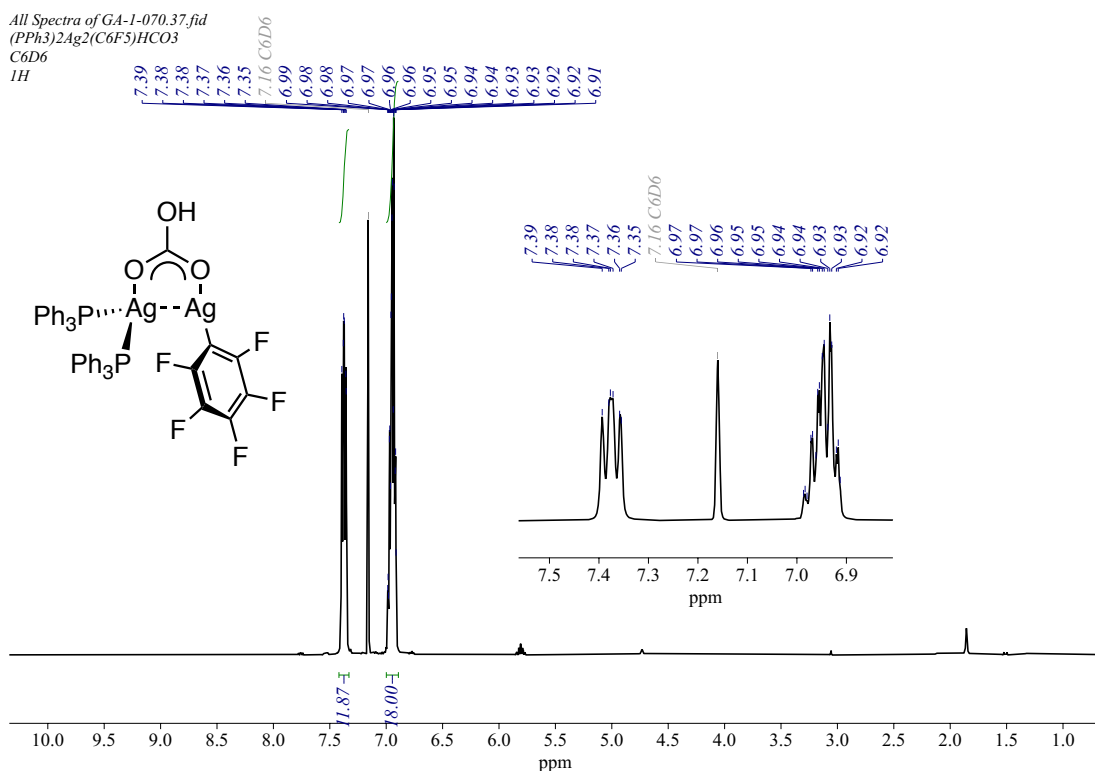


**Figure 208:** <sup>1</sup>H NMR (500 MHz, C<sub>6</sub>D<sub>6</sub>, 25 °C) spectrum of Ag<sub>2</sub>(PPh<sub>3</sub>)<sub>2</sub>(C<sub>6</sub>F<sub>5</sub>)(μ<sub>2</sub>-HCO<sub>3</sub>) **91** (spectrum collected on AV500, saved as 37 under GA-1-070)

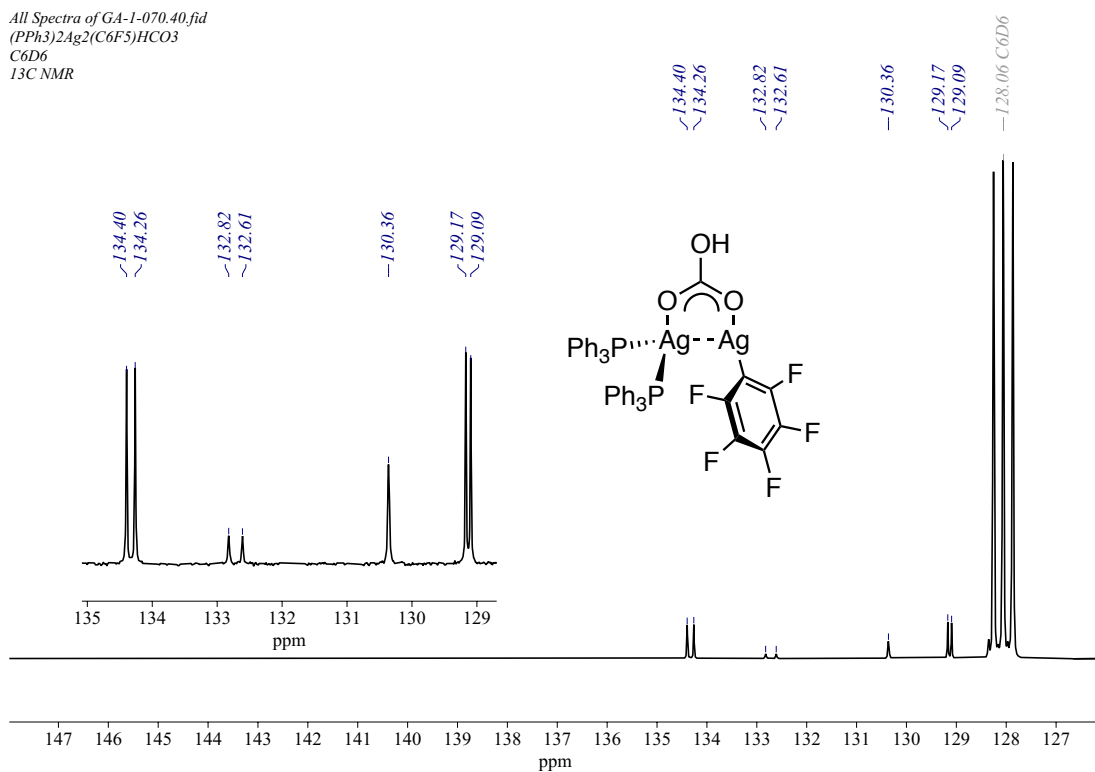


**Figure 209:** <sup>13</sup>C{<sup>1</sup>H} NMR (125.7 MHz, C<sub>6</sub>D<sub>6</sub>, 25 °C) spectrum of Ag<sub>2</sub>(PPh<sub>3</sub>)<sub>2</sub>(C<sub>6</sub>F<sub>5</sub>)(μ<sub>2</sub>-HCO<sub>3</sub>) **91** (spectrum collected on AV500, saved as 40 under GA-1-070)

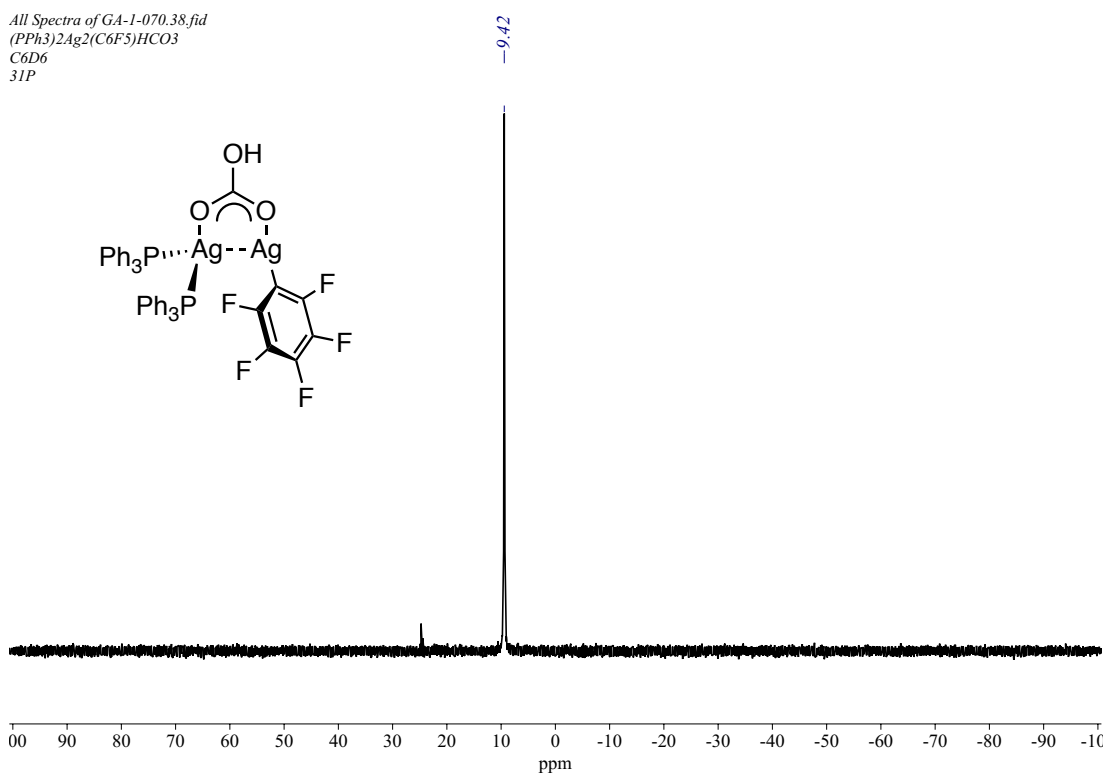


**Figure 210:** <sup>31</sup>P{<sup>1</sup>H} NMR (202 MHz, C<sub>6</sub>D<sub>6</sub>, 25 °C) spectrum of Ag<sub>2</sub>(PPh<sub>3</sub>)<sub>2</sub>(C<sub>6</sub>F<sub>5</sub>)(μ<sub>2</sub>-HCO<sub>3</sub>) **91** (spectrum collected on AV500, saved as 38 under GA-1-070)

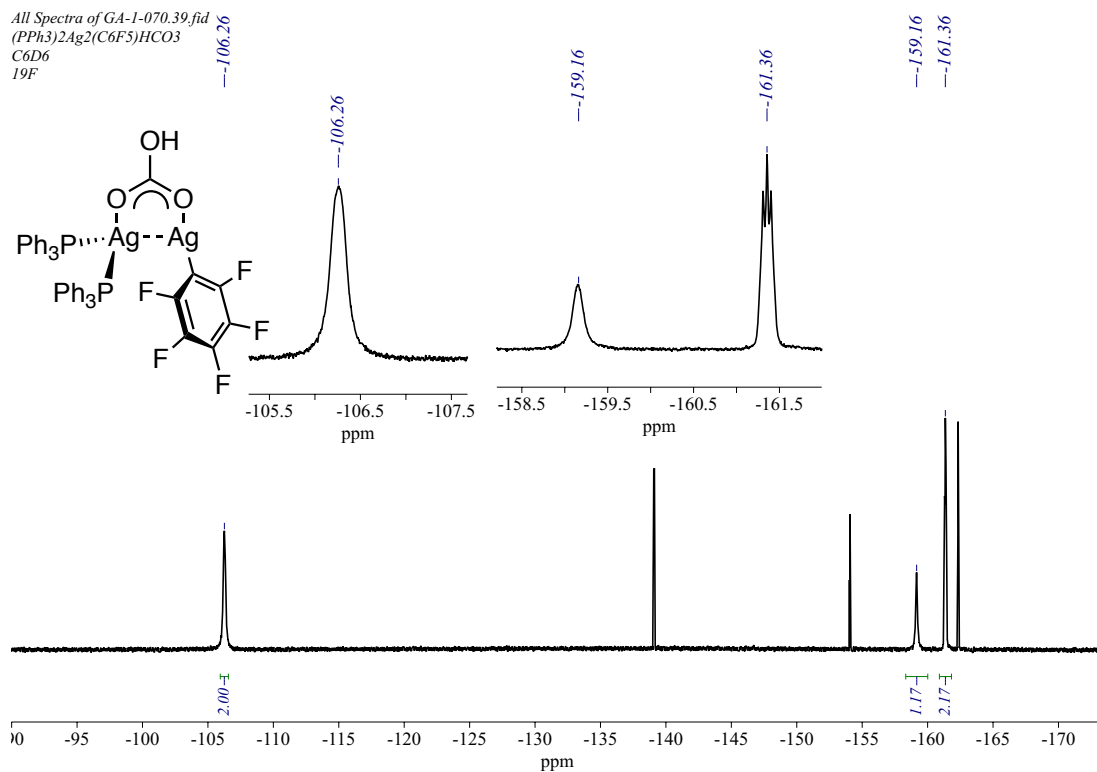


**Figure 211:**  $^{19}\text{F}\{^1\text{H}\}$  NMR (470 MHz,  $\text{C}_6\text{D}_6$ , 25 °C) spectrum of  $\text{Ag}_2(\text{PPh}_3)_2(\text{C}_6\text{F}_5)(\mu_2\text{-HCO}_3)$  **91** (spectrum collected on AV500, saved as 39 under GA-1-070)

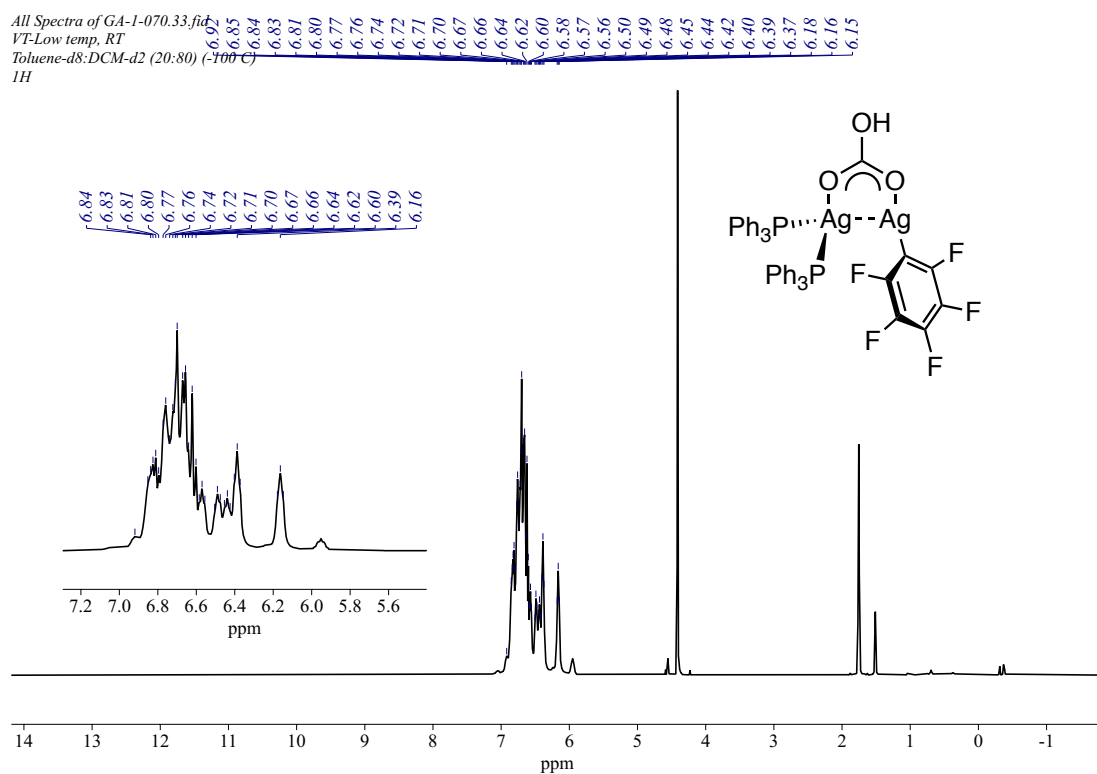


**Figure 212:**  $^1\text{H}$  NMR (500 MHz,  $\text{tol-}d_8$ :dichloromethane- $d_2$  (20:80), -100 °C) spectrum of  $\text{Ag}_2(\text{PPh}_3)_2(\text{C}_6\text{F}_5)(\mu_2\text{-HCO}_3)$  **91** (spectrum collected on AV500, saved as 33 under GA-1-070)

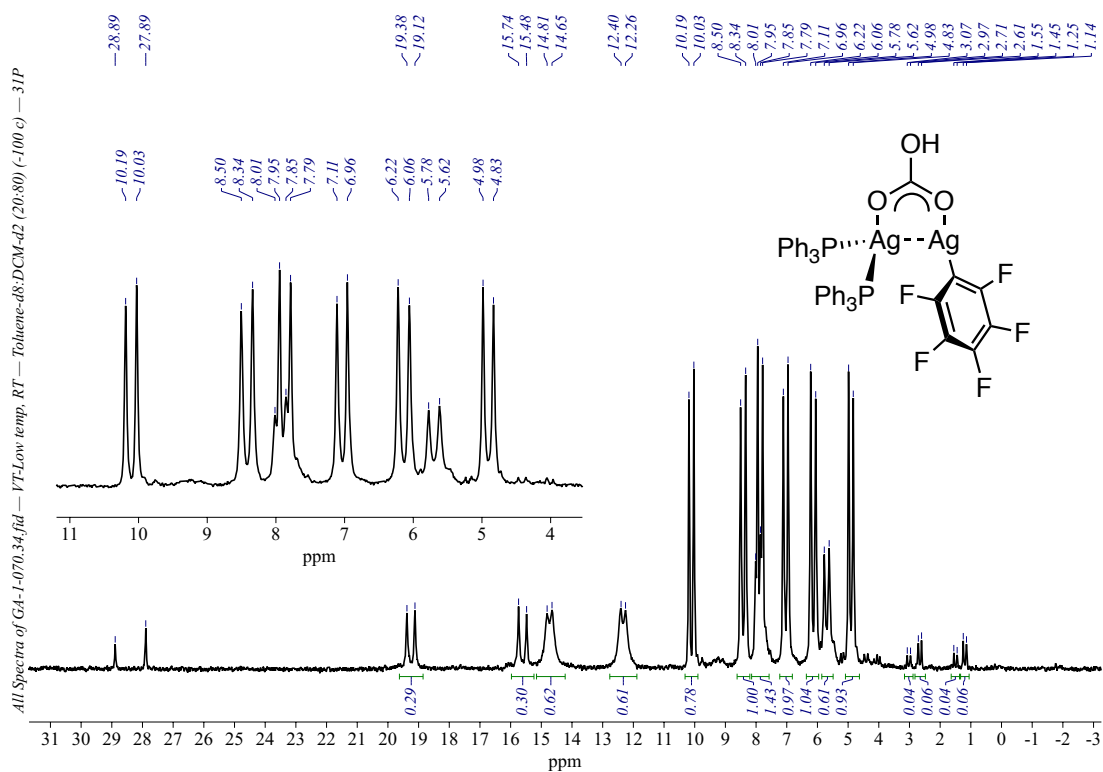


**Figure 213:** <sup>31</sup>P{<sup>1</sup>H} NMR (202 MHz, tol-*d*<sub>8</sub>: dichloromethane-*d*<sub>2</sub> (20:80), -100 °C) spectrum of Ag<sub>2</sub>(PPh<sub>3</sub>)<sub>2</sub>(C<sub>6</sub>F<sub>5</sub>)(μ<sub>2</sub>-HCO<sub>3</sub>) **91** (spectrum collected on AV500, saved as 34 under GA-1-070)

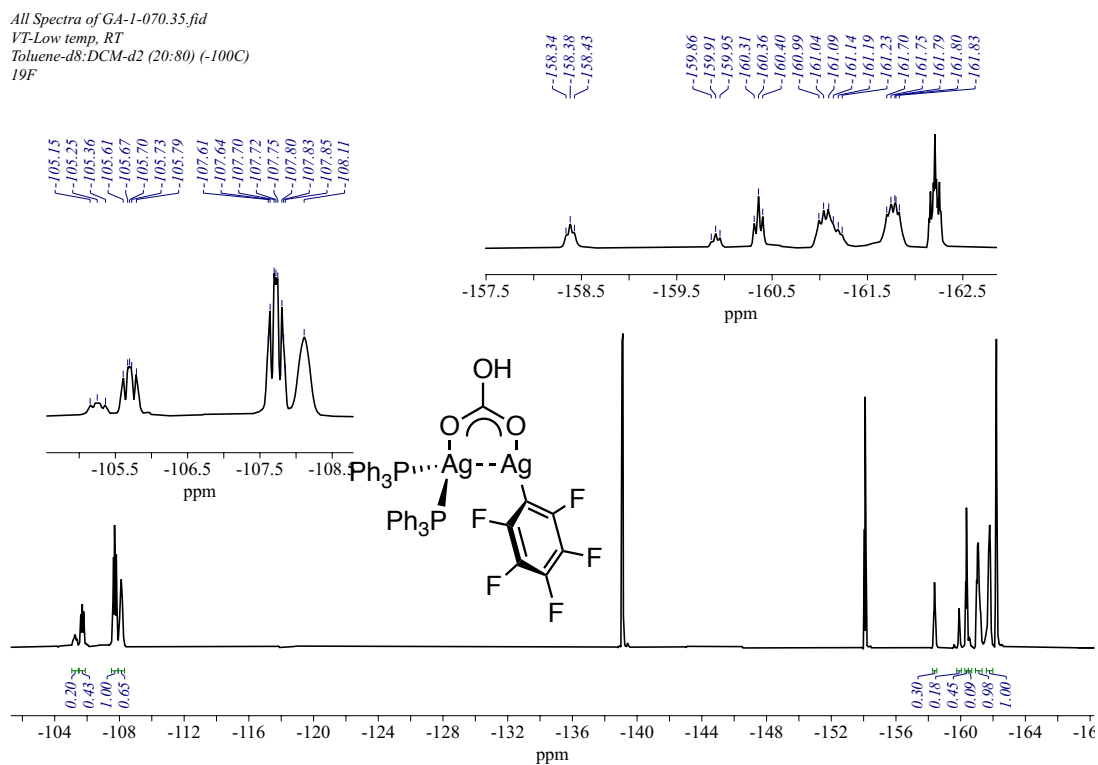


**Figure 214:** <sup>19</sup>F{<sup>1</sup>H} NMR (470 MHz, tol-*d*<sub>8</sub>: dichloromethane-*d*<sub>2</sub> (20:80), -100 °C) spectrum of **91** (spectrum collected on AV500, saved as 35 under GA-1-070)





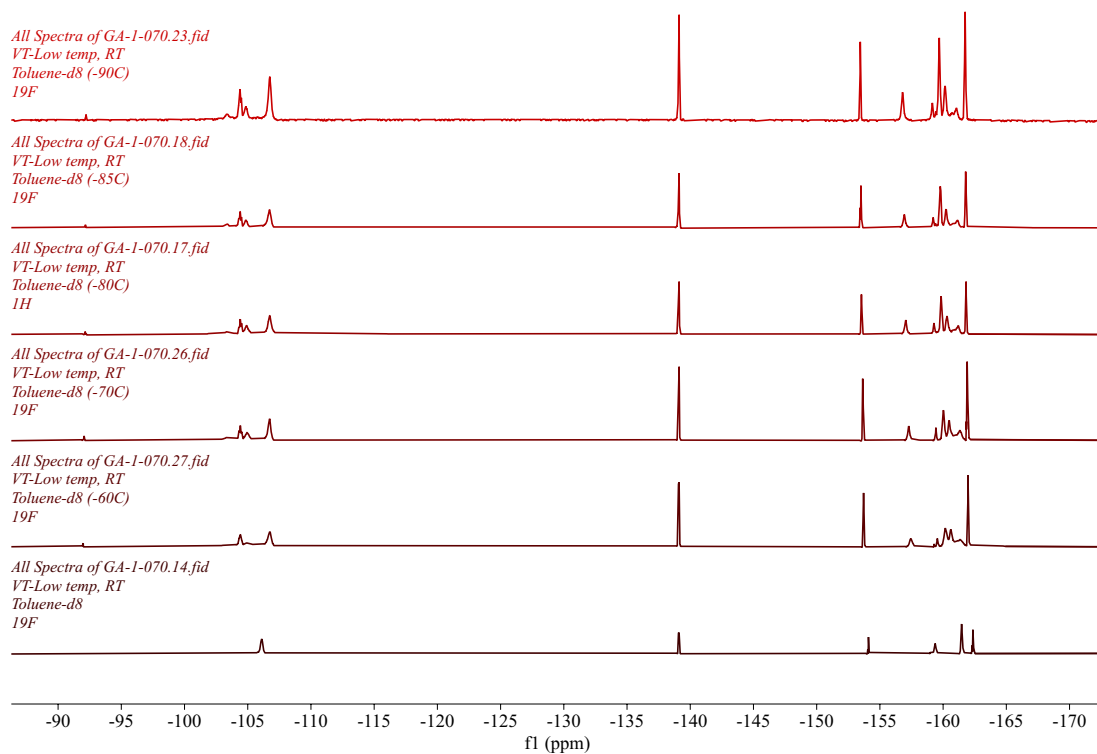


**Figure 217:** The variable-temperature  $^{19}\text{F}\{^1\text{H}\}$  NMR (470 MHz, 64 scans,  $\text{tol-}d_8$ ) spectrum of  $\text{Ag}_2(\text{PPh}_3)_2(\text{C}_6\text{F}_5)(\mu_2\text{-HCO}_3)$  **91** (spectrum collected on AV500 and saved under GA-1-070)

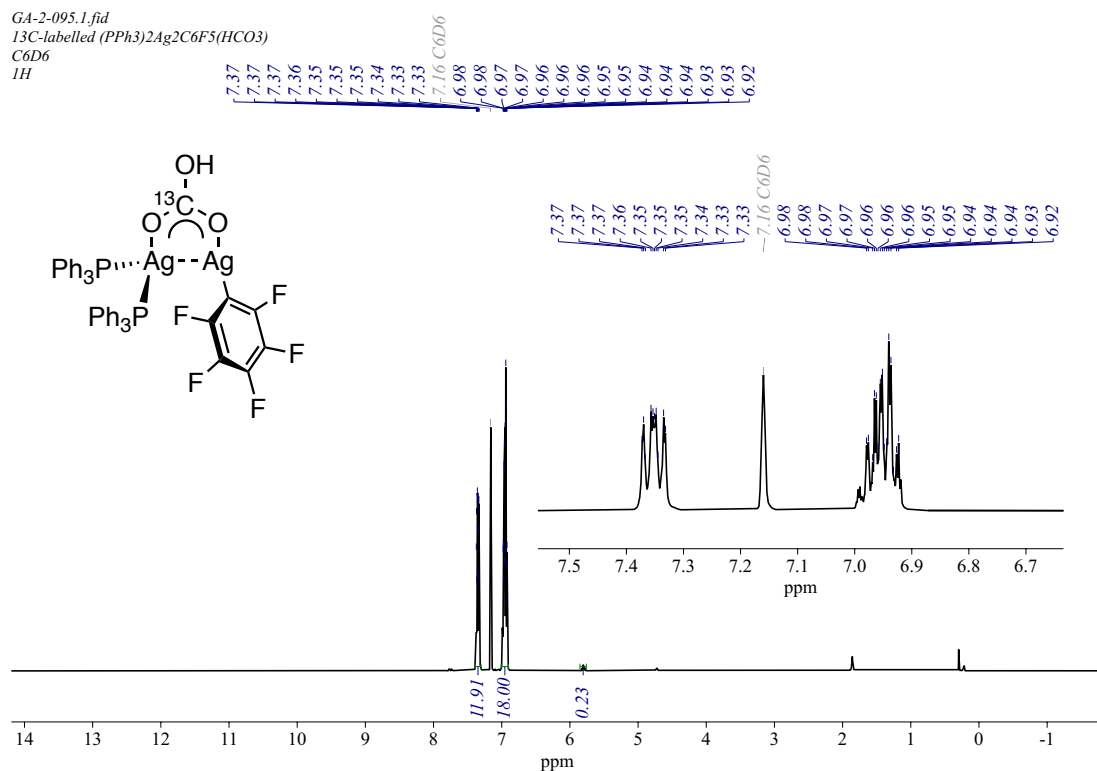


**Figure 218:**  $^1\text{H}$  NMR (500 MHz,  $\text{C}_6\text{D}_6$ , 25 °C) spectrum of  $\text{Ag}_2(\text{PPh}_3)_2(\text{C}_6\text{F}_5)(\mu_2\text{-H}^{13}\text{CO}_3)$  **92** (spectrum collected on AV500, saved as 1 under GA-2-095)

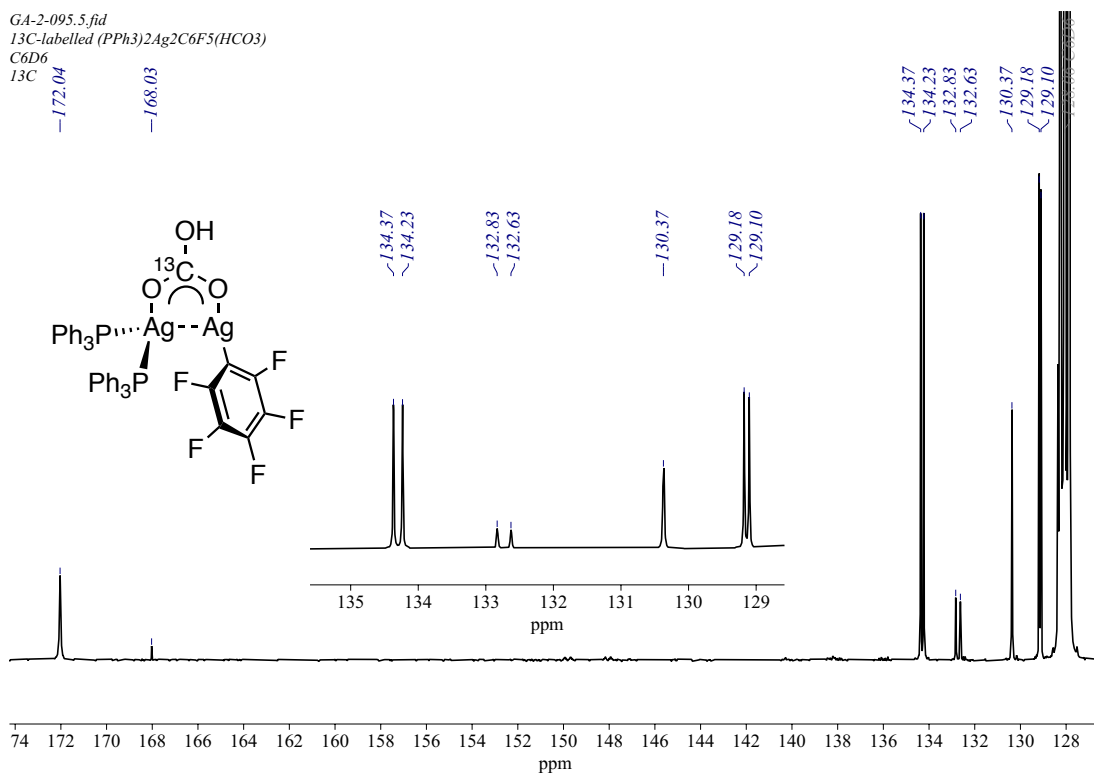


**Figure 219:** <sup>13</sup>C{<sup>1</sup>H} NMR (125.7 MHz, C<sub>6</sub>D<sub>6</sub>, 25 °C) spectrum of Ag<sub>2</sub>(PPh<sub>3</sub>)<sub>2</sub>(C<sub>6</sub>F<sub>5</sub>)(μ<sub>2</sub>-H<sup>13</sup>CO<sub>3</sub>) **92** (spectrum collected on AV500, saved as 5 under GA-2-095)

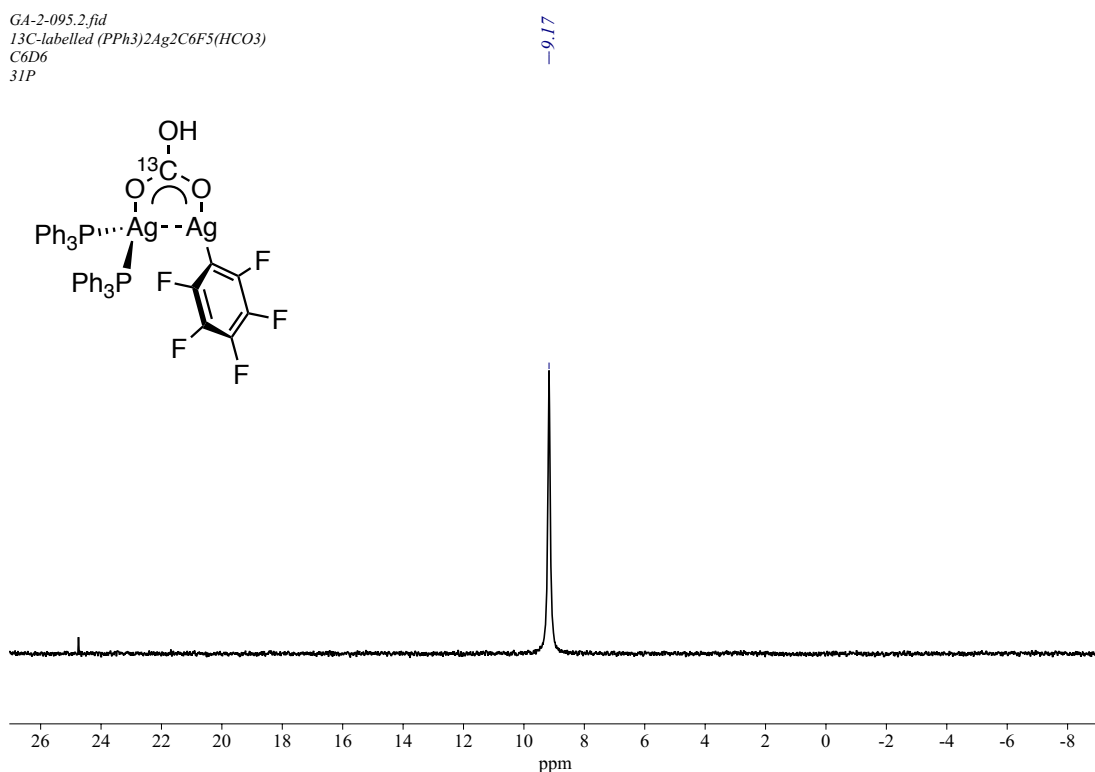


**Figure 220:** <sup>31</sup>P{<sup>1</sup>H} NMR (202 MHz, C<sub>6</sub>D<sub>6</sub>, 25 °C) spectrum of Ag<sub>2</sub>(PPh<sub>3</sub>)<sub>2</sub>(C<sub>6</sub>F<sub>5</sub>)(μ<sub>2</sub>-H<sup>13</sup>CO<sub>3</sub>) **92** (spectrum collected on AV500, saved as 2 under GA-1-095)

Appendix B – NMR Spectroscopic Data for Synthesised Compounds

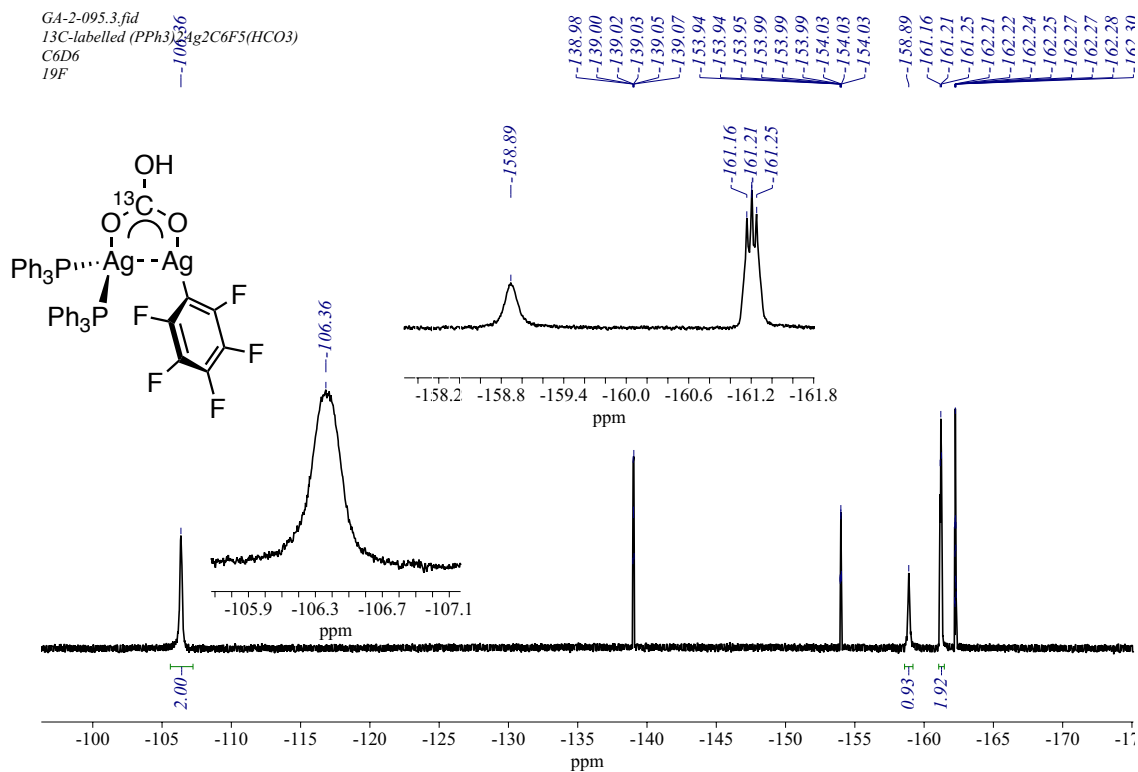


**Figure 221:**  $^{19}\text{F}\{^1\text{H}\}$  NMR (470 MHz,  $\text{C}_6\text{D}_6$ , 25 °C) spectrum of  $\text{Ag}_2(\text{PPh}_3)_2(\text{C}_6\text{F}_5)(\mu_2\text{-H}^{13}\text{CO}_3)$  **92** (spectrum collected on AV500, saved as 3 under GA-1-095)

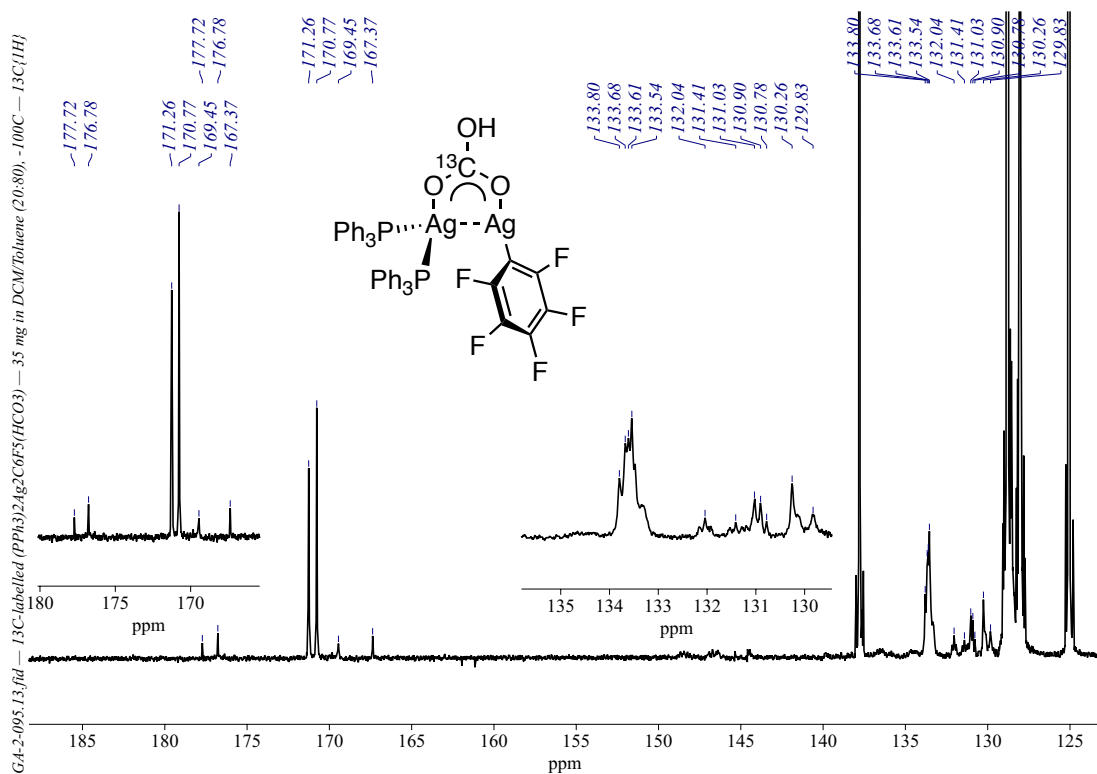


**Figure 222:**  $^{13}\text{C}\{^1\text{H}\}$  NMR (125.7 MHz,  $\text{tol-}d_8$ :dichloromethane- $d_2$  (20:80), -100 °C) spectrum of  $\text{Ag}_2(\text{PPh}_3)_2(\text{C}_6\text{F}_5)(\mu_2\text{-H}^{13}\text{CO}_3)$  **92** (spectrum collected on AV500, saved as 13 under GA-1-095)

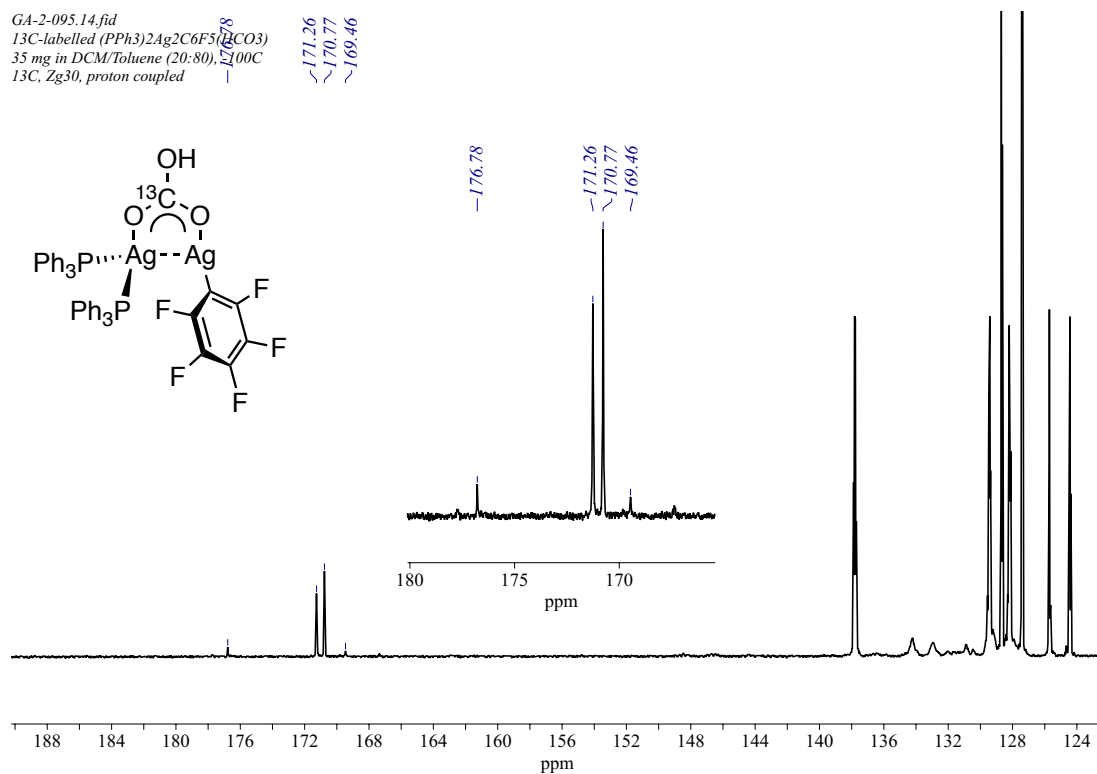


**Figure 223:** <sup>13</sup>C NMR (125.7 MHz, tol-*d*<sub>8</sub>:dichloromethane-*d*<sub>2</sub> (20:80)) spectrum of  $\text{Ag}_2(\text{PPh}_3)_2(\text{C}_6\text{F}_5)(\mu_2\text{-H}^{13}\text{CO}_3)$  **92** (spectrum collected on AV500, saved as 14 under GA-1-095)

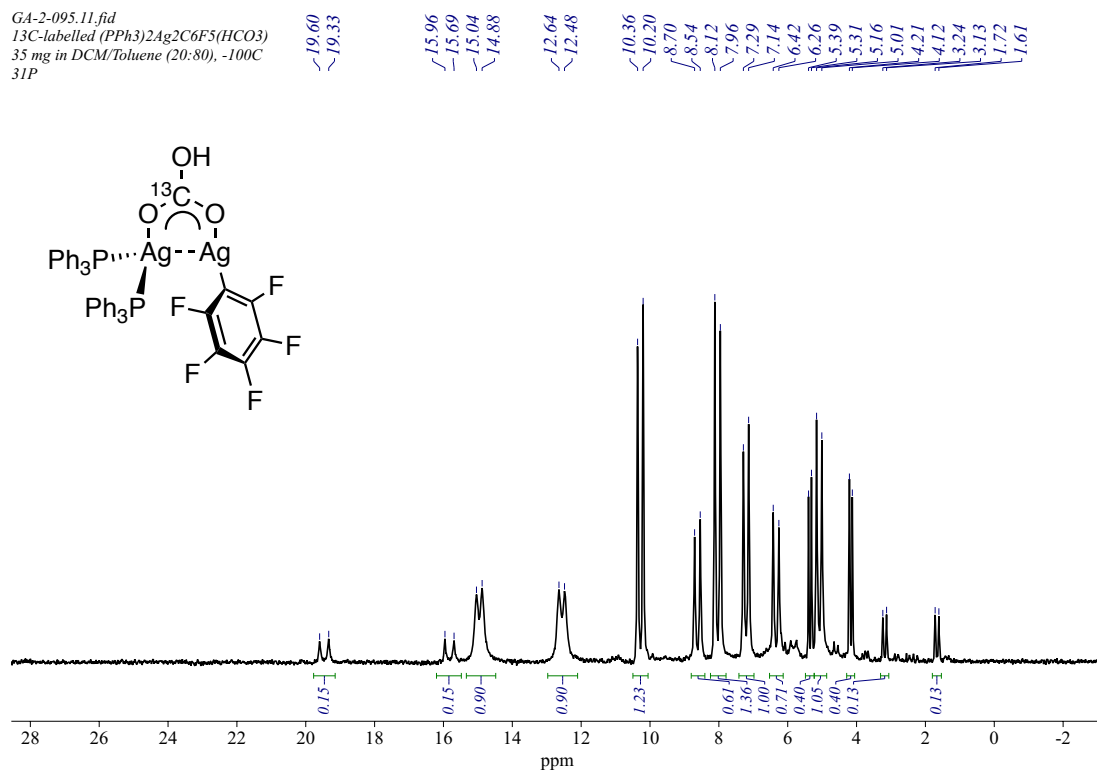
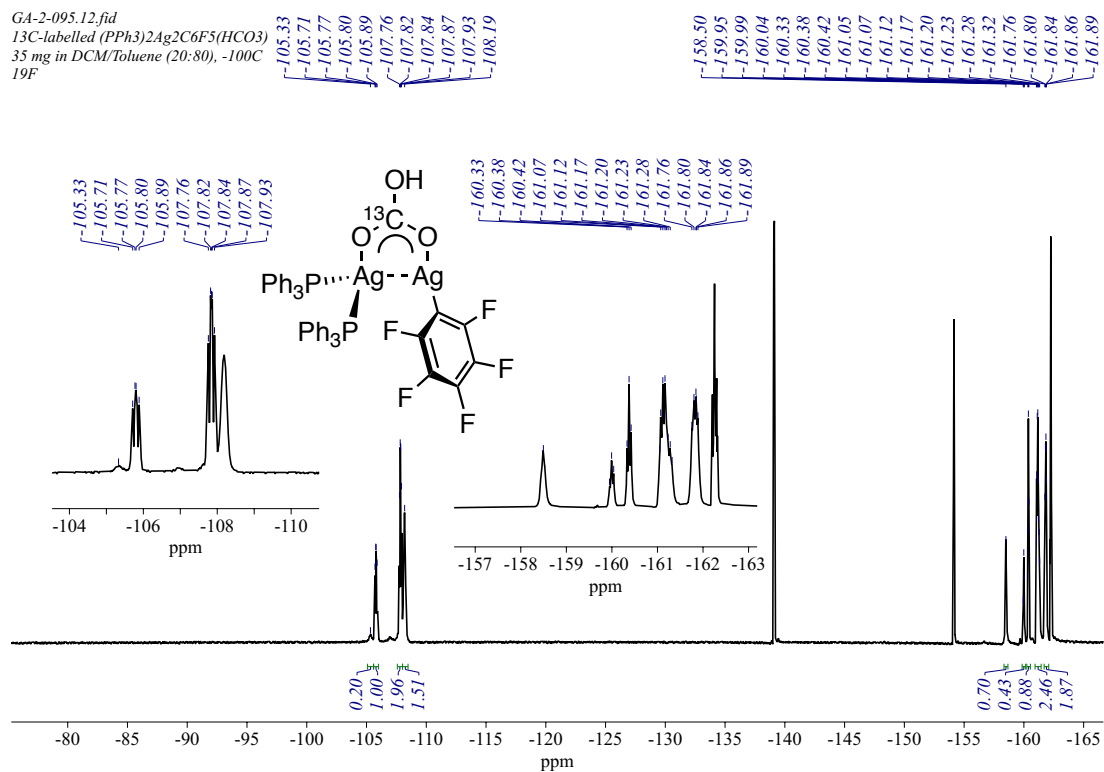
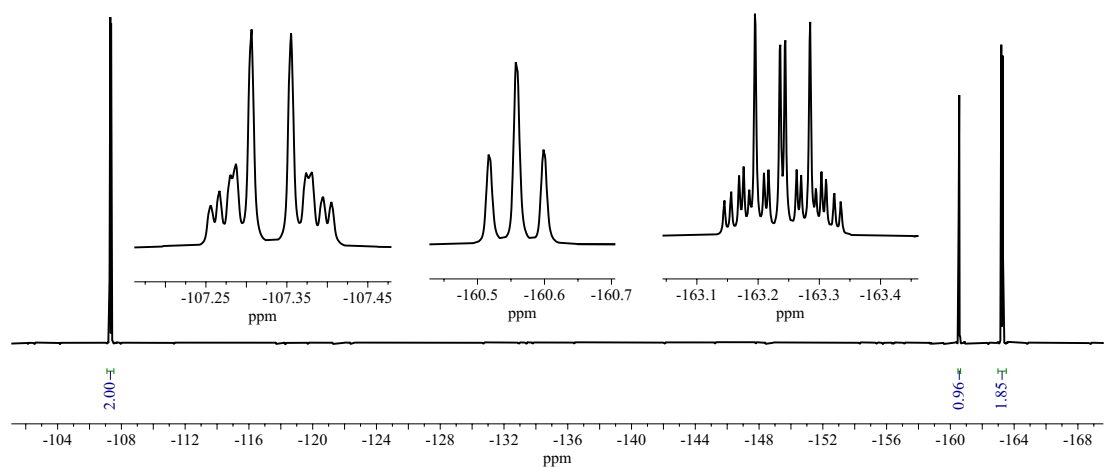


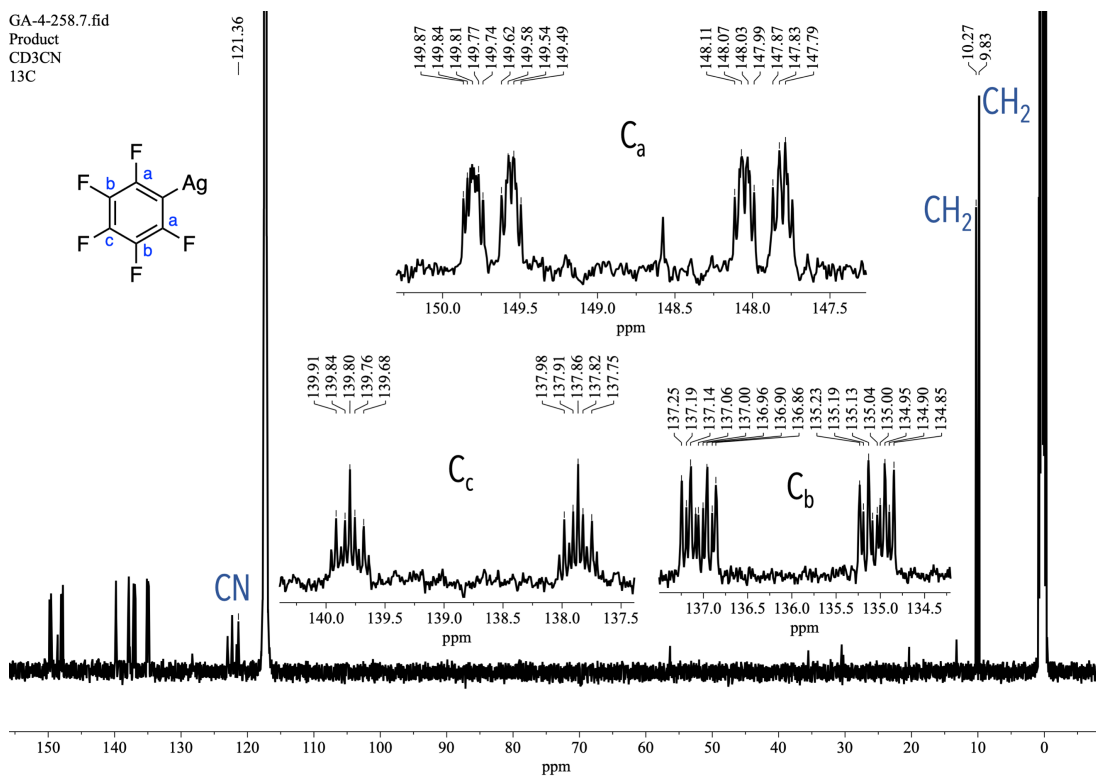
**Figure 224:** <sup>31</sup>P{<sup>1</sup>H} NMR (202 MHz, tol-*d*<sub>8</sub>:dichloromethane-*d*<sub>2</sub> (20:80), -100 °C) spectrum of  $\text{Ag}_2(\text{PPh}_3)_2(\text{C}_6\text{F}_5)(\mu_2\text{-H}^{13}\text{CO}_3)$  **92** (spectrum collected on AV500, saved as 11 under GA-1-095)

Appendix B – NMR Spectroscopic Data for Synthesised Compounds

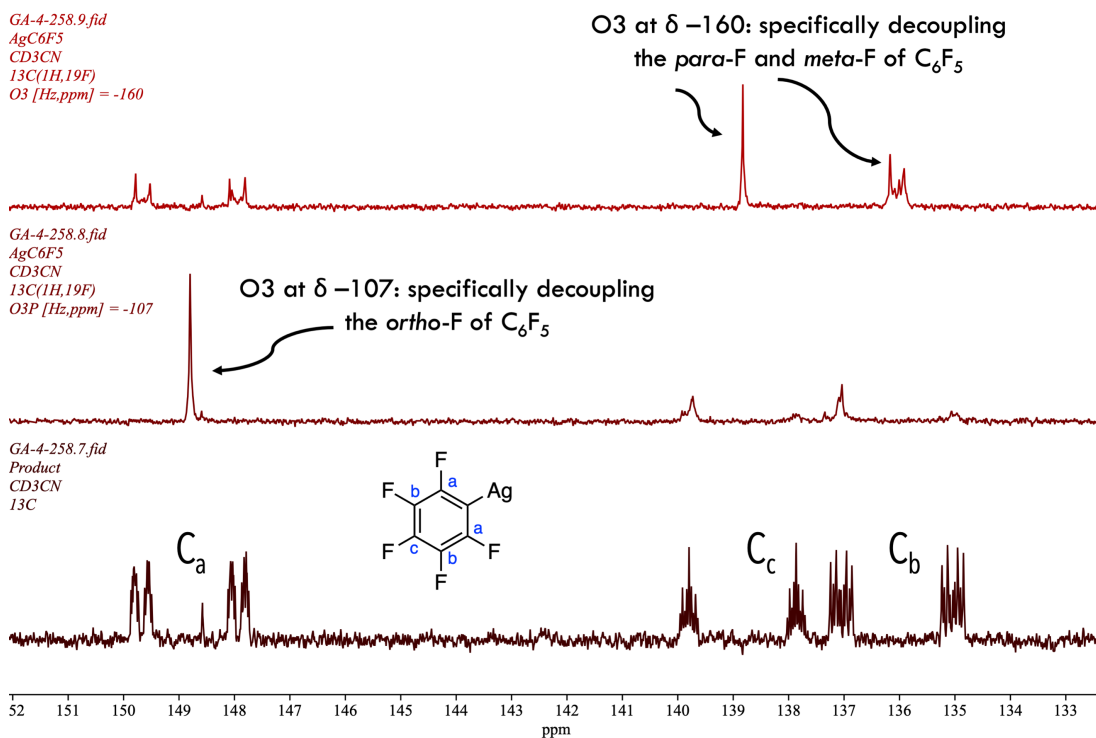


GA-4-258.4.fid  
 AgC<sub>6</sub>F<sub>5</sub>  
 CD<sub>3</sub>CN, 19F

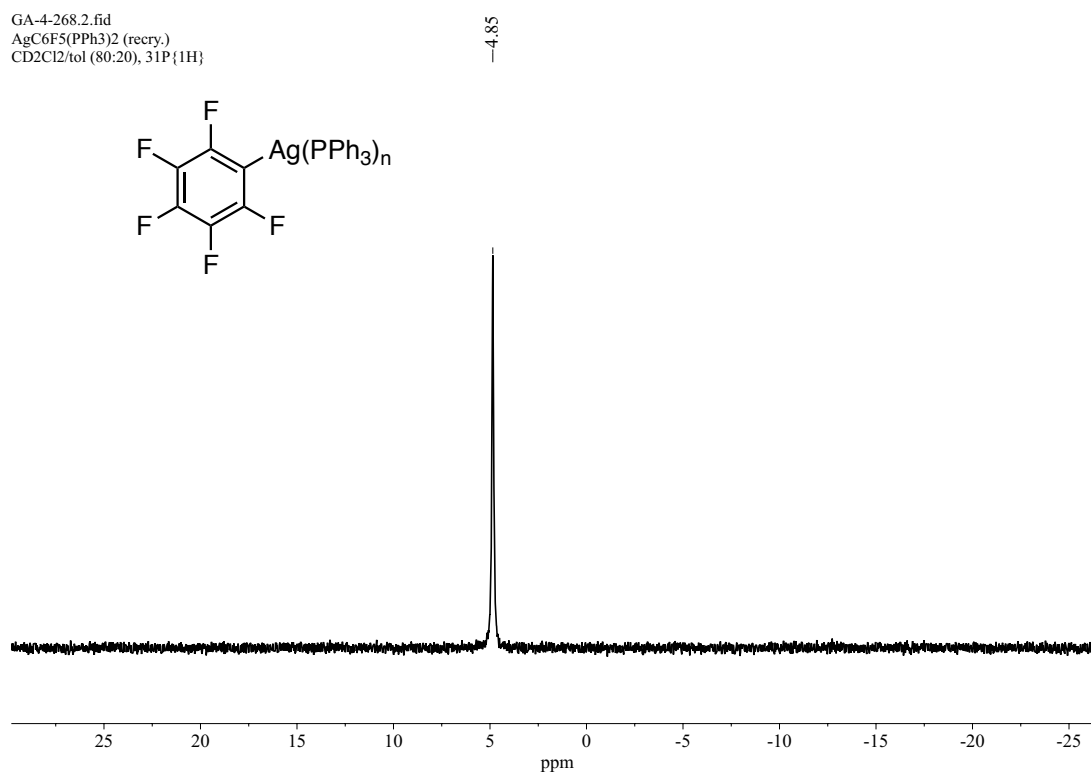




**Figure 227:** The <sup>13</sup>C{<sup>1</sup>H} (125.8 MHz, CD<sub>3</sub>CN, 25 °C) spectrum of AgC<sub>6</sub>F<sub>5</sub> 55. Trace amount of EtCN (blue) is also present in the solution. EtCN and CD<sub>3</sub>CN tend to coordinate strongly with AgC<sub>5</sub>F<sub>6</sub>, the CN <sup>13</sup>C peaks of the coordinated species is also present in the <sup>13</sup>C spectra. (spectrum collected on AV500, saved as 7 under GA-4-258)



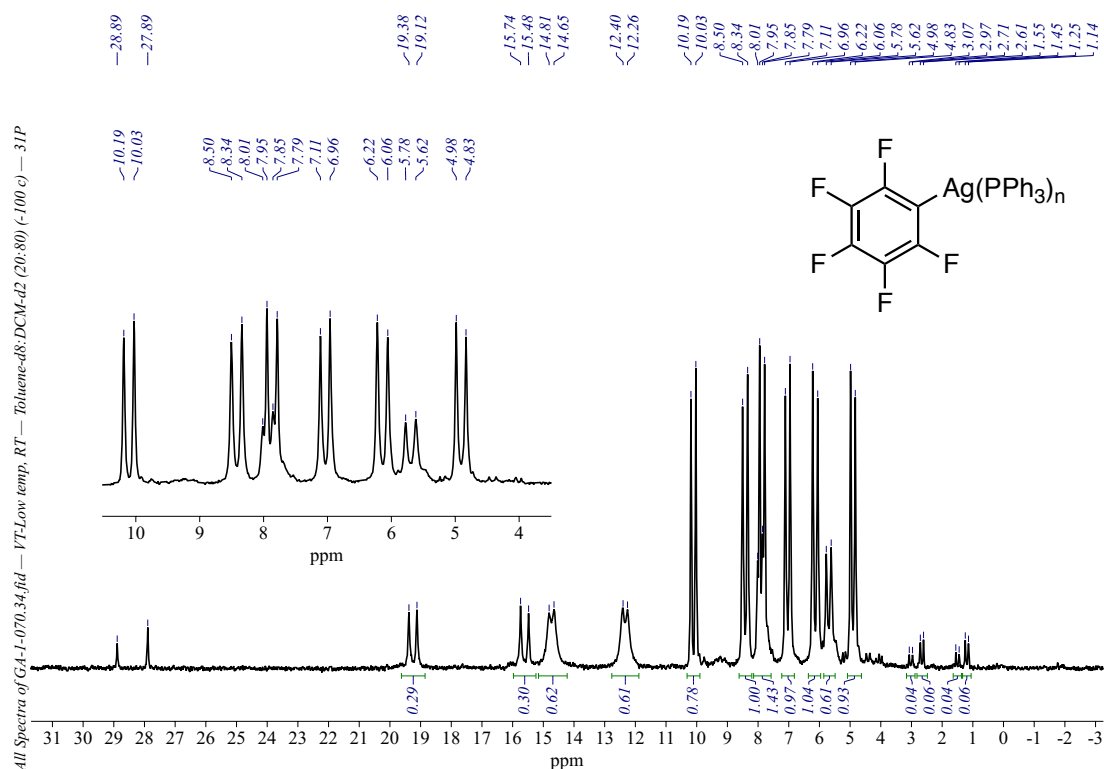
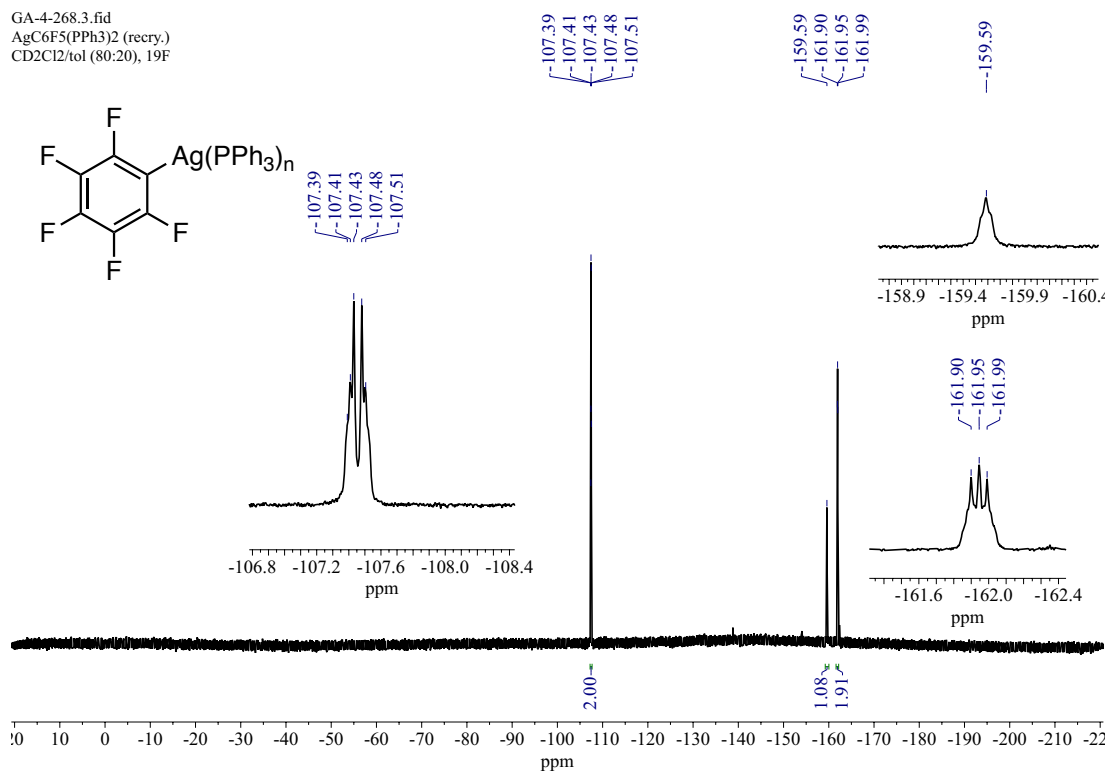
**Figure 228:** The Stack plot of the  $^{13}\text{C}\{^1\text{H}\}$  NMR spectrum (bottom),  $^{13}\text{C}\{^1\text{H}, ^{19}\text{F}\}$  NMR spectrum with O3P = -107 (middle) and  $^{13}\text{C}\{^1\text{H}, ^{19}\text{F}\}$  NMR spectrum (top) of AgC<sub>6</sub>F<sub>5</sub> **55**. (spectra collected on AV500, saved under GA-4-258)

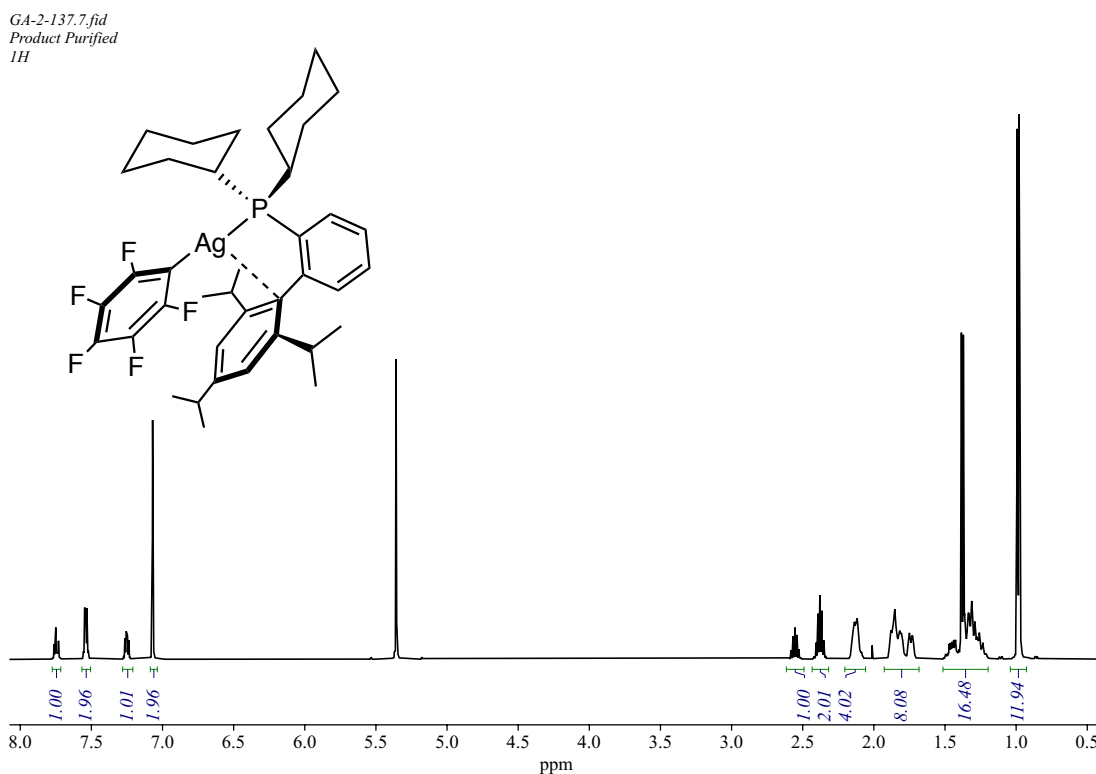
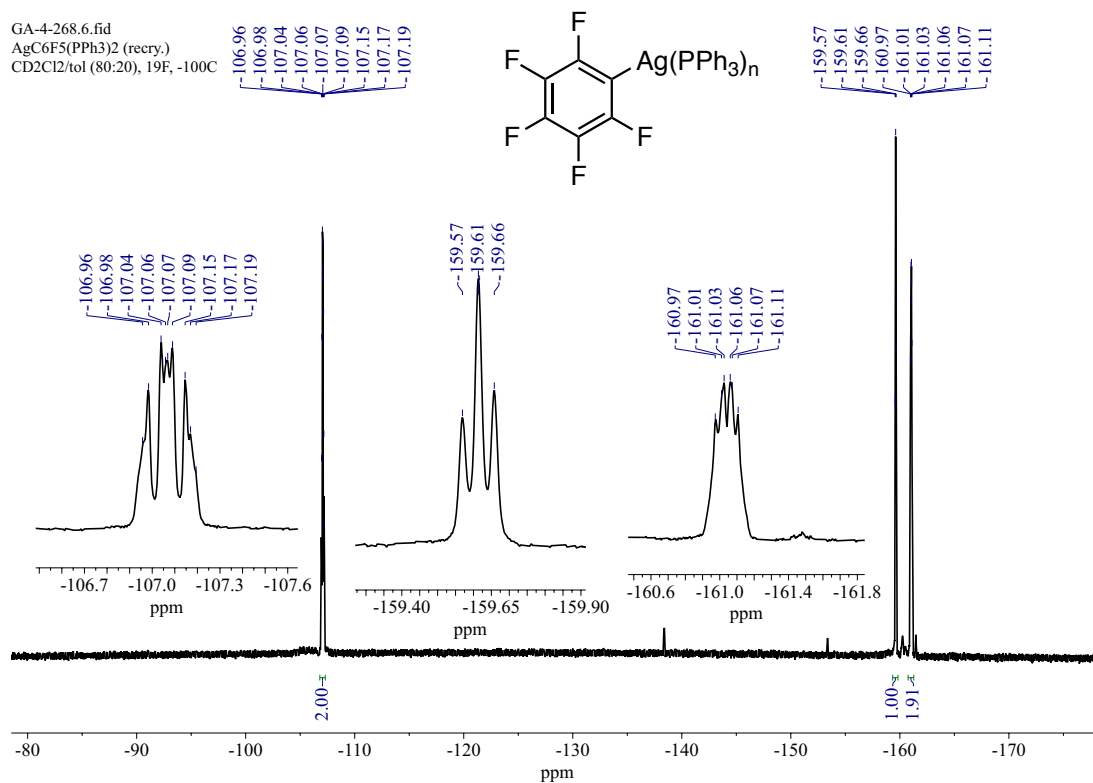


**Figure 229:**  $^{31}\text{P}\{^1\text{H}\}$  NMR (202 MHz, tol-*d*<sub>8</sub>:dichloromethane-*d*<sub>2</sub> (20:80), 25 °C ) spectrum of Ag<sub>2</sub>(PPh<sub>3</sub>)<sub>n</sub>(C<sub>6</sub>F<sub>5</sub>) **93** (spectrum collected on AV500, saved as 2 under GA-4-268)



Appendix B – NMR Spectroscopic Data for Synthesised Compounds





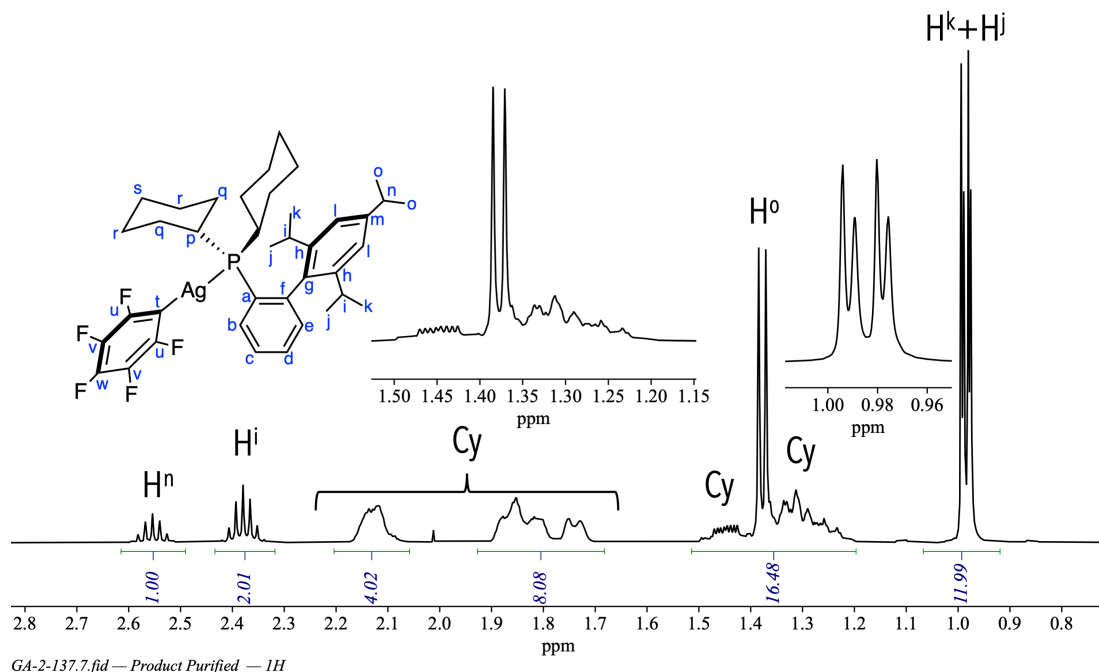


**Figure 234:**  $^1\text{H}$  NMR (500 MHz,  $\text{CD}_2\text{Cl}_2$ ,  $25^\circ\text{C}$ ) spectrum of **101** between  $\delta$  0.7 and  $\delta$  3.00

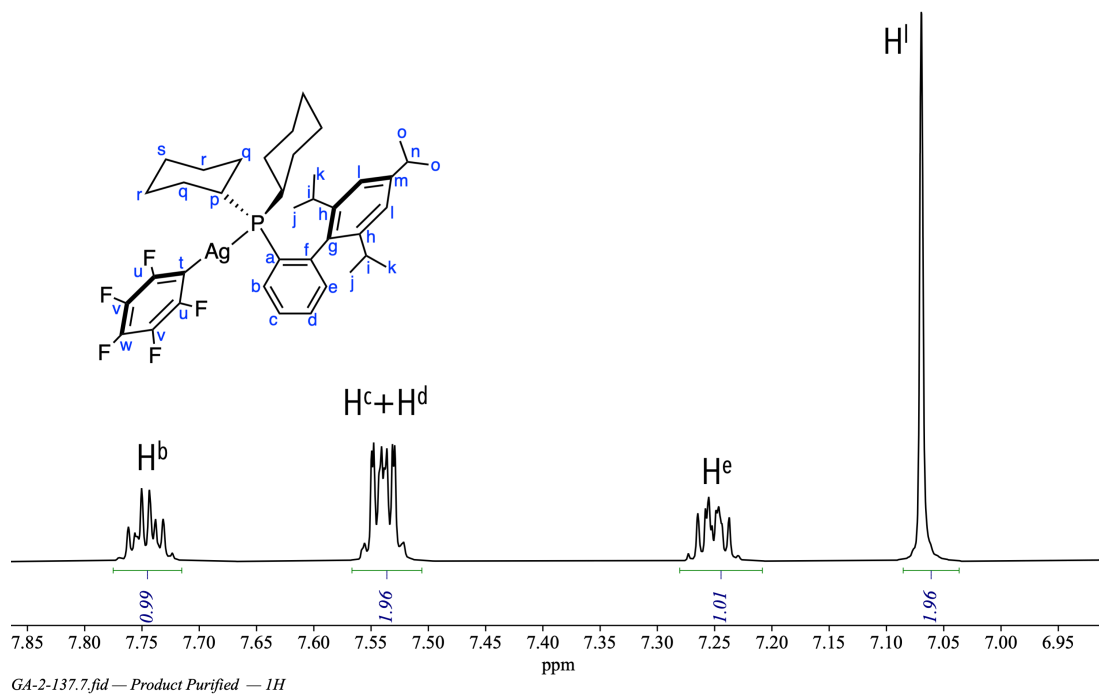


**Figure 235:**  $^1\text{H}$  NMR (500 MHz,  $\text{CD}_2\text{Cl}_2$ ,  $25^\circ\text{C}$ ) spectrum of **101** between  $\delta$  7.00 and  $\delta$  8.00

GA-2-137.8.fid  
Product Purified  
31P

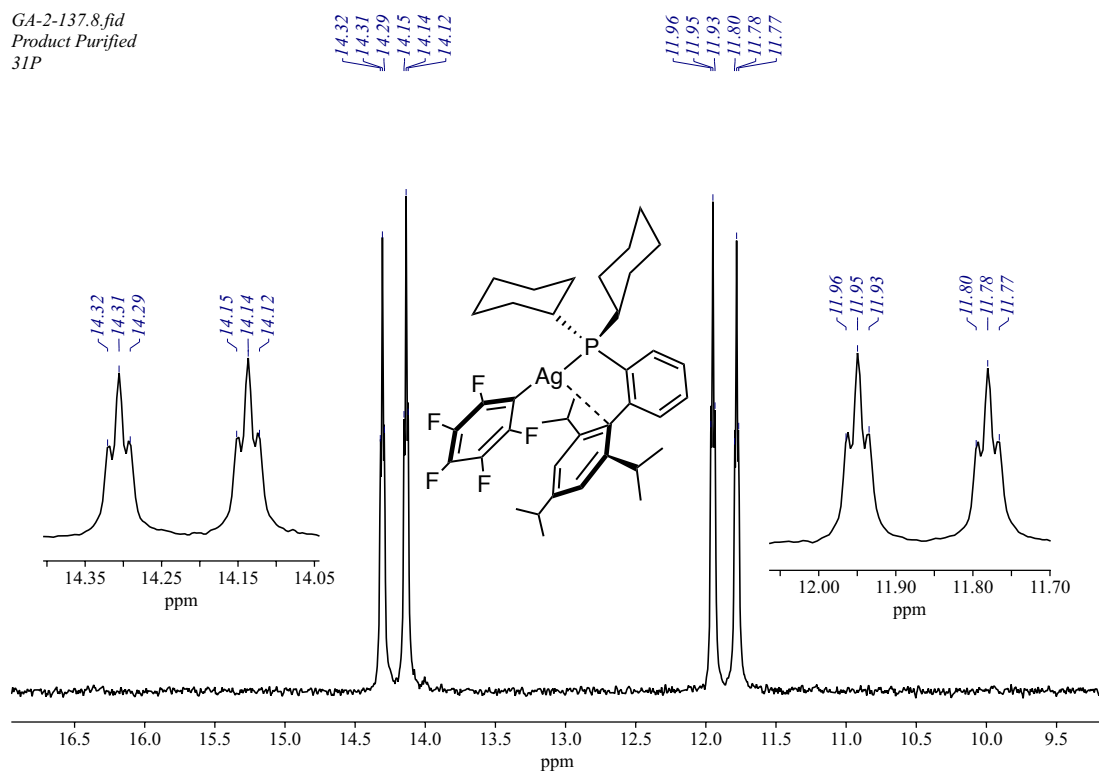


**Figure 236:**  $^{31}\text{P}\{^1\text{H}\}$  (202.5 MHz,  $\text{CD}_2\text{Cl}_2$ , 25 °C) spectrum of **101** (spectrum collected on AV500, saved as 8 under GA-2-137)

GA-2-137.9.fid  
Purified product  
 $^{19}\text{F}$

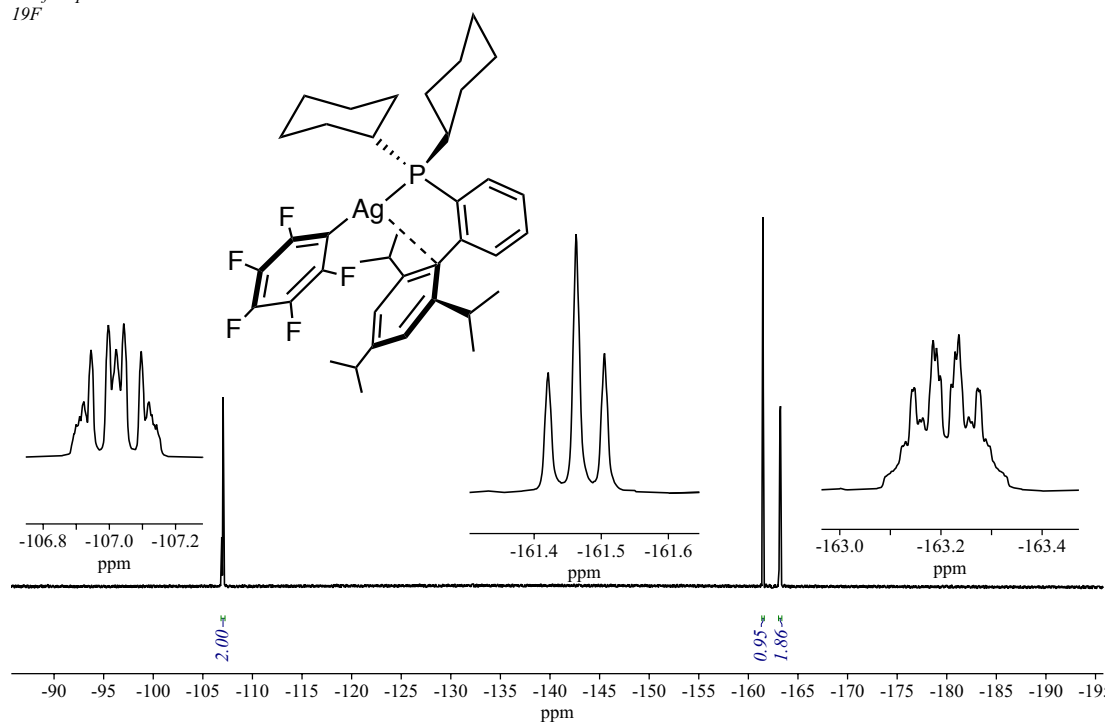


**Figure 237:**  $^{19}\text{F}\{^1\text{H}\}$  NMR (470.6 MHz,  $\text{CD}_2\text{Cl}_2$ , 25 °C) spectrum of **101** (spectrum collected on AV500, saved as 9 under GA-2-137)

Appendix B – NMR Spectroscopic Data for Synthesised Compounds

GA-2-138.15.fid  
 AgC6F5Xphos  
 CD<sub>2</sub>Cl<sub>2</sub>  
 Carbon DEPT - 135

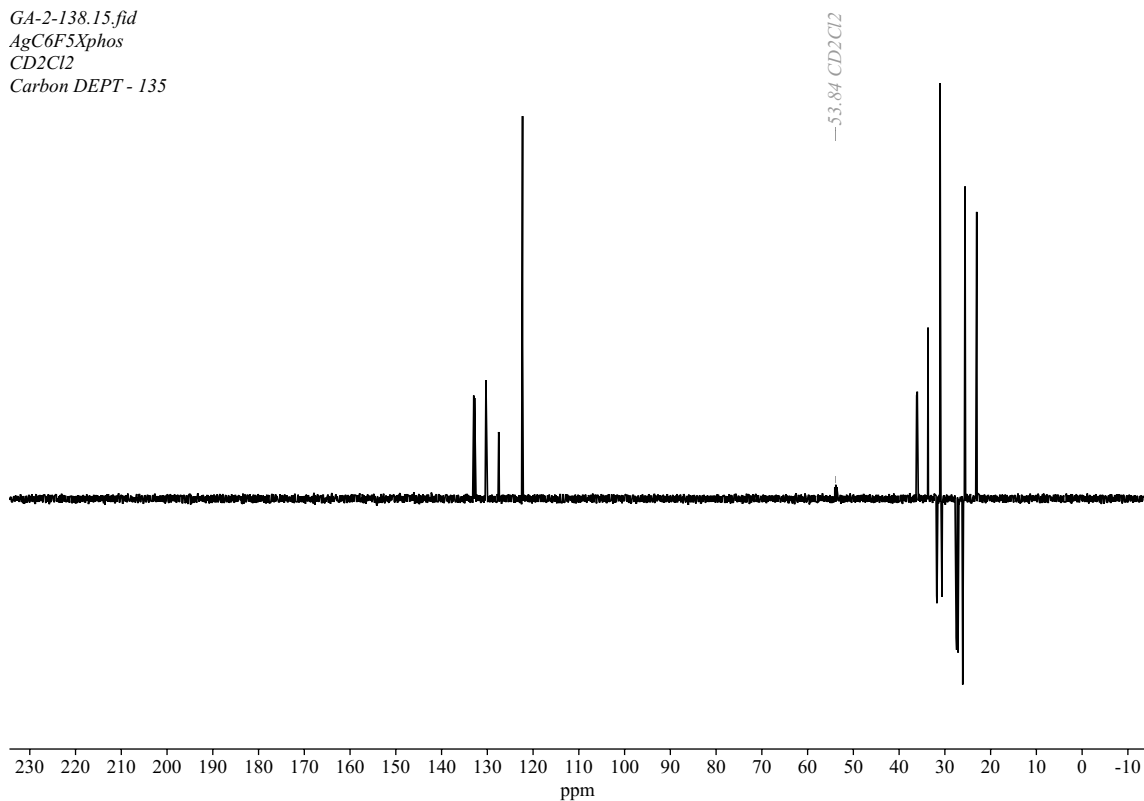


**Figure 238:** <sup>13</sup>C DEPT-135 (125.8 MHz, CD<sub>2</sub>Cl<sub>2</sub>, 25 °C) spectrum of **101** (spectrum collected on AV500, saved as 15 under GA-2-138)

GA-2-138.20.fid  
 AgC6F5Xphos  
 CD<sub>2</sub>Cl<sub>2</sub>  
<sup>13</sup>C

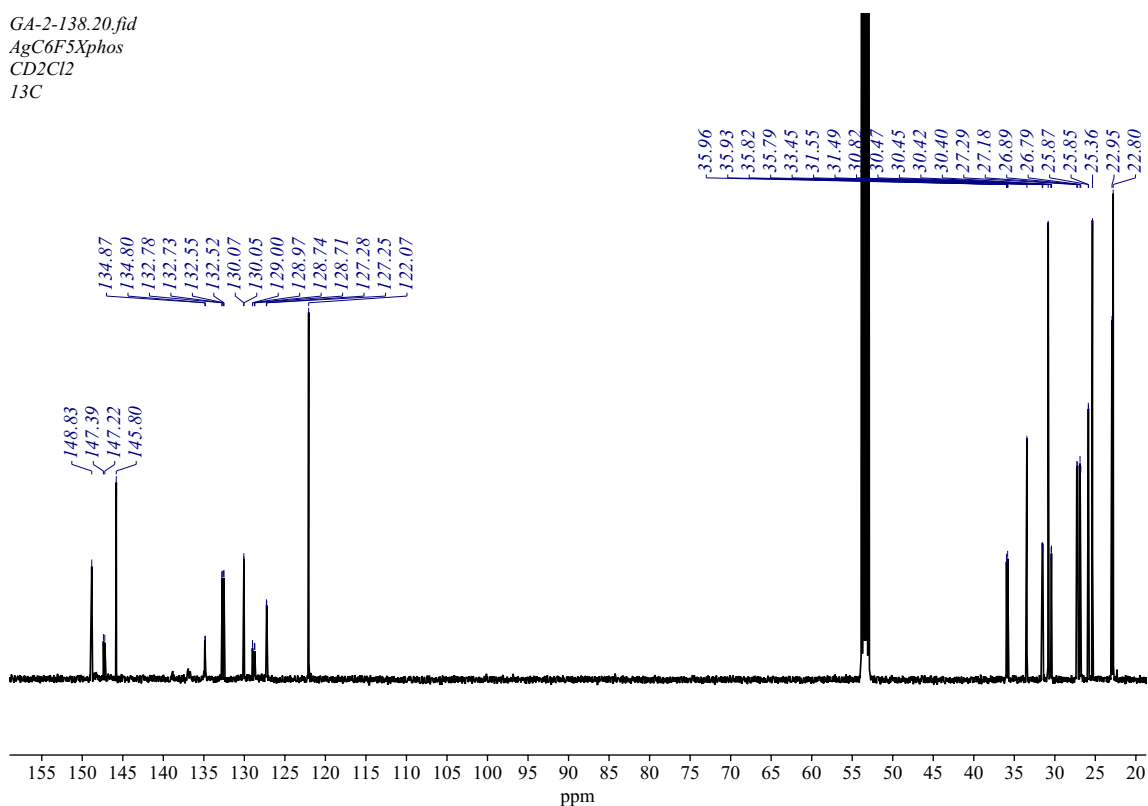


**Figure 239:** <sup>13</sup>C {<sup>1</sup>H} (125.8 MHz, CD<sub>2</sub>Cl<sub>2</sub>, 25 °C) spectrum of **101** (spectrum collected on AV500, saved as 20 under GA-2-138)

GA-2-138.20.fid  
AgC6F5Xphos  
CD<sub>2</sub>Cl<sub>2</sub>  
13C

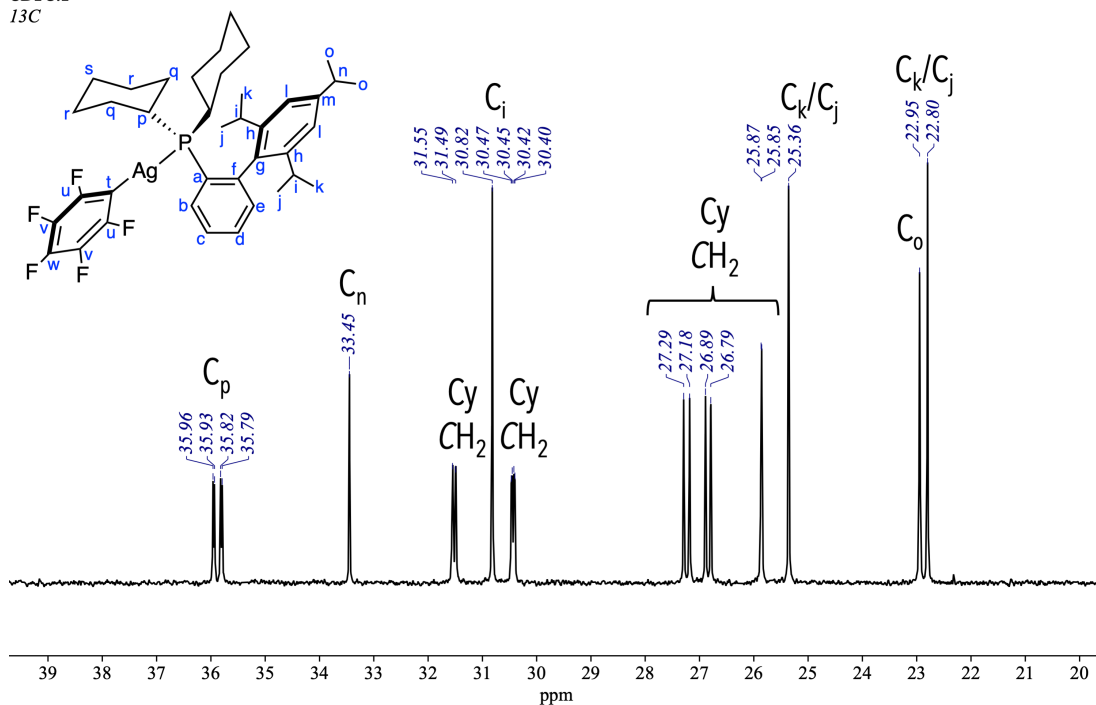


**Figure 240:**  $^{13}\text{C}\{^1\text{H}\}$  (125.8 MHz, CD<sub>2</sub>Cl<sub>2</sub>, 25 °C) spectrum of **101** between  $\delta$  20 and  $\delta$  40

GA-2-138.15.fid  
AgC6F5Xphos  
CD<sub>2</sub>Cl<sub>2</sub>  
Carbon DEPT - 135

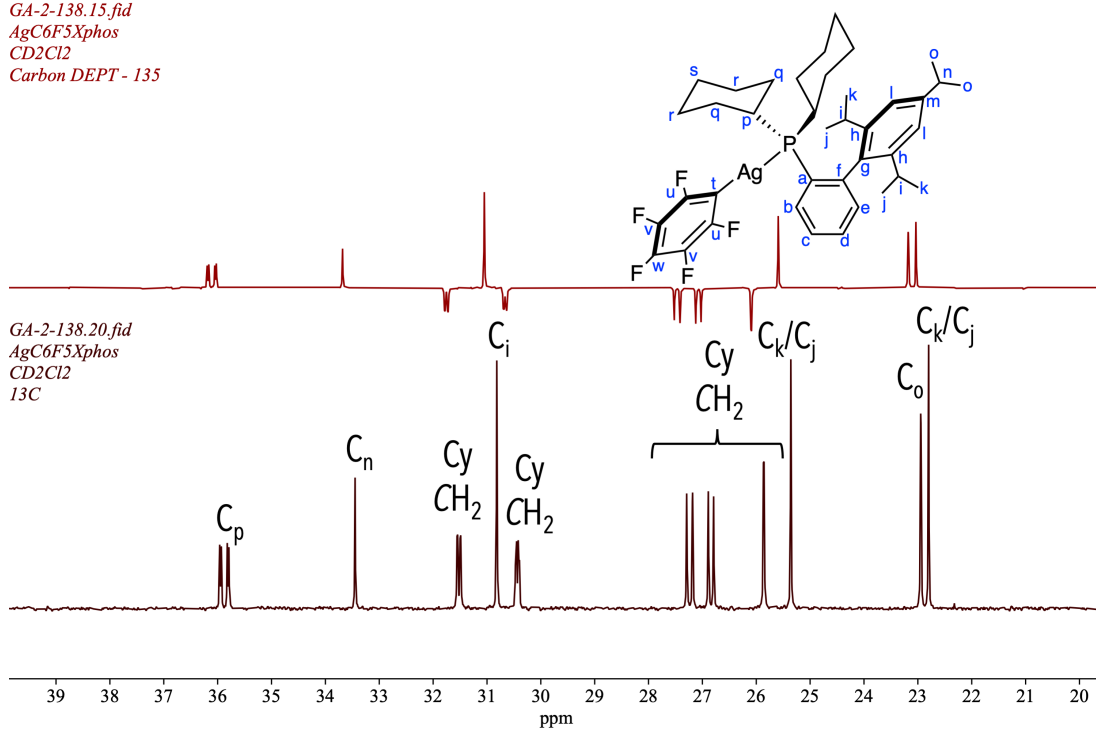


**Figure 241:** Stack plot of the  $^{13}\text{C}\{^1\text{H}\}$  NMR spectrum (bottom) and the  $^{13}\text{C}$  DEPT-135 of **101** between  $\delta$  20 and  $\delta$  40

GA-2-138.20.fid  
 AgC6F5Xphos  
 CD2Cl2  
 13C

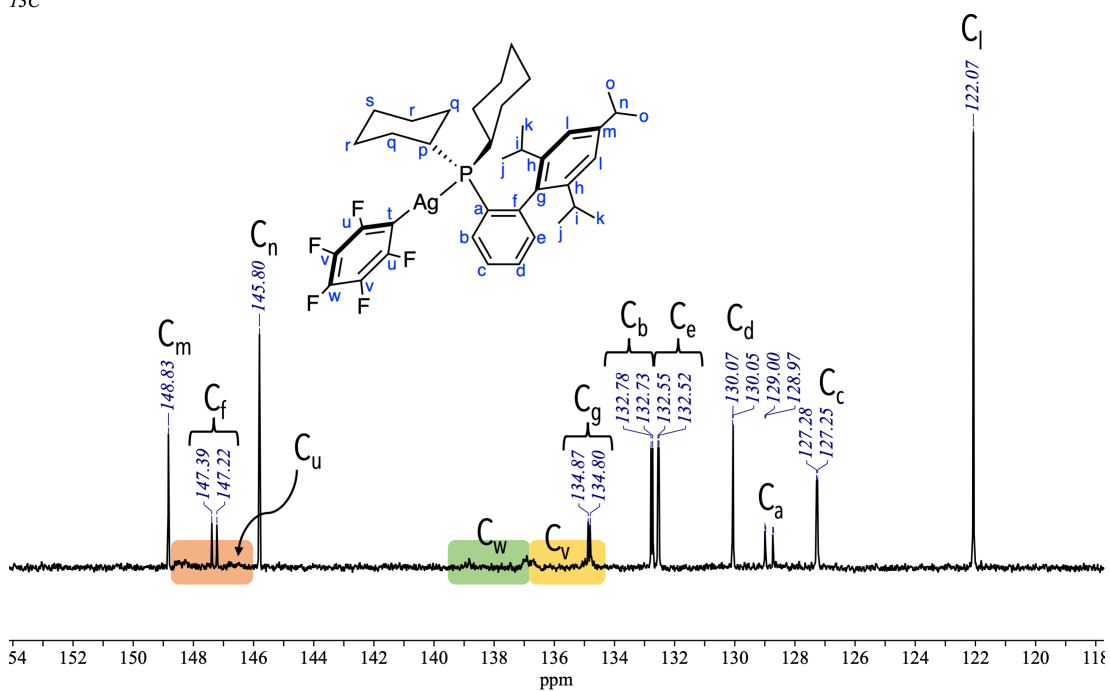


**Figure 242:**  $^{13}\text{C}\{^1\text{H}\}$  (125.8 MHz,  $\text{CD}_2\text{Cl}_2$ , 25 °C) spectrum of **101** between  $\delta$  160 and  $\delta$

110

GA-2-138.15.fid  
 AgC6F5Xphos  
 CD2Cl2  
 Carbon DEPT - 135

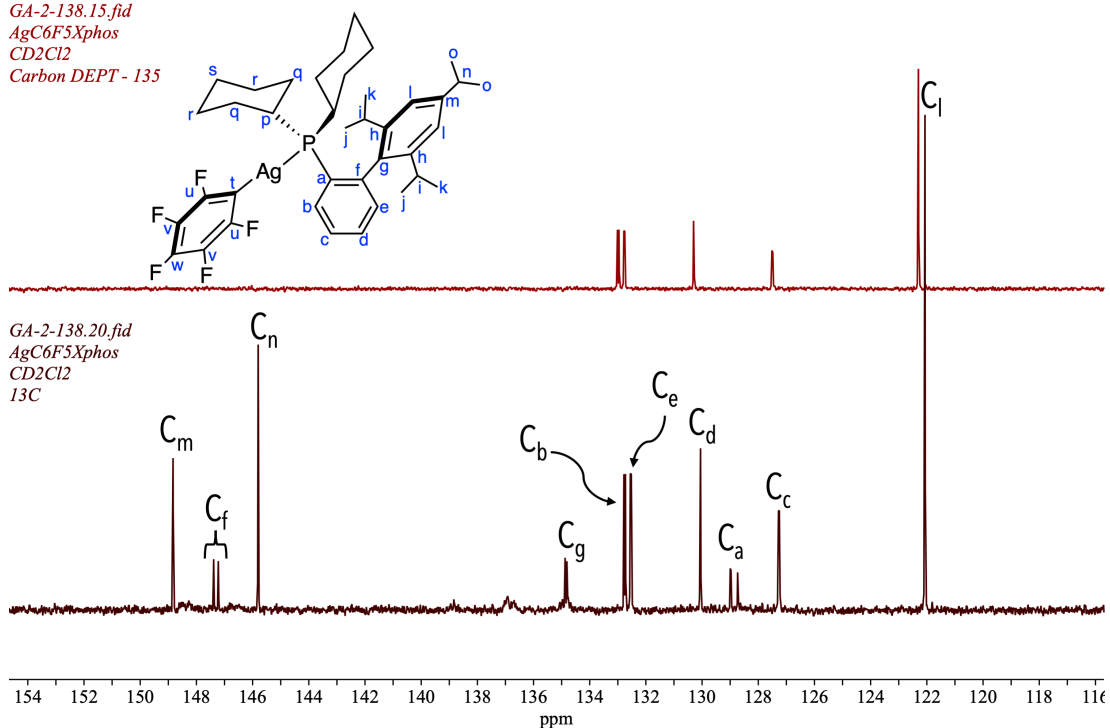


**Figure 243:** Stack plot of the  $^{13}\text{C}\{^1\text{H}\}$  NMR spectrum (below) and the  $^{13}\text{C}$  DEPT-135 (above) of **101** between  $\delta$  160 and  $\delta$  110

The assignment of the  $C_6F_5$  group carbon peaks were done using a  $^{13}C\{^1H,^{19}F\}$  spectrum. Two different  $^{13}C\{^1H,^{19}F\}$  experiments were setup, one with an irradiation frequency offset (O3P) at  $\delta - 107$  and  $\delta - 160$  (for  $^{19}F$ ). The O3P of  $\delta - 107$  specifically decoupled the *ortho*-F from the carbon of  $C_6F_5$  whereas the O3P of  $\delta - 160$  offset decoupled the *meta*- and *para*-F from the carbon of  $C_6F_5$ . The stack plot of the three spectra has been shown in **Figure 244**. To see the  $C_6F_5$  group carbon peaks more clearly, a more concentrated sample of **101** was prepared in  $CDCl_3$  (50 mg dissolved in 0.5 mL  $CDCl_3$ ) as seen in **Figure 245**.

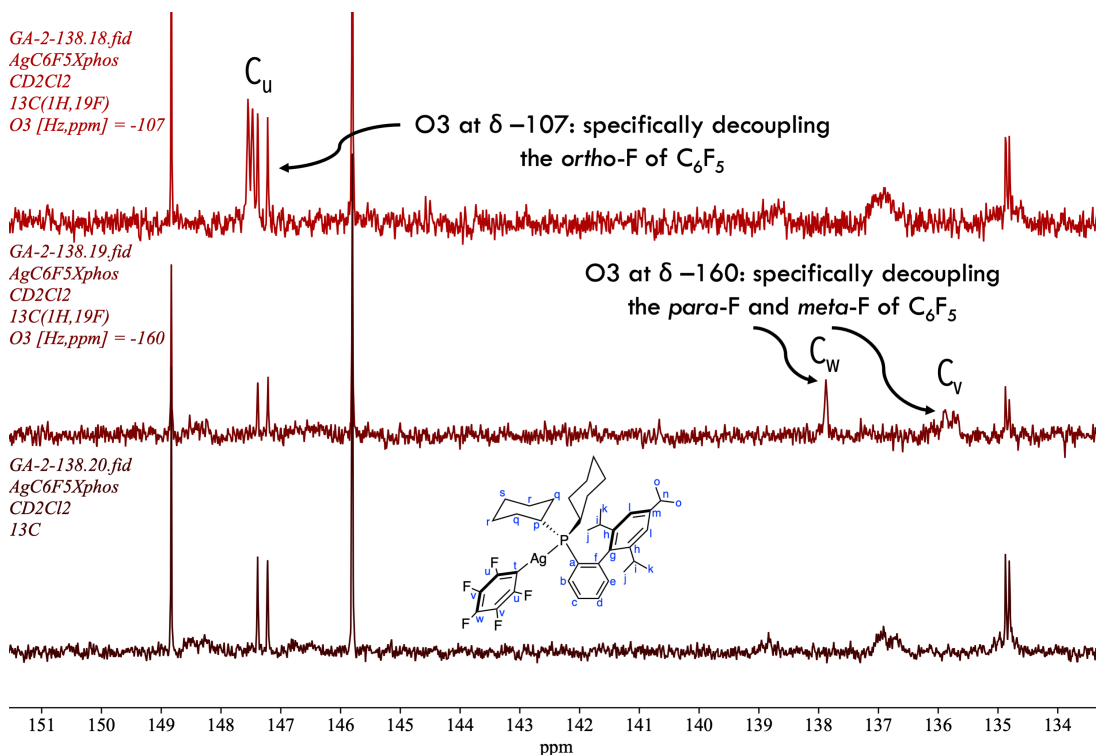


**Figure 244:** Stack plot of the  $^{13}C\{^1H\}$  NMR spectrum (bottom) with the  $^{13}C\{^1H,^{19}F\}$  spectrum with an O3P of  $\delta - 107$  (top) and  $\delta - 160$  (middle) in  $CD_2Cl_2$



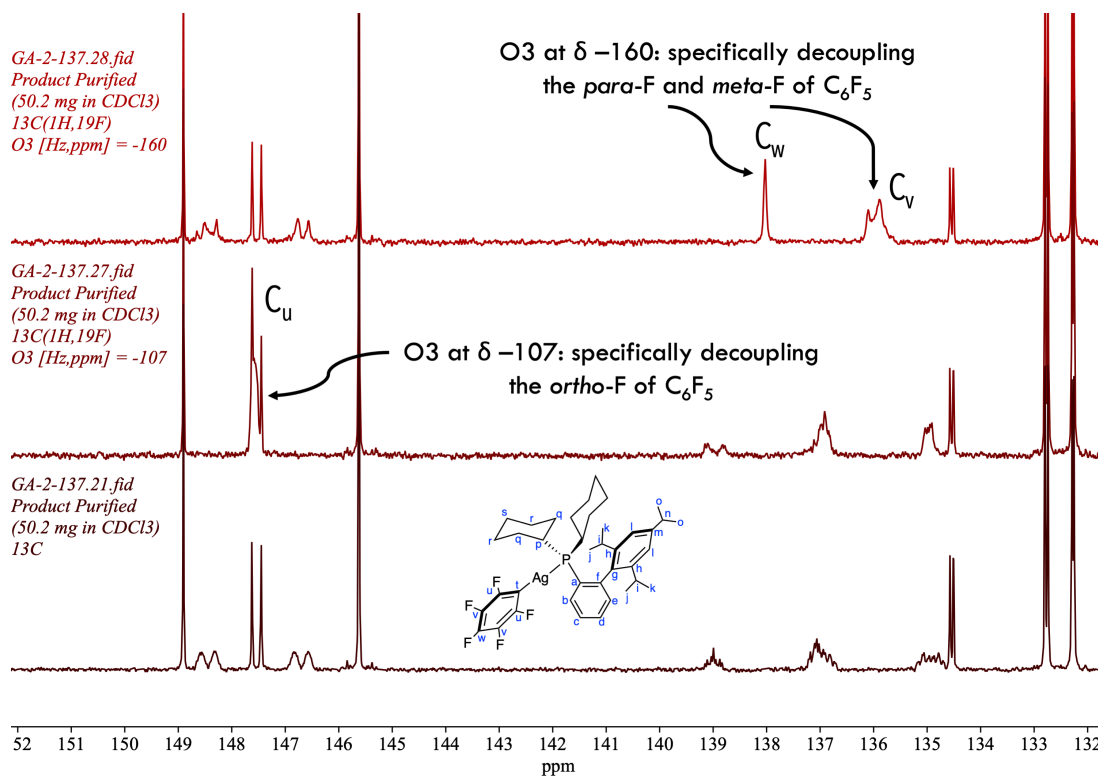


**Figure 245:** Stack plot of the  $^{13}\text{C}\{^1\text{H}\}$  NMR spectrum (bottom) with the  $^{13}\text{C}\{^1\text{H}, ^{19}\text{F}\}$  spectrum with an O3P of  $\delta -107$  (middle) and  $\delta -160$  (top), in CDCl<sub>3</sub>

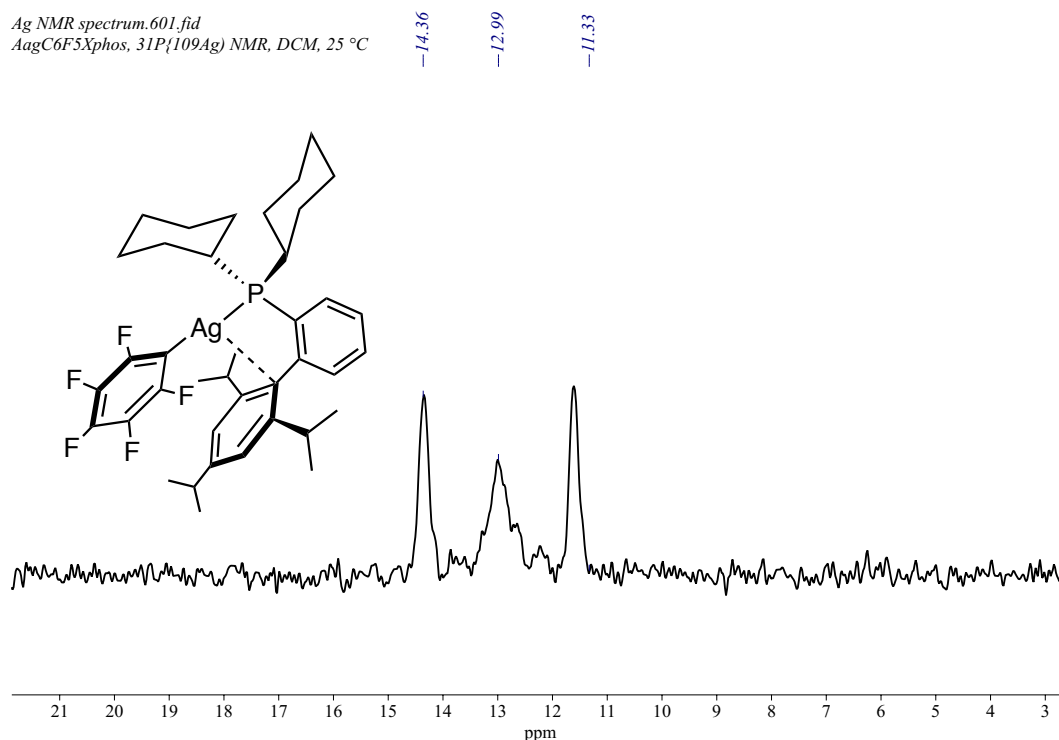


**Figure 246:**  $^{31}\text{P}\{^{109}\text{Ag}\}$  (162 MHz, CD<sub>2</sub>Cl<sub>2</sub>, 25 °C) spectrum of **101**

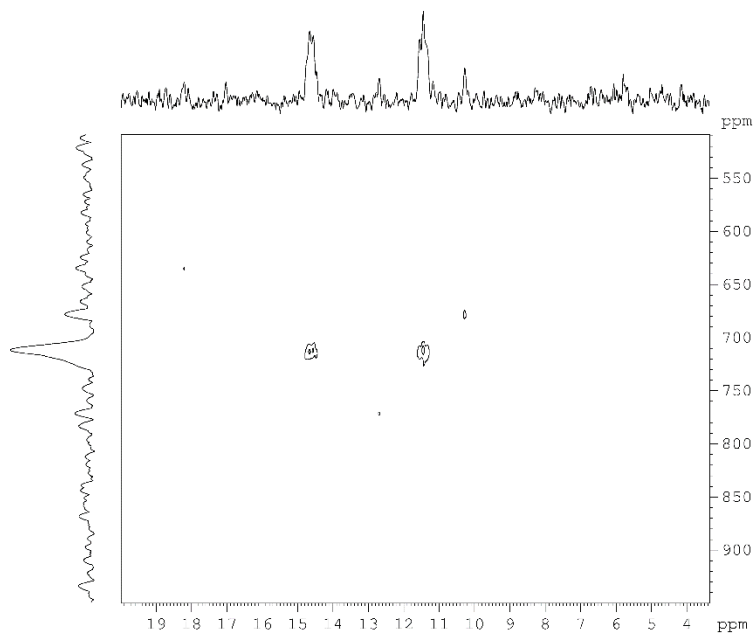


**Figure 247:**  $^{31}\text{P}\{^{109}\text{Ag}\}\text{-}^{109}\text{Ag}$  HMQC spectrum of **101**

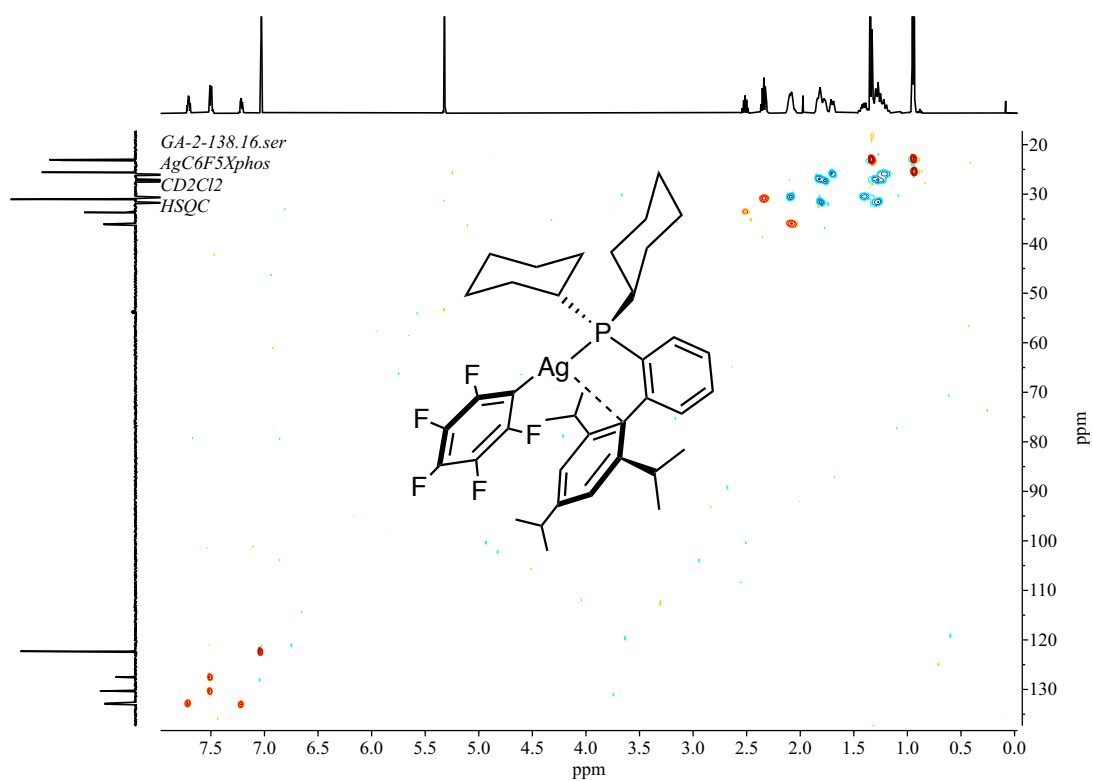


**Figure 248:** HSQC spectrum of **101** in  $\text{CD}_2\text{Cl}_2$  (spectrum collected on AV500, saved as 16 under GA-2-138)

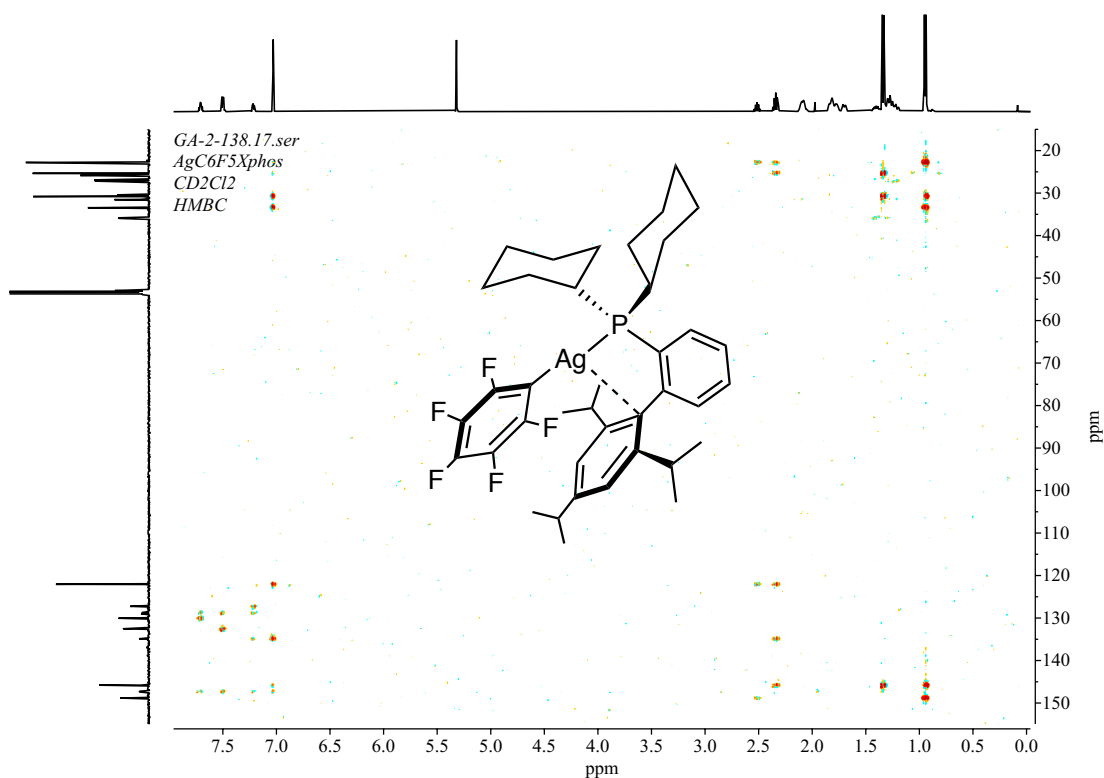


**Figure 249:** HMBC spectrum of **101** in CD<sub>2</sub>Cl<sub>2</sub> (spectrum collected on AV500, saved as 17 under GA-2-138)

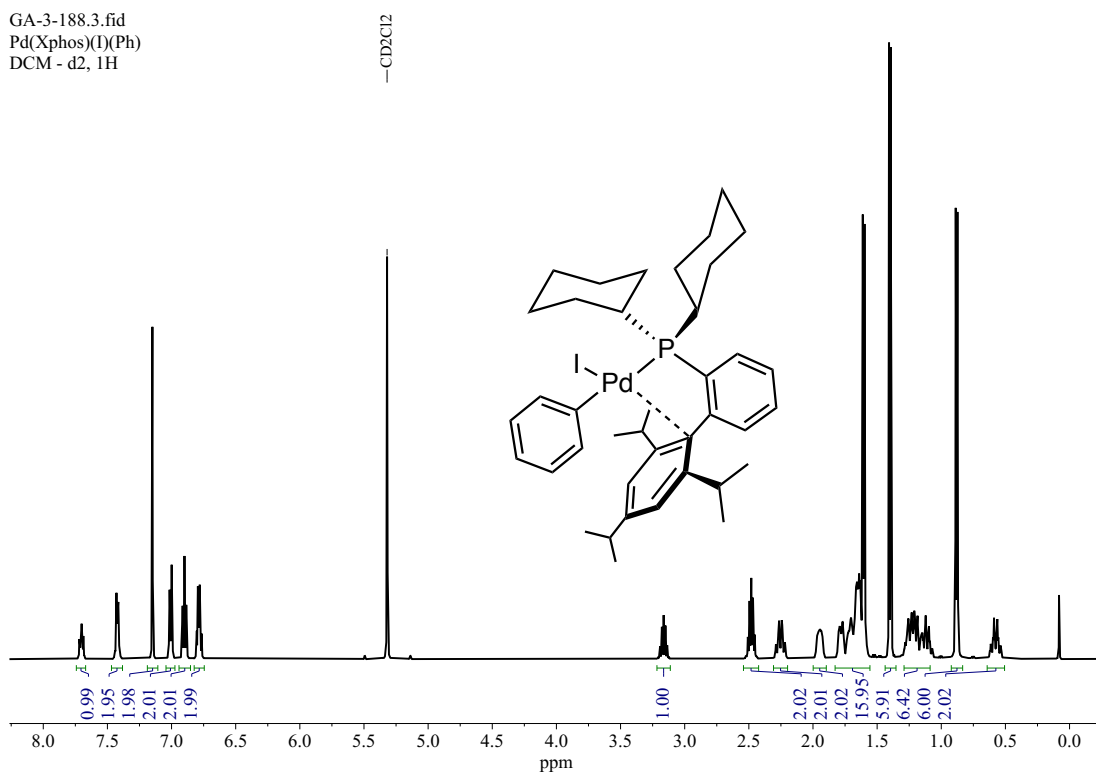


**Figure 250:** <sup>1</sup>H NMR (500 MHz, CD<sub>2</sub>Cl<sub>2</sub>, 25 °C) spectrum of the Pd(I)(Xphos)(Ph) **102** (spectrum collected on AV500, saved as 3 under GA-3-188)

GA-3-188.3.fid  
Pd(Xphos)(I)(Ph)  
DCM - d2, 1H

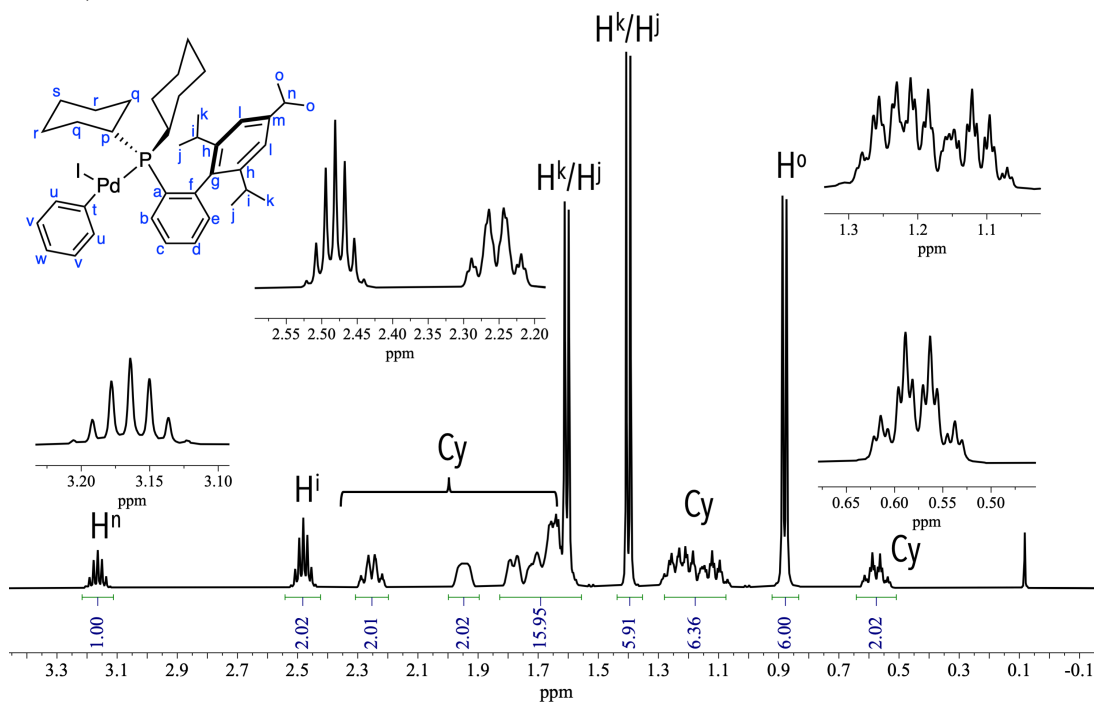


**Figure 251:**  $^1\text{H}$  NMR (500 MHz,  $\text{CD}_2\text{Cl}_2$ , 25 °C) spectrum of **102** between  $\delta$  – 0.2 to  $\delta$  3.5

GA-3-188.3.fid  
Pd(Xphos)(I)(Ph)  
DCM - d2, 1H

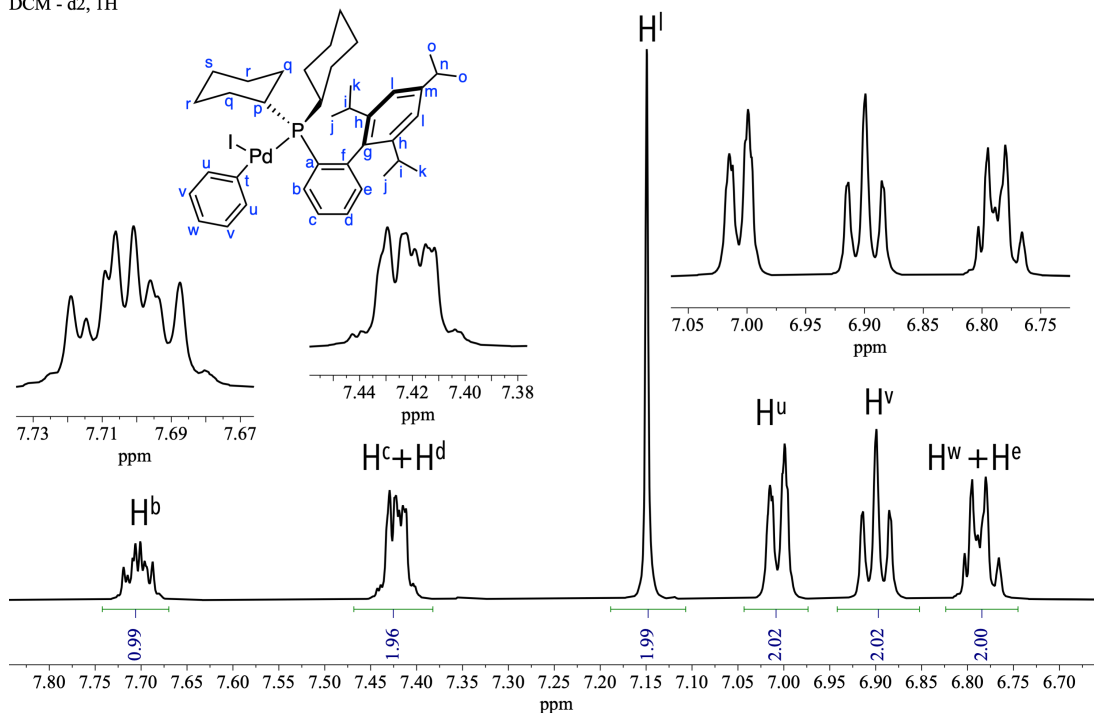


**Figure 252:**  $^1\text{H}$  NMR (500 MHz,  $\text{CD}_2\text{Cl}_2$ , 25 °C) spectrum of **102** between  $\delta$  6.6 to  $\delta$  7.9

GA-3-188.4.fid  
Pd(Xphos)(I)(Ph)  
DCM - d2, 31P{1H}

-21.96

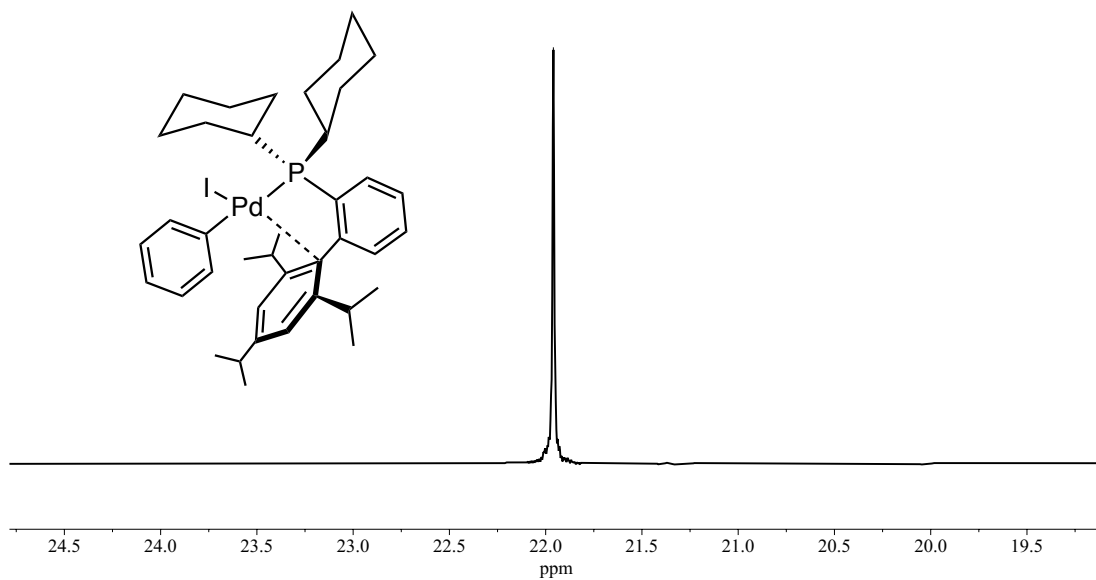


**Figure 253:**  $^{31}\text{P}\{^1\text{H}\}$  (202.5 MHz,  $\text{CD}_2\text{Cl}_2$ , 25 °C) spectrum of **102** (spectrum collected on AV500, saved as 4 under GA-3-188)

GA-3-188.5.fid  
Pd(Xphos)(I)(Ph)  
DCM - d2, DEPT - 135

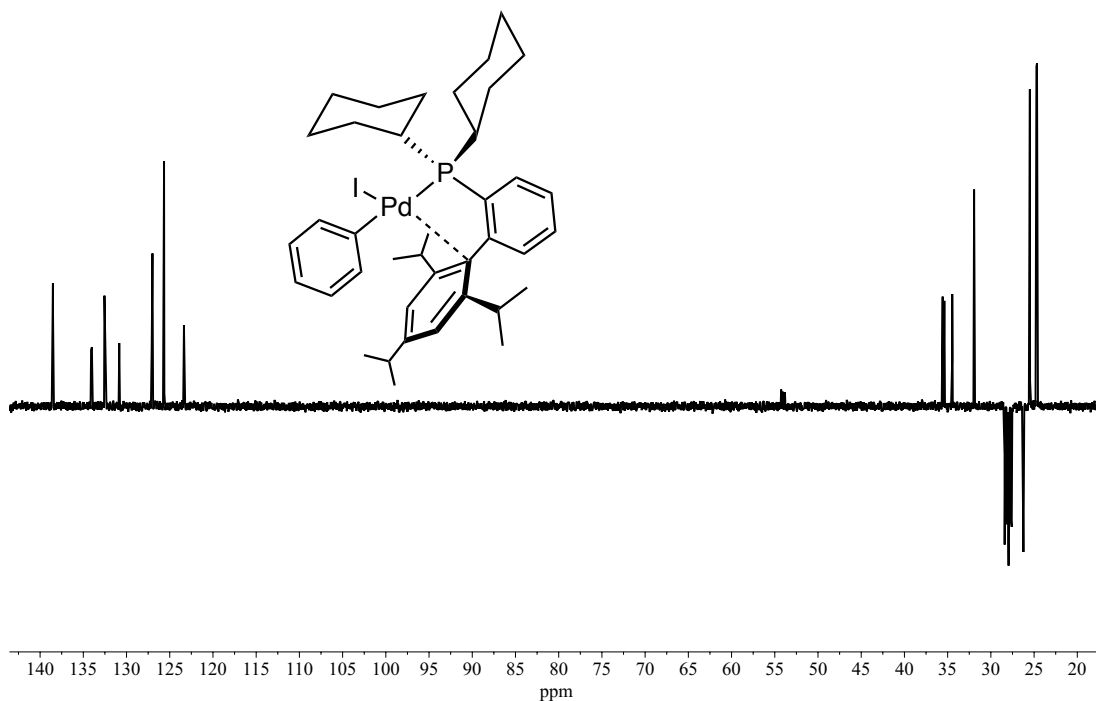


**Figure 254:** DEPT-135 spectrum of **102** (spectrum collected on AV500, saved as 5 under GA-3-188)

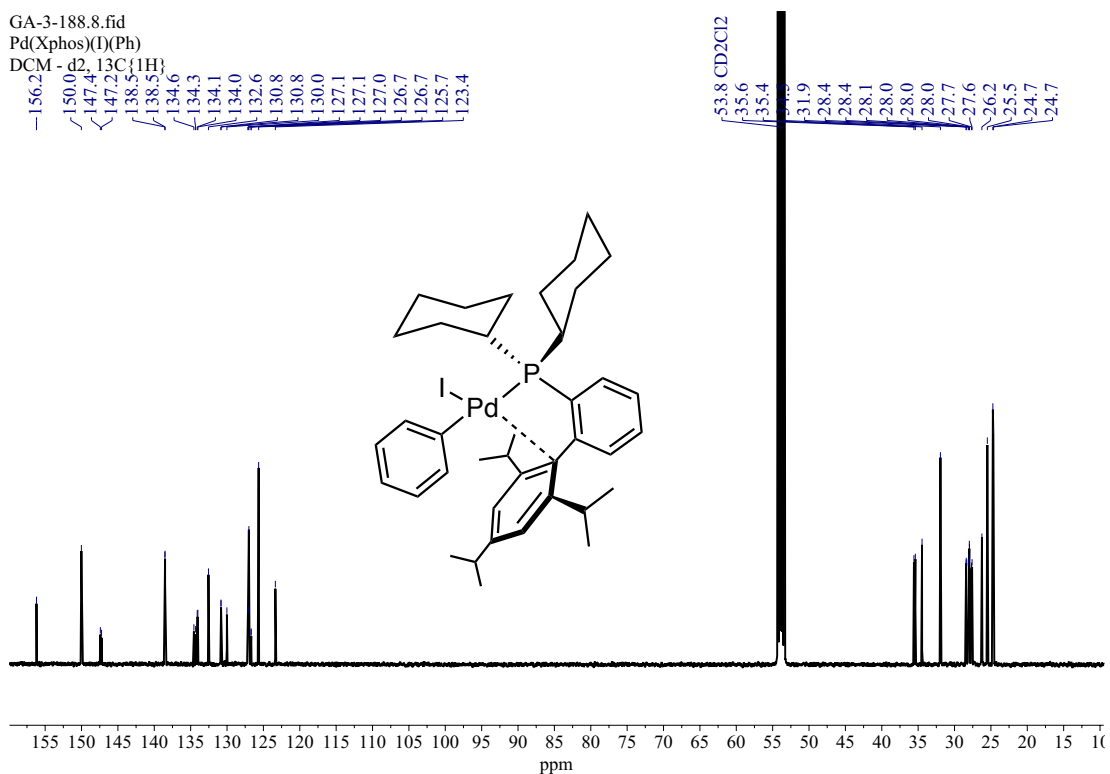


**Figure 255:**  $^{13}\text{C}\{^1\text{H}\}$  (125.8 MHz,  $\text{CD}_2\text{Cl}_2$ , 25 °C) spectrum of **102** (spectrum collected on AV500, saved as 8 under GA-3-188)

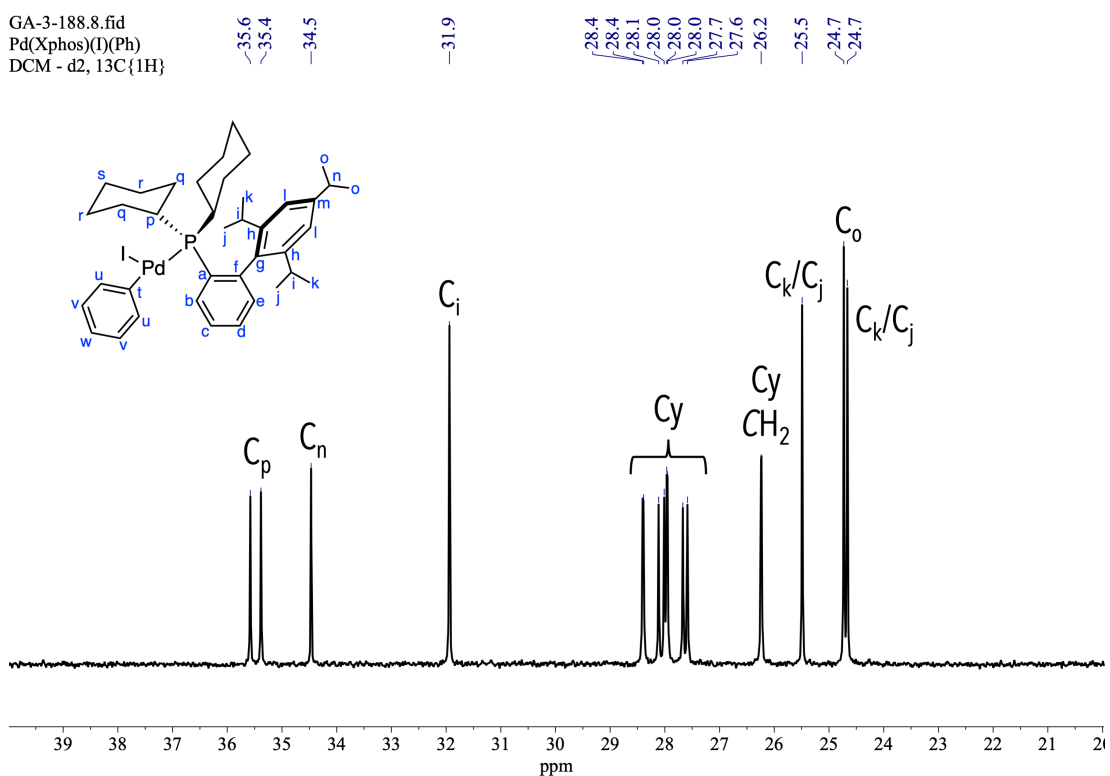


**Figure 256:**  $^{13}\text{C}\{^1\text{H}\}$  (125.8 MHz,  $\text{CD}_2\text{Cl}_2$ , 25 °C) spectrum of **102** between  $\delta$  20 and 40

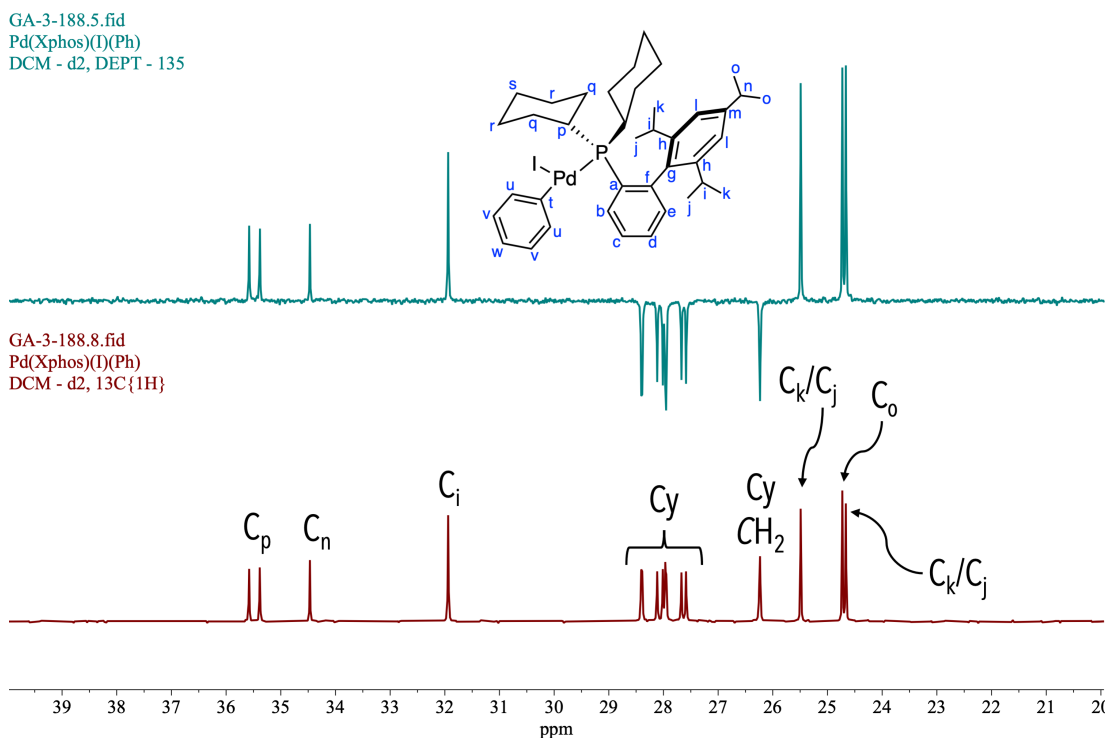


**Figure 257:** Stack plot of the  $^{13}\text{C}$  NMR spectrum (bottom) and DEPT-135 of **102** between  $\delta$  20 and  $\delta$  40

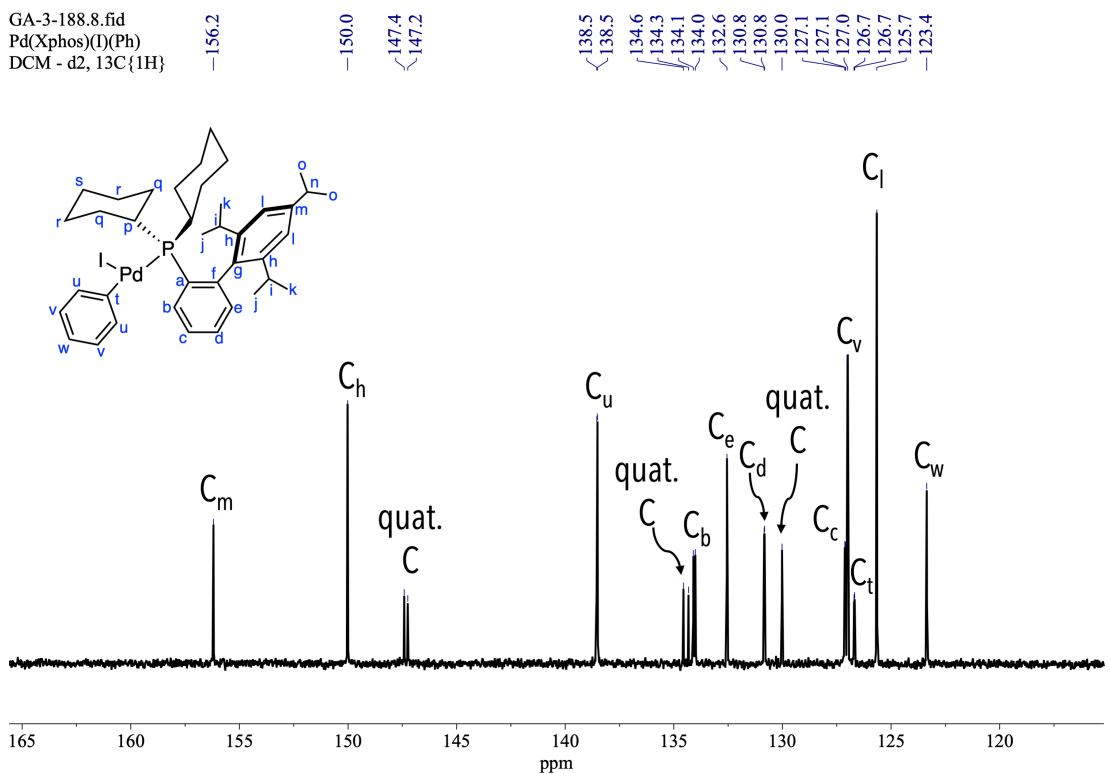


**Figure 258:**  $^{13}\text{C}\{^1\text{H}\}$  (125.8 MHz,  $\text{CD}_2\text{Cl}_2$ , 25 °C) spectrum of **102** between  $\delta$  163 and  $\delta$  117

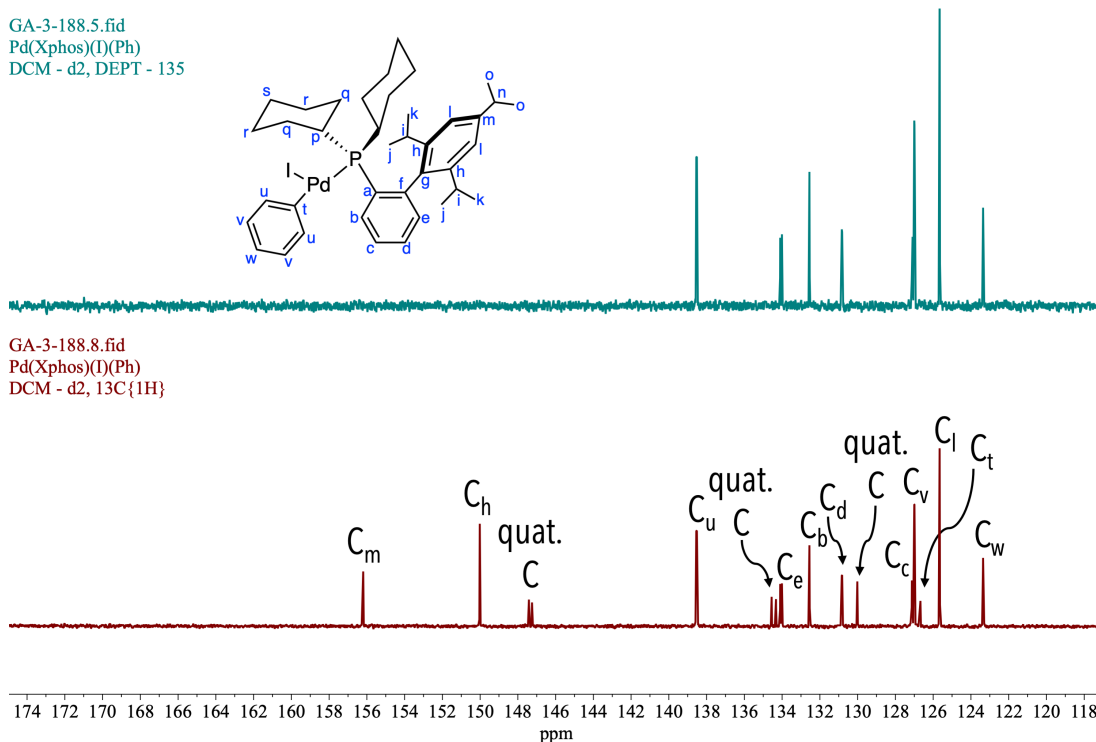


**Figure 259:** Stack plot of the <sup>13</sup>C NMR spectrum (bottom) and DEPT-135 spectrum of **102** between δ 20 and δ 40

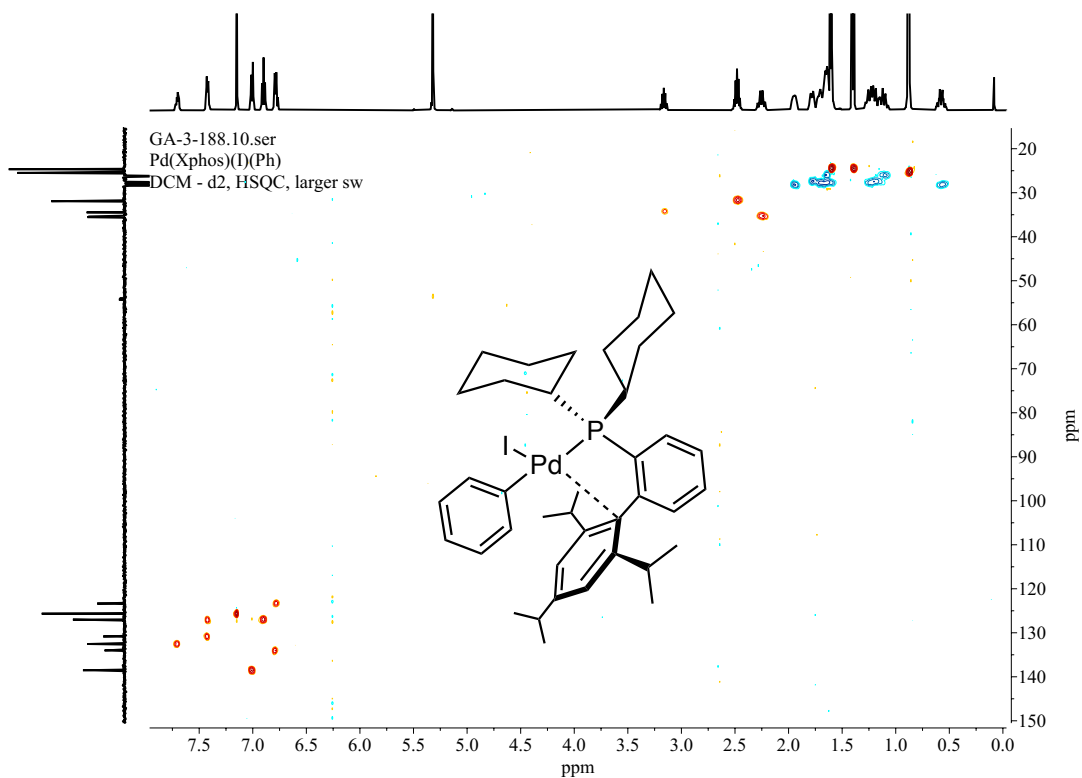


**Figure 260:** HSQC spectrum of **102** (spectrum collected on AV500, saved as 10 under GA-3-188)



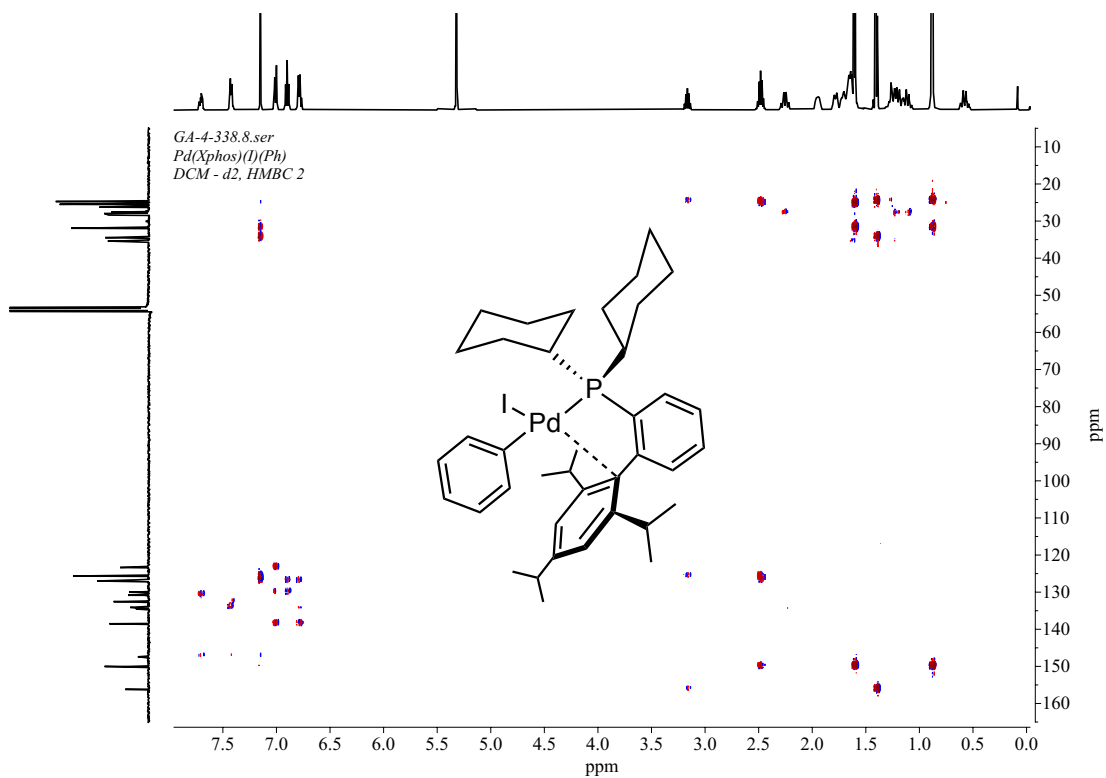


**Figure 261:** HMBC spectrum of **102** (spectrum collected on AV500, saved as 8 under GA-4-338)

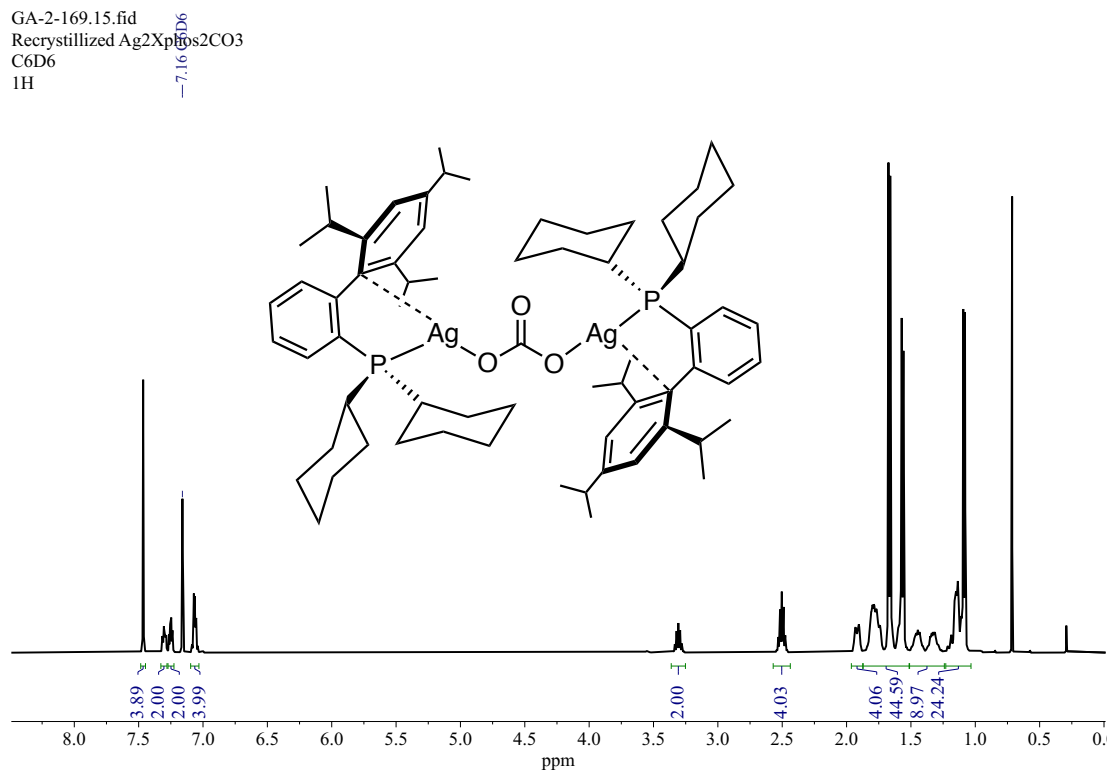


**Figure 262:**  $^1\text{H}$  NMR (500 MHz,  $\text{C}_6\text{D}_6$ , 25 °C) spectrum of the **106** (spectrum collected on AV500, saved as 15 under GA-2-169)

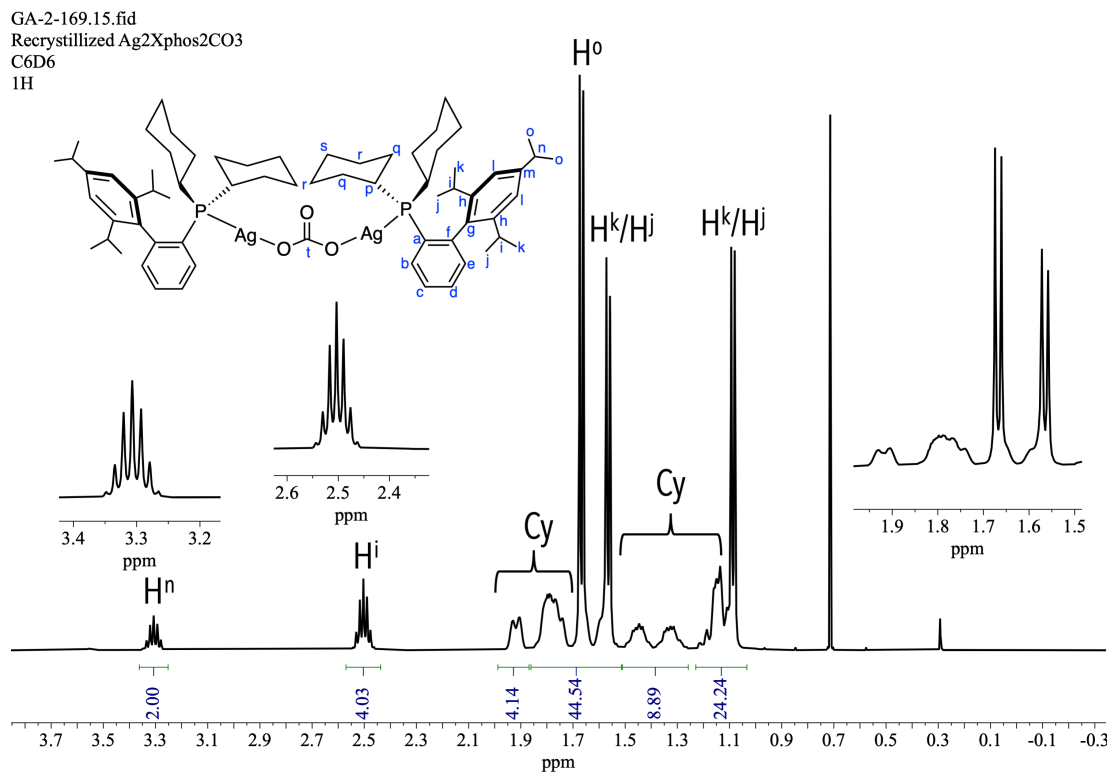


**Figure 263:** <sup>1</sup>H NMR (500 MHz, C<sub>6</sub>D<sub>6</sub>, 25 °C) spectrum of the **106** between δ 0.9 to δ 3.6

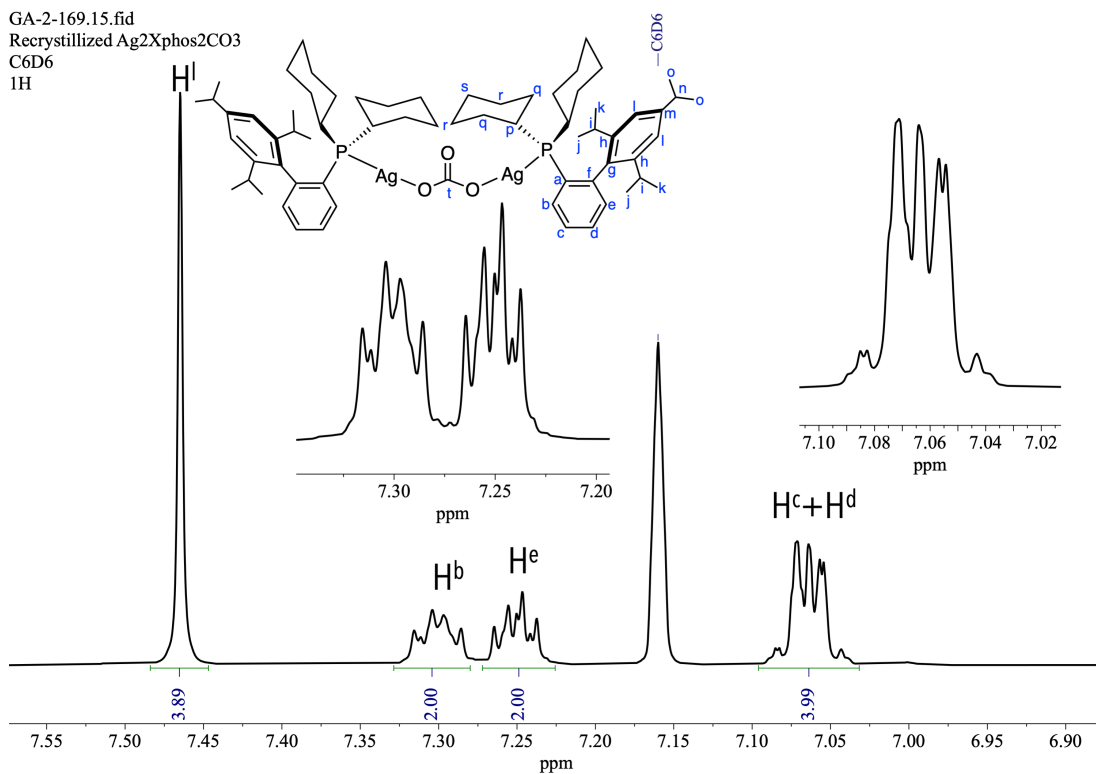


**Figure 264:** <sup>1</sup>H NMR (500 MHz, C<sub>6</sub>D<sub>6</sub>, 25 °C) spectrum of the **106** between δ 0.9 to δ 3.6

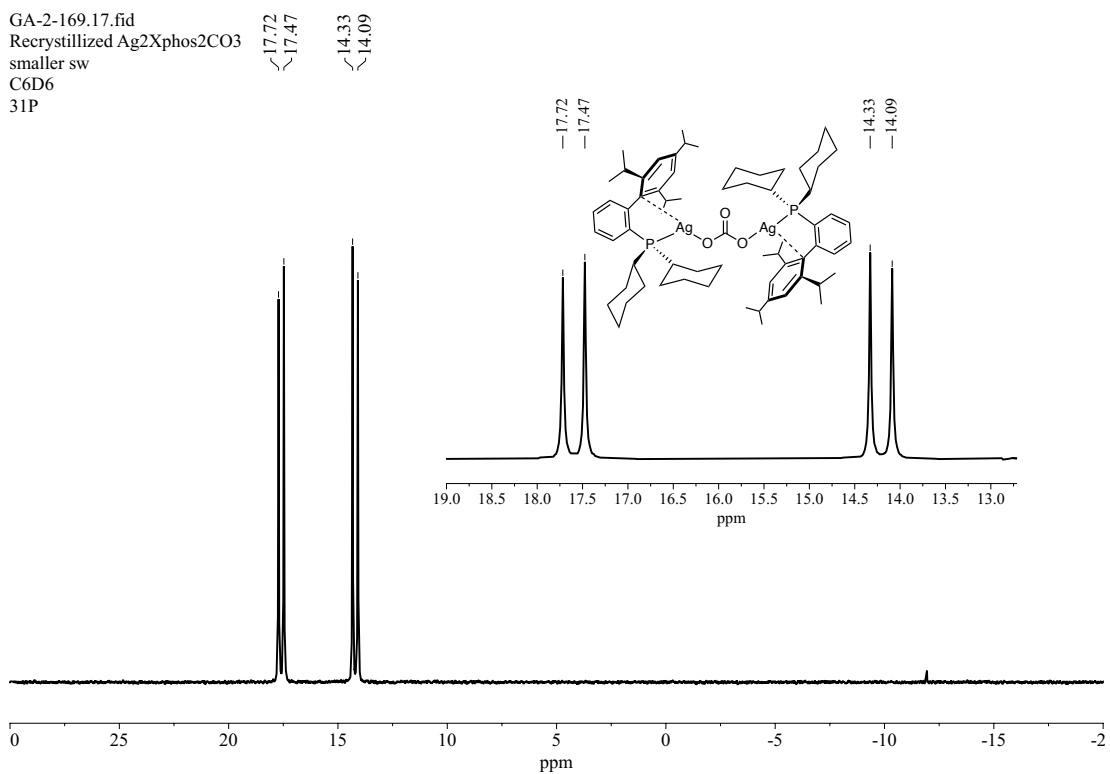


**Figure 265:**  $^{31}\text{P}\{^1\text{H}\}$  (202.5 MHz,  $\text{C}_6\text{D}_6$ , 25 °C) spectrum of the **106** (spectrum collected on AV500, saved as 17 under GA-2-169)

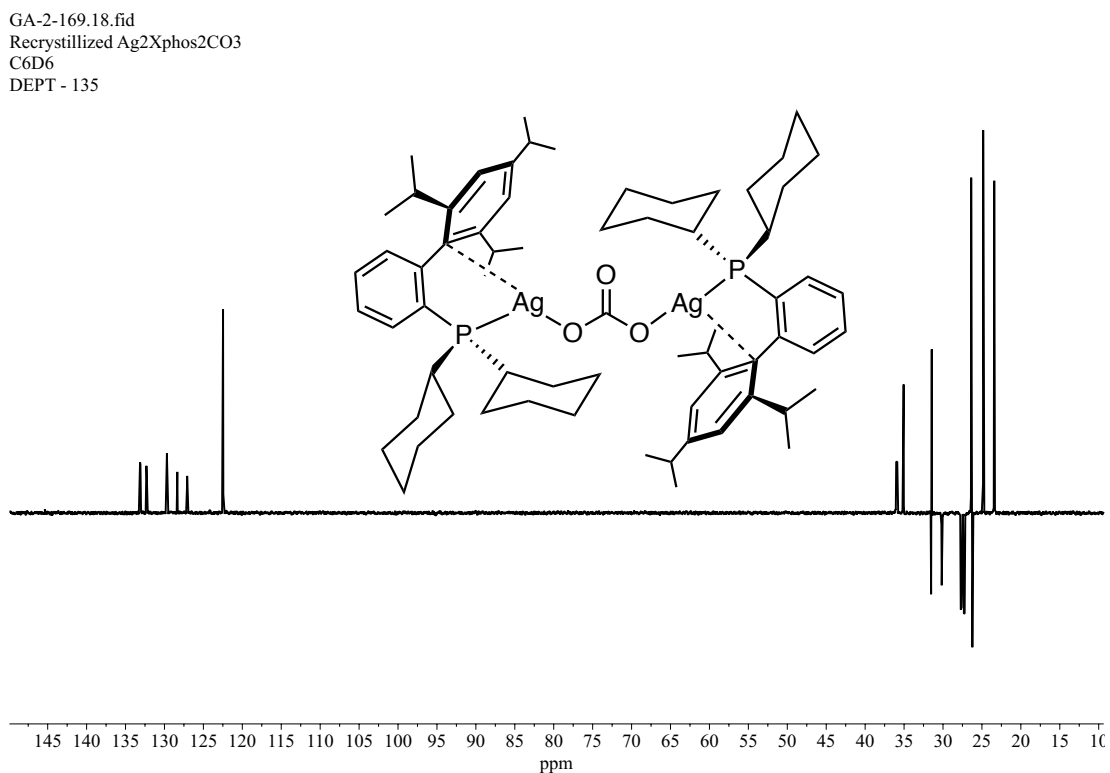


**Figure 266:**  $^{13}\text{C}$  DEPT – 135 (125.8 MHz,  $\text{CD}_2\text{Cl}_2$ , 25 °C) spectrum of **106** (spectrum collected on AV500, saved as 18 under GA-2-169)

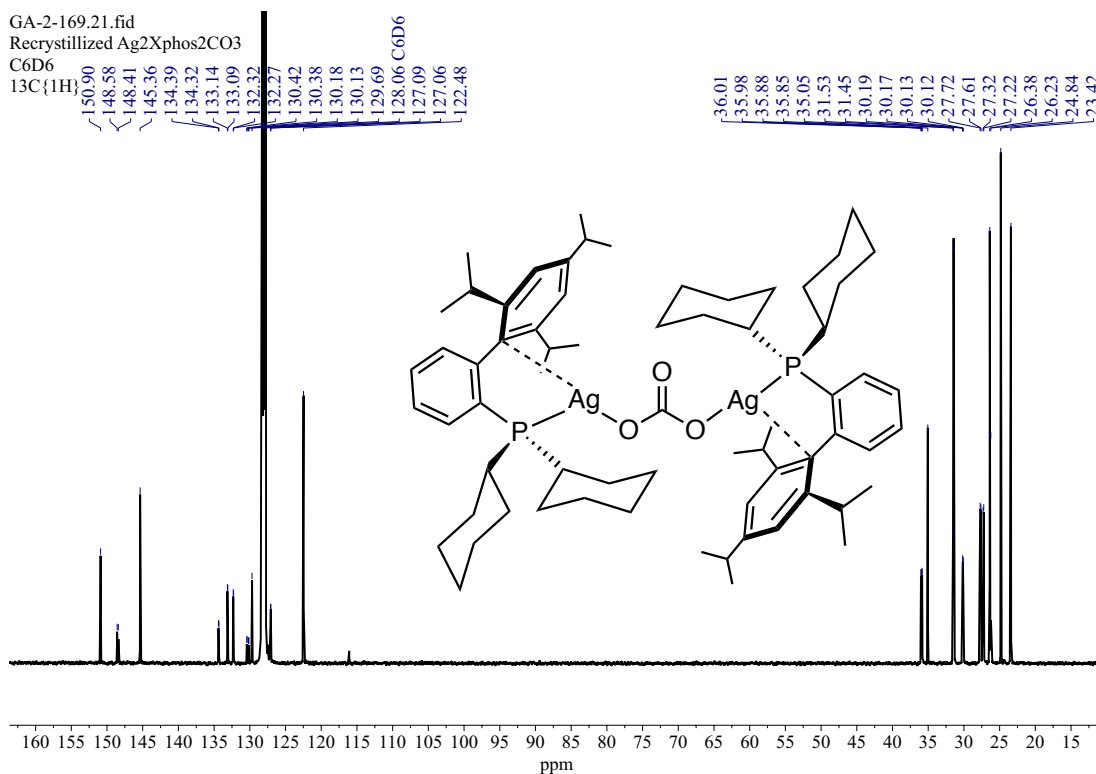


**Figure 267:**  $^{13}\text{C}\{^1\text{H}\}$  (125.8 MHz,  $\text{C}_6\text{D}_6$ , 25 °C) spectrum of **106** (spectrum collected on AV500, saved as 21 under GA-2-169)

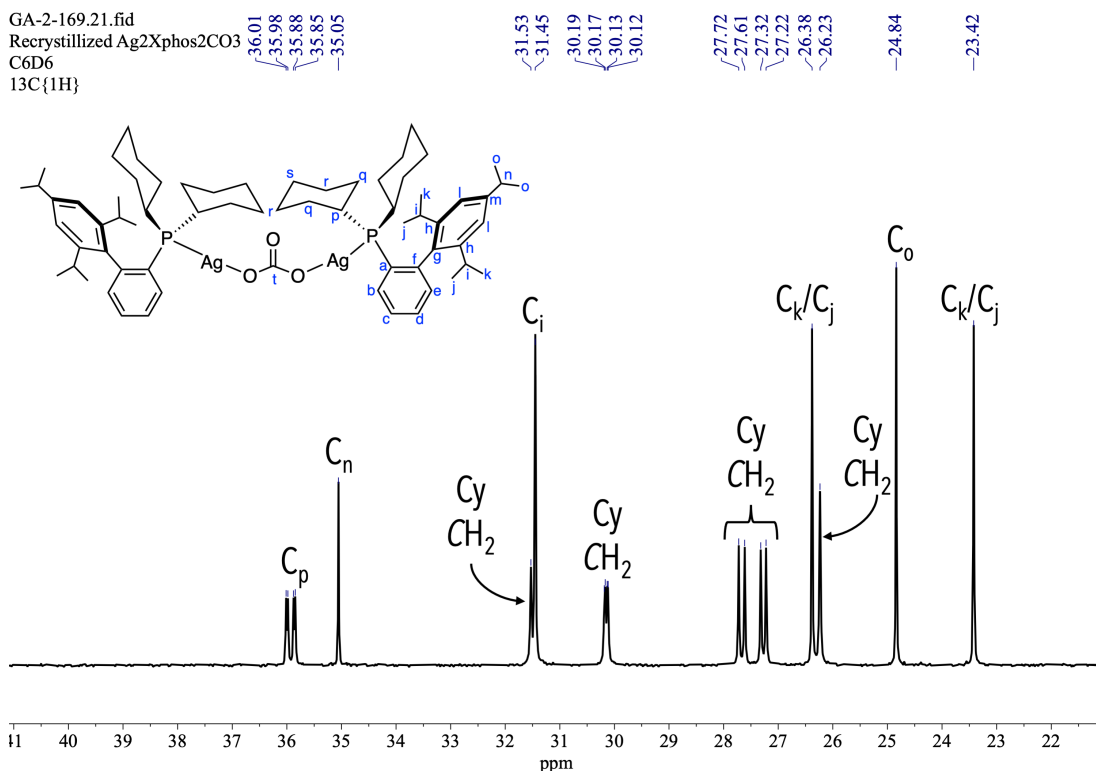


**Figure 268:**  $^{13}\text{C}\{^1\text{H}\}$  (125.8 MHz,  $\text{C}_6\text{D}_6$ , 25 °C) spectrum of **106** between  $\delta$  20 –  $\delta$  40

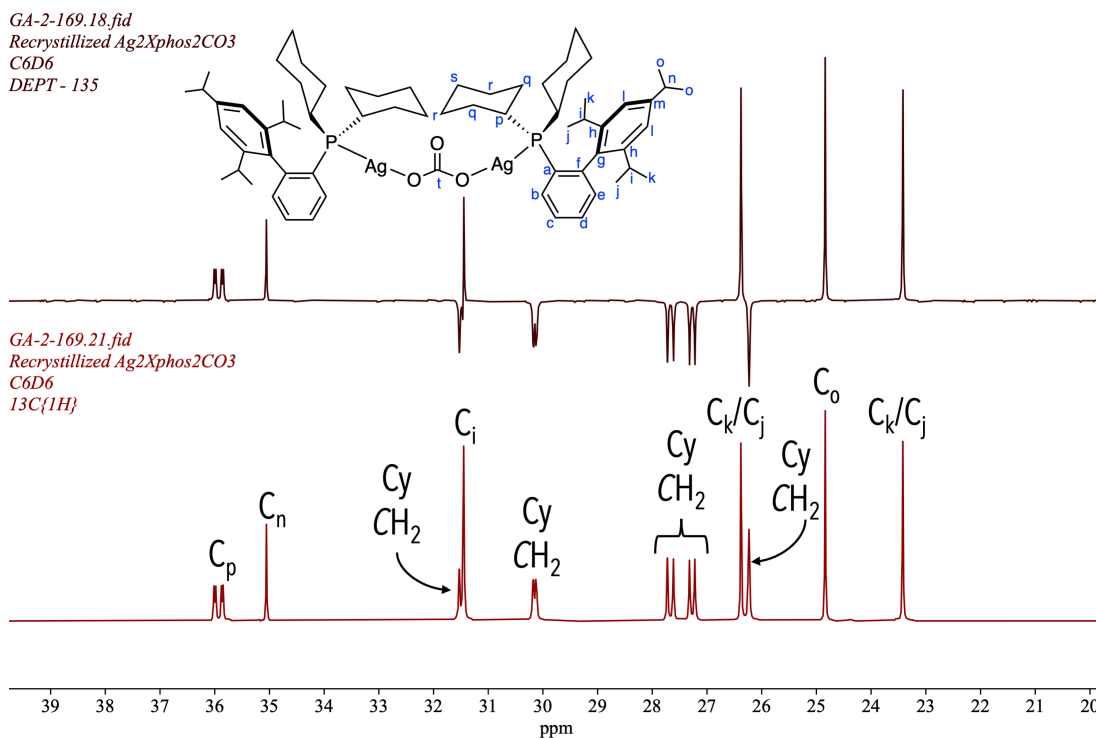


**Figure 269:** Stack plot of the  $^{13}\text{C}\{^1\text{H}\}$  Carbon DEPT spectrum (above) and the  $^{13}\text{C}\{^1\text{H}\}$  spectrum (below) of **106** (between  $\delta$  20 –  $\delta$  40)

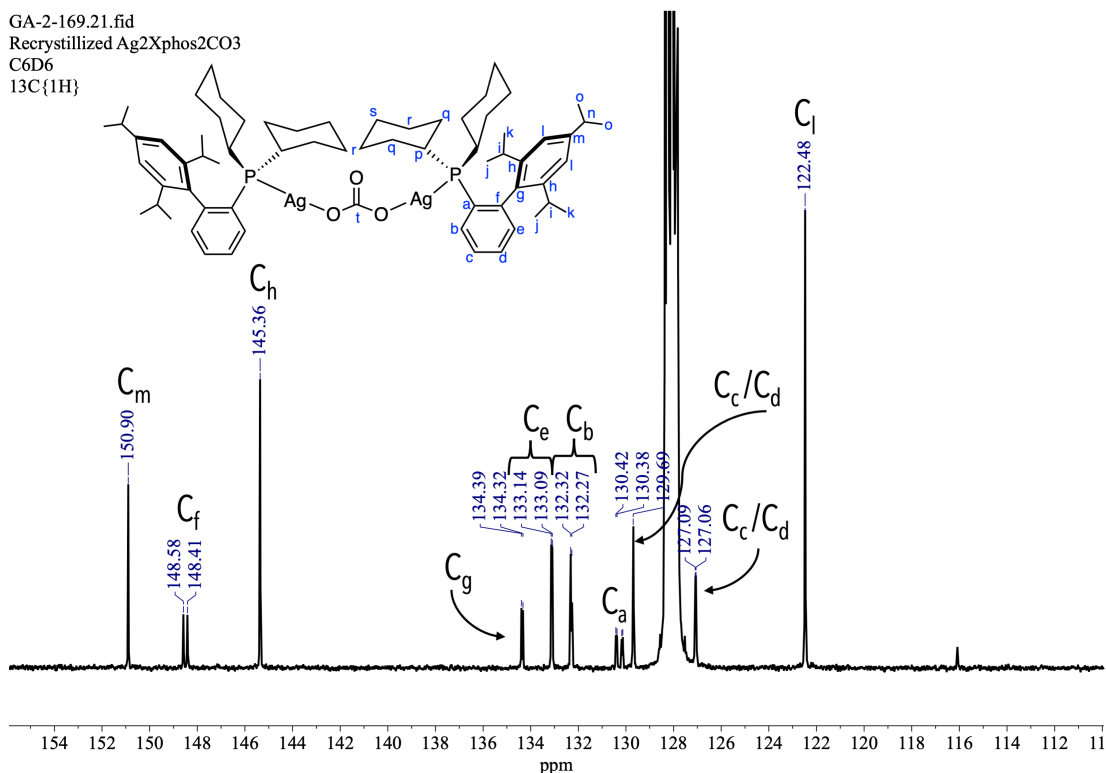


**Figure 270:**  $^{13}\text{C}\{^1\text{H}\}$  (125.8 MHz,  $\text{C}_6\text{D}_6$ , 25 °C) spectrum of **106** between  $\delta$  120 and  $\delta$  156

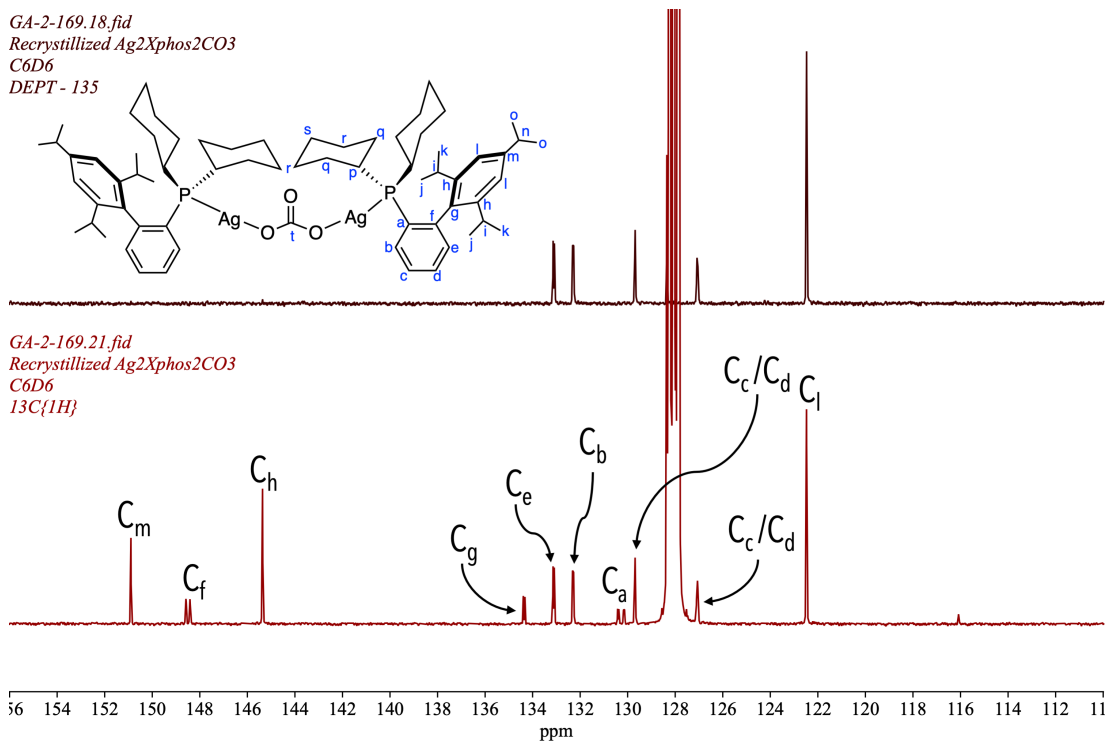


**Figure 271:** Stack plot of the  $^{13}\text{C}\{^1\text{H}\}$  Carbon DEPT spectrum (above) and the  $^{13}\text{C}\{^1\text{H}\}$  spectrum (below) of **106** between  $\delta$  120 and  $\delta$  154

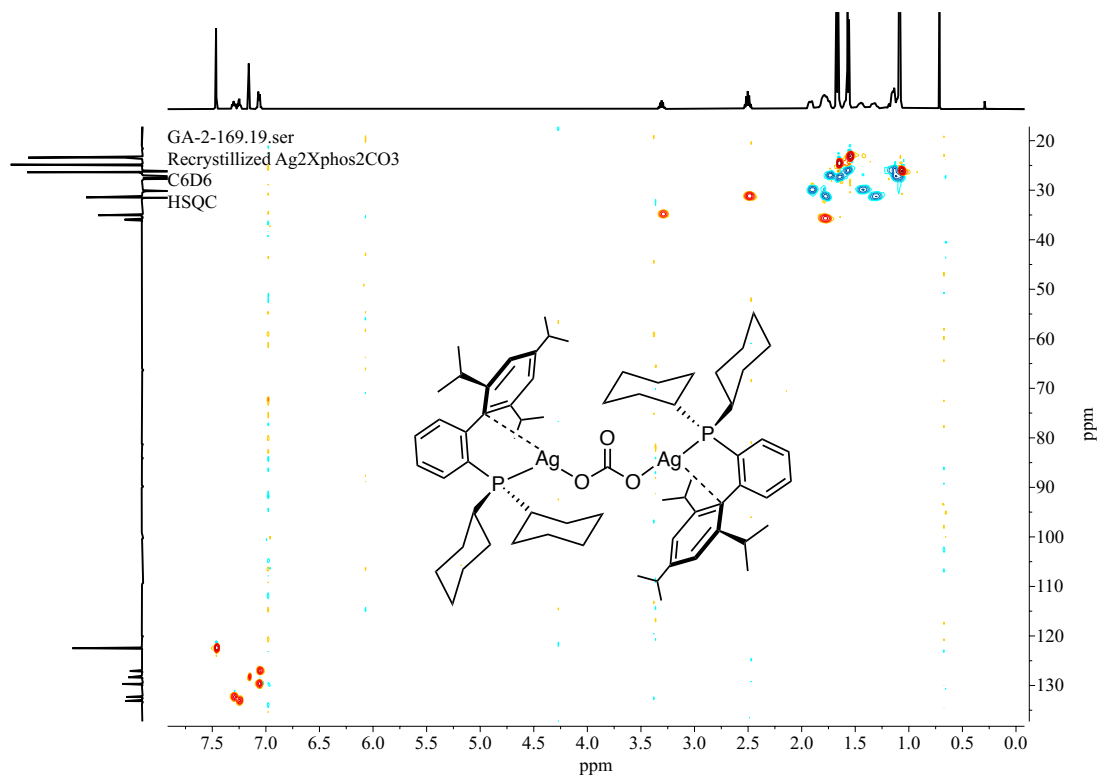


**Figure 272:** HSQC spectrum of **106** (spectrum collected on AV500, saved as 19 under GA-2-169)

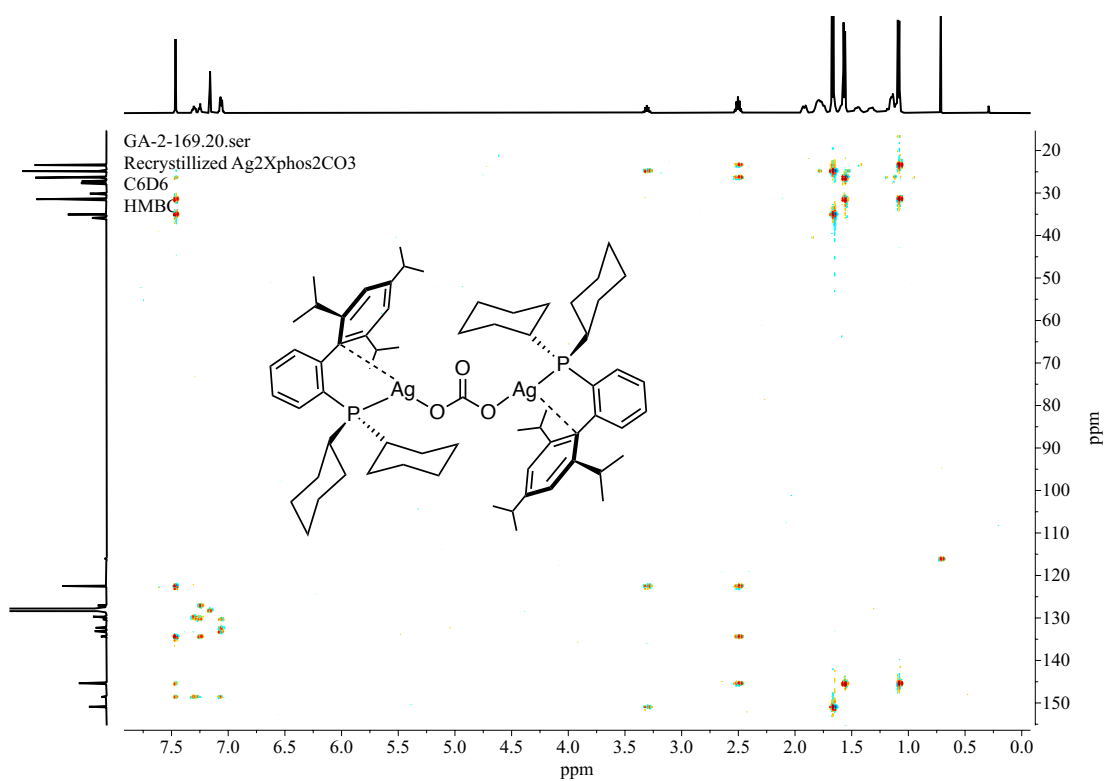


**Figure 273:** HMBC spectrum of **106** (spectrum collected on AV500, saved as 20 under GA-2-169)

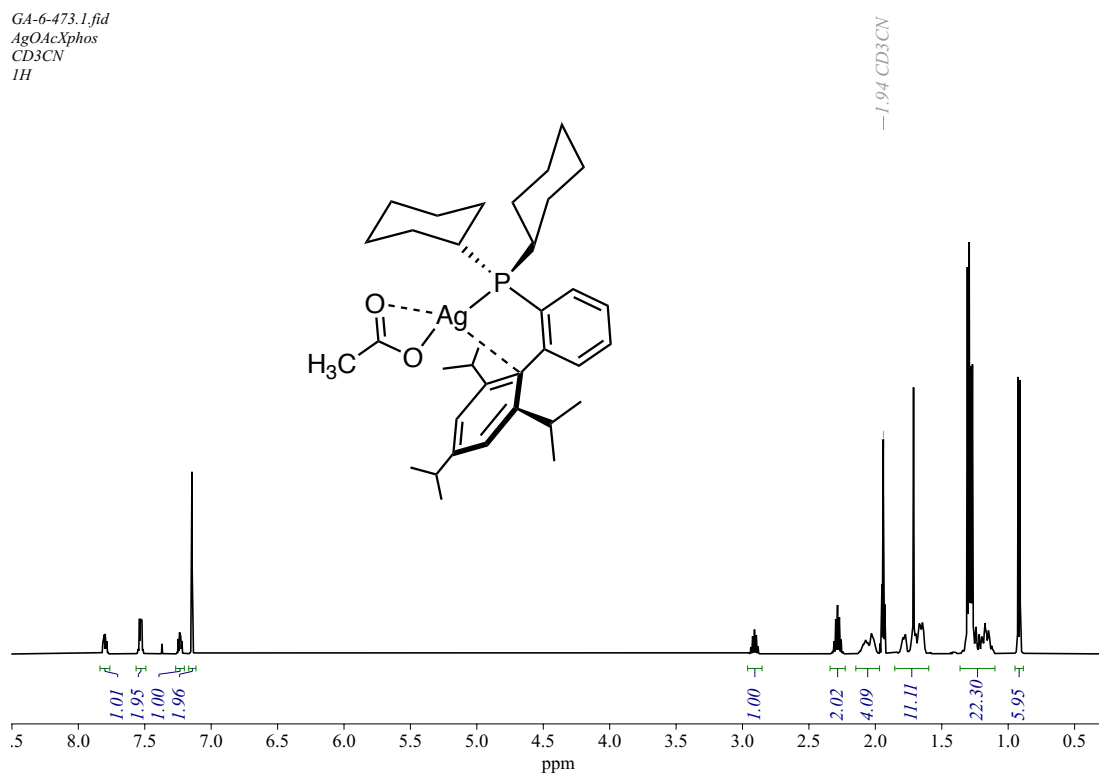


**Figure 274:**  $^1\text{H}$  NMR (500 MHz,  $\text{CD}_3\text{CN}$ , 25 °C) spectrum of **109** (spectrum collected on AV500, saved as 1 under GA-6-473)

GA-6-473.1.fid  
AgOAcXphos  
CD<sub>3</sub>CN  
1H

-1.94 CD<sub>3</sub>CN

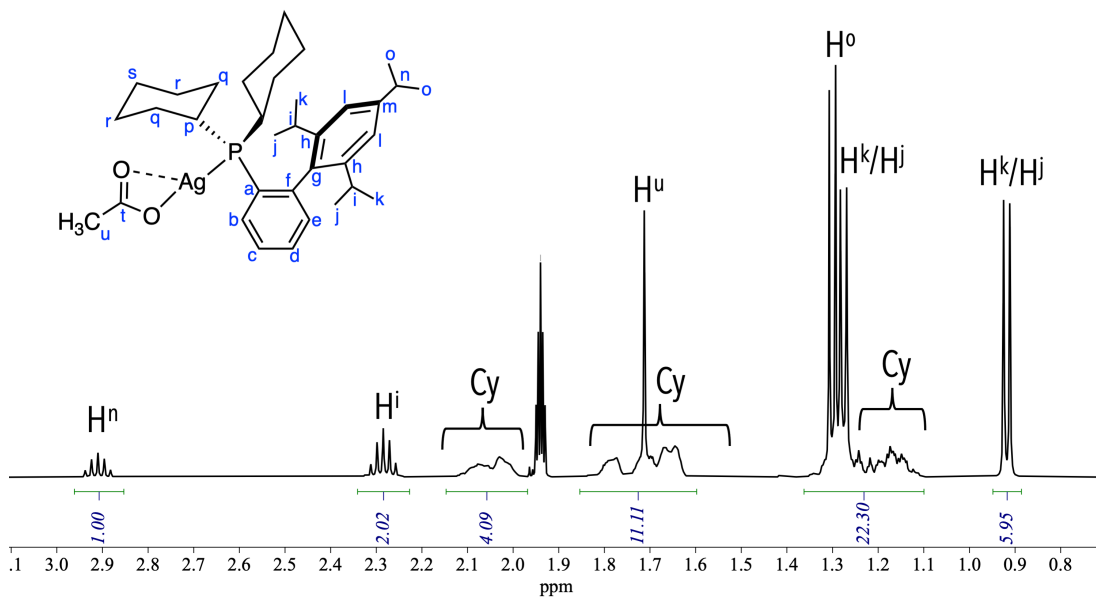


Figure 275: <sup>1</sup>H NMR (500 MHz, CD<sub>3</sub>CN, 25 °C) spectrum of **109** between  $\delta$  0.7 to  $\delta$  3.1

GA-6-473.1.fid  
AgOAcXphos  
CD<sub>3</sub>CN  
1H

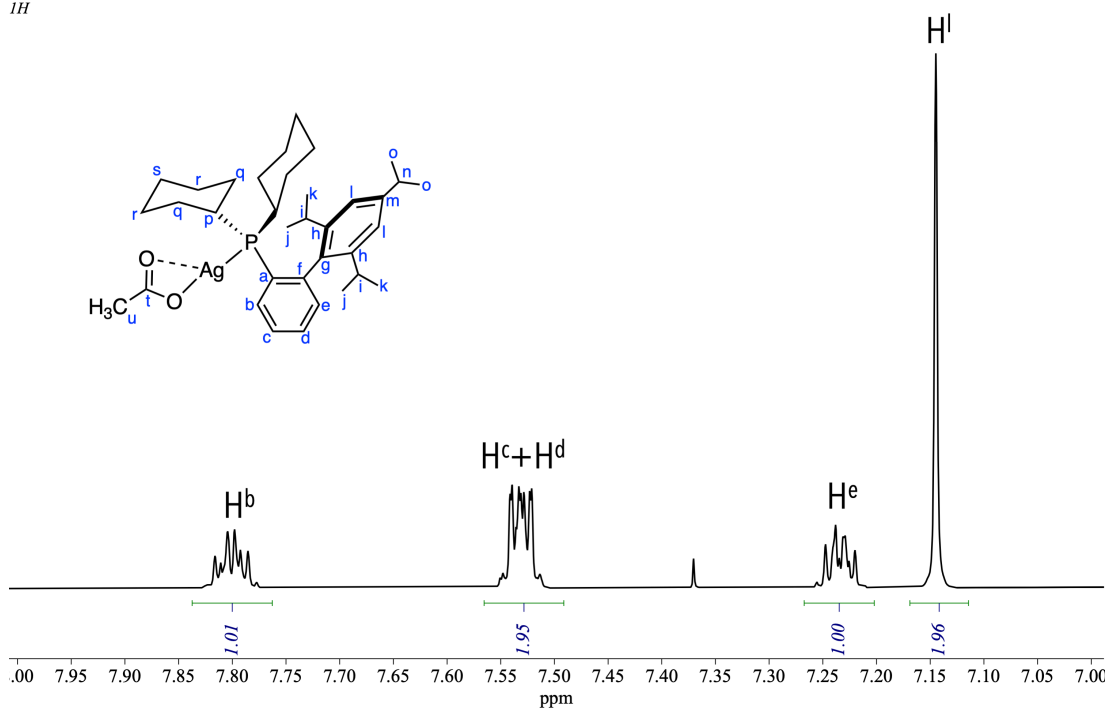
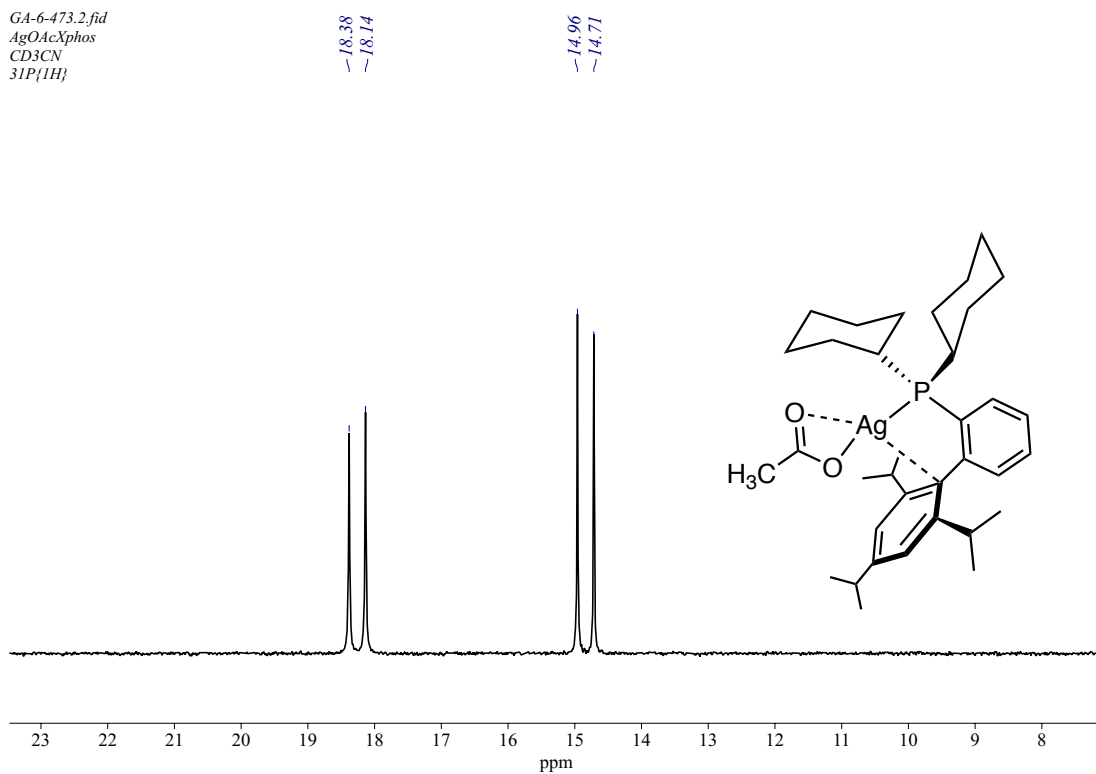
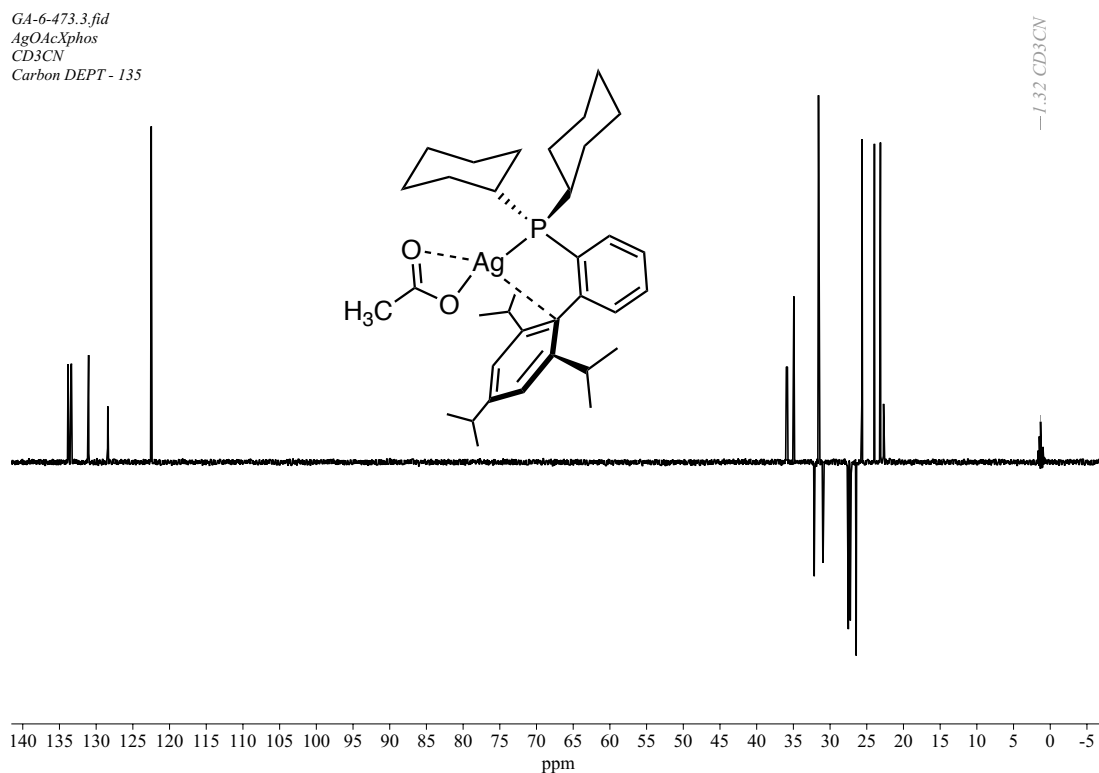


Figure 276: <sup>1</sup>H NMR (500 MHz, CD<sub>3</sub>CN, 25 °C) spectrum of **109** between  $\delta$  7.0 to  $\delta$  8.0





**Figure 277:** <sup>31</sup>P{<sup>1</sup>H} (202.5 MHz, CD<sub>3</sub>CN, 25 °C) spectrum of **109** (spectrum collected on AV500, saved as 2 under GA-6-473)



**Figure 278:** <sup>13</sup>C DEPT-135 (125.8 MHz, CD<sub>3</sub>CN, 25 °C) spectrum of **109** (spectrum collected on AV500, saved as 3 under GA-6-473)

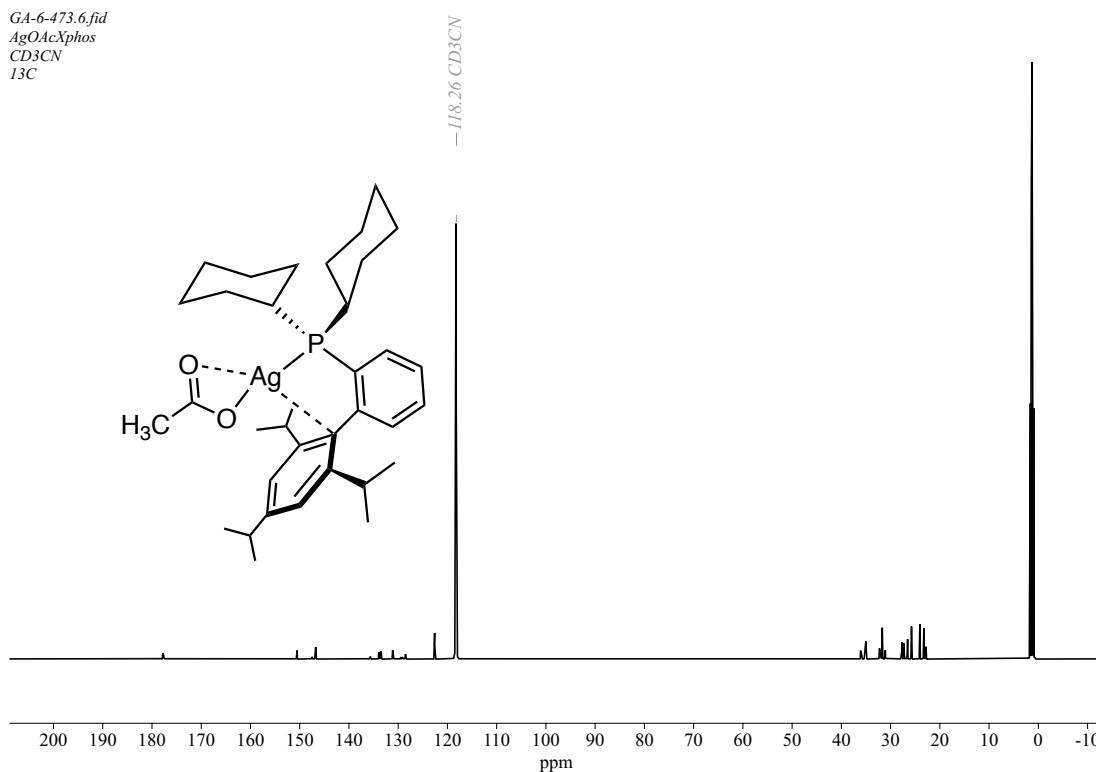


**Figure 279:**  $^{13}\text{C}\{^1\text{H}\}$  (125.8 MHz, CD<sub>3</sub>CN, 25 °C) spectrum of **109** (spectrum collected on AV500, saved as 6 under GA-6-473)

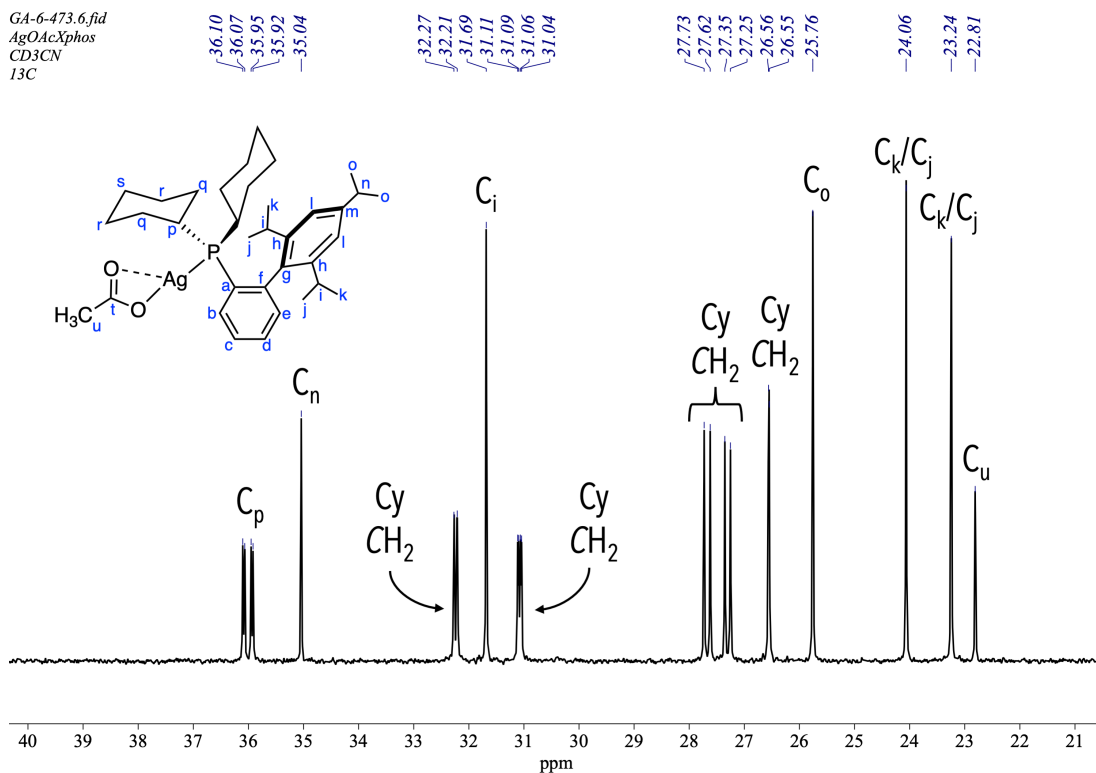


**Figure 280:**  $^{13}\text{C}\{^1\text{H}\}$  (125.8 MHz, CD<sub>3</sub>CN, 25 °C) spectrum of **109** between  $\delta$  20 and  $\delta$  40

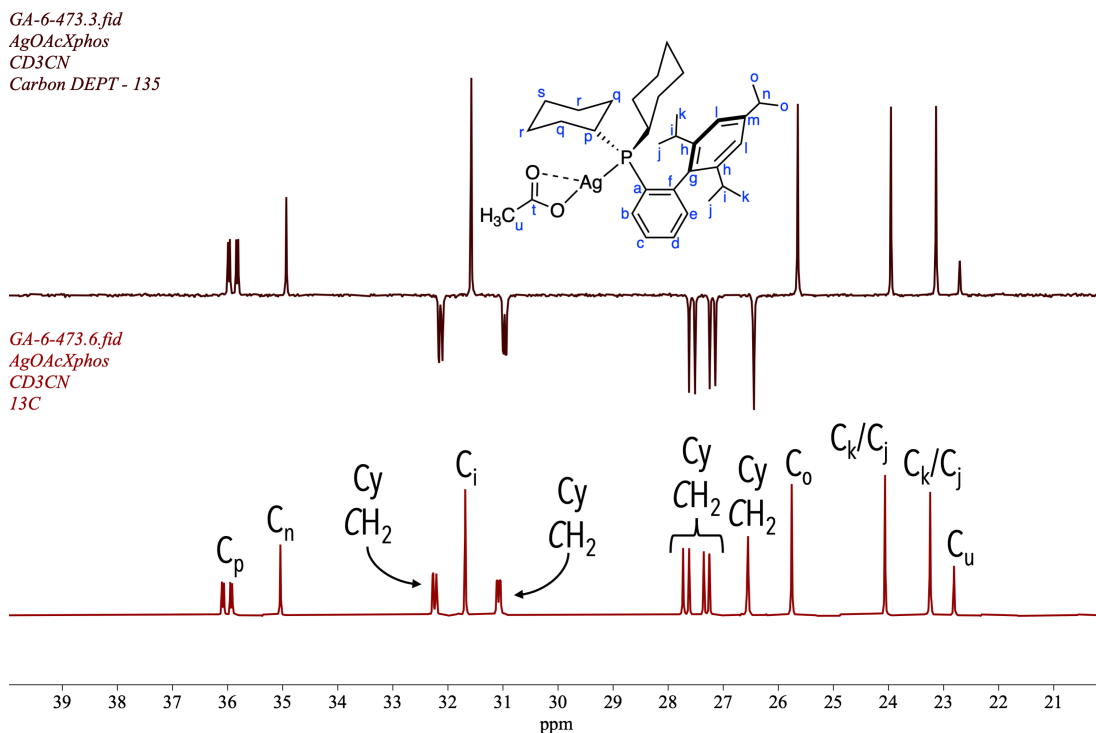


**Figure 281:** Stack plot of the  $^{13}\text{C}\{^1\text{H}\}$  Carbon DEPT spectrum (above) and the  $^{13}\text{C}\{^1\text{H}\}$  spectrum (below) of **109** between  $\delta$  20 and  $\delta$  40

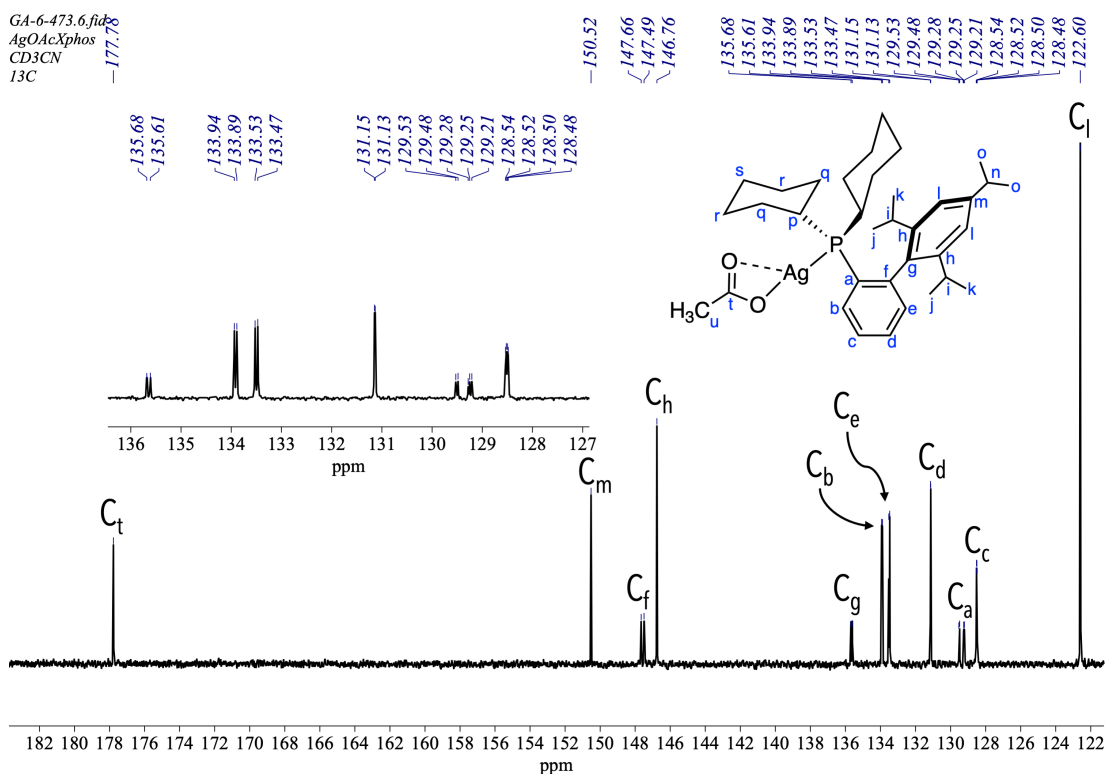


**Figure 282:**  $^{13}\text{C}\{^1\text{H}\}$  (125.8 MHz, CD<sub>3</sub>CN, 25 °C) spectrum of **109** between  $\delta$  120 and  $\delta$

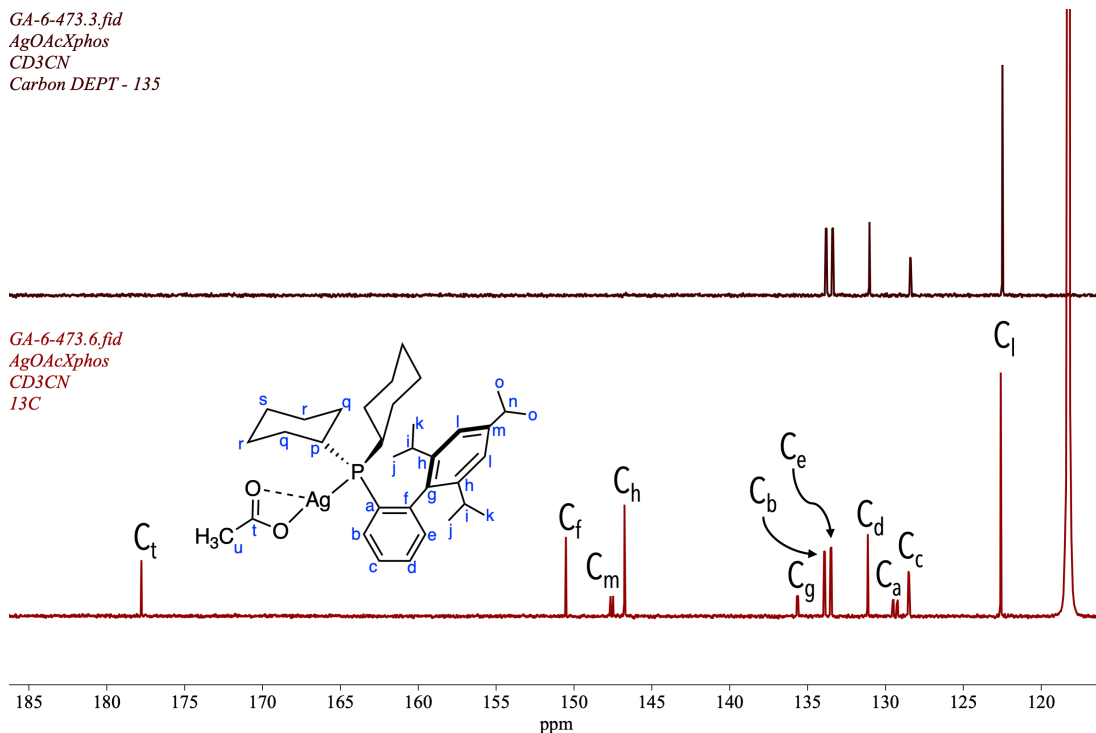


**Figure 283:** Stack plot of the  $^{13}\text{C}\{^1\text{H}\}$  Carbon DEPT spectrum (above) and the  $^{13}\text{C}\{^1\text{H}\}$  spectrum (below) of **109** between  $\delta$  110 and  $\delta$  186

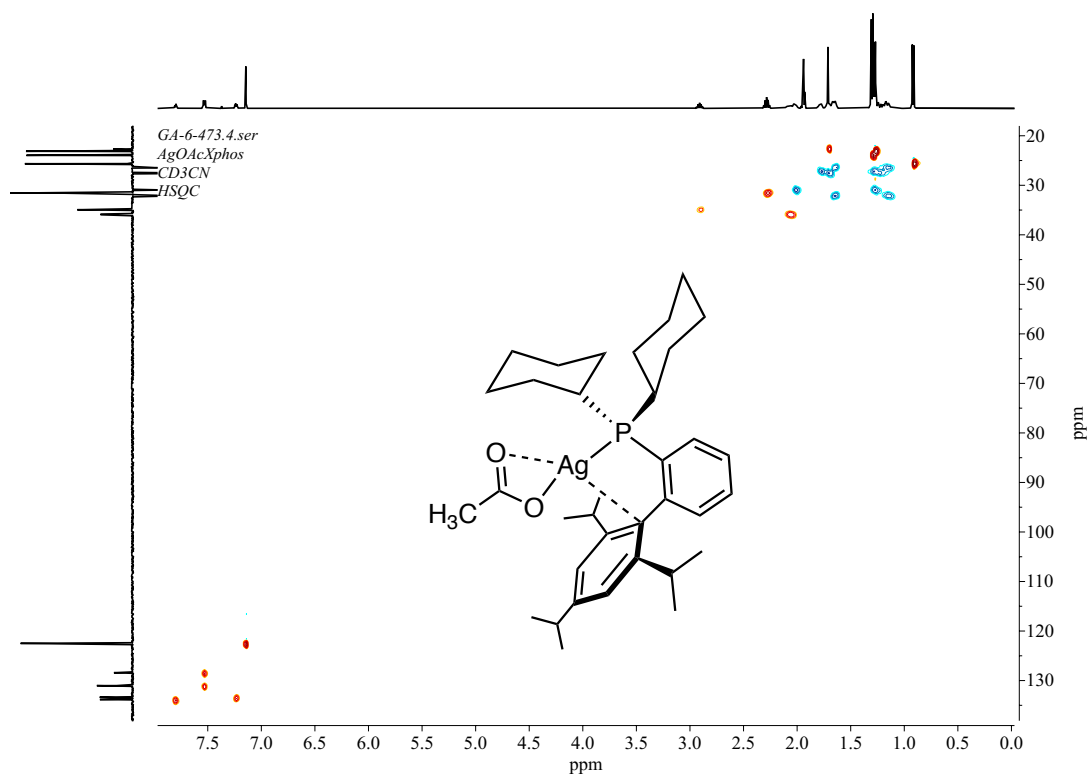


**Figure 284:** HSQC spectrum of **109** (spectrum collected on AV500, saved as 4 under GA-6-473)

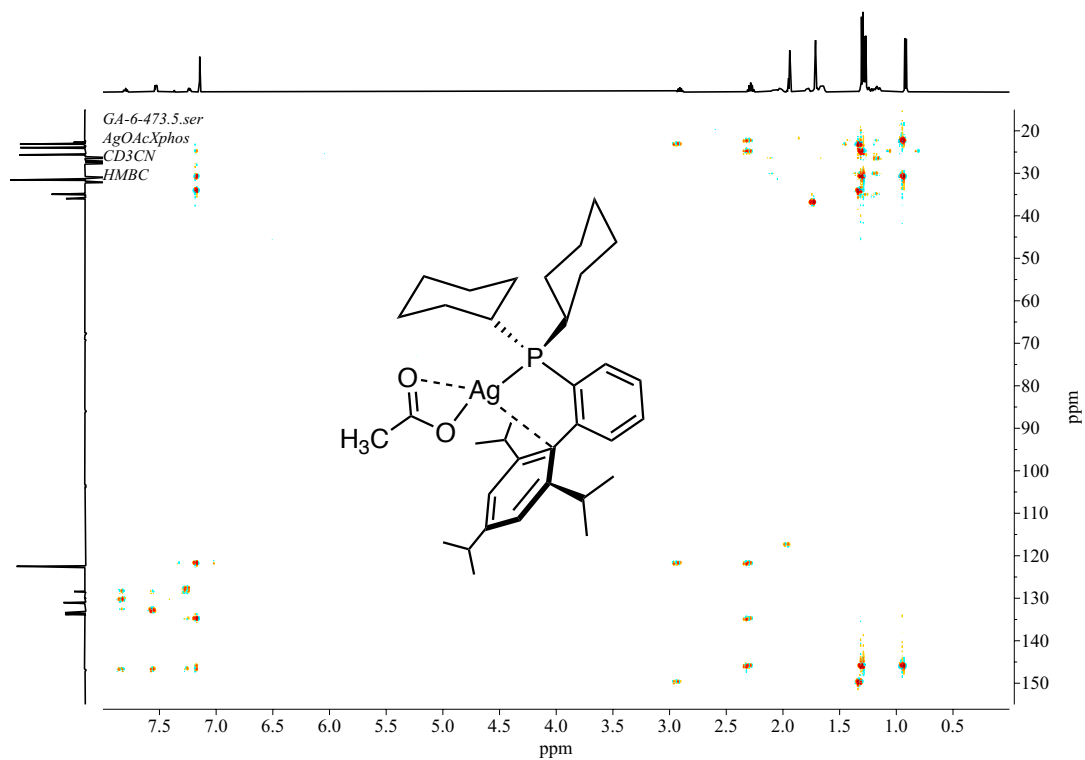


**Figure 285:** HMBC spectrum of **109** (spectrum collected on AV500, saved as 5 under GA-6-473)

GA-2-148.4.fid  
AgIXphos  
1H

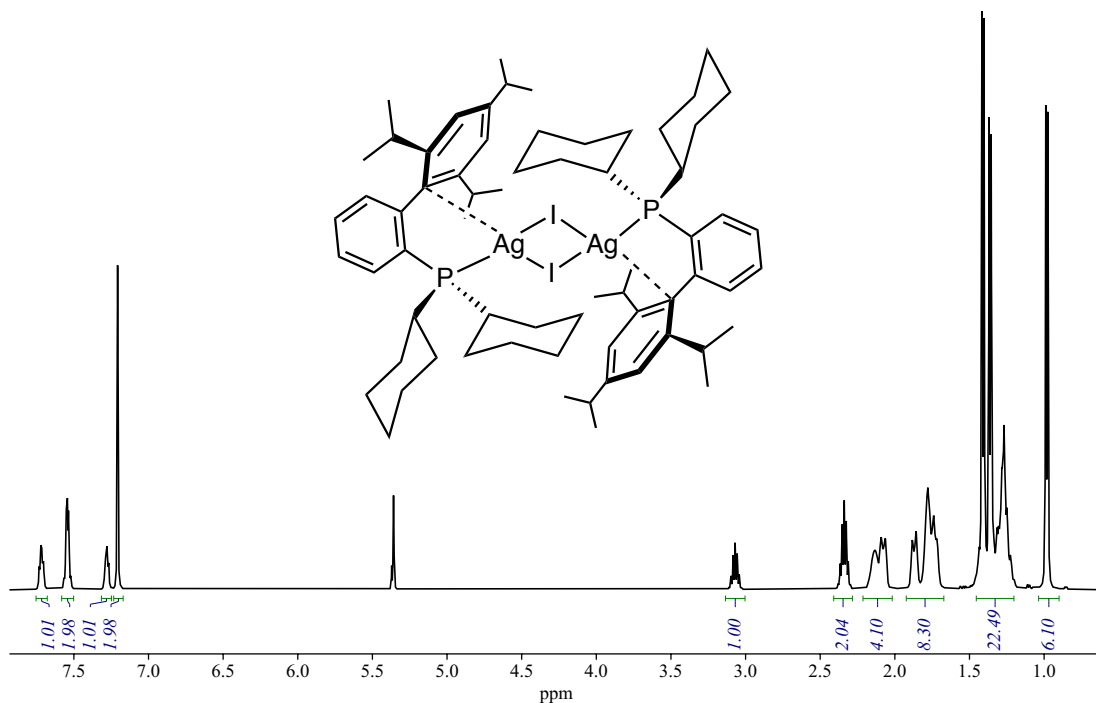


**Figure 286:**  $^1\text{H}$  NMR (500 MHz,  $\text{CD}_2\text{Cl}_2$ , 25 °C) spectrum of **105** (spectrum collected on AV500, saved as 4 under GA-2-148)

GA-2-148.4.fid  
AgIXphos  
1H

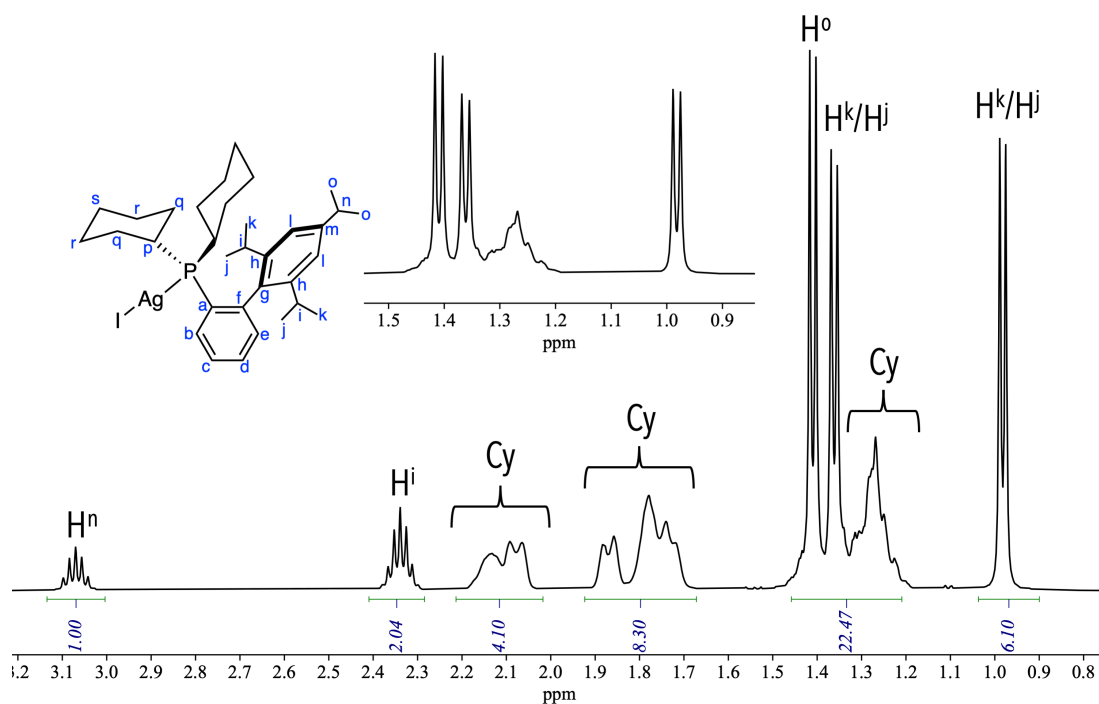


**Figure 287:**  $^1\text{H}$  NMR (500 MHz,  $\text{CD}_2\text{Cl}_2$ , 25 °C) spectrum of **105** between  $\delta$  0.8 and  $\delta$  4.0

GA-2-148.4.fid  
AgIXphos  
1H

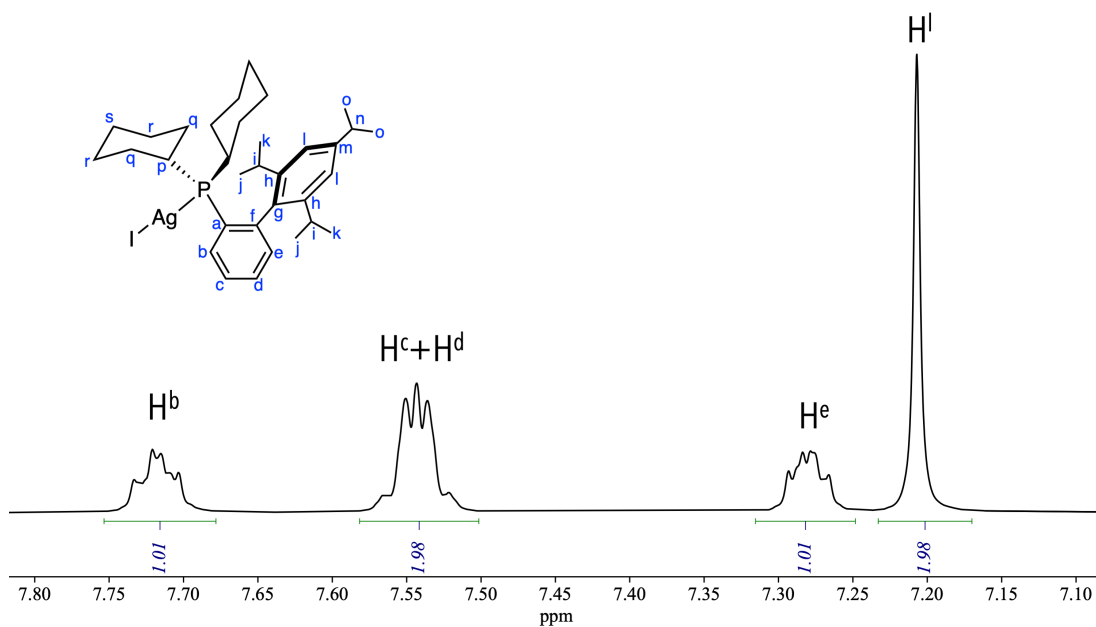


**Figure 288:**  $^1\text{H}$  NMR (500 MHz,  $\text{CD}_2\text{Cl}_2$ , 25 °C) spectrum of **105** between  $\delta$  7.0 and  $\delta$  8.0

GA-2-148.5.fid  
AgIXphos  
31P

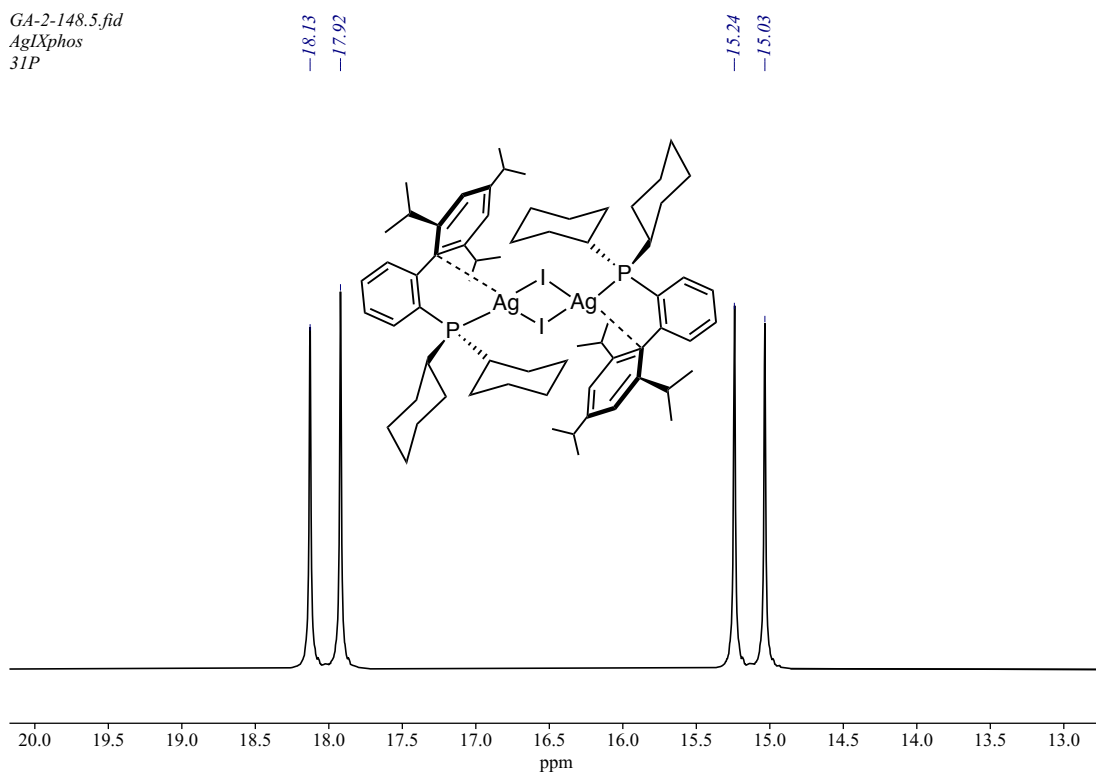


**Figure 289:**  $^{31}\text{P}\{^1\text{H}\}$  (202.5 MHz,  $\text{CD}_2\text{Cl}_2$ , 25 °C) spectrum of **105** (spectrum collected on AV500, saved as 5 under GA-2-148)

GA-2-148.6.fid  
AgIXphos Purified  
 $\text{CD}_2\text{Cl}_2$   
Carbon DEPT - 135

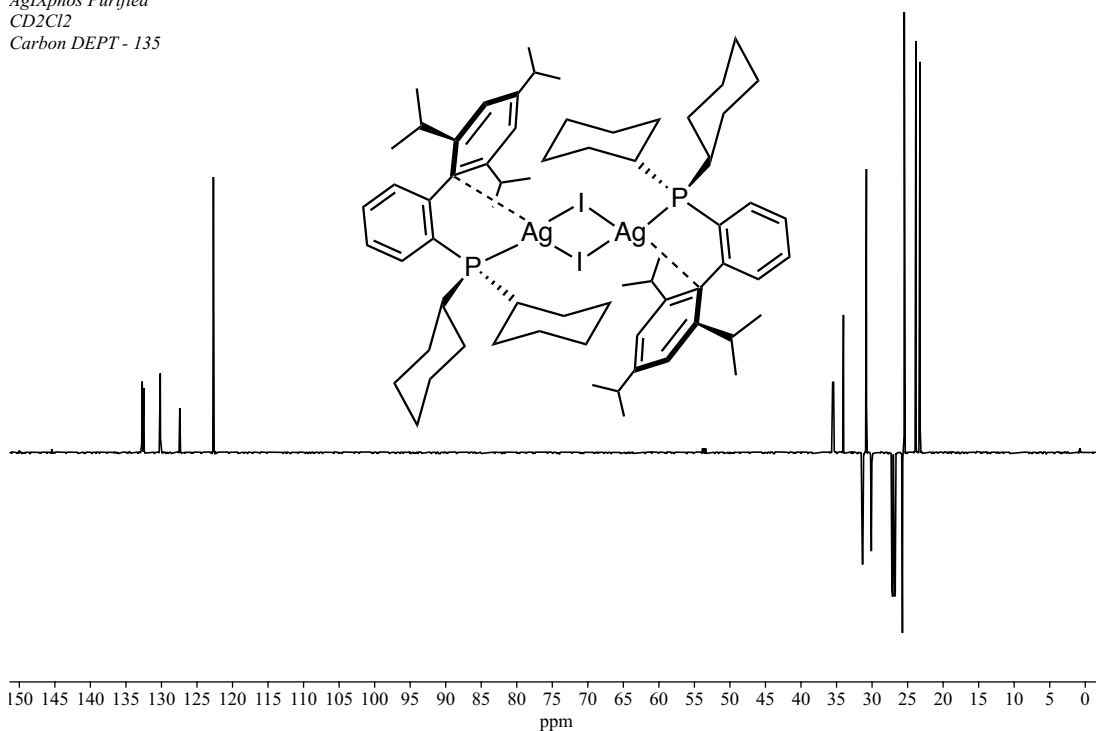


**Figure 290:**  $^{13}\text{C}$  DEPT-135 (125.8 MHz,  $\text{CD}_2\text{Cl}_2$ , 25 °C) spectrum of **105** (spectrum collected on AV500, saved as 6 under GA-2-148)

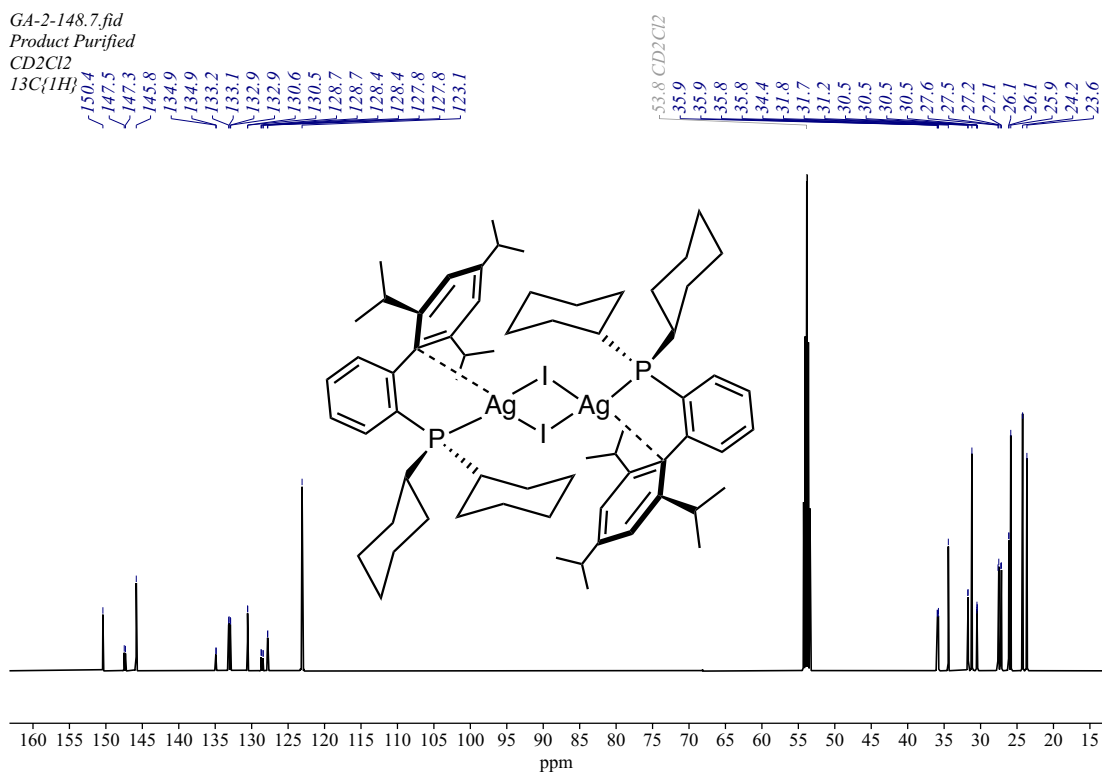


**Figure 291:** <sup>13</sup>C{<sup>1</sup>H} (125.8 MHz, CD<sub>2</sub>Cl<sub>2</sub>, 25 °C) spectrum of **105** (spectrum collected on AV500, saved as 7 under GA-2-148)

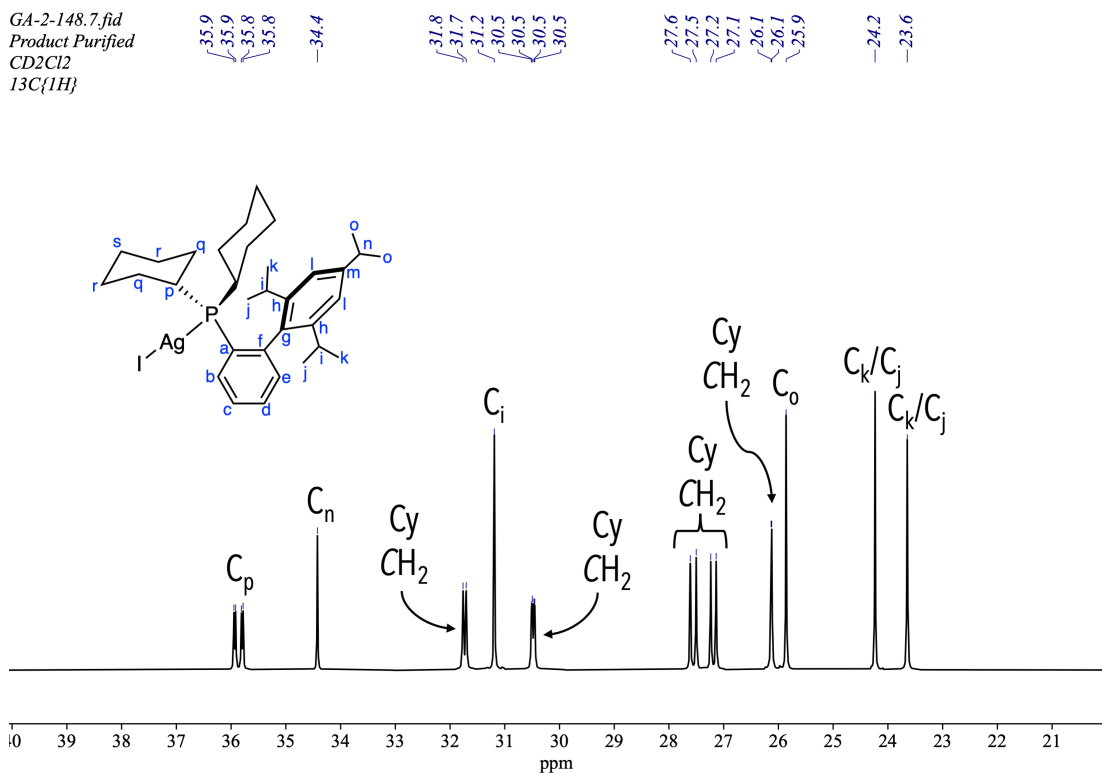


**Figure 292:** <sup>13</sup>C{<sup>1</sup>H} (125.8 MHz, CD<sub>2</sub>Cl<sub>2</sub>, 25 °C) spectrum of **105** between δ 20 and δ 40



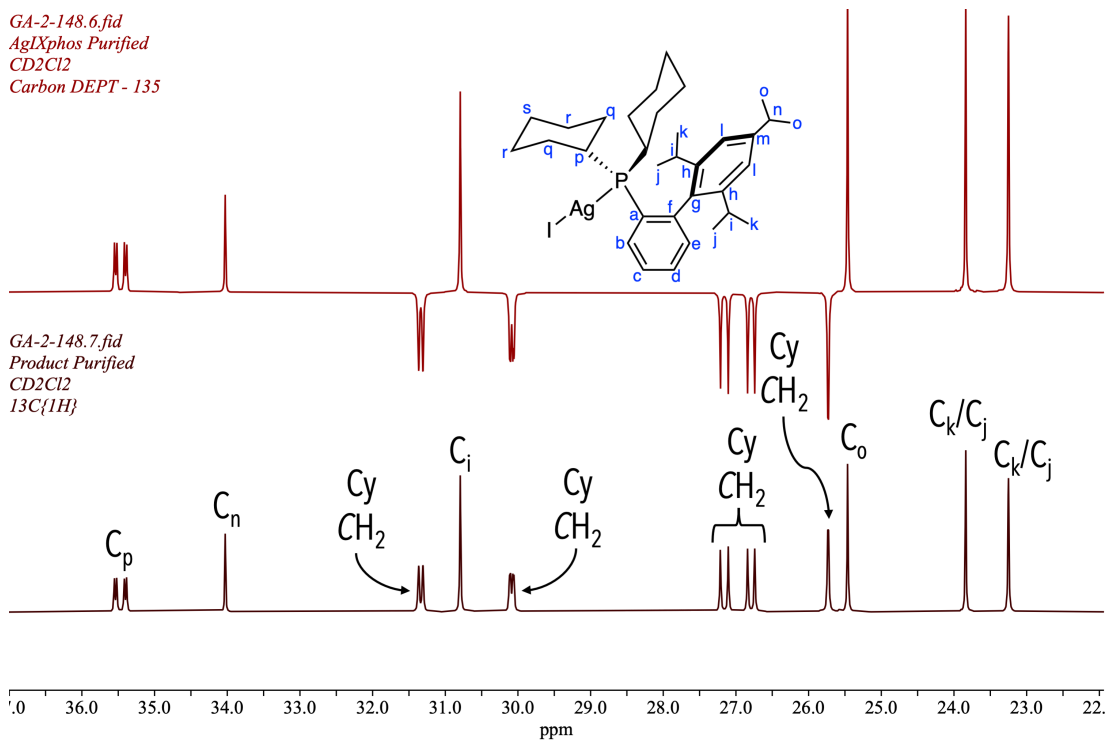


**Figure 293:** Stack plot of the <sup>13</sup>C{<sup>1</sup>H} Carbon DEPT spectrum (above) and the <sup>13</sup>C{<sup>1</sup>H} spectrum (below) of **105** between δ 20 and δ 40

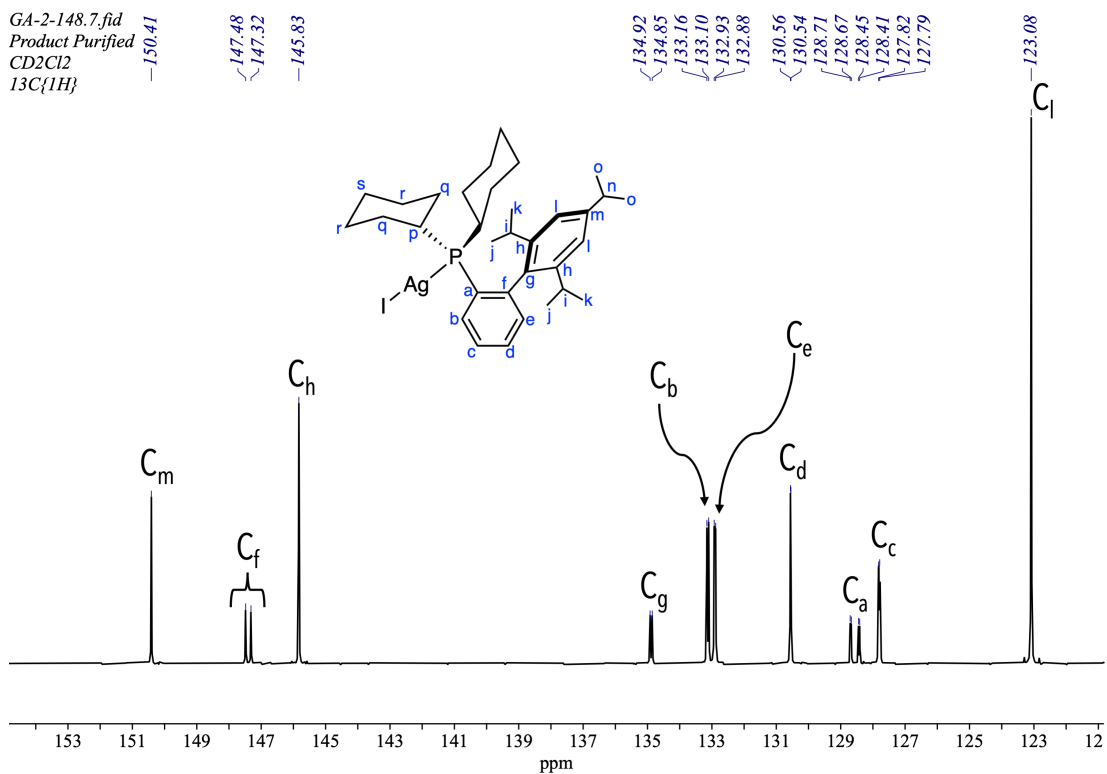
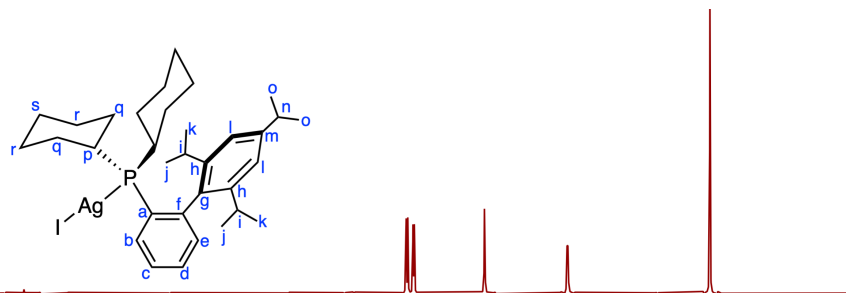


**Figure 294:** <sup>13</sup>C{<sup>1</sup>H} (125.8 MHz, CD<sub>2</sub>Cl<sub>2</sub>, 25 °C) spectrum of **105** between δ 118 and δ 155

GA-2-148.6.fid  
AgIXphos Purified  
CD<sub>2</sub>Cl<sub>2</sub>  
Carbon DEPT - 135



GA-2-148.7.fid  
Product Purified  
CD<sub>2</sub>Cl<sub>2</sub>  
<sup>13</sup>C{<sup>1</sup>H}

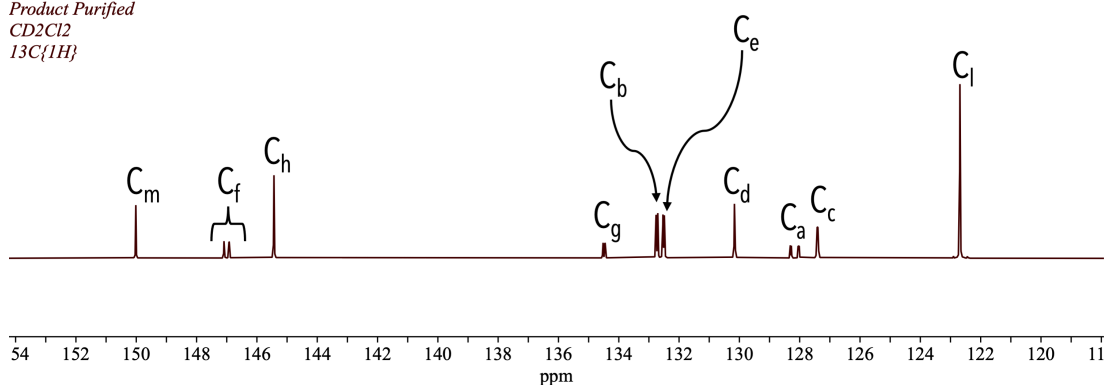


**Figure 295:** Stack plot of the <sup>13</sup>C{<sup>1</sup>H} Carbon DEPT spectrum (above) and the <sup>13</sup>C{<sup>1</sup>H} spectrum (below) of **105** between δ 120 and δ 154

Ag NMR spectrum.401.fid

-18.32  
-16.07  
-14.65

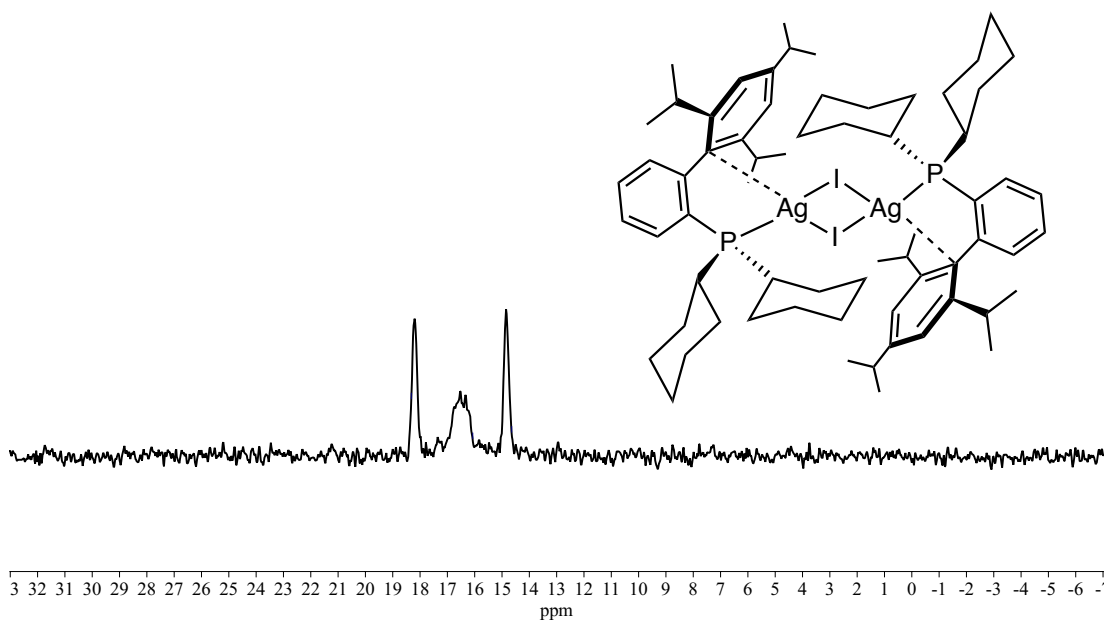


**Figure 296:** <sup>31</sup>P{<sup>109</sup>Ag} (162 MHz, CD<sub>2</sub>Cl<sub>2</sub>, 25 °C) spectrum of **105**

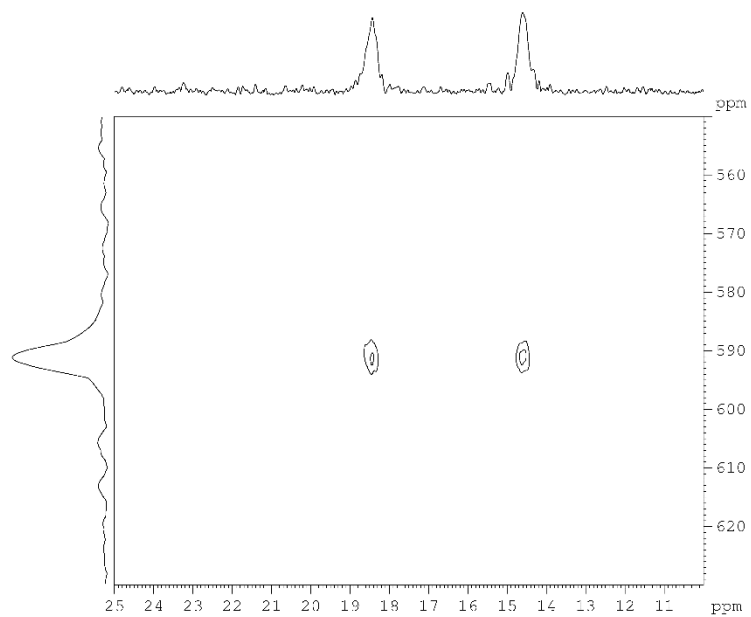


**Figure 297:**  $^{31}\text{P}\{^{109}\text{Ag}\}\text{-}^{109}\text{Ag}$  HMQC spectrum of **105**

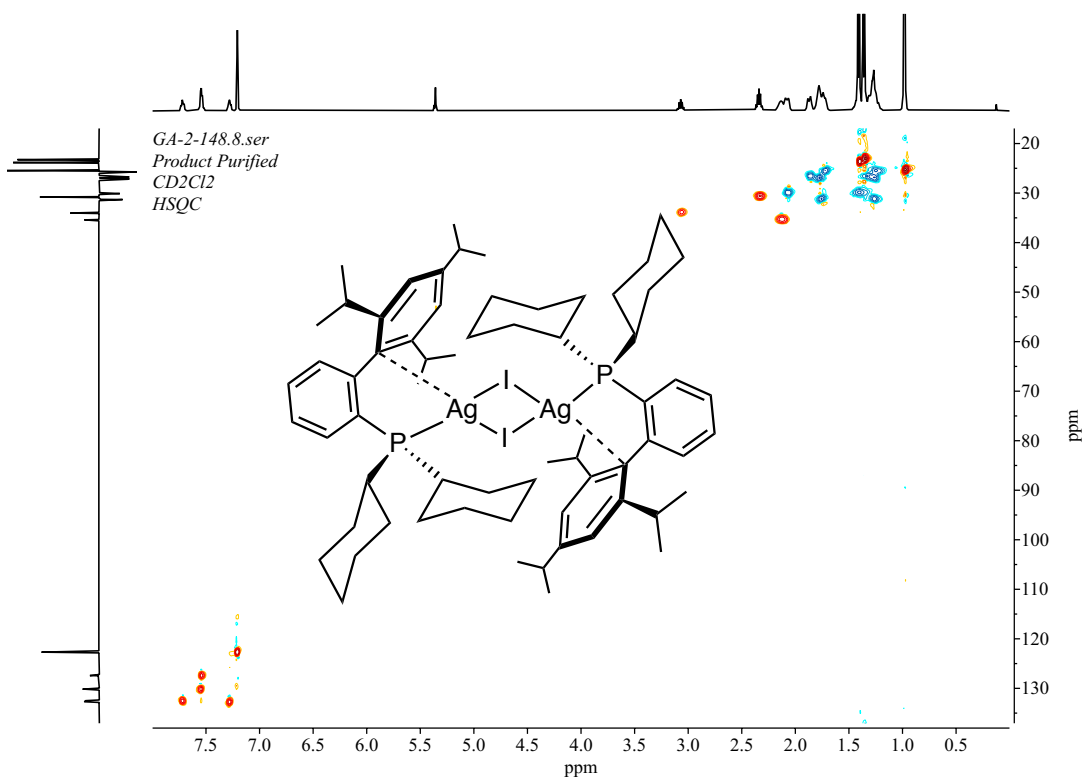


**Figure 298:** HSQC spectrum of **105** (spectrum collected on AV500, saved as 8 under GA-2-148)

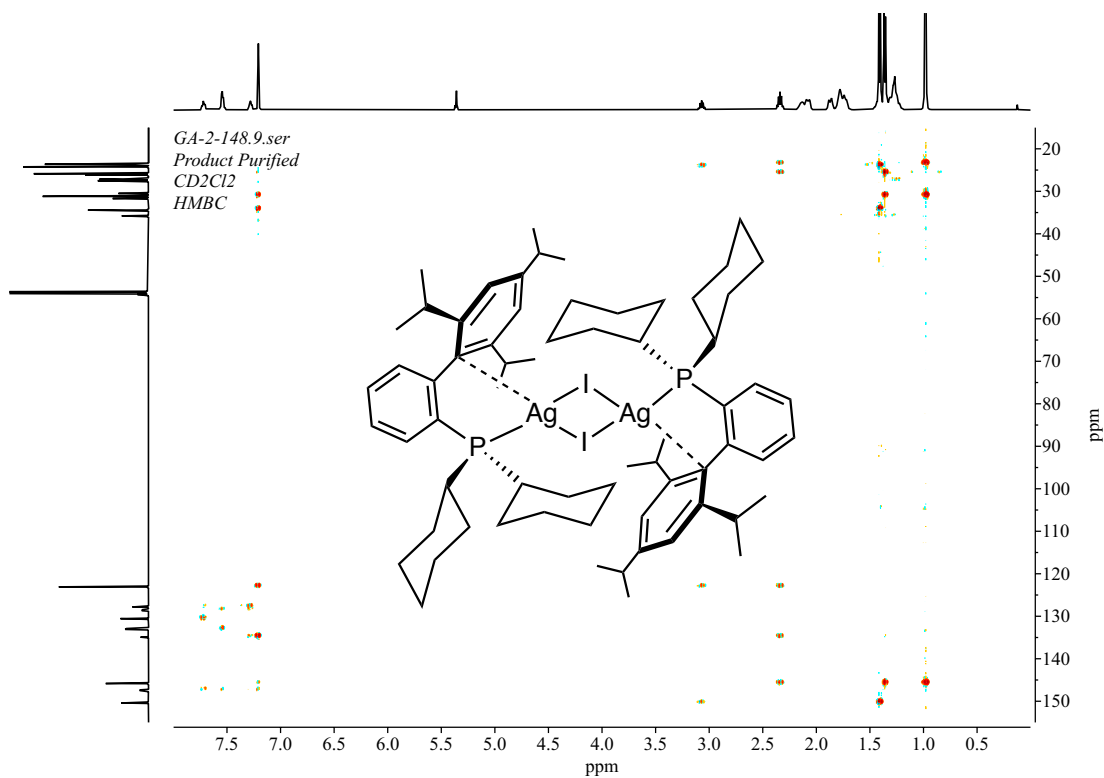


**Figure 299:** HMBC spectrum of **105** (spectrum collected on AV500, saved as 9 under GA-2-148)

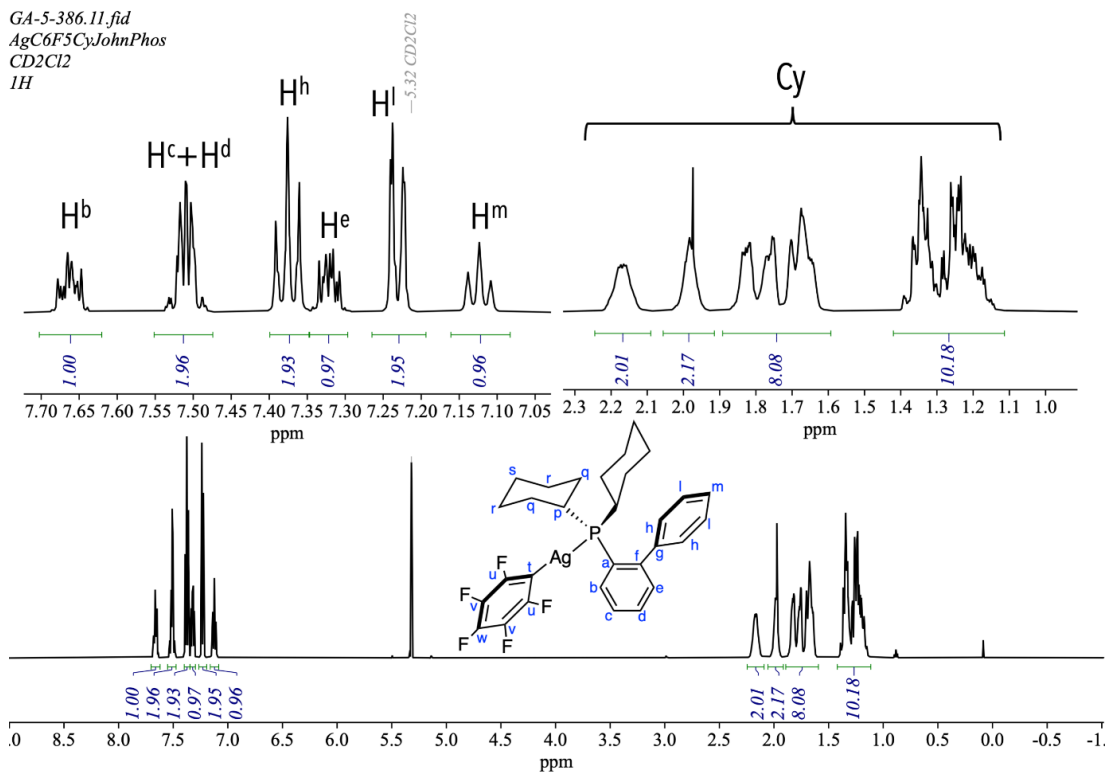


**Figure 300:**  $^1\text{H}$  NMR (500 MHz,  $\text{CD}_2\text{Cl}_2$ , 25 °C) spectrum of  $\text{AgC}_6\text{F}_5\text{CyJohnPhos}$  **122**

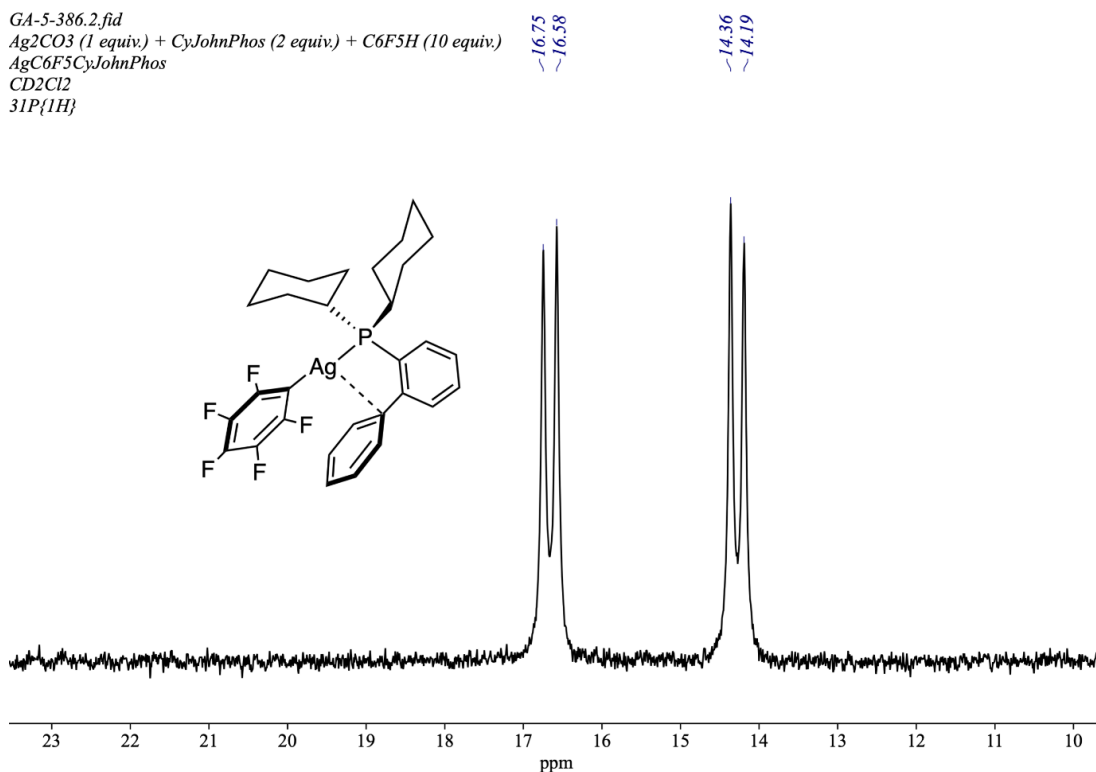


**Figure 301:** <sup>31</sup>P{<sup>1</sup>H} (202.5 MHz, CD<sub>2</sub>Cl<sub>2</sub>, 25 °C) spectrum of AgC<sub>6</sub>F<sub>5</sub>CyJohnPhos **122**

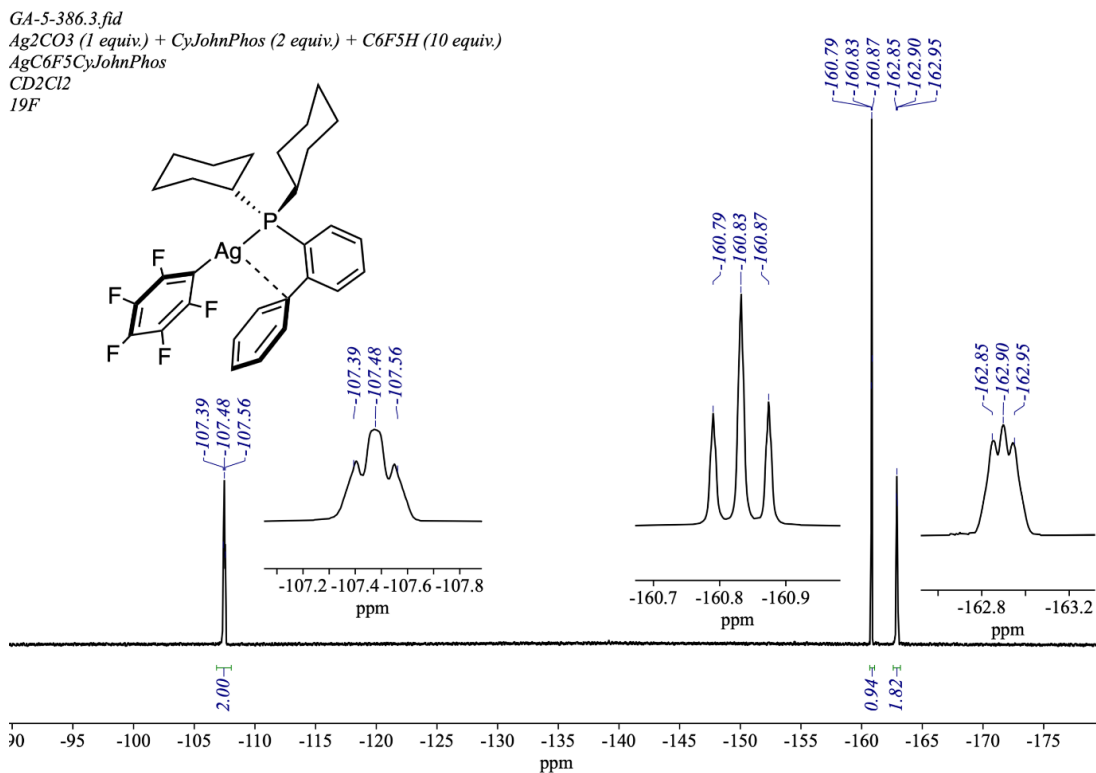


**Figure 302:** <sup>19</sup>F{<sup>1</sup>H} NMR (470.6 MHz, CD<sub>2</sub>Cl<sub>2</sub>, 25 °C) spectrum of AgC<sub>6</sub>F<sub>5</sub>CyJohnPhos **122**

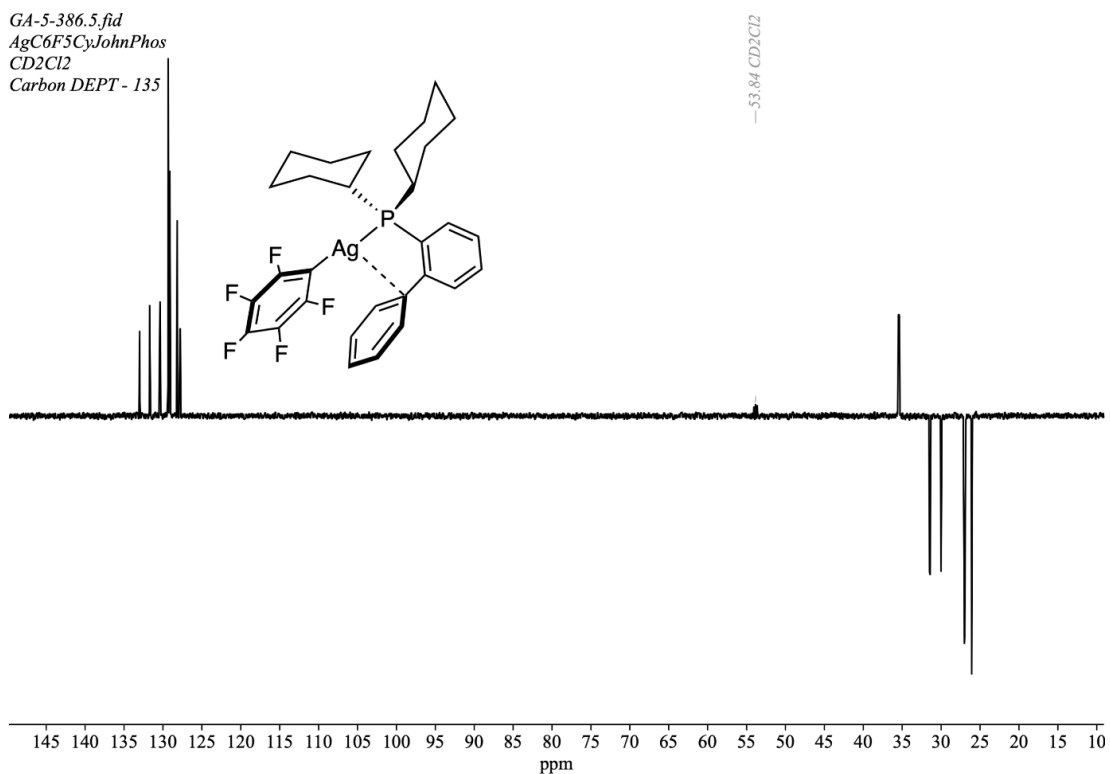


**Figure 303:**  $^{13}\text{C}$  DEPT-135 (125.8 MHz,  $\text{CD}_2\text{Cl}_2$ , 25 °C) spectrum of AgC<sub>6</sub>F<sub>5</sub>CyJohnPhos

**122**

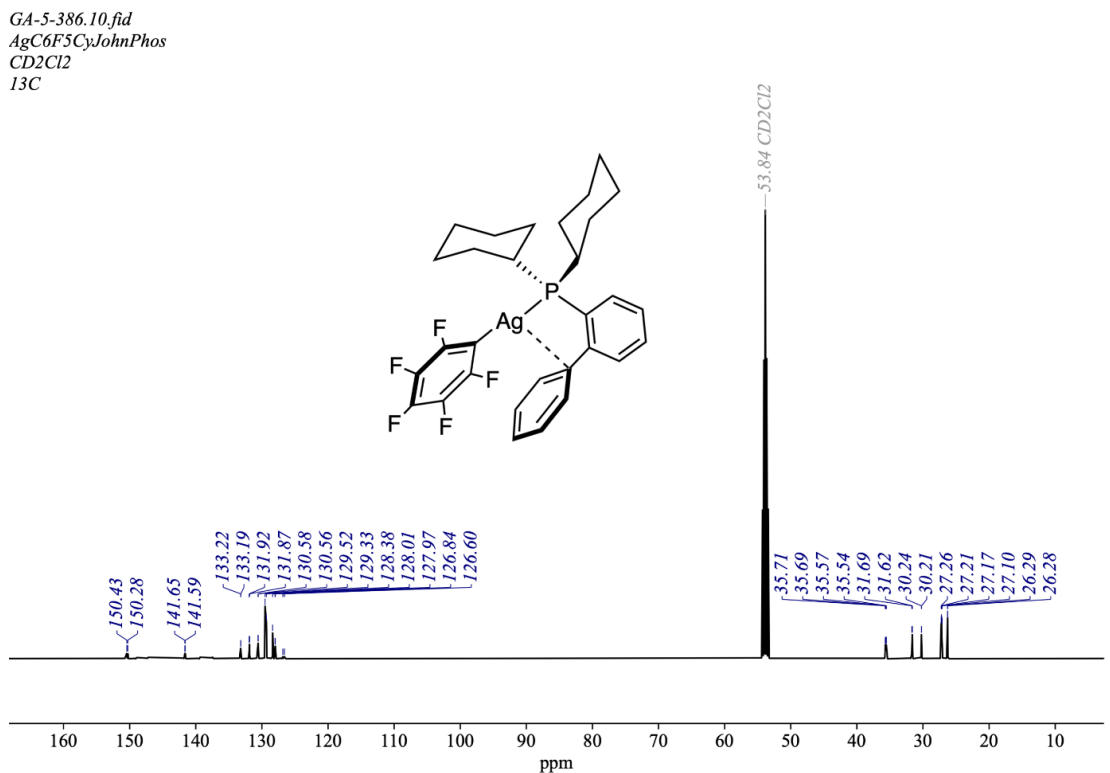


**Figure 304:**  $^{13}\text{C}\{^1\text{H}\}$  (125.8 MHz,  $\text{CD}_2\text{Cl}_2$ , 25 °C) spectrum of AgC<sub>6</sub>F<sub>5</sub>CyJohnPhos **122**

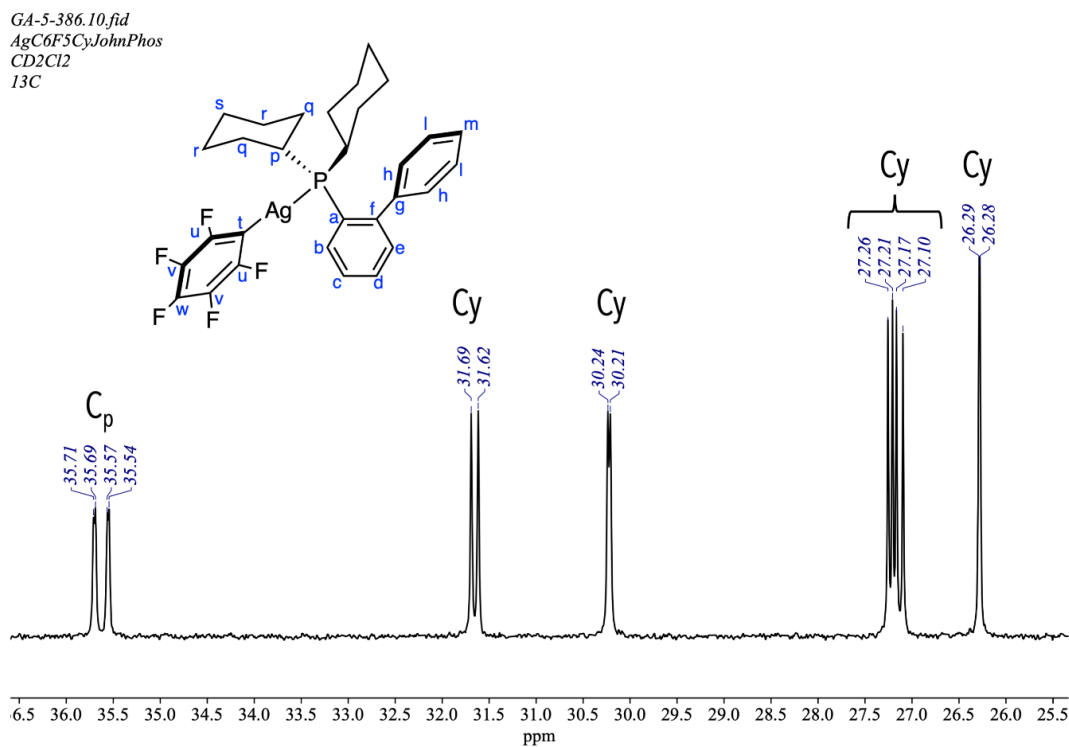


**Figure 305:**  $^{13}\text{C}\{^1\text{H}\}$  (125.8 MHz,  $\text{CD}_2\text{Cl}_2$ ,  $25^\circ\text{C}$ ) spectrum of  $\text{AgC}_6\text{F}_5\text{CyJohnPhos}$  **122** between  $\delta$  25 and  $\delta$  36

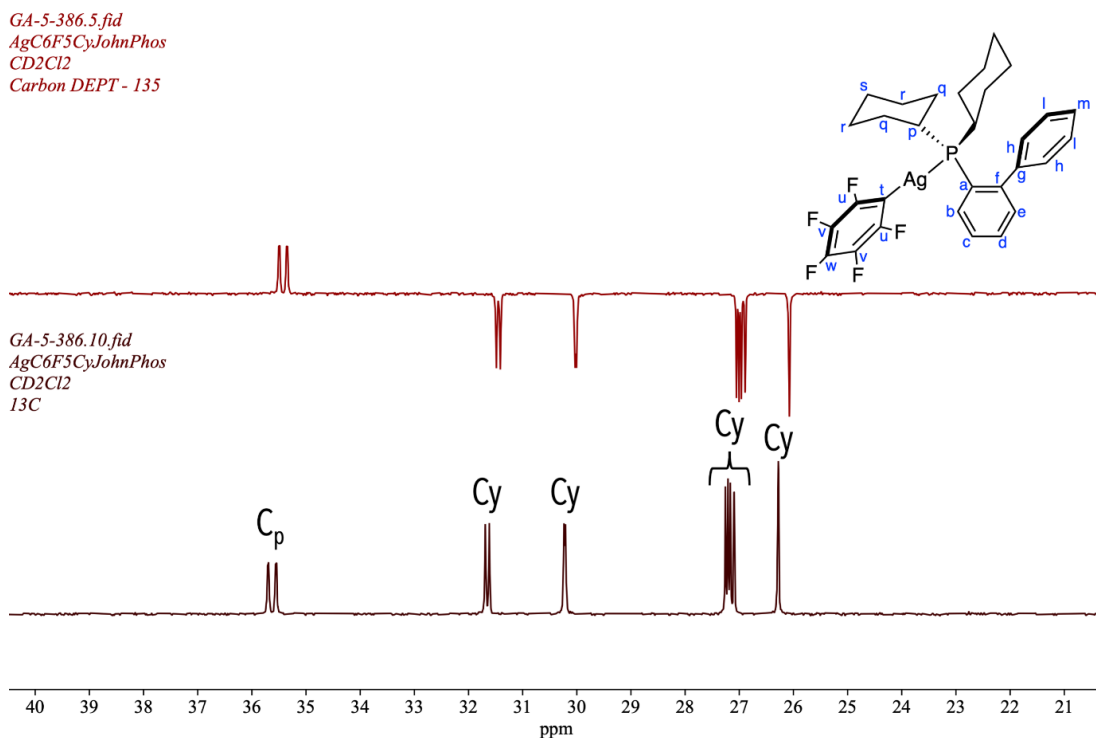


**Figure 306:** Stack plot of the  $^{13}\text{C}\{^1\text{H}\}$  NMR spectrum (bottom) and the  $^{13}\text{C}$  DEPT-135 (top) of  $\text{AgC}_6\text{F}_5\text{CyJohnPhos}$  **122** between  $\delta$  20 and  $\delta$  40

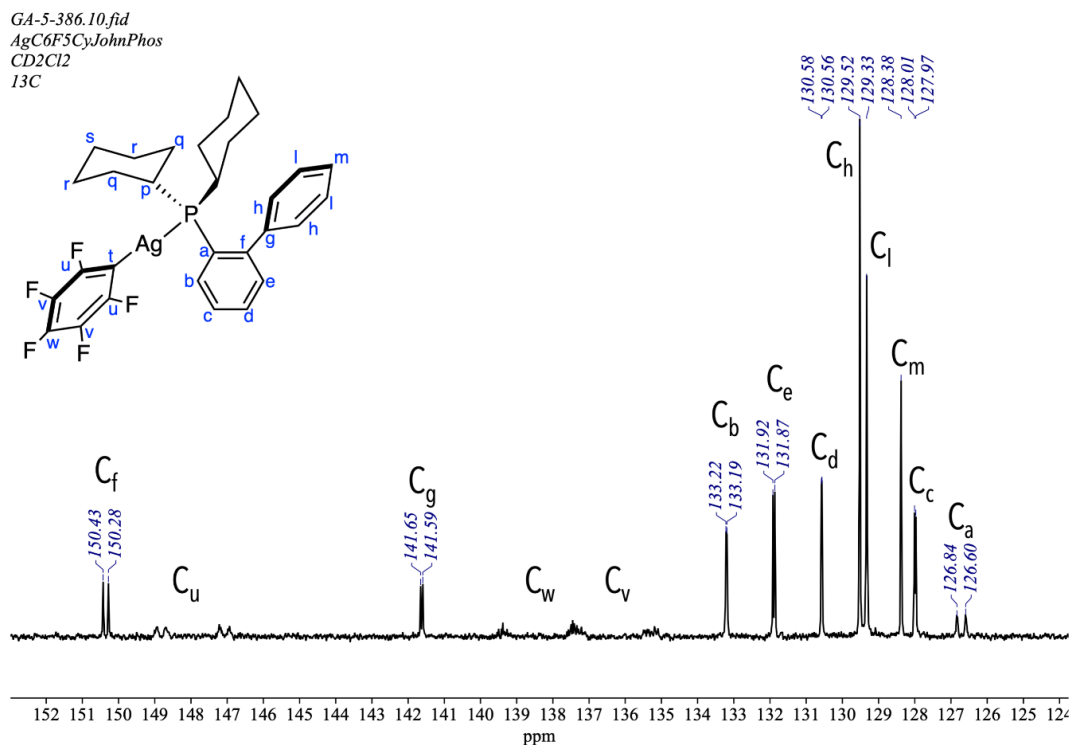


**Figure 307:**  $^{13}\text{C}\{^1\text{H}\}$  (125.8 MHz, CD<sub>2</sub>Cl<sub>2</sub>, 25 °C) spectrum of AgC<sub>6</sub>F<sub>5</sub>CyJohnPhos **122** between  $\delta$  124 and  $\delta$  153

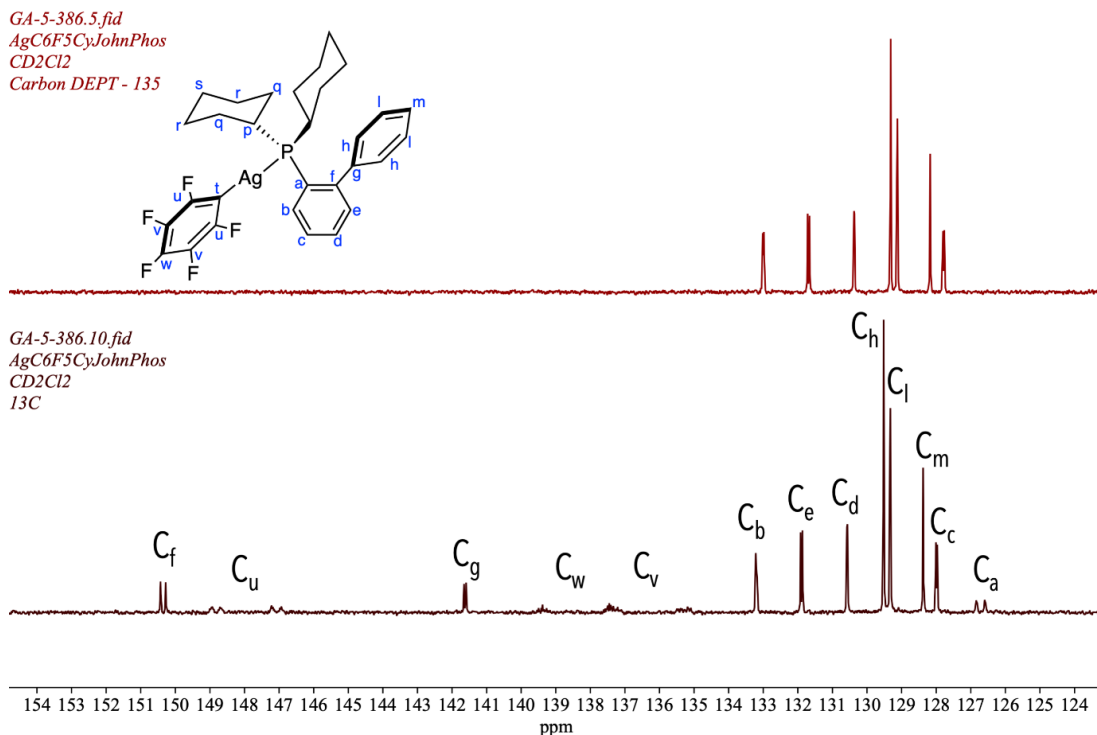


**Figure 308:** Stack plot of the  $^{13}\text{C}\{^1\text{H}\}$  NMR spectrum (below) and the  $^{13}\text{C}$  DEPT-135 (above) of AgC<sub>6</sub>F<sub>5</sub>CyJohnPhos **122** between  $\delta$  160 and  $\delta$  110



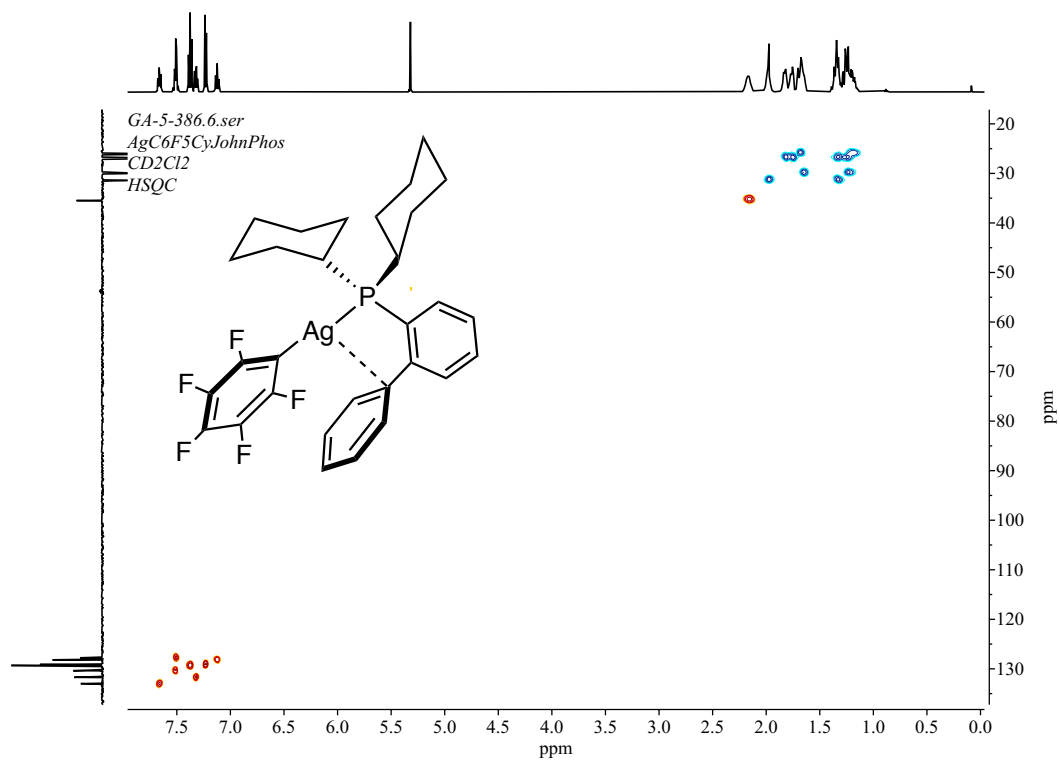


Figure 309: HSQC spectrum of AgC<sub>6</sub>F<sub>5</sub>CyJohnPhos **122** in CD<sub>2</sub>Cl<sub>2</sub>

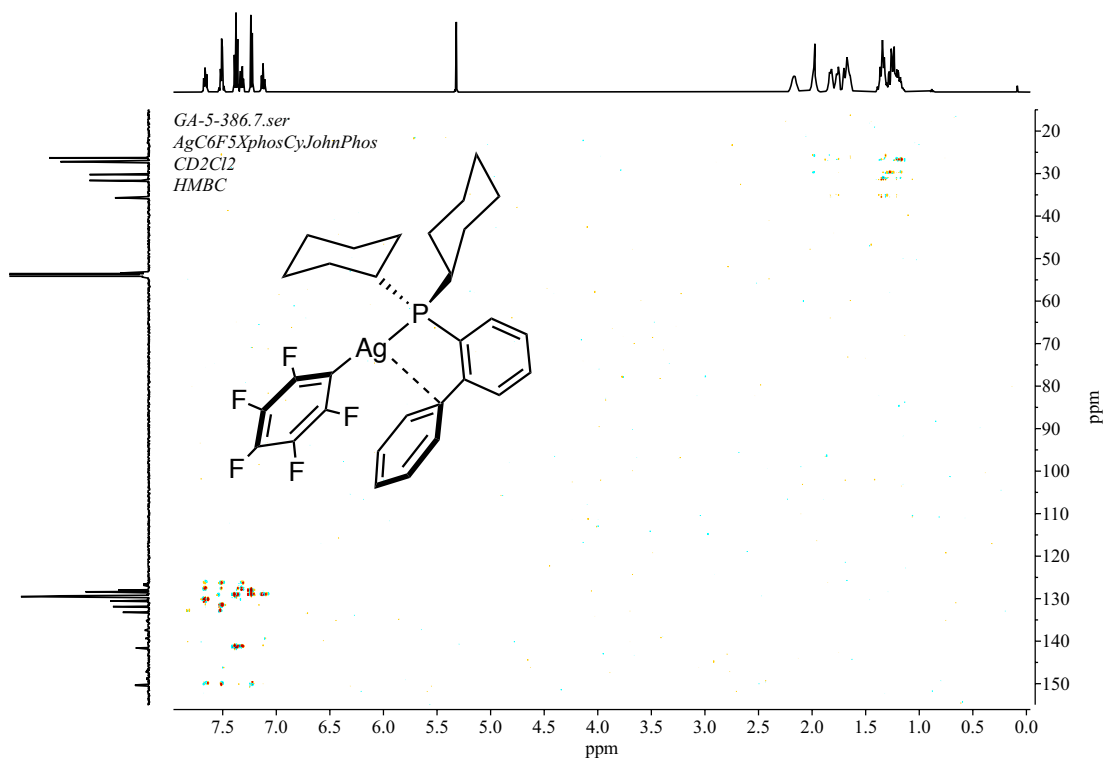
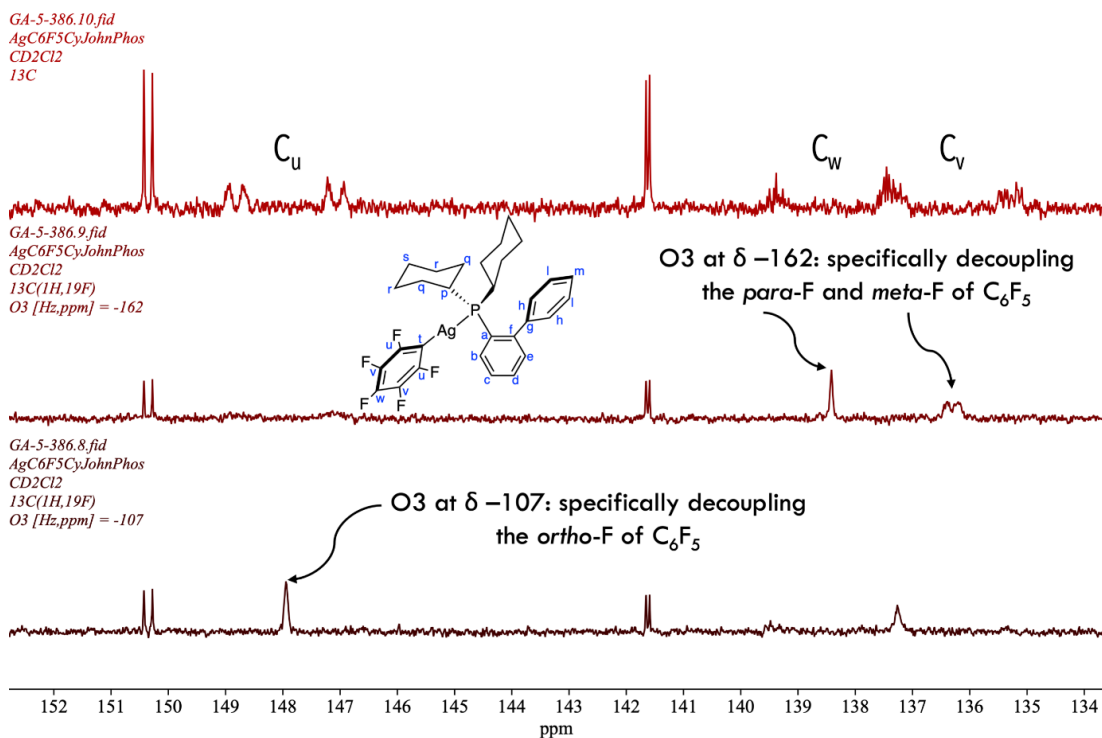
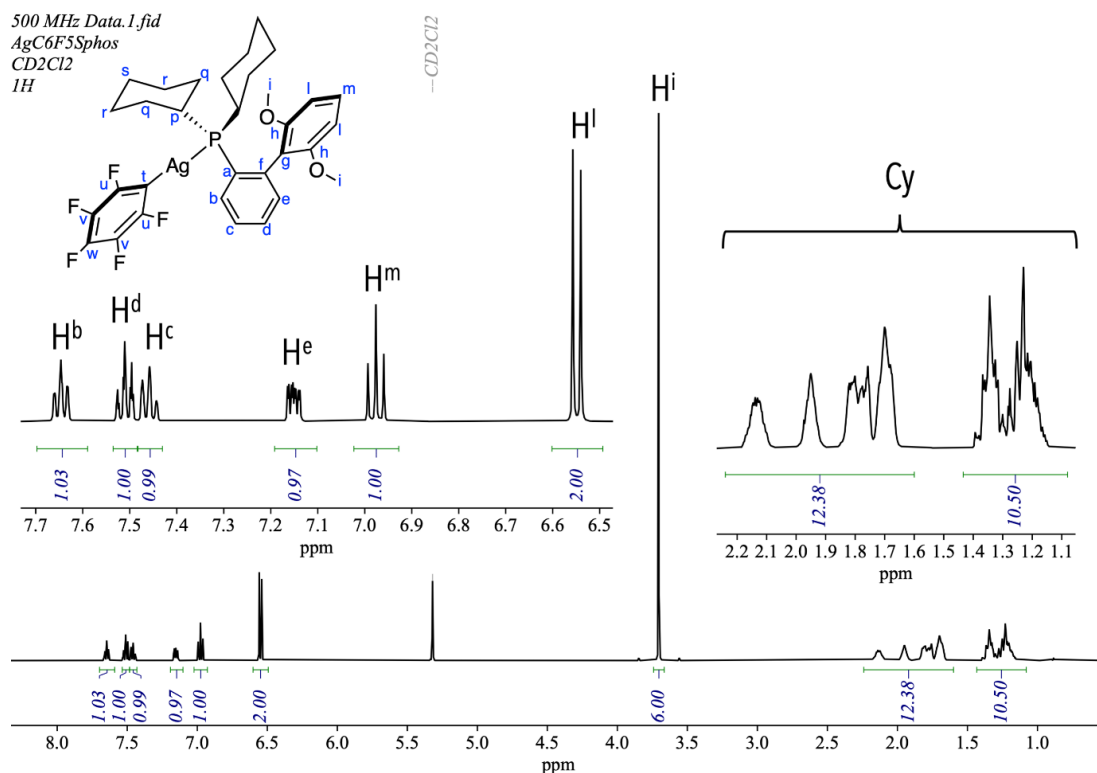


Figure 310: HMBC spectrum of AgC<sub>6</sub>F<sub>5</sub>CyJohnPhos **122** in CD<sub>2</sub>Cl<sub>2</sub>



**Figure 311:** Stack plot of **122** the  $^{13}\text{C}\{^1\text{H}\}$  NMR spectrum (top) with the  $^{13}\text{C}\{^1\text{H}, ^{19}\text{F}\}$  spectrum with specific  $^{19}\text{F}$  coupling of  $^{19}\text{F}$  peak (indicated by O3) at  $\delta -107$  (bottom) and  $\delta -162$  (middle), in  $\text{CD}_2\text{Cl}_2$



**Figure 312:**  $^1\text{H}$  NMR (500 MHz,  $\text{CD}_2\text{Cl}_2$ , 25 °C) spectrum of  $\text{AgC}_6\text{F}_5\text{Sphos}$  **124**

Appendix B – NMR Spectroscopic Data for Synthesised Compounds

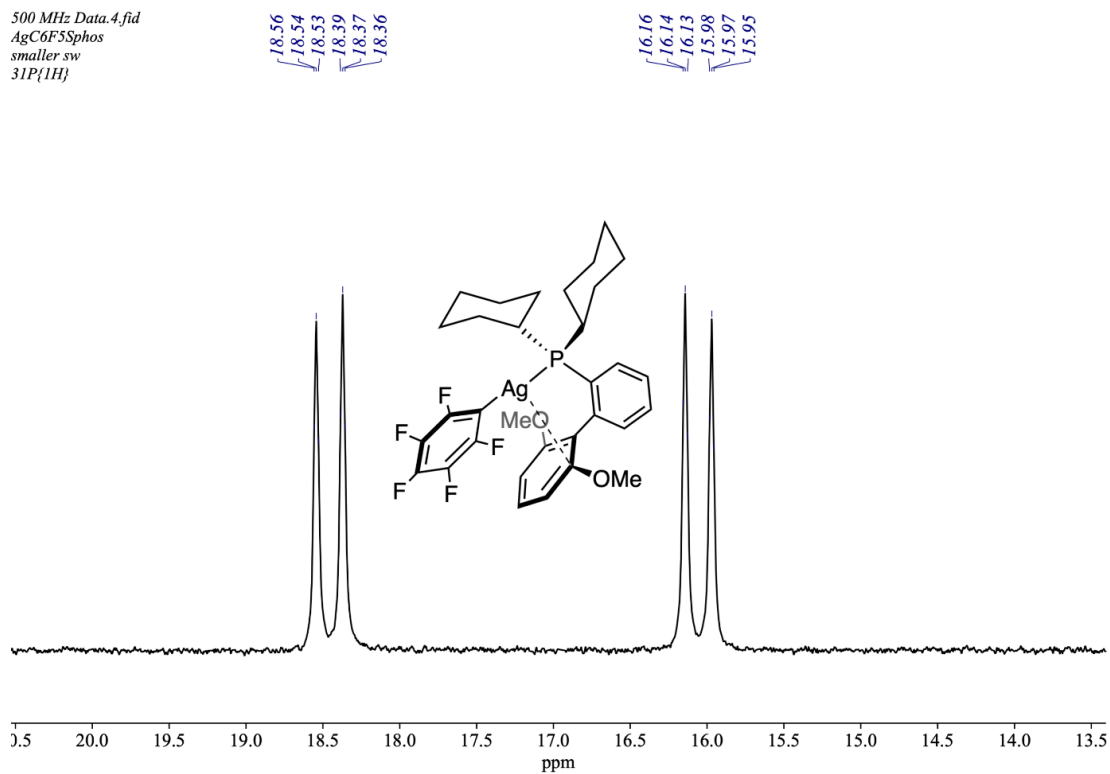


**Figure 313:**  $^{31}\text{P}\{^1\text{H}\}$  (202.5 MHz,  $\text{CD}_2\text{Cl}_2$ , 25 °C) spectrum of  $\text{AgC}_6\text{F}_5\text{Sphos}$  **124**

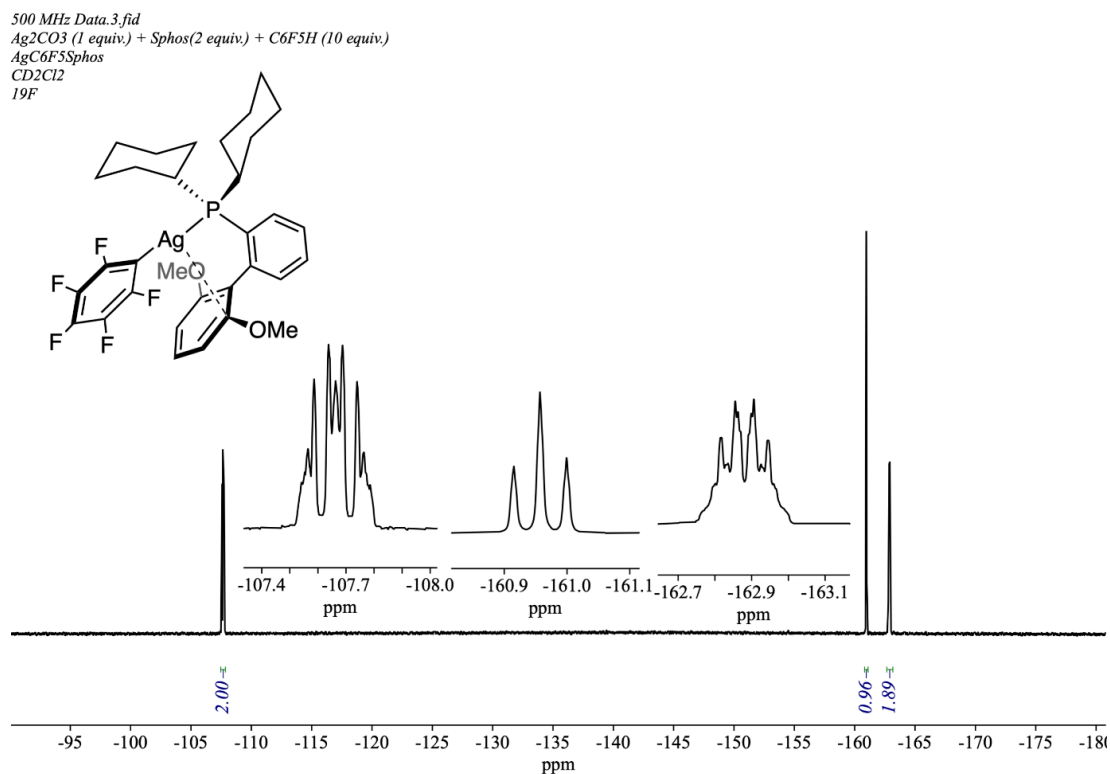


**Figure 314:**  $^{19}\text{F}\{^1\text{H}\}$  NMR (470.6 MHz,  $\text{CD}_2\text{Cl}_2$ , 25 °C) spectrum of  $\text{AgC}_6\text{F}_5\text{Sphos}$  **124**

500 MHz Data.5.fid  
AgC6F5Sphos  
CD2Cl2  
Carbon DEPT - 135

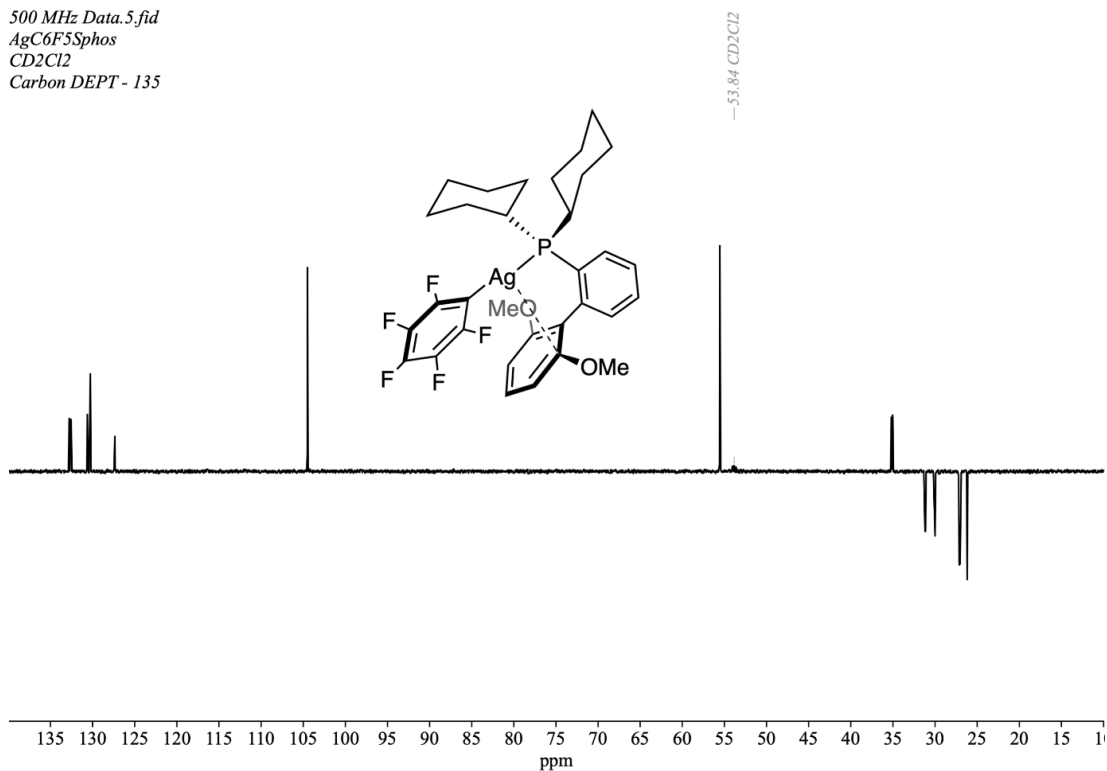


**Figure 315:** <sup>13</sup>C DEPT-135 (125.8 MHz, CD<sub>2</sub>Cl<sub>2</sub>, 25 °C) spectrum of AgC<sub>6</sub>F<sub>5</sub>Sphos 124

500 MHz Data.10.fid  
AgC6F5Sphos  
CD2Cl2  
13C

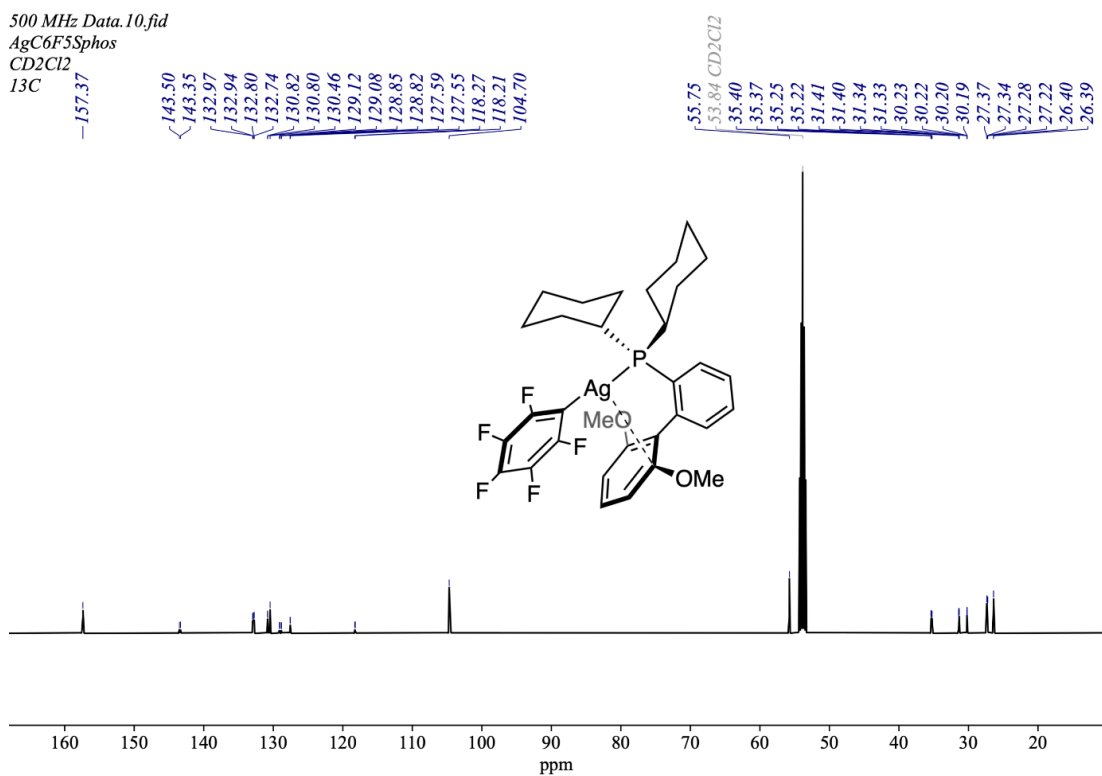


**Figure 316:** <sup>13</sup>C {<sup>1</sup>H} (125.8 MHz, CD<sub>2</sub>Cl<sub>2</sub>, 25 °C) spectrum of AgC<sub>6</sub>F<sub>5</sub>Sphos 124

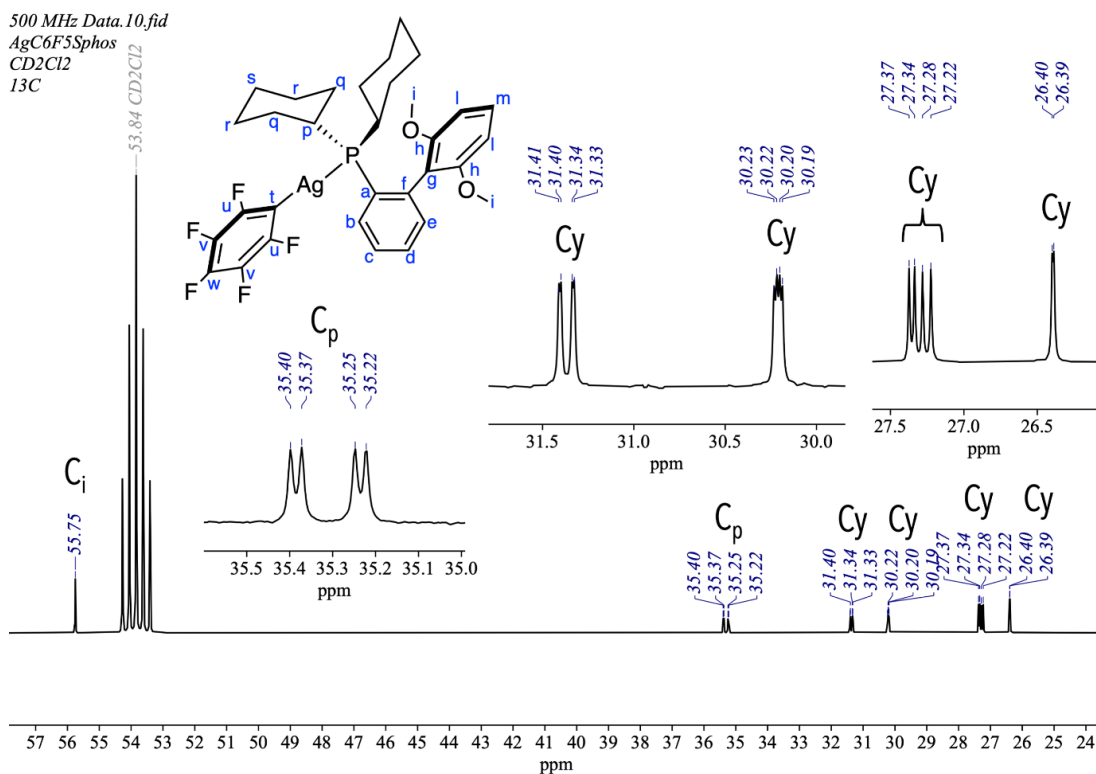


**Figure 317:**  $^{13}\text{C}\{^1\text{H}\}$  (125.8 MHz,  $\text{CD}_2\text{Cl}_2$ , 25 °C) spectrum of **AgC<sub>6</sub>F<sub>5</sub>Sphos 124** between  $\delta$  23 and  $\delta$  58

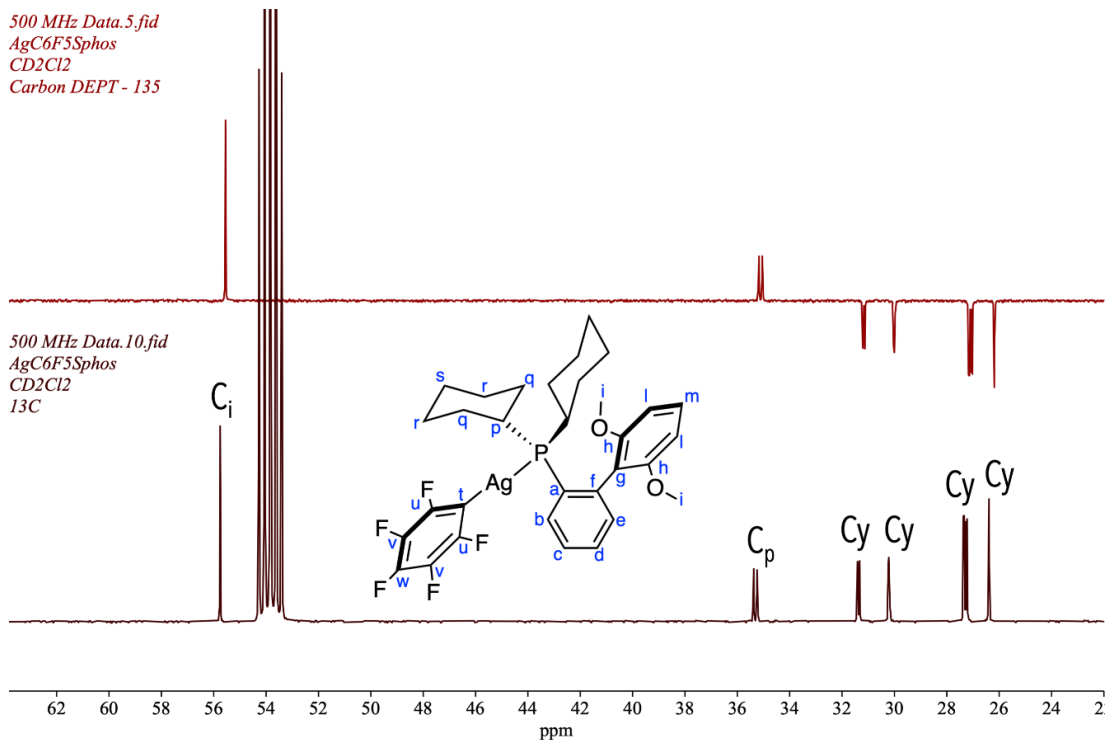


**Figure 318:** Stack plot of the  $^{13}\text{C}\{^1\text{H}\}$  NMR spectrum (bottom) and the  $^{13}\text{C}$  DEPT-135 (top) of **AgC<sub>6</sub>F<sub>5</sub>Sphos 124** between  $\delta$  23 and  $\delta$  58

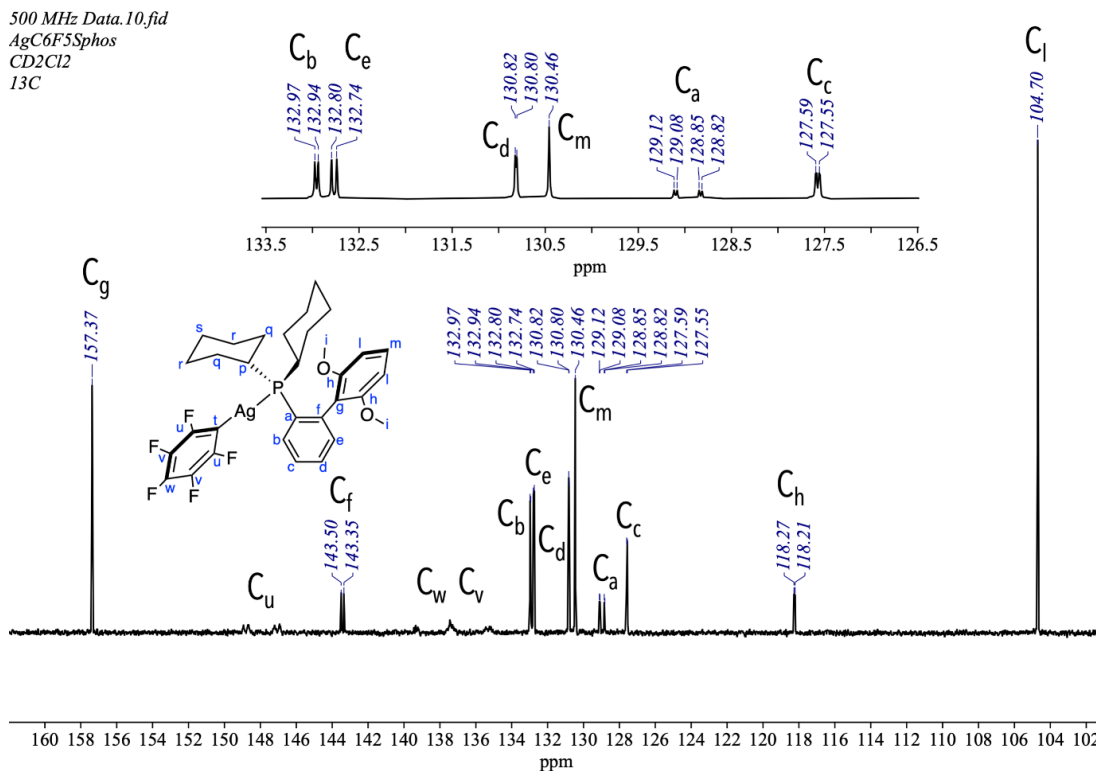


**Figure 319:**  $^{13}\text{C}\{^1\text{H}\}$  (125.8 MHz,  $\text{CD}_2\text{Cl}_2$ , 25 °C) spectrum of AgC6F5Sphos **124** between  $\delta$  20 and  $\delta$  40

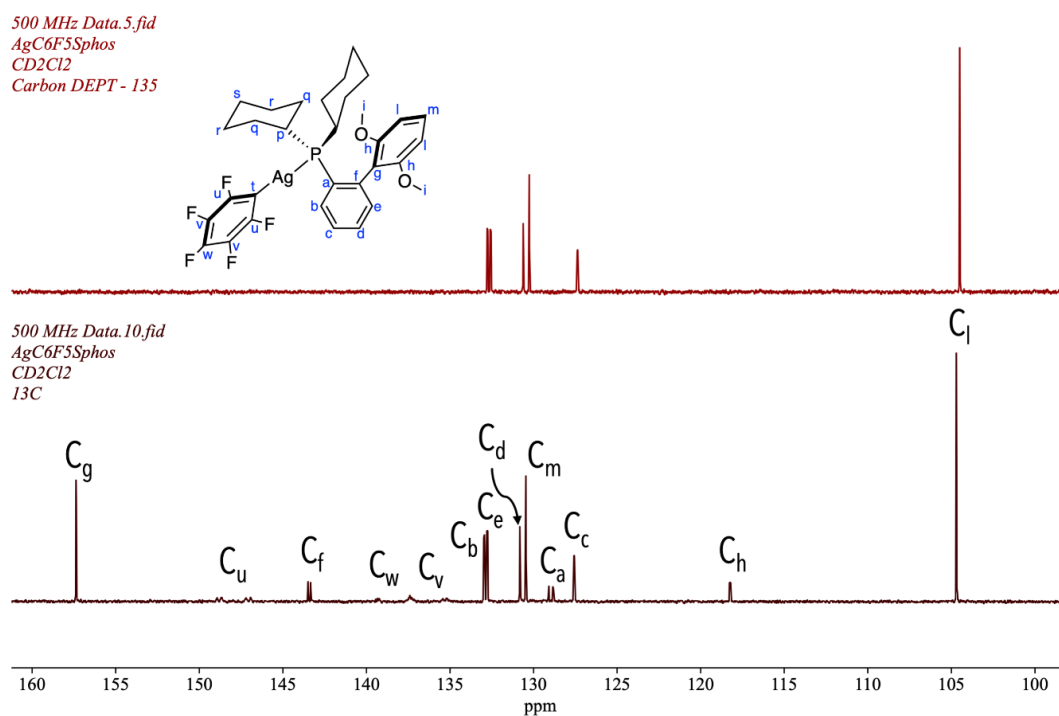


**Figure 320:** Stack plot of the  $^{13}\text{C}\{^1\text{H}\}$  NMR spectrum (bottom) and the  $^{13}\text{C}$  DEPT-135 of AgC6F5Sphos **124** between  $\delta$  20 and  $\delta$  40

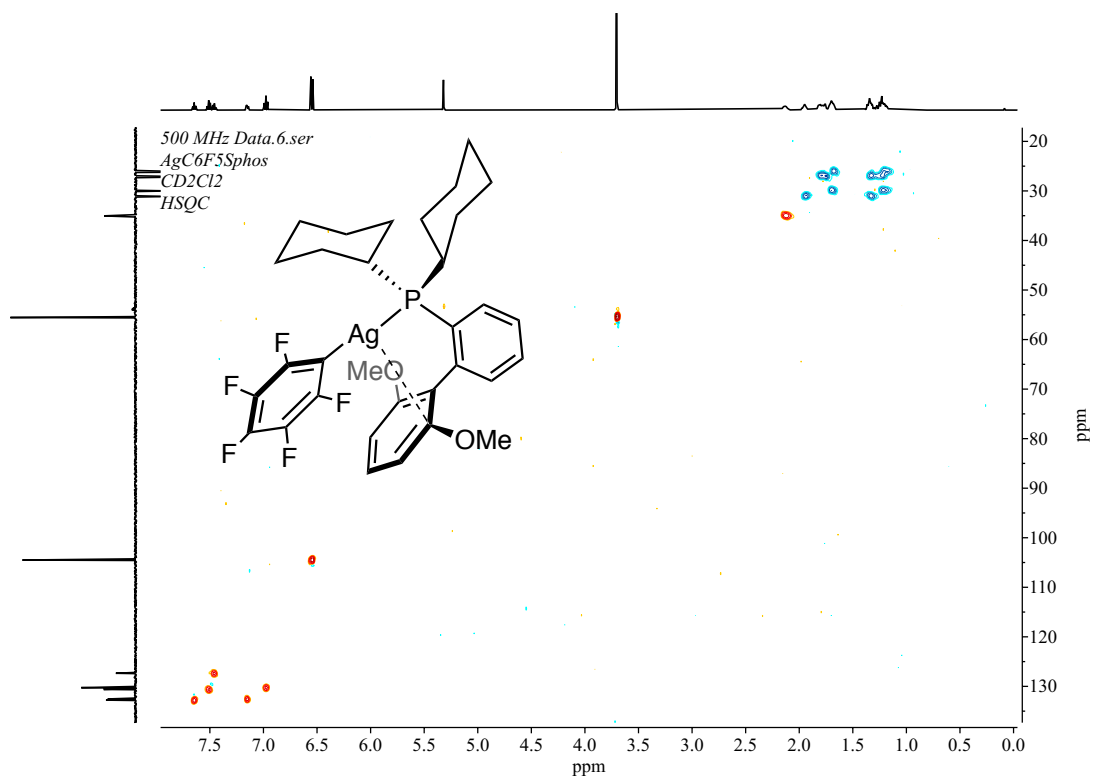


Figure 321: HSQC spectrum of AgC<sub>6</sub>F<sub>5</sub>Sphos **124** in CD<sub>2</sub>Cl<sub>2</sub>

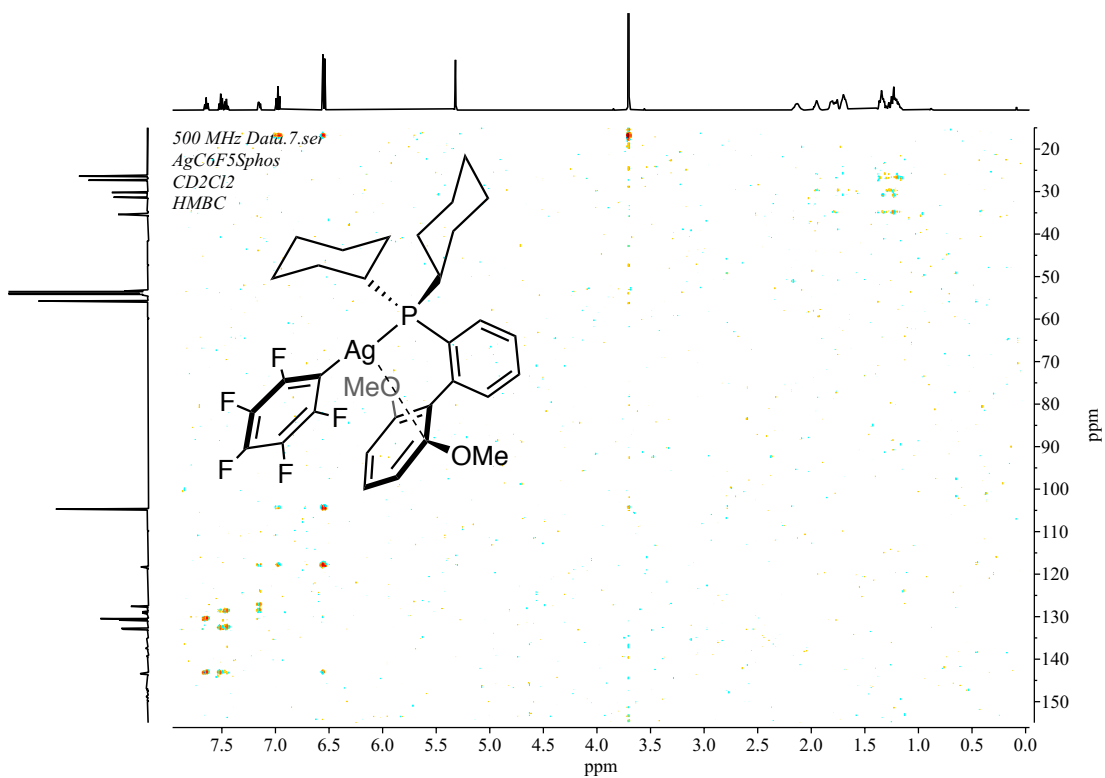
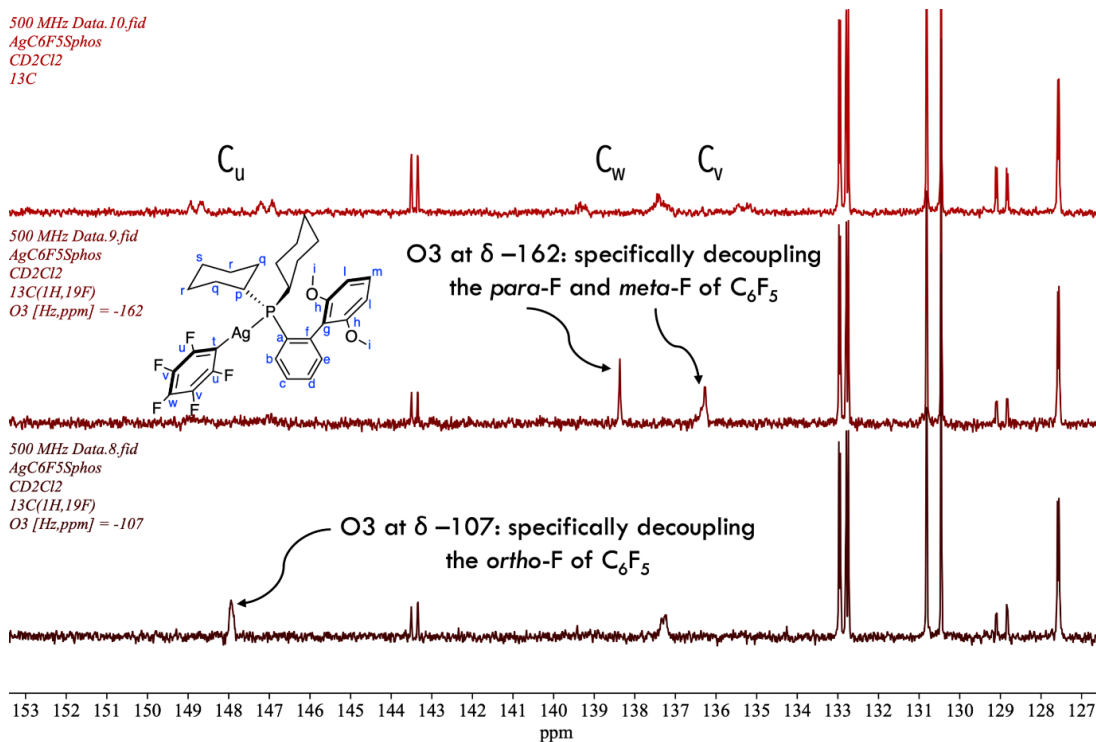
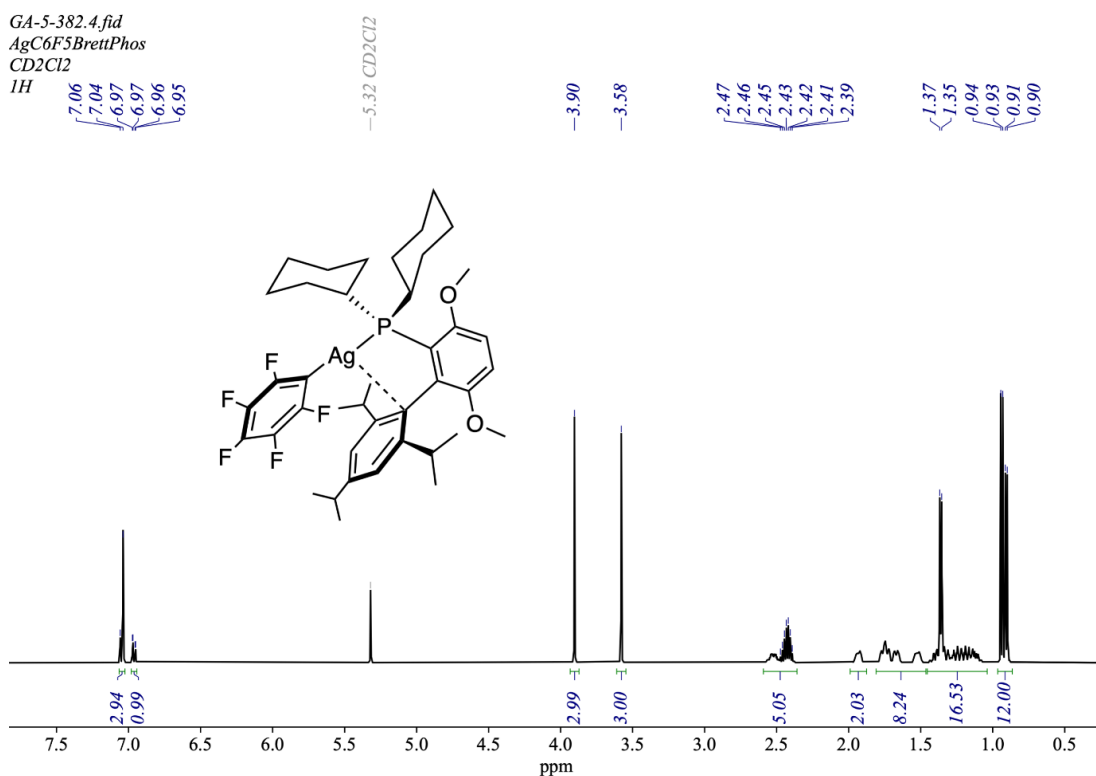


Figure 322: HMBC spectrum of AgC<sub>6</sub>F<sub>5</sub>Sphos **124** in CD<sub>2</sub>Cl<sub>2</sub>

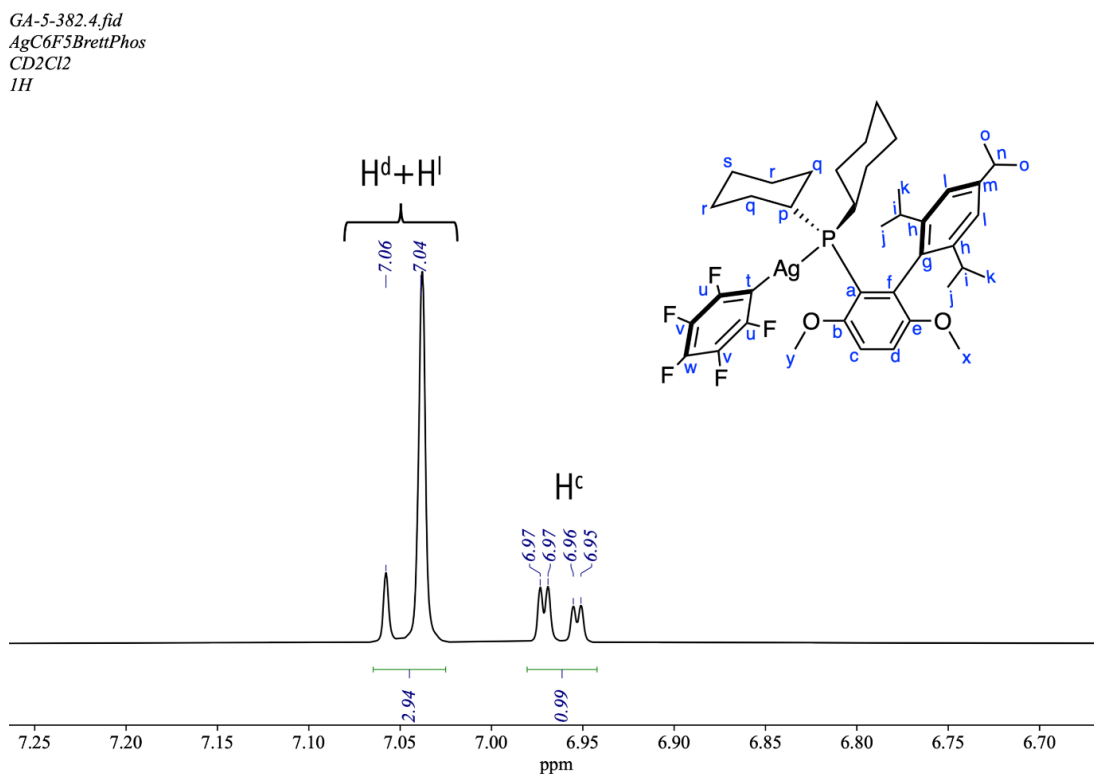
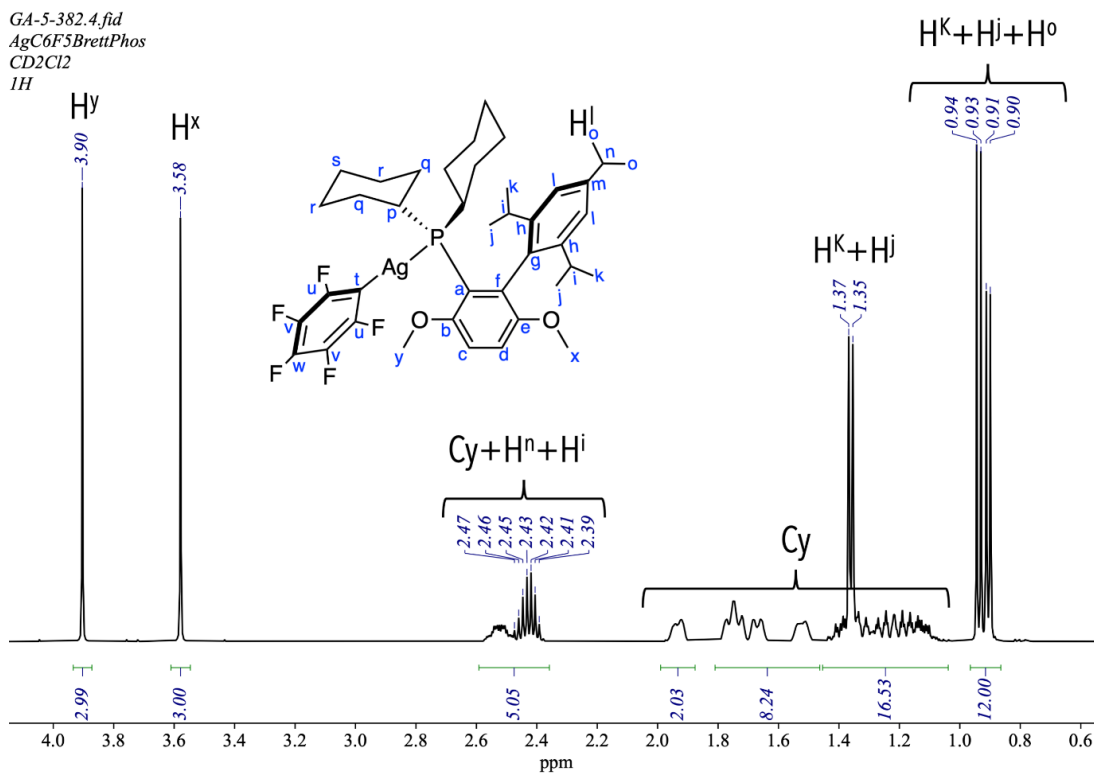


**Figure 323:** Stack plot of **124** the  $^{13}C\{^1H\}$  NMR spectrum (top) with the  $^{13}C\{^1H, ^{19}F\}$  spectrum with specific  $^{19}F$  coupling of  $^{19}F$  peak (indicated by O3) at  $\delta -107$  (bottom) and  $\delta -160$  (middle), in  $CD_2Cl_2$



**Figure 324:**  $^1H$  NMR (500 MHz,  $CD_2Cl_2$ , 25 °C) spectrum of  $Ag(C_6F_5)(BrettPhos)$  **125**





GA-5-382.7.fid  
AgC6F5BrettPhos  
smaller sw  
31P{1H}

19.41  
19.40  
19.39  
19.25  
19.23  
19.22

17.06  
17.05  
17.03  
16.89  
16.88  
16.86

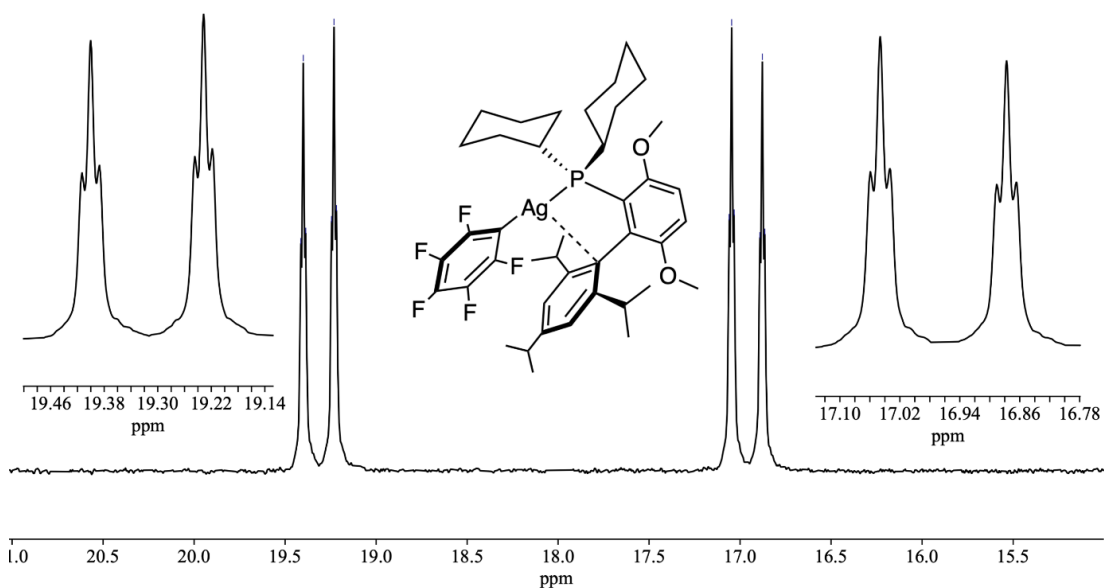


**Figure 327:**  $^{31}\text{P}\{^1\text{H}\}$  (202.5 MHz,  $\text{CD}_2\text{Cl}_2$ , 25 °C) spectrum of  $\text{Ag}(\text{C}_6\text{F}_5)(\text{BrettPhos})$  **125**

GA-5-382.6.fid  
AgC6F5BrettPhos  
CD2Cl2  
19F

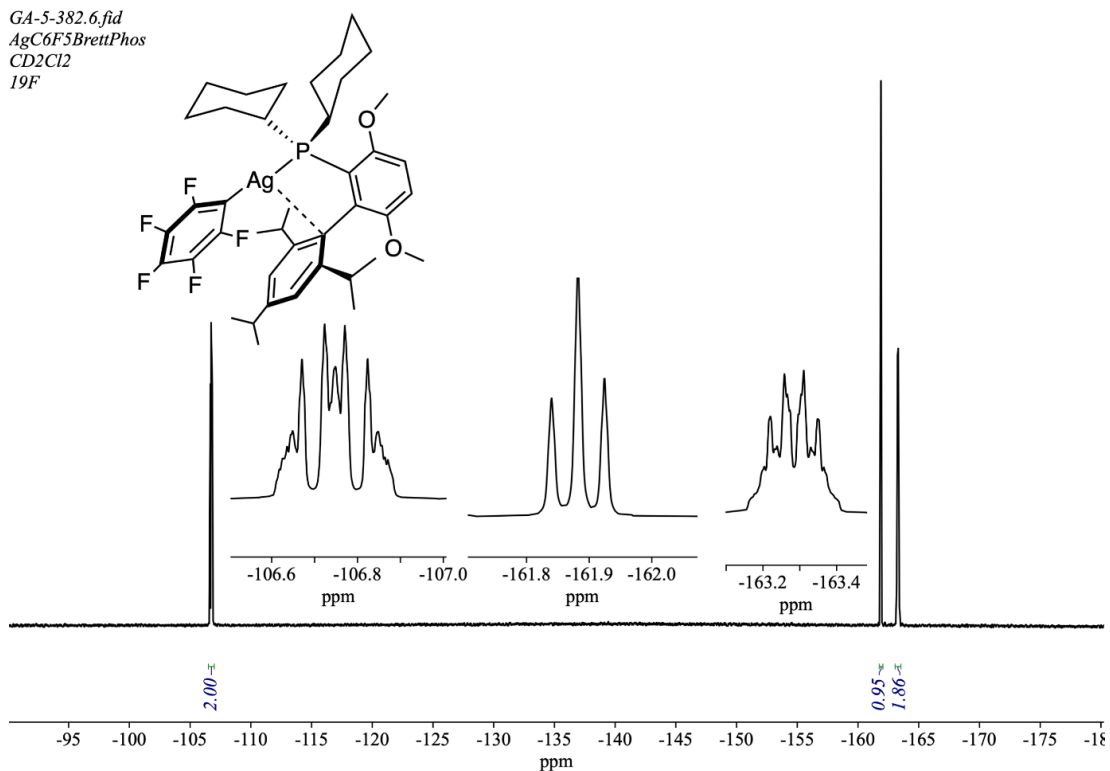


**Figure 328:**  $^{19}\text{F}\{^1\text{H}\}$  NMR (470.6 MHz,  $\text{CD}_2\text{Cl}_2$ , 25 °C) spectrum of  $\text{Ag}(\text{C}_6\text{F}_5)(\text{BrettPhos})$  **125**

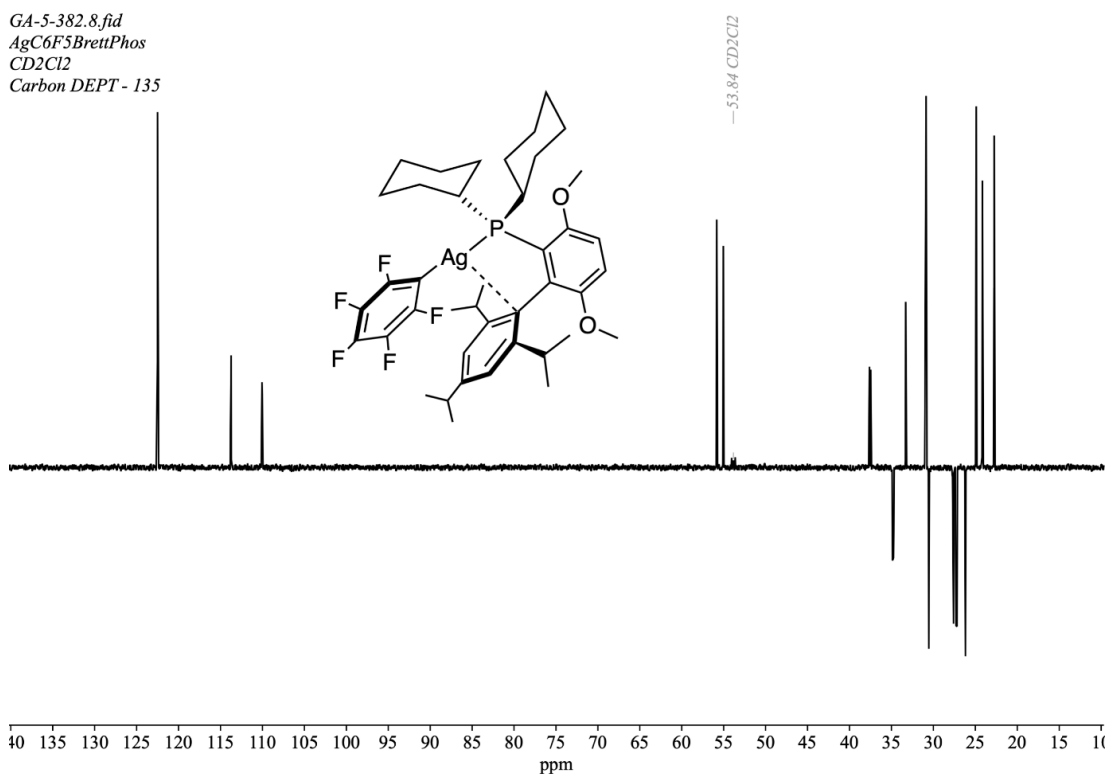


Figure 329:  $^{13}\text{C}$  DEPT-135 (125.8 MHz,  $\text{CD}_2\text{Cl}_2$ , 25 °C) spectrum of  $\text{Ag}(\text{C}_6\text{F}_5)(\text{BrettPhos})$

125

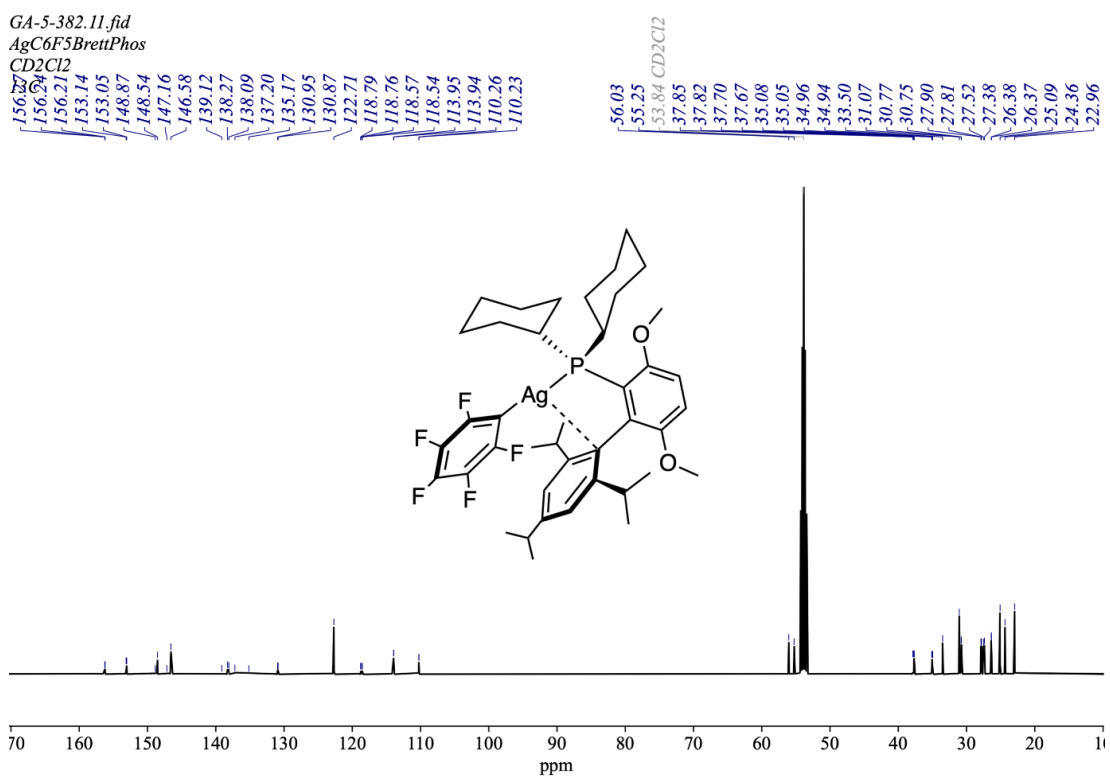
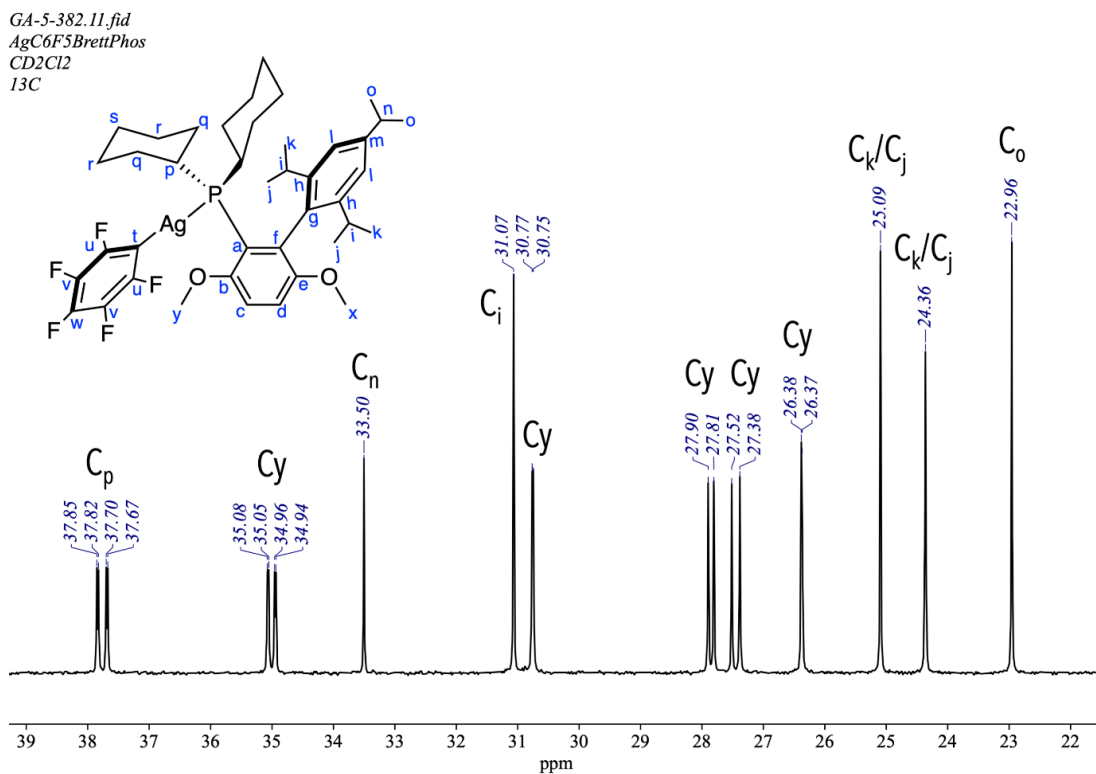
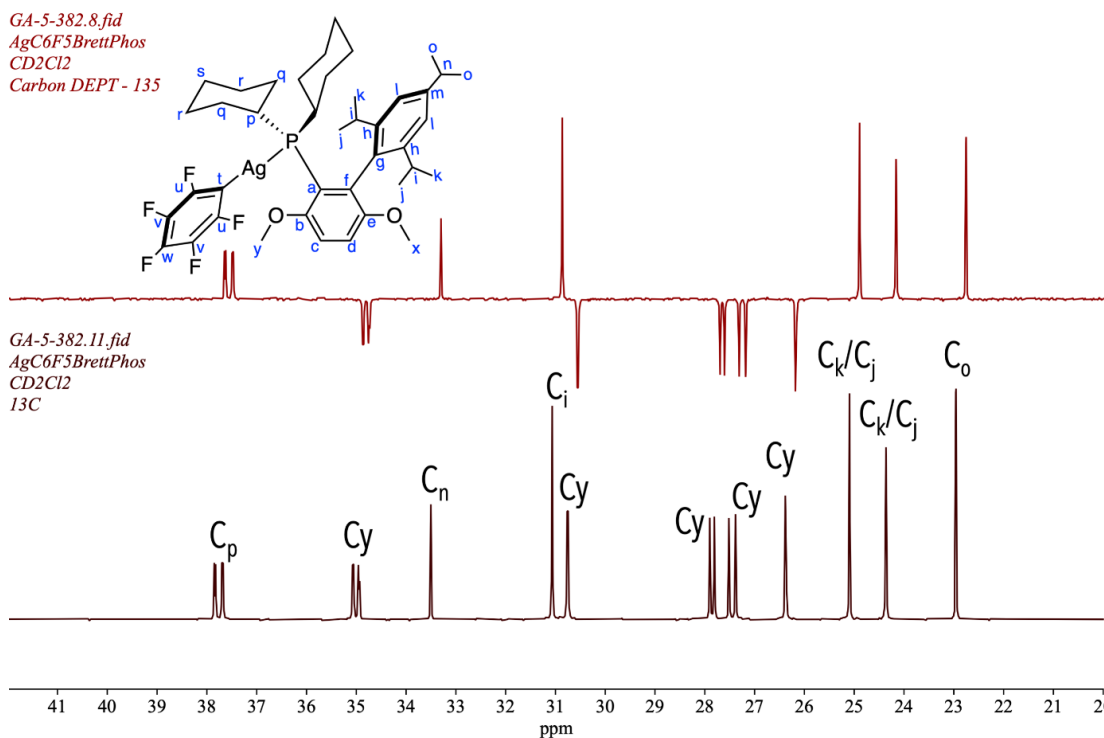


Figure 330:  $^{13}\text{C}\{^1\text{H}\}$  (125.8 MHz,  $\text{CD}_2\text{Cl}_2$ , 25 °C) spectrum of  $\text{Ag}(\text{C}_6\text{F}_5)(\text{BrettPhos})$  125



**Figure 331:** <sup>13</sup>C{<sup>1</sup>H} (125.8 MHz, CD<sub>2</sub>Cl<sub>2</sub>, 25 °C) spectrum of Ag(C<sub>6</sub>F<sub>5</sub>)(BrettPhos) **125** between δ 20 and δ 40



**Figure 332:** Stack plot of the <sup>13</sup>C{<sup>1</sup>H} NMR spectrum (bottom) and the <sup>13</sup>C DEPT-135 (top) of Ag(C<sub>6</sub>F<sub>5</sub>)(BrettPhos) **125** between δ 20 and δ 42

GA-5-382.11.fid  
AgC6F5BrettPhos  
CD2Cl2  
13C

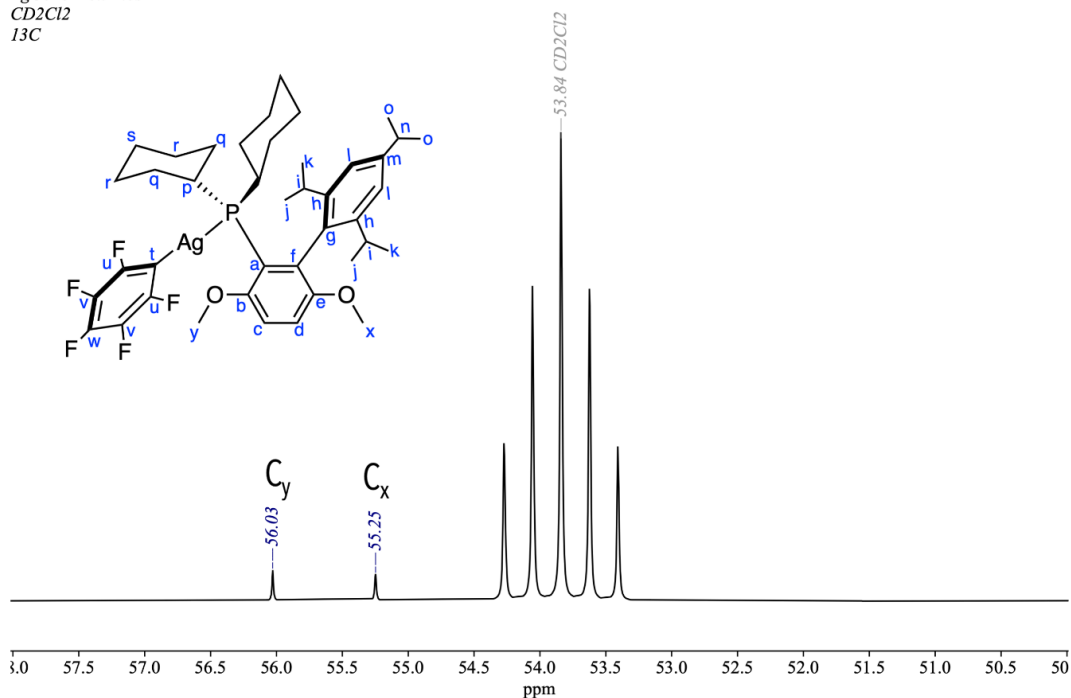


**Figure 333:**  $^{13}\text{C}\{^1\text{H}\}$  (125.8 MHz,  $\text{CD}_2\text{Cl}_2$ , 25 °C) spectrum of  $\text{Ag}(\text{C}_6\text{F}_5)(\text{BrettPhos})$  125 between  $\delta$  50 and  $\delta$  60

GA-5-382.11.fid  
AgC6F5BrettPhos  
CD2Cl2  
13C

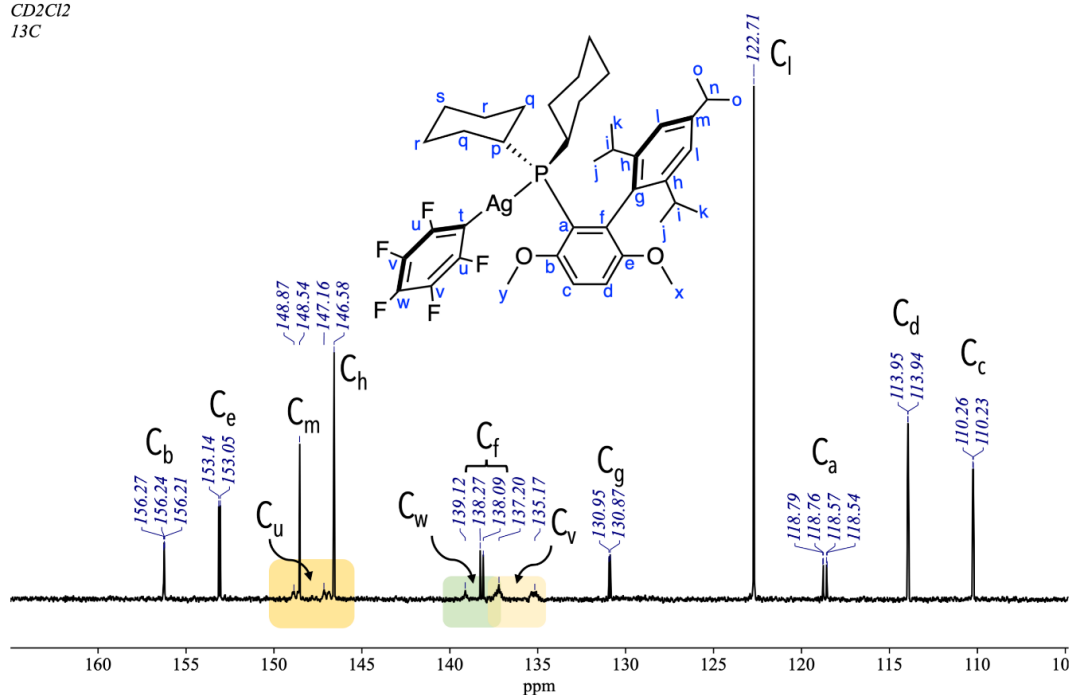


**Figure 334:**  $^{13}\text{C}\{^1\text{H}\}$  (125.8 MHz,  $\text{CD}_2\text{Cl}_2$ , 25 °C) spectrum of  $\text{Ag}(\text{C}_6\text{F}_5)(\text{BrettPhos})$  125 between  $\delta$  108 and  $\delta$  170

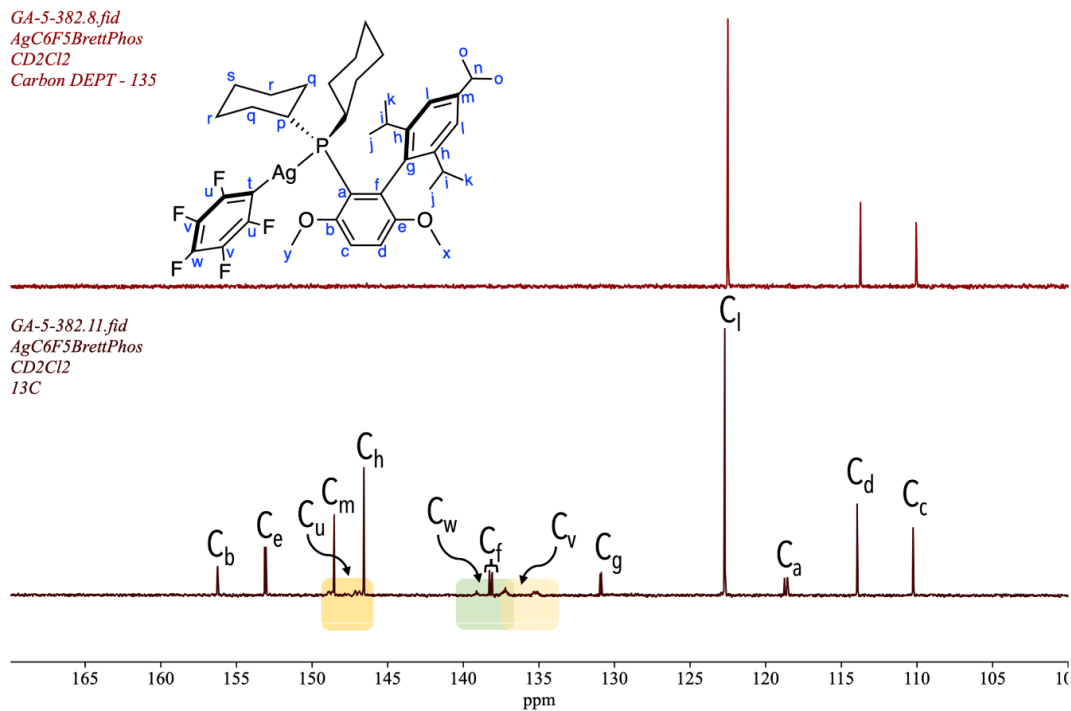


**Figure 335:** Stack plot of the  $^{13}\text{C}\{^1\text{H}\}$  NMR spectrum (bottom) and the  $^{13}\text{C}$  DEPT-135 (top) of  $\text{Ag}(\text{C}_6\text{F}_5)(\text{BrettPhos})$  **125** between  $\delta$  100 and  $\delta$  170

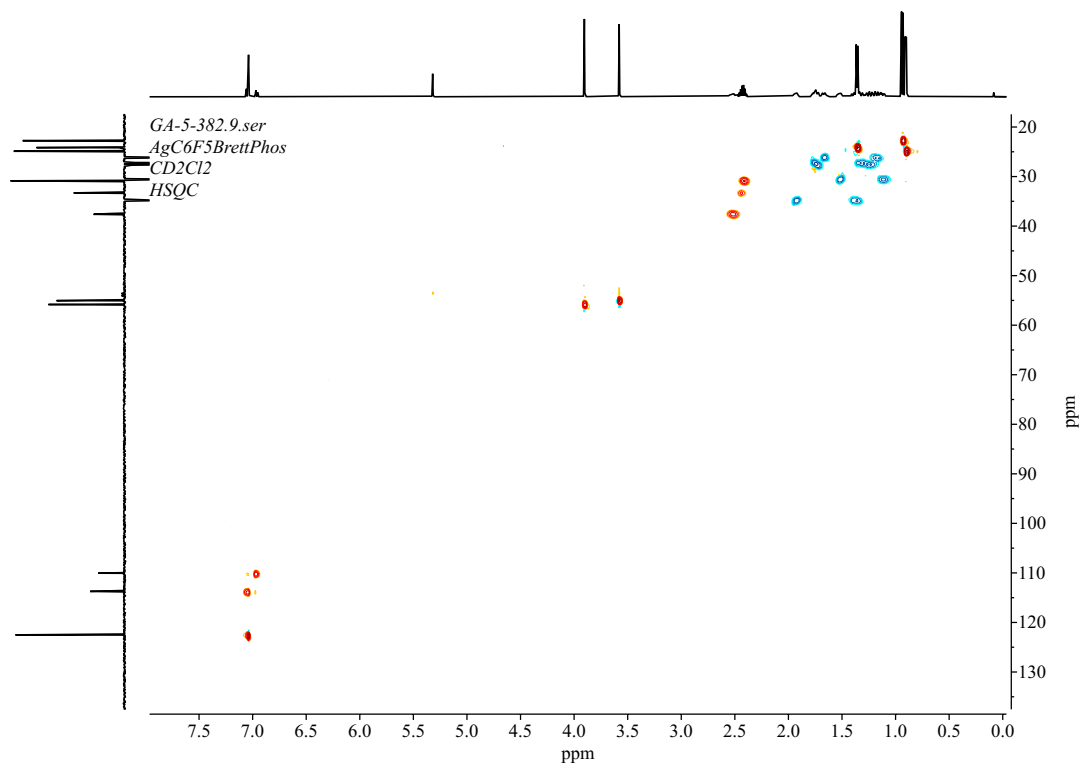


**Figure 336:** HSQC spectrum of  $\text{Ag}(\text{C}_6\text{F}_5)(\text{BrettPhos})$  **125** in  $\text{CD}_2\text{Cl}_2$

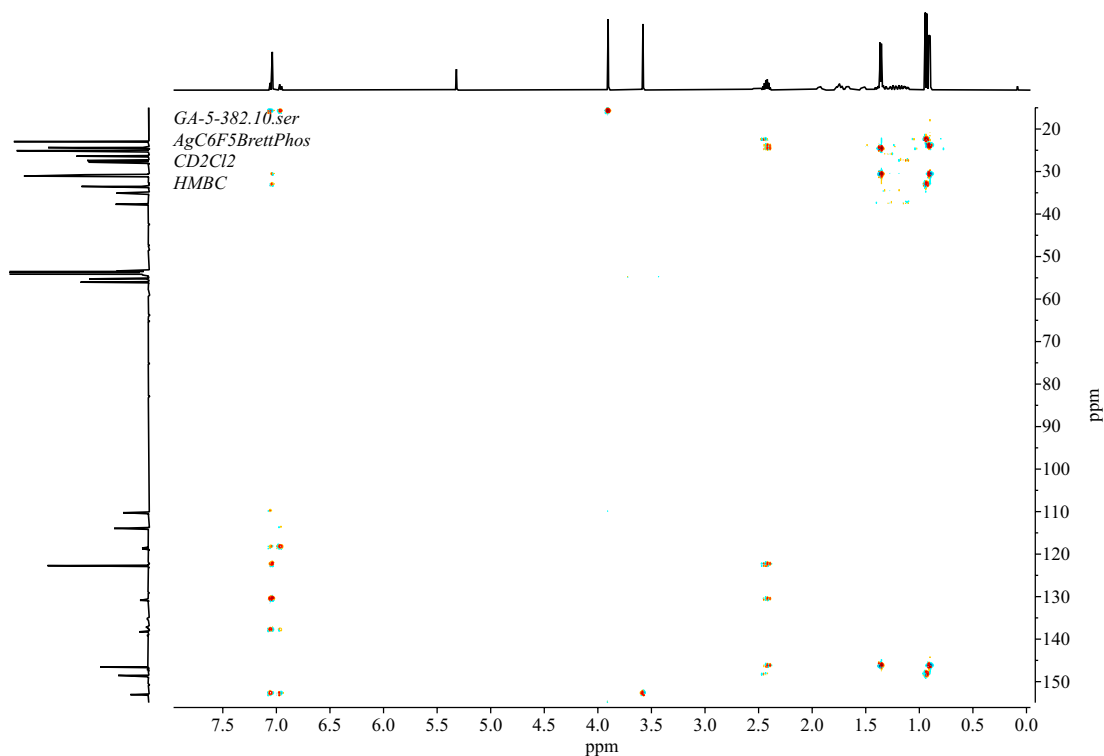


Figure 337: HMBC spectrum of  $\text{Ag}(\text{C}_6\text{F}_5)(\text{BrettPhos})$  **125** in  $\text{CD}_2\text{Cl}_2$

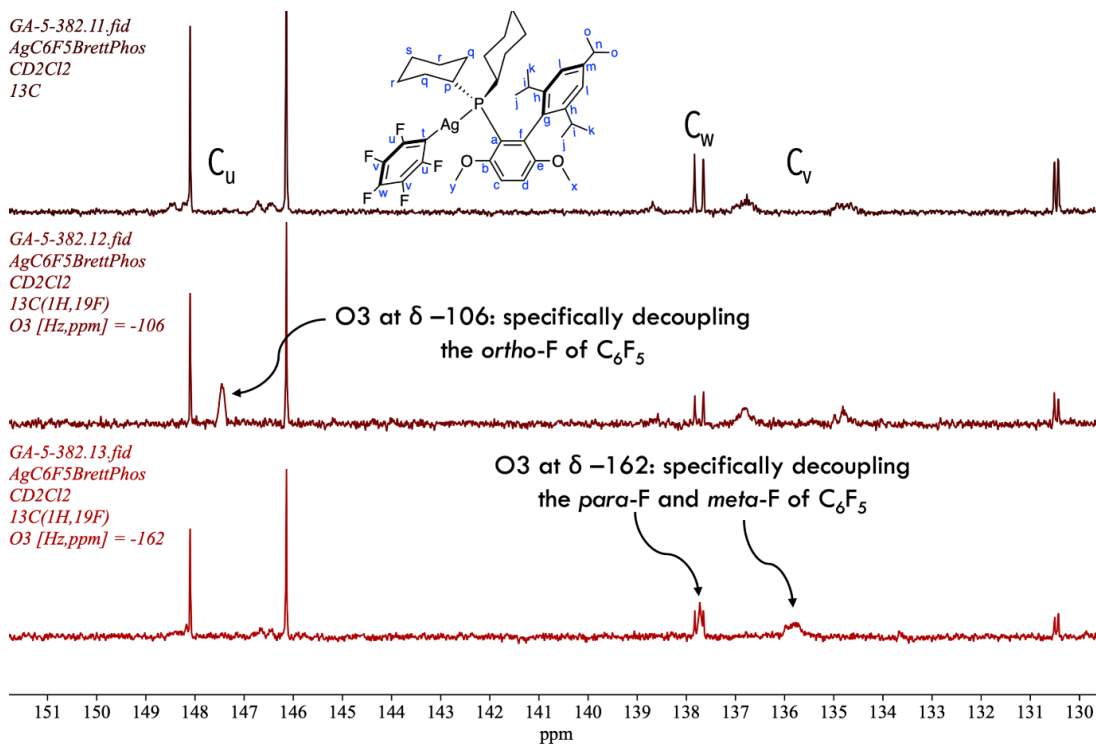
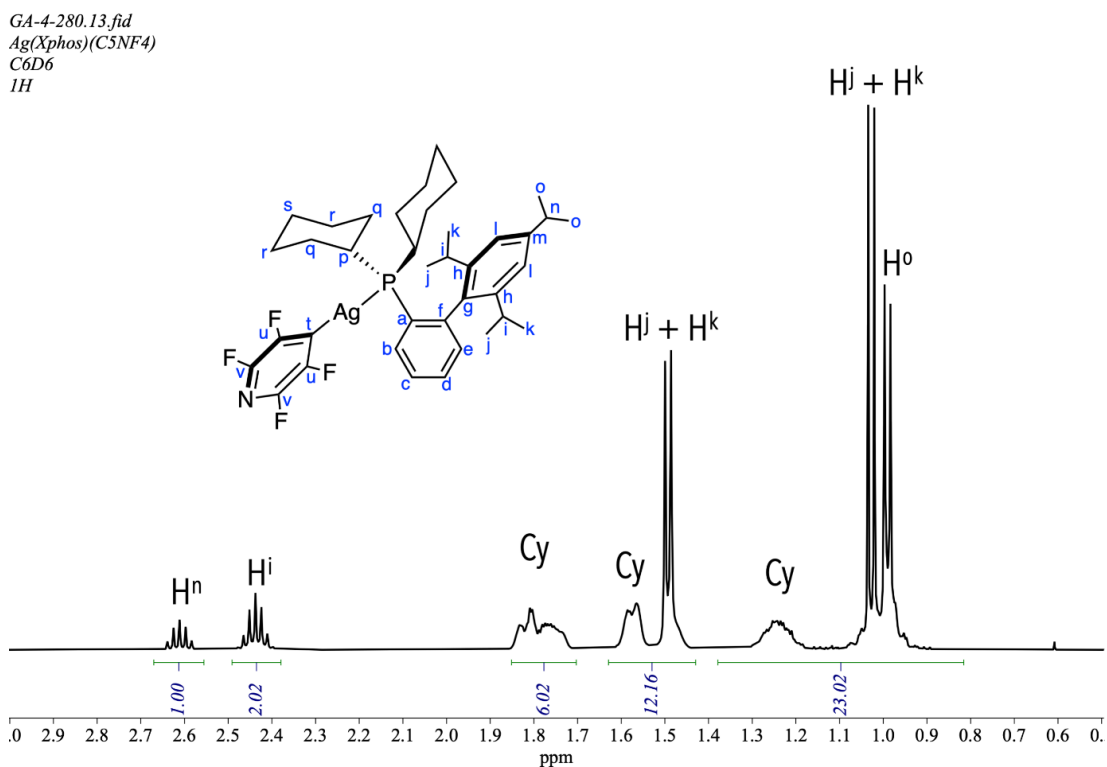
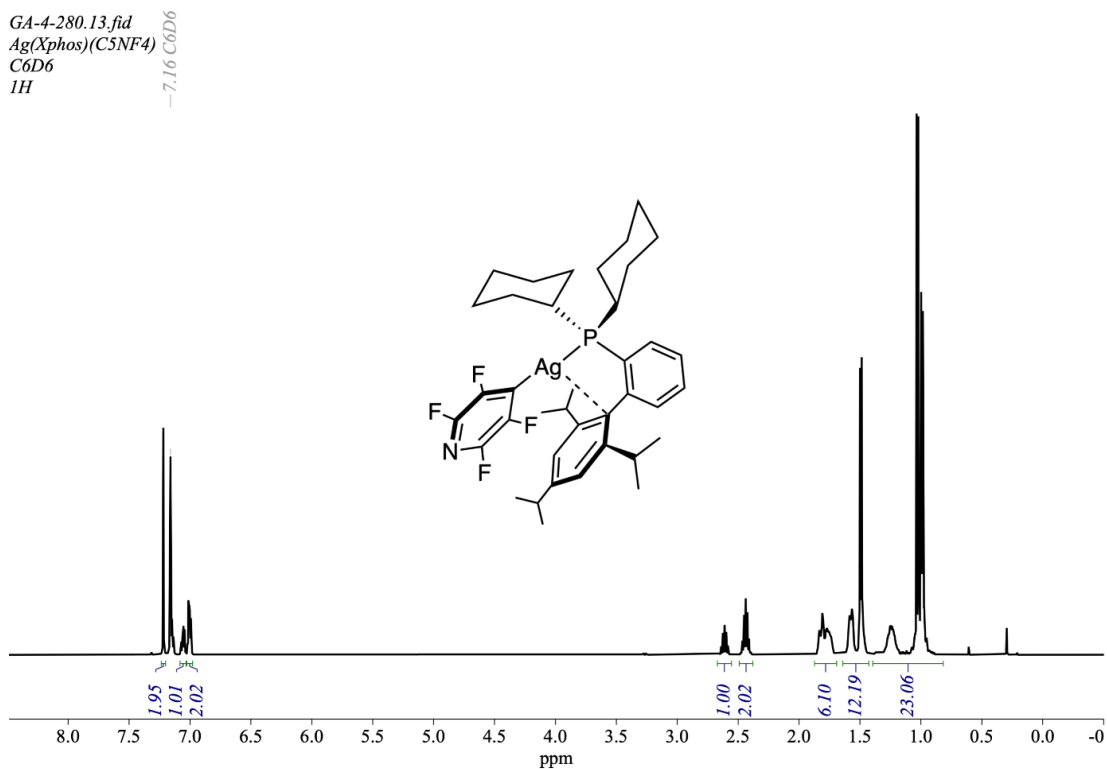
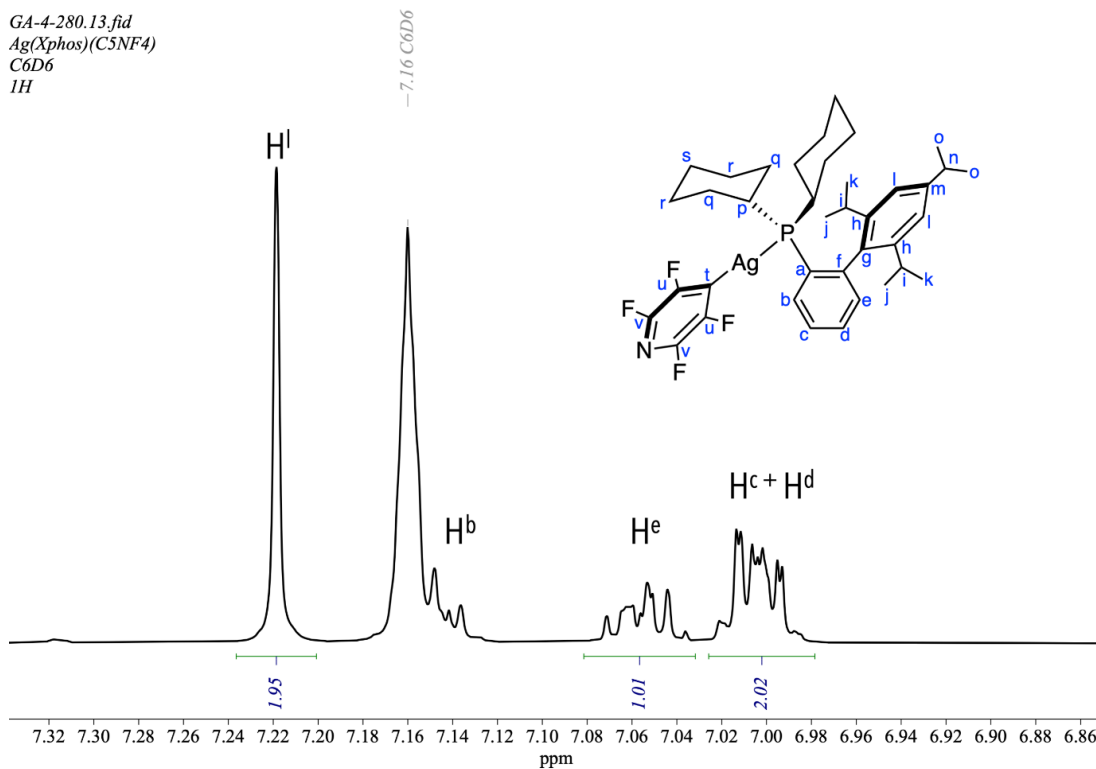


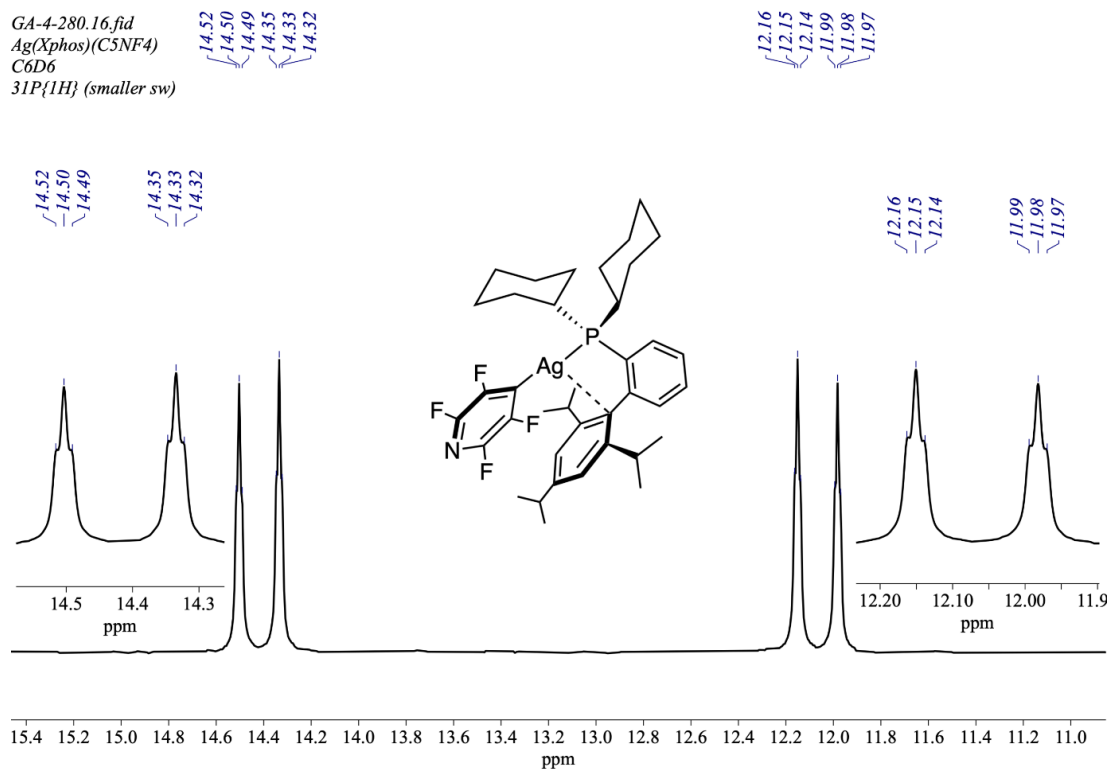
Figure 338: Stack plot of **125** the  $^{13}\text{C}\{^1\text{H}\}$  NMR spectrum (top) with the  $^{13}\text{C}\{^1\text{H}, ^{19}\text{F}\}$  spectrum with specific  $^{19}\text{F}$  coupling of  $^{19}\text{F}$  peak (indicated by O3) at  $\delta -106$  (middle) and  $\delta -162$  (bottom), in  $\text{CD}_2\text{Cl}_2$





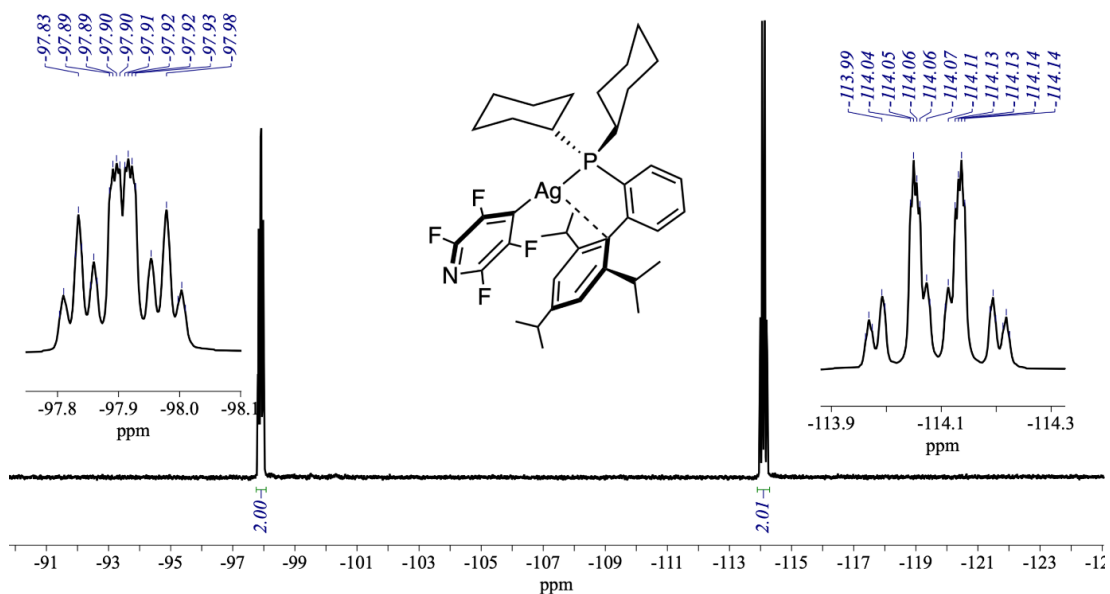


**Figure 341:** <sup>1</sup>H NMR (500 MHz, CD<sub>2</sub>Cl<sub>2</sub>, 25 °C) spectrum of Ag(C<sub>5</sub>F<sub>4</sub>N)(Xphos) **165** between δ 6.8 and δ 7.4



**Figure 342:** <sup>31</sup>P{<sup>1</sup>H} (202.5 MHz, CD<sub>2</sub>Cl<sub>2</sub>, 25 °C) spectrum of Ag(C<sub>5</sub>F<sub>4</sub>N)(Xphos) **165**

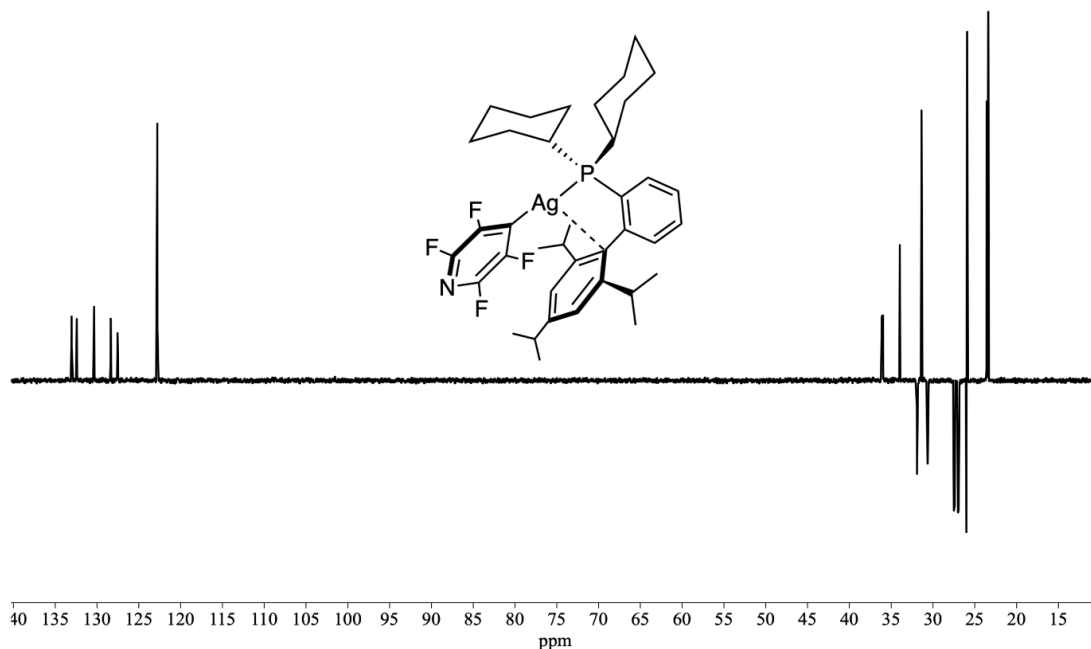
GA-4-280.17.fid  
 Ag(Xphos)(C<sub>5</sub>NF<sub>4</sub>)  
 C<sub>6</sub>D<sub>6</sub>  
 19F (smaller sw)



**Figure 343:** <sup>19</sup>F {<sup>1</sup>H} NMR (470.6 MHz, CD<sub>2</sub>Cl<sub>2</sub>, 25 °C) spectrum of Ag(C<sub>5</sub>F<sub>4</sub>N)(Xphos)

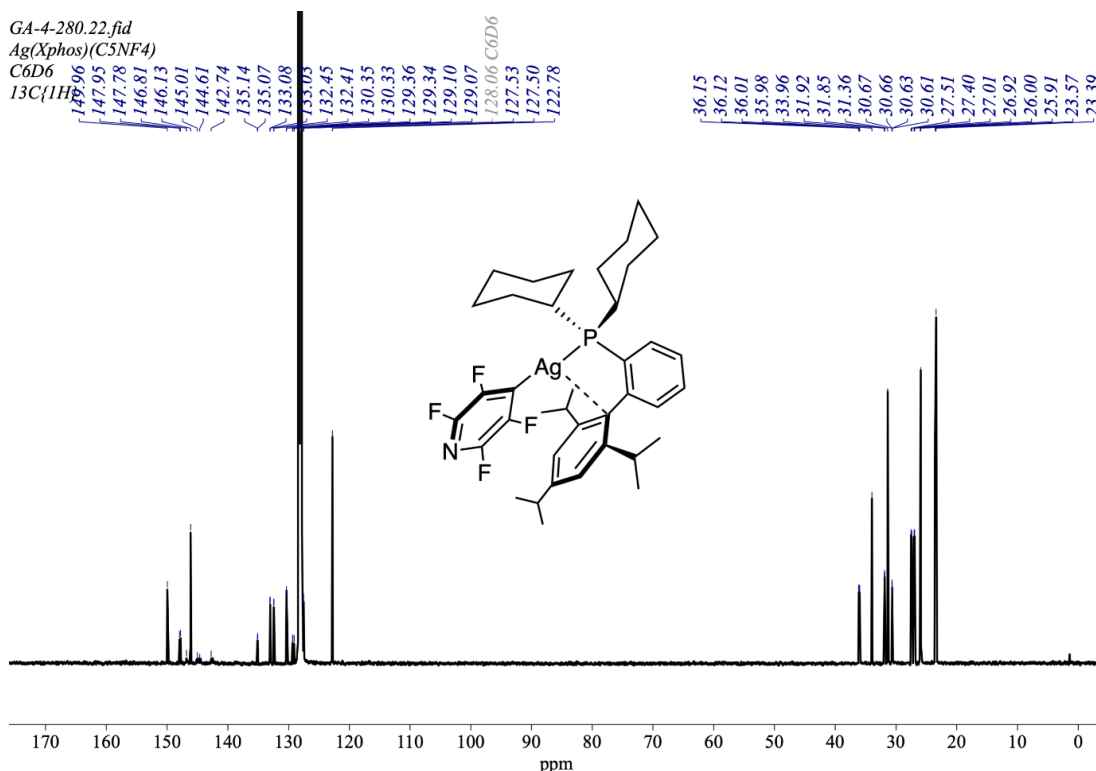
165

GA-4-280.19.fid  
 Ag(Xphos)(C<sub>5</sub>NF<sub>4</sub>)  
 C<sub>6</sub>D<sub>6</sub>  
 Carbon DEPT - 135

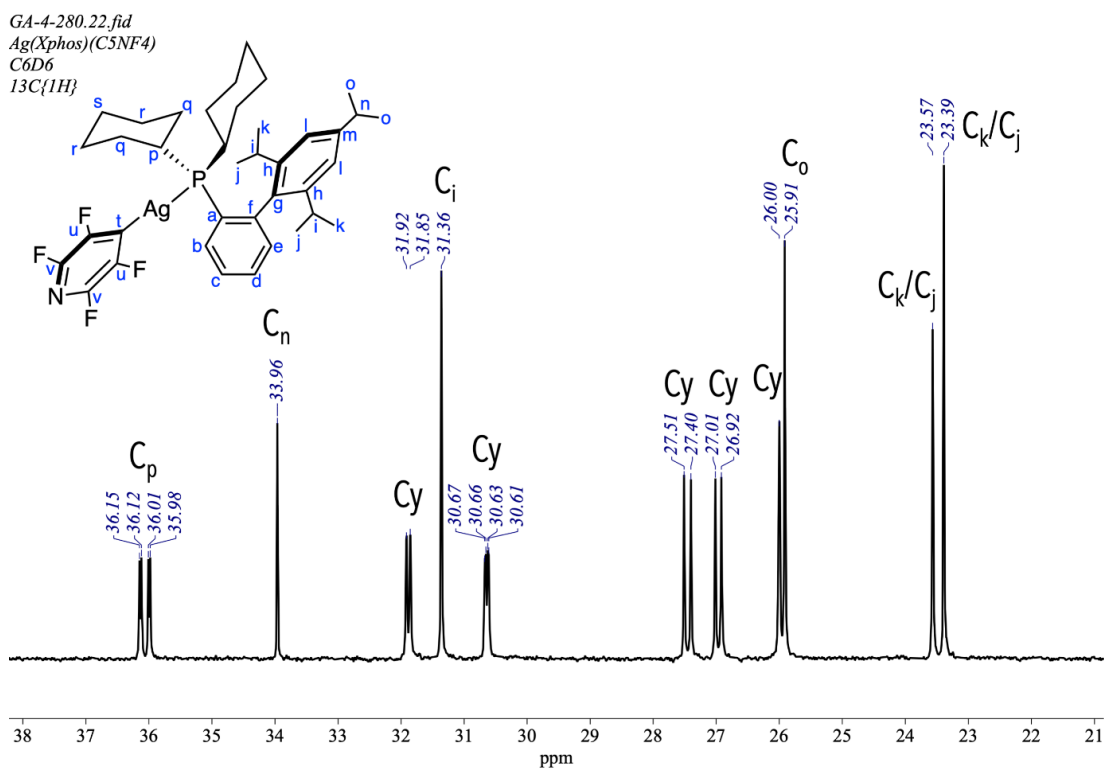


**Figure 344:** <sup>13</sup>C DEPT-135 (125.8 MHz, CD<sub>2</sub>Cl<sub>2</sub>, 25 °C) spectrum of Ag(C<sub>5</sub>F<sub>4</sub>N)(Xphos)

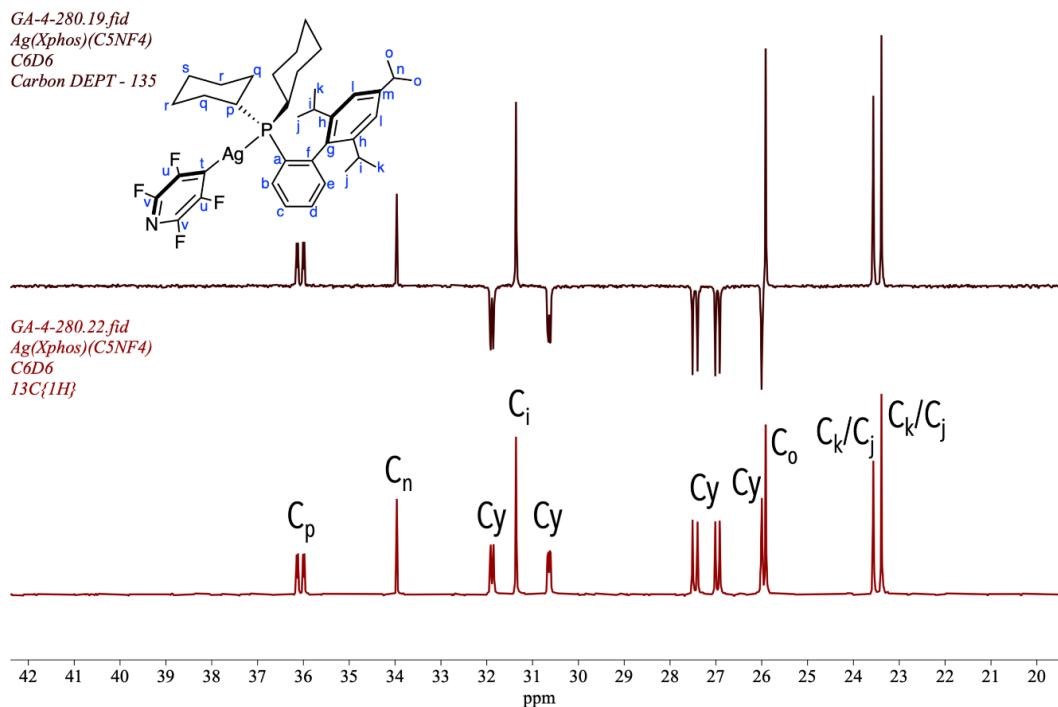
165



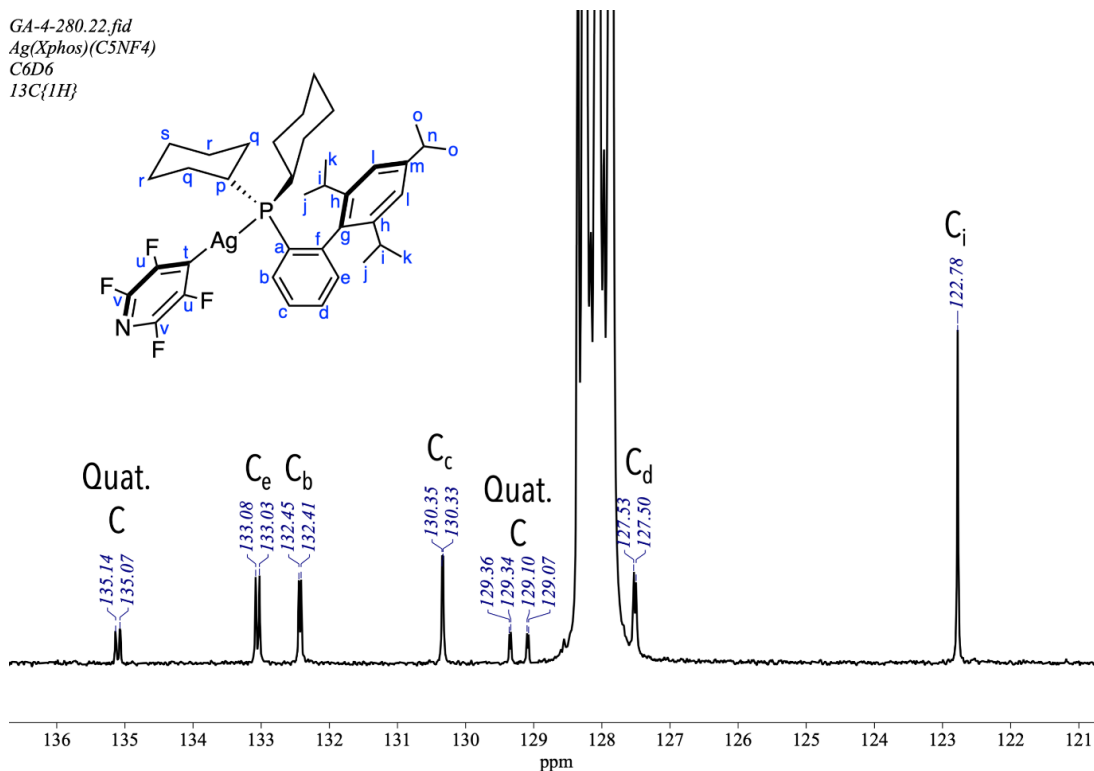
**Figure 345:**  $^{13}\text{C}\{^1\text{H}\}$  (125.8 MHz,  $\text{CD}_2\text{Cl}_2$ , 25 °C) spectrum of  $\text{Ag}(\text{C}_5\text{F}_4\text{N})(\text{Xphos})$  **165**



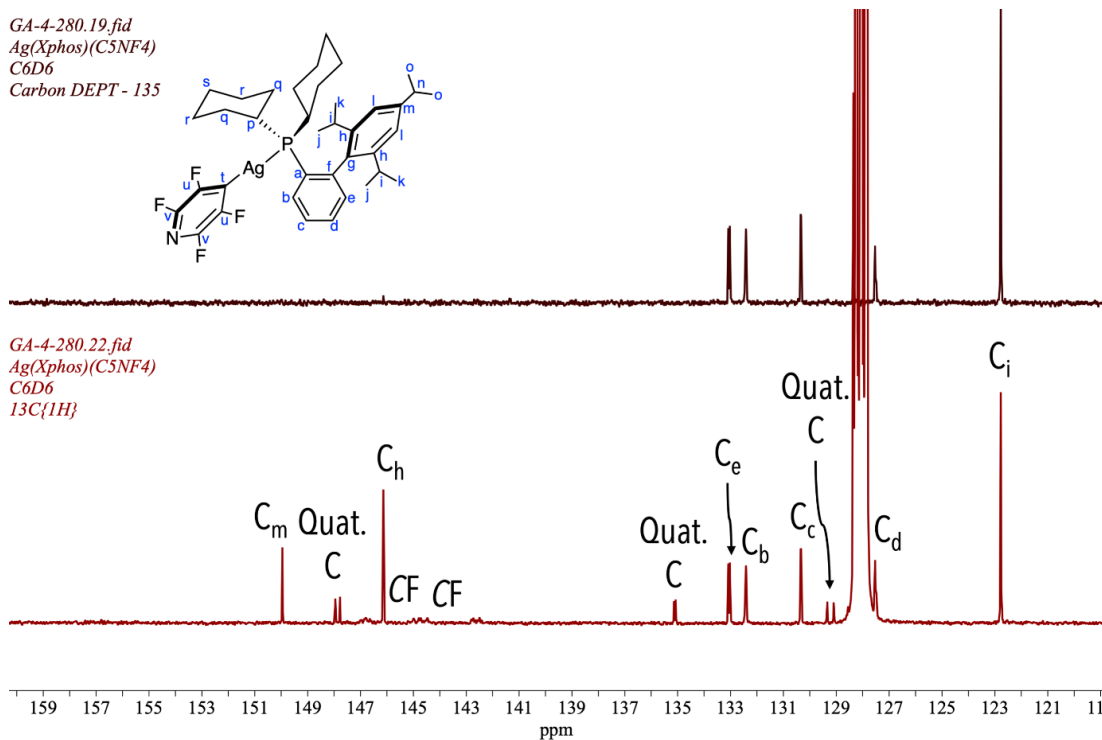
**Figure 346:**  $^{13}\text{C}\{^1\text{H}\}$  (125.8 MHz,  $\text{CD}_2\text{Cl}_2$ , 25 °C) spectrum of  $\text{Ag}(\text{C}_5\text{F}_4\text{N})(\text{Xphos})$  **165** between  $\delta$  20 and  $\delta$  40



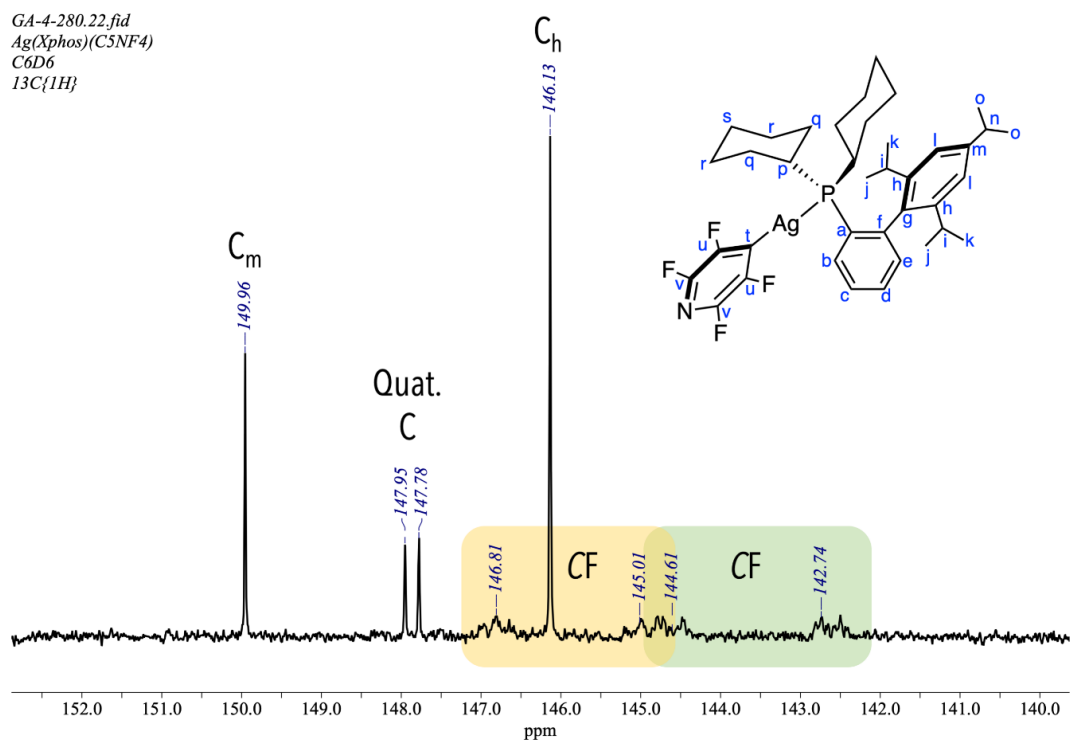
**Figure 347:** Stack plot of the  $^{13}\text{C}\{^1\text{H}\}$  NMR spectrum (bottom) and the  $^{13}\text{C}$  DEPT-135 (top) of Ag(C<sub>5</sub>F<sub>4</sub>N)(Xphos) **165** between  $\delta$  19 and  $\delta$  43



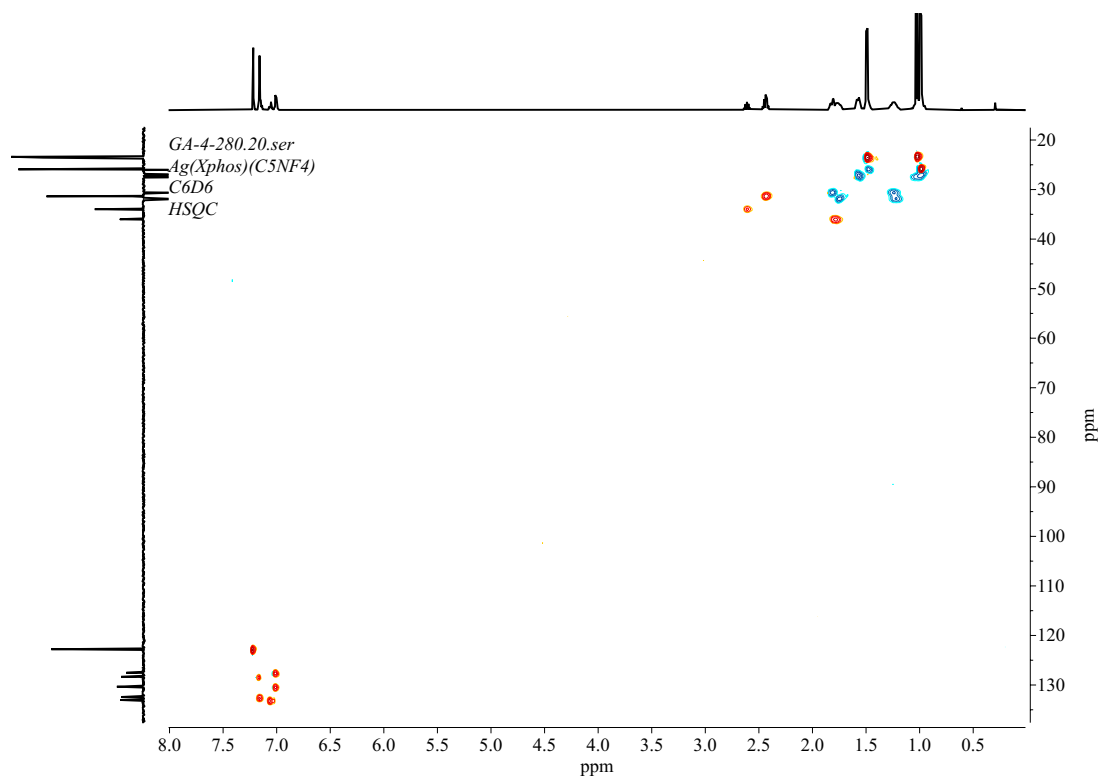
**Figure 348:**  $^{13}\text{C}\{^1\text{H}\}$  (125.8 MHz, CD<sub>2</sub>Cl<sub>2</sub>, 25 °C) spectrum of Ag(C<sub>5</sub>F<sub>4</sub>N)(Xphos) **165** between  $\delta$  120 and  $\delta$  137



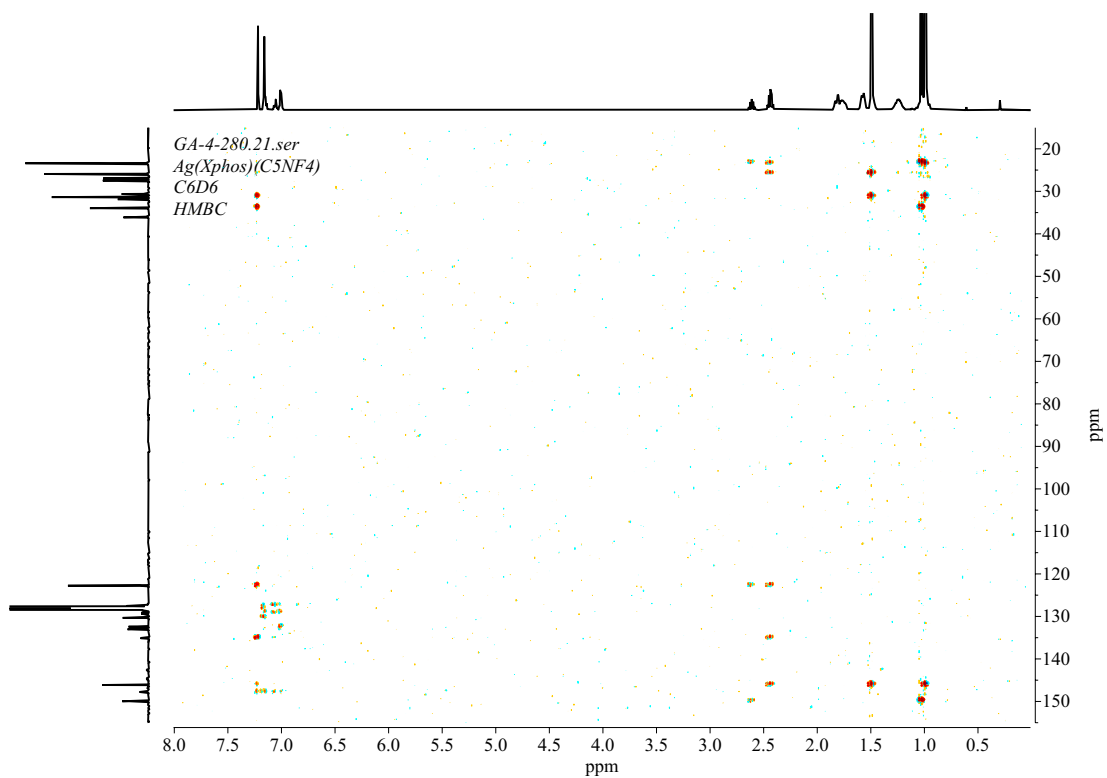
**Figure 349:** Stack plot of the  $^{13}\text{C}\{^1\text{H}\}$  NMR spectrum (bottom) and the  $^{13}\text{C}$  DEPT-135 (top) of Ag(C<sub>5</sub>F<sub>4</sub>N)(Xphos) **165** between  $\delta$  120 and  $\delta$  160



**Figure 350:**  $^{13}\text{C}\{^1\text{H}\}$  (125.8 MHz, CD<sub>2</sub>Cl<sub>2</sub>, 25 °C) spectrum of Ag(C<sub>5</sub>F<sub>4</sub>N)(Xphos) **165** between  $\delta$  138 and  $\delta$  154

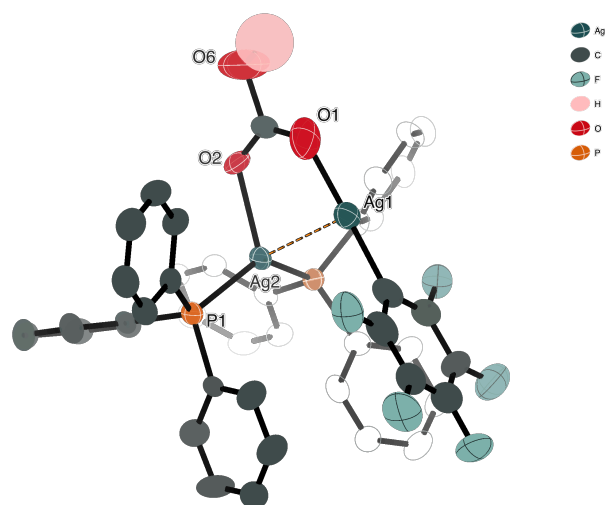


**Figure 351:** HSQC spectrum of Ag(C<sub>5</sub>F<sub>4</sub>N)(Xphos) **165** in CD<sub>2</sub>Cl<sub>2</sub>



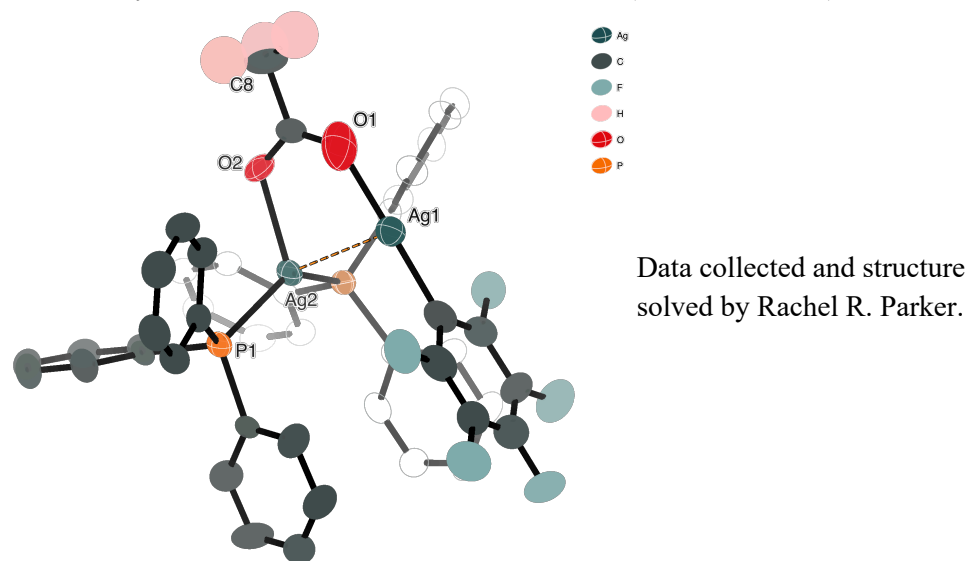
**Figure 352:** HMBC spectrum of Ag(C<sub>5</sub>F<sub>4</sub>N)(Xphos) **165** in CD<sub>2</sub>Cl<sub>2</sub>

## Appendix C – X-Ray Crystallographic Data

**Table 58:** Crystal data and structure refinement for **91** (carbonate structure)

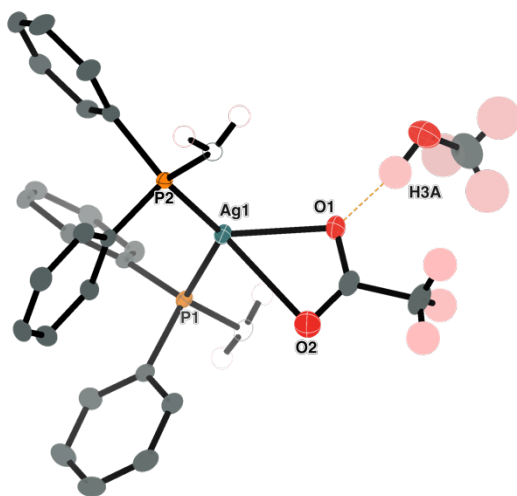
Data collected and refined by  
Adrian C. Whitwood. Post-  
refinement adjustments by  
Theo Tanner.

Identification code	ijsf1911 (GA-1-051)
Empirical formula	C <sub>43</sub> H <sub>31</sub> Ag <sub>2</sub> F <sub>5</sub> O <sub>3</sub> P <sub>2</sub>
Formula weight	968.36
Temperature/K	110.05(10)
Crystal system	monoclinic
Space group	P2 <sub>1</sub> /n
a/Å	23.4916(5)
b/Å	12.5001(2)
c/Å	31.2799(6)
α/°	90
β/°	110.123(2)
γ/°	90
Volume/Å <sup>3</sup>	8624.6(3)
Z	8
ρ <sub>calc</sub> /cm <sup>3</sup>	1.492
μ/mm <sup>-1</sup>	8.483
F(000)	3856.0
Crystal size/mm <sup>3</sup>	0.244 × 0.182 × 0.062
Radiation	Cu Kα (λ = 1.54184)
2θ range for data collection/°	7.686 to 134.156
Index ranges	-21 ≤ h ≤ 28, -14 ≤ k ≤ 14, -37 ≤ l ≤ 37
Reflections collected	33620
Independent reflections	15365 [R <sub>int</sub> = 0.0422, R <sub>sigma</sub> = 0.0493]
Data/restraints/parameters	15365/39/1016
Goodness-of-fit on F <sup>2</sup>	1.053
Final R indexes [I >= 2σ (I)]	R <sub>1</sub> = 0.0778, wR <sub>2</sub> = 0.2014
Final R indexes [all data]	R <sub>1</sub> = 0.0885, wR <sub>2</sub> = 0.2097
Largest diff. peak/hole / e Å <sup>-3</sup>	2.53/-1.60

**Table 59:** Crystal data and structure refinement for **91** (acetate structure)

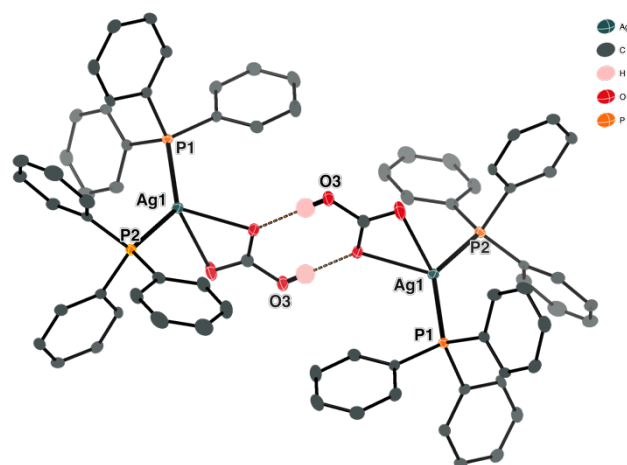
Identification code	ijsf1911 (GA-1-051)
Empirical formula	C <sub>44</sub> H <sub>33</sub> Ag <sub>2</sub> F <sub>5</sub> O <sub>2</sub> P <sub>2</sub>
Formula weight	966.38
Temperature/K	110.05(10)
Crystal system	monoclinic
Space group	P2 <sub>1</sub> /n
a/Å	23.4916(5)
b/Å	12.5001(2)
c/Å	31.2799(6)
α/°	90
β/°	110.123(2)
γ/°	90
Volume/Å <sup>3</sup>	8624.6(3)
Z	8
ρ <sub>calc</sub> /cm <sup>3</sup>	1.489
μ/mm <sup>-1</sup>	8.463
F(000)	3856.0
Crystal size/mm <sup>3</sup>	0.244 × 0.182 × 0.062
Radiation	CuKα (λ = 1.54184)
2θ range for data collection/°	7.686 to 134.156
Index ranges	-21 ≤ h ≤ 28, -14 ≤ k ≤ 14, -37 ≤ l ≤ 37
Reflections collected	33620
Independent reflections	15365 [R <sub>int</sub> = 0.0422, R <sub>sigma</sub> = 0.0493]
Data/restraints/parameters	15365/39/1016
Goodness-of-fit on F <sup>2</sup>	1.085
Final R indexes [I ≥ 2σ (I)]	R <sub>1</sub> = 0.0774, wR <sub>2</sub> = 0.2025
Final R indexes [all data]	R <sub>1</sub> = 0.0881, wR <sub>2</sub> = 0.2108
Largest diff. peak/hole / e Å <sup>-3</sup>	2.53/-1.60



**Table 60:** Crystal data and structure refinement for **95**

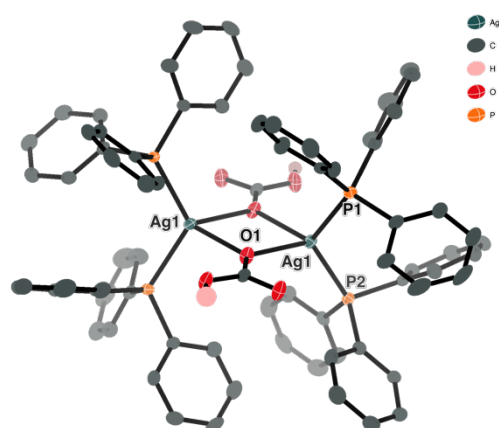
Data collected, solved,  
and refined by Sam  
Hart.

Identification code	ijsf1903 (GA-1-016)
Empirical formula	C <sub>29</sub> H <sub>31</sub> AgO <sub>3</sub> P <sub>2</sub>
Formula weight	597.35
Temperature/K	110.05(10)
Crystal system	triclinic
Space group	P-1
a/Å	10.0772(4)
b/Å	12.4552(5)
c/Å	12.4615(4)
$\alpha$ /°	119.615(4)
$\beta$ /°	101.157(3)
$\gamma$ /°	90.581(3)
Volume/Å <sup>3</sup>	1323.77(10)
Z	2
$\rho_{\text{calc}}$ /cm <sup>3</sup>	1.499
$\mu$ /mm <sup>-1</sup>	7.479
F(000)	612.0
Crystal size/mm <sup>3</sup>	0.179 × 0.168 × 0.038
Radiation	CuK $\alpha$ ( $\lambda$ = 1.54184)
2 $\Theta$ range for data collection/°	8.228 to 141.96
Index ranges	-12 ≤ h ≤ 12, -15 ≤ k ≤ 15, -15 ≤ l ≤ 15
Reflections collected	12779
Independent reflections	4936 [ $R_{\text{int}}$ = 0.0299, $R_{\text{sigma}}$ = 0.0311]
Data/restraints/parameters	4936/0/322
Goodness-of-fit on F <sup>2</sup>	1.087
Final R indexes [ $I \geq 2\sigma(I)$ ]	$R_1$ = 0.0308, $wR_2$ = 0.0801
Final R indexes [all data]	$R_1$ = 0.0314, $wR_2$ = 0.0806
Largest diff. peak/hole / e Å <sup>-3</sup>	1.22/-0.87

**Table 61:** Crystal data and structure refinement for **89**

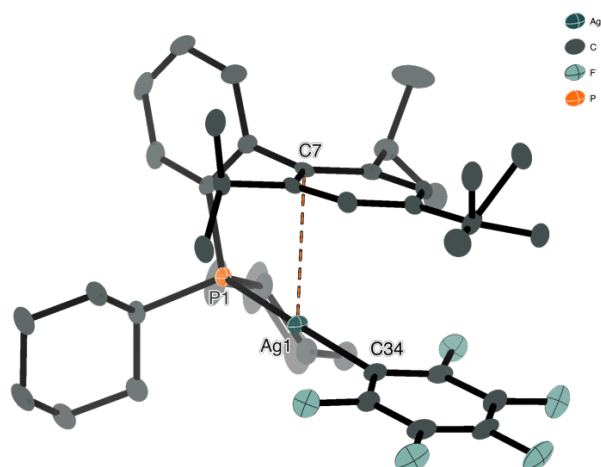
Data collected and  
structure solved by Rachel  
R. Parker.

Identification code	ijsf1914 (GA-2-090)
Empirical formula	$C_{37}H_{31}AgO_3P_2$
Formula weight	693.43
Temperature/K	110.05(10)
Crystal system	triclinic
Space group	P-1
a/Å	10.2263(3)
b/Å	11.9743(5)
c/Å	13.8259(6)
$\alpha/^\circ$	85.939(3)
$\beta/^\circ$	88.049(3)
$\gamma/^\circ$	65.102(4)
Volume/Å <sup>3</sup>	1531.80(11)
Z	2
$\rho_{\text{calc}}/\text{cm}^3$	1.503
$\mu/\text{mm}^{-1}$	0.799
F(000)	708.0
Crystal size/mm <sup>3</sup>	0.143 × 0.13 × 0.119
Radiation	MoK $\alpha$ ( $\lambda = 0.71073$ )
2 $\Theta$ range for data collection/ $^\circ$	6.802 to 52.744
Index ranges	-12 ≤ h ≤ 12, -14 ≤ k ≤ 14, -16 ≤ l ≤ 17
Reflections collected	11159
Independent reflections	6252 [ $R_{\text{int}} = 0.0242$ , $R_{\text{sigma}} = 0.0465$ ]
Data/restraints/parameters	6252/0/392
Goodness-of-fit on F <sup>2</sup>	1.056
Final R indexes [ $I \geq 2\sigma(I)$ ]	$R_1 = 0.0301$ , $wR_2 = 0.0564$
Final R indexes [all data]	$R_1 = 0.0365$ , $wR_2 = 0.0602$
Largest diff. peak/hole / e Å <sup>-3</sup>	0.41/-0.35

**Table 62:** Crystal data and structure refinement for **90**

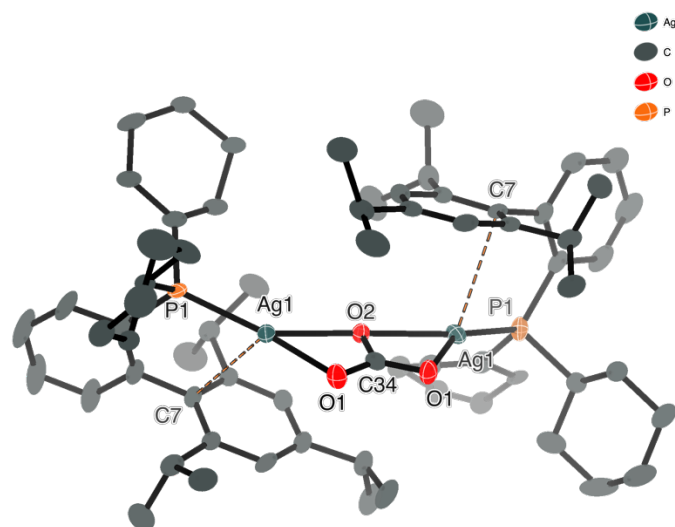
Data collected, solved, and refined by Adrian C Whitwood.

Identification code	ijsf1915 (GA-1-088)
Empirical formula	C <sub>74</sub> H <sub>62</sub> Ag <sub>2</sub> O <sub>6</sub> P <sub>4</sub>
Formula weight	1386.85
Temperature/K	110.05(10)
Crystal system	orthorhombic
Space group	P2 <sub>1</sub> 2 <sub>1</sub> 2
a/Å	23.0838(3)
b/Å	14.87078(17)
c/Å	9.25944(11)
α/°	90
β/°	90
γ/°	90
Volume/Å <sup>3</sup>	3178.53(7)
Z	2
ρ <sub>calc</sub> /cm <sup>3</sup>	1.449
μ/mm <sup>-1</sup>	6.320
F(000)	1416.0
Crystal size/mm <sup>3</sup>	0.149 × 0.049 × 0.045
Radiation	CuKα (λ = 1.54184)
2θ range for data collection/°	7.072 to 134.12
Index ranges	-27 ≤ h ≤ 27, -15 ≤ k ≤ 17, -11 ≤ l ≤ 11
Reflections collected	11910
Independent reflections	5512 [R <sub>int</sub> = 0.0238, R <sub>sigma</sub> = 0.0324]
Data/restraints/parameters	5512/0/392
Goodness-of-fit on F <sup>2</sup>	1.037
Final R indexes [I ≥ 2σ (I)]	R <sub>1</sub> = 0.0197, wR <sub>2</sub> = 0.0443
Final R indexes [all data]	R <sub>1</sub> = 0.0209, wR <sub>2</sub> = 0.0449
Largest diff. peak/hole / e Å <sup>-3</sup>	0.20/-0.29
Flack parameter	-0.026(3)

**Table 63:** Crystal data and structure refinement for **101**

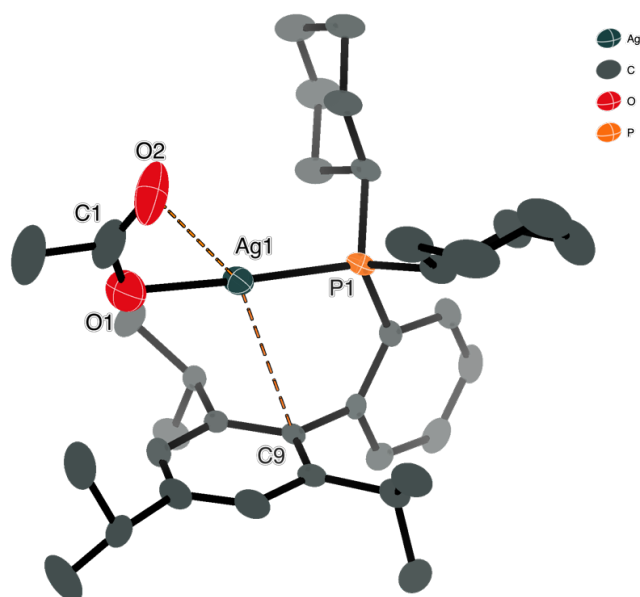
Data collected and refined by Theo Tanner.

CCDC number	2110194
Identification code	ijsf2001 (GA-2-139)
Empirical formula	$C_{39}H_{49}AgF_5P$
Formula weight	751.62
Temperature/K	110.00(14)
Crystal system	monoclinic
Space group	$P2_1/n$
$a/\text{\AA}$	11.22275(16)
$b/\text{\AA}$	17.8780(2)
$c/\text{\AA}$	17.7856(2)
$\alpha/^\circ$	90
$\beta/^\circ$	98.6941(12)
$\gamma/^\circ$	90
Volume/ $\text{\AA}^3$	3527.52(8)
Z	4
$\rho_{\text{calc}}/\text{g cm}^{-3}$	1.415
$\mu/\text{mm}^{-1}$	5.455
F(000)	1560.0
Crystal size/ $\text{mm}^3$	$0.32 \times 0.233 \times 0.148$
Radiation	$\text{CuK}\alpha$ ( $\lambda = 1.54184$ )
$2\theta$ range for data collection/ $^\circ$	7.052 to 142.246
Index ranges	$-13 \leq h \leq 13, -19 \leq k \leq 21, -10 \leq l \leq 21$
Reflections collected	14194
Independent reflections	6697 [ $R_{\text{int}} = 0.0241, R_{\text{sigma}} = 0.0317$ ]
Data/restraints/parameters	6697/0/442
Goodness-of-fit on $F^2$	1.045
Final R indexes [ $I \geq 2\sigma(I)$ ]	$R_1 = 0.0269, wR_2 = 0.0651$
Final R indexes [all data]	$R_1 = 0.0319, wR_2 = 0.0691$
Largest diff. peak/hole / $e \text{\AA}^{-3}$	0.50/-0.57

**Table 64:** Crystal data and structure refinement for **106**

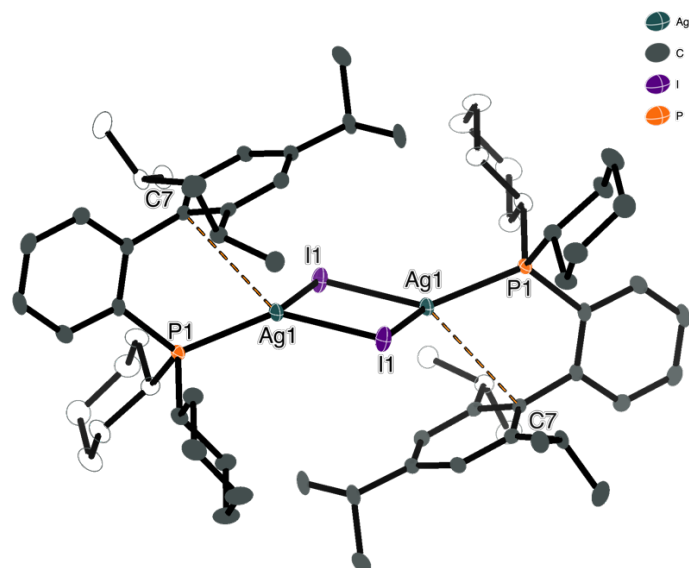
Data collected and  
refined by Theo  
Tanner

CCDC number	2110193
Identification code	ijsf2003 (GA-2-169)
Empirical formula	$C_{69}H_{101}Ag_2NO_3P_2$
Formula weight	1270.18
Temperature/K	110.00(10)
Crystal system	tetragonal
Space group	I-4c2
a/Å	25.0086(2)
b/Å	25.0086(2)
c/Å	20.9083(2)
$\alpha/^\circ$	90
$\beta/^\circ$	90
$\gamma/^\circ$	90
Volume/Å <sup>3</sup>	13076.7(2)
Z	8
$\rho_{\text{calc}}/\text{cm}^3$	1.290
$\mu/\text{mm}^{-1}$	5.599
F(000)	5360.0
Crystal size/mm <sup>3</sup>	0.317 × 0.285 × 0.216
Radiation	Cu K $\alpha$ ( $\lambda = 1.54184$ )
2 $\theta$ range for data collection/ $^\circ$	7.07 to 142.19
Index ranges	-17 ≤ h ≤ 30, -30 ≤ k ≤ 30, -25 ≤ l ≤ 18
Reflections collected	12962
Independent reflections	5403 [ $R_{\text{int}} = 0.0195$ , $R_{\text{sigma}} = 0.0224$ ]
Data/restraints/parameters	5403/0/370
Goodness-of-fit on F <sup>2</sup>	1.039
Final R indexes [ $I \geq 2\sigma(I)$ ]	$R_1 = 0.0240$ , $wR_2 = 0.0633$
Final R indexes [all data]	$R_1 = 0.0248$ , $wR_2 = 0.0639$
Largest diff. peak/hole / e Å <sup>-3</sup>	0.88/-0.36
Flack parameter	-0.020(3)

**Table 65:** Crystal data and structure refinement for **109**

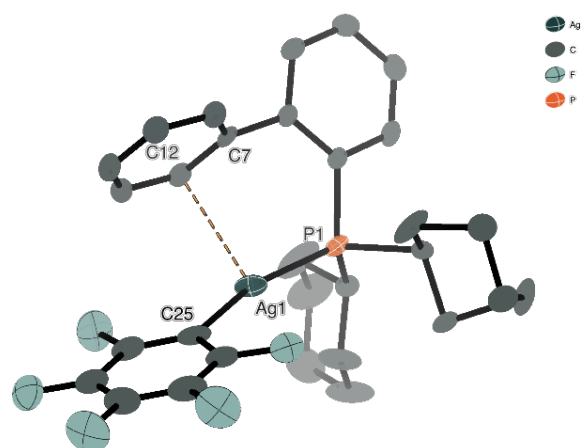
Data collected, solved, and refined by Adrian C Whitwood.

CCDC Number	2160367
Identification code	ijsf21034a (GA-6-454)
Empirical formula	$C_{35}H_{53.61}AgO_{2.8}P$
Formula weight	658.11
Temperature/K	110.00(10)
Crystal system	monoclinic
Space group	$P2_1/c$
a/Å	10.97851(13)
b/Å	17.8546(2)
c/Å	17.7362(2)
$\alpha/^\circ$	90
$\beta/^\circ$	102.1430(12)
$\gamma/^\circ$	90
Volume/Å <sup>3</sup>	3398.83(7)
Z	4
$\rho_{\text{calc}}/\text{cm}^3$	1.286
$\mu/\text{mm}^{-1}$	5.427
F(000)	1392.0
Crystal size/mm <sup>3</sup>	0.156 × 0.137 × 0.045
Radiation	Cu K $\alpha$ ( $\lambda = 1.54184$ )
2 $\theta$ range for data collection/ $^\circ$	7.106 to 134.134
Index ranges	-13 ≤ h ≤ 9, -21 ≤ k ≤ 15, -20 ≤ l ≤ 21
Reflections collected	12530
Independent reflections	6056 [ $R_{\text{int}} = 0.0189$ , $R_{\text{sigma}} = 0.0253$ ]
Data/restraints/parameters	6056/2/420
Goodness-of-fit on F <sup>2</sup>	1.044
Final R indexes [ $I \geq 2\sigma(I)$ ]	$R_1 = 0.0281$ , $wR_2 = 0.0697$
Final R indexes [all data]	$R_1 = 0.0315$ , $wR_2 = 0.0720$
Largest diff. peak/hole / e Å <sup>-3</sup>	0.40/-0.56

**Table 66:** Crystal data and structure refinement for **105**

Data collected,  
solved, and refined  
by Adrian C  
Whitwood

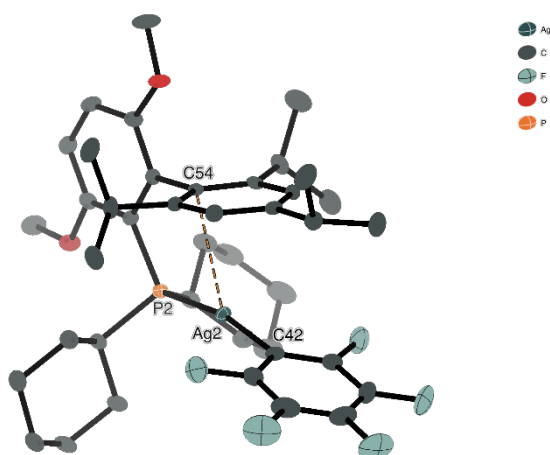
CCDC number	2110192
Identification code	ijsf1926 (GA-2-148)
Empirical formula	$C_{68}H_{102}Ag_2Cl_4I_2P_2$
Formula weight	1592.77
Temperature/K	110.00(10)
Crystal system	monoclinic
Space group	$P2_1/n$
a/Å	13.44088(18)
b/Å	18.7097(2)
c/Å	13.82211(18)
$\alpha/^\circ$	90
$\beta/^\circ$	97.5336(12)
$\gamma/^\circ$	90
Volume/Å <sup>3</sup>	3445.91(8)
Z	2
$\rho_{\text{calc}}/\text{cm}^3$	1.535
$\mu/\text{mm}^{-1}$	13.738
F(000)	1616.0
Crystal size/mm <sup>3</sup>	0.259 × 0.117 × 0.071
Radiation	CuK $\alpha$ ( $\lambda = 1.54184$ )
2 $\theta$ range for data collection/ $^\circ$	7.998 to 134.138
Index ranges	-6 ≤ h ≤ 16, -22 ≤ k ≤ 22, -16 ≤ l ≤ 16
Reflections collected	13120
Independent reflections	6149 [R <sub>int</sub> = 0.0263, R <sub>sigma</sub> = 0.0331]
Data/restraints/parameters	6149/2/372
Goodness-of-fit on F <sup>2</sup>	1.033
Final R indexes [I ≥ 2 $\sigma$ (I)]	R <sub>1</sub> = 0.0251, wR <sub>2</sub> = 0.0588
Final R indexes [all data]	R <sub>1</sub> = 0.0301, wR <sub>2</sub> = 0.0618
Largest diff. peak/hole / e Å <sup>-3</sup>	0.55/-0.59

**Table 67:** Crystal data and structure refinement for **122**

Data collected and  
refined by Theo F N  
Tanner

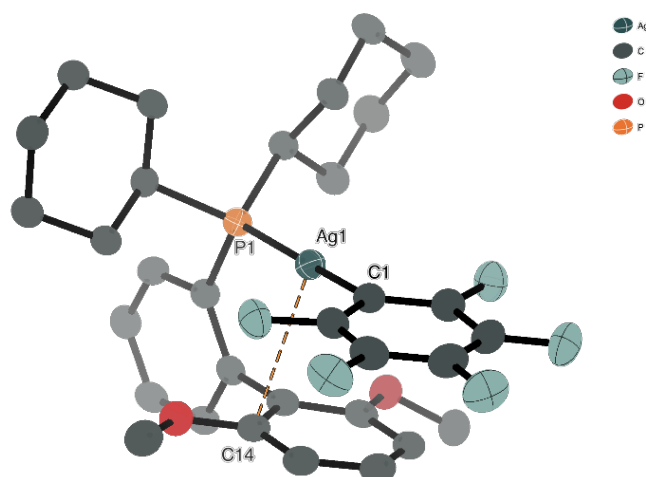
Identification code	ijsf21028b_auto (GA-5-386)
Empirical formula	C <sub>30</sub> H <sub>31</sub> AgF <sub>5</sub> P
Formula weight	625.39
Temperature/K	110.00(10)
Crystal system	orthorhombic
Space group	P2 <sub>1</sub> 2 <sub>1</sub> 2 <sub>1</sub>
a/Å	9.55490(10)
b/Å	14.6927(2)
c/Å	19.2538(2)
α/°	90
β/°	90
γ/°	90
Volume/Å <sup>3</sup>	2702.99(5)
Z	4
ρ <sub>calc</sub> /cm <sup>3</sup>	1.537
μ/mm <sup>-1</sup>	6.998
F(000)	1272.0
Crystal size/mm <sup>3</sup>	0.269 × 0.215 × 0.154
Radiation	Cu Kα (λ = 1.54184)
2θ range for data collection/°	7.568 to 141.926
Index ranges	-9 ≤ h ≤ 11, -16 ≤ k ≤ 17, -23 ≤ l ≤ 17
Reflections collected	9859
Independent reflections	5114 [R <sub>int</sub> = 0.0209, R <sub>sigma</sub> = 0.0260]
Data/restraints/parameters	5114/0/380
Goodness-of-fit on F <sup>2</sup>	1.101
Final R indexes [I ≥ 2σ (I)]	R <sub>1</sub> = 0.0256, wR <sub>2</sub> = 0.0633
Final R indexes [all data]	R <sub>1</sub> = 0.0259, wR <sub>2</sub> = 0.0634
Largest diff. peak/hole / e Å <sup>-3</sup>	0.31/-0.42
Flack parameter	0.035(3)



**Table 68:** Crystal data and structure refinement for **125**

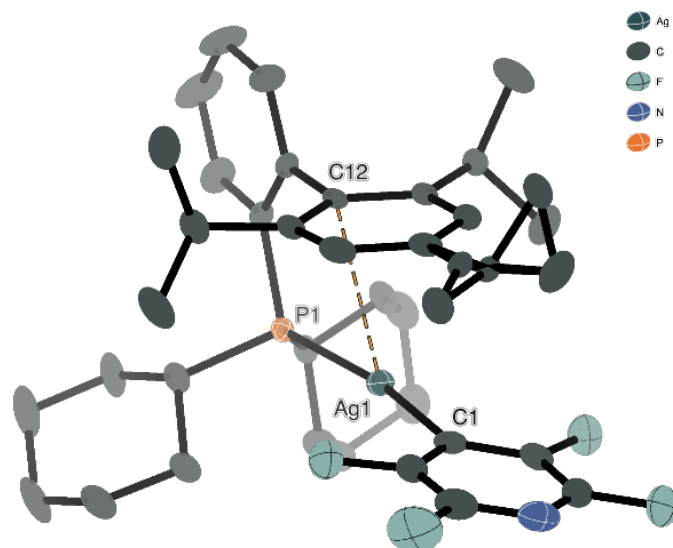
Data collected, solved,  
and refined by Adrian C  
Whitwood

Identification code	ijsf21010 (GA-5-382)
Empirical formula	C <sub>41</sub> H <sub>53</sub> AgF <sub>5</sub> O <sub>2</sub> P
Formula weight	811.67
Temperature/K	110.00(10)
Crystal system	monoclinic
Space group	P2 <sub>1</sub> /c
a/Å	16.70741(8)
b/Å	20.48575(11)
c/Å	22.75069(13)
$\alpha$ /°	90
$\beta$ /°	91.7740(5)
$\gamma$ /°	90
Volume/Å <sup>3</sup>	7783.01(7)
Z	8
$\rho_{\text{calc}}$ /cm <sup>3</sup>	1.385
$\mu$ /mm <sup>-1</sup>	5.026
F(000)	3376.0
Crystal size/mm <sup>3</sup>	0.21 × 0.087 × 0.028
Radiation	Cu K $\alpha$ ( $\lambda$ = 1.54184)
2 $\theta$ range for data collection/°	6.83 to 134.156
Index ranges	-19 ≤ h ≤ 13, -24 ≤ k ≤ 24, -26 ≤ l ≤ 27
Reflections collected	42154
Independent reflections	13887 [R <sub>int</sub> = 0.0244, R <sub>sigma</sub> = 0.0260]
Data/restraints/parameters	13887/0/917
Goodness-of-fit on F <sup>2</sup>	1.035
Final R indexes [I ≥ 2 $\sigma$ (I)]	R <sub>1</sub> = 0.0251, wR <sub>2</sub> = 0.0602
Final R indexes [all data]	R <sub>1</sub> = 0.0303, wR <sub>2</sub> = 0.0627
Largest diff. peak/hole / e Å <sup>-3</sup>	0.55/-0.60

**Table 69:** Crystal data and structure refinement for **124**

Data collected, solved,  
and refined by Adrian  
C Whitwood

Identification code	ijsf21021 (GA-5-383)
Empirical formula	$C_{32}H_{35}AgF_5O_2P$
Formula weight	685.44
Temperature/K	109.95(10)
Crystal system	monoclinic
Space group	$P2_1/n$
a/Å	9.89053(16)
b/Å	15.8072(3)
c/Å	18.8036(3)
$\alpha/^\circ$	90
$\beta/^\circ$	92.1690(14)
$\gamma/^\circ$	90
Volume/Å <sup>3</sup>	2937.67(8)
Z	4
$\rho_{\text{calc}}/\text{cm}^3$	1.550
$\mu/\text{mm}^{-1}$	6.546
F(000)	1400.0
Crystal size/mm <sup>3</sup>	0.129 × 0.111 × 0.028
Radiation	Cu K $\alpha$ ( $\lambda = 1.54184$ )
2 $\theta$ range for data collection/ $^\circ$	7.308 to 134.148
Index ranges	$-11 \leq h \leq 11, -10 \leq k \leq 18, -22 \leq l \leq 22$
Reflections collected	10537
Independent reflections	5238 [ $R_{\text{int}} = 0.0262, R_{\text{sigma}} = 0.0371$ ]
Data/restraints/parameters	5238/0/372
Goodness-of-fit on $F^2$	1.021
Final R indexes [ $I \geq 2\sigma(I)$ ]	$R_1 = 0.0326, wR_2 = 0.0792$
Final R indexes [all data]	$R_1 = 0.0402, wR_2 = 0.0836$
Largest diff. peak/hole / e Å <sup>-3</sup>	0.65/-0.38

**Table 70:** Crystal data and structure refinement for **165**

Data collected, solved, and refined by Adrian C Whitwood.

Identification code	ijsf2025 (GA-4-280)
Empirical formula	C <sub>38</sub> H <sub>49</sub> AgF <sub>4</sub> NP
Formula weight	734.62
Temperature/K	110.00(10)
Crystal system	monoclinic
Space group	P2 <sub>1</sub> /n
a/Å	11.3251(3)
b/Å	17.8552(4)
c/Å	17.4883(4)
α/°	90
β/°	97.944(2)
γ/°	90
Volume/Å <sup>3</sup>	3502.41(13)
Z	4
ρ <sub>calc</sub> /cm <sup>3</sup>	1.393
μ/mm <sup>-1</sup>	5.447
F(000)	1528.0
Crystal size/mm <sup>3</sup>	0.187 × 0.105 × 0.02
Radiation	Cu Kα (λ = 1.54184)
2θ range for data collection/°	7.11 to 134.156
Index ranges	-13 ≤ h ≤ 10, -21 ≤ k ≤ 20, -17 ≤ l ≤ 20
Reflections collected	13257
Independent reflections	6255 [R <sub>int</sub> = 0.0299, R <sub>sigma</sub> = 0.0398]
Data/restraints/parameters	6255/0/600
Goodness-of-fit on F <sup>2</sup>	1.032

## Abbreviation List

$\Delta H^\ddagger$	enthalpy of activation
$\Delta S^\ddagger$	entropy of activation
$\Delta G^\ddagger$	gibbs free energy of activation
Ac	acetyl
Ad	adamantyl
AMLA(4)	4 membered ambiphilic metal-ligand activation
AMLA(6)	6 membered ambiphilic metal-ligand activation
ATR	attenuated total reflectance
CMD	concerted metalation deprotonation
Cod	1,5-cyclooctadiene
COSY	correlation spectroscopy
Cy	cyclohexyl
dba	dibenzylideneacetone
DCM	dichloromethane
DFT	density functional theory
DMF	<i>N,N</i> -dimethylformamide
DPPE	1,2-bis(diphenylphosphino)ethane
dtbyp	4,4'-di- <i>tert</i> -butyl-2,2'-dipyridyl
D1	NMR parameter, relaxation time
EI	electron ionisation
Equiv.	equivalents
Et	ethyl
EXSY	exchange spectroscopy
ESI	electrospray ionization (MS)
EtCN	propionitrile
EtOAc	ethyl acetate
EtOH	ethanol
GC-MS	gas chromatography – mass spectroscopy
HFIP	hexafluoro-2-propanol
HMBC	heteronuclear multiple bond coherence
HMQC	heteronuclear multiple quantum coherence
HOMO	highest occupied molecular orbital
HSQC	heteronuclear single quantum coherence
INEPT	Insensitive nuclei enhanced by polarization transfer
<sup>i</sup> Pr	isopropyl

IR	infrared spectroscopy
LIFDI	liquid injection field desorption ionization
LUMO	lowest unoccupied molecular orbital
[M] <sup>+</sup>	molecular ion (MS)
Me	methyl
MeCN	acetonitrile
MeOH	methanol
MS	mass spectroscopy
m/z	mass to charge ratio
NMR	nuclear magnetic resonance
ns	NMR parameter, number of scans
OAc	acetate
OPiv	pivalate
OTFA	trifluoroacetate
O1p	NMR parameter, transmitter centre (centre of spectra)
Ph	phenyl
ppm	parts per million
R <sub>f</sub>	retention factor
RPKA	reaction progress kinetic analysis
rt or RT	room temperature
r <sub>w</sub>	van der Waals radius
sw	NMR parameter, spectral width
<sup>t</sup> bu	<i>tert</i> -butyl
THF	tetrahydrofuran
Tol	tolyl
TS	transition state
UV	ultraviolet
Vis	visible
VT	variable temperature
VTNA	variable time normalisation analysis
wrt	with respect to
XRD	x-ray diffraction

---

 Abbreviation for dialkylbiarylphosphines
 

---

BrettPhos	2-(dicyclohexylphosphino)3,6-dimethoxy-2',4'6'-triisopropyl-1,1'-biphenyl
CyJohnPhos	2-(dicyclohexylphosphino)biphenyl

DavePhos	2-dicyclohexylphosphino-2'-( <i>N,N</i> -dimethylamino)biphenyl
JohnPhos	2-(di- <i>tert</i> -butylphosphino)biphenyl
RockPhos	2-Di( <i>tert</i> -butyl)phosphino-2',4',6'-triisopropyl-3-methoxy-6-methylbiphenyl
RuPhos	2-dicyclohexylphosphino-2',6'-diisopropoxybiphenyl
Sphos	2-dicyclohexylphosphino-2',6'-dimethoxybiphenyl
<sup>1</sup> BuBrettPhos	2-(di- <i>tert</i> -butylphosphino)-2',4',6'-triisopropyl-3,6-dimethoxy-1,1'-biphenyl
<sup>1</sup> BuXphos	2-di- <i>tert</i> -butylphosphino-2',4',6'-triisopropylbiphenyl
Xphos	2-dicyclohexylphosphino-2',4',6'-triisopropylbiphenyl

---

 Abbreviation for NMR assignments
 

---

s	singlet
d	doublet
t	triplet
q	quartet
qui	quintet
sext	sextet
sept	septet
m	multiplet
br	broad peak

## References

- (1) Baudoin, O. Multiple Catalytic C–H Bond Functionalization for Natural Product Synthesis. *Angew. Chem. Int. Ed.* **2020**, *59*, 17798–17809.
- (2) Yu, C.; Sanjosé-Orduna, J.; Patureau, F. W.; Pérez-Temprano, M. H. Emerging Unconventional Organic Solvents for C-H Bond and Related Functionalization Reactions. *Chem. Soc. Rev.* **2020**, *49*, 1643–1652.
- (3) Rej, S.; Ano, Y.; Chatani, N. Bidentate Directing Groups: An Efficient Tool in C-H Bond Functionalization Chemistry for the Expedient Construction of C-C Bonds. *Chem. Rev.* **2020**, *120*, 1788–1887.
- (4) Ackermann, L. Carboxylate-Assisted Transition-Metal-Catalyzed C-H Bond Functionalizations: Mechanism and Scope. *Chem. Rev.* **2011**, *111*, 1315–1345.
- (5) Bohra, H.; Wang, M. Direct C-H Arylation: A “Greener” Approach towards Facile Synthesis of Organic Semiconducting Molecules and Polymers. *J. Mater. Chem. A* **2017**, *5*, 11550–11571.
- (6) Rossi, R.; Bellina, F.; Lessi, M.; Manzini, C. Cross-Coupling of Heteroarenes by C-H Functionalization: Recent Progress towards Direct Arylation and Heteroarylation Reactions Involving Heteroarenes Containing One Heteroatom. *Adv. Synth. Catal.* **2014**, *356*, 17–117.
- (7) Xu, S.; Kim, E. H.; Wei, A.; Negishi, E. I. Pd- and Ni-Catalyzed Cross-Coupling Reactions in the Synthesis of Organic Electronic Materials. *Sci. Technol. Adv. Mater.* **2014**, *15*.
- (8) Lee, J. A.; Luscombe, C. K. Dual-Catalytic Ag-Pd System for Direct Arylation Polymerization to Synthesize Poly(3-Hexylthiophene). *ACS Macro Lett.* **2018**, *7*, 767–771.
- (9) Kuhl, N.; Hopkinson, M. N.; Wencel-Delord, J.; Glorius, F. Beyond Directing Groups: Transition-Metal-Catalyzed C-H Activation of Simple Arenes. *Angew. Chem. Int. Ed.* **2012**, *51*, 10236–10254.
- (10) Leow, D.; Li, G.; Mei, T. S.; Yu, J. Q. Activation of Remote Meta-C-H Bonds Assisted by an End-on Template. *Nature* **2012**, *486*, 518–522.
- (11) Luo, J.; Preciado, S.; Larrosa, I. Overriding Ortho-Para Selectivity via a Traceless Directing Group Relay Strategy: The Meta-Selective Arylation of Phenols. *J. Am. Chem. Soc.* **2014**, *136*, 4109–4112.
- (12) Wang, X.; Leow, D.; Yu, J. Pd(II)-Catalyzed Para-Selective C–H Arylation of Monosubstituted Arenes. *J. Am. Chem. Soc.* **2011**, *133*, 13864–13867.
- (13) Rani, G.; Luxami, V.; Paul, K. Traceless Directing Groups: A Novel Strategy in Regiodivergent C-H Functionalization. *Chem. Commun.* **2020**, *56*, 12479–12521.

- (14) Davies, H. M. L.; Morton, D. Recent Advances in C-H Functionalization. *J. Org. Chem.* **2016**, *81*, 343–350.
- (15) Liu, Y. J.; Xu, H.; Kong, W. J.; Shang, M.; Dai, H. X.; Yu, J. Q. Overcoming the Limitations of Directed C-H Functionalizations of Heterocycles. *Nature* **2014**, *515*, 389–393.
- (16) Deprez, N. R.; Sanford, M. S. Synthetic and Mechanistic Studies of Pd-Catalyzed C-H Arylation with Diaryliodonium Salts: Evidence for a Bimetallic High Oxidation State Pd Intermediate. *J. Am. Chem. Soc.* **2009**, *131*, 11234–11241.
- (17) Kalyani, D.; Deprez, N. R.; Desai, L. V.; Sanford, M. S. Oxidative C-H Activation/C-C Bond Forming Reactions: Synthetic Scope and Mechanistic Insights. *J. Am. Chem. Soc.* **2005**, *127*, 7330–7331.
- (18) Mendiola, J.; Castellote, I.; Alvarez-Builla, J.; Fernández-Gadea, J.; Gómez, A.; Vaquero, J. J. Palladium-Catalyzed Arylation and Heteroarylation of Azolopyrimidines. *J. Org. Chem.* **2006**, *71*, 1254–1257.
- (19) Seregin, I. V.; Ryabova, V.; Gevorgyan, V. Direct Palladium-Catalyzed Alkynylation of N-Fused Heterocycles. *J. Am. Chem. Soc.* **2007**, *129*, 7742–7743.
- (20) Luo, J.; Preciado, S.; Araromi, S. O.; Larrosa, I. A Domino Oxidation/Arylation/Protodecarboxylation Reaction of Salicylaldehydes: Expanded Access to Meta-Arylphenols. *Chem. Asian J.* **2016**, *11*, 347–350.
- (21) Bedford, R. B.; Coles, S. J.; Hursthouse, M. B.; Limmert, M. E. The Catalytic Intermolecular Orthoarylation of Phenols. *Angew. Chem. Int. Ed.* **2003**, *42*, 112–114.
- (22) Huang, C.; Chattopadhyay, B.; Gevorgyan, V. Silanol: A Traceless Directing Group for Pd-Catalyzed o-Alkenylation of Phenols. *J. Am. Chem. Soc.* **2011**, *133*, 12406–12409.
- (23) Sarkar, D.; Gevorgyan, V. Pd-Catalyzed C–H Alkylation of Arenes Using PyrDipSi, a Transformable and Removable Silicon-Tethered Directing Group. *Chem. Eur. J.* **2016**, *22*, 11201–11204.
- (24) Cai, G.; Fu, Y.; Li, Y.; Wan, X.; Shi, Z. Indirect Ortho Functionalization of Substituted Toluenes through Ortho Olefination of N,N-Dimethylbenzylamines Tuned by the Acidity of Reaction Conditions. *J. Am. Chem. Soc.* **2007**, *129*, 7666–7673.
- (25) Feng, R.; Yao, J.; Liang, Z.; Liu, Z.; Zhang, Y. Cu(II)-Promoted Palladium-Catalyzed C–H Ortho-Arylation of N,N - Dimethylbenzylamines. *J. Org. Chem.* **2013**, *78*, 3688–3696.
- (26) Wang, P.; Verma, P.; Xia, G.; Shi, J.; Qiao, J. X.; Tao, S.; Cheng, P. T. W.; Poss, M. A.; Farmer, M. E.; Yeung, K. S.; Yu, J. Q. Ligand-Accelerated Non-Directed C-H Functionalization of Arenes. *Nature* **2017**, *551*, 489–493.
- (27) Wedi, P.; Farizyan, M.; Bergander, K.; Mück-Lichtenfeld, C.; van Gemmeren, M.



- Mechanism of the Arene-Limited Nondirected C–H Activation of Arenes with Palladium\*\*. *Angew. Chem. Int. Ed.* **2021**, *60*, 15641–15649.
- (28) Milani, J.; Pridmore, N. E.; Whitwood, A. C.; Fairlamb, I. J. S.; Perutz, R. N. The Role of Fluorine Substituents in the Regioselectivity of Intramolecular C–H Bond Functionalization of Benzylamines at Palladium(II). *Organometallics* **2015**, *34*, 4376–4386.
- (29) Hammarback, L. A.; Bishop, A. L.; Jordan, C.; Athavan, G.; Eastwood, J. B.; Burden, T. J.; Bray, J. T. W.; Clarke, F.; Robinson, A.; Krieger, J. P.; Whitwood, A.; Clark, I. P.; Towrie, M.; Lynam, J. M.; Fairlamb, I. J. S. Manganese-Mediated C–H Bond Activation of Fluorinated Aromatics and the Ortho-Fluorine Effect: Kinetic Analysis by In Situ Infrared Spectroscopic Analysis and Time-Resolved Methods. *ACS Catal.* **2022**, *12*, 1532–1544.
- (30) García-Cuadrado, D.; De Mendoza, P.; Braga, A. A. C.; Maseras, F.; Echavarren, A. M. Proton-Abstraction Mechanism in the Palladium-Catalyzed Intramolecular Arylation: Substituent Effects. *J. Am. Chem. Soc.* **2007**, *129*, 6880–6886.
- (31) Guihaumé, J.; Clot, E.; Eisenstein, O.; Perutz, R. N. Importance of Palladium-Carbon Bond Energies in Direct Arylation of Polyfluorinated Benzenes. *Dalton Trans.* **2010**, *39*, 10352–10361.
- (32) He, C. Y.; Fan, S.; Zhang, X. Pd-Catalyzed Oxidative Cross-Coupling of Perfluoroarenes with Aromatic Heterocycles. *J. Am. Chem. Soc.* **2010**, *132*, 12850–12852.
- (33) Li, H.; Liu, J.; Sun, C. L.; Li, B. J.; Shi, Z. J. Palladium-Catalyzed Cross-Coupling of Polyfluoroarenes with Simple Arenes. *Org. Lett.* **2011**, *13*, 276–279.
- (34) Lafrance, M.; Rowley, C. N.; Woo, T. K.; Fagnou, K. Catalytic Intermolecular Direct Arylation of Perfluorobenzenes. *J. Am. Chem. Soc.* **2006**, *128*, 8754–8756.
- (35) Chen, F.; Min, Q. Q.; Zhang, X. Pd-Catalyzed Direct Arylation of Polyfluoroarenes on Water under Mild Conditions Using PPh<sub>3</sub> Ligand. *J. Org. Chem.* **2012**, *77*, 2992–2998.
- (36) Eisenstein, O.; Milani, J.; Perutz, R. N. Selectivity of C–H Activation and Competition between C–H and C–F Bond Activation at Fluorocarbons. *Chem. Rev.* **2017**, *117*, 8710–8753.
- (37) Ma, X.; Liu, Y.; Liu, P.; Xie, J.; Dai, B.; Liu, Z. Palladium-Catalyzed Direct Arylation of Polyfluoroarene and Facile Synthesis of Liquid Crystal Compounds. *Appl. Organomet. Chem.* **2014**, *28*, 180–185.
- (38) Cao, M.; Wu, D.; Su, W.; Cao, R. Palladium Nanocrystals Stabilized by Cucurbit[6]Urils as Efficient Heterogeneous Catalyst for Direct C–H Functionalization of Polyfluoroarenes. *J. Catal.* **2015**, *321*, 62–69.

- (39) Zhou, Y.; Wang, J.; Gu, Z.; Wang, S.; Zhu, W.; Acenã, J. L.; Soloshonok, V. A.; Izawa, K.; Liu, H. Next Generation of Fluorine-Containing Pharmaceuticals, Compounds Currently in Phase II-III Clinical Trials of Major Pharmaceutical Companies: New Structural Trends and Therapeutic Areas. *Chem. Rev.* **2016**, *116*, 422–518.
- (40) Wang, J.; Sánchez-Roselló, M.; Aceña, J. L.; del Pozo, C.; Sorochinsky, A. E.; Fustero, S.; Soloshonok, V. A.; Liu, H. Fluorine in Pharmaceutical Industry: Fluorine-Containing Drugs Introduced to the Market in the Last Decade (2001–2011). *Chem. Rev.* **2014**, *114*, 2432–2506.
- (41) Fujiwara, T.; O'Hagan, D. Successful Fluorine-Containing Herbicide Agrochemicals. *J. Fluor. Chem.* **2014**, *167*, 16–29.
- (42) Wang, Q.; Song, H.; Wang, Q. Fluorine-Containing Agrochemicals in the Last Decade and Approaches for Fluorine Incorporation. *Chin. Chem. Lett.* **2022**, *33*, 626–642.
- (43) Jeschke, P. The Unique Role of Fluorine in the Design of Active Ingredients for Modern Crop Protection. *ChemBioChem* **2004**, *5*, 570–589.
- (44) Cheng, M.; Guo, C.; Gross, M. L. The Application of Fluorine-Containing Reagents in Structural Proteomics. *Angew. Chem. Int. Ed.* **2020**, *59*, 5880–5889.
- (45) Casa, S.; Henary, M. Synthesis and Applications of Selected Fluorine-Containing Fluorophores. *Molecules* **2021**, *26*, 1–37.
- (46) Gimenez, D.; Zhou, G.; Hurley, M. F. D.; Aguilar, J. A.; Voelz, V. A.; Cobb, S. L. Fluorinated Aromatic Monomers as Building Blocks to Control  $\alpha$ -Peptoid Conformation and Structure. *J. Am. Chem. Soc.* **2019**, *141*, 3430–3434.
- (47) Babudri, F.; Farinola, G. M.; Naso, F.; Ragni, R. Fluorinated Organic Materials for Electronic and Optoelectronic Applications: The Role of the Fluorine Atom. *Chem. Commun.* **2007**, No. 10, 1003–1022.
- (48) Berger, R.; Resnati, G.; Metrangolo, P.; Weber, E.; Hulliger, J. Organic Fluorine Compounds: A Great Opportunity for Enhanced Materials Properties. *Chem. Soc. Rev.* **2011**, *40*, 3496–3508.
- (49) Lu, W.; Kuwabara, J.; Iijima, T.; Higashimura, H.; Hayashi, H.; Kanbara, T. Synthesis of  $\pi$ -Conjugated Polymers Containing Fluorinated Arylene Units via Direct Arylation: Efficient Synthetic Method of Materials for Oleds. *Macromolecules* **2012**, *45*, 4128–4133.
- (50) Campo, M. A.; Huang, Q.; Yao, T.; Tian, Q.; Larock, R. C. 1,4-Palladium Migration via C-H Activation, Followed by Arylation: Synthesis of Fused Polycycles. *J. Am. Chem. Soc.* **2003**, *125*, 11506–11507.
- (51) Colletto, C.; Islam, S.; Julia, F. Room-Temperature Direct  $\beta$  - Arylation of Thiophenes and Benzo [ b ] Thiophenes and Kinetic Evidence for a Heck-Type Pathway. *J. Am. Chem. Soc.* **2016**, *138*, 1677–1683.

- (52) Li, W.; Nelson, D. P.; Jensen, M. S.; Scott Hoerrner, R.; Javadi, G. J.; Cai, D.; Larsen, R. D. Palladium-Catalyzed Regioselective Arylation of Imidazo[1,2-a]Pyrimidine. *Org. Lett.* **2003**, *5*, 4835–4837.
- (53) Liégault, B.; Petrov, I.; Gorelsky, S. I.; Fagnou, K. Modulating Reactivity and Diverting Selectivity in Palladium-Catalyzed Heteroaromatic Direct Arylation through the Use of a Chloride Activating/Blocking Group. *J. Org. Chem.* **2010**, *75*, 1047–1060.
- (54) Davies, D. L.; Macgregor, S. A.; McMullin, C. L. Computational Studies of Carboxylate-Assisted C-H Activation and Functionalization at Group 8-10 Transition Metal Centers. *Chem. Rev.* **2017**, *117*, 8649–8709.
- (55) Gorelsky, S. I.; Lapointe, D.; Fagnou, K. Analysis of the Concerted Metalation-Deprotonation Mechanism in Palladium-Catalyzed Direct Arylation across a Broad Range of Aromatic Substrates. *J. Am. Chem. Soc.* **2008**, *130*, 10848–10849.
- (56) García-Cuadrado, D.; Braga, A. A. C.; Maseras, F.; Echavarren, A. M. Proton Abstraction Mechanism for the Palladium-Catalyzed Intramolecular Arylation. *J. Am. Chem. Soc.* **2006**, *128*, 1066–1067.
- (57) Lafrance, M.; Lapointe, D.; Fagnou, K. Mild and Efficient Palladium-Catalyzed Intramolecular Direct Arylation Reactions. *Tetrahedron* **2008**, *64*, 6015–6020.
- (58) Pascual, S.; de Mendoza, P.; Braga, A. A. C.; Maseras, F.; Echavarren, A. M. Bidentate Phosphines as Ligands in the Palladium-Catalyzed Intramolecular Arylation: The Intermolecular Base-Assisted Proton Abstraction Mechanism. *Tetrahedron* **2008**, *64*, 6021–6029.
- (59) Boutadla, Y.; Davies, D. L.; Macgregor, S. A.; Poblador-bahamonde, A. I. Computational and Synthetic Studies on the Cyclometallation Reaction of Dimethylbenzylamine with [IrCl<sub>2</sub>Cp\*]<sub>2</sub>: Role of the Chelating Base. *Dalton Trans.* **2009**, No. 30, 5887–5893.
- (60) Boutadla, Y.; Davies, D. L.; Macgregor, S. A.; Poblador-bahamonde, A. I. Mechanisms of C–H Bond Activation: Rich Synergy between Computation and Experiment. *Dalton Trans.* **2009**, No. 30, 5820–5831.
- (61) Ess, D. H.; Bischof, S. M.; Oxgaard, J.; Periana, R. A.; Goddard, W. A. Transition State Energy Decomposition Study of Acetate-Assisted and Internal Electrophilic Substitution C-H Bond Activation by (Acac-O,O) <sub>2</sub>Ir(X) Complexes (X = CH<sub>3</sub>COO, OH). *Organometallics* **2008**, *27*, 6440–6445.
- (62) Oxgaard, J.; Tenn, W. J.; Nielsen, R. J.; Periana, R. A.; Goddard, W. A. Mechanistic Analysis of Iridium Heteroatom C-H Activation: Evidence for an Internal Electrophilic Substitution Mechanism. *Organometallics* **2007**, *26*, 1565–1567.
- (63) Lapointe, D.; Fagnou, K. Overview of the Mechanistic Work on the Concerted Metallation-Deprotonation Pathway. *Chem. Lett.* **2010**, *39*, 1118–1126.

- (64) Ackermann, L.; Vicente, R.; Althammer, A. Assisted Ruthenium-Catalyzed C-H Bond Activation: Carboxylic Acids as Cocatalysts for Generally Applicable Direct Arylations in Apolar Solvents. *Org. Lett.* **2008**, *10*, 2299–2302.
- (65) Özdemir, I.; Demir, S.; Çetinkaya, B.; Gourlaouen, C.; Maseras, F.; Bruneau, C.; Dixneuf, P. H. Direct Arylation of Arene C-H Bonds by Cooperative Action of NHCarbene-Ruthenium(II) Catalyst and Carbonate via Proton Abstraction Mechanism. *J. Am. Chem. Soc.* **2008**, *130*, 1156–1157.
- (66) Davies, D. L.; Donald, S. M. A.; Al-Duaij, O.; Fawcett, J.; Little, C.; Macgregor, S. A. N-H versus C-H Activation of a Pyrrole Imine at {Cp\*Ir}: A Computational and Experimental Study. *Organometallics* **2006**, *25*, 5976–5978.
- (67) Carrow, B. P.; Sampson, J.; Wang, L. Base-Assisted C–H Bond Cleavage in Cross-Coupling: Recent Insights into Mechanism, Speciation, and Cooperativity. *Isr. J. Chem.* **2020**, *60*, 230–258.
- (68) Platt, G. M. H. Mechanistic Investigation into the Pd-Catalysed C – H Bond Functionalisation of Fluoroarenes: Reaction Kinetics and Intermediate Characterisation, Ph.D. Dissertation, University of York, 2016.
- (69) Blackmond, D. G. Reaction Progress Kinetic Analysis: A Powerful Methodology for Mechanistic Studies of Complex Catalytic Reactions. *Angew. Chem. Int. Ed.* **2005**, *44*, 4302–4320.
- (70) Burés, J. Variable Time Normalization Analysis: General Graphical Elucidation of Reaction Orders from Concentration Profiles. *Angew. Chem. Int. Ed.* **2016**, *55*, 16084–16087.
- (71) Tan, Y.; Hartwig, J. F. Assessment of the Intermediacy of Arylpalladium Carboxylate Complexes in the Direct Arylation of Benzene: Evidence for C-H Bond Cleavage by “Ligandless” Species. *J. Am. Chem. Soc.* **2011**, *133*, 3308–3311.
- (72) Bhattacharya, T.; Dutta, S.; Maiti, D. Deciphering the Role of Silver in Palladium-Catalyzed C-H Functionalizations. *ACS Catal.* **2021**, *11*, 9702–9714.
- (73) Mudarra, Á. L.; Martínez De Salinas, S.; Pérez-Temprano, M. H. Beyond the Traditional Roles of Ag in Catalysis: The Transmetalating Ability of Organosilver(i) Species in Pd-Catalysed Reactions. *Org. Biomol. Chem.* **2019**, *17*, 1655–1667.
- (74) Lotz, M. D.; Camasso, N. M.; Canty, A. J.; Sanford, M. S. Role of Silver Salts in Palladium-Catalyzed Arene and Heteroarene C-H Functionalization Reactions. *Organometallics* **2017**, *36*, 165–171.
- (75) Bay, K. L.; Yang, Y. F.; Houk, K. N. Multiple Roles of Silver Salts in Palladium-Catalyzed C–H Activations. *J. Organomet. Chem.* **2018**, *864*, 19–25.
- (76) Yew, C. N.; Vittal, J. J.; Andy Hor, T. S. Pd(O<sub>2</sub>CCF<sub>2</sub>CF<sub>3</sub>-O)<sub>2</sub>(Dppf) and PdAg(μ-O<sub>2</sub>CCF<sub>2</sub>CF<sub>3</sub>)<sub>2</sub>(O<sub>2</sub>CCF<sub>2</sub>CF<sub>3</sub>-O)- (Dppf)[Dppf] = 1,1'-

- Bis(Diphenylphosphino)Ferrocene]: A Stable Pd(II) Phosphine Carboxylate as a Precursor to Heterobimetallic Carboxylates. *Dalton Trans.* **2002**, 2, 337–342.
- (77) Micksch, M.; Herdtweck, E.; Strassner, T. Synthesis and Structure of a Trinuclear Pd-Ag-Pd Carbene Acetato Complex. *Z. Anorg. Allg. Chem.* **2013**, 639, 1237–1241.
- (78) Kozitsyna, N. Y.; Nefedov, S. E.; Klyagina, A. P.; Markov, A. A.; Dobrokhotova, Z. V.; Velikodny, Y. A.; Kochubey, D. I.; Zyubina, T. S.; Gekhman, A. E.; Vargaftik, M. N.; Moiseev, I. I. Novel Heterometallic Palladium-Silver Complex. *Inorg. Chim. Acta* **2011**, 370, 382–387.
- (79) Yang, Y. F.; Cheng, G. J.; Liu, P.; Leow, D.; Sun, T. Y.; Chen, P.; Zhang, X.; Yu, J. Q.; Wu, Y. D.; Houk, K. N. Palladium-Catalyzed Meta-Selective C-H Bond Activation with a Nitrile-Containing Template: Computational Study on Mechanism and Origins of Selectivity. *J. Am. Chem. Soc.* **2014**, 136, 344–355.
- (80) Fang, L.; Saint-Denis, T. G.; Taylor, B. L. H.; Ahlquist, S.; Hong, K.; Liu, S.; Han, L.; Houk, K. N.; Yu, J. Q. Experimental and Computational Development of a Conformationally Flexible Template for the Meta-C-H Functionalization of Benzoic Acids. *J. Am. Chem. Soc.* **2017**, 139, 10702–10714.
- (81) Zhang, L.; Zhao, C.; Liu, Y.; Xu, J.; Xu, X.; Jin, Z. Activation of Remote Meta-C-H Bonds in Arenes with Tethered Alcohols: A Salicylonitrile Template. *Angew. Chem. Int. Ed.* **2017**, 56, 12245–12249.
- (82) Anand, M.; Sunoj, R. B.; Schaefer, H. F. Non-Innocent Additives in a Palladium(II)-Catalyzed C-H Bond Activation Reaction: Insights into Multimetallic Active Catalysts. *J. Am. Chem. Soc.* **2014**, 136, 5535–5538.
- (83) Anand, M.; Sunoj, R. B.; Schaefer, H. F. Palladium-Silver Cooperativity in an Aryl Amination Reaction through C-H Functionalization. *ACS Catal.* **2016**, 6, 696–708.
- (84) Yoo, E. J.; Ma, S.; Mei, T. S.; Chan, K. S. L.; Yu, J. Q. Pd-Catalyzed Intermolecular C-H Amination with Alkylamines. *J. Am. Chem. Soc.* **2011**, 133, 7652–7655.
- (85) Whitaker, D.; Burés, J.; Larrosa, I. Ag(I)-Catalyzed C-H Activation: The Role of the Ag(I) Salt in Pd/Ag-Mediated C-H Arylation of Electron-Deficient Arenes. *J. Am. Chem. Soc.* **2016**, 138, 8384–8387.
- (86) Whitaker, D.; Burés, J.; Larrosa, I. Ag(I)-Catalyzed C-H Activation: The Role of the Ag(I) Salt in Pd/Ag-Mediated C-H Arylation of Electron-Deficient Arenes. *J. Am. Chem. Soc.* **2016**, 138, 8384–8387.
- (87) Lee, S. Y.; Hartwig, J. F. Palladium-Catalyzed, Site-Selective Direct Allylation of Aryl C-H Bonds by Silver-Mediated C-H Activation: A Synthetic and Mechanistic Investigation. *J. Am. Chem. Soc.* **2016**, 138, 15278–15284.
- (88) Li, W.; Yuan, D.; Wang, G.; Zhao, Y.; Xie, J.; Li, S.; Zhu, C. Cooperative Au/Ag Dual-Catalyzed Cross-Dehydrogenative Biaryl Coupling: Reaction Development and

- Mechanistic Insight. *J. Am. Chem. Soc.* **2019**, *141*, 3187–3197.
- (89) Colletto, C.; Panigrahi, A.; Fernández-Casado, J.; Larrosa, I. Ag(I)-C-H Activation Enables Near-Room-Temperature Direct  $\alpha$ -Arylation of Benzo[ b]Thiophenes. *J. Am. Chem. Soc.* **2018**, *140*, 9638–9643.
- (90) Lyons, T. W.; Sanford, M. S. Palladium-Catalyzed Ligand-Directed C - H Functionalization Reactions. *Chem. Rev.* **2010**, *110*, 1147–1169.
- (91) Leone, A. K.; Goldberg, P. K.; McNeil, A. J. Ring-Walking in Catalyst-Transfer Polymerization. *J. Am. Chem. Soc.* **2018**, *140*, 7846–7850.
- (92) Panigrahi, A.; Whitaker, D.; Vitorica-Yrezabal, I. J.; Larrosa, I. Ag/Pd Cocatalyzed Direct Arylation of Fluoroarene Derivatives with Aryl Bromides. *ACS Catal.* **2020**, *10*, 2100–2107.
- (93) Hu, G. Q.; Li, E. C.; Zhang, H. H.; Huang, W. Ag(i)-Mediated Hydrogen Isotope Exchange of Mono-Fluorinated (Hetero)Arenes. *Org. Biomol. Chem.* **2020**, *18*, 6627–6633.
- (94) Tlahuext-Aca, A.; Hartwig, J. F. Site-Selective Silver-Catalyzed C-H Bond Deuteration of Five-Membered Aromatic Heterocycles and Pharmaceuticals. *ACS Catal.* **2021**, *11*, 1119–1127.
- (95) Tyrra, W.; Wickleder, M. S. Silver Compounds in Synthetic Chemistry. 1. A Facile Preparative Route for Pentafluorophenylsilver, AgC<sub>6</sub>F<sub>5</sub> and Its Use as an Oxidative Pentafluorophenyl Group Transfer Reagent in Reactions with Group 12 to 16 Elements. *Z. Anorg. Allg. Chem.* **2002**, *628*, 1841–1847.
- (96) Penner, G. H.; Li, W. Silver-109 NMR Spectroscopy of Inorganic Solids. *Inorg. Chem.* **2004**, *43*, 5588–5597.
- (97) Zangger, K.; Armitage, I. M. Silver and Gold NMR. *Met. Based. Drugs* **1999**, *6*, 239–245.
- (98) Endo, K.; Yamamoto, K.; Matsushita, K.; Deguchi, K.; Kanda, K.; Nakatsuji, H. Correlation between Metal NMR Physical Quantities and Structures of Metal Complexes. I. 109Ag NMR Spectroscopy of Aqueous Silver Ions Coordinated with Nitroxide Radical. *J. Magn. Reson.* **1985**, *65*, 268–281.
- (99) Létinois-Halbes, U.; Pale, P.; Berger, S. Ag NMR as a Tool for Mechanistic Studies of Ag-Catalyzed Reactions: Evidence for in Situ Formation of Alkyn-1-Yl Silver from Alkynes and Silver Salts. *J. Org. Chem.* **2005**, *70*, 9185–9190.
- (100) Van der Ploeg, A. F. M. J.; Van Koten, G.; Brevard, C. INEPT 109Ag NMR Evidence for Direct Pt-to-Ag Bonding in Dinuclear [[2,6-Me<sub>2</sub>NCH<sub>2</sub>)<sub>2</sub>C<sub>6</sub>H<sub>3</sub>][p-TolNC(H)NR]PtAgBr]. *Inorg. Chem.* **1982**, *21*, 2878–2881.
- (101) Berners-Price, S. J.; Sadler, P. J.; Brevard, C. Tetrahedral, Chelated, Silver(I) Diphosphine Complexes. Rapid Measurements of Chemical Shifts and Couplings by

- Two-dimensional  $^{31}\text{P}$ - $\{^{109}\text{Ag}\}$  NMR Spectroscopy. *Magn. Reson. Chem.* **1990**, *28*, 145–148.
- (102) Bestgen, S.; Fuhr, O.; Breitung, B.; Kiran Chakravadhanula, V. S.; Guthausen, G.; Hennrich, F.; Yu, W.; Kappes, M. M.; Roesky, P. W.; Fenske, D.  $[\text{Ag}_{11}\text{S}_{34}(\text{SCH}_2\text{C}_6\text{H}_4\text{tBu})_4(\text{Dpph})_6]$ : Synthesis, Crystal Structure and NMR Investigations of a Soluble Silver Chalcogenide Nanocluster. *Chem. Sci.* **2017**, *8*, 2235–2240.
- (103) Liannza, F.; Macchionni, A.; Pregosin, P.; Ruegger, H. Multidimensional  $^{109}\text{Ag}$ ,  $^{31}\text{P}$  and  $^1\text{H}$  HMQC and HSQC NMR Studies on a Model Homogeneous Catalyst. Reactions of a Chiral Ferrocenylphosphine with  $\text{Ag}(\text{CF}_3\text{SO}_3)$ . *Inorg. Chem.* **1994**, *33*, 4999–5002.
- (104) Muetterties, E. L.; Alegranti, C. W. Solution Structure and Kinetic Study of Metal–Phosphine and –Phosphite Complexes. I. The Silver(I) System. *J. Am. Chem. Soc.* **1972**, *94*, 6386–6391.
- (105) Patmore, N. J.; Hague, C.; Cotgreave, J. H.; Mahon, M. F.; Frost, C. G.; Weller, A. S. Silver Phosphanes Partnered with Carborane Monoanions: Synthesis, Structures and Use as Highly Active Lewis Acid Catalysts in a Hetero-Diels-Alder Reaction. *Chem. Eur. J.* **2002**, *8*, 2088–2098.
- (106) Keller, S.; Camenzind, T. N.; Abraham, J.; Prescimone, A.; Häussinger, D.; Constable, E. C.; Housecroft, C. E. Self-Assembly of Heteroleptic Dinuclear Silver(I) Complexes Bridged by Bis(Diphenylphosphino)Ethyne. *Dalton Trans.* **2018**, *47*, 946–957.
- (107) Bachman, R. E.; Andretta, D. F. Metal-Ligand Bonding in Coinage Metal-Phosphine Complexes: The Synthesis and Structure of Some Low-Coordinate Silver(I)-Phosphine Complexes. *Inorg. Chem.* **1998**, *37*, 5657–5663.
- (108) Sun, K. K.; Miller, W. T. Perfluorophenylsilver. *J. Am. Chem. Soc.* **1970**, *92*, 6985–6987.
- (109) Utin, R.; Laguna, A.; Abad, J. A. Pentahalophenylargentate(I) Complexes. *J. Organomet. Chem.* **1983**, *246*, 341–345.
- (110) Hofstee, H. K.; Boersma, J.; Van Der Kerk, G. J. M. The Reaction of Diarylzinc Compounds with Silver Salts. *J. Organomet. Chem.* **1979**, *168*, 241–249.
- (111) Beverwijk, C. D. M.; Van Der Kerk, G. J. . The Synthesis and Properties of Phenylsilver. *J. Organomet. Chem.* **1972**, *43*, 11–12.
- (112) Kuprat, M.; Lehmann, M.; Schulz, A.; Villinger, A. Synthesis of Pentafluorophenyl Silver by Means of Lewis Acid Catalysis: Structure of Silver Solvent Complexes. *Organometallics* **2010**, *29*, 1421–1427.
- (113) Ibad, M. F.; Schulz, A.; Villinger, A. Pentafluorophenyl Silver: Structure and Bonding of Arene Solvates. *Organometallics* **2015**, *34*, 3893–3901.

- (114) Floriani, C.; Meyer, E. M.; Gambarotta, S.; Chiesi-Villa, A.; Guastini, C. Polynuclear Aryl Derivatives of Group 11 Metals: Synthesis, Solid State-Solution Structural Relationship, and Reactivity with Phosphines. *Organometallics* **1989**, *8*, 1067–1079.
- (115) Edwards, D. A.; Harker, R. M.; Mahon, M. F.; Molloy, K. C. Crystallographic Analysis of an Intramolecularly Stabilised Organosilver Tetramer  $[\text{Ag}(\text{C}_6\text{H}_4\text{CH}_2\text{NMe}_2)_2]_4$ , and the First Structurally Characterised Silver Siloxide,  $\{[\text{Ag}(\text{PPh}_3)]_2\text{-(M}_4\text{-OMe}_2\text{SiOSiMe}_2\text{O)}\}_2$ . *Dalton Trans.* **1997**, No. 1, 3509–3513.
- (116) Voelker, H.; Labahn, D.; Bohnen, F. M.; Herbst-Irmer, R.; Roesky, H. W.; Stalke, D.; Edelmann, F. T. Structural Diversity in Nonfluoromesityl Chemistry. *New J. Chem.* **1999**, *23*, 905–909.
- (117) Jeffries, P. M.; Wilson, S. R.; Girolami, G. S. Crystal Structure of  $[\text{CF}_3\text{CFC}(\text{CF}_3)\text{Ag}]_4$  and Its Use as a Chemical Vapor Deposition Precursor for Silver Films. *J. Organomet. Chem.* **1993**, *449*, 203–209.
- (118) Hwang, C. S.; Power, P. P. Synthesis and Characterization of the Lithium Organoargentate Salts  $[\text{Li}(\text{THF})_4][\text{Ag}(\text{Triph})_2] \cdot \text{THF}$  and  $[\text{Li}(\text{THF})_4][\text{Ag}(\text{C}_6\text{H}_3\text{-2,6-Mes}_2)_2] \cdot 1/8\text{OEt}_2$  (Triph =  $\text{C}_6\text{H}_2\text{-2,4,6-Ph}_3$ ; Mes =  $\text{C}_6\text{H}_2\text{-2,4,6-Me}_3$ ). *J. Organomet. Chem.* **1999**, *589*, 234–238.
- (119) Usón, R.; Laguna, A.; Usón, A.; Jones, P. G. .; Meyer-Bäse, K. Synthesis of Pentafluorophenyl(Ylide)Silver(I) Complexes: X-Ray Structures of Two Modifications of  $[\text{Ag}(\text{C}_6\text{F}_5)(\text{CH}_2\text{PPh}_3)]$ . *Dalton Trans.* **1988**, 341–345.
- (120) Meijboom, R.; Bowen, R. J.; Berners-Price, S. J. Coordination Complexes of Silver(I) with Tertiary Phosphine and Related Ligands. *Coord. Chem. Rev.* **2009**, *253*, 325–342.
- (121) Bowmaker, G. A.; Effendy; Hanna, J. V.; Healy, P. C.; King, S. P.; Pettinari, C.; Skelton, B. W.; White, A. H. Solution and Mechanochemical Syntheses, and Spectroscopic and Structural Studies in the Silver(i) (Bi-)Carbonate: Triphenylphosphine System. *Dalton Trans.* **2011**, *40*, 7210–7218.
- (122) Sołtys-Brzostek, K.; Terlecki, M.; Sokołowski, K.; Lewiński, J. Chemical Fixation and Conversion of  $\text{CO}_2$  into Cyclic and Cage-Type Metal Carbonates. *Coord. Chem. Rev.* **2017**, *334*, 199–231.
- (123) Edwards, D. A.; Harker, R. M.; Mahon, M. F.; Molloy, K. C. Aerosol-Assisted Chemical Vapour Deposition (AACVD) of Silver Films from Triorganophosphine Adducts of Silver Carboxylates, Including the Structure of  $[\text{Ag}(\text{O}_2\text{CC}_3\text{F}_7)(\text{PPh}_3)_2]$ . *Inorg. Chim. Acta* **2002**, *328*, 134–146.
- (124) Pérez-galán, P.; Delpont, N.; Herrero-Gómez, E.; Maseras, F.; Echavarren, A. M. Metal – Arene Interactions in Dialkylbiarylphosphane Complexes of Copper, Silver, and Gold. *Chem. Eur. J.* **2010**, *16*, 5324–5332.
- (125) Herrero-gómez, E.; Nieto-Oberhuber, C.; López, S.; Benet-Buchholz, J.; Echavarren,



- A. M. Cationic H1/H2-Gold(I) Complexes of Simple Arenes. *Angew. Chem. Int. Ed.* **2006**, *45*, 5455–5459.
- (126) Tyrra, W.; Wickleder, M. S. A Facile Preparative Route for Pentafluorophenylsilver, AgC6F5 and Its Use as an Oxidative Pentafluorophenyl Group Transfer Reagent in Reactions with Group 12 to 16 Elements - the Single Crystal Structure of AgC6F5·EtCN, the First Arylsilver Derivative. *Z. Anorg. Allg. Chem.* **2002**, *628*, 1841–1847.
- (127) Milner, P. J.; Maimone, T. J.; Su, M.; Chen, J.; Müller, P.; Buchwald, S. L. Investigating the Dearomative Rearrangement of Biaryl Phosphine-Ligated Pd(II) Complexes. *J. Am. Chem. Soc.* **2012**, *134*, 19922–19934.
- (128) Ricci, P.; Krämer, K.; Cambeiro, X. C.; Larrosa, I. Arene-Metal  $\pi$ -Complexation as a Traceless Reactivity Enhancer for C-H Arylation. *J. Am. Chem. Soc.* **2013**, *135*, 13258–13261.
- (129) Johnson, S. A.; Taylor, E. T.; Cruise, S. J. A Combined Experimental and Computational Study of Unexpected C-F Bond Activation Intermediates and Selectivity in the Reaction of Pentafluorobenzene with a (PEt3)2Ni Synthon. *Organometallics* **2009**, *28*, 3842–3855.
- (130) Jeener, J. Meier, B.H., Bachmann, P, Ernst, R. R. Investigation of Exchange Process by Two Dimensional NMR Spectroscopy. *J. Chem. Phys.* **1979**, *71*, 4546–4553.
- (131) Larson, P. E. Z.; Kerr, A. B.; Leon Swisher, C.; Pauly, J. M.; Vigneron, D. B. A Rapid Method for Direct Detection of Metabolic Conversion and Magnetization Exchange with Application to Hyperpolarized Substrates. *J. Magn. Reson.* **2012**, *225*, 71–80.
- (132) Aski, S. N.; Takacs, Z.; Kowalewski, J. Inclusion Complexes of Cryptophane-E with Dichloromethane and Chloroform: A Thermodynamic and Kinetic Study Using the 1D-EXSY NMR Method. *Magn. Reson. Chem.* **2008**, *46*, 1135–1140.
- (133) Wilkins, R. G. *Kinetics and Mechanism of Reactions of Transition Metal Complexes*, 2nd ed.; 1992; Vol. 426.
- (134) Scott, N. W. J.; Ford, M. J.; Schotes, C.; Parker, R. R.; Whitwood, A. C.; Fairlamb, I. J. S. The Ubiquitous Cross-Coupling Catalyst System 'Pd(OAc)2'/2PPh3 Forms a Unique Dinuclear PdI Complex: An Important Entry Point into Catalytically Competent Cyclic Pd3 Clusters. *Chem. Sci.* **2019**, *10*, 7898–7906.
- (135) Elkoush, T.; Reich, N. D.; Campbell, M. G. Dinuclear Silver Complexes in Catalysis. *Angew. Chem. Int. Ed.* **2021**, *60*, 22614–22622.
- (136) Pla, D.; Gómez, M. Metal and Metal Oxide Nanoparticles: A Lever for C-H Functionalization. *ACS Catal.* **2016**, *6*, 3537–3552.
- (137) Reay, A. J.; Fairlamb, I. J. S. Catalytic C-H Bond Functionalisation Chemistry: The Case for Quasi-Heterogeneous Catalysis. *Chem. Commun.* **2015**, *51*, 16289–16307.

- (138) Reay, A. J.; Neumann, L. K.; Fairlamb, I. J. S. Catalyst Efficacy of Homogeneous and Heterogeneous Palladium Catalysts in the Direct Arylation of Common Heterocycles. *Synlett* **2016**, *27*, 1211–1216.
- (139) Martin, R.; Buchwald, S. L. Palladium-Catalyzed Suzuki-Miyaura Cross-Coupling Reactions Employing Dialkylbiaryl Phosphine Ligands. *Acc. Chem. Res.* **2008**, *41*, 1461–1473.
- (140) Surry, D. S.; Buchwald, S. L. Dialkylbiaryl Phosphines in Pd-Catalyzed Amination: A User's Guide. *Chem. Sci.* **2011**, *2*, 27–50.
- (141) Surry, D. S.; Buchwald, S. L. Biaryl Phosphane Ligands in Palladium-Catalyzed Amination. *Angew. Chem. Int. Ed.* **2008**, *47*, 6338–6361.
- (142) Kaye, S.; Fox, J. M.; Hicks, F. A.; Buchwald, S. L. The Use of Catalytic Amounts of CuCl and Other Improvements in the Benzyne Route to Biphenyl-Based Phosphine Ligands. *Adv. Synth. Catal.* **2001**, *343*, 789–794.
- (143) Barder, T. E.; Buchwald, S. L. Rationale behind the Resistance of Dialkylbiaryl Phosphines toward Oxidation by Molecular Oxygen. *J. Am. Chem. Soc.* **2007**, *129*, 5096–5101.
- (144) Arrechea, P. L.; Buchwald, S. L. Biaryl Phosphine Based Pd(II) Amido Complexes: The Effect of Ligand Structure on Reductive Elimination. *J. Am. Chem. Soc.* **2016**, *138*, 12486–12493.
- (145) Allgeier, A. M.; Shaw, B. J.; Hwang, T. L.; Milne, J. E.; Tedrow, J. S.; Wilde, C. N. Characterization of Two Stable Degradants of Palladium Tbxphos Catalyst and a Unique Dearomatization Reaction. *Organometallics* **2012**, *31*, 519–522.
- (146) Heald, A. Studying the Effect of Buchward Ligands on a Palladium Catalysed Direct Arylation Reaction with Characterisation of Silver Intermediates, MChem Dissertation, University of York, 2021.
- (147) Chin, R. M.; Dong, L.; Duckett, S. B.; Partridge, M. G.; Jones, W. D.; Perutz, R. N. Control of H<sub>2</sub>-Coordination vs C-H Bond Activation by Rhodium: The Role of Aromatic Resonance Energies. *J. Am. Chem. Soc.* **1993**, No. 115, 7685–7695.
- (148) Lang, H.; Herres, M.; Zsolnai, L. Synthesis and Characterization of Monomeric Bis(H<sub>2</sub>-Alkyne)Silver(I) Compounds: Crystal Structure of {(H<sub>5</sub>-C<sub>5</sub>H<sub>4</sub>SiMe<sub>3</sub>)<sub>2</sub>Ti(CCSiMe<sub>3</sub>)<sub>2</sub>}AgNO<sub>2</sub>. *Organometallics* **1993**, *12*, 5008–5011.
- (149) Jasim, N. A.; Perutz, R. N.; Whitwood, A. C.; Braun, T.; Izundu, J.; Neumann, B.; Rothfeld, S.; Stammler, H. G. Contrasting Reactivity of Fluoropyridines at Palladium and Platinum: C-F Oxidative Addition at Palladium, P-C and C-F Activation at Platinum. *Organometallics* **2004**, *23*, 6140–6149.
- (150) Alharis, R. A.; McMullin, C. L.; Davies, D. L.; Singh, K.; Macgregor, S. A. The Importance of Kinetic and Thermodynamic Control When Assessing Mechanisms of

- Carboxylate-Assisted C-H Activation. *J. Am. Chem. Soc.* **2019**, *141*, 8896–8906.
- (151) Zheng, Q. Z.; Jiao, N. Ag-Catalyzed C-H/C-C Bond Functionalization. *Chem. Soc. Rev.* **2016**, *45*, 4590–4627.
- (152) Myers, A. G.; Tanaka, D.; Mannion, M. R. Development of a Decarboxylative Palladation Reaction and Its Use in a Heck-Type Olefination of Arene Carboxylates. *J. Am. Chem. Soc.* **2002**, *124*, 11250–11251.
- (153) Hossian, A.; Bhunia, S. K.; Jana, R. Substrate-Dependent Mechanistic Divergence in Decarboxylative Heck Reaction at Room Temperature. *J. Org. Chem.* **2016**, *81*, 2521–2533.
- (154) Cornella, J.; Lahlali, H.; Larrosa, I. Decarboxylative Homocoupling of (Hetero)Aromatic Carboxylic Acids. *Chem. Commun.* **2010**, *46*, 8276–8278.
- (155) Hu, P.; Shang, Y.; Su, W. A General Pd-Catalyzed Decarboxylative Cross-Coupling Reaction between Aryl Carboxylic Acids: Synthesis of Biaryl Compounds. *Angew. Chem. Int. Ed.* **2012**, *51*, 5945–5949.
- (156) Tanaka, D.; Romeril, S. P.; Myers, A. G. On the Mechanism of the Palladium(II)-Catalyzed Decarboxylative Olefination of Arene Carboxylic Acids. Crystallographic Characterization of Non-Phosphine Palladium(II) Intermediates and Observation of Their Stepwise Transformation in Heck-like Processes. *J. Am. Chem. Soc.* **2005**, *127*, 10323–10333.
- (157) Rodríguez, N.; Goossen, L. J. Decarboxylative Coupling Reactions: A Modern Strategy for C–C-Bond Formation. *Chem. Soc. Rev.* **2011**, *40*, 5030–5048.
- (158) Lu, P.; Sanchez, C.; Cornella, J.; Larrosa, I. Silver-Catalyzed Protodecarboxylation of Heteroaromatic Carboxylic Acids. *Org. Lett.* **2009**, *11*, 5710–5713.
- (159) Fang, G.; Bi, X. Silver-Catalysed Reactions of Alkynes: Recent Advances. *Chem. Soc. Rev.* **2015**, *44*, 8124–8173.
- (160) Liu, C.; Luo, Y.; Zhang, W.; Qu, J.; Lu, X. DFT Studies on the Silver-Catalyzed Carboxylation of Terminal Alkynes with CO<sub>2</sub>: An Insight into the Catalytically Active Species. *Organometallics* **2014**, *33*, 2984–2989.
- (161) Jover, J.; Maseras, F. Computational Characterization of the Mechanism for Coinage-Metal-Catalyzed Carboxylation of Terminal Alkynes. *J. Org. Chem.* **2014**, *79*, 11981–11987.
- (162) Mo, G.; Tian, Z.; Li, J.; Wen, G.; Yang, X. Silver-Catalyzed Glaser Coupling of Alkynes. *Appl. Organomet. Chem.* **2015**, *29*, 231–233.
- (163) Zhang, X.; Zhang, W. Z.; Ren, X.; Zhang, L. L.; Lu, X. B. Ligand-Free Ag(I)-Catalyzed Carboxylation of Terminal Alkynes with CO<sub>2</sub>. *Org. Lett.* **2011**, *13*, 2402–2405.
- (164) Halbes-Létinois, U.; Pale, P. Pd-Ag Catalyzed Selective Dicomplexing of  $\alpha$ -Trialkylsilyl

- $\alpha,\omega$ -Diyne; the First One-Pot Synthesis of Dienediynes. *J. Organomet. Chem.* **2003**, *687*, 420–424.
- (165) Halbes, U.; Pale, P. A New Mild Procedure for the Direct Coupling of 1-Trimethylsilyl Acetylenes with Vinyl Triflates or Aryl Iodide. *Tetrahedron Lett.* **2002**, *43*, 2039–2042.
- (166) Dillinger, S.; Bertus, P.; Pale, P. First Evidence for the Use of Organosilver Compounds in Pd-Catalyzed Coupling Reactions; A Mechanistic Rationale for the Pd/Ag-Catalyzed Enyne Synthesis? *Org. Lett.* **2001**, *3*, 1661–1664.
- (167) Létinois-Halbes, U.; Pale, P.; Berger, S. Triphenylphosphane Complex Formation with Hexyn-1-Yl Silver. *Magn. Reson. Chem.* **2004**, *42*, 831–834.
- (168) CrysAlisPro, Oxford Diffraction Ltd. Version 1.171.40.84.
- (169) Empirical Absorption Correction Using Spherical Harmonics, Implemented in SCALE3 ABSPACK Scaling Algorithm within CrysAlisPro Software, Oxford Diffraction Ltd. Version 1.171.34.40.
- (170) Sheldrick, G. M. SHELXT – Integrated Space-Group and Crystal-Structure Determination. *Acta Crystallogr. A* **71**, 3–8.
- (171) Sheldrick, G. M. Crystal Structure Refinement with SHELXL. *Acta Crystallogr.* **2015**, *C71*, 3–8.
- (172) Finck, L.; Oestreich, M. Transition-Metal-Free Coupling of Polyfluorinated Arenes and Functionalized, Masked Aryl Nucleophiles. *Chem. Eur. J.* **2021**, *27*, 11061–11064.
- (173) Lafrance, M.; Shore, D.; Fagnou, K. Mild and General Conditions for the Cross-Coupling of Aryl Halides with Pentafluorobenzene and Other Perfluoroaromatics. *Org. Lett.* **2006**, *8*, 5097–5100.
- (174) Chen, Q.; Wu, A.; Qin, S.; Zeng, M.; Le, Z.; Yan, Z.; Zhang, H. Ni-Catalyzed Decarboxylative Cross-Coupling of Potassium Polyfluorobenzoates with Unactivated Phenol and Phenylmethanol Derivatives. *Adv. Synth. Catal.* **2018**, *360*, 3239–3244.
- (175) Burns, M. J.; Thatcher, R. J.; Taylor, R. J. K.; Fairlamb, I. J. S. Pd-Catalysed Regioselective C–H Functionalisation of 2-Pyrones. *Dalton Trans.* **2010**, *39*, 10392–10400.
- (176) Negishi, E. I.; Takahashi, T.; Baba, S.; Van Horn, D. E.; Okukado, N. Palladium- or Nickel-Catalyzed Reactions of Alkenylmetals with Unsaturated Organic Halides as a Selective Route to Arylated Alkenes and Conjugated Dienes: Scope, Limitations, and Mechanism<sup>1,2</sup>. *J. Am. Chem. Soc.* **1987**, *109*, 2393–2401.
- (177) Athavan, G.; Tanner, T. F. N.; Whitwood, A. C.; Fairlamb, I. J. S.; Perutz, R. N. Direct Evidence for Competitive C–H Activation by a Well-Defined Silver XPhos Complex in Palladium-Catalyzed C–H Functionalization. *Organometallics* **2022**.